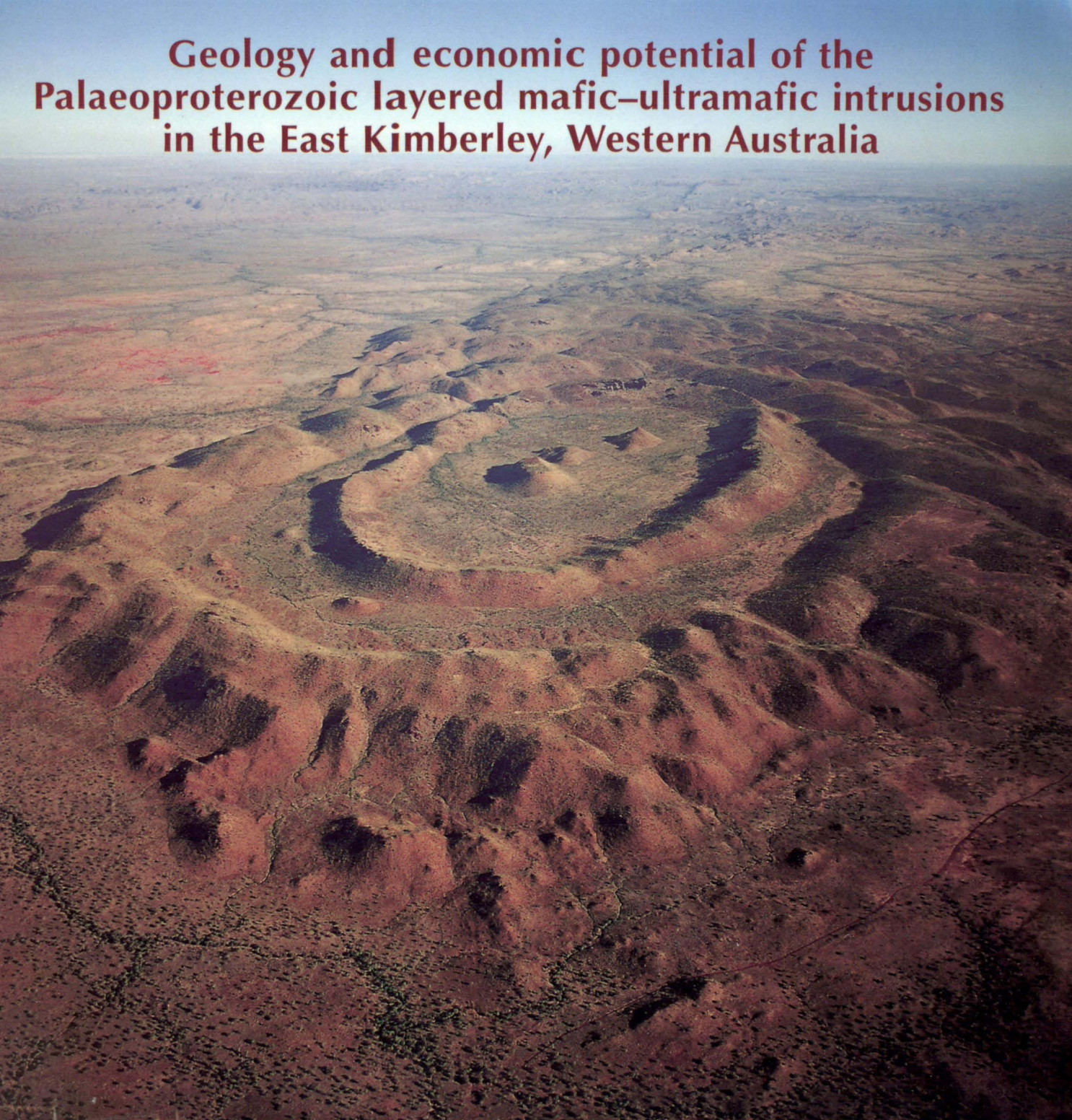
Geology and economic potential of the Palaeoproterozoic layered mafic–ultramafic intrusions in the East Kimberley, Western Australia



BMR
S55
(94)
BUL.45
v.246
copy 3

AGSO

AUSTRALIAN GEOLOGICAL SURVEY ORGANISATION

AGSO BULLETIN 246

GEOLOGICAL SURVEY · WESTERN AUSTRALIA ·

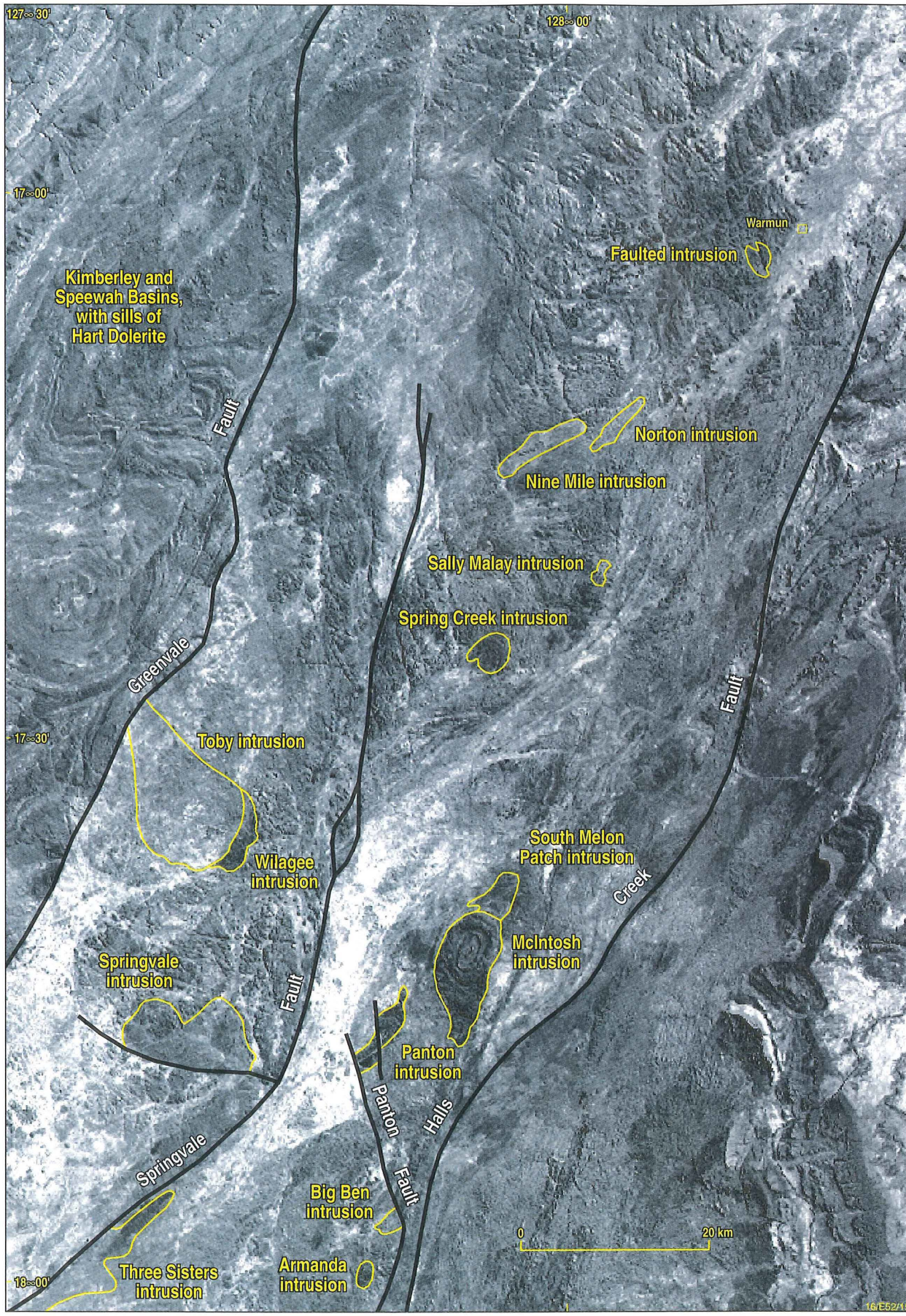
Compiled and edited by Dean M. Hoatson & David H. Blake

BMR
555
(94)
BUL.45
v.246
Copy 3

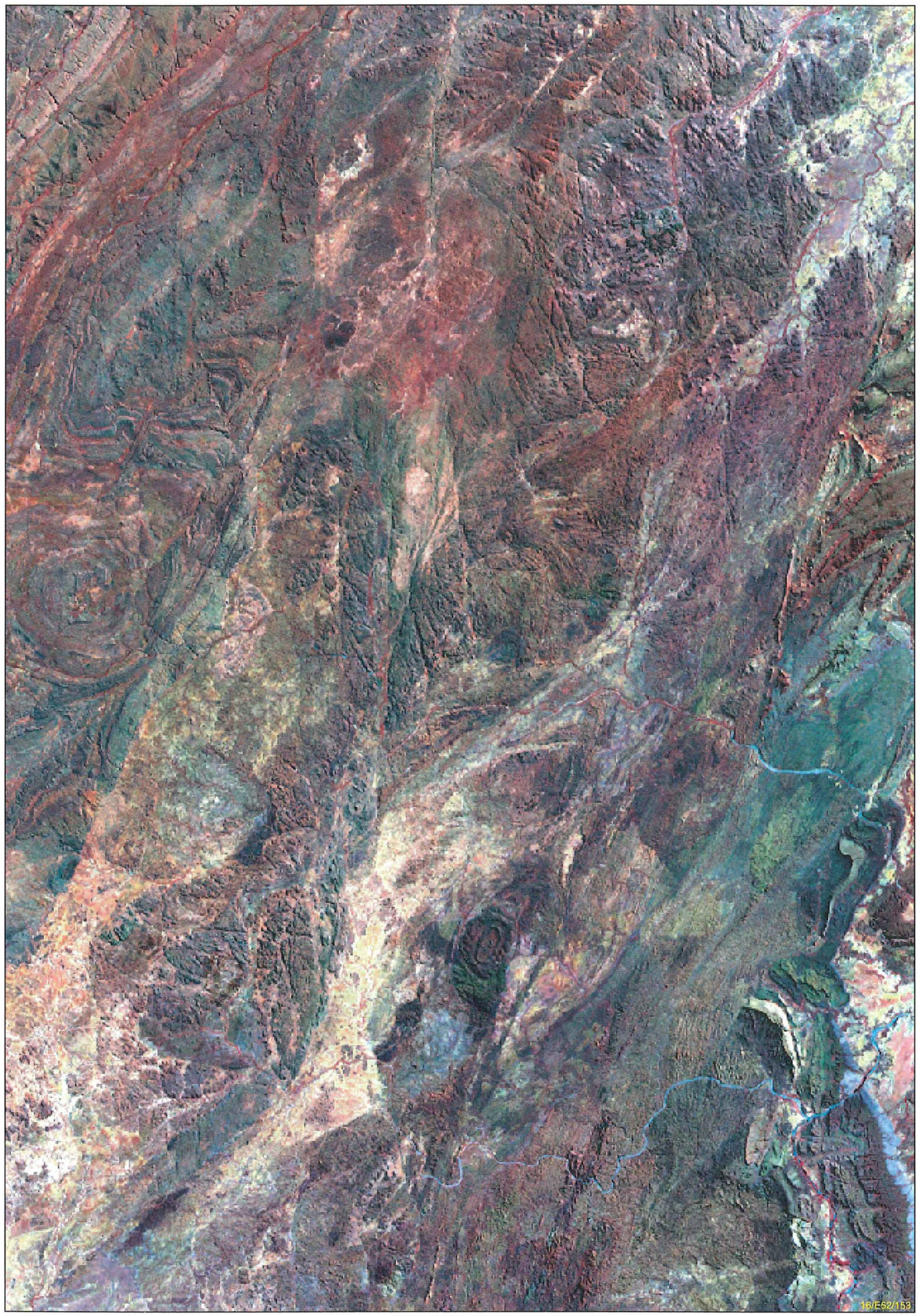
AGSO BULLETIN 246

Geology and economic potential of the Palaeoproterozoic layered mafic–ultramafic intrusions in the East Kimberley, Western Australia





Annotated grey scale image, using band 7, for facing colour Landsat image.



The regional setting of the Palaeoproterozoic layered mafic–ultramafic intrusions in the Halls Creek Orogen described in this *Bulletin*. Landsat Multispectral Scanner (MSS) colour composite image using bands 7, 5, and 4 displayed as red, blue, and green, respectively. The Landsat data, received by the Australian Centre for Remote Sensing, AUSLIG, Canberra (www.auslig.gov.au), is part of a geocoded Landsat MSS mosaic produced by Geoimage Pty Ltd. Image was processed by L.F. Macias (AGSO).

AUSTRALIAN GEOLOGICAL SURVEY ORGANISATION

BULLETIN 246

Geology and economic potential of the Palaeoproterozoic layered mafic–ultramafic intrusions in the East Kimberley, Western Australia

Compiled and edited by Dean M. Hoatson & David H. Blake

Department of Industry, Science & Resources

Minister for Industry, Science & Resources: Senator the Hon. Nick Minchin

Parliamentary Secretary: The Hon. Warren Entsch, MP

Australian Geological Survey Organisation

Chief Executive Officer: Neil Williams

Department of Minerals and Energy, Western Australia

Minister for Mines: The Hon. Norman Moore, MLC

Geological Survey of Western Australia

Director: David Blight

ISSN 0084–7089

ISBN 0 642 39801 1

© Commonwealth of Australia 2000

This work is copyright. Apart from any fair dealings for the purposes of study, research, criticism, or review, as permitted under the *Copyright Act 1968*, no part may be reproduced by any process without written permission. Copyright is the responsibility of the Chief Executive Officer, Australian Geological Survey Organisation. Requests and enquiries should be directed to the Chief Executive Officer, Australian Geological Survey Organisation, GPO Box 378, Canberra, ACT 2601.

AGSO has tried to make the information in this *Bulletin* as accurate as possible. However, it does not guarantee that the information is totally accurate or complete. Therefore, you should not rely solely on this information when making a commercial decision.

Technical editing by Ian Hodgson
Cover design by Karin Weiss (AGSO) and figures prepared by AGSO Information Management Branch
Command E of Adelaide carried out the high-resolution scanning of the cover photographs
Printed in Australia by National Capital Printing, Fyshwick, Canberra, ACT 2609

Recommended bibliographic citation:

Bulletin as a whole:
Hoatson, D.M. & Blake D.H. (editors), 2000. Geology and economic potential of the Palaeoproterozoic layered mafic–ultramafic intrusions in the East Kimberley, Western Australia. Canberra: Australian Geological Survey Organisation Bulletin 246, 496pp.

Individual chapters:
Sproule, R.A., Lambert, D.D. & Hoatson, D.M., 2000. Geochemical and isotopic constraints on the petrogenesis of the Panton and Sally Malay intrusions: implications for exploration. In: Hoatson, D.M. & Blake D.H. (editors), Geology and economic potential of the Palaeoproterozoic layered mafic–ultramafic intrusions in the East Kimberley, Western Australia. Canberra: Australian Geological Survey Organisation Bulletin 246, 250–264pp.

Front cover: Aerial photograph looking south of the group VI McIntosh layered mafic intrusion. Photograph by Ian Oswald-Jacobs.

Back cover: Aerial photograph looking southwest along the synclinal axis of the group I Panton layered mafic–ultramafic intrusion. Photograph by Ian Oswald-Jacobs.

Copies of this *Bulletin* can be purchased from the:
Sales Centre
Australian Geological Survey Organisation
GPO Box 378
Canberra, ACT, 2601, Australia
telephone: 02 6249 9519 (domestic) and +61 2 6249 9519 (international)
facsimile: 02 6249 9982 (domestic) and +61 2 6249 9982 (international)
electronic mail: sales@agso.gov.au
internet: www.agso.gov.au/information/bookshop.html

CONTENTS

Acknowledgements xviii

Abstract xix

Chapter 1. Introduction (Dean M. Hoatson) 1

Introduction 1
Aims, methods of study, and nomenclature 1
Review of mineralisation processes in layered mafic–ultramafic intrusions 5
Acknowledgements 7
References 7

Chapter 2. Exploration history of the East Kimberley, Western Australia (Dean M. Hoatson) 13

Mineral exploration in the East Kimberley 13
Investigations of the mafic–ultramafic intrusions 19
Alice Downs 21
Armanda 23
Big Ben 23
Billymac Yard 23
Black Hills Yard 23
Bow River 23
Bulldust Flat 24
Cattle Creek 24
Corkwood 24
Eastmans Bore 24
Egg 25
Eileen Bore 25
Emull 25
Faulted 25
Fletcher Creek 25
Foal Creek 25
Frog Hollow 25
Greenvale Fault 25
Keller Creek 25
Lamboo 26
Mabel Downs West, Mabel Downs Homestead, and Mabel Downs Southwest 26
McIntosh 26
McKenzie Spring 27
Melon Patch 27
Mini 27
Norton 27
Ord Crossing-Grid A Ni–Cu and Ord Crossing-Grid A North Ti–V 27
Osmond Valley 27
Panton 28
Panton River 28
Paperbark 28
Sally Malay 28
Salt Lick Creek 28
Sandy Creek, Billymac Yard, and Paperbark 28
South Melon Patch 29
Spring Creek 29
Springvale 29
Three Sisters 29
Toby 29
Turkey Creek 29
West McIntosh 30
West Robin Soak 30
White Rock Well West 30
Wilagee 30
Wild Dog Creek 30
Wills Creek 30
Acknowledgements 30
References 30

Chapter 3. Regional geology of the Halls Creek Orogen (David H. Blake, Ian M. Tyler, & Rodney W. Page) 35

Introduction 35
Regional setting 35
Eastern zone of the Halls Creek Orogen 39
Pre-1835 Ma basement 39
Rocks younger than ~1835 Ma 44
Layered mafic–ultramafic intrusions 45
Central zone of the Halls Creek Orogen 45
Pre-1835 Ma basement 45
1835-1805 Ma granite and gabbro 48
Layered mafic–ultramafic intrusions 48
Other rocks younger than ~1835 Ma 48
Western zone of the Halls Creek Orogen 51
Pre-1835 Ma basement 51
Rocks younger than ~1835 Ma 51
Bow River Batholith 52
Orogenic events 53
Regional correlations 54
Economic geology 56
Diamonds 58
Gold 58
Copper–lead–zinc 58
Rare-earth elements and associated rare metals 58
Tungsten 58
Uranium 59
Tin 59
Acknowledgements 59
References 59
Appendix—U-Pb geochronology of Ding Dong Downs Volcanics and Junda Microgranite, eastern zone of the Halls Creek Orogen 62

Chapter 4. Regional geophysical setting and tectonic implications of the mafic–ultramafic intrusions (Russell D. Shaw, Tony J. Meixner, & Alice S. Murray) 63

Introduction 63
Geophysical framework 63
National magnetic, spectrometric, and gravity databases 63
Previous interpretation of the national geophysical data sets 63
Australian crustal elements in the East Kimberley region 66
Classes of crustal elements 70
(i) Highly magnetic elements 70
(ii) Elements corresponding to zones of geophysical overprinting 70
(iii) Elements showing relict geophysical features 70
(iv) Standard elements 70
Mega-elements in the East Kimberley region 70
Halls Creek Orogen—lithospheric plate or subplate boundary? 70
Geophysical interpretation of the Dixon Range and northern Gordon Downs 1:250 000 Sheet areas 73
Crustal element KBE (Kimberley Basin East) and parent crustal element KL (King Leopold Orogen) 73
Crustal subelement HCC (Halls Creek Central) 73
Boundary between the Halls Creek Central and Biscay subelements 80
Crustal subelement HCB (Biscay) 80
Boundary between crustal elements HCB (Biscay) and ST (Sturt) 80
Sturt crustal element (ST) and its subelements STN & STS 81
Crustal element RO (Rosewood) 81
Geophysical characteristics of geological units in the Dixon Range and northern Gordon Downs 1:250 000 Sheet areas 82
Physical properties of rock units 82
Spectrometric expression of geological units 82
Magnetic expression of individual geological units 83
Magnetic and spectrometric expression of structural features: some examples 86
Discussion of tectonic implications 86
Concluding remarks 94
Acknowledgements 95
References 95

Chapter 5. Geological setting, petrography, and geochemistry of the mafic–ultramafic intrusions (Dean M. Hoatson) 99

Introduction 99
Geological setting, petrography, and geochemistry 101
Group I layered mafic–ultramafic intrusions 101
Panton 101
Big Ben 111
Highway 113
Melon Patch 113
Mini 113
South Melon Patch 114
Springvale Track 114
West McIntosh 116
West Panton 116
West Robin Soak 116
Group II layered mafic–ultramafic intrusions 117
Springvale 118
Foal Creek 119
Wilagee 120
Group III layered mafic intrusion 122
Toby 122
Group IV Wild Dog Creek mafic intrusions 124
Group V layered mafic–ultramafic intrusions 124
Sally Malay 124
Corkwood 128
Dave Hill 129
Fletcher Creek 130
Frog Hollow 130
Keller Creek 133
Mabel Downs Homestead 134
Mabel Downs Southwest 134
McKenzie Spring 134
Oxide 137
Spring Creek 137
Three Nuns 139
Wilson Creek 139
Other possible group V layered mafic–ultramafic intrusions 140
Group VI layered mafic intrusions 140
McIntosh 140
Armanda 142
Togo 145
Group VII layered mafic intrusions 145
Black Hills Yard 145
Amphitheatre 146
Egg 146
Other layered mafic intrusions 147
Panton River 147
Three Sisters 147
Corridor gabbro 147
Billymac Yard 148
Faulted 148
Greenvale Fault 149
Juries 149
Mabel Downs West 149
Margaret River 149
Nine Mile 150
Paperbark 150
Sandy Creek 150
Turkey Creek microgabbro-norite 150
Metagabbros of the Tickalara Metamorphics 151
Norton 151

Typical field relationships of the layered intrusions 152
Contact relationships 152
Types of layering 156
(i) Microrhythmic layering 156
(ii) Cryptically graded layers 159
(iii) Modal laminations 160
Distribution of mineralised layered intrusions in the East Kimberley 160
Comparisons with other Palaeoproterozoic provinces in Australia 160
Acknowledgements 161
References 161

Chapter 6. Geochronology of the mafic–ultramafic intrusions (Rodney W. Page & Dean M. Hoatson) 163

Introduction 163
Scope of this study 163
Results 165
Panton mafic–ultramafic intrusion (group I) 165
Intrusive rocks predating and postdating the Panton intrusion 166
(i) Rose Bore Granite 166
(ii) Muscovite pegmatite 166
Springvale mafic intrusion (group II) 166
Toby mafic intrusion (group III) 166
Sally Malay mafic–ultramafic intrusion (group V) 168
McIntosh mafic intrusion (group VI) 169
Discussion 170
Summary 170
Acknowledgements 171
Appendix 171
SHRIMP II analytical techniques 171
References 172

Chapter 7. Geophysical expression of the mafic–ultramafic intrusions and implications for exploration (Russell D. Shaw & Lautaro F. Macias) 173

Introduction 173
Geophysical framework 173
Magnetic data 173
Geophysical expression of the mafic and mafic–ultramafic intrusions 173
General features of the gravity expression 173
General features of the magnetic expression 178
Geophysical and related geological features of individual intrusions 179
Pre-group I intrusions of the Tickalara Metamorphics 179
Group I intrusions 179
Group II intrusions 179
Group III intrusion 179
Group IV intrusions 181
Group V intrusions 182
Group VI intrusions 182
Group VII intrusions 182
Corridor gabbro group 182
Turkey Creek microgabbro-norite group 183
Undivided gabbro 183
Discussion 183
Conclusions 187
Acknowledgements 188
References 188

Chapter 8. Remote sensing of mafic and ultramafic rocks in the McIntosh 1:100 000 sheet area (Lautaro F. Macias) 190

Introduction 190
Scanner data characteristics 190
Weathering and alteration products 190
Spectral reflectance 192
Digital data processing 192
Geology and remote sensing 193
Panton intrusion (group I) 193
Big Ben intrusion (group I) 193
Springvale intrusion (group II) 193
Wilagee intrusion (group II) 193
Toby intrusion (group III) 194
Wild Dog Creek intrusion (group IV) 195
McKenzie Spring intrusion (group V) 197
McIntosh intrusion (group VI) 197
Armanda intrusion (group VI) 197
Gamma-ray spectrometry 197
Discussion and conclusions 198
Acknowledgements 199
References 199

Chapter 9. Depths of emplacement of the mafic–ultramafic intrusions (Alfonso G. Trudu & Dean M. Hoatson) 201

Introduction 201
Previous geobarometric studies of layered intrusions 203
Methods 203
Petrography 204
Gabbronorite 204
Troctolite 207
Norite 207
Plagioclase peridotite 207
Corona textures 207
Type 1 207
Type 2 207
Type 3 207
Type 4 207
Mineral chemistry 207
Amphibole 209
Biotite 209
Clinopyroxene 209
Ilmenite 209
Olivine 209
Orthopyroxene 209
Plagioclase 209
Spinel 210

Origin of coronas and geothermobarometry 210
Relationships between intrusions and country rock migmatites 213
Stratigraphic variations in mineral chemistry 214
Some regional implications and conclusions 215
Acknowledgements 217
References 217

Chapter 10. Comments on relationships of mafic and felsic magmatism (Lesley A.I. Wyborn & David H. Blake) 220

Introduction 220
Bimodal magmatism 220
Chemical characteristics of the granites 220
Generation of the magmas 220
Inheritance 224
Tectonic models 224
Acknowledgements 224
References 225

Chapter 11. Trace-element geochemical and Nd isotopic study of the mafic–ultramafic intrusions: implications for their petrogenesis and tectonic environment (Shen-su Sun & Dean M. Hoatson) 226

Introduction 226
Analytical methods 227
Chemical analyses and trace-element spidergrams 227
Group I 227
Group II 231
Group III 231
Group IV 231
Group V 231
Group VI 235
Corridor gabbro 235
Undivided gabbro 235
Unnamed intrusion 235
Mafic intrusions within the Tickalara Metamorphics 235
Dolerite in the ?Biscay Formation (~1880 Ma) 235
Discussion of geochemical results 236
Neodymium isotope data 238
Mantle-source character versus crustal contamination 238
Compositions of parent magmas 243
Tectonic environments of the mafic–ultramafic intrusions 245
Implications of magma chemistry for PGE and Ni–Cu–Co mineralisation potential 247
Acknowledgements 247
References 247

Chapter 12. Geochemical and isotopic constraints on the petrogenesis of the Panton and Sally Malay intrusions: implications for exploration (Rebecca A. Sproule, David D. Lambert, & Dean M. Hoatson) 250

Introduction 250
Geological setting 250
Panton intrusion 250
Sally Malay intrusion 250
Methods 252
Geochemical and isotopic results 253
Panton intrusion 253
Platinum-group-element data 253
Sm-Nd isotopic data 253
Re-Os isotopic data 253
Sally Malay intrusion 255
Sm-Nd isotopic data 255
Re-Os isotopic data 255
Petrogenesis of the Panton and Sally Malay intrusions 255
Enriched mantle versus crustal contamination 255
R-factor modelling and ore genesis 257
Implications for exploration 260
Conclusions 262
Acknowledgements 262
References 262

Chapter 13. A Laser Raman and electron probe microanalysis study of chromite from Precambrian layered mafic–ultramafic intrusions in northern Western Australia (Terrence P. Mernagh, Alfonso G. Trudu, & Dean M. Hoatson) 265

Introduction 265
Occurrence of chromite in the layered mafic–ultramafic intrusions of the East Kimberley 265
Chromite petrography 266
The vibrational spectrum of spinels 266
Experimental techniques 267
Electron probe microanalysis and Laser Raman microprobe results 268
Electron probe microanalysis 268
Geothermometry 271
Laser Raman microprobe studies 273
Discussion 274
Conclusions 276
Acknowledgements 276
References 276

Chapter 14. Mineralisation and economic potential of the mafic–ultramafic intrusions (Dean M. Hoatson) 278

Introduction 278
Styles of platinum-group-element mineralisation associated with Precambrian layered mafic–ultramafic intrusions in Australia 278

(i) Stratabound sulphide-bearing layers 278
(ii) Stratabound chromitite layers 279
(iii) Basal segregations of Ni–Cu–Co–PGE sulphides 281
(iv) Hydrothermal remobilisation 281
(v) Enrichment in the laterite profile 281
Mineral deposits associated with mafic–ultramafic intrusions in the East Kimberley 284
Chromite association (Cr–PGEs–Ni–Cu±Au) 284
Sulphide association (Ni–Cu–Co±PGEs) 289
Fe–Ti oxide association (Fe–Ti–V) 290
Hydrothermal polymetallic association (Pd, Pt, Cu, Zn, Pb, Au) 292
Comparison of the East Kimberley mafic–ultramafic intrusions with overseas intrusions 293
(i) Voisey's Bay, Canada 295
(ii) Svecofennian domain of the Fennoscandian Shield, Finland 296
Status of sulphur saturation during magma evolution 297
Review of exploration strategies for layered intrusions in the East Kimberley 302
Stratabound PGE-enriched chromitite and sulphide-bearing layers 302
Basal segregations of Ni–Cu–Co sulphides 304
Concluding statements 306
Acknowledgements 306
References 306

Chapter 15. Summary of conclusions and suggestions for further studies (Dean M. Hoatson & David H. Blake) 312

Introduction 312
Summary of major points and conclusions 312
Chapter 2 (exploration history of the East Kimberley) 312
Chapter 3 (regional geology of the Halls Creek Orogen) 312
Chapter 4 (regional geophysical setting and tectonic implications) 313
Chapter 5 (classification and geological setting) 313
Chapter 6 (geochronology) 314
Chapter 7 (geophysical expression) 314
Chapter 8 (remote sensing) 314
Chapter 9 (depths of emplacement) 315
Chapter 10 (relationships of mafic and felsic magmatism in the Halls Creek Orogen) 315
Chapter 11 (geochemistry, isotopes, and tectonic environment) 315
Chapter 12 (geochemistry, isotopes, and petrogenesis of the Panton and Sally Malay intrusions) 315
Chapter 13 (geochemistry of chromite in Precambrian layered intrusions of northern Western Australia) 316
Chapter 14 (mineralisation and economic potential) 316
Suggestions for further studies 316
Geology and geophysics 316
Geochronology 317
Geochemistry 317
Acknowledgements 317

Appendices
1. Analytical procedures 319
2. Whole-rock (major, trace, PGEs) geochemical tables 322
3. Mineral chemical tables 357
4. U-Pb geochronological tables 449
5. Magnetic susceptibility tables 457
6. National Geoscience Mapping Accord bibliography of the East Kimberley 465

FIGURES

1.1. Location of the study area and relevant geological sheets 2
1.2. Regional geological setting of the mafic–ultramafic intrusions in the Halls Creek Orogen 3
2.1. Members of Alexander Forrest's 1879 exploration party 13
2.2. Edward Hardman's camp in the Robinson River, Kimberley 13
2.3. The first geological map of the East Kimberley 14–15
2.4. Distribution of prospective metallogenic corridors, goldfields, and prospects in the western part of the Gordon Downs and Dixon Range 1:250 000 Sheet areas 19
3.1. Regional setting of the Halls Creek Orogen 36
3.2. Locality map of the Halls Creek Orogen 37
3.3. Geological map of the Halls Creek Orogen 38
3.4. Landsat Multispectral Scanner composite image of the Halls Creek Orogen 40–41
3.5. Annotated Landsat Multispectral Scanner composite image of the Halls Creek Orogen 40–41
3.6. Summary diagram of U-Pb geochronology for the Halls Creek Orogen and King Leopold Orogen 44
3.7. Metamorphosed sedimentary and volcanic rocks 46

A. Fragmental volcanic rock of the Maude Headley Member, Olympio Formation
B. Pencil slate in a fold closure within the Olympio Formation
C. Migmatitic hornfels of the Koongie Park Formation
D. Basaltic pillow lava cut by vein of leucogranite within Tickalara Metamorphics
E. Fragmental basalt within Tickalara Metamorphics
F. Banded marble within Tickalara Metamorphics
3.8. Metamorphosed sedimentary and igneous rocks 49
A. Migmatitic metasediments of the Tickalara Metamorphics and mafic dykes of synplutonic type
B. 'Pillowed' mafic dyke intruding remobilised migmatitic pelitic gneiss of the Tickalara Metamorphics
C. Finely banded Fletcher Creek Monzogranite
D. Inclusion of Dougalls suite amphibolite, veined by tonalite, within garnet-bearing Fletcher Creek Monzogranite
E. Tightly folded pelitic migmatite within Tickalara Metamorphics
F. Migmatitic Tickalara Metamorphics
3.9. Migmatitic and igneous rocks 50
A. Dougalls Tonalite of the Tickalara Metamorphics
B. Chaotic metasedimentary migmatite from the Tickalara Metamorphics
C. Net-veined complex from the Paperbark supersuite
D. Mafic pillows in granite of the Sally Downs supersuite
E. Sally Downs Tonalite of the Sally Downs supersuite
F. Porphyritic Paperbark Granite of the Paperbark supersuite
3.10. Correlation diagram of the Halls Creek Orogen and nearby regions 55
3.11. Map of main mines and prospects in the Halls Creek Orogen 57

Appendix
3.A. Concordia diagrams for samples of Ding Dong Downs Volcanics (including Sophie Downs Granophyre Member) and Junda Microgranite 62

4.1. Bouguer gravity image of the Kimberley region 64
4.2. Total magnetic intensity image, reduced to the pole, of the Kimberley region 64
4.3. Total magnetic intensity image, continued upwards to 6000 m, of the Kimberley region 65
4.4. Elevation model image of the Kimberley region 65
4.5. Crustal elements of Australia 66
4.6. Bouguer gravity image of the Kimberley region 66
4.7. Main tectonic units of the Kimberley region 67
4.8. Crustal elements of the Kimberley region 71
4.9. Annotated Bouguer gravity image of the Dixon Range–Gordon Downs 1:250 000 Sheet areas 76
4.10. Total magnetic intensity image, reduced to the pole, of the Dixon Range–Gordon Downs 1:250 000 Sheet areas 76
4.11. Processed total-intensity gamma-ray spectrometric image of the Dixon Range–Gordon Downs 1:250 000 Sheet areas 77
4.12. Processed grey-scale total magnetic intensity image of the Dixon Range–Gordon Downs 1:250 000 Sheet areas 77
4.13. Geological units grouped according to their magnetic character in the Dixon Range–Gordon Downs 1:250 000 Sheet areas 84
4.14. Preliminary interpretation of regional aeromagnetic data of the Dixon Range–Gordon Downs 1:250 000 Sheet areas 85
4.15. Interpreted cross-section of the Halls Creek Orogen 91
4.16. Palaeoproterozoic evolutionary stages in the Kimberley region 93

5.1. Distribution of the Palaeoproterozoic mafic–ultramafic intrusions in the East Kimberley 100
5.2. Photographs of layered mafic–ultramafic intrusions 104
A–B. Group I Panton intrusion
C–D. Group I Big Ben intrusion
E. Group II Springvale intrusion
F. Group VII Black Hills Yard troctolite plugs
5.3. Geological map of the group I Panton mafic–ultramafic intrusion 106
5.4. Major rock types in the group I Panton mafic–ultramafic intrusion 107
A. Dunite
B. Weakly layered gabbro
C. Massive melagabbro
D. Massive ferrogabbro
E. Mottled anorthosite
F. Harzburgite
5.5. Panton intrusion: variations in whole-rock major-element compositions with stratigraphic height 108
5.6. Panton intrusion: variations in whole-rock Al_2O_3 and trace-element compositions with stratigraphic height 109
5.7. Panton intrusion: variations in whole-rock Pt, Pd, Cu, and Ni across the Main 110

Chromitite Layer in diamond holes PS28 and PS39
5.8. Panton intrusion: variations of Pt, Cr, Ni, and Ni/Cu in soils across the Ultramafic Series 111
5.9. Geological map of the group I Big Ben mafic–ultramafic intrusion 112
5.10. Geological map of the group I Panton, Mini, West McIntosh, and South Melon Patch mafic–ultramafic intrusions, group IV Wild Dog Creek mafic intrusion, and group VI McIntosh mafic intrusion 115
5.11. Geological map of the group II Springvale mafic intrusion 117
5.12. Springvale intrusion: variations in whole-rock major-element compositions with stratigraphic height 118
5.13. Springvale intrusion: variations in whole-rock trace-element compositions with stratigraphic height 118
5.14. Geological map of the group II Foal Creek mafic intrusion and the Greenvale Fault mafic intrusion 120
5.15. Geological map of the group II Wilagee mafic–ultramafic intrusion and group III Toby mafic intrusion 121
5.16. Wilagee intrusion: variations in whole-rock major-element compositions with stratigraphic height 122
5.17. Wilagee intrusion: variations in whole-rock trace-element compositions with stratigraphic height 122
5.18. Toby intrusion: variations in whole-rock major-element compositions of mafic rocks with traverse distance 123
5.19. Toby intrusion: variations in whole-rock trace-element compositions of mafic rocks with traverse distance 123
5.20. Geological map of the group V Sally Malay, Dave Hill, and Wilson Creek mafic–ultramafic intrusions 125
5.21. Schematic diagram of subchamber A of the Sally Malay intrusion 126
5.22. Sally Malay intrusion: variations in whole-rock major-element compositions with stratigraphic height 127
5.23. Sally Malay intrusion: variations in whole-rock trace-element compositions with stratigraphic height 127
5.24. Geological map of the group V Corkwood mafic intrusion 129
5.25. Geological map of the group V Fletcher Creek mafic intrusion 131
5.26. Geological map of the group V Frog Hollow mafic intrusion and the Norton metagabbro intrusion 132
5.27. Geological map of the group V Keller Creek mafic intrusion 133
5.28. Geological map of the group V Mabel Downs Homestead and Mabel Downs Southwest mafic intrusions, and the Faulted and Mabel Downs West mafic intrusions 135
5.29. Geological map of the group V McKenzie Spring mafic intrusion 136
5.30. Geological map of the group V Spring Creek mafic intrusion 138
5.31. Spring Creek intrusion: variations in whole-rock major-element compositions with stratigraphic height 139
5.32. Spring Creek intrusion: variations in whole-rock trace-element compositions with stratigraphic height 139
5.33. McIntosh intrusion: variations in whole-rock major-element compositions with stratigraphic height 142
5.34. McIntosh intrusion: variations in whole-rock trace-element compositions with stratigraphic height 142
5.35. Geological map of the group VI Armanda mafic intrusion 143
5.36. Armanda intrusion: variations in whole-rock major-element compositions with stratigraphic height 144
5.37. Armanda intrusion: variations in whole-rock trace-element compositions with stratigraphic height 144
5.38. Geological map of the group VII Black Hills Yard mafic intrusions and the Paperbark mafic intrusion 145
5.39. Geological map of the group VII Amphitheatre mafic intrusion 146
5.40. Norton intrusion: variations in whole-rock major-element compositions with stratigraphic height 151
5.41. Norton intrusion: variations in whole-rock trace-element compositions with stratigraphic height 152
5.42. Contact relationships of mafic and felsic magmas 153
A. Angular mafic fragments in granite, Greenvale Fault intrusion
B. Concentration of irregular pillow-like mafic inclusions, Toby intrusion
C. Closely spaced rounded mafic pillows, Greenvale Fault intrusion
D. Enlargement of Figure 5.42C
E. Dismembered mafic body, Fletcher Creek region
5.43. Contact relationships of mafic and felsic magmas 154
A. Ellipsoidal mafic pillows, Juries intrusion
B. Enlargement of Figure 5.43A
C. Concentration of mafic pillows, Shepherds Bore
D. Concentration of closely spaced mafic enclaves, Toby intrusion
E. Stacked composite sequence of parallel mafic sheets, Greenvale Fault intrusion
F. Angular enclave of hybrid diorite containing a more mafic enclave, Toby intrusion
5.44. Contact relationships of mafic and felsic magmas 155

A. Heterogeneous hybrid rock, Greenvale Fault intrusion
B. Mafic pillows, Greenvale Fault intrusion
C. Irregular contact between granite and massive biotite quartz gabbro of the Paperbark intrusion
D. Homogeneous hybrid biotite diorite at the contact between gabbro of the Paperbark intrusion and granite
E. Massive biotite gabbro in contact with granite, Toby intrusion
F. Leucogranite veins cutting massive gabbro of the Toby intrusion

5.45. Typical country rocks to the East Kimberley mafic–ultramafic intrusions 157
A. Swirly and stromatic paramigmatites
B. Twinned ?cordierite and garnet porphyroblasts in paramigmatite
C. Garnet and biotite-rich segregation in migmatite
D. Retrogressed andalusite porphyroblasts in metapelite
E. Tight to isoclinal folding of marble and calc-silicate rock
F. Folded and boudinaged felsic and biotite-rich bands in migmatite

5.46. Types of layering in the East Kimberley mafic–ultramafic intrusions 158
A. Rhythmically layered gabbro and anorthosite
B. Rhythmically layered gabbro
C. Composite sequence of uniform chromite and olivine-chromite modal layers and modally graded chromite-olivine layers
D. Rhythmically layered and laminated leucogabbro and anorthosite
E. Rhythmically layered leucogabbro and anorthosite
F. Rhythmically layered and laminated leucogabbro and anorthosite

5.47. Types of layering in the East Kimberley mafic–ultramafic intrusions 159
A. Rhythmic grain-size layering in magnetite gabbronorite and leucogabbro
B. Fe-Ti oxide-rich layer in magnetite gabbronorite
C. Microrhythmically layered magnetite gabbronorite and leucogabbro
D. Laminated gabbro

6.1. Palaeoproterozoic mafic–ultramafic intrusions that have been dated in the East Kimberley 164

6.2. Concordia plot of zircon U-Pb data from the Rose Bore Granite 166

6.3. Photomicrographs of zircon and baddeleyite grains from the East Kimberley intrusions in transmitted light or cathodoluminescence imagery 167
A. Panton intrusion
B. Rose Bore Granite
C. Springvale intrusion
D. Toby intrusion
E. Sally Malay intrusion
F. Sally Malay intrusion
G. McIntosh intrusion contact aureole
H. McIntosh intrusion contact aureole

6.4. Concordia plot of zircon U-Pb data from the Toby, Springvale, and Panton intrusions 168

6.5. Plot of Th/U and U in zircons from four of the mafic–ultramafic intrusions in the Halls Creek Orogen 168

6.6. Concordia plot of zircon U-Pb and baddeleyite data from the Sally Malay intrusion. 168

6.7. Field photograph of migmatite from the northwestern contact aureole of the McIntosh mafic intrusion 169

6.8. Concordia plot of zircon U-Pb data from the migmatitic hornfels in the contact aureole of the McIntosh intrusion 169

7.1. Distribution of Palaeoproterozoic mafic–ultramafic intrusions in the East Kimberley, showing their general magnetic response 177

7.2. Processed image of Total Magnetic Intensity data in the region of mafic–ultramafic intrusions, with a NW illumination filter and 'Comtal' pseudocolour 180

7.3. Distribution of Palaeoproterozoic mafic–ultramafic intrusions and structural element boundaries, overprinted on the magnetic image 181

8.1. Reflectance curves for dunite, harzburgite, anorthosite, norite, gabbro, and ferrogabbro 192

8.2. Landsat-5 TM colour composite 5/7, 5/3, and 5 image for the McINTOSH Sheet 194

8.3. Landsat-5 TM colour composite dpc2(4/3,5/7), 5/4, and 1+7 image for the McINTOSH Sheet 195

8.4. Landsat-5 TM colour composite dpc2(4/3,5/7), 5/4, and 1+7 image, with potassium layer 196

8.5. Enlargement of Landsat-5 TM colour composite image shown in Figure 8.2 198

9.1. Regional distribution of Palaeoproterozoic layered mafic–ultramafic intrusions in the East Kimberley 202

9.2. Photomicrographs of coronas surrounding cumulus olivine 208
A. Type 1 corona
B–C. Type 2 corona
D. Type 2 corona under crossed nicols

E. Detail of type 2 corona
F. Type 2 corona under crossed nicols
G–H. Type 4 corona
9.3. Variations of clinopyroxene and spinel compositions for the East Kimberley intrusions 211
A. Variation of Mg-Ca-Fe components for cumulus and intercumulus clinopyroxene
B. Variation of Mg-Fe^{3+}-(Fe^{2+} + Mn) components for spinel in coronas surrounding cumulus olivine
9.4. Relationships of mg number in olivine and associated corona minerals 212
A. Cumulus olivine versus corona orthopyroxene
B. Cumulus olivine versus corona spinel
C. Corona orthopyroxene versus corona spinel
9.5. Variations of mineral chemistry for the Toby and Wilagee intrusions 214
A. mg number of clinopyroxene, orthopyroxene, and olivine
B. Anorthite content of plagioclase
9.6. Variations of mineral chemistry versus stratigraphic height for the Springvale intrusion 215
A. mg number of clinopyroxene, orthopyroxene, and olivine
B. Anorthite content of plagioclase
9.7. Calculated crystallisation pressures for the layered mafic–ultramafic intrusions studied 216

10.1. Histogram of igneous rocks from the Halls Creek Orogen 220
10.2. Spidergrams for typical Sr-depleted and Sr-undepleted granites 223
10.3. Pressure-temperature-depth diagram for dehydration melting of amphibolites 224

11.1. East Kimberley mafic–ultramafic intrusions investigated and isotopic results. 226
A. Sample locations
B. Initial ε_{Nd} values for those samples shown in Figure 11.1A
11.2. Mantle-normalised trace-element diagrams of melt-like samples 232
11.3. Chondrite-normalised rare earth element diagrams of melt-like samples 233
11.4. Ti-Zr-Y discrimination diagram 236
11.5. Nb-Zr-Y discrimination diagram 237
11.6. Plot of initial ε_{Nd} values versus geological age for samples of mafic–ultramafic intrusions and other rocks from the East Kimberley 239
11.7. A–D. Mantle-normalised trace-element diagrams for East Kimberley mafic–ultramafic intrusions and Paperbark supersuite granite 240–241
11.8. Discrimination diagram of Ti content versus Cr# in spinel for different magma types 244

12.1. Geology of the Panton intrusion and locations of diamond drillhole and surface samples 251
12.2. Geology of the Sally Malay intrusion and locations of sampled diamond drillholes 252
12.3. Primitive mantle-normalised PGE patterns for chromitite seams from the Panton and overseas intrusions 253
12.4. Trace-element geochemistry of the Panton and Munni Munni intrusions 254
A. Pd/Ir versus stratigraphic height for the Panton intrusion
B. Cu/Pd versus stratigraphic height for the Panton intrusion
C. Cu/Pd versus stratigraphic height for the Munni Munni intrusion
12.5. Sm-Nd isotopic evolution diagram for samples from the Panton intrusion 254
12.6. Re/Os versus Os isotopic plots for the Panton and overseas intrusions 257
A. Comparison of common Os concentration versus Re/Os ratio for the Panton intrusion with other mafic–ultramafic rocks and mineralised settings
B. Re-Os isotopic evolution diagram for the Panton intrusion
12.7. Re/Os versus Os isotopic plots for the Sally Malay and overseas intrusions 258
A. Comparison of common Os concentration versus Re/Os ratio for the Sally Malay intrusion with other mafic–ultramafic rocks and mineralised settings
B. Re-Os isotopic evolution diagram for the Sally Malay intrusion
12.8. Two component γ_{Os} versus ε_{Nd} contamination diagram 258
12.9. Common Os concentration versus Re/Os ratio for mantle-derived magmas and ores. 259
12.10. Initial γ_{Os} versus Re/Os for massive sulphides from the Sally Malay intrusion and the Panton intrusion A seam chromitites 259
12.11. Model for the formation of magmatic mineralisation in the Sally Malay and Panton intrusions 261

13.1. Locality map showing sampled chromite-bearing intrusions 265
13.2. Combined reflected and transmitted light photomicrographs of chromite 267
A. Tightly packed chromite grains from the Lamboo intrusion
B. Subhedral chromite from the Big Ben intrusion
C. Subhedral chromite from the Mini intrusion
D. Subhedral to euhedral chromite from the Panton intrusion

E. Anhedral chromite from the South Melon Patch intrusion
F. Euhedral chromite from the West McIntosh intrusion
13.3. Part of the spinel structure 268
13.4. A–C. Compositions of chromite from the East Kimberley region in the oxidised-spinel prism and their projections on faces A and B 270
13.5. Variations of Cr-Al-Fe^{3+} in Cr-bearing spinel from various layered intrusions 270
13.6. Cr_2O_3 versus $Al_2O_3/(Al_2O_3 + Cr_2O_3 + Fe_2O_3)$ diagram for intrusions from the East Kimberley, Yilgarn Craton, and overseas 271
13.7. Equilibration temperatures for chromite from East Kimberley intrusions calculated with the Ni-Zn geothermometer 272
13.8. Equilibration temperatures for chromite from East Kimberley intrusions calculated with the Ni-Mn geothermometer 272
13.9. A–C. Selected laser Raman microprobe spectra of East Kimberley chromite 273
13.10. Plot of Lorentzian curves as a function of Cr number (Cr′) for chromite from layered intrusions in the East Kimberley and west Pilbara Craton 274
13.11. Plot of Lorentzian curves as a function of Al number (Al′) for chromite from layered intrusions in the East Kimberley and west Pilbara Craton 274
13.12. Plot of Lorentzian curves as a function of Fe^{3+} number for chromite from layered intrusions in the East Kimberley and west Pilbara Craton 275
13.13. Plot of Lorentzian curves as a function of $Cr + Fe^{3+}/(Cr + Al + Fe^{3+})$ for chromite from layered intrusions in the East Kimberley and west Pilbara Craton 275

14.1. Distribution of platinum-group element mineralisation related to Precambrian layered mafic–ultramafic intrusions in Australia 279
14.2. Chromitites from the East Kimberley layered intrusions 282
A. Massive A chromitite, group I Panton intrusion
B. Stacked chromite and dunite cyclic sequence, Panton intrusion
C. Irregular chromitite in dunite, Panton intrusion
D. Sheared chromitite in dunite lenses, Panton intrusion
E. Isoclinally folded chromitite layers in dunite, Panton intrusion
F. Massive chromitite in dunite, group I Big Ben intrusion
G. Parallel chromitite layers in dunite, group I West McIntosh intrusion
H. Chromitite in troctolite, group II Wilagee intrusion
14.3. Chromitites and sulphides from the East Kimberley layered intrusions 283
A. Serpentinised olivine–chromite cumulate, group I Panton intrusion
B. Serpentinised olivine–chromite cumulate, group I Big Ben intrusion
C. Serpentinised olivine–chromite cumulate, group I West McIntosh intrusion
D. Serpentinised olivine–chromite–plagioclase cumulate, group II Wilagee intrusion
E. Massive sulphides, near the basal contact of the group V Sally Malay intrusion
F. Massive sulphides, near the basal contact of the Sally Malay intrusion
G. Troctolite containing interstitial pyrrhotite, chalcopyrite, and pentlandite, Sally Malay intrusion
H. Enlargement of sulphides shown in Figure 14.3G
14.4. Stratigraphic distribution of chromite, Ni–Cu–Co sulphides, and titaniferous magnetite and ilmenite 288
14.5. Gossans and Fe–Ti–V oxides from the group V mafic–ultramafic intrusions 291
A. Ferruginous gossan at the base of the Sally Malay intrusion
B. Massive goethite-hematite-limonite gossan at the base of the Norton intrusion
C. Ferruginous gossan at the base of the Keller Creek intrusion
D. Partly oxidised Fe-sulphides in leucogabbro from the Dave Hill intrusion
E. Massive lens of ilmenite and titaniferous magnetite in the Frog Hollow intrusion
F. Cyclic layers of titaniferous magnetite in the Mabel Downs Southwest intrusion
14.6. Comparative thicknesses of mafic and ultramafic rocks in layered intrusions from the East Kimberley, the west Pilbara Craton, and overseas 294
14.7. Geology of the Voisey's Bay Ni–Cu–Co sulphide deposit 297
14.8. Logarithmic plots of S, Ni, Cu, and Cr against Zr for East Kimberley mafic–ultramafic intrusions 299
14.9. Logarithmic plots of TiO_2, K_2O, Ba, and Y against Zr for East Kimberley mafic–ultramafic intrusions 299
14.10. Ternary geochemical plots of East Kimberley and other layered intrusions 300
14.11. Summary of the different types of PGE–Cr and Ni–Cu–Co-PGE deposits 303
14.12. Potential mineralisation in the layered intrusions of the East Kimberley 305

TABLES

2.1. Gold production from the East Kimberley 16–17
2.2. Publications and theses relating to the East Kimberley layered mafic–ultramafic intrusions 20
2.3. Significant exploration events relating to the East Kimberley layered mafic–ultramafic intrusions 22

3.1. References for geological maps and accompanying reports of the East Kimberley 39
3.2. Summary of the geological history of the Halls Creek Orogen 42–43

4.1. Crustal elements of the Kimberley region 68–69
4.2. Crustal elements and sub-elements in the Dixon Range and southern Gordon Downs 1:250 000 Sheet areas 74
4.3. Magnetic units and properties for the Dixon Range and southern Gordon Downs 1:250 000 Sheet areas 79–79

5.1. Mafic and mafic–ultramafic intrusions investigated in the East Kimberleys 102–103
5.2. Platinum-group-element and gold geochemistry of chromitite layers in the Ultramafic Series of the Panton intrusion 111

6.1. Summary of U-Pb zircon and baddeleyite SHRIMP results for layered mafic–ultramafic intrusions and associated rocks in the Halls Creek Orogen, East Kimberley 165

7.1. Geophysical features of representative mafic–ultramafic intrusions in the East Kimberley region 174–176

8.1. Wavelengths recorded by Landsat-5 TM 190
8.2. Major lithologies and mineralogy of mafic–ultramafic intrusions 191

9.1. Classification of the layered mafic–ultramafic intrusions in the East Kimberley 201
9.2. Magmatic crystallisation pressures for layered mafic–ultramafic intrusions in the East Kimberley 203
9.3. Magmatic crystallisation pressures for layered mafic–ultramafic intrusions outside the East Kimberley 204
9.4. Petrography of samples 205–206
9.5. Summary of chemical features of minerals analysed 209
9.6. Summary of mineral compositions for layered intrusions in the East Kimberley 210
9.7. Estimated crystallisation pressures for the major layered intrusions in the East Kimberley 213

10.1. Palaeoproterozoic magmatism in the Halls Creek Orogen 221–222

11.1. Major and trace-element geochemistry and Nd isotopic data for melt-like mafic rocks from the East Kimberley 228–230
11.2. Samarium and Nd whole rock and mineral data for samples from the East Kimberley 234
11.3. Estimated mg number of parent magmas for the East Kimberley layered intrusions 243

12.1. Platinum-group-element geochemistry of major rock types in the Panton intrusion 252
12.2. Sm-Nd isotopic data for the Panton and Sally Malay intrusions 255
12.3. Re-Os isotopic data for the Panton and Sally Malay intrusions 256
12.4. R-factor estimates based on Pd, Pt, and Cu concentrations from the Panton and Sally Malay intrusions 259

13.1. Possible superstructures in spinels and the predicted Raman active modes for each structure 268
13.2. Electron microprobe analyses of chromite from chromitite layers in East Kimberley layered mafic–ultramafic intrusions 269
13.3. Calculated equilibration temperatures for chromites from the East Kimberley region 272
13.4. Raman frequencies as a function of ratioed compositions of chromite 276

14.1. Precambrian layered mafic–ultramafic intrusions containing platinum-group elements 280–281
14.2. Platinum-group element resources in Australian Precambrian layered mafic–ultramafic intrusions 285
14.3. Platinum-group-element and trace-element geochemistry of chromitites, sulphides, and other rock types from the East Kimberley layered intrusions 286
14.4. Areal extent of layered mafic–ultramafic intrusions 295
14.5. Sequences of cumulus mineral assemblages in various mafic–ultramafic geological settings 296
14.6. Comparison of Ni–Cu–Co layered intrusions in the East Kimberley and the Svecofennian domain of southern Finland 298

Appendix 1.1. Accuracy of XRFS and AAS data 320
Appendix 1.2. Accuracy of ICP–MS data 321

ACKNOWLEDGEMENTS

This multidisciplinary study of the layered mafic–ultramafic intrusions in the East Kimberley has drawn on data, information, inspiration, and advice provided by many colleagues at AGSO, GSWA, universities, and exploration companies. These include, in addition to the authors of chapters in this *Bulletin,* Morrie Duggan, John Sheraton, Alastair Stewart, and Gladys Warren at AGSO; Steve Sheppard, Alan Thorne, and Tim Griffin at GSWA; Paul Hamlyn (consultant), Tom Marshall (Normandy Poseidon Ltd), Charter Mathison (University of Western Australia, Perth), Robert Mosig (Helix Resources NL), Karin Orth (Key Centre for Ore Deposit and Exploration Studies, University of Tasmania), and Steve Shedden (Gindalbie Gold NL), who provided many hours of stimulating discussion that contributed to a greater understanding of the geology of the intrusions. The *Bulletin* chapters were improved by the constructive criticism of many reviewers (listed at the end of each chapter). Access to company diamond-drill core, geological maps, geochemical data, and logistical support were kindly provided by Clutha Minerals NL, Gindalbie Gold NL, Helix Resources NL, Minsaco Resources Pty Ltd, Normandy Poseidon Ltd, Northern Exploration NL, Peko-Wallsend Operations Ltd, and Precious Metals Australia Ltd. Billiton Australia Pty Ltd and CRA Exploration Pty Ltd kindly made available their exploration base camps in Halls Creek and Kununurra, respectively, for field investigations by AGSO and GSWA.

Many people helped make fieldwork enjoyable as well as productive and also provided valuable geological input. Special thanks are due to: AGSO technical officers Piers Bairstow, Phil Browne, Garth Doblinger, Frank Kane, and Bill Pappas; GSWA technical officers John Bradley, Peter Boner, and Stephen Wallace; Kerry Turnock and Will Dix of Monash University; and Ben Cairns and Katie Jack of the Canberra Institute of Technology.

Nick Ware (Research School of Earth Sciences, Australian National University, Canberra) is gratefully acknowledged for his assistance with the electron microprobe work. At AGSO, Bruce Cruikshank, John Pyke, and Bill Pappas carried out the XRFS-AAS and ICP-MS analyses, and Julie Kamprad, the XRD analyses. Bruce Cruikshank wrote the analytical procedures described in Appendix 1.1. Shane Reeves (University of Melbourne) provided precious-metal analyses. Terry Brown, Chris Fitzgerald, Angie Jaensch, Neale Jeffery, Joe Mifsud, Pat Pratt and, in particular, Lana Murray drafted the line figures, under the guidance of Martyn Moffat at AGSO.

Ian Hodgson carried out the technical editing and Karin Weiss designed the cover of the *Bulletin*.

ABSTRACT

The Palaeoproterozoic layered mafic–ultramafic intrusions in the Halls Creek Orogen (HCO) of the East Kimberley, Western Australia, represent one of the most extensively mineralised igneous associations of their type in Australia. They contain a range of magmatic and hydrothermal deposits of platinum-group elements (PGEs), chromium, nickel, copper, cobalt, titanium, vanadium, iron, and gold. The intrusions are restricted to the central and western zones of the HCO—a well-exposed north-northeasterly trending orogenic belt of variably deformed and metamorphosed sedimentary, volcanic, and intrusive Palaeoproterozoic rocks, and overlapping Proterozoic and Palaeozoic basinal sequences. Marked gravity highs along the HCO can be attributed to large mafic intrusions and high-grade (granulite facies) metamorphic rocks, and most intrusions are moderately to highly magnetic.

The layered intrusions have been assigned to seven major groups (designated I–VII) on the basis of rock types, U–Pb geochronology, contact relations with country rocks, metamorphic-structural history, types of mineralisation, trace-element chemistry, and Sm–Nd isotopic composition. Intrusions that show no compositional layering and generally form small irregular mafic bodies are also common throughout the HCO. The layered intrusions form folded sheets, shallowly dipping basinal bodies, composite multi-chambered bodies, funnel-shaped bodies, steeply plunging plugs, fault-bounded blocks, narrow dyke-like bodies, and screens between granite plutons. Chilled and contaminated margins, contact aureoles, ribbon-like comagmatic satellite intrusions, net-vein complexes (resulting from mingling of mafic and felsic magmas), and feeder conduits indicate that the intrusions crystallised in situ, rather than being tectonically emplaced blocks that crystallised elsewhere, as proposed previously. The layered intrusions were emplaced into the crust at depths ranging from ~8 to 23 km (2.4–6.7 kb) and there were at least three major periods of emplacement—1855 Ma, 1845 Ma, and 1830 Ma. Emplacement of the 1855 Ma intrusions (groups I–III) was contemporaneous with granite plutonism (part of the Bow River Batholith) and felsic volcanism (Whitewater Volcanics) during a major magmatic event that represented a large flux of heat into the crust. Most of the layered intrusions can be classified as late orogenic to postorogenic bodies that were emplaced during quieter phases between periods of active tectonism in a complex orogenic belt.

The mafic–ultramafic intrusions were derived from olivine tholeiite and quartz tholeiite parent magmas of basaltic affinity (i.e. relatively fractionated magmas with mg = 67 or less). Incompatible-trace-element abundances are consistent with compositions ranging from mid-ocean ridge basalt to continental tholeiite. High average S contents (520–1570 ppm) in cumulate rocks from most groups of intrusions indicate early S saturation of the parent magmas.

The regional distribution of the major mineralised intrusions (groups I, II, and V) defines two northeast-trending corridors, which can help focus exploration for Cr–PGEs–Ni–Cu±Au (chromite association) and Ni–Cu–Co±PGEs (sulphide association) mineralisation. Magma mixing, crustal contamination, and the dynamics of magma flow (e.g. fast, slow, turbulent, passive) were significant mineralising processes in the petrogenesis of these intrusions. Landsat–5 Thematic Mapper imagery, using band ratios and directed principal component analysis, is particularly useful in defining favourable stratigraphic levels for mineralisation in those differentiated intrusions comprising mafic and ultramafic sequences. Exploration strategies in the HCO vary considerably for the different styles of stratabound and basal contact mineralisation associated with the intrusions. It is important not to be 'blinkered' by a particular model, but to maintain a flexible innovative approach and consider other unusual styles of magmatic and hydrothermal mineralisation at different stratigraphic levels in the intrusion.

CHAPTER 1

INTRODUCTION

by DEAN M. HOATSON

Introduction

Palaeoproterozoic layered mafic–ultramafic intrusions[1] in the East Kimberley of northern Western Australia have generated considerable exploration interest since the mid 1960s, when Dow & Gemuts (1967) reported the first occurrence of platinum in the Panton mafic–ultramafic intrusion. The East Kimberley is an attractive province to explore for platinum-group elements (PGEs), chromium, nickel, copper, cobalt, titanium, and vanadium since it contains one of the most extensively exposed mafic–ultramafic igneous associations in Australia; only the Giles Complex in the Musgrave Block of central Australia contains a larger area of layered intrusions (Glikson et al. 1996).

The East Kimberley mafic–ultramafic intrusions are confined to the central part of the Halls Creek Orogen (HCO: see Chapter 3), a well-exposed north-northeasterly-trending orogenic belt about 400 km long and at least 120 km wide along the southeastern margin of the Kimberley and Speewah Basins (Tyler et al. 1995). The orogen formed initially during the Palaeoproterozoic between a postulated Kimberley Craton, underlying the Kimberley and Speewah Basins to the west, and a composite craton containing Archaean rocks in the Pine Creek and The Granites–Tanami provinces to the east (Tyler et al. 1995). Much of the composite craton is covered by Mesoproterozoic, Neoproterozoic, and Palaeozoic sedimentary and volcanic sequences. The HCO is a complex province comprising low- to high-grade metasedimentary and metavolcanic rocks, and voluminous granitic, mafic, and mafic–ultramafic intrusions that collectively range in age from about 1910 Ma to 1790 Ma (Page & Hancock 1988, Tyler et al. 1995, Page et al. 1995). Major phases of tectonism occurred along the orogenic belt during the Palaeoproterozoic, Mesoproterozoic, and Neoproterozoic.

The regional tectonic setting of the HCO has been the subject of considerable debate for many years. Hancock & Rutland (1984) postulated that the province developed in an intracontinental setting from initial extension where large areas of thinned Archaean crust were formed, followed by convergence. Tyler et al. (1995) and Sheppard et al. (1999) have made analogies with modern continental margins, with the formation of felsic and basaltic magmas being related to modern-style subduction processes in a magmatic arc environment. Wyborn. L. (pers. comm., 1997, see Chapter 10) on the basis of the geochemistry of Kimberley granites has proposed a model involving underplating and extension. Shaw et al. (see Chapter 4) have highlighted the importance of transpressional and transtensional tectonism in the evolution of the HCO. Proterozoic layered intrusions overseas, such as the Bushveld Complex in South Africa and the Great Dyke in Zimbabwe, are generally believed to have been emplaced in stable intracratonic environments in which rifting occurred (von Gruenewaldt & Harmer 1992). The emplacement of the East Kimberley layered mafic–ultramafic intrusions implies multiple periods of rifting from about 1860 Ma to at least 1830 Ma. The development of large magma chambers (some intrusions are up to 7.8 km-thick and cover 240 km^2), laterally continuous rhythmic layering (over tens of kilometres) and fine-scale cumulate textures also indicate that stable tectonism prevailed for some periods of time during the crystallisation of the East Kimberley layered intrusions. Any model that attempts to explain the tectonic evolution of the HCO must take into consideration the emplacement of the Palaeoproterozoic layered mafic–ultramafic intrusions. The regional geology and tectonic setting of the HCO are discussed in Chapters 3, 4, 10, and 11.

Aims, methods of study, and nomenclature

Despite intensive exploration during the past four decades and the discovery of many prospects, no economic deposits associated with the layered intrusions have been found in the HCO. Some of the more high-profile intrusions (Panton, Sally Malay) contain significant resources of PGEs–Cr and Ni–Cu–Co and have experienced several unsuccessful phases of exploration, hence a major aim of this study was to provide an improved geoscientific framework for a more reliable assessment of the prospectivity and resource potential of the intrusions. Unlike previous investigations that have been largely carried out at the intrusion scale, it was hoped that this study would identify the different phases of mafic–ultramafic magmatism and mineralisation on a regional scale to help focus future exploration.

The Australian Geological Survey Organisation (AGSO) and the Geological Survey of Western Australia (GSWA) commenced investigations of the intrusions in 1992 as part of the National Geoscience Mapping Accord (NGMA) Kimberley–Arunta project that was initiated in 1990. The NGMA, endorsed by the Australian (now Australian and New Zealand) Minerals and Energy Council in August 1990, is a joint Commonwealth/State/Territory initiative to produce, using modern technology, a new generation of geological maps, data sets, and other information on strategically important regions of Australia. A list of publications and maps produced by the NGMA Kimberley–Arunta Project is given in

[1] Taken in this *Bulletin* to include intrusions of mafic and/or ultramafic rocks showing compositional layering and/or primary igneous laminations (see Irvine 1982).

Appendix 6. The general aims of the Kimberley–Arunta project are to:

- determine, through systematic mapping, geochemical and geochronological studies, and interpretation of remotely sensed and geophysical data, the nature, timing, and distribution of significant geological events in and between the western Arunta, The Granites–Tanami, and East Kimberley regions of the North Australian Craton;
- determine the extent of prospective bedrock beneath cover;
- describe styles of mineralisation that can be used as predictive exploration models; and
- provide geological and mineral resource information necessary for land use decisions.

In accordance with the above aims, this multidisciplinary study involved the geological mapping, U–Pb geochronology, petrology, whole-rock major- and trace-element chemistry, mineral chemistry, Sm–Nd and Re–Os isotopic systematics, and airborne geophysical and remote sensing investigations of 46 layered and massive mafic and mafic–ultramafic intrusions in the McINTOSH (Tyler et al. 1997a), MOUNT REMARKABLE (Sheppard et al. 1996), and TURKEY CREEK (Tyler et al. 1997b) 1:100 000 sheet areas[2] (Fig. 1.1). These sheets form components of the Dixon Range 1:250 000 Sheet (Tyler et al. 1998). The regional geological setting of the intrusions is shown in Figure 1.2 and individual intrusions are indicated on Figure 5.1. Since this study formed part of the NGMA mapping program of the East Kimberley, the intrusions were largely investigated at a regional scale. However, more detailed petrological, geochemical, and isotopic investigations of the economically significant Panton and Sally Malay intrusions and of chromitites from other intrusions are included in this *Bulletin* to complement the regional synthesis (see Chapters 12 and 13).

In addition to this *Bulletin*, the principal products related to the intrusions include the relevant parts of the geological maps (at 1:100 000 and 1:250 000 scales) and accompanying explanatory notes, airborne geophysical and remote sensing images, and field, geochemical, geochronological datasets. Findings from this study have also been reported in a number of other publications that discuss the:

- geology (Warren 1992, Blake & Hoatson 1993, Hoatson & Tyler 1993, Blake 1997, Hoatson 1997, Sheppard et al. 1997);
- mineralisation (Hoatson 1993a,b, 1995, 1998a,b, in press, Hoatson et al. 1995, 1997, Sheppard et al. 1997; Sproule et al. 1997a,b,c, 1999);
- geochronology (Page et al. 1995, Page & Hoatson 1997); and
- depths of emplacement (Trudu & Hoatson 1996) of the intrusions.

The mapping of the 46 layered intrusions was conducted by D.M. Hoatson during three field seasons on the following sheet areas:

1992 (12 weeks)—McINTOSH

1993 (4 weeks)—TURKEY CREEK and McINTOSH

1994 (10 weeks)—TURKEY CREEK, MOUNT REMARKABLE, and McINTOSH

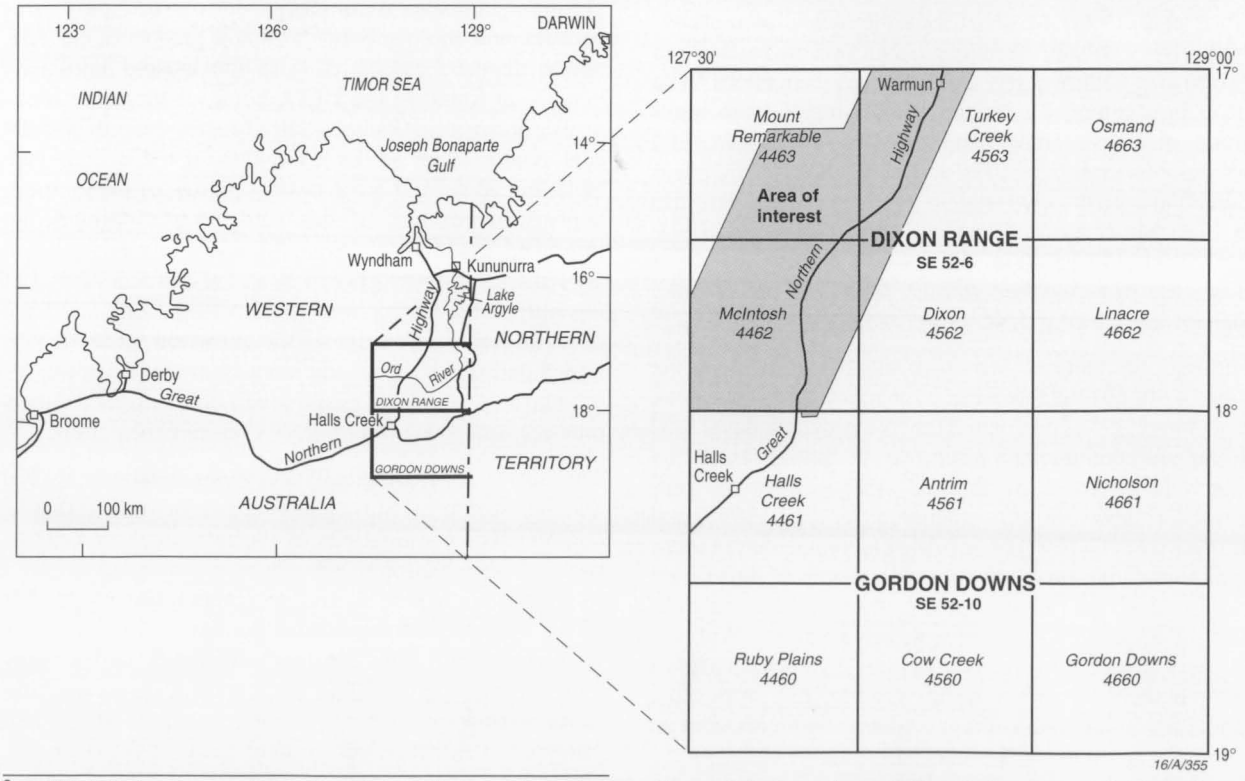


Figure 1.1. Location of the study area and the relevant 1:250 000 (in bold) and 1:100 000 geological sheets.

[2] 1:100 000 sheet names throughout this *Bulletin* are in capital letters to avoid confusion with identical place names and to distinguish them from 1:250 000 sheet names.

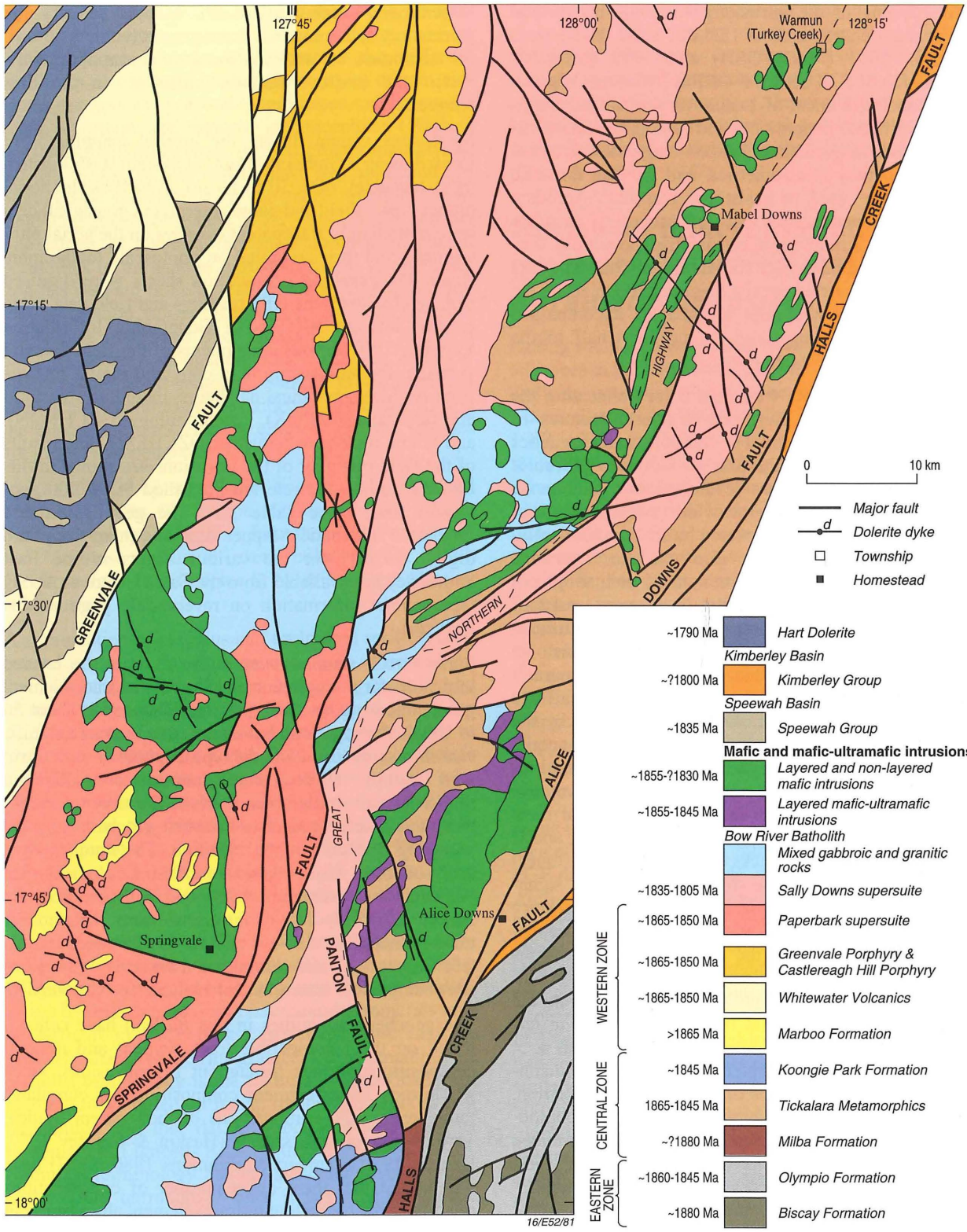


Figure 1.2. Regional geological setting of the mafic and mafic–ultramafic intrusions in the Halls Creek Orogen of the East Kimberley. Names of individual intrusions are indicated on Figure 5.1.

This mapping was done in association with AGSO specialists in the field who undertook geochronological (R.W. Page in 1994), remote sensing imagery (L.F. Macias in 1992 and 1993), and geophysical (R.D. Shaw in 1992 and J. Williams in 1993) studies of the intrusions. These specialist studies were integrated with the regional mapping program which was undertaken by D.H. Blake, D.M. Hoatson, R.G. Warren (all AGSO), I.M. Tyler, S. Sheppard, A.M. Thorne, and T.J. Griffin, (all GSWA). R.G. Warren (AGSO) investigated the Armanda intrusion region in 1992 and T.J. Griffin (GSWA) mapped part of the Toby intrusion in 1992. The

field mapping of the intrusions was done on vertical colour aerial photographs at 1:25 000 scale. These were flown in 1991 (McINTOSH) and 1992 (MOUNT REMARKABLE, TURKEY CREEK) for the Western Australian Department of Lands Administration, Perth. Various airborne geophysical and remote-sensing techniques, such as gradient-enhanced magnetics, gamma-ray (radiometric) spectrometrics, and Landsat thematic imagery, were used to assist the mapping. Aerodata Holdings Limited carried out and processed an aeromagnetic and gamma-ray spectrometric (potassium, thorium, and uranium) survey for AGSO in 1992. The survey, which was carried out at a height of 100 m above the surface along east-west lines 400 m apart, encompassed all of the Dixon Range and the northern half of the Gordon Downs 1:250 000 sheets.

The aeromagnetic data were useful for delineating the regional extent, geometry, and structural features of poorly exposed intrusions. For example, aeromagnetics showed that the magnetite-bearing Corridor gabbro is laterally continuous across several granite plutons on McINTOSH, despite its narrow width (a few hundreds of metres) and it often being covered by shallow black alluvium. Aeromagnetics were also used to determine younging (or fractionation) directions by indicating concentrations of primary magnetite in the upper parts of large evolved mafic intrusions (e.g. McIntosh, Springvale). However, younging directions in mafic–ultramafic intrusions (e.g. Panton) generally could not be determined in this way due to the small size of these bodies and the masking effects caused by the erratically distributed fine-grained secondary magnetite derived from the serpentinisation of olivine in the ultramafic rocks. Composite gamma-ray spectrometric images accurately defined the size and shape of most intrusions, since the low concentrations of K, Th, and U in the mafic–ultramafic rocks (expressed as dark tones) contrast markedly with the strong spectrometric signatures of the granitic and micaceous metasedimentary country rocks. Gamma-ray spectrometrics were particularly useful in defining the extent of the intrusions (Springvale and Toby) enclosed by various granite plutons of the Bow River Batholith and in determining the relative rock proportions in mixed gabbro-granite terrains. Landsat 5 Thematic Mapper imagery (bands 4, 5, 7, and 5/7, 5/3, 5; see Chapter 8) was helpful in distinguishing major rock groups of contrasting composition. For example, peridotite, gabbro, and anorthosite components could be readily distinguished in differentiated mafic–ultramafic intrusions (e.g. Panton, Mini, West McIntosh, and Melon Patch group) on the basis of distinctive colour signatures, and favourable stratigraphic levels for PGE–chromite mineralisation near the contacts of ultramafic and gabbroic sequences in these intrusions could be identified. The Landsat imagery provided useful information on structural features. For example, concentric lineaments in the Toby intrusion, not readily evident on other geophysical images, were revealed in large areas covered by shallow in-situ black soils. The Landsat imagery also depicted alteration in olivine- and feldspar-rich cumulates, geobotanical signatures (black lichen coatings on rocks of specific composition), and cultural influences (fireburns).

In summary, Landsat 5 Thematic Mapper imagery and gamma-ray spectrometrics were generally the most useful techniques for assisting the ground mapping of the mafic and mafic–ultramafic intrusions in the East Kimberley.

Most sites visited during the ground mapping were located using a Global Positioning System (GPS) instrument (accuracy of ± 50 to 80 m) as well as the aerial photographs. Field and photo-interpreted geological data were plotted onto transparent overlays on the aerial photographs and then compiled on photoscale topographic bases. The resulting compilation sheets were digitised and, together with the GPS readings and field data, were entered into an ARC/INFO Geographic Information System (GIS). Various components of the field data are available for purchase in hard-copy and digital formats from AGSO's geological databases, including structural and field data (OZROX), geochronology (OZCHRON), and whole-rock geochemistry (OZCHEM). The results of the field mapping of the intrusions are shown in this *Bulletin* and on the relevant published 1:100 000 geological sheets (see Table 3.1). The geophysical and Landsat 5 Thematic Mapper imagery (hard copy and digital format) for the various sheets in the East Kimberley are available from the Sales Centre at AGSO (see contact information on reverse-title page of this *Bulletin*).

Surface rock samples were collected from the layered intrusions for petrographic and major- and trace-element geochemical studies. Samples were obtained at about 50 to 100 m spacing along traverses across the more significant intrusions (including the type example of each intrusion group) to determine cumulus crystallisation sequences and stratigraphic levels of S and/or Cr saturation, and, where needed, to establish geochemically the younging direction of the intrusion. The samples were analysed for 11 major-elements and 25 trace elements (see Appendix 1.1). Mineralised diamond drill core from the Panton and Sally Malay intrusions were sampled for trace-element and Sm–Nd and Re–Os isotopic analysis (see Chapter 12), and chromitites from several intrusions were sampled for trace-element analysis (see Chapter 13).

The geochemical studies in this *Bulletin* have concentrated on the incompatible trace-element and mineral compositional trends throughout the intrusions, since whole-rock major-element compositions of cumulates rarely reflect the compositions of their parent liquids. Various petrogenetic studies (Haskin & Korotev 1977, Hanson 1980, Lambert & Simmons 1980, 1987) have highlighted that there are a number of complications relating to the modelling of trace-element abundances in cumulate rocks and the minerals that comprise these rocks. These complications include: (1) processes such as subliquidus re-equilibration, infiltration metasomatism, and subsolidus re-equilibration that may have significant effects on trace-element distributions; (2) uncertainties in mineral-melt distribution coefficients (e.g. Kd's) for rocks of different compositions; (3) the percent crystallisation of the solid; (4) assumptions involving the intercumulus material (e.g. determining extent of adcumulus growth); and (5) whether or not one magma was involved. These complications can hinder the interpreta-

tion of such processes as multiple injections, magma mixing, and magma contamination. In addition, the East Kimberley whole-rock data illustrate the different mobilities and redistribution behaviours of certain elements in response to secondary processes such as weathering, alteration, and regional metamorphism (Wallace & Hoatson 1990). Because of their greater mobility, K, Rb, Ba, S, Ce, Sr, Ga, and La have less application as petrogenetic indicators than the more immobile high-field-strength cations, such as Zr, Ti, Al, Y, Se, and Sc. The effects of alteration are most apparent in altered peridotites of the Panton intrusion, where serpentinisation has resulted in Fe_2O_3/FeO ratios as high as 5.2 and loss-on-ignition values of up to 16.12%. Despite these limitations, major and trace elements can be useful in defining gross fractionation trends and the chemical affinities of parent magmas. Sample preparation and analytical procedures are described in Appendix 1.1 and the major- and trace-element chemistry of the samples are given in Appendix 2.

Large (20 to 30 kg) samples of fractionated gabbro and anorthosite from the Panton, Springvale, Toby, Sally Malay intrusions, and gabbro from the contact aureole of the McIntosh intrusion, were collected for U–Pb geochronology (see Chapter 6) by drilling and blasting fresh surface material.

A combination of cumulus and traditional rock classifications is used in this *Bulletin* since both schemes have their advantages. Cumulus terminology as described by Irvine (1982) and Mathison (1989) involves listing the cumulus minerals in order of decreasing abundance as prefixes to Cumulate (e.g. opC is an olivine–plagioclase cumulate with cumulus olivine modally dominant relative to cumulus plagioclase) and a descriptive classification based on the abundance of intercumulus minerals, e.g. adcumulates have up to 7 volume percent intercumulus minerals, mesocumulates 7–25 percent, and orthocumulates 25–50 percent. Abbreviations used for the cumulus minerals are: a (augite: used for clinopyroxene in general), b (bronzite: used for orthopyroxene in general), c (chromite), m (magnetite), o (olivine), and p (plagioclase). It should be emphasised that the identification between cumulus and intercumulus minerals may be difficult in some rocks, especially those that are intensely altered or are fine grained. Complementing the cumulus terminology is the traditional classification of plutonic rocks based on modal mineral contents as recommended by the IUGS Subcommission on the Systematics of Igneous Rocks (Streckeisen 1973, 1976). Cumulate terminology has the advantage over conventional IUGS terminology since it has a better genetic basis in that it recognises crystallisation order and records the crystallisation history of magmas (Mathison 1989). However, conventional terminology, being based on the total mode of the cumulate can provide a clearer indication of the overall composition of the rock. As with tradition, the mineral assemblages of metamorphic rocks described in this *Bulletin* are arranged in ascending modal abundances, i.e. the reverse of cumulate rocks of igneous origin described above.

Individual modal proportions of cumulates are generally not given in this *Bulletin* since these rocks can be very heterogeneous in composition due to their compositional layering (i.e. ranging from dunite to gabbro to anorthosite over a few centimetres). For other features relating to layered intrusions, such as type of layering and descriptions of cumulates, the terminology proposed by Irvine (1982) is used. General geological terms used in this *Bulletin* are as defined in the Glossary of Geology (Bates & Jackson 1987).

Review of mineralisation processes in layered mafic–ultramafic intrusions

During the past few decades there have been important advances in the understanding of the magmatic and mineralising processes that operate in layered intrusions. Classical works by Wager et al. (1960), Jackson (1961, 1967, 1970), and Wager & Brown (1968) provided the foundation for this expanding research by introducing cumulus terminology for the classification of the rocks in layered intrusions. In more recent times, a greater understanding of the mineralisation processes has been achieved by the application of low-temperature experimental studies which simulate the fluid dynamical and fractional crystallisation mechanisms that are believed to occur in magma chambers. Scaled-tank experiments involving aqueous solutions of salts and sugars at various temperatures and densities (Huppert & Sparks 1980, 1984; Huppert & Turner 1981, Sparks et al. 1984, Campbell & Turner 1986, Sparks & Huppert 1987, Huppert et al. 1987, Tait & Kerr 1987) have attempted to simulate various magmatic processes, such as convection, overturning, mixing, and crystallisation.

Some broad generalisations can be made about the geological setting of layered intrusions hosting significant PGE deposits. For example, the intrusions are generally Archaean or Palaeoproterozoic, were emplaced into stable tectonic terranes, and have thicknesses exceeding 5 km. However, in detail there is considerable variation in style, stratigraphic level, and tenor of mineralisation that cannot be explained by a single genetic model. This variation is highlighted by the Bushveld Complex, where PGE enrichment is related to magmatic, hydrothermal, and contamination processes, e.g. (1) in narrow stratabound sulphide-bearing pegmatoidal layers 400 to 500 m above the first major appearance of cumulus plagioclase and in the vicinity of where cumulus augite occurs with cumulus orthopyroxene (e.g. Merensky Reef); (2) in chromitite layers (UG-2 and UG-3 chromitites); (3) in discordant dunite pipes (Onverwacht and Driekop pipes); and (4) in contaminated floor rocks (Platreef). Variations in mineralisation styles may reflect the relative importance of factors such as the chemical heterogeneity of the mantle source (e.g. part of the source may be enriched in PGEs), magma type and magma generation processes (e.g. boninite-type magma, second-stage melting of refractory mantle, timing of sulphur saturation), magma chamber processes (crystal fractionation, sequence of crystallisation, crustal contamination, magma mixing), and post-emplacement mechanisms (adcumulus growth, late magmatic fluids,

hydrothermal remobilisation). It is also important to recognise that significant PGE mineralisation is not restricted to intrusions of Precambrian age. It can occur in younger Phanerozoic intrusions as shown by the Permo-Triassic Ni–Cu deposits of Noril'sk-Talnakh, Russia (Naldrett 1989, 1997) and the Tertiary Skaergaard Intrusion, East Greenland (Nielsen & Brooks 1995).

Mineralising processes that occurred in magma chambers (Naldrett 1989, 1997, Lee 1996) have to be inferred by examination of exhumed intrusions and by extrapolation of laboratory investigations on analogue systems. Various hypotheses relating to the mineralising processes have been proposed. Some of the more important processes which may have relevance to the East Kimberley intrusions include: (1) filter pressing; (2) crustal contamination; (3) crystal fractionation; (4) magma mixing; (5) constitutional zone refining; and (6) hydrothermal processes.

(1) *Filter pressing*. von Gruenewaldt (1979) argued that the PGE tenor of the Merensky Reef sulphides was upgraded by ascending, PGE-enriched, late magmatic intercumulus fluids expelled during compaction of underlying cumulus pile. In these models, sulphides interact with thousands of times their own mass of PGE-undepleted magma. Gain (1985) also used the filter-pressing model to explain the PGE-enrichment of the UG-2 chromitite layer by the upward migration of highly fractionated intercumulus fluids under highly reducing conditions.

(2) *Crustal contamination*. Sulphide precipitation models that have been proposed for the driving of mafic magmas towards S saturation include the direct addition of S by the assimilation of sulphide- or sulphate-bearing country rocks, such as sulphide-bearing iron formations and evaporites, and/or the contamination of mafic magmas (e.g. silicification) by crustal melts (Thornett 1981, Cawthorn et al. 1985a,b, Barton et al. 1986, Peltonen 1995a, Naldrett 1997, Li & Naldrett 1999).

(3) *Crystal fractionation*. The incompatibility of Pt, Pd, and Rh during crystal fractionation of S-undersaturated magmas, and late S saturation in such magmas, are important processes for the development of PGE-enriched layers at high stratigraphic levels in fractionating intrusions (Hoatson & Keays 1989, Wilson & Tredoux 1990, Naldrett et al. 1994, Filho et al. 1995).

(4) *Magma mixing*. Mixing of chemically distinct magmas can induce saturation of sulphide and chromite in layered intrusions (Campbell et al. 1983, Naldrett et al. 1987, 1990; Wilson et al. 1989, Hoatson & Keays 1989, Eales et al. 1990b, Wilson & Tredoux 1990, Cawthorn 1996, Naldrett 1997, Hoatson 1998b). Laterally extensive mineralised layers (Merensky Reef, Munni Munni) are considered to have formed by the mixing of a fractionated density-stratified resident magma with a pulse of hotter and more buoyant primitive magma injected into the magma chamber as a fountain or plume. The formation of a plume or fountain depends largely on the relative densities of the two liquids and the velocity and volume of the injected magma. Campbell & Naldrett (1979) and Naldrett (1989, 1997) have emphasised the importance of a high silicate/sulphide mass ratio (R factor) during turbulent magma mixing for the formation of a PGE-enriched layer. The most favourable condition for producing a high R factor is when a new, hot, buoyant pulse is injected into a density-stratified magma chamber. The pulse convects turbulently as it rises to find its own density level, and then spreads out laterally like a plume to form a hybrid layer. During the early crystallisation of plagioclase, the density of the hybrid layer of the magma increases, and so the density stratification within the hybrid layer may destabilise, resulting in turbulent mixing with the resident magma, thus permitting the equilibration of any immiscible sulphides with large volumes of silicate melt. Because of the large volume of melt and the high partition coefficients of the PGEs for sulphides (in the range 10^3 to 10^5: Campbell & Barnes 1984, Barnes & Naldrett 1985, Peach et al. 1989, Stone et al. 1990, Fleet et al. 1996, 1999), the PGE tenor of the sulphides is maximised. This proposed large-scale magma mixing can account for the very high concentrations of PGEs in mineralised layers (around 10 000 ppb Pt compared to 10 ppb Pt in unmineralised cumulates) and can explain why the mineralised layers occur about 500 m above the stratigraphic level where plagioclase first becomes a cumulus mineral. In an extension of this model, Naldrett et al. (1986) suggested that the Merensky Reef formed from downspouts of a dense mixture of crystals, sulphides, and entrained liquid that spread out across the crystal-pile floor after having originated from the mixing of anorthositic and ultramafic magmas at higher levels in the magma chamber. Irvine et al. (1983), Campbell et al. (1983), and Campbell (1996) have described the fluid dynamics of various mixing models that involved magmas of different relative temperatures and compositions, and their effect on the R factor in plume, jet, and double-diffusive magma mixing systems.

The timing of S saturation in layered intrusions is critical, because if a host magma attains saturation too early in its evolution (i.e. in the mantle or during its ascent into the crust), the PGEs will become rapidly depleted due to their extremely high partition coefficients into sulphide phases. Consequently, early S saturation of a magma will inhibit the effectiveness of processes such as sulphide fractionation and the generation of high R-factor sulphides in the formation of PGE-enriched layers.

Various isotopic systems have been used for studies relating to (1) geochronology, (2) geochemistry of magma source/s, and (3) identification of isotopically distinct magma types in mineralising processes such as magma mixing and crustal contamination. These isotopic systems include: Re–Os and Os–Os (Hart & Kinloch 1989, Lambert et al. 1989, 1990, 1991, 1998a,b, 1999, Hattori et al. 1991, Sproule et al. 1999), Sm–Nd (Lambert et al. 1988, 1989, 1990, 1994, Martin 1989, Sun & Hoatson 1992), O (Schiffries & Rye 1989, 1990, Lee & Ripley 1996, Ripley et al. 1999), Pb (Auret et al. 1989, Wooden et al. 1991), S (Mainwaring & Naldrett 1977, Ripley 1981, 1983, Zientek & Ripley 1990), and Rb–Sr (Sharpe 1985, Lee et al. 1989, Stewart & DePaolo 1990, Eales et al. 1990a,b, Kruger 1994, Nielsen et al. 1996). Isotopic and geochemical studies of feeder-dykes

and marginal rocks (Sharpe 1981, Sharpe & Hulbert 1985, Davies & Tredoux 1985) have supported the hypothesis that the Merensky Reef formed from large-scale mixing of anorthositic (A–type) and ultramafic (U–type) magmas. The A–type magmas were largely tholeiitic, with low incompatible-element concentrations (von Gruenewaldt et al. 1985), whereas the U–type magmas had higher MgO and SiO_2 contents and were relatively enriched in PGEs. Mixing of A–type and U–type magmas has also been proposed for the Stillwater Complex (Todd et al. 1982; Barnes & Naldrett 1986, Lambert & Simmons 1987, 1988), although the U–type magma was more evolved and the A–type magma was silica-undersaturated compared to the equivalent magmas in the Bushveld Complex.

(5) *Constitutional zone refining*. The distribution of breccias, pegmatites, plagioclase-rich gabbro segregations, and extremely fractionated PGE ratios in the Lac des Iles Complex, Ontario was considered by Brügmann et al. (1989) to result from volatile-induced partial melting of cumulates and subsequent S saturation of the melt, a process that McBirney (1987) has referred to as 'constitutional zone refining'. The irregular and non-stratabound mineralisation is thought to have formed from the interaction of water with hot cumulates, causing volatile-induced partial remelting of the overlying cumulates, and resulting in the scavenging of PGEs by a rising melt. As the melt ascended, it became progressively enriched in S until S saturation occurred and PGE-rich sulphides were precipitated.

(6) *Hydrothermal processes*. There has been considerable debate about the relative importance of magmatic processes, sensu stricto, versus fluid-volatile hydrothermal processes in the formation of PGE deposits. Various studies (Boudreau et al. 1986, 1993; Stumpfl 1986, Ballhaus & Stumpfl 1986, Schiffries & Skinner 1987, Watkinson & Melling 1992, Boudreau 1993, 1995a,b; Cawthorn 1994, Watkinson & Jones 1996) have shown that there is a spectrum of PGE deposits, ranging from those dominantly magmatic in origin, through those magmatic deposits which have had various degrees of hydrothermal overprinting, to those deposits which are largely hydrothermal in origin. The occurrence of pegmatoidal bodies, discordant dunite pipes and sulphide zones, alteration veins, high Cl/F ratios in apatite, high Cl in biotite, graphite, intergrowths of sulphides with intercumulus hydrous phases, and fluid inclusions, have all been used as evidence for the importance of fluid-volatile systems in the transport and concentration of PGEs during the cooling history of intrusions. In the hydrothermal systems, hot late-stage fluids exsolve from the solidifying cumulate pile, scavenge and transport PGEs (often by halogen complexing) upwards through the cumulates and into the overlying intercumulus melt, where they interact with S to produce the PGE-rich sulphides. Boudreau & Meurer (1999) interpreted offset PGE and base-metal distribution trends in mineralised layers to have formed from migrating sulphide enrichment-resorption fronts accompanying degassing of interstitial liquids from a compacting and solidifying cumulus pile.

Barnes & Campbell (1988), on the other hand, argue that many hydrothermal-type features are the result of postcumulus processes superimposed on layers whose extensive, uniform PGE concentrations were formed by magmatic cumulus processes. They note (1) the location of PGEs near the bottom of cyclic units and with chromitite layers, indicating a genetic relationship to influxes of new magma; (2) the lateral persistence of grade in the Merensky Reef and UG-2 chromitite; and (3) the systematic stratigraphic controls on PGE contents of sulphides within the UG-2 chromitite. In addition, they claim that the ascending-hydrothermal-fluid models do not account for the paucity of mineralisation in horizons stratigraphically below the Merensky Reef, such as the Pseudoreef and various chromitite horizons. They also note that the highest grades often occur in the margins of some intrusions (e.g. Great Dyke) which do not overlie great thicknesses of ultramafic cumulates. Naldrett et al. (1987) consider that the extreme stratiform nature and constant composition of mineralised layers, like the Merensky Reef, and the difficulties inherent with deriving the PGEs from below, indicate that the PGE-bearing sulphides accumulated from a homogeneous layer of magma during the crystallisation of the enclosing magma.

Acknowledgements

The author would like to thank David Blake, John Sheraton, Alastair Stewart (all AGSO), and Ian Tyler (GSWA) for their constructive comments of earlier drafts of the manuscript. Lana Murray drafted the figures.

References

Auret, J.M., Harmer, R.E., Eglington, B.M. & Sharpe, M.R., 1989. Pb isotope systematics in the Eastern Bushveld Complex. In: Abstracts, Origin of mineralization in Southern African layered complexes. University of Witwatersrand, Johannesburg, South Africa, 21–22.

Ballhaus, C.G. & Stumpfl, E.F., 1986. Sulfide and platinum mineralization in the Merensky Reef: evidence from hydrous silicates and fluid inclusions. Contributions to Mineralogy & Petrology, 94, 193–204.

Barnes, Stephen J. & Campbell, I.H., 1988. Role of late magmatic fluids in Merensky-type platinum deposits: a discussion. Geology, 16, 488–491.

Barnes, Stephen J. & Naldrett, A.J., 1985. Geochemistry of the J-M (Howland) Reef of the Stillwater Complex, Minneapolis Adit Area. I. Sulfide chemistry and sulfide-olivine equilibrium. Economic Geology, 80, 627–645.

Barnes, Stephen J. & Naldrett, A.J., 1986. Geochemistry of the J-M (Howland) Reef of the Stillwater Complex, Minneapolis Adit Area. II. Silicate mineral chemistry and petrogenesis. Journal of Petrology, 27, 791–825.

Barton, J.M., Jr., Cawthorn, R.G. & White, J., 1986. The role of contamination in the evolution of the Platreef of the Bushveld Complex. Economic Geology, 81, 1096–1104.

Bates, R.L. & Jackson, J.A., 1987. Glossary of geology, Third Edition. American Geological Institute, Alexandria, Virginia, 788 pp.

Blake, D.H., 1997. Speculations relating to the layered mafic–ultramafic intrusions of the East Kimberley, Western Australia. AGSO Research Newsletter, 27, 19–21.

Blake, D.H. & Hoatson, D.M., 1993. Granite, gabbro, and migmatite field relationships in the Proterozoic Lamboo Complex of the East Kimberley region, Western Australia. Australian Geological Survey Organisation, Journal, 14/4, 319–330.

Boudreau, A.E., 1993. Chlorine as an exploration guide for the platinum-group elements in layered intrusions. Journal of Geochemical Exploration, 48, 21–37.

Boudreau, A.E., 1995a. Fluid evolution in layered intrusions: Evidence from the chemistry of the halogen-bearing minerals. In: Thompson, J.F.H. (editor), Magmas, fluids, and ore deposits. Mineralogical Association of Canada, Short Course Series, 23. Victoria, British Columbia, 25–45.

Boudreau, A.E., 1995b. Some geochemical considerations for platinum-group element exploration in layered intrusions. Exploration and Mining Geology, 4, 215–225.

Boudreau, A.E., Love, C. & Hoatson, D.M., 1993. Variation in the composition of apatite in the Munni Munni Complex and associated intrusions of the West Pilbara Block, Western Australia. Geochimica et Cosmochimica Acta, 57, 4467–4477.

Boudreau, A.E., Mathez, E.A. & McCallum, I.S., 1986. Halogen geochemistry of the Stillwater and Bushveld Complexes: Evidence for transport of the platinum-group elements by Cl-rich fluids. Journal of Petrology, 27, 967–986.

Boudreau, A.E. & Meurer, W.P. 1999. Chromatographic separation of the platinum-group elements, gold, base metals and sulfur during degassing of a compacting and solidifying igneous crystal pile. Contributions to Mineralogy and Petrology, 134, 174–185.

Brügmann, G.E., Naldrett, A.J. & Macdonald, A.J., 1989. Magma mixing and constitutional zone refining in the Lac des Iles Complex, Ontario: genesis of platinum-group element mineralization. Economic Geology, 84, 1557–1573.

Campbell, I.H., 1996. Fluid dynamic processes in basaltic magma chambers. In: Cawthorn, R.G. (editor), Layered intrusions. Developments in Petrology 15. Elsevier, Amsterdam, 45–76.

Campbell, I.H. & Barnes, Stephen J., 1984. A model for the geochemistry of the platinum group elements in magmatic sulfide deposits. Canadian Mineralogist, 22, 151–160.

Campbell, I.H. & Naldrett, A.J., 1979. The influence of silicate:sulfide ratios on the geochemistry of magmatic sulfides. Economic Geology, 74, 1503–1506.

Campbell, I.H., Naldrett, A.J. & Barnes, S.J., 1983. A model for the origin of the platinum-rich sulphide horizons in the Bushveld and Stillwater Complexes. Journal of Petrology, 24, 133–165.

Campbell, I.H. & Turner, J.S., 1986. The role of convection in the formation of platinum and chromitite deposits in layered intrusions. In: Scarfe, C.M. (editor), Short course in silicate melts. Mineralogical Association of Canada: Ottawa, Canada, 236–278.

Cawthorn, R.G., 1994. Formation of chloro- and fluorapatite in layered intrusions. Mineralogical Magazine, 58, 299–306.

Cawthorn, R.G., 1996. Layered intrusions. Developments in Petrology 15. Elsevier, Amsterdam, 531 pp.

Cawthorn, R.G., Barton, J.M., Jr. & Viljoen, M.J., 1985a. Interaction of floor rocks with the Platreef on Overysel, Potgietersrus, Northern Transvaal. Economic Geology, 80, 988–1006.

Cawthorn, R.G., Barton, J.R., Jr., White, J. & Viljoen, M.J., 1985b. The role of contamination in the evolution of the Platreef of the Bushveld Complex. Fourth International Platinum Symposium, Abstracts, 14-31 July 1985, Toronto, Canada. IGCP Project 161. Canadian Mineralogist, 23, 298–299.

Davies, G. & Tredoux, M., 1985. The platinum-group element and gold contents of the marginal rocks and sills of the Bushveld Complex. Economic Geology, 80, 838–848.

Dow, D.B. & Gemuts, I., 1967. Dixon Range, Western Australia - 1 : 250 000 Geological Series. Bureau of Mineral Resources, Australia, Explanatory Notes SE/52-6, 15 pp.

Eales, H.V., De Klerk, W.J., Butcher, A.R. & Kruger, F.J., 1990a. The cyclic unit beneath the UG1 chromitite (UG1FW unit) at RPM Union Section Platinum Mine-Rosetta Stone of the Bushveld Upper Critical Zone? Mineralogical Magazine, 54, 23–43.

Eales, H.V., De Klerk, W.J. & Teigler, B., 1990b. Evidence for magma mixing processes within the Critical and Lower Zones of the northwestern Bushveld Complex, South Africa. Chemical Geology, 88, 261–278.

Filho, C.F., Naldrett, A.J. & Asif, M., 1995. Distribution of platinum-group elements in the Niquelandia mafic–ultramafic intrusion, Brazil: implications with respect to exploration. Canadian Mineralogist, 33, 165–184.

Fleet, M.E., Crocket, J.H. & Stone, W.E., 1996. Partitioning of platinum-group elements (Os, Ir, Ru, Pt, Pd) and gold between sulfide liquid and basalt melt. Geochimica et Cosmochimica Acta, 60, 2397–2412.

Fleet, M.E., Crocket, J.H., Liu, M. & Stone, W.E. 1999. Laboratory partitioning of platinum-group elements (PGE) and gold with application to magmatic sulfide-PGE deposits. Lithos, 47, 127–142.

Gain, S.B., 1985. The geological setting of the platiniferous UG-2 chromitite layer on the farm Maandagshoek, Eastern Bushveld Complex. Economic Geology, 80, 925–943.

Glikson, A.Y., Stewart, A.J ., Ballhaus, C.G., Clarke, G.L., Feeken, E.H.J., Leven, J.H., Sheraton, J.W. & Sun, S-s., 1996. Geology of the western Musgrave Block, central Australia, with particular reference to the mafic–ultramafic Giles Complex. Australian Geological Survey Organisation Bulletin 239, 206 pp.

Hancock, S.L. & Rutland, R.W.R., 1984. Tectonics of an Early Proterozoic geosuture - the Halls Creek orogenic sub-province, northern Australia. Journal of Geodynamics, 1, 387–432.

Hanson, G.N., 1980. Rare earth elements in petrogenetic studies of igneous systems. Annual Review of Earth & Planetary Sciences, 8, 307–406.

Hart, S.R. & Kinloch, E.D., 1989. Osmium isotope systematics in Witwatersrand and Bushveld ore deposits. Economic Geology, 84, 1651–1655.

Haskin, L.A. & Korotev, R.A., 1977. Test of a model for trace element partitioning during closed-system solidification of a silicate liquid. Geochimica et Cosmochimica Acta, 41, 921–939.

Hattori, K., Cabri, L.J. & Hart, S.R., 1991. Osmium isotope ratios of PGE grains associated with the Freetown layered complex, Sierra Leone, and their origin. Contributions to Mineralogy & Petrology, 109, 10–18.

Hoatson, D.M., 1993a. Correlation of structurally disrupted layered mafic–ultramafic intrusions in the East Kimberley: Is Big Ben part of the Panton intrusion? AGSO Research Newsletter, 19, 9–10.

Hoatson, D.M., 1993b. Summary of geoscientific information for the East Kimberley, Western Australia, with specific reference to the Dixon Range 1:250 000 Sheet (SE/52-6) and Gordon Downs 1:250 000 Sheet (SE/52-10). Australian Geological Survey Organisation, Record 1993/32, 76 pp.

Hoatson, D.M., 1995. New mineral discoveries in the East Kimberley. AGSO Research Newsletter, 22, 9–11.

Hoatson, D.M., 1997. Geology and mineralisation of the Palaeoproterozoic layered mafic–ultramafic intrusions in the Halls Creek Orogen, Western Australia. In: Rutland, R.W.R. & Drummond, B.J. (editors), Palaeoproterozoic tectonics and metallogenesis: comparative analysis of parts of the Australian & Fennoscandian shields. Workshop, Darwin, September, 14-22, 1997. Australian Geological Survey Organisation, Record 1997/44, 61–64.

Hoatson, D.M., 1998a. The geology and economic potential of the Palaeoproterozoic layered mafic–ultramafic intrusions in the East Kimberley, Western Australia. The Geological Society of South Africa and The South African Institute of Mining and Metallurgy, Symposium Series S18. Extended Abstract 8th International Platinum Symposium, Rustenburg, 28 June-3 July 1998, 153–156.

Hoatson, D.M., 1998b. Platinum-group element mineralisation in Australian Precambrian layered mafic–ultramafic intrusions. Special Issue of AGSO Journal of Australian Geology & Geophysics, 17/4, 139–151.

Hoatson, D.M., in press. Exploration strategies for Precambrian layered mafic–ultramafic intrusions in the East Kimberley. AGSO Research Newsletter, 32.

Hoatson, D.M. & Keays, R.R., 1989. Formation of platiniferous sulfide horizons by crystal fractionation and magma mixing in the Munni Munni layered intrusion, west Pilbara Block, Western Australia. Economic Geology, 84, 1775–1804.

Hoatson, D.M., Blake, D., Warren, G., Orth, K. & Tyler, I.M., 1995. Recent NGMA mapping highlights the metallogenic potential of the East Kimberley. AGSO Research Newsletter, 22, 1–2.

Hoatson, D.M., Sproule, R.A. & Lambert, D.D., 1997. Are there Voisey's Bay-type Ni–Cu–Co sulphide deposits in the East Kimberley of Western Australia? AGSO Research Newsletter, 27, 17–19.

Hoatson, D.M. & Tyler, I., 1993. Prospective layered mafic–ultramafic intrusions in the East Kimberley. AGSO Research Newsletter, 18, 8–9.

Huppert, H.E. & Sparks, R.S.J., 1980. The fluid dynamics of a basaltic magma chamber. Contributions to Mineralogy & Petrology, 75, 279–289.

Huppert, H.E. & Sparks, R.S.J., 1984. Double diffusive convection due to crystallisation in magmas. Annual Reviews, Earth & Planetary Science, 12, 11–37.

Huppert, H.E., Sparks, R.S.J., Wilson, J.R., Hallworth, M.A. & Leitch, A.M., 1987. Laboratory experiments with aqueous solutions modelling magma chamber processes - II. Cooling and crystallisation along inclined planes. In: Parsons, I. (editor), Origins of igneous layering. NATO Advanced Science Series, 196. D. Reidel Publishing Company, Dordrecht, 539–568.

Huppert, H.E. & Turner, J.S., 1981. A laboratory model of a replenished magma chamber. Earth & Planetary Science Letters, 54, 144–152.

Irvine, T.N., 1982. Terminology for layered intrusions. Journal of Petrology, 23, 127–162.

Irvine, T.N., Keith, D.W. & Todd, S.G., 1983. The J-M platinum-palladium reef of the Stillwater Complex, Montana: II. Origin by double-diffusive convective magma mixing and implications for the Bushveld Complex. Economic Geology, 78, 1287–1334.

Jackson, E.D., 1961. Primary textures and mineral associations in the Ultramafic Zone of the Stillwater Complex, Montana. United States Geological Survey, Professional Paper 358, 106 pp.

Jackson, E.D., 1967. Ultramafic cumulates in the Stillwater, Great Dyke and Bushveld intrusions. In: Wyllie, P.J. (editor), Ultramafic and related rocks. John Wiley & Sons, New York, 20–38.

Jackson, E.D., 1970. The cyclic units in layered intrusions - a comparison of repetitive stratigraphy in the ultramafic parts of the Stillwater, Muskox, Great Dyke, and Bushveld Complexes. Geological Society of South Africa, Special Publication 1, 391–424.

Kruger, F.J., 1994. The Sr-isotopic stratigraphy of the western Bushveld Complex. South African Journal of Geology, 97, 393–398.

Lambert, D.D., Foster, J.G. & Frick, L.R., 1998a. Geodynamics of magmatic Cu-Ni-PGE sulfide deposits: New insights from the Re–Os isotope system. Economic Geology, 93, 121–136.

Lambert, D.D., Foster, J.G., Frick, L.R., Hoatson, D.M. & Purvis, A.C., 1998b. Application of the Re–Os isotopic system to the study of Precambrian magmatic sulfide deposits of Western Australia. Australian Journal of Earth Sciences, 45, 265–284.

Lambert, D.D., Foster, J.G., Frick, L.R., Li, C. & Naldrett, A.J., 1999. Re–Os isotopic systematics of the Voisey's Bay Ni–Cu–Co magmatic ore system, Labrador, Canada. Lithos, 47, 69–88.

Lambert, D.D., Morgan, J.W., Walker, R.J., Shirey, S.B., Carlson, R.W., Zientek, M.L. & Koski, M.S., 1989. Rhenium-osmium and samarium-neodymium isotopic systematics of the Stillwater Complex, Montana. Science, 244, 1169–1174.

Lambert, D.D., Shirey, S.B., Carlson, R.W., Walker, R.J. & Morgan, J.W., 1990. Re–Os and Sm–Nd isotope geochemistry of the Stillwater Complex, Montana: the role of crustal versus lithospheric mantle sources in layered intrusions. In: Glover, J.E. & Ho, S.E. (compilers), Third International Archaean Symposium, Extended Abstracts. Geoconferences (WA) Incorporated, Perth, 1990, 153–155.

Lambert, D.D., Shirey, S.B., Carlson, R.W., Walker, R.J., Morgan, J.W. & Zientek, M.L., 1991. Applications of the Re–Os isotopic system to platinum-group element ore genesis in the Stillwater Complex, Montana (USA). In: Barnes, Stephen J. (editor), Sixth International Platinum Symposium, Abstracts, July 1991, Perth, WA. IAGOD and the Geological Society of Australia, 30.

Lambert, D.D. & Simmons, E.C., 1980. Cumulate minerals as liquid analogues, a new approach to modelling trace elements in mafic layered intrusions: applications to the Stillwater Complex, Montana. EOS, 61, 410.

Lambert, D.D. & Simmons, E.C., 1987. Magma evolution in the Stillwater Complex, Montana - I. Rare-earth element evidence for the formation of the ultramafic series. American Journal of Science, 287, 1–32.

Lambert, D.D. & Simmons, E.C., 1988. Magma evolution in the Stillwater Complex - II. Rare-earth element evidence for the formation of the J-M Reef. Economic Geology, 83, 1109–1126.

Lambert, D.D., Unruh, D.M. & Gilbert, M.C., 1988. Rb-Sr and Sm–Nd isotopic study of the Glen Mountains layered complex: initiation of rifting within the southern Oklahoma aulacogen. Geology, 16, 13–17.

Lambert, D.D., Walker, R.J., Morgan, J.W., Shirey, S.B., Carlson, R.W., Zientek, M.L., Lipin, B.R., Koski, M.S. & Cooper, R.L., 1994. Re–Os and Sm–Nd isotope geochemistry of the Stillwater Complex, Montana: Implications for the petrogenesis of the J-M Reef. Journal of Petrology, 35, 1717–1753.

Lee, C.A., 1996. A review of mineralization in the Bushveld Complex and some other layered intrusions. In: Cawthorn, R.G. (editor), Layered intrusions. Developments in Petrology 15. Elsevier, Amsterdam, 103–145.

Lee, C.A., Cawthorn, R.G. & Barton, J.M., Jr., 1989. Further Sr-isotope and trace element studies on the Platreef, Bushveld Complex. In: Papunen, H. (editor), 5th International Platinum Symposium, Abstracts. Bulletin of the Geological Society of Finland, 61, Part 1, 1989, 21.

Lee, I. & Ripley, E.M., 1996. Mineralogic and oxygen isotopic studies of open system magmatic processes in the South Kawishiwi intrusion, Spruce Road area, Duluth Complex, Minnesota. Journal of Petrology, 37, 1437–1461.

Li, C. & Naldrett, A.J. 1999. Geology and petrology of the Voisey's Bay intrusion: reaction of olivine with sulfide and silicate liquids. Lithos, 47, 1–31.

Mainwaring, P.R. & Naldrett, A.J., 1977. Country-rock assimilation and the genesis of Cu-Ni sulfides in the Water Hen intrusion, Duluth Complex, Minnesota. Economic Geology, 72, 1269–1284.

Martin, C.E., 1989. Re–Os isotopic investigation of the Stillwater Complex, Montana. Earth & Planetary Science Letters, 93, 336–344.

Mathison, C.I., 1989. Petrological encoding of cumulates. Transactions of the Institution of Mining and Metallurgy, 98, B18–B23.

McBirney, A.R., 1987. Constitutional zone refining of layered intrusions. In: Parsons, I. (editor), Origins of igneous layering. NATO Advanced Science Series, 196. D. Reidel Publishing Company, Dordrecht, 437–452.

Naldrett, A.J., 1989. Magmatic Sulfide Deposits. Clarendon Press; Oxford University Press, New York, 177 pp.

Naldrett, A.J., 1997. Key factors in the genesis of Noril'sk, Sudbury, Jinchuan, Voisey's Bay and other world-class Ni–Cu-PGE deposits: implications for exploration. Australian Journal of Earth Sciences, 44, 283–315.

Naldrett, A.J., Gasparrini, E.C., Barnes, Stephen J., von Gruenewaldt, G. & Sharpe, M.R., 1986. The upper critical zone of the Bushveld Complex and the origin of Merensky-type ores. Economic Geology, 81, 1105–1117.

Naldrett, A.J., Cameron, G., von Gruenewaldt, G. & Sharpe, M.R., 1987. The formation of stratiform PGE deposits in layered intrusions. In: Parsons, I. (editor), Origins of igneous layering. NATO Advanced Science Series, 196. D. Reidel Publishing Company, Dordrecht, 313–398.

Naldrett, A.J., Brügmann, G.E. & Wilson, A.H., 1990. Models for the concentration of PGE in layered intrusions. Canadian Mineralogist, 28, 389–408.

Naldrett, A.J., Asif, M., Scoates, R.J.F., Eckstrand, O.R. & Schwann, P.L., 1994. Platinum-group elements in Fox River Sill, Manitoba, Canada: implications with respect to influxes of fresh magma and exploration for PGE deposits. Transactions of the Institution of Mining and Metallurgy, 103, B10–B21.

Nielsen, T.F.D. & Brooks, C.K., 1995. Precious metals in magmas of East Greenland: Factors important to the mineralization in the Skaergaard Intrusion. Economic Geology, 90, 1911–1917.

Nielsen, F.M., Campbell, I.H., McCulloch, M. & Wilson, J.R., 1996. A strontium isotopic investigation of the Bjerkreim-Sokndal layered intrusion, Southwest Norway. Journal of Petrology, 37, 171–193.

Page, R.W. & Hancock, S.L., 1988. Geochronology of a rapid 1.85-1.86 Ga tectonic transition: Halls Creek Orogen, northern Australia. Precambrian Research, 40/41, 447–467.

Page, R.W. & Hoatson, D.M., 1997. SHRIMP U-Pb geochronology of Palaeoproterozoic layered mafic–ultramafic intrusions, East Kimberley, Western Australia. Abstract GAC/MAC Annual Meeting Ottawa '97, 9-21 May 1997, A 111.

Page, R.W., Hoatson, D.M., Sun, S-s. & Foudoulis, C., 1995. High-precision geochronology of Palaeoproterozoic layered mafic–ultramafic intrusions in the East Kimberley. AGSO Research Newsletter, 22, 7–8.

Peach, C.L., Mathez, E.A. & Keays, R.R., 1989. Sulfide melt-silicate melt distribution coefficients for the noble metals as deduced from MORBs. In: Papunen, H. (editor), 5th International Platinum Symposium,

Abstracts. Bulletin of the Geological Society of Finland, 61, Part 1, 1989, 58.

Peltonen, P., 1995a. Magma-country rock interaction and the genesis of Ni–Cu deposits in the Vammala nickel belt, Southwest Finland. Mineralogy & Petrology, 52, 1–24.

Ripley, E.M., 1981. Sulfur isotopic studies of the Dunka Road Cu-Ni deposit, Duluth Complex, Minnesota. Economic Geology, 76, 610–620.

Ripley, E.M., 1983. Sulfide mineralogy and sulfur isotope geochemistry of layered sills in the Deer Lake Complex, Minnesota. Mineralium Deposita, 18, 3–15.

Ripley, E.M., Park, Y-R., Li, C. & Naldrett, A.J., 1999. Sulfur and oxygen isotopic evidence of country rock contamination in the Voisey's Bay Ni–Cu–Co deposit, Labrador, Canada. Lithos, 47, 53–68.

Schiffries, C.M. & Rye, D.M., 1989. Stable isotopic systematics of the Bushveld Complex: I. Constraints of magmatic processes in layered intrusions. American Journal of Science, 289, 841–873.

Schiffries, C.M. & Rye, D.M., 1990. Stable isotopic systematics of the Bushveld Complex: II. Constraints on hydrothermal processes in layered intrusions. American Journal of Science, 290, 209–245.

Schiffries, C.M. & Skinner, B.J., 1987. The Bushveld hydrothermal system. Field and petrologic evidence. American Journal of Science, 287, 566–596.

Sharpe, M.R., 1981. The chronology of magma influxes to the eastern compartment of the Bushveld Complex as exemplified by its marginal border groups. Journal of the Geological Society of London, 138, 307–326.

Sharpe, M.R., 1985. Strontium isotope evidence for preserved density stratification in the main zone of the Bushveld Complex. Nature, 316, 119–126.

Sharpe, M.R. & Hulbert, L.J., 1985. Ultramafic sills beneath the Eastern Bushveld Complex: mobilized suspensions of early lower zone cumulates in a parental magma with boninitic affinities. Economic Geology, 80, 849–871.

Sheppard, S., Tyler, I.M., Griffin, T.J. & Taylor, W.R., 1999. Palaeoproterozoic subduction-related and passive margin basalts in the Halls Creek Orogen, northwest Australia. Australian Journal of Earth Sciences, 46, 679–690.

Sheppard, S., Tyler, I.M. & Hoatson, D.M., 1996. Mount Remarkable, Western Australia, 1:100 000 geological map (sheet 4463). Geological Survey of Western Australia, Perth.

Sheppard, S., Tyler, I.M. & Hoatson, D.M., 1997. Geology of the Mount Remarkable 1:100 000 sheet: Western Australia Geological Survey, 1:100 000 Geological Series Explanatory Notes, 27 pp.

Sparks, R.S.J. & Huppert, H.E., 1987. Laboratory experiments with aqueous solutions modelling magma chamber processes. I. Discussion of their validity and geological application. In: Parsons, I. (editor), Origins of igneous layering. NATO Advanced Science Series, 196. D. Reidel Publishing Company, Dordrecht, 527–538.

Sparks, R.S.J., Huppert, H.E. & Turner, J.S., 1984. The fluid dynamics of evolving magma chambers. Philosophical Transactions, Royal Society of London, A 310, 511–534.

Sproule, R.A., 1999. Genesis of Palaeoproterozoic mafic–ultramafic intrusions and associated PGE–Cr and Ni–Cu–Co mineralisation in the East Kimberley, Western Australia. Ph.D. thesis, Monash University, Australia (unpublished), 320 pp.

Sproule, R., Lambert, D.D. & Hoatson, D.M., 1997a. Re–Os and Sm–Nd isotopic constraints on the genesis of magmatic ores in the Palaeoproterozoic Panton Intrusion, East Kimberley. New Developments in Research for Ore Deposit Exploration. Third National Conference of the Specialist Group in Economic Geology, Canberra, January 30-31 1997. Geological Society of Australia, Abstracts, 44, 67.

Sproule, R.A., Lambert, D.D. & Hoatson, D.M., 1997b. Guides to PGE and Ni–Cu–Co exploration in the East Kimberley, Western Australia. In: Burroughs, A. (editor), Student and young professionals conference. Australasian Institute of Mining and Metallurgy, Abstract, Ballarat 1997.

Sproule, R.A., Lambert, D.D. & Hoatson, D.M., 1997c. Rhenium-osmium constraints on the genesis of magmatic nickel-copper-cobalt-platinum-group-element ores, East Kimberley, Western Australia. Abstracts. Seven Annual V.M. Goldschmidt Conference, June 2-6, 1997, Tucson, Arizona. LPI contribution number 921, 195–196.

Sproule, R.A., Lambert, D.D. & Hoatson, D.M., 1999. Re–Os isotopic constraints on the genesis of the Sally Malay Ni–Cu–Co deposit, East Kimberley, Western Australia. Lithos, 47, 89–106.

Stewart, B.W. & DePaolo, D.J., 1990. Isotopic studies of processes in mafic magma chambers - II: The Skaergaard intrusion, East Greenland. Contributions to Mineralogy & Petrology, 104, 125–141.

Stone, W.E., Crockett, J.H. & Fleet, M.E., 1990. Partitioning of palladium, iridium, platinum, and gold between sulfide liquid and basalt melt at 1200°C. Geochimica et Cosmochimica Acta, 54, 2341–2344.

Streckeisen, A.L., 1973. Plutonic rocks: classification and nomenclature recommended by the IUGS Subcommission on the systematics of igneous rocks. Geotimes, October 1973, 26–30.

Streckeisen, A.L., 1976. To each plutonic rock its proper name. Earth-Science Reviews, 12, 1–33.

Stumpfl, E.F., 1986. Distribution, transport and concentration of platinum group elements. In: Gallagher, M.J., Ixer, R.A., Neary, C.R. & Prichard, H.M. (editors), Metallogeny of basic and ultrabasic rocks. The Institution of Mining & Metallurgy, London, 379–394.

Sun, S-s. & Hoatson, D.M., 1992. Chemical and isotopic characteristics of parent magmas of the west Pilbara layered intrusions: Implications for petrogenesis, magma mixing, and PGE mineralisation in layered intrusions. In: Hoatson, D.M., Wallace, D.A., Sun, S-s., Macias, L.F., Simpson, C.J. & Keays, R.R., Petrology and platinum-group-element geochemistry of Archaean layered mafic–ultramafic intrusions, west Pilbara Block, Western Australia. Australian Geological Survey Organisation, Bulletin 242, 141–149.

Tait, S.R. & Kerr, R.C., 1987. Experimental modelling of interstitial melt convection in cumulus piles. In: Parsons, I. (editor), Origins of igneous layering. NATO Advanced Science Series, 196. D. Reidel Publishing Company, Dordrecht, 569–587.

Thornett, J.R., 1981. The Sally Malay deposit: gabbroid associated nickel-copper sulfide mineralization in the Halls Creek Mobile Zone, Western Australia. Economic Geology, 76 (6), 1565–1580.

Todd, S.G., Keith, D.W., Le Roy, L.W., Schissel, D.J., Mann, E.L. & Irvine, T.N., 1982. The J-M platinum-palladium reef of the Stillwater Complex, Montana: I. Stratigraphy and petrology. Economic Geology, 77, 1454–1480.

Trudu, A. & Hoatson, D.M., 1996. Depths of emplacement of Precambrian layered intrusions in the East Kimberley. AGSO Research Newsletter, 25, 10–12.

Tyler, I.M., Griffin, T.J., Page, R.W. & Shaw, R.D., 1995. Are there terranes within the Lamboo Complex of the Halls Creek Orogen? Western Australia Geological Survey, Annual Review 1993-94, 37–46.

Tyler, I.M., Hoatson, D.M., Griffin, T.J., Sheppard, S., Blake, D.H. & Warren, R.G., 1997a. McIntosh, Western Australia, 1:100 000 geological map (sheet 4462). Geological Survey of Western Australia, Perth.

Tyler, I.M., Thorne, A.M., Hoatson, D.M. & Blake, D.H., 1997b. Turkey Creek, Western Australia, 1:100 000 geological map (sheet 4563). Geological Survey of Western Australia, Perth.

Tyler, I.M., Thorne, A.M., Sheppard, S., Hoatson, D.M., Griffin, T.J., Blake, D.H. & Warren, R.G., 1998. Geology of the Dixon Range 1:250 000 Sheet. Geological Survey of Western Australia, Perth.

von Gruenewaldt, G., 1979. A review of some recent concepts of the Bushveld Complex, with particular reference to sulfide mineralization. Canadian Mineralogist, 17, 233–256.

von Gruenewaldt, G. & Harmer, R.E., 1992. Tectonic setting of Proterozoic layered intrusions with special reference to the Bushveld Complex. In: Condie, K.C. (editor), Developments in Precambrian geology, 10. Proterozoic crustal evolution. Elsevier, Amsterdam, 181–213.

von Gruenewaldt, G., Sharpe, M.R. & Hatton, C.J., 1985. The Bushveld Complex: introduction and review. Economic Geology, 80, 803–812.

Wager, L.R. & Brown, G.M., 1968. Layered igneous rocks. Oliver & Boyd, Edinburgh & New York, 588 pp.

Wager, L.R., Brown, G.M. & Wadsworth, W.J., 1960. Types of igneous cumulates. Journal of Petrology, 1, 73–85.

Wallace, D.A. & Hoatson, D.M., 1990. Petrology and whole-rock geochemistry of selected mafic and ultramafic suites from the Pilbara Block and Halls Creek Mobile Zone, Western Australia. Bureau of Mineral Resources, Australia, Record 1990/46, 69 pp.

Warren, R.G., 1992. District surrounding the Armanda Sill, Halls Creek Inlier, Western Australia. Australian Geological Survey Organisation, Record 1992/70, 16 pp.

Watkinson, D.H. & Jones, P.C., 1996. Platinum-group minerals in fluid inclusions from the Marathon deposit, Coldwell Complex, Canada. Mineralogy and Petrology, 57, 91–96.

Watkinson, D.H. & Melling, D.R., 1992. Hydrothermal origin of platinum-group mineralization in low-temperature copper sulfide-rich assemblages, Salt Chuck Intrusion, Alaska. Economic Geology, 87, 175–184.

Wilson, A.H., Naldrett, A.J. & Tredoux, M., 1989. Distribution and controls of platinum group element and base metal mineralization in the Darwendale subchamber of the Great Dyke, Zimbabwe. Geology, 17, 649–652.

Wilson, A.H. & Tredoux, M., 1990. Lateral and vertical distribution of platinum-group elements and petrogenetic controls on the sulfide mineralization in the P1 pyroxenite layer of the Darwendale subchamber of the Great Dyke, Zimbabwe. Economic Geology, 85, 556–584.

Wooden, J.L., Czamanske, G.K. & Zientek, M.L., 1991. A lead isotopic study of the Stillwater Complex: constraints on crustal contamination and source regions. Contributions to Mineralogy & Petrology, 107, 80–93.

Zientek, M.L. & Ripley, E.M., 1990. Sulphur isotope studies of the Stillwater Complex and associated rocks, Montana. Economic Geology, 85, 376–391.

EXPLORATION HISTORY OF THE EAST KIMBERLEY, WESTERN AUSTRALIA

by DEAN M. HOATSON

Mineral exploration in the East Kimberley

The mineral potential of the East Kimberley region was first noted in 1879, by the Western Australian explorer and surveyor Alexander Forrest (1849–1901; Fig. 2.1). Forrest worked for the State Survey Department at a time when the Western Australian Government was encouraging the opening up of unsettled land. In 1879 he led an expedition party, which included a government-appointed geologist named Fenton Hill from Victoria, to assess the potential of the northern part of Western Australia for minerals, horse and cattle breeding, and tropical crops.

With 26 horses and rations for six months, Forrest's party began their journey from the De Grey River in the West Pilbara on 25 February 1879. Initially, the party made good progress, but the King Leopold Ranges in the central Kimberley presented an impenetrable barrier, forcing Forrest back to the Fitzroy River and east towards the Overland Telegraph Line in the Northern Territory. On this eastward journey his party found large grassy plains and strongly flowing rivers, one of which would later be called the Ord River.

After five months of travelling, Forrest's party was suffering from ill health and a shortage of rations. They were, therefore, forced to press on through the promising East Kimberley area towards the Northern Territory, which they reached several weeks later. It was Forrest's decision to travel east, against his original instructions, that resulted in the long-term impacts of his expedition.

The report of his journey (Forrest 1880) stimulated interest into the pastoral and mineral potential of the East Kimberley. Forrest's geologist, Fenton Hill, regretted that he was not able *".... to announce the discovery of any large tracts of auriferous lands"*, but that there was *".... good reason to hope that both gold and other minerals, such as tin and copper"* existed (Fenton Hill, Supplement to Forrest's Journal, 1880, p. 43). In addition, Forrest had optimistically noted the similarity between rocks in the East Kimberley and those around the Pine Creek gold mine in the Northern Territory. It was this observation that inspired the manager of the Pine Creek mine, Adam Johns, to embark on an expedition in 1882 with Philip Saunders and an Aboriginal named Crawford to follow Forrest's tracks in the hope of finding gold. Prospecting the upper reaches of the Ord River southeast of the King Leopold Ranges, they found minor gold over a distance of 60 km, although the lack of adequate water for panning and Johns's failing health forced the prospectors to push on east to the Northern Territory. Upon returning to civilisation, Saunders sent a telegram to Forrest, now Surveyor General, advising him of their find. The telegram prompted Forrest to dispatch an expedition headed by a geologist from the Geological Survey of Ireland, Edward T. Hardman (1845–1887; Fig. 2.2). In recognition of his discovery, Saunders received a government pension of one pound ten shillings a week.

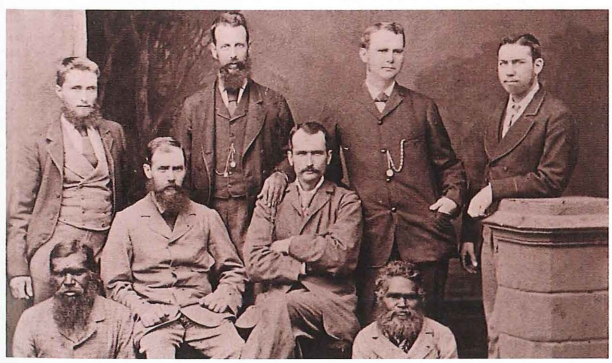
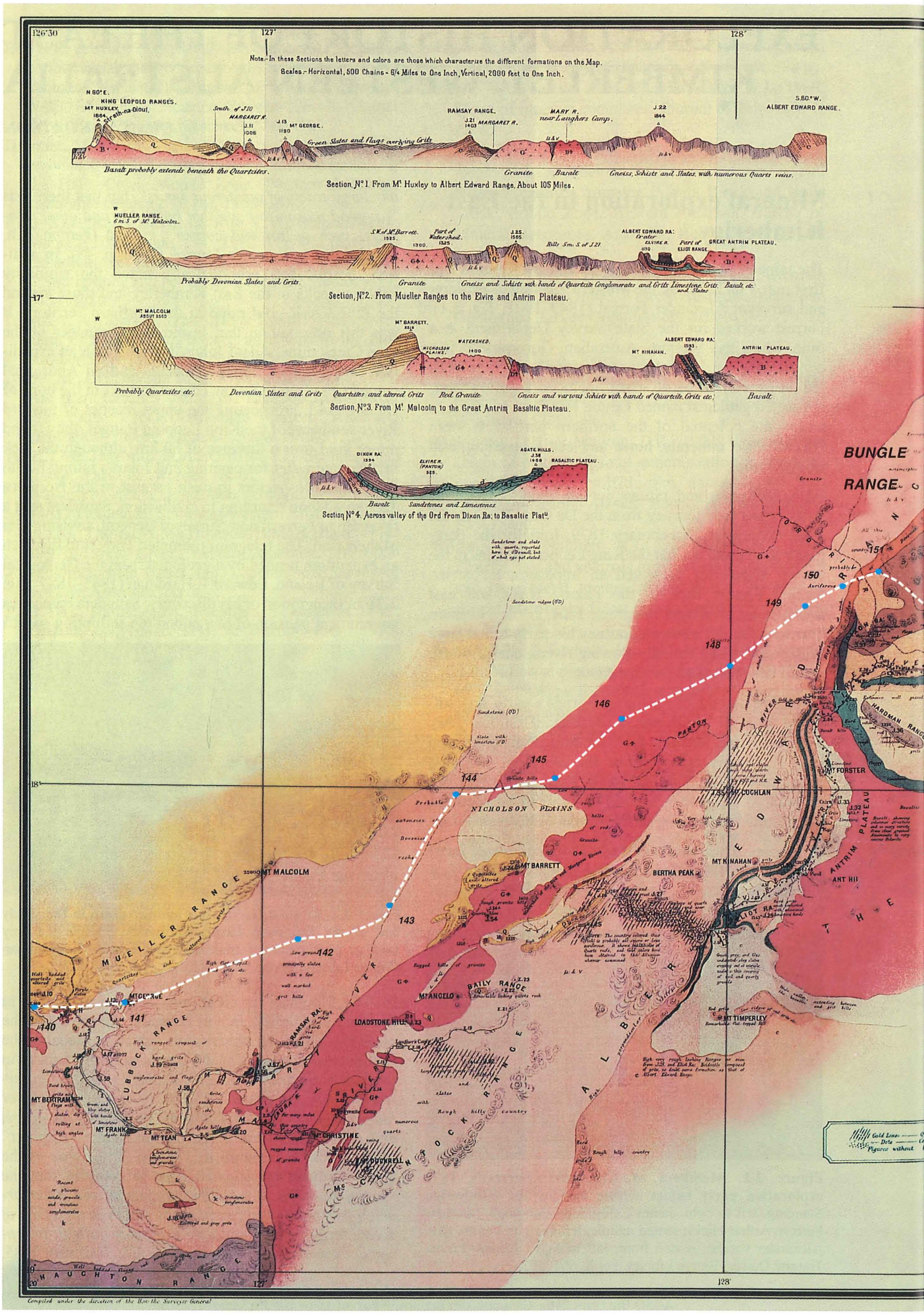


Figure 2.1. Members of Alexander Forrest's 1879 exploration party before setting out for the Kimberley. Standing, left to right: James Carey, John Campbell, Matthew Forrest, Arthur Hicks; seated middle, left to right: Fenton Hill, Alexander Forrest; seated front, left to right: Tommy Pierre, Tommy Dower (Battye Library, Perth: 66175P).



Figure 2.2. Edward Hardman's midday camp in the sandy bed of the Robinson River, Kimberley. This is the only existing photograph of Irish geologist Edward T. Hardman (Battye Library, Perth: 5390B/11).

In 1884, Hardman travelled from the West Kimberley to the East Kimberley. In the Margaret River region, he made the following observation, which is probably the first documentation of mafic intrusive igneous rocks in the East Kimberley. *"Gabbro, diallage rock, and hypersthenic rock are found in large masses on the Upper Margaret about 2 miles below the opening of the gorge, and again, below the gorge on the Lower Margaret"* (observation 217, Hardman 1885, p. 25). Some of the areas Hardman investigated were so complex that the *"....ramifications of the different igneous and metamorphic rocks become so complicated that even on a map of a very large scale it would be extremely difficult to represent them correctly"* (observation 232, Hardman 1885,


126°30
127°
128°
Note.–In these Sections the letters and colors are those which characterize the different formations on the Map.
Scales.–Horizontal, 500 Chains = 6¼ Miles to One Inch, Vertical, 2000 feet to One Inch.
N 60° E.
KING LEOPOLD RANGES.
MT HUXLEY
1864
Streath-na-Dioul
South of J 10
MARGARET R.
J 11
1006
J 13
1190
MT GEORGE.
Green Slates and Flags overlying Grits
RAMSAY RANGE.
J 21
1403
MARGARET R.
MARY R.
near Laughers Camp.
J 22
1844
S 80° W.
ALBERT EDWARD RANGE.
Basalt probably extends beneath the Quartzites.
Granite
Basalt
Gneiss, Schists and Slates, with numerous Quartz veins.
Section N° 1. From Mt Huxley to Albert Edward Range, About 105 Miles.
W
MUELLER RANGE.
6 m S of Mt Malcolm.
S.W. of Mt Barrett.
1525.
1300.
Part of Watershed.
1525.
J 25.
1565.
Hills 5 m S of J 21
ALBERT EDWARD RA.
Crater
ELVIRE R.
1170
Part of ELIOT RANGE.
GREAT ANTRIM PLATEAU.
Probably Devonian Slates and Grits.
Granite
Gneiss and Schists with bands of Quartzite Conglomerates and Grits Limestone Grits and Slates
Basalt etc.
Section, N°2. From Mueller Ranges to the Elvire and Antrim Plateau.
17°
W
MT MALCOLM
ABOUT 3500
MT BARRETT.
8519
NICHOLSON PLAINS.
WATERSHED.
1400
ALBERT EDWARD RA.
1523.
MT KINAHAN.
ANTRIM PLATEAU.
Probably Quartzites etc.
Devonian Slates and Grits
Quartzites and altered Grits
Red Granite
Gneiss and various Schists with bands of Quartzite, Grits etc.
Basalt.
Section, N°3. From Mt Malcolm to the Great Antrim Basaltic Plateau.
DIXON RA.
1334
ELVIRE R. (PANTON)
525.
AGATE HILLS.
J 38
1458
BASALTIC PLATEAU.
Basalt
Sandstones and Limestones
Section N° 4. Across valley of the Ord from Dixon Ra. to Basaltic Plat.
BUNGLE RANGE
Granite
Sandstone and slate with quartz reported here by O'Donnell, but of what age not stated.
Sandstone ridges (OD)
Sandstone (OD)
Slate with limestone (OD)
Granite Hills
Probable extension of Devonian rocks
NICHOLSON PLAINS
hills of red Granite
Quartzites (and altered grits)
Rough granite hills
Rough granite hills country
Low ground principally slates with a few well marked grit hills
Well bedded quartzites and altered grits
Purple slates
High Cliffs of grits etc.
Recent or Pliocene sands, gravels and ironstone conglomerate
Ironstone conglomerates
Limestone and grey grits
Sandstone and grits
Rough hilly country
Rough hills country
Numerous quartz veins
Rough ridges of granite
Slates and Grits
Slates with Rough hills country
Slates and Grits
Slates and Limestone
Slates and Grits
Slates and Limestone
Slates and Grits
Slates and Limestone

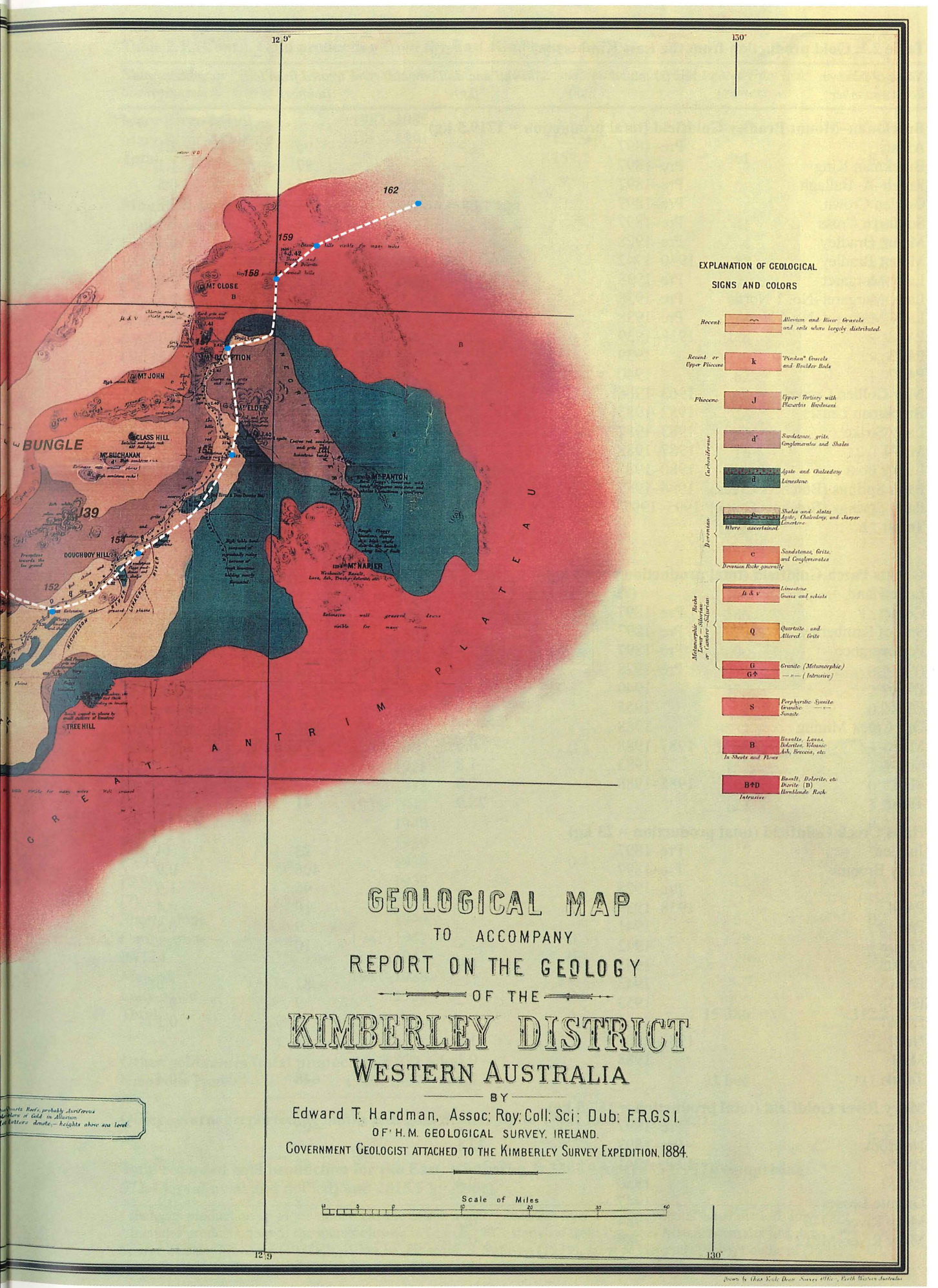


Figure 2.3. The first geological map of the East Kimberley (by Edward Hardman in 1884). The route (dashed line) and campsites of Alexander Forrest's 1879 exploration party have been added.

Table 2.1. Gold production from the East Kimberley.

Name of mine or licence number	*Year(s) mined*	*Alluvial and dollied gold (kg)*	*Ore treated from lode (tonnes)*	*Lode gold (kg)*
Brockman–Mount Bradley Goldfield (total production = 1719.5 kg)				
Afgan	Pre–1897	–	96	2.1
Brockman King	Pre–1897	–	87	1.1
Faugh–A–Ballagh	Pre–1897	–	15	0.5
Golden Crown	Pre–1897	–	1172	39.7
Southern Cross	Pre–1897	–	5	0.1
Mount Bradley	Pre–1928	–	2500	56.4
Mount Bradley	1940–1942	–	196	1.6
Lady Margaret	Pre–1938	–	98.5	7.2
Lady Margaret–No. 1 North	Pre–1938	–	20.8	0.5
Lady Margaret–No.4 North	Pre–1938	–	6.6	0.3
PA78	1938–1939	0.2	–	–
PA93	1939	–	–	0.1
PA97	1940	0.2	7	0.4
New Golden Crown	1963–1966	–	120	1
Brockman Leases	1982–1985	3.7	–	–
Lady Strike	1983–1987	2.6	–	–
M174	1987–1988	0.7	–	–
Lucky Four	1980–1987	3.1	–	–
Palm Springs (Butchers Creek)	1986–1987	23	–	–
Palm Springs (Butchers Creek)	1995–1997[1]	–	735 000	1575
Total		**33.5**	**739 323.9**	**1686**
Grants Patch Goldfield (total production = 42.4 kg)				
Lone Hand	(?)	–	–	8.1
Comet	Pre–1897	–	29	4.6
Star of Kimberley	Pre–1897	–	1	0.1
Perseverance	Pre–1897	–	5	0.1
(?)	Pre–1928	–	3	0.5
PA96	1940	–	3	0.1
PA162	1955	0.2	–	–
Dry Creek Mining	1988	24	–	–
M156	1987–1988	0.1	–	–
M6–9	1983	1.8	–	–
M38	1985–1988	2.8	–	–
Total		**28.9**	**41**	**13.5**
Halls Creek Goldfield (total production = 23 kg)				
Jubilee	Pre–1897	–	23	14
Lady Broome	Pre–1897	–	406	0.9
(?)	Pre–1928	–	96	1.9
PA84	1938–1939	–	10	0.4
PA112	1941	–	9	0.5
PA118	1942	–	10	0.5
PA108	1942	0.9	–	–
PA115	1943	–	82	1.6
PA158	1953	–	9	0.5
PA161	1953	–	3	0.1
No. 1	1981–1982	1.6	–	–
M90	1988	0.1	–	–
Total		**2.6**	**648**	**20.4**
Mary River Goldfield (total production = 167.5 kg)				
Reform	Pre–1897	–	405	6.5
Newlook	Pre–1897	32.1	–	–
PA99	1940–1941	–	48	1.7
PA151	1950	0.4	–	–
Granite Leases	1947	–	8	0.1
Mary River–M46	1984	0.2	–	–
Mary River–M212	1988	0.2	–	–

Table 2.1. (Cont.). Gold production from the East Kimberley.

Name of mine or licence number	*Year(s) mined*	*Alluvial and dollied gold (kg)*	*Ore treated from lode (tonnes)*	*Lode gold (kg)*
Mary River–M199	1987–1988	0.4	–	–
Mary River–M248	1989–1991	125.9	–	–
Total		**159.2**	**461**	**8.3**
Mount Dockrell Goldfield (total production = 45.1 kg)				
Lady Hopetown	Pre–1897	–	41	10
Victoria	Pre–1897	–	4	3.5
PA59	1935	–	37	0.8
(?)	1935	–	–	0.8
Mount Miniard	1936	–	187	5.3
Western Lead	1935–1942	–	219	2.3
Irish Lass	1937–1943	0.7	346	8.3
Old Mac	1938–1940	–	239	5.6
Erin–Go–Bragh	1939–1941	–	62	1.7
PA75	1938	0.6	–	–
PA102	1940	–	26	0.4
PA101	1940–1941	–	83	0.7
(?)	1941	–	16	0.1
Old Golden Dream	1941–1942	–	93	0.8
M194	1988	0.7	–	–
Sundry claims	(?)	–	163	2.8
Total		**2**	**1516**	**43.1**
Ruby Creek Goldfield (total production = 316.4 kg)				
North Ruby Queen	Pre–1897	–	194	5.8
Rising Sun	Pre–1897	–	586	15.2
Sunny Corner	Pre–1897	–	22	1.8
West and Left	Pre–1897	–	690	29.4
West and Left	1938–1941	–	10	0.2
St. Lawerence	Pre–1902	–	383	2.8
St. Lawerence	1938	–	10	0.2
Ruby Queen (claim 61)	Pre–1908	–	9833	192.7
Ruby Queen (claim 97)	1897–1963	0.1	3120	53.7
(?)	Pre–1928	–	153	3.9
PA79	1938	–	93	0.7
Goliath	1938–1942	–	123	3.2
Goliath	1940	–	7	0.2
PA91	1939	–	12	0.1
PA93	1939	0.4	–	–
PA96	1939	–	12	0.1
(?)	1939	0.1	–	–
Shorts Hope	1940	–	51	0.1
Darcys mine	1941–1942	0.5	79	1.9
PA124	1947	0.4	8	0.2
Majeed	1981–1988	2.1	–	–
Lady Myra	1987	0.6	–	–
Total		**4.2**	**15 386**	**312.2**
Other gold mines (total production = 731.6 kg)				
Nicolsons Find	1996–1997[2]	–	**93 000**	**731.6**
Other returns (reported by banks and gold dealers up to 1963: total = 342.4 kg)				
		342	–	**0.4**

Total recorded gold production for the East Kimberley is 3387.9 kg (1885–1997), comprising: 572.4 kg (alluvial and dollied) and 2815.5 kg (lode).

[1] Includes production up to the mine's closure in April 1997; statistics from Precious Metals Australia Ltd, July 1999.
[2] Includes production up to the mine's closure in March 1997; statistics from Precious Metals Australia Ltd, July 1999.
Source of data: Finucane (1938a,b, 1939a,b), Finucane & Sullivan (1939), Dow & Gemuts (1969), Louthean (1991, 1992), Gonnella (1997), Bester (1998), and Sanders (1999).

p. 27). Hardman's 1884 geological map (Fig. 2.3)—the first such map of the East Kimberley—and report are remarkably accurate, considering the reconnaissance nature of his work and the complexity of the geology. Hardman also found many traces of gold, and noted quartz reefs and alluvial gold in the country drained by the Margaret, Mary, Elvire, Panton, and Ord Rivers. He was confident that the area would be found to be *".... auriferous to a payable degree"* (observation 325, Hardman 1885, p. 34).

It was Hardman's report of 1885, which noted promising alluvial prospects over a large area of metamorphic rocks, that resulted in Charles Hall, a Roebourne well sinker and fencer, and his companion, John Slattery, finding the first discovery of payable gold in Western Australia. On 14 July 1885, they found about 8 ounces of gold near the headwaters of the Elvire River, which they named Halls Creek (now called Old Halls Creek). Soon after their discovery, Hall and Slattery arrived in Derby carrying with them 106 ounces of gold. By claiming the one thousand pounds government reward offered at that time to the first finders of payable gold in Western Australia, they started the Kimberley gold rush. This rush reached its peak in late 1886, when thousands of diggers arrived from other parts of Australia and from New Zealand. In the ensuing years, the rich auriferous gravels, which were thin and of limited extent, were rapidly worked out. When Western Australia Government Geologist Woodward (1891) visited the goldfield in 1890, very few alluvial mines were still operating, the gold had been traced to its source, and most fields had been discovered, developed, and abandoned. The small size of the gold reefs, remoteness of the area, lack of fuel and water and, in some cases, the mineralogy of the ores all contributed to the failure of the hard-rock mines. By the early 1890s, most prospectors in the Kimberleys travelled south when major new gold finds were announced in the Pilbara, Murchison, and Ashburton (in 1890), Southern Cross (1891), Coolgardie (1892), and Kalgoorlie (1893) regions of Western Australia.

Total recorded gold production in the East Kimberley from ~1885 to 1997 was about 3388 kg (Table 2.1). More than 68% of this production (2307 kg) has been derived from lode deposits near Halls Creek since 1995. Hard-rock lode mining has produced approximately 2816 kg of gold, whereas alluvial mining operations have been relatively small, accounting for only 572 kg. Historical (pre–1960) hard-rock and alluvial gold production in the East Kimberley was largely restricted to six main areas: Ruby Creek, Brockman–Mount Bradley, Halls Creek, Mary River, Grants Patch, and Mount Dockrell (Dow & Gemuts 1969, Sanders 1999). The Ruby Creek area was the most productive goldfield (total production of 313.7 kg), followed by the Brockman–Mount Bradley Goldfield (110.4 kg), Mount Dockrell Goldfield (44.4 kg), Mary River Goldfield (40.8 kg), Halls Creek Goldfield (21.3 kg), and Grants Patch Goldfield (13.7 kg). These are minimum production totals since the majority of the alluvial production was not recorded. Recent gold production in the East Kimberley has been dominated by the Butchers Creek (Palm Springs operation) and Nicolsons Find hard-rock mines near Halls Creek (Bester 1998). Production at Butchers Creek commenced in April 1995 and about 1575 kg of gold was obtained until mining ceased in April 1997. Mineable reserves at June 1997 were 500 000 t @ 2.26 ppm below 120 m. The small high-grade Nicolsons Find deposit produced about 732 kg Au from early 1996 to its closure in March 1997. It has an inferred underground resource of 279 000 t @ 5.5 ppm. The other major gold prospect in the Halls Creek region is Grants Creek, which has an indicated resource of 67 000 t @ 5 ppm (Bester 1998)

The fault-controlled quartz-lode gold deposits are generally hosted by low-grade metasediments of the Halls Creek Group, and are confined to a narrow stratigraphic zone between the Olympio and Biscay Formations adjacent to sills of Woodward Dolerite (Dow & Gemuts 1969) and/or metamorphosed basalt. In some deposits there is also a close spatial relationship between economic gold mineralisation and alkaline volcanic rocks of the Butchers Gully and Maude Headley Members of the Olympio Formation (Warren 1994a,b, Blake et al. 1999). The gold-bearing quartz veins are related to faults that cut the early folds affecting the Halls Creek Group; i.e. the gold lodes postdate the main phase (1835 Ma) of the Halls Creek Orogeny (Blake et al. 1999). It is believed that the gold was originally disseminated in rocks of the Halls Creek Group, especially in alkaline volcanics, and was mobilised and concentrated by H_2O and CO_2 fluids during later tectonic events (Warren 1994a).

The lodes generally consist of thin (<2 m), steeply dipping quartz veins that are mostly concordant with the bedding. Metamorphosed mudstone and siltstone are the usual hosts, but lodes also occur in metadolerite and metasandstone. Most of the deposits have been worked only in the oxidised zone, where the fine–grained gold occurs free. In the unoxidised zone the gold occurs with pyrite–galena–sphalerite–chalcopyrite mineralisation. The alluvial gold workings occur downstream from most of the quartz-lode gold deposits. Some of these workings occur in creeks that cross alkaline volcanics of the Olympio Formation.

Historical reports by Woodward (1891), Smith (1898), Blatchford (1927a,b), Finucane (1938a,b, 1939a,b), Jones (1938), Finucane & Sullivan (1939), Matheson & Teichert (1948), Matheson & Guppy (1949), Traves (1955), and Harms (1959) provide valuable information on the regional geology and early resource details of individual mines and goldfields in the East Kimberley. More recent reports by Gemuts & Smith (1968), Dow & Gemuts (1969), Gemuts (1971), de Havelland (1985, 1986), and Plumb (1990) describe the geological setting of the alluvial and hard-rock deposits. Warren (1994a,b, 1997) investigated gold mineralisation processes in the light of the revised stratigraphical and structural relationships determined during NGMA[1] mapping.

In addition to the gold deposits described above, other major styles of mineralisation documented in the Halls Creek Orogen (Plumb 1990, Hoatson 1993b, 1995,

[1] National Geoscience Mapping Accord.

Sanders 1999) include stratabound volcanogenic massive base-metal sulphides (Rugless & Vanderplank 1995, Orth 1997, Rea 1997, Sewell 1999), porphyry base metals (Witt & Sanders 1997), volcanogenic Nb and rare-earth elements (Chalmers 1990, Ramsden et al. 1993, Taylor et al. 1995a,b), magmatic Cr–platinum-group elements (PGEs), Ni–Cu–Co, and Fe–Ti–V in layered mafic–ultramafic intrusions (this *Bulletin*), diamondiferous pipes of lamproitic and kimberlitic affinities (Jaques et al. 1986, Atkinson et al. 1990), sediment-hosted uranium (Ruker 1961), pegmatite-hosted tin, niobium, and tantalum (Dow & Gemuts 1969), and psammite-hosted stratabound tungsten (Ririe 1989, Trudu & Ririe 1990). Apart from the world-class Mesoproterozoic Argyle diamond deposit to the north of this study area and some minor alluvial and hard-rock gold operations near Halls Creek, there have been no major deposits mined in recent years.

Figure 2.4 summarises the regional distribution of metallogenic corridors containing rock types believed to be prospective for various types of precious, base-metal, and rare-earth-element mineralisation in the western part of the Gordon Downs and Dixon Range 1:250 000 Sheet areas. The northeasterly trending corridors are broadly zoned towards the southeast as follows: Ni–Cu–Co and Ti–V → PGEs–Cr–Ni–Cu–Au → Ti–V → Cu–Pb–Zn → a mixed mineralised zone of Au and REE.

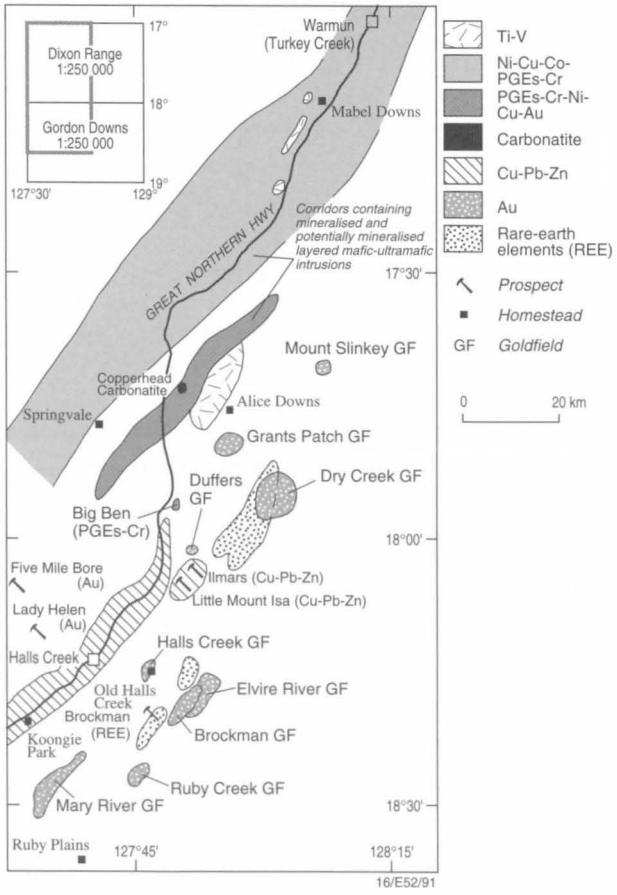


Figure 2.4. Distribution of prospective metallogenic corridors, goldfields, and prospects in the western part of the Gordon Downs and Dixon Range 1:250 000 Sheet areas, East Kimberley.

Investigations of the mafic–ultramafic intrusions

The East Kimberley mafic–ultramafic intrusions were first systematically investigated in 1962–64, during geological mapping of the Precambrian rocks of the Kimberley region (Dow & Gemuts 1969, Gemuts 1971) by the Bureau of Mineral Resources (now AGSO) and the GSWA[2]. Dow & Gemuts (1969) divided the intrusive mafic and ultramafic rocks into three distinct units: tightly folded narrow sills and dykes of dolerite and gabbro (their Woodward Dolerite), competent, broadly warped thick sills, comprising ultramafic rocks (their Alice Downs Ultrabasics), and mafic rocks (their McIntosh Gabbro). They suggested that the Alice Downs Ultrabasics and McIntosh Gabbro were emplaced as a continuous sill-like body, with the former representing a tectonically disrupted, more primitive lower part of the latter. However, subsequent investigations (Hamlyn 1980, Mathison & Hamlyn 1987) and geological mapping and geochronological and geochemical results from this study show that the Alice Downs Ultrabasics and McIntosh Gabbro are neither cogenetic nor coeval. The regional distribution of the intrusions was generally accurately portrayed on the first edition Dixon Range 1:250 000 Sheet, but in some areas that were photo-interpreted, rocks of the Tickalara Metamorphics were incorrectly shown as layered intrusive rocks (e.g. the Big Ben intrusion) and vice versa (southeast of the Nine Mile intrusion). In addition, Dow & Gemuts (1969) did not formally subdivide the Alice Downs Ultrabasics and McIntosh Gabbro units into mafic and ultramafic components or document the mineralisation associated with the intrusions.

Wallace & Hoatson (1990) and Sun et al. (1991) carried out trace-element geochemical and Sm–Nd isotopic studies on the layered intrusions at a regional scale. A number of detailed studies (Table 2.2) have focussed on the stratigraphy, geochemistry, structure, and mineralisation of individual intrusions. These include university theses on the Bow River (Blain 1967), Corkwood (Nevill 1974), Panton (Hamlyn 1977, Bourke 1990, Sproule, 1999), McIntosh (Hamlyn 1977, Sproule 1999), Sally Malay (Thornett 1986, Sproule 1999), and various (Gemuts 1965) intrusions. The geological and mineralisation features of many intrusions are also described in Hoatson & Glaser (1989) and in open-file company exploration reports summarised in Hoatson (1993b) and Sanders 1999.

The layered mafic–ultramafic intrusions in the East Kimberley have been explored for PGEs, Cr, Ni, Cu, Co, Ti, V, and Au since the early 1960s (Table 2.3). Although significant amounts of these commodities have been found in many of the intrusions, no economic deposits have been located to date. The Panton and Sally Malay intrusions are among the most intensively explored Proterozoic layered intrusions in Australia. There have been four major phases of exploration relating to the

[2] Geological Survey of Western Australia.

Table 2.2. Publications, theses, etc., relating to the East Kimberley layered mafic–ultramafic intrusions.

Reference	*Intrusion*	*Investigations*
Blain (1967)	Bow River	Petrology, mineralogy, mineralisation
Nevill (1974)	Corkwood	Structure, petrology, mineralogy, mineralisation
Wilkinson et al. (1975)	Salt Lick Creek	Stratigraphy, mineralogy
Hamlyn (1975, 1980)	Panton	Mineralogy, metamorphism, chromite chemistry
Hamlyn (1977)	Panton, McIntosh	Mineralogy, chromite chemistry
Hamlyn & Keays (1979)	Panton	Mineralogy, chromite chemistry
Halligan & Harris (1980)	Bow River	Stream-sediment, soil and rock geochemistry, mineralisation
Wilding (1980)	Corkwood	Soil and stream-sediment geochemistry, mineralisation
Thornett (1981, 1986)	Sally Malay	Structure, metamorphism, petrology
Mathison & Hamlyn (1987)	McIntosh	Stratigraphy, petrology, mineral chemistry
Bourke (1990)	Panton	Structure, geochemistry, mineralisation
Wallace & Hoatson (1990)	Several intrusions	Petrology, whole-rock geochemistry
Wallace et al. (1990)	Several intrusions	Petrology, whole-rock geochemistry
Barnes et al. (1991)	Several intrusions	Regional setting, mineralisation
Perring & Vogt (1991)	Panton	Stratigraphy, whole-rock geochemistry, mineralisation
Sun et al. (1991)	Several intrusions	Whole-rock and Sm-Nd isotope geochemistry
Blake & Hoatson (1993)	Several intrusions	Contact relationships, net-veining, co-mingling magma
Hoatson (1993a)	Big Ben	Stratigraphy, mineralisation
Hoatson & Tyler (1993)	Several intrusions	Regional setting, mineralisation
Frankcombe et al. (1994)	Sally Malay	Geophysics, exploration
Hoatson (1995)	Frog Hollow, Norton	Stratigraphy, mineralisation
Hoatson et al. (1995)	Several intrusions	Regional setting, mineralisation
Page et al. (1995)	Several intrusions	U-Pb zircon geochronology
Shedden & Barnes (1996)	Sally Malay	Exploration, stratigraphy, mineralisation
Trudu & Hoatson (1996)	Several intrusions	Geothermobarometry
Blake (1997)	Several intrusions	Regional setting, tectonics
Hoatson (1997)	Several intrusions	Regional setting, mineralisation
Hoatson et al. (1997)	Sally Malay	Geology, mineralisation
Sproule et al. (1997a)	Panton	Re-Os and Sm-Nd isotope geochemistry
Sproule et al. (1997b)	Panton, Sally Malay	Re-Os and Sm-Nd isotope geochemistry
Sproule et al. (1997c)	Sally Malay	Re-Os isotope geochemistry
Hoatson (1998a,b)	Several intrusions	Geology, mineralisation
Sproule (1999)	Panton, Sally Malay, McIntosh	Re-Os and Sm-Nd isotope geochemistry
Sproule et al. (1999)	Sally Malay	Re-Os isotope geochemistry mineralisation
Hoatson (in press)	Several intrusions	Mineralisation, exploration

intrusions in the East Kimberley during the last four decades. Interest was stimulated during:

- *the 1960s*, by the first systematic geological mapping of the region (mainly for Cr–PGEs, Fe–Ti–V, and Ni–Cu–Co);
- *the early 1970s (the 'nickel boom years')*, by the discovery of komatiite-hosted Ni–Cu deposits in the Yilgarn Craton, Western Australia (Ni–Cu–Co);
- *the mid to late 1980s*, by buoyant world PGE metal prices (Cr–PGEs); and
- *the mid to late 1990s*, by the NGMA geological mapping of the region and the discovery of world-class deposits overseas, such as Voisey's Bay in Canada (Ni–Cu–Co, Cr–PGEs).

Interest in the PGE–Cr potential of the intrusions was stimulated in the mid 1960s, when Dow & Gemuts (1967) reported PGE-bearing chromitites in the Panton intrusion during the first generation geological mapping of the Dixon Range 1:250 000 geological sheet area by BMR and GSWA. They noted anomalous amounts of Pt and Ni in primary chromitite bands and secondary chromite veins in the ultramafic sequences. The primary bands, which consist of alternating chromitite layers (2.5 cm thick) and altered ultramafic rocks, were reported to be up to 10 m thick and assaying 0.4 dwt/long ton (0.6 ppm) Pt and 0.15% Ni. The secondary chromite-rich

veins in magnesite were up to 100 m long and 0.7 m wide, and contained a maximum of 2.0 dwt/long ton (3.1 ppm) Pt and 0.2% Ni.

Intensive exploration of the Panton intrusion since 1967 has delineated a PGE-enriched chromitite layer directly below the ultramafic–gabbroic zone contact. An indicated and inferred resource of 2 Mt @ 6.02 ppm Pt+Pd+Au and 0.28% Ni has been defined from the main chromitite layer on the northwestern side of the intrusion (Perring & Vogt 1991). In Australia, only the Munni Munni intrusion in the west Pilbara Craton (Hoatson et al. 1992) has a larger primary resource of PGEs associated with a layered intrusion (Hoatson 1998a,b).

The discovery of PGE-enriched chromitite layers associated with ultramafic cumulates in the Panton intrusion had a profound influence on the direction of exploration in the East Kimberley. Mineral exploration companies focussed their exploration strategies on finding stratabound chromitite layers in the ultramafic zones. PGE-bearing chromitite layers were found in the Eastmans Bore, Lamboo, Mini, West McIntosh, South Melon Patch, and Melon Patch intrusions (Table 2.3), but all were subeconomic. For many years, exploration companies new to the East Kimberley often duplicated previous exploration programs, and other styles of magmatic or hydrothermal mineralisation at higher stratigraphic levels in the intrusions, or in the country rocks, were rarely evaluated or even considered. Open-file company reports at the Western Australian Department of Minerals and Energy indicate that most mineral exploration companies were searching for large tonnage stratabound mineralised layers similar to those in the Bushveld Complex of South Africa, such as the Merensky Reef and the UG-2 chromitite layer.

Pickands Mather[3] and Australian Anglo American[4] carried out some of the earliest regional exploration programs in the East Kimberley from the early 1960s to the mid 1970s. Stream-sediment geochemical and gossan search programs over large areas of the province led to the discovery of several sub-economic Ni–Cu–Co and PGE–Cr deposits associated with the mafic–ultramafic intrusions. One of the more significant discoveries was the Sally Malay deposit in 1974 by Australian Anglo American (see below). This deposit contains the largest Ni–Cu–Co resource (3.85 Mt @ 1.79% Ni, 0.73% Cu, and 0.10% Co: Shedden & Barnes 1996) in the East Kimberley, and highlights the potential of the intrusions to host sulphide and/or oxide (chromite, titaniferous magnetite) associations. Similar, but smaller sulphide deposits were found in other mafic intrusions, such as McKenzie Spring, Keller Creek, Dave Hill, Corkwood, and Bow River.

Another major influence on exploration directions in the East Kimberley was the discovery of Ni–Cu deposits in the Eastern Goldfields Province of the Yilgarn Craton during the 'nickel boom' of the early 1970s. During this period, mineral exploration companies in the East Kimberley were exploring for Ni–Cu sulphide deposits near the basal contacts of intrusions. Gossan search and stream-sediment geochemical sampling, together with geophysical surveys, were commonly used. Frankcombe et al. (1994) showed in their geophysical study of the Sally Malay deposit that electromagnetic, ground magnetic, and induced polarisation surveys are the most useful methods for locating and mapping basal concentrations of Ni–Cu sulphides.

Exploration for precious metals intensified again in the mid to late 1980s, when PGE metal prices increased, but no major new deposits were found. Exploration interest waned until the mid 1990s, when the regional setting and economic potential of the intrusions were reinterpreted during the second generation geological mapping of the East Kimberley by AGSO and GSWA. These new investigations resulted in the identification of several types of layered intrusions of different ages with the potential to host various styles of base and precious metal mineralisation at different stratigraphic levels (Hoatson 1993a, Hoatson & Tyler 1993, Hoatson et al. 1995, Page et al. 1995, Trudu & Hoatson 1996). The recognition of a possible mineralised feeder conduit in the Sally Malay intrusion (Hoatson et al. 1997) and the similarity of the geological setting of this intrusion to the world-class Voisey's Bay Ni–Cu–Co sulphide deposit in Canada also increased the economic potential and exploration interest of the East Kimberley intrusions. There has been a recent trend for companies (e.g. BHP Minerals) to quickly evaluate large areas of prospective ground for sulphide mineralisation by airborne electromagnetic surveys.

Prior to 1992, very few mafic–ultramafic intrusions were being explored; however, with new ideas and products being generated by the NGMA program, all significant occurrences of mafic–ultramafic rocks are now covered by exploration title. The East Kimberley is now recognised as one of the most prospective and actively explored provinces in Australia.

The following section summaries the different phases of company exploration and the significant results obtained for most of the intrusions investigated in this study. Further details are in Marston (1979, 1984), Hoatson (1993b), Sanders (1999), Chapter 5 of this *Bulletin*, and in unpublished open-file reports in the Western Australian Department of Minerals and Energy, Perth. The number in brackets after the name of the intrusion refers to the number of the intrusion in Figure 5.1. Several other mineralised East Kimberley intrusions (Alice Downs, Bow River, Bulldust Flat, Cattle Creek, Eastmans Bore, Eileen Bore, Emull, Lamboo, Ord Crossing, Osmond Valley, Salt Lick Creek, Turkey Creek, White Rock Well West, Wills Creek) that were not investigated in this study are also briefly described below. Further details on mineral deposits associated with these intrusions can be found in Sanders (1999).

Alice Downs (not investigated in this study; AMG ~928473 on McINTOSH[5]). The Alice Downs Ni–Cu

[3] Pickands Mather & Company International.

[4] Australian Anglo American Limited.

[5] 1:100 000 sheet names throughout this *Bulletin* are in capital letters to avoid confusion with identical place names and to distinguish them from 1:250 000 sheet names.

Table 2.3. Significant exploration events relating to the East Kimberley layered mafic–ultramafic intrusions.

Year	*Intrusion*	*Event*	*Discovery method*	*Company/ Organisation*	*Reference*
1965	Bow River	Discovery of basal Cu–Ni sulphides	Stream sediment geochemistry	Pickands Mather & Co International	Bell (1966), Halligan & Harris (1980)
1965	Springvale	Discovery of gossans	Mapping, rock sampling	Pickands Mather & Co International	Pickands Mather & Co (1965–1968c)
1967	Panton	Discovery of PGE-bearing chromitites	Mapping, rock sampling	BMR-GSWA	Dow & Gemuts (1967)
1969[1]	Eastmans Bore	Discovery of PGE-bearing chromitites	Mapping, rock sampling	Kennecott Australia Pty. Ltd.	Barnes et al. (1991)
1969[1]	West Robin Soak	Discovery of Ni–Cu gossans	Mapping, rock sampling	Westmex Ltd.	Mosig & Mills (1971)
1970[1]	McKenzie Spring	Investigation of Ni–Cu gossans	Mapping, gossan search, rock sampling	Stratin Minerals Pty. Ltd. and Dampier Mining Co. Ltd	Dampier Mining Co. Ltd. (1971–1973)
1972	Billymac Yard	Discovery of Ni–Cu gossans	Mapping, rock sampling	Stratin Minerals Pty. Ltd.	Lewis (1972)
1972	Corkwood	Discovery of Ni–Cu gossans	Mapping, gossan search	Australian Anglo American Ltd.	Nevill (1974), Wilding (1980)
1972	Melon Patch	Reporting of Cu–Ni sulphides and gossans	Mapping, gossan search	Stratin Minerals Pty. Ltd.	Stratin Minerals Pty. Ltd. (1971–1973)
1973	Keller Creek	Discovery of Ni–Cu gossans	Mapping, gossan search	Broken Hill Pty Co. Ltd.	Anon. (1975)
1974	Sally Malay	Discovery of gossan and basal Ni–Cu sulphides	Stream sediment geochemistry, gossan search	Australian Anglo American Ltd.	Shedden & Barnes (1996)
1976	Lamboo	Investigation of PGE-bearing chromitites	Mapping, rock sampling	Kennecott Australia Pty. Ltd. and Broken Hill Pty. Co. Ltd.	Barnes et al. (1991)
1977	West McIntosh	Discovery of PGE-bearing chromitites	Mapping, stream sediment and soil geochemistry	Australian Anglo American Ltd.	Codner (1979)
1977	Mini	Discovery of PGE-bearing chromitites	Mapping, stream sediment and soil geochemistry	Australian Anglo American Ltd.	Codner (1979)
1981	Springvale	Discovery of chromite-bearing rocks	Mapping, rock sampling, soil sampling	Inco Australia Ltd.	Geopeko Ltd. (1986–1989)
1986	West Robin Soak	Identification of Ni–Cu gossans and chromitites	Mapping, rock sampling	Argold Holdings Pty. Ltd. and Hadowill Pty. Ltd.	Kenway (1988)
1989	Wilagee	Discovery of PGE-bearing chromitite	Mapping, rock sampling	Geopeko Ltd.	Geopeko Ltd. (1986–1990)
1993	Big Ben	Recognition of fault-displaced part of the Panton intrusion and discovery of PGE-bearing chromitites	Regional mapping, rock sampling	AGSO	Hoatson (1993a)
1994	Norton	Discovery of Ni–Cu gossans	Regional mapping, rock sampling	AGSO	Hoatson (1995)
1994	Frog Hollow	Identification of Fe–Ti–V oxide lenses	Regional mapping, rock sampling	AGSO	Hoatson (1995)

[1] approximate year of discovery.

prospect (Sanders 1999) is located just east of the Alice Downs Fault about 6 km north-northeast of Fourteen Mile Well. Investigations by Western Mining Corporation (WMC) Ltd from 1974 to 1979 and by Delta Gold in 1991 involved soil and rock chip geochemistry, induced polarisation, transient electromagnetics, ground magnetics, and percussion (24 holes) and diamond drilling (2 holes). Sanders (1999) notes that disseminated and massive Ni–Cu sulphides are hosted by irregular elongate (up to 240 m wide and 700 m long) pyroxenite and peridotite intrusives, and minor Cu mineralisation occurs in more continuous metagabbro that envelopes the ultramafic rocks. The intrusions are partially concordant with the regional foliation in banded felsic and mafic gneiss, pelitic schist, and calc-silicate country rocks of the Tickalara Metamorphics. Six prospects (Cabernet, Malbec, Shiraz, Palamino, Grenache, and Mataro) have been identified in the ultramafic intrusions. Rock chip sampling has defined values up to 1.95% Ni, 1.55% Cu, 61 ppb Au, and 46 ppb Pt at Cabernet and Shiraz, and 3.25% Ni and 2.3% Cu at Malbec. Percussion drilling at Cabernet by WMC Ltd intersected massive sulphides that returned 4 m @ 2.38% Ni and 1.3% Cu within a 16 m-wide zone that averaged 1.4% Ni and 0.94% Cu. Follow-up drilling and transient electromagnetics failed to locate further significant mineralisation.

Armanda (46). In the late 1960s, while carrying out regional stream-sediment geochemical and mapping programs for Ni–Cu in gabbroic sills and Cu–Pb–Zn in metamorphosed carbonate rocks, Pickands Mather (1965–68a) defined an elliptical sill, 3 km long, of uralitised gabbro, bounded by metasediments, metavolcanics and porphyry. No pronounced geochemical anomalies were found in the intrusion, the maximum assays being 150 ppm Cu, 100 ppm Ni, and 50 ppm Co. Black limestone and calcareous gossans, interpreted to be part of the Tickalara Metamorphics near the intrusion, were found to contain up to 200 ppm Pb, 125 ppm Cu, and 150 ppm Zn, and anomalous Ag.

Big Ben (43). PGE-bearing chromitite layers were discovered in 1993 during the NGMA mapping of McINTOSH (Hoatson 1993a). The stratigraphy, mineralisation, and precious metal ratios of the chromitites indicate that the Big Ben intrusion is possibly a fault-displaced part of the mineralised Panton intrusion. Reconstruction of the pre-faulting disposition of the country rocks in the vicinity of the intrusions is consistent with the Big Ben body being displaced 15 km south along the Panton Fault. The Big Ben intrusion was incorrectly shown on the first edition Dixon Range 1:250 000 map as metasediments and amphibolite of the Tickalara Metamorphics. Preliminary investigations in 1994 by Northern Exploration NL showed that two major chromitite layers contained 20 and 26% Cr_2O_3, 540 and 640 ppm Ni, 580 and 760 ppb Pd, 450 and 520 ppb Pt, and 7 and 15 ppb Au.

Billymac Yard (27). See Sandy Creek.

Black Hills Yard (29). Pickands Mather, in 1968, carried out stream-sediment geochemical surveys over a group of small troctolite bodies surrounded by various granite plutons of the Bow River Batholith. High Ni values were found in the troctolite, but no anomalous Cu or sulphide mineralisation was found.

Bow River (not investigated in this study; AMG ~290345 on BOW RIVER). The poorly exposed Bow River mafic intrusion, 4 km south-southwest of the junction of Bow River and Turkey Creek, covers an area of about 2.5 by 6.5 km. The northeast-trending body dips steeply north and is intruded by contaminated granite in the north (Marston 1979). It has been metamorphosed to granulite facies and has been assigned to the Tickalara Metamorphics by Sheppard et al. (1999). The dominant rock type was originally norite, with minor leucogabbro and troctolite. The mafic granulites have preserved primary igneous layering and superimposed metamorphic foliation and granuloblastic textures. Garnet-bearing migmatitic and pelitic gneiss of the Tickalara Metamorphics country rocks crop out nearby. The Bow River intrusion appears to show similar textural and mineralisation features to the Corkwood (10) and Keller Creek (9) intrusions and may be of similar age to the granulite facies Norton metagabbro intrusion (6), which forms part of the Tickalara Metamorphics on TURKEY CREEK. However, if the intrusion was emplaced after the metamorphic peak and is of sub-granulite facies, it may be similar to the highly prospective group V intrusions, such as the Sally Malay intrusion (12). The Bow River Cu–Ni prospect was discovered by Pickands Mather in 1965, after following up weak Cu (100 ppm) and Ni (60 ppm) anomalies in stream sediments. The mineralised part of the intrusion is roughly lenticular, measuring some 300 m by 900 m. Scattered pods of malachite and chrysocolla-stained limonite gossan contain up to 28% Cu (Bell 1966). The gossans were evaluated by 16 drillholes, trenching, and induced polarisation surveys. All drillholes intersected primary and remobilised sulphides, the average grade being 0.20% Cu and 0.15% Ni over 64 m. Local Ni enrichment of up to 1.5% occurs in narrow shear zones less than 1 m wide. Coarse-grained pyrrhotite, subordinate chalcopyrite, and minor pentlandite are primary sulphides that form thin massive bands and disseminated grains in mafic granulites. Remobilised chalcopyrite and pyrrhotite veins and stringers occur on the margins of younger dolerite and granitic pegmatite dykes and in small joints (Halligan & Harris 1980). No concentration of massive sulphides was found along the margins of the intrusion. In the late 1970s and early 1980s, Australian Anglo American undertook aeromagnetic, ground magnetic, and airborne electromagnetic surveys, soil and rock sampling for geochemistry, and diamond drilling over the prospect (Lemcke 1981). The drilling showed that the contact of the mineralised norite with the surrounding rocks is complex, there is no concentration of sulphides at the southern contact, and Cu and Ni contents in the low-grade disseminated sulphides are relatively constant, whereas those of the richer disseminated and massive zones are extremely variable—often having antipathetic relationships (Sanders 1999). It was concluded that the Bow River intrusion hosts low-grade primary disseminated sulphide with metamorphic and tectonic effects causing local remobilisation of the sulphides into small, enriched, disseminated and massive pockets. The Bow

River intrusion and nearby Salt Lick Creek intrusion still appear to have potential for segregations of Ni–Cu–Co sulphide mineralisation in depressions along the basal contact and in possible feeder conduits, and also for remobilised mineralisation. Detailed drilling and geophysical programs would be required to identify these favourable environments, particularly in areas of poor exposure.

Bulldust Flat (not investigated in this study; AMG ~039720 on TURKEY CREEK). Australian Anglo American from 1971 to 1976 carried out geological mapping, soil and stream sediment sampling, electromagnetic surveys, costeaning, and diamond drilling (2 holes) at the Bulldust Flat prospect (Sanders 1999), 9 km northeast of Dougalls Bore. Broad, irregular Ni anomalies from the stream-sediment program indicated minor disseminated Cu–Ni mineralisation in a poorly exposed pod-like granulite (actually norite) intrusion. The 120 m-wide body, which strikes north and dips steeply (60 to 70°) west, intrudes a north-trending Tickalara Metamorphics sequence of amphibolite, metasediments, and carbonate lenses. The metamorphosed intrusion appears to be differentiated with leuco and mafic variants being reported. Ferruginous gossans stained with malachite, chrysocolla, and garnierite contained up to 1.2% Cu, 0.78% Ni, and 0.02% Co. Broad zones of low-grade mineralisation were defined in costeans (17 m @ 0.51% Cu, 0.26% Ni) and diamond drilling (4 m @ 0.17% Cu, 0.33% Ni). Australian Anglo American concluded that the mineralisation was due to surface enrichment.

Cattle Creek (not investigated in this study; AMG ~028681 on TURKEY CREEK). Australian Anglo American from 1976 to 1977 undertook mapping, soil geochemistry, and rock-chip sampling at the Cattle Creek Cu–Ni prospect (Sanders 1999), about 3.5 km south of Bulldust Flat. Malachite-stained gossans occur in a poorly exposed 60 m-wide by 300 m-long mafic granulite body (actually norite) that intrudes metasediments of the Tickalara Metamorphics. Gossans near the contact of the intrusion with amphibolitic metasediments returned 1.3% Ni, 0.36% Cu, and 470 ppm Co.

Corkwood (10). In 1972, Australian Anglo American discovered discontinuous linear malachite-bearing gossans containing up to 1.3% Ni and 0.3% Cu in zones 220 m long and 5 m wide (Nevill 1974, Wilding 1980). A mise-à-la-masse induced polarisation survey successfully delineated sulphide mineralisation to the north of the gossans. In 1973, 10 diamond drillholes encountered narrow massive bands, veins, fracture fillings, and disseminations of pyrrhotite, pyrite, pentlandite/violarite, and chalcopyrite in recrystallised metagabbro enveloped by amphibolite. The sulphide body plunges 10^{o} towards 35^{o} and individual sulphide bands are subparallel to the north-northeast-trending foliation in the amphibolites. Most sulphides are restricted to areas of non-foliated metagabbro, indicating possible metamorphic remobilisation of sulphides towards the least recrystallised, low-stress areas. The mineralisation ranged from 0.3 to 2.6% Ni, 0.1 to 0.5% Cu, and 0.02 to 0.1% Co over true widths of 1.5 to 4 m, with the highest grades occurring over the narrowest widths (Marston 1984). Electromagnetic surveys showed that some of the best electrical conductors were graphitic shales and further work was abandoned (Briggs 1976). During the early 1990s, anomalous Au (13 ppb) and Pt (480 ppb) concentrations were defined in a stream sediment program by the Poseidon Group Trading Ltd (Barnes 1994).

Eastmans Bore (also called Louisa Downs; not investigated in this study; AMG ~475295 on RAMSAY). This PGE–Cr prospect, 4 km northeast of Eastmans Bore and 11 km west of Louisa Downs homestead, has experienced several phases of exploration by various mineral exploration companies. The mafic–ultramafic intrusion is a steeply dipping folded sill, 950 m thick, that is exposed for 6 km along its northeast strike and extends under shallow cover for a further 2 km. Helix Resources NL documented three principal zones comprising a basal ultramafic zone of dunite, peridotite, orthopyroxenite, and several thin PGE-bearing chromitites, overlain by a mafic–ultramafic zone of anorthosite and norite containing lenses of chromite-bearing ultramafics, and an upper mafic zone containing a thick sequence of gabbro. Country rocks include felsic volcanics and metasediments assigned to the 1843 Ma Koongie Park Formation. The Eastman Granite truncates the western end of the layered intrusion. The intrusion is overturned and dips steeply to the south (Barnes et al. 1991). East-northeast and northwest-trending faults have displaced the chromitites by up to 1.2 km and divided the intrusion into separate blocks. The chromitite layers were discovered by Kennecott Explorations Australia Ltd in the late 1960s during a regional base metal program, but no further work was undertaken until the mid 1970s, when Union Corporation Pty Ltd conducted mapping, soil and rock geochemistry, and magnetic surveys. No drilling was carried out, but Pt and Pd abundances of up to 7.5 ppm were found in chromitites 1 m thick. From the 1970s to the 1980s, the intrusion was investigated by several mineral exploration companies, including Strategic Minerals Corporation NL, Valiant Consolidated Ltd, International Nickel Company of Canada, and BHP[6]. Inco Australia Pty Ltd completed four shallow diamond drillholes from 1980 to 1982. Three holes failed to intersect the massive chromitite layers, which were consequently believed to be sheared out, whereas the fourth hole intersected multiple narrow chromitites with low PGE abundances. In 1983, Freeport of Australia Incorporated and Inco Australia Pty Ltd drilled the chromitite layers with three diamond holes, 100 m either side of the Inco holes. These holes also failed to intersect the chromitites. National Strategic NL and Helix Resources NL reassessed the intrusion from the mid 1980s to the early 1990s. In addition to the PGE–chromitite association, these companies also investigated the PGE potential of anorthositic and gabbroic sequences and structurally controlled mineralisation. Highest PGE concentrations were found within chromitite layers in the ultramafic zone. The chromitites generally form 5 to 30 cm-thick (maximum 1 m) layers and lenses that rapidly thicken and thin over distances of

[6] Broken Hill Proprietary Limited.

tens of metres along strike. Typical PGE grades are 1–6 ppm, at a Pt/Pd ratio of about 1:1 (Barnes et al. 1991). Helix Resources NL indicated that the chromitites offer the greatest potential, but their limited width and extent down-grades the commercial viability of the deposit.

Egg (21). In 1968, Pickands Mather carried out a stream-sediment geochemical survey over this small plug of troctolite and peridotite. High Ni and Co abundances were found in streams draining both rock types, but no sulphide mineralisation was identified.

Eileen Bore (not investigated in this study; AMG ~894400 on McINTOSH). In 1977, Australian Anglo American discovered the Eileen Bore Cu–Ni–PGEs–Au prospect (Sanders 1999) on a large alluvium plain just east of the Alice Downs Fault, 4.2 km north-northeast of Alice Downs Homestead. The mineralisation was discovered during a regional input electromagnetic survey, and was followed up by stream sediment and soil sampling, mapping, percussion and diamond drilling (10 holes), and airborne electromagnetics and magnetics. Residual soils up to 3 m thick cover the metamorphosed intrusion with limited outcrop restricted to nearby steeply dipping folded metacarbonate and quartzite. Semi-concordant bodies of sulphide-bearing felsic, mafic and ultramafic rocks intrude metasedimentary and metamafic rocks of the Tickalara Metamorphics. Hornblende mafic variants, pyroxenite, and serpentinised peridotite are the major rocks. Airborne magnetic data indicate that the intrusion is a south-closing synform with a north-northeasterly trending axial plane. Mineralisation is hosted by a 70 m-wide sulphide-rich hornblendite unit, with best drillhole intersections of 10 m @ 1.35% Cu and 0.41% Ni and 38 m @ 0.91% Cu and 0.34% Ni. Drilling by Dry Creek Mining in 1986–87 obtained 35 m @ 0.78% Cu, 0.36% Ni, 0.17 ppm Au, 0.15 ppm Pt, and 0.46 ppm Pd from 15 m depth. Main sulphide zone dips moderately (30 to 50°) to the east. Mineralisation consists of primary disseminated (up to 15%) chalcopyrite, pyrrhotite, and pentlandite, and supergene pyrite, violarite, and marcasite.

Emull (not investigated in this study; AMG ~204617 on ANGELO; see Chapter 14).

Faulted (1). In 1968, Pickands Mather carried out regional mapping and geochemical rock sampling for Ni–Cu mineralisation.

Fletcher Creek (15). In the late 1960s, Pickands Mather (1965–69) carried out regional stream-sediment geochemical and mapping programs for Ni–Cu in gabbroic sills and Cu–Pb–Zn in metamorphosed carbonate rocks. They defined a north–south-trending gabbroic sill abutting a zone of calc-silicate marble and interbedded quartz–biotite–garnet gneiss. A steeply dipping sequence of peridotite, troctolite, olivine gabbro, and leucogabbro was identified near Tickalara Bore. No pronounced anomalies were defined by stream-sediment geochemistry, maximum assays being 60 ppm Cu, 160 ppm Ni, 90 ppm Co, and 90 ppm Zn. In another geochemical program, a stream-sediment sample 3 km east of Tickalara Bore assayed 600 ppm Ni. A further three adjacent samples, each with 160 ppm Ni, defined a zone of outcropping troctolite, probably belonging to a southwestern extension of the Fletcher Creek intrusion.

Foal Creek (8). Pickands Mather in 1968 carried out a regional mapping and rock sampling program for Ni–Cu mineralisation.

Frog Hollow (7). In 1994 ilmenite- and titaniferous magnetite-bearing lenses were discovered in a fractionated gabbro of the Frog Hollow intrusion during the NGMA mapping of TURKEY CREEK (Hoatson 1995). The intrusion occurs in the Violet Valley Aboriginal Reserve. Ferrogabbroic rocks in the upper southwestern part of the intrusion contain some of the thickest lenses of Fe–Ti oxides known in the Kimberleys, with the largest lens about 20 m wide by 30 m long. This oxide lens is characterised by high TiO_2 (39.4%), total Fe as Fe_2O_3 (52.5%), V (0.23%), and Cr (0.08%). Another oxide lens, lower down in the gabbroic stratigraphy, contains less TiO_2 (22.1%), but higher contents of total Fe as Fe_2O_3 (60.6%), V (0.99%) and Cr (0.93%). Cyprus Minerals and Stockdale Holdings held title over the area from 1980 to 1983 for base metals and diamond exploration, respectively, and this area was also covered by Poseidon Ltd's Sally Malay tenements in the early 1990s (Hughes 1996). The prospect was evaluated in the late 1990s by Gindalbie Gold NL.

Greenvale Fault (11). In 1968, Pickands Mather carried out regional mapping and geochemical rock sampling for Ni–Cu mineralisation.

Keller Creek (9). Several companies since the early 1970s have used geological mapping, rock and soil sampling, ground magnetics, costeaning, and diamond drilling to explore for Ni–Cu sulphide mineralisation. BHP from 1973 to 1975, defined a strongly magnetic, 100 m-long, low-grade sulphide lens of disseminated pyrrhotite, chalcopyrite, and pentlandite near the base of a gabbroic lens within an east-west trending sequence of paramigmatites and mafic granulites of the Tickalara Metamorphics. Similar mineralisation also occurs in a quartz monzonite stock which has intruded the gabbroic rocks and metasedimentary country rocks (Anon. 1975). The best diamond drillhole intersection (7.8 m @ 1.0% Ni and 0.26% Cu) is in the felsic stock (Marston 1984). BHP carried out further exploration aimed at extending the known mineralisation; however, they concluded that the sulphides represent a lens of limited size. Australian Anglo American acquired the prospect in 1976 and continued exploration to 1981 (Gaunt 1977). Egerton Gold NL took over the prospect in 1994 as part of a larger exploration tenement, but no results are available (Hughes 1996). Gindalbie Gold NL indicated in 1996 that only 300 m of a total 1400 m of prospective footwall had been tested by drilling. Previous explorers had defined massive sulphides over narrow widths in 6 of 14 reconnaissance drillholes. Assays of 246 samples from previously unsampled stringer sulphide zones in diamond drill core defined an intersection of 1 m @ 0.2% Ni, 0.02% Cu, 0.02% Co, and 0.2 ppm Pt. Samples of the Keller Creek gossan yielded maximum values of 0.25% Ni, 0.52% Cu, 0.30% Co, and 20 ppb Au (Gindalbie Gold NL 1997). In late 1998, Gindalbie Gold NL, in a joint venture with Egerton Gold NL, planned to

undertake follow-up ground geophysical and geochemical sampling of four targets identified in airborne geophysical surveys.

Lamboo (also called Loadstone Hill; not investigated in this study; AMG ~235575 on ANGELO). The Lamboo mafic–ultramafic intrusion, 2 km west of Lamboo homestead, is an oval body about 6 km long and 3 km wide, comprising a lower, 1500 m thick, ultramafic series of serpentinised peridotite and an upper, 1000+ m thick, mafic series of massive anorthosite, leucogabbro gabbro, and magnetite-bearing granophyre (Barnes et al. 1991). The granophyre consists of a monotonous quartz diorite to adamellite sequence that may be a separate intrusive phase. The mafic–ultramafic rocks (renamed the Lamboo Ultramafics) are interpreted by Griffin et al. (1998) to intrude low to medium-grade metasediments and metavolcanics of the ~1843 Ma Koongie Park Formation. The intrusion is tightly folded into an S-shaped outcrop pattern, and most contacts with the country rocks are sheared. The folding occurred prior to the mafic–ultramafic body being intruded at its northeastern end by felsic rocks of the ~1827 Ma Loadstone Monzogranite (Griffin et al. 1998). The peridotites are often covered by silcrete, although chromitite layers in these recessive ultramafic rocks generally have positive relief. Primary igneous layering on the southern margin of the intrusion dips 60° towards the south (Gemuts 1971). Griffin & Tyler (1994) initially thought the intrusion formed a north-northeasterly plunging syncline; however, Griffin et al. (1998) reinterpreted the structure to be a south-southwesterly plunging anticline with steeply dipping limbs. The poorly exposed eastern limb can be traced as a magnetic feature as far south as the Mary River. Despite its apparent younger age (between 1827 Ma and 1843 Ma), the Lamboo intrusion contains similar rock types and mineralisation to the 1856 Ma Panton intrusion further north. Chromitites are best exposed in the central and western parts of the Lamboo intrusion, where they form two 20–30 m thick zones separated by an 80 m interval of serpentinised peridotite in the upper part of the ultramafic series (Griffin et al 1998). Both zones contain about 6–7 chromitite layers, ranging in thickness from 0.2 to 1.5 m. Local thickening is due to folding and faulting. The chromitites are sometimes weakly to strongly magnetic due to the chromite grains (0.1–0.5 mm) in the serpentine matrix having oxidation rims of iron-rich phases, such as magnetite and hematite. Since the early 1970s, the intrusion has been explored by many companies for Cr, PGEs, chrysotile, and Au. The first investigation of the chromitites by Union Corporation Pty Ltd in 1974–75 reported PGE concentrations of 2.5 ppm. In 1976, Kennecott Explorations Australia Ltd and BHP investigated the Cr and chrysotile potential of the western and central parts of the intrusion. Mapping, diamond drilling (2 holes) and trenching (27 costeans) indicated a subeconomic resource of about 1.5 Mt of chromite within 30 m of the surface and along a 13 km strike length. The chromitites have Cr_2O_3 contents below chemical grade ore (40–46% Cr_2O_3) and FeO contents too high for refractory ore. Gencor Pty Ltd and Union Corporation Pty Ltd between 1981 and 1984 assessed the Cr potential of the eastern limb and the PGE potential of the upper mafic units. In the late 1980s, West Coast Holdings Ltd and Hunter Resources Ltd used soil sampling to define broad zones of low-grade PGE mineralisation associated with narrow (<15 cm) laterally discontinuous chromitite layers in the upper 300 m of the ultramafic series. Typical grades of about 500 ppb combined Pt and Pd over 40 m, and maximum grades of 2.5 ppm over 0.5–2 m intervals were indicated (Barnes et al. 1991). The higher grade intervals extend laterally for less than 400 m. The PGE mineralisation generally corresponds to the interval containing the chromitite layers, but there is no direct correlation between abundance of chromite and PGEs. The mineralisation consists of disseminated to massive chromite and traces of chalcopyrite, pyrrhotite, pyrite, and pentlandite. Extensive drilling failed to find a significant PGE resource (Barnes et al. 1991). The general coincidence of chromitites with elevated PGEs, Ni, and Cu abundances in peridotites provides a useful exploration tool. Hunter Resources Ltd also reported shear-related gold mineralisation in metasedimentary country rocks and other weathered ferruginous rocks on the northern side of the intrusion. The quartz-vein mineralisation occurs over 1.5 km along strike, and local high grades of 17 m @ 8.6 ppm Au were defined in trenches. It is not known if this mineralisation has any genetic or temporal relationship with the Lamboo intrusion.

Mabel Downs West (2), Mabel Downs Homestead (3), and Mabel Downs Southwest (4). In 1968 Pickands Mather carried out regional mapping and geochemical rock sampling for Ni–Cu mineralisation.

McIntosh (34). Pickands Mather (1965–71) explored the intrusion and surrounding rocks for Ni–Cu mineralisation. The McIntosh A prospect was discovered in 1971 during investigation of a low-order regional stream geochemical anomaly (60 ppm Cu, 60 ppm Ni). The prospect consists of a sporadically mineralised gabbro horizon in an area of low relief and alluvium about 5 km northeast of the centre of the intrusion (precise location is unknown; could occur in the Wild Dog Creek intrusion that is faulted against the eastern margin of the McIntosh intrusion). The gabbro is cut by numerous shear zones, narrow biotite amphibolite dykes, and quartz veins. Primary igneous layering trends northeast. The mineralisation consists of remobilised copper as malachite and chalcopyrite in shears and joints, and as minor disseminations in gabbro over an area of 170 by 200 m. Soil sampling showed a >500 ppm Cu (maximum values of 2800 ppm Cu and 60 ppm Ni) anomaly over a 60 m by 150 m area near the contact of the gabbro with gneiss. Pickands Mather concluded that the mineralisation is of low-grade magmatic origin and was remobilised and upgraded into fault zones. Australian Anglo American, in 1977, tested coincident electromagnetic/magnetic and soil/stream-sediment geochemical anomalies for Ni–Cu mineralisation. Most anomalies were attributed to graphitic metasediments in the nearby Tickalara Metamorphics. Bands of ultramafic rock with associated geochemical anomalies and Ni–Cu gossans were identified in the Queensland Creek area, but were too small to be of economic interest. Mathison & Hamlyn (1987) reported disseminated sulphide blebs throughout the McIntosh intrusion, indicating that the

magma forming the intrusion was sulphur saturated throughout and, therefore, had low potential for PGEs.

McKenzie Spring (20). Stratin Minerals Pty Ltd and Dampier Mining Company Ltd (1971–1973) used mapping, induced polarisation, magnetic, and geochemical methods during the initial investigations of the intrusion in the early 1970s. More than 25 gossans (up to 11% Cu and 1.25% Ni), some with a strike length of more than 200 m, were defined at different stratigraphic levels in the intrusion. BHP drilled six percussion holes into the main gossan in 1973 and intersected mafic–ultramafic rocks containing anomalous Ni (up to 2600 ppm) and Cu (1400 ppm). Australian Anglo American continued exploration from 1976 to 1980 with mapping, stream-sediment geochemistry, and airborne electromagnetic and magnetic surveys. Peko-Wallsend Operations Ltd began investigations, but budget cuts halted exploration at a preliminary stage. Noranda Australia Ltd carried out mapping, drainage and rock chip sampling for PGEs from 1986 to 1987. Results of the stream-sediment geochemical program were negative. Delta Gold NL commenced a phase of exploration in 1991 (Hughes 1996).

Melon Patch (26). In the early 1970s, Stratin Minerals Pty Ltd (1971–1973) undertook mapping, ground magnetics, and percussion drilling and reported four areas of extensive Cu–Ni mineralisation (up to 22.5% Cu and 2.35% Ni) in gossans associated with ultramafics, 4.5 to 5.5 km east of Melon Patch Well. The gossans typically consist of massive limonite with abundant malachite and azurite staining and rare chalcopyrite. They occur at the contact of peridotite and gneissic granite or in fractures over an exposed area of 12 m by 30 m. Costeaning and drilling showed the gossans were of narrow width and the intersection of gneissic granite at shallow depths indicated limited depth potential. In 1977, Australian Anglo American tested coincident electromagnetic/magnetic and soil/stream-sediment geochemical anomalies for Ni–Cu mineralisation. Results were disappointing, and most geophysical anomalies were attributed to graphitic metasediments in the Tickalara Metamorphics. In 1989, Peko-Wallsend Operations Ltd carried out detailed mapping of chromitite layers in olivine-rich ultramafic units and stream-sediment sampling throughout the region.

Mini (33: also called Mini M). In the 1970s, Australian Anglo American carried out mapping, ground magnetic, electromagnetic, and stream-sediment and soil geochemical programs for base-metal sulphides and chromitites in this small folded ultramafic sill. Initial interest in the intrusion was based on anomalous Ni and Cu anomalies defined in a regional stream sediment program. Chromitite layers were found at four different stratigraphic levels and malachite-stained gossans occur in shears at the northwestern end of the body. The chromitites are up to 10 cm thick, about 20 m along strike, and contain a maximum of 5 ppm Pd, 2 ppm Pt, 1100 ppm Ni, and 300 ppm Cu (Codner 1979). In 1989, Peko-Wallsend Operations Ltd undertook further detailed mapping, sampling, and drilling of the chromitites.

Norton (6). Cyprus Minerals and Stockdale Holdings held title over the area that includes the Norton intrusion from 1980 to 1983 as part of their respective regional surveys for base metals and diamonds, and the area was also covered by Poseidon Ltd's Sally Malay tenements in the early 1990s (Hughes 1996). In 1994, during the NGMA mapping of TURKEY CREEK, Hoatson (1995) discovered limonitic gossans that extend for at least 4 km along the basal contact of a homogeneous mafic granulite body representing a metamorphosed gabbroic intrusion. The gossans occur in the Violet Valley Aboriginal Reserve and have not been evaluated. Gindalbie Gold NL in 1996 and 1997 carried out mapping, rock geochemistry, and a stream-sediment orientation survey of the intrusion. Their mapping showed that the basal gossan was a cluster of subparallel gossanous zones extending for 6.5 km along the entire strike extent of the intrusion. Maximum values from 126 rock samples analyses were 980 ppm Ni, 580 ppm Cu, and 100 ppm Co. Stream-sediment samples contained coarse detrital platinum shedding from an identified source within the intrusion. Maximum values reported were 1.5 ppm Pt (Gindalbie Gold NL 1997).

Ord Crossing—Grid A Ni–Cu (not investigated in this study; AMG ~877685 on MOUNT REMARKABLE) and **Ord Crossing—Grid A North Ti–V** (not investigated in this study; AMG ~892700 on MOUNT REMARKABLE). Pickands Mather discovered in 1969 the Ord Crossing—Grid A Ni–Cu prospect, and 2 km further northeast, the Ord Crossing—Grid A North Ti–V prospect. Gossans associated with a northeasterly striking gabbroic intrusion (probably northeast strike extension of the McKenzie Spring intrusion) have maximum Ni and Cu concentrations of 0.45% and 0.80%, respectively (Sanders 1999). The Ord Crossing—Grid A Ti–V deposit consists of multiple oxide lenses, up to 150 m long and 30 m wide, in uralitised gabbro and minor amphibolite. A composite channel sample returned 15.2% TiO_2, 41.9% Fe_2O_3, and 0.03% V. Pickands Mather inferred a potential oxide resource of 25 000 t/vertical metre.

Osmond Valley (not investigated in this study; AMG ~220965 on TURKEY CREEK). Australian Anglo American discovered the Osmond Cu–Ni prospect (Sanders 1999) in 1972 during a geological mapping, soil sampling, electromagnetic, and induced polarisation survey. Low-grade mineralisation occurs in three arcuate exposures of a 600 m-wide altered (amphibole-chlorite) metagabbro that intrudes metasedimentary rocks of the Winnama Formation (Tyler et al. 1997). The gabbro has been metamorphosed to lower amphibolite facies and contains a silica–sericite–carbonate alteration assemblage. The southern and northern contacts are truncated by the 1827 Ma McHale Granodiorite and parts of the northern contact are masked by a ferruginous breccia horizon. Small (2 by 10 m) malachite-stained gossans overlying altered gabbro contain up to 4300 ppm Cu and 3650 ppm Ni, whereas those associated with nearby epidote-rich metasedimentary rocks have 3500 ppm Cu and only 250 ppm Ni. Much of the mineralisation in the gabbro and metasediments appears to be related to hydrothermal activity related to the McHale Granodiorite.

Panton (39). Many companies have investigated the PGE–Cr–Ni–Au potential of this intrusion since chromite was first reported by Dow & Gemuts (1967). The intrusion was highlighted in a large (80 000 km^2) stream-sediment geochemical exploration of the Kimberleys managed in the 1960s by Pickands Mather. From the 1970s to the early 1980s, Minsaco Resources Pty Ltd mapped the intrusion in detail, and identified and drilled the main PGE-bearing chromitite layer. During 1989–91, Pancontinental Mining Ltd and Degussa Explorations GmbH carried out further investigations of the chromitites. Closely spaced drilling of stratabound chromitite layers on the northwestern side of the intrusion has defined a significant resource of 2 Mt @ 6.02 ppm Pt+Pd+Au, 0.28% Ni, 0.06% Cu, and 8.49% Cr (using 3 ppm PGEs+Au cut-off: Perring & Vogt 1991, Helix Resources 1993); In the mid 1990s, Helix Resources NL focussed their exploration efforts on styles of magmatic and hydrothermal PGE mineralisation not considered by previous explorers. A stream-sediment geochemical orientation survey over the intrusion in 1994 identified anomalous Pt, Pd, Au, Ni, Cu, and Cr in the <4 mm fraction of samples. A review of the open-cut potential of the PGE resource was carried out in 1997, but results were discouraging.

Panton River (42). In the late 1960s, Pickands Mather (1965–68b, 1968) carried out reconnaissance mapping and stream-sediment sampling of the northern half of the intrusion. Limonitic gossans derived from massive pyrite–pyrrhotite bodies were reported in the nearby Tickalara Metamorphics, but no mineralisation related to the intrusion was found. In 1984, West Coast Holdings Ltd investigated the potential for skarn mineralisation in marble and calc-silicate rock units of the Tickalara Metamorphics that occur as inclusions in the intrusion.

Paperbark (31). See Sandy Creek.

Sally Malay (12). A regional reconnaissance stream-sediment program in 1973 by Australian Anglo American delineated seven geochemical targets. One of these, the SM2 anomaly at Sally Malay, contained elevated concentrations of Ni (maximum 142 ppm) and Cu (81 ppm). Follow-up work in 1974 revealed a prominent gossan with up to 2.1% Ni and 1.4% Cu. Diamond drilling defined massive, disseminated, and brecciated Fe–Ni–Cu sulphides near the base of a thin cyclic sequence of mafic–ultramafic cumulates. Australian Anglo American ceased exploration in 1978, following the completion of 95 diamond drillholes, and Normandy Poseidon Ltd acquired the prospect in 1989. They reviewed the existing data and tested for extensions of the mineralisation along strike at depth. During the mid 1990s, Gindalbie Gold NL published an in-situ indicated and inferred resource, from 30 000 m of drilling in 106 holes, of 3.85 Mt @ 1.79% Ni, 0.73% Cu, and 0.10% Co. A further 2.41 Mt @ 1.05% Ni, 0.61% Cu, and 0.05% Co are classed as potential resources. The resource is closed along strike, but open at 900 m vertical depth (Shedden & Barnes 1996). In the late 1990s, a joint venture between Gindalbie Gold NL and BHP Minerals focussed on the Sally Malay and several other East Kimberley intrusions for Voisey's Bay-type, Canada, Ni–Cu–Co mineralisation. Airborne geophysical (GEOTEM and electromagnetic) and stream-sediment geochemical programs were used to identify potential targets.

Salt Lick Creek (not investigated in this study; AMG ~290445 on BOW RIVER; note: location given by Wilkinson et al. (1975) as 16°47′S and 128°2′E should be 16°47′S and 128°20′E). This well-exposed oval-shaped mafic–ultramafic intrusion, about 3.3 km in diameter, occurs about 5 km east of the Great Northern Highway and 10 km north of the Bow River intrusion. It intrudes low-grade metasedimentary rocks of the ~1870 Ma Marboo Formation and is cut by granites possibly belonging to the ~1835–1800 Ma Sally Downs supersuite (Sheppard et al. 1999). In their detailed petrological and mineralogical study, Wilkinson et al. (1975) divided the body into two well-defined zones, the Basal Zone and Main Zone. The Basal Zone, 360 m thick, contains rhythmically layered olivine and plagioclase–olivine cumulates (troctolite, olivine gabbronorite, leucogabbro, plagioclase dunite), and the Main Zone, 540 m thick, is largely composed of plagioclase–orthopyroxene cumulates (norite, gabbronorite, leucogabbro) which grade upwards into plagioclase cumulates (anorthosite). No olivine is present in the Main Zone. Chromite is restricted to the olivine-rich cumulates of the Basal Zone and sulphides (pentlandite, pyrrhotite, chalcopyrite, valleriite, bornite, cubanite, and siegenite) form a trace component of most rocks. The ultramafic cumulates of the Basal Zone crop out along the southern rim of the intrusion and dip northwards at about 30°. Layering varies from fine scale to units up to 4 m thick. The cumulus minerals display limited and sometimes inconsistent cryptic variation with stratigraphic height. Olivine ranges in composition from Fo_{81} to Fo_{84}, orthopyroxene from mg_{80} to mg_{85}, clinopyroxene from mg_{85} to mg_{88}, and plagioclase from An_{84} to An_{88}. The parent magma to the intrusion is interpreted to be a high-alumina, subalkaline tholeiitic mafic magma that was strongly olivine- and plagioclase-normative. It is not known how thoroughly this intrusion and the nearby Bow River intrusion have been explored in recent years, but depressions in the basal contact and possible feeder conduits should be high priorities for Ni–Cu–Co sulphide mineralisation.

Sandy Creek (23), Billymac Yard (27), and Paperbark (31). These three contiguous intrusions are part of the poorly exposed Corridor gabbro on McINTOSH. In 1972, Stratin Minerals Pty Ltd reported limonitic gossans in the Billymac Yard area with up to 5% Cu and 0.5% Ni, exposed discontinuously for over 2 km near the basal contact of an northeast-trending differentiated sequence of gabbro, norite, and ultramafic rocks (Lewis 1972). BHP, in 1973, undertook a mapping, soil sampling, mapping, costeaning, induced polarisation, and percussion drilling (8 holes) program that defined gossans over a strike length of up to 600 m. From 1978 to 1980 (Anon. 1980), Western Mining Corporation Ltd identified 15 stream-sediment geochemical and two TEM geophysical anomalies, and their percussion drillhole, BP1, intersected disseminated sulphide in gabbro and norite and pyrrhotite-rich sulphides (20 to 40%)

between 62 and 64 m with up to 4560 ppm Ni and 1200 ppm Cu. Peko-Wallsend Operation Ltd reported magnetite seams 1 m wide in gabbroic rocks west of Billymac Yard (Sherrington 1985, Geopeko Ltd 1986–90). In the early 1990s, Delta Gold NL and Australian Anglo American explored the area for Ni–Cu–PGEs, and sampled gossanous gabbro containing up to 1450 ppm Ni, 2.95% Cu, 39 ppb Au, and 100 ppb Pd (Keeley 1991).

South Melon Patch (30). In 1977, Australian Anglo American tested coincident electromagnetic/magnetic and soil/stream-sediment geochemical anomalies for Ni–Cu mineralisation. Most anomalies were attributed to graphitic metasediments in the Tickalara Metamorphics. Freeport of Australia Incorporated carried out rock sampling, costeaning, and diamond drilling to evaluate several chromitite layers in the ultramafic units. In 1989, Peko-Wallsend Operations Ltd undertook further detailed mapping, sampling, and drilling of the chromitites.

Spring Creek (19). Australian Anglo American carried out preliminary mapping and sampling in the area in the 1970s. They identified a sequence of alternating norite, olivine norite, and minor peridotite. A stream-sediment geochemical survey over the entire intrusion defined low abundances of Ni and Cu, but there were no follow-up investigations. National Strategic NL explored for stratabound PGE–sulphide and chromitite deposits, without success in the mid 1980s. From 1986 to 1989, Peko-Wallsend Operation Ltd and Australmin Holdings Ltd assessed the PGE potential of the intrusion (Barrett 1989). A stratigraphic diamond drillhole near the centre of the intrusion, just south of Spring Creek, produced a maximum of 15 ppb Pd at the base of an olivine cumulate unit.

Springvale (37). Pickands Mather (1965–68c) and Australian Anglo American identified several limonitic gossans during a reconnaissance exploration program for Ni and Cu from the mid 1960s to the early 1970s. Induced polarisation and electromagnetic surveys over the gossans were unsuccessful. In 1972, Stratin Minerals Pty Ltd reported large gossans with up to 1520 ppm Cu and 800 ppm Ni near the southern basal contact and in the eastern part of the intrusion. During 1981–82, Inco Australia Ltd explored for PGEs, Ni, and Cu. A program of aeromagnetic, ground magnetic, stream sediment, gossan and soil sampling, and mapping defined two PGE-bearing chromite prospects in the northwest of the intrusion. The more significant prospect consists of trace to minor disseminated chromite in troctolite and anorthosite layers, 1.5 m thick, which have up to 0.5 ppm Pt+Pd, and anomalous Ni and Cu (however, later check sampling and ICP–MS analyses by Geopeko Ltd revealed only 30 ppb Pt and 38 ppb Pd). This occurrence and the Wilagee intrusion farther north are the only known examples of plagioclase-rich cumulates hosting chromite mineralisation in the East Kimberley. Inco Australia Ltd and Freeport of Australia Incorporated tested the chromite-bearing layers and gossans with four diamond drillholes in 1983. The highest PGE assay was 90 ppb Pd in SVD2. Peko-Wallsend Operations Ltd and National Strategic NL investigated the stratabound PGE–sulphide and chromitite potential of the intrusion in the mid 1980s (Geopeko Ltd 1986–89). Two holes (SV1 and SV2) tested the PGE potential of troctolite cyclic units from different stratigraphic levels in the intrusion. Peko-Wallsend reported that the PGE contents of samples from their drillholes and those of earlier explorers were uniformly low (maximum of 15 ppb Pt, 27 ppb Pd), irrespective of rock type or stratigraphic position. Several zones of anomalous Cu (up to 390 ppm) were defined in interlayered anorthosite. In the mid 1990s, Clutha Minerals NL investigated the building-stone potential of the gabbroic rocks in the intrusion.

Three Sisters (45: also includes the Moola Bulla intrusion). In 1968, Pickands Mather explored parts of a north-northeast-trending linear belt of fragmented gabbroic intrusions extending from near Moola Bulla homestead to Three Sisters Hill in the north. The economic potential of the mafic intrusions, which lie close to the Springvale Fault, was downgraded when no ultramafic rocks or sulphide mineralisation were found in their regional survey. In 1973, Australian Anglo American investigated an area of high magnetic background near the southern end of the belt; soil sampling defined Ni (up to 2300 ppm) and Cu (up to 205 ppm) anomalies, and weathered bedrock in a costean assayed 1.3% Ni and 600 ppm Cu over 1.53 m. One of three percussion holes drilled to test the soil anomalies intersected anomalous Ni (maximum of 6000 ppm) and Cu over its entire length (Davies 1974). In 1988, Peko-Wallsend Operations Ltd and Australmin Holdings Ltd investigated the PGE potential of the Three Sisters intrusion (Barrett 1988). They concluded that the prospect required further work, but exploration was stopped by land right disputes. Northern Exploration NL carried out preliminary investigations of the Three Sisters intrusion for PGEs, Ni, Cu, and Au in 1994.

Toby (22). From 1964 to 1968, Pickands Mather carried out a regional stream-sediment geochemical survey over the intrusion. Little variation in rock types was noted and no geochemical anomalies were identified. Australian Anglo American undertook geological mapping, stream, soil and rock chip sampling, and geophysical surveys near Martys Bore on the northern side of the intrusion. Gem Exploration and Minerals Ltd assayed samples derived from the adjacent granites for cassiterite and scheelite, but no significant anomalies were reported. In the late 1980s, National Strategic NL and Peko-Wallsend Operations Ltd carried out a stream sediment and outcrop sampling program for stratabound PGE–sulphide and chromitite mineralisation (Geopeko Ltd. 1986–90). They found that most rocks were non-cumulates, came from very high stratigraphic levels in the intrusion, and had no potential for PGEs. Northern Exploration NL carried out preliminary investigations for PGEs, Ni, Cu, and Au over the southeastern part of the intrusion in 1994.

Turkey Creek (not investigated in this study; AMG ~234128 on TURKEY CREEK). Australian Anglo American in the early 1970s located a narrow (0.3 to 0.6 m) malachite-stained gossan in mafic granulite at the Turkey Creek prospect (Sanders 1999) about 1.8 km south-southeast of Killarney Bore. The granulite forms

part of a north-northeast striking sequence of paramigmatite, amphibolite, carbonate, and tonalite of the Tickalara Metamorphics adjacent to the eastern margin of the Mabel Downs Tonalite—similar setting to the Corkwood intrusion further south. Samples of the gossan, which extends 100 m along strike, returned 1.1% Ni and 0.6% Cu. Follow up stream and soil geochemistry, mapping, and electromagnetics failed to locate extensions of the outcropping mineralisation. Australian Anglo American concluded there was little potential for economic mineralisation.

West McIntosh (32: also called Melon South or Togo 5). From 1977 to 1978, Australian Anglo American undertook mapping, stream sediment and soil geochemistry for base-metal sulphide and chromitite mineralisation. Interest in the intrusion was initiated by three stream-sediment geochemical anomalies. Codner (1979) reported gossan float containing 0.11 ppm Pt, 605 ppm Ni, and 465 ppm Cu. Massive chromitites a few centimetres thick and a few tens of metres along strike in the ultramafics contained a maximum of 34.1% Cr_2O_3, 0.15 ppm Pt, 715 ppm Ni, and 205 ppm Cu. In 1989, Peko-Wallsend Operations Ltd undertook detailed mapping, sampling, and drilling of the chromitite layers that are hosted by the olivine-rich ultramafic units.

West Robin Soak (41). This area was initially explored in the late 1960s for Ni and Cu by Westmex Ltd, who found gossans and siliceous gossanous caprock with up to 1.6% Ni and 0.18% Cu along the basal margins of mafic–ultramafic sills over a strike length of 14 km. Several thin chromitite–magnetite bands were also reported. Northern Mining Corporation NL and Westcharter held tenements covering the strike extension of the intrusion and southeastern flank of the Westmex Ltd tenement block. In 1971, Northern Mining Corporation NL carried out aerial photography, reconnaissance geology, and stream-sediment sampling for Ni–Cu deposits (Mosig & Mills 1971). No ultramafic rocks were identified, but a vein of oxidised lead, 15 cm wide and 30 m long, was found near the eastern boundary of their claims. From 1986 to 1988, Argold Holdings Pty Ltd and Hadowill Pty Ltd undertook geological mapping and rock chip sampling for PGEs, Au, Cu, and Cr (Kenway 1988). They identified two zones of ultramafic–mafic intrusions hosting Ni–Cu gossans and chromitite bands. Ferruginous rocks in these intrusions contained 0.05–0.6 ppm Au, up to 5 ppb Pt, up to 10 ppb Pd, 33–940 ppm Ni, and 24–1100 ppm Cu. Australian Anglo American searched unsuccessfully for base metals in 1991.

White Rock Well West (not investigated in this study; AMG ~890517 on McINTOSH). The White Rock Well West Cu–Ni prospect (Sanders 1999), just north of the South Melon Patch intrusion, was discovered by Australian Anglo American in 1976 through coincident stream-sediment geochemical and airborne electomagnetic anomalies. Soil sampling, ground magnetics, and electromagnetics defined a 50 m-long malachite stained gossan hosted by norite and gabbronorite. High Cu values (25%) associated with low Ni (0.4%) and Co (180 ppm) indicate possible secondary remobilisation. Australian Anglo American concluded that the small pods of Cu-rich sulphides were of no economic importance.

Wilagee (24). Pickands Mather carried out a regional stream-sediment program for Ni and Cu in the 1960s, and Western Mining Corporation Ltd undertook a similar, but more detailed program over the Wilagee intrusion and eastern part of the Toby intrusion from 1978 to 1979. No mineralisation was found, but a differentiated sequence of norite, troctolite, pyroxenite, and peridotite was documented. From 1986 to 1989, Peko-Wallsend Operations Ltd and National Strategic NL carried out a geophysical, stream sediment, outcrop sampling, and diamond drilling program for stratabound PGE–sulphide and chromitite mineralisation. Low-order Pd anomalies near Tobys Dam and a 10–15 cm-thick chromitite in leucogabbro were tested by three diamond drillholes. Low-order PGE anomalies (up to 92 ppb Pt and 240 ppb Pd) were intersected in two holes (Geopeko Ltd. 1986–90). Northern Exploration NL undertook preliminary investigations in 1994 for PGEs, Ni, Cu, and Au.

Wild Dog Creek (40). In 1973, Western Mining Corporation Ltd carried out a regional stream-sediment geochemical survey over the intrusion on the eastern side of the McIntosh intrusion from Fourteen Mile Bore to White Rock Well, but results were disappointing. See also McIntosh A prospect under McIntosh intrusion entry.

Wills Creek (not investigated in this study; AMG ~007676 on TURKEY CREEK). In the late 1970s, Western Mining Corporation Ltd and Australian Anglo American evaluated several Ni–Cu occurrences, discovered in a regional stream-sediment survey, just south of the Ord River about 3.7 km east-northeast of Dougalls Bore (Sanders 1999). The mineralisation (Alpha and Beta Grids) occurs in upper amphibolite facies mafic rocks that intruded folded and faulted metasediments and amphibolites of the Tickalara Metamorphics. Gabbroic to pyroxenitic bodies contain malachite-stained gossans that crop out over 30 m by 120 m. Sparse disseminated sulphides occur in massive biotite pods in gabbro, in metaperidotite, and in amphibole–talc–chlorite dykes prominent in the basal part of the intrusion.

Acknowledgements

The author would like to thank David Blake, John Sheraton, Alastair Stewart (all AGSO), and Ian Tyler (GSWA) for their constructive comments on earlier drafts of the manuscript.

References

Anon., 1975. Final annual report for 1974–1975 on Temporary Reserve 5946, Mabel Downs and Mineral Claims 80/4538–41, Keller Creek, East Kimberley area, Western Australia. Broken Hill Proprietary Company Limited internal report (unpublished) for the Department of Minerals and Energy, Western Australia (Item 740, AN6139).

Anon., 1980. Sandy Creek terminal report. Western Mining Corporation Limited internal report (unpublished) for the Department of Minerals and Energy, Western Australia (Item 1640, AN9091).

Atkinson, W.J., Smith, C.B., Danchin, R.V. & Janse, A.J.A., 1990. Diamond deposits of Australia. In: Hughes, F.E. (editor), Geology of the mineral deposits of Australia and

Papua New Guinea. Australasian Institute of Mining and Metallurgy, Melbourne, Monograph 14, 69–76.

Barnes, G.J., 1994. Surrender report E80/1450 – Corkwood Project. Poseidon Group Trading Ltd internal report number 6490 (unpublished) for the Department of Minerals and Energy, Western Australia (Item 7511, AN40093).

Barnes, Stephen.J., Perring, R.J. & Bunting, J.A., 1991. Mafic–ultramafic intrusions of the East Kimberley region. In: Barnes, S.J. & Hill, R.E.T. (editors), Mafic–ultramafic complexes of Western Australia, Excursion Guidebook No. 3. Sixth International Platinum Symposium, July, 1991, Perth, Western Australia. IAGOD and the Geological Society of Australia, 10–13.

Barrett, F.M., 1988. Annual report on Exploration Licence 80/787 (Three Sisters) for the period January 20 1987 to January 19 1988. Geopeko Pty Ltd report (unpublished) for the Department of Minerals and Energy, Western Australia (Item 4936, AN24171).

Barrett, F.M., 1989. Annual report on Exploration Licence 80/681 (Spring) for the period November 28 1988 to November 27 1989. Geopeko Pty Ltd report (unpublished) for the Department of Minerals and Energy, Western Australia (Item 5866, AN29517).

Bell, A.J., 1966. Final report on the Bow River region, Western Australia. Pickands Mather & Co International internal report (unpublished) for the Department of Minerals and Energy, Western Australia (Item 251A, AN464).

Bester, G, (editor), 1998. Gold. In: Register of Australian mining, 1998/99. Resource Information Unit Ltd, Perth, 276.

Blain, C.F., 1967. Petrology and mineralogy of the Bow River copper–nickel occurrence. BSc.(Hons.) thesis, University of Western Australia.

Blake, D.H., 1997. Speculations relating to the layered mafic–ultramafic intrusions of the East Kimberley, Western Australia. AGSO Research Newsletter, 27, 19–21.

Blake, D.H. & Hoatson, D.M., 1993. Granite, gabbro, and migmatite field relationships in the Proterozoic Lamboo Complex of the East Kimberley region, Western Australia. AGSO Journal of Australian Geology & Geophysics, 14(4), 319–330.

Blake, D.H., Tyler, I.M., Griffin, T.J., Sheppard, S., Thorne, A.M. & Warren, G.W., 1999. Geology of the Halls Creek 1:100 000 sheet area (4461), Western Australia. Explanatory Notes. Australian Geological Survey Organisation, Canberra, 36 pp.

Blatchford, T., 1927a. Geological observations between the Pentecost and King Rivers, then eastwards to Argyle Station. Western Australia Geological Survey, Annual Report 1927, 10–15.

Blatchford, T., 1927b. The geology of portions of the Kimberley Division, with special reference to the Fitzroy Basin and the possibilities of the occurrence of mineral oil. Western Australia Geological Survey, Bulletin 93.

Bourke, P.R., 1990. The geochemistry and structure of a sequence of PGE-bearing chromitite seams at the Panton Sill layered intrusion, East Kimberley Region, Western Australia. BSc.(Hons.) thesis, University of Western Australia.

Briggs, I., 1976. Final report – Corkwood. Australian Anglo American internal report (unpublished) for the Department of Minerals and Energy, Western Australia (Item 617, AN4615).

Chalmers, D.I., 1990. Brockman multi-metal and rare-earth deposit. In: Hughes, F.E. (editor), Geology of the mineral deposits of Australia and Papua New Guinea. Australasian Institute of Mining and Metallurgy, Melbourne, Monograph 14, 707–709.

Codner, C.C., 1979. Final report on Mini M and Togo 5 prospects. Results of exploration on mineral claims 80/5986 to 80/5992 inclusive. Australian Anglo American Limited internal report (unpublished) for the Department of Minerals and Energy, Western Australia (Item 878, AN8463).

Dampier Mining Company Limited, 1971–1973. McKenzies Spring and McKenzies East nickel–copper exploration. Dampier Mining Company Limited and Stratin Minerals Pty Ltd internal report (unpublished) for the Department of Minerals and Energy, Western Australia (Item 738/E, Microfilm roll 215–M1250/5).

Davies, H., 1974. Halls Creek South regional project, Moola Bulla Prospect, final report. Results of exploration of Mineral Claims during 1973. Australian Anglo American Limited internal report (unpublished) for the Department of Minerals and Energy, Western Australia (Item 617, AN5207).

De Havelland, D.W., 1985. Gold & ghosts—a prospectors guide to metal detecting in Australia and history of the Australian goldfields. Volume 1—Western Australia. Hesperian Press, Western Australia, 326 pp.

De Havelland, D.W., 1986. Gold & ghosts—a prospectors guide to metal detecting in Australia and history of the Australian goldfields. Volume 2—Western Australia. Hesperian Press, Western Australia, 382 pp.

Dow, D.B. & Gemuts, I., 1967. Dixon Range, Western Australia, 1:250 000 Geological Series. Bureau of Mineral Resources, Australia, Explanatory Notes SE/52–6, 15 pp.

Dow, D.B. & Gemuts, I., 1969. Geology of the Kimberley Region, Western Australia: The East Kimberley. Bureau of Mineral Resources, Australia, Bulletin 106, 135 pp.

Finucane, K.J., 1938a. The Halls Creek–Ruby Creek area, East Kimberley District. Aerial, Geological and Geophysical Survey of Northern Australia. Western Australia, Report 27.

Finucane, K.J., 1938b. The Mount Dockrell gold mining centre, East Kimberley District. Aerial, Geological and Geophysical Survey of Northern Australia. Western Australia, Report 29.

Finucane, K.J., 1939a. The Grants Creek gold mining centre (Panton River), East Kimberley District. Aerial, Geological and Geophysical Survey of Northern Australia. Western Australia, Report 40, 8 pp.

Finucane, K.J., 1939b. The twelve-mile alluvial workings and Elvire River dredging reserves (893H and 948H), Halls Creek, East Kimberley District. Aerial, Geological and Geophysical Survey of Northern Australia. Western Australia, Report 42.

Finucane, K.J. & Sullivan, C.T., 1939. The Mary River gold mining centre, East Kimberley District. Aerial, Geological and Geophysical Survey of Northern Australia. Western Australia, Report 41.

Forrest, A., 1880. North-west exploration. Journal of expedition from DeGrey to Port Darwin. Government Printer, Perth, 43 pp (includes Hill, F.W., Geological report no.2. From Beagle Bay to Katherine Station. pp. 42–43.).

Frankcombe, K., Barnes, G. & Trussell, D., 1994. Geophysical signature of the Sally Malay nickel deposit, Western Australia. In: Dentith, M.C. et al. (editors),

Geophysical signatures of Western Australian mineral deposits. Geology and Geophysics Department & UWA Extension, University of Western Australia, 26, 157–168.

Gaunt, F.McA., 1977. Keller Creek final report. Results of exploration of Mineral Claims 80/5209, 5302–5319 inclusive. Australian Anglo American Limited internal report (unpublished) for the Department of Minerals and Energy, Western Australia (Item 742, AN7692).

Gemuts, I., 1965. Metamorphism and igneous activity in the Lamboo Complex, East Kimberley area, Western Australia. MSc. thesis, University of Sydney, 85 pp.

Gemuts, I., 1971. Metamorphic and igneous rocks of the Lamboo Complex, East Kimberley region, Western Australia. Bureau of Mineral Resources, Australia, Bulletin 107, 71 pp.

Gemuts, I. & Smith, J.W., 1968. Gordon Downs, Western Australia – 1:250 000 Geological Series. Bureau of Mineral Resources, Australia, Explanatory Notes SE/52–10, 23 pp.

Geopeko Ltd., 1986–1989. Springvale platinum/chromite exploration. Geopeko Ltd internal report (unpublished) for the Department of Minerals and Energy, Western Australia (Item 4592, Fiche 6447–6448).

Geopeko Ltd., 1986–1990. Toby Sill platinum exploration. Geopeko Ltd internal report (unpublished) for the Department of Minerals and Energy, Western Australia (Item 4326, Fiche 5755–5757–M4713).

Gindalbie Gold NL, 1997. Quarterly report (unpublished) by Gindalbie Gold NL for the three months period ended 31 December 1996 to the Australian Stock Exchange, 1–9.

Gonnella, P. (editor), 1997. Gold. In: Register of Australian mining, 1997/98. Resource Information Unit Ltd, Perth, 152.

Griffin, T.J. & Tyler, I.M., 1994. Angelo, Western Australia, 1:100 000 geological map (sheet 4361). Geological Survey of Western Australia, Perth.

Griffin, T.J., Tyler, I.M., Sheppard, S. & Orth, K., 1998. Geology of the Angelo 1:100 000 sheet: Western Australia Geological Survey, 1:100 000 Geological Series Explanatory Notes, 27 pp.

Halligan, R. & Harris, J.L., 1980. Bow River Cu-Ni deposit, Halls Creek Province, Western Australia. Journal of Geochemical Exploration, 12 (2/3), 214–217.

Hamlyn, P.R., 1975. Chromite alteration in the Panton Sill, East Kimberley region, Western Australia. Mineralogical Magazine, 40, 181–192.

Hamlyn, P.R., 1977. Petrology of the Panton and McIntosh layered intrusions, Western Australia, with particular reference to the genesis of the Panton chromite deposit. Ph.D. thesis, University of Melbourne, 389 pp.

Hamlyn, P.R., 1980. Equilibration history and phase chemistry of the Panton Sill, Western Australia. American Journal of Science, 280/7, 631–668.

Hamlyn, P.R. & Keays, R.R., 1979. Origin of chromite compositional variation in the Panton Sill, Western Australia. Contributions to Mineralogy and Petrology, 69/1, 75–82.

Hardman, E.T., 1885. Report on the geology of the Kimberley District, Western Australia, Report 34. Government Printer, Perth, 38 pp.

Harms, J.E., 1959. The geology of the Kimberley Division, Western Australia, and of an adjacent area of the Northern Territory. MSc. thesis, Adelaide University.

Helix Resources NL, 1993. 8th Annual Report, 36 pp.

Hoatson, D.M., 1993a. Correlation of structurally disrupted layered mafic–ultramafic intrusions in the East Kimberley: Is Big Ben part of the Panton intrusion? AGSO Research Newsletter, 19, 9–10.

Hoatson, D.M., 1993b. Summary of geoscientific information for the East Kimberley, Western Australia, with specific reference to the Dixon Range 1:250 000 Sheet (SE/52–6) and Gordon Downs 1:250 000 Sheet (SE/52–10). Australian Geological Survey Organisation, Record 1993/32, 76 pp.

Hoatson, D.M., 1995. New mineral discoveries in the East Kimberley. AGSO Research Newsletter, 22, 9–11.

Hoatson, D.M., 1997. Geology and mineralisation of the Palaeoproterozoic layered mafic–ultramafic intrusions in the Halls Creek Orogen, Western Australia. In: Rutland, R.W.R. & Drummond, B.J. (editors), Palaeoproterozoic tectonics and metallogenesis: comparative analysis of parts of the Australian & Fennoscandian shields. Workshop, Darwin, September, 14–22, 1997. Australian Geological Survey Organisation, Record 1997/44, 61–64.

Hoatson, D.M., 1998a. The geology and economic potential of the Palaeoproterozoic layered mafic–ultramafic intrusions in the East Kimberley, Western Australia. The Geological Society of South Africa and The South African Institute of Mining and Metallurgy, Symposium Series S18. Extended Abstract 8th International Platinum Symposium, Rustenburg, 28 June-3 July 1998, 153–156.

Hoatson, D.M., 1998b. Platinum-group element mineralisation in Australian Precambrian layered mafic–ultramafic intrusions. AGSO Journal of Australian Geology & Geophysics, 17(4), 139–151.

Hoatson, D.M., in press. Exploration strategies for Precambrian layered mafic–ultramafic intrusions in the East Kimberley. AGSO Research Newsletter, 32.

Hoatson, D.M. & Glaser, L.M., 1989. The geology and economics of platinum-group metals in Australia. Bureau of Mineral Resources, Australia, Resource Report 5, 81 pp.

Hoatson, D.M. & Tyler, I., 1993. Prospective layered mafic–ultramafic intrusions in the East Kimberley. AGSO Research Newsletter, 18, 8–9.

Hoatson, D.M., Wallace, D.A., Sun, S-s., Macias, L.F., Simpson, C.J. & Keays, R.R., 1992. Petrology and platinum-group-element geochemistry of Archaean layered mafic–ultramafic intrusions, west Pilbara block, Western Australia. Australian Geological Survey Organisation, Bulletin 242, 319 pp.

Hoatson, D.M., Blake, D., Warren, G., Orth, K. & Tyler, I.M., 1995. Recent NGMA mapping highlights the metallogenic potential of the East Kimberley. AGSO Research Newsletter, 22, 1–2.

Hoatson, D.M., Sproule, R.A. & Lambert, D.D., 1997. Are there Voisey's Bay-type Ni–Cu–Co sulphide deposits in the East Kimberley of Western Australia? AGSO Research Newsletter, 27, 17–19.

Hughes, S.L.M., 1996. Sally Malay Nickel NL. Independent consulting geologists report on the East Kimberley Nickel Project produced for Gindalbie Gold NL (unpublished), 43 pp.

Jaques, A.L., Lewis, J.D. & Smith, C.B., 1986. The kimberlites and lamproites of Western Australia. Western Australia Geological Survey, Bulletin 132.

Jones, F.H., 1938. The Mount Amherst gold and silver–lead deposits. Aerial, Geological and Geophysical Survey of Northern Australia. Western Australia, Report 31.

Keeley, G., 1991. Billymac Prospect E80/1393, Kimberley Mineral Field, Western Australia. Internal report (unpublished) for the Department of Minerals and Energy, Western Australia (Item 6425, AN34824).

Kenway, G.S., 1988. Annual report for the year ending 8th September 1988 on exploration licence 80/757—

"Springvale", Kimberley Mineral Field, Western Australia. Argold Holdings Pty Ltd internal report (unpublished) for the Department of Minerals and Energy, Western Australia (Item 3796, Fiche 4222–4223–M5018).

Lemcke, D.L., 1981. Bow River Prospect. Final report to the Mines Department, Western Australia. Mineral Claims 80/5899–5903, 5922, 6610, 6611. Australian Anglo American Prospecting Proprietary Limited internal report (unpublished) for the Department of Minerals and Energy, Western Australia (Item 1591, AN9748).

Lewis, P.G., 1972. Stratin Minerals Pty Ltd mineral claim locations. Internal report (unpublished) for the Department of Minerals and Energy, Western Australia (Item 738, AN5687).

Louthean, R., 1991 (editor), Register of Australian mining, 1990/91. Resource Information Unit Ltd, Perth.

Louthean, R., 1992. (editor), Register of Australian mining, 1991/92. Resource Information Unit Ltd, Perth.

Marston, R.J., 1979. Copper mineralization in Western Australia. Western Australia Geological Survey, Mineral Resources Bulletin 13, 208 pp.

Marston, R.J., 1984. Nickel mineralization in Western Australia. Geological Survey of Western Australia, Mineral Resources Bulletin 14, 271 pp.

Matheson, R.S. & Guppy, D.J., 1949. Geological reconnaissance in the Mount Ramsay area, Kimberley Division, Western Australia. Bureau of Mineral Resources, Australia, Record 1949/48, 24 pp.

Matheson, R.S. & Teichert, C., 1948. Geological reconnaissance in the eastern portion of the Kimberley Division, Western Australia. Western Australia Geological Survey, Annual Report 1945, 27–41.

Mathison, C.I. & Hamlyn, P.R., 1987. The McIntosh layered troctolite–olivine gabbro intrusion, east Kimberley, Western Australia. Journal of Petrology, 28, 211–234.

Mosig, R.W. & Mills, B.G., 1971. Reconnaissance geological mapping and stream sediment geochemistry—Panton River Prospect, Western Australia. Northern Mining Corporation NL internal report (unpublished) for the Department of Minerals and Energy, Western Australia (Item 737, AN2120).

Nevill, M.W., 1974. The geology and mineralisation of the Corkwood prospect area, Lamboo Complex, East Kimberley, Western Australia. BSc.(Hons.) thesis, University of Western Australia, 72 pp.

Orth, K., 1997. Notes on the geology of the Koongie Park formation southwest of Halls Creek, Western Australia. Australian Geological Survey Organisation, Record 1997/25, 18 pp.

Page, R.W., Hoatson, D.M., Sun, S-s. & Foudoulis, C., 1995. High-precision geochronology of Palaeoproterozoic layered mafic–ultramafic intrusions in the East Kimberley. AGSO Research Newsletter, 22, 7–8.

Perring, R.J. & Vogt, J.H., 1991. The Panton Sill. In: Barnes, S.J. & Hill, R.E.T. (editors), Mafic–ultramafic complexes of Western Australia. Excursion Guidebook 3. Sixth International Platinum Symposium, July 1991, Perth, Western Australia. IAGOD and the Geological Society of Australia, 97–106.

Pickands Mather & Company International, 1965–68a. Armanda Sill nickel–copper/copper–lead–zinc exploration. Pickands Mather & Company International internal report (unpublished) for the Department of Minerals and Energy, Western Australia (Item 251/cj, Microfilm roll 126–M67/61).

Pickands Mather & Company International, 1965–68b. Moola Bulla/Little Panton nickel–copper exploration. Pickands Mather & Company International internal report (unpublished) for the Department of Minerals and Energy, Western Australia (Item 3064, Fiche 2623–M67/68).

Pickands Mather & Company International, 1965–68c. Springvale Sill prospect nickel–copper exploration. Pickands Mather & Company International internal report (unpublished) for the Department of Minerals and Energy, Western Australia (Item 251/cn, Microfilm roll 127–M67/65).

Pickands Mather & Company International, 1965–69. Fletcher Creek nickel–copper–lead–zinc exploration. Pickands Mather & Company International internal report (unpublished) for the Department of Minerals and Energy, Western Australia (Item 251/ci, Microfilm roll 126–M67/60).

Pickands Mather & Company International, 1965–71. McIntosh Sill Prospect nickel–copper exploration. Pickands Mather & Company International internal report (unpublished) for the Department of Minerals and Energy, Western Australia (Item 251/cp, Microfilm roll 126–M67/67).

Pickands Mather & Company International, 1968. Annual Report 1968 Moola Bulla – Little Panton areas nickel–copper exploration, East Kimberley region. Pickands Mather & Company International internal report (unpublished) for the Department of Minerals and Energy, Western Australia (Item 3064, Fiche 2623–M67/68).

Plumb, K.A., 1990. Halls Creek Province and The Granites–Tanami Inlier: regional geology and mineralisation. In: Hughes, F.E. (editor), Geology of the mineral deposits of Australia and Papua New Guinea. Australasian Institute of Mining and Metallurgy, Melbourne, Monograph 14, 681–695.

Ramsden, A.R., French, D.H. & Chalmers, D.I., 1993. The volcanic-hosted rare-metals deposit at Brockman, Western Australia: mineralogy and geochemistry of the Niobium Tuff. Mineralium Deposita, 28, 1–12.

Rea, P.S., 1997. Aspects of the geology and mineralisation of Proterozoic VHMS systems in Koongie Park, Western Australia. New Developments in Research for Ore Deposit Exploration. Third National Conference of the Specialist Group in Economic Geology, Canberra, January 30–31 1997. Geological Society of Australia, Abstracts, 44, 61.

Ririe, G.T., 1989. Evaporites and strata-bound tungsten mineralization. Geology, 17, 139–143.

Rugless, C.S. & Vanderplank, A., 1995. Multi-element geochemical approach to recognising VMS polymetallic mineralisation at regional and mine scales in the East Kimberley and Pilbara regions, Western Australia. In: Ho, S.E. & Amann, W.J. (editors), Recent developments in base metal geology and exploration. Australian Institute of Geoscientists Bulletin 16, Australian Institute of Geoscientists Seminar, 29 November 1995, Perth, 59–74.

Ruker, R.A., 1961. The Saunders Creek radioactive prospect, Halls Creek district, Western Australia. Bureau of Mineral Resources, Australia, Record 1961/103, 21 pp.

Sanders T.S., 1999. Mineralization of the Halls Creek Orogen, east Kimberley region, Western Australia. Geological Survey of Western Australia, Report 66, 44 pp.

Sewell, D., 1999. The Koongie Park and Little Mount Isa zinc–copper–lead deposits East Kimberley Region, Western Australia. In: Ferguson, K.M., Lead, zinc and silver deposits of Western Australia. Geological Survey

of Western Australia, Mineral Resources Bulletin 15, 139–155.

Shedden, S.H. & Barnes, G.J., 1996. East Kimberley nickel province. Characteristics and origin of the Sally Malay Ni-Cu-Co deposit, East Kimberley, Western Australia. In: Grimsey, E.J. & Neuss, I. (editors), Nickel 96—Mineral to market. Australasian Institute of Mining and Metallurgy, Publication Series 6/96, November 27–29, Kalgoorlie, Western Australia, 145–155.

Sheppard, S., Thorne, A.M. & Tyler, I.M. 1999. Geology of the Bow 1:100 000 sheet: Western Australia Geological Survey, 1:100 000 Geological Series Explanatory Notes, 36 pp.

Sherrington, G.H., 1985. Final report on the Exploration Licence 80/368—Billymac Yard, for the period 30 March 1984 to 14 September 1984. Geopeko, Division of Peko-Wallsend Operations Limited internal report. Western Australia Geological Survey M-series Open File, item 2177, AN15391 (unpublished).

Smith, R.N., 1898. State of mining in the Kimberley District. Western Australia Geological Survey, Bulletin 2.

Sproule, R.A., 1999. Genesis of Palaeoproterozoic mafic–ultramafic intrusions and associated PGE-Cr and Ni-Cu-Co mineralisation in the East Kimberley, Western Australia. Ph.D. thesis, Monash University, Melbourne, 320 pp.

Sproule, R., Lambert, D.D. & Hoatson, D.M., 1997a. Re–Os and Sm–Nd isotopic constraints on the genesis of magmatic ores in the Palaeoproterozoic Panton Intrusion, East Kimberley. New Developments in Research for Ore Deposit Exploration. Third National Conference of the Specialist Group in Economic Geology, Canberra, January 30–31 1997. Geological Society of Australia, Abstracts, 44, 67.

Sproule, R.A., Lambert, D.D. & Hoatson, D.M., 1997b. Guides to PGE and Ni-Cu-Co exploration in the East Kimberley, Western Australia. In: Burroughs, A. (editor), Student and young professionals conference, Ballarat 1997. Australasian Institute of Mining and Metallurgy, Abstract.

Sproule, R.A., Lambert, D.D. & Hoatson, D.M., 1997c. Rhenium–osmium constraints on the genesis of magmatic nickel–copper–cobalt–platinum–group–element ores, East Kimberley, Western Australia. Abstracts, Seventh Annual V. M. Goldschmidt Conference, June 2–6, 1997, Tucson, Arizona. LPI Contribution number 921, 195–196.

Sproule, R.A., Lambert, D.D. & Hoatson, D.M., 1999. Re–Os isotopic constraints on the genesis of the Sally Malay Ni–Cu–Co deposit, East Kimberley, Western Australia. Lithos, 47, 89–106.

Stratin Minerals Proprietary Limited, 1971–1973. Melon Patch nickel–copper exploration, Western Australia. Stratin Minerals Proprietary Limited internal report (unpublished) for the Department of Minerals and Energy, Western Australia (Item 738F, Microfilm roll 215–M1250/6).

Sun, S-s., Wallace, D.A., Hoatson, D.M., Glikson, A.Y. & Keays, R.R., 1991. Use of geochemistry as a guide to platinum group element potential of mafic–ultramafic rocks: examples from the west Pilbara Block and Halls Creek Mobile Zone, Western Australia. Precambrian Research, 50, 1–35.

Taylor, W.R., Page, R.W., Esslemont, G., Rock, N.M.S. & Chalmers, D.I., 1995a. Geology of the volcanic-hosted Brockman rare-metals deposit, Halls Creek Mobile Zone, northwest Australia: I. Volcanic environment, geochronology and petrography of the Brockman volcanics. Mineralogy and Petrology, 52, 209–230.

Taylor, W.R., Esslemont, G. & Sun, S-s. 1995b. Geology of the volcanic-hosted Brockman rare-metals deposit, Halls Creek Mobile Zone, northwest Australia: II. Geochemistry and petrogenesis of the Brockman volcanics. Mineralogy and Petrology, 52, 231–255.

Thornett, J.R., 1981. The Sally Malay deposit: gabbroid associated nickel–copper sulfide mineralization in the Halls Creek Mobile Zone, Western Australia. Economic Geology, 76(6), 1565–1580.

Thornett, J.R., 1986. Evolution of a high-grade metamorphic terrain in the Proterozoic Halls Creek Mobile Zone, Western Australia. Ph.D. thesis, University of Western Australia, 350 pp.

Traves, D.M., 1955. The geology of the Ord–Victoria region, Northern Australia. Bureau of Mineral Resources, Australia, Bulletin 27, 133 pp.

Trudu, A. & Hoatson, D.M., 1996. Depths of emplacement of Precambrian layered intrusions in the East Kimberley. AGSO Research Newsletter, 25, 10–12.

Trudu, A. & Ririe, G.T., 1990. Comment and reply on 'Evaporite and strata-bound tungsten mineralization'. Geology, 18, 188–189.

Tyler, I.M., Thorne, A.M., Hoatson, D.M. & Blake, D.H., 1997. Turkey Creek, Western Australia, 1:100 000 geological map (sheet 4563). Geological Survey of Western Australia, Perth.

Wallace, D.A. & Hoatson, D.M., 1990. Petrology and whole-rock geochemistry of selected mafic and ultramafic suites from the Pilbara Block and Halls Creek Mobile Zone, Western Australia. Bureau of Mineral Resources, Australia, Record 1990/46, 69 pp.

Wallace, D.A. Hoatson, D.M., Sun, S-s. & Keays, R.R., 1990. The geochemistry and PGE potential of selected East Kimberley and West Pilbara mafic–ultramafic intrusives and related rocks. Tenth Australian Geological Convention, Hobart—Gondwana: terranes and resources. Geological Society of Australia, Abstracts, 25, 1–2.

Warren, R.G., 1994a. Gold mineralisation in the northern East Kimberley gold district, Western Australia. Australasian Institute of Mining and Metallurgy, Conference, Darwin, 5–9 August 1994, 117–121.

Warren, R.G., 1994b. Role of early extensional faults in the Grants Patch district, East Kimberley, Western Australia. Geological Society of Australia, Abstracts, 37, 453–454.

Warren, R.G., 1997. Reconnaissance geological mapping in Dixon, SE McIntosh and northernmost Halls Creek 1:100 000 Sheet areas, East Kimberley, W. A., 1992–93. Australian Geological Survey Organisation, Record 1997/26, 54 pp.

Wilding, I.G.P., 1980. Corkwood Cu-Ni prospect, Halls Creek Province, WA. In: Butt, C. R.M. & Smith, R.E.(editors), Conceptual models in exploration geochemistry. Journal of Geochemical Exploration, 12, 220–224.

Wilkinson, J.F.G., Duggan, M.B., Herbert, H.K. & Kalocsai, G.I.Z., 1975. The Salt Lick Creek layered intrusion, East Kimberley region, Western Australia. Contributions to Mineralogy and Petrology, 50, 1–23.

Witt, W.K. & Sanders, T., 1997. Magmatic–hydrothermal breccia dykes and hydrothermal alteration in the McHale Granodiorite, Halls Creek Orogen: a possible porphyry system. Western Australia Geological Survey, Annual Review 1995–96, 104–110.

Woodward, H.P., 1891. Report on the goldfields of the Kimberley District. Western Australia Parliamentary Paper 18.

REGIONAL GEOLOGY OF THE HALLS CREEK OROGEN

by DAVID H. BLAKE, IAN M. TYLER, & RODNEY W. PAGE

Introduction

The layered mafic–ultramafic intrusions of the East Kimberley are confined to the central and western zones of the north-northeasterly trending Halls Creek Orogen (HCO) of Griffin & Grey (1990). This orogen (Fig. 3.1) is a composite linear belt consisting of variably deformed and metamorphosed sedimentary, volcanic, and intrusive Palaeoproterozoic rocks, including the mafic–ultramafic intrusions, and overlapping sequences laid down in Palaeoproterozoic, Mesoproterozoic, Neoproterozoic, and Palaeozoic basins. It is equivalent to the Halls Creek Mobile Belt of Dow & Gemuts (1969) and the Halls Creek orogenic sub-province of Hancock & Rutland (1984).

The first systematic mapping of the Precambrian rocks of the HCO was carried out by the Bureau of Mineral Resources, now the Australian Geological Survey Organisation (AGSO), and the Geological Survey of Western Australia (GSWA) in the 1960s (Dow & Gemuts 1969, Gemuts 1971). Most of the HCO was remapped between 1990 and 1995 by AGSO and GSWA as part of the Kimberley-Arunta NGMA project. A major objective of the NGMA project was to develop a better understanding of the geology and mineral potential of the Kimberley to Arunta region, enabling more effective mineral exploration in the area. A study of the layered mafic–ultramafic intrusions in the Dixon Range 1:250 000 Sheet area was included as an important part of the project because of the potential of these intrusions for economic deposits of platinum-group elements and other metals.

The 1:100 000 map sheets[1] and 1:250 000 map sheets covering the East Kimberley are shown in Figure 3.2. The generalised geology of the HCO is shown in Figure 3.3. Available geological maps, and accompanying reports giving detailed descriptions of the geology, are listed in Table 3.1. A comprehensive listing of geoscientific publications on the East Kimberley up to 1992 is given by Hoatson (1993). All references on the East Kimberley relating to the Kimberley–Arunta NGMA Project are in Appendix 6 of this *Bulletin*.

Figure 3.4 shows a coloured Landsat image covering most of the HCO. The same Landsat image, but in shades of grey, is shown in Figure 3.5 with some prominent geological and topographic features annotated.

Isotopic ages quoted, unless stated otherwise, are results of U–Pb zircon SHRIMP analyses undertaken by R.W. Page during the NGMA project. Details are in AGSO's OZCHRON database. The isotopic dating of volcanic and intrusive units indicates that the Palaeoproterozoic rocks of the HCO range in age from ~1910 Ma to ~1790 Ma (Fig. 3.6). Although the Palaeoproterozoic part of the HCO is now one of the best-dated Precambrian orogenic belts in northern Australia, the dated units represent only a small proportion of the total units mapped; for example, only 5 of the many layered mafic–ultramafic intrusions described in this *Bulletin* have been dated isotopically. Consequently, it should be borne in mind that many of the undated units could be significantly different in age from their dated 'correlatives'.

Regional setting

The HCO merges in the southwest with the west-northwesterly trending King Leopold Orogen of the West Kimberley (Fig. 3.1). The two orogens flank the eastern and southern sides of the Kimberley Craton, where late Archaean (~2500 Ma) to early Palaeoproterozoic (~1870 Ma) rocks are concealed beneath flat-lying younger Palaeoproterozoic sedimentary and igneous rocks (Tyler et al. 1999). Both orogens consist of Palaeoproterozoic rocks and relatively minor younger units. The only older rocks exposed in the Kimberley region are late Archaean metamorphics to the southeast of the HCO (Page et al. 1995a, Blake et al. in press a,b), in the Browns Range Dome of The Granites–Tanami region.

The HCO comprises three north-northeasterly trending belts, termed the eastern, central, and western zones[2], which are separated from one another by major strike-slip faults (Tyler et al. 1995). Each of the three zones had a different geological history prior to 1835 Ma. Hence the faults separating them can be considered to coincide with the boundaries between three different basement (pre-1835 Ma) terranes (Tyler et al. 1995, Thorne & Tyler 1996). The three basement terranes are made up of weakly to strongly deformed and metamorphosed sedimentary, volcanic, and intrusive rocks, including voluminous granites and several layered mafic–ultramafic intrusions. Younger Palaeoproterozoic rocks include granite, gabbro, and mafic–ultramafic intrusions emplaced between 1835 and 1790 Ma. All the layered

[1] 1:100 000 sheet names throughout this *Bulletin* are in capital letters to avoid confusion with identical place names and to distinguish them from 1:250 000 sheet names.

[2] The terms 'eastern zone', 'central zone' and 'western zone' are used for geographical parts of the HCO, and hence differ from the terms 'Eastern zone', 'Central zone' and 'Western zone' used in post-1995 GSWA publications (e.g. Sheppard et al. 1996, 1997a, Tyler et al. 1997a,b, 1998a). The terms as used in these GSWA publications have geological connotations as they refer only to rocks of the HCO that are older than ~1835 Ma. These rocks, which correspond to the basement, according to this Chapter, and the 1835–1805 Ma igneous rocks in the HCO are referred to by GSWA as the Lamboo Complex, a name not used in this *Bulletin*.

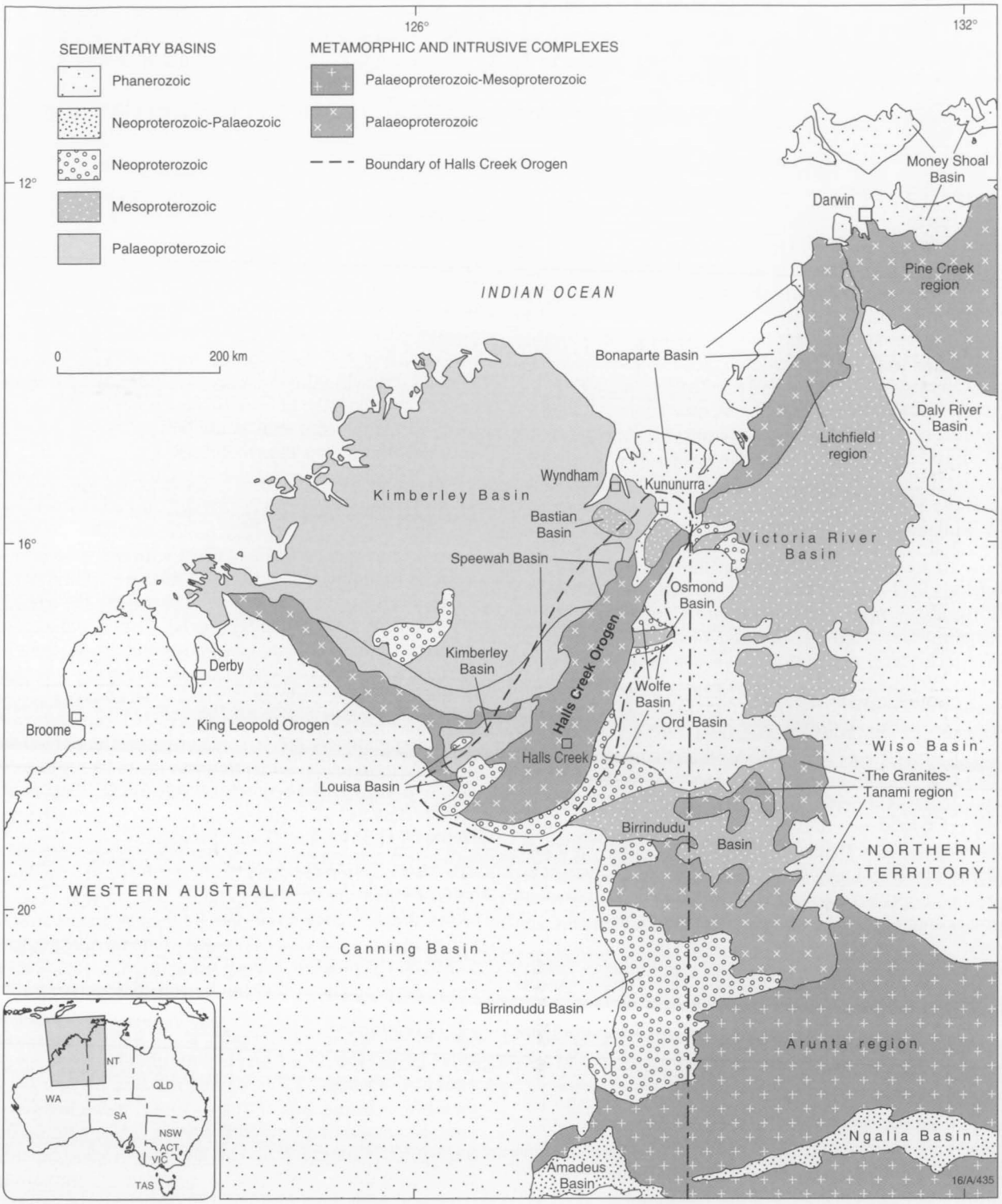


Figure 3.1. Regional setting of the Halls Creek Orogen.

mafic–ultramafic intrusions are confined to the central and western zones of the HCO. The granitic and some gabbroic intrusions in these two zones, whether part of the basement or younger, are grouped together as the Bow River Batholith (Sheppard et al. 1997b). In all three zones there are younger rocks that were laid down in Mesoproterozoic, Neoproterozoic, and Palaeozoic basins.

Major deformations affected the western zone of the HCO between 1870 and 1850 Ma (Hooper Orogeny), the central zone between 1863 and 1845 Ma and both the central and eastern zones between 1840 and 1805 Ma (Halls Creek Orogeny). Later deformations, probably affecting all three zones, took place at ~1000 Ma (Yampi Orogeny), ~560 Ma (King Leopold Orogeny), and ~ 300 Ma (Alice Springs Orogeny).

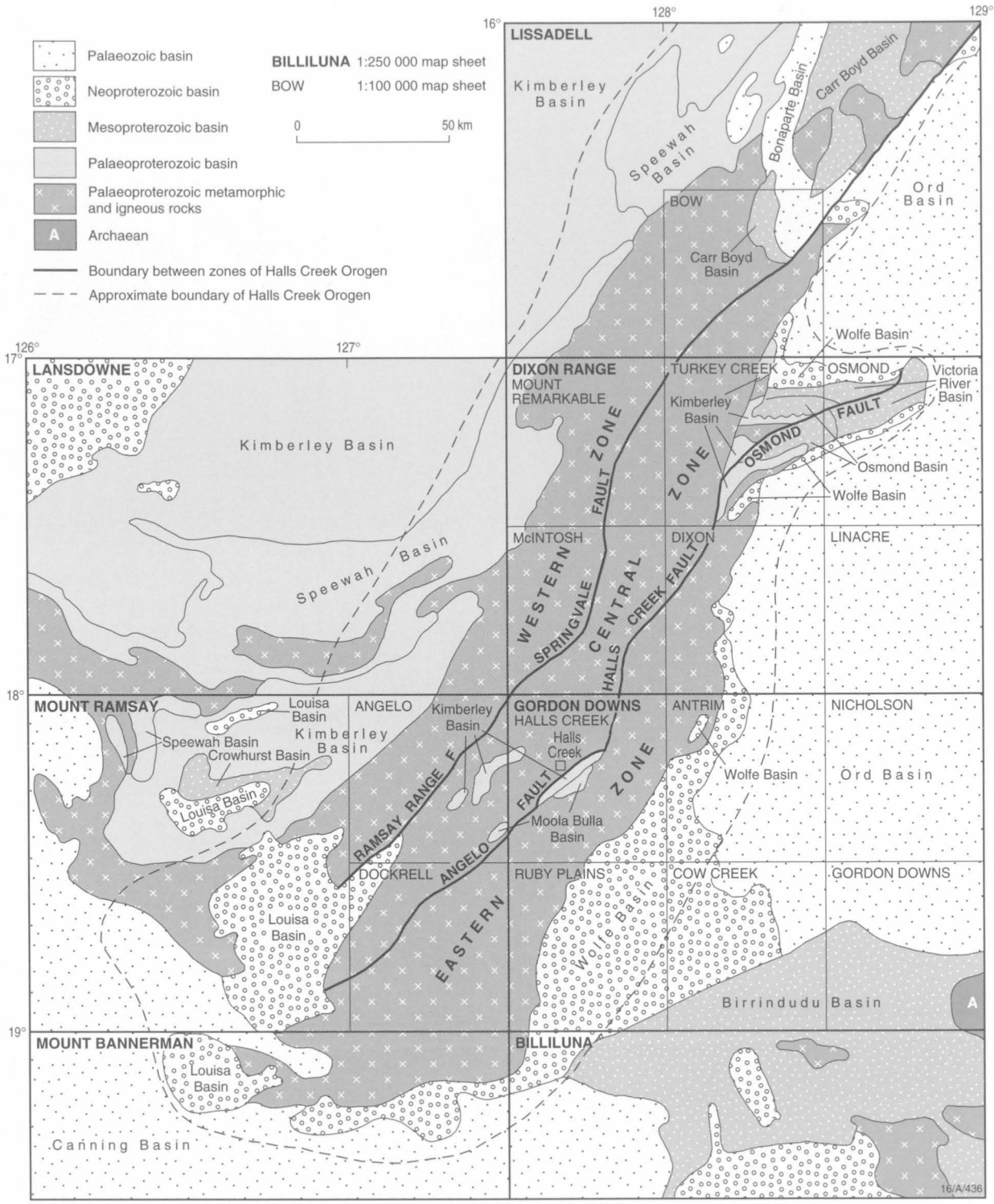


Figure 3.2. Locality map of the Halls Creek Orogen.

The faults separating the three zones of the HCO are part of a regional strike-slip system thought to have been activated during the Mesoproterozoic Yampi Orogeny and reactivated several times since (Tyler et al. 1995, Thorne & Tyler 1996). Rocks predating this orogeny are inferred to have been displaced greater distances than younger rocks by the strike-slip fault system. Following Tyler et al. (1995), the boundary between the eastern and central zones (Figs 3.2–3.5) is taken to be a combination of the north-northeasterly trending Halls Creek Fault and two major splays—the southwest-trending Angelo Fault splay in the south, and the northeast-trending Osmond Fault in the north. The boundary between the central and western zones (Figs 3.2–3.5) is taken to be a combination of (from south to north) the Ramsay Range Fault, part of the Springvale Fault, and the northern part of the

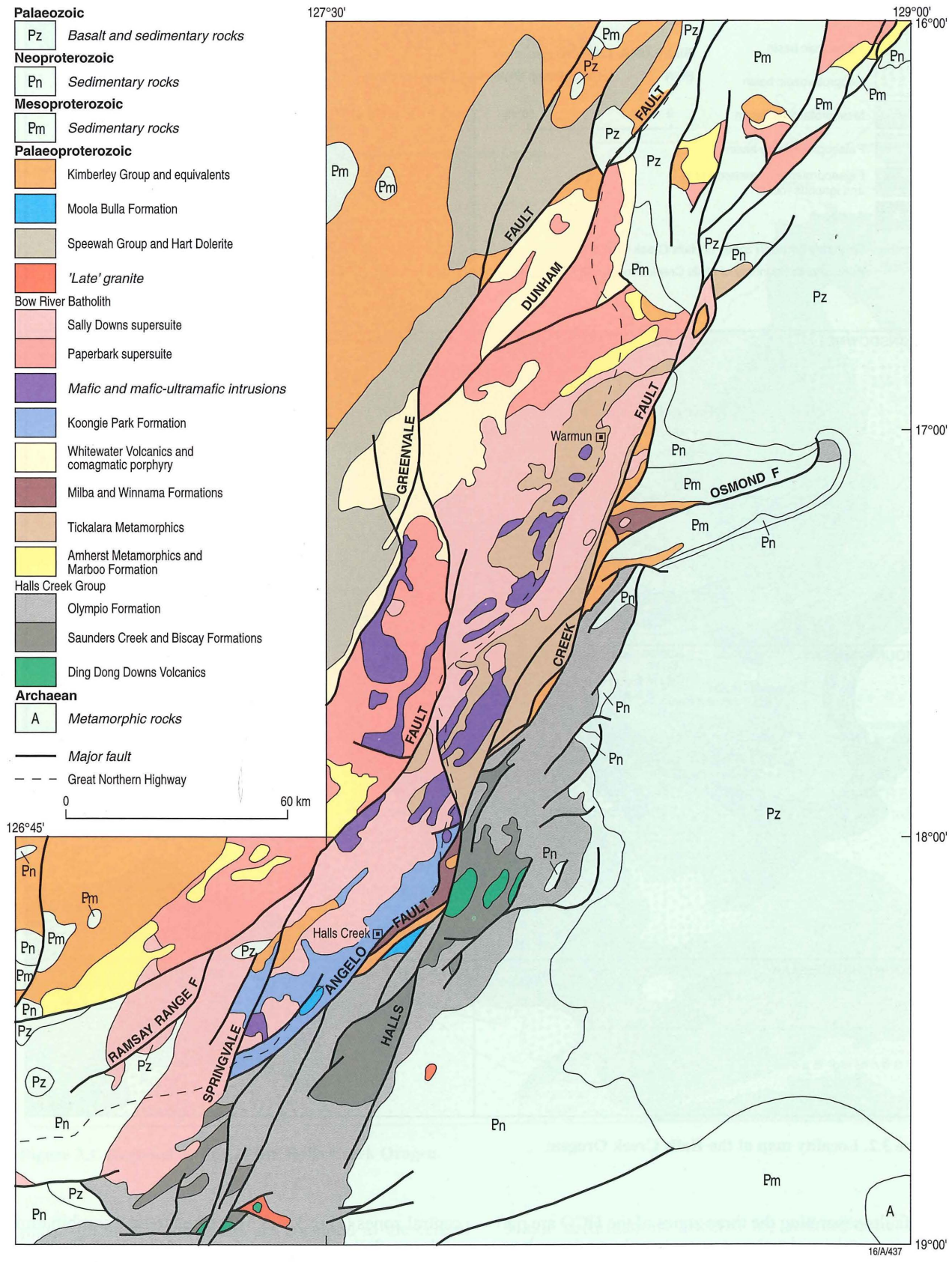


Figure 3.3. Geological map of the Halls Creek Orogen (Gordon Downs, Dixon Range, Lissadell and eastern part of Mount Ramsay sheet areas).

Table 3.1. References for geological maps and accompanying reports of the East Kimberley.

1:250 000 map sheets	**References**
Dixon Range	First edition map and explanatory notes: Dow & Gemuts (1967). Second edition map: Tyler et al. (1998c)
Gordon Downs	First edition map and explanatory notes: Gemuts & Smith (1968). Second edition map and explanatory notes: Blake et al. (in press a,b)
Lansdowne	First edition map and explanatory notes: Gellatly & Derrick (1967)
Lissadell	First edition map and explanatory notes: Plumb (1968). Second edition map and explanatory notes: Thorne et al. (1998, 1999)
Mount Ramsay	First edition map and explanatory notes: Roberts et al. (1968). Second edition map: Tyler et al. (1998a)
1:100 000 map sheets	
ANGELO	First edition map: Griffin & Tyler (1994). Explanatory notes: Griffin et al. (1998)
ANTRIM	Print-on-demand map: Blake & Warren (1996a)
BOW	First edition map and explanatory notes: Sheppard et al. (1997c and 1999)
COW CREEK	Print-on-demand map: (Blake 1996b)
DIXON	First edition map: Tyler et al. (1998b)
DOCKRELL	First edition map: Tyler & Griffin (1994). Explanatory notes: Tyler et al. (1998d)
GORDON DOWNS	Print-on-demand map: (Blake 1996c)
HALLS CREEK	First edition map and explanatory notes: Blake et al. (1999a and 1999b)
McINTOSH	First edition map: Tyler et al. (1997a)
MOUNT REMARKABLE	First edition map and explanatory notes: Sheppard et al. (1996 and 1997a)
NICHOLSON	Print-on-demand map: (Blake & Warren 1996)
RUBY PLAINS	First edition map and explanatory notes: Blake et al. (1997a and 1997b)
TURKEY CREEK	First edition map: Tyler et al. (1997b).

Halls Creek Fault. The Angelo and Osmond Faults are regarded by Thorne & Tyler (1996) as segments of a major fault that has been offset about 90 km by the Halls Creek Fault. The bounding faults are generally well defined, but are obscured in places by stitching plutons of 1830–1805 Ma granite (e.g. in DOCKRELL and MOUNT REMARKABLE). These plutons give minimum ages for major displacements along the stitched parts of the boundary faults and indicate that these parts were not involved in much strike-slip displacement during the Yampi Orogeny and younger tectonic events.

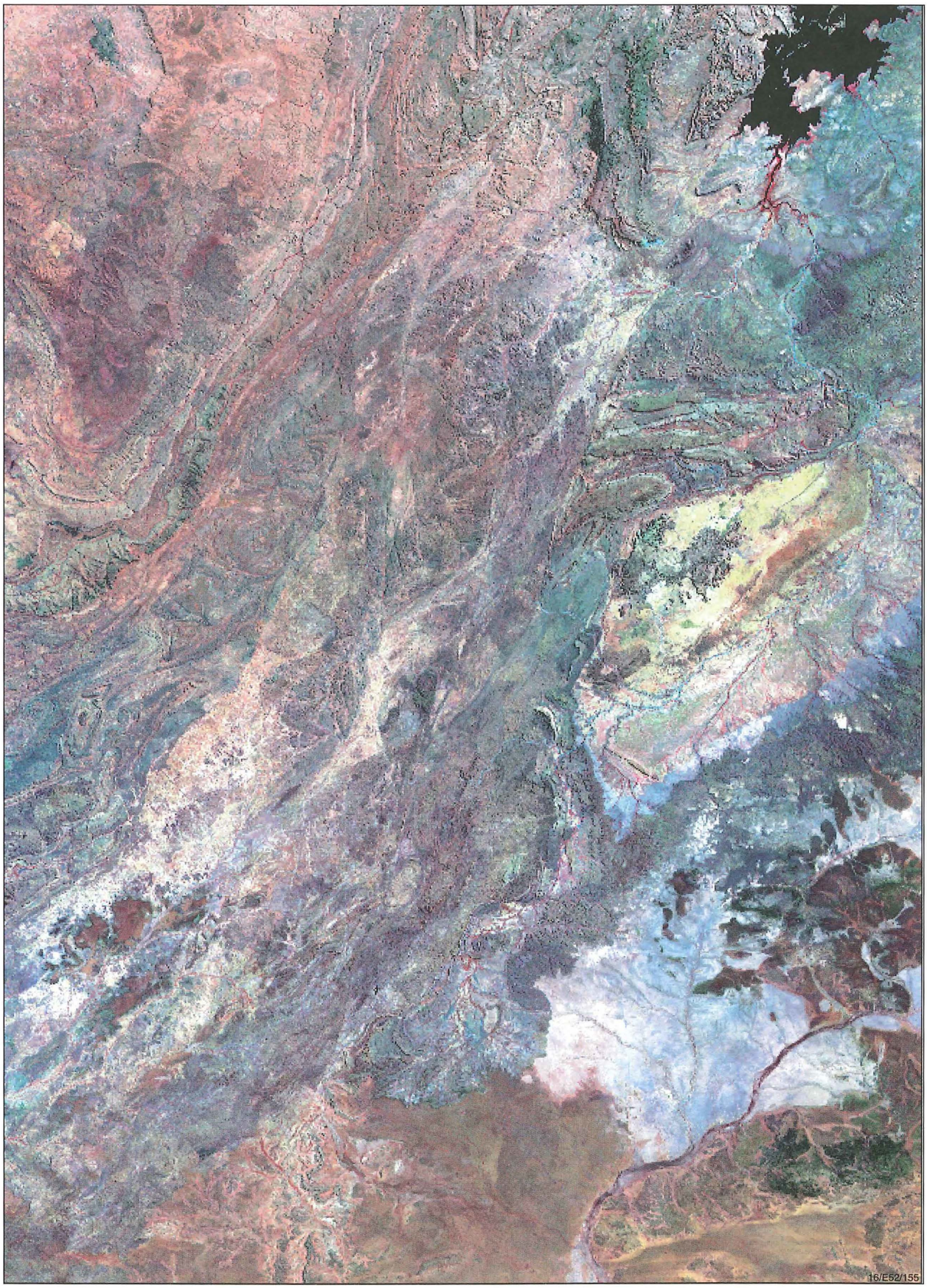
Several post-basement depositional basins are represented in the HCO. The largest in the area covered by Figure 3.2 are the Palaeoproterozoic Speewah Basin (~1835 Ma) and Kimberley Basin (~1800 Ma), which extend into the orogen from the Kimberley Craton to the west, the Mesoproterozoic Carr Boyd Basin and ?Mesoproterozoic Osmond Basin in the northeast, the Mesoproterozoic to possibly Neoproterozoic Victoria River Basin, which extends into the HCO from the northeast, the Neoproterozoic Louisa Basin in the southwest and Wolfe Basin in the south and east, and the Palaeozoic Bonaparte, Ord, and Canning Basins, which extend into the HCO from the north, east, and south, respectively (Fig. 3.1). There are also some small, or remnants of large, Palaeoproterozoic basins overlying basement rocks. One of these is the Moola Bulla Basin near Halls Creek, which predates the Kimberley Basin. The others are the Red Rock and Texas Downs Basins, which are regarded by Tyler et al. (1997b, 1998b) as probably equivalent to the Kimberley Basin and by Blake (1997a) as essentially part of the Kimberley Basin, and the Revolver Creek Basin of Sheppard et al. (1997c) and Thorne et al. (1998), which may also be equivalent to the Kimberley Basin. Near the western margin of the HCO, the Kimberley Basin is overlain by Mesoproterozoic sediments of the Bastian Basin in the north (Fig. 3.1) and the Crowhurst Basin in the south (Fig. 3.2).

The stratigraphy, magmatism, and deformation in the three zones of the HCO are summarised in Table 3.2, and the results of U–Pb zircon geochronology carried out by Page are summarised in Figure 3.6.

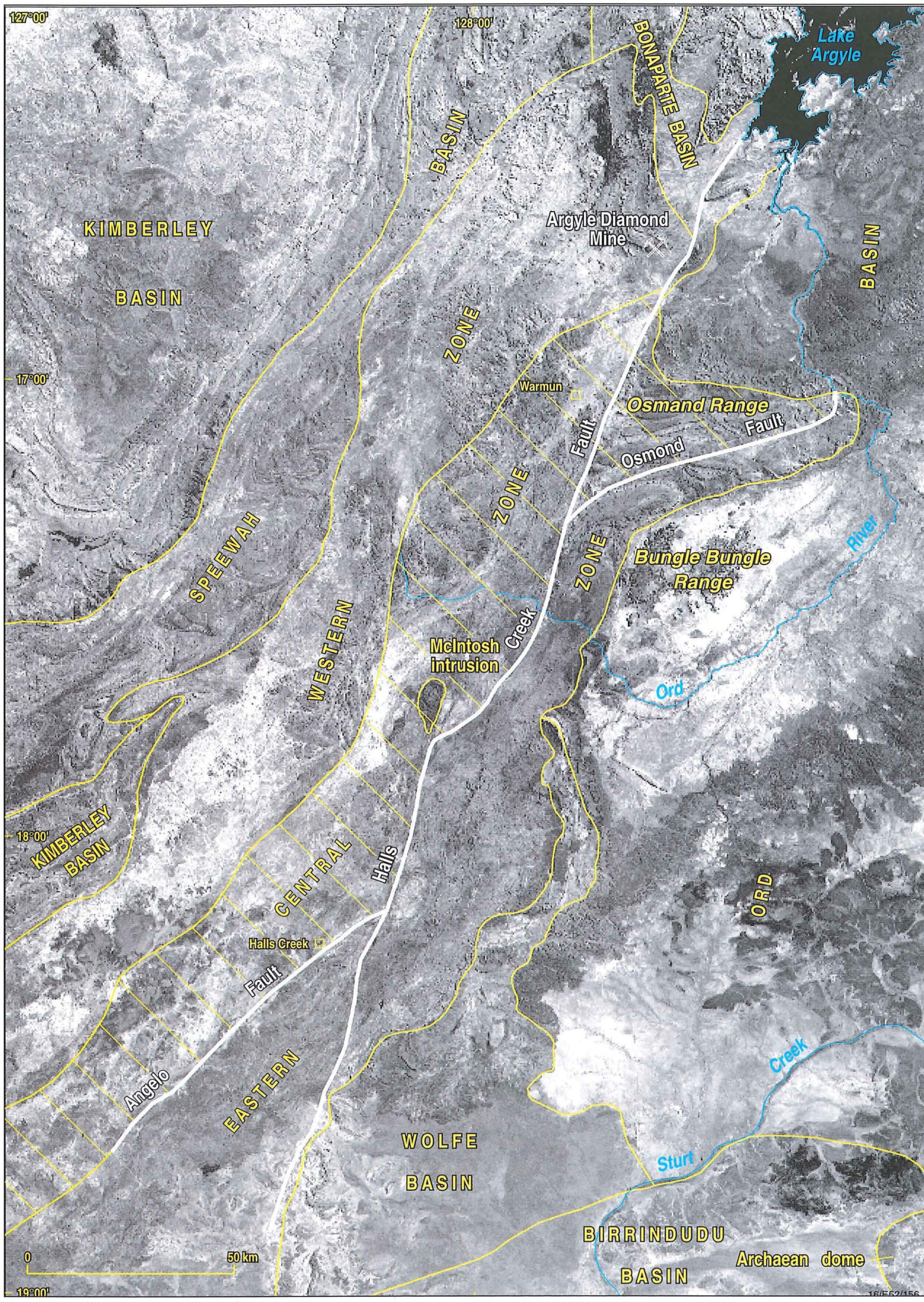
Eastern zone of the Halls Creek Orogen

Pre-1835 Ma basement

The basement in the eastern zone consists mainly of the ~1880–1845 Ma Halls Creek Group, but also contains the oldest rocks known in the HCO. These are the bimodal **Ding Dong Downs Volcanics** and the **Junda Microgranite**, both dated at ~1910 Ma (see appendix at the end of this chapter), and the **Esaw Monzogranite**. They are exposed in the cores of anticlines and structural domes northeast and southwest of Halls Creek (in HALLS CREEK and DOCKRELL), where they are separated from



Figures 3.4 and 3.5. Landsat Multispectral Scanner (MSS) colour composite image of most of the Halls Creek Orogen, using bands 7, 5, and 4 displayed as red, blue, and green, respectively (Fig. 3.4), and grey scale image, using band 7, showing some annotated geological and topographic features (Fig. 3.5, opposite). The Landsat data, received by the Australian Centre for Remote Sensing, Canberra, is part of a geocoded Landsat MSS mosaic produced by Geoimage Pty Ltd. Processed by L.F. Macias (AGSO).


127°00'
128°00'
17°00'
18°00'
19°00'
Lake Argyle
BONAPARTE BASIN
BASIN
KIMBERLEY
BASIN
Argyle Diamond Mine
BASIN
ZONE
Warmun
Osmand Range
Fault
Osmond
Fault
ZONE
ZONE
Bungle Bungle Range
River
SPEEWAH
WESTERN
McIntosh intrusion
Creek
Ord
KIMBERLEY BASIN
CENTRAL
Halls
ORD
Halls Creek
Fault
Angelo
EASTERN
Creek
WOLFE
BASIN
Sturt
BIRRINDUDU
BASIN
Archaean dome
0
50 km

the overlying Halls Creek Group by an unconformity representing a time gap of about 30 Ma (Fig. 3.6). The Ding Dong Downs Volcanics include the **Sophie Downs Granophyre Member**, previously known as the Sophie Downs Granite, exposed northeast of Halls Creek. This member may be subvolcanic to partly extrusive (Blake et al. 1999a).

The **Halls Creek Group** is represented by three formations. The **Saunders Creek Formation** at the base, lying unconformably on the older basement rocks, is a fluvial to possibly shallow marine unit of mainly quartz sandstone and conglomerate. Sandstone near the base of this formation in HALLS CREEK has a Sm–Nd TDM model age of 3230 Ma and contains detrital zircon ranging in age from ~3590 Ma to ~2500 Ma (U–Pb SHRIMP data from 79 analyses), indicating derivation from an Archaean source area (Page & Sun 1994). The conformably overlying **Biscay Formation** consists of mafic and subordinate felsic volcanic rocks, fine to medium-grained clastic sedimentary rocks, carbonates, and chert. A felsic volcanic rock from this formation near the Ilmars Cu–Pb–Zn prospect (Blake et al. 1999a) has been dated at 1880±3 Ma. The Biscay Formation probably represents shallow-marine shelf sedimentation and subaqueous to subaerial volcanism, either on a passive continental margin, as suggested by Sheppard et al. (1999), or in an intracratonic setting. Contacts between the Biscay Formation and the overlying **Olympio Formation**, the youngest formation of the Halls Creek Group, generally appear to be conformable, but isotopic dating indicates that a time gap of up to 20 Ma may separate the two formations. The Olympio Formation consists mainly of turbiditic greywacke and mudstone (submarine fan deposits: Hancock & Rutland 1984), but also includes two units of subaqueous alkaline volcanics. These are the **Maude Headley Member** (Fig. 3.7A), which is dated at ~1857 Ma, in the central part of the eastern zone, and the **Butchers Gully Member** to the south, pillow lava from which is dated at ~1848 Ma. Both these members are underlain and overlain by turbidites. The niobium tuff of Chalmers (1990), which contains euhedral volcanic-type zircon grains dated at ~1870 Ma (Taylor at al. 1995), lies at the base of the Butchers Gully Member at the Brockman rare-earth elements and rare-metals prospect southeast of Halls Creek. The significance of the 1870 Ma age is unclear (Blake et al. 1999a). In the north, in southern TURKEY CREEK, the Olympio Formation is taken to include calcareous, dolomitic, and chloritic metasediments containing bands of chert and jasper, as well as conformably overlying turbidites with, near the base, some felsic fragmental volcanic rocks.

The Ding Dong Downs Volcanics and Halls Creek Group were intruded by sill-like bodies of **Woodward Dolerite** before they were tightly folded and regionally metamorphosed to greenschist and, locally, amphibolite

Table 3.2. Summary of geological history of the Halls Creek Orogen.

Age (Ma)	*Western zone*	*Central zone*	*Eastern zone*
~300-0	Prolonged erosion apart from Permian sedimentation in *Bonaparte Basin* and Permian to Triassic sedimentation in *Canning Basin.* Laterite formation during early Cainozoic	Prolonged erosion. Laterite formation during early Cainozoic	Prolonged erosion. Laterite formation during early Cainozoic
~300	Folding, faulting—**Alice Springs Orogeny**	Folding, faulting—**Alice Springs Orogeny**	Folding, faulting—**Alice Springs Orogeny**
370-320	Sedimentation in *Bonaparte Basin, Canning Basin*		
~370	Sedimentation in *Bonaparte Basin*		Sedimentation, Mahony Group in *Ord Basin*
~500	Sedimentation in *Bonaparte Basin*	Sedimentation, Goose Hole Group in *Ord Basin*	Sedimentation, Goose Hole Group in *Ord Basin*
~540	Basaltic volcanism, Antrim Plateau Volcanics in *Bonaparte Basin* and in southwest	Basaltic volcanism, Antrim Plateau Volcanics in *Ord Basin*	Basaltic volcanism, Antrim Plateau Volcanics in *Ord Basin*
~560	Folding, faulting—**King Leopold Orogeny**	Folding, faulting—**King Leopold Orogeny**	Folding, faulting—**King Leopold Orogeny**
~700-600	Sedimentation (incl. glacial), Louisa Downs and Kuniandi Groups in *Louisa Basin*	Sedimentation (incl. glacial), Louisa Downs and Kuniandi Groups in *Louisa Basin*	Sedimentation (incl. glacial), Albert Edward and Duerdin Groups in *Wolfe Basin* and Louisa Downs Group in *Louisa Basin*
~800			Sedimentation, Ruby Plains Group in *Wolfe Basin*
~900?		Sedimentation in *Victoria River Basin*	Sedimentation in *Victoria River Basin*
~1000	Faulting—**Yampi Orogeny**	Folding and faulting—**Yampi Orogeny**	Folding and faulting—**Yampi Orogeny**

Table 3.2. (Cont.) Summary of geological history of the Halls Creek Orogen.

Age (Ma)	*Western zone*	*Central zone*	*Eastern zone*
~1200	Sedimentation, Carr Boyd Group in *Carr Boyd Basin*		
~1500?		Sedimentation in *Osmand Basin*	Sedimentation in *Osmand Basin*
~1790	Mafic intrusion, Hart Dolerite		Emplacement of granite, San Sou Monzogranite
~1800	Sedimentation and basaltic volcanism, Kimberley Group and probable correlatives in *Kimberley Basin* and *Revolver Creek Basin*	Sedimentation and basaltic volcanism, Kimberley Group and probable correlatives in *Kimberley Basin, Texas Downs Basin,* and *Red Rock Basin*	Sedimentation and basaltic volcanism, Kimberley Group and probable correlatives in *Kimberley Basin* and *Red Rock Basin*
~1835-1805	Emplacement of granite and gabbro, Sally Downs supersuite of *Bow River Batholith*	Emplacement of granite and gabbro, Sally Downs supersuite of *Bow River Batholith,* and group VI and younger layered mafic intrusions. Sedimentation, Moola Bulla Formation in *Moola Bulla Basin*	Emplacement of granite of Sally Downs supersuite of *Bow River Batholith* and possibly of unnamed granite in south. Sedimentation, Moola Bulla Formation in *Moola Bulla Basin*
~1835	Sedimentation and minor felsic volcanism, Speewah Group in *Speewah Basin*	Regional deformation and metamorphism—**Halls Creek Orogeny**	Regional deformation and metamorphism—**Halls Creek Orogeny**
~1845		Sedimentation and bimodal volcanism, Koongie Park Formation and possibly Milba and Winnama Formations. Emplacement of group V layered mafic intrusions. VMS mineralisation, Koongie Park Formation	Possible turbidite sedimentation, upper part of Olympio Formation of Halls Creek Group
~1855-1845	?Regional deformation—**Hooper Orogeny**, late phase	Emplacement of felsic and mafic intrusions, possibly including group IV layered intrusions. Deformation and metamorphism, Tickalara Metamorphics	Turbidite sedimentation and alkaline volcanism, Olympio Formation, including Butchers Gully Member. Intrusion of mafic sills, Woodward Dolerite
~1860-1850	Felsic volcanism, Whitewater Volcanics. Emplacement of porphyry, granite, and gabbro, Paperbark supersuite of *Bow River Batholith,* and layered mafic intrusions of groups II and III	Emplacement of group I mafic–ultramafic intrusions. Deformation and metamorphism	Turbidite sedimentation and alkaline volcanism, Olympio Formation, including Maude Headley Member. Intrusion of mafic sills, Woodward Dolerite
~1865	Folding and metamorphism—**Hooper Orogeny**, early phase	Sedimentation, mafic volcanism and granite intrusion, protoliths of Tickalara Metamorphics	?Turbidite sedimentation, Olympio Formation
~1880-1865	Turbidite sedimentation, Marboo Formation (and intrusion of Ruins Dolerite in King Leopold Orogen)		Sedimentation, Saunders Creek Formation and Biscay Formation, Halls Creek Group. Bimodal volcanism and VMS mineralisation, Biscay Formation. Intrusion of mafic sills, Woodward Dolerite
~1910			Bimodal magmatism, Ding Dong Downs Volcanics (incl. Sophie Downs Granophyre Member), Junda Microgranite and possibly some Woodward Dolerite

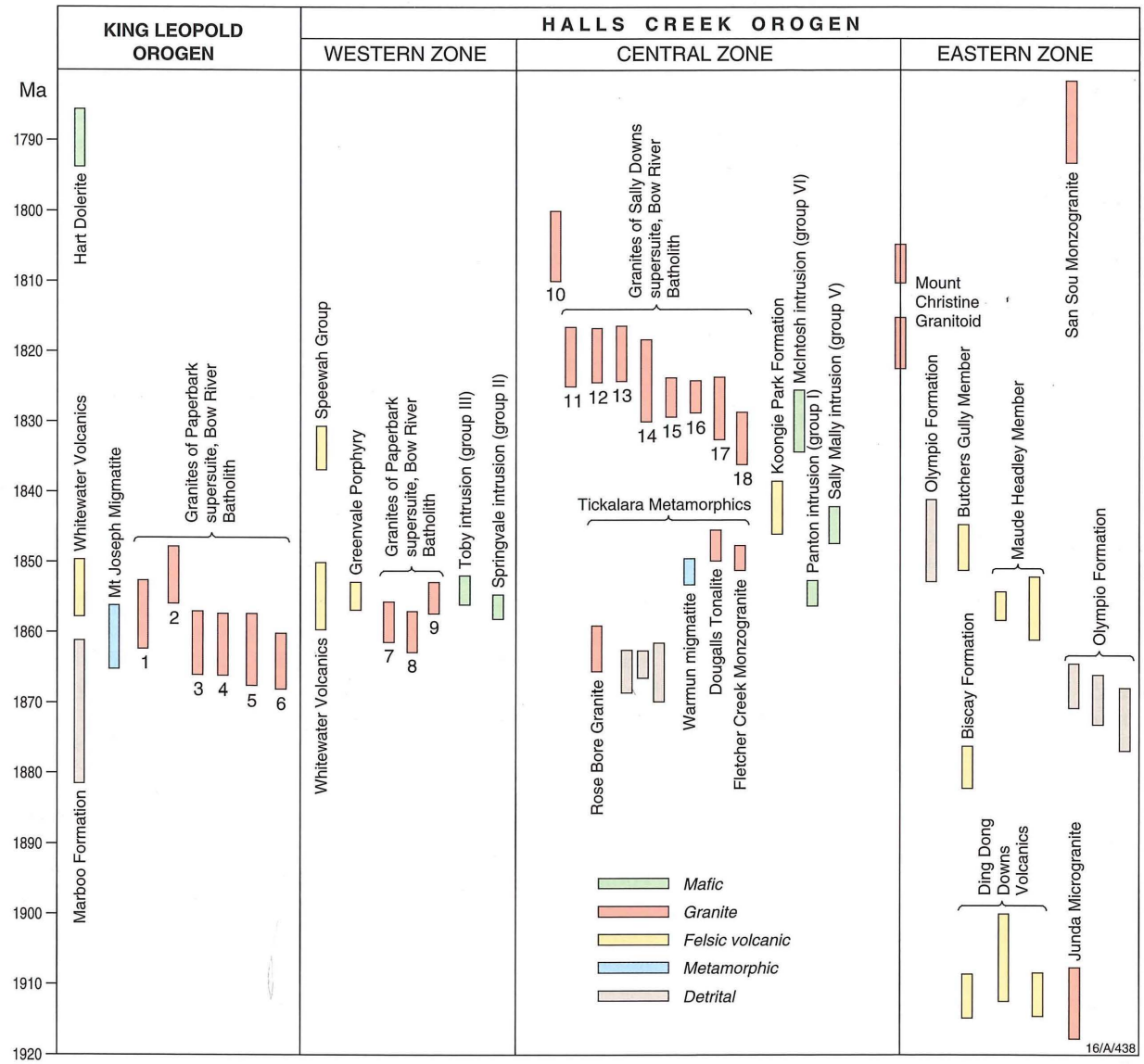


Figure 3.6. Summary of U–Pb geochronology for the Halls Creek Orogen and King Leopold Orogen (West Kimberley).

1, Richenda Microgranite; 2, Kongorow Granite; 3, McSherrys Granodiorite; 4, Mondooma Granite; 5 & 6, Lennard Granite; 7, Nyalassy Granite; 8, Neville Granodiorite; 9, Paperbark Granite; 10, Eastmans Granite; 11, Copperhead Albitite 'Carbonatite' Complex; 12, Sally Downs Tonalite; 13, leucogranite vein cutting Mabel Downs Tonalite; 14, pegmatite vein cutting the Panton layered mafic–ultramafic intrusion; 15, Loadstone Monzogranite; 16, McHale Granodiorite; 17, leucotonalite vein cutting Tickalara Metamorphics; 18, Mabel Downs Tonalite.

facies during the main folding event of the **Halls Creek Orogeny**, which took place at ~1835 Ma (e.g. Blake et al. 1999a). As some sill intrusion probably took place during the mafic volcanism represented by basalt lavas in the Ding Dong Downs Volcanics and Halls Creek Group, the Woodward Dolerite sills could have been intruded at various times between ~1910 and ~1835 Ma. The Halls Creek Orogeny has been attributed to the coming together of the basement in the eastern zone and basement in the central zone of the HCO (e.g. Griffin et al. 1998, Blake et al. 1999a), and is considered by Tyler & Page (1996) to be part of the final stages of a collision between the Kimberley Craton and the rest of the North Australian Craton. Most of the basement rocks in the eastern zone are well cleaved to schistose as a result of the deformation, but their primary sedimentary, volcanic, or intrusive character is generally readily apparent. Spectacular pencil slates resulting from the intersection of bedding and strongly oblique cleavage are present locally in fold closures within the Olympio Formation (Fig. 3.7B).

Rocks younger than ~1835 Ma

Tightly folded rocks of the Olympio Formation in HALLS CREEK are overlain unconformably by the **Moola Bulla Formation**, a unit of fluvial and lacustrine or shallow marine (deltaic) sandstone, conglomerate and mudstone derived from a granitic and metasedimentary source to the southwest (Blake et al. 1999a, Griffin et al. 1998). This formation may represent molasse-type sedi-

ments (Blake 1991) deposited in a local basin, the Moola Bulla Basin (Blake et al. 1999a, Griffin et al. 1998), shortly after the main folding event of the Halls Creek Orogeny. Dow & Gemuts (1969) and Griffin & Tyler (1992) suggested that it was deposited at about the same time as the ~1835 Ma Speewah Group in the Speewah Basin on the west side of the Halls Creek Orogen. The Moola Bulla Formation is overlain unconformably by sandstone and basalt assigned to either the **Kimberley Group** or the **Red Rock Formation** (Blake 1997a, Blake et al. 1999a, Tyler et al. 1997b). The Kimberley Group west of the HCO is intruded by sills of Hart Dolerite, one of which has been dated at ~1790 Ma, and in the central zone of the HCO (see below) the group overlies ~1827 Ma granite, indicating that it is probably close to 1800 Ma in age.

Intrusions in the eastern zone that postdate the main folding of the Halls Creek Orogeny include ~1820 Ma and ~1810 Ma phases of the **Mount Christine Granitoid** and the ~1790 Ma **San Sou Monzogranite** in the Mount Ramsay 1:250 000 Sheet area, and unnamed granite (in RUBY PLAINS), and granite veins east of Halls Creek in the Gordon Downs 1:250 000 Sheet area. The Mount Christine Granitoid is the only one of these intrusions regarded as part of the 1835–1805 Ma Sally Downs supersuite of the Bow River Batholith (Tyler et al. 1998a).

In the northern part of the eastern zone, in the Osmand Range area of TURKEY CREEK, the Palaeoproterozoic rocks mapped as Kimberley Group by Blake (1997a) and Red Rock Formation by Tyler et al. (1997b) are overlain unconformably by the **Mount Parker Sandstone** and **Bungle Bungle Dolomite** of the ?Mesoproterozoic Osmond Basin sequence. These formations are overlain in turn by the **Wade Creek Formation**, **Ahern Formation**, and **Helicopter Siltstone** of the Mesoproterozoic to ?Neoproterozoic Victoria River Basin sequence (Thorne & Tyler 1996, Tyler et al. 1997b). Unconformities separate the Helicopter Siltstone from overlying glacial sedimentary rocks of the Neoproterozoic **Duerdin Group** and this group from overlying basalts of the early Cambrian **Antrim Plateau Volcanics**, the basal formation of the Palaeozoic Ord Basin succession (Mory & Beere 1988).

Along the eastern margin of the eastern zone south of the Osmand Range, folded turbidites of the basement Olympio Formation are overlain directly by generally gently dipping sedimentary rocks of the **Ruby Plains**, **Duerdin**, and **Albert Edward Groups**, which were laid down in the Neoproterozoic Wolfe Basin. Tillite at the base of the Duerdin Group locally lies directly on the Olympio Formation. A low-angle unconformity separates the Albert Edward Group from the overlying Cambrian and Devonian sedimentary succession of the Ord Basin.

In the southwest of the eastern zone the Neoproterozoic **Kuniandi** and **Louisa Downs Groups**, correlatives of the Duerdin and Albert Edward Groups, respectively, were deposited in the Louisa Basin, unconformably on folded rocks of the Olympio Formation (Yeates & Muhling 1997, Tyler et al. 1998a).

Layered mafic–ultramafic intrusions

No layered mafic–ultramafic intrusions have been found in the eastern zone of the HCO. One explanation—that there has been insufficient erosion to expose such intrusions in this zone—is perhaps supported by airborne magnetic data, which indicate the possible presence of some concealed layered intrusions here (see Chapter 4). However, the absence of layered intrusions, like the paucity of granite plutons, may be a real feature of the eastern zone, marking a major difference in Palaeoproterozoic geology between this zone and the central and western zones of the HCO.

Central zone of the Halls Creek Orogen

The central zone of the HCO, bounded to the east and south by the Halls Creek, Osmond, and Angelo Faults and to the west by the Springvale Fault and the Ramsay Range Fault, contains pre-1835 Ma basement rocks, post-1835 Ma plutons of the Bow River Batholith and layered mafic–ultramafic intrusions, and younger rocks laid down in Proterozoic and Palaeozoic basins (Table 3.2 and Fig. 3.3).

Pre-1835 Ma basement

The basement rocks in the central zone range in age from pre-1863 Ma to probably about 1840 Ma. They comprise the Milba Formation, Winnama Formation, Koongie Park Formation, Angelo Microgranite, Tickalara Metamorphics, and layered mafic–ultramafic intrusions of groups I, IV, and V (typified by the Panton, Wild Dog Creek, and Sally Malay intrusions, respectively).

The **Milba Formation** is confined to narrow fault-bounded blocks in the eastern part of the central zone in northern HALLS CREEK and southern McINTOSH. All contacts with adjacent Proterozoic units are faulted. The formation consists of tightly folded turbiditic greywacke, siltstone and mudstone, lithic and minor quartz sandstone, pure to impure calcareous rocks, chert, and minor mafic lavas and sills. These rocks have been metamorphosed to greenschist or lower amphibolite facies, and are commonly phyllitic or schistose. The formation could be similar in age to the Winnama Formation, Koongie Park Formation and parts of the Tickalara Metamorphics in the central zone, parts of the Halls Creek Group in the eastern zone, and the Marboo Formation in the western zone.

The **Winnama Formation**, which is similar in lithology, deformation, metamorphism and, possibly, age to the Milba Formation, is exposed north of the Osmond Fault and east of the Halls Creek Fault in TURKEY CREEK. It was folded and metamorphosed before being intruded by the ~1827 Ma McHale Granodiorite, and was subsequently overlain unconformably by sandstone and basalt mapped as Kimberley Group by Blake (1997a) and as Red Rock and Texas Downs Formations by Tyler et al. (1997b).

The **Koongie Park Formation,** exposed in the southern part of the central zone, consists of folded and metamor-

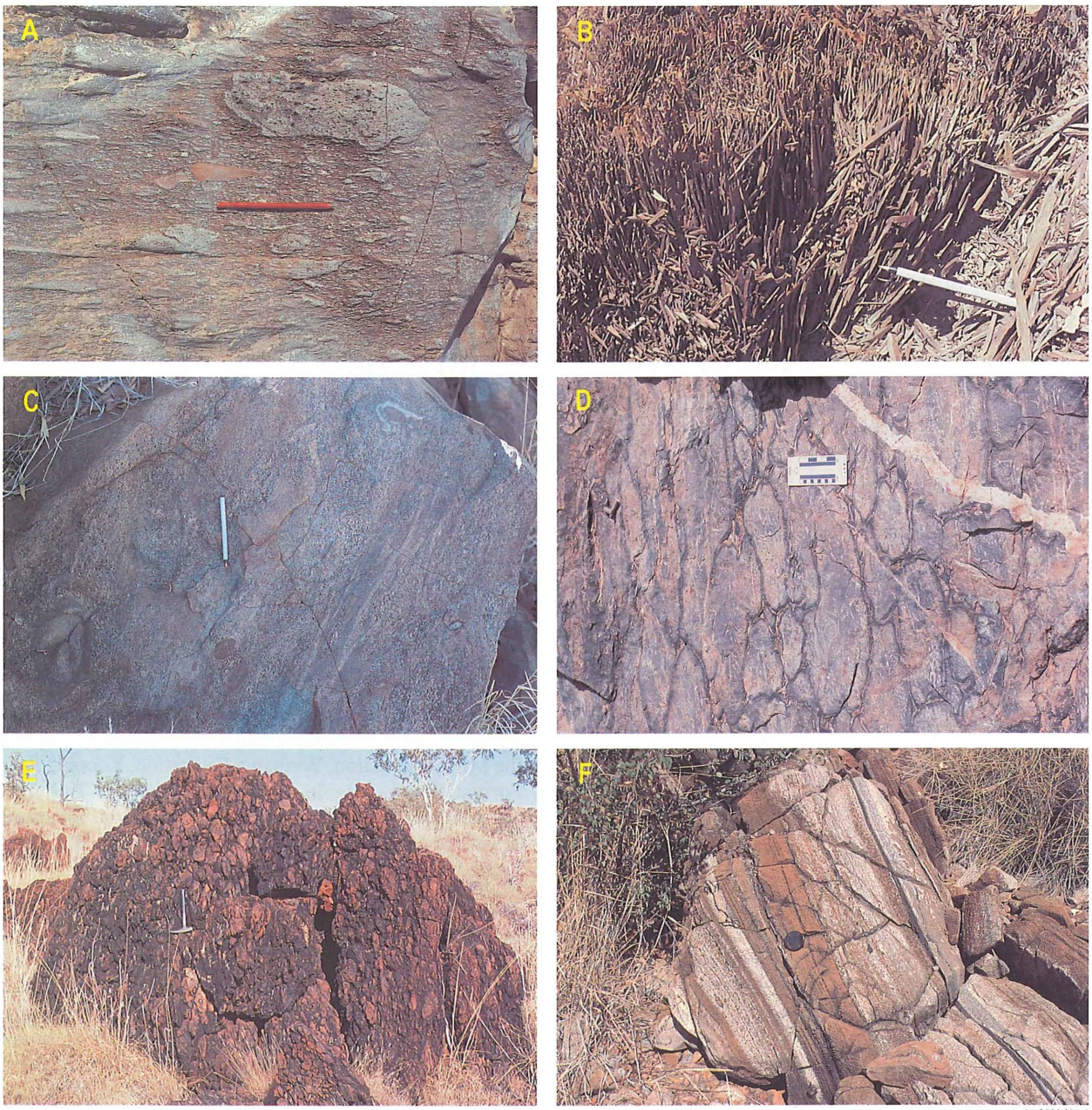


Figure 3.7. Metamorphosed sedimentary and volcanic rocks.

A. Fragmental volcanic rock of the Maude Headley Member, Olympio Formation, in the eastern zone of the HCO (McINTOSH AMG ~913152) (photograph by D.H. Blake).

B. Pencil slate in a fold closure in the Olympio Formation, in the eastern zone of the HCO (TURKEY CREEK AMG ~103704) (photograph by D.H.Blake).

C. Migmatitic hornfels (metasediment), Koongie Park Formation in the central zone of the HCO (McINTOSH AMG ~642103) (photograph by D.H.Blake).

D. Basaltic pillow lava cut by irregular vein of leucogranite in medium-grade Tickalara Metamorphics, in the central zone of the HCO (McINTOSH AMG ~937540) (photograph by I.M.Tyler).

E. Fragmental basalt in medium-grade Tickalara Metamorphics, in the central zone of the HCO (McINTOSH AMG ~830319) (photograph by I.M.Tyler).

F. Banded marble in medium to high-grade Tickalara Metamorphics, in the central zone of the HCO (TURKEY CREEK AMG ~031719) (photograph by I.M.Tyler).

phosed turbidites, carbonates, volcaniclastic rocks, black shale, chert, basalt, and rhyolite. Zircons from three samples of rhyolite indicate an age for the formation of ~1843 Ma (Page et al. 1994). This shows that the formation is younger than any dated rocks of the Tickalara Metamorphics in the central zone, younger than the ~1855 Ma felsic Whitewater Volcanics in the western zone of the HCO, and also younger than the youngest dated suite of detrital zircon, at ~1848 Ma, in turbidites of the Olympio Formation in the Halls Creek Group of the eastern zone. However, the rhyolite date is clearly older than a ~1835 Ma felsic volcanic rock in the Speewah Group of the Speewah Basin to the west. Possible correlatives of the Koongie Park Formation include some undated metavolcanic rocks mapped as Tickalara Metamorphics in the eastern part of the central zone to the north (see Chapter 5).

The Koongie Park Formation was tightly folded and regionally metamorphosed to greenschist facies before it was intruded by plutons of the Sally Downs supersuite of the Bow River Batholith, including the ~1827 Ma Loadstone Monzogranite, and by the group VI (~1830 Ma) Armanda layered mafic intrusion. Contact metamorphism of the Koongie Park Formation accompanied emplacement of the granitic and gabbroic intrusions, in places resulting in partial melting and the development of migmatitic rocks (Fig. 3.7C). The formation is of considerable interest to mineral exploration companies, as it hosts several volcanogenic massive sulphide deposits of Zn, Cu, and Pb (mainly in the Onedin Member: Orth 1997) that are currently subeconomic, and it is intruded in ANGELO by the **Angelo Microgranite**, host for subeconomic Cu mineralisation of possibly porphyry type. The Angelo Microgranite is a high-level intrusion, which may be comagmatic with felsic volcanic and subvolcanic rocks of the Koongie Park Formation.

The **Tickalara Metamorphics** are a complex unit of amphibolite and granulite facies metasedimentary and meta-igneous rocks confined to the basement of the central zone. These rocks are exposed mainly in McINTOSH, DIXON, MOUNT REMARKABLE, TURKEY CREEK, and BOW, but also occur to the south, in DOCKRELL. Rocks previously mapped as Tickalara Metamorphics in ANGELO (Griffin & Tyler 1994) are now regarded as part of the Koongie Park Formation (Griffin et al. 1998). If correct, this indicates that the Lamboo layered mafic–ultramafic intrusion in ANGELO intrudes the Koongie Park Formation, rather than the Tickalara Metamorphics, and is, therefore, considerably younger (<1843 Ma) than the otherwise similar Panton layered intrusion to the northeast, which is dated at ~1855 Ma.

The Tickalara Metamorphics have been deformed several times, and most, if not all, have undergone more than one phase of medium to high-grade metamorphism. Sedimentary protoliths include turbiditic interbedded mudstone, siltstone, and greywacke, together with quartz sandstone, carbonates (now marble and calc-silicate rocks), chert, and banded iron-formation. Igneous protoliths include mafic volcanics and mafic and felsic sheet-like intrusives; DHB believes that felsic volcanic rocks are also present. Mafic rocks in the Tickalara Metamorphics include those forming the Norton and Bow River intrusions, described by Hoatson in Chapters 2 and 5. In medium-grade areas, the sedimentary rocks preserve primary bedding features (Fig. 3.7F) and the mafic volcanic rocks show primary amygdaloidal, pillow (Fig. 3.7D) and fragmental textures (Fig. 3.7E). Sheppard et al. (1999) consider that the whole-rock geochemistry of the mafic volcanic rocks indicates an oceanic island arc/back arc basin or an ensialic marginal basin setting.

Detrital zircons from the metasedimentary rocks indicate a maximum depositional age of ~1865 Ma (Page et al. 1995b, Bodorkos et al. 1998). The oldest dated intrusion in the Tickalara Metamorphics, the recrystallised and locally gneissic **Rose Bore Granite**, was emplaced at ~1863 Ma, giving a minimum age for deposition and a maximum age for the earliest layer-parallel deformation (Tyler & Page 1996). The Rose Bore Granite and its country rocks are intruded by the group I ~1856 Ma Panton layered mafic–ultramafic body (see Chapter 6).

The regional metamorphic grade generally increases from southwest to northeast along the central zone (Gemuts 1971, Tyler & Page 1996). In the northeast, the Tickalara Metamorphics have been regionally metamorphosed under high temperature/low to moderate pressure granulite facies conditions—up to 875°C and 6 kb in Thornett (1981), 840°C and 5 kb in Thornett (1986), 800°C and 5 kb in Bodorkos et al. (1999). Here they consist predominantly of migmatitic pelitic gneisses, which display structures typical of large-scale in-situ anatexis and contain discontinuous layers, pods, and rafts of psammitic gneiss, mafic granulite, and calc-silicate rock (Gemuts 1971, Thornett 1986, Sheppard et al. 1997a, 1999). Metamorphic minerals present include cordierite, sillimanite, garnet, spinel, biotite, microcline, plagioclase, and quartz. Migmatisation near Warmun has been dated at ~1852 Ma (Page & Sun 1994). Prominent bands of granuloblastic mafic granulite, up to 300 m thick in this part of the area, and the thicker Norton and Bow River mafic bodies (see Chapters 2 and 5) may represent thick sills (Sheppard et al. 1997a). Some mafic intrusions were either emplaced before the migmatitic country rocks had completely solidified or they caused remobilisation of the migmatite (e.g. Blake & Hoatson 1993, Blake 1994, 1997b, Oliver & Barr 1997, Bodorkos et al. 1998, 1999, Oliver et al. 1998, also Figs 3.8A, 3.8B). Leucosomes containing zircon with overgrowths as young as ~1835 Ma suggest that temperatures remained elevated for 10 Ma (Oliver et al. 1998, Bodorkos et al. 1999) or longer.

In the central part of the central zone, the metamorphic grade is transitional between high and medium grade. Metamorphic minerals in migmatitic pelites include garnet, cordierite, sillimanite, biotite, plagioclase, and quartz (Plumb et al. 1985, Sheppard et al. 1997a). Those in amphibolites include green hornblende, clinopyroxene, garnet, plagioclase, and quartz.

To the southwest, metamorphic minerals in medium-grade pelitic schists include sillimanite, andalusite, garnet, staurolite, biotite, muscovite, plagioclase, and quartz (Plumb et al. 1985, Sheppard et al. 1997a). The

~1856 Ma Panton layered mafic–ultramafic intrusion in McINTOSH truncates large-scale folds and is in contact with both medium and high-grade country rocks, suggesting that deformation and regional metamorphism of the country rocks here predated this intrusion. Some of the deformation and metamorphism, though, might have accompanied emplacement of the Panton intrusion (Fig. 3.8F).

The Tickalara Metamorphics include sheet-like bodies of **Fletcher Creek Monzogranite** and tonalite, quartz diorite, trondhjemite, and gabbro of the Dougalls suite of Sheppard et al. (1997d) in the central part of the Dixon Range 1:250 000 Sheet area (Tyler et al. 1998c). The Fletcher Creek Monzogranite and the **Dougalls Tonalite** of the Dougalls suite have been dated at ~1850 Ma (Tyler & Page 1996). Blake considers that at least part of the Fletcher Creek Monzogranite is a metamorphosed felsic volcanic rock (Blake 1994, Fig. 3.8C), even though intrusive relationships (e.g. Fig. 3.8D) and a contact aureole have been reported by Bodorkos et al. (1999). The Dougalls suite includes intrusions of variably deformed and metamorphosed quartz diorite and dolerite/gabbro, which are veined by tonalite and trondhjemite, and also locally abundant inclusions of metasedimentary country rocks (Fig. 3.9A). In areas of low strain, the relationship between the melanocratic and leucocratic phases in intrusions of the Dougalls suite is consistent with mingling of mafic and felsic magmas, like that described by Blake & Hoatson (1993) and Sheppard (1996). The geochemistry of the Dougalls suite (Sheppard et al. 1995, 1997b) is similar to that of Phanerozoic tonalite–trondhjemite suites in island arcs and convergent continental margin settings (Sheppard et al. 1997d).

All the intrusions of the Tickalara Metamorphics are metamorphosed and display a prominent tectonic fabric. Those in the central part of the central zone show a peak regional metamorphism dated at ~1845 Ma by Bodorkos et al. (1999).

The high temperature/low to medium pressure nature of the regional metamorphism of the Tickalara Metamorphics is consistent with the addition of heat into the crust by large-scale magmatism. A major gravity high that underlies the northeastern part of the central zone may be a result of this magmatism (Hancock & Rutland 1984, see Chapter 4). Thornett (1986) attributed heating to mantle upwelling associated with rifting in an intracratonic setting, whereas Tyler & Page (1996) suggested that the metamorphism might reflect igneous underplating at an active plate margin. The apparent diachronous nature of peak regional metamorphism (Tyler & Page 1996), which ranges from pre or syn 1856 Ma to ~1845 Ma, may reflect local prolonging of elevated temperatures by repeated intrusions of mafic magma (cf. Huppert & Sparks 1988).

Restricted, very low to low pressure/medium to high temperature contact aureoles are present around layered mafic–ultramafic intrusions and post-1835 Ma granite plutons throughout the Tickalara Metamorphics outcrop area. The aureoles overprint the regional metamorphic mineral assemblages and associated tectonic structures (Thornett 1986, Tyler & Page 1996, Sheppard et al. 1997a, 1999), and are characterised by the occurrence of andalusite–cordierite–K-feldspar±spinel assemblages and chaotic migmatitic hornfels. Metamorphic zircon from chaotic migmatitic hornfels (Fig. 3.9B) in the contact aureole of the McIntosh intrusion has been interpreted as recording the age of this intrusion at ~1830 Ma (see Chapter 6 and Page et al. 1995b).

1835-1805 Ma granite and gabbro

The basement rocks in the central zone are intruded by post-1835 Ma granite and gabbro plutons of the Sally Downs supersuite of the Bow River Batholith, layered mafic intrusions of groups VI and VII, and bodies of Corridor gabbro and Turkey Creek microgabbro–norite. The ~1832 Ma **Mabel Downs Tonalite** and the ~1820 Ma component of the **Mount Christine Granitoid** of the Bow River Batholith have been pervasively foliated and metamorphosed under amphibolite facies conditions. Other dated post-1835 Ma intrusions are the McIntosh layered mafic intrusion at 1830 Ma, the **Loadstone Monzogranite** and **McHale Granodiorite**, both at ~1827 Ma, the **Sally Downs Tonalite** and **Copperhead Albitite 'Carbonatite' Complex** at ~1820 Ma, the younger component of the Mount Christine Granitoid at ~1808 Ma, and the **Eastmans Granite** at ~1805 Ma. The ages of many other 'young' granitic and gabbroic intrusions in the central zone that have not been dated can be expected to range between 1835 and 1805 Ma.

Layered mafic–ultramafic intrusions

The central zone of the HCO contains most of the layered mafic–ultramafic intrusions of the East Kimberley. Those of groups I, IV, and V, and the Norton and Bow River mafic intrusions in the north, are older than 1835 Ma and, hence, are part of the basement. The intrusions were emplaced at depths estimated at about 8–23 km, the deepest being those of group V, typified by the ~1845 Ma Sally Malay intrusion (see Chapter 9). Country rocks include the Tickalara Metamorphics, Koongie Park Formation, and also previously emplaced mafic–ultramafic intrusions. The ~1830 Ma McIntosh intrusion of group VI, for example, intrudes Tickalara Metamorphics and gabbro of the group IV Wild Dog Creek intrusions. The presence of laterally extensive rhythmic layering in many of the mafic–ultramafic intrusions implies relatively stable crustal conditions during their emplacement, whether this was before or after the ~1835 Ma deformation of the Halls Creek Orogeny (Blake 1997b).

Other rocks younger than ~1835 Ma

In the southern part of the central zone, in ANGELO and HALLS CREEK, the 1843 Ma Koongie Park Formation is overlain unconformably by clastic sedimentary rocks of the **Moola Bulla Formation** and, together with granitic rocks of the Sally Downs supersuite, by sandstone and basalt of the ~1800 Ma **Kimberley Group**. In TURKEY CREEK, to the north, the Kimberley Group of Blake (1997a) and similar rocks of the **Red Rock Formation** and **Texas Downs Formation** of Tyler et al. (1997b) lie unconformably on the Winnama Formation, gabbro, and ~1827 Ma McHale Granodiorite and are

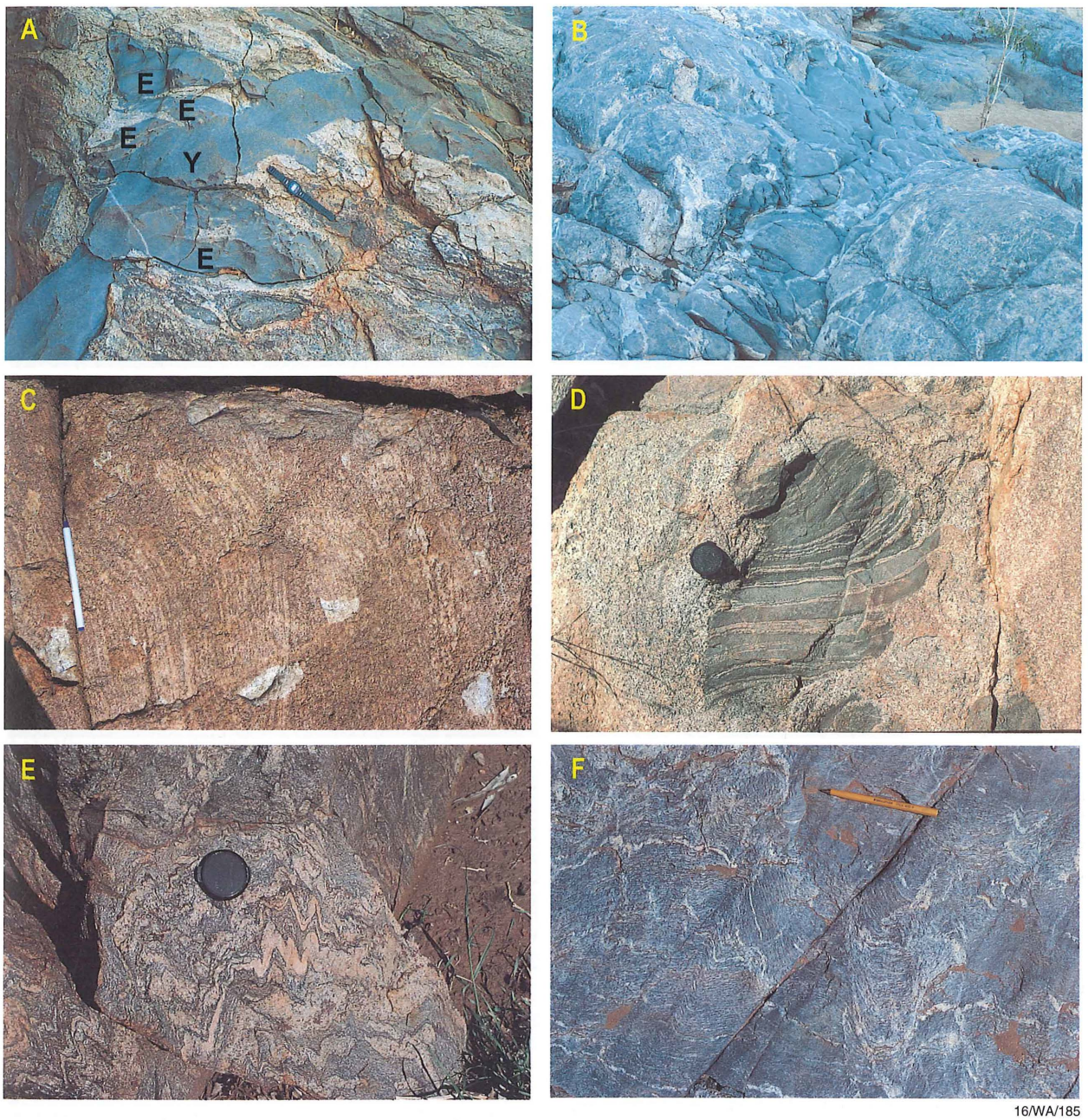


Figure 3.8. Metamorphosed sedimentary and igneous rocks.

A Migmatitic metasediments of the Tickalara Metamorphics and irregular mafic dykes of synplutonic type that were intruded before the migmatite had solidified (according to DHB), west of Warmun in the central zone of the HCO (TURKEY CREEK AMG ~146168). The youngest dyke (Y) cuts what DHB considers to be earlier dismembered dykes (E). The last rock to crystallise was the leucogranite vein (photograph by D.H.Blake).

B. 'Pillowed' mafic dyke intruding remobilised migmatitic pelitic gneiss of the Tickalara Metamorphics in the central zone of the HCO (TURKEY CREEK AMG ~937865) (photograph by I.M.Tyler).

C. Finely banded Fletcher Creek Monzogranite (a metarhyolite, according to DHB), dated at ~1850 Ma, in the central zone of the HCO (McINTOSH AMG ~944643) (photograph by D.H.Blake).

D. Inclusion of Dougalls suite amphibolite, veined by tonalite, in garnet-bearing Fletcher Creek Monzogranite in the central zone of the HCO (DIXON AMG ~942637) (photograph by I.M.Tyler).

E. Tightly folded pelitic migmatite in medium- to high-grade Tickalara Metamorphics in the central zone of the HCO (McINTOSH AMG ~972687) (photograph by I.M.Tyler).

F. Migmatitic Tickalara Metamorphics exposed in the Panton River on the southeastern side of the Panton mafic–ultramafic layered intrusion, in the central zone of the HCO (McINTOSH AMG ~750317). The protoliths were either ~1863 Ma Rose Bore Granite (favoured by IMT) or sedimentary rocks intruded by this granite (favoured by DHB), and were metamorphosed to migmatite either before (IMT) or during (DHB) emplacement of the Panton intrusion (photograph by D.H.Blake).



Figure 3.9. Migmatitic and igneous rocks.

A. Heterogeneous Dougalls Tonalite in the central zone of the HCO (DIXON AMG ~948630). Igneous zircon from this site has been dated at ~1848 Ma (photograph by D.H.Blake).

B. Chaotic metasedimentary migmatite, Tickalara Metamorphics, at the margin of the McIntosh layered mafic intrusion in the central zone of the HCO (McINTOSH AMG ~845477). Leucosomes in the migmatite contain two main populations of zircon, one dated at ~1830 Ma, which is presumed to be the emplacement age of the layered intrusion, and the other, interpreted as detrital, at ~1865 Ma (Page et al. 1995b, and Chapter 6) (photograph by D.H.Blake).

C. Net-veined complex formed where three adjacent mafic dykes, one of which contains feldspar phenocrysts, have been intruded into partly molten granite of the Paperbark supersuite, Bow River Batholith, in the western zone of the HCO (MOUNT REMARKABLE AMG ~646918) (photograph by D.H.Blake).

D. Mafic pillows in granite of the Sally Downs supersuite at a net-veined complex west of Halls Creek, in the central zone of the HCO (HALLS CREEK AMG ~550890) (photograph by D.H.Blake).

E. Sally Downs Tonalite of the Sally Downs supersuite, with mafic inclusion, Bow River Batholith, in the central zone of the HCO (McINTOSH AMG ~880630. The tonalite here is dated at ~1821 Ma (photograph by D.H.Blake).

F. Densely porphyritic Paperbark Granite of the Paperbark supersuite, Bow River Batholith, in the western zone of the HCO (McINTOSH AMG ~488453). The granite at this site is dated at ~1854 Ma (photograph by D.H.Blake).

overlain unconformably by the ?Mesoproterozoic **Mount Parker Sandstone** and **Bungle Bungle Dolomite** of the Osmond Basin succession. Farther north, this succession and older rocks are overlain by ?Mesoproterozoic, Neoproterozoic, and Palaeozoic rocks of the Victoria River, Wolfe, and Ord Basins (Thorne et al. 1998). In the southwest, the Palaeoproterozoic rocks of the central zone are overlain by the Neoproterozoic **Louisa Downs Group,** early Cambrian **Antrim Plateau Volcanics** and Palaeozoic sedimentary rocks of the Canning Basin sequence (Tyler et al. 1998a).

Western zone of the Halls Creek Orogen

This zone of the HCO merges westwards with the Kimberley Craton and the west-northwest-trending King Leopold Orogen of the West Kimberley (Tyler et al. 1995). As well as basement (older than ~1835 Ma), which correlates with the Hooper Complex of the King Leopold Orogen, it includes the overlying Speewah and Kimberley Groups, granites of the post-1835 Ma Sally Downs supersuite of the Bow River Batholith, the Black Hills Yard (group VII) and Salt Lick layered intrusions (see Chapters 2 and 5), and, in the southwest, Neoproterozoic and Palaeozoic units.

Pre-1835 Ma basement

The basement is represented by the ~1870 Ma Marboo Formation (Griffin et al. 1993, Tyler et al. 1999) and probably correlative Amherst Metamorphics (Griffin et al. 1998), the ~1855 Ma Whitewater Volcanics and comagmatic high-level porphyry intrusions, the 1865–1850 Ma granitic plutons of the Bow River Batholith (Paperbark supersuite of Sheppard et al. 1997a), ~1855 Ma layered mafic–ultramafic intrusions of groups II and III, and, possibly, the mafic intrusions assigned to the Corridor gabbro (see Chapter 5). The Corridor gabbro intrusions commonly form spectacular net-veined complexes with granite at their contacts with plutons of the Paperbark supersuite. This indicates, according to DHB, that these mafic bodies were probably intruded after the adjacent granite plutons had been emplaced (see section on Bow River Batholith below) and, hence, could range in age from ~1860 Ma to younger than 1835 Ma.

The **Marboo Formation** consists of turbiditic mudstone, siltstone, greywacke, and quartz wacke, which were probably deposited as part of a submarine fan system (Hancock 1991, Griffin et al. 1993, Tyler et al. 1999). Ages of detrital zircons indicate that sedimentation took place after ~1872 Ma, and that some detritus was derived from latest Archaean to early Palaeoproterozoic sources (Tyler et al. 1999). In the Lansdowne 1:250 000 Sheet area, Hancock (1991) recorded palaeocurrent data that indicate a depositional slope from the north and northeast, and also recognised downward-facing structures that suggest the presence of early recumbent folds. These recumbent folds represent the first phase of deformation and accompanying greenschist facies metamorphism of the Hooper Orogeny. This phase predates the emplacement of the earliest granite plutons of the Paperbark supersuite at ~1865 Ma (Page & Sun 1994). Upright folding between 1865 and 1850 Ma, during a later phase of the Hooper Orogeny, affected the Marboo Formation and also the ~1855 Ma Whitewater Volcanics near Lake Argyle in the HCO (Thorne et al. 1999). The Marboo Formation has been metamorphosed at medium- to high-grade in contact aureoles of granite plutons and, in places, has become migmatitic (e.g. Griffin et al. 1998).

The **Amherst Metamorphics** in ANGELO consist of medium to high-grade, locally migmatitic, paragneiss and orthogneiss. These gneisses have been interpreted as Marboo Formation and intrusive granitic rocks of the Paperbark supersuite that were metamorphosed under low pressure/medium to high temperature conditions between 1860 and 1805 Ma (Griffin et al. 1998), the possible heat source being a large mafic intrusion at depth.

The felsic **Whitewater Volcanics**, dated at ~1855 Ma, lie unconformably on folded Marboo Formation and are overlain unconformably by the ~1835 Ma Speewah Group (e.g. Thorne et al. 1999). The volcanics are intruded by comagmatic **Castlereagh Hill Porphyry**, ~1855 Ma **Greenvale Porphyry,** and granites of the Paperbark supersuite. They have not been tightly folded nor much metamorphosed in the western zone west of the Greenvale and Dunham Faults, unlike near Lake Argyle to the east and in the King Leopold Orogen of the West Kimberley. Porphyritic dacitic to rhyolitic ignimbrites predominate over lava flows in the Whitewater Volcanics, indicating that the volcanism was probably subaerial.

The **layered mafic intrusions of groups II and III**, typified by the Springvale and Toby intrusions, respectively, are similar in age to the Whitewater Volcanics and comagmatic felsic intrusions in the western zone, and also to the Panton layered mafic–ultramafic intrusion in the central zone, all of which have been dated at ~1855 Ma. The Springvale and Toby intrusions were emplaced at depths of 8–18 km (see Chapter 9), intruding the Marboo Formation and granites of the Paperbark supersuite east of the Greenvale Fault (Fig. 3.3). This fault separates them from Whitewater Volcanics to the west. Although they predate the Halls Creek Orogeny and, hence, are part of the basement, the layered intrusions of groups II and III appear to be much less deformed than the coeval group I layered intrusions in the basement of the central zone; however, they may be metamorphosed to amphibolite facies (see Chapter 5), like the group I intrusions. The presence of layered intrusions of similar age in the western zone and adjacent part of the central zone of the HCO may be significant, as it favours the possibility, according to DHB, that these two zones were relatively close together when the intrusions were emplaced.

Rocks younger than ~1835 Ma

Palaeoproterozoic rocks younger than ~1835 Ma include granitic and gabbroic rocks of the 1835–1805 Ma Sally Downs supersuite of the Bow River Batholith, which extends into the western zone from the central zone of

the HCO, the Speewah and Kimberley Groups, the Revolver Creek Formation, the Hart Dolerite, and, possibly, some intrusions of Corridor gabbro. These predate the Mesoproterozoic Carr Boyd and Bastian Groups in the north of the western zone and the Mesoproterozoic Crowhurst Group in the southwest (Tyler et al. 1998a).

The **Speewah Group** was deposited in the Speewah Basin, which extends eastwards from the Kimberley Craton into the western zone of the HCO as far as the Greenvale and Dunham Faults (Fig. 3.2). The group is made up mainly of fluvial to shallow marine sandstone and siltstone, but includes some felsic volcanics (in the Valentine Siltstone) dated at ~1835 Ma, indicating that the group is about 20 Ma younger than the underlying Whitewater Volcanics. Palaeocurrent directions determined from cross bedding in the Speewah Group indicate transport from the northeast and east (Gellatly et al. 1970, Plumb et al. 1981). The Speewah Group is overlain disconformably or with a very low-angle unconformity by the ~1800 Ma **Kimberley Group** (Griffin et al. 1993), which consists of sandstone, siltstone, and a formation of basaltic lavas (Carson Volcanics) laid down in the Kimberley Basin. Both groups have maximum thickness of at least 2000 m and both are intruded by sills of **Hart Dolerite**, one of which has been dated at ~1790 Ma. The Kimberley Group, but not the Speewah Group, extends eastwards into the central zone of the HCO and, according to Blake (1997a), also into the eastern zone. Cross bedding in sandstone of the Kimberley Group indicates palaeocurrents from the north and northwest (Gellatly et al. 1970, Plumb & Gemuts 1976). The palaeocurrent measurements indicate that although some detritus in the Speewah Group may have come from the HCO, the detritus in Kimberley Group was derived from outside the present confines of the HCO.

The **Revolver Creek Formation**, a possible correlative of the Kimberley Group, lies unconformably on the Marboo Formation, Whitewater Volcanics, and granite of the Paperbark supersuite in the north, to the east of the Dunham Fault in the Lissadell 1:250 000 Sheet area. It consists of feldspathic sandstone, siltstone, conglomerate, and basaltic volcanic rocks, and was laid down in a fluvial to deltaic environment (Thorne et al. 1999). The formation is overlain by the Mesoproterozoic (~1200 Ma) **Carr Boyd Group**.

In the north, the Palaeoproterozoic and Mesoproterozoic rocks of the western zone are overlain by the Palaeozoic Bonaparte Basin succession (Thorne et al. 1998). In the southwest they are overlain by Neoproterozoic sedimentary rocks laid down in the Louisa Basin, by early Cambrian basalt and conglomerate, and by younger Palaeozoic sedimentary rocks of the Canning Basin succession.

Bow River Batholith

The Bow River Batholith in the HCO is made up of granite and subordinate gabbro intrusions assigned to the Paperbark and Sally Downs supersuites (Sheppard et al. 1997b). The granites, mainly unfractionated I-types, commonly contain abundant country rock xenoliths and mafic enclaves. Net-veined complexes of intimately mixed granitic, gabbroic, and hybrid dioritic rocks (Figs 3.9C, 3.9D) are common, especially in contact zones between granite and gabbro intrusions. These complexes indicate either contemporaneous emplacement of granitic and mafic magmas (Sheppard 1996) or intrusion of mafic magma into previously emplaced granite that had not completely crystallised or had been melted by the intruding mafic magma (e.g. Blake & Hoatson 1993). No granite plutons of the batholith show marked compositional zoning and none are known to host economically important mineral deposits. Pegmatite and aplite veins are common, but no greisens have been reported. The intrusive rocks range from strongly foliated and recrystallised, especially near major faults, to apparently undeformed, although all the granites contain strained and partly recrystallised quartz. Adjacent country rocks are contact metamorphosed to hornfels and, where some partial melting has taken place, to migmatite (Fig. 3.7C).

Several gabbro bodies regarded as layered intrusions by Hoatson (see Chapter 5) are shown as part of the Bow River Batholith on the recently published geological maps of McINTOSH, MOUNT REMARKABLE, and TURKEY CREEK. They include the Toby intrusion of group III, where Hoatson has recognised large-scale concentric lineaments and rare compositional layering, and Wild Dog Creek intrusions of group IV, which in places show a well-developed igneous lamination.

The granite plutons of the **Paperbark supersuite** in the HCO are confined to the western zone. Those isotopically dated range in age from ~1860 Ma to ~1850 Ma, indicating that they are coeval with the layered intrusions of groups II and III in this zone and group I in the central zone, and are part of the pre ~1835 Ma basement. The plutons intrude previously folded and metamorphosed Marboo Formation and also the comagmatic Whitewater Volcanics, Greenvale Porphyry, and Castlereagh Hill Porphyry. The main granitic rock types present are monzogranite, syenogranite, and granodiorite containing K-feldspar phenocrysts (Fig. 3.9F); tonalite is less common. Biotite is the dominant ferromagnesian mineral and hornblende is present in only a few plutons (Sheppard et al. 1995). Like most other Palaeoproterozoic granites of Australia, those of the Paperbark supersuite have high K_2O, Rb, Y, Th, and K_2O/Na_2O contents and low Sr, Sr/Y, and K/Rb values (Sheppard et al. 1995, 1997d, Wyborn 1988, and Chapter 10).

The Paperbark supersuite includes the granite plutons of the Hooper Complex in the King Leopold Orogen of the West Kimberley (Sheppard et al. 1997b). These plutons range in age from about 1865 Ma to 1850 Ma and they intrude comagmatic felsic extrusives of the Whitewater Volcanics, which are folded and metamorphosed. Here and also in the north of the HCO (Sheppard et al. 1999), granitic plutonism, felsic volcanism, folding and metamorphism took place together.

Plutons of the ~1835–1805 Ma **Sally Downs supersuite** are concentrated in the central zone of the HCO, where they intrude the Tickalara Metamorphics, Winnama

Formation, and Koongie Park Formation. Some plutons extend into the western zone, mainly in MOUNT REMARKABLE and ANGELO, where they intrude the Marboo Formation and granite of the Paperbark supersuite, and into the eastern zone in DOCKRELL, where they intrude the Halls Creek Group. Three suites have been recognised in the supersuite (Sheppard et al. 1997d). These are the Kevins Dam suite, the most voluminous, which consists of even-grained and porphyritic biotite monzogranite and syenogranite; the relatively mafic Mabel Downs suite, consisting mainly of porphyritic hornblende-biotite tonalite and granodiorite; and the Syenite Camp suite of even-grained, porphyritic and weakly porphyritic biotite granodiorite and tonalite, subordinate biotite monzogranite, and minor hornblende-bearing granodiorite and monzogranite. The main pluton of the Mabel Downs suite, formed of Mabel Downs Tonalite, is a north-northeasterly trending body extending northwards from the Ord River for about 80 km, between the Great Northern Highway and the Halls Creek Fault to the east. The pluton, dated at ~1832 Ma, has a pervasive foliation, which almost everywhere dips steeply to the west, and is considered by Bodorkos et al. (1998) to have been emplaced contemporaneously with deformation under mid-amphibolite facies conditions. The foliation is cut by veins of pegmatitic to aplitic leucogranite, one of which has been dated at ~1821 Ma. This is the same age as the Sally Downs Tonalite (Fig. 3.9E) to the south, which is also part of the Mabel Downs suite.

According to Sheppard et al. (1997d), the granites of the Kevins Dam suite of the Sally Downs supersuite are geochemically indistinguishable from those of the Paperbark supersuite. Those of the Mabel Downs suite (Mabel Downs Tonalite, Sally Downs Tonalite, and McHale Granodiorite) are characterised by high Al_2O_3, Na_2O, and Sr, and low Y and Yb values, and in these respects they resemble Archaean high-Al tonalite–trondhjemite–granodiorite suites and their Phanerozoic equivalents. Granites in the Syenite Camp suite have major and trace-element abundances similar to those of the Coastal Batholith of Peru.

Orogenic events

The earliest period of orogenesis recorded in the HCO took place between ~1872 and 1850 Ma, mainly in the western zone of the HCO, following deposition of the Marboo Formation. It involved deformation, metamorphism, and magmatism and is attributed to the **Hooper Orogeny** recognised in the King Leopold Orogen of the West Kimberley (Griffin et al. 1993, Page & Sun 1994, Tyler & Page 1996). The main deformation event of this orogeny in the western zone of the HCO postdated deposition of the ~1870 Ma Marboo Formation and predated emplacement of the ~1855 Ma Springvale (group II) and Toby (group III) layered mafic intrusions. Deformation and metamorphism in the central zone between ~1863 and ~1856 Ma, the emplacement ages of the Rose Bore Granite and Panton layered intrusion, respectively, may also be related to the Hooper Orogeny. That affecting the Tickalara Metamorphics between ~1850 and 1845 Ma in the central zone does not appear to have any equivalents in the western or eastern zones.

The oldest orogenic event recorded in the eastern zone of the HCO was the main deformation phase of the **Halls Creek Orogeny** at around 1835 Ma. During this phase the ~1910 Ma Ding Dong Downs Volcanics, the overlying ~1880–1845 Ma Halls Creek Group, and sills of Woodward Dolerite were tightly folded about moderately inclined to upright axial planes trending north-northeast, and were metamorphosed to mainly greenschist facies. The folding, which may be part of an easterly verging fold and thrust system, and associated pervasive axial planar cleavage were preceded in places by a bedding-parallel foliation, possibly related to low-angle extensional faults (Warren 1994a). The main deformation took place before the emplacement of the Mount Christine Granitoid, dated at ~1820 Ma and ~1810 Ma, which extends into the eastern zone from the central zone in DOCKRELL.

A comparable phase of folding and greenschist facies metamorphism in the central zone of the HCO affected the Milba, Winnama, and ~1843 Ma Koongie Park Formations of the basement and predated emplacement of the ~1827 Ma Loadstone Monzogranite and McHale Granodiorite. This phase is attributed to the ~1835 Ma deformation of the Halls Creek Orogeny (Tyler & Page 1996, Blake et al. 1999a). Its effects included the amphibolite-facies metamorphism and pervasive foliation in the ~1832 Ma Mabel Downs Tonalite and comparable metamorphism and deformation in the Tickalara Metamorphics.

In the western zone of the HCO, there is no evidence of regional folding at ~1835 Ma, when the main deformation of the Halls Creek Orogeny was taking place in the central and eastern zones. Extension, though, may have occurred in the north of this zone, contemporaneously with deposition of the ~1835 Ma Speewah Group in the Speewah Basin. No regional folding or metamorphic events other than minor tilting separate the ~1855 Ma Whitewater Volcanics from the overlying ~1835 Ma Speewah Group or the Speewah Group from the overlying ~1800 Ma Kimberley Group.

Tyler et al. (1995) and Sheppard et al. (1997a,d, 1999) attribute the Hooper Orogeny in the King Leopold Orogen and the western zone of the HCO, including the 1865–1850 Ma felsic magmatism of the Paperbark supersuite, to the coming together of the basement in this zone, on the eastern margin of a Kimberley Craton continent, with an oceanic island arc to the east, represented by the Tickalara Metamorphics of the central zone. Similarly, they attribute the Halls Creek Orogeny and post-1835 Ma felsic magmatism to a northwestward directed collision at ~1835 Ma of the eastern zone of the HCO, on the western margin of the North Australian Craton, with the central zone now on the eastern margin of the Kimberley Craton. Sheppard et al (1999) consider that much of the 1910–1790 Ma magmatism in the HCO can be related to subduction associated with the continent collision. In summary, this interpretation involves the accretion of an island arc onto a continental margin to the west, and subsequent northwestward

subduction of oceanic crust during collision of two continental masses that were previously widely separated. Support is given by the suggestion of Gunn & Meixner (1998) that a linear zone of dense, magnetic, northwesterly dipping material under the southeastern edge of the Kimberley craton could be due to 'ophiolitic' material associated with a subduction process.

An alternative interpretation is that the Hooper and Halls Creek Orogenies and Palaeoproterozoic magmatism in the Halls Creek Orogen took place in an intracratonic setting and were essentially ensialic (e.g. Etheridge et al. 1987, Wyborn 1988, and Chapter 10). Underplating of mafic magma at the base of the crust below the HCO, perhaps as a result of small-scale mantle convection, caused heating and melting of the lower crust and crustal extension and thinning. This led to bimodal magmatism (cf. Huppert & Sparks 1988) and magma mingling, and also to basin formation, but not to significant ocean-floor spreading or generation of oceanic crust. Cooling of the underplated magma triggered crust–mantle delamination, providing driving force for two compressional orogenies: the older, the Hooper Orogeny, which has mainly west-northwesterly trending structures in the King Leopold Orogen, and the younger, the Halls Creek Orogeny, dominated by north-northeasterly trending structures in the HCO to the east.

In another interpretation, Shaw et al. (Chapter 4) consider that the geophysical data for the East Kimberley can be explained by the HCO representing a major crustal boundary and also a lithospheric plate boundary between about 1860 and 1800 Ma. They suggest that a major elongate gravity high within the HCO could be the result of repeated emplacement of mafic–ultramafic intrusions into dilational pockets formed during complex transcurrent movements along the length of the orogen. They also suggest that transcurrent movements, both transtensional and transpressional, could explain many other tectonic features of the HCO.

Deciding which one of these or other possible interpretations of the tectonic setting of the East Kimberley between ~1910 and ~1800 Ma is the most likely requires more research. It depends, for example, on finding further evidence for or against subduction of oceanic crust during this period and on determining the effects of strike-slip faulting both before and after 1800 Ma.

Several folding and faulting events postdate the ~1835 Ma deformation of the Halls Creek Orogeny. Most of these can be attributed to the Yampi Orogeny, which took place at around 1000 Ma (Thorne & Tyler 1996), the King Leopold Orogeny at ~560 Ma (Shaw et al. 1992a), and the main phase of the Alice Springs Orogeny at ~300 Ma (Shaw et al. 1992b). An exception is a folding event between 1830 and 1805 Ma that affected the Tickalara Metamorphics and may have caused tilting of the Moola Bulla Formation prior to deposition of the Kimberley Group and correlatives. This event represents a late stage of the Halls Creek Orogeny (Tyler & Page 1996).

The major strike-slip fault system of the HCO is thought to have been initiated during the **Yampi Orogeny**, with some of these faults being reactivated Palaeoproterozoic terrane boundaries (Tyler et al. 1995). The strike-slip faulting postdates deposition of the ~1200 Ma Carr Boyd Group (Thorne & Tyler 1996). Other structures which may be attributed to the Yampi Orogeny include a major northwest-trending, tight syncline of Kimberley Group rocks near Halls Creek and the doubly plunging Sophie Downs Dome, Brim Anticline, Saunders Creek Dome, and Castle Creek Anticline to the east (Blake et al. 1999a). Folding of the Kimberley Group on Mount Barrett, west of Halls Creek, may be of Yampi Orogeny age or younger. Folding, tilting, and thrusting of the Kimberley Group (the Red Rock Formation and Texas Downs Formation of Tyler et al. 1997b) reported by Blake (1997a) in TURKEY CREEK predates the Mount Parker Sandstone and Bungle Bungle Dolomite of the ?Mesoproterozoic Osmond Basin sequence, so are probably older than the Yampi Orogeny.

Tight to very gentle refolding of folds formed during the Halls Creek Orogeny and Yampi Orogeny, folding and faulting (including thrusting) in the Neoproterozoic Wolfe Basin, and reactivation of the major strike-slip fault system of the HCO may have taken place during the **King Leopold Orogeny** and/or the **Alice Springs Orogeny.** Folding and most faulting and tilting of the Palaeozoic Ord Basin sequence in the east is attributed to the Alice Springs Orogeny. Strike-slip faulting that controlled late Devonian sedimentation in the northern part of the HCO may reflect an early phase of this orogeny (Thorne & Tyler 1996). Faulting and tilting of Miocene sediments at White Mountain, east of the Bungle Bungle Range (e.g. Blake 1996a), indicate that there has also been tectonism during the Cainozoic in the East Kimberley.

Regional correlations

Correlations of stratigraphic and intrusive units in the HCO and between the HCO and nearby regions are shown diagrammatically in Figure 3.10 (see also Table 3.2).

The oldest rocks exposed in the HCO, the ~1910 Ma Ding Dong Downs Volcanics and Junda Microgranite in the eastern zone, are older than any rocks known in the King Leopold Orogen to the west, but may have some correlatives in the Tanami Complex of The Granites–Tanami region to the southeast (at Tanami, RWP unpublished data). The lower part of the overlying Halls Creek Group (the Saunders Creek Formation and ~1880 Ma Biscay Formation) may be older than any units exposed in the central and western zones of the HCO, although the Milba and Winnama Formations in the central zone cannot be discounted as possible correlatives.

Turbidites of several different ages are present in the pre-1835 Ma basement of all three zones of the HCO. Those of the Marboo Formation in the western zone are older than ~1865 Ma, as they are intruded by granite of this age in the King Leopold Orogen, but are not much older, as they contain detrital zircon dated at ~1870 Ma (Tyler et al. 1999). They are probably older than turbidites containing ~1865 Ma detrital zircon in the Tickalara Metamorphics, and are certainly older than turbidites

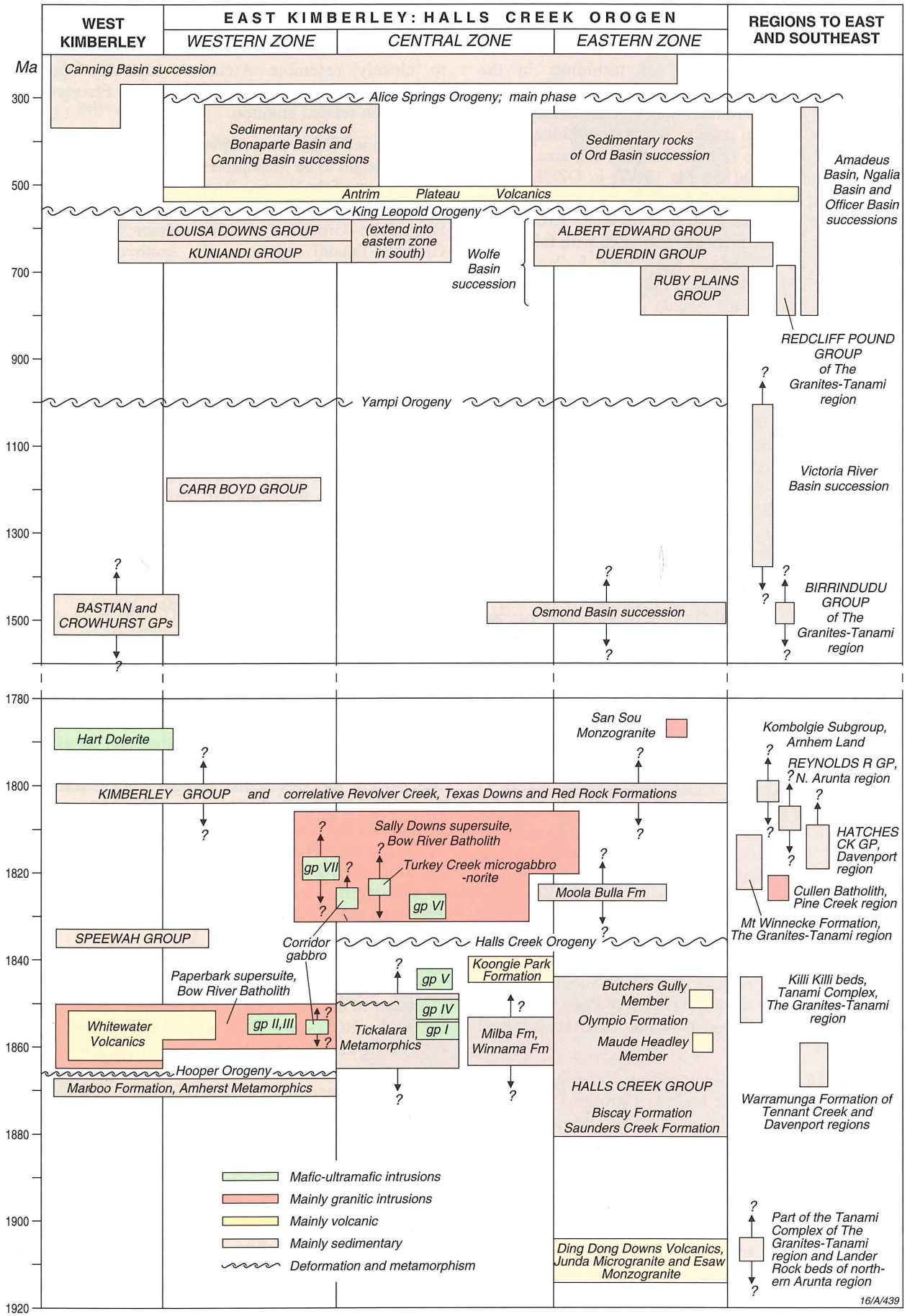


Figure 3.10. Correlation diagram for the Halls Creek Orogen and nearby regions.

interlayered with ~1843 Ma felsic volcanics in the Koongie Park Formation in the central zone. Turbidites in the Milba and Winnama Formations in the central zone could be correlatives of turbidites in the ~1860–1845 Ma Olympio Formation of the eastern zone. The Olympio turbidites may extend southeast into The Granites–Tanami region, where a turbidite in the Killi Killi beds of the Tanami Complex contains detrital zircon as young as ~1850 Ma (RWP, in OZCHRON). They appear to be younger than turbidites in the Warramunga Formation of the Tennant Creek and Davenport regions, which are associated with felsic volcanics dated at ~1870-1860 Ma (Blake & Page 1988, Compston 1995). Turbidites in the Lander Rock beds in the northern part of the Arunta region are somewhat older, as they predate a major deformation dated at ~1880 Ma (Young et al. 1995). The Olympio Formation is the only one of these turbiditic units that also contains some alkaline volcanic rocks.

U–Pb zircon geochronology shows that the ~1843 Ma Koongie Park Formation in the central zone of the HCO, previously assigned on lithological evidence to the Biscay Formation and Olympio Formation of the Halls Creek Group in the eastern zone, is younger than this group, and has no correlatives in either the eastern or western zone. The volcanics in the Koongie Park Formation are younger those of the ~1855 Ma Whitewater Volcanics in the western zone and those of the Halls Creek Group in the eastern zone, and they are older than ~1835 Ma felsic volcanics in the Speewah Group to the northwest.

The Moola Bulla Formation in the central and eastern zones is a possible correlative of the Speewah Group. However, it was probably deposited in a separate sedimentary basin, and is more likely to be a younger unit.

The Kimberley Group, which extends into the HCO from the Kimberley Craton to the west, and the probably correlative Red Rock, Texas Downs, and Revolver Creek Formations, all characterised by quartz-rich sandstone and interlayered basaltic lava, are similar in lithology and age constraints (younger than 1827 Ma and older than 1790 Ma) to extensive stratigraphic units in the Northern Territory. These possible correlatives include the lower part of the Kombolgie Subgroup in Arnhem Land (Sweet et al. 1999), the Wauchope Subgroup in the Davenport region to the south (Blake & Page 1988), and the Reynolds Range Group in the northern Arunta region (Young et al. 1995).

Of the Palaeoproterozoic intrusions, the large well-layered mafic–ultramafic bodies of groups I, II, III, V, and VI are confined to the central zone and eastern part of the western zone of the HCO, and have no known correlatives elsewhere. Most of the plutons making up the Bow River Batholith (those of the 1865–1850 Ma Paperbark supersuite and 1835–1805 Ma Sally Downs supersuite) consist predominantly of I (granodiorite)-type granitic rocks and can be broadly correlated with plutons of similar composition and age in other parts of northern Australia; for example, in the King Leopold Orogen to the west of the HCO and in the Pine Creek, Tennant Creek, and Mount Isa regions to the east. Exceptions are the plutons of the Mabel Downs and Syenite Camp suites of the Sally Downs supersuite, which are considered by Sheppard et al. (1997d) to closely resemble Archaean high-Al tonalite–trondhjemite–granodiorite suites and Phanerozoic subduction-related granites.

The Osmond Basin succession east of the Halls Creek Fault, thought to be Mesoproterozoic, has been correlated with part of the Victoria River Basin succession to the east (Sweet 1977) and is also a possible correlative of the Birrindudu Group of the Birrindudu Basin in The Granites–Tanami region to the south and southeast (Blake et al. 1994). Its age relative to that of the ~1200 Ma Carr Boyd Group (Thorne & Tyler 1996) west of the Halls Creek Fault is uncertain.

The Neoproterozoic Wolfe Basin succession along the eastern and southern margins of the HCO is equivalent to Supersequences 1 and 3 of the Centralian Superbasin of Walter et al. (1995). The Ruby Plains Group at the base correlates with basal units of the Amadeus Basin, Ngalia Basin, and Officer Basin successions (Grey & Blake 1999) and, hence, is equivalent to Supersequence 1 and also to the Redcliff Pound Group in The Granites–Tanami region (Blake et al. 1979). The overlying Duerdin and Albert Edward Groups, equivalent to Supersequence 3, are correlatives of the Kuniandi and Louisa Downs Group, respectively, exposed in the southwest of the HCO (Tyler et al. 1998a).

The partly correlative Palaeozoic sedimentary sequences of the Bonaparte Basin in the north and the Ord Basin to the east (Mory & Beere 1988) are underlain by basalt lavas of the early Cambrian Antrim Plateau Volcanics. These volcanics are also exposed in the southwestern part of the HCO. Non-marine sandstone and conglomerate of the Devonian Mahony Group in the Ord Basin, which form the spectacular Bungle Bungle Range of Purnululu National Park (Hoatson et al. 1997), and correlatives in the Bonaparte Basin are probably similar in age to marine reef carbonates of the Napier Range along the southern side of the King Leopold Orogen, and also to non-marine sandstone and conglomerate in the Amadeus and Ngalia Basins of central Australia.

Economic geology

Accounts of the history of mining and prospecting activity in the HCO have been given by Dow & Gemuts (1969), De Havelland (1985, 1986), Hoatson (1993 and Chapter 2), and Sanders (1999). The mineral potential of the Dixon Range and Gordon Downs 1:250 000 sheet areas has been discussed by Hoatson et al. (1995). The locations of the main mines and prospects are shown in Figure 3.11.

The only recorded mineral production in the HCO has come from the world-class Argyle diamond deposit and the nearby Bow River diamond deposit in the north of the central zone (in BOW) and from alluvial and lode gold deposits well to the south, mainly in the eastern zone. However, as discussed by Hoatson et al. (1995) and Hoatson (see Chapter 2), the layered mafic–ultramafic intrusions in the central and western zones of the

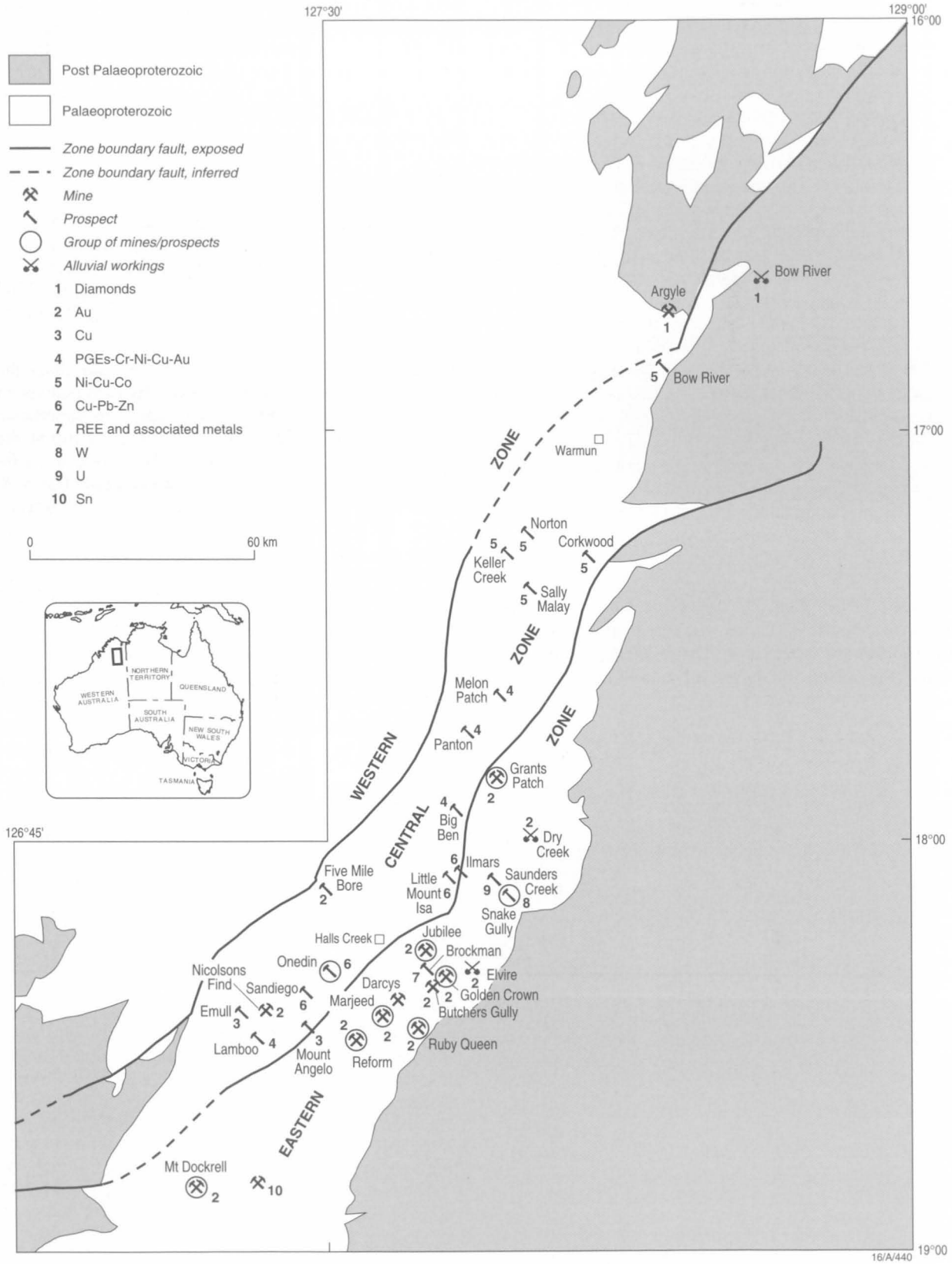


Figure 3.11. Map of main mines and prospects in the Halls Creek Orogen.

orogen are prospective for various styles of platinum-group elements, chromium, nickel, copper, cobalt, gold, titanium, and vanadium mineralisation. The HCO also contains subeconomic deposits of copper–lead–zinc and of rare-earth elements and associated rare metals.

Diamonds

The diamonds at the Argyle diamond mine come from an olivine lamproite pipe in the Carr Boyd Group in the north of the HCO. The deposit was discovered in 1979 and the open-cut mine was opened in 1985. The Argyle pipe, dated at ~1200 Ma, is filled with pyroclastic and reworked pyroclastic material and cut by rare dykes (Boxer & Jaques 1990). The mine produced about 29.7 million carats of diamonds in 1999, down from 40.8 million carats in 1998. Alluvium and soils downstream, at the Bow River Mine, supplied about 7 million carats of diamonds from 1988 to 1995.

Gold

The first payable gold in Western Australia was found near Halls Creek in 1885, and led to a short-lived gold rush that peaked in late 1886. Gold mining, both alluvial and lode, continued sporadically on a minor scale until a resurgence in the 1990s, marked by the opening of the Butchers Creek mine south of Old Halls Creek in HALLS CREEK and the Nicolsons Find mine to the west, in ANGELO, and by increased production from several alluvial operations. The Butchers Creek mine (Palm Springs operation) produced 1575 kg Au between April 1995 and its closure in April 1997. Details of individual mines and prospects in the HCO are given by Sanders (1999) and Chapter 2. Warren (1994b, 1997) has described the gold mineralisation in the eastern zone of the HCO in McINTOSH and DIXON.

All lode gold mined up to 1997 in the eastern zone of the HCO has come from quartz vein deposits in either the lower part of the Olympio Formation or the upper part of the underlying Biscay Formation of the Halls Creek Group (e.g. Dow & Gemuts 1969, Blake et al. 1999a, Warren 1997). Many of the lodes in the Olympio Formation are either hosted by alkaline volcanics of the Butchers Gully Member or are located close to this member or to the Maude Headley Member. Lodes in the Biscay Formation are spatially associated with metabasalt and/or metadolerite (Woodward Dolerite). Alluvial gold workings are located downstream from gold-bearing quartz veins and also in creeks crossing alkaline volcanics of the Maude Headley and Butchers Gully Members of the Olympio Formation. The association with alkaline volcanics indicates that much of the gold may be derived from these volcanics.

The main gold mine in the central zone of the HCO is Nicolsons Find, which commenced production in 1996. Representing an inferred resource of 279 000 t of ore containing 5.54 ppm Au, this mine had produced 731.6 kg from 93 000 tonnes of ore by the time it closed in March 1997. The mineralisation is restricted to quartz veins cutting altered felsic volcaniclastic rocks of the Koongie Park Formation close to a sheared contact with Loadstone Monzogranite.

The gold-bearing quartz veins of the HCO are epigenetic and related to faulting that postdates the Halls Creek Orogeny. The gold was probably mobilised and concentrated in tensional veins with quartz (structural traps) during the Mesoproterozoic Yampi Orogeny, the late Neoproterozoic King Leopold Orogeny and/or the late Palaeozoic Alice Springs Orogeny.

Copper–lead–zinc

Several subeconomic copper–lead–zinc deposits are hosted by the Koongie Park Formation in the central zone and by the Biscay Formation in the eastern zone (Sewell 1999) in ANGELO and HALLS CREEK. In ANGELO, the Koongie Park Formation is also the host for some copper–gold and uranium–copper prospects. The sulphide mineralisation in the Koongie Park Formation is mainly in carbonate lenses, banded ironstone, and mudstone spatially associated with ~1843 Ma felsic volcanics. It is pre-metamorphic and probably of volcanogenic massive sulphide (VMS) type (Orth 1997). The deposits in the ~1880 Ma Biscay Formation, at the Ilmars and Little Mount Isa prospects close to the Halls Creek Fault in HALLS CREEK, may also be of VMS type, as they are hosted by carbonates, calc-silicate rocks, and chert in a sequence that includes felsic volcanics.

Traces of copper–lead–zinc mineralisation have been reported from several localities elsewhere within the Biscay Formation, mainly in carbonates, and also in metabasalt of the Ding Dong Downs Volcanics and basalt of the Antrim Plateau Volcanics (e.g. Dow & Gemuts 1969, Marston 1979, Hoatson 1993).

A possible porphyry system with potential epithermal copper and gold mineralisation in the central zone has been described by Witt & Sanders (1996). It is in the McHale Granodiorite of the Sally Downs supersuite, Bow River Batholith, in TURKEY CREEK.

Rare-earth elements and associated rare metals

A subeconomic resource of rare-earth elements and associated rare metals occurs in the eastern zone of the HCO at the Brockman deposit in HALLS CREEK (Chalmers 1990, Ramsden et al. 1993, Taylor et al. 1995). Metals present in significant quantities include zirconium, yttrium, niobium, tantalum, hafnium, gallium, and heavy rare-earth elements such as terbium and dysprosium. The mineralisation is hosted by a fluorite-bearing volcaniclastic unit known as the 'niobium tuff', which occurs at the base of the Butchers Gully Member of the Olympio Formation. The mineralised rocks contain volcanic or detrital zircon dated at ~1870 Ma (Taylor et al. 1995) and are overlain by a sequence of trachytic to rhyolitic volcanics, which include pillow lava dated at ~1848 Ma (Blake et al. 1999a).

Tungsten

Stratabound scheelite mineralisation occurs in discontinuous lenses in quartzite of the Saunders Creek Formation, Halls Creek Group, on the flanks of the Castle Creek Anticline in the eastern zone, Gordon Downs 1:250 000 Sheet area. Ririe (1989) proposed an evaporitic origin for the mineralisation, which predates

the regional metamorphism, but Trudu (Trudu & Ririe 1990) questions this. Diamond drilling found no economically significant tungsten values.

Uranium

The presence of uranium-bearing conglomerate at the base of the Saunders Creek Formation at the northern end of the Saunders Creek Dome in HALLS CREEK has been known since the 1950s (Dow & Gemuts 1969). The uranium values are too low to be of economic interest.

Tin

Small amounts of tin have been obtained from pegmatites and alluvial deposits in the eastern zone of the HCO in DOCKRELL.

Acknowledgements

This chapter follows numerous fruitful discussions with many other geoscientists, in particular Dean Hoatson, Russell Shaw, Gladys Warren, Shen-su Sun, Lesley Wyborn, and Taro Macias (all AGSO) and Tim Griffin, Steve Sheppard, and Alan Thorne (all GSWA). Figures were drawn at AGSO, mainly by Lana Murray, but also by Neale Jeffery. Ian Sweet, Russell Shaw, and Dean Hoatson (all AGSO) are gratefully acknowledged for their constructive reviews of the manuscript.

References

Blake, D.H., 1991. Notes on the geology of the Halls Creek 1:100 000 sheet area, East Kimberley, Western Australia: results of 1990 fieldwork. Bureau of Mineral Resources, Australia, Record 1991/94, 12 pp.

Blake, D.H., 1994. Migmatites, magma mingling, mylonites and other myths in the East Kimberley, WA. Geological Society of Australia, Abstracts, 37, 29–30.

Blake, D.H., 1996a. How ancient is the Bungle Bungle Range of the East Kimberley, Western Australia? AGSO Research Newsletter, 24, 4–6.

Blake, D.H., 1996b. Cow Creek, Western Australia, 1:100 000 geological map (sheet 4560; preliminary edition). Australian Geological Survey Organisation, Canberra.

Blake, D.H., 1996c. Gordon Downs, Western Australia, 1:100 000 geological map (sheet 4660; preliminary edition). Australian Geological Survey Organisation, Canberra.

Blake, D.H., 1997a. Proterozoic thrusting in the Osmand Range area of the East Kimberley, Western Australia. AGSO Research Newsletter, 26, 4–7.

Blake, D.H., 1997b. Speculations relating to the layered mafic–ultramafic intrusions of the East Kimberley, Western Australia. AGSO Research Newsletter, 27, 19–21.

Blake, D.H. & Hoatson, D.M., 1993. Granite, gabbro, and migmatite field relationships in the Proterozoic Lamboo Complex of the East Kimberley region, Western Australia. AGSO Journal of Australian Geology & Geophysics, 14, 319–330.

Blake, D.H. & Page, R.W., 1988. The Proterozoic Davenport province: regional geology and geochronology. Precambrian Research, 40/41, 329–340.

Blake, D.H. & Warren, R.G., 1996a. Antrim, Western Australia, 1:100 000 geological map (sheet 4561; preliminary edition). Australian Geological Survey Organisation, Canberra.

Blake, D.H. & Warren, R.G., 1996b. Nicholson, Western Australia, 1:100 000 geological map (sheet 4661; preliminary edition). Australian Geological Survey Organisation, Canberra.

Blake, D.H., Hodgson, I.M. & Muhling, P.C., 1979. Geology of The Granites–Tanami region, Northern Territory and Western Australia. Bureau of Mineral Resources, Australia, Bulletin 197, 99 pp.

Blake, D.H., Page, R.W., Shaw, R.D. & Warren, R.G., 1994. Correlating geological events between the Proterozoic Arunta and East Kimberley regions. Geological Society of Australia, Abstracts, 37, 31.

Blake, D.H., Tyler, I.M. & Griffin, T.J., 1997a. Ruby Plains, Western Australia, 1:100 000 geological map (sheet 4460). Australian Geological Survey Organisation, Canberra.

Blake, D.H., Tyler, I.M. & Sheppard, S., 1997b. Geology of the Ruby Plains 1:100 000 Sheet area (4460), Western Australia. Australian Geological Survey Organisation, Canberra, 15 pp.

Blake, D.H., Tyler, I.M., Griffin, T.J., Sheppard, S., Thorne, A.M. & Warren, R.G., 1999a. Geology of the Halls Creek 1:100 000 Sheet area (4461), Western Australia. Australian Geological Survey Organisation, Canberra, 36 pp.

Blake, D.H., Griffin, T.J., Tyler, I.M., Thorne, A.M. & Warren, R.G., 1999b. Halls Creek, Western Australia, 1:100 000 geological map (sheet 4461). Australian Geological Survey Organisation, Canberra.

Blake, D.H., Tyler, I.M. & Warren, R.G., (in press a). Gordon Downs, Western Australia—1:250 000 geological map (sheet SE/52-10). Australian Geological Survey Organisation, Canberra (second edition).

Blake, D.H., Tyler, I.M. & Warren, R.G., (in press b). Gordon Downs, Western Australia (second edition): 1:250 000 Geological Series. Australian Geological Survey Organisation, Explanatory Notes SE/52–10.

Bodorkos, S., Carwood, P.A. & Oliver, N.H.S., 1998. Thermal evolution of the central Halls Creek Orogen, W.A: field, petrological and geochronological constraints. Geological Society of Australia, Abstracts 45, 46

Bodorkos, S., Oliver, N.H.S. & Cawood, P.A., 1999. Thermal evolution of the central Halls Creek Orogen, northern Australia. Australian Journal of Earth Sciences, 46, 453–466.

Boxer, G.L. & Jaques, A.L., 1990. Argyle (AK1) diamond deposit. In: Hughes, F.E. (editor), Geology of the mineral deposits of Australia and Papua New Guinea. Australasian Institute of Mining and Metallurgy, Monograph 14, vol. 1, 697–706.

Chalmers, D.I., 1990. Brockman multi-metal and rare earth deposit. In: Hughes, F.E. (editor), Geology of the mineral deposits of Australia and Papua New Guinea. Australasian Institute of Mining and Metallurgy, Monograph, 14, vol. 1, 707–709.

Compston, D.M., 1995. Time constraints on the evolution of the Tennant Creek Block, northern Australia. Precambrian Research, 71, 107–129.

De Havelland, D.W., 1985. Gold and ghosts—a prospectors guide to metal detecting in Australia. Volume 1—Western Australia. Hesperian Press, Western Australia, 326 pp.

De Havelland, D.W., 1986. Gold and ghosts—a prospectors guide to metal detecting in Australia. Volume 2—Western Australia. Hesperian Press, Western Australia, 382 pp.

Dow, D.B. & Gemuts, I., 1967. Dixon Range Western Australia—1:250 000 Geological Series. Bureau of Mineral Resources, Australia, Explanatory Notes SE/52–6, 15 pp.

Dow, D.B. & Gemuts, I., 1969. Geology of the Kimberley region, Western Australia: the East Kimberley. Bureau of

Mineral Resources, Australia, Bulletin 106, & Geological Survey of Western Australia, Bulletin 120, 135 pp.

Etheridge, M.A, Rutland, R.W.R. & Wyborn, L.A.I., 1987. Orogenesis and tectonic process in the early to middle Proterozoic of northern Australia. American Geophysical Union, Geodynamic Series, 17, 131–147.

Gellatly, D.C. & Derrick, G.M., 1967. Lansdowne, Western Australia—1:250 000 Geological Series. Bureau of Mineral Resources, Australia, Explanatory Notes SE/52–5, 28 pp.

Gellatly, D.C., Derrick, G.M. & Plumb, K.A., 1970. Proterozoic palaeocurrent directions in the Kimberley region, northwestern Australia. Geological Magazine, 107, 249–257.

Gemuts, I., 1971. Metamorphic and igneous rocks of the Lamboo Complex, East Kimberley Region, Western Australia. Bureau of Mineral Resources, Australia, Bulletin 107, 71 pp.

Gemuts, I. & Smith, J.W., 1968. Gordon Downs, Western Australia—1:250 000 Geological Series. Bureau of Mineral Resources, Australia, Explanatory Notes SE/52–10, 23 pp.

Grey, K. & Blake, D.H., 1999. Neoproterozoic (Cryogenian) stromatolites from the Wolfe basin, East Kimberley, Western Australia; correlation with the Centralian Superbasin. Australian Journal of Earth Sciences, 46, 329–341.

Griffin, T.J. & Grey, K, 1990. King Leopold and Halls Creek Orogens. In: Geology and mineral resources of Western Australia. Geological Survey of Western Australia, Memoir 3, 232–253.

Griffin, T.J. & Tyler, I.M., 1992. Geology of the southern Halls Creek Orogen—a summary of field work in 1992. Geological Survey of Western Australia, Record 1992/17, 28 pp.

Griffin, T.J. & Tyler, I.M., 1994. Angelo, Western Australia, 1:100 000 geological map (sheet 4361). Geological Survey of Western Australia, Perth.

Griffin, T.J. & Tyler, I.M., 1995. Geological map of the King Leopold Orogen, West Kimberley region. Geological Survey of Western Australia, Bulletin 143, plate 1.

Griffin, T.J., Tyler, I.M. & Playford, P.E., 1993. Lennard River, Western Australia—1:250 000 Geological Series. Geological Survey of Western Australia, Explanatory Notes SE/51–8 (third edition), 56 pp.

Griffin, T.J., Tyler, I.M., Orth, K. & Sheppard, S., 1998. Geology of the Angelo 1:100 000 sheet. Geological Survey of Western Australia, 1:100 000 Geological Series Explanatory Notes, 27 pp.

Gunn, P. & Meixner, A., 1998. The nature of the basement to the Kimberley Block, northwestern Australia. Exploration Geophysics, 29, 506–511.

Hancock, S.L., 1991. Tectonic development of the Lower Proterozoic basement in the Kimberley district of northwestern Australia. PhD thesis, University of Adelaide.

Hancock, S.L. & Rutland, R.W.R., 1984. Tectonics of an early Proterozoic geosuture: the Halls Creek orogenic subprovince, northern Australia. Journal of Geodynamics, 1, 387–432.

Hoatson, D.M., 1993. Summary of geoscientific information for the East Kimberley, Western Australia, with specific reference to the Dixon Range 1:250 000 Sheet (SE/52–6) and Gordon Downs 1:250 000 Sheet (SE/52–10). Australian Geological Survey Organisation, Record 1993/32, 76 pp.

Hoatson, D.M., Blake, D.H., Warren, R.G., Orth, K. & Tyler, I.M., 1995. Recent NGMA mapping highlights the metallogenic potential of the East Kimberley. AGSO Research Newsletter, 22, 1–2.

Hoatson, D.M., Blake, D.H., Mory, A.J., Tyler, I.M., Pittavino, M., Allen, B., Kamprad, J. & Oswald-Jacobs, I., 1997. Bungle Bungle Range, Purnululu National Park, East Kimberley, Western Australia: a guide to the rocks, landforms, plants, animals, and human impact. Australian Geological Survey Organisation, Canberra, 83 pp.

Huppert, H.E. & Sparks, R.S.J., 1988. The generation of granitic magmas by intrusion of basalt into continental crust. Journal of Petrology, 29, 599–624.

Marston, R.J., 1979. Copper mineralization in Western Australia. Geological Survey of Western Australia, Mineral Resources Bulletin 13, 208 pp.

Mory, A.J. & Beere, G.M., 1988. Geology of the onshore Bonaparte and Ord basins in Western Australia. Geological Survey of Western Australia, Bulletin 134, 184 pp.

Oliver, N.H.S. & Barr, T.D., 1997. The geometry and evolution of magma pathways through migmatites of the Halls Creek Orogen, Western Australia. Mineralogical Magazine, 61, 3–14.

Oliver, N.H.S., Bodorkos, S., Nemchin, A.A., Kinny, P.D. & Watt, G.R., 1998. Differential renewal of U-Pb patterns in zircons during anatexis of Kimberleys pelites: implications for granite genesis. Geological Society of Australia, Abstracts 49, 339.

Orth, K., 1997. Notes on the geology of the Koongie Park Formation southwest of Halls Creek, Western Australia. Australian Geological Survey Organisation, Record 1997/25, 18 pp.

Page, R.W. & Sun, S-s., 1994. Evolution of the Kimberley region, W.A. and adjacent Proterozoic inliers—new geochronological constraints. Geological Society of Australia, Abstracts 37, 332–333.

Page, R.W., Blake, D.H., Sun, S-s., Tyler, I.M., Griffin, T.J. & Thorne, A.M., 1994, New geological and geochronological constraints on volcanogenic massive sulphide prospectivity near Halls Creek (WA). AGSO Research Newsletter, 20, 5–7.

Page, R.W., Sun, S-s., Blake, D.H., Edgecombe, D. & Pearcey, D., 1995a. Geochronology of an exposed late Archaean basement terrane in The Granites–Tanami region. AGSO Research Newsletter, 22, 19–20.

Page, R.W., Hoatson, D.M., Sun, S-s. & Foudoulis, C., 1995b. High-precision geochronology of Palaeoproterozoic layered mafic–ultramafic intrusions in the East Kimberley. AGSO Research Newsletter, 22, 7–8.

Plumb, K.A., 1968. Lissadell, Western Australia—1:250 000 Geological Series. Bureau of Mineral Resources, Australia, Explanatory Notes SE/52–2, 31 pp.

Plumb, K.A. & Gemuts, I., 1976. Precambrian geology of the Kimberley region, Western Australia. 25th International Geological Congress Excursion Guide 44c, 69 pp.

Plumb, K.A., Derrick, G.M., Needham, R.S. & Shaw, R.D., 1981. The Proterozoic of northern Australia. In Hunter, D.R. (Editor): Precambrian of the Southern Hemisphere. Developments in Precambrian Geology, 2. Elsevier, Amsterdam, 205–307.

Plumb, K.A., Allen, R. & Hancock, S.L., 1985. Excursion guide: Proterozoic evolution of the Halls Creek province, Western Australia. Bureau of Mineral Resources, Australia, Record 1985/25, 87 pp.

Ramsden, A.R., French, D.H. & Chalmers, D.I., 1993. The volcanic-hosted rare-metals deposit at Brockman, Western Australia: mineralogy and geochemistry of the Niobium Tuff. Mineralium Deposita, 28, 1–12.

Ririe, G.T., 1989. Evaporites and strata-bound tungsten mineralization. Geology, 17, 139–143.

Roberts, H.G., Halligan, R, & Playford, P.E., 1968. Mount Ramsay, Western Australia—1:250 000 Geological Series.

Bureau of Mineral Resources, Australia, Explanatory Notes SE/52–9, 24 pp.

Sanders, T.S., 1999. Mineralization of the Halls Creek Orogen, east Kimberley region, Western Australia. Geological Survey of Western Australia, Report 66, 44 pp.

Sewell, D., 1999. The Koongie Park and Little Mount Isa zinc–copper–lead deposits, East Kimberley region. Western Australia. In: Ferguson, K.M. (editor), Lead-zinc (silver) deposits of Western Australia. Geological Survey of Western Australia, Mineral Resources Bulletin 16, 139–155.

Shaw, R.D., Tyler, I.M., Griffin, T. J. & Webb, A., 1992a. New K–Ar constraints on the onset of subsidence in the Canning Basin, Western Australia. BMR Journal of Australian Geology & Geophysics, 13, 31–35.

Shaw, R.D., Zeitler, P.K., McDougall, I. & Tingate, P.R., 1992b. The Palaeozoic history of an unusual intracratonic thrust belt in central Australia based on ^{40}Ar–^{39}Ar, K–Ar and fission track dating. Journal of the Geological Society of London, 149, 937–954.

Sheppard, S., 1996. Mafic-felsic magma mingling in the Bow River batholith of the Halls Creek Orogen. Geological Survey of Western Australia, Annual Review 1995–96, 56–60.

Sheppard, S., Griffin, T.J. & Tyler, I.M., 1995. Geochemistry of felsic igneous rocks from the southern Halls Creek Orogen. Geological Survey of Western Australia, Record 1995/4, 81 pp.

Sheppard, S., Tyler, I.M. & Hoatson, D.M., 1996. Mount Remarkable, Western Australia, 1:100 000 geological map (sheet 4463). Geological Survey of Western Australia, Perth.

Sheppard, S., Tyler, I.M. & Hoatson, D.M., 1997a. Geology of the Mount Remarkable 1:100 000 sheet. Geological Survey of Western Australia, 1:100 000 Geological Series Explanatory Notes, 27 pp.

Sheppard, S., Griffin, T.J. & Tyler, I.M., 1997b. Compilation of whole-rock geochemical data for the King Leopold and Halls Creek Orogens. Geological Survey of Western Australia, Record 1977/4, 138 pp.

Sheppard, S., Thorne, A.M. & Tyler, I.M., 1997c. Bow, Western Australia, 1:100 000 geological map (sheet 4564). Geological Survey of Western Australia, Perth.

Sheppard, S., Griffin, T.J. & Tyler, I.M., 1997d. The tectonic setting of granites in the Halls Creek and King Leopold Orogens, northwest Australia. Australian Geological Survey Organisation, Record 1997/44, 107–109.

Sheppard, S., Thorne, A.M. & Tyler, I.M., 1999. Geology of the Bow 1:100 000 sheet. Geological Survey of Western Australia, 1:100 000 Geological Series Explanatory Notes, 36 pp.

Sheppard, S., Tyler, I.M., Griffin, T.J. & Taylor, W.R., 1999. Palaeoproterozoic subduction-related and passive margin basalt in the Halls Creek Orogen, northwest Australia. Australian Journal of Earth Sciences, 46, 679–690.

Sweet, I.P., 1977. The Precambrian geology of the Victoria River region, Northern Territory. Bureau of Mineral Resources, Australia, Bulletin 168, 73 pp.

Sweet, I.P., Brakel, A.T. & Carson, L., 1999. The Kombolgie Subgroup—a new look at an old 'formation'. AGSO Research Newsletter, 30, 26–28.

Taylor, J.R. 1982. An introduction to error analysis: the study of uncertainties in physical measurement. Oxford University Press, 270 pp.

Taylor, W.R., Page, R.W., Esslemont, G., Rock, N.M.S. & Chalmers, D.I., 1995. Geology of the volcanic-hosted Brockman rare-metals deposit, Halls Creek Mobile Zone, northwest Australia, Part I—Volcanic environment, geochronology and petrography of the Brockman volcanics. Mineralogy and Petrology, 52, 209–230.

Thorne, A.M. & Tyler, I.M., 1996. Mesoproterozoic and Phanerozoic sedimentary basins in the northern Halls Creek Orogen: constraints on the timing of strike-slip movement on the Halls Creek Fault system. Geological Survey of Western Australia, Annual Review 1995–96, 156–168.

Thorne, A.M., Sheppard, S. & Tyler, I.M., 1998b. Lissadell, Western Australia—1:250 000 geological map (sheet SE/52-2). Geological Survey of Western Australia, Perth (second edition).

Thorne, A.M., Sheppard, S. & Tyler, I.M. 1999. Lissadell, Western Australia (second edition): Western Australia Geological Survey, 1:250 000 Geological Series Explanatory Notes, 68 pp.

Thornett, J.R., 1981. The Sally Malay deposit: gabbroid associated nickel-copper sulfide mineralization in the Halls Creek Mobile Zone, Western Australia. Economic Geology, 76 (6), 1565–1580.

Thornett, J.R., 1986. Evolution of a high-grade metamorphic terrain in the Proterozoic Halls Creek Mobile Zone, Western Australia. PhD thesis, University of Western Australia, Australia, 350 pp.

Trudu, A.G. & Ririe, G.T., 1990. Comment and reply on "Evaporite and strata-bound tungsten mineralization". Geology, 18, 188–189.

Tyler, I.M. & Griffin, T.J., 1994. Dockrell, Western Australia, 1:100 000 geological map (sheet 4360). Geological Survey of Western Australia, Perth.

Tyler, I.M. & Page, R.W., 1996. Palaeoproterozoic deformation, metamorphism and igneous intrusion in the central zone of the Lamboo Complex, Halls Creek Orogen. Geological Society of Australia, Abstracts, 41, 450.

Tyler, I.M., Griffin, T.J., Page, R.W. & Shaw, R.D., 1995. Are there terranes within the Lamboo Complex of the Halls Creek Orogen? Geological Survey of Western Australia, Annual Review 1993-94, 37–46.

Tyler, I.M., Hoatson, D.M., Griffin, T.J., Sheppard, S., Blake, D.H. & Warren, R.G., 1997a. McIntosh, Western Australia, 1:100 000 geological map (sheet 4462). Geological Survey of Western Australia, Perth.

Tyler, I.M., Thorne, A.M., Hoatson, D.M. & Blake, D.H., 1997b. Turkey Creek, Western Australia, 1:100 000 geological map (sheet 4563). Geological Survey of Western Australia, Perth.

Tyler, I.M., Griffin, T.J., Playford, P.E. & Hocking, R.M., 1998a. Mount Ramsay, Western Australia - 1:250 000 geological map (sheet SE/52–9). Geological Survey of Western Australia, Perth (second edition).

Tyler, I.M., Warren, R.G. & Blake, D.H., 1998b. Dixon, Western Australia, 1:100 000 geological map (sheet 4562). Geological Survey of Western Australia, Perth.

Tyler, I.M., Thorne, A.M., Sheppard, S., Hoatson, D.M., Griffin, T.J., Blake, D.H. & Warren, R.G., 1998c. Dixon Range, Western Australia—1:250 000 geological map (sheet SE/52/6). Geological Survey of Western Australia, Perth (second edition).

Tyler, I.M., Griffin, T.J. & Sheppard, S., 1998d. Geology of the Dockrell 1:100 000 Sheet (4360). Geological Survey of Western Australia, 1:100 000 Geological Series Explanatory Notes, 24 pp.

Tyler, I.M., Page, R.W. & Griffin, T.J., 1999. Depositional age and provenance of the Marboo Formation from SHRIMP U–Pb zircon geochronology: implications for the early Palaeoproterozoic tectonic evolution of the Kimberley region, Western Australia. Precambrian Research, 95, 225–243.

Walter, M.J., Veevers, J.J., Calver, C.R. & Grey, K., 1995. Late Proterozoic stratigraphy of the Centralian Superbasin, Australia. Precambrian Research, 73, 173–195.

Warren, R.G., 1994a. Role of early extensional faults in the Grants Patch district, East Kimberley, Western Australia. Geological Society of Australia, Abstracts, 37, 453–452.

Warren, R.G., 1994b, Gold mineralisation in the northern East Kimberley gold district, Western Australia. Australasian Institute of Mining & Metallurgy, Annual Conference, Darwin, 5–9 August 1994, 117–121.

Warren, R.G., 1997. Reconnaissance geological mapping in Dixon, SE McIntosh and northernmost Halls Creek 1:100 000 Sheet areas, East Kimberley, W.A. 1992–3. Australian Geological Survey Organisation, Record 1997/26, 54 pp.

Witt, W.K. & Sanders, T., 1996. Magmatic-hydrothermal breccia dykes and hydrothermal alteration in the McHale Granodiorite, Halls Creek Orogen: a possible porphyry system. Geological Survey of Western Australia, Annual Review 1995–96, 104–110.

Wyborn, L.A.I., 1988. Petrology, geochemistry and origin of a major Australian 1880–1840 Ma felsic volcanoplutonic suite: a model for intracontinental felsic magma generation. Precambrian Research, 40/41, 37–60.

Yeates, A.N. & Muhling, P.C., 1977. Mount Bannerman, Western Australia, 1:250 000 Geological Series. Bureau of Mineral Resources, Australia, Explanatory Notes SE/52–13 (second edition), 24 pp.

Young, D.N., Edgoose, C.J., Blake, D.H. & Shaw, R.D., 1995. Mount Doreen—1:250 000 Geological Series. Northern Territory Geological Survey, Explanatory Notes SF/52–12 (second edition), 55 pp.

Appendix

U–Pb geochronology of Ding Dong Downs Volcanics and Junda Microgranite, eastern zone of the Halls Creek Orogen

Two samples of foliated felsic metavolcanic rocks from the Ding Dong Downs Volcanics and one of recrystallised granophyre from the Sophie Downs Granophyre Member, all from northeast HALLS CREEK, and a sample of Junda Microgranite from DOCKRELL to the southwest have been dated by SHRIMP U–Pb zircon geochronology (Fig. 3.A). Descriptions of the HALLS CREEK samples are given in Table 1 of Blake et al (1999a). Details of analyses are in AGSO's OZCHRON database.

The SHRIMP data for felsic volcanic rock sample 88598005 are generally concordant. Uranium in the analysed zircons is in the range 63–764 ppm, and many grains have high Th/U. Although analyses of low-U grains have large individual errors in $^{207}Pb/^{206}Pb$, the pooled $^{207}Pb/^{206}Pb$ data are coherent to within experimental error. The indicated zircon crystallisation age from all 24 analyses (χ^2 0.56) is 1907±6 Ma. (Note that χ^2, normally close to unity for a normal distribution of data, is a measure of the degree of fit for the population in the normal distribution; Taylor 1982).

U contents and Th/U for zircons from the other felsic volcanic rock (sample 93526009) are similar; 34 of the 35 analyses of zircons from this rock are well grouped in $^{207}Pb/^{206}Pb$, and indicate a zircon crystallisation age of 1912±3 Ma. The one aberrant grain is a 2505 Ma xenocryst.

Zircons from the sample of Sophie Downs Granophyre Member (no. 87598029) have generally higher common Pb, and individual age errors are, thus, somewhat higher. Like the volcanic zircons, they have high Th/U. All 34 zircon analyses from this sample form a single concordant population (χ^2 0.43), giving an age of 1912±5 Ma, which is interpreted as the time of magmatic crystallisation for the granophyre.

Th/U and U–Pb ages of clear euhedral zircons from the sample of Junda Microgranite (GSWA no. 108547) are similar to those of the zircons from the Ding Dong Downs Volcanics; 16 analyses of zircons from this sample form a concordant to sub-concordant array (χ^2 1.05) with an indicated $^{207}Pb/^{206}Pb$ age of 1913±5 Ma. One analysis, 78.1, is somewhat younger than the others, but its deletion does not significantly affect the resultant age for the microgranite.

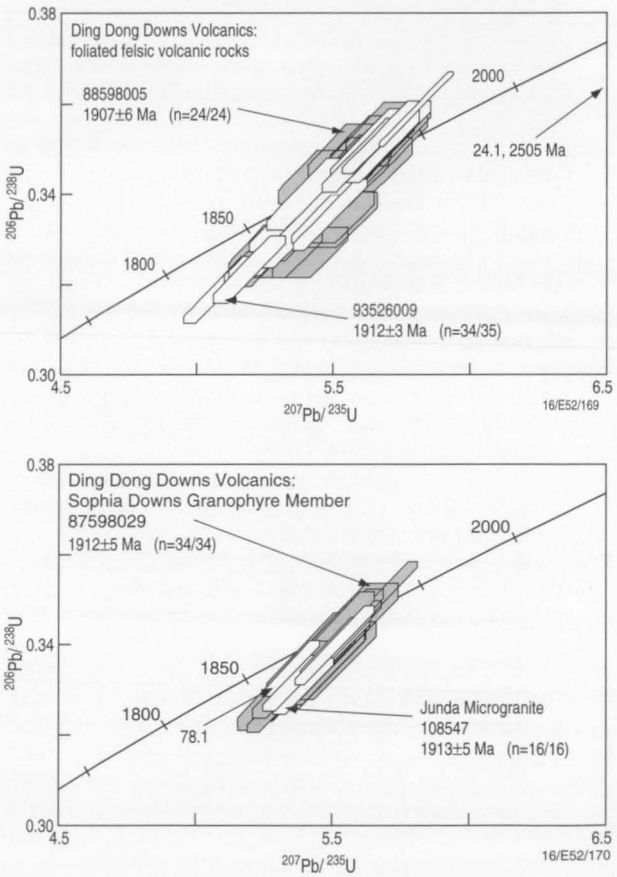


Figure 3.A. Concordia diagrams for samples of Ding Dong Downs Volcanics (including Sophie Downs Granophyre Member) and Junda Microgranite.

REGIONAL GEOPHYSICAL SETTING AND TECTONIC IMPLICATIONS OF THE MAFIC–ULTRAMAFIC INTRUSIONS

by RUSSELL D. SHAW, TONY J. MEIXNER, & ALICE S. MURRAY

Introduction

This study, started in 1992, was undertaken to support the Kimberley-Arunta project as part of the National Geoscience Mapping Accord (NGMA).

In this chapter we attempt to place the mafic–ultramafic intrusions and their geophysical expression into their tectonic context and provide new insights into the crustal structure and tectonic evolution of the Halls Creek Orogen. We focus, in particular, on the Dixon Range and northern half of Gordon Downs 1:250 000 Sheet areas, complementing the geophysical study of the Kimberley Basin and its underlying basement by Gunn & Meixner (1998).

Geophysical framework

National magnetic, spectrometric, and gravity databases

The magnetic, gamma-ray spectrometric (radiometric), and gravity data used in this study are available from the AGSO National Geophysical Database (AGSO 1997). Bouguer gravity data from the national data set have been gridded at 90 s of arc (about 2.5 km). A gravity image of the Kimberley region at 1:5 000 000 scale is shown in Figure 4.1.

Magnetic and gamma-ray spectrometric data have been assembled from various airborne surveys covering the Kimberley region. The digital data set is gridded at 3 s of arc (about 80 m), using a minimum-curvature method (Meixner 1997). Three regional images of the Kimberley region have been derived from these data:

(i) a total magnetic intensity (TMI) image (Fig. 4.2) reduced to the pole to remove the asymmetrical stigmatism of the Earth's magnetic field, with a northerly illumination to accentuate the structural grain;

(ii) a magnetic image (Fig. 4.3) in which the magnetic data have been transformed by *upward continuation* (Blakely 1996, p. 313) to give an indication of what the anomalies would look like if the magnetic field was observed from 6000 m above the ground surface; and

(iii) a digital terrain image (Fig. 4.4), with northeasterly illumination, which shows there is only a small change in elevation across the main tectonic features of the Halls Creek Orogen, consistent with the region being close to isostatic balance.

For the Dixon Range and northern half of the Gordon Downs 1:250 000 Sheet areas, magnetic and gamma-ray spectrometric data were acquired for AGSO in 1991 by Aerodata Holdings Limited (survey project 584). The data were collected using a crystal volume of 33.546 L and a sample interval of 70 m, on E–W flight lines at 400 m intervals and a nominal height of 100 m above ground level; tie-line spacing was 4000 m. The airborne instruments recorded digital position-located magnetic data every 0.2 s (~14 m) and digital position-located gamma-ray spectrometric data every 1 s (70 m). A satellite global-positioning system (GPS) recorded navigational data, including aircraft height. A grid of the data was produced with a cell spacing of 100 m.

In 1993, AGSO carried out two gravity traverses across parts of the Halls Creek Orogen in the Dixon Range and Gordon Downs 1:250 000 Sheet areas, to provide more detail on the gravity expression of the mafic–ultramafic intrusions and major regional faults, including the Halls Creek Fault[1]. Gravity and altitude readings were taken at about 1 km intervals. These data have been incorporated into the AGSO National Gravity Database (AGSO 1997). Also in 1993, Shaw carried out geological sampling along the gravity traverses.

Previous interpretation of the national geophysical data sets

Previous Australia-wide geophysical studies, which included the Kimberley region, focussed on gravity data. Wellman (1976) assessed the relative ages of broad gravity domains, on the basis of cross-cutting gravity trends. Fraser et al. (1977) were the first to subdivide the Australia continent, including the Kimberley region, into a set of Bouguer gravity domains, which they attempted to correlate with regional geological features. Wellman (1978) described how major gravity 'dipole' anomalies could be used to recognise changes across crustal block boundaries, and Wellman (1988) applied these concepts to an interpretation of the development of Australian Proterozoic provinces.

Mathur & Shaw (1982), in attempting to relate patterns of gravity highs and lows to the evolution of orogenic belts, realised that unusually dense rocks, perhaps including ultramafic rocks, were needed to account for marked gravity highs in the East Kimberley region. They speculated that the mafic–ultramafic component of the Halls Creek Orogen was intruded into a localised tensional region within a zone of major strike-slip movement. Shaw et al. (1995, 1996) and Wellman (1998) sub-

[1] In this Chapter 'Halls Creek Fault' refers to the zone of faulting of which the Halls Creek Fault is the dominant element.

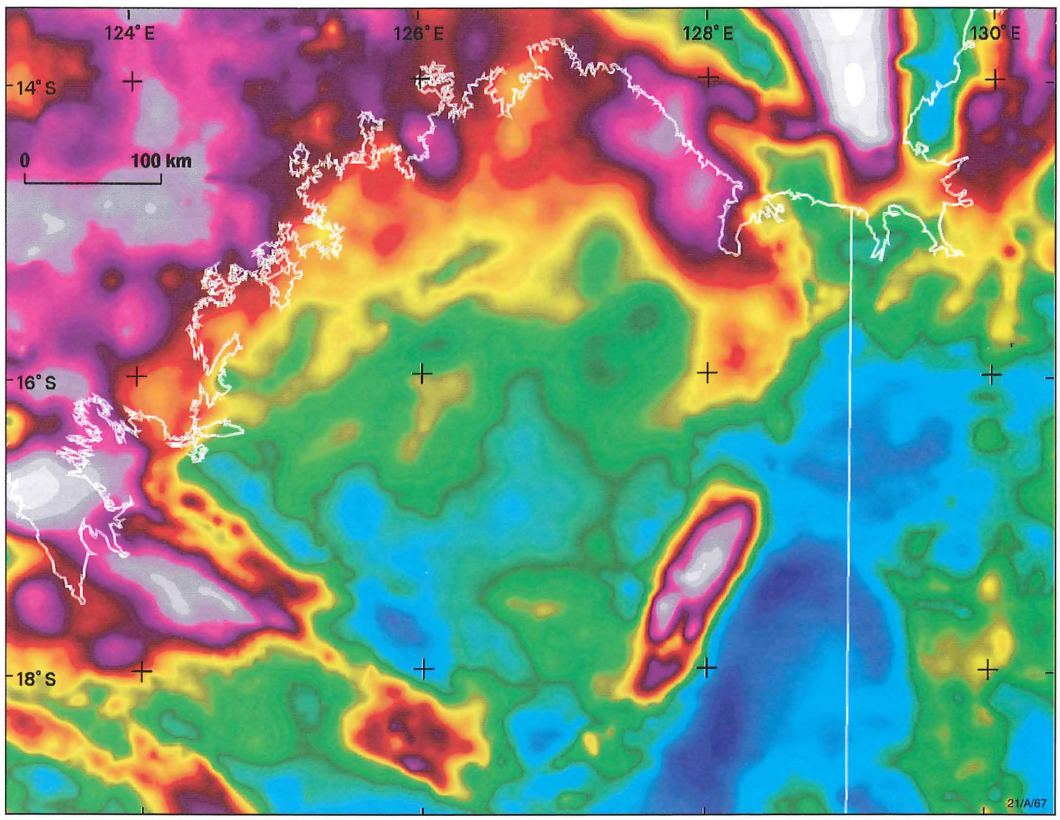


Figure 4.1. Image of simplified Bouguer anomalies of the Kimberley region, designed to facilitate comparison with Total Magnetic Intensity data. Lambert Conformal Conic Projection (WGS84) with standard parallels at 14°S and 18°S and central meridian at 127.5° (image by AJM, derived from the Australian National Geophysical Database).

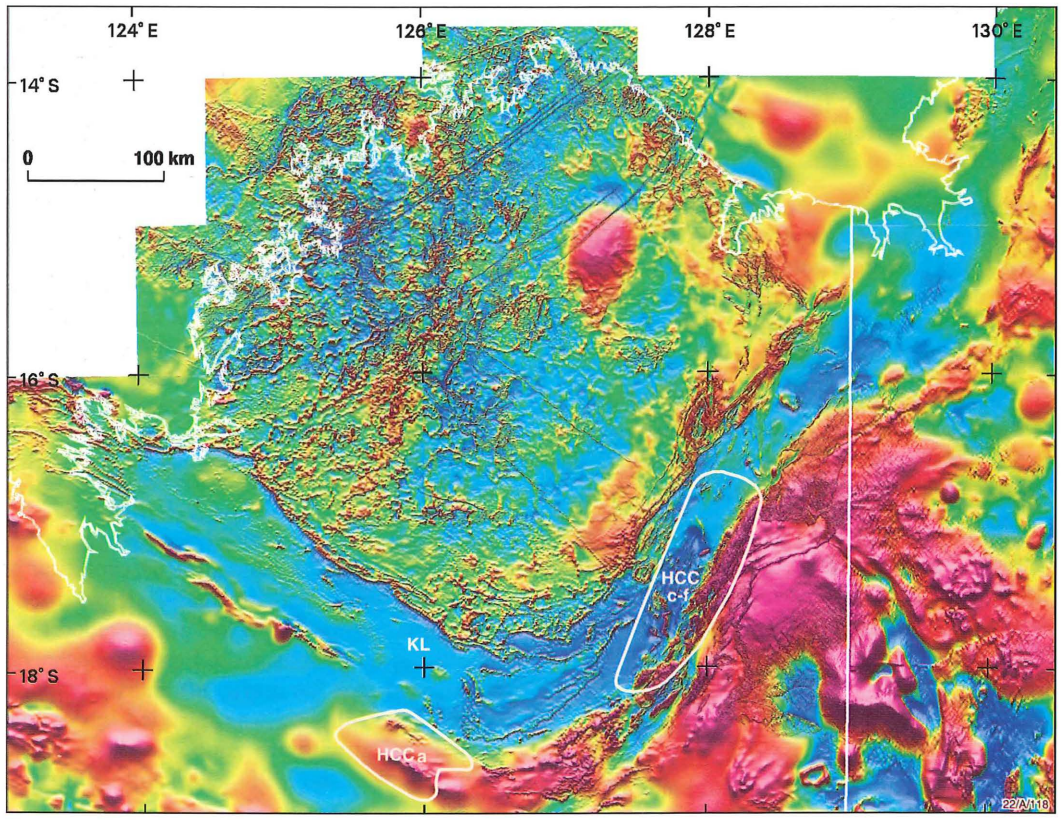


Figure 4.2. Image of Total Magnetic Intensity, reduced to the pole, of the Kimberley region with gradient enhancement and illumination from the north. Outlined are the two regional gravity highs discussed in the text (crustal microelements HCCc–f and HCCa, see Fig. 4.8). Also labelled is the regional magnetic low corresponding to crustal element KL and its northeasterly extension. Magnetic intensity values range from about 6000 to 4800 nT. Lambert Conformal Conic Projection (WGS84) with standard parallels at 14°S and 18°S and central meridian at 127.5° (image by AJM, derived from the Australian National Geophysical Database).

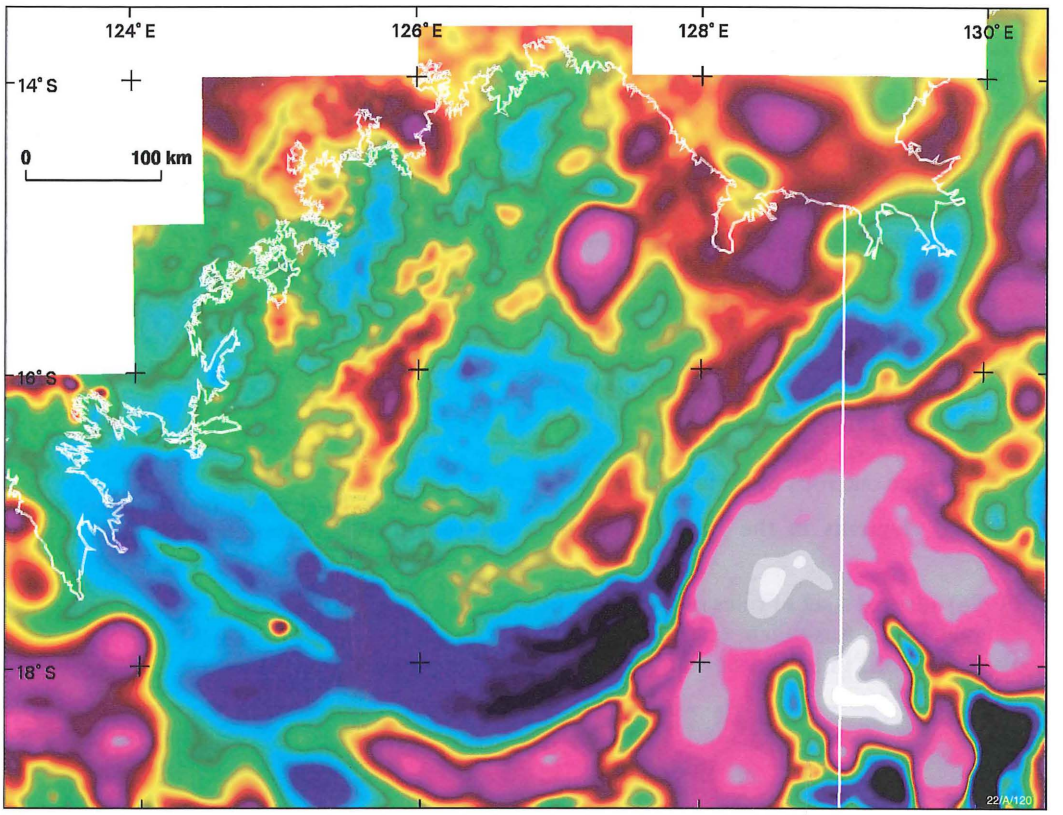


Figure 4.3. Image of Total Magnetic Intensity continued upwards to 6000 m. Lambert Conformal Conic Projection (WGS84) with standard parallels at 14°S and 18°S and central meridian at 127.5° (image by AJM, derived from the Australian National Geophysical Database).

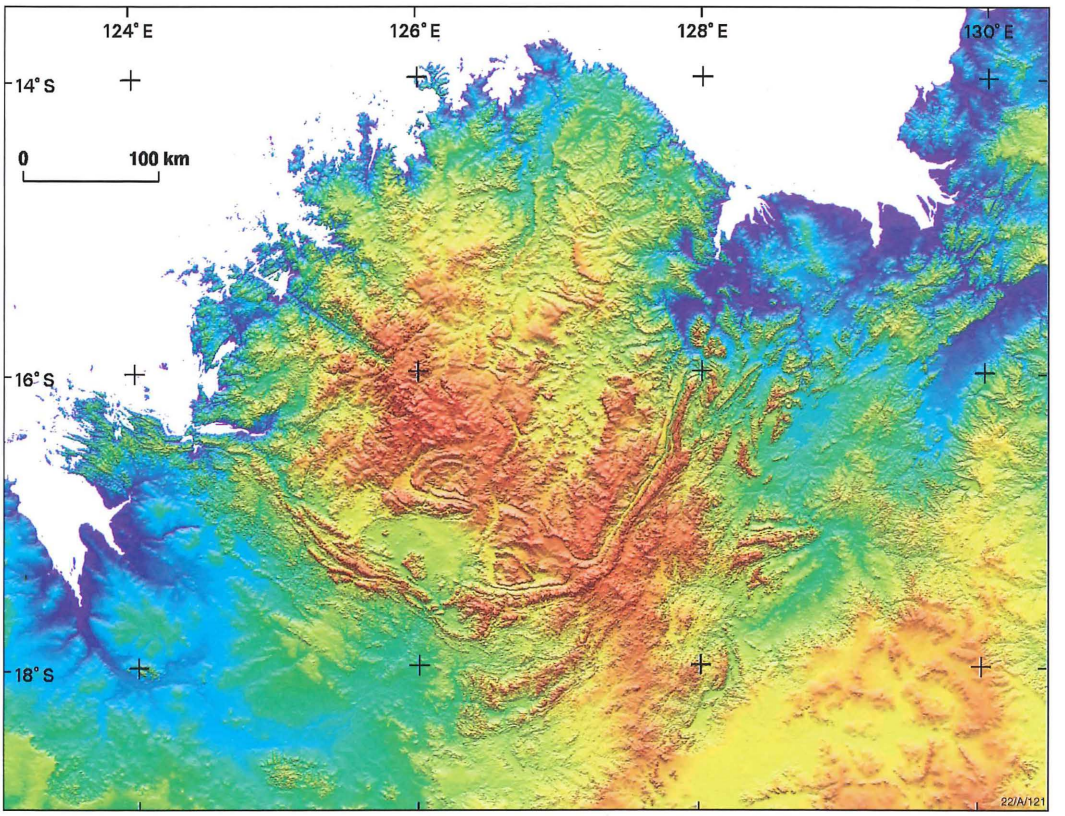


Figure 4.4. Digital elevation model for the Kimberley region, illuminated from the northeast. Lambert Conformal Conic Projection (WGS84) with standard parallels at 14°S and 18°S and central meridian at 127.5° (image by AJM, derived from the Australian National Geophysical Database).

sequently used continental-scale gravity and magnetic data sets to subdivide the continent into crustal mega-elements (Fig. 4.5) and their constituent geophysical domains or elements.

Gunn & Meixner (1998) have divided the basement of the Kimberley Basin into five lithological zones based on magnetic and gravity characteristics. The zones, one of which included a possible ophiolite slice on the south-east margin of the Kimberley Basin next to a granitic terrain to the northwest, are interpreted to have formed by convergence of a Kimberley 'microcontinent' with the main Australian continent. Gunn & Meixner (1998) also recognise a major gravity anomaly beneath the Halls Creek Orogen. Lacking a magnetic anomaly, it is interpreted as a large non-serpentinised mafic–ultramafic intrusion underlying the outcrops of ultramafic rocks.

Australian crustal elements in the East Kimberley region

Shaw et al. (1996) adopted a set of rules or principles in the interpretation of the Australian crustal elements. Crustal elements, mapped initially using magnetic and



Figure 4.5. Mega-elements that represent groupings of the Australian crustal elements (after Shaw et al. 1995, 1996). The boundaries between mega-elements are considered to mark significant changes in composition and/or structural pattern (tectonic style) of the crust. CA, Central Australia; NA, North Australia; NE, New England; P, Pinjarra; SA, South Australia; T, Tasman; WA, West Australia.

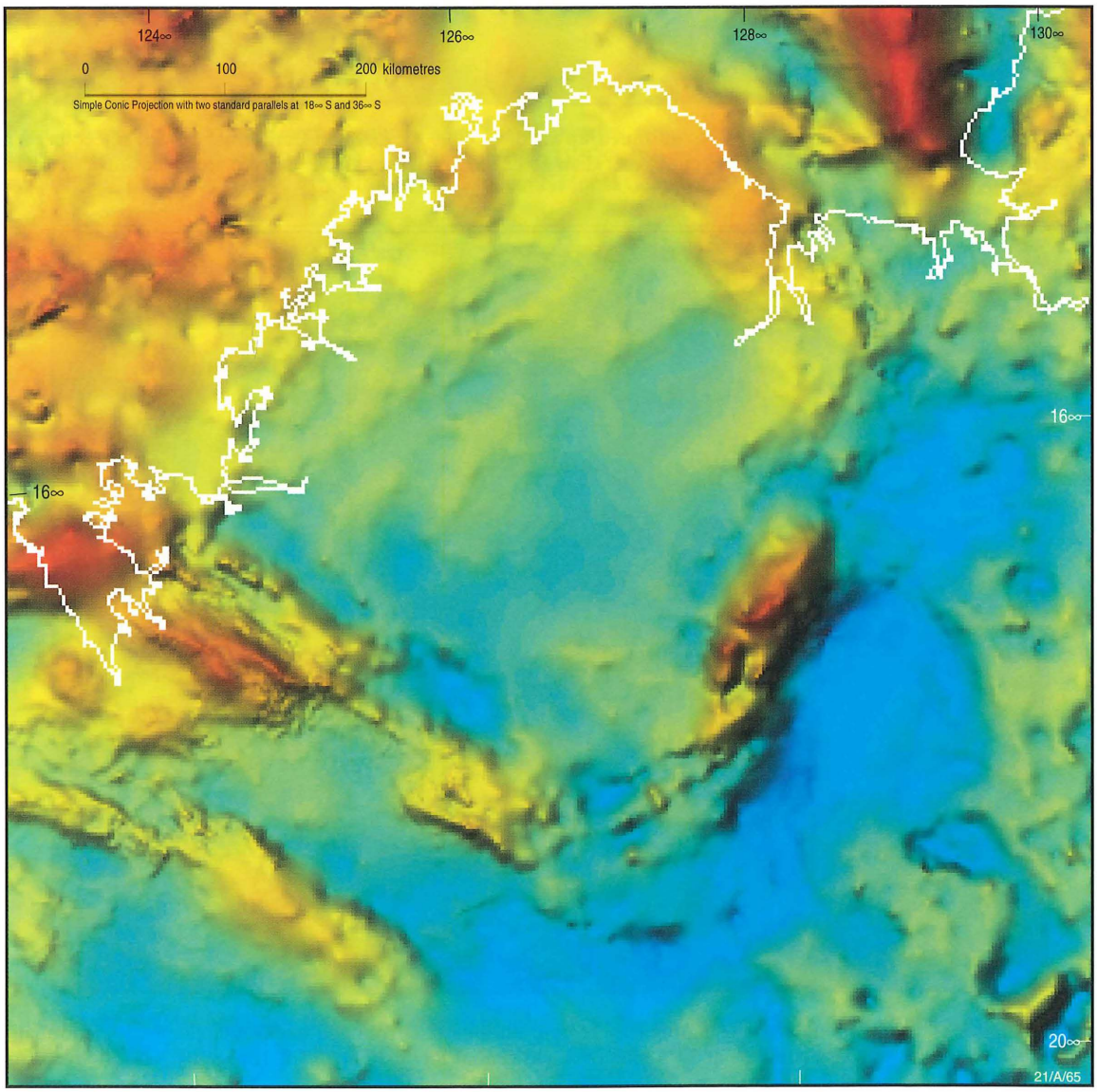


Figure 4.6. Image of Bouguer anomalies designed to emphasis their relationship to crustal elements shown in Figure 4.8. Simple Conic Projection with standard parallels at 18°S and 36°S; hill-shaded to highlight gravity gradients and processed to accentuate minor features. Gravity values range from about to 500 to –700 μm/s² (for a density of 2.67 t/m³) (image by ASM).

gravity data, are considered to represent distinct pieces of upper crust with some overall commonality of physical properties. The age range for the source rocks of each element is thought to fit within the same broad range, although this is not an essential criterion. Their validity can be tested and refined against a variety of geophysical and geological data sets, such as seismic reflection and refraction data, in addition to magnetic and gravity data. They tend to track upper crustal features because their boundaries are commonly defined in the more detailed magnetic data. Where there is a choice of boundaries, the one favoured is that which most closely corresponds to a mapped geological province boundary.

The various crustal elements are referred to here by symbol, but corresponding tectonic features, such as Halls Creek Orogen and King Leopold Orogen, are named in full. Figure 4.6 is an image of the Bouguer anomalies for the Kimberley region (after Murray et al. 1997). Figure 4.7 is a sketch map of tectonic features based on the regional geology (after Tyler et al. 1995), many of which approximately match the crustal elements shown in Figure 4.8. Table 4.1 summarises the relationships between the various crustal elements, indicating their gravity and magnetic expression, their correlation with tectonic features, such as basement provinces and sedi-

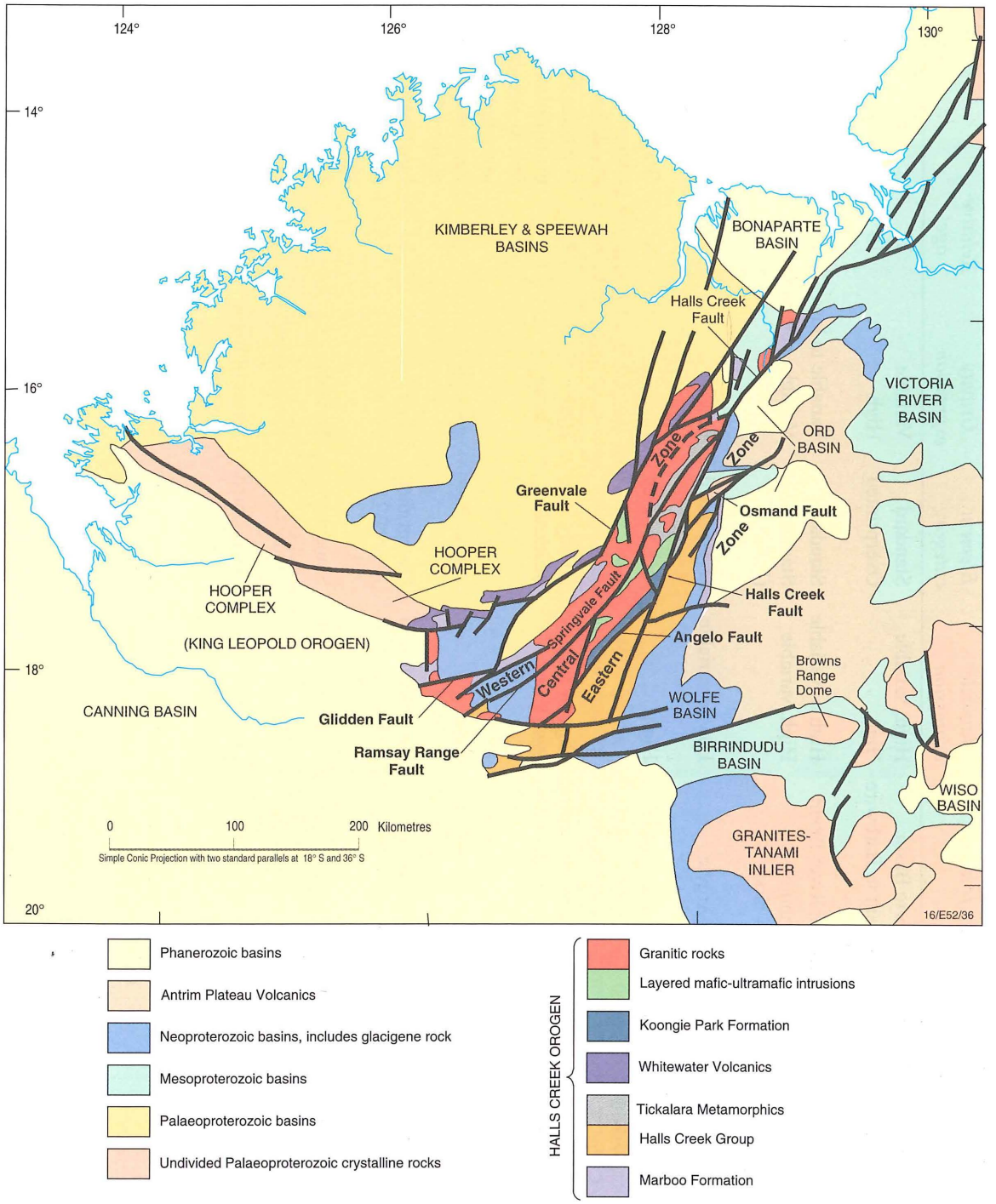


Figure 4.7. Sketch map of the main tectonic units of the Kimberley region. The eastern, central, and western zones of the Halls Creek Orogen are exaggerated for clarity (compiled by RDS, after Tyler et al. 1995).

Table 4.1. Crustal elements of the Kimberley region (see Fig. 4.8).

Crustal element	*Symbol derivation*	*Tectonic feature*	*Magnetic expression*	*Element category*	*Gravity expression*	*Relative age*[1]	*Comments*
BN	Bonaparte Basin	Bonaparte Basin	High, variable	Standard	Variable	27	
BR	Barbwire	Basement to Barbwire Terrace	High	Overprinted	High	10	Northeast margin corresponds to Fenton Fault
BU	Buchan	Victoria River Basin	High to variable	Standard	Variable to low	12	
GT	Granites Tanami	The Granites–Tanami block	High, variable	Standard (Relict)	Variable, complex	8	Numerous small gravity and magnetic lows correlate with granites; poor correlation between gravity and magnetic patterns
HCA	Halls Creek: Argyle	HCO[2]: Argyle segment	Low to variable	Overprinted	Low	20	Segmented into two gravity lows
HCB	Halls Creek: Biscay	HCO: eastern zone[3]	High	Overprinted	High	8	Gravity gradient with segmented features; western edge corresponds to Angelo Fault and the Halls Creek Fault north of the Angelo Fault
HCC	Halls Creek: Central	HCO: western, central, and eastern zones[3]	High in east only; low in west	Highly magnetic	High	8	Segmented gravity highs (micro-elements b-f explained in text and Fig. 4.8); magnetic ridge (micro-elements c, f) only in eastern part corresponding to the central zone, its western limit approximating the Ramsay Range and Springvale Faults; linked to crustal element NK
HCF	Halls Creek: Fitzmaurice	HCO: Fitzmaurice Fault Zone	Variable, low in south	Overprinted	High	8	Low links with crustal element HCA; details of magnetic and gravity signals masked by sedimentary cover of Victoria River Basin
K	Kimberley Basin	Kimberley Basin	Variable	Standard (Relict)	Variable	9	A number of small, poorly correlating gravity and magnetic highs; lows in central and southern parts may reflect thicker sedimentary fill
KBE	Kimberley: East	Kimberley Basin overlying KLO[4]	Low, high along northern margin	Overprinted	Series of highs and lows	20	Gravity high in centre, thin sedimentary veneer (Neoproterozoic glacigene rocks and Kimberley Basin); low corresponds to basement of KLO
KL	King Leopold	KLO (west of Halls Creek region)	Marked, continuous low	Overprinted	Low to variable	8	Gravity segmented: high in northwest, lows correlate with granite; feature overlaps with basement to Lennard Shelf, Canning Basin
LA	LaGrange	Basement to Broome Platform, Canning Basin	Variable	Standard	Variable to low	24	Corresponds to shallow basement under Broome Platform, Canning Basin
MB	Mount Bannerman	Fitzroy Trough, Canning Basin	Low	Standard	Low	12	Gravity low link with crustal elements STS and STN

MWN (?)	Mount Winnecke	Mount Winnecke region, Granites–Tanami province	Low	Standard	Low	9	Magnetic expression segmented; magnetic and gravity lows correspond to late granites; poorly defined in gravity pattern
NK	Nookoonbah	Central Fitzroy Trough, Canning Basin	Low	Standard	Variable gradient	12	Transition between crustal elements O and MB, linked to crustal element HCC
O	Oscar	Basement to western Fitzroy Trough, Canning Basin	Low	Standard	High	8	Isolated, marked gravity highs
RO	Roseberry	Basement to Victoria River Basin	Regional plateau	Standard	Regional low	9	Transitional contact with crustal element HCC suggests east-dipping boundary; corresponds to central zone of the HCO overlain by Victoria River Basin
STN	Sturt: North	Granites–Tanami basement province: northeastern part	High	Standard	Marked low	12	Gravity low with central gravity ridge; strength of low consistent with thick sedimentary fill or thickened crust; northern part of low corresponds to Kimberley and Victoria River Basins
STS	Sturt: South	Granites–Tanami basement province: southwestern part	High	Standard	Marked low	12	Boundary with crustal element STN is a weak gravity lineament
TNW	Tanami West	Southern margin of Granites–Tanami province	Low	Overprinted	Variable	31	Corresponds to zone of thrust faulting at margin of The Granites–Tanami province
V	Victoria	Basement to Victoria River Basin	Variable	Standard	Variable	12	

[1] Relative ages of Australia Crustal Elements deduced on the basis of geophysical criteria (Shaw et al. 1996). Approximate age ranges of magnetic source rocks are: 8 = 1920–1850 Ma; 9 = 1840–1780 Ma; 10 = 1780–1730 Ma; 12 = 1840–1700 Ma; 20 = 1530–1400 Ma; 24 = 1000–600 Ma; 27 = 545–470 Ma; 31 = 420–300 Ma.

[2] Halls Creek Orogen.

[3] Classification of zones from Tyler et al. (1995).

[4] King Leopold Orogen.

mentary basins, and the mega-element to which they belong.

Crustal elements are ranked according to size and significance, namely: mega-elements, elements, subelements and micro-elements. They generally correlate with tectonic provinces: mega-elements with larger cratonic regions made up of several provinces, subelements and their micro-elements with smaller geological features. The mega-elements represent the maximum extent of cratonisation within each major region of the continent (Shaw et al. 1995, 1996, Wellman 1998).

The boundaries between mega-elements and between many other crustal elements are generally associated with two kinds of geophysical anomaly. One is a major change in mean density or mean apparent magnetic susceptibility of the crust, giving rise to paired high and low gravity or magnetic anomalies along the boundary. The other is a structural zone boundary, resulting from interactive processes at the boundary; it includes three main types of zone:

(i) zones of geophysical overprinting, in which trends within one element replace those of another; these commonly correlate with wide composite shear zones;

(ii) zones of overprinting characterised by extensive magnetic lows, resulting from processes such as demagnetisation associated with metamorphism of the older element (e.g. where a younger and potentially hotter crust has been thrust over older and cooler crust); and

(iii) zones where the middle and the lower crust of the younger element has been thrust over an older element. These zones are characterised by major gravity and magnetic highs formed along the margin of the younger element.

Classes of crustal element

(i) Highly magnetic elements (diamond pattern in Fig. 4.8). These elements are generally characterised by regionally extensive zones of high magnetisation, and generally correspond to uplifted regions of mid to lower crust. They correspond to geological zones characterised by regional-scale addition of material (e.g. magma), or pervasive deformation and high-grade metamorphism, or all of these. Crustal subelement HCC (central zone subelement of the Halls Creek element, shown as overprint pattern of diamond-shapes in Figure 4.8) was assigned to the highly magnetised class of geophysical zone by Shaw et al. (1995, 1996), based on the data available at the time. However, it is now known to consist of two regional gravity highs connected by a segmented belt of gravity highs and lows (Fig. 4.1, cf. features outlined as HCCa & HCCc–f in Fig. 4.2). Only the eastern part corresponds to a highly magnetised belt. Elsewhere in Australia, highly magnetised crustal elements can be correlated with orogenic zones, as is the case for part of the subelement HCC, which, as part of the central zone of the Halls Creek element, corresponds to part of the Halls Creek Orogen that was produced during the Hooper and Halls Creek orogenies.

(ii) Elements corresponding to zones of geophysical overprinting (dot patterns in Fig. 4.8). These are zones where the geophysical signatures, commonly developed in regions with a complex pattern of magnetisation, reflect younger tectonic events overprinted on older, and commonly more regional, geophysical features at a major crustal boundary. Grouped into this class are crustal elements KBE (Kimberley East at the eastern margin of the Kimberley Basin) and HCA (Argyle subelement of Halls Creek element), which appear to display the effects of demagnetisation. Examples of more complex zones of overprinting are crustal elements KL (King Leopold) and two subelements of HC (corresponding to the Halls Creek Orogen), namely HCF (Fitzmaurice) and HCB (Biscay zone).

(iii) Elements showing relict geophysical features (cross-pattern in Fig. 4.8). Relict elements commonly have a gravity pattern related to older, deep rocks, which differs substantially from magnetic patterns that reflect properties and structures of younger, shallower rocks units. Elements K and GT are examples.

(iv) Standard elements (not patterned in Fig. 4.8). These elements have geophysical signatures that lack evidence of substantial modification by superimposed tectonic events. An example is the Oscar crustal element (O). Although the Sturt element, ST (subelements STN & STS) and the Mount Bannerman element, MB are classed as standard elements in the Crustal Elements Map of Australia (Shaw et al. 1995, 1996); their classification is uncertain because of the masking effect of thick Palaeozoic and Neoproterozoic sedimentary fill (see Fig. 4.7) and they may be classified as *covered elements.*

Mega-elements in the East Kimberley region

Parts of two mega-elements are recognised in the East Kimberley region: the north Australian mega-element, corresponding to the North Australian Craton of Myers et al. (1996), is represented (i) the basement beneath the Speewah and Kimberley Basins (K, KBE) in the west and (ii) the Halls Creek and King Leopold Orogens along the eastern and southern sides of these basins; and the central Australian mega-element, corresponding in part to the intracratonic Centralian Superbasin (Walter et al. 1995, Myers et al. 1996), is represented by the Canning Basin.

Halls Creek Orogen—lithospheric plate or subplate boundary?

The geophysical features at the margins of the Halls Creek Orogen and King Leopold Orogen, such as the dipole gravity anomalies and the bordering zones of geophysical overprinting, are typical of those associated with major crustal boundaries. Such features may also mark the preserved position of lithospheric plate boundaries (Thomas & Gibbs 1985). However, they were nor portrayed as such by Shaw et al. (1996) because they are discontinuous, perhaps because of post-Palaeoproterozoic faulting, which may have continued until the Devonian.

Crustal element HC (Halls Creek) corresponds to the Halls Creek Orogen (Tyler et al. 1995) and comprises subelements HCA, HCB, HCC, HCF and HCL (Fig. 4.8). HCC differs from surrounding subelements in that it corresponds to a regional high Bouguer anomaly. Its eastern part shows high magnetisation, reflecting the effects of a shallower crustal block. It appears to correlate with those parts of the central and western zones of the Halls Creek Orogen that are characterised by relatively dense rocks. No one rock type can account for the regional gravity high. Exposed rocks in the region of the gravity high that have above crustal average density include various metamorphosed rocks, such as granites of tonalitic to granodioritic composition, metapelites, mafic granulites, and amphibolites, and some mafic–ultramafic intrusions. HCC also correlates spatially with the distribution of unmetamorphosed mafic–ultramafic intrusions, although, volumetrically, these and their potentially high-density ultramafic components in particular, are not sufficient to account for the high regional Bouguer anomaly on their own. The granites of the Paperbark supersuite in the western zone of the Halls Creek Orogen are not obviously related to HCC, as they are not particularly dense or strongly magnetised.

Crustal element HC and subelement HCC, in particular, are bordered to the east and west by zones of geophysical overprinting which align with major linear gravity 'dipole' anomalies of a type that commonly indicates a major change in crustal composition. These 'dipole' anomalies correspond to the limit of an uplifted block of

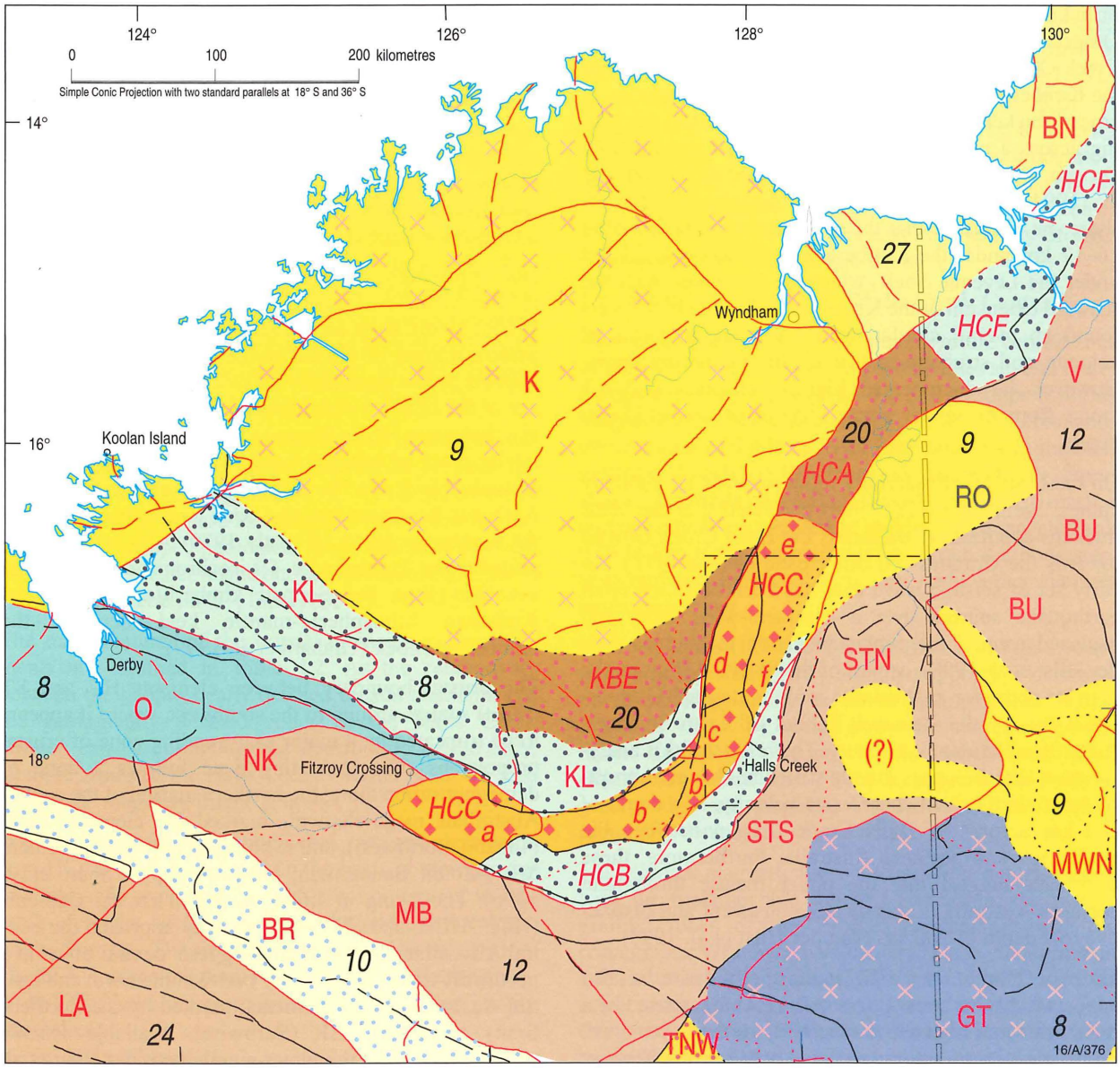


Figure 4.8. Crustal elements of the Kimberley region. These represent the composite geophysical domains mapped by Shaw et al. (1995, 1996) and are considered to represent pieces of upper crust with different physical properties, including bulk density and magnetic properties. The elements, labelled in red and outlined by colour, are summarised in Table 4.1, which includes a listing of their relative ages, shown as black numbers on the figure. Gravity boundaries are in red and magnetic boundaries in black (compiled by RDS).

mid-crustal rocks, which differs from the neighbouring blocks to the east and west in its physical properties, which, in turn, reflect differences in rock composition.

West of HCC and element K (in the Kimberley Basin), seismic refraction and reflection data, as well as the gravity pattern, show that the offshore extension of the Kimberley Basin to the northwest has a crust (K in Fig. 4.8) that seismically resembles the Archaean Yilgarn and Pilbara cratons. Symonds et al. (1994) estimated a crustal thickness of ~30–35 km (11.4s TWT) under the Kimberley Basin. Their crustal model consists of an upper 10 km layer with a seismic velocity of 5.8 km/s, an underlying basement layer up to 13 km thick (inferred to be Archaean) with a velocity of 6.2 km/s, and a lower crustal layer, 12 km thick, with a velocity in the range 6.8–7.4 km/s.

Recently acquired refraction seismic data (Sawyers in Struckmeyer et al. 1998) shows that the King Leopold Orogen (KL in Fig. 4.8), which is linked to the Halls Creek Orogen, has a crustal character not unlike that of the Kimberley Basin, but differs in showing evidence of crustal thickening. Sawyers documented crustal thickening across a presumed extension of the King Leopold Orogen, well south of the Yampi traverse of Symonds et al. (1994). Using refraction data mainly collected offshore, he estimated that the lower crust thickened from 16–17 km under the Kimberley Basin to up to 24 km under the Leveque Shelf, which he correlated with the seaward extension of the King Leopold Orogen. Sawyers found an overall similar crustal section, in terms of velocity and structure to that of the Kimberley Basin. However, he documented higher velocities (5.5–6.1 km/s) from the upper part of the crust above 15 km depth.

On the basis of substantially reduced Bouguer anomaly values, Wellman (1978, 1988) predicted that the crust thickens southeastwards across the Halls Creek Orogen towards the Granites–Tanami crustal element (GT). An early set of seismic wave data has been collected from earthquake sources over a continent-wide array and analysed using tomographic inversion techniques (van der Hilst et al. 1998), as part of the SKIPPY Project, the popular name for an Australia-wide tomographic experiment run by the Research School of Earth Sciences, Australian National University. The results of this analysis show that the upper mantle structure changes abruptly, from slow to fast shear-wave velocity, at a depth of 200 km across the Halls Creek Orogen between the Kimberley and northern Australia. Furthermore, these new data suggest that the upper mantle throughout northern Australia is seismically consistent and distinctive to a depth of 200 km (van der Hilst et al. 1998).

Like the mantle, the crust in northern Australia also appears to have a consistent structure, characterised by a thick crust and high seismic velocity in the lower crust. From seismic refraction traverses between the Tennant Creek and Mt Isa Inliers, Collins (1983) estimated that the crust is 50–55 km thick and that high velocities (Vp) dominate in the lower crust, implying a predominantly mafic lower crustal layer. More widespread seismic refraction data, summarised by Finlayson (1982) similarly revealed that the region is characterised by relatively high refraction velocity in the lower crust. These findings accord with the interpretation of granite geochemistry in terms of magmatic underplating at the base of the crust (Wyborn et al. 1992) over much of northern Australia. From the combined seismic data sets for the lithosphere, including the magnetic and gravity data, we can expect that the crustal structure in the region of The Granites–Tanami Inlier (Fig. 4.7) is similar to that of most of northern Australia and unlike that of either the Kimberley Basin or the Halls Creek Orogen. That is, the Halls Creek Orogen coincides with lithospheric changes that appear to mark an ancient plate or sub-plate boundary.

In detail, crustal elements K (Kimberley) and GT (Granites–Tanami) both show indications of having older substrata at depth, as their gravity and magnetic patterns are not coherent. That is, their magnetic pattern generally reflects shallow source rocks and their gravity pattern, which tends to reflect deeper crustal features, does not match in the same region. These elements also contrast markedly from each other in their composite gravity and magnetic patterns. Taken together, these features suggest that K and GT represent pieces of crust which, while they both have older elements, have very different geological histories and incorporate older elements.

Not surprisingly, Archaean ages have been documented in The Granites–Tanami Inlier (Fig. 4.7, Page et al. 1995b, 1996). Also, an Archaean basement at or near the eastern margin of crustal element HC (Halls Creek) is implied by the anomalous 2200–2300 Ma Pb–Pb model age at the Ilmars volcanogenic massive sulphide deposit in subelement HCB (Biscay) (Sun et al. 1996). This particular piece of basement may well belong to the same cratonic block as The Granites–Tanami province. An Archaean basement has also been long suspected under the Kimberley Basin (Gellatly 1970). This view is supported by an Archaean Re–Os isochron age for chromite xenoliths from the Seppelt kimberlite, implying an Archaean lithospheric-mantle keel beneath the Kimberley Block (Graham et al. 1999).

The crustal boundary between elements HC and ST (Sturt) swings around to the southwest, where it appears to be truncated by a major east-trending zone of crustal proportions. The truncating zone follows a zone of demagnetisation along the northern margin of the central Australian mega-element, marked by element TNW (Tanami Northwest), and is linked to the west to element MB (Mount Bannerman; see also map in Shaw et al. 1996). The swing in strike of several crustal elements (HCC, HCB, and SDT–MD) as they approach the central Australian mega-element suggests dextral offset at a northwest-trending boundary between the north and central Australian mega-elements, marked by the northern limits of element BR (Barbwire). Available seismic velocity data from the upper mantle (van der Hilst et al. 1998) also show a change in character in this region south of the King Leopold Orogen. However, there are also important changes in mantle character across a north-trending zone, which aligns with the extrapolated southward trend of the Halls Creek Orogen. Because

sedimentary rocks of the Canning Basin cover all these features, their relationships to one another are difficult to assess.

From an assessment of combined teleseismic, gravity, and magnetic data, we conclude that the Halls Creek Orogen marks not only a complex crustal boundary, but a lithospheric boundary as well. However, because there are gaps in the various data sets and three-dimensional complexities in the mid to upper crust, it is difficult to pinpoint with certainty any particular feature in the orogen as a plate or sub-plate boundary. Available geophysical data are consistent with the view that the Halls Creek Orogen represents a zone of interaction between two separate Archaean cratons (cf. Tyler & Page 1996, Myers et al. 1996).

Geophysical interpretation of the Dixon Range and northern Gordon Downs 1:250 000 Sheet areas

Our regional approach to geophysical interpretation has been to document physical properties of rocks, to build up qualitative information on the expected magnetic signature of rock units and to establish links between the different geophysical and geological data sets. This process aids our understanding of the geophysical expression of the tectonic and mapped geological units in the region. Particular emphasis has been placed on the magnetic and gravity expression of the layered mafic–ultramafic intrusions (see also Chapter 7).

Firstly, we examine the internal features of each crustal element and the nature of the boundaries between the elements (Table 4.2, Figs 4.9, 4.10, 4.11). Secondly, in the next section, we use the magnetic and spectrometric character of mapped geological units, and their physical properties, to further refine our interpretation in terms of a set of 'magnetic units' (Table 4.3; Figs 4.9–4.14).

The main features of the crustal elements and subelements are outlined in Table 4.2. As the relationship between the geophysically defined crustal elements and the geologically defined zones of the Halls Creek Orogen can be confusing, the distribution of the three tectonic zones of the Halls Creek Orogen is shown as a grey-scale magnetic image (Fig. 4.11).

Some subelements are subdivided into microelements (e.g. HCCa–HCCf), defined on the basis of their gravity and magnetic expression, which can correspond to tectonic elements such as fault blocks and stratotectonic units. For the Dixon Range–Gordon Downs region, Figure 4.9 shows the main tectonic features (white annotation) that have an expression in the Bouguer gravity anomalies.

Crustal element KBE (Kimberley Basin East) and parent crustal element KL (King Leopold Orogen)

Element KL, corresponding to the King Leopold Orogen, a stratotectonic unit dominated by the Hooper Complex (Fig. 4.7), is characterised by a series of gravity highs and lows (Figs 4.1, 4.6) and a marked, regional magnetic low (Figs 4.2, 4.3). The gravity lows in KL are known to correlate with granite and, to a lesser extent, metamorphic rocks of the Marboo Formation, both of the Hooper Complex (cf. Figs 4.6, 4.8). The source of the main gravity high in KL (in the northwestern part, outlined by the red gravity boundary in Fig. 4.8) is unknown, as sedimentary rocks of the Canning Basin (Fig. 4.7) cover it.

KBE (Kimberley Basin East) is a subelement of K, but corresponds to the southeast part of the Kimberley Basin and its underling basement (cf. Figs 4.7, 4.8). Its magnetic expression (Fig. 4.2) and, to a lesser extent, its gravity expression (Fig. 4.6) are like those of KL. It shows evidence of geophysical overprinting ('reworking') in that its magnetic expression shows local evidence of demagnetisation (correlating with thrust slices). The transitional character of KBE is well illustrated by the image (Fig. 4.3) showing an upward-continuation of the anomalies to 6000 m, where most of KBE lies within the marked magnetic low of KL. The short-wavelength magnetic expression of KBE is thought to result from the thin cover of the Kimberley and Speewah Basins, which include two moderately magnetic (and dense) units—the Hart Dolerite, mainly intruding the Speewah Group, and the Carson Volcanics of the Kimberley Group. The eastern boundary of KBE corresponds to the Greenvale Fault.

Crustal subelement HCC (Halls Creek Central)

This subelement corresponds mainly to the central zone of the Halls Creek Orogen. It encompasses several major elongate gravity highs (Fig. 4.9) and overlaps a highly magnetic zone in the east (Fig. 4.10). HCC corresponds to the region of the Bow River Batholith, which includes granites of both the Paperbark and Sally Downs supersuites. The limits of the Bow River Batholith are marked by the dashed line labelled g* and by the Greenvale Fault (GF in Fig. 4.9). The main mafic–ultramafic bodies are also outlined in Fig. 4.9, as are some other features explained below.

Microelements HCCd and HCCe (d & e in Fig. 4.9) are parts of a regional gravity high that appears to overlap a much more regionally extensive magnetic low (KL in Figs 4.2, 4.9, 4.10), which otherwise characterises element KL (King Leopold) and subelement KBE (Kimberley Basin East). This is because the regional gravity high and magnetic low are related to different regionally distributed source rocks.

The regional magnetic low correlates here and elsewhere with the metamorphic Marboo Formation, the mainly granitic rocks of the Paperbark supersuite and the comagmatic Whitewater Volcanics. That is, the dominant surface units in the region of HCCd and HCCe are the same group of rocks that make up the King Leopold Orogen, which corresponds to element KL. The weak magnetisation of the Paperbark supersuite is typical of similar, generally siliceous and high-K granites, showing Sr-depleted and Y-undepleted patterns, such as the Kalkadoon batholith of the Mount Isa region, and may reflect the reduced nature (oxygen fugacity) of the primary source rocks. Wyborn et al. (1992) regarded these

Table 4.2. Crustal elements and sub-elements in the Dixon Range and southern Gordon Downs 1:250 000 Sheet areas.

Element–subelement (Figs 4.8 & 4.9)	*Micro-element (Figs 4.8 & 4.9)*	*Gravity expression*	*Magnetic expression*	*Lithological associations (magnetic units in Table 4.3 & Fig. 4.13)*	*Facies of associated metamorphic rocks*	*Inferred age of metamorphism (Ma)*	*Mafic–ultramafic intrusions, (age in Ma)*
HCC	b	Complex	Segmented ridge and gradient	Koongie Park Formation (10b)	Greenschist	1845–1835	Rare
HCC	c	Moderate high	Variable, linear highs and lows	Tonalite–granodiorite (7), high -grade metamorphic rocks (10b)	Amphibolite	1840–1830	Big Ben (small), Armanda (small)
HCC	d	Narrow ridge, with peak near Toby intrusion	Trough with local subdued highs	Tonalite–granite, migmatite (6c)–younger granites	Amphibolite	1865	Toby (1855), Springvale (1857), Sandy Creek-Paperbark (?1830)
HCC	e-west	Broad gravity ridge	Trough	Monzogranite, granodiorite, tonalite (6b)–younger granites	Amphibolite	?1865	Nine Mile (dyke), Spring Creek, Foal Creek
HCC	e-east	Broad gravity ridge, peak in southeast	Variable, but moderate, linear highs and lows	Granulites (10a)	Granulite	1850–30	Norton, Frog Hollow
HCC	f^{+}	Gradient, lower values to east	Low	Milba Formation (10a)	Greenschist	uncertain	None
HCC	f	Complex high with gradient to east	High to variable, linear highs and lows	Tonalite–granodiorite (7), high-grade metamorphic rocks (10a)	Amphibolite	1860, 1850–1845, 1830	McIntosh (1830), Panton (small; 1856)
HCB		Eastern margin to regional ridge, segmented highs or gradient	Low in west and south, high in east	Turbidites, basalt–rhyolite (11, 12)	Greenschist	1840–1830	None
KBE		Includes gradient at western margin to regional ridge	Regional low; moderate to high short-wavelength ridges	Sedimentary rocks, minor dolerite, basalt (5a, 5b, 6d)	Not metamorphosed		None
RO		Regional plateau	Segmented high plateau	Sedimentary rocks, shallow basement (3a, 3c, 5c, 10a, ?11)	Not metamorphosed		None
STN		Trough	Broad high (deep source)	Sedimentary rocks (1b)	Not metamorphosed		Intrusions, sills or volcanics in sub-surface
STS		Trough	Broad high (deep source)	Sedimentary rocks (3c)	Not metamorphosed		None

granites as derived from restite-dominant magmas. Sheppard et al. (1997a) disputed the restite model and suggested that the granites could have been intruded into an extensional basin behind an oceanic arc to the east. Griffin et al. (in press) also dispute the restite model, citing the paucity of inherited zircons and emphasising possible subduction-related features, such as LILE/HFSE (the proportion of large ion lithophile elements relative to high field-strength elements). They suggest that the granites could be the result of remelted crust formed during an earlier period of subduction (at? 2100–1940 Ma).

The regional gravity anomaly used to define HCC has a different origin to this regional magnetic low. This unusual situation is thought to be due to three-dimensional factors and is discussed at length in this chapter. The magnitude and wavelength of the regional gravity anomaly (Fig. 4.6) characterising microelements HCCd and HCCe indicate that a mass excess derived from one or several dense rock bodies may continue to at least mid-crustal depths. Multiple sources are indicated within the combined region of the western and central zones of the Halls Creek Orogen, considered to represent an uplifted crustal block. Within the north-northeast-trending regional gravity ridge that characterises microelements HCCd and HCCe, three of the four main gravity peaks and one subsidiary peak are associated with layered mafic–ultramafic intrusions (Fig. 4.9). Otherwise, much of the zone containing HCCd and HCCe aligns with exposures of the Paperbark supersuite of the Bow River Batholith, characterised mainly by granite and monzogranite, rather than denser tonalite and granodiorite.

Of greater significance is the fact that the eastern part of the prominent positive gravity anomalies in HCCe corresponds to a belt of granulites, traditionally placed in the Tickalara Metamorphics, that are characterised by rocks of high density, such as mafic granulite and garnet-bearing metapelite. The boundary that separates HCCe and HCCf aligns with the Highway Shear Zone (HS in Fig. 4.9), which is linked to the Springvale Fault (SF in Fig. 4.9). The geophysical expression of this boundary appears to be more important than the splays of the Springvale Fault that have been taken as the eastern boundary of the western zone of the Halls Creek Orogen by Tyler et al. (1995, 1997a). If the Highway Shear Zone is the correct tectonic boundary, then the metapelites and mafic granulites immediately west of the Highway Shear Zone may not be part of the Tickalara Metamorphics exposed to the east. They are made up of granulite facies rocks, rather than the amphibolite facies rocks typifying the Tickalara Metamorphics to the east, and approximate the high-grade gneissic sub-zone IIc of Hancock & Rutland (1984). They are less magnetic than rocks mapped as Tickalara Metamorphics to the west, but more magnetic the Marboo Formation to the southwest. The informal term, 'Violet Valley zone' is adopted in this study for this zone of high-grade metamorphic rocks with its distinct pattern of magnetisation (VVZ between HS and t* in Figs 4.9 & 4.11). The 'Violet Valley zone' has no obvious fault boundary to the west, but is intruded by a variety of granites, largely assigned to the Sally Downs supersuite, which show extremely weak magnetisation (Fig. 4.11).

Microelements HCCc and HCCf (Fig. 4.9) are, for the most part, highly magnetised (Fig. 4.10), but also highly variable in their magnetisation. The observed general pattern is a correlation between increasing metamorphic grade and both variability in magnetisation and number of magnetic anomaly highs with extreme values (see Gemuts 1971 for data on metamorphic grade). One coincident magnetic and gravity anomaly in HCCf aligns with the McIntosh mafic intrusion (McI in Fig. 4.9). A similar and broader gravity anomaly in HCCc to the southwest could represent another mafic–ultramafic intrusion at depth, but the lack of a coincident magnetic anomaly is more consistent with the presence at depth of higher grade metamorphic rocks of the Tickalara Metamorphics.

Several markedly linear magnetic anomalies in HCCf align with belts of pelitic gneiss and, in some cases, amphibolite. Other important magnetic source rocks are the more mafic components of the tonalite-dominated Sally Downs supersuite, such as partly recrystallised rocks of the Mabel Downs Tonalite (Ord River Tonalite of Ogasawara 1988) as well as several granite phases of the Dougalls suite (Sheppard et al. 1997b).

Highly magnetic banded iron formations (BIFs) also produce prominent anomalies. An example is the spot anomaly associated with the Upper Panton River BIF occurrence (east of the Panton Fault at 127°50.5'E, 17° 50.5'S). This iron formation is intercalated with mafic volcanics of the Tickalara Metamorphics and, in places, with felsic intrusions (Hoatson 1995, unit PmTi on McINTOSH: Tyler et al. 1997a). All these rock types are likely to have moderate to high density.

The boundary separating the HCCc and HCCf aligns with the north-trending Panton Fault (PF in Fig. 4.9), which lines up to the northwest with a splay of the Springvale Fault. The Koongie Park Formation, which is dominated by low-grade metasedimentary rocks and felsic volcanics, corresponds to some of the lower gravity values and weaker magnetic anomalies on the southeastern margin of HCCc. Hornfelsed parts of the Koongie Park Formation are more highly magnetised.

The narrow micro-element labelled HCCf+ (f+ in Fig. 4.9) represents the southwestern extension of the western margin of subelement HCCf and corresponds to the Milba Formation, a unit of metamorphosed clastics of uncertain age. HCCf+ is bounded to the southeast by the Angelo Fault (AF in Fig. 4.9) and to the northwest by the Highway Fault (WF in Fig. 4.9; see also Blake et al. 1999).

The much higher magnetisation and somewhat lower average Bouguer anomaly values of HCCc and HCCf, compared to HCCd and HCCe, are consistent with them having a much higher proportion of magnetic tonalitic granites and variably magnetised metamorphic rocks of lower metamorphic grade and density.

HCCb corresponds to a southward continuation of the highly magnetised belt (Fig. 4.2) that characterises HCCc (Fig. 4.8) and microelement labelled b (Fig. 4.9),

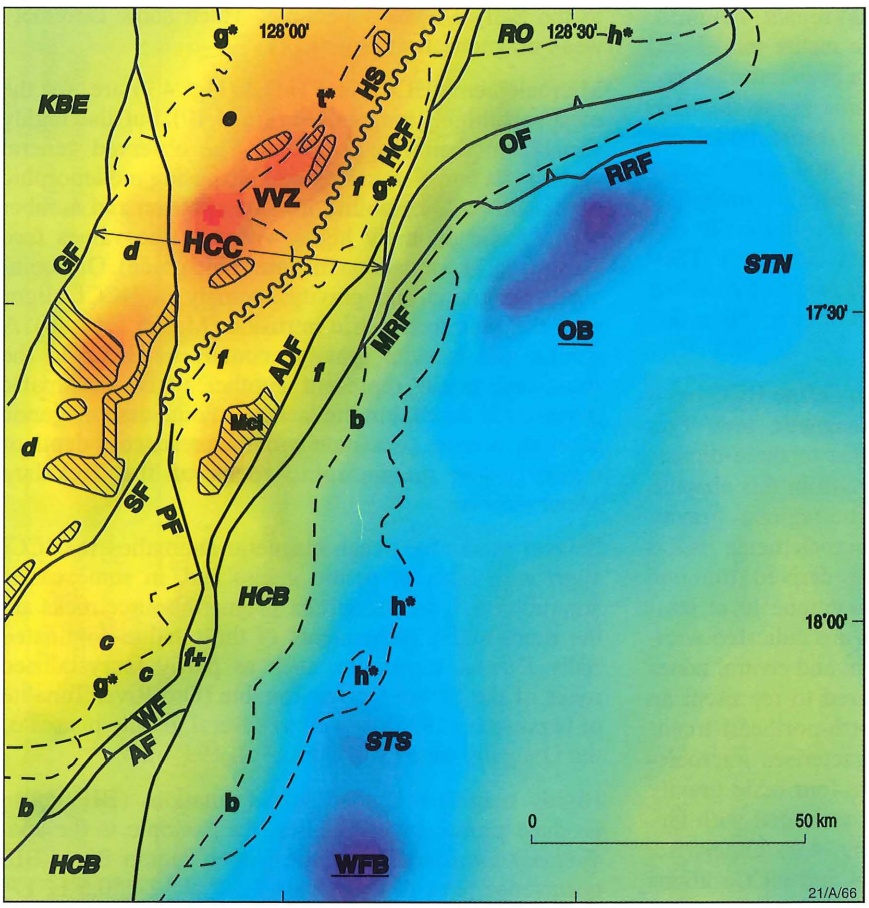


Figure 4.9. Bouguer anomalies in the Dixon Range and Gordon Downs 1:250 000 Sheet areas, showing geophysical subelements KBE, HCB, RO, STN, & STS and geophysical microelements of HCC (b, c, d, e, f, & f+). Gravity values range from about +500 to –700 μm/s² (for a density of 2.67 t/m³). Pixel image by ASM, after Murray et al. (1997); annotation by RDS. VVZ, Violet Valley zone; WFB, Wolfe Basin; OB, Ord Basin; ---line 'b', eastern limit of subelement HCB; unlabelled continuous lines enclosing white diagonal dashes, main mafic–ultramafic intrusions, including the McIntosh intrusion (McI); dashed lines g*, limits of Bow River Batholith (granitic and gabbroic rocks), where this is not the Greenvale Fault; h*, eastern limits of basement rocks of the Halls Creek Group, taken to be the base of the Wolfe Basin or its equivalent (unit 3b or 3c in Fig. 4.13); t*, western limit of the Violet Valley zone of Tickalara Metamorphics (west of the Highway Shear Zone, HS); continuous lines, ADF, Alice Downs Fault; AF, Angelo Fault; GF, Greenvale Fault; HCF, Halls Creek Fault; HS, Highway Shear Zone; MRF, Mount Ramsay Fault; OF, Osmand Fault; PF, Panton Fault; RRF, Red Rock Fault; SF, Springvale Fault; WF, Highway Fault.

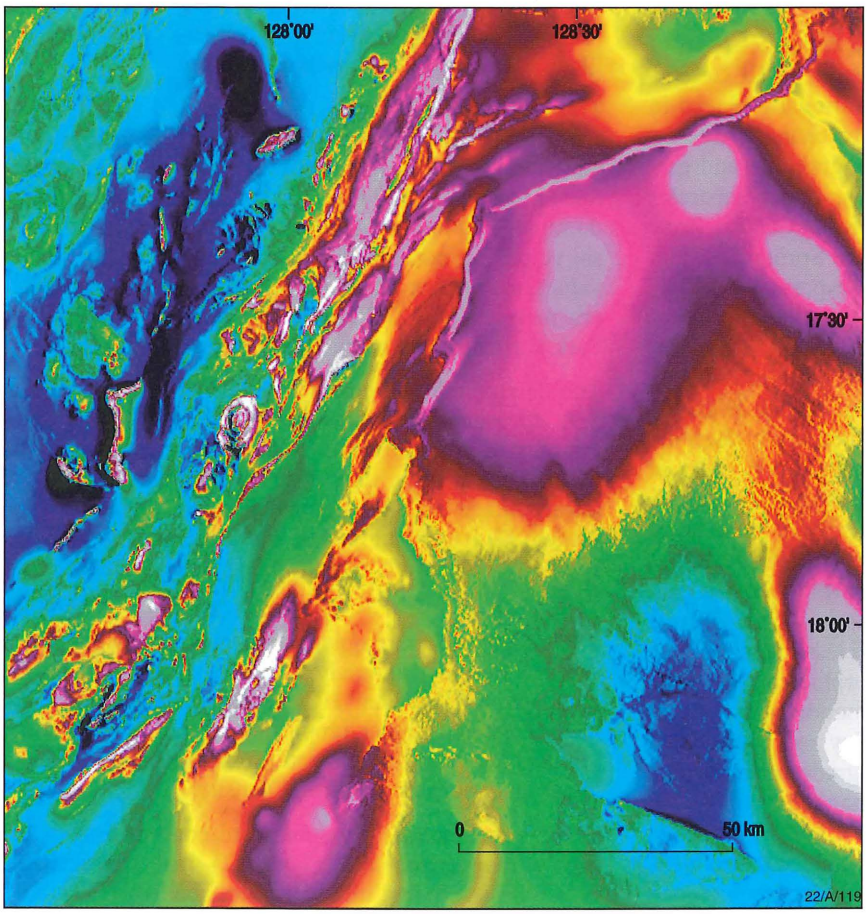


Figure 4.10. Total Magnetic Intensity, reduced to the pole, of the Dixon Range and Gordon Downs 1:250 000 Sheet areas, East Kimberley (image by AJM).

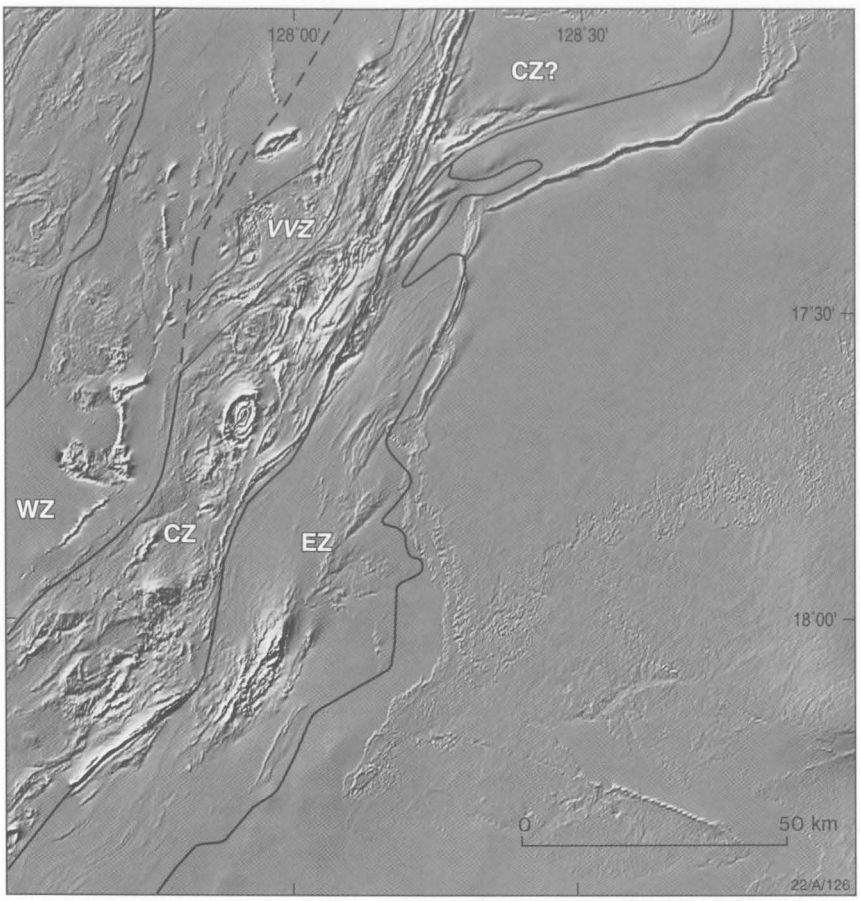


Figure 4.11. Processed grey-scale Total Magnetic Intensity image of the Dixon Range and Gordon Downs 1:250 000 Sheet areas, with a NW illumination filter to emphasise short-wavelength magnetic features. WZ, western zone; CZ, CZ?, central zone; EZ, eastern zone of the Halls Creek Orogen, and the more magnetic part of the Violet Valley zone (VVZ) within the central zone. Dashed line is the approximate position of the boundary between the western and central zones (see Chapter 3). The western boundary of the western zone is not well defined and is placed here at the Greenvale Fault, although others place the boundary farther west to include the preserved limits of the Whitewater Volcanics (see Chapter 3) (image by Taro Macias, AGSO).



1 *Palaeozoic sedimentary rock, basalt*

2 *Neoproterozoic and Mesoproterozoic sedimentary rock*

3 *Palaeoproterozoic sedimentary and felsic extrusive rocks*

4 *Palaeoproterozoic mafic and layered mafic-ultramafic intrusions, gabbro*

5B/5A *Palaeoproterozoic igneous and metamorphic rocks*

6 *Palaeoproterozoic felsic magmatic basement rocks >1900 Ma*

Geological boundary

Fault

Figure 4.12. Processed total-intensity gamma-ray spectrometric image displayed as a background to a simplified solid geology map of the Dixon Range and northern half of the Gordon Downs 1:250 000 Sheet areas (image by RDS). A, Sophie Creek Dome; B, Saunders Creek Dome; C, Castle Creek Anticline; D, trachytic volcanics at Dry Creek and Grants Patch; E, Brockman rare-earth element prospect. Labelled boxes mark the NW corners of 1:100 000 Sheet areas—AN, ANTRIM; DX, DIXON; HC, HALLS CREEK; LI, LINACRE; MI, McINTOSH; MR, MOUNT REMARKABLE; NI, NICHOLSON; OS, OSMAND; TC, TURKEY CREEK.

Table 4.3. Magnetic units and their properties for the Dixon Range and southern Gordon Downs 1:250 000 Sheet areas.

Magnetic unit (Fig 4.13)	*Group/Suite*	*Key geological unit(s)*[1]	*Dominant lithology*	*Magnetic response*	*Magnetic susceptibility range (SI*10^{-6} units)*	*Structural element (Figs 4.7 & 4.8)*	*Gamma-ray response (unit, Fig. 4.12)*	*Counts/ sec*	*Comment (magnetic susceptibility, SI*10^{-6} units)*
1b	Mahony Group	Purralili Sandstone, Glass Hill Sandstone, Boll Conglomerate	Sandstone, conglomerate	Weak	0–10	Ord Basin	Very weak (1)	2–7	
1a	Goose Hole Group	Elder and Negri Subgroups	Limestone, siltstone, shale	Weak	0–10	Ord Basin	Very weak to weak (1)	3–15	
2 upper		Antrim Plateau Volcanics	Fragmental basalt	Variable	1500–30 000	Ord Basin	Weak (1)	7–14	Potassic feldspar matrix; remanent magnetism recorded locally steeply inclined to northeast
2 lower		Antrim Plateau Volcanics	Amydaloidal basalt	Variable	200–30 000	Ord Basin	Very weak (1)	3–13	450–500 m thick
3c	Albert Edward and Duerdin Groups	Timperley Shale, Mount Forster Sandstone, Ranford Formation, Fargoo Tillite	Lithic sandstone, siltstone, mudstone, tillite	Weak	10–170	Wolfe Basin	Variable (2)	5–23	
3b	Ruby Plains Group	Illjarra Sandstone, Eliot Range Dolomite, Mount Kenahan Sandstone	Sandstone, dolomite, siltstone	Weak	150–500	Wolfe Basin	Very weak (2)	2–5	
3a	NA[2]	Wade Creek Sandstone, Helicopter Siltstone	Sandstone, siltstone	Weak	150–500	Osmand region	Variable (2)	5–20	
4	NA	Bungle Bungle Dolomite, Mount Parker Sandstone, Gardiner Sandstone	Dolomite, sandstone	Weak	150–500	Osmand region	Very weak to weak (2)	2–15	
5c	NA	Hart Dolerite	Dolerite	Moderate to variable	200–6000	Kimberley Basin	Very weak (4)	2–10	
5b	NA	King Leopold Sandstone, Texas Downs Formation, Red Rock Formation, Moola Bulla Formation	Sandstone	Weak	10–200	Kimberley and Speewah Basins	Variable (3)	5–21	Includes units of the Kimberley Basin and units correlated with these in the Osmand Range region, west of the Halls Creek Fault
5a	NA	Carson Volcanics, basalt within Red Rock Formation	Basalt	Variable	150–30 000	Kimberley and Speewah Basins	Weak (3)	4–14	Magnetically either a magnetic ridge or, if altered, magnetically weak. Magnetic susceptibility shows bimodal distribution
6d	Whitewater Volcanics suite	Greenvale and Castlereagh Porphyries, Whitewater Volcanics	Felsic volcanics	Weak	50–9000	Western zone of the HCO[3]	Moderate to high (5A)	10–21	Magnetic susceptibility generally low (less than 70)
6c	Mainly granites of Kevins Dam suite	Kevins Dam Monzogranite, Violet Valley Tonalite	Monzogranite, granodiorite, tonalite	Weak	50–9000	Western zone of HCO	Moderate to high (5A)	10–21	Mapped as a late phase of the Sally Downs Supersuite; Magnetic susceptibility generally low (less than 70)
6b	Granites of Paperbark supersuite (1860–1850 Ma)	Mainly granites of Paperbark supersuite	Monzogranite granite, granodiorite, tonalite, diorite	Weak	50–9000	Western zone of HCO	Moderate to high (5A)	10–21	Magnetic susceptibility variable; generally, but not always low (measured values less than 70)
6a		Marboo Formation	Pelitic metasediment (migmatised)	Weak	10–200	Western zone of HCO	Moderate to high (5A)	10–21	Magnetic susceptibility generally low (measured values less than 100)

7	NA	Unnamed	Metadolerite, gabbro	Weak	200–750	Central zone of HCO; Osmand Valley basement	Very weak (NA)	2–5	Dykes cutting Tickalara Metamorphics and Winnama Formation; too narrow to show on map
7	Granites and gabbro of the Sally Downs supersuite (1830–1820 Ma)	Sally Downs Granite, Mabel Downs Granite, McHale Granodiorite	Tonalite, granodiorite, granite, monzogranite, gabbro	High	200–40 000	Central zone of HCO; Osmand Valley basement	Very weak to weak (5B)	2–14	Corrara Granite in southwest could be mixed with a variety of rock types
8c	Mafic–ultramafic intrusions of groups TM, V, VI, Ug, and Cg	Norton (TM), Wilson Creek (V), Frog Hollow (V), Three Sisters (Ug), Armanda (VI), and Greenvale Fault (Cg) intrusions, other gabbroic intrusions	Mafic–ultramafic rocks, biotite quartz gabbro	Weak	200–600	Central and western zones of HCO	Very weak (NA)	2–10	Greenvale Fault (low)—biotite quartz gabbro; Armanda (low)—weakly layered olivine gabbro; Frog Hollow (high)—olivine gabbro and ferrogabbro; Norton—contains thin, basal intermittent gossanous unit
8b	Mafic–ultramafic intrusions of groups IV–VII, and Cg	Wild Dog Creek (IV), Sally Malay (V), Spring Creek (V), McIntosh (VI), Nine Mile (Cg), Black Hills Yard (VII) intrusions	Mafic–ultramafic rocks	High	12000–20 000	Central and western zones of HCO	Very weak (4)	2–10	Maximum magnetic susceptibility value recorded (42 500) in magnetite gabbro
8a	Mafic intrusions of groups II and III	Springvale (II) and Toby (III) intrusions	Mafic rocks, quartz-biotite gabbro	Moderate to high	2000–12 000+	Western zone of HCO	Very weak (4)	2–10	Toby has moderate magnetic response; Springvale has variable response
9	Mafic–ultramafic intrusions of group 1	Panton, South Melon Patch, and West McIntosh intrusions (all I)	Mafic–ultramafic rocks	Weak to variable	50–1000 (35 000)	Central zone of HCO	Very weak (4)	2–10	Highest values (>5000) in lower serpentinised dunite and harzburgite units; mainly less than about 1000
10b	NA	Koongie Park Formation, Milba Formation (in east)	Metavolcanic and meta-sedimentary rocks	Low to variable	20–5000	Central zone of HCO; Osmand Valley basement	Weak to moderate (5B)	4–16	Locally extreme (50 000+) magnetic values recorded in ironstones, associated with impure calcareous rocks and felsic volcanics
10a	Igneous and sedimentary rocks of Tickalara Metamorphics	Tickalara Metamorphics, Winnama Formation, Dougalls Tonalite, Milba Formation	Meta-greywacke, meta-mafic -intermediate intrusions, migmatite	Variable	100–60 000	Central zone of HCO	Variable (5B)	3–18	Milba Formation (2000–5000); Winnama Formation (20–3500)
11	NA	Woodward Dolerite	Metadolerite	Weak	200–600	Eastern zone of HCO	Very weak? (NA)	2–5	Too small to show on map
11 (east)	Halls Creek Group	Upper Olympio Formation (in east)	Metamorphosed turbiditic sedimentary rocks	Moderate	3000–7000	Eastern zone of HCO	Weak-moderate (5A)	6–16	Magnetite is secondary
11 (west)	Halls Creek Group	Lower Olympio Formation (in west)	Metamorphosed turbiditic sedimentary rock, alkaline volcanics	Weak	10–800	Eastern zone of HCO	Variable (5A)	3–23	Volcanics are not notably magnetic, but are prominent in spectrometric data
12	Halls Creek Group	Saunders Creek Formation, Biscay Formation	Mainly felsic volcanics, meta-sedimentary rocks	Moderate	30–40 000	Eastern zone of HCO	Variable (5B)	3–19	
13	NA	Sophie Downs Granophyre Member	Felsic volcanics	Weak	50	Eastern zone of HCO	Moderate to high (6)	17–22	
14	NA	Ding Dong Downs Volcanics	Bimodal volcanics	High	600++	Eastern zone of HCO	Very weak to weak (6)	5–10	

[1] Group numbers (I to VII: see Chapter 5) for mafic–ultramafic intrusions are indicated in parenthesis; TM = Tickalara Metamorphics; Ug = Undivided gabbro; Cg = Corridor gabbro.
[2] Not Applicable.
[3] Halls Creek Orogen.

but, like HCCa located farther to the southwest, it is a broader and more magnetised belt. The northern margin of HCCb approximates the Glidden and Lubbock Faults, and the southern margin, the Angelo Fault (Fig. 4.7; Tyler et al. 1995). The magnetised units are all monzogranites (Loadstone Monzogranite, Dillinger Monzogranite, Mount Christine Granitoid) and form part of the more oxidised, and locally magnetite-bearing Sally Downs supersuite (Sheppard et al. 1995, 1997a). HCCb has a more complex gravity expression. It forms a segmented belt of gravity anomaly highs as well as a parallel belt of lows (Fig. 4.6). A linear gravity anomaly feature within the belt aligns approximately with the trace of the Ramsay Range Fault (Fig. 4.7; see Tyler et al. 1998a for map details). In keeping with a generally weak gravity expression, it lacks high-grade metamorphic rocks and contains only a few small mafic–ultramafic intrusions (see Tyler et al. 1995 for map details).

Boundary between the Halls Creek Central and Biscay subelements

A marked and broad gravity gradient occupies a wide region between the Halls Creek Central (HCC) and Biscay (HCB) crustal subelements, and corresponds to the Halls Creek Fault and related faults (HCK, ADF, AF, & WF in Fig. 4.9). The gradient can be accounted for by the progressive down-stepping eastwards, across a series of subvertical faults, of one or more density boundaries; for example, a progressive increase downwards in metamorphic grade. Another explanation could be that there are a series of fault slices separating zones that decrease in metamorphic grade and degree of consolidation (stratigraphic age) from the granulites west of the Highway Shear Zone to sedimentary rocks of the Ord and Wolfe Basins in the east. Less well-defined gravity gradients correspond to both the Angelo Fault and its extension, the Mount Ramsay Fault in the southwest, and to the Osmand Fault and Red Rock Fault to the northeast (AF, MRF, OF & RRF in Fig. 4.9). Along these faults there is local evidence of their dipping steeply to the northwest or west, consistent with them being slightly reversed and, hence, contractional (Tyler et al. 1998b).

Crustal subelement HCB (Biscay)

This subelement corresponds to the eastern zone of the Halls Creek Orogen. It lies on the eastern margin of a prominent gravity gradient between the crustal elements labelled HCC and STS (b in Fig. 4.9). Several small, but prominent, elongate magnetic highs lie in what is otherwise a zone of low magnetisation and magnetisation variability (a magnetically 'quiet' region; Fig. 4.10).

HCB correlates with the mainly low-grade metamorphic rocks of the Halls Creek Group. It is cut by magnetic lineaments that correspond to faults; the most obvious of which is the southern continuation of the Halls Creek Fault (Figs 4.7, 4.9, 4.10, 4.13). The lack of a marked gradient in Bouguer anomaly values over this segment of the Halls Creek Fault (Figs 4.7, 4.9) accords with the view that it is the Angelo Fault that has taken up most of the displacement (Tyler et al. 1995).

Features (see Figs 4.9–4.13) to note within subelement HCB are:

(i) A series of basement domes exhibiting a range of magnetic patterns, reflecting a variety of localised, mainly volcanic sources (e.g. Ding Dong Downs Volcanics, unit 14 in Table 4.3, Fig. 4.13). The westernmost dome, containing the Sophie Downs Granophyre Member (unit 13; Blake et al. 1999) has a subdued, uniform magnetisation, whereas the magnetisation of the eastern domes is much higher.

(ii) The area corresponding to the Biscay Formation (unit 12 in Table 4.3, Fig. 4.13) displays a variable and generally moderate level of magnetisation attributed to a high content of basaltic volcanic and volcaniclastic rocks.

(iii) Thin units of ferruginous chert and trachytic volcanics near the base of the Olympio Formation are not resolved in the airborne data.

(iv) The amplitude and extent of a magnetic low where the Biscay Formation borders the Halls Creek Fault north of the Sophie Downs Dome are indicative of a region of weakly magnetised rocks, like the calc-silicate unit mapped along strike to the south (Blake et al. 1999).

(v) The western part of the outcropping Olympio Formation (unit 11 in Table 4.3, Fig. 4.13) is weakly magnetised, as might be expected for metasedimentary rocks (see below for information on the eastern part).

Boundary between crustal elements HCB (Biscay) and ST (Sturt)

The boundary between HCB (Biscay) and ST (Sturt) is complex and is thought to involve three-dimensional factors. The magnetic patterns reflect shallower sources of the Olympio Formation, whereas those causing the gravity low, used to delineate the crustal element boundary, appear to reflect an underlying low density rock unit, possibly an underthrust wedge of Neoproterozoic sedimentary rocks of the Wolfe Basin. However, the surface trace of the crustal element boundary, appears, from gravity data, to separate the eastern part of the Olympio Formation from the western part.

The slightly stronger and more variable magnetisation (Fig. 4.10) in the easternmost part of the Olympio Formation (Fig. 4.13) implies that the unit is relatively rich in more magnetic rocks, perhaps volcaniclastic rocks like those of the Biscay Formation (cf. Fig 4.10 & Fig. 4.13). As Neoproterozoic sedimentary rocks directly overlie the eastern part of the Olympio Formation (Table 4.3, Fig. 4.13), this easternmost unit is taken to be a separate, younger unit of the Olympio Formation (Blake et al. 1999).

It is useful to examine the factors that could have produced this unusual crustal boundary in more detail. Possible explanations for the gravity low (western STS) are that it represents:

(i) A Palaeoproterozoic sedimentary trough, made up of Olympio Formation, which thickens eastward underneath the Neoproterozoic sedimentary rocks of the Wolfe Basin. In this model, the southeastern margin of HCB would approximate the near-surface margin of the trough, flanked to the west by a

'basement' made up of the Biscay Formation and possibly the Ding Dong Downs Volcanics at shallow depths (Blake et al. 1999).

(ii) A Mesoproterozoic sedimentary trough underlying the Wolfe Basin, such as the Victoria River or Birrindudu Basins, which has been overthrust by the Halls Creek Group from the east. For such a model to be valid, the transport direction of the thrust would need to be oblique to the north-northeasterly-trending margin of the basin.

(iii) An underthrust wedge of rocks of a lower relative density, such as an even older trough lying beneath the exposed rocks of the Halls Creek Group.

(iv) The Halls Creek Group has been thrust over sedimentary rocks of the Wolfe Basin.

The first explanation—that the gravity low represents the margin of a trough filled with Olympio Formation continues under the Wolfe Basin—is the simplest one and is consistent with the geological mapping. This explanation would require the Olympio Formation to be considerably less dense than the Biscay Formation and any underlying units. However, the presence of a segmented homocline (monoclinal structure) at the contact between basement, made up of Olympio Formation, and the Wolfe Basin (Blake et al. 1999) implies the presence of a complex thrust zone of the type that typically marks a 'mountain front' (Vann et al. 1986, Erslev 1986). For this reason, the model where HCCb is thrust over sedimentary rocks of the Wolfe Basin (iv above) is favoured.

Sturt crustal element (ST) and its subelements STN & STS

Regional large-amplitude gravity lows east of HCB (Biscay) correlate with the thick parts of Neoproterozoic and Palaeozoic sedimentary successions (Fig. 4.9). A northern low, centred on the thickest preserved part of the Ord Basin, is labelled STN, and a low in the southwest, corresponding to the Neoproterozoic Wolfe Basin, is labelled STS. The magnitude and extent of a more extensive gravity low, which includes elements RO and V (Fig. 4.8), suggest that sedimentary rocks of the older Birrindudu Basin and/or the Roper Group of the Victoria River Basin, may also contribute to the low (Figs 4.7, 4.8). The higher Bouguer anomaly value to the southeast (Fig. 4.9) may be due to shallow older Palaeoproterozoic or Archaean basement in the region of The Granites–Tanami Inlier (Fig. 4.7), like that exposed in the Browns Range Dome (Page et al. 1995b, 1996).

Subelement STS (Sturt) in the southwest extends into an area mapped as Halls Creek Group (Blake et al. 1999), indicating a complex and transitional relationship with the Biscay subelement HCB.

Features to note in ST are:

(i) For the most part, units nearer the surface are very poorly magnetised and correspond to unmetamorphosed sedimentary rocks such as sandstone and limestone.

(ii) Flat-lying Antrim Plateau Volcanics show weak magnetisation, for the most part, and are visible only in images enhancing the high frequency signal, so in this area we can 'see' through to older deeper units. Narrow high-amplitude anomalies ('magnetic ridges') correspond to zones where the basalt is steeply dipping.

(iii) Prominent high-amplitude, long-wavelength magnetic anomalies in subelements STN and STS (Fig. 4.10) are not related to the Antrim Plateau Volcanics, but to a much deeper source. As they are not coincident with any positive gravity features, they may represent an extensive volcanic unit, either a felsic volcanic or a thin mafic volcanic unit within or at the base of a deep sedimentary trough. The felsic volcanic rocks of the Ding Dong Downs Volcanics underlying the Halls Creek Group are probably of sufficient magnetic intensity to account for these anomalies. These areas of high magnetisation do not align with any known bodies of magnetised granite in the region. In the Tanami region to the southeast (GT, Fig. 4.8), prominent magnetic highs correlate with basalt near the base of the Mount Charles beds (Blake et al. 1979). Such basalt could also account for the long-wavelength magnetic anomalies if they extend in the subsurface into the Gordon Downs Sheet area.

(iv) Moderate and more variable magnetisation in the easternmost part of Olympio Formation outcrop area belongs, strictly speaking, to subelement STS, as it overlies the gravity low defining this.

Crustal element RO (Rosewood)

This crustal element, which is centred on the Osmand Range region, is characterised by a marked regional gravity low (Fig. 4.9) and a prominent magnetic high (Figs 4.2 & 4.6). Near its southern boundary, magnetisation is higher in the west than in the east (cf. Figs 4.9, 4.10).

The crustal element correlates in part with metamorphic rocks of the Winnama Formation exposed in the Osmand Range. Fault slivers of gabbro, dolerite, and some basalt can explain narrow, elongate magnetic anomalies (magnetic 'ridges'), which are part of a fault system centred on the Osmand Fault (Tyler et al. 1997b, Blake 1997). This faulting repeats a volcanic unit in the Red Rock Formation, previously called the Fish Hole Dolerite (Tyler et al. 1997b), which may correlate with the Carson Volcanics of the Kimberley Basin (see Chapter 3). Tyler et al. (1995) placed these rocks in the central zone of the Halls Creek Orogen (Fig. 4.11).

A gravity gradient along the southern margin of the domain is considered to reflect a zone of southward thrusting at the northern margin of the Palaeozoic Ord Basin. Palaeoproterozoic rocks are interleaved with Neoproterozoic rocks in the area between the Osmand and Red Rock Faults, and the complexity of the magnetic patterns here (Figs 4.10, 4.11) indicates that slivers of these may be thrust over the Palaeozoic rocks of the Ord Basin.

Geophysical characteristics of geological units in the Dixon Range and northern Gordon Downs 1:250 000 Sheet areas

Physical properties of rock units

Summaries of the physical properties of geological units, grouped to emphasise their regional magnetic expression, are given in Table 4.3. Details of selected field and laboratory measurements are given in Appendix 5. Measurements include:

(i) magnetic susceptibility—field and laboratory measurements;

(ii) magnitude and relative inclination of normal remanent magnetism;

(iii) bulk specific gravity (dry density); and

(iv) relative gamma-ray spectrometric response in the field.

On the basis of the variation in the physical properties of mapped rock units, it is possible to combine units in various ways and erect regional rock units that have a more obvious regional pattern of magnetisation. These units and their physical properties are listed as 'magnetic units' in Table 4.3.

The relationship between these 'magnetic units' and units mapped geologically at the formation level is not always exact. For example, unit 10a, characterised by a variable magnetisation and corresponding to the Tickalara Metamorphics as a whole (Table 4.3), includes some of the more highly magnetised rocks in the region, including metapelites and some of the metamorphosed mafic rocks and rocks of the Dougalls suite granites.

In another regional magnetic group in the central zone are the granites of the 1830–1820 Ma Sally Downs supersuite (subunit 7, Table 4.3), which show a more variable but characteristic pattern of magnetisation. This regional unit includes uniformly magnetised granites, such as the Sally Downs Tonalite (Ogasawara 1988) and the Mabel Downs Tonalite (Sheppard et al. 1995).

In contrast, in the western zone, the granites of the 1860–1850 Ma Paperbark supersuite (Sheppard et al. 1995, 1997a,b) are placed in another separate unit, designated magnetic unit 6b (Table 4.3). These are not easily distinguished in the aeromagnetic data from granites of the younger Kevins Dam suite (Sheppard et al. 1995, 1997a,b), which are placed in magnetic subunit 6c (Table 4.3) and separated from subunit 6b by a zone of faulting. The problem is that both granite suites are poorly magnetised.

The mafic–ultramafic intrusions generally show moderate to high magnetic susceptibility. In Table 4.3 they are subdivided magnetically into unit 9 and subunits 8a, 8b, and 8c which have only a weak correlation with the regional geological classification of Hoatson (Chapter 5) and Trudu & Hoatson (1996; cf. earlier classifications of Hoatson 1993 and Hoatson & Tyler 1993).

Despite subtle discrepancies, the 'magnetic unit' approach, aids interpretation by allowing rapid comparison of the geological and geophysical data (cf. Figs 4.10, 4.13).

Spectrometric expression of geological units

The grey-scale image of total-count gamma-ray spectrometric data (Fig. 4.12) has the advantage that its tonal range can be related to ground measurements of total count (see Table 4.3). For example, near-black regions correspond to rock types with low count rates, such as sandstones of the Mahony Group in the Ord Basin (unit 1, Fig. 4.12) and the mafic–ultramafic rocks in the Halls Creek Orogen. Near-white regions correspond to the Olympio Formation; a remarkably homogeneous unit of turbidites derived from a common source region with high K, U, and Th. Potential sources include the granites of the Paperbark supersuite in the western zone of the Halls Creek Orogen (unit 5A, Fig. 4.12), the felsic Whitewater Volcanics (or its equivalent; unit 3), or some unit of similar composition that lay opposite the Biscay trough at the time of deposition.

In contrast, the Tickalara Metamorphics (also unit 5B, Fig. 4.12) corresponds to a zone with a wide range of tonal values, indicating intercalation of igneous and sedimentary components with different spectrometric count rates. Darker tones (with low count rates) in this zone correspond to calc-silicate rock, mafic volcaniclastic rock, metavolcanic rocks, gabbro, and dolerite. A similar spectrometric pattern east of the Halls Creek Fault corresponds to the Biscay Formation, which contains mafic and felsic volcanics. Four domes in this eastern region (the larger of which are labelled A, B, & C in Fig. 4.12) correspond to older igneous rocks: each dome has distinct spectrometric characteristics, implying compositional differences (Blake et al. 1999).

Discrimination of most units is clearer in red–green–blue (RGB) and other images of composite K, U, and Th spectrometric data. For example, trachytic volcanics in the Dry Creek–Grants Patch region and at the Brockman rare-earth element prospect (localities D & E, respectively, in Fig. 4.12) show up as blue features in RGB images, owing to their thorium content. The reason why these images are so well defined relative to other parts of Australia is that the region has undergone relatively recent uplift and erosion (Fig. 4.4), thereby removing the deep and complex regolith which otherwise masks the gamma-ray spectrometric characteristics of bedrock.

The continuity of anomalies in areas of soil cover implies colluvium, elluvial, and soil formed more or less in situ. However, in two areas the spectrometric response of units is complicated by a strong Th overprint. In one area, north of Halls Creek (near white region in unit marked 5B and mapped as clay and silt of black soil plains unit Czb in HALLS CREEK[2]; NI in Fig. 4.12), this is related to laterite development. In the other area (near white regions in unit marked 1 NICHOLSON, NI in Fig. 4.12) it corresponds to a cover of black soil (mapped as clay and silt of black soil plains unit Czb or unit Czba) and scattered exposures of Antrim Plateau Volcanics.

Magnetic expression of individual geological units

The distribution of stratigraphic units established at the end of the mapping program (Fig. 4.13) corresponds well with the distribution of magnetic units shown in Figure 4.14, based on a 1992 interpretation of airborne data.

The pattern of aeromagnetic anomalies as recorded in the TMI image (Fig. 4.10) is extensively influenced by anomalies due to igneous units. For example, the Cambrian Antrim Plateau Volcanics (basalt, unit 2, Fig. 4.14) and Palaeoprotesozoic basalt of unit 5 (Fig. 4.14) show strong, but variable, magnetisation.

Palaeoproterozoic basalt (unit 5, Fig. 4.14, unit 5a in Table 4.3) in the Osmand Range area is associated with a higher and more variable degree of magnetisation. Their similar magnetic expression and distinctive style of alteration raise the possibility that the Carson Volcanics and the basalt in the Red Rock Formation are correlatives (also compare unit 5a in Fig. 4.13 with the TMI image in Fig. 4.10).

Surprisingly, the Hart Dolerite, which intrudes the Kimberley and Speewah Basins, shows only a moderate level of magnetisation, which is quite variable.

The highest-amplitude magnetic anomalies correlate with the mafic intrusions, such as the gabbros of the McIntosh intrusion, a funnel-shaped mafic body (unit 8, Fig. 4.14) which corresponds to a series of concentric 'bulls-eye' anomalies (Figs 4.10, 4.11). The smaller mafic–ultramafic bodies, such as the Panton intrusion (unit 9, Fig. 4.14), are poorly magnetised, except for small serpentinised bodies (Fig. 4.10).

Several generations of linear magnetic anomalies in the area of granite in northeastern MOUNT REMARKABLE correlate with late-stage north and northwest-trending narrow gabbro intrusions and, less commonly, dolerite dykes (cf. Fig 4.10 with 'thin gabbro bodies' in Fig. 4.14). These dyke-like intrusions could be localised along early splay faults linked to a proto-Springvale Fault.

In the Halls Creek Orogen (Figs 4.9, 4.11) many of the granites of the Sally Downs supersuite, such as the Mabel Downs Tonalite (unit 7, Fig. 4.13), are associated with moderate to high magnetisation. This association is in keeping with their more mafic composition and their deformed and metamorphosed character, which tends to accompany the presence of magnetite.

Rocks mapped as Tickalara Metamorphics (unit 10, Fig. 4.14) are associated with more variable, but generally higher, magnetisation. The variability of magnetisation is inferred to result from the intercalation of a variety of rock types. These include markedly magnetic calc-silicate rocks and related para-amphibolites, weakly magnetic, sill-like, foliated, medium to coarse-grained ortho-amphibolites, and weakly magnetic, fine-grained to aphanitic metabasalt. Poorly magnetised to very weakly magnetised parts are dominated by metasedimentary rocks of various types, including metaturbidites and minor marble. Migmatitic sillimanite-bearing gneisses, such as those surrounding the Mabel Downs Tonalite, are commonly associated with high magnetisation.

Numerous sill-like bodies of variable magnetic granites of the Dougalls suite are not readily differentiated, and, are included in magnetic unit 10 (Fig. 4.13, Table 4.3) and placed in the Tickalara Metamorphics of current mapping. Magnetic phases of these granites include the Fletcher Creek Monzogranite, containing garnet, magnetite, biotite, and muscovite, and components of the Dead Finish Tonalite (Tyler et al. 1998b). Surprisingly, some of these granite bodies that are of tonalitic composition are only poorly magnetised.

In general, a high proportion of the sedimentary and metasedimentary rocks appear to show very weak to negligible magnetic expression, including the rocks of the Wolfe and Ord Basins and the higher-grade rocks of the Marboo Formation. Exceptions include some metasedimentary rocks in the higher grade Tickalara Metamorphics, much of the low-grade Biscay Formation and parts of the Olympio Formation.

Also showing little in the way of magnetisation are most granitic phases of the Paperbark supersuite (unit 6 in Fig. 4.14, unit 6b in Fig. 4.13) and late phases of the Sally Downs supersuite, including the monzogranite and minor tonalite of the Kevins Dam suite (unit 6c in Fig. 4.13).

East of the Halls Creek Fault, the low-grade metasedimentary rocks of the Biscay Formation (unit 12, Figs 4.13 & 4.14) are associated with moderate but variable magnetisation, reflecting the high volcaniclastic content of the unit (see also Blake et al. 1999). Mafic extrusives in the lower part of this formation show a weak to moderate magnetic expression. However, accompanying, but minor, felsic volcanics, recognised from their high gamma-ray spectrometric total count, are variably magnetised, with increasing magnetisation towards domes of Ding Dong Downs Volcanics (alongside units 14 in Fig. 4.14). Thin BIFs (banded iron formations) associated with the Ilmars and Little Mount Isa Cu–Pb–Zn prospects in the Biscay Formation bordering the Halls Creek Fault (Hoatson et al. 1995) are not resolved in the regional magnetic data.

The domes east of the Halls Creek Fault in HALLS CREEK show contrasting magnetic expressions, consistent with their lithological differences. In the Sophie Downs Dome (A in Fig. 4.12), a complex magnetic pattern suggests a mixture of mafic and felsic rocks (Ding Dong Downs Volcanics; unit 13 in Fig. 4.14). Here, the Sophie Downs Granophyre is marked by a small magnetic low (unit 13 in Figs 4.13, 4.14). In contrast, in the Saunders Creek Dome (B in Fig. 4.12, unit 14 in Fig. 4.13), mafic and felsic volcanics give rise to a complex pattern of magnetisation masked by magnetisation related to broader wavelength anomalies related to deeper bodies (unit 14 in Fig. 4.14). To the east, in the Castle Creek Anticline (C in Fig. 4.12), a set of small, narrow,

[2] 1:100 000 sheet names throughout this *Bulletin* are in capital letters to avoid confusion with identical place names and to distinguish them from 1:250 000 sheet names.

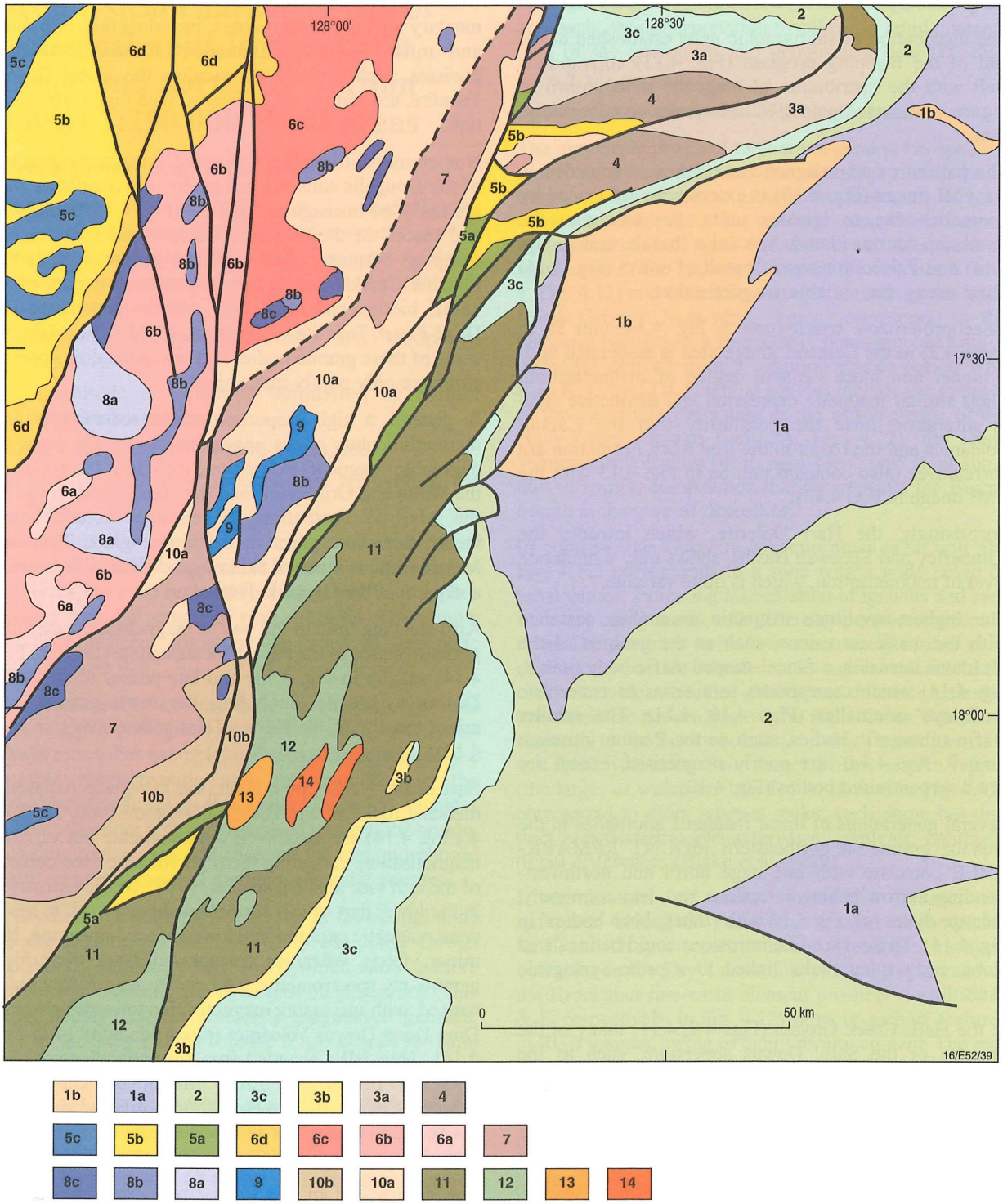
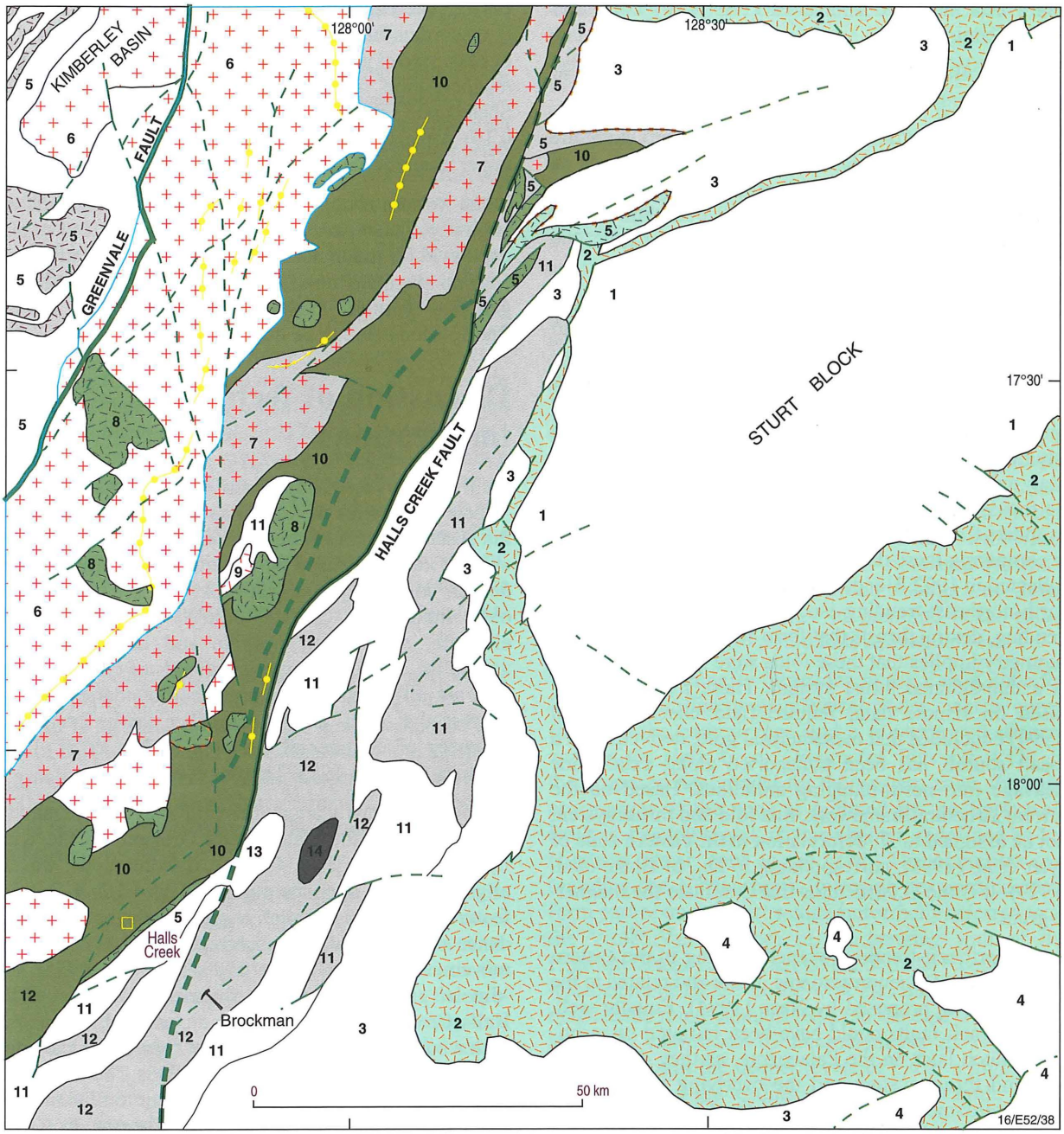


Figure 4.13. Geological units, grouped according to their magnetic character to produce a simplified geological map of the Dixon Range and Gordon Downs 1:250 000 Sheet areas. See Table 4.3 for magnetic unit descriptions (compiled by RDS from 1:100 000-scale maps).



MAGNETIC SIGNATURE

Dominant lithology	High	Moderate	Weak	Variable	Age (Ma)
Sedimentary rocks, some volcanic rocks					Base 300
Granite, felsic extrusive					530
Granites, (tonalite, granodiorite, granite, granitic gneiss)					800
Mafic igneous rocks (basalt, gabbro, ultramafics)					1750
					1860-1870
					1900

Geological boundary
Inferred fault
Thin gabbro body
Block / province boundary
Boundary to deep magnetic body

STRATIGRAPHIC INTERPRETATION

KIMBERLEY BASIN	HALLS CREEK OROGEN	STURT BLOCK
		1
		2
		3
		4
5	5	5
6	6	
	7	
	8	
	9	
	10	
	11	11
	12	
	13	
	14	

Figure 4.14. Preliminary 1992 interpretation of regional aeromagnetic data of the Dixon Range and Gordon Downs 1:250 000 Sheet areas in terms of magnetic signature of various lithological associations (compiled by RDS from magnetic data).

segmented magnetic anomalies (Fig. 4.10) correlates with volcanics.

Magnetic and spectrometric expression of structural features: some examples

Structural information can be obtained by correlating the magnetic grain with regional schistosity and trends of fold–thrust systems, and the discordant magnetic lineaments with faults. Such information is best extracted by viewing grey-scale pixel images that accentuate the high-frequency content of the data (Fig. 4.11).

Correlation with airborne data sets is easier when the structure has been mapped in detail. It can be used to extract information from regions lacking obvious lithological differentiation and to extrapolate the result along strike. For example, in the eastern zone, in a study of controls on the distribution of gold in the Biscay and Olympio Formations, Nash (1994) processed and analysed spectrometric, air-photo and Landsat TM data. He focussed on the Dry Creek area north and east of the Saunders Creek Dome (unit 14 in Fig. 4.13), with a view to comparing these data with the airborne magnetic data collected in 1992. He identified east-verging, overturned north-northeast-trending isoclinal folds and northwest-trending, dextral thrusts that form strike-slip ramps. This geometry implies that these folds were generated as part of a thin-skinned thrust system. These interpretations, based on remote data, require field checking. Nash (1994) concluded that mesothermal gold, derived from a basalt source, has been transported along axial-plane cleavage into north-plunging anticlines. Based on the current structural framework, this fold and thrust system can be assigned to D_2 deformation in the eastern zone of Tyler et al. (1995), corresponding to D_{H2} of Blake et al. (1999). It is the D_2 structures that dominate the magnetic grain.

North-northeast-trending wrench faulting in the eastern zone could be Palaeoproterozoic in age and related to the D_2 folding, as proposed by Nash (1994). Equally well, these wrench faults could have been initiated or reactivated much later, in the Palaeozoic, as they disrupt the fold and thrust system and the overlying rocks of the Neoproterozoic Wolfe Basin and the Cambrian Antrim Plateau Volcanics (Tyler et al. 1998c). Disruption of these and older formation boundaries indicates that late wrench faulting has a dextral shear-sense. Neoproterozoic activity on this wrench fault is indicated by the discontinuous distribution along strike of some Neoproterozoic units (e.g. Mount Kinahan Sandstone) and by the thickening and thinning of units towards the fault (e.g. Ranford Formation; Tyler et al. 1998b). The wrench fault system appears to branch from the Halls Creek fault system and swing northeast to converge with the thrust system of which the Osmand Fault (OF in Fig. 4.9) forms a major component (compare Figs 4.10 & 4.11 with Fig. 4.13). These fault systems are readily apparent in the magnetic data.

Within the central zone, east of the Springvale Fault (SF in Fig. 4.9) and the Highway Shear Zone (HS in Fig. 4.9), the main magnetic grain (Figs 4.10, 4.11) correlates with the marked D_3 fabric and high-grade M_3 metamorphic assemblages and migmatisation of Tyler et al. (1995). The Highway Shear Zone, marked by a regionally discordant magnetic grain, possibly represents the D_4 of Sheppard et al. (1997b), or a younger event. A drop in magnetisation on the southeast side of the Highway Shear Zone, immediately bordering the shear zone, (Fig. 4.10) correlates with a drop in metamorphic grade to upper amphibolite facies (see Sheppard et al. 1997b).

In the western zone, west of the Springvale Fault and the Highway Shear Zone, the magnetisation is too poorly expressed for much detailed information to be interpreted from magnetic trends, as much of this region is homogeneous granite. However, several splays of the Springvale Fault can be distinguished.

Discussion of tectonic implications

Wellman (1978, 1988) described how major gravity 'dipole' anomalies in Australia, including that marking the eastern margin of the Halls Creek Orogen, could be used to identify crustal block boundaries formed where denser, commonly younger, crust has been thrust over older lithosphere. Gravity 'dipoles' are paired, major, elongate, subparallel, positive and negative gravity anomalies. In the Precambrian shields of Canada, many (but not all) of the major province boundaries that are expressed as such 'dipole' anomalies can be interpreted in terms of continental collision (Gibbs et al. 1983, Thomas & Gibbs 1985, Thomas et al. 1988).

The 'dipole' gravity anomalies (Fig. 4.6) associated with the margins of the Halls Creek Orogen and the King Leopold Orogen (Fig. 4.7) are discontinuous, do not align and are of opposite polarity (Figs 4.1 & 4.6). Such features indicate a complex origin, which geological evidence shows involved transcurrent as well as orthogonal movements (Griffin & Grey 1990, Tyler et al. 1995). The 'dipole' gravity anomaly at the eastern margin of the Halls Creek Orogen is of a type commonly associated with a sub-plate or plate boundary, representing a major collisional suture (Gibbs et al. 1983, Thomas et al. 1988), possibly a continent–continent collision with basement reactivation (Fig. 4.3a; Thomas & Gibbs 1985). That is, the complex boundary between crustal subelements HCC–HCB and subelements STS–STN could be a crustal block boundary. Analysis of new seismic wave speed data by van der Hilst et al. (1998, SKIPPY Project) reveals abrupt changes in shear-wave velocity in the upper mantle across the Halls Creek Orogen, suggesting the multifaceted Halls Creek Orogen overlies a boundary of lithospheric extent. The implication is that the Halls Creek Orogen is a complex orogenic wedge preserved at a Proterozoic plate boundary.

Subelement HCB forms a complex transitional feature (Fig. 4.9) and could represent an imbricate thrust wedge on the foreland (proactive) side of the orogen. The lack of strike continuity at the boundary between the basement of the western zone of the Halls Creek Orogen and the sedimentary cover rocks to the east can be explained in terms of offsets, commonly with a sinistral shear sense, produced in a series of fault movements during

the Mesoproterozoic, Palaeoproterozoic, and Palaeozoic (White & Muir 1989, Thorne & Tyler 1997).

That the eastern margin of the central zone could represent a province boundary of crustal proportions is supported by the different geological and structural histories across the margin (Tyler et al. 1995). It is also supported by the chemical character of the ~1850 Ma tonalite and trondhjemite of the Dougalls suite in the central zone, which resembles that of tonalite and trondhjemites found in island arcs (TTG or low-Al tonalite–trondhjemite–granodiorite suite) or along continental margins related to subsidiary back-arc spreading during subduction (Sheppard et al. 1995, 1997a). Granites of the ~1830–1805 Ma Sally Downs supersuite in the central zone include variants such as the 'Ord River tonalite suite' and 'Mabel Downs tonalite suite' of Ogasawara (1988) and Sheppard et al. (1997a), which have trace-element characteristics suggesting possible derivation from a source where garnet was stable (Sheppard et al. 1997a). These source rocks could have been underthrust to the depth of garnet stability in the early stages of the Halls Creek Orogeny or during an earlier event. Irrespective of whether a plate boundary is indicated, the eastern margin of the central zone is a major crustal boundary.

The centre of the gravity gradient forming part of the 'dipole' partly aligns with the Halls Creek Fault. The gradient is distributed over a wide zone to the east and west of the fault zone and passes eastwards into a regional gravity low centred over the western margin of the Wolfe Basin. The gradient is most marked in the section of the fault zone lying between the Osmand and Angelo Faults (Fig. 4.9, cf. Fig. 4.6).

To explain the width of the gravity gradient and why the composite gravity low overlaps the basement–cover boundary, it is postulated that an imbricate thrust complex fans out from the Halls Creek Fault towards the Wolfe Basin. The presence of a homocline at the preserved western margin of the Wolfe Basin points to a concealed trapezoid wedge or triangular zone of disrupted sedimentary rocks that marks the front of the imbricate thrust complex. Such a geometrical relationship is well documented in numerous examples, typical of many 'mountain fronts' (Prucha et al. 1965, Vann et al. 1986, Erslev 1986, Shaw et al. 1991, Leven & Lindsay 1995). In this type of structure the sedimentary succession has been disrupted by the wedge and back-thrust over a homocline. The segmented monoclinal structure marking the preserved edge of the homocline may been developed along the western margin of the Wolfe Basin. Evidence for accompanying back-thrusting is suggested by a number of bedding-parallel detachment zones, which are documented in the Palm Spring region on HALLS CREEK (Blake et al. 1999) and ANTRIM. The segmented nature of the homocline can be explained by compartmentalisation of the thrust complex, which could be the result of reactivation of several basement wrench faults during the King Leopold Orogeny at the close of the Precambrian. These basement wrench faults could have initially formed in the eastern zone of the Halls Creek Orogen during transpressional tectonism in the Palaeoproterozoic (Nash 1994).

The gravity gradient, centred on the Halls Creek Fault, that forms the central part of the linear 'dipole' gravity anomaly also forms part of the eastern margin of the main regional gravity high (Fig. 4.6), so the magnitude of the gradient is, in part, a reflection of the magnitude of the regional gravity high (Fig. 4.6). The 'dipole' gravity anomaly is similar in magnitude and form to that associated with the boundary between the Yilgarn Craton and the Albany–Fraser province (Murray et al. 1997, Shaw et al. 1995, 1996). This latter boundary is considered to mark the site of a collisional orogeny between the South and West Australian cratons during the assembly of Rodinia at about 1300–1200 Ma (Myers et al. 1996) or possibly earlier.

The regional gravity high (Fig. 4.6, crustal microelement HCCc–f) is associated with the mafic–ultramafic intrusions and the Tickalara Metamorphics (northern part of HCC in Fig. 4.8). It is of an unusually large magnitude compared with other anomalies on the Australian continent (Murray et al. 1997). It is comparable, in its segmented expression and magnitude, to that of the Giles Complex in the Musgrave Block of central Australia (Glikson et al. 1996), which comprises large mafic–ultramafic complexes in granulite belts, which have been uplifted from mid to lower crustal levels.

The mafic–ultramafic intrusions in the East Kimberley fall in two different geophysical zones, which correspond to the central zone and a reinterpreted western zone of the Halls Creek Orogen (cf. Figs 4.9, 4.11). In the proposed new model for the western zone, the eastern margin of the zone is outlined by the Springvale Fault in the south and, in this chapter, redefined as the Highway Shear Zone in the north. The granulites surrounding the Norton mafic intrusion are considered to form part of an upthrust wedge (informally referred to as the Violet Valley zone) in the hanging wall of the Highway Shear Zone. That is, the boundary between the microelement HCCe in the west and the largely poorly magnetised microelement HCCf in the east (Fig. 4.9, cf. magnetic expression of microelements in Fig. 4.10) could represent the deeper levels of either a high-angle reverse fault or the leading edge of a thrust fault.

Along the Highway Shear Zone, lower crustal granulites and mafic–ultramafic intrusions have been uplifted in a series of movements. During the Halls Creek Orogeny at about 1835 Ma, synchronous with intrusion of the Mabel Downs Tonalite (cf. Tyler & Page 1996), strike-slip movements dominated activity within the Highway Shear Zone, both extensional and compressional phases being probable. Sheppard et al. (1997b, pp. 19–20) consider that the main activity on the Highway Shear Zone was a transpressional sinistral movement during D_4 under conditions of upper greenschist to lower amphibolite facies (M_4).

When extrapolated regionally to the southwest and then west, this boundary corresponds to the southern margin of crustal element KL, which equates with the King Leopold Orogen (Figs 4.7, 4.8). In this southwestern region, the southern boundary of crustal element KL is seen to be discordant to a series of subparallel boundaries to the south, against elements O (including the

transitional Oscar inlier segment at its northern margins) and HCC (Figs 4.2, 4.8). The discordant relationship suggests that this boundary between elements KL and HCC (Fig. 4.8) is also a major province boundary and could have been a Proterozoic plate boundary disrupted by extensive and recurrent reactivation, including strike-slip faulting.

In such a tectonic situation it is possible that large mafic–ultramafic bodies have been intruded into zones of weakness along this plate boundary dominated by strike-slip fault movements, that this boundary was subsequently overthrust from the northwest by granites of the Paperbark supersuite, and that the thrust front corresponds to the Highway Shear Zone, the reactivated boundary between the western and central zones of the Halls Creek Orogen (Fig. 4.11).

The mafic–ultramafic rock bodies appear to have been intruded during late syn to post-orogenic events. The first probably followed the main ~1860 Ma deformation and metamorphism of the Hooper Orogeny (Tyler & Griffin 1993, Sheppard et al. 1997b) in the western zone of the Halls Creek Orogen. The second largely followed the main ~1835 Ma deformation of the Halls Creek Orogeny in the central zone (Tyler & Page 1996, Myers et al. 1996, Griffin et al. 1998). The Halls Creek Orogeny is thought to have brought the Kimberley (K in Fig. 4.8) and Sturt–Tanami (STN–STS/GT in Fig. 4.8) plates together (Tyler & Page 1996, Myers et al. 1996, cf. Tyler et al. 1995).

In order to explain the close temporal and spatial relationship between the granites emplaced during the Halls Creek Orogeny and the Highway Shear Zone, we propose that strike-slip movements were an important part of the Halls Creek Orogeny in the central zone of the Halls Creek Orogen (cf. Myers et al. 1996: Fig. 6). Several features suggest that the relationship of the Mabel Downs Tonalite to the Highway Shear Zone is analogous to the relationship of the Donegal Granite to the Knockateen Slide in northwest Ireland, interpreted as having been emplaced into a transcurrent shear zone (Hutton 1990). Analogous features include the elongation of the granites parallel to and contiguous with the master shear zone, the similar geometry and style of the foliations in both granite and shear zone, and similar ages of activity in both granite and shear zone. In the Halls Creek Orogen, both the northeasterly trending Mabel Downs Tonalite and the Highway Shear Zone show steeply northwest-dipping foliations and down-dip lineations (Tyler et al. 1998b) and both tonalite and shear were active at ~1830 Ma (Tyler & Page 1996, Sheppard et al. 1997b). Farther southeast the Corrana Granite shows a similar relationship to the ductile part of the Springvale Fault, which we equate with the Highway Shear Zone (Tyler et al. 1998b). Supporting evidence for a transpressional style of tectonic activity in this zone is provided by Sheppard et al. (1997b), who have documented continuing transpressional movement on the Highway Shear Zone (their D_4) and by Kendrick et al. (1999), who provide local field evidence for synchronous transpression and magmatism in this zone, although the timing of these activities may need refinement. Those ~1845 Ma Sally Malay mafic–ultramafic intrusions that parallel the Highway Shear Zone (Chapter 5) could have a similar origin to the granites, as could similar mafic–ultramafic intrusions parallel to the Springvale Fault. In theory, tensional cracks and dilational jogs within a strike-slip fault system (Tikoff & Teyssier 1992, Hutton 1990) could have initially focussed intrusion of both granite and mafic–ultramafic plutons. Alternatively, an en-echelon P-shear array, a type of complex set of second-order, second-generation shears related to Riedel shears (Naylor et al. 1986, Sylvester 1988), could provide continuous zones of dilation within a transpressional orogenic zone, as argued by Tikoff & Teyssier (1992). We envisage that pockets of dilation are formed during switches from orthogonal to oblique tectonism in an overall strike-slip fault system (see also Chapter 7).

Similarly, during the final stages of the Hooper Orogeny, we suggested that emplacement at depth of several large bodies of mafic–ultramafic rock, such as the exposed Toby, Springvale, Panton, and Big Ben intrusions, could have been initially focussed into pockets of dilation within the Halls Creek Orogen. Pockets of dilation could have formed where the proto-Springvale Fault interacted with some complex restraining feature, such as a set of cross-faults. At such depths, the proto-Springvale Fault could have represented a steeply dipping plate boundary, which at the surface approximates the present position of the boundary between the central and western zones. Complex stresses conducive to localised transtension could have been generated in this region if the proto-Springvale Fault zone was linked to and interacting with a proto-Panton Fault zone to produce a fault complex akin to a restraining bend within the overall north-northwest-trending strike-slip fault zone. A possible analogous structure is the Lebanese restraining bend in the Dead Sea region (Butler et al. 1998). In the East Kimberley case, the apparent fanning of faults or possible faults near the intersection of the proto-Springvale and proto-Panton Faults could be explained by localised fault-block rotation. Gabbros of the Corridor group appear to have intruded some of these fault splays, which show evidence of subsequent reactivation.

Note that, as revised, microelement HCCe continues on a northeasterly trend, as shown in Figures 4.8 and 4.9, and does not follow the Springvale Fault northwards, as shown on the map of the Australian Crustal Elements (Shaw et al. 1996). We consider that the Highway Shear Zone represents the effective continuation of the wide zone of shearing developed to the south along the margin of the proto-Springvale Fault. On the other hand, Sheppard et al. (1997b) implied that the upper levels of the proto-Springvale Fault north of the Panton Fault were overprinted by intrusion of granites of the Sally Downs supersuite at about 1835–1805 Ma, when the central and western zones were 'stitched' (cf. Griffin et al. 1998). The presently exposed Springvale Fault continues northwards as a set of fault splays that presumably represent later reactivation, under brittle conditions, possibly during the Yampi Orogeny (Tyler et al. 1995, Thorne & Tyler 1997) at 1450–1000 Ma (Shaw et al. 1992, Sheppard et al. 1997b). The splay that has the most northerly trend is traditionally labelled as the continuation of the

Springvale Fault (Dow & Gemuts 1969, Sheppard et al. 1997b), but we argue that the northerly continuation of the Springvale Fault is more complex.

Within the western zone of the Halls Creek Orogen, dense high-grade metamorphic rocks and a variety of mafic intrusive rocks that underlie the exposed granites can account for the regional positive gravity high. As the western zone is characterised by a regional magnetic low, any mafic–ultramafic intrusions at mid-crustal or deeper levels are likely to be either small bodies or high-grade metamorphic rocks (granulites) that are weakly magnetised, otherwise they should show up in the magnetic data. If olivine is present in any accompanying mafic–ultramafic intrusions, its alteration to magnetite has been inhibited. It is postulated that the dominant magnetic mineral in these deeply buried high-grade metamorphic rocks could be 'ilmenite' rather than 'magnetite'. At depths of 20–25 km or more, equivalent to pressures in excess of 6–7 kb (at 600–700 MPa), metamorphic olivine is not necessarily stable in gabbroic compositions (Green & Ringwood 1967), so olivine may not be present, and, as a consequence, magnetite would not be expected as an alteration product. That is, these high-grade rocks would have been subject to pressure in excess of those indicated for the mafic–ultramafic intrusions presently exposed at the surface (cf. Trudu & Hoatson 1996, and Chapter 9 for pressure and temperature estimates of exposed mafic–ultramafic intrusions). The magnetic expression of deeper rocks could also be masked by a terrain of thick granite bodies of lower density and weak magnetism (Paperbark supersuite). This terrain could have been emplaced in part by the thrusting of Paperbark supersuite rocks over denser, high-grade metamorphic rocks, thereby masking any magnetism. This complex of dense rocks underlying the granites of the western zone could include small, magnetised, but unmetamorphosed mafic–ultramafic intrusions, like Frog Hollow and Sally Malay, which, at mid-crustal depths, would be unrecognisable in the magnetic data. The postulated complex of dense rocks could be the westward down-dip continuation of the Violet Valley zone (equivalent to subzone IIc of Hancock & Rutland 1984). The Violet Valley zone is distinctly less magnetic than the belt immediately to the east of the Highway Shear Zone and this could be because the formation of magnetite is inhibited by the presence of graphite (see discussion below, Hoatson et al. 1997, and Thornett 1981 for record of graphite).

The metamorphic rocks of the Marboo Formation in the western zone of the Halls Creek Orogen are poorly magnetised, as is generally the case in the King Leopold Orogen. In metamorphic rocks, the formation of magnetite is related not only to the rock composition, but also to the ratio of ferrous to ferric iron, the oxygen fugacity, and several other poorly understood factors (Frost 1991). It is suggested that the weak magnetisation of these rocks is because the original sedimentary rocks were deposited in a carbon-rich, reducing environment. The presence of carbon as graphite potentially controls the oxygen fugacity, along with the original lithological composition. So, in the absence of a high fluid flux, the original reduced state of the sedimentary rocks tends to be maintained, thereby restricting reactions that could lead to the formation of oxidised ferromagnetic minerals, such as magnetite, during metamorphism (Fyfe et al. 1978). In principle, at higher metamorphic grades, in situations where TiO_2 is sufficiently abundant, ilmenite-bearing assemblages, characterised by poor magnetisation, will tend be favoured over more oxidised assemblages containing titaniferous magnetite or magnetite-bearing assemblages, characterised by high magnetisation (cf. Rumble 1973).

The granites of the Paperbark Supersuite and the Kevin's Dam suite of the Sally Downs supersuite in the western zone of the Halls Creek Orogen (Sheppard et al. 1995, 1997a,b) also tend to be weakly magnetised. It is postulated that these have either been thrust over dense high-grade metamorphic rocks and several mafic intrusions at depth, or they have been emplaced at a higher crustal-level than the high-grade metamorphic rocks, or some combination of both processes. This tectonic emplacement could have taken place during two events, following the peak of the Hooper Orogeny (Tyler & Griffin 1993) and during D_5 of the Halls Creek Orogeny (Tyler & Page 1996, Sheppard et al. 1997b), following intrusion of the Mabel Downs Tonalite.

In contrast, there is an abundance of magnetite in the central zone of the Halls Creek Orogen east of the Highway Shear Zone and its southwesterly continuation as the Springvale Fault. The diverse rocks of the central zone are highly variable in their degree of magnetisation and, in places, show intense magnetisation (see Appendix 5), consistent with them representing rocks uplifted from mid to lower crustal levels (Mutton & Shaw 1979). The most magnetised rock types include sillimanite-bearing pelitic gneiss, some of the calc-silicate gneisses, and rare banded magnetite quartzite. Neither the rocks of meta-igneous origin (e.g. pyroxene mafic granulite, amphibolite, and metadiorite), nor the para-amphibolites are particularly highly magnetised (Appendix 5). Some of the magnetite appears to have formed during metamorphism (M_3) accompanying the Halls Creek Orogeny, particularly in pelitic gneisses and parts of the Mabel Downs Tonalite that have been deformed and metamorphosed. The magnetic properties of the mafic–ultramafic intrusions in the central zone are highly variable, and are discussed in Chapter 7.

The high gamma-ray spectrometric total count rate of the granites in the western zone of the Halls Creek Orogen (Fig. 4.12) is consistent with their high potassium content and more felsic overall composition compared with those in the central zone (Sheppard et al. 1995, 1997a). The weakly magnetised bodies in the western zone imply that the gabbros associated with these granites are actually hybrid rocks (biotite gabbro, diorite, and tonalite) that form discontinuous, and arguably thin, bodies, which do not contribute significantly to the magnetic expression of the western zone. The geophysical expression of the western zone accords with the view that most of the granites belong to either the Paperbark supersuite (older part of the Bow River Batholith, Sheppard et al. 1995, 1997a,b) or granites derived from a similar source. The geochemistry of these granites is consistent with the view that they have been

emplaced in an extensional setting, either along a continental margin or behind an island arc (i.e. in a back arc; cf. Sheppard et al. 1995, 1997a).

The geophysical expression of the granites of the Paperbark supersuite in the western zone of the Halls Creek Orogen is like that of the granites of the King Leopold Orogen. Hancock & Rutland (1984) referred informally to these granites as the Bow Batholith. They are typical of the high K_2O/SiO_2 granites of northern Australia and are not considered to be as mafic as the bulk of granites making up the Sally Downs supersuite (Sheppard et al. 1995, 1997a,b).

The tectonic framework we have deduced from the geophysical data agrees in broad outline with the sedimentological, petrological, and structural analysis of Hancock & Rutland (1984) to the extent that strike-slip fault movements dominate the tectonic zones of the Halls Creek Orogen. As a consequence, the characteristics of collision orogeny are limited. We differ from them to the extent that we suggest there are two major subparallel sub-plate boundaries: a westernmost one, which separates the Halls Creek Orogen from the King Leopold Orogen, and a eastern one, separating the central and east zones of the Halls Creek Orogen. It is conceivable that these two sub-plate boundaries form part of a crustal wedge and merge at depth to form a single complex zone of lithospheric plate interaction. The Halls Creek Orogen and King Leopold Orogen are not regarded as forming a conjugate pair, as suggested by Hancock & Rutland (1984). Rather, the geophysical pattern of the Halls Creek Orogen is more in keeping with a complex, but continuous, transcurrent plate boundary, developed in two orogenic stages, which has been distorted by later plate movements.

We are in broad agreement with the proposition of Tyler et al. (1995) that a terrane boundary separates the central and eastern zones of the Halls Creek Orogen. We also agree with Tyler & Page's (1996) suggestion that these terranes were 'stitched' during the Halls Creek Orogeny at about 1840–1830 Ma (see also Myers et al. 1996). However, a number of the geophysical and related geological features are, in our view, more easily explained if transpressional and transtensional tectonism played an important part in the early history of the Halls Creek Orogen as well as the later stages, as recognised by Tyler & Page (1996).

The ideas developed from the current study are summarised in Figure 4.15, which shows an interpreted, schematic model of a crustal scale section across the Halls Creek Orogen, and indicates possible relationships of exposed rock bodies to the Bouguer and TMI anomalies. We are concerned in this figure with what geological features and events are important to the construction of a crustal scale cross-section of the region. Of particular interest is how and when the various crustal components came into place and contributed to both the regional Bouguer anomaly and the major, linear, 'dipole' anomaly. Processes such as uplift of deep crustal blocks and the intrusion of mafic and, to a lesser extent, intermediate rocks can increase the mass excess in the crust. Several features of the model are speculative and require further testing or refinement by rigorous geophysical modelling and further geological research. However, the section takes into account the exposed geology and the distribution of gravity and magnetic anomalies, and it incorporates the following suppositions about the tectonic evolution of the region:

(i) Early in its history, either the eastern or western margin of the Halls Creek Orogen was subject to underthrusting, involving crustal thickening at a plate or sub-plate boundary–compare Hancock & Rutland (1984) with Sheppard et al. (1997a,b) and Griffin et al. (in press).

(ii) Stretching at this lithospheric plate or sub-plate boundary resulted in heating of the evolving sedimentary pile, melting of the lower crust, and generation of the voluminous and dominantly felsic magmas of the Paperbark supersuite. These granites could have originated in an extensional setting, possibly behind an oceanic island arc to the east, as suggested by Sheppard et al. (1997a, Wyborn et al. 1992) or above a fossil subduction zone, as suggested by Griffin et al. (in press). Some of the mafic igneous rocks preserved in the Tickalara Metamorphics could represent this evolutionary stage. However, further geochemical studies are needed to resolve their tectonic setting, which could be that of an oceanic arc or ensialic marginal basin (see Chapter 7, cf. Sheppard et al. 1997a, Griffin et al. in press).

(iii) In a series of magmatic pulses between about 1857 Ma and 1845 Ma (see Chapters 5–7) more focussed extension, possible in a transtensional setting, resulted in a localised mafic underplate. As a result, primary mafic tholeiitic magma pooled at the base of the crust in a postulated zone of dislocation, approximating a proto-Springvale Fault, aligned on a more northerly and slightly oblique trend to that of the regional fault system of the developing orogen. The progressive influx of mafic magma may have provided additional heat for the high-grade regional metamorphism at this time. The deeper mafic intrusions (e.g. Norton) were metamorphosed and deformed during the Hooper Orogeny (Tyler & Griffin 1993), which peaked at or before ~1850 Ma, whereas intrusions at higher levels in the crust (e.g. Springvale and Toby) escaped major metamorphism and deformation. It was in the shallower intrusions that conditions of tectonic quiescence allowed layering and intricate cumulus textures to develop in the mafic–ultramafic intrusions.

(iv) By about 1845–1840 Ma in the central zone of the Halls Creek Orogen, dilational conditions existed locally, leading to the subsidence and volcanism recorded by the Koongie Park Formation (Blake et al. 1999).

(v) By the time of the Halls Creek Orogeny (1840–1835 Ma, D_3 of Tyler & Page 1996, Tyler et al. 1995; D_{H2} of Blake et al. 1999), a fold–thrust complex had formed. A thrust front migrated eastwards from the

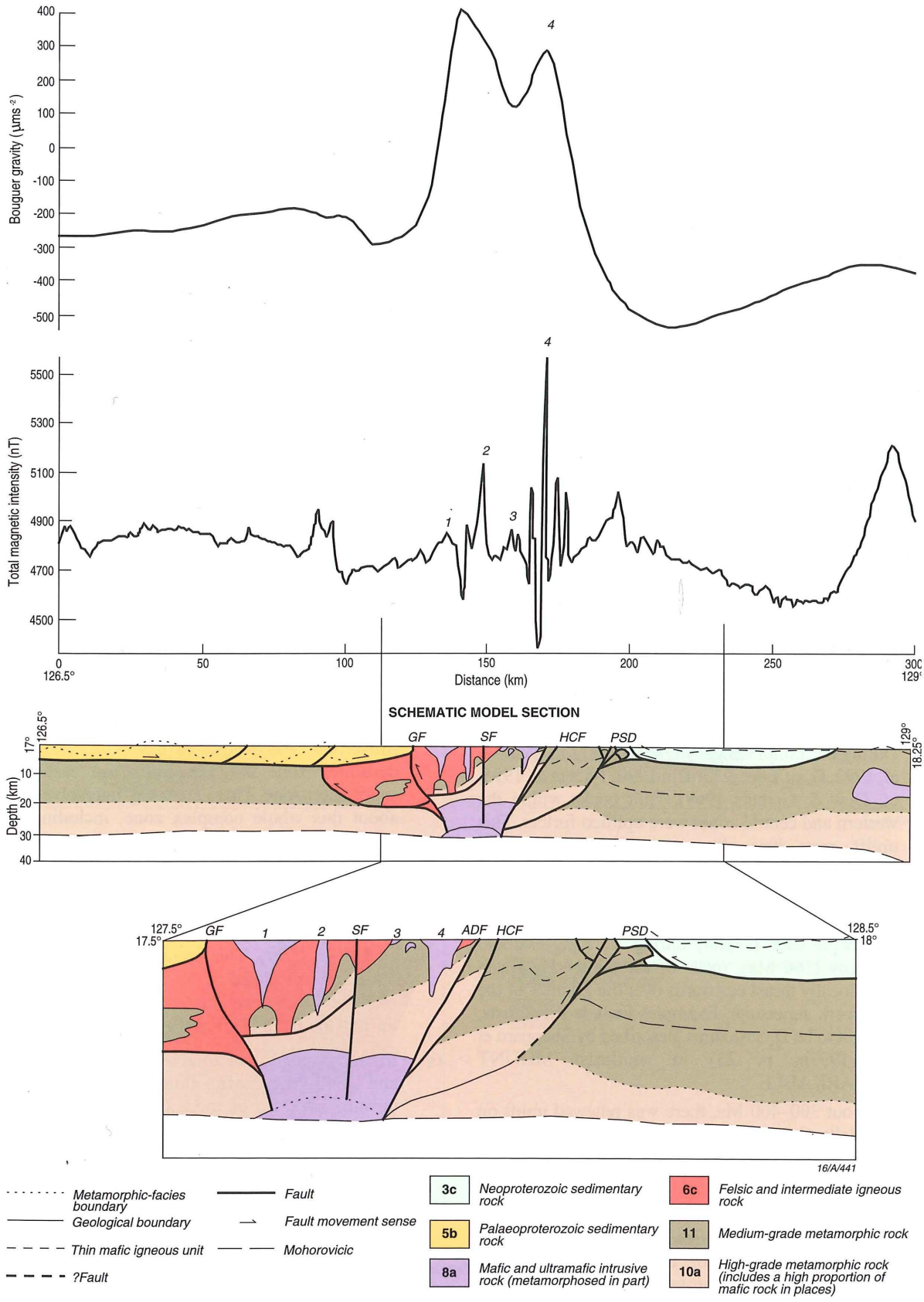


Figure 4.15. Interpretational model of a crustal-scale cross-section for the Halls Creek Orogen, showing possible relationships of rock bodies to Bouguer and Total Magnetic Intensity anomalies. The total section line is from 126.5°E 17.0°S to 129°E, 18.25°S. The enlarged segment extends from 127.5°E 17.5°S to 128.5°E 18°S. Mafic–ultramafic intrusions and their corresponding anomalies are: 1, Toby intrusion; 2, Corridor gabbro; 3, Panton-type intrusion; 4, McIntosh intrusion. ADF, Alice Downs Fault; GF, Greenvale Fault; HCF, Halls Creek Fault; SF, Springvale Fault; PSD, the equivalent of detachment zones in the Palm Spring region.

Halls Creek Fault, resulting in the deformation of the Biscay and Olympio Formations (cf. Nash 1994).

(vi) At about 1835–1830 Ma, west of the main orogenic zone, there may well have been a switch from a contractional to an extensional regime, leading to the subsidence that initiated the Speewah Basin.

(vii) At about 1830 Ma, in the central zone of the Halls Creek Orogen, transtensional movements along the proto-Highway Shear Zone facilitated the emplacement of the Mabel Downs Tonalite and other granitic rocks of the Sally Downs supersuite, characterised by intermediate compositions (cf. Sheppard et al. 1997b). The 1830 Ma McIntosh intrusion (Page et al. 1995a) was emplaced alongside the Halls Creek Fault.

(viii) As a result of a switch to transpressional movement on the Highway Shear Zone (~1805–1800 Ma, D_4, see Sheppard et al. 1997b, p. 19), there was tilting and uplift on the eastern margin of the western zone and, possibly, further uplift along the Halls Creek Fault (Griffin et al. 1998).

(ix) By about 1800 Ma, the metamorphic rocks of the western zone of the Halls Creek Orogen had been uplifted to the surface, possibly as part of an uplifted crustal wedge. This structure resembled a 'flower structure' in which the bounding faults approximate the marked regional gravity gradients.

(x) By 1790 Ma, widespread subsidence had been initiated, leading to the accumulation of sedimentary rocks in the Kimberley Basin (Sheppard et al. 1997b).

(xi) During the Yampi Orogeny (1450–1000 Ma, Shaw et al. 1992, D_5 of Tyler & Griffin 1990, Tyler et al. 1995, cf. Dow & Gemuts 1969), fault bocks within the western and central zones were uplifted further. This uplift may have been a result of sinistral transpressional fault movements on the Greenvale, Springvale, Angelo, and Halls Creek Faults (see Sheppard et al. 1997b).

(xii) Somewhat later, possibly during the King Leopold Orogeny (560 Ma), rocks of the Kimberley Basin were locally thrust eastwards over the granites of the Paperbark supersuite. Examples include the thrusts, thought to be D_5 structures, described by Sheppard et al. (1997b, p. 23) in southeast MOUNT REMARKABLE.

(xiii) At about 300–400 Ma, there was renewed uplift on the Halls Creek Fault and on the possibly linked thrust front, postulated to control the segmented homocline marking the western margin of the Wolfe Basin.

Figure 4.16 shows, in plan view, a scenario of how the main crustal components of the region could have evolved during the Palaeoproterozoic. Throughout its history the Kimberley 'block' can be envisaged as a rotating indenter. The following proposed evolutionary stages are those considered important in the construction of Figure 4.16:

(i) By 1880 Ma (Fig. 4.16A), a plate or sub-plate boundary, possibly in a cordilleran-like transcurrent setting, had formed. This boundary separated a proto-Kimberley 'block' (K in Figs 4.8, 4.16) from a proto-Tanami 'block' (MB-ST-GT in Fig. 4.16).

(ii) These two blocks, together with the Oscar 'block' (O in Figs 4.8, 4.16), appear to have been progressively bent and rotated as a result of interaction with another plate margin to the south (crustal element BR, Barbwire Zone, Fig. 4.8). The age range and structure of this southern zone are not known as Palaeozoic rocks of the Canning Basin cover it.

(iii) 1870–1840 Ma (Fig. 4.16B), extensional spreading between the proto-Kimberley 'block' and the proto-Tanami 'block' led to the formation of a deep marine trough, now preserved as the Marboo Formation. It also eventually led to the generation in the lower crust of the associated granites of the Paperbark supersuite (KL in Fig. 4.16) (Sheppard et al. 1997a).

(iv) It is postulated that this spreading, which eventually evolved into the Hooper Orogeny, either preceded or was concurrent with an active plate margin to the south and east. A possible plate boundary is recognised in seismic data to the south (SPZ in Fig. 4.16B) (Braun & Shaw 1998). The boundary is identified as a fault surface in deep seismic reflection data collected across the Canning Basin (Shaw et al. 1994). It is a southwest-dipping crustal-scale feature and may continue to the northeast and link with either a complex subvertical to steeply east-dipping transcurrent deformed zone or, conceivably, an east-dipping subduction zone. There are many unresolved issues about this whole complex zone, including when and how it was initiated. A subduction zone could account for the tonalite and trondhjemite sheets (>1850 Ma, possibly arc-related, TTG or low-Al tonalite–trondhjemite–granodiorite suite) of the Dougalls suite (cf. tectonic setting of Sheppard et al. 1997a, 1999). This complex zone, now deeply buried, is postulated by us to have evolved rapidly into the deep-seated parent of what became the Springvale Fault (SVF in Fig. 4.16B).

(v) In this regional fault zone between about 1855 Ma and 1840 Ma, mafic–ultramafic magma moved upward into two or more complex transtensional segments. One of these fault segments formed at the bend of the orogen (see (ii) above). Another, much larger, complex transtensional segment, located within the central part of what became the Halls Creek Orogen, appears to have been the deep-seated precursor to the Springvale Fault. The complex jostling of blocks at the intersection of the proto-Springvale Fault and some restraining crustal feature (e.g. its intersection with a proto-Panton Fault extension) could have focussed processes such as intrusion of mafic–ultramafic magmas/rocks, regional metamorphism and block uplift. The fanning of regional structures away from these two transtensional fault zones implies

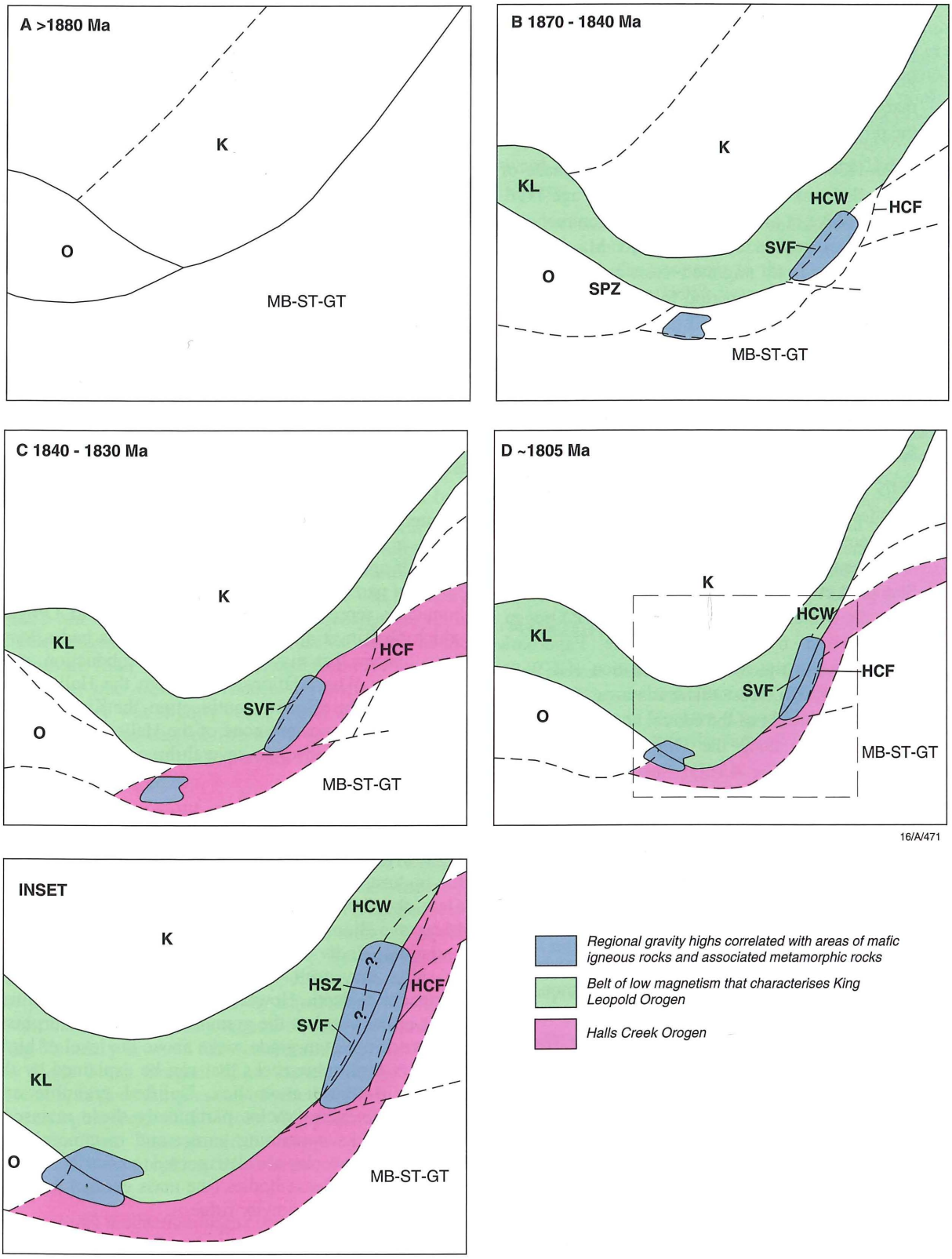


Figure 4.16. Palaeoproterozoic evolutionary stages in the Kimberley region (plan views).

A. Pre 1880 Ma—lithospheric plates or sub-plates beginning to interact.

B. 1870–1840 Ma—extensional spreading in belt that evolved into the King Leopold Orogen.

C. 1840-1830 Ma—main phase of the Halls Creek Orogeny.

D & Inset. ~1805 Ma—sinistral transpression, including movement along the Highway Shear Zone. HCF, Halls Creek Fault; HCW, western zone of the Halls Creek Orogen; HSZ, Highway Shear Zone; K, proto-Kimberley 'block'; KL, proto-King Leopold Orogen; MB-ST-GT–proto-Tanami 'block' (composite feature); O, Oscar 'block'; SPZ, proto-Spielers Shear Zone; SVF, proto-Springvale Fault.

some degree of rotational strain with the orogen. By this time, the western and central zones of the Halls Creek Orogen could have been already juxtaposed and, by the end of this period, the active margin could have moved farther east, to the site of the proto-Halls Creek Fault (HCF in Fig. 4.16B).

(vi) 1840–1830 Ma (Fig. 4.16C)—the main phase of the Halls Creek Orogeny (D_3 of Tyler & Page 1996, D_{H2} of Blake et al. 1999). The main contractional phase (D_3) peaked at about 1835 Ma and the deformation front migrated eastwards from the Halls Creek Fault. A period followed when strain was locally dilational and the McIntosh mafic intrusion and the series of granites that make up the Sally Downs supersuite were emplaced. Dykes of the Corridor gabbro type could have been intruded into early dilational splays of a reactivated proto-Springvale Fault.

(vii) 1805 Ma (Fig. 4.16D)—intrusion of post-tectonic granites of the Sally Downs supersuite terminated by increasing sinistral transpression, including movement along the Highway Shear Zone (cf. Sheppard et al. 1997b). It is proposed that, at this time, the western zone of the Halls Creek Orogen, characterised by granites of the Paperbark supersuite and the Marboo Formation (HCW in Fig. 4.16D), was thrust eastwards over high-grade metamorphic rocks of the central zone of the Halls Creek Orogen along the Highway Shear Zone (HSZ in inset of Fig. 4.16D). Such thrusting could partly explain why the regional gravity high, associated at the surface with high-grade metamorphic rocks, including mafic granulite and amphibolite, extends westwards into a belt of low magnetism that characterises the King Leopold Orogen to the southwest.

The scenario suggested above for the evolution of the Halls Creek Orogen has several features in common with current models for the tectonic evolution of the Svecofennian Orogen in Sweden and Finland (Nironen 1997, Peltonen 1995, Lahtinen & Huhma 1997, Peltonen & Huhma 1997). Common features include their timing, the nature of the mafic–ultramafic intrusions, for example the Ni–Cu-bearing bodies of the Vammala Nickel Belt, and in the apparent nature of some of the magmatic processes involved (see Chapter 14). However, there are also differences, as the mafic–ultramafic intrusions in the Halls Creek Orogen are less obviously related to juvenile arc-forming processes in that their Nd TDM model ages are 450 Ma or more older than the emplacement ages (see Chapter 11, Sun 1997). Also, the Halls Creek Orogen appears to have been dominated by two or more orogenies in a complex transcurrent setting, whereas large horizontal convergence characterised orogenic events in the Svecofennian domain (Gaal 1990, Gaal & Gorbatschev 1987).

Concluding remarks

A re-examination of the geophysical data used to delineate crustal elements in the East Kimberley suggests that the boundary between crustal elements HCC–HCB and STS–STN (Fig. 4.8) represents a complex boundary between crustal blocks. Analysis of new seismic wave speed data by van der Hilst et al. (1998, SKIPPY Project) revealed abrupt changes in shear-wave velocity in the upper mantle across the Halls Creek Orogen, suggesting the Halls Creek Orogen could have formed on a boundary of lithospheric extent. The 'dipole' gravity anomaly at the eastern margin of the Halls Creek Orogen is of a type commonly associated with a sub-plate or plate boundary. This boundary could represent a major collisional suture (cf. Gibbs et al. 1983, Thomas et al. 1988), possibly, a continent–continent collision involving basement reactivation. Although the 'dipole' gravity anomaly is discontinuous, this can be explained by repeated reactivation along the Halls Creek Fault in the Palaeoproterozoic, Mesoproterozoic, Neoproterozoic, and Palaeozoic (cf. Fig. 4.16). The Halls Creek Orogen is interpreted as a complex orogenic wedge preserved above a Proterozoic plate or sub-plate boundary (Fig. 4.15). It appears to have formed as a result of reactivation of a part of an earlier Proterozoic plate or sub-plate boundary represented by the King Leopold Orogen, which Griffin et al. (in press) suggest has had a long-lived history that may have involved subduction at an early stage. The relationship between the Halls Creek Orogen and the effective continuation, the King Leopold Orogen, as the western zone of the Halls Creek Orogen is complex as it involves several three-dimensional tectonic features.

As recognised by Mathur & Shaw (1982), unusually dense rocks are needed to account for marked gravity highs in the East Kimberley region, as these are amongst the highest magnitude Bouguer anomalies in Australia. Only the layered mafic–ultramafic intrusions of the Musgrave Block in central Australia have a comparable magnitude. Individual gravity peaks in a regional gravity ridge may well represent large mafic–ultramafic intrusions at depth. However, most of the exposed intrusions either postdate the granulite-facies metamorphism or intrude medium-grade rocks above the level of high-grade metamorphic rocks that can be explained by the highest Bouguer anomalies. Uplifted granulite and amphibolite facies rocks, particularly those metasedimentary rocks containing garnet and metamorphosed mafic igneous rocks, are all expected to contribute to the distribution of dense bodies (the mass excess) that give rise to the regional gravity ridge.

If there is a greater volume of mafic–ultramafic intrusions at depth than at the surface in the western zone of the Halls Creek Orogen, it is puzzling that there is no matching set of long-wavelength magnetic anomalies. A possible explanation is that iron and titanium are hosted in ilmenite or iron-spinel rather than in magnetite, but any olivine present would have had to escape serpentinisation. Another factor is that the western zone of the Halls Creek Orogen, dominated by units with weak magnetisation, such as granites of the Paperbark supersuite

and the Marboo Formation, has been thrust over part of the central zone. In this way, the magnetic signal of a unit similar to the granulites exposed west of the Highway Shear Zone could be masked by a thrust-wedge of less magnetic rocks. This masking would broaden the anomaly, but would not normally eliminate it. The regional gravity high would, in this case, represent the deeper mass excess generated by these high-grade metamorphic rocks with their high proportion of relatively dense rocks. These rocks include metamorphosed magnetic mafic–ultramafic intrusions like the Norton intrusion, as well as other dense, but less magnetic rocks, such as mafic granulite, amphibolite, calc-silicate rocks and garnet-bearing pelitic gneisses, like those of the Tickalara Metamorphics. The composite density of such rocks could be of sufficient magnitude to explain the regional gravity anomaly (Fig. 4.15). However, in view of the exceptional magnitude of this anomaly, it seems possible that the exposed mafic–ultramafic intrusions are satellite bodies linked at depth to mantle-derived parent bodies, which pooled at or near the crust-mantle boundary, as portrayed in Fig. 4.15.

Figure 4.16 is an attempt to explain the gravity and magnetic features associated with the mafic–ultramafic intrusions in terms of the evolving tectonic setting. It is suggested that a larger transtensional zone was active by ~1855 Ma in the central part of what became the Halls Creek Orogen, as a precursor to what we regard as the Springvale Fault. This zone of transtension (or localised extension) into which the mafic–ultramafic intrusions were intruded was slightly younger and deeper, and was displaced to the east of the more regional zone into which the granites of the Paperbark supersuite were continuing to be emplaced.

From a geological point of view, it is difficult to be certain about the relative importance of the Highway Shear Zone as a boundary between the central and western zones in the northern part of the Halls Creek Orogen. It could represent a late-stage reactivation of a deeper seated, transcurrent fault zone, located immediately to the west, which has been obliterated by the later granite intrusions of the Sally Downs supersuite. There is also the possibility that the Highway Shear Zone is a backthrust that overrides a sub-vertical or even eastward-dipping boundary between the western and central zones of the Halls Creek Orogen. These issues warrant further research, as does the question of whether the high-grade metamorphic rocks of the Violet Valley Zone west of the Highway Shear Zone should be mapped as part of the Tickalara Metamorphics, the Marboo Formation, or a separate unit.

The regional magnetic trough corresponding to the western zone of the Halls Creek Orogen is so similar to that of the King Leopold Orogen that it is hard not to equate these features (Figs 4.2, 4.3). Near the southwestern extension of the Ramsay Range Fault (Fig. 4.7; see Tyler et al. 1998a) the regional magnetic low (Fig. 4.3), which geophysically characterises the King Leopold Orogen, overlaps a prominent rectilinear Bouguer high (labelled HCCa in Figs 4.2, 4.8). This relationship is similar to that described above for the boundary region between the western and central zones of the Halls Creek Orogen (see crustal model, Fig. 4.15). The gravity high in the southwest is complex. It is centred near the Pillara Inlier on the Lennard Shelf of the Canning Basin (Shaw et al. 1994). This relationship to the southwest is analogous to that marked by the Highway Shear Zone to the north. It could be explained if rocks of the King Leopold Orogen are thrust over a belt that could be equivalent to a westward extension of the central zone of the Halls Creek Orogen.

The current study is only a preliminary interpretation of the region and complements the wider geophysical study focussed on the basement to the Kimberley Basin by Gunn & Meixner (1998). It would be desirable to obtain more comprehensive and detailed data on rock properties, as well as on the origin and history of magnetic minerals in both regional geological units and in the mineral deposits in addition to that listed in this chapter. Also, any crustal model would be more accurately constrained if the velocity structure of the crust across this part of the Halls Creek Orogen were better defined by more localised probing. Once key parameters, such as these, are established, geophysical modelling of potential field data will be better able to test and refine ideas on the crustal structure, thereby constraining the tectonic setting of the mafic–ultramafic intrusions.

Acknowledgements

The present work has benefited from discussions with many colleagues at AGSO and GSWA, and the critical reviews of Dean Hoatson, David Blake, Alan Whitaker, Shen-su Sun, Alastair Stewart (all AGSO) and Ian Tyler (GSWA).

References

AGSO, 1997. National Gravity Database, 1997. Australian Geological Survey Organisation, Canberra.

Blake, D.H., 1997. Proterozoic thrusting in the Osmand Range area of the East Kimberley, Western Australia. AGSO Research Newsletter, 26, 4–7.

Blake, D.H., Hodgson, I.M. & Muhling, P.C., 1979. Geology of The Granites–Tanami region, Northern Territory and Western Australia. Bureau of Mineral Resources, Australia, Bulletin 197, 91 pp.

Blake, D.H., Tyler, I.M., Griffin, T.J., Sheppard, S., Thorne, A.M. & Warren, G.W., 1999. Geology of the Halls Creek 1:100 000 sheet area (4461), Western Australia. Australian Geological Survey Organisation, Canberra, 36 pp.

Blakely, R.B., 1996. Potential theory in gravity and magnetic applications. Cambridge University Press, Cambridge, 441 pp.

Braun, J. & Shaw, R.D., 1998. Extension in the Fitzroy Trough, Western Australia: an example of reactivation tectonics. In: Braun, J. et al. (editors), Structure and evolution of the Australian continent. American Geophysical Union, Geodynamics, 26, 157–174.

Butler, R.W.H., Spencer, S. & Griffiths, H.M., 1998. The structural response to evolving plate kinematics during transpression: evolution of the Lebanese restraining bend of the Dead Sea transform. In: Holdworth,

R.E., Strachan, R.A. & Dewey, J.F. (editors), Continental transpressional and transtensional tectonics. Geological Society, London, Special Publication 135, 81–106.

Collins, C.D.N., 1983. Crustal structure of the southern McArthur Basin from deep seismic soundings. BMR Journal of Australian Geology & Geophysics, 8, 19–34.

Dow, D.H. & Gemuts, I., 1969. Geology of the Kimberley region, Western Australia: the East Kimberley. Bureau of Mineral Resources, Australia, Bulletin 106, 135 pp.

Erslev, E.A., 1986. Basement balancing of Rocky Mountain foreland uplifts. Geology, 14, 257–262.

Finlayson, D.M., 1982. Seismic crustal structure of the Proterozoic North Australian Craton between Tennant Creek and Mount Isa. Journal of Geophysical Research, 87 (B13), 10 569–10 578.

Fraser, A.R., Darby, F. & Vale, K.R., 1977. The reconnaissance gravity survey of Australia: a qualitative analysis of results. Bureau of Mineral Resources, Australia, Report 198, Microform MF15.

Frost, B.R., 1991. Magnetic petrology: Factors that control the occurrence of magnetite in crustal rocks. In: Lindsay, D.H. (editor), Oxide minerals: petrologic and magmatic significance. Mineralogical Society of America, Chelsea, MI, 25, 489–506.

Fyfe, W.S., Price, N.J. & Thompson, A.B., 1978. Fluids in the Earth's crust. Elsevier, Amsterdam, 382 pp.

Gaal, G., 1990. Tectonic styles of Early Proterozoic ore deposition in the Fennoscandian Shield. Precambrian Research, 46, 83–114.

Gaal, G. & Gorbatschev, R., 1987. An outline of the Precambrian evolution of the Baltic shield. Precambrian Research, 35, 15–52.

Gellatly, D.C., 1970. Archaean(?) rocks of the Kimberley region, Western Australia. Geological Society of Australia, General Meeting and Symposium, Perth, May 23–26, Abstracts, 36–37.

Gemuts, I., 1971. Metamorphic and igneous rocks of the Lamboo Complex: East Kimberley region, Western Australia. Bureau of Mineral Resources, Australia, Bulletin 107, 71 pp.

Gibbs, R.A., Thomas, M.D., Lapointe, P.L. & Mukhopadhyay, M., 1983. Geophysics of proposed Proterozoic sutures in Canada. Precambrian Research, 19, 349–384.

Glikson, A.Y., Stewart, A.J., Ballhaus, C.G., Clarke, C.G., Feeken, E.H.J., Leven, J.H., Sheraton, J.W. & Sun, S-s., 1996. Geology of the western Musgrave Block, central Australia, with particular reference to the mafic–ultramafic Giles Complex. Australian Geological Survey Organisation, Bulletin 239, 206 pp.

Graham, S., Lambert, D.D., Shee, S.R., Smith, C.B. & Reeves, S., 1999. Re-Os isotopic evidence for Archean lithospheric mantle beneath the Kimberley block, Western Australia. Geology, 27, 431–434.

Green, D.H. & Ringwood, A.E., 1967. An experimental investigation of the gabbro to eclogite transformation and its petrological applications. Geochimica et Cosmochimica Acta, 31, 767–833.

Griffin, T.J. & Grey, K., 1990. King Leopold and Halls Creek Orogens. In: Geology and mineral resources of Western Australia. Western Australia Geological Survey, Memoir 3, 232–253.

Griffin, T.J., Tyler, I.M., Sheppard, S. & Orth, K., 1998. Geology of the Angelo 1:100 000 sheet: Western Australia Geological Survey, 1:100 000 Geological Series Explanatory Notes, 27 pp.

Griffin, T.J., Page, R.W., Sheppard, S. & Tyler, I.M., in press. Palaeoproterozoic high-K granites and felsic volcanics formed above a fossil subduction zone, Kimberley region, northeastern Australia. Precambrian Research.

Gunn, P.J. & Meixner, A.J., 1998. The nature of the basement to the Kimberley Block, Northwestern Australia. Exploration Geophysics, 29, 506–511.

Hancock, S.L. & Rutland, R.W.R., 1984. Tectonics of an early Proterozoic suture: the Halls Creek orogenic sub-province, Northern Australia. Journal of Geodynamics, 1, 387–432.

Hoatson, D.M., 1993. Correlation of structurally disrupted layered mafic–ultramafic intrusions in the East Kimberley. AGSO Research Newsletter, 19, 9–10.

Hoatson, D.M., 1995. New mineral discoveries in the East Kimberley. AGSO Research Newsletter, 22, 9–11.

Hoatson, D.M. & Tyler, I.M., 1993. Prospective layered mafic–ultramafic intrusions in the East Kimberley. Is Big Ben part of the Panton intrusion? AGSO Research Newsletter, 18, 8–9.

Hoatson, D.M., Blake, D.H., Warren, R.G., Orth, K. & Tyler, I.M., 1995. Recent NGMA mapping highlights the metallogenic potential of the East Kimberley. AGSO Research Newsletter, 22, 1–2.

Hoatson, D.M., Sproule, R.A. & Lambert, D.D., 1997. Are there Voisey's Bay-type Ni–Cu–Co sulphide deposits in the East Kimberley of Western Australia? AGSO Research Newsletter, 27, 17–19.

Hutton, D.H.W., 1990. A new mechanism of granite emplacement: Intrusion in active extensional shear zones. Nature, 343, 452–455.

Kendrick, T., Rey, P., Costa, S., Masur, G. & Foley, B., 1999. Synchronous transpression and magmatism in the Halls Creek Mobile Belt (East Kimberley, WA). Geological Society of Australia, Abstracts, 53, 131–133.

Lahtinen, R. & Huhma, H., 1997. Isotopic and geochemical constraints on the evolution of the 1.93–1.79 Ga Svecofennian crust and mantle in Finland. Precambrian Research, 82, 13–34.

Leven, J.H. & Lindsay, J.F., 1995. A geophysical investigation of the southern margin of the Musgrave Block, South Australia. AGSO Journal of Australian Geology & Geophysics, 16 (1/2), 155–161.

Mathur, S.P. & Shaw, R.D., 1982. Australian orogenic belts. Evidence of evolving plate tectonics. Earth Evolution Sciences, 4, 281–308.

Meixner, A.J., 1997. Total magnetic intensity, reduced to the pole, pixel image of the Kimberley Region, WA and NT, scale 1:1 000 000, Australian Geological Survey Organisation, Canberra.

Murray, A.S., Morse, M.P., Milligan, P.R., Mackey, T.E., 1997. Gravity anomaly map of the Australian region, (2nd edition) scale 1:5 000 000. Australian Geological Survey Organisation, Canberra.

Mutton, A.J. & Shaw, R.D., 1979. Physical property measurements as an aid to magnetic interpretation in basement terrains. Australian Society of Exploration Geophysics, Bulletin, 10, 769–791.

Myers, J.S., Shaw, R.D. & Tyler, I.M., 1996. Tectonic evolution of Proterozoic Australia. Tectonics, 15, 1431–1446.

Nash, C., 1994. New structures from old images: Photogeological methods for remapping Australia Proterozoic terrains. Proceedings of 7th Australian Remote Sensing Conference, 1–4 March 1994, Melbourne, Australia.

Naylor, M.A., Mandl, G. & Sijpesteijin, C.H.K., 1986. Fault geometries in basement-induced wrench faulting under different initial stress states. Journal of Structural Geology, 8(7), 737–752.

Nironen, M., 1997. The Svecofennian Orogen: a tectonic model. Precambrian Research, 86, 21–44.

Ogasawara, M., 1988. Geochemistry of the Early Proterozoic granitoids in the Halls Creek Orogenic province, Northern Australia. Precambrian Research, 40/41, 469–486.

Page, R.W., Hoatson, D.M. & Foudoulis, C., 1995a. High-precision geochronology of Palaeoproteroic layered mafic–ultramafic intrusions in the East Kimberley. AGSO Research Newsletter, 22, 7–8.

Page, R.W., Sun, S-s., Blake, D.H., Edgecombe, D. & Percey, D., 1995b. Geochronology of an exposed late Archaean basement terrane in The Granites-Tanami region. AGSO Research Newsletter, 22, 19–20.

Page, R.W., Sun, S-s., Blake, D.H., Edgcombe, D.R. & Percey, D.P., 1996. Exposed Late-Archaean basement terrains in The Granites–Tanami region, Northern Territory. Geological Society of Australia, Abstract, 38, 334.

Peltonen, P., 1995. Petrogenesis of ultramafic rocks in the Vammal Nickel Belt: implications for crustal evolution of the early Proterozoic Svecofennian arc terrane. Lithos, 34, 253–274.

Peltonen, P. & Huhma, H. 1997. Overview of the Svecofennian mafic magmatism in Finland. Australian Geological Survey Organisation, Record 1997/44, 95–97.

Prucha, J.J., Graham, J.A. & Nickelsen, R.P., 1965. Basement controlled deformation in Wyoming Province of Rocky Mountains foreland. American Association of Petroleum Geologists, Bulletin, 49, 966–992.

Rumble, III, D., 1973. Fe–Ti oxide minerals from regionally metamorphosed quartzites of western New Hampshire. Contributions to Mineralogy and Petrology, 42, 181–195.

Shaw, R.D., Goleby, B., Korsch, R.J. & Wright, C., 1991. Seismic interpretation and thrust tectonics of the Amadeus Basin, central Australia, along the BMR regional seismic line. In: Korsch, R.J. & Kennard, J.M. (editors), Geological and geophysical studies in the Amadeus Basin, central Australia. Bureau of Mineral Resources, Australia, Bulletin 236, 385–408.

Shaw, R.D., Tyler, I.M., Griffin, T.J. & Webb, A., 1992. New K–Ar constraints on the onset of subsidence in the Canning Basin, Western Australia. BMR Journal of Australian Geology & Geophysics, 13, 31–35.

Shaw, R.D., Sexton, M.J. & Zeilinger, I., 1994. The tectonic framework of the Canning Basin, Western Australia, including the 1:2 million structural elements map of the Canning Basin. Australian Geological Survey Organisation, Record 1994/48, 89 pp.

Shaw, R.D., Wellman, P., Gunn, P., Whitaker, A.J., Tarlowski, C. & Morse, M., 1995. Australian Crustal Element' map; a geophysical model for the tectonic framework of the continent. AGSO Research Newsletter, 23, 1–3.

Shaw, R.D., Wellman, P., Gunn, P., Whitaker, A.J., Tarlowski, C. & Morse, M., 1996. Guide to using the Australian Crustal Elements map. Australian Geological Survey Organisation, Record 1996/30, 49 pp.

Sheppard, S., Griffin, T.J. & Tyler, I.M., 1995. Geochemistry of felsic igneous rocks from the southern Halls Creek Orogen. Western Australia Geological Survey, Record 1995/4, 81 pp.

Sheppard, S., Griffin, T.J. & Tyler, I.M., 1997a. The tectonic setting of granites in the Halls Creek and King Leopold Orogens, northwest Australia. In: Rutland, R.W.R. & Drummond, B.J. (editors), Palaeoproterozoic tectonics and metallogenesis: comparative analysis of parts of the Australian & Fennoscandian shields. Workshop, Darwin, September, 14-22, 1997. Australian Geological Survey Organisation, Record 1997/44, 107–109.

Sheppard, S., Tyler, I.M. & Hoatson, D.M., 1997b. Geology of the Mount Remarkable 1:100 000 sheet, Western Australia. Western Australia Geological Survey, 1:100 000 Geological Series Explanatory Notes, 27 pp.

Sheppard, S., Tyler, I.M., Griffin, T.J. & Taylor, W.R., 1999. Palaeoproterozoic subduction-related and passive margin basalts in the Halls Creek Orogen, northwest Australia. Australian Journal of Earth Sciences, 46, 679–690.

Struckmeyer, H.I.M., Blevin, J.E., Sayers, J., Totterdell, J.M., Baxter, K. & Cathro, D.L., 1998. Structural evolution of the Browse Basin, North West Shelf: New concepts from deep-seismic data. In: Purcell, P.G. & Purcell, R.R. (editors), The sedimentary basins of Western Australia 2. Proceedings of the Petroleum Exploration Society of Australia, 1988, Perth, WA, 345–367.

Sun, S-s., 1997. Chemical and isotopic features of Palaeoproterozoic mafic igneous rocks of Australia: implications for tectonic processes. In: Rutland, R.W.R. & Drummond, B.J. (editors), Palaeoproterozoic tectonics and metallogenesis: comparative analysis of parts of the Australian & Fennoscandian shields. Workshop, Darwin, 14–22 September, Australian Geological Survey Organisation, Record 1997/44, 119–122.

Sun, S-s., Carr, G.R. & Page, R.W., 1996. A continued effort to improve lead-isotope model ages. AGSO Research Newsletter, 24, 19–20.

Sylvester, A.G., 1988. Strike-slip faults. Geological Society of America, Bulletin, 100, 1666–1703.

Symonds, P.A., Collins, C.D.N. & Bradshaw, J., 1994. Deep structure of the Browse Basin: Implications for basin development and petroleum exploration. In: Purcell, P.G. & Purcell, R.R. (editors), The Canning Basin, Western Australia. Proceedings of the West Australian Basins Symposium. Petroleum Exploration Society of Australia, Perth, Western Australia, 315–331.

Thomas, M.D. & Gibbs, R.A., 1985. Proterozoic plate subduction and collision: processes for reactivation of Archaean crust in the Churchill Province. In: Ayes, L.D., Thurston, P.C., Card, K.D. & Webster, W. (editors), Evolution of Archaean supracrustal sequences. Geological Association of Canada, Special Paper, 28, 263–279.

Thomas, M.D., Grieve, R.A.F. & Sharpton, V.L., 1988. Gravity domains and the assembly of North American continent by collisional tectonics. Nature, 331, 333–334.

Thorne, A.M. & Tyler, I.M. 1997. Mesoproterozoic and Phanerozoic sedimentary basins of the northern Halls Creek Orogen: constraints on the timing of strike-slip movement on the Halls Creek Fault System. Western Australian Geological Survey, Annual Review 1995–96, 156–168.

Thornett, J.R., 1981. The Sally Malay deposit: gabbroid associated nickel–copper sulfide mineralization in the Halls Creek Mobile Zone, Western Australia. Economic Geology, 76 (6), 1565–1580.

Tikoff, B. & Teyssier, C., 1992. Crustal-scale, en echelon "P-shear" tensional bridges: A possible solution to the batholith room problem. Geology, 20, 927–930.

Trudu, A. & Hoatson, D.M., 1996. Depths of emplacement of Precambrian intrusions in the East Kimberley. AGSO Research Newsletter, 25, 10–12.

Tyler, I.M. & Griffin, T.J., 1990. Structural development of the King Leopold Orogen, Kimberley region, Western Australia. Journal of Structural Geology, 12, (5/6), 703–714.

Tyler, I.M. & Griffin, T.J., 1993. Explanatory Notes on the Yampi 1:250 000 geological series (2nd edition). Western Australian Geological Survey, Record 1992/26.

Tyler, I.M. & Page, R.W. 1996. Palaeoproterozoic deformation, metamorphism and igneous intrusion in the central zone of the Lamboo Complex, Halls Creek Orogen. Geological Society of Australia, Abstracts, 41, 450–451.

Tyler, I.M., Griffin, T.J., Page, R.W. & Shaw, R.D., 1995. Are their terranes within the Lamboo Complex of the Halls Creek Orogen? Geological Survey of Western Australia, Annual Review 1993-94, 37–46.

Tyler, I.M., Hoatson, D.M., Griffin, T.J., Sheppard, S., Blake, D.H. & Warren, R.G., 1997a. McIntosh, Western Australia(1:100 000 geological map (sheet 4462). Geological Survey of Western Australia, Perth.

Tyler, I.M., Thorne, A.M., Hoatson, D.M. & Blake, D.H., 1997b. Turkey Creek, Western Australia(1:100 000 geological map (sheet 4563). Geological Survey of Western Australia, Perth.

Tyler, I.M., Playford, P.E. & Hocking, R.M. 1998a. Mount Ramsay, Western Australia(1:250 000 geological map (SE/52-9), 2nd edition. Geological Survey of Western Australia, Perth.

Tyler, I.M., Thorne, A.M., Sheppard, S., Hoatson, D.M., Griffin, T.L., Blake, D.H. & Warren, R.G., 1998b. Dixon Range, Western Australia(1:250 000 geological map sheet (SE 52-6). Geological Survey of Western Australia, Perth.

Tyler, I.M., Warren, R.G. & Blake, D.H., 1998c. Dixon, Western Australia(1:100 000 geological map (sheet 4562). Geological Survey of Western Australia, Perth.

van der Hilst, R.D., Kennett, B.L.K. & Shibutani, T., 1998. Upper mantle structure beneath Australia from portable array deployments. In: Braun, J., Dooley, J., Goleby, B., van der Hilst, R. & Klootwijk, C. (editors), Structure and evolution of the Australian continent. American Geophysical Union, Geodynamics Series, 26, 39–57.

Vann, I.R., Graham, R.H. & Hayward, A.B., 1986. The structure of mountain fronts. Journal of Structural Geology, 8, 215–277.

Walter, M.R., Veevers, J.J., Calver, C.R. & Grey, K., 1995. Neoproterozoic stratigraphy of the Centralian Superbasin, Australia. Precambrian Research, 73, 173–195.

Wellman, P., 1976. Regional variations of gravity and isostatic equilibrium of the Australia crust. BMR Journal of Australian Geology & Geophysics, 1, 294–302.

Wellman, P., 1978. Gravity evidence for abrupt changes in mean crustal density at the junction of Australian blocks. BMR Journal of Australian Geology & Geophysics, 3, 153–162.

Wellman, P., 1988. Development of the Australian Proterozoic crust as inferred from gravity and magnetic anomalies. Precambrian Research, 40/41, 89–100.

Wellman, P., 1998. Mapping of geophysical domains in the Australian continent using gravity and magnetic anomalies. In: Braun, J. et al. (editors), Structure and evolution of the Australian continent. American Geophysical Union, Geodynamics 26, 59–71.

White, S.H. & Muir, M.D., 1989. Multiple reactivation of coupled orthogonal fault systems: an example from the Kimberley region in northern Western Australia. Geology, 17, 618–621.

Wyborn, L.A.I., Wyborn, D., Warren, R.G. & Drummond, B.J., 1992. Proterozoic granite types in Australia: implications for lower crustal compositions, structure and evolution. Royal Society of Edinburgh, Earth Science Transactions, 83, 210–209.

GEOLOGICAL SETTING, PETROGRAPHY, AND GEOCHEMISTRY OF THE MAFIC–ULTRAMAFIC INTRUSIONS

by DEAN M. HOATSON

Introduction

The Palaeoproterozoic layered mafic–ultramafic intrusions of the Halls Creek Orogen (HCO) in the East Kimberley were regarded by Dow & Gemuts (1969) as competent, broadly warped thick sills comprising ultramafic rocks of the Alice Downs Ultrabasics and mafic rocks of the McIntosh Gabbro. They suggested that they were emplaced at considerable depth as a single large differentiated sill comprising a basal ultrabasic part and an overlying gabbroic part. During partial crystallisation, the sill was dismembered by faulting and folding and the differentiated portion of the magma was intruded at higher crustal levels to form the Alice Downs Ultrabasics and McIntosh Gabbro. In their regional tectonic studies of the East Kimberley, Hancock & Rutland (1984) considered the layered intrusions to be exotic bodies that were emplaced tectonically by thrusting. However, recent investigations by the Australian Geological Survey Organisation (AGSO) and the Geological Survey of Western Australia (see Chapter 1) have shown that the intrusions of the Alice Downs Ultrabasics and McIntosh Gabbro are of different ages, are not comagmatic, and in most cases are not sills, sensu stricto. In addition, many of the layered intrusions display a range of contact relationships that indicate they have not been tectonically uplifted, relative to the country rocks, since their emplacement.

The layered intrusions of the HCO have been assigned to seven major groups (designated I to VII: Fig. 5.1, Table 5.1) on the basis of U–Pb geochronology, contact relationships with country rocks, range of rock types, metamorphic–structural histories, types of mineralisation, assemblages of cumulus minerals, trace-element chemistry, and Sm–Nd isotopic compositions. Intrusions that show no primary compositional layering and generally form irregular massive bodies (those of Corridor gabbro and Turkey Creek microgabbro-norite), or are assigned to the Tickalara Metamorphics (Norton metagabbro: Fig. 5.1) are not included in these groups. Some groups are coeval (groups I, II, and III), and some may be comagmatic (the group III Toby intrusion may represent the evolved upper part of group II intrusions). U–Pb zircon and baddeleyite geochronology (Page et al. 1995, see Chapter 6) has shown that there were at least three major periods of emplacement of the layered intrusions: ~1855 Ma (groups I–III), ~1845 Ma (group V), and ~1830 Ma (group VI). Further geochronological studies are likely to reveal other major periods of mafic magmatism in the HCO. Groups I, II, and V, in particular, have economic potential for magmatic and hydrothermal precious-metal and base-metal mineralisation (Hoatson & Tyler 1993, Hoatson 1993, 1995, 1998, Hoatson et al. 1995, 1997, Sheppard et al. 1997, Trudu & Hoatson 1996, see Chapter 14).

The well-preserved layered intrusions (Fig. 5.2) form folded sheets, shallowly dipping basins, composite multi-chambered bodies, large funnel-shaped bodies, steeply plunging plugs, fault-bounded blocks, and narrow dyke-like bodies and screens between granite plutons. The intrusions are confined to the central and western zones of the HCO (see Chapter 3). Those in the central zone (approximately 75%) are elongated parallel to the regional north-northeast structural trend of the Tickalara Metamorphics, whereas those in the western zone were largely emplaced at different orientations in granite plutons belonging to the ~1865–1850 Ma Paperbark supersuite of the Bow River Batholith (see Chapter 3). Very few intrusions occur in granites of the ~1835–1805 Ma Sally Downs supersuite, which occurs in both the central and western zones. Most intrusions crosscut structural fabrics in the country rocks and in some cases they form thick bodies with stratigraphic thicknesses up to 7.8 km; thus, the term 'sill', frequently used in the literature, is not generally applicable.

The metamorphic grade of the intrusions ranges from amphibolite facies in McINTOSH[1] (most intrusions), to transitional amphibolite/granulite facies (Keller Creek and Corkwood) in the central parts of MOUNT REMARKABLE and TURKEY CREEK, to granulite facies (Norton, Bow River) further north. Primary igneous minerals and cumulus textures are generally well preserved in amphibolite facies bodies, whereas granuloblastic and pervasive recrystallisation fabrics characterise the more massive granulite bodies. With the exception of the group I mafic–ultramafic intrusions, which are folded and have a penetrative axial plane cleavage, most layered intrusions show little evidence of intense deformation. The effects of metamorphism and deformation were diminished by the large size of some intrusions (McIntosh), whereas others (Springvale, Toby) were protected by large bodies of homogeneous competent country rocks, such as granite in the western zone.

[1] 1:100 000 sheet names throughout this *Bulletin* are in capital letters to avoid confusion with identical place names and to distinguish them from 1:250 000 sheet names.

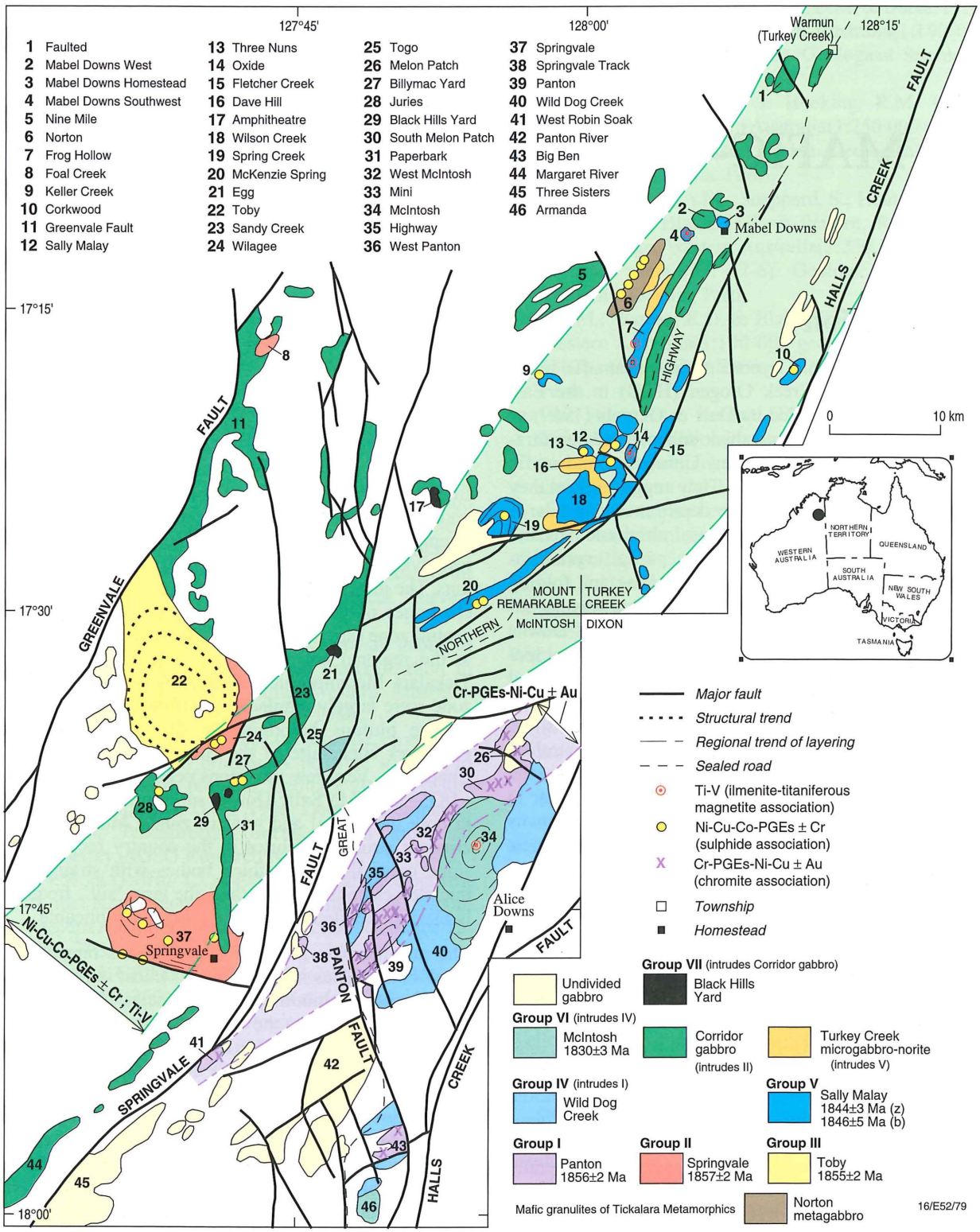


Figure 5.1. Distribution of the Palaeoproterozoic mafic–ultramafic intrusions in the Dixon Range 1:250 000 sheet area, East Kimberley. The two northeast-trending metallogenic corridors containing mineralised intrusions are shown as green and purple zones. The junction of the relevant 1:100 000 sheets are indicated in upper case near the right centre of the figure.

The East Kimberley layered intrusions have chilled and contaminated margins, narrow contact aureoles, ribbon-like comagmatic satellite intrusions, associated net-vein complexes resulting from mingling of mafic and felsic magmas, and feeder conduits, all indicating that the intrusions generally crystallised in situ (Hoatson & Tyler 1993) rather than being tectonically displaced fragments of a larger body, as proposed by previous investigators.

The major aims of this chapter are:

1. to describe and classify the mafic–ultramafic intrusions of the HCO so that their regional correlations and economic potential (see Chapter 14) can be assessed; and
2. to provide basic geological information for more specialised studies described in other chapters of this *Bulletin*.

Geological setting, petrography, and geochemistry

This section summarises the age, stratigraphy, layering, structure, contact relationships, mineralisation, petrography, and whole-rock major and trace-element geochemistry of the layered intrusions in groups I–VII and the other more massive mafic intrusions investigated in this study. A brief introduction describing the general features of each group is followed by descriptions of firstly the type example for each group and then the other intrusions of the group in alphabetical order. Additional details of the intrusions can be found elsewhere in this *Bulletin*: exploration history and mineralisation (Chapters 2, 3, 14), geochronology (Chapter 6, Appendix 4), geophysics and remote sensing (Chapters 4, 7, 8), mineral chemistry (Chapters 9, 13, Appendix 3), and whole-rock geochemistry (Chapters 10, 11, 12, 13, Appendix 2). The definitions of ratios used for the whole-rock and mineral chemistry appear in Appendices 2 and 3, respectively.

Group I layered mafic–ultramafic intrusions

Group I layered intrusions are strongly differentiated mafic–ultramafic bodies that have the highest ratio of ultramafic to mafic cumulates of all the groups (5.5:1 to 0.5:1). The type example is the Panton intrusion, which has been dated at 1856±2 Ma. The other intrusions of the group are considered to be of similar age, making the intrusions of group I coeval with those of groups II and III. Group I intrusions have undergone considerable exploration for stratabound chromitite layers and they also have potential for structurally controlled hydrothermal mineralisation (see Chapter 14). They have been deformed by tight upright northeasterly trending folds to produce steeply dipping bodies up to 2 km thick, and have been metamorphosed to amphibolite facies.

Nine major group I layered intrusions are located in a narrow northeast-trending corridor on McINTOSH, in the central zone of the HCO (Fig. 5.1). The largest of these intrusions (Panton, Mini, West McIntosh, and South Melon Patch) occur along the western side of the group VI McIntosh intrusion. They range in shape from syncline (Panton), anticline (South Melon Patch), folded sill (Mini), to steeply dipping sheet (West McIntosh). These particular bodies may represent 'tectonically disrupted' components of a single large sheet-like body, but detailed geochemical and structural studies are required to confirm this suggestion. The other group I intrusions in the corridor are smaller discontinuous ribbon-like bodies in two parallel zones, 1.5 to 3 km apart, extending northeastwards for 45 km from near the Springvale Fault in the southwest (West Robin Soak, Springvale Track), across the Great Northern Highway (Highway, West Panton), to just east of Mabel Hill (unnamed intrusions), before appearing to terminate near the northeast corner of McINTOSH (Melon Patch).

The only group I body outside the northeast-trending corridor is the Big Ben intrusion in central southern McINTOSH. This fault-bounded block is considered by the author to be the western part of the Panton intrusion displaced 15 km to the south along the Panton Fault. All group I intrusions are considered to be comagmatic because of their strikingly similar rock types, stratigraphy, layering, and platinum-group element (PGE)–chromitite mineralisation.

Two other intrusions with similar characteristics in the HCO, south of the area studied, may also belong to group I: Lamboo and Eastmans Bore mafic–ultramafic intrusions in the Mount Ramsay Sheet area (see Chapter 2).

Group I intrusions described below are Panton, Big Ben, Highway, Melon Patch, Mini, South Melon Patch, Springvale Track, West McIntosh, West Panton, and West Robin Soak.

Panton mafic–ultramafic intrusion *(39 in Fig. 5.1, Fig. 5.3, back cover of this* Bulletin*)*

Centre of intrusion. Central McINTOSH at AMG ~762355.

Age. U–Pb age of 1856±2 Ma determined for zircon from mottled anorthosite in the Upper Mafic Zone of the intrusion (see Chapter 6).

Form, structure, and areal extent. Steep-sided asymmetric syncline, 10.5 km long by 2.5 km wide, plunging moderately southwest; three small isolated ultramafic outcrops at northern end; truncated in southwest by the Panton Fault; elongate shape attributed to tight, upright, northeasterly trending folding of an original lopolith; layering on the southeastern limb dips towards the centre of the intrusion at 60–68°, northwestern limb has steeper to locally overturned dips, and axial region has inward dips of 30–45°; ultramafic cumulates have steeply dipping axial plane cleavage; parallel north-northwest-trending faults with sinistral strike-slip and vertical displacements cut the intrusion (Fig. 5.3); different amounts of movement along these faults suggest that strain dissipated northeastwards from the Panton Fault; metamorphic grade is middle amphibolite facies.

Thickness. 1550 m.

Stratigraphy and main rock types. Strongly differentiated, well layered mafic–ultramafic intrusion comprising a

Table 5.1. Mafic and mafic–ultramafic intrusions investigated in the East Kimberleys.

Intrusion (group)	*Areal extent (km)*	*Approximate thickness (km)*	*Form*	*Surrounding rocks*	*Major rock types*	*Mineralisation*
(1) Faulted (C g)	2 x 4	1.4	Steeply dipping basin	Metasediments, migmatite	BiotGabn, BiotGab, MtGab, HbGab	
(2) Mabel Downs West (C g)	1.5 x 2.2	?1	?Steeply plunging plug	Granite, gabbro, migmatite	BiotGabn, BiotGab, MtGab, Ton	
(3) Mabel Downs Homestead (V)	0.5 x 1	0.5	Steeply dipping sheet	Gabbro (C g), granite, migmatite	OGab, Gab, LGab, An	
(4) Mabel Downs Southwest (V)	0.8 x 1.2	1	Steeply dipping sheet	Gabbro (C g), granite, migmatite	MtGab, BiotGab, OGab	Ti, V
(5) Nine Mile (C g)	2.5 x 8	?2	Elongate body	Granite, metasediments, migmatite	MtGab, BiotGab, OGab	
(6) Norton (T M)	1.5 x 9	1	Steeply dipping elongate body	Metasediments, migmatite, granulite	MGran, HbMGab, HbMtMGab	Ni, Cu, Co, PGEs
(7) Frog Hollow (V)	1 x 8	?0.8	Steeply dipping elongate body	Metasediments, migmatite, granite	MtGab, Gab, OGab, LGab, An	Ti, V
(8) Foal Creek (II)	1 x 2.2	?1	Dipping sheet	Gabbro (C g), granite	OGab, Gab, Troc, LGab, An	
(9) Keller Creek (V)	0.3 x 1.5	0.3	Folded lens	Pelite, migmatite, granulite, granite	OGab, LGab	Ni, Cu, Co
(10) Corkwood (V)	0.2 x 2.2	0.2	Steeply dipping sheet	Pelite, marble, migmatite, granulite	MGab, OMGab, OGab, Amph	Ni, Cu, Co
(11) Greenvale Fault (C g)	3 x 28	?	Irregular ?sheet	Felsic volcanics, granite	BiotGabn, BiotGab, MtGab, Ton	
(12) Sally Malay (V)	1.5 x 3	1.7	Elliptical sub-chambers & feeders	Metasediments, migmatite, granulite	Du, Troc, OGab, LGab, N, An	Ni, Cu, Co
(13) Three Nuns (V)	0.3 x 0.3	?0.2	?Lens	Granulite, metasediments, migmatite	MGab, OMGab, Amph	Ni, Cu, Co
(14) Oxide (V)	0.3 x 0.3	?0.2	?Lens	Metasediments, migmatite, granulite	MtGab, Gab	Ti, V
(15) Fletcher Creek (V)	0.5 x 9	?0.3	Composite lenticular sill	Metasediments, migmatite, marble, granite	OGab, Troc, LGab,	Cu
(16) Dave Hill (V)	1 x 3.5	0.8	Steeply dipping folded sheet	Migmatite, granulite, gabbro (T Ck)	OGab, OGabn, Troc, LGab, An, Du	Ni, Cu, Co
(17) Amphitheatre (VII)	0.2 x 0.8	0.2	Steeply plunging plug	Gabbro (C g), granite	OGabn, OGab, Troc	
(18) Wilson Creek (V)	3 x 6	?2	Steeply plunging plugs & irregular lobate body	Gabbro (T Ck), granite, migmatite	OGab, An, Du, OGabn, Troc, LGab	Ni, Cu
(19) Spring Creek (V)	4 x 4	2.5	Moderately dipping ovoid body	Gabbro, granite	OGab, OGabn, Troc, LGab, An	Ni, Cu
(20) McKenzie Spring (V)	1.2 x 15	?1	Lenticular sill	Metasediments, granite, amphibolite	OGab, MtGab, Troc, An, LGab, Pyrox	Ni, Cu, Co
(21) Egg (VII)	0.7 x 1	?0.5	Steeply plunging plug	Granite, gabbro (C g)	Troc, OGab, OGabn, Gab	
(22) Toby (III)	12 x 20	?2	Shallow-dipping basin	Granite, gabbro (group II)	BiotGab, OGab, Du, non-cumulates	
(23) Sandy Creek (C g)	2 x 14	?1	Irregular dyke	Granite	OGab, BiotGab, MtGab, LGab, An	Cu, Ni, PGEs
(24) Wilagee (II)	2 x 10	1.3	Fault-bounded block & sheet	Granite, gabbro (group III)	OGab, Troc, LGab, An, N, Du, Cr	Cr, PGEs, Ni

(25) Togo (VI)	1.5 x 3.5	?0.5	Fault-bounded block	Granite, amphibolite, metasediments	Gab, OGab, LGab, An	
(26) Melon Patch (I)	0.6 x 3	?0.5	Steeply dipping lenses	Metavolcanics, calc-silicate, amphibolite, granite	Du, Amph, Tr-An, Gab, An, N, Cr	Cr, PGEs, Ni
(27) Billymac Yard (C g)	1 x 6	?0.5	Moderately dipping dyke	Granite	MtGab, BiotGab, LGab, An, N	Cu, Ni, PGEs
(28) Juries (C g)	3 x 4	?1	Folded & faulted sheets	Granite, metasediments	Gab, OGab, BiotGab	Cu
(29) Black Hills Yard (VII)	0.4 x 1	?0.3	Plugs & sheets	Gabbro (C g), granite	Troc, OGab, LGab, BiotGab, Lherz	
(30) South Melon Patch (I)	2.5 x 5.5	1	Plunging anticline	Granite, amphibolite, metasediments, gabbro (groups IV & VI)	Du, Cr, Ha, Amph, Tr-An, Gab, Gabn, N, LGab, An	Cr, PGEs, Ni
(31) Paperbark (C g)	1 x 11	?0.5	Irregular dyke	Granite	MtGab, Gab, BiotGab	
(32) West McIntosh (I)	0.5 x 8	0.5	Steeply dipping sheet	Metasediments, gabbro (group VI)	Du, Cr, Amph, Tr-An, Gab, Gabn, N, An	Cr, PGEs, Ni, Cu
(33) Mini (I)	0.3 x 2.5	0.2	Folded sill	Metasediments, granite	Du, Cr, Amph, Tr-An, Gab, N	Cr, PGEs
(34) McIntosh (VI)	6 x 14	7.8	Shallow- to steeply dipping funnel	Gabbro (groups I & IV), calc-silicate, metavolcanic, granite	OGab, OGabn, Troc, MtGab, LGab, Lherz	Ti, V
(35) Highway (I)	0.3 x 2.2	0.2	Steeply dipping sheet	Metasediments, granite, gabbro (group IV)	Du, Cr, Amph, Tr-An, An, Gab	Cr, PGEs
(36) West Panton (I)	0.5 x 1.2	0.5	Steeply dipping sheet	Metasediments, gabbro (group IV)	Du, Cr, Amph, Tr-An, Gab, An	Cr, PGEs
(37) Springvale (II)	6 x 13	2	Moderately dipping lobes	Granite, metasediments, gabbro (C g)	Gab, OGab, Troc, LGab, An	Cr, PGEs, Cu, Ni
(38) Springvale Track (I)	0.2 x 0.6	?0.2	Discontinuous lenses	Amphibolite, metasediments	Du, Tr-An	
(39) Panton (I)	2.5 x 10.5	1.6	Plunging syncline	Metasediments, amphibolite, granite	Du, Ha, Cr, Tr-An, Gab, Gabn, N, LGab, An, FGab	Cr, PGEs, Cu, Ni, Au
(40) Wild Dog Creek (IV)	6 x 10	?2	Shallow-dipping sheets	Metavolcanics, calc-silicate, granite, gabbro (groups I & VI)	MtGab, BiotGab, OGab, Ton, Amph	
(41) West Robin Soak (I)	0.2 x 0.8	?0.1	Discontinuous lenses	Amphibolite, metasediments, granite	Du, Tr-An, Gab	Cr, PGEs, Ni, Cu
(42) Panton River (U g)	5 x 8	?2	Fault-bounded ?sheet	Granite, gabbro, metavolcanics	OGab, Gab, LGab	
(43) Big Ben (I)	2.5 x 2.5	2	Fault-bounded block	Metavolcanics, gabbro (group IV), granite	Du, Tr-An, An, Gab, LGab, Pyrox	Cr, PGEs, Cu, Ni, Au
(44) Margaret River (C g)	1 x 4	?	Irregular dyke	Metasediments, granite	Gab, LGab	
(45) Three Sisters (U g)	2 x 10	?1.5	Moderately dipping sheet	Granite, metavolcanics, gabbro	Gab, OGab, LGab, An	
(46) Armanda (VI)	1.5 x 2.5	0.7	Moderately dipping sheet	Metavolcanics, metasediments	OGab, OGabn, Gab, LGab, An	

(C g) = Corridor gabbro; (T Ck) = Turkey Creek microgabbro-norite; (T M) = Tickalara Metamorphics; (U g) = Undivided gabbro. Major rock types are arranged in approximate order of decreasing abundance. Amph = amphibolite; An = anorthosite; BiotGab = biotite gabbro; BiotGabn = biotite gabbronorite; Cr = chromitite; Du = dunite; FGab = ferrogabbro; Gab = gabbro; Gabn = gabbronorite; Ha = harzburgite; HbGab = hornblende gabbro; HbMGab = hornblende metagabbro; HbMtMGab = hornblende-magnetite metagabbro; LGab = leucogabbro; Lherz = lherzolite; MGab = metagabbro; MGran = mafic granulite; MtGab = magnetite±ilmenite gabbro; N = norite; OGab = olivine gabbro; OGabn = olivine gabbronorite; OMGab = olivine metagabbro; Pyrox = pyroxenite; Ton = tonalite; Tr-An = tremolite-anthophyllite peridotite; Troc = troctolite.

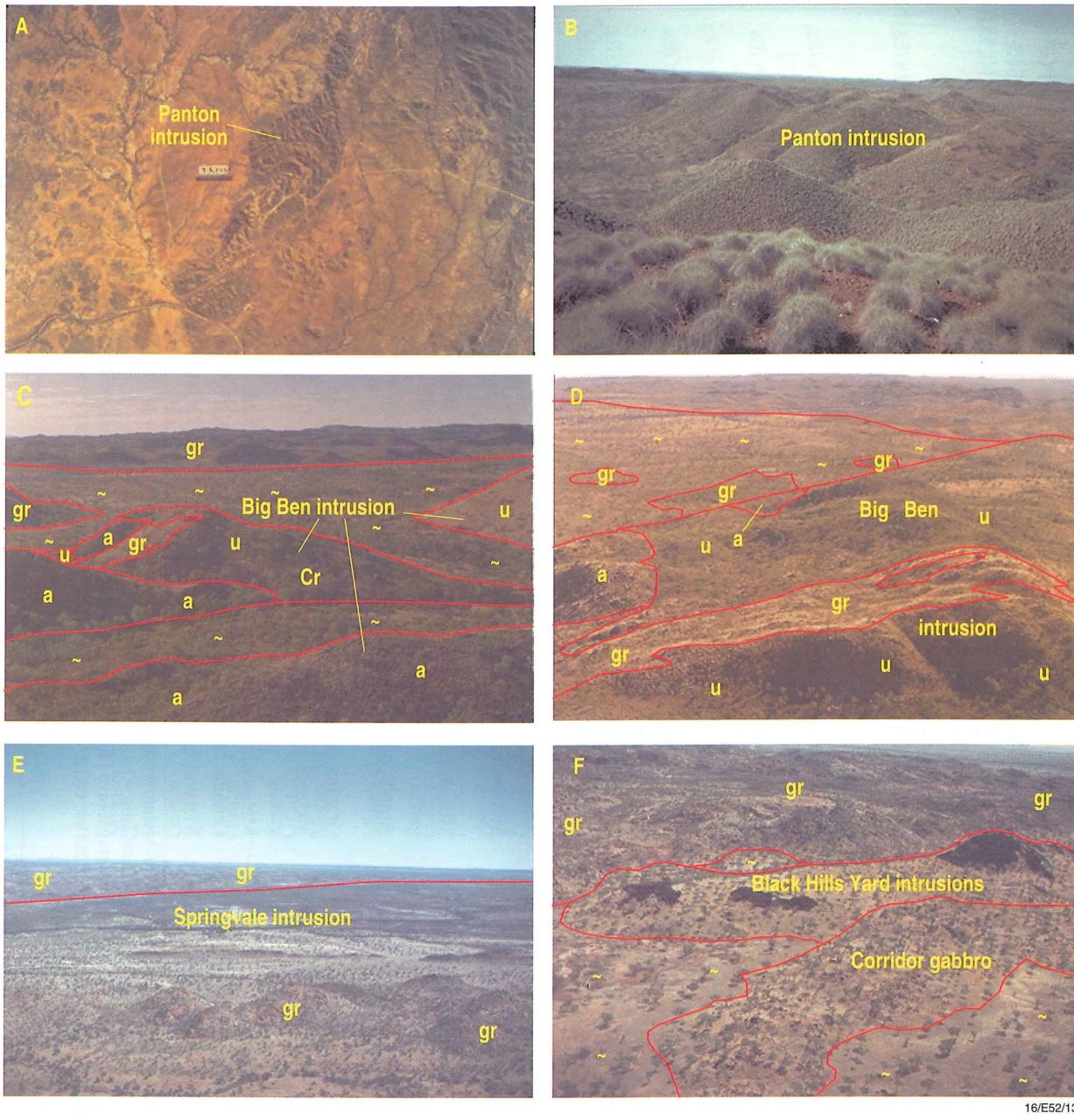


Figure 5.2. Layered mafic–ultramafic intrusions in the East Kimberley.

A. Vertical aerial photograph of the group I Panton mafic–ultramafic intrusion, a steep-sided asymmetric syncline plunging moderately towards the bottom left. The dark tones in the top right corner are ridge-forming gabbroic rocks of the group VI McIntosh mafic intrusion. Poorly outcropping rocks include gabbros of the Wild Dog Creek intrusion between the Panton and McIntosh intrusions, and granite, gabbro, and metasediments of the Tickalara Metamorphics to the left of the Panton intrusion. Scale bar under the Panton intrusion name represents 1 km. North is to the top of the photograph.

B. Low rounded bouldery hills with spinifex clumps, rubbly soil, and closely spaced gullies are typical of the ultramafic rocks in the Panton intrusion.

C. Aerial view looking northwest across the group I Big Ben mafic–ultramafic intrusion. Ultramafic rocks (u) are intruded by granite (gr) of the Sally Downs supersuite, and chromitite (Cr) layers are hosted by peridotite in the upper part of the ultramafic sequence below gabbro and anorthosite (a).

D. Aerial view looking north across the central part of Big Ben intrusion. Same legend as C.

E. Aerial view looking west across poorly exposed gabbroic rocks and black soil plains of the eastern and western lobes of the group II Springvale mafic intrusion. Boulder-strewn hills of granite (gr) of the Paperbark supersuite are in the foreground and background.

F. Aerial view looking west across the distinctive black hills of the group VII Black Hills Yard troctolite plugs. The plugs intrude biotite gabbro of the Corridor gabbro and granite (gr) of the Paperbark supersuite.

lower Ultramafic Series, 650 m thick, of contaminated basal contact rocks and a homogeneous ultramafic cumulate sequence, and an upper Gabbroic Series, 900 m thick, of mafic and minor ultramafic cumulates (Fig. 5.4A–F); Ultramafic and Gabbroic Series divided on the basis of the distribution of cumulus olivine and cumulus plagioclase, with the Gabbroic Series further subdivided into Lower, Middle, and Upper Mafic Zones according to different rock types and field relationships; complete cumulate sequence and both floor and roof rocks of intrusion are well exposed.

Ultramafic Series: basal sequence of shallowly dipping dunite (Fig. 5.4A) and porphyritic harzburgite (Fig. 5.4F); harzburgite is a distinctive unit containing large oikocrysts of orthopyroxene, which is most abundant along the northern margin of the intrusion; its close spatial association with margins of the intrusion and its irregular distribution indicate that siliceous contamination of the primitive magma by felsic country rocks initiated orthopyroxene crystallisation at the expense of olivine; most of the Ultramafic Series consists of cyclic units of massive and well-layered medium-grained dunite with minor lherzolite and chromitite more prominent in the upper part of the series.

Gabbroic Series: contains a range of rock types indicating periodic replenishment by influxes of new magma of contrasting composition; rhythmically layered and laminated gabbro (Fig. 5.4B), gabbronorite, and minor norite are the major cumulates in the Lower Mafic Zone; replacement of clinopyroxene by Fe-rich clinoamphibole imparts a distinctive dark green colour to the outcrops, or red-brown where deeply weathered; the Middle Mafic Zone consists of melagabbro, gabbronorite, and chromite-bearing dunite lenses; the gabbros of this zone form massive dark grey to black outcrops (Fig. 5.4C); the Upper Mafic Zone consists of a composite sequence of foliated ferrogabbro (Fig. 5.4D) and mottled anorthosite (Fig. 5.4E)—these are the most fractionated cumulates in the intrusion and their cyclic distribution indicates rapid changes in composition of magma pulses into the chamber.

Relationships. The Panton intrusion generally crosscuts and hence post-dates the main structural fabrics in the andalusite–muscovite–feldspar–quartz schist country rocks of the Tickalara Metamorphics; homogeneous schistose biotite granite along the synclinal axis of the southern part of the intrusion is interpreted as a remnant of deformed country rocks forming the roof of the intrusion; the biotite granite resembles migmatised Rose Bore Granite, which crops out along the southeastern margin of the intrusion; gabbro of the Wild Dog Creek unit and hybrid biotite granite and tonalite of the Sally Downs supersuite intrude dunite of the Panton intrusion on the northwestern margin of the southern block (Fig. 5.3).

Contact aureole: a weakly defined contact aureole, ~50 m-wide, comprising late-crystallising sillimanite overprinting andalusite porphyroblasts of regional metamorphic origin in hornfelsed pelitic migmatite and schist of the Tickalara Metamorphics, along sections of the northwestern contact of the northern block; in a contact aureole on the southeastern margin of the southern block, the contact metamorphic minerals have been largely hydrated to upper greenschist facies mineral assemblages during subsequent regional metamorphism (R.G. Warren, AGSO, 1995, pers. comm.); inconspicuous sillimanite–garnet-bearing ?paragneiss forms a ~50 m wide zone between the intrusion and a biotite-rich banded migmatitic granite (Rose Bore Granite) that forms rock pavements in the Upper Panton River; the migmatite consists of knots of biotite and muscovite in a matrix of quartz, plagioclase, sillimanite (mostly fibrolite), and minor garnet (Fig. 5.45F); complex folding and boudinage features imply considerable shortening during deformation and melting; the proportion of leucosome decreases progressively away from the contact of the Panton intrusion, and no leucosome is present in schistose rocks several hundred metres from the intrusion; the Rose Bore Granite has a U–Pb zircon age of 1863±4 Ma (see Chapter 6), which constrains the maximum emplacement age of the Panton intrusion.

Chilled margin: quartz–hornblende microgabbro and quartz dolerite locally form a contaminated chilled zone (Fig. 5.3), ~10 m-wide, to the basal peridotites of the Ultramafic Series in the northern block.

Mineralisation. Subeconomic resource of 2 Mt @ 6.02 ppm Pt+Pd+Au, 0.28% Ni, 0.06% Cu, and 8.49% Cr (using 3 ppm PGEs+Au cut-off) in stratabound chromitite layers on the northwestern side of the intrusion (Perring & Vogt 1991, Helix Resources 1993); chromitite layers (see Chapter 14) occur at three major stratigraphic levels in the intrusion: (1) Lower Chromitite Group in the basal part of the Ultramafic Series—thin (<10 cm) discontinuous layers in harzburgite and dunite, (2) Middle Chromitite Group about 120–150 m below the contact of the Ultramafic and Gabbroic Series—economically important package of PGE-enriched layers in dunite that includes the Main Chromitite Layer (MCL; also called A chromitite layer by Perring & Vogt 1991), 0.1–2.4 m thick over a strike length of 12 km, and (3) Upper Chromitite Group in the Middle Mafic Zone of the Gabbroic Series—intensely fractured, locally thickened (up to 0.3 m) layers in a stacked sequence of arcuate dunite lenses that traverse the synclinal axis of the intrusion; in addition thin (millimetre to centimetre) chromitite layers, stringers, and lenses occur throughout the intrusion, particularly in the upper half of the Ultramafic Series.

Petrography. *Ultramafic Series:* chilled marginal rocks contain hornblende after clinopyroxene, plagioclase, graphic intergrowths of quartz and feldspar, interstitial quartz, minor apatite, magnetite, chlorite, and trace sulphide; high quartz content and fractionated Fe-rich composition of the marginal rocks are considered to be due to alteration by fluid activity and/or SiO_2 contamination from the country rocks; dominant rocks of the series are intensely serpentinised ultramafic cumulates containing only two cumulus minerals—olivine and/or chromite (oC, ocC, cC); there is a complete gradation from dunite containing no chromite, to chromite-bearing dunite, to chromitites with no silicate minerals; adcumulus granular textures are preserved in the dunites as a tight interlocking array of subhedral olivine grains (1–3 mm)

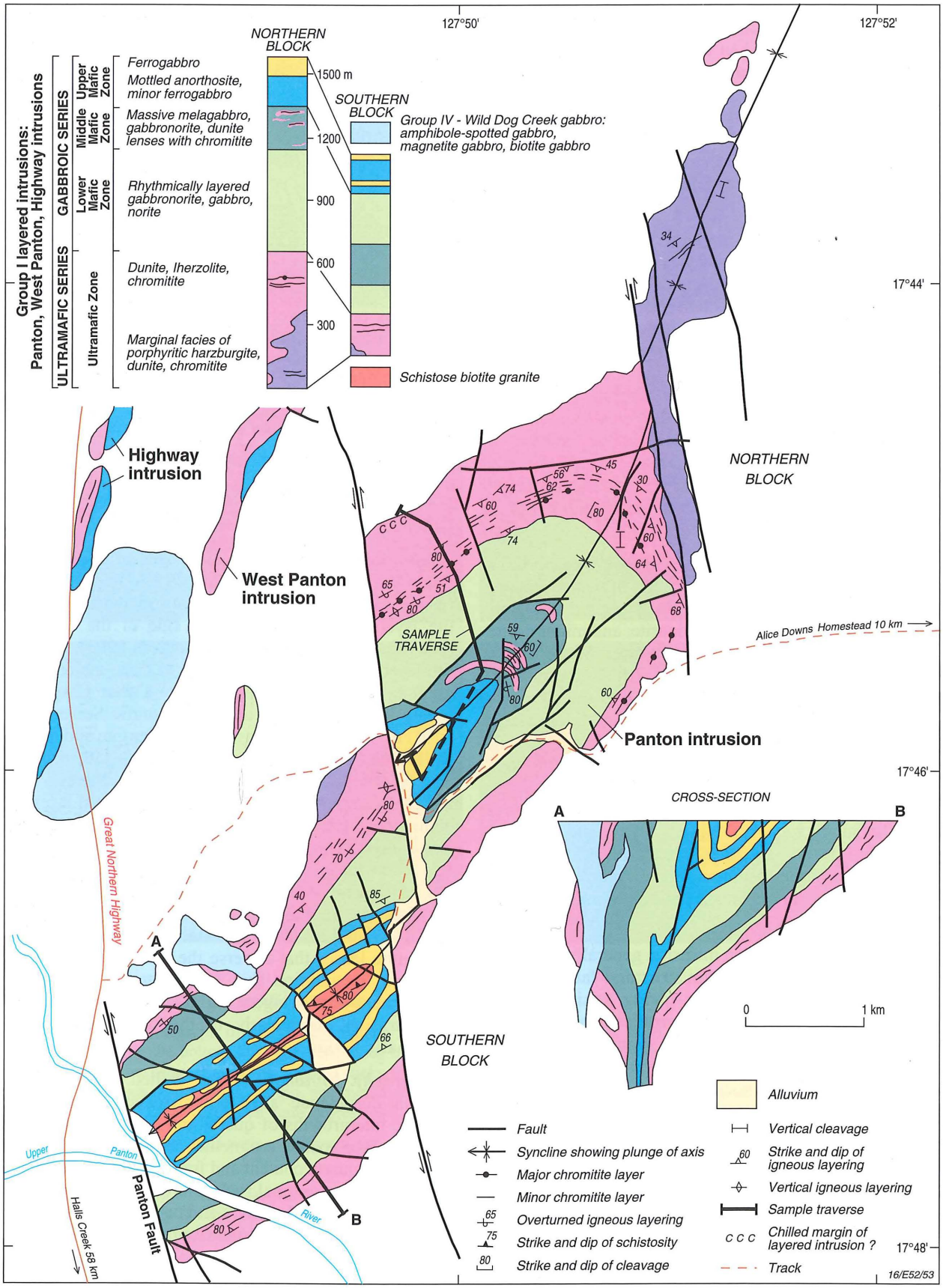
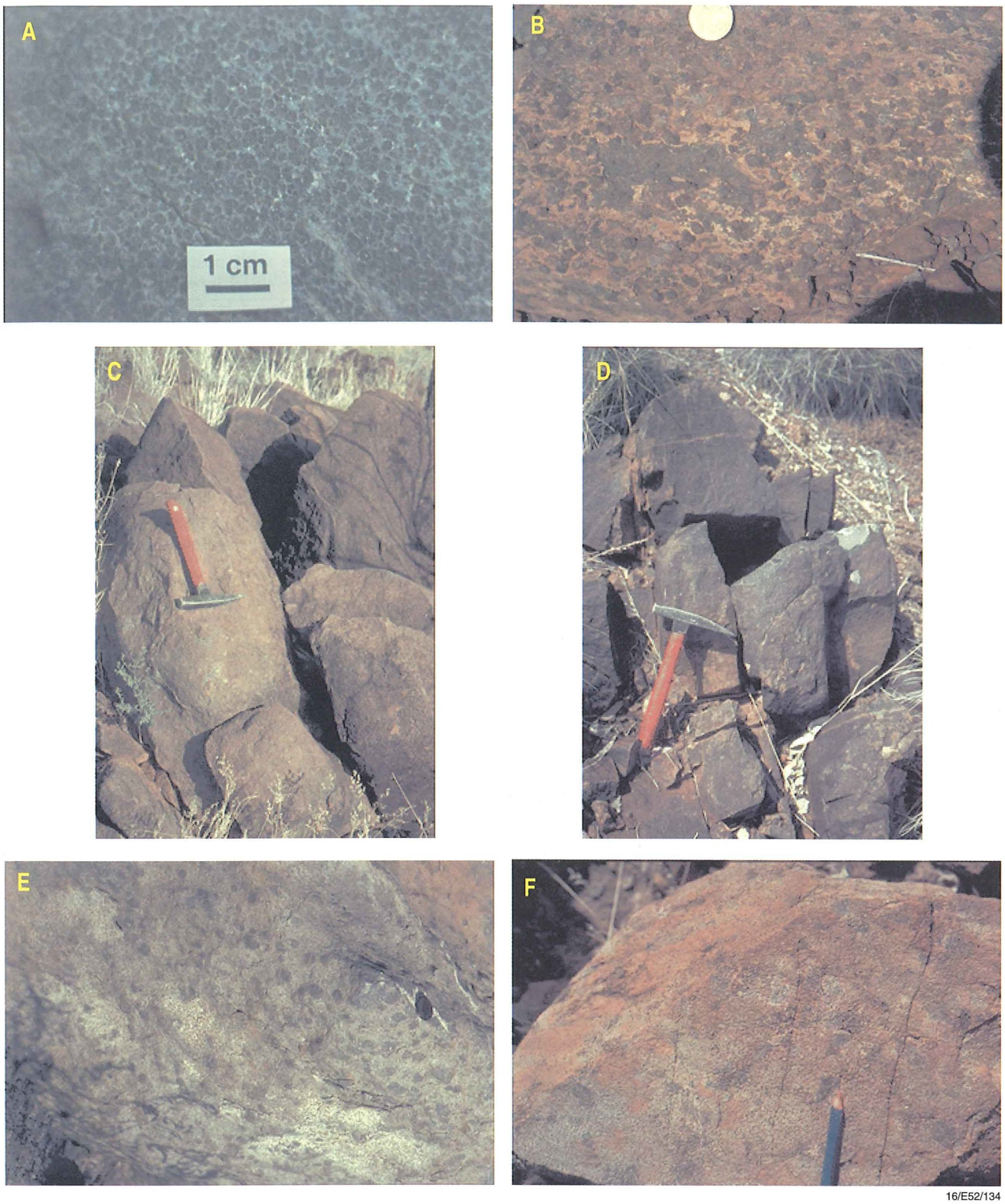


Figure 5.3. Geological map and schematic cross-section of the group I Panton mafic–ultramafic intrusion. The southern parts of the group I Highway and West Panton intrusions are also shown.



16/E52/134

Figure 5.4. Major rock types in the group I Panton mafic–ultramafic intrusion.

A. Dunite typical of the Ultramafic Series (photograph by R. Perring, Normandy Exploration Ltd).

B. Weakly layered gabbro consisting of uralitised equant clinopyroxene (dark green) and sericitised plagioclase (pinkish white) in the Lower Mafic Zone (McINTOSH AMG ~769365).

C. Massive melagabbro in the Middle Mafic Zone (McINTOSH AMG ~741333).

D. Massive ferrogabbro in the Upper Mafic Zone (McINTOSH AMG ~740323).

E. Mottled anorthosite in the Upper Mafic Zone (McINTOSH AMG ~763358).

F. Harzburgite with dark oikocrysts of orthopyroxene at the base of the Ultramafic Series (McINTOSH AMG ~778382).

surrounded by discontinuous trains of euhedral chromite grains; chromite also occurs as rare subhedral inclusions in olivine; olivine locally has well-developed coronas of amphibole, Al spinel, and chlorite (similar coronas occur in the Big Ben intrusion: see below); Hamlyn (1975) and Hamlyn & Keays (1979) reported narrow Al–Mg-enrichment and Fe–Cr–Ti-depletion alteration zones along the margins and fractures of chromite grains, and olivine is altered to serpentine minerals, magnetite, hematite, chlorite, iddingsite, calcite, and magnesite; intercumulus minerals are rarely preserved in dunite, but clinozoisite aggregates may indicate the former presence of plagioclase (Hamlyn 1980); cumulus plagioclase is restricted to rare chromite-bearing ultramafics from the 375–425 m stratigraphic interval; orthopyroxene forms large (up to 3 cm) oikocrysts in harzburgite near the base of the intrusion and, with clinopyroxene, forms a minor cumulus component in rare lherzolite (oabC) mesocumulates near the top of the Ultramafic Series (Perring & Vogt 1991); S-saturated conditions for most ultramafic cumulates are indicated by trace amounts of pentlandite, chalcopyrite, pyrite, and pyrrhotite in veinlets and as small anhedra at grain boundaries of silicates.

Chromitites: the MCL is a fine to medium-grained (0.1–2 mm) massive adcumulate (cC), comprising tightly packed fragmented and fractured chromite anhedra in a groundmass of serpentine, carbonate, tremolite, chlorite, and iddingsite; some chromite grains are embayed and doughnut-shaped; pyrite, pentlandite, pyrrhotite, chalcopyrite, bornite, and covellite form trace anhedral interstitial grains, and dominant platinum-group minerals are platinum arsenides (sperrylite), palladium sulphides, tellurides, and bismuthinides; Cr_2O_3 concentration is fairly constant across the MCL, which contains 24% Cr_2O_3, 0.31% Ni, and 0.06% Cu (Perring & Vogt 1991); chromitites with a greater abundance of olivine (ocC, coC) about 20 m below the MCL have net textures, comprising disseminated chromite subhedra mantling olivine grains that are replaced by magnesite and lesser serpentine; chromitites of the Lower Chromitite Group contain fine-grained (0.1–0.3 mm) euhedral chromite grains, brittle fracturing is restricted to thin (<0.5 mm) shear zones, and carbonate alteration of olivine is subordinate to serpentinisation; the very low sulphide content for most chromitites in the Ultramafic Series relative to adjacent S-saturated cumulates may be due to remobilisation of sulphides during intense serpentinisation of Cr–Fe–Mg-rich assemblages; Hamlyn & Keays (1979) attributed olivine's more primitive compositions in chromite-rich peridotite (mg_{84-91}), compared to chromite-poor peridotite (mg_{81-85}), to the postcumulus re-equilibration of olivine with the surrounding magma.

Gabbroic Series: defined by the introduction of cumulus plagioclase at the expense of cumulus olivine; medium-grained gabbro, melagabbro, gabbronorite, and minor norite adcumulates in the Lower and Middle Mafic Zones contain similar cumulus assemblages (paC, pabC), but are subdivided on the basis of contrasting layering and outcrop features (see *Stratigraphy and main rock types*); gabbros of these two zones contain subhedral to anhedral tabular plagioclase, uralitised clinopyroxene and orthopyroxene, accessory apatite, zircon, granular green spinel, sphene, chromite, and sulphides, and very rare Fe–Ti oxides and primary biotite; widespread uralitisation and sericitisation, and local tourmalinisation alteration have often destroyed cumulus textures and primary mineralogy; Hamlyn (1980) described deformational features such as undulose extinction, bent lamellae twins, local subgrain recrystallisation, and metamorphic schistosity of prismatic amphibole overprinting igneous lamination of aligned plagioclase laths; mottled textures in anorthosite (pC) mesocumulate from the Upper Mafic Zone are defined by large (up to 5 mm) broad plagioclase laths with postcumulus overgrowths enclosed by centimetre-sized intercumulus clinopyroxene grains that are replaced by hornblende, magnetite, tremolite, chlorite, clinozoisite, and epidote; primary accessory apatite, zircon, and brown biotite are prominent in the middle part of the zone; foliated ferrogabbro cyclic units at the top of the Upper Mafic Zone contain decussate aggregates of poikilitic hornblende with associated Fe–Ti oxide and sphene anhedra, and fine-grained interstitial plagioclase; Hamlyn (1977, 1980) attributed calcic compositions of plagioclase (An_{83-100}) in the Gabbroic Series to the metamorphic re-equilibration of this mineral with adjacent hornblende.

Geochemistry. *Regional trends:* variations in the major oxides largely reflect gross modal changes, as defined

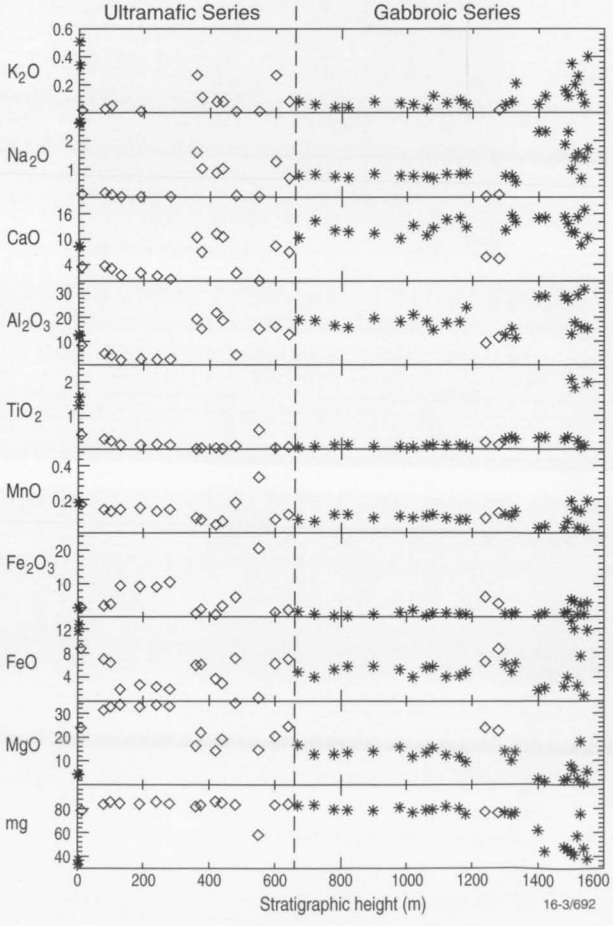


Figure 5.5. Panton intrusion: variation in whole-rock major-element composition (in weight %) with stratigraphic height. Open diamond—ultramafic cumulate; star—mafic cumulate.

by the variable proportions of olivine, chromite, and, to a lesser extent, plagioclase in the Ultramafic Series, and plagioclase, clinopyroxene, orthopyroxene, and Fe–Ti oxides in the Gabbroic Series; fractionated compositions of the chilled basal ultramafic rocks (high FeO, MnO, TiO_2, Al_2O_3, Na_2O, and K_2O and low $mg_{32.6–36.5}$) relative to the overlying dunites (Fig. 5.5) are attributed to rapid cooling and contamination along the basal contact; Hamlyn et al. (1988) recognised two megacyclic units for the main part of the Ultramafic Series—lowermost unit is delineated by increasing Al_2O_3 and decreasing Cr, Ir, and Ni abundances to approximately the 400 m level (Fig. 5.6), where rare cumulus plagioclase is present (see *Petrography)*; an abrupt discontinuity at this level defines the base of the second megacyclic unit, above which the highly compatible behaviour of decreasing Cr, Ir, and Ni indicate closed-system fractionation to 950 m; pronounced fluctuations in Cr, Ir, Pt, and Pd concentrations from 950 m to about 1350 m coincide with more open-system fractionation, involving the reappearance of thin dunite lenses in gabbro hosting chromitite layers;

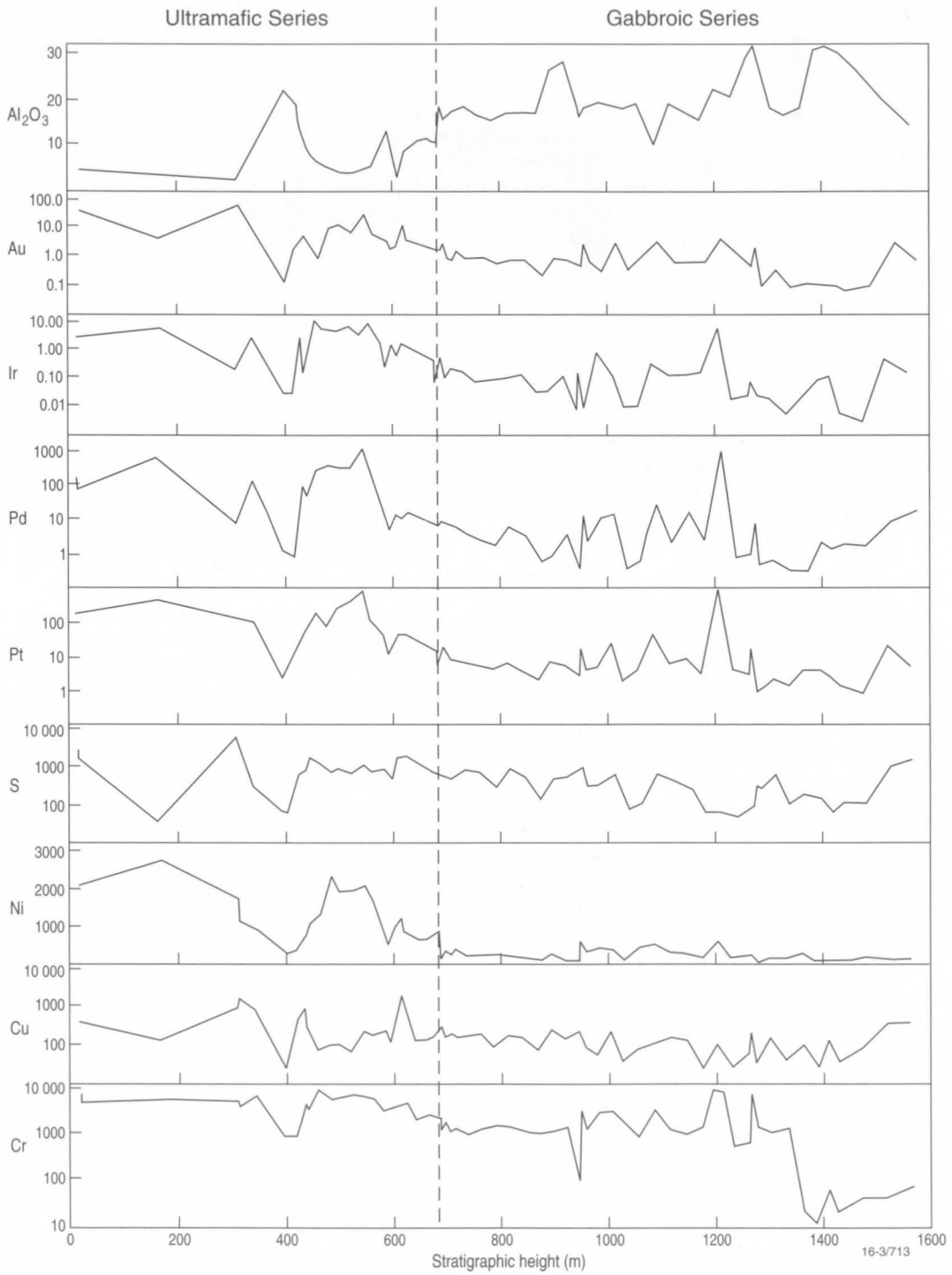


Figure 5.6. Panton intrusion: variation in whole-rock Al_2O_3 (in wt. %) and trace-element composition (in ppm) with stratigraphic height. Reproduced with permission from P. Hamlyn (Hamlyn et al. 1988).

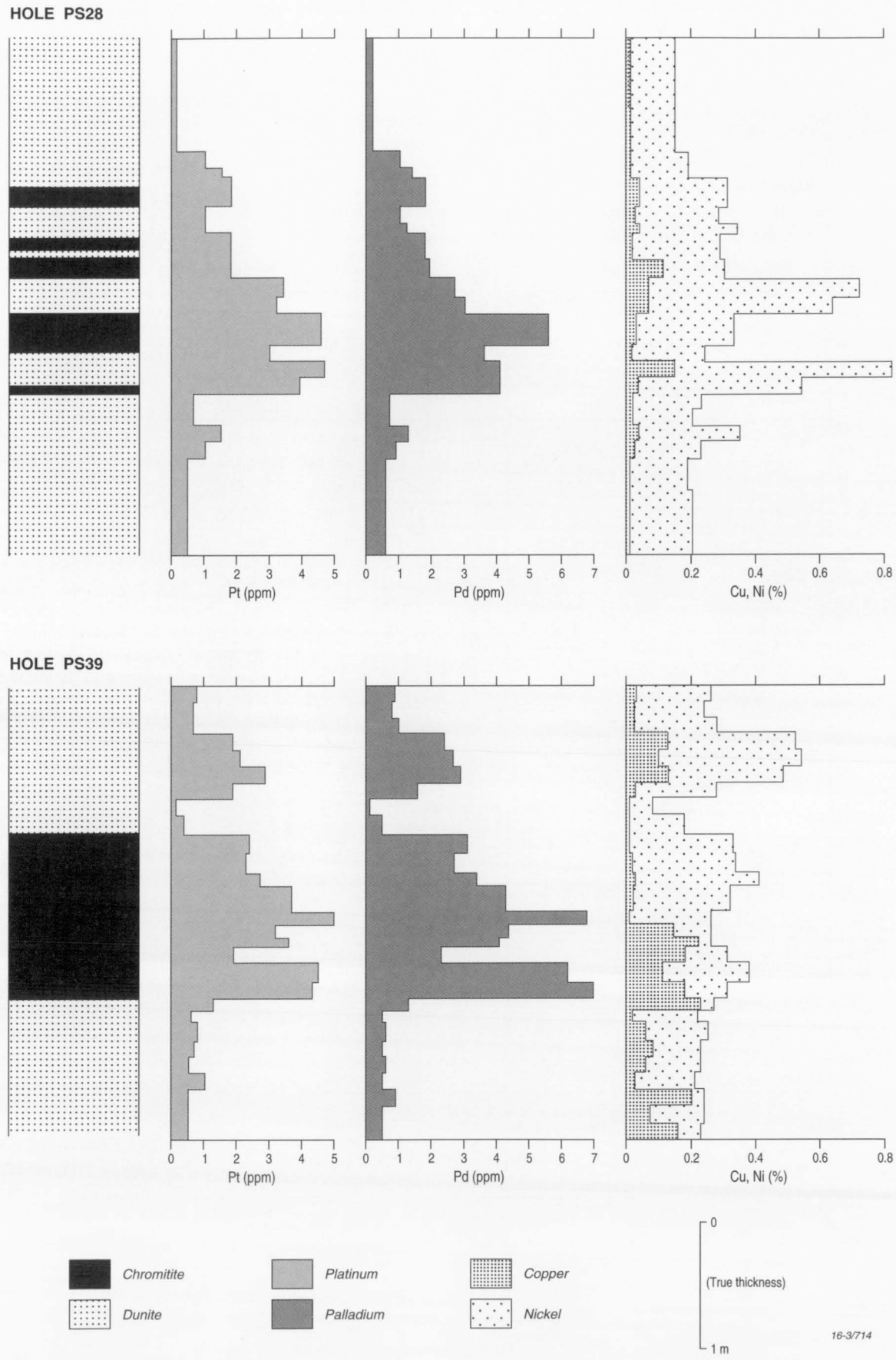


Figure 5.7. Panton intrusion: variation in whole-rock Pt and Pd (in ppm), Cu and Ni (in wt. %) across the Main Chromitite Layer (A chromitite layer of Perring & Vogt 1991) in diamond holes PS28 and PS39. Modified after Perring & Vogt (1991).

Table 5.2. Platinum-group-element (ppb) and gold (ppb) geochemistry of chromitite layers in the Ultramafic Series of the Panton intrusion (modified after Perring & Vogt 1991).

Chromitite Layer[1]	*Stratigraphic height (m)*[2]	*Thickness (cm)*	*Pt*	*Pd*	*Rh*	*Ru*	*Ir*	*Os*	*Au*	*Pt/Pd*	*Pd/Ir*	*(Pt+Pd)/(Ru+Ir+Os)*
A	530	80	3175	3730	70	140	62	92	53	0.85	60.2	23.5
B	515	10	2070	1785	82	132	56	66	108	1.16	31.9	15.2
C	500	15	295	440	42	85	30	32	30	0.67	14.7	5
D	40	10	1215	1350	80	250	80	76	50	0.90	16.9	6.3
E	15	10	1500	1975	125	310	75	100	55	0.76	26.3	7.2

[1] Classification of chromitites by Perring & Vogt (1991).

In this *Bulletin*: Chromitite layers A, B, and C are equivalent to the Middle Chromitite Group, where chromitite A is equivalent to the Main Chromitite Layer (MCL); and Chromitite layers D and E are equivalent to the Lower Chromitite Group.

[2] The contact between the Gabbroic Series and the underlying Ultramafic Series is at the 650 m stratigraphic level.

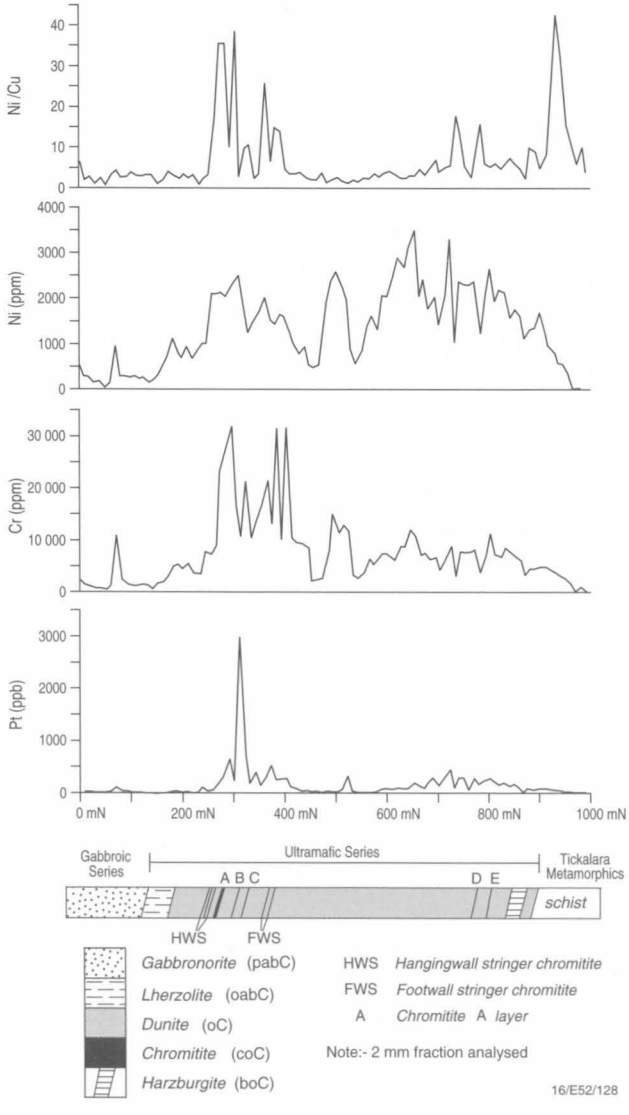


Figure 5.8. Panton intrusion: variation of Pt (ppb), Cr and Ni (in ppm), and Ni/Cu in soils across the Ultramafic Series. Modified after Perring & Vogt (1991).

marked changes in K_2O, Na_2O, Al_2O_3, TiO_2, mg (Fig. 5.5), and increases in most trace-element abundances (Fig. 5.6) above 1350 m correlate with fractionated anorthosite and ferrogabbro cyclic units of the Upper Mafic Zone.

Mineralisation trends: the two major stratigraphic levels of chromitite in the intrusion (Lower and Middle Chromitite Groups: see *Mineralisation*) define approximately the basal parts of the two megacyclic units; Pt, Pd, Ir, and Au generally show sympathetic decreasing trends with S throughout the intrusion, and no marked discontinuity at the contact of the Ultramafic Series and Gabbroic Series; high S contents of most ultramafic (300–1750 ppm) and gabbroic (340–920 ppm) cumulates testify to S-saturated conditions, which were probably induced by repeated mixing between slightly evolved resident magma and influxes of hotter more primitive magma; chromitite layers in the Ultramafic Series have markedly different concentrations and ratios of PGEs and Au (Table 5.2); Pt and Pd show similar enrichment trends in the lower parts of the MCL (Fig. 5.7), whereas Cu and Ni show weak and no correlation, respectively; soil geochemistry (Fig. 5.8) indicates that the most sensitive indicators of PGE-enriched chromitites are Pt and Cr, with elevated Ni/Cu ratios directly above the MCL due to preferential partitioning of Cu into sulphide minerals in the chromitite; Ni is not a useful indicator of mineralisation, since its broad distribution reflects its association with both sulphides and olivine.

Other comments. Most intensively explored intrusion in the East Kimberley, with PGE-enriched stratabound chromitites being the focus of several phases of exploration since the potential of the intrusion was first realised in the mid-1960s.

Big Ben mafic–ultramafic intrusion (43 in Fig. 5.1, Fig. 5.9)

Centre of intrusion. Southern McINTOSH at AMG ~767160.

Age. Correlated with the 1856±2 Ma Panton intrusion.

Form, structure, and areal extent. Fault-bounded wedge, 2.5 x 2.5 km, on western side of Panton Fault; chromitites strike east-southeast and dip about 65°S; general differentiation trend of mafic and ultramafic cumulates indicates younging south.

Thickness. 2 km.

Stratigraphy and main rock types. Stratigraphy similar to the southwestern part of the Panton intrusion; has the thickest sequence of ultramafic cumulates of all group I intrusions; Ultramafic Zone, ~1700 m thick, of serpentinised dunite, peridotite, lherzolite, tremolite-actinolite schist, chromitite, and minor pyroxenite is overlain by Mafic Zone, ~300 m thick, of mottled anorthosite, foliated gabbro, gabbronorite, and norite.

Relationships. Intrudes partly sheared mafic and felsic metavolcanics, and quartz–feldspar–muscovite schist assigned to Tickalara Metamorphics (see *Other comments*), and gabbroic sills of the Wild Dog Creek intrusion in south; alluvium masks northwestern contact and eastern contact is faulted; contact between the Ultramafic and Mafic Zones is intruded by massive and foliated equigranular hornblende–biotite granite of the Sally Downs supersuite and aplitic dykes; in places the felsic bodies have also disrupted the strike trends of the chromitites; similar granites intrude the northwestern margin of the southern block of the Panton intrusion.

Mineralisation. Steeply dipping chromitite layers are hosted by olivine cumulates in lower and upper parts of the Ultramafic Zone (as in other thick group I intrusions); thickest chromitite layers (up to 15 cm) in the upper part extend for several hundred metres along strike.

Petrography. Intensely serpentinised medium-grained (0.25–2 mm) ultramafic mesocumulates and orthocumulates (opC, oC, ocC) contain cumulus olivine, chromite, and minor plagioclase, and intercumulus and, locally, oikocrystic orthopyroxene; deeply embayed olivine anhedra adjoining plagioclase have coronas (see Chapter 9) of inner granular pale green Ca-amphibole surrounded by fine to coarse-grained green spinel anhedra; chromitite in upper part of Ultramafic Zone contains chromite subhedra (0.02–0.4 mm) mantling serpentinised cumulus olivine; mottled textures in anorthosite (pC) consist of sericitised plagioclase laths (2–3 mm) and clots of intercumulus clinopyroxene replaced by hornblende or actinolite.

Geochemistry. Well-differentiated sequence, comprising dunite ($mg_{79.5}$, 1901 ppm Cr), pyroxenite ($mg_{75.4}$, 827 ppm Cr), plagioclase peridotite ($mg_{72.3}$, 26 ppm Cr), and anorthosite ($mg_{53.9}$, 21 ppm Cr); variable S content (20–910 ppm) partly reflects variable intensity of serpentinisation; chromitites in upper part of Ultramafic Zone directly below Mafic Zone are enriched in Pd (1080 ppb) and Pt (583 ppb) and contain anomalous Au (8 ppb).

Other comments. Big Ben intrusion is the only group I body outside the Cr–PGEs–Ni–Cu±Au metallogenic corridor (Fig. 5.1, Hoatson 1993). Restoration of common rock units (gabbro of the Wild Dog Creek intrusion and granite of the Sally Downs supersuite) across the

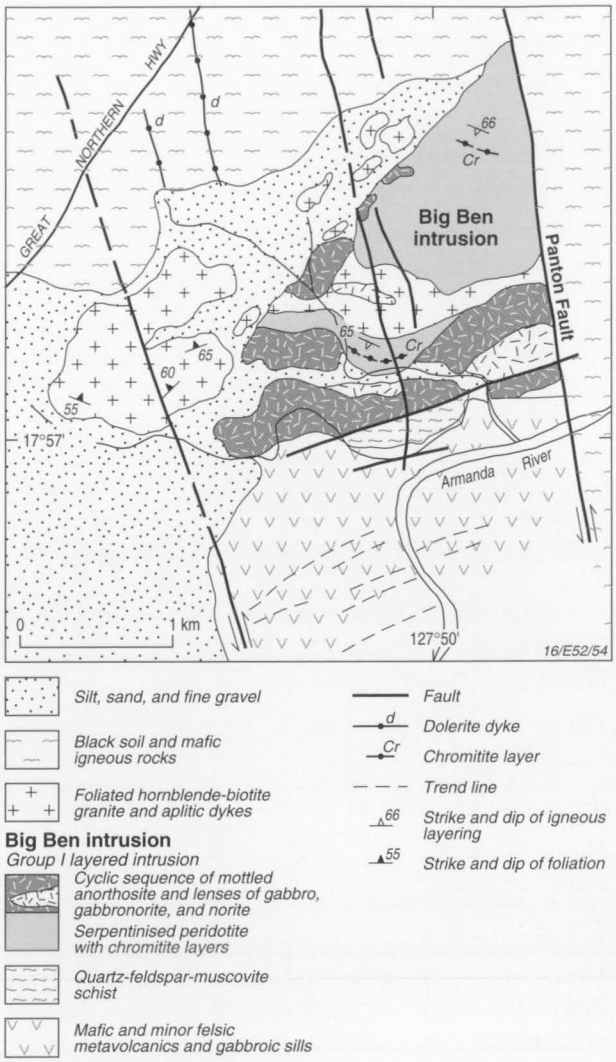


Figure 5.9. Geological map of the group I Big Ben mafic–ultramafic intrusion.

Panton Fault, and similar mineralogical and chemical features (see below) indicate that the Big Ben intrusion is probably a transposed fault-bounded block that was originally part of the mineralised Panton intrusion (Hoatson 1993). Sinistral displacement of about 15 km along the Panton Fault accounts for it being outside the metallogenic corridor: 'tectonic fragmentation' of the southwestern end of the Panton intrusion is also indicated by another smaller transposed mafic–ultramafic block just east of the Panton Fault, about 2.5 km south-southeast of the Panton intrusion. The high ratio of ultramafic to mafic cumulates in the Big Ben intrusion (5.5:1) relative to the Panton intrusion (0.7:1) is probably due to deeper erosion of the former intrusion caused by upward dip-slip movement along the Panton Fault. The Big Ben and Panton intrusions have similar:

- cumulus assemblages in the ultramafic (cumulus olivine, chromite, and, locally, plagioclase, intercumulus orthopyroxene) and gabbroic (cumulus plagioclase, clinopyroxene, and orthopyroxene) zones;
- coronas of amphibole and Al spinel around embayed olivine;

- unusual calcic compositions (Big Ben—An_{89-100}, Panton—An_{83-100}) for plagioclase, owing to its re-equilibration with metamorphic hornblende;
- Pt/Pd ratios for chromitites in the ultramafic zones (Big Ben—0.54–0.90, Panton—0.67–1.16: Tables 5.2 and 14.3); and
- depths of emplacement (around 11 km: see Chapter 9).

If the Big Ben and Panton intrusions were originally part of the same body, the metavolcanics (Peb) shown as the 1843±2 Koongie Park Formation south of the Big Ben intrusion on McINTOSH (Tyler et al. 1997) should be assigned to the pre-1860 Ma Tickalara Metamorphics. Similarly, unassigned felsic volcanics (Pgf) east of the Panton Fault and north of the Big Ben intrusion may correlate when restored along the Panton Fault with felsic volcanics (Pef) of the Koongie Park Formation east of the Armanda intrusion (46 in Fig. 5.1) to the south.

Highway mafic–ultramafic intrusion (35 in Fig. 5.1, Fig. 5.3)

Centre of intrusion. Central McINTOSH at AMG ~733371.

Age. Correlated with the 1856±2 Ma Panton intrusion.

Form, structure, and areal extent. Steeply dipping mafic–ultramafic lens, 300 m wide by 2.2 km long.

Thickness. 200 m.

Stratigraphy and main rock types. Basal Ultramafic Zone, 100 m thick, of serpentinised peridotite in west overlain to east by similar thickness of mottled and massive uralitised anorthosite and minor gabbro.

Relationships. Contacts with country rocks not exposed; surrounded by foliated granite of Sally Downs supersuite, metagabbro of the Wild Dog Creek, and metasediments of the Tickalara Metamorphics.

Mineralisation. Thin (1–5 cm) chromitite layers, tens of metres long, directly below contact of peridotite and anorthosite.

Petrography. Peridotite (ocC, oC) consists of intensely serpentinised cumulus olivine and chromite grains; mottled anorthosite (pC) consists of tightly packed squat plagioclase laths (2–3 mm) with deformed lenticular and bent twinning and smaller clinopyroxene anhedra replaced by hornblende, calcite, and clinozoisite.

Geochemistry. Single anorthosite sample (92522116 in Appendix 2) has similar composition ($mg_{55.6}$, 29 ppm Cr, 21 ppm Ni, 50 ppm S) to anorthosite in the upper part of the Panton intrusion.

Other comments. Crops out along the Great Northern Highway and contains similar rock types and chromite mineralisation to the nearby Panton and West Panton intrusions.

Melon Patch mafic–ultramafic intrusions (26 in Fig. 5.1)

Centre of intrusions. Northeastern McINTOSH at AMG ~875540 and 882523.

Age. Correlated with the 1856±2 Ma Panton intrusion.

Form, structure, and areal extent. Two northeast-trending, steeply dipping (65°), elongate bodies that dip and young to the southeast; southern intrusion is an irregular ultramafic body, 2 km long by 600 m wide, and the northern intrusion is a mafic–ultramafic intrusion 3 km long by 500 m wide.

Thickness. ?500 m.

Stratigraphy and main rock types. Southern intrusion contains serpentinised peridotite and tremolite–anthophyllite–chlorite schist, and the northern intrusion contains foliated mottled anorthosite, uralitised gabbro, and serpentinised dunite.

Relationships. Both bodies intrude amphibolite, schistose metasediments, and foliated biotite granite of the Tickalara Metamorphics, and are intruded by various hybrid granitic and gabbroic rocks of the Sally Downs supersuite.

Mineralisation. Chromitite layers (1–3 cm thick) occur in dunite at different stratigraphic levels at the southwestern end of the southern intrusion and near the contact between dunite and anorthosite in the northern intrusion.

Other comments. Melon Patch intrusions are the most northerly group I bodies studied.

Mini ultramafic intrusion (33 in Fig. 5.1, Fig 5.10; also known as Mini M)

Centre of intrusion. Central McINTOSH at AMG ~791428.

Age. Correlated with the 1856±2 Ma Panton intrusion.

Form, structure, and areal extent. Sill, 2.5 km long by 300 m wide, folded about southwest-plunging anticlinal axis on western margin of the McIntosh intrusion; dips 70–82° to the south and southwest, and both ends of body displaced by faults.

Thickness. 200 m.

Stratigraphy and main rock types. Sheared tremolite–anthophyllite–chlorite schist and serpentinised peridotite are the major ultramafic rocks (180 m thick), with rare thin (10 m) uratilised gabbro units restricted to the southwestern side of the sill; carbonate alteration locally prominent; Codner (1979) described brecciated and variably deformed ultramafic rocks and small ultramafic apophyses in metasediments on the northeastern side of the sill.

Relationships. Intrudes and concordant with andalusite–garnet–muscovite–feldspar–quartz schist and gneiss of the Tickalara Metamorphics; intrusion and country rocks are cut by numerous aplite and dolerite dykes, and minor pegmatite and quartz veins.

Mineralisation. Discontinuous thin chromitite layers are common on the southern and southwestern sides of the sill (Codner 1979); sheared massive chromitite layers, 1–10 cm thick, can be traced along strike for tens of metres in the tremolite–anthophyllite–chlorite schist and peridotite; four different stratigraphic levels of chromitites have been recognised, and disseminated chromite also occurs within the ultramafic rocks; Codner (1979) found that Pt (0.6→0.7→1.5→2 ppm) and Pd (2→0.15→3→5 ppm) concentrations and Pt/Cr x 10 ratios (0.36→0.44→0.75→1.2) increased upwards (southwards) in the chromitites—these trends and the relative position of the chromitites on the 'upper' side of the sill led Codner to believe that the sill was overturned; however, the most PGE-rich chromitites in other group I intrusions (e.g. Panton) occur high in the ultramafic sequence directly below the Mafic Zone and Ultramafic Zone contact, similar to the Mini intrusion; gossans in shears and quartz veins at northwestern end of sill contain >1% Cu.

Petrography. Chromitites consist of disseminated fine-grained (<0.2 mm) chromite anhedra and subhedra in a groundmass of tremolite, anthophyllite, chlorite, and minor serpentine; disseminated blebs of pyrrhotite with minor exsolved pentlandite, chalcopyrite, and pentlandite occur in the least sheared ultramafic rocks.

Geochemistry. Chromitites in upper part of Ultramafic Zone directly below Mafic Zone contain 122 ppb Pd, 43.4 ppb Pt, and 1 ppb Au.

Other comments. The Mini intrusion is a rare example of a folded ultramafic sill, sensu stricto, in the East Kimberley.

South Melon Patch mafic–ultramafic intrusion (30 in Fig. 5.1, Fig. 5. 10)

Centre of intrusion. Northeastern McINTOSH at AMG ~863490.

Age. Correlated with the 1856±2 Ma Panton intrusion.

Form, structure, and areal extent. Tight southwesterly plunging anticline, 5.5 km long by 2.5 km wide, on north side of the group VI McIntosh intrusion; appears to be coaxial with the group I Mini intrusion to the southwest.

Thickness. 1 km.

Stratigraphy and main rock types. Complete sequence of differentiated mafic and ultramafic rocks, together with roof and floor rocks, is exposed (similar to the Panton intrusion); axis of anticline consists of metasediments of the Tickalara Metamorphics, ovoid bodies of foliated leucogranite, dolerite dykes, and a basal ultramafic sequence, 300 m thick, of serpentinised peridotite, dunite, chromitite, and minor harzburgite, which is overlain by a mafic sequence, 700 m thick, comprising gabbro, gabbronorite, and minor norite (400 m), followed by foliated amphibolite and melagabbro (150 m), and, at top, mottled anorthosite and leucogabbro (150 m); thin plagioclase-bearing tremolite–anthophyllite–hercynite schist unit occurs near transition between ultramafic and mafic sequences; coarse ?hercynite octahedral euhedra (up to 4 cm across) with alteration rims of chlorite and amphibole are locally found loose on the weathered surface of peridotite.

Relationships. Migmatitic garnet-bearing metasediments and foliated biotite metagranite (probably Rose Bore Granite equivalent) of the Tickalara Metamorphics to the south; deformed metagranite wraps around nose of anticlinal structure to flank the northern side of intrusion; mainly discordant massive gabbros of the Wild Dog Creek intrusion to the east; north-trending dextral fault displaces the middle part of the intrusion 150 m southward, and the eastern end of the intrusion is partly truncated by a regional northwest-trending sinistral fault.

Mineralisation. Thin (2–5 cm) chromitite layers, up to 2 km long, just below contact of ultramafic rocks with mafic rocks on northern limb of anticline and in other parts of ultramafic sequence.

Petrography. Peridotite (oacC) consists of serpentinised and uralitised cumulus olivine, with secondary tremolite, actinolite, anthophyllite, dark green spinel (?hercynite), magnetite, chlorite, and carbonates; gabbro (paC) has intergranular adcumulate textures, and foliated amphibolite has granuloblastic polygonal textures attributed to greater partitioning of strain during amphibolite/granulite facies metamorphism; foliated melagabbro contains decussate prismatic hornblende layers alternating with discontinuous layers of polygonal plagioclase grains; mottled anorthosite consists of small (<1mm) equant plagioclase grains and larger (1.5 mm) poikilitic hornblende anhedra, which host small magnetite and plagioclase inclusions; coarse blades of epidote cut a foliation defined by alignment of plagioclase grains.

Geochemistry. Well-fractionated sequence of peridotite ($mg_{78.6–82}$, 2438–7235 ppm Cr) melagabbro and gabbro ($mg_{57.4–78.3}$, 60–1951 ppm Cr), and leucogabbro ($mg_{42.1}$, 10 ppm Cr); chromitite and chromite-bearing peridotite in the upper part of Ultramafic Zone directly below Gabbroic Zone are enriched in Pt (527 and 91.6 ppb), Pd (283 and 179 ppb), and Au (38 and 3 ppb); variable S content (40–1350 ppm) of mafic and ultramafic cumulates partly reflects varying intensities of serpentinisation and uralitisation.

Springvale Track ultramafic intrusion (38 in Fig. 5.1)

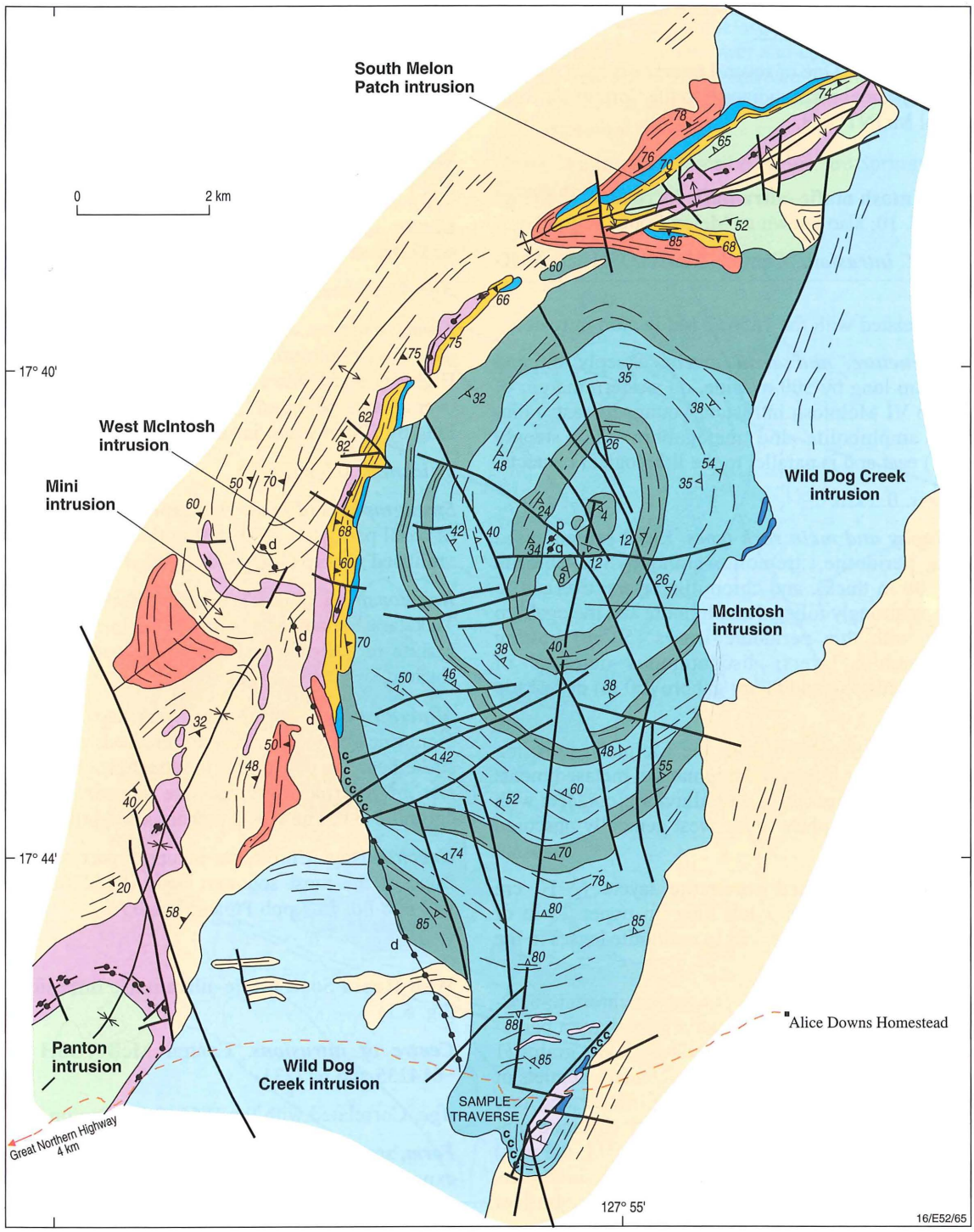
Centre of intrusion. Central McINTOSH at AMG ~685336.

Age. Correlated with the 1856±2 Ma Panton intrusion.

Form, structure, and areal extent. ultramafic lens, 600 m long by 200 m wide, forming low rounded hills on alluvium plain.

Thickness. ?0.2 km.

Stratigraphy and main rock types. Massive intensely serpentinised peridotite and dunite and, in contrast to most other group I intrusions, no gabbroic rocks or chromitites are known.



McIntosh intrusion
Group VI layered intrusion
- *Magnetite gabbro, magnetite olivine gabbro*
- *Olivine gabbro, olivine gabbronorite, troctolite*
- *Anorthosite, leucogabbro*
- *Peridotite, troctolite*

Wild Dog Creek intrusion
Group IV layered intrusion
- *Gabbro, magnetite gabbro, magnetite olivine gabbro*

Panton, Mini, West McIntosh, South Melon Patch intrusions
Group I layered intrusions
- *Anorthosite, leucogabbro*
- *Amphibolite, metagabbro, norite*
- *Gabbro, gabbronorite, norite*
- *Peridotite, serpentinised ultramafic rocks, chromitite*

Tickalara Metamorphics
- *Biotite-quartz-feldspar schist (metagranite)*
- *Metasediments, mafic and felsic meta-volcanics, tonalite, diorite*

- *Dolerite dyke, pegmatite dyke, quartz vein*
- *Chilled margin of layered intrusion*
- *Chromitite layer*
- *Strike and dip of igneous layering*
- *Strike and dip of foliation*
- *Trend of layering or foliation*
- *Sample traverse*
- *Track*

Figure 5.10. Geological map of the group I Panton (part of), Mini, West McIntosh, and South Melon Patch mafic–ultramafic intrusions, group IV Wild Dog Creek (part of) mafic intrusion, and group VI McIntosh mafic intrusion.

Relationships. Intrudes amphibolite and metasediments of Tickalara Metamorphics.

Other comments. One of several poorly exposed group I bodies on alluvial plains adjacent to the Springvale Fault in central McINTOSH.

West McIntosh mafic–ultramafic intrusion (32 in Fig. 5.1, Fig. 5. 10; also known as Melon South or Togo 5).

Centre of intrusion. Central McINTOSH at AMG ~807430.

Age. Correlated with the 1856±2 Ma Panton intrusion.

Form, structure, and areal extent. Steeply dipping sheet, 8 km long by 500 m wide, on western margin of the group VI McIntosh intrusion; youngs to east; foliation in amphibolite and metagabbro dips steeply (60–75°) east and is parallel to the lithological contacts.

Thickness. 0.5 km.

Stratigraphy and main rock types. Basal serpentinised foliated peridotite, tremolite–anthophyllite–chlorite schist (200 m thick), and chromitite layers, overlain to the east by strongly foliated amphibolite and metagabbro (200 m) with thin peridotite lenses (50 m) hosting thin chromitite layers; discontinuous outcrops of mottled anorthosite and minor gabbro (50 m) define top of intrusion.

Relationships. Separated from the McIntosh intrusion by screens of poorly exposed migmatised metasediments of Tickalara Metamorphics and alluvium; contacts with Tickalara Metamorphics to the west generally obscured by alluvium.

Mineralisation. Stacked chromitite layers (2–10 cm thick), some more than 3 km long, in upper 20 m of basal ultramafic sequence, and in peridotite lenses in the foliated mafic sequence.

Petrography. Peridotite (ocC) consists of chromite-bearing adcumulate and mesocumulate, which have a pervasive foliation defined by aligned ovoid olivine grains (1 x 2 mm) parallel to closely spaced secondary veinlets of serpentine, iddingsite, and magnetite; olivine and rare intercumulus orthopyroxene contain small chromite subhedra; chromitite consists of fine-grained (0.1–0.3 mm) disseminated chromite grains enclosing subrounded serpentinised olivine ('doughnut' texture); margins of chromite grains are irregular and embayed, owing to blades of serpentine minerals in the groundmass; fine-grained anorthosite (pC) mesocumulates contain small (<1.5 mm) aligned plagioclase (An_{62}) laths enclosed by intercumulus clinopyroxene which has been replaced by hornblende.

Geochemistry. Chromitite in upper part of ultramafic sequence contains anomalous Pt (333 and 662 ppb), Pd (79 and 488 ppb), and Au (2 and 6 ppb).

Other comments. Davies (in Gemuts 1971) described the intrusion as a faulted anorthosite–pyroxenite sill, which probably represents the basal ultramafic component of the McIntosh sill, but U–Pb zircon age dating and trace-element geochemistry indicate that the intrusions are neither cogenetic nor coeval. The West McIntosh intrusion is similar in stratigraphy, lithology, and mineralisation to the nearby comagmatic Panton and South Melon Patch intrusions.

West Panton mafic–ultramafic intrusions (36 in Fig. 5.1, Fig. 5.3)

Centre of intrusions. Central McINTOSH at AMG ~747380 and 744356.

Age. Correlated with the 1856±2 Ma Panton intrusion.

Form, structure, and areal extent. Group of small elongate mafic–ultramafic bodies midway between the Highway and Panton intrusions; outcrop is intermittent over an area of 500 m by 3.5 km; largest body is 1.2 km long by 500 m wide; intrusions young to east.

Thickness. 0.5 km.

Stratigraphy and main rock types. Most bodies consist of basal peridotite (100–300 m thick) overlain by either uralitised gabbro (150 m) or mottled anorthosite (50 m).

Relationships. Inferred to intrude metasediments of the Tickalara Metamorphics and to be intruded by foliated granite of Sally Downs supersuite; contacts commonly sheared.

Mineralisation. Chromitite layers and stringers up to 5 cm thick extend for several hundreds of metres along strike near top of ultramafic sequence; chromitites consist of alternating grain-size laminae of anhedral chromite (<0.5 mm) and serpentinised olivine.

Geochemistry. Chromitite in upper part of Ultramafic Zone of the most southern body (92522068) contains 142 ppb Pd, 75.7 ppb Pt, and 7 ppb Au.

West Robin Soak mafic–ultramafic intrusions (41 in Fig. 5.1)

Centre of intrusions. Central McINTOSH at AMG ~614235 and 627231.

Age. Correlated with the 1856±2 Ma Panton intrusion.

Form, structure, and areal extent. Several small poorly exposed northeast-trending mafic–ultramafic bodies flanking the Springvale Fault; elongate bodies occur in two parallel zones (western and eastern), 1.5–2 km apart, with individual bodies up to 800 m long and 200 m wide.

Thickness. ?100 m.

Stratigraphy and main rock types. Intrusions of western zone consist predominantly of serpentinised peridotite, those of eastern zone contain uralitised gabbro and pyroxenite.

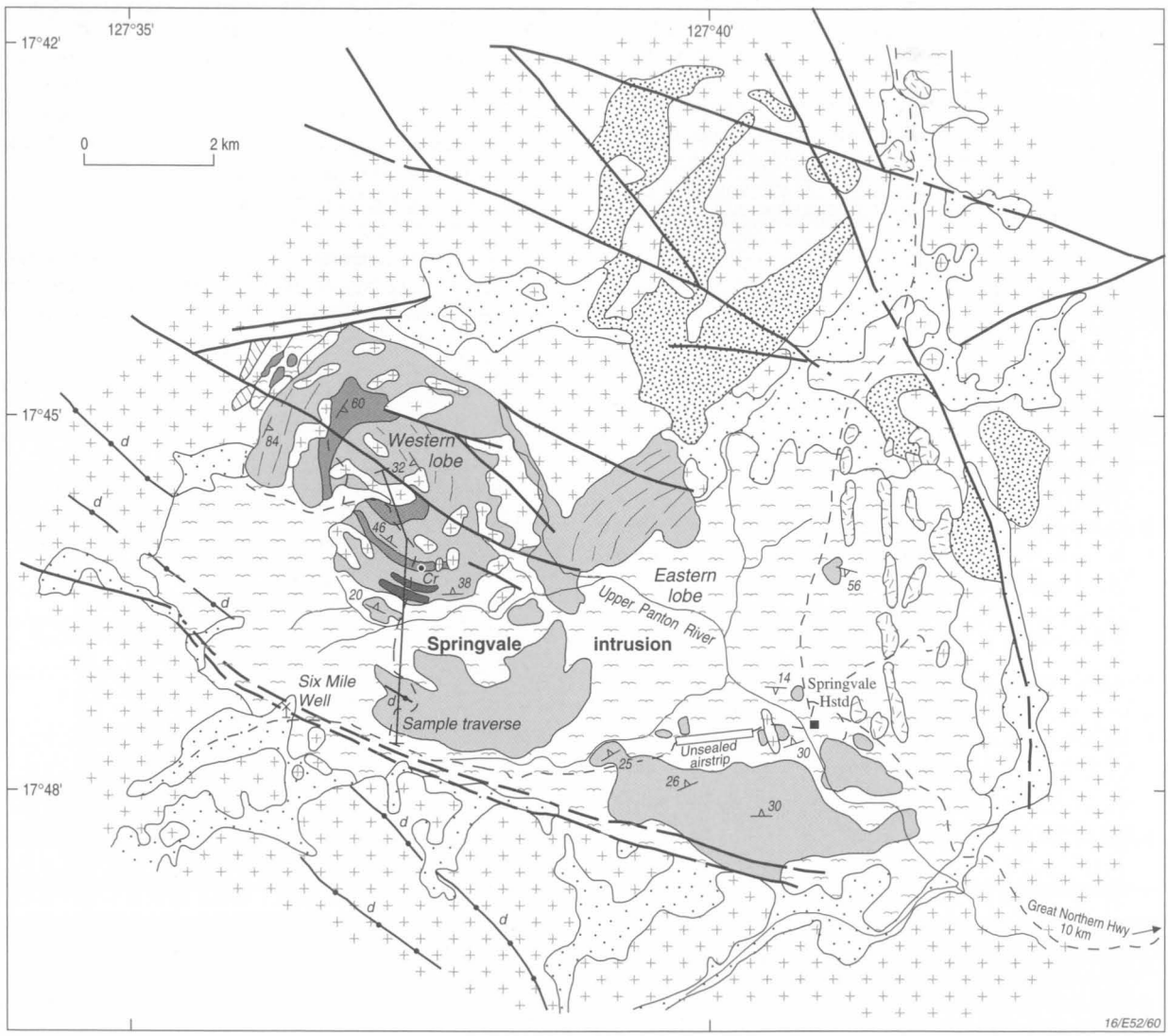
Relationships. Bodies intrude metasediments, amphibolite, mafic ?granulite, and calc-silicate rocks of the Tickalara Metamorphics; western and eastern zones separated by granitic to doleritic rocks mapped as part of the Sally Downs supersuite of the Bow River Batholith; relationship between the zones is not clear.

Mineralisation. Rare thin (1–2 cm) chromitite layers in peridotite in western zone; siliceous Ni–Cu gossans along margins of intrusions in the eastern zone.

Group II layered mafic–ultramafic intrusions

Group II layered intrusions typified by the 1857±2 Ma Springvale intrusion occur on McINTOSH and MOUNT REMARKABLE in the western zone of the HCO. They are moderately dipping sheet-like bodies, coeval with or slightly younger than adjacent granite plutons of the Paperbark supersuite. Weakly anomalous concentrations of Ni, Cu, and PGEs are reported to be associated with chromite in cyclic plagioclase-rich cumulates (troctolite and anorthosite) in the lower and upper parts of group II bodies, and the Wilagee intrusion contains one of the few chromitites in the East Kimberley hosted by a plagioclase-rich cumulate.

Group II intrusions described below are Springvale, Foal Creek, and Wilagee.



Black soil on mafic rocks
Silt, sand, gravel
Corridor gabbro
Biotite-magnetite gabbro, quartz gabbro, tonalite
Bow River Batholith
Biotite granite, biotite granodiorite, leucogranite
Springvale intrusion
Group II layered intrusion
Troctolite, leucogabbro, anorthosite, gabbro
Olivine gabbro, olivine gabbronorite, troctolite, gabbro, gabbronorite
Marboo Formation
Mudstone, siltstone, greywacke, schist, psammite
Mafic granulite
Metasomatic cordierite-spinel-sillimanite rock
Fault
Dolerite dyke
Trend of layering
Strike and dip of igneous layering
Chromite
Track

Figure 5.11. Geological map of the group II Springvale mafic intrusion.

Springvale mafic intrusion (37 in Fig. 5.1, Fig. 5.11)

Centre of intrusion. Central western McINTOSH at AMG ~570340.

Age. U–Pb age of 1857±2 Ma determined for zircon from mottled anorthosite in the upper northwestern part of intrusion (see Chapter 6).

Form, structure, and areal extent. Two partly concealed contiguous lobes (western and eastern lobes), which together extend over 6 x 13 km; prominent arcuate layering and cyclic unit trends in the western lobe appear to be cut by macrolayering trends in the eastern lobe; dip of layering in the northern part of the western lobe generally decreases inwards from 84° in the outer part to 15° in the centre of the lobe; cyclic mafic units and layering in the western lobe are locally distorted by large irregular granite bodies; the eastern lobe displays a dip reversal from shallow (30°) northward, near the southern basal contact, to variable (15–55°) southward, in the centre of the lobe.

Thickness. 2 km.

Stratigraphy and main rock types. Western lobe consists of olivine-bearing gabbroic rocks (1200 m thick) along the southern sheared basal contact, overlain to the north by a well-exposed arcuate cyclic mafic sequence of troctolite and anorthosite (80 m), olivine gabbro (220 m), troctolite (120 m), olivine gabbro, leucogabbro, and minor troctolite (380 m); massive porphyritic olivine gabbro and gabbronorite (containing large poikilitic amphibole grains replacing clinopyroxene) along the southern basal contact are overlain by weakly layered equigranular olivine gabbro and minor magnetite gabbro; cyclic mafic rock types in the upper part of the western lobe are more variable in composition than the gabbros from the lower succession; at least three major troctolite–anorthosite cyclic units are associated with minor leucogabbro, olivine gabbronorite, olivine gabbro, and norite; cyclic units have well-defined arcuate trends, which are conformable with the regional concentric structure of the lobe; Landsat thematic-mapper imagery indicates several other thin troctolite–anorthosite cyclic units in the upper part of the intrusion; gabbroic rocks in the intrusion are generally massive, but anorthosite and leucogabbro locally display well-developed rhythmic modal layering (centimetre scale) and igneous lamination; several stratigraphic levels in the western lobe contains rafts of metasedimentary rock; narrow elongate rafts are hosted by olivine gabbro and olivine gabbronorite on the southern central side of the lobe—the 30–80 m wide rafts extend for over 1 km along strike and have a slight arcuate trend, conformable with the layering in overlying troctolite–anorthosite cyclic units; rafts consist of fine-grained massive cordierite–spinel±silli-

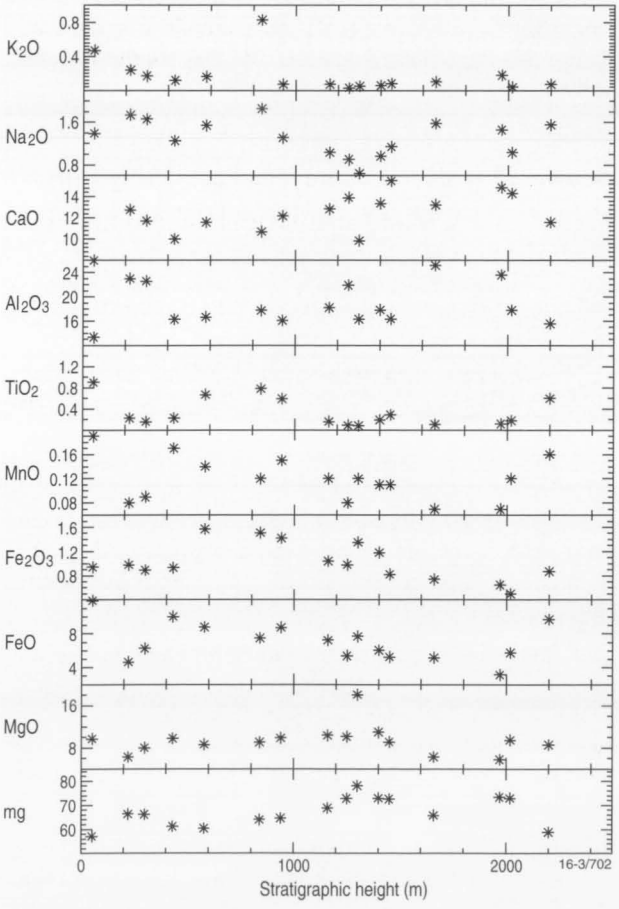


Figure 5.12. Springvale intrusion: variation in whole-rock major-element composition (in wt. %) of mafic cumulates with stratigraphic height.

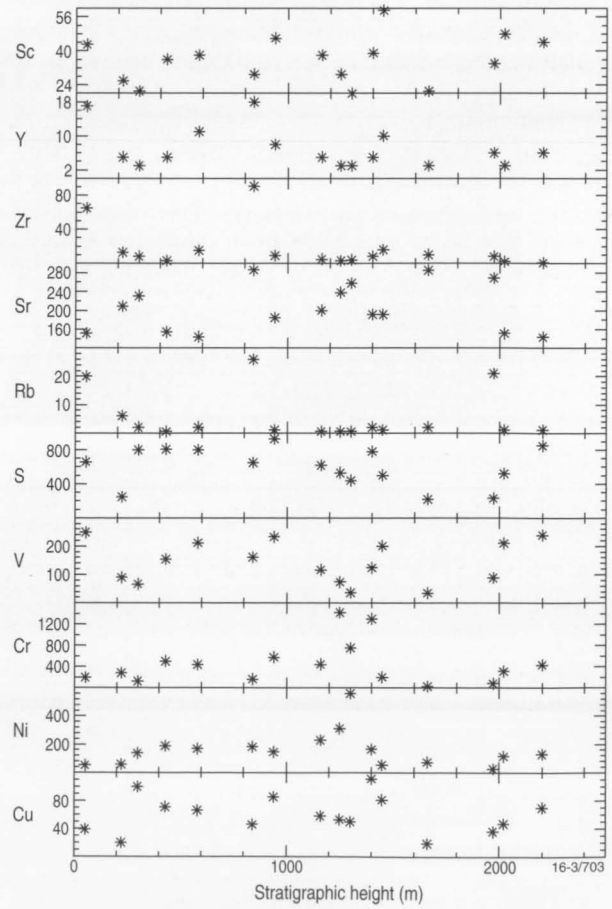


Figure 5.13. Springvale intrusion: variation in whole-rock trace-element composition (in ppm) of mafic cumulates with stratigraphic height.

manite±corundum assemblages and are recessive relative to the host gabbros; the deep purple cordierite has a well-developed conchoidal fracture and is finely spotted with disseminated spinel; rafts of mafic ?granulite hornfels, up to 300 m long, are enclosed by granite of the Paperbark supersuite on the northwestern margin of the intrusion; the ?granulites are fine grained and display tight folds in pyroxene-rich bedding laminae, so they may be recrystallised mafic sedimentary rocks.

Relationships. Intrudes and is faulted against different granite plutons of the Paperbark supersuite; western lobe is cut by large irregular bodies of leucogranite and veins of pegmatite and quartz; a major west-northwest-trending shear zone along the southern basal contact with the Airfield Granodiorite and Top Water Tonalite (both Paperbark supersuite) is marked by uralititised gabbro and intensely altered mafic rocks.

Mineralisation. Weakly mineralised iron-rich gossans (see Chapter 2) occur in the shear zone along the southern basal contact; exploration companies have reported trace amounts of disseminated chromite with up to 0.5 ppm Pt+Pd (subsequent analyses revealed lower PGE concentrations; see Chapter 2) and anomalous Ni and Cu in the lower troctolite-anorthosite cyclic unit in the upper part of the western lobe; no chromitite layers have been identified in the intrusion.

Petrography. Gabbroic rocks (poC) from the lower part of the intrusion are medium-grained equigranular adcumulates and mesocumulates containing cumulus plagioclase ($An_{53–81}$) and minor cumulus olivine; orthopyroxene containing fine exsolution lamellae of Ca-pyroxene is cumulus in olivine-free gabbros (pbC), and clinopyroxene is intercumulus in most gabbros; red-brown biotite and spatially associated magnetite–ilmenite grains increase in size and abundance up the gabbroic sequence; Fe–Ti oxides in troctolite-anorthosite cyclic units in the upper part of the intrusion are less abundant and clinopyroxene becomes more prominent as centimetre-size oikocrysts enclosing anhedral plagioclase at the expense of cumulus prismatic orthopyroxene—this imparts a mottled or spotted appearance to the plagioclase-rich rocks; trace amounts of disseminated chromite are associated with the upper troctolite–anorthosite cyclic units; small (<0.1 mm) trace amounts of irregular to subspherical blebs of chalcopyrite–pyrrhotite–pentlandite and some pyrite subhedra at grain boundaries of silicates in most rocks testify to the S-saturated character of the intrusion.

Geochemistry. Weak geochemical break near the 1200 m stratigraphic level (Fig. 5.12) defines a boundary between a lower megacyclic sequence dominated by olivine gabbro and gabbronorite ($mg_{57.6–69.3}$), and an upper, more primitive (most samples $mg_{73–78.4}$) megacyclic sequence of troctolite and olivine gabbro containing relatively low TiO_2 (<0.29%) and K_2O (<0.18%); maximum Cr concentration (1418 ppm) in olivine gabbro defines the basal part of the upper megacyclic unit (Fig. 5.13); sustained S-saturation conditions are indicated by high S abundance (generally >400 ppm), low Pt (<1.9 ppb), Pd (<4.2 ppb), and Au (<2 ppb), and the absence of any systematic trends for Cu and Ni; fluctuating trend of V reflects heterogeneous distribution of Fe–Ti oxides, owing to regular influxes of new magma; Sanders (1999) also noted a trend of more primitive composition up the succession, namely: (1) the lowest troctolite cyclic unit of the western lobe is the most evolved based on olivine compositions ($mg_{63–67}$), the presence of magnetite and ilmenite, and the absence of chromite; (2) the central troctolite unit contains more primitive olivine and some low-Cr chromites in addition to ilmenite and magnetite; and (3) the upper chromite-bearing troctolite unit contains the most primitive olivine ($mg_{74–82}$).

Other comments. The Springvale intrusion is the largest group II intrusion. Black soil plains cover about two-thirds of the intrusion, with most outcrop in the western lobe. Some of the poorly exposed fractionated biotite gabbro of the eastern lobe may not be part of the Springvale intrusion, but may belong to the younger Corridor gabbro cutting the eastern margin of the intrusion. The cordierite-bearing rafts in the western lobe are interpreted as blocks of metasomatised aluminous metasedimentary country rock that were either detached from the walls of the feeder conduit during magma emplacement or fell from the roof into the upper parts of the intrusion. The rafts may be derived from an extensive sequence of aluminous metasediments of the >1865 Ma Marboo Formation on the north side of the intrusion. The potential for accumulation of massive Ni–Cu–Co sulphides in the Springvale intrusion is downgraded, owing to the sheared nature of the southern basal contact.

Foal Creek mafic intrusion (8 in Fig. 5.1, Fig. 5.14)

Centre of intrusion. Central MOUNT REMARKABLE at AMG ~645894.

Age. Correlated with the 1857±2 Ma Springvale intrusion.

Form, structure, and areal extent. Differentiated mafic sheet, 1 km wide by 2.2 km long, that strikes northeast and youngs to the southeast.

Thickness. ?1 km.

Stratigraphy and main rock types. Massive to rarely layered gabbro, olivine gabbro, and coarse-grained amphibole-bearing melagabbro, overlain by massive troctolite, leucogabbro, and anorthosite.

Relationships. Located at contact between granitic rocks of the Survey Creek Monzogranite (Paperbark supersuite) and biotite gabbro of the Greenvale Fault intrusion; mafic–felsic net-vein complexes occur near the eastern contact of the Foal Creek intrusion with the granites.

Petrography. Gabbro (paC) mesocumulates contain large (up to 8 mm) subhedral clinopyroxene grains, uralitised to actinolite/tremolite, hornblende, and chlorite, and intensely sericitised and chloritised plagioclase (An_{60}); troctolite (poC) orthocumulates consist of cumulus plagioclase (An_{58}) and olivine, and intercumulus clinopyroxene, inverted pigeonite, and biotite; coronas

of orthopyroxene rims fringed by radial intergrowths of green spinel and Ca-clinopyroxene or ?amphibole occur at contacts between olivine and plagioclase grains; inverted pigeonite grains, which typically contain two generations of exsolved Ca-clinopyroxene lamellae at high angles to each other, indicate slow crystallisation conditions in a fairly evolved magma.

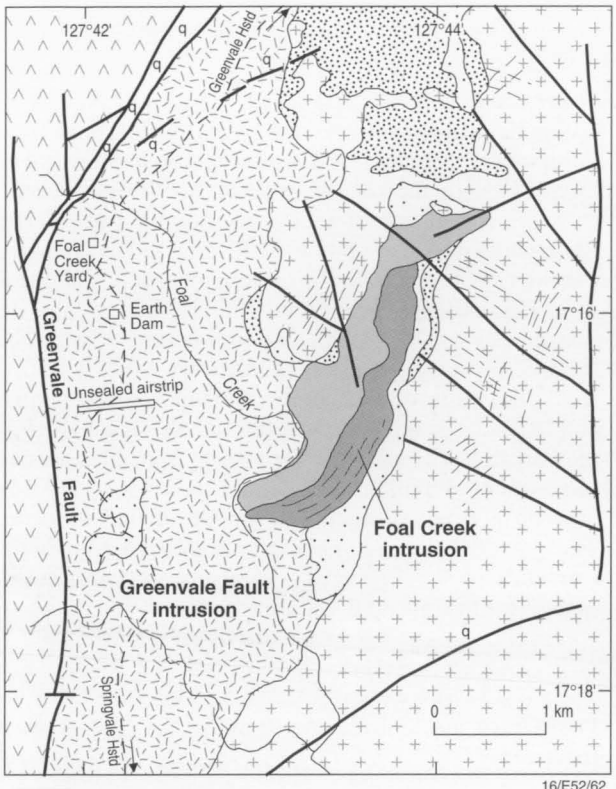


Figure 5.14. Geological map of the group II Foal Creek mafic intrusion and the Greenvale Fault mafic intrusion (Corridor gabbro).

Wilagee mafic–ultramafic intrusion (24 in Fig. 5.1, Fig. 5.15)

Centre of intrusion. Northwestern McINTOSH at AMG ~622545.

Age. Correlated with the 1857±2 Ma Springvale intrusion.

Form, structure, and areal extent. Arcuate body, 10 km long by 2 km wide, on the southeastern side of the group III Toby intrusion; divided into southern and northern parts by northeasterly trending fault; southern part strikes northeast and appears to dip steeply and young towards the southeast, i.e. opposite to that of the Toby intrusion; attitude of northern part is unknown.

Thickness. 1.3 km.

Stratigraphy and main rock types. Southern part contains two differentiated mafic–ultramafic megacycles, each comprising discontinuous basal units, 20–50 m thick, of serpentinised plagioclase peridotite overlain to southeast by 50–500 m units of olivine gabbro, troctolite, anorthosite, and leucogabbro; primitive cumulates near the base of each megacycle indicate open fractionation systems, involving magma pulses with olivine and plagioclase on the liquidus; northern part consists of a homogeneous sequence of troctolite and olivine gabbro similar to the upper parts of megacycles in the southern part.

Relationships. Southern part is faulted against Paperbark Granite of the Paperbark supersuite to the east and fine-grained gabbros of the Toby intrusion to the west, and northern part intrudes and forms chilled margins and net-vein complexes with different granites of the Paperbark supersuite.

Mineralisation. Chromitite lens (see Chapter 2), 15–20 cm thick, in pegmatitic troctolite near middle of lower megacycle in southern part.

Petrography. Peridotite (opC) mesocumulates contain cumulus olivine and minor cumulus plagioclase (An_{58}) grains enclosed by centimetre-sized oikocrysts of orthopyroxene; olivine forms rounded and embayed anhedra with curvilinear contacts with orthopyroxene, indicating that some of the orthopyroxene was derived from the reaction of olivine with a SiO_2-saturated (basaltic) melt; trace minerals include clinopyroxene, green spinel, chromite, ilmenite, magnetite, pentlandite, chalcopyrite, and pyrrhotite; troctolite (oC, opC) mesocumulates from higher in the sequence have cumulus olivine, cumulus or intercumulus plagioclase, and minor intercumulus orthopyroxene; disseminated chromite subhedra occur in olivine or at contacts between olivine and plagioclase; in contrast to the peridotites, olivine is euhedral to subhedral and has very thin coronas of finely intergrown amphibole and spinel (see Chapter 9); gabbro is intensely uralitised, chloritised, sericitised, and in places contains coarse-grained blue-green tourmaline; chromitite in troctolite contain small (<0.5 mm) dark brown to black chromite euhedra that enclose serpentinised cumulus olivine grains and sericitised plagioclase laths.

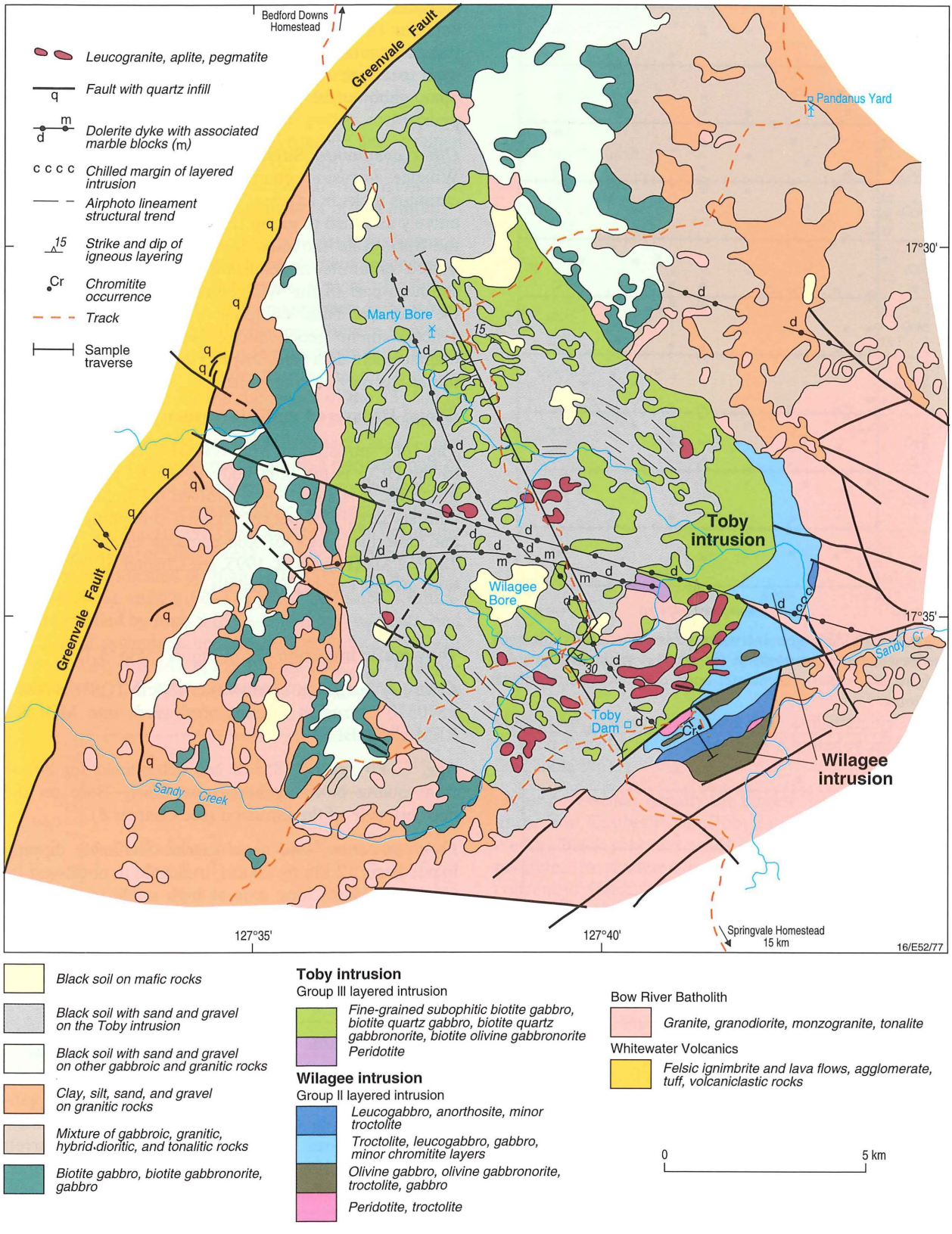


Figure 5.15. Geological map of the group II Wilagee mafic–ultramafic intrusion and group III Toby mafic intrusion.

Geochemistry. Lower megacyclic unit (also includes chilled sample 92522533 from northern part of intrusion, but excludes basal peridotite unit: Fig. 5.15) consists of fractionated chilled biotite gabbro ($mg_{56.4}$) at the basal contact and steady fractionation upwards through primitive troctolite ($mg_{77.2–81.4}$) and olivine gabbro ($mg_{74.3–78.8}$) (Fig. 5.16); decreasing mg values and increasing abundances of TiO_2 and incompatible elements Y, Zr, V, and Sc (Fig. 5.17) up the sequence are consistent with closed fractionation of a single megacyclic unit;

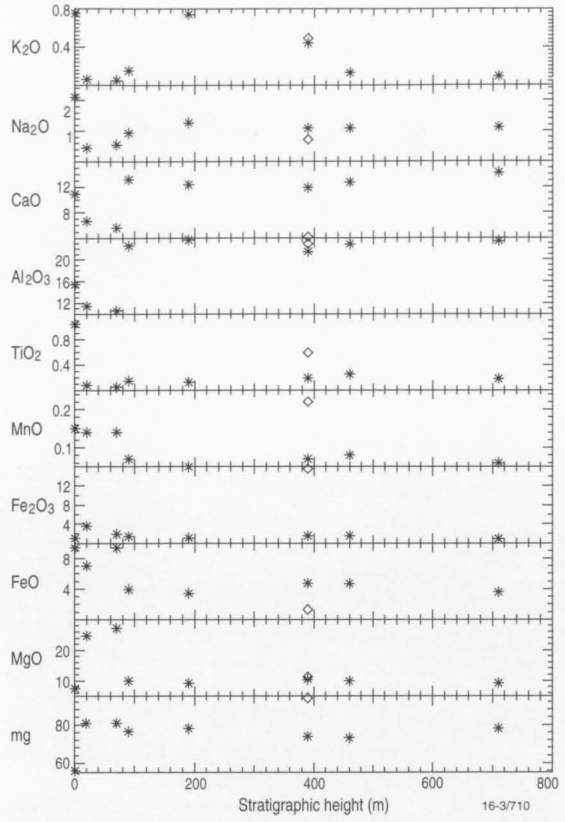


Figure 5.16. Wilagee intrusion: variation in whole-rock major-element composition (in wt. %) with stratigraphic height. Star—mafic cumulate; open diamond—chromitite in troctolite.

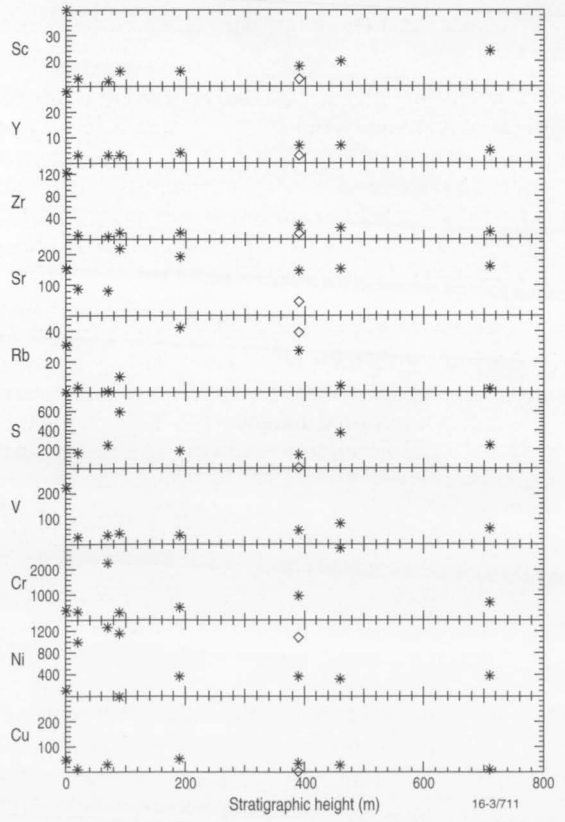


Figure 5.17. Wilagee intrusion: variation in whole-rock trace-element composition (in ppm) with stratigraphic height. Symbols as in Figure 5.16.

chromitite in troctolite at the 390 m stratigraphic level contains 148 ppb Pd, 57.4 ppb Pt, and 1 ppb Au; Cr-rich parent magma is indicated by anomalous Cr contents for most rock types (leucogabbro 2843 ppm, troctolite 2256 ppm, gabbro 959 ppm, and olivine gabbronorite 716 ppm).

Other comments. Strongly differentiated cumulates in Wilagee intrusion contrast with homogeneous non-cumulus rocks in adjacent Toby intrusion. Although tentatively assigned to group II on the basis of similarity to the Springvale intrusion in rock types and troctolite-hosted chromite mineralisation (see Chapter 6), the southern part of the Wilagee intrusion could represent the primitive basal component of the Toby intrusion. Trace-element geochemical, isotopic, and depth of emplacement data (see Chapters 9 & 11) suggest the two intrusions may be comagmatic.

Group III layered mafic intrusion

The Toby intrusion on McINTOSH in the western zone of the HCO is the only body in the HCO assigned to group III. It is a high-level evolved mafic intrusion that consists largely of poorly exposed subophitic gabbroic and doleritic rocks of non-cumulus origin. Dated at 1855±2 Ma (Page et al. 1995, see Chapter 6), it is coeval with groups I and II intrusions.

Toby mafic intrusion (22 in Fig. 5.1, Fig. 5.15)

Centre of intrusion. Northwestern McINTOSH at AMG ~570570 (intrusion extends northwards into MOUNT REMARKABLE).

Age. U–Pb age of 1855±2 Ma determined for zircon from quartz–biotite gabbro near Marty Bore on the northern side of the intrusion (see Chapter 6).

Form, structure, and areal extent. Shallowly dipping lobate basin,12 km by 20 km, truncated in northwest by Greenvale Fault; long axis at high angle to dominant north-northeast structural trend of the HCO; rare compositional layering generally dips inwards towards the centre of the body at 10–20° (e.g. near Marty Bore), although dips locally increase to 40° on the southern side of the intrusion.

Thickness. ?2 km.

Main rock types. Fine-grained (<1.5 mm) quartz–biotite gabbro, biotite gabbro, biotite gabbronorite, olivine gabbronorite, and doleritic gabbro with subophitic to intergranular textures of non-cumulus origin; Barrett (Geopeko Ltd 1986–1990) identified minor troctolite, pyroxenite, gabbro, and olivine norite interlayered with the non-cumulus gabbroic rocks near the centre of the intrusion; serpentinised ultramafic rocks crop out along prominent faults near the centre of the intrusion.

Relationships. Enclosed by granite plutons of Paperbark supersuite, mixed granite–gabbro, and the group II Wilagee mafic–ultramafic intrusion on its southeastern margin; spectacular magma mingling relationships with granite on southern contact indicate intrusion is probably younger than adjacent granite.

Petrography. Fine-grained gabbro contains an unusually large number of minerals, e.g. plagioclase, clinopyroxene, orthopyroxene, inverted pigeonite, olivine, biotite, quartz, alkali feldspar, apatite, zircon, ilmenite, magnetite, and sulphides; plagioclase forms randomly orientated tabular laths (1.5 x 0.2 mm) partly enclosed by uralitised clinopyroxene, orthopyroxene, and strained quartz; rare olivine is small (<0.5 mm) and rounded; magnetite–ilmenite forms anhedral inclusions in clinopyroxene and in decussate mats of brown biotite.

Geochemistry. One of the most fractionated mafic intrusions in the HCO; major and trace-element geochemical profiles show subtle to flat trends, typical of a broad shallowly dipping body of homogeneous composition (Figs 5.18, 5.19); mg initially decreases up the sequence from $mg_{56.6}$ to $mg_{51.8}$, until it is reset to more primitive values ($mg_{57.7}$) at the ~5200 m traverse height, and then it remains fairly flat for the remainder of the 13 500 m long traverse; geochemical break at ~5200 m coincides with two major west-northwest-trending faults—this implies that the slightly more primitive northern half of the intrusion may be thrown up relative to the southern half; Al_2O_3, TiO_2, incompatible trace elements Y and Zr, and mineral compositions (see Chapter 9) also define the geochemical–structural break; evolved character of intrusion is indicated by high TiO_2 (0.99–1.43%), P_2O_5 (0.12–0.27%), and Zr (90–141 ppm); sustained S saturation is implied by high S (830–1050 ppm) contents, and the lack of systematic enrichment trends by Cu (50–72 ppm) and Ni (61–141 ppm); olivine (mg_{52-63}), clinopyroxene (mg_{65-73}), orthopyroxene (mg_{49-74}), and plagioclase (An_{45-86}) compositions are considerably more evolved than for most other East Kimberley intrusions (see Table 9.6).

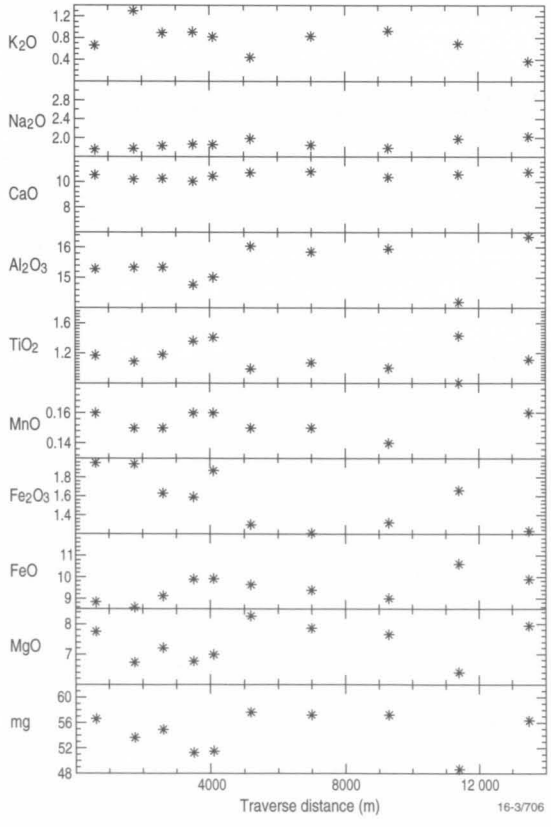


Figure 5.18. Toby intrusion: variation in whole-rock major-element composition (in wt. %) of mafic rocks with traverse distance.

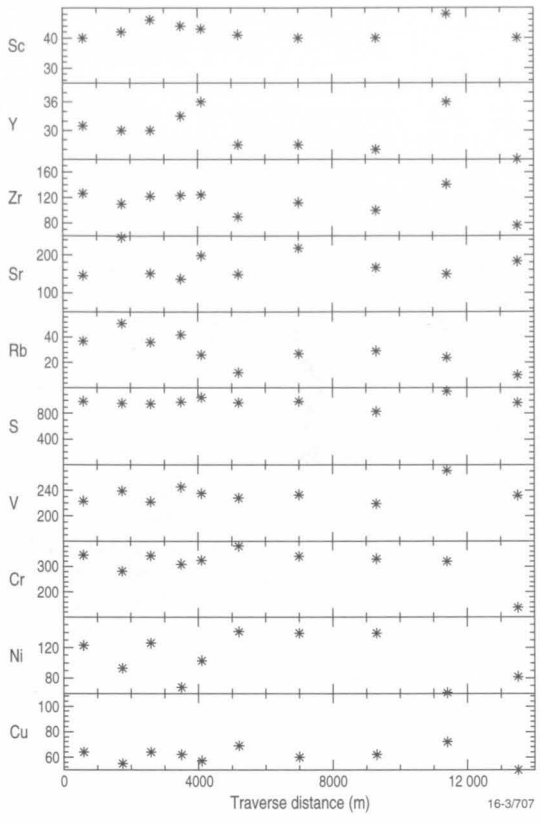


Figure 5.19. Toby intrusion: variation in whole-rock trace-element composition (in ppm) of mafic rocks with traverse distance.

Other comments. Areally the largest 'layered' intrusion in the East Kimberley, the Toby intrusion is largely covered by black clay and sandy soils, with most exposure restricted to scattered recessive outcrops. Large-scale concentric lineaments parallel to the margins of the intrusion are evident on aerial photographs, aeromagnetics, and Landsat Thematic Mapper images, but are rarely obvious on the ground. Bodies of leucogranite in the southeast are generally subparallel to the lineaments, whereas ubiquitous dolerite dykes, infilling faults, cut the lineaments. The subophitic gabbros contain variable, but minor disseminated magnetite, which may explain the concentric structures evident on aeromagnetic images. Alternatively, they may be concentric ring fractures formed during subsidence or partial collapse of the upper part of the intrusion, owing to withdrawal of magma. This process may be similar that responsible for the arcuate structures developed during the downsagging of volcanic calderas (Branney 1995). Blocks of recrystallised carbonate rock that persist for several hundred metres along west-northwest-trending faults crossing the centre of the intrusion may represent country rock material fallen from the roof of the intrusion during the collapse. The fractionated and fine-grained character of the gabbro suggests that the Toby intrusion is a highly evolved body that was emplaced into the upper crust at a shallow depth (~8 km: see Chapter 9).

Group IV Wild Dog Creek mafic intrusions

The group IV Wild Dog Creek intrusions are large homogeneous sheet-like gabbroic bodies spatially associated with groups I and VI intrusions on McINTOSH in the central zone of the HCO. No Wild Dog Creek intrusions have been dated, but one intrudes the 1856 Ma Panton intrusion, another is cut by the 1830 Ma McIntosh intrusion, and another is chilled against felsic volcanics of the 1843 Ma Koongie Park Formation, indicating that the Wild Dog Creek intrusions were probably emplaced between 1843 and 1830 Ma.

Compositional rhythmic layering was not observed in the Wild Dog Creek intrusions, but the gabbroic rocks locally have a strong 'layered' appearance, owing to a primary igneous lamination, defined by crystallographic alignment of tabular plagioclase laths. This lamination is commonly subparallel to a metamorphic fabric of aligned amphibole and biotite porphyroblasts. For this reason, the Wild Dog Creek intrusions have been included in the classification of the East Kimberley layered intrusions.

A large Wild Dog Creek body east of the Panton intrusion (40 in Fig. 5.1, Figs 5.2A, 5.10) is exposed as isolated clusters of small rounded black boulders on low hills and black soil plains with shallowly incised creeks containing abundant detrital Fe–Ti oxide grains. The abundance of heavy minerals testifies to the highly fractionated composition of the mafic rocks. The most common rock types are biotite–magnetite gabbro and magnetite quartz gabbronorite that contain anhedral plates (2–5 mm) of red-brown biotite sieved with inclusions of anhedral plagioclase and opaque grains, subaligned sodic plagioclase laths, granular titaniferous augite, orthopyroxene, titaniferous magnetite moulded around augite, deformed interstitial quartz, and accessory apatite. Associated rocks include biotite diorite, biotite tonalite, and hybrid variants. A metamorphic fabric is commonly defined by prominent amphibole porphyroblasts (up to 5 cm) aligned sub-parallel to a primary igneous lamination of aligned plagioclase laths. With the exception of the Fe–Ti oxide content, the gabbroic rocks appear to be uniform in composition, which may indicate that this particular gabbroic sheet is gently dipping to subhorizontal. A magnetite quartz gabbronorite sample (92522437) has a fractionated composition (mg51, 1.44% Na_2O, 1.45% TiO_2, 0.18% P_2O_5, 89 ppm Zr, 36 ppm Y) and high S content (1170 ppm) typical of group IV intrusions.

The large homogeneous Wild Dog Creek body (Fig. 5.10) northeast of the McIntosh intrusion is regarded as the northeast extension of the large mafic body east of the Panton intrusion. This is supported by the similarity of rock types and both areas have comparable Landsat Thematic Mapper signatures. Partly uralitised gabbro in this northeastern body has a weak primary igneous lamination, comprising large (3–4 mm) subaligned plagioclase (An_{52}) laths and smaller aggregates of clinopyroxene rimmed by hornblende. Fine-grained subophitic intergranular and equigranular types are also present. Compositionally, they range from evolved magnetite gabbro ($mg_{57.1}$, 2.46% Na_2O, 1.19% TiO_2, 0.21% P_2O_5, 49 ppm Zr, 16 ppm Y) to more primitive olivine gabbronorite ($mg_{74.8}$, 1.59% Na_2O, 0.24% TiO_2, 0.02% P_2O_5, 12 ppm Zr); high S (360–920 ppm) associated with low Pd (2.5 ppb), Pt (2.3 ppb), and Au (1 ppb) concentrations indicate S-saturated magmas.

Other intrusions of group IV include thin mafic sheets intercalated with volcanic rocks south of the group I Big Ben intrusion and northwest of the group VI Armanda intrusion (Fig. 5.35). Chilled magnetite quartz gabbro from the margin of one of the latter bodies has similar Na_2O (2%), TiO_2 (1.27%), P_2O_5 (0.12%), and Zr (38 ppm) contents to the fractionated magnetite gabbros from the Wild Dog Creek bodies further north. Generally, the Wild Dog Creek intrusions are believed to have little potential for base-metal or precious-metal mineralisation because of their lack of compositional layering, high degree of fractionation, and thin sheet-like shapes.

Group V layered mafic–ultramafic intrusions

Group V layered mafic–ultramafic intrusions, of which the 1844±3 Ma Sally Malay intrusion is the type example, occur on southern TURKEY CREEK and MOUNT REMARKABLE and northern McINTOSH, in the central zone of the HCO. These differentiated intrusions typically form elongate to ovoid mafic bodies emplaced in paramigmatite and mafic granulite of the Tickalara Metamorphics after the main peak of high-grade metamorphism at about 1850 Ma. Ultramafic lithologies form a minor component in the lower parts of the thicker intrusions. Group V intrusions have generated considerable exploration interest for massive and disseminated Ni–Cu–Co sulphides near the basal contacts of peridotite–troctolite–gabbro–anorthosite cycles and in feeder conduits (Sally Malay), and in homogeneous olivine gabbroic sequences (Corkwood, Keller Creek). Ilmenite and titaniferous magnetite lenses characterise the upper parts of more evolved gabbroic bodies (Frog Hollow, Mabel Downs Southwest). The sulphide-rich nature and pervasive faulting of group V intrusions also indicate potential for hydrothermally remobilised mineralisation (see Chapter 14).

Group V intrusions described below are Sally Malay, Corkwood, Dave Hill, Fletcher Creek, Frog Hollow, Keller Creek, Mabel Down Homestead, Mabel Downs Southwest, McKenzie Spring, Oxide, Spring Creek, Three Nuns, and Wilson Creek.

Sally Malay mafic–ultramafic intrusion (12 in Fig. 5.1, Fig. 5.20)

Centre of intrusion. Southwestern TURKEY CREEK at AMG ~962820.

Age. U–Pb ages of 1844±3 Ma and 1846±5 Ma determined for zircon and baddeleyite, respectively, from mottled anorthosite in the upper part of megacycle I of subchamber A (Fig. 5.20; see Chapter 6).

Form, structure, and areal extent. Multi-chambered body, 1.5 km by 3 km; comprising four subchambers (A–D) separated from each other by screens of paramigmatite of the Tickalara Metamorphics; sub-

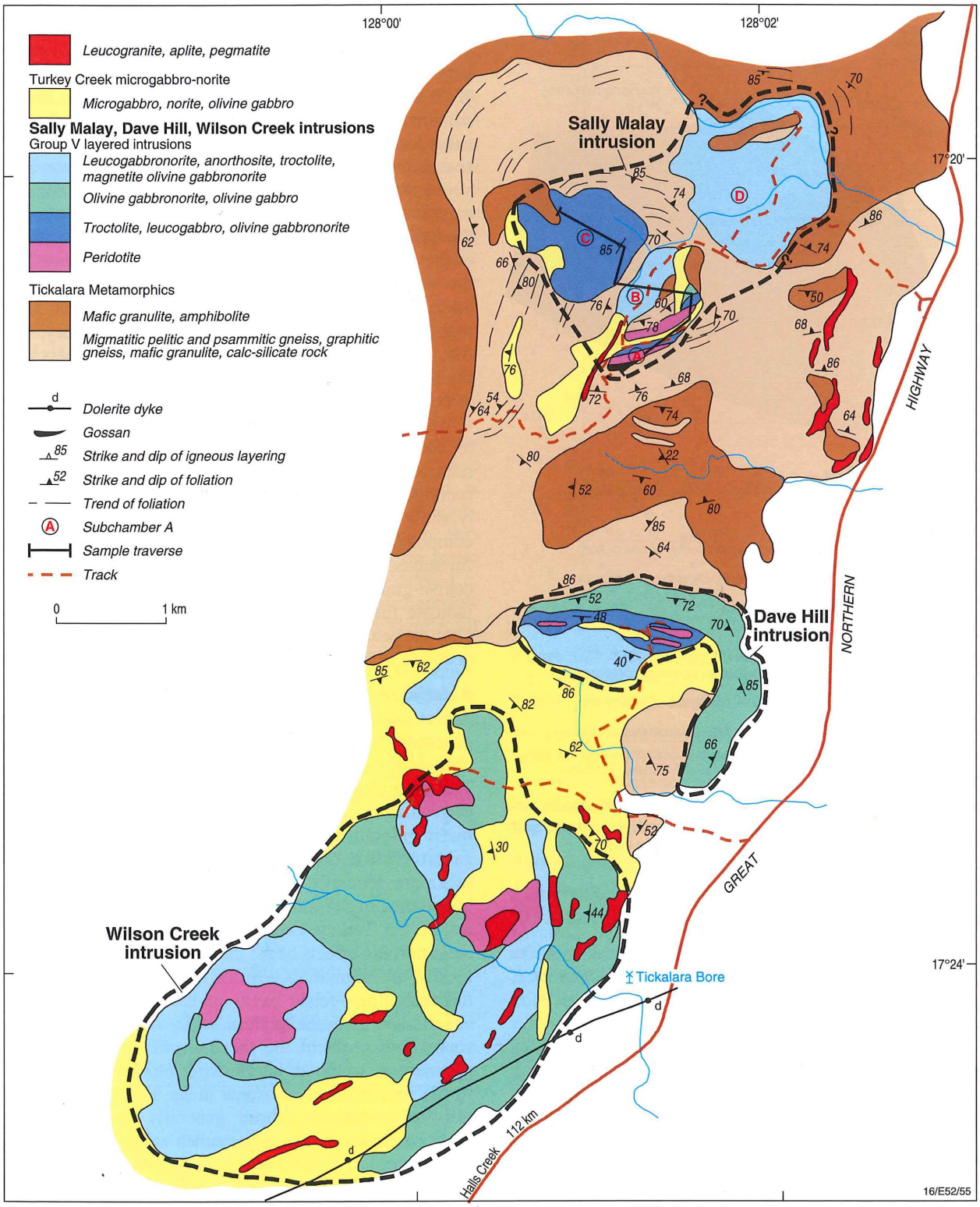


Figure 5.20. Geological map of the group V Sally Malay, Dave Hill, and Wilson Creek mafic–ultramafic intrusions and the Turkey-Creek microgabbro-norite rock unit.

chambers may have been emplaced at slightly different levels in the crust and connected by a network of feeder conduits; each subchamber had open fractionation systems, involving regular pulses of magma; layering is most prominent in plagioclase-rich rocks in the upper parts of each subchamber; Thornett (1981) described rhythmically layered troctolite with alternating olivine- and plagioclase-rich layers, 0.5–1 cm thick; gabbroic rocks show an igneous lamination of aligned plagioclase laths; dips of layers and laminations range between subvertical and moderate to the northwest, and, together with gross compositional trends, indicate that the intrusion youngs to the northwest; intrusive rocks generally

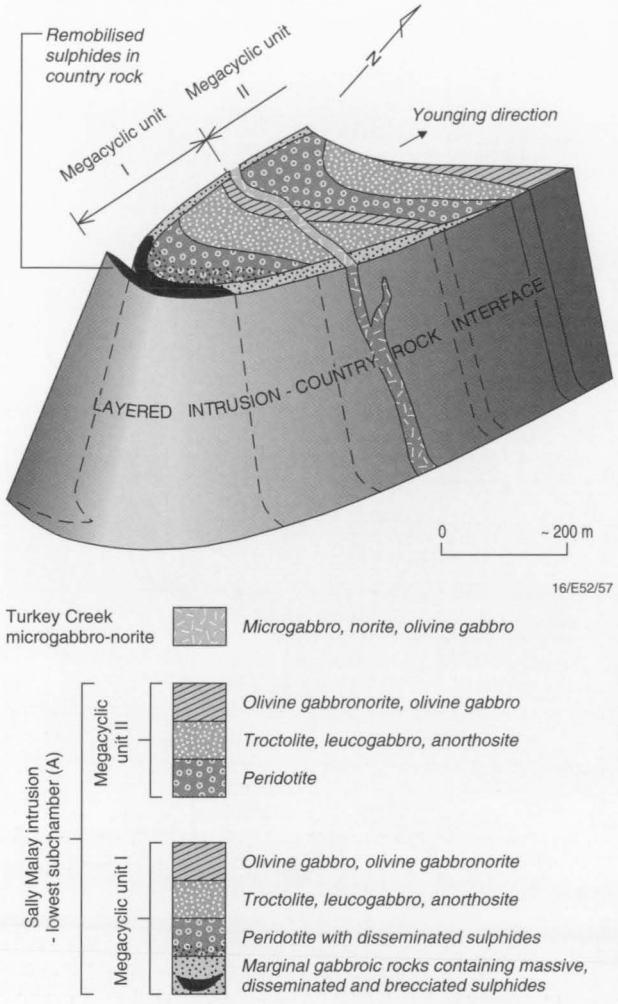


Figure 5.21. Schematic diagram of megacyclic units and different mineralisation styles in subchamber A of the Sally Malay intrusion (modified after Thornett 1981).

form recessive units in the valleys, whereas country rock migmatite and granulite form steep-sided conical hills.

Thickness. 1.7 km, comprising subchamber A (~500 m thick), subchamber B (~150 m thick), subchamber C (~800 m thick), and subchamber D (at least ~250 m thick).

Stratigraphy and main rock types. Subchamber A contains the most primitive and economically important rocks in the intrusion; it is a northeast-trending gently arcuate body, 400 m wide by 1200 m long, and is interpreted to be a feeder conduit to the other more evolved and ovoidal subchambers of the intrusion (Hoatson et al. 1997); it contains two differentiated megacyclic units (I and II: Fig. 5.21) of serpentinised peridotite and minor gabbroic rocks at the base, followed by mottled troctolite and anorthosite and, at top, various olivine-bearing gabbroic rocks; fractionated basal gabbroic rocks between the peridotites of megacycle I and the paramigmatite country rocks host the massive Ni–Cu–Co sulphide mineralisation (see *Mineralisation*); subchamber B is an elongate mafic body, 250 m wide, of olivine-free leucogabbro and anorthosite along the main access track between subchambers A and C; subchamber C is a lobate body, 1200 m wide, 1 km northwest of subchamber A, containing interlayered troctolite and olivine gabbronorite similar to those in the upper part of subchamber A; subchamber D is a poorly exposed lobate body, 1500 m wide, 2 km northeast of subchamber A, which contains olivine-free leucogabbro and anorthosite, and ridge-forming uralitised magnetite gabbronorite; recessive rocks of subchamber D were previously shown as a younger norite suite by Thornett (1981), but are considered in this study to be the most evolved component of the Sally Malay intrusion; plagioclase-rich compositions of the gabbros in subchambers B and D are indicated by the widespread sericitisation and kaolinisation alteration, which show as patchy white tones on aerial photographs and Landsat Thematic Mapper imagery; the overlap of common rock types in the subchambers and the shapes of the subchambers suggest that subchamber A could be a feeder to the olivine-bearing subchamber C, and the olivine-free subchamber B could be a feeder to the olivine-free subchamber D—indicating that the relative age of subchambers is A (oldest), C, B, and D (youngest); most rock types in the subchambers generally show well-preserved primary cumulus textures, rare compositional layering, and no obvious overprinting foliations, in addition, sulphides in subchamber A are coarse-grained and not recrystallised; all these features indicate that the Sally Malay intrusion was emplaced after the peak of high-grade regional metamorphism that occurred at about 1850 Ma.

Relationships. Intrudes largely granulite facies garnet–cordierite–biotite–alkali feldspar–plagioclase–quartz±sillimanite±graphite paramigmatite, mafic granulite, and minor retrogressive schist and carbonate of the Tickalara Metamorphics; migmatites were probably derived from sub-aluminous pelites and psammites and mafic granulites may represent conformable doleritic or gabbroic sills; metamorphic foliations in the country rocks are generally at a high to moderate angle to the boundaries of the intrusion; the intrusion is cut by bodies of the Turkey Creek microgabbro–norite; contact metamorphic effects of the intrusion are weak, although, locally, the migmatites near the intrusion underwent partial remelting—felsic bands of the migmatite become chaotic and coalesce to form swirly remobilised leucosomes that crosscut the metamorphic banding of the migmatites; irregular interlocking blocks are enclosed by the remobilised leucosome melts; blocky (agmatitic) raft-type migmatite fabrics generally merge into the more consistent banded migmatites within a few metres of the contact; basal units of intrusion are cut by net-veins rich in sodic plagioclase, orthopyroxene, phlogopite, and quartz, which represent fractures infiltrated by felsic magma formed from remelting of country rock migmatites; partially melted stoped migmatite fragments containing cordierite–plagioclase–hercynite–sillimanite, and resorbed garnet and cordierite xenocrysts are common in the basal mineralised rocks; no chilled margins of the intrusion have been found; results of two-pyroxene thermometry in the mafic rocks and reaction coronas in contact paramigmatites indicate that emplacement followed the peak of regional metamorphism (Thornett 1981).

Mineralisation. Contains the largest Ni–Cu–Co sulphide resource in the East Kimberley with an indicated and inferred resource of 3.85 Mt @ 1.79% Ni, 0.73% Cu, and 0.10% Co (see Chapter 2; Shedden & Barnes 1996); basal sulphide mineralisation is defined at the surface by a 300 x 20 m limonite–goethite gossan with oxidation extending to about 30 m depth; primary mineralisation (Thornett 1981, Shedden & Barnes 1996) consists of two steeply dipping massive sulphide lenses, which have an overall keel shape at the base of the intrusion; in places, low-angle faults offset the lenses or duplicate them vertically and, at the western end of the deposit, the two lenses partially merge; thickness of the ore horizon is 3–40 m; most sulphides are hosted by gabbroic rocks, 5–40 m thick, along the basal contact; these rocks consist largely of microgabbro and norite, which pass upward into peridotite, harzburgite, and lherzolite, which have closely packed olivine grains; the main zone of mineralisation typically consists of interstitial sulphides interspersed with barren zones and sporadically developed massive and matrix sulphides; massive pyrrhotite–chalcopyrite–pentlandite mineralisation is enveloped by subordinate stringer and matrix chalcopyrite–pyrrhotite–pentlandite mineralisation, which persists into the lower parts of the peridotite units; the grade of the massive sulphides is 2–2.7% Ni, 0.5–1.5% Cu, and 0.1–0.2% Co, whereas the grade of the stringer sulphide is 0.5–2% Ni, 2.5% Cu, and <0.1% Co; significant sulphides also occur in offset sulphide breccia zones in the migmatites, which are interpreted to represent fault-remobilised contact sulphides; sulphides from higher in the intrusion are restricted to very sparse disseminations, interstitial to olivine and thin veinlets; four major textural types of sulphide (massive basal, matrix and disseminated, breccia matrix, and remobilised) in the intrusion are described in Chapter 14.

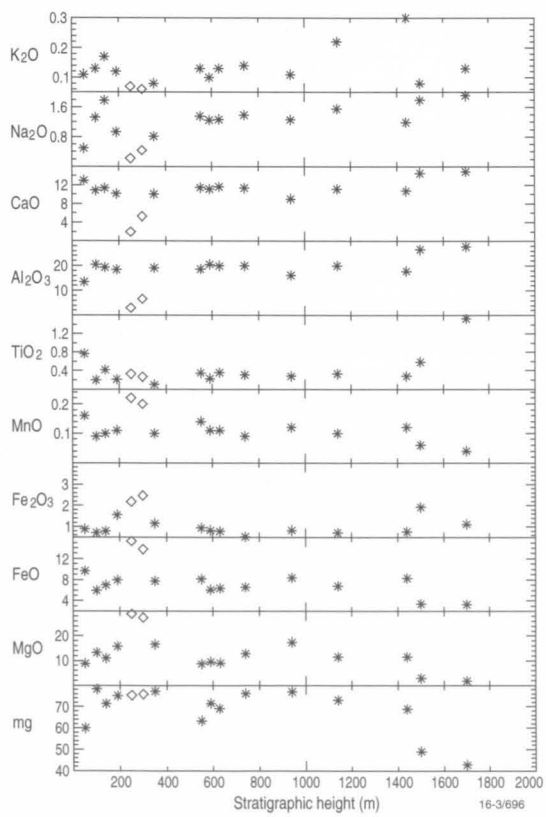


Figure 5.22. Sally Malay intrusion: variation in whole-rock major-element composition (in wt. %) with stratigraphic height. Open diamond—ultramafic cumulate; star—mafic cumulate.

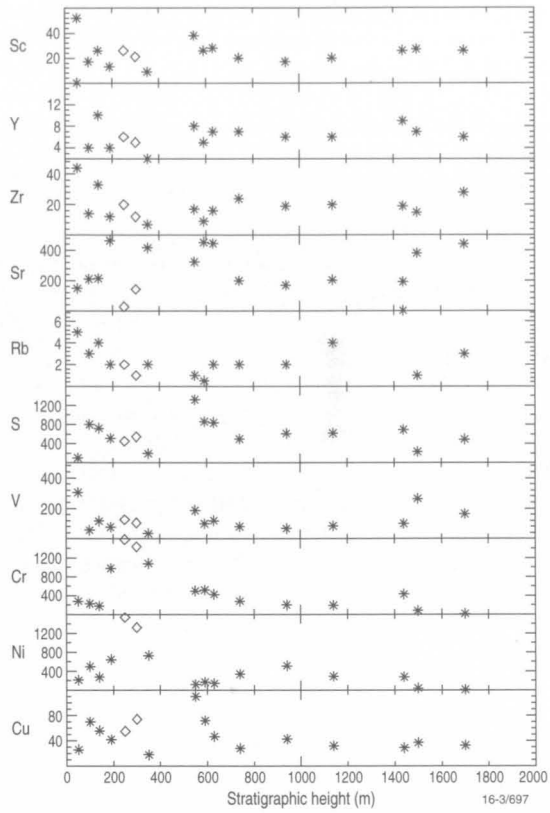


Figure 5.23. Sally Malay intrusion: variation in whole-rock trace-element composition (in ppm) with stratigraphic height. Symbols as in Figure 5.22.

Petrography. Basal contact rocks are fine grained (<0.5 mm) equigranular gabbro, gabbronorite and norite, containing plagioclase, clinopyroxene, orthopyroxene, inverted pigeonite, phlogopite or biotite, microcline, olivine, quartz, magnetite, ilmenite, sulphides, and apatite; Thornett (1981) described these rocks from drill core as ophitic in texture (plagioclase ($An_{49–72}$) laths enveloped by pyroxene anhedra), and grading upwards into mafic rocks having euhedral prismatic orthopyroxene and poikilitic reverse-zoned plagioclase ($An_{60–75}$); resorbed garnet and cordierite xenocrysts and plagioclase–sillimanite–spinel–cordierite xenoliths also occur in the basal gabbros; overlying these are medium-grained (2–3 mm) peridotite (oC) mesocumulates and orthocumulates with plagioclase ($An_{71–82}$), amphibole-replaced clinopyroxene, and orthopyroxene intercumulus to equant olivine grains, which contain chromite inclusions; higher in the sequence, medium-grained troctolite (poC) contains cumulus calcic plagioclase and olivine, intercumulus orthopyroxene, red-brown biotite, magnetite, and ilmenite; olivine–plagioclase grain contacts are embayed and scalloped with well-developed orthopyroxene–amphibole–spinel coronas (see Chapter 9); gabbro (paoC, pabC) is mineralogically similar to the troctolite except that uralitised clinopyroxene and orthopyroxene may be cumulus or intercumulus and

coarse dark-green spinel anhedra are locally prominent; in the more fractionated gabbroic rocks, minor disseminated magnetite–ilmenite is moulded around cumulus clinopyroxene and cumulus orthopyroxene; sulphides in the upper level mafic rocks occur as irregular blebs of pyrrhotite–pentlandite and/or chalcopyrite at grain boundaries of silicates, indicating that S-saturated conditions prevailed throughout the intrusion.

Geochemistry. Distinctive fractionation trends in the subchambers and chemical reversals (Figs 5.22, 5.23) between the subchambers favour open system mechanisms involving progressive influxes of slightly more fractionated mafic magma; with the exception of gabbroic rocks along the basal contact (most fractionated rocks in subchambers A, B, and C with $mg_{60.1}$, 51.46% SiO_2, 9.67% FeO, 0.77% TiO_2) and in subchamber B (500–650 m), there is an overall progression to more evolved compositions ($mg_{78.3}$ to $mg_{41.9}$) up the 1750 m thick succession; the rate of fractionation (mg, Na_2O, TiO_2) increases up the succession; marked discontinuities in mg, MgO, MnO, TiO_2, Ni, and S occur between subchambers A–B (500 m), B–C (650 m), and C–D (1450 m); the anomalous evolved composition of leucogabbros in subchamber B relative to the overall fractionation trend supports the suggestion above that subchamber B may be a feeder to subchamber D; although there is a general increase in Ni, Cu, and S concentrations towards the base of the intrusion, detailed trends are masked by regular magma replenishment; most cumulates contain 450–1320 ppm S, indicating sustained S saturation throughout the intrusion; massive Ni–Cu–Co sulphides appear to have lower Pt (0.8 ppb), Pd (102 ppb), and Au (16 ppb) concentrations relative to disseminated sulphides (40.5 ppb Pt, 336 ppb Pd, 176 ppb Au).

Other comments. Located in the middle of the Ni–Cu–Co–PGEs metallogenic corridor as defined by Hoatson (1993), near the intersection of two major regional structural trends displayed by the Tickalara Metamorphic country rocks and other group V intrusions. An east-west trend, which is also reflected in the elongated shapes of the nearby Keller Creek and Dave Hill intrusions, is truncated by a later north-northeast trend just east of the Sally Malay intrusion. The Sally Malay and Panton intrusions are the most intensively explored bodies in the East Kimberley.

Corkwood mafic intrusion (10 in Fig. 5.1, Fig. 5.24)

Centre of intrusion. Central TURKEY CREEK at AMG ~135878.

Age. Correlated with the 1844±3 Ma Sally Malay intrusion, but may be older (>1850 Ma).

Form, structure, and areal extent. Steeply dipping mafic sheet, 2.2 km long by 0.2 km wide, in a north-northeast-striking narrow zone of high-grade Tickalara Metamorphics bounded by the Halls Creek Fault to the east and the Mabel Downs Tonalite to the west; foliation in the intrusion dips steeply to the northwest, which is generally concordant with the foliation in the country rocks (58–88°) of the Tickalara Metamorphics.

Thickness. 200 m.

Stratigraphy and main rock types. Weakly foliated to massive homogeneous sequence of metagabbro, olivine metagabbro, and metagabbronorite; no marked compositional layering or ultramafics have been identified.

Relationships. Intrudes pelitic schist, graphitic schist, psammite, migmatitic gneiss, marble, calc-silicate, foliated amphibolite, and mafic granulite of the Tickalara Metamorphics; there is a regional increase from low metamorphic grade east of the intrusion to higher grade garnet–biotite–feldspar–quartz gneiss and migmatitic gneiss next to the Mabel Downs Tonalite in the west; carbonate layers in Tickalara Metamorphics display complex tight folding and boudinage features, resulting from the greater partitioning of deformation relative to the adjacent gneissic and pelitic rocks.

Mineralisation. A recessive limonitic gossan, 220 x 10 m, with fine boxwork textures and malachite and chrysocolla staining in lower part of intrusion; also small pods of gossan along strike for most of the length of the intrusion; sulphide body plunges 10° towards 35° with sulphide bands below the main gossan generally subparallel to the regional north-northeast-trending foliation; sulphides are concentrated in massive and weakly foliated metagabbro, indicating possible metamorphic remobilisation of sulphides towards low-strain regions.

Petrography. Metagabbros are fine to medium-grained (1–2 mm), weakly foliated uralitised rocks, containing plagioclase, clinopyroxene, orthopyroxene, and minor Fe–Ti oxides, rutile, sulphides, quartz, and biotite; orthopyroxene predominates over clinopyroxene in some gabbronorite variants; brown and green amphibole replaces both clinopyroxene and orthopyroxene; sulphides occur as massive concentrations of pyrrhotite, pyrite, pentlandite, and chalcopyrite, and as a matrix to silicates; sulphide concentration typically varies dramatically over a few centimetres; pyrrhotite contains exsolved pentlandite, which is altered to violarite, pyrite is secondary after pyrrhotite, and chalcopyrite forms small grains and fine stringers in fractures and cleavages of silicates (Sanders 1999).

Geochemistry. Metagabbro ranges from MgO-rich variants ($mg_{76.4}$, 17.07% MgO, 0.48% TiO_2, 0.05% P_2O_5, 1503 ppm Cr, 40 ppm Zr) to more evolved types (mg_{51}, 6.91% MgO, 1.08% TiO_2, 0.1% P_2O_5, 75 ppm Cr, 59 ppm Zr); S-saturated conditions are indicated by sustained high S content (960–2090 ppm); chilled gabbro ($mg_{66.2}$) has elevated S (1720 ppm) and Ni (227 ppm) abundances.

Other comments. Metagabbro has recrystallisation and mineralogical features indicative of transitional amphibolite to granulite facies metamorphism, similar to the Keller Creek intrusion. Both these intrusions are similar to mafic granulite bodies in the Tickalara Metamorphics. According to Barnes (1994), (1) the Corkwood gossans are the product of remobilised sulphides concentrated along lithologic boundaries that became parallel during the peak of granulite metamorphism, and (2), mineralogical reconstitution of the intrusive rocks during granulite metamorphism released Ni from olivine, which

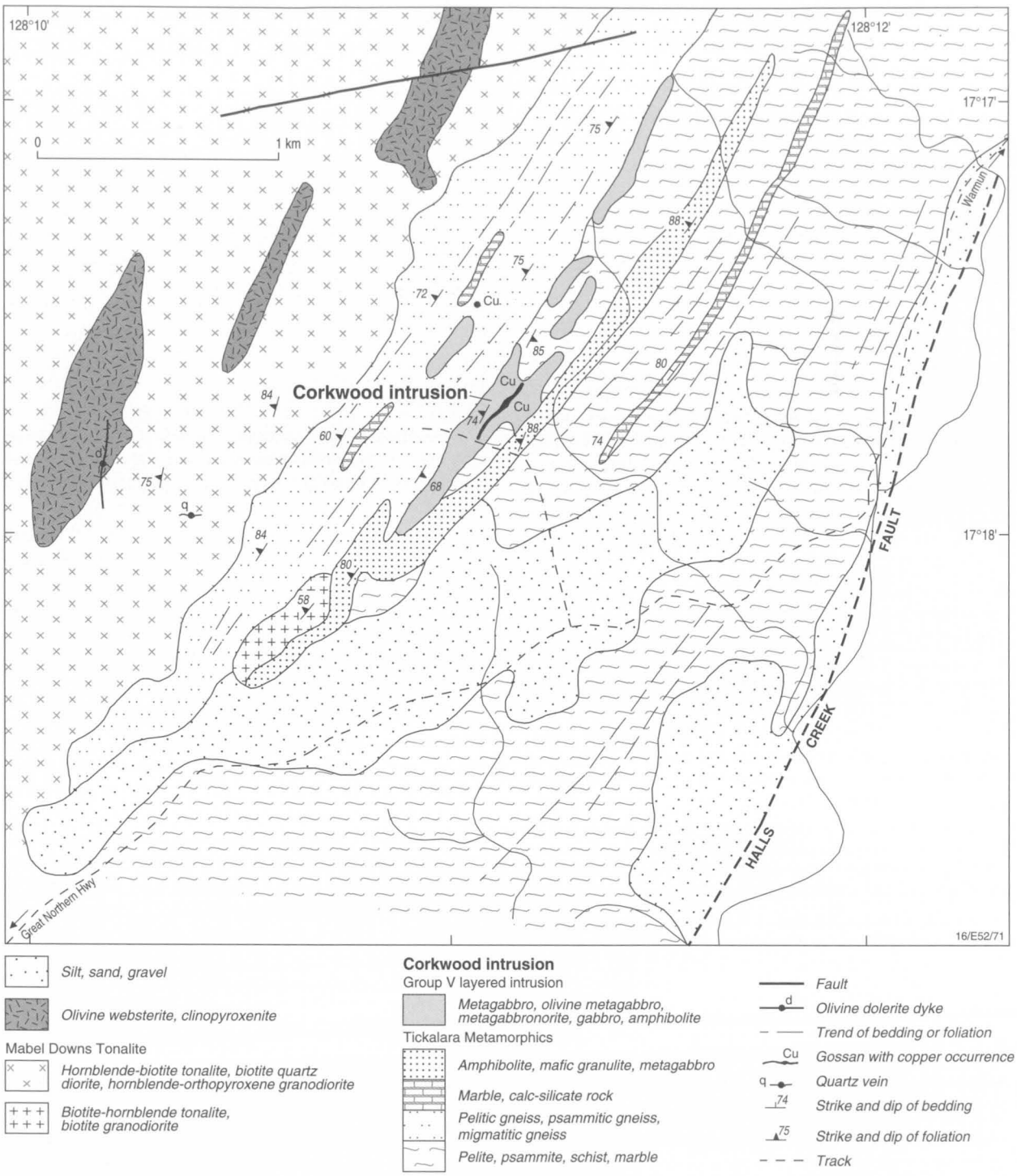


Figure 5.24. Geological map of the group V Corkwood mafic intrusion.

subsequently partitioned with sulphide liberated from graphitic schists, resulting in the development of massive Ni sulphides.

Dave Hill mafic–ultramafic intrusion (16 in Fig. 5.1, Fig. 5.20)

Centre of intrusion. Southwestern TURKEY CREEK at AMG ~961790.

Age. Correlated with the 1844±3 Ma Sally Malay intrusion.

Form, structure, and areal extent. Arcuate mafic sheet, 1 km wide by 3.5 km long, correlated with the fractionated gabbroic units in the upper part of the Sally Malay intrusion; layering dips between 40 and 85° towards the south and west.

Thickness. 0.8 km.

Stratigraphy and main rock types. A ridge-forming sequence, ~250 m thick, of rhythmically layered olivine gabbro and olivine gabbronorite at the base is overlain by a recessive cyclic mafic sequence, ~250 m thick, of troctolite, leucogabbro, and mottled anorthosite containing prominent limonite spots after oxidised disseminated sulphides; thin serpentinised plagioclase-bearing peridotite and pyroxenite lenses are interlayered with the cyclic mafic units; a ridge-forming sequence, ~300 m thick, of homogeneous leucogabbro and minor anorthosite south of the recessive mafic sequence defines the highest exposed part of the intrusion.

Relationships. Intrudes granulite facies garnet–cordierite–biotite–alkali feldspar–plagioclase–quartz±sillimanite±graphite paramigmatite, mafic granulite, and minor retrogressive schist and carbonate of the Tickalara Metamorphics; intruded by lenses of Turkey Creek microgabbro–norite and by veins of north-trending quartz, granite pegmatite, aplite, and microgranite.

Petrography. Troctolite and olivine gabbro (poC) adcumulates contain cumulus plagioclase (An_{86}) and olivine, with minor intercumulus orthopyroxene and clinopyroxene; well-developed coronas of orthopyroxene, amphibole, and green spinel (see Chapter 9), up to 0.3 mm wide, occur at most olivine and plagioclase contacts; smaller coronas of spinel and amphibole surround sulphide blebs; leucogabbro (pabC) in upper part of the intrusion is an equigranular medium-grained (2 mm) adcumulate.

Geochemistry. Normal fractionation trends ($mg_{78.3–73.8}$, 0.08–0.21% TiO_2) reflect upward decrease in modal olivine throughout mafic sequence; extremely low P_2O_5 (<0.01%) and Zr (<11 ppm) contents indicate that even the most fractionated mafic cumulates are too primitive for the crystallisation of apatite and zircon; persistent high S concentration (1030–2760 ppm), erratic Cu and Ni trends, and low Pd (2.1 ppb), Pt (1.4 ppb), and Au (4 ppb) contents imply sustained S saturation.

Fletcher Creek mafic intrusion (15 in Fig. 5.1, Fig. 5.25)

Centre of intrusion. Southwestern TURKEY CREEK at AMG ~983773.

Age. Correlated with the 1844±3 Ma Sally Malay intrusion.

Form, structure, and areal extent. Northeast-trending composite sill, at least 9 km long and only 0.5 km wide; may be the northeast strike extension of the McKenzie Spring intrusion.

Thickness. ?0.3 km.

Stratigraphy and main rock types. Southwestern part comprises low-ridge-forming steeply dipping leucogabbro and anorthosite, with minor olivine gabbro, olivine gabbronorite, and troctolite; Pickands Mather & Company International (1965–1969) also reported peridotite along the northwestern basal contact, but these rocks were not observed during the present study; gabbroic units form weakly layered lenticular bodies within leucogabbro and anorthosite; troctolite is associated with olivine gabbro in a small ovoid body near the northeastern end of the sill; the northeastern part consists of a uniform sequence of weakly layered olivine gabbronorite and olivine gabbro, largely covered by black soils and colluvium.

Relationships. Northwest-trending fault with both dip-slip and strike-slip sinistral (~300 m) displacements separates the southwestern part from the more primitive northeastern part of the intrusion; concordant with ridge-forming garnet–sillimanite–biotite–microcline–plagioclase–quartz paramigmatite and lenses of mafic granulite units of the Tickalara Metamorphics to west and a prominent 15 m ridge of marble, calc-silicate, and dolomite to east; further east, the carbonates are faulted against foliated biotite granite and tonalite of the Mabel Downs Tonalite; chilled biotite gabbro and malachite-stained garnet–epidote calc-silicate skarns along east side of the northeastern part of the intrusion with carbonates indicate the intrusion postdates the Tickalara Metamorphics.

Petrography. Plagioclase, uralitised clinopyroxene, and minor olivine are generally cumulus in gabbro (paoC), whereas clinopyroxene is intercumulus to coarse-grained plagioclase in leucogabbro and anorthosite (pC); olivine in the troctolite (poC) mesocumulates has very thin (<0.05 mm) orthopyroxene–amphibole–spinel coronas where it touches plagioclase.

Geochemistry. Chilled gabbro from the eastern contact of the northeastern part of the intrusion has fractionated mafic composition ($mg_{53.7–56.7}$, 7.38–7.87% MgO, 0.82–1.47% TiO_2, and up to 0.22% P_2O_5, 120 ppm Zr, and 30 ppm Y); contrasting Na_2O/CaO ratios (0.1 and 0.03) in the two chilled samples suggest plagioclase has variable composition; high S (670–1190 ppm) and low Pd (2.8 ppb), Pt (0.5 ppb), and Au (1 ppb) contents indicate S-saturated conditions.

Frog Hollow mafic intrusion (7 in Fig. 5.1, Fig. 5.26)

Centre of intrusion. Central western TURKEY CREEK at AMG ~985905.

Age. Correlated with the upper parts of the 1844±3 Ma Sally Malay intrusion.

Form, structure, and areal extent. Irregular elongate body, 8 km long by 1 km wide, of fractionated gabbroic rocks similar to those in subchamber D of the Sally Malay intrusion (Hoatson 1995).

Thickness. ?0.8 km.

Stratigraphy and main rock types. Mafic units include weakly layered olivine gabbro, melagabbro, leucogabbro, anorthosite, and ferrogabbro; discontinuous irregular anorthosite bodies are most prominent in the central and eastern parts of the intrusion; at least two stratigraphic levels of Fe–Ti–V oxides in ferrogabbroic rocks in the south; the oxide lenses are drained by creeks containing abundant oxide alluvium.

Relationships. Intrudes granulite facies garnet–cordierite–biotite–alkali feldspar–plagioclase–quartz±

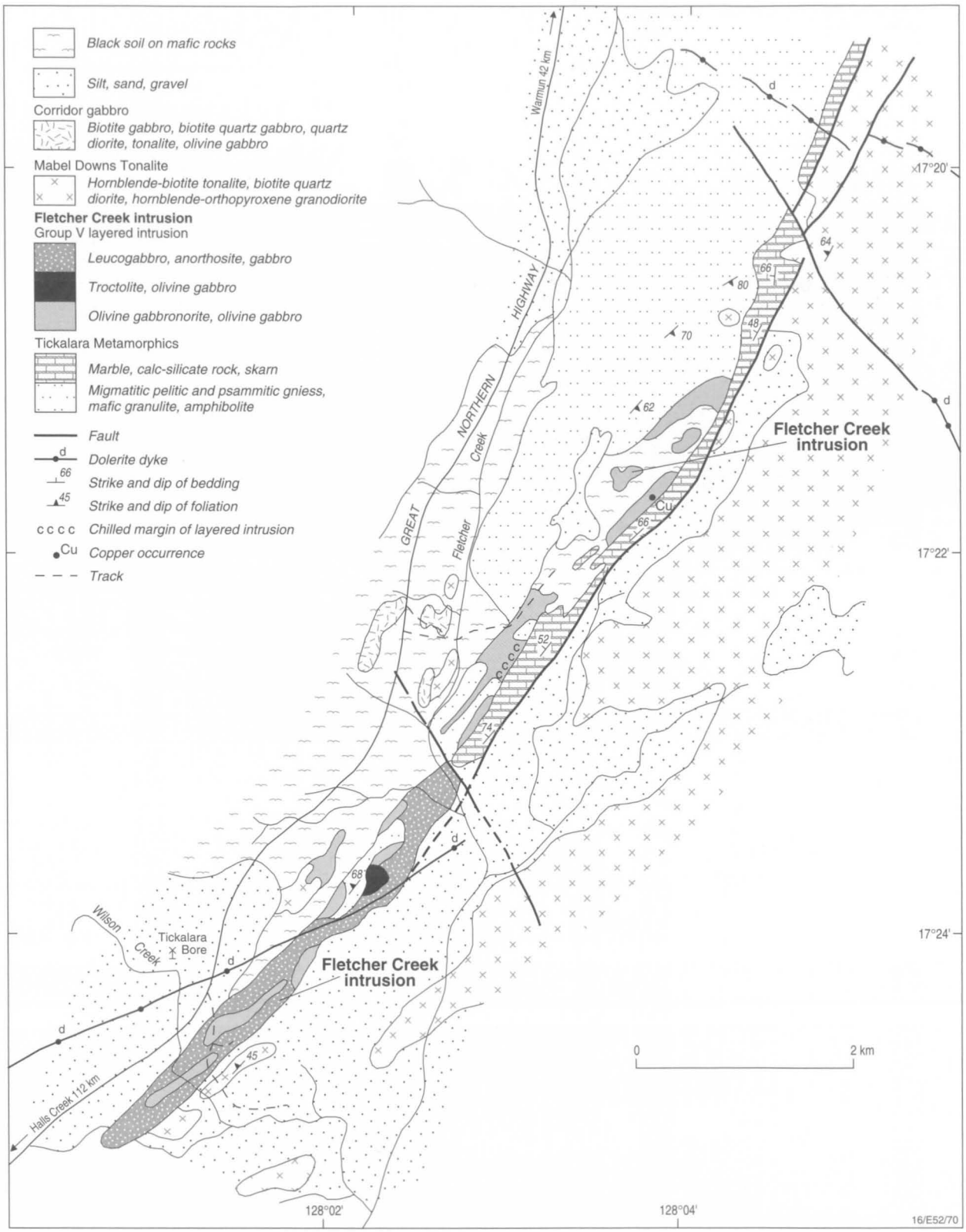
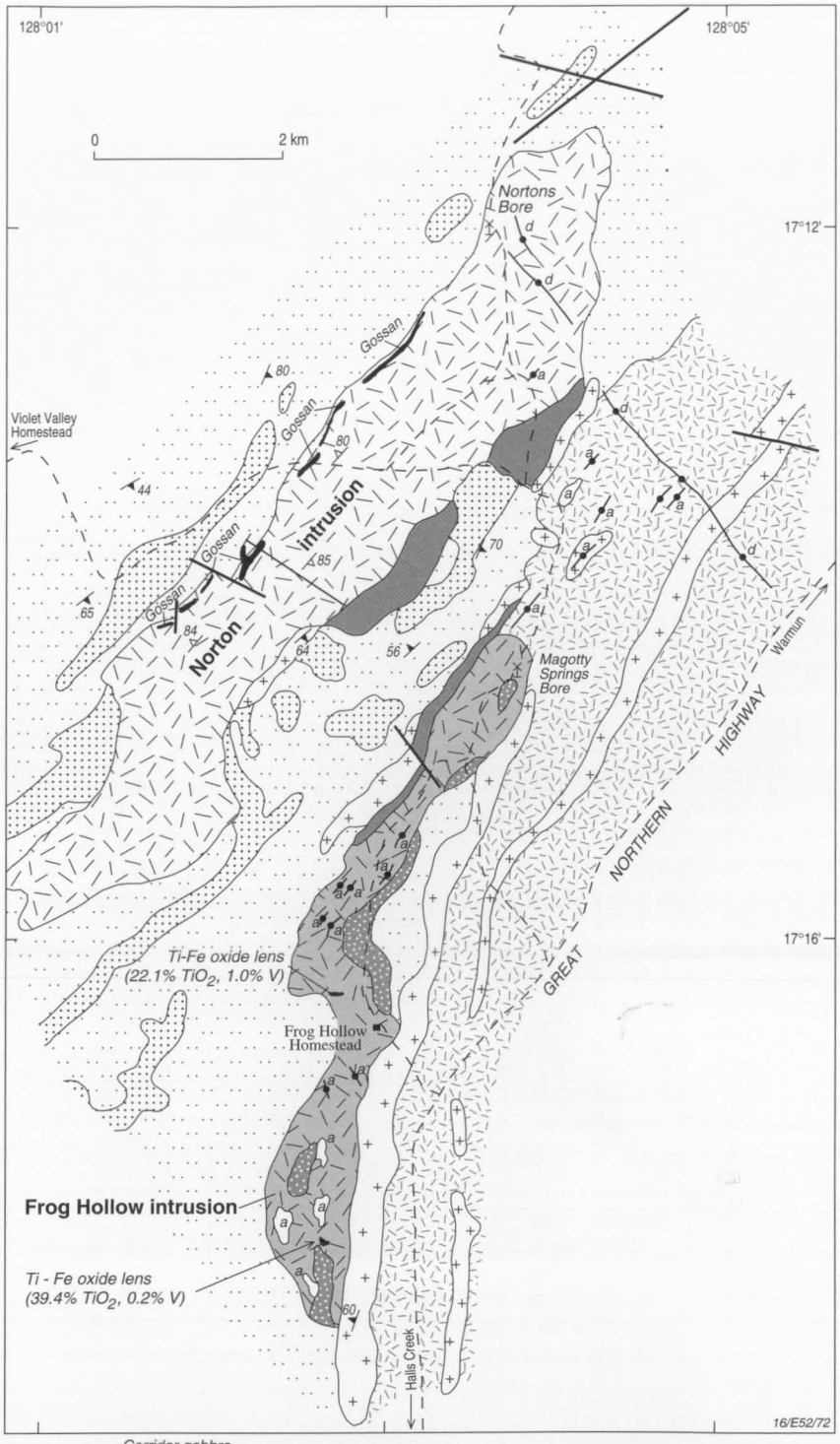


Figure 5.25. Geological map of the group V Fletcher Creek mafic intrusion.

sillimanite paramigmatite and mafic granulite, and minor retrogressive schist and carbonate of the Tickalara Metamorphics; intruded in north by Turkey Creek microgabbro–norite and in east by granite of Sally Downs supersuite; cut by irregular bodies of aplitic granite, and veins of aplite, pegmatite, and quartz.

Mineralisation. Ferrogabbro in the southern part contains some of the thickest lenses of Fe–Ti oxides known in the Kimberleys; largest lens is ~20 m wide by 30 m long and forms a prominent 15 m-high hill.

Petrography. Largest oxide lens contains deformed coarse-grained (up to 4 mm) aggregates of ilmenite



Corridor gabbro
Biotite gabbro, biotite quartz gabbro, quartz diorite, tonalite, olivine gabbronorite
Turkey Creek microgabbro-norite
Microgabbro, biotite norite, gabbronorite
Biotite monzogranite, hornblende-biotite granodiorite
Frog Hollow intrusion
Group V layered intrusion
Leucogabbro, anorthosite
Olivine gabbro, gabbro, ilmenite and titaniferous magnetite-bearing gabbro, quartz diorite
Tickalara Metamorphics
Norton intrusion
Hornblende metagabbro, hornblende-magnetite metagabbronorite, olivine metagabbro
Mafic granulite, amphibolite
Migmatitic pelitic and psammitic gneiss

Strike and dip of igneous layering
Strike and dip of foliation
Dolerite dyke
Aplitic granite, aplite, pegmatite, quartz vein
Track
Sample traverse

Figure 5.26. Geological map of the group V Frog Hollow mafic intrusion and the Norton metagabbro intrusion (Tickalara Metamorphics).

(55% vol.), secondary tremolite–actinolite (40%) after clinopyroxene, and minor titaniferous magnetite (5%).

Geochemistry. Largest oxide lens contains TiO_2 (39.4%), total Fe as Fe_2O_3 (52.5%), V (0.23%), and Cr (0.08%); another lens lower in the intrusion contains less TiO_2 (22.1%), but more total Fe as Fe_2O_3 (60.6%), V (0.99%), and Cr (0.93%); coarse grain size and high TiO_2 grades of the deformed oxides may reflect high-temperature subsolidus annealing and grain enlargement processes related to metamorphism.

Other comments. The Frog Hollow Fe–Ti–V deposit compares favourably with other major Australian titaniferous magnetite deposits associated with layered intrusions, which typically contain 3–30% TiO_2 and 0.1–0.7% V (1986 Australian Mineral Industry Quarterly 39(1), p.7).

Keller Creek mafic intrusion (9 in Fig. 5.1, Fig. 5.27)

Centre of intrusion. Central eastern MOUNT REMARKABLE at AMG ~904865.

Age. Correlated with the 1844±3 Ma Sally Malay intrusion, but may be older (>1850 Ma).

Form, structure, and areal extent. Gabbroic lens, 0.3 km wide by 1.5 km long, folded around the northwestern end of a small elongate biotite monzogranite stock ('Misery Hill granite'); folded western part of intrusion occupies the hinge of a regional east-trending overturned anticline that extends eastwards towards the Sally Malay intrusion (Gaunt 1977); intrusion is generally concordant with adjacent mafic granulite and paramigmatite of the Tickalara Metamorphics and is not strongly discordant as reported in Sheppard et al. (1997); this reinterpretation has important implications since it suggests the Keller Creek intrusion may belong to the older Tickalara Metamorphics (i.e. Norton-type) rather than being a group V intrusion; this is supported by similar flat trace-element geochemical patterns and initial eNd values for the Keller Creek and Norton intrusions (see Chapter 11).

Thickness. 0.3 km.

Stratigraphy and main rock types. Massive and weakly layered olivine gabbro, melagabbro, and minor leucogabbro; an unrelated coarse-grained amphibole-spotted melagabbro locally present below base of the intrusion; no ultramafics have been identified.

Relationships. Concordant with paramigmatite and mafic granulite of the Tickalara Metamorphics, cut by biotite monzogranite of the Sally Downs supersuite and numerous pegmatite and quartz veins.

Mineralisation. Disseminated low-grade Ni–Cu sulphide mineralisation along the northwestern basal contact beneath the thickest part of the mafic sequence; a lens, 100 m long, of disseminated pyrrhotite, chalcopyrite, and pentlandite beneath a limonitic gossan that crops out for about 400 m along strike; sulphide mineralisation locally remobilised into structurally favourable sites in adjacent paragneiss and contact aureole of the monzogranite stock; the best drillhole intersection of 7.8 m @ 1.0% Ni and 0.26% Cu is in a marginal apophysis

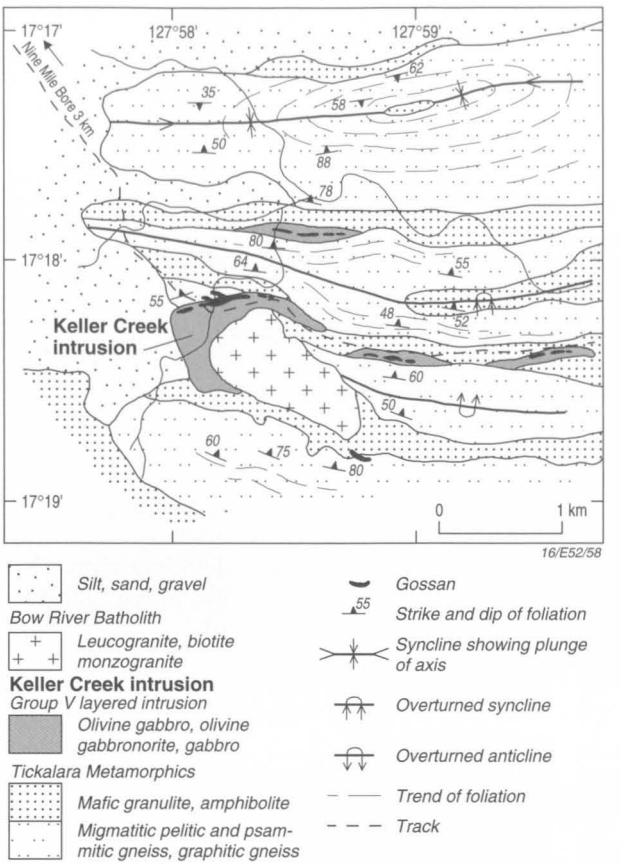


Figure 5.27. Geological map of the group V Keller Creek mafic intrusion.

to the granite; thin gossans cut paramigmatites of the Tickalara Metamorphics near the southeast end of the felsic stock, indicating that the granitic stock may have been an important source of heat and fluids for remobilisation of the sulphides; thin gossans also occur in small gabbroic lenses 1.5 and 2.5 km along strike to the east of the Keller Creek intrusion.

Petrography. Weakly layered gabbros are transitional in metamorphic grade between upper amphibolite and granulite facies; coarse minerals contain primary igneous features, such as plagioclase and opaque inclusions in coarse poikilitic olivine anhedra (up to 20 vol. %), primary twinning and exsolution in clinopyroxene, and compositionally zoned plagioclase; however, the groundmass, which contains no olivine, consists of recrystallised tightly packed granular clinopyroxene and plagioclase aggregates, which display triple point junctions and annealing fabrics that are not typical of adcumulus growth processes; Sanders (1999) describes the development of biotite and pyroxene porphyroblasts and uralitisation near the contact with the granite; recrystallisation textures therefore may be related to the contact metamorphic effects of the monzogranite stock, regional metamorphism, and/or autometamorphism; dominant sulphide phase in the gabbros is pyrrhotite, which occurs as discrete and composite blebs, and in fractures with trace amounts of chalcopyrite and pyrite, pentlandite forms exsolved flames in pyrrhotite rather than discrete grains, chalcopyrite is interstitial to, and

rims, pyrrhotite blebs, and infills irregular fractures and stringers in shear zones (Sanders 1999).

Geochemistry. Olivine gabbro and olivine gabbronorite have fractionated compositions ($mg_{38.4–58.2}$, 5.66–8.98% MgO, 0.98–1.68% TiO_2, and up to 0.14% P_2O_5, 62 ppm Zr, and 27 ppm Y); S-saturated conditions are indicated by sustained high S contents (1410–3320 ppm); exceptionally low Ba (4–17 ppm) contents are typical of mafic granulites in the Tickalara Metamorphics (see Norton intrusion).

Other comments. The Keller Creek intrusion has a similar geological setting to the Corkwood intrusion—thin lenticular mafic bodies containing a restricted range of gabbroic rocks, largely concordant relationships with amphibolite and mafic granulite of the Tickalara Metamorphics, transitional amphibolite to granulite metamorphic facies, similar recrystallisation features, metamorphic remobilisation of sulphides, and low Ni/Cu ratio (~<3:1) of sulphides. Both intrusions have affinities with mafic granulite bodies in the Tickalara Metamorphics (e.g. Norton intrusion).

Mabel Downs Homestead mafic intrusion (3 in Fig. 5.1, Fig. 5.28)

Centre of intrusion. Central western TURKEY CREEK at AMG ~064008.

Age. Correlated with the 1844±3 Ma Sally Malay intrusion.

Form, structure, and areal extent. Irregular mafic body, 0.5 km by 1 km, immediately north of Mabel Downs Homestead.

Thickness. 0.5 km.

Stratigraphy and main rock types. Ridge-forming cyclic sequence of coarse-grained mottled anorthosite and uralitised gabbro, with minor leucogabbro and magnetite gabbro; intergranular, poikilitic, and pegmatoidal textures are common, but compositional layering is not well developed; weathered gabbroic units have a distinctive red oxidation colour that reflects their Fe-rich compositions; mafic stratigraphy is similar to that of the evolved subchambers of the Sally Malay intrusion.

Relationships. Contacts largely concealed by alluvium.

Other comments. Most northerly group V intrusion investigated in this study.

Mabel Downs Southwest mafic intrusion (4 in Fig. 5.1, Fig. 5.28)

Centre of intrusion. Central western TURKEY CREEK at AMG ~032000.

Age. Correlated with the upper parts of the 1844±3 Ma Sally Malay intrusion.

Form, structure, and areal extent. Fractionated mafic sheet, 0.8 km by 1.2 km; multiple Fe–Ti–V oxide layers dip steeply (75°) north in the upper part of intrusion.

Thickness. 1 km.

Stratigraphy and main rock types. Biotite gabbro, gabbro, magnetite gabbro, and tonalite; zone, ~150 m wide, in northern part of the body contains at least three major cyclic units, each comprising multiple thin layers (2–5 cm; see Fig. 14.5F) of titaniferous magnetite and ilmenite.

Relationships. Intrudes paramigmatites of the Tickalara Metamorphics to west and south and is intruded by foliated porphyritic granite of the Sally Downs supersuite to east and north.

Mineralisation. Multiple Fe–Ti–V oxide layers in upper part can be followed along strike for hundreds of metres.

Petrography. Fe–Ti–V oxide layers comprise equally abundant 1–1.5 mm anhedral subgrains of titaniferous magnetite and ilmenite with minor plagioclase, clinopyroxene, inverted pigeonite, biotite, and brown-green amphibole developed at plagioclase–oxide grain contacts.

Geochemistry. Oxide layer contains 15.46% TiO_2, 16.96% Fe_2O_3, 19.89% FeO, 1693 ppm V, and 495 ppm Cr.

Other comments. Evolved rock types and Fe–Ti–V oxide mineralisation are similar to the group V Frog Hollow intrusion.

McKenzie Spring mafic intrusion (20 in Fig. 5.1, Fig. 5.29)

Centre of intrusion. Southeastern MOUNT REMARKABLE at AMG ~843661 (intrusion extends southwestwards into McINTOSH).

Age. Correlated with the 1844±3 Ma Sally Malay intrusion.

Form, structure, and areal extent. Northeast-trending lenticular mafic sill, 1.2 km by up to 16 km, which may be the southwest strike extension of the Fletcher Creek intrusion.

Thickness. ?1 km.

Stratigraphy and main rock types. Weakly layered olivine gabbronorite, olivine–magnetite gabbronorite, troctolite, leucogabbro, uralitised and feldspathic pyroxenite, norite, and anorthosite; no obvious cyclic distribution or younging direction, but an increase in magnetite content in fractionated gabbros towards the northwest, and the presence of the largest gossans on the southeast contact indicate that the intrusion probably youngs northwest; plugs of ?unrelated peridotite and minor troctolite and olivine gabbro occur northwest of the intrusion near the Ord River.

Relationships. Intrudes garnet–cordierite–sillimanite–spinel–biotite–feldspar–quartz paragneiss and deformed foliated mafic igneous rocks of the Tickalara Metamorphics to the northwest of the Highway Shear Zone; cut by fine-grained leucogranite and pegmatite.

Mineralisation. Thin stratiform gossanous zones of massive and vuggy limonite/goethite crop out along the hangingwall and footwall contacts; hangingwall gossan

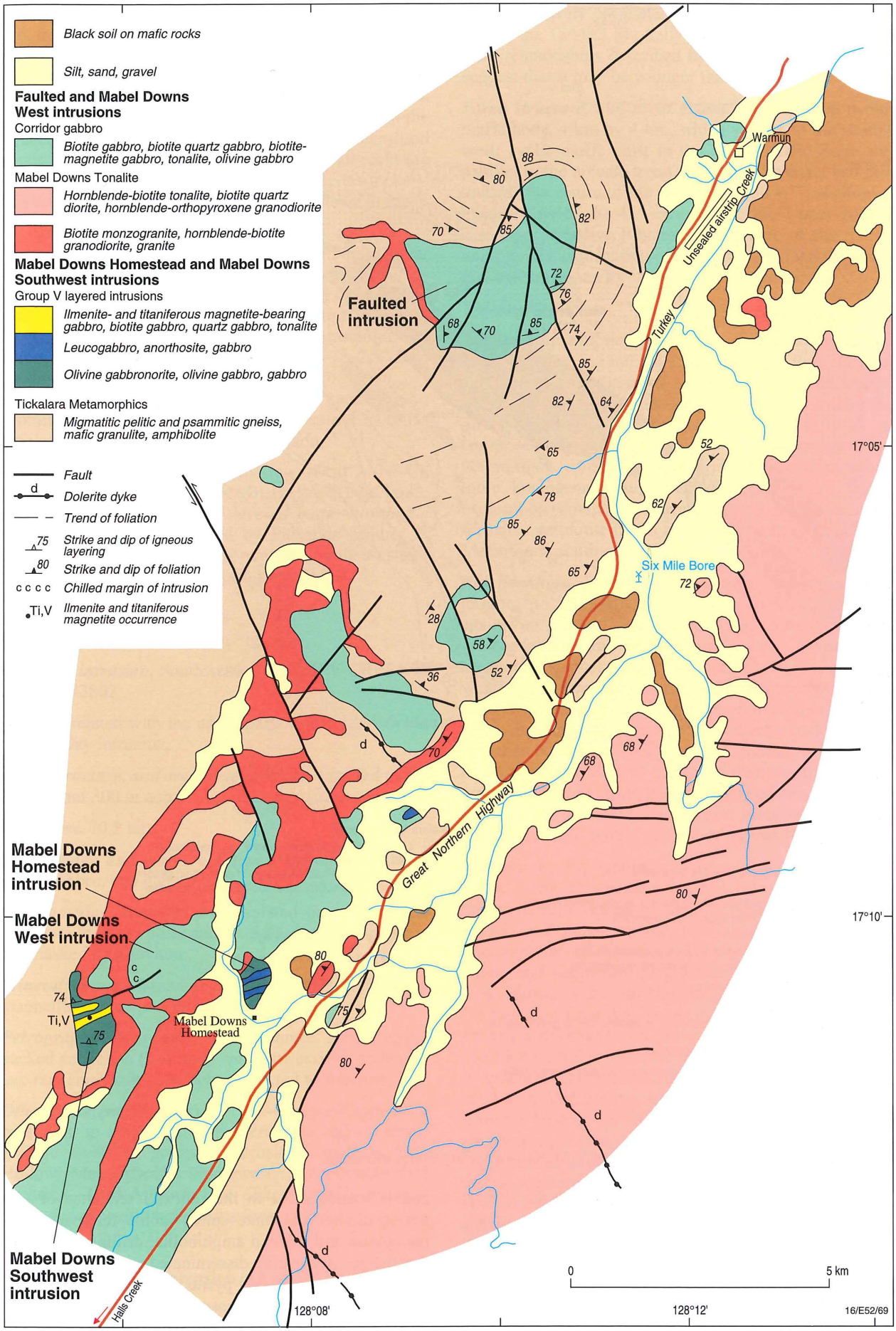


Figure 5.28. Geological map of the group V Mabel Downs Homestead and Mabel Downs Southwest mafic intrusions, and the Faulted and Mabel Downs West mafic intrusions (Corridor gabbro).

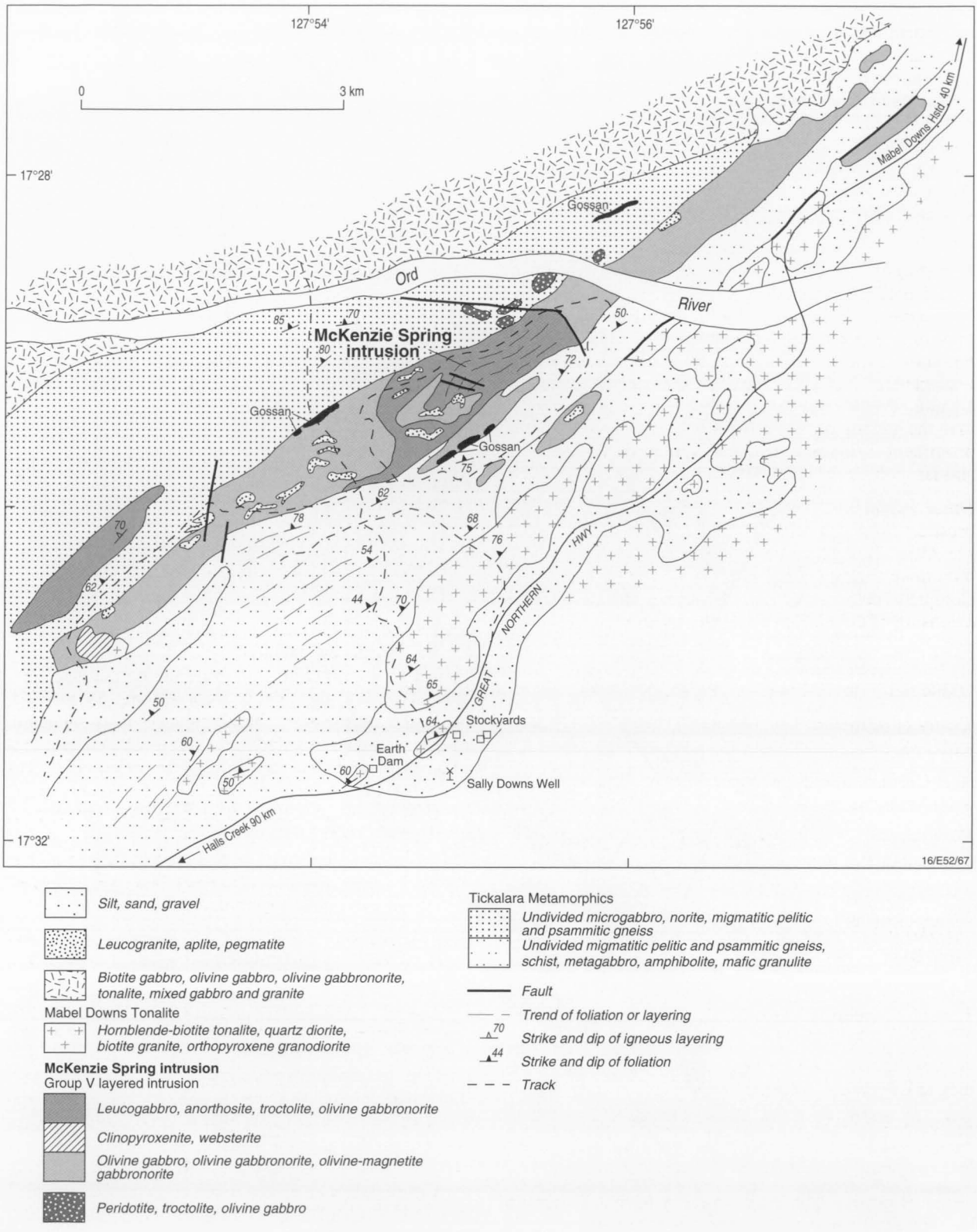


Figure 5.29. Geological map of the group V McKenzie Spring mafic intrusion.

(Fig. 5.29) crops out for over 150 m along the contact between the magnetite gabbro and the country rocks, comprising migmatitic paragneiss and microgabbro; gossans also persist intermittently for several hundred metres along strike in a large structural embayment on the southeastern margin (Fig. 5.29); the 1600 m long re-entrant embayment or trough is probably fault-controlled and is transgressive to the footwall sequence of garnet–cordierite–sillimanite–spinel–biotite–feldspar–quartz paragneiss and foliated amphibolite; drilling has shown that the gossans overlie disseminated and stringer primary sulphides, comprising pyrite, chalcopyrite, and pentlandite (see Chapter 2); gossans occur near the widest part of the intrusion (i.e. thickest sequence of cumulates)

beneath a weakly layered mafic sequence of olivine gabbro, troctolite, leucogabbro, and anorthosite; exploration companies have also reported weakly anomalous Ni and Cu concentrations from stratabound gossans at higher stratigraphic levels in the intrusion, from gossans associated with quartz veins, and from small gossans in the country rocks; it is also significant that most mineralised zones in the intrusion occur where the footwall rocks are dominantly metasediments, rather than igneous rocks—this association is evident for most mineralised group V intrusions.

Petrography. Gabbroic rocks (paboC) are equigranular (1–1.5 mm) adcumulates and mesocumulates of cumulus plagioclase (An_{60}) and olivine, cumulus or intercumulus orthopyroxene and clinopyroxene, and accessory Fe–Ti oxides, green spinel, and sulphides; troctolite and leucogabbro (poC) are coarser grained (2–2.5 mm) adcumulates that have more calcic plagioclase ($An_{65–77}$) than the gabbro; olivine–plagioclase grain contacts have prominent orthopyroxene–amphibole–spinel coronas similar to those in the Dave Hill intrusion.

Other comments. The Ord Crossing—Grid A Ni–Cu prospect (MOUNT REMARKABLE at AMG ~877685; see *Other possible group V layered mafic–ultramafic intrusions*, below) discovered by Pickands Mather & Company International in 1969 may be a northeast strike extension of the McKenzie Spring intrusion.

Oxide mafic intrusion (14 in Fig. 5.1)

Centre of intrusion. Southwestern TURKEY CREEK at AMG ~973802.

Age. Correlated with the upper parts of the 1844±3 Ma Sally Malay intrusion.

Form, structure, and areal extent. Poorly exposed mafic body about 300 m across.

Thickness. ?0.2 km.

Stratigraphy and main rock types. Ferrogabbro, magnetite gabbro, and gabbro.

Relationships. Contacts with isolated outcrops of the Tickalara Metamorphics and the Sally Downs supersuite are masked by alluvium.

Mineralisation. Massive segregations of Fe–Ti oxides in magnetite gabbro and ferrogabbro.

Petrography. Magnetite and ilmenite form tightly packed subgrains (2–4 mm) with fine exsolution lamellae; rare small sulphide blebs restricted to ilmenite.

Other comments. The Oxide Fe–Ti–V deposit appears to be similar to others that characterise the highest stratigraphic levels of group V intrusions, such as Frog Hollow, Mabel Downs Southwest, and possibly Ord Crossing—Grid A North (see *Other possible group V layered mafic–ultramafic intrusions*, below).

Spring Creek mafic intrusion (19 in Fig. 5.1, Fig. 5.30)

Centre of intrusion. Southeastern MOUNT REMARKABLE at AMG ~860735.

Age. Tentatively correlated with the upper fractionated part of the 1844±3 Ma Sally Malay intrusion; however, field relationships described by Sheppard et al. (1997) suggest that it may be younger than 1820 Ma.

Form, structure, and areal extent. Well-exposed ovoid mafic body, 4 km by 4 km, which youngs to the southwest; cyclic mafic units in the Lower Mafic Zone are parallel to the arcuate trend of the basal contact and dip towards the centre of the intrusion at 50–65°; shallower inward dips of 20–45° characterise the Upper Mafic Zone; no pervasive foliation or cleavage of the mafic units; spatial distribution of cyclic units reflects the original basinal geometry of the magma chamber.

Thickness. 2.5 km.

Stratigraphy and main rock types. Lower Mafic Zone, 1650 m thick, of interlayered olivine gabbro, olivine gabbronorite, leucogabbro, and anorthosite, and Upper Mafic Zone, 850 m thick, of poorly layered troctolite, olivine gabbro, and leucogabbro; Lower Mafic Zone comprises two megacyclic units—a lower megacycle, 900 m thick, comprising interlayered mafic units, and a more homogeneous upper megacycle, 750 m thick; exploration companies have reported rare thin conformable peridotite layers in the lower part of the Upper Mafic Zone south of Spring Creek.

Relationships. Intrudes a co-mingled gabbro–granite terrane; northwestern basal contact is locally chilled against porphyritic biotite granite, and co-mingled fine-grained gabbro and granite form a zone, 50 m wide, along the northeastern basal contact; it is uncertain whether these co-mingled rocks represent a contaminated partly melted zone related to the intrusion or are part of the older mixed gabbro–granite country rocks; cut by irregular bodies and veins of leucogranite, aplite, pegmatite, and quartz infill faults and fractures that radiate across the intrusion; southwestern part of the intrusion is intruded by unrelated fractionated body of laminated melagabbro and biotite gabbronorite.

Petrography. Equigranular gabbros (paoC) of the Lower Mafic Zone are medium-grained mesocumulates and adcumulates, containing cumulus plagioclase, clinopyroxene, and minor olivine, and accessory cumulus or intercumulus orthopyroxene, biotite, apatite, zircon, sulphide, and magnetite; plagioclase in the Lower Mafic Zone shows sodic enrichment trends consistent with fractionation from An_{65} (most calcic composition determined) at the base to An_{58} near the top of the zone; concomitant with this trend are increases in the abundances of apatite and zircon and a decrease in olivine; relative to the Lower Mafic Zone, troctolite and anorthosite (poC) from the base of the Upper Mafic Zone have more calcic plagioclase (An_{65}), an increase in olivine abundance, and a change in clinopyroxene from cumulus to intercumulus—features indicating a possible major pulse of new magma; both rock types have mottled textures consisting of cumulus plagioclase and olivine and intercumulus clinopyroxene; olivine is partially altered to serpentine minerals, magnetite, iddingsite, and chlorite; clinopyroxene is variably uralitised; and plagioclase shows incipient alteration to sericite and epidote; in contrast, gabbro intruding the central part of the Upper

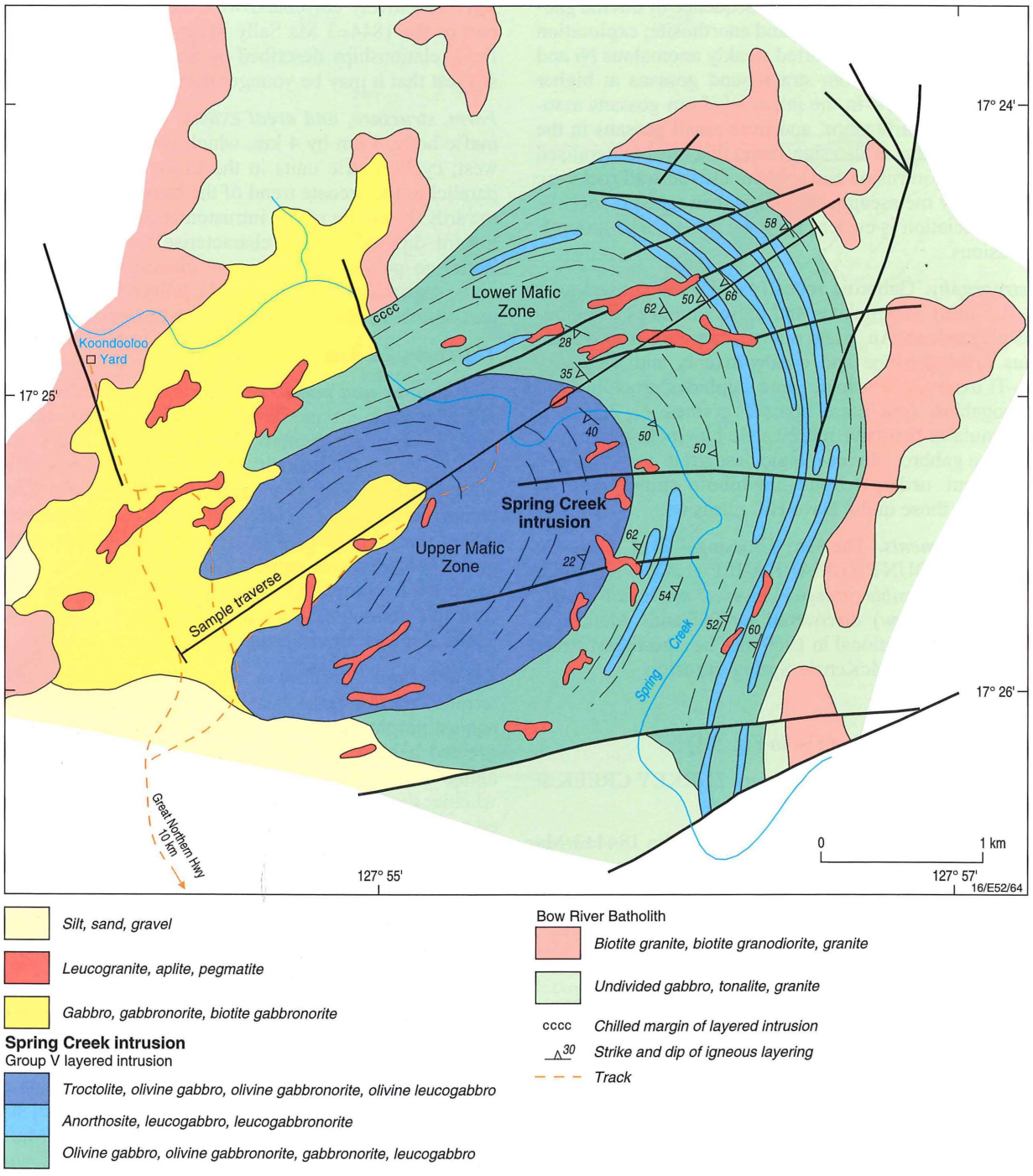


Figure 5.30. Geological map of the group V Spring Creek mafic intrusion.

Mafic Zone has prominent laminated and subophitic textures, with more evolved composition indicated by the absence of olivine and an increase in abundance of pleochroic Fe-rich hypersthene, quartz, titaniferous magnetite, sphene, and biotite.

Geochemistry. Fluctuating major and trace-element trends (Figs 5.31, 5.32) reflect regular magma injection into the Lower Mafic Zone (0–1650 m), whereas slightly more consistent MgO, CaO, and MnO trends in the Upper Mafic Zone (1650–2500 m) indicate limited magma input; FeO, MnO, Al_2O_3, and, in particular, Sr trends suggest that the Lower Mafic Zone may be composed of two megacycles separated at the ~900 m stratigraphic level; except for Na_2O, V, and Sr, there is no major chemical discontinuity across both zones at 1650 m; high S concentration in the Lower Mafic Zone (450–1010 ppm) and Upper Mafic Zone (550–1150 ppm) and the absence of systematic Cu and Ni trends imply sustained S saturation; unrelated laminated gabbro (2500–3290 m) intruding Upper Mafic Zone is relatively more fractionated with lower mg ($mg_{57.9–64.1}$), Al_2O_3 (13.47–17.81%), and higher Zr (29–124 ppm), Y (12–31 ppm), K_2O (0.31–0.68%), TiO_2 (0.58–1.28%), and P_2O_5 (0.04–0.24%).

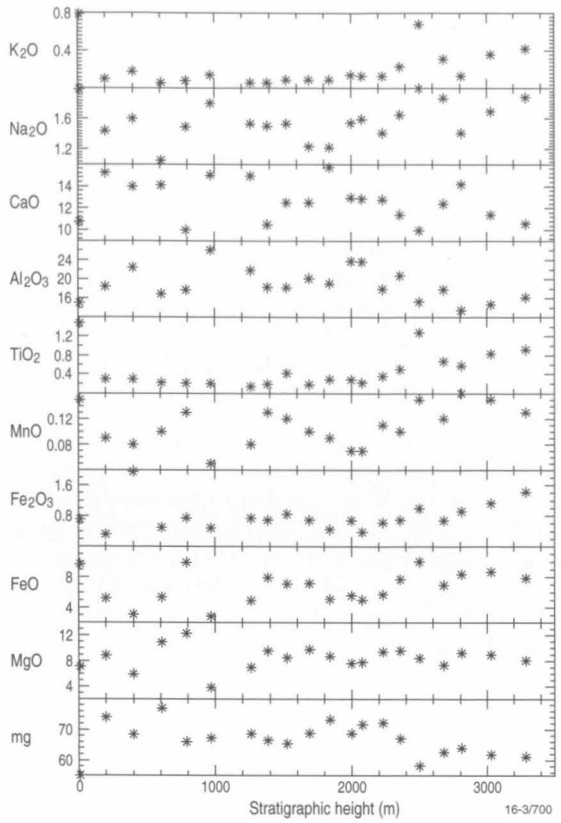


Figure 5.31. Spring Creek intrusion: variation in whole-rock major-element composition (in wt. %) of mafic cumulates with stratigraphic height.

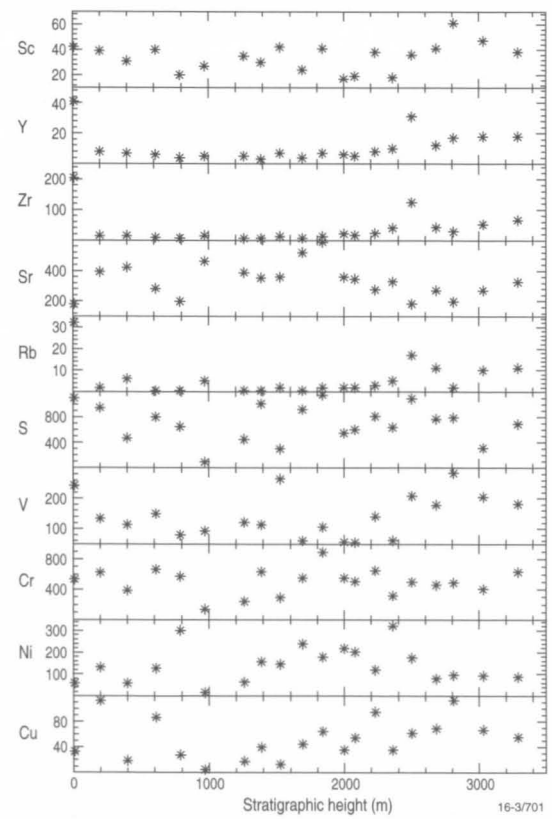


Figure 5.32. Spring Creek intrusion: variation in whole-rock trace-element composition (in ppm) of mafic cumulates with stratigraphic height.

Three Nuns mafic intrusion (13 in Fig. 5.1)

Centre of intrusion. Central western TURKEY CREEK at AMG ~942812.

Age. Correlated with the 1844±3 Ma Sally Malay intrusion.

Form, structure, and areal extent. At least two small north-trending ?lenses, about 300 m by 300 m.

Thickness. ?0.2 km.

Stratigraphy and main rock types. Poorly exposed metagabbro and olivine metagabbro.

Relationships. Concordant with the major structures of the surrounding mafic granulites of the Tickalara Metamorphics.

Mineralisation. Recessive limonitic/hematitic gossans, up to 100 m long and 20 m wide, are associated with metagabbroic rocks.

Other comments. The metamorphic grade of these recrystallised gabbroic rocks is unknown; however, they may be of sub-granulite to granulite facies. If this is correct, the Three Nuns intrusion should be reclassified as a Tickalara Metamorphics intrusion (similar to the Norton and ?Keller Creek intrusions) rather than being a post-metamorphic group V intrusion. Many of the thin limonitic gossans associated with granulitic bodies of the Tickalara Metamorphics appear to be derived from pyrite–pyrrhotite bodies containing very low abundances of Ni, Cu, and Co.

Wilson Creek mafic–ultramafic intrusion (18 in Fig. 5.1, Fig. 5.20)

Centre of intrusion. Southeastern MOUNT REMARKABLE at AMG ~938765 (intrusion extends eastwards into TURKEY CREEK).

Age. Correlated with the 1844±3 Ma Sally Malay intrusion.

Form, structure, and areal extent. Lobate intrusion, 3 km by 6 km, comprising weakly layered mafic sheets intruded by irregular plug-like ultramafic bodies.

Thickness. ?2 km.

Stratigraphy and main rock types. Stratigraphy is not well defined, although irregular ovoid bodies of massive serpentinised peridotite appear to cut mottled anorthosite, leucogabbro, and troctolite; ridge-forming units of coarse-grained, locally pegmatitic, amphibole-spotted gabbro, olivine gabbro, and olivine gabbronorite are interlayered with anorthosite; serpentinisation and magnesite alteration are intense in peridotite.

Relationships. Intruded by massive and foliated fine-grained olivine microgabbro and norite (Turkey Creek microgabbro–norite in Fig. 5.20) and ovoid bodies and dykes of leucogranite and aplite, and veins of quartz and pegmatite; eastern contact is largely masked by alluvium.

Petrography. Coarse-grained (3–5 mm) peridotite (oC) mesocumulates and orthocumulates have large equant cumulus olivine grains enclosed by intercumulus orthopyroxene, clinopyroxene, and minor plagioclase (An*58*); minor chromite subhedra inclusions in olivine and in brown phlogopite; troctolite (poC) mesocumulates contain cumulus plagioclase and olivine, and gabbroic variants also contain minor intercumulus clinopyroxene and orthopyroxene; olivine is deeply embayed where it touches plagioclase and is surrounded by thin coronas of orthopyroxene, green spinel, and Ca-clinopyroxene or amphibole; common accessory minerals include biotite, titaniferous magnetite, and small disseminated sulphide blebs.

Geochemistry. Olivine-bearing mafic cumulates (gabbronorite, troctolite) are considerably more primitive ($mg_{66.2–70}$, 9.42–15.81% MgO, 0.25–0.66% TiO_2, 0.01–0.05% P_2O_5, 11–51 ppm Zr) than a gabbronorite sample (mg_{52}, 7.82% MgO, 1.22% TiO_2, 0.14% P_2O_5, 90 ppm Zr); high S (360–1430 ppm) and low Pt (0.5 ppb), Pd (<0.5 ppb), and Au (1 ppb) abundances suggest S-saturated magma conditions.

Other comments. Compared with the other group V intrusions, the Wilson Creek intrusion contains the largest area of ultramafic rocks.

Other possible group V layered mafic–ultramafic intrusions

Pickands Mather & Company International, in 1969, discovered a northeasterly striking gabbroic intrusion near the Ord River that hosted Ni–Cu sulphide and Fe–Ti–V oxide mineralisation. The Ord Crossing—Grid A Ni–Cu (MOUNT REMARKABLE at AMG ~877685), and 2 km further northeast, the Ord Crossing—Grid A North Fe–Ti–V (MOUNT REMARKABLE at AMG ~892700) deposits occur in a steeply dipping, layered gabbroic body, 400–1200 m wide, which is probably the northeast strike extension of the group V McKenzie Spring intrusion. Major rock types are gabbro, norite, olivine gabbro, and pyroxenite. Gossans near the contact between fine and coarse-grained gabbro have a strike length of 300 m and maximum Ni and Cu concentrations of 0.45% and 0.80%, respectively (Sanders 1999). The Ord Crossing—Grid A Fe–Ti–V deposit (Sanders 1999) appears to be similar to those that characterise the highest stratigraphic levels of other group V intrusions, such as Oxide, Frog Hollow, and Mabel Downs Southwest. The oxide lenses occur in two northeast-trending gabbro zones, separated by a narrow zone of norite, that extend from 5 km northeast of the Ord River to 3 km southwest of the river. Individual lenses are up to 150 m long and 30 m wide, with primary oxide segregations trending 240° and having variable dips of 25–85° to the northwest. The main prospect consists of massive oxide lenses over a 60 by 300 m area in uralitised gabbro and minor amphibolite after pyroxenite. A composite channel sample returned 15.2% TiO_2, 41.9% Fe_2O_3, and 0.03% V. Pickands Mather & Company International inferred a potential oxide resource of 25 000 t/vertical metre.

Other small lenticular and ovoid mafic intrusions (Fig. 5.1; see Chapter 2) that have been tentatively correlated with group V occur along the southeastern and northwestern margins of the Mabel Downs Tonalite, in the southwest corner of TURKEY CREEK. Olivine gabbro, metagabbro, leucogabbro, and anorthosite are the major rock types that intrude metasediments, amphibolite, and mafic granulite of the Tickalara Metamorphics. The intrusions are located along strike from the Corkwood intrusion near Sally Malay Bore (AMG ~100823), as a group of ovoid bodies near the junction of Fletcher Creek and Ord River (AMG ~994668), and about 6 km north-northeast of the Fletcher Creek intrusion (AMG ~020864).

Several other Ni–Cu-bearing mafic intrusions not investigated in this study (Sanders 1999, see Chapter 2) may belong to group V or are mafic granulite bodies that should be assigned to the Tickalara Metamorphics. These include Bulldust Flat (TURKEY CREEK at AMG ~039720), Cattle Creek (TURKEY CREEK at AMG ~028681), Eileen Bore (McINTOSH at AMG ~894400), Osmond Valley (TURKEY CREEK at AMG ~220965), White Rock Well West (McINTOSH at AMG ~890517), and Wills Creek (TURKEY CREEK at AMG ~007676).

Group VI layered mafic intrusions

Group VI comprises the 1830±3 Ma McIntosh intrusion (type example) and correlative intrusions on McINTOSH, in the central zone of the HCO. These are large funnel-shaped and smaller sheet-like gabbroic bodies that intrude group IV intrusions, Tickalara Metamorphics, and the 1843±2 Ma Koongie Park Formation (Page et al. 1994). Despite thicknesses of up to 7.8 km and well-developed macrorhythmic cyclic units, the group VI intrusions have a restricted range of olivine-bearing and magnetite-bearing gabbroic cumulates. The basal contact and feeder regions of the thicker S-saturated intrusions have potential for Ni–Cu sulphide mineralisation, and their upper more fractionated parts are prospective for stratabound titaniferous magnetite layers and remobilised Au–Pd–Cu mineralisation, similar to the Platinova Reef of the Skaergaard intrusion, East Greenland (Bird et al. 1991, Brooks et al. 1999).

Group VI intrusions described below are McIntosh, Armanda, and Togo.

McIntosh mafic intrusion (34 in Fig. 5.1, Fig. 5.10, front cover of this *Bulletin*)

Centre of intrusion. Central eastern McINTOSH at AMG ~846437.

Age. U–Pb zircon age of 1830±3 Ma determined for zircon from migmatitic hornfels of the Tickalara Metamorphics in the northwestern contact aureole of the intrusion (see Chapter 6).

Form, structure, and areal extent. Covering an area of 6 km by 14 km, this is one of the most striking landforms in the East Kimberley—the distinctive concentric pattern of alternating ridges and valleys readily visible on satellite and geophysical images is due to differential erosion of macrocyclic units—valleys generally corre-

sponding to olivine-rich cumulates (troctolite, rare peridotite), and ridges up to 170 m high in the lower 6000 m of the intrusion composed of pyroxene-bearing mafic cumulates (olivine gabbro, olivine gabbronorite, gabbro) and those in the upper 1800 m formed of magnetite-bearing mafic cumulates (magnetite gabbro); Dow & Gemuts (1969) interpreted a sill-like body folded into a structural basin, but it is now known (Mathison & Hamlyn 1987, this study) to be a discordant, steep-sided, funnel-shaped body, comprising a northern ovoid part ('cross-section of an onion') and a southern part that narrows into a keel-shaped dyke-like body ('ice-cream cone'); macrorhythmic cyclic units along the eastern and western margins of the ovoid part of the intrusion have inward dips from 35–55°; the dips decrease towards the centre of the intrusion, where they are sub-horizontal; macrorhythmic units in the southern part, which contains the most primitive lowermost units of the intrusion and may include a possible concealed feeder conduit, are steeply dipping (60–90°) to locally overturned, as a result of post-emplacement tilting.

Thickness. 7.8 km; Mathison & Hamlyn (1987) measured a stratigraphic thickness of 6 km, but did not include an additional 1300 m sequence south of the Alice Downs road.

Stratigraphy and main rock types. Despite its size and cyclic character, the McIntosh intrusion does not contain a wide range of rock types; mafic rocks which show minor variation in modal plagioclase, olivine, augite, orthopyroxene, and magnetite dominate; the lower 3000 m of the exposed sequence consists of troctolite, olivine gabbro, and olivine gabbronorite; ultramafic rocks, which account for less than 2% of the total thickness, are near the base; minor peridotite occurs with olivine-rich troctolite and anorthosite along a northeast-trending ridge crossing the Alice Downs road, and further north, concordant lenses up to 20 m thick of peridotite and harzburgite are interlayered with gabbroic rocks—these lenses are thought to represent primitive magma crystallised in situ rather than accidental blocks incorporated in the gabbro; the general increase of ultramafic rocks to the south, combined with geophysical studies (see Chapter 7), indicates that other related prospective components of the intrusion (e.g. base of ultramafic zone, subchamber, feeder conduit) may be concealed near the southern end of the intrusion; olivine gabbro and olivine gabbronorite are the major rocks in the middle 3000–6000 m stratigraphic interval, and are joined by magnetite gabbro and magnetite gabbronorite for the highest stratigraphic interval from 6000–7800 m; the intrusion is essentially a macrolayered mafic body comprising alternating troctolite and olivine gabbro with minor gabbronorite and rare peridotite; north of the Alice Downs road, Mathison & Hamlyn (1987) identified at least 96 macrolayers, comprising 44 troctolite, 38 olivine gabbro, and 14 gabbronorite layers, and 40 cyclic units (50–200 m thick), comprising troctolite and overlying olivine gabbro; sharp contacts between the cycles are defined by the upward change of augite or orthopyroxene from intercumulus to cumulus, or vice versa, and by changes in the modal proportions of augite, olivine, orthopyroxene, and Fe–Ti oxides—thus the contacts represent combinations of changes in mineral phases, mode, and texture (Irvine 1982).

Relationships. Preferentially emplaced along the contacts of a variety of rock types immediately west of the Alice Downs Fault—it intrudes felsic intrusive sheets (Dead Finish Tonalite) and mafic metavolcanics of the Tickalara Metamorphics, group I West McIntosh and South Melon Patch intrusions, and group IV Wild Dog Creek intrusions; eastern margin has a linear trend subparallel to the Alice Downs Fault, indicating it is possibly faulted against parts of the Wild Dog Creek body and the felsic intrusive sheets of the Tickalara Metamorphics; gabbro along the eastern contact of the McIntosh intrusion is often intensely uralitised, reflecting increased water activity along the ?faulted margin; thin chilled gabbroic zones are locally present at contacts with mafic metavolcanics of the Tickalara Metamorphics in south and southwest (Fig. 5.10); Mathison & Hamlyn (1987) described rounded chilled gabbroic pillows in a slightly coarser gabbroic matrix in the northwest at a contact with sheared gneiss (Tickalara Metamorphics); gabbro becomes progressively coarser grained for 100 m inwards from this chilled margin; isolated outcrops of migmatitic garnet–cordierite–sillimanite–spinel–biotite–alkali feldspar–plagioclase–quartz hornfels (Tickalara Metamorphics) define a contact aureole in the northwest (see Chapter 6); as is typical of most East Kimberley intrusions, a prominent contact thermal aureole is absent.

Petrography. Most mafic rocks display well-preserved primary mineralogy and cumulus textures; uralitisation and weak recrystallisation features, such as deformation lamellae and strained extinction in olivine, and bent and lenticular twinning in plagioclase, are more prominent towards the margins of the intrusion (Mathison & Hamlyn 1987)—these features may be due to post-emplacement metamorphism or hydration and deformation that were focussed along the margins during emplacement; troctolites (poC) are coarse-grained mesocumulates and adcumulates, consisting of cumulus olivine and plagioclase and minor intercumulus clinopyroxene and orthopyroxene; coronas (0.3 mm wide), comprising an inner shell of orthopyroxene or radiating brown amphibole surrounded by an outer symplectite zone of amphibole and vermicular green spinel rods (see Chapter 9), are often well developed at olivine–plagioclase grain contacts; clinopyroxene and orthopyroxene are cumulus in olivine gabbro (paoC) and olivine gabbronorite (paboC); compared to troctolite, the gabbros are medium-grained adcumulates, equigranular to porphyritic, and the coronas around olivine are much thinner (<0.1 mm); olivine in troctolite and the more primitive gabbros is generally anhedral, owing to postcumulus overgrowths; accessory biotite, magnetite, ilmenite, sulphides, zircon, apatite, and alkali feldspar are surprisingly very low in abundance; magnetite becomes a significant cumulus mineral at the expense of olivine in the most fractionated rocks—magnetite gabbro (pamC) and magnetite gabbronorite (pabmC); in most of these rocks, disseminated cumulus magnetite with late crystallising ilmenite averages 6 vol. %, whereas it is the dominant cumulus mineral in thin segregated layers in the most

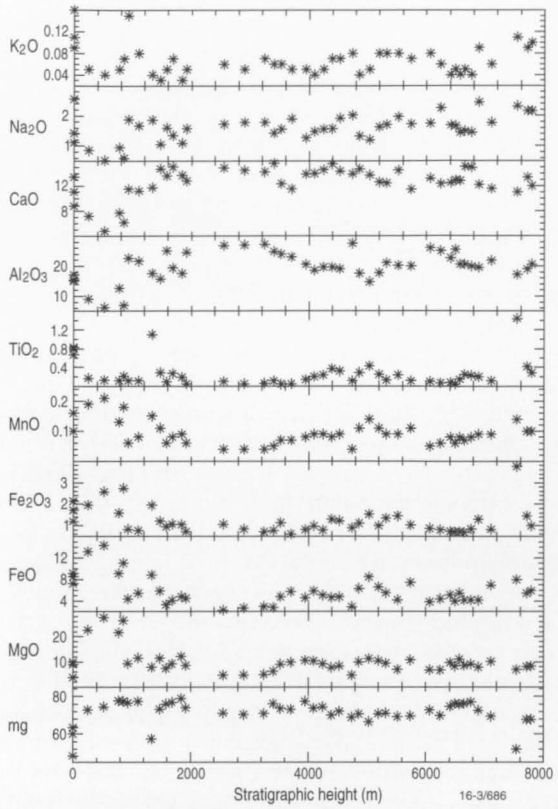


Figure 5.33. McIntosh intrusion: variation in whole-rock major-element composition (in weight %) of mafic cumulates with stratigraphic height.

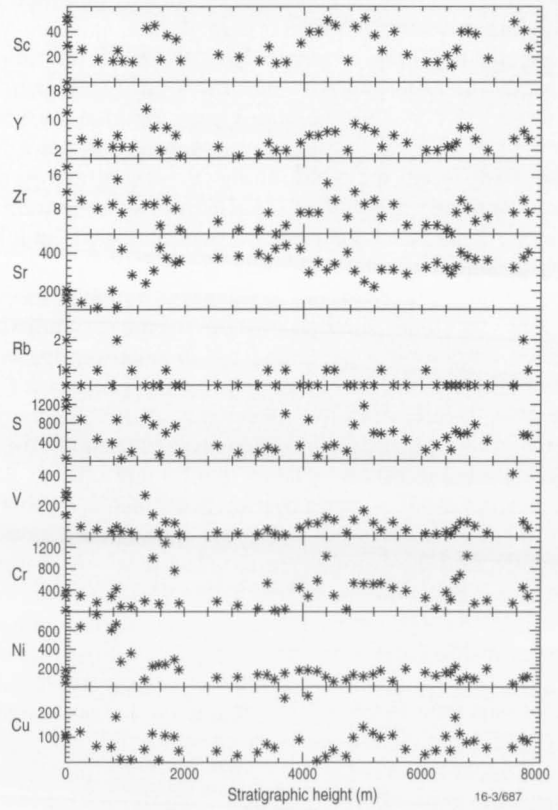


Figure 5.34. McIntosh intrusion: variation in whole-rock trace-element composition (in ppm) of mafic cumulates with stratigraphic height.

evolved gabbros; general distribution of rock types in the intrusion indicates an upward sequence of cumulus assemblages from poC to paoC to paboC to pabmC; Mathison & Hamlyn (1987) noted that the overall ranges of cumulus mineral compositions in the intrusion are plagioclase ($An_{51–83}$), olivine ($mg_{56–79}$), clinopyroxene ($mg_{64–82}$), and orthopyroxene ($mg_{52–80}$), with the most fractionated minerals occurring in magnetite gabbronorite.

Geochemistry. Regularly fluctuating trends of major and trace-elements (Figs 5.33, 5.34) indicate an open fractionation system involving repeated influxes of magma not markedly different in composition from the resident magma; chilled gabbro near the basal contact and magnetite gabbroic rocks above 6800 m display the most obvious deviations in regional trends—chilled gabbro is considerably more fractionated ($mg_{60.1–63}$, 46.9–48.3% SiO_2, 12–18 ppm Zr, up to 0.05% P_2O_5) than overlying olivine gabbro, olivine gabbronorite ($mg_{67.1–79}$) and troctolite ($mg_{70.1–74.7}$); magnetite gabbro ($mg_{52.1–70.2}$) is highly evolved, containing up to 1.44% TiO_2 and 417 ppm V; Al_2O_3 and MnO have distinctive antipathetic saw-tooth trends, reflecting megacycles of olivine gabbro and troctolite; high S content of chilled gabbro (1140–1290 ppm), olivine gabbro (200–1160 ppm), troctolite (160–870 ppm), and magnetite gabbro (540–1590 ppm) indicates sustained S saturation throughout the intrusion—this is supported by low concentrations of Pt (<4.8 ppb), Pd (<2.3 ppb), and Au (<4 ppb) in coarse-grained cumulates and in chilled olivine gabbro (1.9 ppb Pt, 1.6 ppb Pd, and 2 ppb Au).

Other comments. The McIntosh body is the thickest intrusion in the East Kimberley and the second largest in area after the Toby intrusion (see Table 14.4). Because of its size and S-saturated character, the intrusion has potential for Ni–Cu–Co sulphides, particularly in embayments along the basal contact or in the feeder conduit (see Chapter 14). Geophysics (see Chapter 7) would play an important role in locating these unexposed prospective components, which if present, may be atconsiderable depth.

Armanda mafic intrusion (46 in Fig. 5.1, Fig. 5.35)

Centre of intrusion. Central southern McINTOSH at AMG ~745107.

Age. Correlated with the 1830±3 Ma McIntosh intrusion.

Form, structure, and areal extent. Moderately dipping mafic sheet, 2.5 km by 1.5 km, which is much smaller than the previously mapped fault-bounded composite sill (Gemuts 1971); redefined here to exclude the quartz–feldspar porphyry, granite, and dolerite; rhythmic layering is generally parallel to the arcuate western margin, with dips of 25–45° towards the east and southeast; intrusion youngs towards the southeast.

Thickness. 700 m.

Stratigraphy and main rock types. A lower rhythmically layered sequence of olivine gabbro, olivine gabbronorite, gabbro, and minor leucogabbro is overlain by

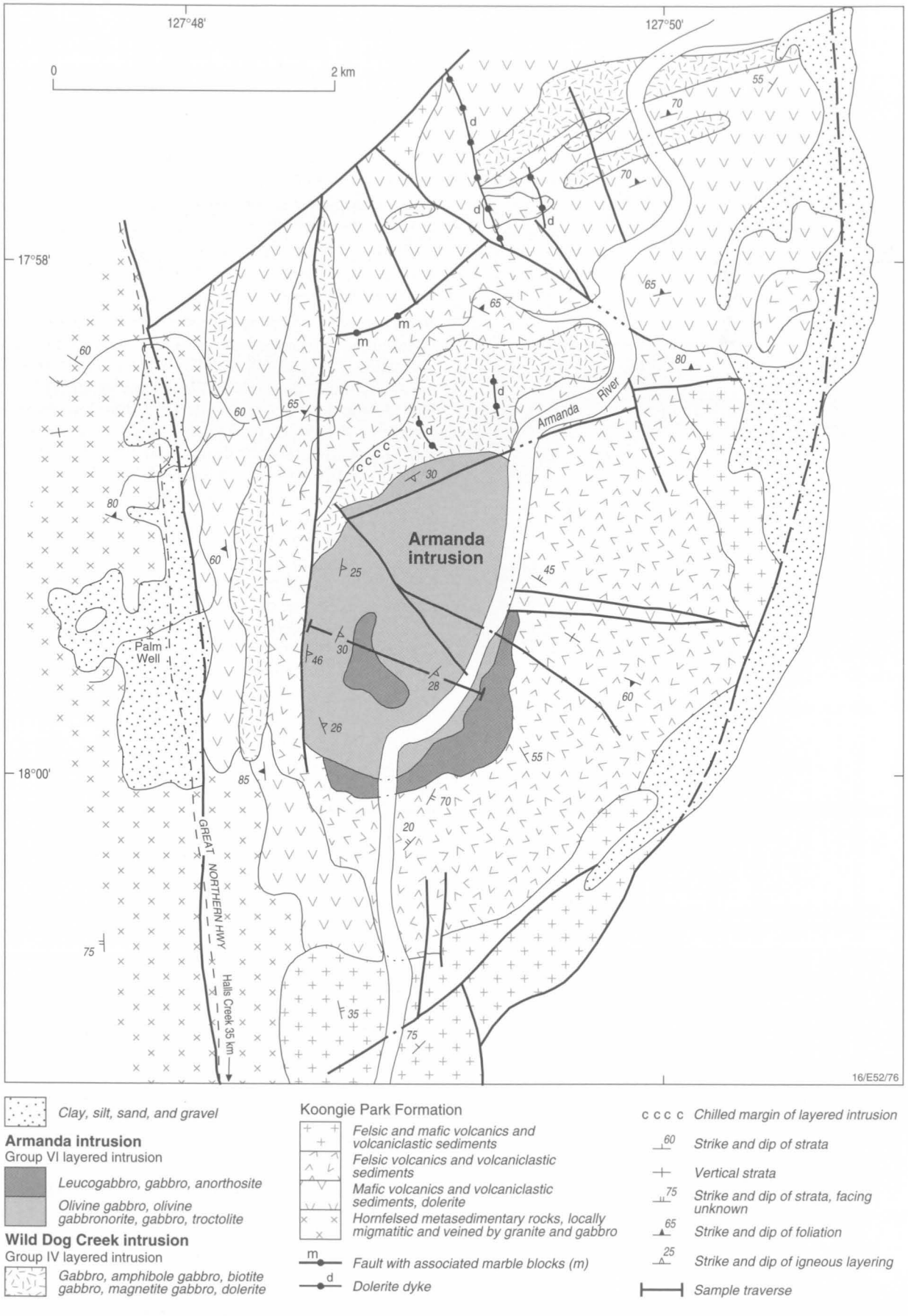


Figure 5.35. Geological map of the group VI Armanda mafic intrusion.

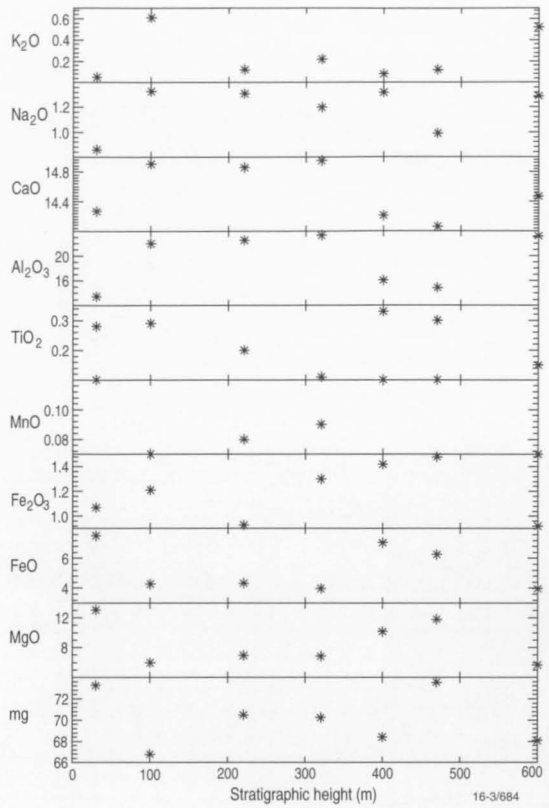


Figure 5.36. Armanda intrusion: variation in whole-rock major-element composition (in weight %) of mafic cumulates with stratigraphic height.

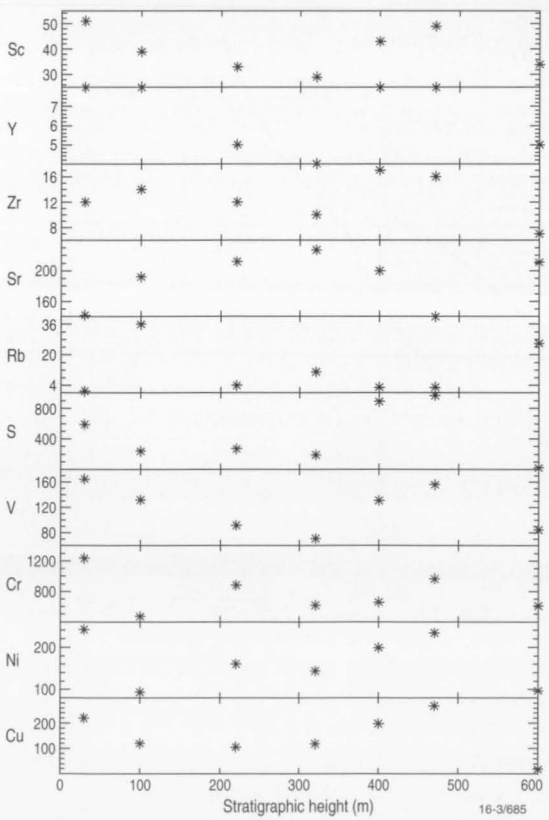


Figure 5.37. Armanda intrusion: variation in whole-rock trace-element composition (in ppm) of mafic cumulates with stratigraphic height.

an upper sequence of leucogabbro and minor anorthosite; these fractionated mafic units are intercalated with felsic metavolcanic country rock and may represent high-level felsic sills near the roof of the intrusion; most gabbroic rocks coarse grained (up to 6 mm), but some finer grained variants along eastern margin; rhythmic layering is generally not prominent, but locally it comprises alternating diffuse layers of olivine gabbro and leucogabbro containing variable amounts of plagioclase, clinopyroxene, orthopyroxene, and olivine; gabbros are increasingly uralitised towards the margins, owing to increased fluid activity along the contacts during emplacement of the intrusion and/or amphibolite facies metamorphism.

Relationships. Intrudes felsic metavolcanics and metasediments mapped as 1843±2 Ma Koongie Park Formation (Page et al. 1994) and amphibole-spotted melagabbro and doleritic gabbro of the group IV Wild Dog Creek intrusion; contact metamorphic features (Warren 1992, Blake & Hoatson 1993) of the Koongie Park Formation felsic volcanics on the southern and eastern margins include hornfelsing to quartz–feldspar–muscovite assemblages, cordierite porphyroblasts, incorporation of mafic blocks and enclaves, angular and pillow-like blocks of the gabbro separated by back veining of remelted felsic material, and net-vein complexes formed from mingling of mafic and felsic magmas; distinctive coarse cordierite porphyroblasts (up to 4 cm) are retrogressed to biotite, chlorite, and muscovite in the felsic metavolcanics on the southern margin of the intrusion; the western margin of the intrusion is partly sheared against a north-trending sequence of mafic-felsic volcanics and sediments of the Koongie Park Formation and gabbroic sills.

Petrography. Gabbros (poC) are coarse-grained granular to intergranular adcumulates and mesocumulates containing cumulus plagioclase and olivine and intercumulus clinopyroxene and orthopyroxene; plagioclase ($An_{76–80}$) forms broad tabular subhedral to anhedral laths partly altered to sericite clinozoisite, chlorite, epidote, calcite, and clays; interstitial clinopyroxene is variably uralitised to mats of green fibrous clinoamphibole; anhedral olivine grains have embayed margins and coronas where they touch plagioclase (see Chapter 9); the coronas consist of a thin (<0.02 mm) inner discontinuous shell of orthopyroxene, surrounded by a green-brown amphibole zone, grading outwards into a radiating symplectite zone of green amphibole and vermicular green spinel rods (<0.05 mm), and an outermost zone of a plagioclase–spinel symplectite of variable thickness; tiny amphibole prisms display a radiating texture around olivine in some coronas where the orthopyroxene shell is absent.

Geochemistry. Limited sampling indicates a moderately differentiated mafic sequence comprising three possible megacyclic units (Figs 5.36, 5.37); mg (67.8–73.3), Ni (94–242 ppm), Cr (470–1233 ppm), and Cu (18–268 ppm) display sympathetic saw-tooth trends which have discontinuities at the base of the megacycles near the ~0 m, ~150 m, and ~450 m stratigraphic levels; maximum Cu (268 ppm) and Cr (1233 ppm) concentrations are similar to those in the McIntosh intrusion (265 ppm Cu,

1271 ppm Cr); variable, but high S (20–970 ppm) and low Pt (<1.3 ppb), Pd (<1 ppb), and Au (<3 ppb) contents indicate sustained S-saturation conditions in the intrusion.

Other comments. Similar to the McIntosh intrusion in stratigraphy, lithology, mineralogical features (e.g. olivine coronas), and contact relationship to the Wild Dog Creek intrusion.

Togo mafic intrusion (25 in Fig. 5.1)

Centre of intrusion. Central McINTOSH at AMG ~715523.

Age. Correlated with the 1830±3 Ma McIntosh intrusion.

Form, structure, and areal extent. Fault-bounded block, 3.5 km by 1.5 km, between the Springvale Fault and north-trending arcuate splay.

Thickness. ?0.5 km.

Stratigraphy and main rock types. The central ovoid part of the intrusion, 1.2 km wide, has a distinctive white tone on aerial photographs, which correlates with intensely sericitised leucogabbro, gabbro, and minor anorthosite; surrounding these altered rocks is a more primitive sequence of coarse-grained massive melagabbro, olivine gabbro, and olivine gabbronorite.

Relationships. Faulted against Togo Monzogranite of the Paperbark supersuite to the west and mixed granite-gabbro of the Sally Downs supersuite to the east; cut by east-trending faults, along which fluid movement may have intensely altered the central leucocratic rocks.

Other comments. Tentatively classified as a group VI intrusion on the basis of similar ovoid shape and lithologies to the McIntosh and Armanda intrusions.

Group VII layered mafic intrusions

Group VII intrusions (type example: Black Hills Yard intrusion) are small steeply plunging troctolite and olivine gabbro plugs cutting the Corridor gabbro on McINTOSH and MOUNT REMARKABLE, in the western zone of the HCO. The clustering of plug-like and elongate dyke-like bodies is a characteristic feature of this group. They are not markedly metamorphosed and they probably post-date the ~1835 Ma Halls Creek Orogeny and the 1830 Ma group VI layered intrusions. There is no obvious concentric zonation of rock types and compositional layering is restricted to the Egg intrusion. All group VII intrusions have a distinctive 1–3 mm-thick black skin of 'lichen' (?cyanobacteria) on exposed surfaces. Group VII intrusions have limited economic potential because of their small size and limited range of composition.

Group VII intrusions described below are Black Hills Yard, Amphitheatre, and Egg.

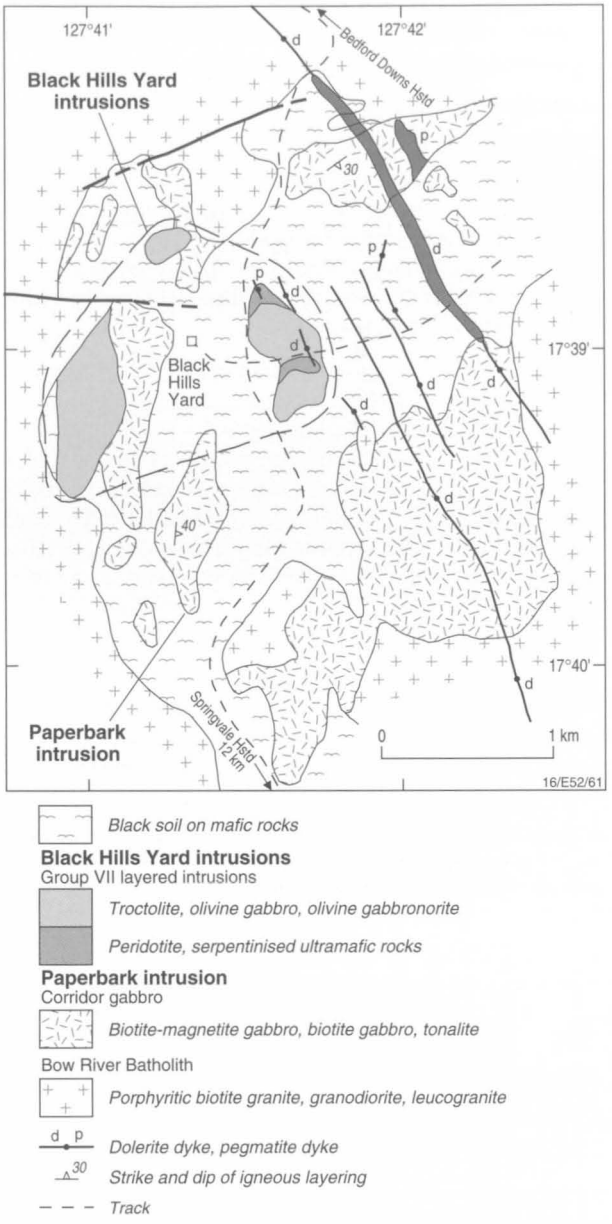


Figure 5.38. Geological map of the group VII Black Hills Yard mafic intrusions and the Paperbark mafic intrusion (Corridor gabbro).

Black Hills Yard mafic intrusions (29 in Fig. 5.1, Fig. 5.38)

Centre of intrusions. Central McINTOSH at AMG ~613481 and 602477.

Age. <?1830 Ma.

Form, structure, and areal extent. Three plug-like troctolite bodies near a north to northeast bend of the dyke-like Corridor gabbro; Subrounded body, 250 m wide, and two larger elongate bodies, up to 1 km by 400 m, form prominent black conical hills, ~60 m high (Fig. 5.2F).

Thickness. ?0.5 km.

Stratigraphy and main rock types. Massive troctolite and olivine gabbro with distinctive mottled and dimpled surface appearance, owing to large oikocrysts of plagio-

clase and preferential weathering of olivine; biotite-bearing variants are also locally prominent; some thin magnesite-altered peridotite units in easterly plug.

Relationships. Intrude biotite gabbro of the Paperbark intrusion (Corridor gabbro).

Petrography. Granular troctolite (oC) mesocumulates have cumulus olivine, oikocrysts of plagioclase, deep red-brown biotite anhedra enclosing rounded olivine grains, minor clinopyroxene and orthopyroxene, and trace amounts of disseminated subhedral chromite inclusions in olivine and clinopyroxene.

Geochemistry. A troctolite sample (92522517) has primitive characteristics (high $mg_{79.1}$, MgO–26.52%, and low P_2O_5 –0.06%, Y–10 ppm) and high Cr (3179 ppm) and low Al_2O_3 (5.11%) relative to troctolites in the older groups of intrusions; low S (280 ppm) and above background Pd (16.1 ppb), Pt (8.5 ppb), and Ni (851 ppm) concentrations indicate these plug-like bodies may have been derived from S-undersaturated sub-aluminous magmas.

Other comments. The Black Hills Yard intrusions may be rare examples of a S-undersaturated mafic body in the East Kimberley. Despite the favourable status of S saturation and the anomalous PGE concentrations, the small dimensions of these plug-like bodies downgrades their economic potential.

Amphitheatre mafic intrusion (17 in Fig. 5.1, Fig. 5.39)

Centre of intrusion. Southeastern MOUNT REMARKABLE at AMG ~811752.

Age. <?1830 Ma.

Form, structure, and areal extent. Irregular steeply plunging plug, 800 m by 200 m.

Thickness. 0.2 km.

Stratigraphy and main rock types. Massive troctolite and olivine gabbronorite are the dominant rocks; biotite-bearing variants are also locally prominent.

Relationships. Intrudes biotite gabbro and tonalite of the Corridor gabbro; separated by black soil plains from granite of the Koondooloo Monzogranite (Sally Downs supersuite).

Petrography. Troctolite consists of cumulus plagioclase (An_{56}) and olivine, with minor clinopyroxene, orthopyroxene, biotite, and trace apatite and zircon; chromite occurs as small sparse euhedral inclusions in olivine.

Geochemistry. In contrast to the Black Hills Yard intrusions, the high S (1280 ppm) content of a fractionated olivine gabbronorite ($mg_{61.8}$) suggests the Amphitheatre intrusion was derived from an evolved S-saturated mafic magma; high P_2O_5 (0.30%), Zr (109 ppm), and Cr (805 ppm) contents reflect the crystallisation of apatite, zircon, and chromite, respectively.

Other comments. Correlated with the Black Hills Yard and Egg intrusions on the basis of similar lithologies, small plug-like forms, and discordant relationships with the Corridor gabbro. One of the few intrusions in the East Kimberley occurring in granites of the ~1835–1805 Ma Sally Downs supersuite. Irregular black mafic bodies similar to the Amphitheatre intrusion are present throughout the co-mingled gabbro–granite terrains on MOUNT REMARKABLE (e.g. north of the Spring Creek intrusion), but have more fractionated compositions of olivine-free biotite–quartz diorite, biotite tonalite, and biotite gabbro.

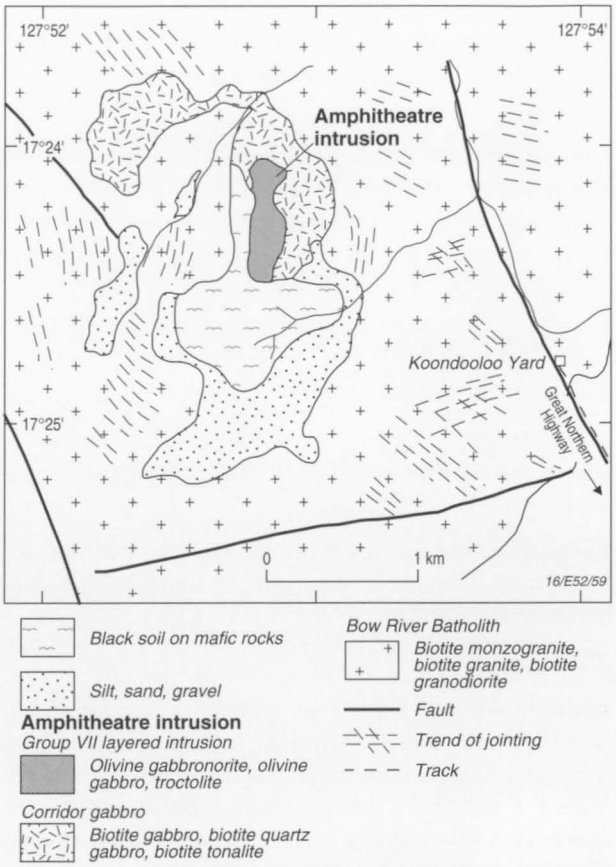


Figure 5.39. Geological map of the group VII Amphitheatre mafic intrusion.

Egg mafic intrusion (21 in Fig. 5.1)

Centre of intrusion. Central northern McINTOSH at AMG ~713613.

Age. <?1830 Ma.

Form, structure, and areal extent. Steeply plunging ovoid body, 1000 m by 700 m, which forms a distinctive black-capped hill about 50 m high.

Thickness. ?0.5 km.

Stratigraphy and main rock types. Olivine gabbro and troctolite are coated by a thin black skin of ?cyanobacteria and have a dimpled surface, similar to the other group VII intrusions; rare peridotite reported by Pickands Mather & Company International in 1968; gabbroic rocks are generally massive, but compositional rhythmic layering is present near the eastern margin.

Relationships. Intrudes contact between granite of the Togo Monzogranite (Paperbark supersuite) and gabbro of the Corridor gabbro; contact with the granite is masked by alluvium, and the western end of the intrusion is faulted, as indicated by magnesite veins up to 1 m thick in the more olivine-rich rocks, the abundance of fine-grained dolerite dykes, and intense shearing.

Other comments. Like other layered intrusions emplaced in granite of the Bow River Batholith (e.g. Springvale, Toby), the Egg intrusion is orientated at a high angle to the general north-northeast structural trend of the HCO. Another group VII intrusion occurs immediately southwest of the Egg intrusion. It is a narrow, 700 m long, northeast-trending dyke-like body of troctolite and olivine gabbro that cuts, and hence postdates, biotite gabbro of the Corridor gabbro.

Other layered mafic intrusions

Two large layered mafic bodies in the south of McINTOSH (Panton River and Three Sisters intrusions) have been classified as Undivided gabbro. Field relationships and geochemical evidence indicate that both intrusions could be similar in age or younger than the 1830 Ma group VI McIntosh intrusion.

Panton River mafic intrusion (42 in Fig. 5.1)

Centre of intrusion. Central McINTOSH at AMG ~720240.

Age. ?1830±3 Ma.

Form, structure, and areal extent. Fault-bounded mafic sheet, over 5 km by 8 km; restricted compositional range of gabbroic rocks suggests the intrusion is shallow dipping to sub-horizontal; gabbros typically form a northeast-trending series of parallel low ridges and valleys—in places a steeply dipping foliation (60–82°) in the gabbros is generally parallel to this northeast trend.

Thickness. ?2 km.

Stratigraphy and main rock types. Uralitised olivine gabbro, olivine gabbronorite, and leucogabbro are the major rock types; rafts of pelitic schist and gneissic metasediments (Tickalara Metamorphics) are locally intercalated with the gabbroic rocks.

Relationships. Faulted contacts with adjacent metasediments and amphibolite of the Tickalara Metamorphics, and granitic and gabbroic rocks of the Sally Downs supersuite.

Mineralisation. Some pods of massive limonitic gossan (up to 2 m wide and several hundred metres long) are associated with the metasedimentary rafts.

Three Sisters mafic intrusion (45 in Fig. 5.1)

Centre of intrusion. Southwestern McINTOSH at AMG ~520160.

Age. ?1830±3 Ma.

Form, structure, and areal extent. Northeast-trending elongate body, 10 km long and, locally, 2 km wide, along the southeastern side of the Springvale Fault; may extend southwest beneath black soil plains into HALLS CREEK; layering in gabbroic rocks dips 28–58° southeast.

Thickness. ?1.5 km.

Stratigraphy and main rock types. Mafic sequence of biotite gabbronorite, biotite quartz gabbro, leucogabbro, and minor anorthosite; rhythmic modal layering defined by alternating plagioclase and plagioclase–pyroxene layers is well developed in the upper parts of the mafic sequence—these rocks also show an igneous lamination, with plagioclase and pyroxene grains having a preferred crystallographic alignment parallel to the compositional layering; some low-angle cross bedding, comprising thin wispy plagioclase layers truncated by thicker plagioclase layers.

Relationships. Flanks the southeastern side of a series of aligned narrow ridges of quartz-veined siliceous rocks (called the Three Sisters) that define the Springvale Fault; porphyritic biotite granite of the Sally Downs supersuite and metavolcanics of the Tickalara Metamorphics are the major rocks along the irregular southeastern margin of the intrusion.

Petrography. Gabbroic rocks are equigranular (2–3 mm) adcumulates, containing cumulus sodic plagioclase, clinopyroxene, orthopyroxene, minor biotite, quartz, magnetite, ilmenite, apatite, and zircon; plagioclase grains are commonly strained and have lenticular albite twinning, quartz has undulose extinction, and many calcic exsolution lamellae in orthopyroxene are wavy, owing to deformation related to possible movement along the Springvale Fault.

Geochemistry. Gabbros have a wide range of $mg_{49–72}$, owing to variable amounts of pyroxene, but a restricted range of CaO (10.3–11.87%) and Na_2O (1.68–1.88%) related to the crystallisation of plagioclase; greater variations in TiO_2 (0.29–1.88%), P_2O_5 (0.01–0.4%), and Zr (12–177 ppm) reflect variable amounts of accessory Fe–Ti oxides, apatite, and zircon, respectively; high S contents (640–1490 ppm) for all rock types and low Pt (0.9 ppb), Pd (<0.5 ppb), and Au (2 ppb) for a magnetite gabbro sample (93522007) imply S-saturated magma conditions.

Corridor gabbro

The Corridor gabbro (Fig. 5.1) comprises many massive gabbroic and hybrid mafic intrusions of different ages on McINTOSH, MOUNT REMARKABLE, and TURKEY CREEK, in the western and central zones of the HCO. In these sheet areas it equates with many of the bodies shown as PgPog, PgPob, PgSog, and PgSob. It is the only group of mafic intrusions that crops out on both sides of the Springvale Fault, which forms the boundary between the western and central zones. The Corridor gabbro intrusions west of the Springvale Fault are coeval with or younger than enclosing granites of the ~1865–1850 Ma Paperbark supersuite, whereas those east of the fault are coeval with or younger than enclosing granites of the ~1835–1805 Ma Sally Downs supersuite. Thus, the Corridor gabbro consists of two major geographical and temporal groups of mafic intrusions

that collectively range in age from about 1865 to 1800 Ma.

The Corridor gabbro intrusions typically are long dyke-like mafic bodies that have northeast to north trends that are parallel or sub-parallel to the Springvale and Greenvale Faults. Many of the bodies have intruded different fault splays related to these major fault systems. In the western zone on McINTOSH, they form laterally continuous bodies for 70 km along a narrow corridor (hence their name) between granite plutons of the Paperbark supersuite, and they appear to cut the eastern part of the 1857 Ma Springvale intrusion of group II. The Corridor gabbro intrusions can be broadly subdivided on the basis of their aeromagnetic signature, which varies from strong to weak and reflects variable amounts of disseminated magnetite. In the north, intrusions lie along major faults, boundaries between plutons of the Paperbark and Sally Downs supersuites, and contacts between the Sally Downs supersuite plutons and Tickalara Metamorphics.

The Corridor intrusions contain a variety of fractionated and contaminated medium-grained massive gabbroic and hybrid mafic rocks, such as magnetite gabbro, magnetite–biotite gabbro, biotite quartz gabbro, quartz gabbro, biotite tonalite, diorite, and mixtures of gabbroic and granitic rocks. Most bodies are massive with rhythmic compositional layering and igneous lamination restricted to the Paperbark, Billymac Yard, and Faulted intrusions. Intergranular and porphyritic textures predominate, and net-veining, magma mingling, and heterogeneous hybrid rocks (see Contact relationships on page 152) are commonly developed at contacts with granite. Quartz is a common accessory mineral in those intrusions emplaced into quartz-bearing paramigmatites rather than into granites. Evolved hybrid compositions and magma mingling relationships indicate extensive contamination of the mafic parent magmas of the Corridor gabbro by felsic crustal rocks.

Billymac Yard mafic intrusion (27 in Fig. 5.1)

Centre of intrusion. Central McINTOSH at AMG ~637499.

Age. ?1865–1850 Ma.

Form, structure, and areal extent. Northeast-trending elongate body, 6 km by 1 km, dipping southeast at 40–58°.

Thickness. ?0.5 km.

Stratigraphy and main rock types. Equigranular massive magnetite gabbro, biotite gabbro, and biotite gabbronorite are prominent, with leucogabbro, norite, and rare anorthosite forming low rubbly hills at the northeastern end of the intrusion—these more felsic rocks display rhythmic compositional layering defined by alternating plagioclase–pyroxene and plagioclase layers, 1–5 cm thick; companies (see Chapter 2) have also reported thin lenses of pyroxenite and peridotite in the gabbro, and an upper foliated gabbroic sequence containing coarse (up to 1 cm) biotite and abundant (5%) disseminated ilmenite and magnetite grains.

Relationships. Outcrop is restricted to the northwestern side of the intrusion, where biotite granites of the Paperbark Granite and Sandy Dam Monzogranite (both Paperbark supersuite) are the major country rocks; contacts with these felsic rocks are generally covered by alluvium; several northwest-trending dolerite and pegmatite dykes cut the intrusion.

Mineralisation. Lewis (1992) described ferruginous gossans and malachite-stained norite 100 m south of the northwestern contact between the intrusion and the granite (see Chapter 2); cellular limonitic gossans, exposed discontinuously over 2 km, are associated with extensive magnetite-rich segregations in the gabbros and with apophyses of granitic rocks.

Other comments. The Billymac Yard intrusion is one of the few Corridor gabbro bodies that contains an extensive sequence of rhythmically layered gabbroic rocks. Abundant magnetite in these rocks produces one of the most intense aeromagnetic signatures of all intrusions on McINTOSH.

Faulted mafic intrusion (1 in Fig. 5.1, Fig. 5.28)

Centre of intrusion. Northwestern TURKEY CREEK at AMG ~116142.

Age. ?1835–1805 Ma.

Form, structure, and areal extent. Basin, 2 km by 4 km; rare compositional layering and igneous laminations generally dip steeply inwards (65–85°), but some subvertical outward dips near margins; steeply dipping garnet-bearing paramigmatite country rocks are generally concordant with the basin; several faults of various orientations cut the intrusion, including a sinistral fault (hence the name of the intrusion), which displaces the eastern part of the intrusion 500 m to the north.

Thickness. 1.4 km.

Stratigraphy and main rock types. Homogeneous sequence of fine-grained (1–2 mm) equigranular biotite gabbronorite, magnetite–biotite gabbronorite, biotite gabbro, and biotite quartz gabbro.

Relationships. Intrudes paramigmatite of the Tickalara Metamorphics and irregular bodies of biotite granite of the Magotty Springs Monzogranite (Sally Downs supersuite); cut by aplite, quartz, and other felsic dykes in the western half of the intrusion.

Petrography. Gabbroic rocks contain small squat plagioclase laths, uralitised granular clinopyroxene, prismatic orthopyroxene with fine exsolution lamellae of Ca-pyroxene, red-brown biotite, disseminated Fe–Ti oxides, strained interstitial quartz, and minor apatite and zircon; quartz content (up to 8 vol. %) increases towards contacts with Tickalara Metamorphics, probably due to contamination.

Geochemistry. Fractionated gabbroic rocks with variable composition ($mg_{50.2-70}$, 6.90–13.51% MgO, 0.21–1.11% TiO_2, 0.03–0.47% P_2O_5, 341–1252 ppm Cr, 10–79 ppm Zr); absence of marked systematic trends up the sequence and variable compositions may be due to

contamination of magma by country rocks; high S (840–2090 ppm) and low Cu (<50 ppm) and Ni (<147 ppm) contents indicate S-saturated conditions.

Greenvale Fault mafic intrusion (11 in Fig. 5.1, Fig. 5.14)

Centre of intrusion. Southwestern MOUNT REMARKABLE at AMG ~560710 (intrusion extends southwards into McINTOSH).

Age. ?1865–1850 Ma.

Form, structure, and areal extent. Irregular mafic body, generally less than 3 km wide, extending 28 km northwards from the Toby intrusion on McINTOSH to north of the group II Foal Creek intrusion on MOUNT REMARKABLE.

Thickness. Unknown.

Stratigraphy and main rock types. Biotite gabbro, biotite quartz gabbro, tonalite, various mixed mafic–felsic rocks, and associated extensive black soil plains; weak aeromagnetic signature indicates gabbros have low magnetite content.

Relationships. Faulted (Greenvale Fault) against felsic rocks of the Whitewater Volcanics to the west and inferred to intrude granite plutons of the Paperbark supersuite to the east because of the presence of net-veining complexes and magma mingling.

Petrography. Generally fine to medium-grained equigranular and subophitic massive gabbros, containing tabular plagioclase, subhedral clinopyroxene, and lesser orthopyroxene; abundant accessory biotite, magnetite–ilmenite, quartz, zircon, and apatite indicate evolved composition.

Geochemistry. Most rocks have a similar evolved composition ($mg_{55.4–63.5}$, 49.01–51.76% SiO_2, 6.90–8.24% MgO, 0.68–1.17% TiO_2, 0.08–0.15% P_2O_5, 181–497 ppm Cr, 58–118 ppm Zr, 180–1180 ppm S) to the more fractionated gabbros of the Faulted intrusion.

Juries mafic intrusion (28 in Fig. 5.1)

Centre of intrusion. Northwestern McINTOSH at AMG ~555474.

Age. ?1865–1850 Ma.

Form, structure, and areal extent. Irregular sheet-like body intercalated with granite over an area of 3 km by 4 km.

Thickness. ?1 km.

Stratigraphy and main rock types. Northern part consists of fine-grained homogeneous massive gabbro with irregular blocks of porphyritic biotite granite; the middle part is represented by shallow sands and black soils; and the southern arcuate part consists of discontinuous outcrops of massive gabbro interspersed with thin sheets of granite; in contrast to other Corridor gabbro intrusions, magnetite gabbro and biotite gabbro are minor components of the Juries intrusion.

Relationships. Classic net-veined complexes, especially in northeast, indicate gabbro was emplaced at same time, or later than, associated granite of the Paperbark Granite (Paperbark supersuite).

Mineralisation. Secondary copper carbonates locally present in narrow (<1 m wide) shear zones in gabbro near the northeastern corner of the intrusion.

Mabel Downs West mafic intrusion (2 in Fig. 5.1, Fig. 5.28)

Centre of intrusion. Central western TURKEY CREEK at AMG ~038014.

Age. ?1835–1805 Ma.

Form, structure, and areal extent. Irregular ovoid mafic body, 1.5 km by 2.2 km.

Thickness. ?1 km

Stratigraphy and main rock types. Massive fine to coarse-grained equigranular to porphyritic biotite gabbro, biotite–magnetite gabbro, biotite–magnetite gabbronorite, and biotite tonalite.

Relationships. Surrounded by foliated biotite granites of the Magotty Springs Monzogranite (Sally Downs supersuite) with contacts often masked by alluvium; chilled zone, 2 m wide, (Fig. 5.28) of uralitised subophitic biotite gabbro occurs at the contact with foliated porphyritic granite on the southwestern side of the intrusion.

Petrography. Highly evolved composition of the gabbros is indicated by inverted pigeonite and lesser clinopyroxene anhedra moulded around tabular sodic plagioclase laths, and abundant brown biotite, and accessory Fe–Ti oxides, quartz, and apatite.

Geochemistry. Gabbros have evolved composition ($mg_{45.2–47.2}$, 45.4–50.22% SiO_2, 6.34–7.11% MgO, 0.14–0.23% P_2O_5, 48–88 ppm Zr, 130–2040 ppm S) typical of the Corridor gabbro intrusions; high TiO_2 (1.97–4.72%) contents indicate abundant Fe–Ti oxides; chilled magnetite gabbro has similar SiO_2 (47.63%), MgO (7%), and TiO_2 (2.01%), but slightly higher P_2O_5 (0.41%) and Zr (114 ppm) contents compared with the coarser-grained gabbros.

Margaret River mafic intrusion (44 in Fig. 5.1)

Centre of intrusion. Southwestern McINTOSH at AMG ~438133.

Age. ?1865–1850 Ma.

Form, structure, and areal extent. Series of northeast-trending elongate outcrops, 1 km by up to 4 km, that parallel the nearby Springvale Fault to the east; may be the southwestern extension of the Corridor gabbro forming the Paperbark intrusion.

Thickness. Unknown.

Stratigraphy and main rock types. Poorly exposed gabbroic rocks (partly concealed by black soil plains).

Relationships. Intrudes pelitic metasediments of the Marboo Formation and granite of the Paperbark supersuite.

Nine Mile mafic intrusion (5 in Fig. 5.1)

Centre of intrusion. Central eastern MOUNT REMARKABLE at AMG ~920955 (intrusion extends eastwards into TURKEY CREEK).

Age. ?1835–1805 Ma.

Form, structure, and areal extent. Poorly exposed ?steeply dipping elongate body covering 2.5 km by 8 km; exposed as isolated outcrops on sand and black soil plains.

Thickness. ?2 km.

Stratigraphy and main rock types. Medium-grained magnetite gabbro and magnetite–biotite gabbro; an intense magnetic signature indicates that magnetite gabbros underlie the shallow alluvium cover.

Relationships. Intrudes regional contact between metasediments of the Tickalara Metamorphics and granites of the Sally Downs supersuite; large rafts of both these rock types are present near the centre of the intrusion.

Petrography. Equigranular gabbros are composed of tabular plagioclase laths enclosed by late-crystallising uralitised clinopyroxene, and abundant magnetite–ilmenite anhedra.

Geochemistry. Single gabbro sample (94522129) has similar evolved composition ($mg_{51.1}$, 48.05% SiO_2, 5.88% MgO, 1.26% TiO_2, 0.05% P_2O_5, 180 ppm Cr, 29 ppm Zr, 1300 ppm S) to gabbro of the Faulted and Greenvale Fault intrusions.

Paperbark mafic intrusion (31 in Fig. 5.1, Fig. 5.38: not to be confused with the Paperbark supersuite of the Bow River Batholith)

Centre of intrusion. Central McINTOSH at AMG ~618397.

Age. ?1865–1850 Ma.

Form, structure, and areal extent. Over 90% of this north-trending, 1–3 km wide, dyke-like intrusion, which extends 11 km north from near Paperbark Dam to Black Hills Yard, is covered by sandy alluvium derived from the granites of the Paperbark supersuite on both sides of the intrusion, and by black soils derived from the mafic rocks.

Thickness. ?0.5 km.

Stratigraphy and main rock types. Medium-grained equigranular massive gabbro, biotite gabbro, biotite–magnetite gabbro, biotite quartz gabbronorite, and various hybrid mafic rocks; prominent aeromagnetic signatures reflect the abundant magnetite content of the gabbros; the magnetite forms disseminated grains and rare thin segregated layers in the fractionated gabbros.

Relationships. Intrudes contact between the Paperbark Granite and Sandy Dam Monzogranite, both of the Paperbark supersuite.

Petrography. Red-brown anhedral plates of biotite, up to 5 mm across, containing magnetite–ilmenite, plagioclase, and apatite inclusions characterise the gabbroic rocks; intergranular textures are defined by compositionally zoned sodic plagioclase laths partly enclosing similar amounts of anhedral clinopyroxene and orthopyroxene, strained quartz, and minor apatite and zircon.

Geochemistry. Similar evolved composition ($mg_{58.3}$, 51.43% SiO_2, 7.78% MgO, 1.08% TiO_2, 0.32% P_2O_5, 451 ppm Cr, 196 ppm Zr, 740 ppm S) to the other intrusions in this group (Nine Mile, Greenvale Fault, Faulted)

Sandy Creek mafic intrusion (23 in Fig. 5.1)

Centre of intrusion. Central northern McINTOSH at AMG ~685575.

Age. ?1865–1850 Ma.

Form, structure, and areal extent. Elongate mafic body, 14 km long, which extends north of the Billymac Yard intrusion, past the Egg intrusion, to become a broader irregular body in the south of MOUNT REMARKABLE; strong linear aeromagnetic anomalies further north along strike from the Sandy Creek intrusion indicate that this part of the Corridor gabbro may extend a further 25 km to the centre of MOUNT REMARKABLE; width of the intrusion varies from less than 0.5 km to over 5 km; partly bounded by north-trending splays off the Springvale Fault.

Thickness. ?1 km.

Stratigraphy and main rock types. Rock types are similar to those in the Paperbark intrusion, with massive sericitised biotite gabbro, biotite gabbronorite, and various hybrid mafic rocks prominent; there is a marked decrease in magnetite content of these equigranular gabbros compared to the rocks in the contiguous Billymac Yard intrusion; aeromagnetic signature of the southern part of the Sandy Creek intrusion is relatively featureless, with small local aeromagnetic highs restricted to the area north of the crosscutting group VII Egg intrusion.

Relationships. Intrudes contact between the Paperbark Granite and Togo Monzogranite, both of the Paperbark supersuite; irregular western contact with the granites contrasts with the straighter, partly faulted eastern contact.

Other comments. Similar geological setting to the Margaret River, Paperbark, and Billymac Yard intrusions.

Turkey Creek microgabbro–norite

Fine-grained massive gabbroic rocks of the Turkey Creek microgabbro–norite are restricted to the southern parts of TURKEY CREEK and MOUNT REMARKABLE (Fig. 5.1). Previously classified the 'Younger Norite Suite' by Thornett (1981, 1986), the Turkey Creek microgabbro–norite intrudes group V layered intrusions,

the upper part of the Norton metagabbro intrusion, and hybrid gabbroic rocks of the Corridor gabbro. In the Sally Malay intrusion, it intrudes the contact between two megacyclic mafic–ultramafic units in subchamber A, and in the Dave Hill intrusion it is closely associated with peridotite lenses (Fig. 5.20). The crosscutting relationships with these group V intrusions constrain the maximum emplacement age of the Turkey Creek microgabbro–norite to ~1845 Ma. It is also cut by aphanitic and amphibole-spotted doleritic and felsic dykes, larger ovoid bodies of leucogranite, and veins of aplite, and pegmatite. Some of the granitic bodies may belong to the ~1835–1805 Ma Sally Downs supersuite.

The Turkey Creek microgabbro–norite typically forms irregular elongate bodies with arcuate boundaries. The type example occurs in creek exposures through hilly terrain southwest of the Wilson Creek intrusion (MOUNT REMARKABLE at AMG ~918738). Its most distinctive features are the fine grain size (<2 mm and generally <1 mm) and its fawn brown to dark brown rounded bouldery outcrop. Compositional layering is absent, and except for foliated and recrystallised variants in mylonite zones, it is generally massive. Dominant rock types include subophitic to equigranular biotite and/or quartz-bearing gabbro, gabbronorite, and norite. On the southwestern side of the Wilson Creek intrusion are small rounded pillows of fine-grained gabbro of the Turkey Creek microgabbro–norite hosted by medium-grained gabbro (group V intrusions?).

Metagabbros of the Tickalara Metamorphics

Norton metagabbro intrusion (6 in Fig. 5.1, Fig. 5.26)

Centre of intrusion. Central western TURKEY CREEK at AMG ~985950.

Age. ?1850 Ma.

Form, structure, and areal extent. North-northeasterly-trending mafic body, 9 km long by 1.5 km wide.

Thickness. 1 km.

Stratigraphy and main rock types. Mafic granulites show little variation in composition across the intrusion with hornblende metagabbro and hornblende–magnetite metagabbronorite the most common rock types; rare preserved primary compositional layering in the granulites is generally steeply dipping and parallel to a pervasive metamorphic foliation defined by the crystallographic alignment of pyroxene and amphibole.

Relationships. Intrudes garnet-bearing paramigmatites of the Tickalara Metamorphics; intruded by Turkey Creek microgabbro–norite.

Mineralisation. Basal 80 m of the mafic sequence exposed in the northwest of the intrusion contains a cluster of subparallel ferruginous gossans, which persist intermittently along strike for 6.5 km; in places, thin gossanous veins also cut the footwall paramigmatite, indicating some later remobilisation of the sulphides; the gossans consist of goethite, hematite, traces of magnetite and/or maghemite, quartz, and montmorillonite; maximum Ni and Cu concentrations in two analysed gossan samples of 79 ppm and 139 ppm, respectively, indicate either that the gossans were derived from the oxidation

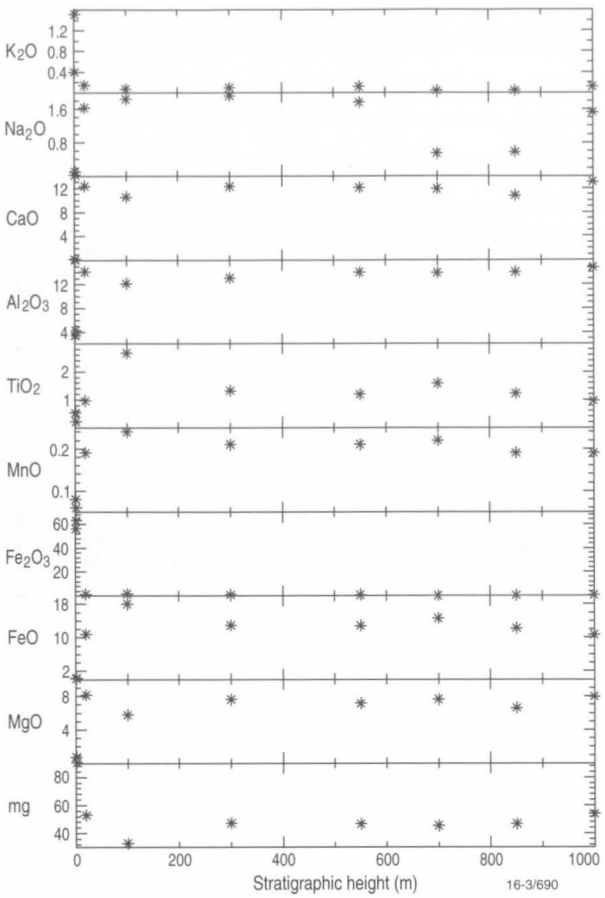


Figure 5.40. Norton intrusion: variation in whole-rock major-element composition (in wt. %) of mafic cumulates with stratigraphic height.

of disseminated Ni–Cu-poor, Fe-rich sulphide assemblages (e.g. pyrite and/or pyrrhotite) or that any base metals originally present have been leached by acidic ground water; Gindalbie Gold NL obtained anomalous Ni (980 ppm) and Cu (580 ppm) concentrations from rock samples and coarse detrital platinum (1.5 ppm) from stream-sediment samples (see Chapter 2); lateral continuity and basal contact setting of the gossans and the proximity of similar Ni–Cu prospects indicate that the Norton intrusion has potential for basal segregations of Ni–Cu–Co sulphide mineralisation—most prospective parts are considered to be embayments in the footwall contact (where sulphides may accumulate by gravitational and/or thermal erosion/contamination processes) in the central part of the intrusion, where the overlying cumulate sequence is thickest; however, the thinness and very long strike extent of the gossans may indicate that favourable basal structural traps for the concentration of massive sulphides were not present.

Petrography. Mafic rocks metamorphosed to granulite facies, with recrystallised khaki green-brown hornblende, orthopyroxene, clinopyroxene, and plagioclase showing foliated equigranular and granuloblastic polygonal textures—this contrasts with the amphibolite facies group V intrusions nearby, which typically contain abundant olivine, have well-preserved cumulus igneous textures, and contain massive sulphides, which show little evidence of recrystallisation; accessory minerals are apatite, magnetite, ilmenite, and disseminated sulphides.

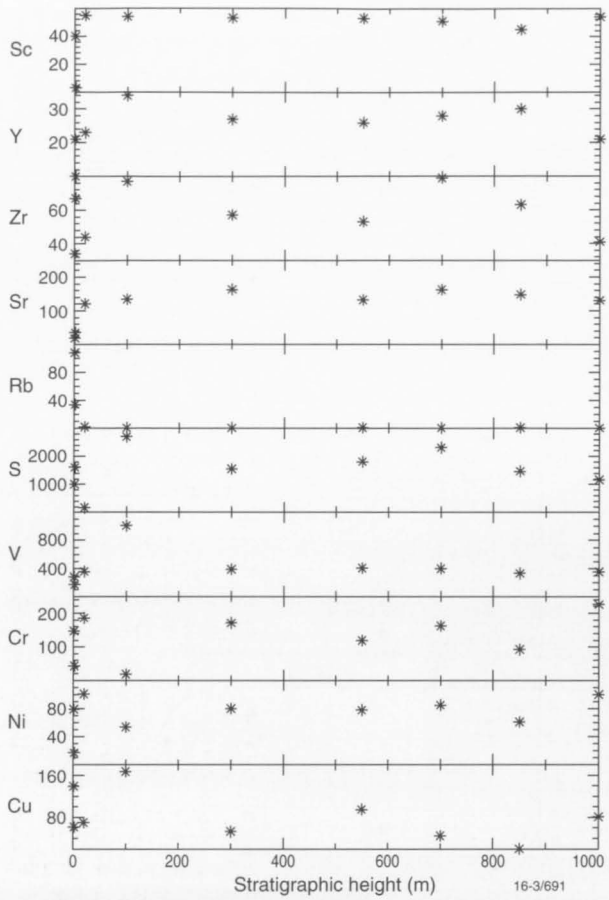


Figure 5.41. Norton intrusion: variation in whole-rock trace-element composition (in ppm) of mafic cumulates with stratigraphic height.

Geochemistry. Fairly flat fractionation trends, with most metagabbros up the stratigraphy having a restricted range of mg (48.4–55.5), MnO (0.19–0.22%), Al_2O_3 (13.04–14.80%), CaO (10.75–13.07%), Sr (121–163 ppm), Zr (41–79 ppm), and Sc (45–55 ppm) (Figs 5.40, 5.41); the exceptionally low mg values are typical of mafic granulite intrusions in the Tickalara Metamorphics—these, with the Corridor gabbro, represent some of the most evolved compositions documented for gabbros in this study; another characteristic feature of the metagabbros is their low Ba (<4–23 ppm) content; Cu, Ni, and V show local enrichment towards the basal contact and high S concentrations (1160–2700 ppm) throughout the intrusion indicate S-saturated conditions.

Other comments. The Norton intrusion is the largest mafic body assigned to the Tickalara Metamorphics investigated in this study. Considered to be older than the 1845 Ma group V intrusions, since it predates granulite metamorphism of the Tickalara Metamorphics at about 1850 Ma. The absence of ultramafic cumulates does not downgrade the economic potential of the body, as thick olivine-rich sequences are also absent from nearby Corkwood and Keller Creek Ni–Cu prospects, and the host rocks to some of the largest magmatic Ni–Cu deposits in the world, such as the Sudbury deposit in Ontario and Voisey's Bay in Canada, are dominantly mafic rather than ultramafic.

Typical field relationships of the layered intrusions

Contact relationships

The East Kimberley layered intrusions display a range of contact relationships (Figs 5.42–5.44) that indicate they were emplaced in situ (Hoatson & Tyler 1993) rather than being emplaced tectonically by thrusting (Hancock & Rutland 1984). Those emplaced into metasediments of the Tickalara Metamorphics and the Koongie Park Formation in the central zone and into granites in the western zone of the HCO have: thin chilled and contaminated margins, narrow contact aureoles, ribbon-like comagmatic satellite intrusions, and net-vein complexes indicating mingling of mafic and felsic magmas. The type of contact is largely related to the composition of the country rock, and is independent of magma type and depth of emplacement.

Chilled margins up to 10 m wide have been recognised around the Fletcher Creek, Mabel Downs West, McIntosh, Panton, Spring Creek, Wilagee, and Wild Dog Creek intrusions. Fine-grained (0.1–0.4 mm) quartz hornblende gabbro, hornblende gabbronorite, magnetite gabbro, and doleritic gabbro are the major rock types found in the chilled margins. They have fractionated compositions, indicating that they have been extensively altered by fluid activity and/or SiO_2 contamination from the country rocks. Contaminated porphyritic harzburgite containing large poikilitic orthopyroxene is largely restricted to basal contacts of group I and group V intrusions. The crystallisation of orthopyroxene at the expense of olivine in these rocks was probably initiated by SiO_2 contamination of the primitive magma by the country rocks.

Contact aureoles up to 50 m wide are largely restricted to those 'hotter' intrusions containing an ultramafic component (Panton, Sally Malay) or a thick mafic sequence (McIntosh). Alkali feldspar–plagioclase–cordierite–garnet–quartz-bearing pelitic migmatites containing late-crystallising sillimanite overprinting andalusite occur in a contact aureole, 10–50 m wide, along parts of the northwestern contact of the Panton intrusion. Local remelting of country rock migmatites below the base of the Sally Malay intrusion has resulted in the formation of felsic net-vein complexes rich in alkali-bearing minerals. Partially melted migmatite fragments and resorbed garnet and cordierite xenocrysts from the country rocks also occur in the basal mineralised rocks. 'Blow-torch' type contact paramigmatites (see Figs 5.45A, 6.7) characterise the northwestern contact aureole of the McIntosh intrusion.

In contrast to the central zone, most mafic intrusions in the western zone are associated with granite plutons of the 1865–1850 Ma Paperbark supersuite. U–Pb geochronology and field relationships indicate that the groups II and III mafic intrusions are coeval or younger than most adjacent granite intrusions and, consequently, there are many types of contact relationships related to magma mixing processes that occurred at high levels in the crust (Blake & Hoatson 1993, Sheppard 1996).

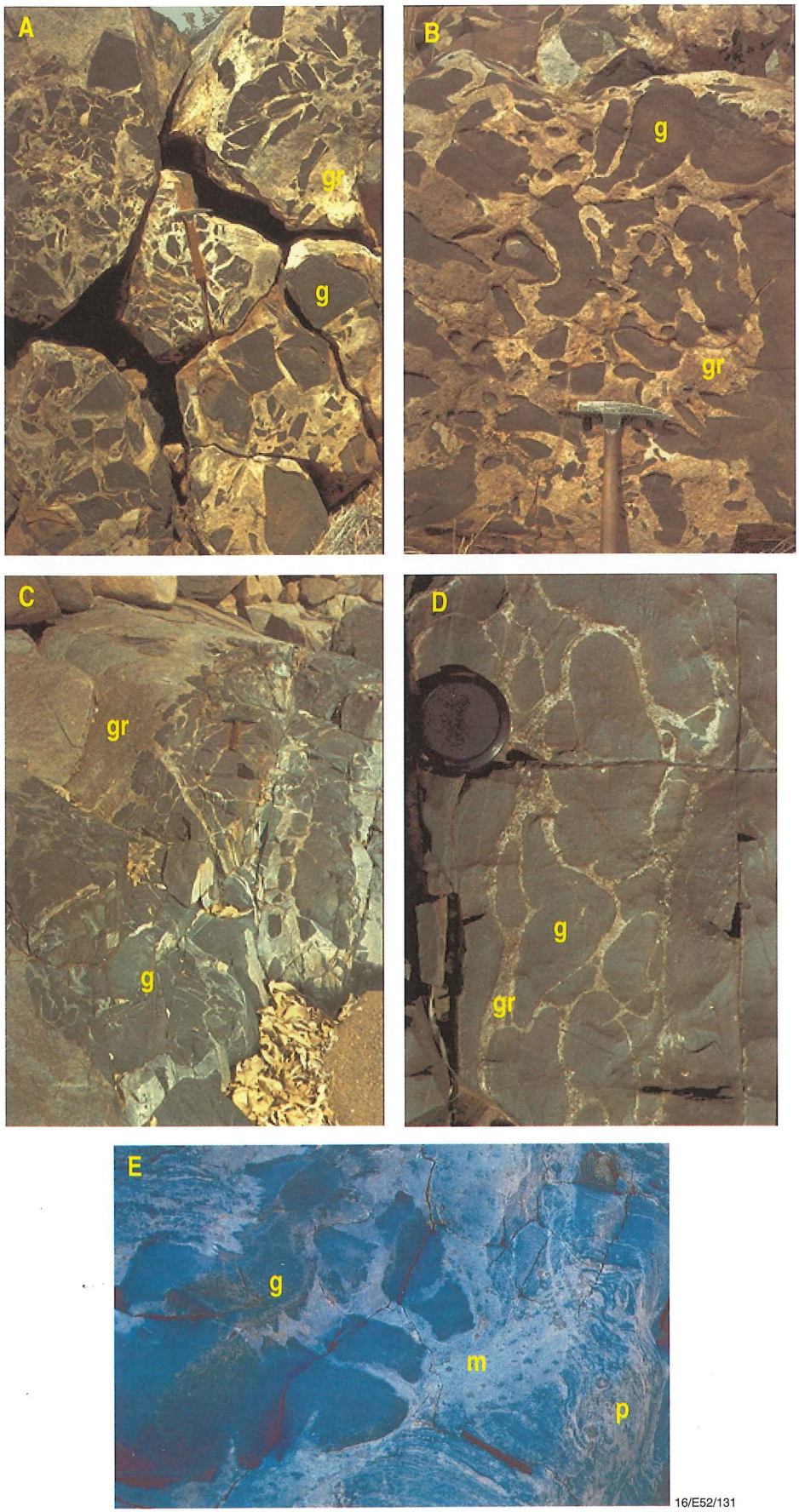


Figure 5.42. Contact relationships of mafic and felsic magmas.

A. Angular fragments of mafic rocks (g) enclosed in leucogranite (gr), Greenvale Fault mafic intrusion (MOUNT REMARKABLE AMG ~636903).

B. Concentration of irregular pillow-like mafic inclusions (g) in granite (gr), Toby mafic intrusion (McINTOSH AMG ~585514).

C. Closely spaced rounded mafic pillows (g) forming 1.5 m wide dyke that intruded granite (gr), which it partially melted and formed interstitial microgranite, Greenvale Fault mafic intrusion (MOUNT REMARKABLE AMG ~646918).

D. Enlargement of middle part of dyke in C, showing rounded mafic pillows (g) and interstitial microgranite (gr).

E. Dismembered mafic body (g) that has partially melted stromatic paramigmatite (p) to form a felsic leucosome-rich contact migmatite (m), Fletcher Creek, ~3 km east of the Keller Creek mafic intrusion (photograph by N. Oliver, James Cook University).

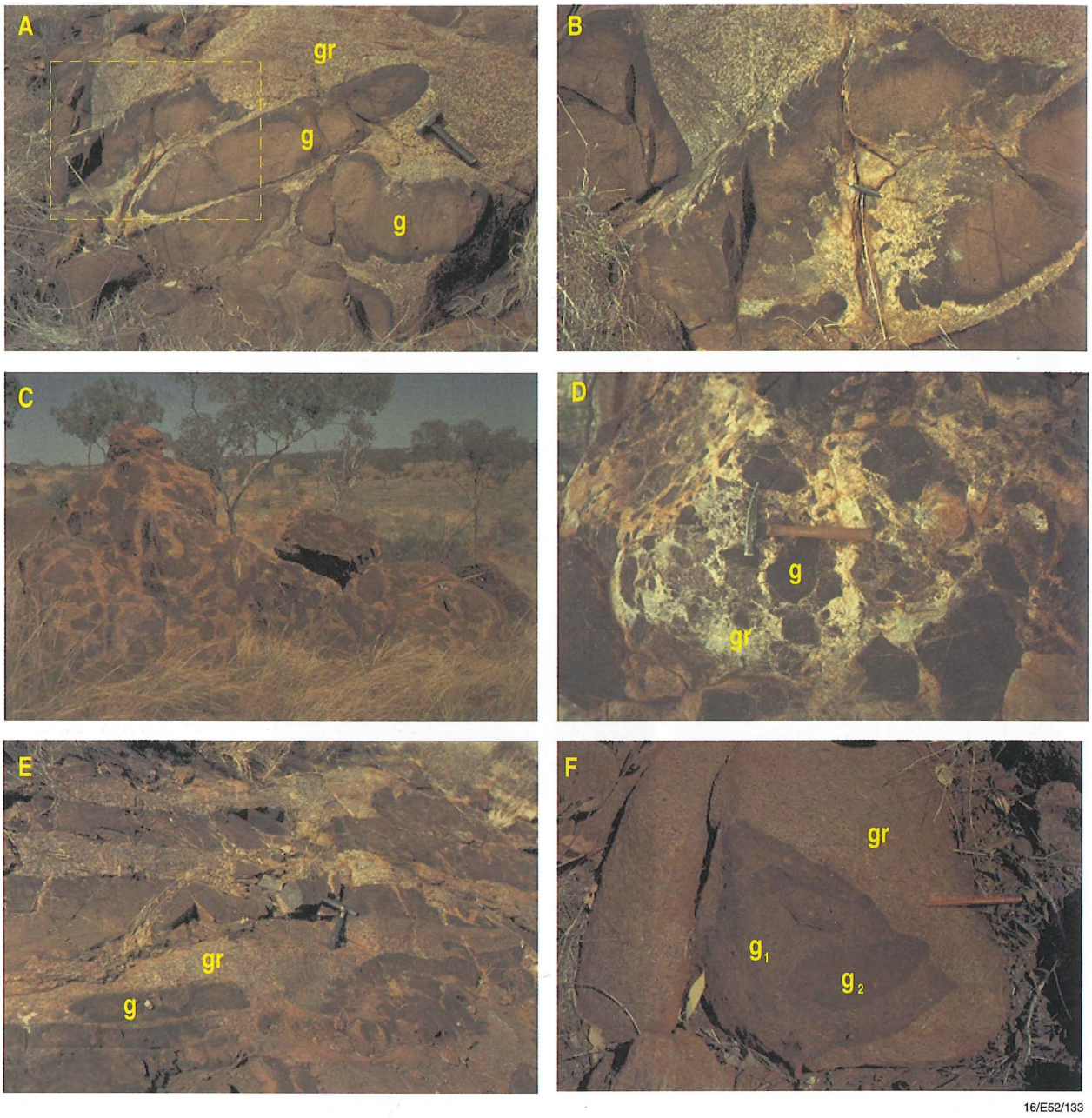


Figure 5.43. Contact relationships of mafic and felsic magmas.

A. Ellipsoidal mafic pillows (g) with dark biotite-rich margins in partly hybridised granite (gr), Juries mafic intrusion (McINTOSH AMG ~576476).

B. Enlargement of top left part of A, showing intricate cuspate contacts, indicative of liquid–liquid relationships between mafic pillows and enclosing granite.

C. Concentration of mafic pillows in coarse-grained granite near Shepherds Bore (photograph by D. Blake, AGSO: HALLS CREEK AMG ~542910).

D. Concentration of closely spaced mafic enclaves (g), showing various stages of assimilation in leucogranite (gr) at the southeastern margin of the Toby mafic intrusion (McINTOSH AMG ~598526).

E. Stacked composite sequence of pillow-like mafic sheets with biotite-rich margins intrusive into coarse-grained granite, Greenvale Fault mafic intrusion (MOUNT REMARKABLE AMG ~669779).

F. Angular composite enclave of hybrid diorite (g_1) containing a more mafic enclave (g_2) in leucogranite (gr) at the southeastern margin of the Toby mafic intrusion (photograph by D. Blake, AGSO: McINTOSH AMG ~589515).

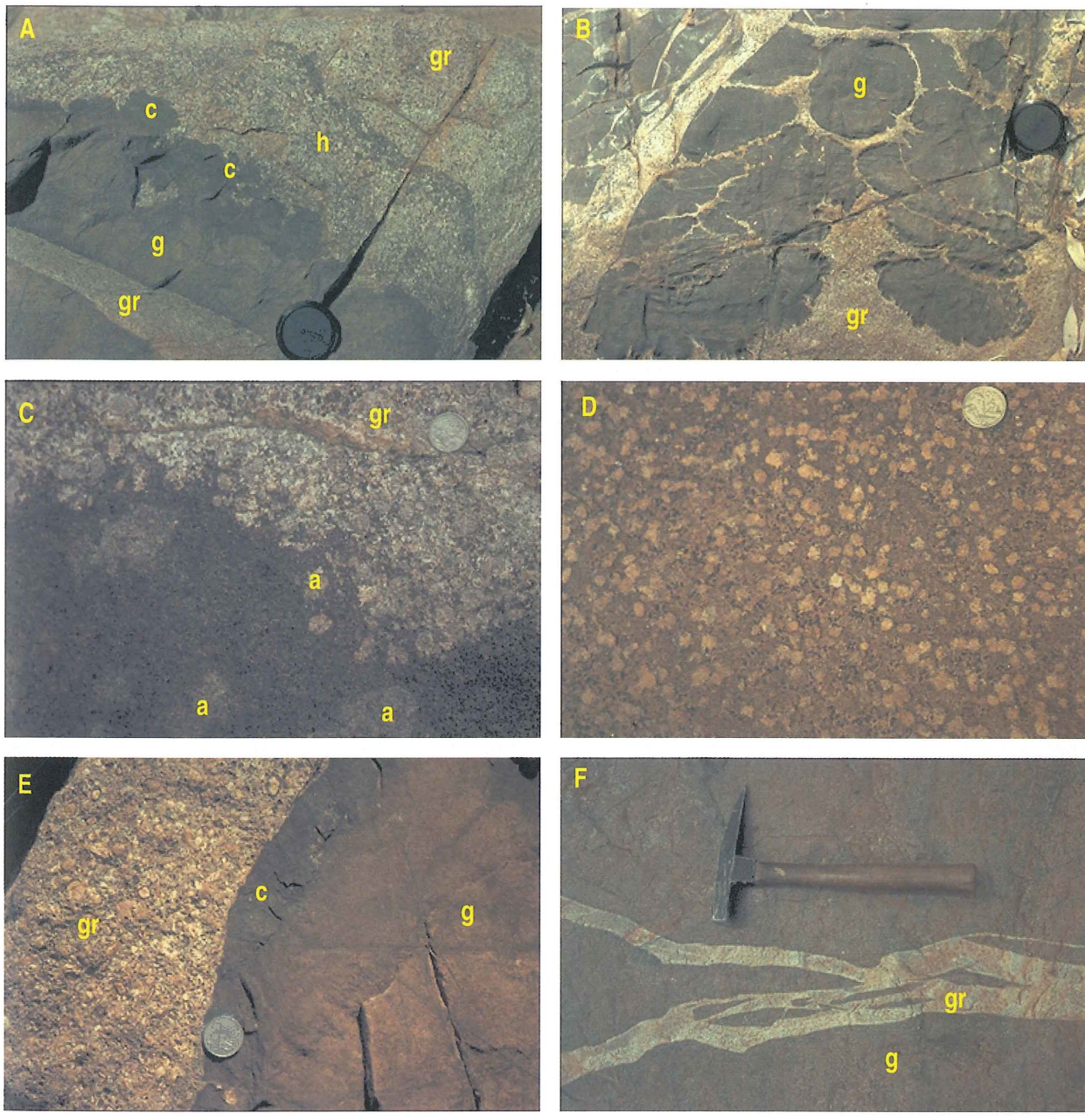


Figure 5.44. Contact relationships of mafic and felsic magmas.

A. Heterogeneous hybrid rock (h) between a mafic pillow (g) with biotite-rich crenulate to cuspate margins (c) and medium-grained biotite granite (gr). A vein of fine-grained granite (gr) cuts the pillow at the bottom left corner, Greenvale Fault mafic intrusion (MOUNT REMARKABLE AMG ~646918).

B. Rounded and subrounded mafic pillows (g) with highly irregular crenulate to cuspate margins, in granite (gr), and, to left, cross-cutting veins of leucogranite, Greenvale Fault mafic intrusion (MOUNT REMARKABLE AMG ~646918).

C. Irregular contact between coarse-grained biotite granite (gr) and massive biotite quartz gabbro of the Paperbark mafic intrusion. The quartz gabbro contains red biotite and partly resorbed alkali feldspar crystals (a) derived from the granite (McINTOSH AMG ~610488).

D. Homogeneous hybrid biotite diorite with abundant partly resorbed alkali feldspar phenocrysts at the contact between gabbro of the Paperbark mafic intrusion and coarse-grained granite (McINTOSH AMG ~629469).

E. Fine-grained massive biotite gabbro (g) with dark biotite-rich chilled margin (c) in contact with medium-grained porphyritic granite (gr) near the southwest side of the Toby mafic intrusion (McINTOSH AMG ~532517).

F. Fine-grained leucogranite (gr) veins cutting medium-grained massive gabbro (g), Toby mafic intrusion (McINTOSH AMG ~600563).

Magma mixing is a progressive process, which commences with the physical interaction or mingling of two magmas, where both components are still recognisable, and ends when the different components lose their identity during mixing and become a homogeneous hybrid magma (Metcalf et al. 1995, Weinberg 1997). Magma mixing features at the margins of the East Kimberley intrusions (Figs 5.42–5.44) include small irregular globular-shaped mafic enclaves in granitic rocks, small-scale streaky magma mingling on a millimetre to centimetre scale, net-vein complexes up to 100 m wide, comprising complete or fragmented rounded mafic pillows on a metre scale, which have curvilinear to cuspate and contaminated chilled margins, and homogeneous hybrid tonalitic and dioritic rocks that contain abundant biotite and partly resorbed ovoid phenocrysts of alkali feldspar. These hybrid rocks, which represent the end member of the mixing process, are enriched in SiO_2, Fe_2O_3, Na_2O, K_2O, Ba, Rb, Zr, Y, and light rare-earth elements La, Ce, Pr, and Nd compared with adjacent gabbro. The mixing features are associated with group III (Toby) and Corridor gabbro (Greenvale Fault, Juries, Paperbark) intrusions emplaced in granites of the Paperbark supersuite and group VI (Armanda) intrusions emplaced in felsic rocks of the Koongie Park Formation. The mingling and net-vein complexes have been described in detail by Blake & Hoatson (1993), Sheppard (1996), and Sheppard et al. (1997).

There are also many examples where layered intrusions are cut by much younger granite. In such cases, the granite cuts across layering and has sharp intrusive contacts with the older mafic rock. The different contact relationships highlight the broad coeval relationships between mafic and felsic magmatism in the East Kimberley (see Chapter 10).

The apparent absence of extensive contact aureoles around the East Kimberley layered intrusions may be attributed to such factors as: 1. temperature and volume of the intruding magma; 2. metamorphic grade and composition of country rocks; and/or 3. temperature of country rocks.

1. Extensive contact aureoles are generally developed adjacent to volumetrically large intrusions that formed from hot primitive mafic magmas with liquidus temperatures of at least 1200ºC, or with those intrusions that have had a rapid flow of magma over a prolonged period of time; e.g. contact aureoles of the Noril'sk feeder intrusions in Siberia extend further into the country rocks than the thickness of the intrusions themselves (Naldrett 1997, 1999). With the exception of the 7.8 km thick tabular McIntosh intrusion, most East Kimberley intrusions are sheet or dyke-like bodies less than 2.5 km thick. They are unlikely to have introduced large amounts of heat over a protracted period of time due to the small volumes of magma involved.

2. The most common country rocks (Fig. 5.45) to the intrusions in the central zone of the HCO are medium to high-grade metasediments of the Tickalara Metamorphics, so that little change in mineralogy occurs during contact metamorphism. In addition, the quartzofeldspathic composition of other common country rocks—paramigmatite, psammite, and granite—is not suitable for the development of distinctive minerals. Other physical features of the relatively high-grade country rocks, such as thermal conductivity, density, low water content, and preferred orientation of platy minerals may have also been important in controlling the widths of contact aureoles in the East Kimberleys.

3. Intrusion of a body of hot magma into initially cold country rocks favours the development of a pronounced temperature gradient, and so the effects of contact metamorphism are likely to be conspicuous. However, if the intrusion is emplaced into deep-seated rocks where regional temperatures are several hundred degrees C, contact effects may be indistinguishable (Turner 1968). High regional geothermal gradients are indicated for the East Kimberley crustal rocks by the deep emplacement of the intrusions (8–23 km: see Chapter 9), spatially associated coeval granite intrusions, and prolonged metamorphism (see Chapter 3). Hot country rocks with small temperature gradients would also inhibit the formation of extensive chilled margins around the intrusions.

Types of layering

Groups I–VII intrusions of the East Kimberley display a range of rhythmic compositional layering and primary igneous laminated textures (Figs 5.46, 5.47), which are typical of tholeiitic bodies intruded into the middle to upper crust. The layering is developed in both mafic and ultramafic cumulates at scales ranging from large-scale macrorhythmic layering, which controls the regional configuration of intrusions (e.g. the concentric pattern of the McIntosh intrusion visible on satellite imagery), to cyclically layered units that extend across the width of the intrusions (Panton), to outcrop-scale layering components, such as microrhythmic layering, modal layering, cryptically graded layers, and modal laminations (Irvine 1982). Macrorhythmic layering is most prominent in the larger intrusions, such as Toby, Springvale, McIntosh, Panton, and Spring Creek.

(i) Microrhythmic layering. One of the most common forms of layering displayed in the intrusions is microrhythmic layering, i.e. the systematic recurrence of distinctive layers or sequences of layers. Individual layers range in thickness from a few millimetres for grain-size laminae up to tens of centimetres for modally graded layers. Gabbroic rocks from the lower parts of mafic zones in group I intrusions have alternating plagioclase and plagioclase–clinopyroxene laminae, a couple of millimetres thick, interlayered with more massive plagioclase-rich layers, 1–20 cm thick. The upper parts of ultramafic zones of group I intrusions contain composite sequences of uniform modal layers and modally graded layers that involve only cumulus chromite and olivine. Uniform modal layers have an even distribution of both minerals, whereas modally graded layers have chromite-rich bases and olivine-rich tops. Contacts between layers with different proportions of olivine and chromite are gradational (modal contact), and those between chromite and chromite–olivine layers are more abrupt (phase contact). Grain-size graded layers and texturally graded layers are generally rare.

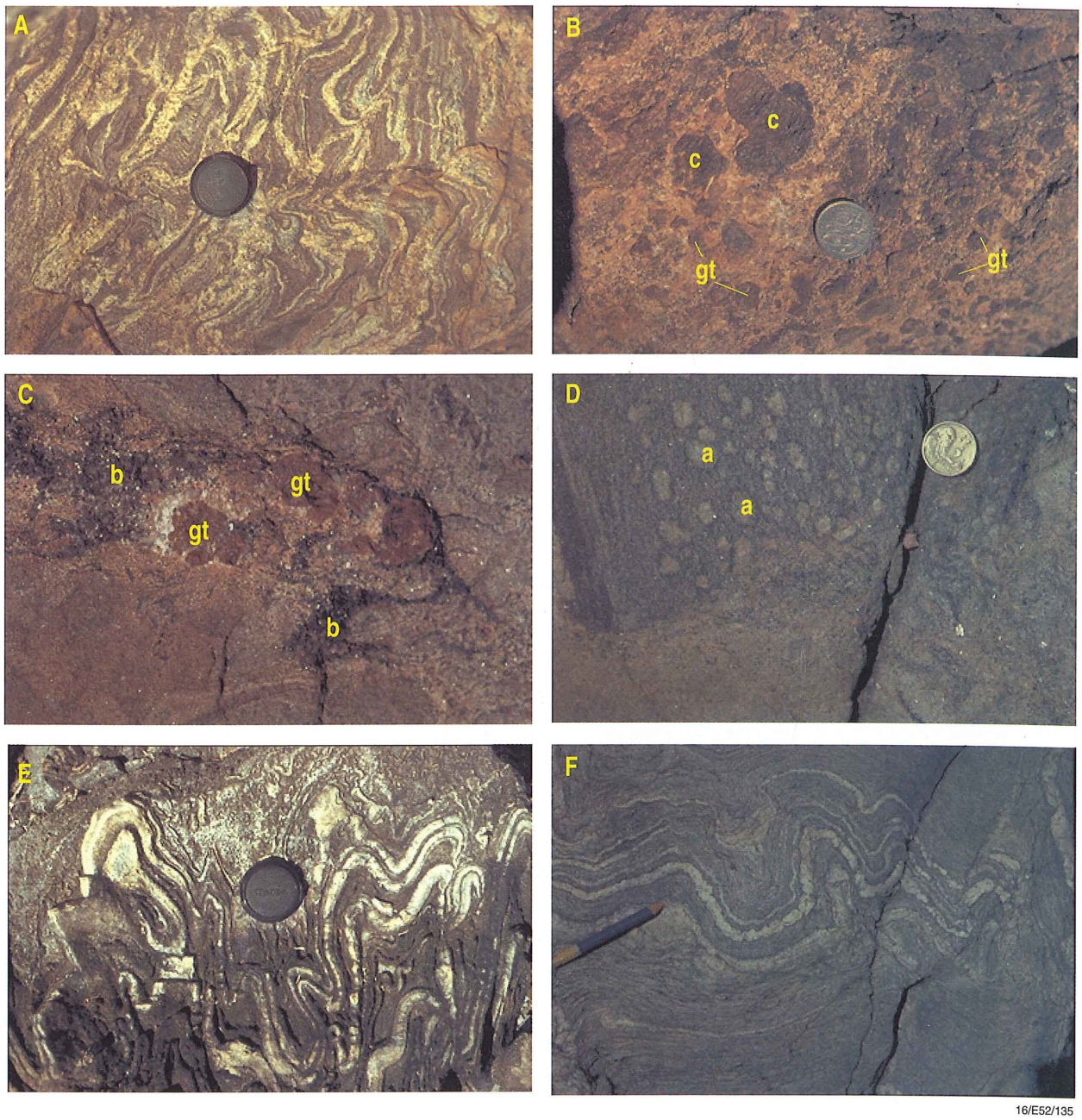


Figure 5.45. Typical country rocks (Tickalara Metamorphics) to the East Kimberley mafic–ultramafic intrusions.

A. Swirly and stromatic garnet–cordierite–sillimanite–spinel–biotite–feldspar–quartz paramigmatites are the most common country rocks to the layered intrusions in the northern part of the study area (TURKEY CREEK AMG ~138167).

B. Large ?cordierite (c) and smaller equant garnet (gt) porphyroblasts in paramigmatite in the southern contact aureole of the Sally Malay mafic–ultramafic intrusion (TURKEY CREEK AMG ~960813).

C. Garnet (gt) and biotite (b)-rich segregation in garnet–cordierite–sillimanite–spinel–biotite–alkali feldspar–plagioclase–quartz migmatite at the northwestern contact aureole of the McIntosh mafic intrusion (McINTOSH AMG ~845477).

D. Andalusite (a) porphyroblasts retrogressed to sericite in metapelite in the southern contact aureole of the Panton mafic–ultramafic intrusion (McINTOSH AMG ~751315).

E. Tight to isoclinal folding in marble and calc-silicate rock at the western contact of the Corkwood mafic intrusion (TURKEY CREEK AMG ~132882).

F. Folded and boudinaged felsic and biotite-rich bands in muscovite–garnet–sillimanite–biotite–plagioclase–quartz migmatite (Rose Bore Granite) in the southern contact aureole of the Panton mafic–ultramafic intrusion (McINTOSH AMG ~751315).

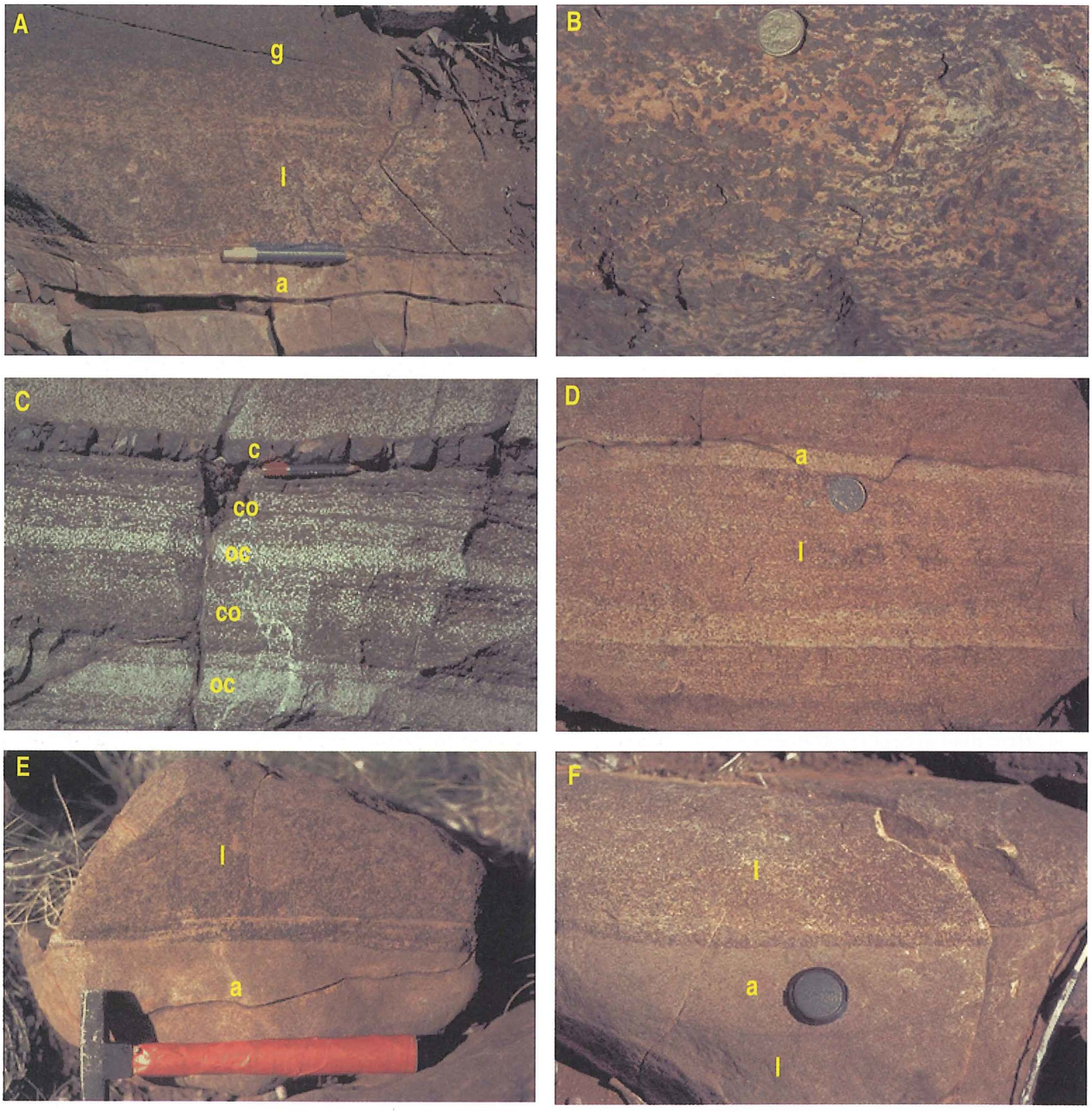


Figure 5.46. Types of layering in the East Kimberley mafic–ultramafic intrusions.

A. Rhythmically layered gabbro (g), leucogabbro (l), and anorthosite (a) in the Lower Mafic Zone of the Panton mafic–ultramafic intrusion (McINTOSH AMG ~756340).

B. Rhythmically layered gabbro, consisting of uralitised equant clinopyroxene (dark green) and sericitised plagioclase (pinkish white) in the Lower Mafic Zone of the Panton mafic–ultramafic intrusion (McINTOSH AMG ~769365).

C. Composite sequence of uniform chromite (c) and olivine–chromite (oc) modal layers and modally graded chromite–olivine (co) layers in the upper part of the Ultramafic Zone of the Panton mafic–ultramafic intrusion. Olivine has been totally replaced by white magnesite (McINTOSH AMG ~771372).

D. Rhythmically layered and laminated leucogabbro (l) and anorthosite (a) in the upper part of the Springvale mafic intrusion (McINTOSH AMG ~531366).

E. Rhythmically layered leucogabbro (l) and anorthosite (a) in the Three Sisters mafic intrusion (McINTOSH AMG ~542176).

F. Rhythmically layered and laminated leucogabbro (l) and anorthosite (a) in the middle part of the Spring Creek mafic intrusion (MOUNT REMARKABLE AMG ~861743).

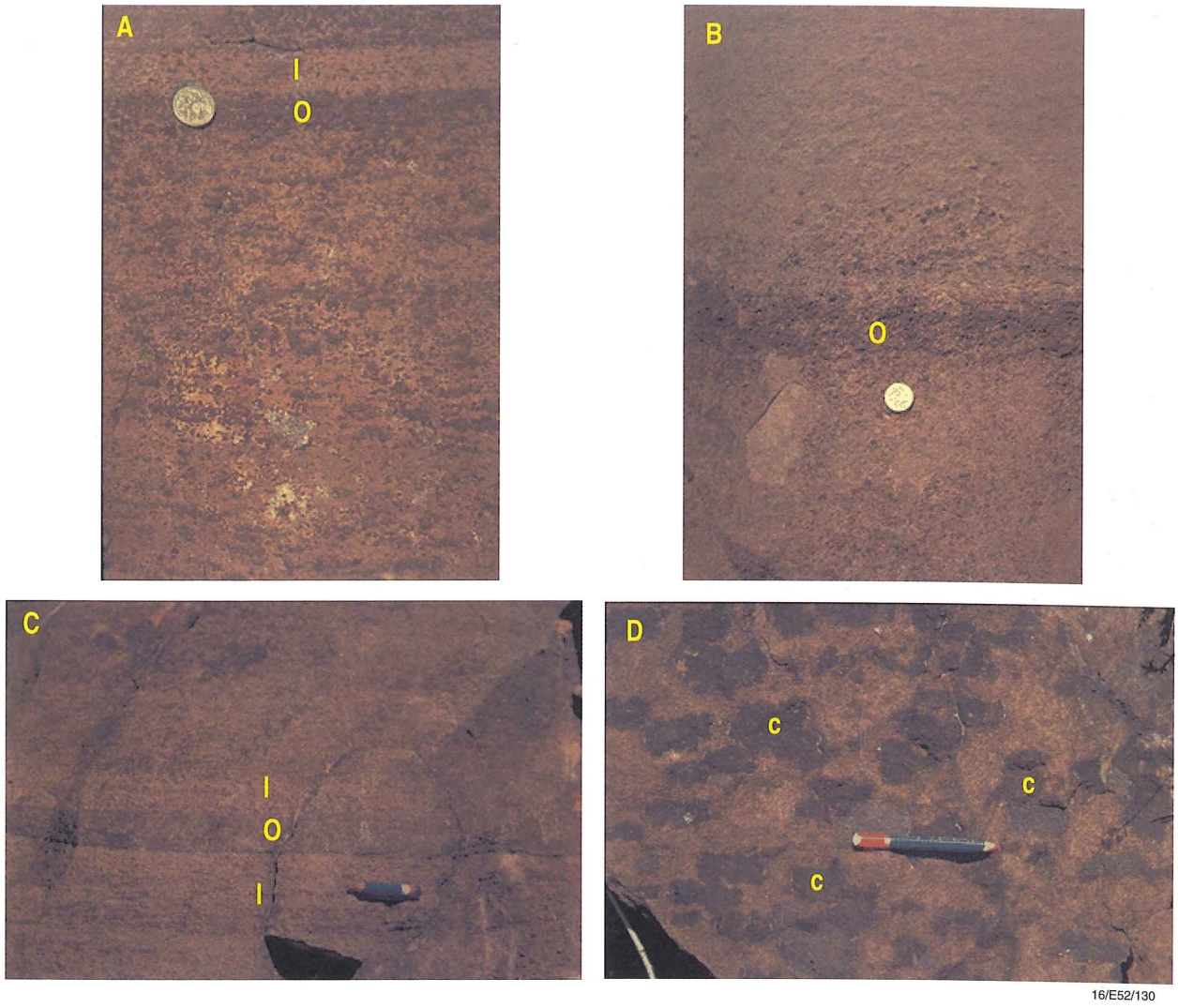


Figure 5.47. Types of layering in the East Kimberley mafic–ultramafic intrusions.

A. Rhythmic grain-size layering, consisting of wispy laminae of Fe–Ti oxides (o) in magnetite gabbronorite and leucogabbro (l) in the upper part of the McIntosh intrusion (McINTOSH AMG ~836437).

B. Fe–Ti oxide-rich layer (o) with diffuse margins in magnetite gabbronorite near the southwest side of the McIntosh intrusion (McINTOSH AMG ~821382).

C. Microrhythmically layered magnetite gabbronorite and leucogabbro (l) with centimetre-thick modally graded Fe–Ti oxide layers (o) and wispy grainsize-thick Fe–Ti oxide laminae near the southwest side of the McIntosh intrusion (McINTOSH AMG ~822383).

D. Laminated gabbro consisting of aligned clinoamphibole (c) porphyroblasts subparallel to a primary igneous lamination of plagioclase laths (visible in thin section) in the Wild Dog Creek intrusion (McINTOSH AMG ~736362).

Mathison & Hamlyn (1987) defined sharp layer contacts between cyclic units of troctolite and olivine gabbro in the McIntosh intrusion by the upward change of texture of augite or orthopyroxene from post-cumulus to cumulus, or vice versa, and by changes in the modal proportions of augite, olivine, orthopyroxene, and Fe–Ti oxides. Thus the layer contacts represent combinations of phase contacts, textural contacts, and modal contacts. Fractionated gabbros from the western margin and upper parts of the McIntosh intrusion contain rhythmically layered concentrations of Fe–Ti oxide. The 1–4 cm thick uniform modal and modally graded oxide layers commonly have diffuse irregular contacts and are associated with thin discontinuous wispy oxide laminae.

(ii) Cryptically graded layers. Cryptic layering, involving changes in the chemical compositions of cumulus minerals with stratigraphic height, has been documented in the McIntosh and Sally Malay intrusions. Mathison & Hamlyn (1987) found that the most sensitive parameters for indicating the degree of fractionation in the McIntosh intrusion were anorthite (An) content in plagioclase, mg number in olivine, augite, and orthopyroxene, Cr_2O_3 content in magnetite and augite, and NiO content in olivine. Cryptic variations in mafic rocks, except the

very fractionated oxide-bearing gabbros, include a slight overall fractionation of plagioclase (An_{80-70}) and olivine (mg_{78-68}) from the base to the top of the intrusion. The limited fractionation of 10 mol % for these minerals was attributed to repeated influxes of new magma coupled with possible losses of fractionated magma. Irregularly fluctuating cryptic trends, involving combinations of rapidly increased normal fractionation and reversed fractionation trends with height, occur throughout the intrusion. These fluctuations were due to the reappearance of fractionated magnetite gabbronorite in the layered sequence.

Thornett (1981) described cryptic trends within and between various subchambers of the Sally Malay intrusion and noted a general decrease in olivine compositions (mg_{82-69}) up the intrusion. Reversions to slightly more primitive compositions (mg_{72}–mg_{78}) across some subchambers were ascribed to magma replenishment.

(iii) Modal laminations. The platy alignment or lamination of tabular minerals parallel to compositional layers is a feature of gabbroic cumulates in mafic intrusions of group II and Undivided gabbro. The preferred alignment of plagioclase laths and clinopyroxene prisms characterises leucogabbro and anorthosite from the middle to upper parts of the Springvale and Three Sisters intrusions. The laminated sequences are commonly associated with uniform modal layers and modally graded layers comprising varying amounts of plagioclase and pyroxene. Biotite–magnetite gabbro from the group IV Wild Dog Creek intrusions also has aligned igneous plagioclase laths subparallel to a metamorphic lamination defined by the crystallographic alignment of coarse clinoamphibole and biotite.

Distribution of mineralised layered intrusions in the East Kimberley

The major mineralised layered intrusions (groups I, II, and V) in the East Kimberley occur in two northeast-trending 'metallogenic corridors' (Fig. 5.1), one characterised by Cr–PGEs–Ni–Cu±Au (chromite association) and the other, by Ni–Cu–Co±PGEs (sulphide association). The mineralised group I intrusions (e.g. Panton) containing the chromite association are restricted to a narrow corridor across McINTOSH, whereas the sulphide-bearing group II and V (Sally Malay) intrusions occur in a longer and wider corridor, about 15 km to the northwest, on McINTOSH, MOUNT REMARKABLE, and TURKEY CREEK. Only the mineralised group I Big Ben intrusion, which has been displaced by the Panton Fault, lies outside the two corridors. There is potential for finding other mineralised intrusions, particularly those which are poorly exposed within the corridors, or those which are further along strike of the corridors. The 'metallogenic corridors' indicate that magmatism for the mineralised intrusions generally youngs towards the northeast of the HCO, and that the sulphide association became dominant with time relative to the chromite association.

The 1080 Ma layered mafic–ultramafic intrusions of the Giles Complex in the Musgrave Block of central Australia (Glikson et al. 1996) show a regional zoned distribution which is interpreted to reflect different levels of individual magma chambers in the crust, the level being controlled by magma density. The ratio of mafic to ultramafic components for the intrusions of the Giles Complex increases south-southwestwards, implying decreasing density with progressively shallower crustal levels. However, this does not appear to be applicable to the East Kimberleys, where the intrusions are of different ages and those with the highest proportion of dense ultramafic rocks (group I) occur at higher crustal levels than the mafic intrusions with little or no ultramafics (groups II, V, and VI). Also, the two East Kimberley corridors do not represent different crustal levels, because, within the sulphide association corridor, there are mineralised intrusions emplaced at shallow (Billymac Yard), moderate (Wilagee), and deep (all group V) crustal depths (see Chapter 9).

The Ni–Cu–Co–PGEs±Cr corridor appears to cut across the Springvale Fault that separates the central zone from the western zone of the HCO (Tyler et al. 1995). However, if Shaw et al's (see Chapter 4) suggested boundary between the central and western zones, the Highway Shear Zone, is correct, then most of the Ni–Cu–Co deposits are confined to the western zone. Shaw & Macias (see Chapter 7) propose that the mineralised corridors reflect different histories and metamorphic conditions of the western and central zones.

Comparisons with other Palaeoproterozoic provinces in Australia

Palaeoproterozoic layered mafic–ultramafic intrusions are more abundant and larger in the HCO, and contain more styles of mineralisation, than those elsewhere in Australia. Palaeoproterozoic layered intrusions are present in the Arunta, Gascoyne, Mount Isa, Paterson, Pine Creek, Tennant Creek, The Granites–Tanami, and Willyama provinces, but these are mainly thin mafic bodies with no significant mineralisation. Even those that are relatively large, such as the Lunch Creek Gabbro (Derrick 1980) in the Mount Isa Inlier and the Anburla Anorthosite (Warren & Shaw 1995) in the Arunta Block, are not particularly well layered or differentiated. The large volume of magmas and extensive mineralisation that characterise the East Kimberley intrusions probably indicate large-scale mantle-crustal processes and primary magmatic controls, the relative significance of which are beyond the scope of this *Bulletin*. High crustal geothermal gradients (see Chapter 10), intense fracturing, and mantle plume activity could facilitate the upward movement of magma through the crust. A feature of the HCO is an intense array of major strike-slip faults (Halls Creek, Mount Angelo, Springvale, and Highway) that extend for long distances and have had a long history of activity. Most of these faults postdate the intrusions, but older faults may have penetrated deep into the crust to assist the ascent of magma and the development of magma chambers. The apparent absence in the province

of rocks crystallised from high-temperature ultramafic magmas typical of mantle plumes, such as picrite and komatiite, sensu stricto, or of cumulus minerals with high mg numbers, suggest that such plume activity was not responsible for the emplacement of the East Kimberley layered intrusions. However, it is conceivable that the voluminous Hart Dolerite, which occurs throughout much of the Kimberley Basin to the west of the HCO, formed from a fractionated mafic magma related to mantle plume activity at 1790 Ma, some 70 to 40 million years after the emplacement of the East Kimberley layered intrusions (S-s. Sun, personal communication, AGSO, 1998).

The tectonic setting of the HCO may account for the abundance, shape, and grouping of the intrusions. Shaw & Macias (see Chapter 7) suggest that the large volume of intrusions is in accord with their emplacement in a transtensional tectonic setting at a plate or sub-plate boundary.

Another factor, which may explain the large volume of layered intrusions in the HCO relative to other provinces, is the considerable depth to which the crust is eroded. In contrast, the Mount Isa and Pine Creek provinces, for example, are eroded to much shallower depths, below which intrusions may well be present. In addition, geobarometric studies of the HCO intrusions by Trudu & Hoatson (see Chapter 9) show there is a gradient from relatively shallower crustal depths of emplacement of around 8 km in the southwestern part of the study area to 23 km in the northeastern part of the area. This gradient implies that the crust has been tilted to provide a cross-section through upper to middle crust levels.

The abundance and variety of mineralisation (see Chapter 14) in the HCO may reflect the relative importance of such factors as:

- chemical heterogeneity of the mantle source (e.g. patchy enrichment in PGEs, Ni, and Cu), although recent geochemical evidence (Solomon & Sun 1997) suggests that this is unlikely to be a significant factor;
- magma generation processes (second-stage melting of refractory mantle, timing of S saturation) and the contamination of the magma with favourable S-bearing rocks during ascent in the conduit or after emplacement in the magma chamber;
- geodynamic processes of magma flow in the conduit and changes in the magma flow regime in the chamber (fast, slow, turbulent, passive); and
- magma chamber processes (crystal fractionation, filter pressing, magma mixing) and post-emplacement mechanisms (introduction of late magmatic fluids, hydrothermal remobilisation).

It is difficult to quantify the relative importance of these processes for mineralisation, however, it is likely that both the timing and mechanism of sulphide saturation, and the dynamics of the magma flow played significant roles in the East Kimberley. The geochemical and isotopic studies of Sun et al. (1991), Sproule et al. and Sun & Hoatson (see Chapters 11 & 12) have highlighted the importance of crustal contamination and magma mixing processes in initiating mineralisation in the Sally Malay and Panton intrusions, and probably in most other mineralised intrusions in the HCO.

Acknowledgements

The author would like to thank David Blake, Alastair Stewart (both of AGSO), and Steve Sheppard (GSWA) for their constructive comments on earlier drafts of the manuscript. Lana Murray, Joe Mifsud, Neale Jeffery, and Angie Jaensch drafted the figures.

References

Barnes, G.J., 1994. Surrender report E80/1450—Corkwood Project. Poseidon Group Trading Ltd internal report number 6490 (unpublished) for the Department of Minerals and Energy, Western Australia (Item 7511, AN40093).

Bird, D.K., Brooks, C.K., Gannicott, R.A. & Turner, P.A., 1991. A gold-bearing horizon in the Skaergaard intrusion, East Greenland. Economic Geology, 86, 1083–1092.

Blake, D.H. & Hoatson, D.M., 1993. Granite, gabbro, and migmatite field relationships in the Proterozoic Lamboo Complex of the East Kimberley region, Western Australia. AGSO Journal of Australian Geology & Geophysics, 14(4), 319–330.

Branney, M.J., 1995. Downsag and extension at calderas: new perspectives on collapse geometries from ice-melt, mining, and volcanic subsidence. Bulletin of Volcanology, 57, 303–318.

Codner, C.C., 1979. Final report on Mini M and Togo 5 prospects. Results of exploration on mineral claims 80/5986 to 80/5992 inclusive. Australian Anglo American Limited internal report (unpublished) for the Department of Minerals and Energy, Western Australia (Item 878, AN8463).

Derrick, G.M., 1980. Marraba, Queensland - 1:100 000 Geological Series. Bureau of Mineral Resources, Australia, Explanatory Notes 6956, 33 pp.

Dow, D.B. & Gemuts, I., 1969. Geology of the Kimberley Region, Western Australia: The East Kimberley. Bureau of Mineral Resources, Australia, Bulletin 106, 135 pp.

Frost, T.R. & Mahood, G.A., 1987. Field, chemical and physical constraints on mafic-felsic magma interaction in the Lamarck Granodiorite, Sierra Nevada, California. Geological Society of America, Bulletin 99, 272–291.

Gaunt, F. McA., 1977. Keller Creek final report. Results of exploration of Mineral Claims 80/5209, 5302-5319 inclusive. Australian Anglo American Limited internal report (unpublished) for the Department of Minerals and Energy, Western Australia (Item 742, AN7692).

Gemuts, I., 1971. Metamorphic and igneous rocks of the Lamboo Complex: East Kimberley region, Western Australia. Bureau of Mineral Resources, Australia, Bulletin 107, 71 pp.

Geopeko Ltd., 1986–1990. Toby Sill platinum exploration. Geopeko Ltd internal report (unpublished) for the Department of Minerals and Energy, Western Australia (Item 4326, Fiche 5755–5757–M4713).

Glikson, A.Y., Stewart, A.J., Ballhaus, C.G., Clarke, G.L., Feeken, E.H.J., Leven, J.H., Sheraton, J.W. & Sun, S-s., 1996. Geology of the western Musgrave Block, central Australia, with particular reference to the mafic–ultramafic Giles Complex. Australian Geological Survey Organisation, Bulletin 239, 206 pp.

Hamlyn, P.R., 1975. Chromite alteration in the Panton Sill, East Kimberley region, Western Australia. Mineralogical Magazine, 40, 181–192.

Hamlyn, P.R., 1977. Petrology of the Panton and McIntosh layered intrusions, Western Australia, with particular reference to the genesis of the Panton chromite deposit. PhD thesis, University of Melbourne, 389 pp.

Hamlyn, P.R., 1980. Equilibration history and phase chemistry of the Panton Sill, Western Australia. American Journal of Science, 280/7, 631–668.

Hamlyn, P.R. & Keays, R.R., 1979. Origin of chromite compositional variation in the Panton Sill, Western Australia. Contributions to Mineralogy and Petrology, 69/1, 75–82.

Hamlyn, P.R., Keays, R.R., Peck, D.C. & Reeves, S.J. 1988. Geochemical criteria for platinum metal exploration. Australian Mineral Industries Research Association Limited, Final Report 85/P228 (unpublished), 215 pp.

Hancock, S.L. & Rutland, R.W.R., 1984. Tectonics of an Early Proterozoic geosuture - the Halls Creek orogenic subprovince, northern Australia. Journal of Geodynamics, 1, 387–432.

Helix Resources N.L., 1993. 8th Annual Report, 36 pp.

Hoatson, D.M., 1993. Correlation of structurally disrupted layered mafic–ultramafic intrusions in the East Kimberley: Is Big Ben part of the Panton intrusion? AGSO Research Newsletter, 19, 9–10.

Hoatson, D.M., 1995. New mineral discoveries in the East Kimberley. AGSO Research Newsletter, 22, 9–11.

Hoatson, D.M., 1998. Platinum-group element mineralisation in Australian Precambrian layered mafic–ultramafic intrusions. AGSO Journal of Australian Geology & Geophysics, 17(4), 139–151.

Hoatson, D.M. & Tyler, I., 1993. Prospective layered mafic–ultramafic intrusions in the East Kimberley. AGSO Research Newsletter, 18, 8–9.

Hoatson, D.M., Blake, D., Warren, R.G., Orth, K. & Tyler, I.M., 1995. Recent NGMA mapping highlights the metallogenic potential of the East Kimberley. AGSO Research Newsletter, 22, 1–2.

Hoatson, D.M., Sproule, R.A. & Lambert, D.D., 1997. Are there Voisey's Bay-type Ni–Cu–Co sulphide deposits in the East Kimberley of Western Australia? AGSO Research Newsletter, 27, 17–19.

Irvine, T.N., 1982. Terminology for layered intrusions. Journal of Petrology, 23, 127–162.

Lewis, P.G., 1972. Stratin Minerals Pty Ltd mineral claim locations. Internal report (unpublished) for the Department of Minerals and Energy, Western Australia (Item 738, AN5687).

Mathison, C.I. & Hamlyn, P.R., 1987. The McIntosh layered troctolite-olivine gabbro intrusion, east Kimberley, Western Australia. Journal of Petrology, 28, 211–234.

Metcalf, R.V., Smith, E.I., Walker, J.D., Reed, R.C. & Gonzales, D.A., 1995. Isotopic disequilibrium among commingled hybrid magmas: evidence for a two-stage magma mixing–commingling process in the Mt. Perkins pluton, Arizona. Journal of Geology, 103, 509–527.

Naldrett, A.J., 1997. Key factors in the genesis of Noril'sk, Sudbury, Jinchuan, Voisey's Bay and other world-class Ni-Cu-PGE deposits: implications for exploration. Australian Journal of Earth Sciences, 44, 283–315.

Naldrett, A.J., 1999. World-class Ni-Cu-PGE deposits: key factors in their genesis. Mineralium Deposita, 34, 227–240.

Page, R.W., Blake, D.H., Sun, S-s., Tyler, I.M., Griffin, T.J. & Thorne A.M., 1994. New geological and geochronological constraints on volcanogenic massive sulphide prospectivity near Halls Creek, W.A. AGSO Research Newsletter, 20, 5–7.

Page, R.W., Hoatson, D.M., Sun, S-s. & Foudoulis, C., 1995. High-precision geochronology of Palaeoproterozoic layered mafic–ultramafic intrusions in the East Kimberley. AGSO Research Newsletter, 22, 7–8.

Perring, R.J. & Vogt, J.H., 1991. The Panton Sill. In: Barnes, S.J. & Hill, R.E.T. (editors), Mafic–ultramafic complexes of Western Australia. Excursion Guidebook 3. Sixth International Platinum Symposium, July 1991, Perth, Western Australia. IAGOD and the Geological Society of Australia, 97–106.

Pickands Mather & Company International, 1965-1969. Fletcher Creek nickel-copper-lead-zinc exploration. Pickands Mather & Company International internal report (unpublished) for the Department of Minerals and Energy, Western Australia (Item 251/ci, Microfilm roll 126–M67/60).

Sanders T.S., 1999. Mineralization of the Halls Creek Orogen, east Kimberley region, Western Australia. Geological Survey of Western Australia, Report 66 and Appendix, 44 pp.

Shedden, S.H. & Barnes, G.J., 1996. East Kimberley Nickel Province — Characteristics and origin of the Sally Malay Ni-Cu-Co deposit, East Kimberley, Western Australia. In: Grimsey, E.J. & Neuss, I. (editors), Nickel 96—Mineral to market. Australasian Institute of Mining and Metallurgy, Publication Series 6/96, November 27-29, Kalgoorlie, Western Australia, 145–155.

Sheppard, S., 1996. Mafic-felsic magma mingling in the Bow River batholith of the Halls Creek Orogen. Western Australia Geological Survey, Annual Review 1995-96, 56–59.

Sheppard, S., Tyler, I.M. & Hoatson, D.M., 1997. Geology of the Mount Remarkable 1:100 000 sheet: Western Australia Geological Survey, 1:100 000 Geological Series Explanatory Notes, 27 pp.

Solomon, M. & Sun, S-s., 1997. Earth's evolution and mineral resources, with particular reference on volcanic-hosted massive sulphide deposits and banded iron formations. AGSO Journal of Australian Geology & Geophysics, 17(1), 33–48.

Sun, S-s., Wallace, D.A., Hoatson, D.M., Glikson, A.Y. & Keays, R.R., 1991. Use of geochemistry as a guide to platinum group element potential of mafic–ultramafic rocks: examples from the west Pilbara Block and Halls Creek Mobile Zone, Western Australia. Precambrian Research, 50, 1–35.

Thornett, J.R., 1981. The Sally Malay deposit: gabbroid associated nickel-copper sulfide mineralization in the Halls Creek Mobile Zone, Western Australia. Economic Geology, 76 (6), 1565–1580.

Thornett, J.R., 1986. Evolution of a high-grade metamorphic terrain in the Proterozoic Halls Creek Mobile Zone, Western Australia, PhD thesis, University of Western Australia, Perth, 350 pp.

Trudu, A. & Hoatson, D.M., 1996. Depths of emplacement of Precambrian layered intrusions in the East Kimberley. AGSO Research Newsletter, 25, 10–12.

Turner, F.J., 1968. Metamorphic petrology. Mineralogical and field aspects. McGraw-Hill Company, New York. 403 pp.

Tyler, I.M., Griffin, T.J., Page, R.W. & Shaw, R.D., 1995. Are there terranes within the Lamboo Complex of the Halls Creek Orogen? Western Australia Geological Survey, Annual Review 1993-94, 37–46.

Tyler, I.M., Hoatson, D.M. Griffin, T.J., Sheppard, S., Blake, D.H. & Warren, R.G., 1997. McIntosh, Western Australia, 1:100 000 geological map (sheet 4462). Geological Survey of Western Australia, Perth.

Warren, R.G., 1992. District surrounding the Armanda Sill, Halls Creek Inlier, Western Australia. Australian Geological Survey Organisation, Record 1992/70, 16 pp.

Warren, R.G. & Shaw, R.D., 1995. Geology of the HERMANNSBURG 1:250 000 sheet (SF 53-13). Australian Geological Survey Organisation, 1:250 000 Geological Series Explanatory Notes, 81 pp.

Weinberg, R.F., 1997. The disruption of a diorite magma pool by intruding granite: The Sobu body, Ladakh Batholith, Indian Himalayas. Journal of Geology, 105, 87–98.

GEOCHRONOLOGY OF THE MAFIC–ULTRAMAFIC INTRUSIONS

by RODNEY W. PAGE & DEAN M. HOATSON

Introduction

Plutonic and metamorphic rocks are major components of the Halls Creek Orogen (HCO) in the East Kimberley of Western Australia. The widespread distribution of large layered mafic–ultramafic intrusions in the central and western zones of the orogen and the existence of granulite-facies rocks in the central zone (Tyler et al. 1995, see Chapter 3) distinguish this orogen from most other Palaeoproterozoic terrains of northern Australia. Are these two characteristics of the orogen fundamentally related?

The layered intrusions of the HCO (Fig. 6.1) represent one of the most extensively exposed mafic–ultramafic igneous associations in Australia, and imply significant input of heat into the crust. The nature and tectonic significance of the relationship between igneous intrusions, migmatites, and other high-grade metamorphic rocks have been investigated in the HCO and elsewhere (e.g. Thornett 1986, Wickham 1987, Barton & Hanson 1989, Thompson 1989, Looseveld & Etheridge 1990, De Yoreo et al. 1991, Amato et al. 1994). It has long been debated whether the migmatites in the East Kimberley are of regional or contact metamorphic origin. Dow & Gemuts (1969), Gemuts (1971), Thornett (1986), and Tyler et al. (1995) considered that the high-grade metamorphic rocks and migmatites of the Tickalara Metamorphics (see Chapter 3) were produced under conditions of low-pressure and high-temperature regional metamorphism. However, Blake (Blake & Hoatson 1993, see Chapter 3) suggests that the migmatites may have formed directly from contact metamorphism resulting from the granitic and mafic–ultramafic intrusions.

This study endeavours to determine crystallisation ages for the more important mafic–ultramafic intrusions, the relative timing of these intrusions and granite plutonism, and possible links between mafic–ultramafic and felsic magmatism and high-grade metamorphism. The new SHRIMP U–Pb dating is integrated with field relationships, petrology, and geochemistry of the mafic–ultramafic intrusions.

The Palaeoproterozoic layered intrusions in the HCO were collectively grouped by Dow & Gemuts (1969) into the Alice Downs Ultrabasics and the McIntosh Gabbro. However, different contact relations, degrees of fractionation, styles and intensity of deformation, and types of mineralisation indicate that the intrusions represent more than the two major types of Dow & Gemuts. On the basis of field relationships and U–Pb geochronological data reported below, seven major groups (I–VII) of mafic and mafic–ultramafic intrusions, at least three of which appear to be coeval (Fig. 6.1), can be recognised in the East Kimberley.

Geochronological results are reported here for five of the largest and economically most important layered intrusions in the McINTOSH, MOUNT REMARKABLE, and TURKEY CREEK sheet areas[1] (see Fig 1.1; Fig. 6.1; Table 6.1) of the East Kimberley. Geological and mineralisation features of the intrusions are described in Hoatson (1993), Hoatson & Tyler (1993), Trudu & Hoatson (1996), Sheppard et al. (1997), and Chapters 5 and 14 of this *Bulletin*. The dated intrusions include the type examples of groups I (Panton), II (Springvale), III (Toby), V (Sally Malay), and VI (McIntosh). The East Kimberley intrusions have variable forms, ranging from folded sheets, shallow-dipping sheets or basins, composite multi-chambered bodies, funnel-shaped bodies, broad dyke-like bodies, to steeply plunging plugs. Metamorphic overprinting of most intrusions ranges from lower to upper amphibolite facies, but, although the intrusions have been variously recrystallised, primary igneous cumulus textures are generally well preserved.

The Panton and Sally Malay intrusions contain the largest resources of platinum-group elements (PGEs)–Cr–Ni–Cu–Au and Ni–Cu–Co, respectively, in the East Kimberley. The Springvale mafic intrusion hosts minor amounts of chromite and the McIntosh mafic intrusion has potential for Fe–Ti–V and Au mineralisation. The relative ages of these bodies and other such intrusions in the geological framework of the HCO are, therefore, clearly relevant to understanding the region's metallogenic potential.

Scope of this study

Fractionated anorthositic and gabbroic cumulates in the intrusions contain magmatic zircon ($ZrSiO_4$) and, in one case, coexisting baddeleyite (ZrO_2). These minerals were once thought to be rare, absent, or only xenocrystic components in mafic and ultramafic rocks—unrelated to the crystallisation history. However, they are now proving increasingly useful for dating mafic and ultramafic magmatism. The general difficulties of identifying magmatic zircon in mafic rocks and using it to successfully date mafic magmatic events were outlined by Black et al. (1991). The benefits and high-precision ages that can be derived from magmatic zircon and baddeleyite are now well known (Paces & Miller

[1] 1:100 000 sheet names throughout this *Bulletin* are in capital letters to avoid confusion with identical place names and to distinguish them from 1:250 000 sheet names.

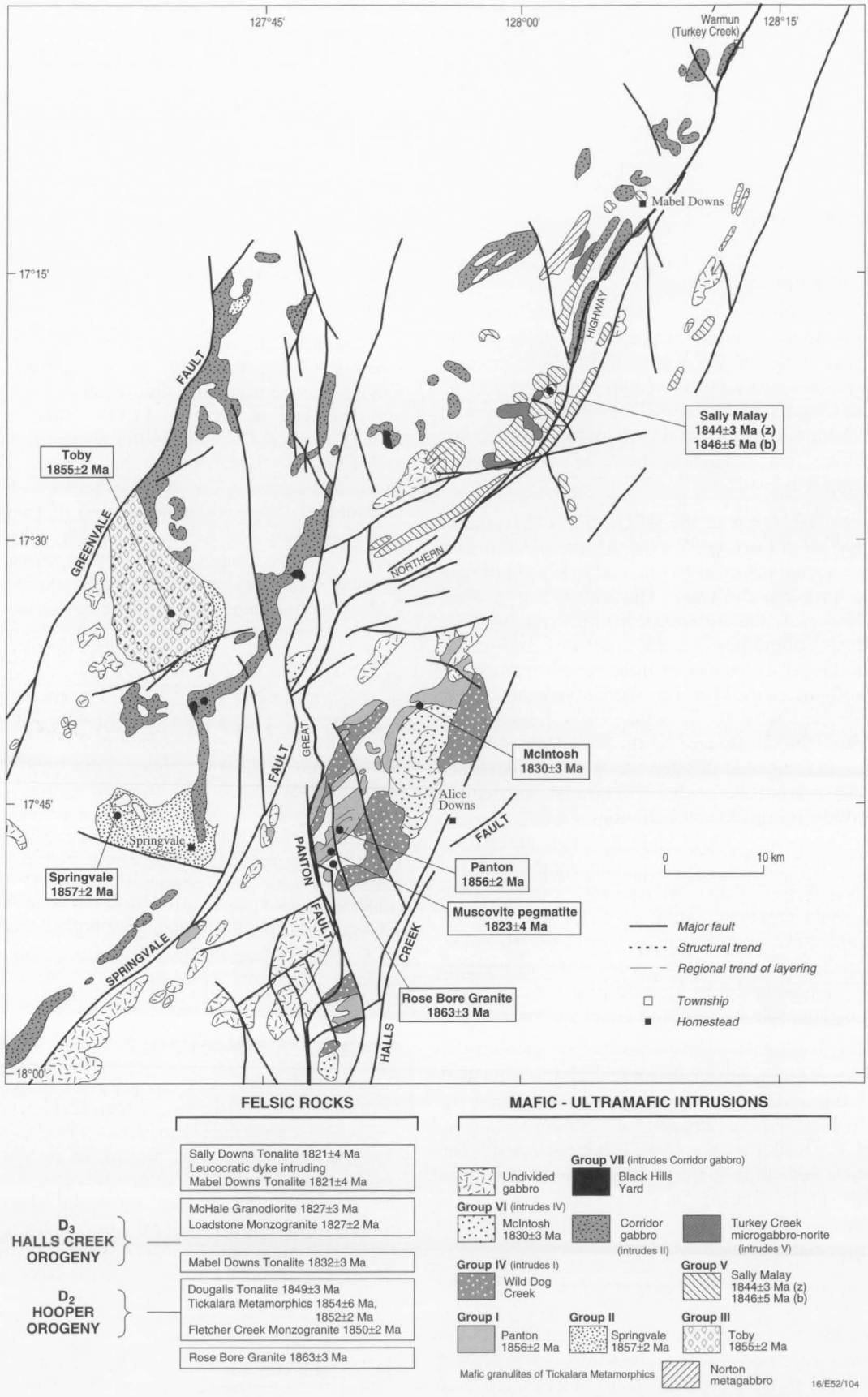


Figure 6.1. Palaeoproterozoic mafic–ultramafic intrusions that have been dated in the East Kimberley. The temporal framework, determined from field relationships and SHRIMP dating, of mafic–ultramafic intrusions and interpreted orogenic episodes in the Halls Creek Orogen is also shown. Those intrusions forming large layered or weakly layered bodies are assigned to groups I–VII. The type example of the intrusion and its SHRIMP U–Pb zircon (z) or baddeleyite (b) age (where determined) are indicated, and sample locations are shown. Other unassigned mafic–ultramafic formations shown generally form small massive irregular intrusive bodies of undefined age.

Table 6.1. Summary of U–Pb zircon and baddeleyite SHRIMP results for layered mafic–ultramafic intrusions and associated rocks in the Halls Creek Orogen, East Kimberley.

Igneous unit	*Sample number*	*Lithology*	*Easting*[1]	*Northing*[1]	*U-Pb Age (Ma)*
Rose Bore Granite (zirc)	113439	Gneissic granite	374866	8031584	1863±3
Pegmatite dyke cutting Panton intrusion (zirc)	93526031	Muscovite pegmatite	375473	8032534	1825±10
Panton intrusion (zirc)	93526033	Mottled anorthosite	375877	8034974	1856±2
Springvale intrusion (zirc)	93526022	Leucogabbro	354261	8035097	1857±2
Toby intrusion (zirc)	93526017	Quartz gabbro	357120	8058510	1855±2
Sally Malay intrusion (zirc)	94522307	Mottled anorthosite	396074	8081664	1844±3
Sally Malay intrusion (bad)	94522307	Mottled anorthosite	396074	8081664	1846±5
McIntosh intrusion (leuocosome zirc)	93525043	Garnet paramigmatite	384510	8047730	1830±3
McIntosh intrusion (palaeosome zirc)	93525043	Garnet paramigmatite	384510	8047730	1865±3, ~1910, 2250, 2610

zirc = zircon, bad = baddeleyite.
[1]Australian Map Grid Zone 52 co-ordinates.
Locations of samples are shown in Figure 6.1.

1993, Heaman & LeCheminant 1993). Precise zircon dates from Archaean layered intrusions in Western Australia have been reported from meta-anorthosite in the Manfred Complex of the Western Gneiss Terrain (Kinny et al. 1988) and from plagioclase websterite in the Munni Munni intrusion of the west Pilbara Craton (Sun & Hoatson 1992). Wingate et al. (1998) have used both zircon and baddeleyite to date Proterozoic mafic dyke swarms in the Broken Hill region.

In this study, fractionated anorthositic and high-Zr-bearing gabbroic cumulates (containing up to 140 ppm Zr) from the upper parts of the Panton, Springvale, Toby, and Sally Malay intrusions (Fig. 6.1, see Chapter 5) were sampled for magmatic zircon. In the Sally Malay intrusion, baddeleyite coexists with zircon. Granite (Rose Bore Granite) and pegmatite that, respectively, predate and postdate the Panton intrusion were sampled to further constrain the age of this intrusion and test the internal consistency of the ages obtained against unambiguous field geological relationships. A migmatitic hornfels from the contact aureole of the McIntosh intrusion was sampled to provide an indirect means of determining the emplacement age of this intrusion.

Results

Panton mafic–ultramafic intrusion (group I)

The Panton intrusion is a synclinal body that consists of a lower, 650 m thick, ultramafic sequence (Ultramafic Series) of olivine and chromite cumulates and an overlying, 900 m thick, mafic sequence (Gabbroic Series) of gabbro, norite, anorthosite, and ferrogabbro. The thickest and economically most important group I body, it intrudes the gneissic Rose Bore Granite, which has an emplacement age of 1863±3 Ma (see below).

The dated zircons come from a fractionated mottled anorthosite in the upper part of the Gabbroic Series near the centre of the Panton intrusion (Fig. 6.1). The mottled texture is commonly displayed by fractionated mafic cumulates of groups I and V intrusions. It is defined by centimetre-scale irregular clots of uralitised intercumulus clinopyroxene within partly sericitised cumulus plagioclase.

The distinctive suite of zircons from the mottled anorthosite form partly altered, squat, euhedral to subhedral grains (Fig. 6.3A). In general, the most highly altered domains were avoided in the SHRIMP analysis by focussing the 30 μm ion microprobe beam onto clear unaltered regions. Some zircon grains are moderately zoned; others appear unzoned. All analyses (Appendix Table 4.1; Figs 6.4, 6.5) have very high U (2360–5930 ppm), high Th/U (1.0–3.1) and are highly radiogenic with very large measured $^{206}Pb/^{204}Pb$.

Despite their high-U and irregular alteration, the zircon Pb–U systems are concordant in all 16 analysed grains. Grain 207 has an aberrantly young $^{207}Pb/^{206}Pb$ age (1841 Ma), but the remaining 15 grains are 1853–1858 Ma, with a weighted mean of 1856±2 Ma (χ^2 1.41)[2]. This result is in accord with the age constraints (see below) given by the older Rose Bore Granite (1863±3 Ma) and a younger pegmatite dyke (~1823 Ma).

The internal coherence and concordance of the data indicate that the measured age is the igneous crystallisation age of the Panton intrusion. An alternative explanation, that all these grains are xenocrysts derived from 1856 Ma felsic rocks underlying the intrusion, cannot be seriously considered, given the morphology

[2] Note: χ^2, normally close to unity for a normal distribution of data, is a measure of the degree of fit for the population in the normal distribution (Taylor 1982).

and unusual Th/U chemistry (up to 3.1) of the zircons. It will be become apparent that high Th/U zircons are characteristic of other mafic–ultramafic intrusions in the East Kimberley.

Intrusive rocks predating and postdating the Panton intrusion

(i) Rose Bore Granite. The deformed Rose Bore Granite (Fig. 6.1) crops out in the Panton River, where it is intruded by the southern end of the Panton body. It is a strongly gneissic muscovite–biotite–quartz–feldspar migmatitic granite that displays evidence of intense small-scale folding and local partial melting adjacent to the Panton intrusion. Migmatised metasediments of the Tickalara Metamorphics are also associated with the granite in the contact aureole.

Most zircons from the Rose Bore Granite are clear, pale, subhedral grains with partly resorbed crystal faces, probably caused by metamorphism (Fig. 6.3B). About 10%, though, are darker anhedral grains. Two xenocrystic grains, which have much lower Th/U ratios (a factor of 15 lower than the average) and ages of 2048 Ma (grain 11) and 1873 Ma (grain 12), are much older than the main magmatic suite (Appendix Table 4.2; Fig. 6.2). Rejecting these and the youngest result (8.1, which overlapped a crack across the grain), the remaining 19 data points define a coherent, normal distribution in $^{207}Pb/^{206}Pb$, giving an age of 1863±3 Ma (χ^2 1.39). This age is considered to be the magmatic age for the granite, but it is possible that the actual age is slightly older, since some of the data (with slightly younger $^{207}Pb/^{206}Pb$) are a few per cent discordant. If these are ignored, the concordant group of 10 remaining data points indicates a magmatic age of 1867±3 Ma (χ^2 0.6). However, this is considered an unrealistically close grouping and the 1863±3 Ma age is preferred for the crystallisation age of the Rose Bore Granite and a minimum age for the host paragneisses and schists of the Tickalara Metamorphics.

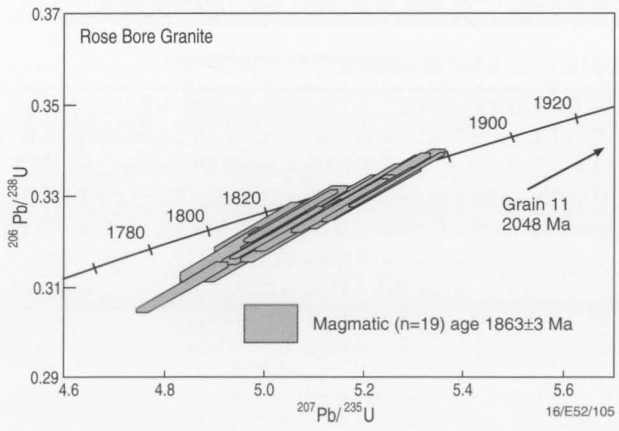


Figure 6.2. Concordia plot of zircon U–Pb data from the Rose Bore Granite adjacent to and intruded by the Panton mafic–ultramafic intrusion. SHRIMP error boxes in this and subsequent concordia figures are 1σ analytical limits, although quoted age errors are at the 95% confidence level.

(ii) Muscovite pegmatite. A muscovite–tourmaline pegmatite dyke, about 50 m long and 3 m wide, cuts serpentinised peridotite in the southeast of the Panton intrusion (Fig. 6.1). Like many K-rich pegmatites, it contains zircons that are altered and have very high U and significant common Pb (Appendix Table 4.2). The two zircon grains that were measured are concordant to sub-concordant, giving a weighted mean $^{207}Pb/^{206}Pb$ age of 1823±4 Ma (1σ). Although the age obtained cannot be regarded as a particularly accurate crystallisation age for the pegmatite, it is consistent with the geological relationships of the Panton intrusion. This pegmatite could well be an apophysis from a nearby granite belonging to the 1835–1805 Ma Sally Downs supersuite of the Bow River Batholith (Sheppard et al. 1995, 1997).

Springvale mafic intrusion (group II)

The Springvale intrusion is a moderately dipping mafic sheet, comprising olivine gabbro, gabbronorite, troctolite, leucogabbro, and anorthosite. About 40 brown, transparent, subhedral zircons (Fig. 6.3C) were recovered from 15 kg of mottled uratilised leucogabbro from the northwest part of the intrusion. Most zircons are inclusion-free and unaltered. A few grains have some euhedral crystal faces and show a weak internal magmatic zonation.

The zircons have variable Th/U (0.14–2.0) and U (Appendix Table 4.3; Figs 6.4, 6.5). Although U is not as high as in the Panton zircon suite, some grains have 2500–3000 ppm U; however, these are indistinguishable from the remainder in colour, morphology, and Th/U and $^{207}Pb/^{206}Pb$ ratios (Fig. 6.4). All 18 data points are concordant, and range in $^{207}Pb/^{206}Pb$ age from 1845 Ma to 1859 Ma. The weighted mean of 1857±2 Ma (χ^2 1.32) reflects the igneous crystallisation age of these zircons, approximating the emplacement time for the Springvale intrusion. This age is the same as that for the Panton intrusion and is also within error of the 1854±3 Ma age for the nearby Paperbark Granite (Sheppard et al. 1995).

Toby mafic intrusion (group III)

The Toby mafic intrusion is a shallowly dipping basinal body, 16 km north of the Springvale intrusion. In area, it is the largest of the intrusions (12 x 20 km) in the East Kimberley and it is enclosed by granites of the Bow River Batholith (Fig. 6.1). The intrusion is undeformed except in thin biotite–chlorite-rich shear zones. A high-level sub-ophitic quartz–biotite gabbro with an anomalously high Zr (140 ppm) was dated from the central part of the intrusion.

The gabbro contains abundant, clear, inclusion-free, light-brown zircons (Fig. 6.3D). The generally euhedral nature and lower U (85–460 ppm) and Th/U (0.5–1.0) ratios of the zircon grains distinguish this suite from the zircon suites in the Panton and Springvale intrusions (Appendix Table 4.4; Fig. 6.5). However, the isotopic data overlap those of the other two suites, and the zircon crystallisation age of 1855±2 Ma determined for the Toby intrusion is indistinguishable from the ages for the Panton and Springvale intrusions. The Toby intrusion age is based on all 24 analysed grains (age range

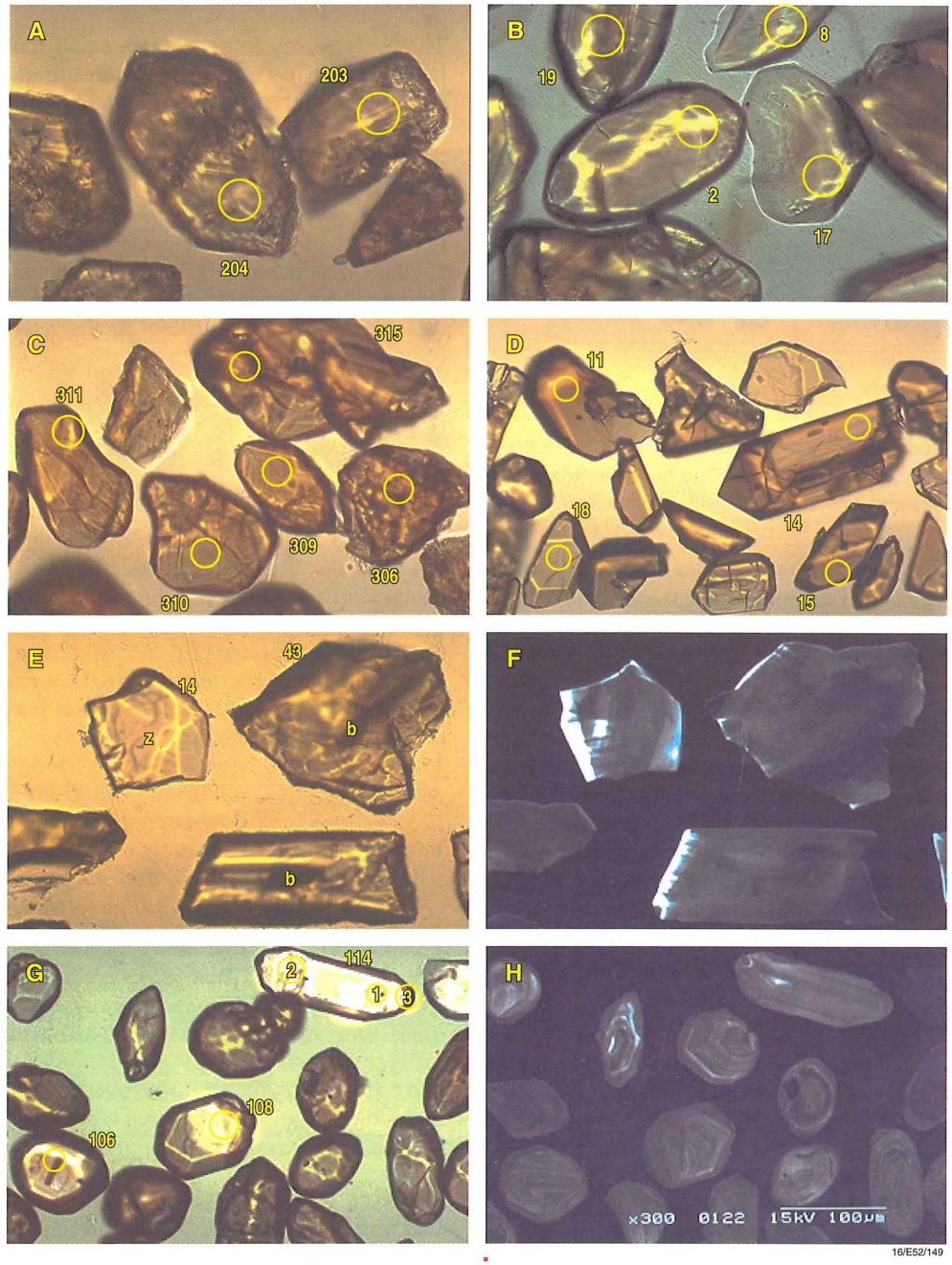


Figure 6.3. Photomicrographs of zircon and baddeleyite grains from the East Kimberley mafic–ultramafic intrusions in transmitted light or cathodoluminescence imagery. Clear, unaltered grain areas were selectively targeted in the SHRIMP analyses, as indicated by the 30 µm diameter circled areas for the numbered grains. Details of these analyses are listed in the tables of Appendices 4.1–4.7.

A. Panton intrusion, euhedral to subhedral zircon grains with high U content and displaying a variably altered appearance (transmitted light).

B. Rose Bore Granite, clear subhedral zircon grains (transmitted light).

C. Springvale intrusion, subhedral and a few euhedral clear cracked zircon grains (transmitted light).

D. Toby intrusion, clear, brown to colourless euhedral zircon grains (transmitted light).

E. Sally Malay intrusion, clear generally shapeless zircon (z) and baddeleyite (b) grains, with the latter grains having a higher reflectance (transmitted light).

F. Sally Malay intrusion, cathodoluminescence (CL) image of zircon and baddeleyite grains shown in Figure 6.3E.

G. McIntosh intrusion contact aureole, newly formed (1830 Ma leucosome) zircon group are generally clear, inclusion-free and colourless, whereas the inherited (detrital) zircon group (1865 Ma palaeosome and older grains) consists of brown subhedral grains with some resorption and corrosion features (transmitted light).

H. McIntosh intrusion contact aureole, cathodoluminescence (CL) image of zircon grains shown in G; the younger ~1830 Ma group of mainly clear, colourless euhedral grains have no compositional zoning or very weak zoning in a few grains under CL, as in transmitted light; many of the older palaeosome zircons show some zoning in transmitted light, whereas this zoning is always evident under CL.

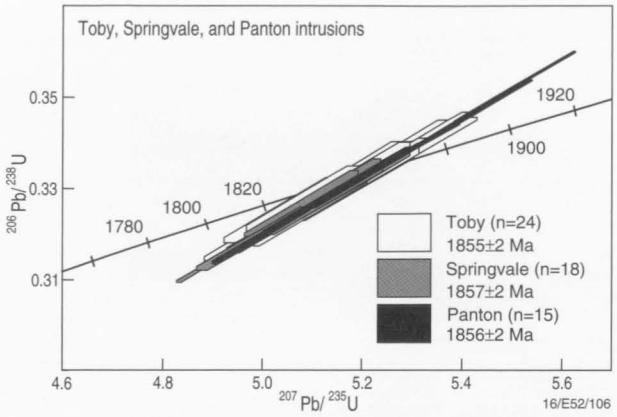


Figure 6.4. Concordia plot of zircon U–Pb data from the Toby, Springvale, and Panton mafic–ultramafic intrusions. The number of individual zircon analyses is indicated, and the pooled $^{207}Pb/^{206}Pb$ ages have errors quoted at the 95% confidence level.

1840–1864 Ma), the analyses being concordant and forming a single population in $^{207}Pb/^{206}Pb$ (χ^2 1.49).

On the concordia plot (Fig. 6.4) individual Toby intrusion zircons have larger errors than the higher-U zircons from the Panton and Springvale intrusions, but there is an overlap and close correspondence of the three magmatic ages at 1855±2 Ma, 1856±2 Ma, and 1857±2 Ma, respectively. As earlier mentioned, these ~1855 Ma layered mafic intrusions and the felsic rocks of the Paperbark supersuite and Whitewater Volcanics (~1865–1850 Ma) are fairly close in age, possibly coeval, and represent a major period of magmatic activity in the HCO.

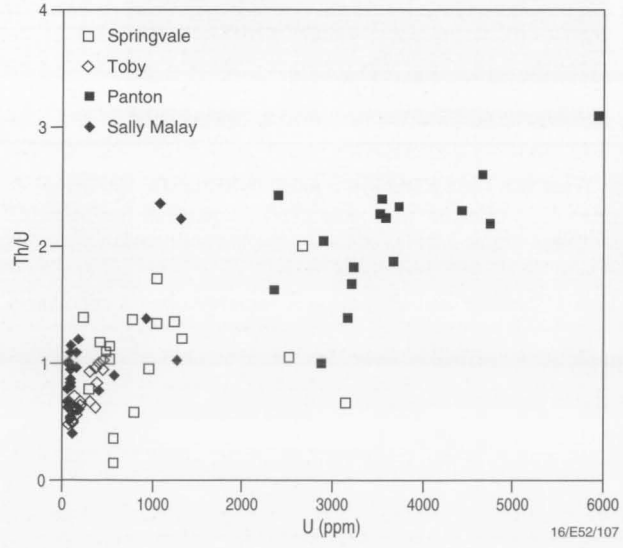


Figure 6.5. Plot of Th/U in zircons from four of the mafic-ultramafic intrusions in the Halls Creek Orogen, indicating very elevated U and Th, especially for the Panton and Springvale zircon suites.

Sally Malay mafic–ultramafic intrusion (group V)

The Sally Malay intrusion is a small multi-chambered layered mafic–ultramafic body that contains a significant, but subeconomic, resource of Ni–Cu–Co sulphides. Located on the TURKEY CREEK sheet northeast of the other dated intrusions (Fig. 6.1), it comprises cyclic units of peridotite, troctolite, olivine gabbro, and anorthosite. Mottled anorthosite from the upper part of the lowest cycle (which hosts the basal sulphides) contains about equal amounts of primary magmatic zircon and baddeleyite (Figs 6.3E,F).

The zircons are anhedral, clear, and colourless to pale brown. Their Th/U ratios (Appendix Table 4.5) overlap those of zircons from the Springvale and Toby intrusions (Fig. 6.5). The 23 analysed zircons range in age from 1834 to 1854 Ma, with a weighted mean $^{207}Pb/^{206}Pb$ age of 1844±3 Ma (Fig. 6.6); they do not define a normal distribution in $^{207}Pb/^{206}Pb$ (χ^2 1.79). Replicate analyses of grain 13 show it to have relatively high Th/U and U, but it is not aberrant in any other way and was not discarded from the main age group. A single population (χ^2 1.49) is, however, defined when the four most discordant data points (5.2, 8.1, 10.2, 15.1) are rejected. The mean age of the remaining 19 concordant analyses is unchanged at 1844±3 Ma, which is interpreted as the magmatic age of the zircon suite.

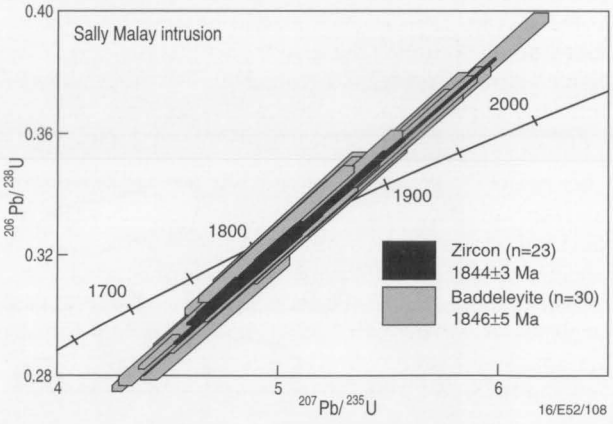


Figure 6.6. Concordia plot of zircon U–Pb and baddeleyite data from the Sally Malay mafic–ultramafic intrusion.

Baddeleyite in the anorthosite occurs as subhedral, light-brown grains. In many physical respects the baddeleyite resembles the zircon, but the former has a brighter reflectance and, in some cases, fine striations parallel to the prism faces. In the absence of a Pb/U baddeleyite standard, there is no absolute control on Pb/U in the baddeleyite analyses (Appendix Table 4.6), which were calibrated to the SL13 zircon standard, only for graphical representation in Figure 6.6.

The baddeleyite data straddle the concordia and overlap the zircon data in $^{207}Pb/^{206}Pb$. Individual baddeleyite analyses are generally less precise in $^{207}Pb/^{206}Pb$ measurement, but the pooling of the 30 data points suggests a single magmatic population with a weighted mean age of 1846±5 Ma (χ^2 0.85). This is in good agreement with the zircon crystallisation age of 1844±3 Ma. The zircon and baddeleyite data together provide a

reliable age for crystallisation and emplacement of the Sally Malay intrusion.

McIntosh mafic intrusion (group VI)

The McIntosh intrusion is a mafic body, 7.8 km thick, of cyclic units of olivine gabbro, olivine gabbronorite, troctolite, magnetite gabbro, and minor leucogabbro and peridotite. A large sample of gabbro on the northwestern side of the intrusion was found to be devoid of zircon and baddeleyite, and hence could not be directly dated.

However, a migmatitic garnet–cordierite–sillimanite–biotite–plagioclase–alkali feldspar–quartz hornfels (Fig. 6.7) of the Tickalara Metamorphics in the northwestern contact aureole of the intrusion (Fig. 6.1) contains zircon that crystallised in complexly folded, felsic leucosome 'sweat' bands. Dating of these zircons provides an alternative way of determining the emplacement age of the intrusion. The metamorphic mineral assemblage and associated rocks in the area indicate that the protolith to the migmatite was probably of sedimentary origin.

The recovered zircon population (Fig. 6.3G) contains two equal groups, readily distinguished using cathodoluminescence (CL) imagery (Fig. 6.3H). One group (which was found to be the younger) consists mainly of clear, colourless, euhedral grains, which display very weak or no compositional zoning in transmitted light and CL. The second group consists of colourless to light-brown euhedral to subhedral grains, many of which show zoning in transmitted light and CL. Some grains in the second group have discordant rims of unzoned zircon; such selvedges were too thin for satisfactory analysis with the SHRIMP ion beam.

The zircon U–Pb data fall into two groups (Fig. 6.8), corresponding to the two groups with the different physical attributes described above. Most of the analyses are concordant or near-concordant, and, in general, there is very good $^{207}Pb/^{206}Pb$ agreement in the replicate analyses (Appendix Table 4.7). The U values for the two groups overlap and Th/U ratios are also similar, although tending to be somewhat lower in the second group.

All 14 analyses of the generally unzoned first group define a $^{207}Pb/^{206}Pb$ age of 1830±3 Ma (χ^2 0.93). This is



16/E52/152

Figure 6.7. Field photograph of garnet–cordierite–sillimanite–biotite–feldspar–quartz migmatite from the northwestern contact aureole of the McIntosh mafic intrusion.

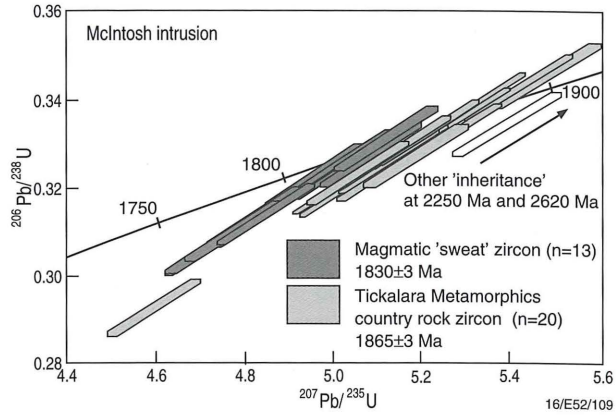


Figure 6.8. Concordia plot of zircon U–Pb data from the migmatitic hornfels (see Fig. 6.7) in the contact aureole of the McIntosh mafic intrusion. Thirteen data points define the 1830±3 Ma age for the felsic melt (leucosome) fraction of the contact migmatite, and this is regarded as the emplacement age of the mafic intrusion. The Tickalara Metamorphics country rock contains zircon age components of about 2620 Ma, 2250 Ma, 1910 Ma, and 1865±3 Ma, with the latter age component providing a maximum age for the migmatite's precursor rock.

the age of new zircon growth in the leucosome material and is interpreted to be the age of contact metamorphism/partial melting and, hence, the age of emplacement of the McIntosh intrusion. This intrusion, therefore, is significantly younger than the other four dated intrusions, and the age is in accord with its younger classification as group VI type—that is, the age is consistent with the field observations that the McIntosh intrusion cuts the Wild Dog intrusion, which cuts the Panton intrusion.

The second group of zoned zircons in the migmatite are grains that predate the contact metamorphic melting event. These zircons are interpreted as inherited (detrital) grains, which give the age(s) for the sedimentary provenance of the country rock, the Tickalara Metamorphics. Discordant rims (not analysed) are evident in CL imagery in grains 117, 119, 124, 128, and 130. The inherited zircons include several late Archaean and Palaeoproterozoic grains (2611 Ma, 2254 Ma, and 1911 Ma). The remaining 21 grains are between 1855 and 1882 Ma. However, they do not form a single age population unless the youngest grain (123) and the three oldest grains (100, 105, 130) at ~1880 Ma are discarded. The dominant population (n = 17) gives an age of 1865±3 Ma (χ^2 1.68). This is a reasonably coherent suite of restite zircons, considering the unconfirmed genesis of the migmatite and the fact that it has been contact metamorphosed to upper amphibolite facies.

The ~1880 Ma and 1911 Ma relic zircon in the Tickalara Metamorphics may be derived from the Biscay Formation of the Halls Creek Group or equivalents and from the Ding Dong Downs Formation, which contain felsic volcanics dated at about 1880 Ma and 1910 Ma, respectively.

The 1865±3 Ma age of the main inherited suite of detrital zircons in the migmatitic hornfels gives a

maximum depositional age for this part of the Tickalara Metamorphics. This age is similar to that of the Rose Bore Granite (1863±3 Ma), which gives a minimum age for the Tickalara Metamorphic country rocks on the south side of the Panton intrusion. Using these results, one can deduce depositional age constraints for the Tickalara Metamorphics in this part of the East Kimberley at close to 1865 Ma.

Discussion

The geochronological data, which have refined the relative age relationships of the intrusions as determined from field observations, show that the layered intrusions of the East Kimberley range in age from at least as old as 1857±2 Ma to at least as young as 1830±3 Ma. They predate and postdate the main folding event of the Halls Creek Orogeny (see Chapter 3). Three of the largest intrusions–Panton, Springvale, and Toby–were emplaced within a few million years of each other, at 1856±2 Ma, 1857±2 Ma, and 1855±2 Ma, respectively. However, as shown by Trudu & Hoatson (1996, see Chapter 9), emplacement depths for these 'coeval' intrusions range from 8 to 18 km. This implies that a thick section of the crust was subjected to a major influx of heat from the intrusions at around 1855 Ma. In addition, the age of emplacement of these three intrusions coincides with felsic magmatic ages in the Paperbark supersuite and Whitewater Volcanics (both ~1865–1850 Ma). These represent a very significant magmatic event or events that extend over a distance of at least 400 km. Thus, mafic, mafic–ultramafic, and felsic magmatism collectively contributed to heating large parts of the crust (both vertically and laterally) in the East Kimberley from 1865 to 1850 Ma. This magmatic event is also close to the best timing estimates for granulite-facies metamorphism (around 1850 Ma), suggesting that this magmatism also had a role in the high-grade regional metamorphic episode.

A mottled anorthosite unit from the multi-chambered Sally Malay intrusion contains primary zircon and baddeleyite. Their respective $^{207}Pb/^{206}Pb$ ages of 1844±3 Ma and 1846±5 Ma are indistinguishable, suggesting that both are magmatic ages and that the Sally Malay intrusion is about 10 million years younger than the Panton, Springvale, and Toby intrusions.

The McIntosh mafic intrusion postdates the main D_3 folding event of the Halls Creek orogeny at ~1835 Ma (see Chapter 3). As it contained no primary zircon or baddeleyite, this intrusion was dated indirectly, using migmatitic hornfels from its northwestern contact aureole. Zircon that crystallised in leucosome bands in this migmatite defines an age of 1830±3 Ma. This is interpreted as the time of partial melting and, hence, the emplacement age of the intrusion. Zircon in the palaeosome component of the migmatite records inheritance ages at around 1910 Ma, 2250 Ma, and 2620 Ma; however, the major inherited suite, dated at 1865±3 Ma, provides a maximum depositional age for the Tickalara Metamorphics country rocks in this region.

The 1855 Ma (groups I–III) and 1830 Ma (group VI) layered intrusions of the East Kimberley are similar in age to the granites of the Paperbark and Sally Downs supersuites of the Bow River Batholith, respectively (Sheppard et al. 1995). However, whole-rock geochemical and isotopic data (Sheppard 1996, Chapter 11) indicate that the mafic–ultramafic and felsic rocks of these major magmatic events are not comagmatic. Simultaneous intrusion of mafic–ultramafic and felsic magmatism from different sources was followed by crystal fractionation and limited magma mingling in the crust.

Summary

SHRIMP U–Pb zircon and baddeleyite ages have been obtained for fractionated anorthositic and gabbroic cumulates and related contact aureole rocks from five layered mafic–ultramafic intrusions in the HCO of the East Kimberley (Table 6.1). The abundance of suitable zircon in these rocks and the precision of ages obtained (±2 and ±3 Ma) indicate that U–Pb geochronology can be used successfully for the dating of Proterozoic mafic–ultramafic intrusions in this province. With the exception of the McIntosh body, all the investigated intrusions contain zircon believed to have crystallised from fractionating mafic magmas. The coexistence of baddeleyite and zircon in some fractionated mafic cumulates is also useful, since the dating of both minerals provides further checks on the consistency of the U–Pb geochronology.

Zircons from the East Kimberley intrusions have distinctive chemical and isotopic features. Those in the Panton, Springvale, and Sally Malay intrusions have unusually high Th/U ratios (up to 3.1), and in some cases very high U contents (2360–5930 ppm), and highly radiogenic Pb compositions. Cathodoluminescence imagery highlights the unzoned nature of zircons in the intrusions, whereas those from the Tickalara Metamorphics country rocks are commonly zoned.

The geochronological data obtained in this study (summarised in Table 6.1) highlight a number of important points relating to the geological evolution and mineralisation potential of mafic–ultramafic magmatism in the East Kimberley. These include:

- at least three major periods of mafic–ultramafic magmatism have been identified in this study, namely 1855 Ma, 1845 Ma, and 1830 Ma. Three major groups (I–III) of layered intrusions were emplaced over a very narrow time span close to 1855 Ma ago;
- some phases of mafic magmatism older than 1850 Ma (not investigated in this study) are represented by metagabbroic and metadoleritic sills in the Tickalara Metamorphics and the Woodward Dolerite. The Norton intrusion (Hoatson 1995) on TURKEY CREEK is one of the largest granulite facies mafic bodies of the Tickalara Metamorphics that was emplaced prior to the peak of metamorphism at about 1850 Ma. The last major stage of mafic magmatism in the East Kimberley is illustrated by the extensive mafic sills of the 1790±4 Ma Hart Dolerite

(OZCHRON, AGSO's geochronological database) in the Kimberley Basin;

- there is an apparent relationship between mineralisation and time (see Chapter 5). This secular variation consists of Cr–PGEs in the 1855 Ma intrusions of groups I (Panton) and II (Springvale), Ni–Cu–Co in the 1845 Ma intrusions of group V (Sally Malay), and Fe–Ti–V in the 1830 Ma intrusions of group VI (McIntosh);
- there is a correlation between depth of emplacement and age for the layered intrusions of greatest economic significance in the East Kimberley (see Chapter 9). The 1855 Ma group I intrusions (PGEs–Cr–Ni–Au) crystallised at crustal levels of ~11 km, whereas the 1845 Ma group V intrusions (Ni–Cu–Co) were emplaced at deeper crustal levels of 20–23 km (see Chapter 9). There also appears to be a migration of magmatism northwards along the HCO for these two economically important groups;
- ultramafic magmatism became subordinate to mafic magmatism with time;
- the distinctive chemical features of the zircons, the narrow age range for the emplacement of the intrusions (mostly 1855–1845 Ma), the close spatial association of the various groups of intrusions, and field evidence (see Chapter 5) support the idea that these bodies crystallised in situ and are not tectonically emplaced bodies derived from fragmentation of different 'parent' intrusions of different ages;
- with the exception of the granulite mafic bodies in the Tickalara Metamorphics, there is no apparent relationship between intensity of deformation and age of the layered intrusion. For example, the most deformed body, the 1855 Ma Panton intrusion, is coeval with the largely undeformed Toby intrusion. This paradox may reflect heterogeneity of deformation across the central and western zones of the HCO (discussed in terms of a terrane boundary by Tyler et al. 1995), and/or the size, composition, and geological setting of the intrusions. For example, a small ultramafic body (i.e. containing serpentinised peridotites) surrounded by mixed sedimentary and volcanic rocks will be more susceptible to deformation than a large homogeneous mafic body emplaced into a competent granite batholith; and
- emplacement of the large 1855 Ma group I–III layered intrusions was contemporaneous with the emplacement of granitic plutons of the Paperbark supersuite in the Bow River Batholith, with eruption of the Whitewater Volcanics taking place between 1865 and 1850 Ma, and with granulite-facies metamorphism at around 1850 Ma. Together, the emplacement of the mafic, mafic–ultramafic, and felsic magmas represents a huge flux of heat into the Earth's crust, indicating that this magmatism also probably played a major role in the high-grade regional metamorphism that affected the East Kimberley.

Acknowledgements

Frank Kane is thanked for assistance with field sample collection. The skilful and labour-intensive work by Lance Keast and Tas Armstrong (both AGSO) in separating zircon and baddeleyite is greatly appreciated. Chris Foudoulis (AGSO) is thanked for the long hours he spent preparing and documenting samples, providing the cathodoluminescence images, and generating much of the SHRIMP II data. The present work has benefited from discussions with many colleagues at AGSO and GSWA, and the critical reviews of Lance Black, David Blake, Alastair Stewart (all AGSO), and Ian Tyler (GSWA).

Appendix

SHRIMP II analytical techniques

The ion microprobe study used the SHRIMP II in the Research School of Earth Sciences, ANU. Detailed description of the analytical techniques for zircon U–Th–Pb analysis using SHRIMP is given by Compston et al. (1984) and Williams & Claesson (1987).

Zircon and baddeleyite grains were separated by conventional gravity and magnetic techniques, and mounted with fragments of SL13 standard in an epoxy-resin disk, which was coated with a ~50 Å layer of Au. A 30 μm primary beam of singly negatively charged O_2 was used for the production of positively charged secondary ions. Operation at a mass resolution in excess of 6500 ensured that there were no significant spectral interferences.

Corrections were made for initial Pb in the zircons, using values from Cumming & Richards (1975), based upon measured $^{204}Pb/^{206}Pb$. Pb/U was determined by reference to standard zircon SL13 (572 Ma, $^{206}Pb/^{238}U$ 0.0928). In this study, data on standards and unknowns were collected in sets of 7 scans through the species of interest. Errors were augmented according to the degree of non-collinearity of the ratioed species. Uncertainties in Pb/U and Pb/Th included an additional component derived from uncertainty in the calibration curve for the standard for each session. This component, which dominated the uncertainty in these ratios, was about 2.2 to 2.0% (1σ). The data for the Panton, Springvale, Toby, and McIntosh intrusions were collected over a SHRIMP session of 72 hours and the 25 standards have 1σ uncertainty of 2.2%.

Decay constants are those recommended by the IUGS Subcommission on Geochronology (Steiger & Jäger 1977). Uncertainties in calculated ages are quoted as 95% confidence limits, although analytical errors for individual analyses in the tables of Appendices 4.1–4.7 are quoted at the 1σ level. The analytical dataset (Appendix Tables 4.1–4.7) is available in OZCHRON, AGSO's geochronological database.

References

Amato, J.M., Wright, J.E., Gans, P.B. & Miller, E.L., 1994. Magmatically induced metamorphism and deformation in the Kigluaik gneiss dome, Seward Peninsula, Alaska. Tectonics, 13, 515–527.

Barton, M.D. & Hanson, R.B., 1989. Magmatism and the development of low-pressure metamorphic belts: Implications from the western United States and thermal modeling. Geological Society of America Bulletin, 101, 1051–1065.

Black, L.P., Kinny, P.D. & Sheraton, J.W., 1991. The difficulties of dating mafic dykes: an Antarctic example. Contributions to Mineralogy and Petrology, 109, 183–194.

Blake, D.H. & Hoatson, D.M., 1993. Granite, gabbro, and migmatite field relationships in the Proterozoic Lamboo Complex of the East Kimberley region, Western Australia. AGSO Journal of Australian Geology & Geophysics, 14(4), 319–330.

Compston, W., Williams, I.S. & Meyer, C., 1984. U–Pb Geochronology of zircons from Lunar breccia 73217 using a sensitive high mass-resolution ion microprobe. Proceedings 14th Lunar & Planetary Science Conference, Part 2. Journal of Geophysical Research, 89, Supp. B525–B534.

Cumming, G.L. & Richards, J.R., 1975. Ore lead isotopes in a continuously changing Earth. Earth and Planetary Science Letters, 28, 155–171.

De Yoreo, J.J., Lux, D.R. & Guidotti, C.V., 1991. Thermal modelling in low-pressure/high-temperature metamorphic belts. Tectonophysics, 188, 209–238.

Dow, D.B. & Gemuts, I., 1969. Geology of the Kimberley region, Western Australia: the East Kimberley. Bureau of Mineral Resources Australia Bulletin 106, 135 pp.

Gemuts, I., 1971. Metamorphic and igneous rocks of the Lamboo Complex, East Kimberley region, Western Australia. Bureau of Mineral Resources, Australia, Bulletin 107, 69 pp.

Heaman, L.M. & LeCheminant, A.N., 1993. Paragenesis and U–Pb systematics of baddeleyite (ZrO^2). Chemical Geology, 110, 95–126.

Hoatson, D.M., 1993. Correlation of structurally disrupted layered mafic–ultramafic intrusions in the East Kimberley: Is Big Ben part of the Panton intrusion? AGSO Research Newsletter, 19, 9–10.

Hoatson, D.M., 1995. New mineral discoveries in the East Kimberley. AGSO Research Newsletter, 22, 9–11.

Hoatson, D.M. & Tyler, I.M, 1993. Prospective layered mafic–ultramafic intrusions in the East Kimberley. AGSO Research Newsletter, 18, 8–9.

Kinny, P.D., Williams, I.S., Froude, D.O., Ireland, T.R. & Compston, W., 1988. Early Archaean zircon ages from orthogneisses and anorthosites at Mount Narryer, Western Australia. Precambrian Research, 38, 325–341.

Looseveld, R.J.H. & Etheridge, M.A., 1990. A model for low-pressure facies metamorphism during crustal thickening. Journal of Metamorphic Geology, 8, 257–267.

Paces, J.B. & Miller, J.D., 1993. Precise U–Pb ages of Duluth Complex and related mafic intrusions, northeastern Minnesota: geochronological insights to physical, petrogenetic, paleomagnetic, and tectonomagmatic processes associated with the 1.1 Ga midcontinent rift system. Journal of Geophysical Research, 98, no. B8, 13997–14013.

Sheppard, S., 1996. Mafic-felsic magma mingling in the Bow River Batholith of the Halls Creek Orogen. Western Australia Geological Survey, Annual Review 1995–96, 56–59.

Sheppard, S., Griffin, T.J. & Tyler, I.M., 1995. Geochemistry of felsic igneous rocks from the southern Halls Creek Orogen. Geological Survey of Western Australia, Record 1995/4, 81 pp.

Sheppard, S., Tyler, I.M. & Hoatson, D.M., 1997. Geology of the Mount Remarkable 1:100 000 sheet: Western Australia Geological Survey, 1:100 000 Geological Series Explanatory Notes, 27 pp.

Steiger, R.H. & Jäger, E., 1977. Subcommission on geochronology: convention on the use of decay constants in geo- and cosmochronology. Earth and Planetary Science Letters, 36, 359–362.

Sun, S-s. & Hoatson, D.M., 1992. Chemical and isotopic characteristics of parent magmas of the west Pilbara layered intrusions: Implications for petrogenesis, magma mixing, and PGE mineralisation in layered intrusions. In: Hoatson, D.M., Wallace, D.A., Sun, S-s., Macias, L.F., Simpson, C.J. & Keays, R.R., Petrology and platinum-group-element geochemistry of Archaean layered mafic–ultramafic intrusions, west Pilbara Block, Western Australia. Australian Geological Survey Organisation, Bulletin 242, 141–149.

Taylor, J.R. 1982. An introduction to error analysis: the study of uncertainties in physical measurement. Oxford University Press, Oxford, 270 pp.

Thompson, P.H., 1989. Moderate overthickening of thinned sialic crust and the origin of granitic magmatism and regional metamorphism in low-P–high-T terranes. Geology, 17, 520–523.

Thornett, J.R., 1986. Evolution of a high-grade metamorphic terrain in the Proterozoic Halls Creek Mobile Zone, Western Australia. Ph.D. thesis, University of Western Australia, 350 pp.

Trudu, A. & Hoatson, D.M., 1996. Depths of emplacement of Precambrian layered intrusions in the East Kimberley. AGSO Research Newsletter, 25, 10–12.

Tyler, I.M., Griffin, T.J., Page, R.W. & Shaw, R.D., 1995. Are there terranes within the Lamboo Complex of the Halls Creek Orogen? Western Australia Geological Survey, Annual Review 1993-94, 37–46.

Wickham, S.M., 1987. Crustal anatexis and granite petrogenesis during low pressure regional metamorphism: the Trois Seigneurs Massif, Pyrenees, France. Journal of Petrology, 28, 127–169.

Williams, I.S. & Claesson, S., 1987. Isotopic evidence for the Precambrian provenance and Caledonian metamorphism of the high grade paragneisses from the Seve Nappes, Scandinavian Caledonides. II. Ion microprobe zircon U–Th–Pb. Contributions to Mineralogy and Petrology, 97, 205–217.

Wingate, M.T.D., Campbell, I.H., Compston, W. & Gibson, G.M., 1998. Ion microprobe U-Pb ages for Neoproterozoic basaltic magmatism in south-central Australia and implications for the breakup of Rodinia. Precambrian Research, 87, 135–159.

GEOPHYSICAL EXPRESSION OF THE MAFIC–ULTRAMAFIC INTRUSIONS AND IMPLICATIONS FOR EXPLORATION

by RUSSELL D. SHAW & LAUTARO F. MACIAS

Introduction

This chapter provides an outline of the geophysical expression of mafic–ultramafic intrusions in the East Kimberley. It follows on from the regional studies of the geophysical and tectonic setting of the mafic–ultramafic intrusions within the Halls Creek Orogen (HCO) by Shaw et al. (see Chapter 4) and the geophysical and tectonic setting of the Kimberley Basin by Gunn & Meixner (1998).

Studying the geophysical expression of the different types of mafic–ultramafic intrusions provides information on their composition, alteration history, three-dimensional shapes, and depth extent. Such studies can also aid correlations with similar intrusions of economic potential (Hoatson et al. 1995).

The principle aims of this study are to:

- describe the geophysical expression of a representative set of mafic–ultramafic intrusions;
- place some constraints on the likely distribution of types of mafic–ultramafic intrusions that could have mineral potential; and
- examine the possible relationships between the tectonic setting and the mineral potential of the intrusions.

Geophysical framework

This study builds on the regional geophysical framework established for the East Kimberley region by Shaw et al. (see Chapter 4). That study was based on an earlier Australia-wide study (Shaw et al. 1996), which mapped crustal elements. These are composite geophysical domains based on distinctive patterns of magnetic and gravity anomalies that have been delineated to emphasise, where possible, their relationships to recognised geological provinces. This chapter aims to add to our understanding of the compositional variation, geometry, and tectonic setting of the mafic–ultramafic intrusions.

Magnetic data

The magnetic data used in this study are derived from the AGSO National Geophysical Database (AGSO 1997). The data were acquired for AGSO in 1991 and were collected on east-west flight lines spaced at 400–m intervals and at a nominal height of 100 m above ground level. The tie-line spacing was 4000 m. The digital data set had been gridded to a cell size of about 80 m, using the standard AGSO minimum curvature method.

Geophysical expression of the mafic and mafic–ultramafic intrusions

Figure 7.1 shows the distribution and generalised magnetic response of Palaeoproterozoic mafic–ultramafic intrusions in the East Kimberley. Figure 7.2 is a processed Total Magnetic Intensity (TMI) image of the region and includes most of the mafic–ultramafic intrusions in the East Kimberley. In Figure 7.3 the boundaries of some of the mafic–ultramafic intrusions, as well as major faults, are shown overlying the TMI image. The numbering used to identify each intrusion follows that adopted by Hoatson (see Chapter 5).

In constructing the overlay for Figure 7.3, the boundaries of the mafic and mafic–ultramafic intrusions were refined slightly using a processed gamma-ray spectrometric (radiometric) image (cf. Fig. 4.12) in which the limits of the intrusions are commonly clearly expressed as dark tones.

Geophysical features of the intrusions are summarised in Table 7.1 where the intrusions are grouped according to the classifications of Hoatson & Tyler (1993), Hoatson (1993), Trudu & Hoatson (1996), and as updated in Chapter 5.

General features of the gravity expression

The ultramafic rocks have no obvious expression as individual gravity anomalies, because of their small size and tendency to spatially align with the margins of long-wavelength gravity anomalies.

The East Kimberley is dominated by a large-wavelength regional gravity ridge which is unusually large in magnitude. Its source appears to be some mixture of rocks dominated by pelitic and mafic granulite, carbonates, para-amphibolites and tonalite, together with some mafic–ultramafic intrusions—all uplifted from mid-crustal depths.

As explained in the section on gravity features in Chapter 4 (see Fig. 4.9), the regional gravity ridge can be partly related to uplifted deep-seated crustal blocks within the western and central zones (see Chapter 3) of the HCO. At mid- to lower-crustal depths, these blocks, as presently preserved, are considered to contain a high proportion of mafic rocks with relatively high densities, including metamorphosed mafic–ultramafic intrusions, as well as other dense rocks such as garnet-bearing pelitic gneisses and calc-silicate rocks.

Table 7.1. Geophysical features of representative mafic–ultramafic intrusions in the East Kimberley region. Locations of numbered intrusions are shown in Figs 7.1 and 7.3.

No.	*Name*	*Group*	*Magnetic expression*	*Magnetic source*	*Age (Ma)*[1]	*Depth of emplacement (km)*[2]	Comment
1	Faulted	Cg	High	Disseminated magnetite			Small magnetic anomaly in centre of body
2	Mabel Downs West	Cg	Variable	Disseminated magnetite in gabbro			Remnant magnetism (?)
3	Mabel Downs Homestead	V	Localised low	Disseminated magnetite			
4	Mabel Downs Southwest	V	Localised high	Ilmenite-titaniferous magnetite in gabbro			Remnant magnetism (?); along strike from Frog Hollow intrusion (7)
5	Nine Mile	Cg	Intense, complex high, with internal lows	Disseminated magnetite			Some magnetite may have formed from contamination of mafic magma by rafts of granite and metasediments
6	Norton	TM	Moderate to weak	Coarse-grained ?metamorphic magnetite	>1850		No obvious magnetic response from gossans or from associated sulphides at depth
7	Frog Hollow	V	Narrow ridge	Ilmenite-titaniferous magnetite in gabbro			Massive ilmenite–titaniferous magnetite lenses near top of intrusion
8	Foal Creek	II	Magnetically transparent				
9	Keller Creek	V	Magnetically transparent	Magnetite in gabbro		21	Possible magnetic contribution from pyrrhotite in Ni–Cu–Co sulphides near basal contact
10	Corkwood	V	Near broad high	Magnetite in gabbro			Possible magnetic contribution from pyrrhotite in Ni–Cu–Co sulphides near basal contact
11	Greenvale Fault	Cg	Magnetically transparent	Magnetite in gabbro			
12	Sally Malay	V	Near small high	Pyrrhotite and magnetite in sulphides; disseminated magnetite in gabbro	1844±3 1846±5	22	Small intrusion containing massive and disseminated pyrrhotite, pentlandite, chalcopyrite, and magnetite
13	Three Nuns	V	Indistinct				Too small to have geophysical signature
14	Oxide	V	Weak low	Ilmenite-titaniferous magnetite in gabbro			
15	Fletcher Creek	V	Narrow ridge	Magnetite in olivine gabbro and gabbro			Along strike from McKenzie Spring intrusion (20)
16	Dave Hill	V	Intense low and folded narrow ridge	Not known			Remnant magnetism (?) associated with norite, leuconorite, and leucogabbronorite
17	Amphitheatre	VII	Magnetically transparent	Not known			Probably too small to have geophysical signature
18	Wilson Creek	V	Magnetically transparent	Not known		22	

19	Spring Creek	V	Small high surrounded by low			20?	
20	McKenzie Spring	V	Narrow ridge	Magnetite in gabbro and/or pyrrhotite in sulphides?		23	Ni–Cu–Co sulphides along basal contact
21	Egg	VII	Small intense low, with high rim	Not known			Remnant magnetism (?)
22	Toby	III	Complex, high-frequency signal	Disseminated magnetite in quartz-bearing biotite gabbro	1855±2	8	Magnetic pattern is characteristic of thin, subhorizontal magnetic layer; eastern part of Toby intrusion and Wilagee intrusion overlies gravity high
23	Sandy Creek	Cg	Weak narrow ridge	Disseminated magnetite in fractionated and altered gabbro			Dyke-like body similar to the strongly magnetic Billymac Yard (27), Paperbark (31), and Margaret River (44) intrusions
24	Wilagee	II	Complex, high-frequency signal	Magnetite in peridotite and troctolite		10	May represent basal part of the Toby intrusion; overlies gravity high
25	Togo	VI	Magnetically transparent	Trace magnetite in leucogabbro			
26	Melon Patch	I	Narrow ridge	Disseminated magnetite after serpentinised olivine			Not easily related to regional magnetic pattern; intense serpentinisation of ultramafic rocks
27	Billymac Yard	Cg	Prominent narrow ridge	Abundant magnetite in gabbro			Dyke-like body; continuation of strongly magnetic Paperbark intrusion (31)
28	Juries	Cg	Complex high	Magnetite in gabbro			Contaminated mafic body formed from extensive commingling with granite
29	Black Hills Yard	VII	Uncertain	Not known			Small plug-like mafic bodies with no significant geophysical signature
30	South Melon Patch	I	Magnetically transparent	Disseminated magnetite after serpentinised olivine			Intense serpentinisation of ultramafic rocks
31	Paperbark	Cg	Prominent narrow ridge	Abundant magnetite			Gabbro dyke, asymmetry of magnetic anomaly suggests western dip
32	West McIntosh	I	Weak	Disseminated magnetite after serpentinised olivine			Intense serpentinisation of ultramafic rocks
33	Mini	I	High	Disseminated magnetite after serpentinised olivine			Intense serpentinisation of ultramafic rocks
34N	McIntosh	VI	Circular pattern of alternative highs and lows	Disseminated and cyclic units of ilmenite-titaniferous magnetite in gabbro	1830±3	18	Ilmenite–titaniferous magnetite in gabbro near top of intrusion and also along western and northern margins; northern part of gravity ridge
34S	McIntosh	VI	Curvilinear, discontinuous high surrounding central low	Magnetite in gabbro	1830 (?)	>18?	Possible feeder in southern part of McIntosh intrusion near Alice Downs Fault; northern part of gravity ridge

35	Highway	I	Small elongate high	Disseminated magnetite after serpentinised olivine			Magnetic high restricted to southern part of thin mafic–ultramafic intrusion; intense serpentinisation of ultramafic rocks
36	West Panton	I	Indistinct	Disseminated magnetite after serpentinised olivine			Intense serpentinisation of ultramafic rocks; possible satellite intrusion to Panton intrusion (39)
37E	Springvale (East)	II	Moderate to weak	Negative magnetic response possibly due to remnant magnetism		18?	Southern edge of gravity ridge; slight misalignment between the magnetic and gravity anomalies suggests intrusion may plunge to north
37W	Springvale (West)	II	Complex high containing small lows; sharp southern boundary probably marks a fault	Disseminated magnetite in olivine-bearing gabbro	1857±2	18	Southern edge of gravity ridge
38	Springvale Track	I	Magnetically transparent	Disseminated magnetite after serpentinised olivine			Mafic–ultramafic intrusion with small exposures of ultramafic rocks strongly serpentinised
39 39u	Panton	I	Curvilinear, discontinuous high surrounding a low	Disseminated magnetite after serpentinised olivine	1856±2	11	Magnetic high follows ultramafic rocks at base of synformal intrusion; intense serpentinisation of ultramafic rocks
40	Wild Dog Creek	IV	Weak and complex	Magnetite gabbro and magnetite quartz gabbro			Several of these mafic bodies have heterogeneous magnetic expression
41	West Robin Soak	I	Includes weak ridge	Disseminated magnetite after serpentinised olivine			Borders the Springvale Fault; intense serpentinisation of ultramafic rocks
42	Panton River	Ug	Magnetically transparent	Disseminated magnetite in fractionated gabbro			Weak magnetic expression suggests thin sheet-like intrusion
43	Big Ben	I	Weak	Disseminated magnetite after serpentinised olivine	1856?	11	Weak magnetic expression suggests thin intrusion; intense serpentinisation of ultramafic rocks
44	Margaret River	Cg	Prominent ridge	Abundant magnetite in gabbro			Dyke-like body; continuation of strongly magnetic Paperbark intrusion (31)
45	Three Sisters	Ug	Includes weak ridge	Disseminated magnetite in fractionated gabbro			
46	Armanda	VI	Magnetically transparent	Disseminated magnetite in olivine gabbro and gabbronorite		10	

[1] Age estimates from Page et al. (1995).
[2] Depth estimates from Trudu & Hoatson (1996).
For details of Cg = Corridor gabbro; Ug = Undivided gabbro; TM = Tickalara Metamorphics, and groups I to VII: see Trudu & Hoatson (1996) and Chapter 5.

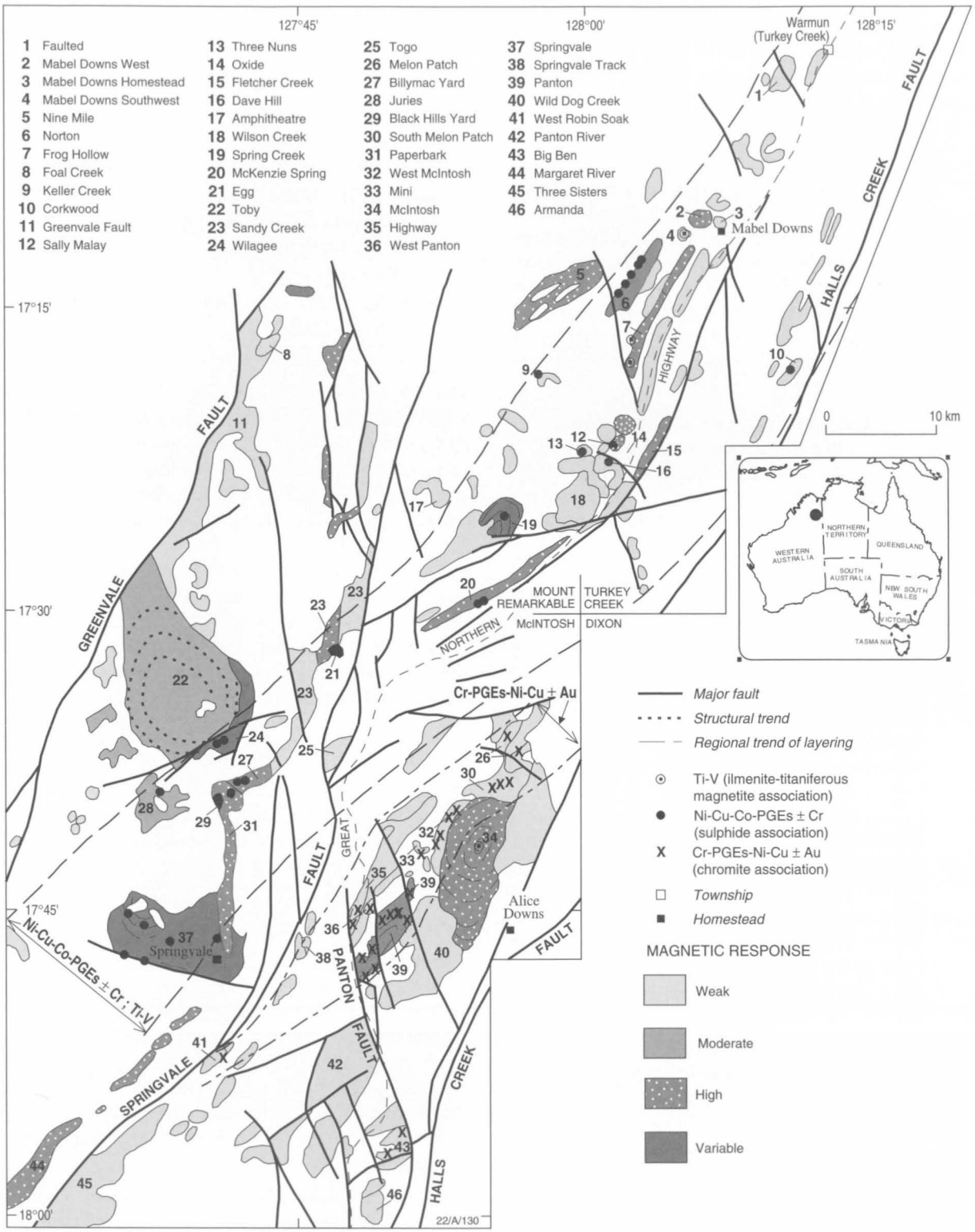


Figure 7.1. Distribution of Palaeoproterozoic mafic–ultramafic intrusions in the East Kimberley, showing their general magnetic response. Two northeast-trending parallel corridors containing mineralised intrusions are bounded by dashed lines (after Trudu & Hoatson 1996, and Chapters 4 & 5). General magnetic responses (SI*10^{-6} units) are: Weak = 10–2000; Moderate = 2000–12 000; High = 12 000–20 000+; Variable = 100–60 000 (values can vary widely over short distances).

Of the individual major Bouguer gravity anomalies that are superimposed as shorter wavelength features on the regional gravity ridge, the most prominent anomaly is in a region where there are no large mafic–ultramafic intrusions. This anomaly corresponds to outcropping garnet-bearing metapelites. So, these metapelites could be the densest of the regionally distributed rocks in that region. The mafic–ultramafic intrusions that could be related to an individual gravity anomaly are the McIntosh, Springvale, and Toby intrusions—although

none of them are directly centred over an individual gravity high. The eastern part of the Toby intrusion overlies a gravity high that could reflect a large, related magma chamber at depth. The Springvale intrusion corresponds to the southern edge of a gravity ridge that may link to the anomaly that partly overlaps the Toby intrusion.

The McIntosh intrusion corresponds to the northern part of a gravity ridge, but not to the peak of the anomaly, which is to the southwest and could reflect a related larger parent magma chamber at depth. The other possibility, that the gravity ridge is an expression not of the McIntosh intrusion, but of the Wild Dog Creek intrusion, is unlikely as other examples of the group IV Wild Dog Creek intrusions are not associated with gravity highs.

Another broader gravity anomaly within subelement HCC to the south corresponds to microelement HCCc (Fig. 4.9). It is not readily explained in terms of exposed rock units and appears to reflect a deeper source, possibly a hybrid set of rock bodies ranging in composition from gabbro to granite.

General features of the magnetic expression

Several of the mafic–ultramafic intrusions are moderately to highly magnetic (Fig. 7.1), reflecting their highly evolved tholeiitic character. Several mafic–ultramafic intrusions also have a highly variable magnetic expression, which, in addition to factors such as the shape, size, and thickness of bodies, depends on the distribution of secondary magnetite formed during serpentinisation of olivine and on the presence of primary magnetite in evolved gabbroic units. Olivine is abundant in the more primitive group I mafic–ultramafic bodies, such as the Panton intrusion (39 in Figs 7.1 & 7.3). However, olivine is more likely to be an accessory mineral of late-stage, more fractionated components of mafic intrusions, as is the case for the numerous gabbroic pulses characterising the group V (Sally Malay: 12 in Fig. 7.1) and VI (McIntosh: 34 in Fig. 7.1) intrusions.

In contrast to the more evolved rock types, plagioclase and clinopyroxene-rich cumulate rock types, such as anorthosite, gabbronorite, and troctolite (plagioclase-olivine cumulate containing little or no pyroxene), tend to be weakly magnetic or non-magnetic. These rock types are present in various proportions in several of the intrusions, such as parts of the Panton (39), Springvale (37), and Togo (25) intrusions (see Chapter 5).

Some of the biotite-bearing gabbros of the Corridor gabbro group (31, 27, & 23 in Fig. 7.1) are highly magnetic. The magnetite and biotite are possibly a consequence of SiO_2 contamination of the primary mafic magma.

Processes favouring the formation of magnetite in the mafic–ultramafic and mafic intrusions are:

- late stage, low-grade alteration of olivine in the more primitive ultramafic rocks (e.g. dunite, lherzolite, and peridotite) resulting in fine-grained disseminated magnetite;
- increase in the Ti and Fe contents of tholeiitic mafic magmas during fractionation, leading ultimately to the crystallisation of ilmenite-titaniferous magnetite as a primary phase—the ilmenite-titaniferous magnetite association of Hoatson (see Chapter 5);
- slight SiO_2 contamination of the primitive mafic magma suppressing olivine crystallisation, thereby enhancing the crystallisation of orthopyroxene and magnetite; and
- excessive SiO_2 contamination suppressing clinopyroxene crystallisation to produce abundant magnetite along with orthopyroxene.

The net outcome of these processes is that more magmatically evolved rock types—such as plagioclase-rich gabbro, gabbronorite, and norite—may contain coarse-grained primary magmatic magnetite or ilmenite in various combinations and are commonly the most magnetic rocks. The magnetite-rich gabbroic rocks of the McIntosh (43N in Fig. 7.3) and Frog Hollow (7) intrusions are examples. The more primitive olivine-rich rock types, such as peridotite and dunite, contain fine-grained, secondary magnetite after olivine that readily alters to Fe-rich products and results in rocks that are generally only weakly magnetic. The Panton intrusion (39 in Figs 7.1 & 7.3) is an example.

In general, the intrusions with the thickest ultramafic components (e.g. Panton intrusion) are weakly magnetic to non-magnetic and are small, whereas the more evolved and generally larger mafic intrusions, such as the McIntosh intrusion, are moderately to intensely magnetic (Figs 7.2 & 7.3).

Particular problems in the regional interpretation of the mafic–ultramafic intrusions are:

1. The mafic–ultramafic intrusions in the western zone of the HCO show as distinct bodies in TMI images (Figs 7.2 & 7.3), but deeper parent bodies are not evident in the long-wavelength magnetic data. This observation implies that either these particular bodies are not linked to a large chamber at depth, or the associated magma chambers have a different magnetic mineralogy, or there is some other complicating factor.
2. If it can be presumed that the mafic–ultramafic intrusions in the central zone of the HCO are similar to those in the western zone, their spatial correlation with the regional gravity high may mean that this regional gravity high represents underplated mafic material deep in the crust, where olivine has not been altered to form magnetite. If so, the deep-seated mafic material extends westwards underneath a thickness of granitic crust. What is possibly an east-dipping crustal boundary fault is marked in the magnetic data by a sharp drop-off in magnetic intensity values.

Geophysical and related geological features of individual intrusions

The following notes, complemented by those in Table 7.1, describe the geology and geophysical character of individually numbered mafic and mafic–ultramafic intrusions shown in Figures 7.1 and 7.3. The intrusions are grouped according to the classification of Hoatson (see Chapter 5), which is based on lithological association and the deduced relative age of the intrusion, and modified from the progressively updated classifications of Hoatson & Tyler (1993), Hoatson (1993), and Trudu & Hoatson (1996). Additional information on the petrophysical properties of the rocks in the Gordon Downs–Dixon Range 1:250 000 Sheet area, including the magnetic properties of some of the intrusions, is given in Appendix 5. General petrophysical information about other rocks types in the region is discussed in Chapter 4. For the most part, the descriptive notes that follow focus on type-examples of each group. Geological comment is added where it helps to understand the geophysical expression of the intrusions.

Pre-group I intrusions of the Tickalara Metamorphics

- These are deformed and folded bodies of amphibolite and mafic granulite mapped as part of the Tickalara Metamorphics.

- Apart from the Norton intrusion, they have low magnetic susceptibilities (<500 SI*10^{-6} units).

- The country rocks are generally amphibolite to granulite facies metapelites and psammites with relatively high densities (2.75–2.8 g/cm^3, see Appendix 5).

Key example – Norton intrusion (6):

- This is a moderately to weakly magnetic body (Figs 7.1 & 7.3) intimately associated with mafic granulites, some of which contain accessory magnetite.

- Altered ferruginous gossans, which intermittently persist along the northwestern basal contact of the intrusion, contain goethite, hematite, traces of magnetite and/or maghemite, and—as well as major silicate minerals—quartz and montmorillonite (Hoatson 1995).

- Neither the gossans nor possible sulphides at depth have a regional magnetic response.

- A thin moderately magnetic horizon that persists near the northwestern basal contact of the Norton intrusion probably represents another mafic granulite unit of the Tickalara Metamorphics.

- The intrusion can be expected to have a density considerably greater than most of the garnet-bearing pelitic gneiss country rocks, which are likely to have a relatively high density (2.75–2.8 g/cc, see Appendix 5).

Group I intrusions

- These are deformed and folded bodies of amphibolite facies with the highest component of ultramafic rocks of any intrusion that crops out in the East Kimberley.

- The country rocks are generally amphibolite facies metapelites, psammites, and metavolcanic rocks of the Tickalara Metamorphics.

- These are the most primitive intrusions (32, 33, 35, 36, 38, 39, 41, 43) in the East Kimberley with the olivine-rich cumulates commonly intensely serpentinised and, hence, containing fine-grained disseminated magnetite.

- Measured magnetic susceptibilities from the mafic–ultramafic rocks are in the range 50–1000 SI*10^{-6} units.

Key example – Panton intrusion (39):

- Moderately high magnetic susceptibility values (2000–5000 SI*10^{-6} units) are estimated for the lower units of serpentinised dunite, lherzolite, and harzburgite, which often host chromitite layers.

- The intrusion is a sill-like body, which has been deformed into a tight syncline, so is not expected to persist at depth.

Group II intrusions

- This group includes the Wilagee intrusion (24) and, arguably, the Foal Creek intrusion (8), both showing a weak magnetic response. The Springvale intrusion is the main member of this group (see below).

- The intrusions show primary cumulus textures not indicative of a strong metamorphic overprint.

Key example – Springvale intrusion (37):

- The intrusion is made up of two lobes:

- Much of the eastern lobe (37E) is covered by black soils, so its stratigraphy is uncertain.

- The low magnetism exhibited by the eastern lobe could be the result of remanent magnetism.

- For the eastern lobe, the slight misalignment between the magnetic and gravity anomalies suggests a northerly plunge to the body.

- Field relationships suggest that the eastern lobe is discordant to the western lobe and that the southern margin of the intrusion is faulted.

- The western lobe (37W) has a variable magnetic response, magnetic susceptibility values expected to be in the 2000–5000 SI*10^{-6} unit range.

- The western lobe is more highly magnetic at its margins and dips and becomes progressively younger to the north.

- Marked aligned gravity and magnetic gradients correspond to the fault on the southern margin, implying that this is a deep-seated fault.

Group III intrusion

- The only intrusion in this group is the Toby intrusion.

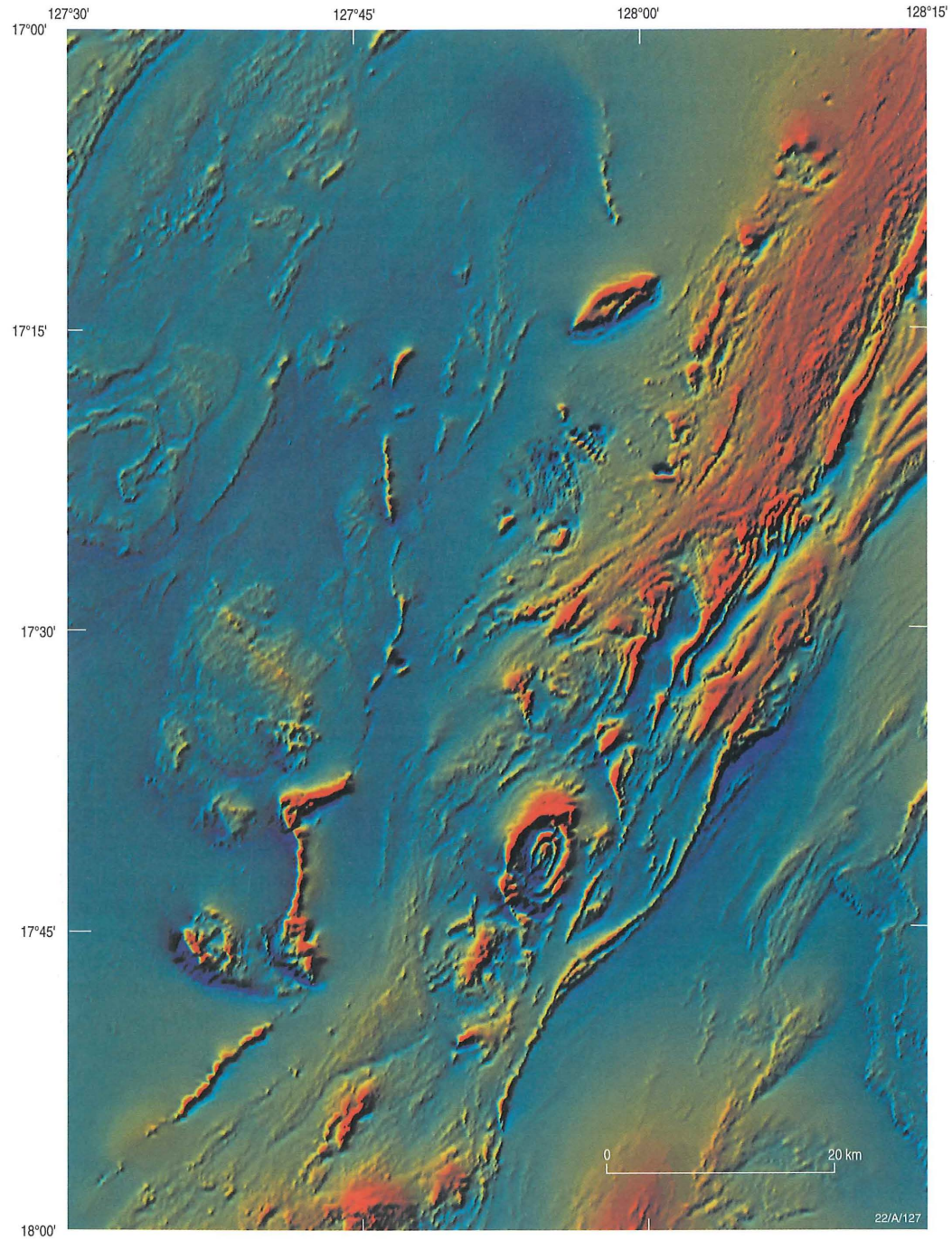


Figure 7.2. Processed image of Total Magnetic Intensity data in the region of the mafic–ultramafic intrusions (McINTOSH, TURKEY CREEK, & MOUNT REMARKABLE), with a NW illumination filter and 'Comtal' pseudocolour (~1: 1:500 000 image by L. Macias).

Key example – Toby intrusion (22):

- Surface structure suggests that the Toby intrusion is a saucer-shaped body, semi-circular in plan, with local shallow dips of less than 20°.

- The intrusion is about 2 km thick (see Chapter 5).

- As over two-thirds of the body is covered by black soil plain, the nature and details of the structure of the body are not well constrained.

- There is a slight misalignment between the magnetic and gravity anomalies, which suggests a northerly plunge to an underlying magma chamber at depth.

- The body is moderately to highly magnetic, (2000–12000 SI*10^{-6} units) and has several magnetite-rich units in the more fractionated part, which could include the adjacent Wilagee intrusion (24) to the southeast.

- The weak concentric grain visible on TMI (Figs 7.2 & 7.3) and Landsat (see Chapter 8) images probably reflects subtle variations of magnetite content in the gabbroic rocks (cf. Fig. 7.1). The variation could be either a primary feature or the result of alteration along concentric fractures (see Chapter 5).

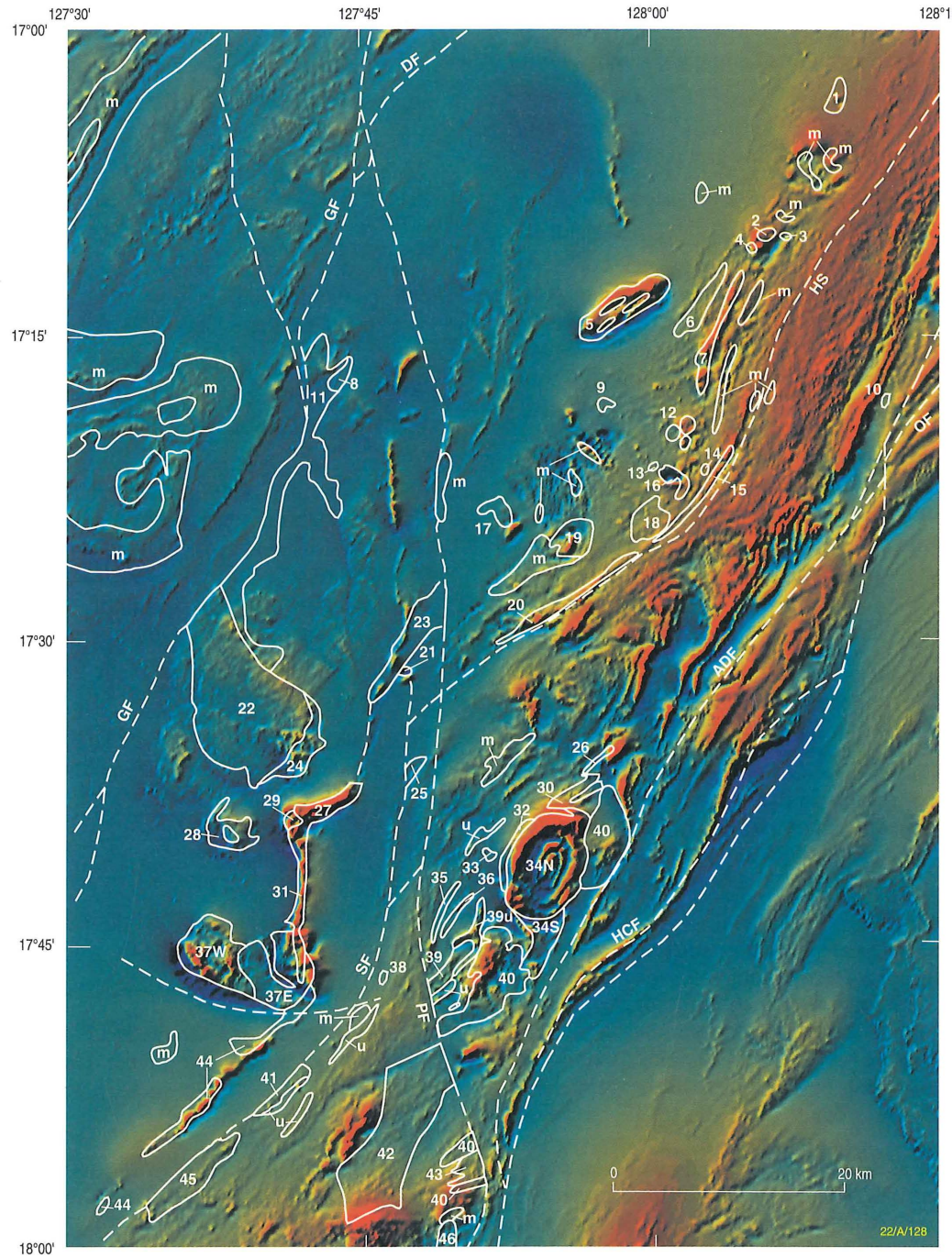


Figure 7.3. Distribution of Palaeoproterozoic mafic–ultramafic intrusions and structural element boundaries, overprinted on the magnetic image displayed in Figure 7.2 (annotation by RDS). Geophysical features of the numbered intrusions are summarised in Table 7.1. Unnamed ultramafic intrusions are labeled 'u' and mafic intrusions 'm'. Large mafic bodies in the west are sills of Hart Dolerite. The boundaries of the mafic and mafic–ultramafic intrusions differ slightly from those shown in Figure 7.1 in that they are based on a processed gamma-ray spectrometric (radiometric) image. The labelled structural features are ADF = Alice Downs Fault; DF = Dunham Fault; GF = Greenvale Fault; HCF = Halls Creek Fault; HS = Highway Shear Zone; OF = Osmond Fault; PF = Panton Fault; and SF = Springvale Fault.

Group IV intrusions

- The largest of the mafic bodies of this group are spatially associated with the McIntosh and the Panton (39) intrusions, but have a very different character that reflects extensive amphibolite-facies metamorphism.

- These intrusions are cut by the McIntosh intrusion and therefore are older than 1830 Ma, and they intrude the western margin of the Panton intrusion, and therefore are younger than 1855 Ma (Tyler et al. 1997a; see Chapter 5).

- The body northeast of the McIntosh intrusion is probably a shallow-dipping, sheet-like body; it contains biotite gabbro, tonalite, and diorite.

- The poorly exposed body east of the Panton intrusion consists of low hills and extensive black soil plains, containing abundant Fe–Ti oxides.

- The magnetite/ilmenite content in associated hybrid mafic rocks of the Wild Dog Creek intrusions is associated with the formation of amphibole and seems to be heterogeneous.

- These hybrid rocks account for much of the variability in the magnetic expression of this group of intrusions.

Key example – Wild Dog Creek intrusion (40):

- There is a suggestion that the strongly magnetic northwestern part of the Wild Dog Creek body east of the Panton intrusion may be more evolved than the southeastern part which has a weaker magnetic character, i.e. the intrusion may young to the northwest.

Group V intrusions

- Together with the group 1 intrusions (e.g. Panton intrusion), these sulphide-bearing intrusions appear to be the most prospective group in the East Kimberley.

- Unlike the Panton group of intrusions, the group V bodies intrude gneisses and granulites of high metamorphic grade, so their different history is expected to reflect some residence time in the lower crust.

- Group V intrusions are commonly small and have either a weak magnetic response (3, 9, 10, 13, 14, 16, and 19) or contain thin moderately to highly magnetic units (4, 7, 10, 12, 15, 18, and 20).

- Olivine, where present in these intrusions (12, 15, 16, 19, 20), is generally intensely serpentinised in the ultramafic rocks and partly serpentinised in the mafic rocks, resulting in finely disseminated secondary magnetite.

- Coarse-grained Fe–Ti oxides are characteristic of highly fractionated mafic variants of this group, such as Frog Hollow. This intrusion is strongly magnetic, with disseminated magnetite in metagabbro, and it contains small discontinuous lenses of ilmenite and titaniferous magnetite associated with clinopyroxene cumulates (Hoatson 1995).

Key example – Sally Malay intrusion (12):

- The main mineralised interval consists of massive Ni–Cu–Co-bearing sulphides hosted by thin gabbroic rocks along the basal contact.

- Disseminated and stringers of sulphides occur in ultramafic and mafic rocks above the massive sulphides (Hoatson et al. 1997).

- The mineralised assemblage—pyrrhotite, pentlandite, chalcopyrite—has magnetic susceptibility, conductivity, and density values that are well above those of both the country rock gneisses and the mafic–ultramafic intrusive rocks (Frankcombe et al. 1994).

Group VI intrusions

- Apart from the McIntosh intrusion, the Armanda intrusion is the only other intrusion in this group.

- The Armanda intrusion is a small layered mafic intrusion (Warren 1992) with a weak magnetic response.

Key example – McIntosh intrusion (34):

- There is a subsurface extension of the main McIntosh body to the north, but otherwise the magnetic anomaly closely matches the mapped geological boundary.

- Magnetite is prominent in the highly evolved upper parts of this large 7.8 km thick (see Chapter 5) mafic body.

- Magnetite, possibly formed as a result of country rock contamination, is also abundant along the western and northern margins of the body.

- There is a slight misalignment between the centre of the intrusion marked by the concentric magnetic anomalies and the peak of a gravity ridge, which aligns with the strike of the intrusion, but is not centred over the intrusion.

- This geometrical relationship suggests that there is a related, less magnetic intrusion at depth to the southwest to account for the gravity ridge.

- The small, more ultramafic phases of the intrusion, exposed in the far southern part of the outcrop-area (see Chapter 5), are less magnetic and unrelated to the gravity ridge.

- Their small outcrop area indicates they would not have a significant geophysical signature.

Group VII intrusions

- Most of these intrusions are too small to show on the map, generally being less than 200 m across.

- They include troctolite and olivine gabbro plugs that intrude hybrid mafic rocks of the Corridor gabbro.

Key example – Black Hills Yard intrusion (29):

- Due to its small size, the magnetic response of this body is swamped by that of the adjacent Corridor gabbro.

Corridor gabbro group

- Many of these intrusions are expressed prominently in the TMI image (Fig. 7.2).

- One set of dyke-like intrusions (31, 27, & 23 in Fig. 7.1) appears to follow an old trace of the Springvale Fault and swings from north-northeast to north, northeast of the Toby intrusion (Figs 7.2 & 7.3, cf. Fig. 4.11).

- They form a set of dyke rocks that are confined to western zone of the HCO, where they cut granites of the Paperbark supersuite.

- These intrusions are of different ages (~1855 Ma to ~1835–1805 Ma) and include a wide variety of rock types from quartz norite, biotite gabbro, diorite, to tonalite.

- Their contacts with granite show a gradual change in mixed rock types and contain anomalous amounts of biotite, clinopyroxene, magnetite, plagioclase, and resorbed alkali feldspar xenocrysts from the granite.

- The biotite in these hybrid mafic rocks appears to have formed by hydrous reaction with melted granite (Sheppard et al. 1997b), so these dyke rocks are probably similar in age to some of the ~1865–1850 Ma Paperbark supersuite and 1835–1805 Ma Sally Downs supersuite granites (see Chapter 3) they intrude;

- The general conclusion is that they are highly contaminated by SiO_2 at their margins with granite and that much of the magnetite was probably introduced during contamination.

- They lack olivine since they are highly evolved and contaminated.

Key example – Nine-Mile intrusion (5):

- The intrusion contains biotite-bearing gabbro, norite and tonalite, which are highly magnetic hybrid rocks formed by reaction of the mafic intrusion with adjacent granite and metasedimentary rocks.

Turkey Creek microgabbro-norite group

- This is a complex group of fine-grained metamorphosed and unmetamorphosed rocks that intrude the Sally Malay intrusion and are, therefore, younger than 1845 Ma (Trudu & Hoatson 1996).

- These intrusions are possibly temporally and spatially related to granite of the Sally Downs supersuite (Sheppard et al. 1997b, Tyler et al. 1997b).

- They are an unusual and not very significant group of intrusions largely confined to the region between the Wilson Creek (18) and Norton (6) intrusions in TURKEY CREEK and MOUNT REMARKABLE[1].

- They generally form small mafic bodies (<few km^2), thus their magnetic expression in the regional magnetic data is weak or absent.

Key intrusion – microgabbro-norite body cutting the Sally Malay intrusion:

- Fine grained gabbroic and noritic rocks of this body intrude the contact between the megacyclic units and also the western end of the mineralised subchamber A of the Sally Malay intrusion. The intrusion has an irregular dyke-like form.

Undivided gabbro

- These gabbro bodies are mainly mapped as unit PgSog in McINTOSH (Tyler et al. 1997a).

- Many of these intrusions could belong to the same group as the McIntosh intrusion, but unlike the McIntosh intrusion, they have a weak magnetic expression.

Key example – Three Sisters intrusion (45):

- A fractionated gabbro containing disseminated magnetite is expressed as a weak magnetic ridge.

[1] 1:100 000 sheet names throughout this *Bulletin* are in capital letters to avoid confusion with identical place names and to distinguish them from 1:250 000 sheet names.

Discussion

The mafic–ultramafic intrusions fall within two contrasting geophysical zones, which correspond to the central zone and a reinterpreted western zone of the HCO (see discussion in Chapter 4). In the proposed new model for the western zone of the HCO, the eastern margin of the zone is outlined by the Springvale Fault in the south and redefined as the Highway Shear Zone in the north (Fig. 7.3 and see Fig. 4.9).

In the central zone of the HCO, the mafic–ultramafic intrusions (e.g. Panton and McIntosh intrusions) overlap in age with numerous granites, including the Dougalls suite, dominated, by tonalitic compositions (Sheppard et al. 1995, 1997a), which was emplaced between 1865 and 1850 Ma (Page et al. 1995). These granites intrude and are spatially associated with the high-grade metamorphosed sedimentary rocks and mafic volcanics deposited initially at about 1870 Ma. These metamorphic rocks have a highly variable and, in places intense, magnetic character that is similar to rocks in the central and southern tectonic zones of the Arunta Block and is in keeping with them representing rocks uplifted from mid- to lower-crustal levels (cf. Mutton & Shaw 1979).

Based on geochemical features, Sheppard et al. (1995, 1997a) have suggested that the granitic rocks of the Dougalls suite, mainly tonalite and trondhjemite, were generated in the central zone in a different setting to the granites of the Paperbark supersuite in the western zone. They suggest these granitic rocks could be subduction-related (Sheppard et al. 1995, 1997a).

In the western zone of the HCO, the mafic–ultramafic intrusions (e.g. Toby and Springvale intrusions) overlap in their age of emplacement with the voluminous, largely non-magnetic granites of the Paperbark supersuite and the associated Whitewater Volcanics. However, the mafic–ultramafic intrusions are not comagmatic with the granites of the Paperbark supersuite (Sheppard 1996). Wyborn et al. (1992) regard the granites of this supersuite as restite-dominated bodies that could have been emplaced in an extensional (or transtensional) rift-like setting. On the other hand, Sheppard et al. (1995) suggest that these granites were emplaced in an extensional setting to the west behind an island arc to the east. In their model, the island arc is represented by some of the mafic igneous rocks of the Tickalara Metamorphics and by granitic rocks of the Dougalls suite.

The granites of the Paperbark supersuite intrude high-grade metamorphosed sedimentary rocks (Marboo Formation and rocks mapped as Tickalara Metamorphics west of the Highway Shear Zone) deposited initially at about 1870 Ma. It is argued that these metamorphic rocks were deposited in a very different tectonic environment to those in the central and western zones. Their weak magnetic character is in keeping with the suggestion that they were deposited in a deep trough in a reducing environment. In such a situation minerals, such as carbon preserved as graphite, were present as accessories phases, thereby tending to effectively control

the oxygen fugacity in favour of initial redox state and, thereby, influencing the development of ferric oxides (for further discussion see Chapter 4). Graphite and pyrrhotite, for example, are preserved as mineral phases in country rocks to the Sally Malay intrusion, west of the Highway Shear Zone (see Thornett 1981, Shedden & Barnes 1996, Hoatson et al. 1997). The presence of graphite and pyrrhotite indicates a reducing environment. A similar reduced environment is predicted for the protolith of the Marboo Formation. For this reason Shaw et al. (see Chapter 4) regard Tickalara Metamorphics west of the Highway Shear Zone as better placed in the western zone.

The eastern zone of the HCO, characterised by rocks that have different compositions and a different tectonic history to the those of the central zone (Tyler et al. 1995), is significantly devoid of mafic–ultramafic intrusions (for further discussion see Chapter 4).

The mafic–ultramafic intrusions in the central and western zones are localised near several gravity gradients that probably represent deep-seated faults, such as the Halls Creek Fault, the Highway Shear Zone, the Springvale Fault, and the Greenvale Fault (see Figs 4.9 & 4.15). Those mafic–ultramafic intrusions uplifted as part of a regional fault block from the greatest depth (Table 7.1, data of Trudu & Hoatson 1996) tend to be on the southeastern or southern side of major fault blocks. Even those that are unrelated to these major faults, such as the Corridor gabbro in the Black Hills Yard region (Fig. 7.1) and other dyke rocks, could be related to reactivation of a series of splays of the Springvale Fault.

Mathur & Shaw (1982) speculated that the HCO may have acted as an aborted rift-like structure early in its history and that the mafic–ultramafic intrusions were emplaced into tensional pockets within a major deformed zone dominated by strike-slip movements. Recent geological mapping has tended to confirm the view that the mafic–ultramafic intrusions were emplaced in an extensional or transtensional setting. The intrusions in the East Kimberley tend to be late-tectonic to post-tectonic, being emplaced in pulses, following episodes of contractile deformation and slightly after the peak of two or more regional metamorphisms. As pointed out by Sun et al. (1991), the mafic–ultramafic intrusions in the HCO have parent magmas with a chemical affinity to tholeiites generated in a continental rift setting. Several features of the mafic–ultramafic intrusions—such as the large number of small intrusions of variable size and type, an overlap in the range of rock compositions (ranging from gabbro to troctolite to anorthosite) and Ni–Cu mineralisation—suggest some similarity to the Duluth Complex in North America, which is regarded as plume related (White & McKenzie 1995) and, at the same time, rift related (Naldrett 1997). These emplacement mechanisms are not mutually exclusive and could occur at the same time. However, the East Kimberley intrusions are smaller in size and mostly lack ultramafic components such as pyroxenite and peridotite. Exceptions are the small Panton intrusion, which contains dunite, lherzolite, and harzburgite, and the even smaller Sally Malay intrusion, which contains a thin lower unit of serpentinised peridotite (Hoatson et al. 1997).

The older mafic–ultramafic intrusions of the East Kimberley, formed at 1860–1855 Ma (Panton, Springvale, and Toby), could be regarded as 'rift-related' to the extent that they were emplaced during the late stages of the Hooper Orogeny and they are similar in age to the 1864–1855 Ma Whitewater Volcanics. Similarly, those intruded at about 1830 Ma (McIntosh, Armanda), during the late stages of the Halls Creek Orogeny, probably overlap in age with subsidence in the 1835 Ma Speewah Basin, which could be an extensional basin containing rhyolitic ashstone and tuff of the Valentine Siltstone.

Elsewhere in the world, platinum-group elements (PGEs), Ni, Cu, Co, Ti, V, and other commodities that can be associated with mafic–ultramafic intrusions commonly accompany huge bodies of tholeiitic magma. Examples include (1) the Voisey's Bay deposit in Canada associated with a large intrusive complex, (2) the Noril'sk deposit associated with intrusions linked to the flood basalts of the Siberian Trap, (3) the PGE-bearing Merensky Reef in the Bushveld Complex in South Africa and (4) numerous Keweenawan deposits in North America, such as the Duluth Complex, associated with a crustal-scale graben (mid-continental ridge) containing volcanic and sedimentary rocks (Naldrett 1997). Many, if not most, of these mafic–ultramafic intrusive complexes can be interpreted as plume-related, and can be linked, in some way, to lithospheric extension to a greater or less extent (White & McKenzie 1995). In the case of the Keweenawan magmatism the extension was expressed as crustal-scale rifting.

Key questions for the East Kimberley are therefore: (1) what is the depth extent of the mafic–ultramafic intrusions, and (2) are there any larger magma chambers at depth in the crust that could have fed magma to the exposed intrusions?

In the western zone of the HCO, the centre of the Toby gabbroic intrusion, as outlined by lithological trends (Trudu & Hoatson 1996), aligns with the peak of a positive gravity anomaly of moderate magnitude. However, the anomaly extends to the east, well beyond the margins of the intrusion. From this geometry, a reasonable interpretation is to assume that the anomaly represents the gravity expression of a feeder conduit to a sub-horizontal, sheet-like body. The close spatial association between the two lobes making up the Springvale intrusion and the southern margin of the regional gravity high implies that the intrusion lies close to the southern margin of a more complex set of dense rocks producing the regional mass excess. The source of the excess of mass could be an uplifted block of granulites which includes mafic igneous rocks, but is dominated by metasedimentary rocks. The lack of an individual gravity anomaly at the site of the Springvale intrusion implies that this intrusion is a thin, subhorizontal body.

As there are no significant magnetic highs in the western zone of the HCO other than those associated with the Toby, Springvale, and Corridor gabbro intrusions, it is

unlikely that there are any hidden large post-orogenic mafic–ultramafic intrusions at shallow to mid-crustal depths, as these would be expected to produce magnetic anomalies. The presence of magnetite-bearing intrusions of the Norton-type that have any regional extent can also be ruled out, as they should also show up in the magnetic data. However, at greater depths, the mafic–ultramafic intrusions could be non-magnetic if their Fe–Ti oxide phases were dominated by ilmenite or spinel, but it seems unlikely that the buried mafic–ultramafic intrusions would differ dramatically from the exposed intrusions, most of which are magnetic. The exception is the group of intrusions containing the thickest sequences of ultramafic rocks, the Panton group I intrusions, but as these are small and regionally less significant bodies, they are unlikely to make a major contribution to the regional geophysical picture.

The close alignment between the gabbros of the Corridor group and a sharp magnetic ridge indicates that these intrusions are part of a northeast-trending subvertical dyke system. This system is parallel to the southern segment of the Springvale Fault, but fans to the northeast into a diverging set of dykes, evidenced by a set of narrow magnetic ridges. An even younger north to northwesterly trending splay of the same fault system, which could be related to the Panton Fault, truncates this fanning system of dykes.

The gravity high and gradient in the central zone of the HCO can be accounted for by metamorphic rocks, including mafic granulites (Tickalara Metamorphics), and by abundant tonalitic granite (1835–1805 Ma Sally Downs supersuite). These rocks were deformed, metamorphosed and uplifted at ~1835 Ma and deformed and uplifted at ~1810–1800 Ma during and immediately following the Halls Creek Orogeny. In this zone the largest layered body is the McIntosh intrusion. Its association with a positive gravity anomaly of moderate magnitude indicates that it has a significant depth extent.

Intrusions with a significant content of ultramafic rocks, such as Panton and Sally Malay, are too small to have an obvious expression in either the regional magnetic data or the gravity data. If they represent satellite bodies linked to a larger magma chamber at lower crustal depths, the chamber has no obvious coincident expression in the gravity (see Fig. 4.9) and magnetic (see Fig. 4.10) data. It is conceivable that large unexposed intrusions are centred near the Amphitheatre mafic intrusion (17 in Fig. 7.3), about 10 to 15 km southwest of the Sally Malay intrusion (12 in Fig. 7.3), as this would explain the large gravity anomaly in that region. However, if this were the case, it is difficult to explain why there is no coincident magnetic anomaly for these intrusions, unless their Fe–Ti oxides are dominated by ilmenite or iron spinel (e.g. hercynite).

Another possible buried mafic–ultramafic intrusion that may correspond to an intense magnetic high of moderate wavelength lies about 5-km west-northwest of the Armanda intrusion (46 in Fig. 7.1). This anomaly is not represented by any exposed mafic–ultramafic intrusions, but its high magnetic response suggests it could represent a magnetite-bearing mafic body. The intrusion appears to be faulted on its eastern side and its depth extent is probably limited, since it does not correspond to a distinctive gravity anomaly.

A possible deep-seated group of parent bodies that could accord with the geophysical data of the HCO would be a number of tholeiitic olivine-bearing bodies similar to those of the Duluth or Voisey's Bay intrusions of North America. In such a hypothetical group of bodies, a special set of conditions would be necessary to explain why there is no regional magnetic anomaly associated with large parent mafic–ultramafic bodies at depth. Presumably, any Fe–Ti oxides would need to be dominantly ilmenite (or the Fe is in a spinel such as hercynite), the effects of normal remanent magnetism (NRM) would need to be small, olivine would need to be unserpentinised so that fine-grained secondary magnetite is not produced or the intrusion was emplaced in a dry, reduced environment where olivine is less subject to serpentinisation. Alternatively, the gravity highs could be explained by the presence of granulites of high density. A possible candidate for such a high-density rock type is a garnet-bearing metasedimentary rock. In this particular case, the appearance of abundant magnetite is suppressed by the presence of graphite, as has been recorded in the country rocks of the Sally Malay intrusion (Thornett 1981, Shedden & Barnes 1996).

Shaw et al. (see Fig. 4.15) have developed a crustal-scale model showing the relationship of the mafic–ultramafic intrusions to a possible mafic igneous underplate. This model is still to be tested by geophysical modelling.

The fact that the Panton intrusion contains Cr–PGE mineralisation and the Sally Malay intrusion contains Ni–Cu–Co mineralisation—a hypothesis developed by Trudu & Hoatson (1996) to explain two distinct mineralising corridors—may be a function of the differing histories of what are two different tectonic zones. The further segmentation of these zones into smaller blocks, corresponding to a set of microelements (Figs 4.8 & 4.9), may also be a factor influencing the distribution and history of mineralisation.

As recognised by Mathur & Shaw (1982), unusually dense rocks are needed to account for marked gravity highs in the East Kimberley region: these are amongst the highest magnitude Bouguer gravity anomalies in Australia. Only the layered mafic–ultramafic intrusions of the Musgrave Block in central Australia have a comparable magnitude. Individual gravity peaks within a regional gravity ridge may well represent large mafic–ultramafic intrusions at depth. However, most of the exposed mafic–ultramafic intrusions either postdate a granulite facies metamorphism, or intrude medium-grade rocks above the level of high-grade rocks that align with the highest Bouguer gravity anomalies. Uplifted granulite and amphibolite facies rocks, particularly metasedimentary rocks containing garnet and metamorphosed mafic igneous rocks, will also contribute to the distribution of dense bodies (the excess of mass) that gives rise to the regional gravity ridge. If there is a greater volume of mafic–ultramafic intrusions at depth than at the surface in the western zone of the

HCO, then it is puzzling that there is no matching set of long-wavelength magnetic anomalies. Another complicating factor is that the western zone of the HCO, characterised by granites of the Paperbark supersuite and the Marboo Formation, has been thrust eastwards over the central zone of the HCO. This overthrusted block could mask the magnetisation of any mafic–ultramafic intrusions, but would not eliminate any regional magnetic anomaly (see Chapter 4 for discussion). Such thrusting could have taken place in two phases, the first conceivably before ~1855 Ma, after which the main phase of mafic–ultramafic intrusion took place, and the second at about ~1805 Ma, when the Highway Shear Zone is considered to have been active.

The shape, grouping, and potentially huge volume of the mafic–ultramafic intrusions, suggested by the pattern of geophysical anomalies, would be in keeping with their emplacement in a transtensional tectonic setting at a plate or sub-plate boundary. Transtension is a mode of deformation that combines the two elements of extension and strike-slip motion. In a transtensional regime, pockets of dilation develop along distortions in the fault system at depth, analogous to pull-apart basins at the surface, and these are conducive to magma injection. Laxroix et al. (1998) discuss this type of tectonic setting in relation to pluton emplacement within the late Archaean Abitibi greenstone belt in Canada. Tikoff & de Saint Blanquat (1997) describe another example from the Late Cretaceous Sierra Nevada of active plutonism in a strike-slip setting in which, contraction occurred concurrently with emplacement. An extensional setting would be in accord with the tholeiitic character of the intrusions, implying high-level fractionation within a thinned and stretched lithosphere. Their distribution and range of ages suggests that there was more than one tensional pulse and that the clustering of intrusions was different for each pulse, according with varying degrees of transtension. Dilation can also develop in a transpressional setting, a scenario discussed in Chapter 4.

A drop in pressure within the central transtensional axis of a proto-Springvale Fault zone at about 1855 Ma could have allowed large degrees of asthenospheric mantle melting and led to magma intrusion at shallow depths within a thinned lithospheric cap. As discussed by Sun & Hoatson (see Chapter 11), such a process could explain how mafic–ultramafic intrusions, such as the subsequently metamorphosed Norton group of intrusions, as well as the Panton and Keller Creek intrusions, were generated with low incompatible element abundances. This setting suggests a model in which the mafic magmas preferentially migrated up a proto-Springvale fault which could have been a transtensional zone of crustal proportions. If outside the axis of the transtension zone, the lithospheric thickness would have been much greater, and, this could explain why the mafic intrusions, such as the Springvale and Toby intrusions, are relatively enriched in incompatible elements (see Chapter 11). Those mafic intrusions lying at the margin of the proposed transtensional zone intruded the barely crystallised granites of the Paperbark supersuite to the west. A rising asthenosphere and accompanying influx of a large volume of tholeiitic magma may have been the heat source for the regional high-grade metamorphism, which peaked at ~1850 Ma (Tyler & Page 1996).

In detail, such a transtensional model suggests that more localised pockets of dilation could have recurred during later pulses and resulted in focussing the emplacement of mafic–ultramafic intrusions like the ~1845 Ma Sally Malay group of intrusions. Chemical and isotopic data for the Sally Malay intrusion suggest high degrees of crustal contamination (see Chapter 12). The contamination would be enhanced if the intrusion represents a satellite body at some distance from the main magma chamber.

The magnetic and gravity data can help focus exploration effort for PGE–Cr and Ni–Cu–Co mineralisation in the East Kimberley region. As suggested by Hoatson et al. (1997), a prospective region for Voisey's Bay-type intrusions is a narrow zone associated with garnet-bearing granulites northwest of the Highway Shear Zone. Another prospective region is a major gravity anomaly near the Amphitheatre mafic intrusion (17 in Fig. 7.1). Satellite bodies of a Voisey's Bay-type would be expected to give rise to small magnetic highs, like that of the Sally Malay intrusion. Potentially mineralised feeder conduits similar to that at Voisey's Bay would be very difficult to identify in the regional AGSO magnetic or gravity data sets, even if the conduits were tilted onto their sides.

The regional magnetic low (trough) corresponding to the western zone of the HCO is remarkably similar to that of the King Leopold Orogen (KL in Fig. 4.8) in the West Kimberley. It is so similar that it is hard not to equate these features (Figs 4.2 & 4.3).

A similar relationship to the prospective boundary region between the western and central zones of the HCO within Dixon Range and Gordon Downs Sheet areas also occurs at the northeast margin of the Canning Basin in the West Kimberley. The region in question is near the southwestern extension of the Ramsay Range Fault (see Fig. 4.7). Here, the regional magnetic low characterising the King Leopold Orogen (Fig. 4.3) overlaps a prominent rectilinear complex Bouguer gravity high (Fig. 4.6; microelement HCCa at the western end of HCC in Fig. 4.8). A gravity high that could indicate a mafic–ultramafic intrusion at depth is located near the Pillara Inlier on the Lennard Shelf of the Canning Basin (see Shaw et al. 1994) and extends from the layered intrusion near the Sparks Range Fault (Tyler et al. 1998). This region could also be considered as a potential exploration area for Voisey's Bay-type Ni–Cu–Co sulphide deposits accompanying group V-type intrusions. This type of mineralisation is amenable to prospecting using electrical, ground magnetic and detailed gravity methods (cf. Frankcombe et al. 1994).

A major difference in geophysical features is recognised across the Highway Shear Zone (cf. microelements HCCe and HCCf in Figs 4.8 & 4.9). This shear zone could represent a major thrust boundary, and possibly even a subplate boundary. If it does represent a major tectonic boundary the Tickalara Metamorphics west of

the shear zone may not be the same metamorphic unit as the Tickalara Metamorphics to the east. The metamorphic unit in question is of a higher metamorphic grade compared to that to the east and its protolith may have been deposited in a reduction environment as argued above (see also Chapter 4). This issue requires further investigation.

East of the Highway Shear Zone (within microelements HCCf and HCCc in Fig. 4.9), the older metamorphosed mafic intrusions form thin discontinuous bodies of mafic granulite of limited exploration interest. PGE–Cr mineralisation accompanying group I intrusions has less obvious targets that show a magnetic expression. The ultramafic rocks hosting the chromitite layers in the Panton intrusion (39 in Fig. 7.1 & 39u in Fig. 7.3) have a distinct and complex magnetic expression, similar to that of mafic–ultramafic rocks in other group I bodies (26, 30, 32, & 33) along the western and northern margins of the McIntosh intrusion (34). Because it forms very thin layers with no distinctive geophysical properties, the chromite mineralisation is more amenable to exploration by geochemical techniques than by using geophysical methods.

Hoatson in Trudu & Hoatson (1996) has recognised two distinct metallogenic corridors in the East Kimberley, one represented by a Cr–PGE oxide association (typified by the Panton intrusion) and the other by a Ni–Cu–Co sulphide association (Sally Malay intrusion). However, these contrasting corridors may not reflect different sources or types of mineralisation, but simply be a function of the differing histories and metamorphic conditions in what are two different tectonic zones separated by the Highway Shear Zone. Also, although these two tectonic zones continue to the south (as microelements HCCd and HCCc, see Figs 4.8 & 4.9), their geophysical expression changes (represented by microelements HCCe and HCCf). The sinistral offset on the Panton Fault does not continue to the northwest and is not considered a sufficient reason for these differences in geophysical expression. This different expression is considered to be of sufficient magnitude to suggest a major change in geology across both the Panton Fault and an aligned NNW-trending splay of the Springvale Fault, and questions the proposition by Trudu & Hoatson (1996) that the mineralising corridors continue to the southwest. The possibility that there was a complex jostling of fault blocks in this region at an early stage in the history of the HCO is discussed in Chapter 4.

Conclusions

The main conclusions of this geophysical study are:

1. Cr–PGE mineralisation in the East Kimberley appears to be associated with mafic–ultramafic intrusions rather than mafic intrusions, and the more prospective intrusions are both rare and difficult to identify in the gravity and magnetic data.
2. Ni–Cu–Co mineralisation is potentially easier to explore for as it could be associated with geophysical anomalies, like the small, local anomaly at the Sally Malay intrusion. Ni–Cu–Co sulphide mineralisation associated with Sally Malay-type intrusions is amenable to prospecting using electrical, ground magnetic, and detailed gravity methods (see Frankcombe et al. 1994).
3. Exploration for gossanous ironstone bodies, like that associated with the Norton intrusion (Hoatson 1995), is difficult as these are only a few metres thick and unlikely to have a marked geophysical signature. Exploration could be aided by looking in detailed magnetic data for dispersed, intermittent, but aligned, magnetic anomalies like those at the Norton deposit.
4. The mafic–ultramafic intrusions, including probable satellite bodies, appear to be concentrated near and along major faults and cross-faults. These faults commonly correspond to marked gravity gradients and lineaments.
5. The two distinct mineralising corridors proposed by Trudu & Hoatson (1996) and discussed in Chapters 5 and 9) correspond to two different geophysical zones (crustal microelements HCCe and HCCf in Fig. 4.9). In the Trudu & Hoatson (1996) proposal, one is characterised by Cr–PGE mineralisation (e.g. Panton intrusion) in the central zone of the HCO and the other by Ni–Cu–Co sulphide mineralisation (e.g. Sally Malay intrusion) in the revised western zone, west of the Highway Shear Zone.
6. The mineralising corridors could extend to the northeast, but probably have a more limited extent to the southwest (as discussed above and in Chapter 4). Although the geophysical zones that correlate with the mineralising corridors have a more regional extent, there is a marked change along-strike to the south in the geophysical and geological character of crustal blocks. That is, there is a marked change in the geology and geophysical expression to the south of the Panton intrusion across the Panton Fault. There is a similar change south of the Sally Malay intrusion across a splay of the Springvale Fault on the northwest side of the Highway Shear Zone (crustal microelements HCCc and HCCd on Fig. 4.9).
7. The exposed mafic–ultramafic intrusions are likely to be connected to larger parent bodies at deeper crustal levels. The regional gravity anomaly mapped as crustal subelement HCC (Shaw et al. 1996, Chapter 4) is likely to be associated with mafic–ultramafic intrusions. However, other rock types are likely to contribute to the gravity anomaly. These include uplifted dense high-grade metamorphic rocks, including mafic granulites and garnet-bearing metasediments, like those in the Tickalara Metamorphics.
8. A similar relationship to the boundary between the western and central zones of the HCO is repeated near the southwestern extension of the Ramsay Range Fault. This region extends from the layered intrusion near the Sparks Range Fault (Tyler et al. 1998) westwards to close to the Pillara Inlier on the Lennard Shelf of the Canning Basin in the West Kimberley (see Shaw et al. 1994 and microelement HCCa in Fig. 4.8, cf. Figs 4.6 & 4.7). This region

contains a prominent complex group of Bouguer anomalies like those associated with the mafic–ultramafic intrusions in the East Kimberley. Because several of the lithological and tectonic ingredients appear to be similar in the two regions, this southwestern region on the Lennard Shelf could also be considered as potentially prospective for Voisey's Bay-type Ni–Cu–Co sulphide deposits accompanying group V-type intrusions.

9. The mafic–ultramafic intrusions have an unusual tectonic setting in that they appear to be late tectonic or post-tectonic. They are considered to represent two or more pulses of mafic magma within a transtensional or a transpressional tectonic setting. Such settings would be conducive to the tectonic quiescence that seems to be a common characteristic of many large PGE– and Ni–Cu-bearing intrusions (cf. Naldrett 1997).

10. While the emplacement of mafic–ultramafic intrusions in the East Kimberley follows contractile episodes, they appear to occupy transtensional pockets and to have formed within an evolving, transcurrent, crustal-scale deformed zone. This transcurrent zone is interpreted to mark a possible plate or sub-plate boundary (Tyler et al. 1995, Chapter 4). This tectonic setting differs from other regions where large PGE and Ni–Cu deposits are mined (cf. Naldrett 1997).

Acknowledgements

The present work has benefited from discussions with many colleagues at AGSO and GSWA, and the critical reviews of earlier versions of the manuscript by Dean Hoatson, David Blake, David Maidment, Greg Ewers, Shen-Su Sun (all AGSO), and Ian Tyler (GSWA).

References

AGSO, 1997. National Geophysical Database, 1997. Australian Geological Survey Organisation, Canberra.

Frankcombe, K.F., Barnes, G. & Trussell, D., 1994. Geophysical signature of the Sally Malay nickel deposit, Western Australia. In: Dentith, M.C., Frankcombe, K.F., Ho, S.E., Shepherd, J.M., Groves, D.I. & Trench, A. (editors), Geophysical signature of Western Australian Mineral Deposits. Australian Society of Exploration Geophysicists, 7, 157–168.

Gunn, P.J. & Meixner, A.J., 1998. The nature of the basement to the Kimberley Block, northwestern Australia. Australian Society of Exploration Geophysicists, 29, 506–511.

Hoatson, D.M., 1993. Correlation of structurally disrupted layered mafic–ultramafic intrusions in the East Kimberley. AGSO Research Newsletter, 19, 9–10.

Hoatson, D.M., 1995. New mineral discoveries in the East Kimberley. AGSO Research Newsletter, 22, 9–11.

Hoatson, D.M. & Tyler, I.M., 1993. Prospective layered mafic–ultramafic intrusions in the East Kimberley. Is Big Ben part of the Panton intrusion? AGSO Research Newsletter, 18, 8–9.

Hoatson, D.M., Blake, D.H., Warren, R.G., Orth, K. & Tyler, I.M., 1995. Recent NGMA mapping highlights the metallogenic potential of the East Kimberley. AGSO Research Newsletter, 22, 1–2.

Hoatson, D.M., Sproule, R.A. & Lambert, D.D., 1997. Are there Voisey's Bay-type Ni–Cu–Co sulphide deposits in the East Kimberley of Western Australia? AGSO Research Newsletter, 27, 17–19.

Laxroix, S., Sawyer, E.W. & Chown, H., 1998. Pluton emplacement within an extensional transfer zone during dextral strike-slip faulting: an example from the late Archaean Abitibi Greenstone Belt. Journal of Structural Geology, 20, 43–59.

Mathur, S.P. & Shaw, R.D., 1982. Australian orogenic belts. Evidence of evolving plate tectonics. Earth Evolution Sciences, 4, 281–308.

Mutton, A. & Shaw, R.D., 1979. Physical property measurements as an aid to magnetic interpretation in basement terrains. Australian Society of Exploration Geophysics, Bulletin, 10, 769–791.

Naldrett, A.J., 1997. Key factors in the genesis of Noril'sk, Sudbury, Jinchuan, Voisey's Bay and other world-class Ni-Cu-PGE deposits: Implications for exploration. Australian Journal of Earth Sciences, 44, 283–315.

Page, R.W., Hoatson, D.M. & Foudoulis, C., 1995. High-precision geochronology of Palaeoproterozoic layered mafic–ultramafic intrusions in the East Kimberley. AGSO Research Newsletter, 22, 7–8.

Shaw, R.D., Sexton, M.J. & Zeilinger, I., 1994. The tectonic framework of the Canning Basin, Western Australia, including the 1:2 million structural elements map of the Canning Basin. Australian Geological Survey Organisation, Record, 1994/48, 89 pp.

Shaw, R.D., Wellman, P., Gunn, P., Whitaker, A.J., Tarlowski, C. & Morse, M., 1996. Guide to using the Australian Crustal Elements map. Australian Geological Survey Organisation, Record, 1996/30, 49 pp.

Shedden, S.H. & Barnes, G.J., 1996. East Kimberley nickel province—Characteristics and origin of the Sally Malay Ni-Cu-Co deposit, East Kimberley, Western Australia. In: Grimsey, E.J. & Neuss, I. (editors), Nickel 96 - Mineral to market. Australasian Institute of Mining and Metallurgy, Publication Series 6/96, November 27-29, Kalgoorlie, Western Australia, 145–155.

Sheppard, S., 1996. Mafic and felsic magma mingling in the Bow River batholith of the Halls Creek Province. Geological Survey of Western Australia, Annual Review, 1995-96, 56–60.

Sheppard, S., Griffin, T.J. & Tyler, I.M., 1995. Geochemistry of felsic igneous rocks from the southern Halls Creek Orogen. Geological Survey of Western Australia, Record, 1995/4, 81 pp.

Sheppard, S., Griffin, T.J. & Tyler, I.M., 1997a. The tectonic setting of granites in the Halls Creek and King Leopold Orogens, northwest Australia. In: Rutland, R.W.R. & Drummond, B.J. (editors), Palaeoproterozoic tectonics and metallogenesis: Comparative analysis of parts of the Australian and Fennoscandian Shields. Australian Geological Survey Organisation, Record, 1997/44, 107–109.

Sheppard, S., Tyler, I.M. & Hoatson, D.M., 1997b. Geology of the Mount Remarkable 1:100 000 sheet, Western Australia. Western Australia Geological Survey, 1:100 000 Geological Series Explanatory Notes, 27 pp.

Sun, S-s., Wallace, D.A., Hoatson, D.M., Glikson, A.Y. & Keays, R.R., 1991. Use of geochemistry as a guide to platinum group element potential of mafic–ultramafic rocks: examples from the west Pilbara and Halls Creek Mobile Zone, Western Australia. Precambrian Research, 50, 1–35.

Thornett, J.R., 1981. The Sally Malay deposit: Gabbroid-associated nickel-copper sulphide mineralisation in the Halls Creek Mobile Zone, Western Australia. Economic Geology, 76, 1565–1580.

Tikoff, B. & de Saint Blanquat, M., 1997. Transpressional shearing and strike-slip partitioning in the Late Cretaceous Sierra Nevada magmatic arc, California. Tectonics, 16, 442–459.

Trudu, A. & Hoatson, D.M., 1996. Depths of emplacement of Precambrian intrusions in the East Kimberley. AGSO Research Newsletter, 25, 10–12.

Tyler, I.M. & Page, R.W. 1996. Palaeoproterozoic deformation, metamorphism and igneous intrusion in the central zone of the Lamboo Complex, Halls Creek Orogen. Geological Society of Australia, Abstracts, 41, 37–46.

Tyler, I.M., Griffin, T.J., Page, R.W. & Shaw, R.D., 1995. Are there terranes within the Lamboo Complex of the Halls Creek Orogen? Western Australian Geological Survey, Annual Review 1993-94, 37–46.

Tyler, I.M., Hoatson, D.M., Griffin, T.J., Sheppard, S., Blake, D.H. & Warren, R.G. 1997a. McIntosh, Western Australia, 1:100 000 geological map (sheet 4462) Geological Survey of Western Australia.

Tyler, I.M., Thorne, A.M., Hoatson, D.M. & Blake, D.H., 1997b. Turkey Creek 1:100 000 Sheet, Western Australia. Geological Survey of Western Australia, Perth.

Tyler, I.M., Playford, P.E. & Hocking, R.M. 1998. Mount Ramsay, Western Australia (1:250 000 Geological Map (SE/52-9) second edition. Geological Survey of Western Australia, Perth.

Warren, R.G., 1992. District surrounding the Armanda Sill, Halls Creek Inlier, Western Australia. Australian Geological Survey Organisation, Record, 1992/70, 16 pp.

White, R.S. & McKenzie, D., 1995. Mantle plumes and flood basalts. Journal of Geophysical Research, 100, 17543–17586.

Wyborn, L.A.I., Wyborn, D., Warren, R.G. & Drummond, B.J., 1992. Proterozoic granite types in Australia: implications for lower crustal compositions, structure and evolution. Royal Society of Edinburgh, Earth Science Transactions, 83, 210–209.

CHAPTER 8

REMOTE SENSING OF MAFIC AND ULTRAMAFIC ROCKS IN THE McINTOSH 1:100 000 SHEET AREA

by LAUTARO F. MACIAS

Introduction

Landsat-5 Thematic Mapper imagery has been used to assist geological mapping of the Palaeoproterozoic layered mafic–ultramafic intrusions in the East Kimberley, and to investigate correlations between lithology and spectral information on McINTOSH[1]. This has resulted in the successful partial discrimination of mafic and ultramafic rocks. Studies on the discrimination of mafic–ultramafic rocks by multispectral scanner data in Australian terranes have been published by Macias et al. (1987), Macias & Simpson (1990, 1992), Macias (1995), and Glikson & Creasey (1995), and elsewhere by Raines & Wyn (1982), Rothery (1984a,b, 1987), Abrams (1986), Sultan et al. (1986), Rothery et al. (1988), Abrams et al. (1988), Harding et al. (1989), Birnie et al. (1989), Pontual (1990), and Van Der Meer et al. (1997).

The following mafic–ultramafic intrusions were investigated in this study:

- Panton and Big Ben intrusions of the group I intrusions of Hoatson (see Fig. 5.1);
- Springvale and Wilagee intrusions of group II;
- Toby intrusion of group III;
- Wild Dog Creek intrusion of group IV;
- McKenzie Spring intrusion of group V; and
- McIntosh and Armanda intrusions of group VI.

The intrusive bodies consist of both mafic and ultramafic types with the main rocks being peridotite, troctolite, olivine gabbro, gabbronorite, and anorthosite. The intrusions are in a semi-arid region, with spinifex as the main vegetation cover (which, together with weathering and soil cover, makes lithologic discrimination difficult). Little correlation between geology and vegetation was observed. The spinifex grows on hills and scree slopes, whereas trees are largely restricted to stream courses. Lichen grows on some gabbroic and hybrid gabbroic–granitic rocks.

Band-ratio composite imagery was prepared for field reconnaissance and locating areas for collecting spectral data with a portable spectroradiometer. The spectral data were used to help discriminate the mafic and ultramafic rocks. Data were processed using the directed principal component analysis (DPCA) to prepare imagery for final analysis. The processed Landsat imagery was integrated with gamma-ray spectrometric data to separate mafic and ultramafic rocks from rocks of other compositions. This resulted in an improved differentiation of granitic, metamorphic, and sedimentary rocks.

[1] 1:100 000 sheet names throughout this *Bulletin* are in capital letters to avoid confusion with identical place names and to distinguish them from 1:250 000 sheet names.

Scanner data characteristics

The Landsat-5 TM sensor acquires data in the electromagnetic spectrum between 400 and 2500 nm in six discrete bands, with a ground pixel resolution of 30 x 30 m, and also in one band in the thermal infrared part of the spectrum, with a ground pixel resolution of 120 by 120 m. Details of the bands are given in Table 8.1.

Table 8.1. Wavelengths recorded by Landsat-5 TM.

Band	*Range (nm)*	*Centre line (nm)*	
1	450–520	485	
2	520–600	560	Visible (VIS)
3	630–690	660	
4	760–900	835	Near infrared (NIR)
5	1550–1750	1650	Shortwave infrared (SWIR)
7	2080–2350	2215	
6	10 400–12 500	11 450	Thermal infrared (TI)

Weathering and alteration products

The lithology and mineralogy of the layered mafic–ultramafic intrusions on McINTOSH are summarised in Table 8.2. The intrusions are weathered to varying degrees. The Panton, Big Ben, Wilagee, and McIntosh intrusions are mostly well exposed, with some scree-covered slopes and minor shallow soil and alluvium, while the Springvale, Toby, and Wild Creek Dog intrusions are characterised by isolated exposures between extensive areas of shallow black soil and alluvium.

The main primary minerals in the intrusions are calcic plagioclase, olivine, clinopyroxene (augite), minor orthopyroxene (hypersthene), hornblende, and biotite. The breakdown of these minerals, by weathering or by hydrothermal alteration, results in the following products (Deer et al. 1966):

1. olivine → serpentine + magnetite → talc, carbonates, clays (saponite);
2. orthopyroxene → serpentine + talc;
3. clinopyroxene → clinoamphibole, chlorite, epidote, carbonates, saponite; and
4. plagioclase → clays (montmorillonite → kaolinite).

Table 8.2. Major lithologies and mineralogy of mafic–ultramafic intrusions.

Intrusions	*Panton*	*BigBen*	*Springvale*	*Wilagee*	*Toby*	*Wild Dog Creek*	*McKenzie Spring*	*McIntosh*	*Armanda*
Ultramafic rocks									
Chromitite	M	m							
Olivine chromitite	M	m		m					
Dunite	M	M		m	m		m	m	
Harzburgite	M								
Pyroxenite (cpx)	m	m			m		m		
Lherzolite	m	M		m				m	
Peridotite	M	M		m	m		m	m	
Plagioclase peridotite	m	m						m	
Tremolite–anthophyllite peridotite	M	M		m			m		
Mafic rocks									
Amphibolite						M	M		
Anorthosite	M	M	M	M			m	m	m
Diorite						m			
Gabbro	M	M	M	M	m	M	M	M	M
Biotite gabbro					M	M			
Doleritic gabbro					M				
Ferrogabbro	m							m	
Magnetite gabbro			m		M	M		M	m
Olivine gabbro		m	M	M	m	m	M	M	M
Quartz–biotite gabbro					M	M			
Gabbronorite	M	M	M	M		m	m	M	M
Biotite gabbronorite					M	M			
Magnetite quartz					M	M			
Olivine gabbronorite			M	M	m		m	M	M
Olivine–magnetite gabbronorite					m		m	M	
Norite	m	m	m						
Olivine norite					m			m	
Troctolite			M	M			m	M	
Major primary minerals									
Biotite		✓	✓	✓	✓	✓	✓	✓	✓
Clinopyroxene	✓	✓	✓	✓	✓	✓	✓	✓	✓
Hornblende	✓		✓			✓	✓		✓
Magnetite	✓				✓	✓		✓	
Olivine	✓	✓	✓	✓	✓		✓	✓	✓
Orthopyroxene	✓	✓			✓	✓	✓	✓	✓
Plagioclase	✓	✓	✓	✓	✓	✓	✓	✓	✓
Quartz					✓	✓			
Secondary minerals									
Carbonates	✓	✓		✓					
Clays	✓	✓	✓	✓	✓	✓	✓	✓	✓
Serpentine group	✓	✓		✓			✓	✓	
Tremolite–actinolite	✓	✓		✓			✓		
Image discrimination									
Band ratio (Fig. 8.2)	g	p	f-p	g	p	f	p	g	p
DPCA (Fig. 8.3)	g	p	f	g	f-g	f	p	g	p-f

M = major; m = minor; (cpx) = clinopyroxene dominant; g = good; p = poor; f-g = fair-good; p-f = poor-fair.

The spectral curves for the mafic and ultramafic rocks on McINTOSH indicate that there are sufficient mineralogical differences to enable lithological discriminations to be made using the Landsat-5 TM sensing bands.

Spectral reflectance

Spectral-reflectance measurements of weathered rocks and soils from the intrusions were carried out both in the field and in the laboratory, using the Infrared Intelligent Spectroradiometer (IRIS). Sample measurements are relative to a Halon standard. Absorption features were determined by the Hull-quotient procedure (Green & Craig 1985). This procedure removes the sloping spectral curve background and allows the absorption features to be better defined than on the corresponding reflectance curves.

Figure 8.1 shows the reflectance curves for representative mafic and ultramafic rocks from the intrusions. Spectra of weathered mafic and ultramafic rocks are strongly influenced by the presence of iron in the 800–1000 nm region; iron oxides are concentrated on weathered surfaces. Spectral reflectance of weathered dunite ranges from about 85%, at about 1300 nm, to about 50% in the short-wavelength infrared (SWIR) at 950 nm, and about 30% at 490 nm. The Hull-quotient curve shows absorption features at 2387, 2310, and 1391 nm, indicating talc. It shows a water absorption feature at 1949 nm and a broad undefined feature centred at 950 nm. In the case of weathered harzburgite, the spectral reflectance reaches a maximum of 65% at about 1700 nm, dropping to about 27% in the SWIR at 980 nm, and about 13% at 490 nm. Its main absorption features are at 2330, 1945, and 1409 nm, with a broad feature centred at 984 nm, and minor features at 2402 and 2218 nm.

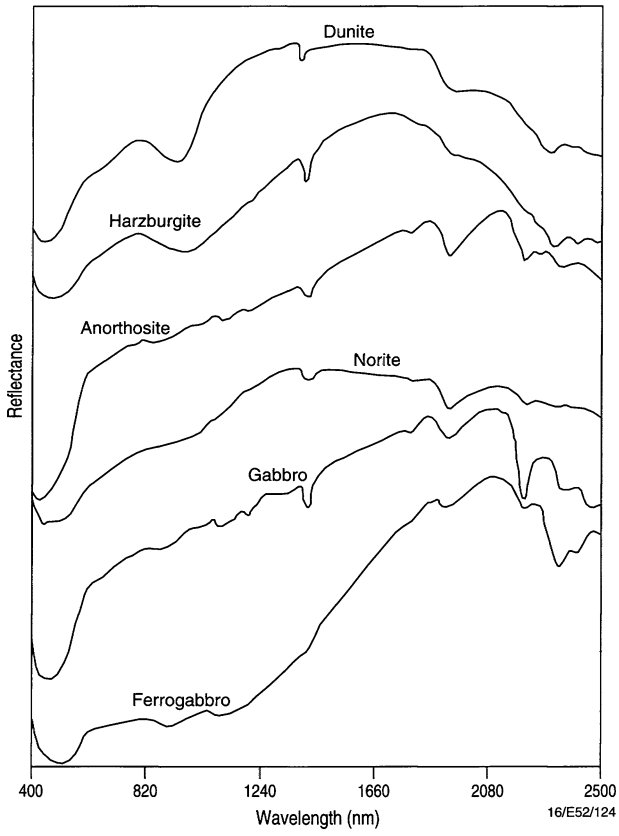


Figure 8.1. Reflectance curves for dunite, harzburgite, anorthosite, norite, gabbro, and ferrogabbro.

The spectral curves of mafic rocks are varied, but all show an absorption feature at 2220 nm, indicating the presence of clay, which is likely to be derived from the weathering of plagioclase. Weathered gabbro shows a maximum reflectance of 65% at 2100 nm. The reflectance drops to 50% towards the SWIR, and to about 20% at 448 nm. It shows absorption features at 246, 236, and 2220 nm, weaker features at 1938 and 1420 nm, and a broad feature centred at 870 nm. Reflectance of weathered ferrogabbro ranges from a maximum of 56% at 2095, dropping rapidly to 18% at 1000 nm, owing to the influence of iron, to about 40% in the SWIR region. It shows absorption features at 2412, 2343, 2220, 1938, and 1416 nm, and a broad feature centred at 901 nm. Anorthosite shows a reflectance maximum of 120% at about 2140 nm, dropping to 29% at 410 nm, and 100% in the SWIR region, with absorption features centred at 2352, 2273, 2220, 1938, and 1422 nm. The reflectance of norite shows a maximum of 62% at 1375 nm, dropping to 45% in the SWIR region and 14% at about 460 nm, with main absorption features at 2220, 1938, 1420, and a broad feature centred at 977 nm.

Digital data processing

Landsat-5 TM Standard-Frame scenes, Path 110, Row 077 and Path 110, Row 078, acquired on 22 August 1986, were used to prepare the imagery for McINTOSH. Preliminary data processing involved image geo-rectification to AMG coordinates and the subtraction of dark pixel values from all bands to correct for additive atmospheric scatter. Two image-processing techniques were used in the preparation of the imagery, Band Ratios and DPCA.

The use of band ratios to discriminate clay materials in arid terrains has been documented by several authors (Abrams et al. 1977, Prost 1980, Podwysocki et al. 1983). For the preliminary phase of this study, a composite image (Fig. 8.2) was generated by ratioing TM band 5 over TM band 7 (5/7) to discriminate clays, TM band 5 over TM band 3 (5/3) to discriminate iron oxides, and using band 5 for the vegetation; these were displayed as red, green, and blue, respectively. However, in vegetated terrains, the spectral response of minerals in Landsat-5 TM data is mixed with the spectral response from vegetation, and ratio images, in particular 5/7, do not provide a good discrimination of the lithological components. This problem was overcame to a large extent by using the DPCA (Fraser & Green 1987). This technique directs a principal component analysis at an input of two specific band-ratio images, in this case ratios 4/3, which enhances vegetation, and 5/7, which enhances the mixed response of clay materials and vegetation; the notation for the resultant image is dpc2(4/3,5/7). The dpc2(4/3,5/7) image was integrated with the band-ratio image 5/4 to discriminate iron

oxides, and bands 1 and 7 were added to discriminate silica (Fig. 8.3). The composite image was integrated with gamma-ray spectrometric data by using the individual potassium, thorium, and uranium channels as intensity layers (Fig. 8.4).

Geology and remote sensing

Panton intrusion (group I)

The 1856 Ma Panton intrusion (number 39 in Fig. 8.2) consists of a 1550 m thick sequence of mafic and ultramafic rocks exposed over an area of 11 km by 2.5 km. The intrusion forms a southwesterly plunging syncline and is disrupted by NNW-trending faults, which divide it into the northern and southern blocks. The intrusion consists of a lower Ultramafic Series and an overlying Gabbroic Series (see Chapter 5). The Ultramafic Series forms just less than half the total thickness of the intrusion, and consists mainly of dunite and porphyritic harzburgite (along the eastern contact of the northern block). The Panton intrusion has been metamorphosed to amphibolite facies, which is similar to all group I intrusions. Sulphide-bearing chromitites occur in harzburgite and dunite near the base of the intrusion and also as laterally continuous layers in dunite some 150 m below the mafic–ultramafic contact. The Gabbroic Series comprises three zones: a Lower Mafic Zone of layered gabbronorite, gabbro, and norite; a Middle Mafic Zone of gabbro and chromite-bearing dunite lenses; and an Upper Mafic Zone of anorthosite and ferrogabbro (Hoatson 1992).

The ultramafic and gabbroic rocks of the Panton intrusion and younger McIntosh intrusion are effectively discriminated in the band-ratio composite images of Figures 8.2 and 8.5. In the Panton intrusion, dunite and harzburgite are displayed as deep brown to magenta. Gabbro, gabbronorite, and norite are displayed as red to yellow, owing to the response of clay and vegetation and iron oxides, and green–yellow to light green to cyan, on scree-covered slopes, owing to a predominant response from iron oxides. Anorthosite and ferrogabbro are both displayed as red to dark brown. North of the Panton intrusion, and to the west and north of the McIntosh intrusion, small group I peridotitic bodies, similar to the Panton intrusion, are displayed mainly as red and minor yellow, indicating the mixed response of carbonates and vegetation.

In contrast, for the DPCA image of Figure 8.3, dunite and harzburgite are displayed as red-magenta, with some red areas, which may represent carbonates, in harzburgite; norite and gabbro are displayed as red-magenta to pink; anorthosite and ferrogabbro are displayed as light red-magenta. Valleys and streams cutting the intrusion are displayed as green, indicating mixed response from iron oxides and lichen. Peridotitic rocks north of the intrusion are displayed as light red, indicating an overall carbonate response and a much reduced vegetation response in comparison with Figure 8.2.

Big Ben intrusion (group I)

The Big Ben intrusion (43 in Fig. 8.2) is 2 km thick. A lower ultramafic zone, 1500 m thick, comprising serpentinised dunite, chromitite, lherzolite, pyroxenite, and tremolite-anthophyllite ultramafic rock, is overlain by 500 m of mafic cumulate sequence, consisting of anorthosite, gabbro, gabbronorite, and norite. Chromitite layers, up to 15 cm thick, occur in serpentinised dunite in the lower and upper parts of the ultramafic zone. The contact between ultramafic and mafic rocks is intruded by hornblende-biotite granite and aplitic leucogranite.

The Big Ben intrusion is a fault-bounded block on the western side of the Panton Fault, and, on the basis of lithological, structural, and mineralogical considerations, is believed to have been originally part of the Panton intrusion (see Chapter 5).

Figures 8.2 and 8.3 show poor or no discrimination of the mafic–ultramafic intrusion from the country rocks. This is due to extensive weathering and the abundance of other similar mafic rocks (belonging to the Wild Dog Creek intrusion and the Tickalara Metamorphics) surrounding the intrusion.

Springvale intrusion (group II)

The 1857 Ma Springvale intrusion (37 in Fig. 8.2) consists of two mafic lobes, eastern and western, each about 6 x 6 km. The western lobe consists of a 2 km-thick sequence of olivine gabbro, olivine gabbronorite, gabbro, troctolite, anorthosite, and minor leucogabbro. Shallow dark clays and soils cover most of the gabbroic rocks of the eastern lobe and the southern part of the western lobe. The northwestern part of the intrusion contains irregular bodies of granite, and is cut by veins of pegmatite and quartz (see Chapter 5).

The image shown in Figure 8.2 provides a fair to good discrimination of the different rock types in the western lobe of the intrusion. Outcrops of gabbroic rocks are displayed as brown to grey, and areas of anorthosite as blue to magenta. Granitic rocks in the intrusion are discriminated as dark blue-grey. Gabbro in the eastern lobe is well discriminated as red, where it is well exposed, to green, where the gabbro is covered by alluvium. The red colour is probably a mixed response of gabbro and vegetation.

Gabbroic rocks in the western lobe for Figure 8.3 are displayed as deep brown, and anorthosite as red-magenta. Granitic bodies are differentiated as pale red-magenta and are difficult to distinguish from anorthosite. In the eastern lobe, the sparse outcrops of gabbro are displayed as light brown, whereas the surficial cover is displayed as light green and yellow. A comparison of the images in Figures 8.2 and 8.3 indicates that the clay response in the ratio 5/7 has been enhanced by the DPCA.

Wilagee intrusion (group II)

The Wilagee intrusion (24 in Fig. 8.2) is a differentiated mafic–ultramafic body located along the southeastern and eastern margins of the Toby intrusion. The southern part, separated from the Toby intrusion by a northeast-trending fault, is 1300 m thick; it consists of a thin basal

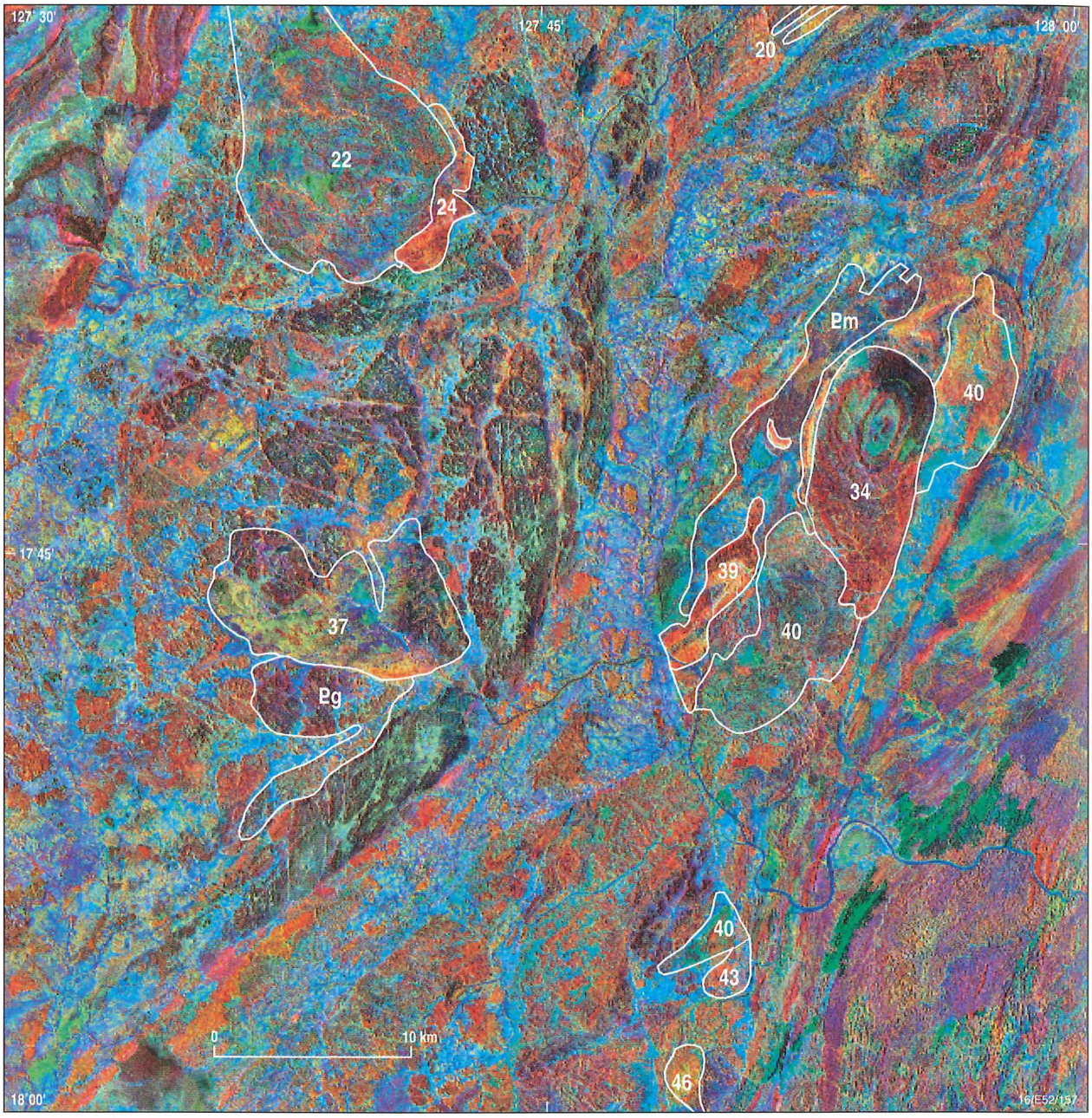


Figure 8.2. McINTOSH 1:100 000 Sheet 4462, Western Australia—Landsat-5 TM (path 107 row 72) colour composite 5/7, 5/3, and 5 image, displayed as red, green, and blue, respectively. Mafic–ultramafic intrusions shown are: McKenzie Spring (20), Toby (22), Wilagee (24), McIntosh (34), Springvale (37), Panton (39), Wild Dog Creek (40), Big Ben (43), and Armanda (46). Other areas annotated include the Airfield Granodiorite (Eg) and a part of the Tickalara Metamorphics (Em).

peridotite unit overlain by thicker units of troctolite and olivine gabbro, anorthosite and leucogabbro, and melagabbro. The northern part of the Wilagee intrusion extends 6 km along the eastern contact of the Toby intrusion, and consists of troctolite and olivine gabbro. These are likely to be the northern extension of the mafic units of the southern part of the intrusion (see Chapter 5).

Both the band-ratio and DPCA composite images (Figs 8.2, 8.3, respectively) provide good discrimination of this intrusion from the Toby intrusion and from the surrounding granitic country rocks. Figure 8.2 displays the intrusion as red-brown with a central red sliver, which may be a result of a spectral response dominated by vegetation. The intrusion in Figure 8.3 is displayed as brownish red, indicating a predominantly clay response, and minor yellow, indicating a mixed response of clay and iron oxides. Neither image discriminates between the mafic and ultramafic rocks since the latter rocks are too thin and have limited strike extent.

Toby intrusion (group III)

The 1855 Ma Toby intrusion (22 in Fig. 8.2) is 2 km thick and occupies an area of about 240 km^2. It consists of quartz–biotite gabbro, biotite gabbro, biotite gabbronorite, olivine gabbronorite, and subophitic

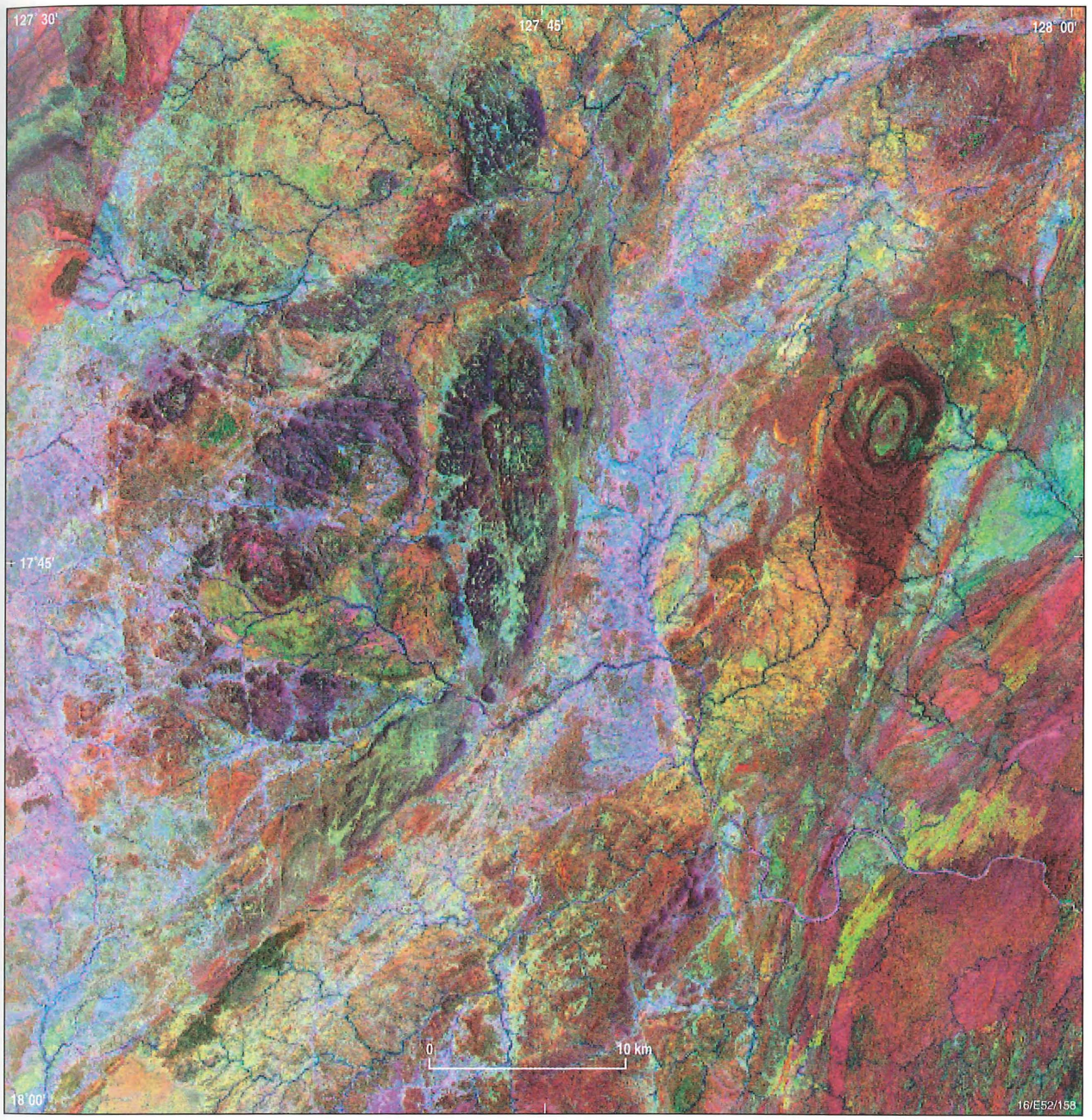


Figure 8.3. McINTOSH 1:100 000 Sheet 4462, Western Australia—Landsat-5 TM (path 107 row 72) colour composite dpc2(4/3,5/7), 5/4, and 1+7 image, displayed as red, green, and blue, enhancing clays, iron oxides, and silica, respectively.

gabbro interlayered with minor troctolite and olivine norite. Rare ultramafic rocks and blocks of marble occur near faults in the centre of the intrusion. Most of the intrusion is covered by alluvium and soil, with recessive outcrops in the central and southwestern parts. It contains concentric lineaments parallel to its margins, and is intruded by dolerite dykes, and by elongate granitic bodies in the southeast (see Chapter 5).

The geometry of the intrusion is well displayed in the images, owing to the concentric layering effect created by arcuate lineaments (see Chapter 5). In Figure 8.2 the gabbroic rocks are poorly discriminated, and are displayed from brown-red in outcrop areas, indicating a predominantly clay response over iron oxides, to brownish grey in areas covered by in-situ soil. The gabbroic rocks in Figure 8.3 are displayed as pinkish red in outcrop areas, and as pink in areas of sparse outcrop or covered by in-situ soil, indicating a dominant clay response over iron oxides. Granitic rocks are shown as dark red-brown. Neither image differentiates the ultramafic rocks from the main gabbro units along faults, and this is probably because of the small size of the outcrops.

Wild Dog Creek intrusion (group IV)

The largest Wild Dog Creek intrusion (40 in Fig. 8.2) crops out to the northeast and southwest of the McIntosh intrusion. Smaller gabbroic bodies correlated with the Wild Dog Creek intrusion occur further south near the Big Ben and Armanda intrusions. Major rock types

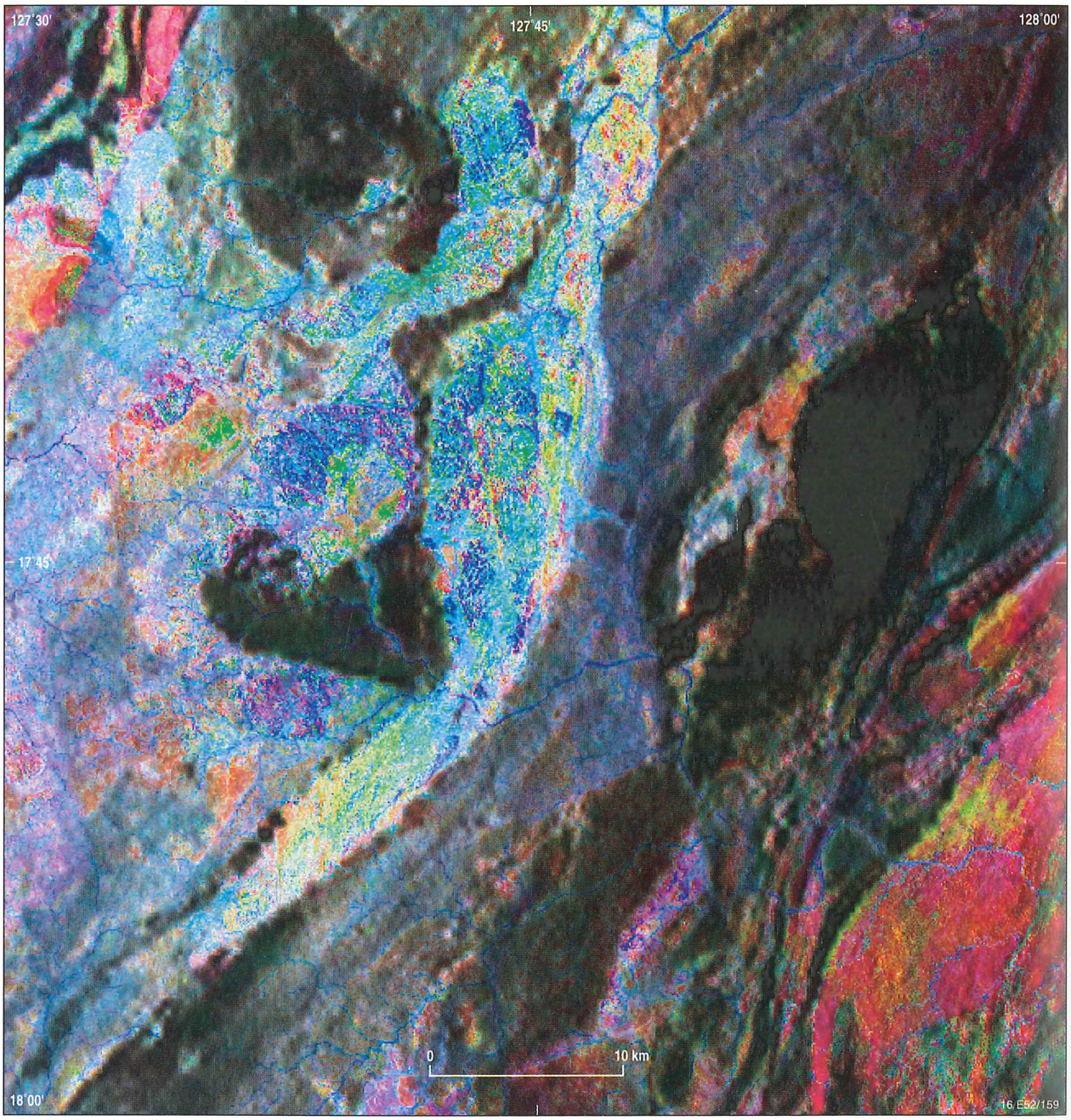


Figure 8.4. McINTOSH 1:100 000 Sheet 4462, Western Australia—Landsat-5 TM (path 107 row 72) colour composite dpc2(4/3,5/7), 5/4, and 1+7 image, displayed as red, green, and blue, enhancing clays, iron oxides, and silica, respectively, with the potassium channel from gamma-ray spectrometric data as the intensity layer.

include magnetite gabbro, magnetite–quartz gabbronorite, biotite gabbro, amphibolite, and various hybrid rocks of dioritic and tonalitic composition. Rhythmic compositional layering is absent, but in places a primary igneous lamination parallel to a preferred fabric defined by the alignment of metamorphic amphibole is present. In terms of outcrop, the Wild Dog Creek intrusion near the McIntosh intrusion is similar to the Springvale intrusion; the northeast part is hilly and covered by spinifex, whereas the southwest part is covered by grassy alluvial plains with shallow soils, containing abundant concentrations of Fe–Ti oxides, and sparse low-lying exposures of bedrock.

The northeast part of the Wild Dog Creek intrusion in Figure 8.2 is brownish red to yellow indicating a strong mixed response from clay and iron oxides. The mostly soil-covered southwest part is predominantly brown-grey, with sparse clay-bearing outcrops showing as brownish red. In Figure 8.3, the gabbroic rocks in the northeast part are brown-red to pink; areas of soil cover and alluvium are green to cyan, indicating the presence of iron oxides and silica; and the southwest part has a more uniform display than Figure 8.2; areas of soil are shown in light brown and yellow-green, sparse gabbroic outcrops are brown, and areas of alluvium are light green to yellow.

McKenzie Spring intrusion (group V)

The McKenzie Spring intrusion (20 in Fig. 8.2) is a northeast-trending lenticular mafic sill, 1 km thick. Only the southwestern part of the intrusion occurs on the northern central margin of McINTOSH. The intrusion consists mainly of weakly layered olivine gabbro, olivine gabbronorite, olivine–magnetite gabbronorite, melagabbro, leucogabbro, troctolite, amphibolite, and minor pyroxenite, with gabbros showing an increase in magnetite content northwest of McINTOSH. Limonite–goethite gossan zones occur near the thickest portion of the cumulates, under a sequence of olivine gabbro, troctolite, and anorthosite. The host rocks are enclosed by a garnet–cordierite–sillimanite–spinel–biotite–feldspar–quartz migmatitic pelitic gneiss of the Tickalara Metamorphics and various mafic igneous rocks (see Chapter 5).

The gabbroic rocks are not discriminated from the country rocks in Figure 8.2. The layered, iron-rich, sequence of olivine gabbro, olivine gabbronorite, gabbronorite, and leucogabbro is displayed as predominantly green in Figure 8.3.

McIntosh intrusion (group VI)

The 1830 Ma McIntosh intrusion (34 in Fig. 8.2) is a large ovoid mafic body about 14 km long from north to south and 6 km wide. It consists of alternating layers of olivine gabbro, olivine gabbronorite, troctolite, magnetite gabbro, and minor leucogabbro and anorthosite, and has a total stratigraphic thickness of about 7800 m. Thin peridotite lenses occur in the lower part of the intrusion. The layering is expressed topographically as concentric strike ridges and valleys. In the upper 2500 m of the intrusion, magnetite gabbro and gabbronorite form the ridges, whereas the olivine-bearing units—troctolite and olivine gabbro—underlie the valleys. In the lower part of intrusion, the ridges are formed by gabbro and gabbronorite, and valleys are underlain by troctolite (Mathison & Hamlyn 1987).

Figures 8.2 and 8.5 highlight the concentric layering of the intrusion, discriminating it from the surrounding gabbros of the Wild Dog Creek intrusion and the Tickalara Metamorphics. The gabbroic rocks in the intrusion are not discriminated from each other and are displayed as red-brown. A large, dark brown area in the northeast probably represents a fireburn. Areas in blue represent soil and vegetation. In Figure 8.3 the masking effect of vegetation has been largely removed, and some discrimination within the gabbroic sequence is evident. Some pinkish red areas represent magnesium-bearing carbonates in an olivine-rich gabbroic unit. Ridges of magnetite gabbro, magnetite gabbronorite, magnetite olivine gabbro, and olivine gabbro are displayed as dark greenish brown; probably due to lichen on the rock surfaces. Areas in light green to green represent soils rich in iron oxides. Emerald green represents either the response of dense lichen on rock surfaces or iron oxide-rich weathered surfaces of magnetite-bearing rocks (Glikson & Creasey 1995). Pegmatitic rocks at the centre of the intrusion are displayed as light red-magenta (cf. blue in Fig. 8.2).

Armanda intrusion (group VI)

The Armanda intrusion (46 in Fig. 8.2) is an ovoid-shaped body, 2.5 km by 1.5 km, 750 m thick, that is correlated with the 1830 Ma McIntosh intrusion. It comprises a weakly layered mafic sequence of olivine gabbro, olivine gabbronorite, gabbro, and minor leucogabbro. The layering is due to variable amounts of plagioclase, clinopyroxene, orthopyroxene, and minor olivine. 'Sills' of leucogabbro and minor anorthosite are intercalated with felsic metavolcanic country rock in the southeastern corner of the intrusion east of the Armanda River (see Chapter 5).

Figure 8.2 gives a poor discrimination of the intrusion. The gabbroic rocks, displayed as red-brown and pale yellowish green, can be distinguished from the metamorphosed felsic volcanics (Koongie Park Formation) to the east, which are displayed as predominantly blue magenta, but they cannot be differentiated from the similar gabbroic rocks of the Wild Dog Creek body to the north of the intrusion. However, Figure 8.3 provides a fair to good discrimination of the intrusion from the surrounding country rocks. The gabbroic rocks are displayed as green with brown patches, which probably represent anorthositic rocks. The metamorphosed felsic volcanics to the east are displayed as red magenta to pink.

Gamma-ray spectrometry

Gamma-ray spectrometric data (K, Th, and U) covering the area of the Dixon Range and Gordon Downs 1:250 000 map sheets was acquired by AGSO in 1992. Aerodata flew and compiled the airborne geophysical survey, and carried out some image processing. The survey, flown at 100 m height, with a traverse spacing of 400 m in an east–west direction, was micro-levelled, and has both a data grid cell and an image pixel size of 125 m.

Figure 8.4 shows the results of the integration of the Landsat image shown in Figure 8.3 with the K channel. Because of the low spectrometric response of mafic and ultramafic rocks, the image provides a quick method of discriminating mafic–ultramafic rocks (dark brown to black) from granitic, metamorphic, and sedimentary rocks.

The well-exposed Airfield Granodiorite, south of the Springvale intrusion (Pg in Fig. 8.2) consists largely of granodiorite and monzogranite, but includes parts that have a very low response to K and also to U, indicating that it is probably a composite body which could be further subdivided.

The Tickalara Metamorphics shown as Pm in Figure 8.2 consist mainly of muscovite ± biotite ± plagioclase ± quartz ± andalusite ± sillimanite ± garnet schist. The central and northern parts in Figure 8.2 are red brown, brown, and dark blue, whereas the southern part is light blue to blue. In Figure 8.3 the central and northern parts are brown, whereas the southern part is pale to pinkish blue. One possible explanation for these differences is a change in the mineralogy of the schist from north to south (e.g. sillimanite to andalusite). However, in Figure

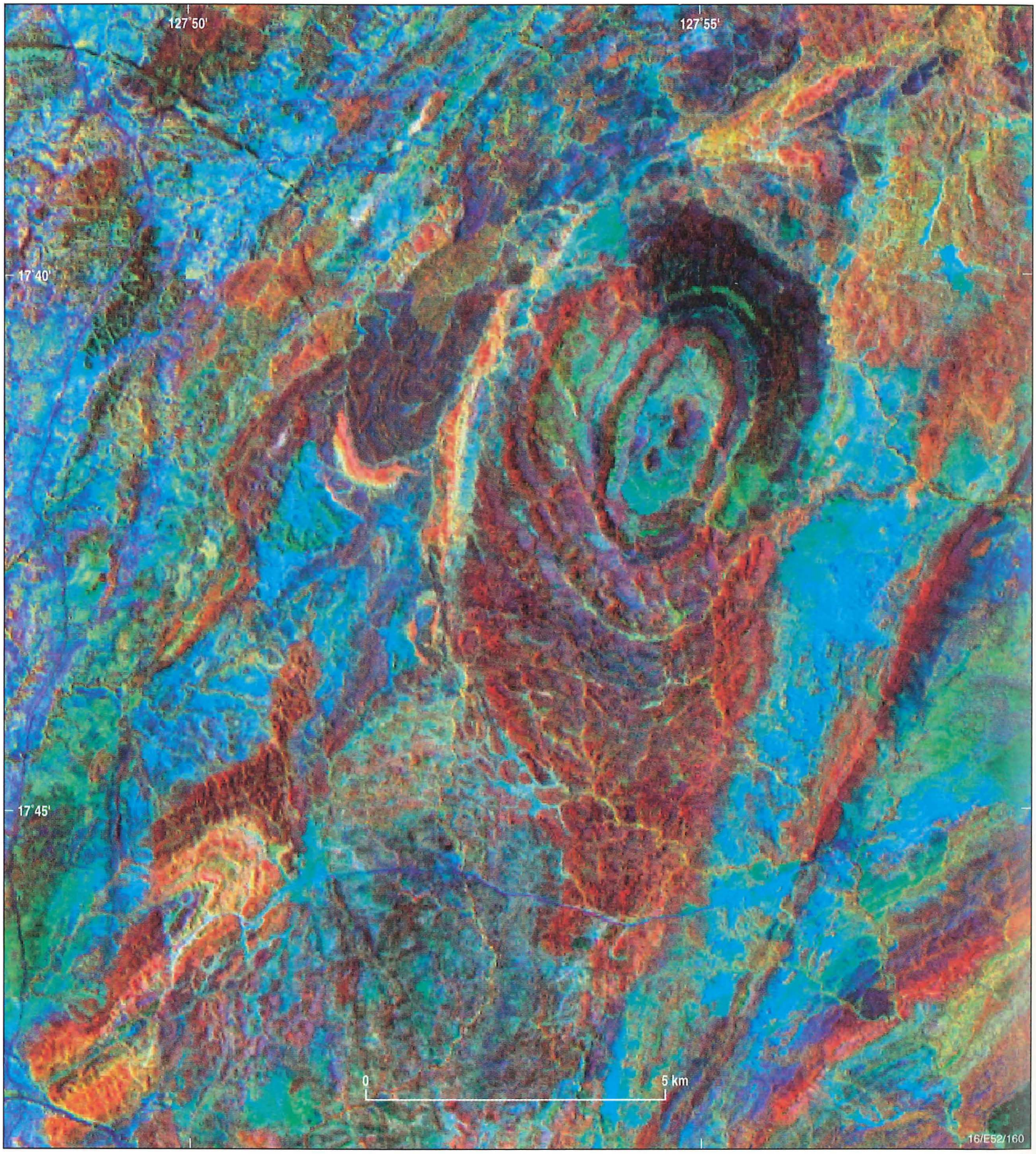


Figure 8.5. Landsat-5 TM (path 107 row 72) colour composite 5/7, 5/3, and 5 image, displayed as red, green, and blue, respectively. This particular image (enlarged right central part of Figure 8.2) highlights the differentiated nature of the Panton intrusion and associated smaller group I intrusions further north, and the concentric form of the large McIntosh intrusion.

8.4, the central part of the unit shows a greater K response, with yellow–red colours, while the southern and northern parts are displayed mainly as blue and grey. The central part consists of hilly terrain, but the other parts have a lower relief, are more weathered, and are partly covered by soil. Hence the differing K responses could be due to differences in weathering and soil cover, rather than to differences in lithology, as suggested by Figure 8.3.

Discussion and conclusions

Landsat-5 Thematic Mapper imagery, using band ratios and DPCA, proved to be a very useful tool in the geological mapping of McINTOSH, as it enabled different lithologies to be distinguished at a regional scale. The analysis of band-ratio imagery is limited to some extent by the mixed spectral response of vegetation and surface materials. Field measurements in other parts

of inland Australia (Macias et al. 1987) show that spinifex density of 30–40% can largely mask the reflectance from underlying soil and/or rock. Interpretation of this imagery is also hampered by younger spinifex regrowth and fireburn patterns of different ages (Simpson 1990). These masking effects, though, are significantly reduced with DPCA imagery.

The mafic and ultramafic intrusions on McINTOSH can be discriminated to varying extents by Landsat-5 TM data. Lithological discrimination depends on a number of factors: e.g. the presence of weathering products from plagioclase-rich gabbroic and anorthositic units, as in the case of the Panton intrusion and the western part of the Springvale intrusion; the presence of carbonates derived from ultramafic rocks; and the nature of the terrain, as is the case for the Wild Dog Creek intrusion; and the presence of lichen, which seems to favour iron oxide-rich outcrops, as is the case for the McIntosh intrusion. The hilly northeastern part of the Wild Dog Creek intrusion is red in Figure 8.3, owing to the predominance of clay on weathered gabbro, whereas the flat, soil-covered southwestern part is mainly red–yellow and green, indicating a response to iron oxides in the soils. Where the layered mafic–ultramafic intrusions are poorly exposed and/or are surrounded by country rocks with similar mineralogy, discrimination is poor or non-existent, as is the case for the Big Ben and Armanda intrusions.

Acknowledgements

I thank Dean Hoatson (AGSO) for providing the geological information on the mafic and ultramafic intrusive rocks, and John Creasey, John Wilford, Alastair Stewart, David Blake (all AGSO), and Ian Tyler (GSWA), whose comments helped to improve the text.

References

Abrams, M.J., 1986. Mapping the Oman ophiolite using TM data. In: Proceedings of the thematic conference, 5th, remote sensing for exploration geology (Reno, Nevada, 29 September-2 October, 1986). Environmental Research Institute and Ann Arbor, Michigan, 85–95.

Abrams, M.J., Ashley, R.P., Rowan, L.C. Goetz, A.F.H. & Kahle, A.B., 1977. Mapping of hydrothermal alteration in the Cuprite mining district, Nevada, using aircraft scanner images for the spectral region 0.46 to 2.36μm. Geology, 5, 713–718.

Abrams, M.J., Rothery, D.A. & Pontual, A., 1988. Mapping in the Oman ophiolite using enhanced Landsat Thematic Mapper images. Tectophysics, 151, 387–401.

Birnie, R.W., Parr, J.P., Naslund, H.R., Nichols, J.D. & Turner, P.A., 1989. Applications of Landsat Thematic Mapper and ground-based spectrometer data to a study of the Skaergaard and other mafic intrusions of East Greenland. Remote Sensing of the Environment, 28, 297–304.

Deer, W.A., Howie, R.A. & Zussman, J., 1966. An introduction to the rock-forming minerals. Longmans, Green & Co. Ltd, London, 528 pp.

Fraser, S.J. & Green, A.A., 1987. A software defoliant for geological analysis of band ratios. International Journal of Remote Sensing, 8, 525–532.

Glikson, A.Y. & Creasey, J.W., 1995. Application of Landsat-5 TM imagery to mapping of the Giles Complex and associated granulites, Tomkinson Ranges, Western Musgrave Block, central Australia. AGSO Journal of Australian Geology & Geophysics, 16, 173–193.

Green, A.A. & Craig, M.D., 1985. Analysis of aircraft data with logarithmic residual. Proceedings of the Airborne Imaging Spectrometer Data Analysis Workshop. Jet Propulsion Laboratory, Publication 85-41, 111–119.

Harding, D.J., Wirth, K.R. & Bird, J.M., 1989. Spectral mapping of Alaskan ophiolites using Landsat Thematic Mapper data. Remote Sensing of the Environment. 28, 219–232.

Hoatson, D.M., 1992. East Kimberley: Panton Intrusion. AGSO 92, Yearbook of the Australian Geological Survey Organisation, 78–80.

Macias, L.F., 1995. Remote Sensing of mafic–ultramafic rocks: examples from Australian Precambrian terranes. AGSO Journal of Australian Geology & Geophysics, 16, 163–171.

Macias, L.F. & Simpson, C.J., 1990. Image processing of TM data over ultramafic complexes. Proceedings of the 5th Australasian Remote Sensing Conference, 1. Committee of the 5th Australasian Remote Sensing Incorporated 1990, Western Australia, 612–627.

Macias, L.F. & Simpson, C.J., 1992. Geological Remote Sensing of the Munni Munni and Andover Complexes. In: Hoatson, D.M., Wallace, D.A., Sun, S-s., Macias, L.F., Simpson, C.J. & Keays, R.R., Petrology and platinum-group-element geochemistry of Archaean layered mafic–ultramafic intrusions, west Pilbara Block, Western Australia. Australian Geological Survey Organisation, Bulletin 242, 167–177.

Macias, L.F., Simpson, C.J. & Moore, R.F., 1987. Differentiation of mafic and ultramafic rock types using NS001 and TIMS data. In: Bruce, D. (editor), Proceedings of the 4th international remote sensing conference, 1. Committee of the 4th Australasian Remote Sensing Conference Incorporated, 1987, 364–370.

Mathison, C.I. & Hamlyn, P.R., 1987. The Mcintosh layered troctolite–olivine gabbro intrusion, East Kimberley, Western Australia. Journal of Petrology, 28, 211–234.

Podwysocki, M.H., Segal, D.B. & Abrams, M.J., 1983. Use of multispectral scanner images for assessment of hydrothermal alteration in the Marysvale, Utah, mining area. Economic Geology, 78, 675–687.

Pontual, A., 1990. Constraining the patterns of hydrothermal circulation cells in ophiolitic terrain by application of digitally enhanced Landsat Thematic Mapper data. Proceedings of the 5th Australasian Remote Sensing Conference 1. Committee of the 5th Australasian Remote Sensing Incorporated 1990, Western Australia, 628–635.

Prost, G., 1980. Alteration mapping with airborne multispectral scanners. Economic Geology, 75, 894–906.

Raines, G.L. & Wyn, J.C., 1982. Mapping of the ultramafic rocks in a heavily vegetated terrain using Landsat data. Economic Geology, 77, 1755–1769.

Rothery, D.A., 1984a. The role of Landsat Multispectral Scanner (MSS) imagery in mapping the Oman Ophiolite. In: Gass, I.G. et al. (editors), Ophiolites and oceanic lithosphere. Geological Society of London, Special Publication 13, 405–413.

Rothery, D.A., 1984b. Reflectance of ophiolite rocks in the Landsat MSS bands: relevance to lithological mapping by remote sensing. Journal of the Geological Society of London, 141, 933–969.

Rothery, D.A., 1987. Improved discrimination of rocks units using Landsat Thematic imagery of the Oman Ophiolite. Journal of the Geological Society of London, 144, 587–597.

Rothery, D.A., Abrams, M.J. & Pontual, A., 1988. Subdivision of mapped units in the Oman Ophiolite using enhanced Landsat Thematic Mapper images. Proceedings, Troodos 87, Ophiolites & Oceanic Lithosphere, Nicosia, Cyprus, 4–10.

Simpson, C.J., 1990. Deep weathering, vegetation and fire burn. Significant obstacles to geoscience remote sensing in Australia. International Journal of Remote Sensing, 11, 2019–2034.

Sultan, M., Arvidson, R.E. & Sturchio, N.C., 1986. Mapping of serpentinites in the Eastern Desert of Egypt by using Landsat thematic mapper data. Geology, 14, 995–999.

Van Der Meer, F., Vazquez-Torres, M. & Van Dijk, P.M., 1997. Spectral characterisation of ophiolite lithologies in the Troodos Ophiolite complex of Cyprus and its potential in prospecting for massive sulphide deposits. International Journal of Remote Sensing, 18, 1245–1257.

DEPTHS OF EMPLACEMENT OF THE MAFIC–ULTRAMAFIC INTRUSIONS

by ALFONSO G. TRUDU[1] & DEAN M. HOATSON

Introduction

The main aim of this geobarometric study is to determine the depth of emplacement of the Palaeoproterozoic layered mafic–ultramafic intrusions in the East Kimberley, Western Australia. To this end, we have determined the pressure (and hence crustal depth) at which crystallisation and/or subsolidus reactions (magmatic coronas and symplectites) took place in gabbroic rocks of the intrusions. It is hoped that these new findings will:

1. explain the spatial distribution of the mineralised members of the intrusive suite;
2. provide information about the petrogenesis of the migmatitic country rocks; and
3. help constrain interpretations of the geological evolution of the East Kimberley.

Geothermobarometric investigations were carried out on 13 layered mafic and mafic–ultramafic intrusions representing groups I, II, III, V, and VI of Hoatson (see Chapter 5; Fig. 9.1). The intrusions are: Big Ben and Panton (group I); Springvale and Wilagee (II); Toby (III); Dave Hill, Keller Creek, McKenzie Spring, Sally Malay, Spring Creek, and Wilson Creek (V); and Armanda and McIntosh (VI). U–Pb zircon dating of fractionated gabbroic rocks by Page et al. (1995) and Page & Hoatson (see Chapter 6) has shown that the intrusions were emplaced during a brief geological period in the Palaeoproterozoic from about 1860 to 1825 Ma. The typical features of the type examples of the seven groups are summarised in Table 9.1, and their geological settings are described by Hoatson (1993, 1995), Hoatson & Tyler (1993), Hoatson et al. (1995, 1997), Blake (1997), and in Chapter 5.

Most of the rocks used for this study are mafic cumulates (olivine gabbronorite, troctolite, norite), the exceptions being a plagioclase peridotite (Big Ben) and a subophitic (non-cumulate) gabbronorite (Toby). The mafic cumulates consist mainly of cumulus olivine and cumulus plagioclase, whereas orthopyroxene and clinopyroxene, where present, tend to form intercumulus phases.

Geothermobarometric calculations are based on electron probe microanalyses of Ca-bearing amphibole from coronas around olivine and from magmatic amphibole replacing clinopyroxene. The Ti content of amphibole in the coronas is used to determine its temperature of formation (Otten 1984) and the Al content of the same

Table 9.1. Classification of the layered mafic–ultramafic intrusions in the East Kimberley.

	Type example U–Pb zircon age[a]	*Thickness (km)*	*Form*	*Major rock types*	*Mineralisation*
Group I	Panton 1856±2 Ma	0.2–2.0	Steeply dipping folded sheets, faulted blocks	Du, Ha, Cr, Tr–An, Amph, Gab, Gabn, N, AnG, An, Fg	Cr, PGE, Ni, Cu, Au
Group II	Springvale 1857±2 Ma	2.0	Moderately dipping sheets	OGab, OGabn, Gab, Troc, AnG, Lherz	Ni, Cu, Cr, PGE
Group III	Toby 1855±2 Ma	2.0	Shallow-dipping basin	BiotGab, OGab, Gab, Du	None known
Group IV	Wild Dog Creek	0.5–2.0	Shallow-dipping sheets	MtGab, BiotGab, Dior	None known
Group V	Sally Malay 1844±3 Ma	0.2–2.0	Composite sub-chambers, dipping sheets	OGab, Troc, Gab, Gabn, N, AnG, An, Lherz, Du	Ni, Cu, Co, PGE Ti, V
Group VI	McIntosh 1830±3 Ma	0.5–8.0	Dipping sheets, basins, funnels, faulted blocks	OGab, OGabn, Troc, MtGab, AnG, Lherz	Cu, Ti, V
Group VII	Black Hills Yard	0.2–1.0	Steeply plunging plugs	Troc, OGab, OGabn, Gab, BiotGab	None known

[a] Geochronology of intrusions from Page & Hoatson (see Chapter 6) and Page et al. (1995).

Major rock types are arranged in order of decreasing abundance. Amph = amphibolite; Cr = chromitite; Du = dunite; Ha = harzburgite; Lherz = lherzolite; Tr-An = tremolite-anthophyllite peridotite; BiotGab = biotite gabbro; OGab = olivine gabbro; Gab = gabbro; OGabn = olivine gabbronorite; Gabn = gabbronorite; MtGab = magnetite gabbro; Troc = troctolite; N = norite; AnG = anorthositic gabbro; An = anorthosite; Fg = ferrogabbro; Dior = diorite.

[1] Department of Earth Sciences, Monash University, Clayton, Victoria 3168.
Present address: CSIRO Minerals, PO Box 883, Kenmore, Queensland 4069

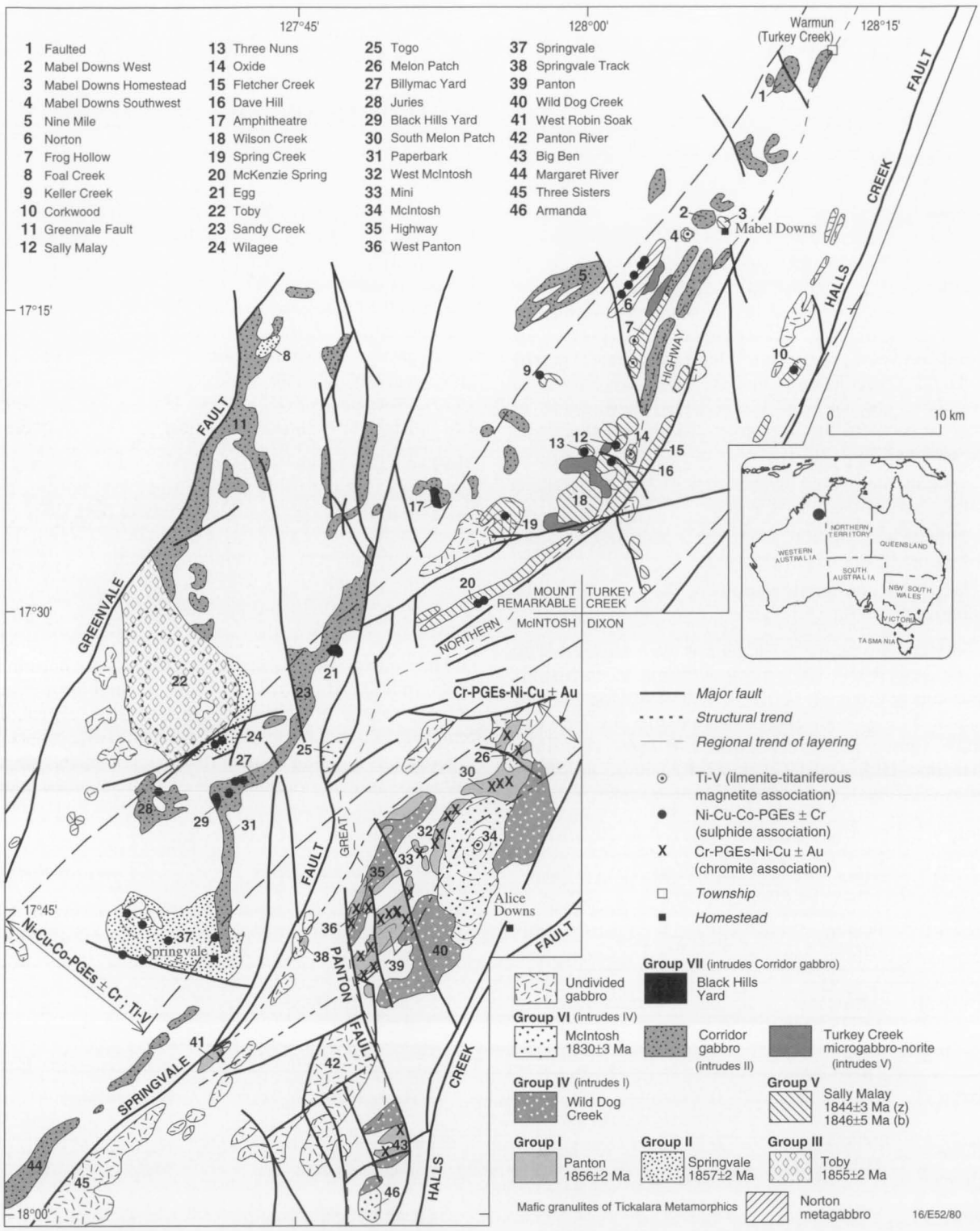


Figure 9.1. Regional distribution of Palaeoproterozoic layered mafic–ultramafic intrusions in the East Kimberley. The intrusions investigated in this study are: Keller Creek (9), Sally Malay (12), Dave Hill (16), Wilson Creek (18), Spring Creek (19), McKenzie Spring (20), Toby (22), Wilagee (24), McIntosh (34), Springvale (37), Panton (39), Big Ben (43), and Armanda (46).

mineral is used to estimate pressure (Hammarstrom & Zen 1986, Anderson & Smith 1995). In a few samples where the coronas were poorly developed or the Ti content of the clinoamphibole in the corona was too low (<~0.1% TiO_2), the Ti content of late high-temperature magmatic amphibole replacing clinopyroxene was used.

Variations in mineral chemistry across parts of the stratigraphy of the Springvale, Toby, and Wilagee intrusions were also investigated in this study to provide additional information about the petrogenesis of the intrusions (e.g. primitive character of intrusions, cryptic variations of mineral chemistry, open or closed fractionation systems).

Previous geobarometric studies of layered intrusions

Directly estimating crystallisation pressures of layered mafic–ultramafic intrusions is difficult, because mineral assemblages in these intrusions are rarely suitable for geothermobarometry. The best examples of using the composition of minerals from the intrusion are those of Ballhaus & Berry (1991) for the Wingellina Hills intrusion, Musgrave Block, central Australia, and Hoatson et al. (1992) for the Munni Munni intrusion, Pilbara Craton, Western Australia. More indirect geothermobarometric methods include reference to: (1) contact metamorphic conditions of either pelitic country rocks (e.g. Nell 1985, for the Bushveld Complex, South Africa) or xenoliths in mafic–ultramafic rocks (e.g. Wallmach et al. 1989, for the Bushveld Complex); (2) petrography and phase diagrams (e.g. Mathison & Hamlyn 1987, for the McIntosh intrusion, East Kimberley); (3) estimates from experiments (e.g. Helz 1995, for the Stillwater Complex, Montana, USA); and (4) the stratigraphic column overlying the intrusions (e.g. McGuire & Coleman 1986 for the Jabal Tirf, Saudi Arabia). Compilations of geobarometric data on the layered intrusions of the East Kimberley and elsewhere in the world, appear in Tables 9.2 and 9.3, respectively.

Geobarometric studies of four layered intrusions in the East Kimberley (Table 9.2) were undertaken prior to this study: they dealt with the McIntosh (Mathison & Hamlyn 1987, Warren pers. comm. 1995), Panton (Hamlyn 1980), Sally Malay (Thornett 1981, 1986, Warren pers. comm. 1995) and Springvale (Warren pers. comm. 1995) intrusions. Results from these studies, which used contact hornfelses, exotic rafts, or phase diagrams, indicate pressures ranging from 1.5 to 9 kb.

Table 9.3 shows the crystallisation pressure of twelve layered intrusions outside the East Kimberley, with values ranging from as low as 0.25±0.05 kb for the Rhum Complex (Greenwood et al. 1990) to 7.2±2 kb for the Wingellina Hills Complex (Ballhaus & Berry 1991). The spread of data for each intrusion tends to be large (1–3 kb). The highest pressures, 6.4–7.2 (± 2) kb, were obtained for olivine–plagioclase–pyroxene–spinel cumulate assemblages in the Wingellina Hills intrusion (Ballhaus & Berry 1991) using the THERMOCALC program of Powell & Holland (1985, 1988) and an updated database of Holland & Powell (1990).

It is interesting to observe that for the Bushveld and Stillwater complexes for which two sets of data exist, the more recent pressure estimates are significantly lower than the older estimates. Although the low pressures (1–2 kb) characterising the Jabal Tirf, Kap Edvald Holm, and Skaergaard complexes were initially considered to be doubtful because of poorly constrained estimates of the thickness of stratigraphic units overlying the intrusions, there is now more evidence (e.g. studies of the Bushveld by Wallmach et al. 1989) that these pressure could be meaningful. The major mineralised intrusions of the world (Bushveld, Stillwater) appear to have been emplaced at fairly moderate pressures in the crust (<5 kb), indicating a possible correlation between mineralisation and depth of emplacement. It is also interesting that most of the very shallow intrusions are much younger (Mesozoic–Tertiary) than most of the others (Proterozoic). However, there is no suggestion here that the younger intrusions are generally emplaced at shallower depths than the Proterozoic intrusions, since other factors, such as tectonic setting, would also have an important influence.

Methods

About 200 thin sections from 18 layered intrusions in the East Kimberley were examined for magmatic and late magmatic mineral assemblages suitable for electron

Table 9.2. Magmatic crystallisation pressures for layered mafic–ultramafic intrusions in the East Kimberley.

Intrusion	*Estimated pressure (kb)*	*Methodology*	*Source of data*
McIntosh	5–6	Geobarometry of hornfels (a, e)	Warren (AGSO, pers. comm. 1995)
McIntosh	<6	Petrography and phase diagrams	Mathison & Hamlyn (1987)
Panton	8–9	Based on phase diagrams from experiments (b)	Hamlyn (1980)
Sally Malay	4–5	Geobarometry of hornfels (a, e)	Warren (AGSO, pers. comm. 1995)
Sally Malay	max. 6	Geobarometry of hornfels (a, d)	Thornett (1981)
Sally Malay	3–5	Geobarometry of hornfels (a, d)	Thornett (1986)
Springvale	~4	Geobarometry of pelitic xenoliths (e)	Warren (AGSO, pers. comm. 1995)

(a) Samples of migmatitic metasediments were collected from the country rocks immediately adjacent to the intrusion and have been contact metamorphosed during the emplacement of the layered intrusion. (b) Experiments by Kushiro & Yoder (1966) and Emslie (1970). (c) Based on orthopyroxene–cordierite geobarometer of Harris & Holland (1984). (d) Based on garnet–cordierite geobarometer of Hensen & Green (1973), which Ashworth & Chinner (1978) considered to yield pressure estimates that are 2 to 3 kb too high. (e) Based on the garnet–cordierite geobarometer discussed by Hensen & Green (1973), Lonker (1981), and Carey (1995).

Table 9.3. Magmatic crystallisation pressures for layered mafic–ultramafic intrusions outside the East Kimberley.

Intrusion	*Estimated pressure (kb)*	*Methodology*	*Source*
Bushveld (South Africa)	4–5	Geobarometry of hornfels (a)	Nell (1985)
Bushveld (critical zone)	0.6–1.6	Geobarometry of calc-silicate xenoliths	Wallmach et al. (1989)
Bushveld (marginal zone)	1.1–2.4	Geobarometry of calc-silicate xenoliths	Wallmach et al. (1989)
Fongen-Hyllingen (Norway)	5–6	Geobarometry of hornfels (b)	Olesen et al. (1973)
Jabal Tirf (Saudi Arabia)	1	Estimate from stratigraphy	McGuire & Coleman (1986)
Kap Edvald Holm (Greenland)	1–2	Estimate from petrography	Bernstein et al. (1996)
Kiglapait (Canada)	4	Geobarometry of hornfels (c)	Berg (1977)
Mulkahy Lake (Canada)	2–5	Estimate from petrography	Morrison et al. (1986)
Munni Munni (Australia)	3.5–5	Geobarometry of gabbro (d)	Hoatson et al. (1992)
Newer Gabbros (Scotland)	4.4–4.7	Geobarometry of hornfels (e)	Droop & Charnley (1985)
Rhum (Scotland)	0.25	Geobarometry of hornfels	Greenwood et al. (1990)
Skaergaard (Greenland)	1–2	Estimate from stratigraphy	Manning (pers. com. 1995)
Stillwater (USA)	3–4	Geobarometry of hornfels (f)	Labotka (1985)
	1.5–3	Estimate from experiments	Helz (1995)
Wingellina Hills (Australia)	6.4–7.2±2	THERMOCALC (g)	Ballhaus & Berry (1991)

(a) Geobarometer of Hensen & Green (1972) on cordierite–orthopyroxene–garnet–quartz. (b) Andalusite, sillimanite, and cordierite zones. (c) Pressure estimates based on experimental data for the olivine–hypersthene–quartz assemblage by Smith (1971). (d) Geobarometer of Ellis (1980) on anorthite–clinopyroxene–quartz. (e) Garnet–cordierite–sillimanite–quartz/spinel. (f) Geobarometers of Newton (1983) on cordierite–garnet–sillimanite–quartz, Lindsley (1983) on pigeonite, and Bohlen & Boettcher (1981) on orthopyroxene compositions in olivine–orthopyroxene–quartz. (g) Calculated from cumulate assemblages.

probe microanalysis. Twenty-one representative gabbroic and peridotitic rocks (Table 9.4) were selected on the basis of: (a) the largest number of different cumulus and intercumulus minerals; (b) suitable corona textures around olivine; and (c) the least amount of post-magmatic mineral assemblages (see the mineralogy column of Table 9.4). Post-magmatic minerals refer to those formed during later metamorphic events or during weathering, and include such minerals as talc, chlorite, sericite, serpentine minerals, iron oxides, and various clays, etc.

Various geobarometers (Ellis & Green 1979, Harley 1984) require coexisting assemblages of garnet, plagioclase, pyroxene, quartz, and/or primary amphibole. For most East Kimberley intrusions, garnet occurs as a rare xenocrystal mineral, quartz has a restricted distribution in the more evolved mafic bodies, and coarse-grained primary amphibole is rare. However, primary amphibole in coronas around olivine was used for this study, since these coronas are generally well developed and occur in most mafic intrusions.

One representative sample from each of the Armanda, Big Ben, Dave Hill, Keller Creek, McKenzie Spring, McIntosh, Sally Malay, Spring Creek, and Wilson Creek intrusions was chosen for the geothermobarometric study. Five polished thin sections of samples from both the Springvale and Toby intrusions and two from the Wilagee intrusion were analysed to investigate the chemical variation of the cumulus and intercumulus phases with stratigraphic height in each intrusion. Samples from the Corkwood, Highway, Mini, Panton, Springvale Track, South Melon Patch, and West McIntosh intrusions were generally too altered for the study. Chemical data for amphibole from the Panton intrusion were obtained from Hamlyn (1977).

Cumulus, intercumulus, and corona mineral compositions were determined with the Cameca electron probe at the Research School of Earth Sciences, Australian National University. Details of the operating conditions for the electron probe are given in Appendix 1.2.

Petrography

Samples of gabbronorite, troctolite, norite, and plagioclase peridotite were used for this study. All samples have retained their original igneous mineralogy and textures, although some show incipient alteration (Table 9.4).

Gabbronorite

Gabbronorite samples were subdivided into three general categories: gabbronorite, olivine gabbronorite, and subophitic gabbronorite.

Gabbronorite (one sample from the Springvale intrusion) consists mainly of cumulus plagioclase (up to 1.5 mm), cumulus (up to 2.5 mm) or intercumulus (up to 1.5 mm) orthopyroxene, and relatively abundant intercumulus clinopyroxene (up to 1.5 mm). The orthopyroxene and clinopyroxene contain exsolution lamellae of clinopyroxene and inverted pigeonite, respectively. Trace intercumulus minerals are biotite, magnetite, chalcopyrite, and pyrite.

Olivine gabbronorite and olivine gabbro (samples from the Armanda, Keller Creek, McKenzie Spring,

Table 9.4. Petrography of samples used for this study.

Intrusion	*Sample number*	*Grid reference*	*Stratigraphic height (m)*	*Lithology*	*Alteration index*	*Mineralogy*
Armanda	92522493	374600-8010200	400	Olivine gabbronorite	7	Cumulus: plg (50%), ol (8%) Intercumulus: cpx (15%), opx (10%), ilm (tr) Corona (3%): opx, amph, sp Alteration: amph (14%), chl-mag (tr)
Big Ben	93522031	375838-8015723	N/D	Plagioclase peridotite	6	Cumulus: plg (20%), ol (10%) Intercumulus: opx (1%) Corona (1%): opx, amph, sp Alteration: amph (30%), plg (30%), sp (8%)
Dave Hill	93522114	397040-8078472	N/D	Troctolite	8	Cumulus: plg (60%), ol (20%) Intercumulus: opx (5%) Corona (8%): opx, amph, sp Alteration: amph (7%)
Keller Creek	94522089	390275-8086600	N/D	Olivine gabbro	7	Cumulus: plg (55%), ol (10%) Intercumulus: cpy (34%), po-ilm (tr) Corona (1%): opx, amph, sp
McKenzie Spring	94522022	383679-8065549	N/D	Olivine gabbro	7	Cumulus: plg (65%), ol (20%) Intercumulus: cpx (10%), po (tr) Corona (5%): opx, amph, sp Alteration: amph-biot-calc (tr)
McIntosh	92622273	383860-8035050	1100	Olivine gabbro	6	Cumulus: plg (60%), ol (15%) Intercumulus: cpx (10%), po (tr) Corona (5%): opx, amph, sp Alteration: amph (10%), calc (tr)
Sally Malay	93522066	396590-8082045	350	Troctolite	7	Cumulus: plg (66%), ol (22%) Intercumulus: ap (1%) Corona (6%): opx, amph, sp, biot Alteration: amph (4%), sp (1%)
Spring Creek	94522062	385527-8073550	2080	Olivine gabbronorite	7	Cumulus: plg (65%), ol (10%) Intercumulus: opx (15%), cpx (5%), ilm-po-pent (tr) Corona (tr): opx, amph, sp Alteration: amph (5%), biot (tr)
Springvale	92522439	361720-8031550	650	Gabbronorite	8	Cumulus: plg (50%), opx (25%) Intercumulus: cpx (20%), biot (1%), mag-py-cpy (tr) Alteration: ser (4%)
Springvale	92522446	354200-8034650	940	Olivine gabbronorite	7	Cumulus: plg (55%), ol (10%) Intercumulus: opx (20%), cpx (10%), ilm (2%), biot-mag (tr) Alteration: idd (3%)
Springvale	92522454	354390-8032050	50	Norite	6	Cumulus: plg (35%), opx (20%) Intercumulus: biot-ilm-mag (tr) Alteration: amph (30%), ser (10%), chl (5%)
Springvale	92522461	354000-8034300	840	Biotite olivine gabbronorite	8	Cumulus: plg (35%), ol (10%) Intercumulus: cpx (25%), opx (15%), biot (10%), ilm-po-cpy (tr) Alteration: amph (4%), idd (1%)
Springvale	92522475	353030-8036420	2020	Gabbronorite	9	Cumulus: plg (55%) Intercumulus: cpx (25%), opx (15%), mag-po-cpy-pent (tr) Alteration: amph (5%)
Toby	92522513	358400-8053130	1750[1]	Subophitic biotite quartz gabbronorite	7	Non-cumulate rock: plg (40%), cpx (15%), biot (15%), opx (5%), qtz (5%), ilm-mag-zir (tr) Alteration: amph (20%)

Table 9.4 (cont.). Petrography of samples used for this study.

Intrusion	*Sample number*	*Grid reference*	*Stratigraphic height (m)*	*Lithology*	*Alteration index*	*Mineralogy*
Toby	92522518	357600-8054700	3500[1]	Subophitic biotite quartz gabbronorite	7	Non-cumulate rock: plg (45%), cpx (30%), biot (10%) opx (5%), qtz (5%), ilm (3%), zir (tr) Alteration: amph (2%)
Toby	92522520	357650-8056450	5200[1]	Subophitic biotite gabbronorite	9	Non-cumulate rock: plg (50%), cpx (30%), opx (10%) ol (5%), biot (2%), mag (1%), ilm-po (tr) Alteration: idd (2%), chl (tr)
Toby	92522523	355700-8060200	9300[1]	Subophitic biotite gabbronorite	8	Non-cumulate rock: plg (40%), cpx (20%), opx (20%), biot (10%), ilm (3%), mag (1%) Alteration: amph (6%)
Toby	92522524	355280-8062150	11400[1]	Subophitic biotite quartz gabbronorite	8	Non-cumulate rock: plg (45%), cpx (25%), opx (10%), biot (10%), qtz (5%), mag (3%) Alteration: amph (2%)
Wilagee	92522502	361200-8052300	710	Olivine gabbronorite	8	Cumulus: plg (65%), ol (20%), opx (5%), chrom (tr) Intercumulus: cpx (10%), ilm-po (tr) Alteration: chl-ser (tr)
Wilagee	92522506	360450-8052900	70	Troctolite	8	Cumulus: ol (50%), chrom (tr) Intercumulus: plg (40%), mag-po-cpy (tr), Corona (tr): opx, sp Alteration: amph (7%), sp (2%), chl (1%)
Wilson Creek	93522126	394142-8077447	N/D	Olivine gabbronorite	7	Cumulus: plg (50%), ol (10%) Intercumulus: cpx (6%), opx (6%) Corona (3%): opx, amph, sp Alteration: amph (25%), sp (tr)

For the Panton intrusion, electron microprobe analyses of amphibole from Hamlyn (1977) have been used for geothermobarometry. amph = amphibole; ap = apatite; biot = biotite; calc = calcite; chl = chlorite; chrom = chromite; cpx = clinopyroxene; cpy = chalcopyrite; idd = iddingsite; ilm = ilmenite; mag = magnetite; musc = muscovite; ol = olivine; opx = orthopyroxene; pent = pentlandite; plg = plagioclase; py = pyrite; po = pyrrhotite; qtz = quartz; ser = sericite; sp = spinel; zir = zircon.
Alteration index is a semi-quantitative scale that ranks the intensity of alteration on a scale of 1 (most altered) to 10 (unaltered). N/D = not determined.

[1] Traverse distance.

McIntosh, Spring Creek, Springvale, Wilagee, and Wilson Creek intrusions; Table 9.4) generally contain cumulus olivine and plagioclase, and intercumulus clinopyroxene and orthopyroxene. Orthopyroxene (up to 2.3 mm) and chromite (up to 0.2 mm) are also cumulus in the Wilagee intrusion. Olivine has a wide range of size (0.5–4.2 mm) except in the Springvale and the Spring Creek intrusions (0.5–1.3 mm) and shows pronounced embayments. Plagioclase (up to 4.2 mm) is generally twinned, but in the Keller Creek intrusion it is small (0.1 mm), untwinned, and forms a recrystallised polygonal groundmass. The Keller Creek body has been tentatively classified as a group V intrusion on the basis of its basal Ni–Cu sulphide mineralisation, but the gabbroic rocks have similar recrystallised textural and mineralogical features to the Norton metagabbro, which is a granulite facies mafic body of the Tickalara Metamorphics. Intercumulus clinopyroxene is present in all samples (up to 4 mm, but mostly 1–2 mm; up to 33 vol. %); it shows exsolution lamellae in the sample from the Keller Creek intrusion and is often partly altered to amphibole. Intercumulus orthopyroxene (up to 2.5 mm) is restricted to the Spring Creek, Springvale, and Wilson Creek intrusions. Trace amounts of intercumulus ilmenite, pyrrhotite, magnetite, and chalcopyrite are present, and exsolution lamellae of pentlandite in pyrrhotite occur in the Spring Creek intrusion. Important textures in the olivine-bearing gabbroic rocks of this study are coronas around olivine in contact with plagioclase (described below).

Fine-grained subophitic gabbronorite is restricted to the Toby intrusion, where it is characterised by a large number of minor phases, indicating a highly evolved mafic rock of non-cumulus origin (see Chapter 5). Early crystallising major phases are plagioclase (up to 2.5 mm) and subordinate orthopyroxene (up to 0.5 mm); in one sample, olivine (up to 0.5 mm) is present. Clinopyroxene (up to 0.9 mm), biotite (up to 1.5 mm) and orthopyroxene (up to 1.4 mm) are generally late

crystallising minor phases, together with quartz, apatite, magnetite, ilmenite, pyrrhotite, and euhedral zircon up to 0.2 mm in size. Clinopyroxene displays exsolution lamellae of pigeonite and is affected by amphibole alteration.

Troctolite

Three troctolite samples from the Dave Hill, Sally Malay, and Wilagee intrusions were studied. Troctolites from the Dave Hill and Sally Malay intrusions have similar modal cumulus olivine (20–22 vol. %; 1–2 mm) and cumulus plagioclase (60–66 vol. %; 0.3–3 mm), and minor apatite for the latter troctolite. Most olivine grains are surrounded by coronas similar to those in olivine gabbronorite. However, olive green spinel in the Sally Malay sample forms large (up to 0.1 mm) anhedral grains hosted by amphibole, which occur with olivine and biotite in some coronas.

Troctolite from the group II Wilagee intrusion has abundant coarse-grained olivine (50 vol. %; up to 3 mm), less plagioclase (40 vol. %; up to 3 mm), chromite, and no apatite, indicating that it is more primitive than the troctolite from the group V Dave Hill and Sally Malay intrusions. Intercumulus magnetite, pyrrhotite, and chalcopyrite are very minor. Olivine is locally surrounded by a corona (see below for detailed discussion) and rarely by orthopyroxene alone.

Norite

The only norite sample studied was from the lowermost part of the Springvale intrusion. It consists of cumulus plagioclase and lesser orthopyroxene of similar size (0.25–2 mm), and rare intercumulus biotite, ilmenite, and magnetite. Orthopyroxene is partly replaced by amphibole, which, in turn, is replaced by chlorite, and plagioclase is replaced by white mica.

Plagioclase peridotite

The only plagioclase peridotite sample studied was from the Big Ben intrusion. It consists essentially of cumulus subhedral plagioclase (0.25–2 mm) and anhedral olivine (0.25–1 mm), and intercumulus orthopyroxene, which surrounds the olivine. There is extensive alteration to an amphibole–plagioclase–spinel assemblage. Amphibole and spinel tend to surround olivine and there is evidence that amphibole has pseudomorphed olivine. Spinel occurs as blue-green anhedra of unusually large size (up to 1 mm).

Corona textures

Corona textures occur around cumulus olivine where it is in contact with cogenetic plagioclase in olivine gabbronorite, troctolite, and plagioclase peridotite. On the basis of their morphology and mineralogy, the coronas have been subdivided into four types, which are interpreted as representing progressive stages (1–4) in the replacement of olivine.

Type 1 coronas (Fig. 9.2A) are restricted to troctolite of the group II Wilagee intrusion. Olivine is surrounded by thin (up to 0.03 mm) pale green symplectitic coronas or fringes, which are difficult to resolve optically into their components. The pale green colour of the coronas in plain polarised light suggests that they may consist of an intergrowth of amphibole and spinel. In a few places the thin coronas consist of only pure Ca-amphibole between the olivine and plagioclase grains. The coronas are continuous around the olivine grains except where an olivine grain abuts pyroxene and no reaction is observed. Type 1 coronas represent the least developed coronas, as the margins of the olivine host are generally not embayed and thin orthopyroxene shells on the olivine grains are rare.

Type 2 coronas (Figs 9.2B–F) are the most common type and are typical of gabbroic rocks from the group V Dave Hill and Sally Malay and group VI McIntosh and Armanda intrusions. These well-developed coronas consist of an inner thin shell (up to 0.02 mm) of orthopyroxene, surrounded by a green-brown amphibole zone grading outwards into a radiating symplectite zone of green amphibole and vermicular blue-green spinel rods (up to 0.3 mm long), and an outermost zone of a plagioclase–spinel symplectite of variable thickness. The orthopyroxene shell appears to be optically continuous around the partly embayed margins of the host olivine and, similarly, the inner amphibole zone is optically continuous with the surrounding symplectitic amphibole. Where the orthopyroxene shell is absent, its place is taken by tiny amphibole prisms displaying a radiating texture. The same feature is also present in the spinel of the symplectite zones, although this mineral also forms blue-green anhedral grains in plain polarised light.

Type 3 coronas characterise partially recrystallised gabbro from the group V Keller Creek intrusion. Olivine grains in contact with plagioclase have zones, 0.02–0.04 mm thick, of brown amphibole and, in some cases, an incipient symplectite of green amphibole and vermicular spinel. Coarse grains of deep green spinel are disseminated throughout the amphibole zones. Rarely, the olivine grains are surrounded by a very thin (up to 0.015 mm) orthopyroxene shell.

Type 4 coronas (Figs 9.2G–H) are restricted to plagioclase peridotite from the group I Big Ben intrusion. They generally consist of granular Ca-amphibole surrounding deeply embayed olivine, then a zone of blue-green spinel anhedra, which are mostly finer grained than the amphibole. There is also evidence that amphibole has pseudomorphed olivine. In some cases, a fine spotted appearance is imparted to the peridotite where olivine is completely replaced by amphibole and/or sub-circular concentrations of spinel anhedra. No orthopyroxene shell or outer symplectite is present in these most advanced coronas.

Mineral chemistry

Electron probe microanalyses were carried out on the cores and rims of cumulus minerals, intercumulus minerals, and corona minerals, including amphibole, biotite, clinopyroxene, ilmenite, olivine, orthopyroxene, plagioclase, and spinel, in samples from thirteen intrusions. Up to five representative samples were

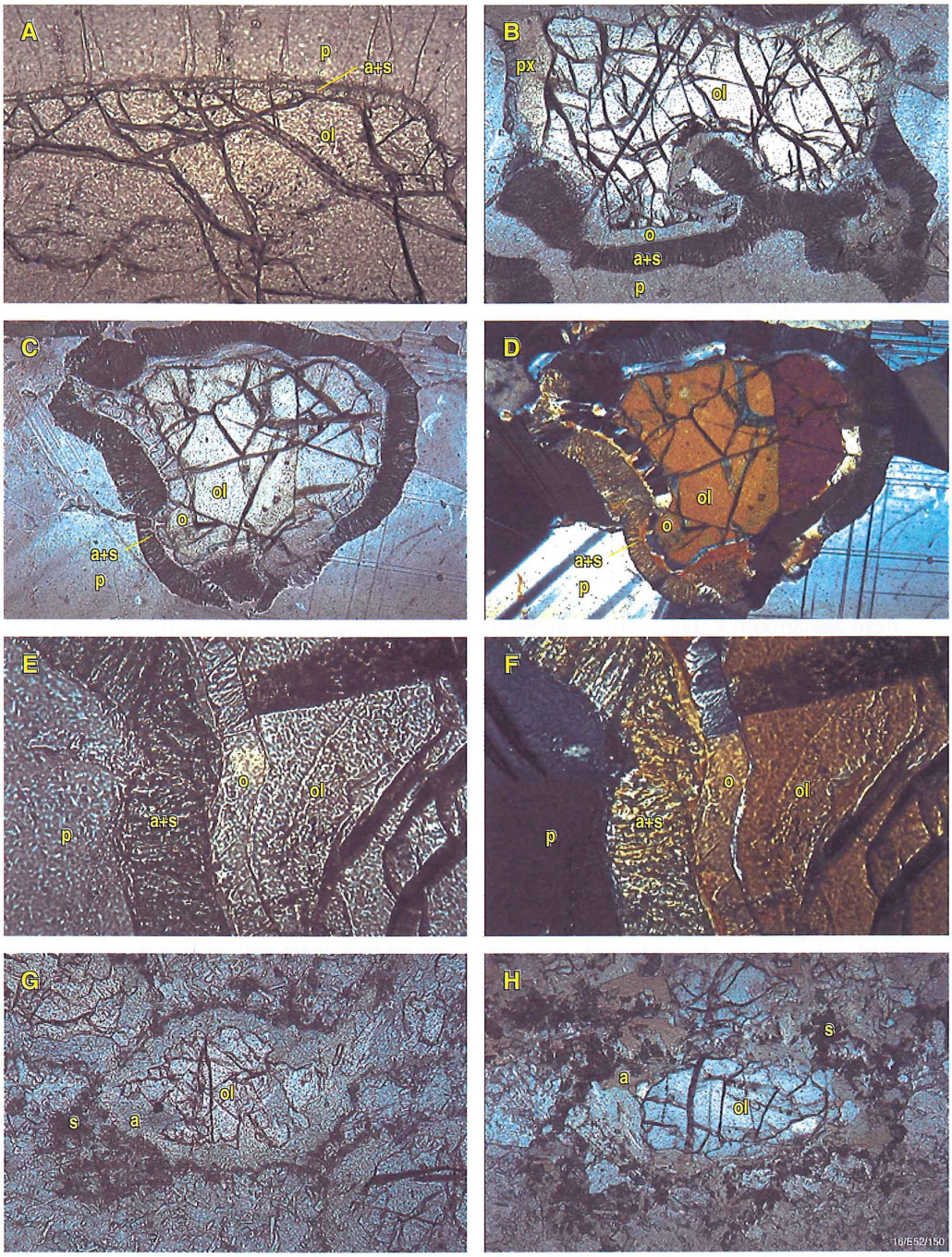


Figure 9.2. Photomicrographs of coronas surrounding cumulus olivine.

A. Type 1 corona: thin corona comprising intergrowth of Ca-amphibole and spinel (a+s) between olivine (ol) and plagioclase (p) (Wilagee intrusion, olivine gabbronorite, 92522502, plane-polarised light, width of view is 0.7 mm).

B. Type 2 corona: embayed olivine (ol) partly surrounded by inner shell of orthopyroxene (o) and a thicker radiating Ca-amphibole-spinel symplectite (a+s). Note that no corona is developed where the olivine abuts early crystallising pyroxene (px) rather than plagioclase (p) (Dave Hill intrusion, troctolite, 93522114, plane-polarised light, width of view is 1.3 mm).

C. Type 2 corona: embayed olivine (ol) surrounded by inner shell of orthopyroxene (o) and Ca-amphibole-spinel (a+s) symplectite abutting plagioclase (p) (Dave Hill intrusion, troctolite, 93522114, plane-polarised light, width of view is 1.3 mm).

D. Same as C, but crossed nicols.

E. Detail of type 2 corona: olivine (ol) surrounded by inner shell of orthopyroxene (o) and radiating Ca-amphibole-spinel symplectite (a+s) abutting plagioclase (p) (Dave Hill intrusion, troctolite, 93522114, plane-polarised light, width of view is 0.3 mm).

F. Same as E, but crossed nicols.

G and H. Type 4 corona: embayed olivine (ol) with zone of granular Ca-amphibole (a) and irregular halo of coarse blue-green spinel (s) grains. No orthopyroxene or amphibole-spinel symplectite is present (Big Ben intrusion, plagioclase peridotite, 93522031, plane-polarised light, width of view is 1.3 mm).

Table 9.5. Summary of chemical features of minerals analysed in this study.

Intrusion	*Olivine mg core*	*Olivine mg rim*	*Clinopyroxene mg core*	*Clinopyroxene mg rim*	*Orthopyroxene mg core*	*Orthopyroxene mg rim*	*Orthopyroxene mg corona*	*Plagioclase An core*	*Plagioclase An rim*
Armanda	67	66–67	75–80	75	N/P	N/P	72–74	76–80	75–82
Big Ben	70–71	70–71	N/P	N/P	75–76	N/D	75–76	93–100	89–95
Dave Hill	72	72–73	N/P	N/P	77	77	73–77	86	86–87
Keller Creek	40–42	40–41	66–69	66	N/P	N/P	57–58	75–80	N/D
McKenzie Spring	68–70	67–68	74–76	N/D	N/P	N/P	71–74	65–77	96–98
McIntosh	78–79	78–79	N/D	N/D	N/P	N/P	79–81	78–79	73–79
Sally Malay	77–78	78–79	N/P	N/P	N/P	N/P	80–81	90–97	88–92
Spring Creek	72–74	71–72	73–80	N/D	N/D	N/D	75–78	76–80	79–90
Springvale	61–63	60–65	N/P	N/P	66–76	65–74	N/P	53–81	57–82
Toby	52–55	N/D	65–73	68	49–63	62–64	N/P	48–86	45–73
Wilagee	79–84	80–83	82–91	82–85	82–83	82	N/P	79–87	80–83
Wilson Creek	61–64	62–63	N/D	N/D	68–71	N/D	N/P	67–73	66–72

mg = 100 x Mg(Mg + Fe^{2+}); An = 100 x Ca(Ca + Na + K); N/D = not determined, N/P = not present.

For the Panton intrusion, electron microprobe analyses of amphibole from Hamlyn (1977) have been used for geothermobarometry.

selected from each intrusion. A summary of the mineral compositions is presented in Table 9.5 and all compositional data are included in the tables of Appendix 3. Data from Table 9.5 are incorporated into Table 9.6, which is a compilation of mineral compositions derived from this and other studies of the East Kimberley intrusions.

Amphibole

Amphibole occurs as an alteration product replacing pyroxene and in coronas surrounding olivine (described above) in most intrusions investigated. Most of the analysed amphiboles are calcic varieties (hornblende and tschermakite) and homogeneous in composition; a notable exception is the variation in Al content (0.4–2.6 atoms per formula unit—afu) in the coronas of the Armanda intrusion. Fe–Mg-rich amphibole (cummingtonite) is present in the Springvale norite and coexists with calcic amphibole in coronas in olivine gabbronorite of the group V Spring Creek intrusion.

Biotite

Late-crystallising euhedral biotite occurs in the Springvale and Toby intrusions, and also forms fibrous fringes in the olivine coronas of the group V Sally Malay intrusion. The contrasting mg numbers (abbreviated to mg; see Appendix 3 for the definitions of mg for the different minerals) for biotite in the Springvale (55–73) and Toby (49–57) samples highlight the different fractionation levels of these two intrusions.

Clinopyroxene

Clinopyroxene occurs in seven intrusions as an intercumulus mineral. Figure 9.3A shows the variation of clinopyroxene composition on a Ca–Fe–Mg diagram. The mg ranges from 65 to 91 (Table 9.5), with the highest mg (82–91) being in the Wilagee intrusion, supporting the interpretation that this body may be an uplifted, more primitive part of the Toby intrusion. The Toby intrusion has evolved mg (65–73) compositions, overlapping with those of the Keller Creek intrusion (66–69).

Ilmenite

Ilmenite, common as an intercumulus mineral, is close to its ideal formula in composition, with only minor substitutions of Mg (up to 0.094 afu) and Mn (up to 0.033 afu.) for Fe.

Olivine

Olivine is present in all samples except most of those from the Springvale and Toby intrusions; its mg ranges from 40 to 84, with the Keller Creek (40–42) and Toby (52–55) intrusions having the lowest values, and the Wilagee (79–84), McIntosh (78–79), and Sally Malay (77–79) intrusions having the highest (most primitive values). All grains analysed were unzoned. Most of the analyses show a slight cationic deficiency in the M_2 and Si sites, probably owing to the presence of ferric iron (Gaite & Hafner 1984). Therefore, the structural formulae shown in the tables of Appendix 3 were calculated to include ferric iron.

Orthopyroxene

Orthopyroxene, present as unzoned cumulus, intercumulus, and corona phases, has mg ranging from 49 to 83. It occurs both as an intercumulus phase and in coronas, with essentially the same compositions in the Big Ben and Dave Hill intrusions. Figure 9.4A shows there is direct correlation between the mg of olivine and orthopyroxene in an adjacent corona.

Plagioclase

Cumulus plagioclase is ubiquitous and generally very calcic ($An_{75–100}$) in most intrusions, but is more evolved ($An_{45–75}$) in the Toby, Keller Creek, Springvale, and Wilson Creek intrusions. It is one of the few minerals that displays compositional zoning. This is evident in plagioclase in the McKenzie Spring and Spring Creek intrusions which has anorthite contents of 65-77 (cores)

Table 9.6. Summary of mineral compositions for layered intrusions in the East Kimberley.

	Intrusion	*Olivine (mg)*	*Clinopyroxene (mg)*	*Orthopyroxene (mg)*	*Plagioclase (An)*	*Reference*
Group I	Panton	81–85[1] 84–91[2]	89	85	83–100	Hamlyn (1977)
	Big Ben	70–71	–	75–76	89–100	This study
Group II	Springvale	63–82	–	–	80–82	Geopeko (1986–1989)
		61–65	–	65–76	53–82	This study
	Wilagee	79–84	82–91	82–83	79–87	This study
Group III	Toby	59–63	–	54–74	55–83	Geopeko (1986–1990)
		52–55	65–73	49–64	45–86	This study
Group V	Sally Malay	69–82	–	–	–	Thornett (1981)
		77–79	–	–	88–97	This study
	Dave Hill	72–73	–	77	86–87	This study
	Spring Creek	71–74	73–80	–	76–90	This study
	McKenzie Spring	67–70	–	–	65–77, 96–98	This study
	Wilson Creek	61–64	–	68–71	66–73	This study
	Keller Creek	40–42	66–69	–	75–80	This study
Group VI	McIntosh	56–79	64–82	52–80	51–83	Mathison & Hamlyn (1987)
		78–79	–	–	73–79	This study
	Armanda	66–67	75–80	–	75–82	This study
Other intrusions:	Salt Lick Creek	81–84	85–88	80–85	84–88	Wilkinson et al. (1975)

mg of olivine = 100 x Mg/(Mg + Fe^{2+}); mg of clinopyroxene = 100 x Mg/(Mg + Fe^{2+}); mg of orthopyroxene = 100 x Mg/(Mg + Fe^{2+}); An of plagioclase = 100 x Ca/(Ca + Na + K). Some mg numbers have minor variations in ratios (e.g. inclusion of Mn). [1] = chromite-poor olivine cumulates, [2] = chromite-rich olivine cumulates.

and 96–98 (rims) in the former, and 76–80 (cores) and 79–90 (rims) in the latter. Gabbros from the Springvale, Toby, and Wilagee intrusions also have zoned plagioclase. Plagioclase shows the most calcic compositions (An_{93-100}) in the Big Ben intrusion, which is a similar anorthite content to that documented for the Panton intrusion (An_{83-100}) by Hamlyn (1977, 1980). The very calcic composition of plagioclase in both intrusions is believed to have resulted from the partial re-equilibration of plagioclase with adjacent hornblende during amphibolite facies metamorphism (Hamlyn 1980). These unusually high calcic compositions support the suggestion that the Panton and Big Ben intrusions were once part of the same body (see Chapter 5).

Spinel

Three major types of spinel were investigated during this study: cumulus chromite (sensu stricto) grains (see Chapter 13), hercynite in coronas, and magnetite in coronas and as disseminated grains. A minor occurrence of exsolved ulvöspinel in ilmenite in the Springvale intrusion was also analysed. The spinels in the coronas are hercynite and spinel (sensu stricto), with Mg/(Fe^{2+}+Mg) ratios of 45–65.

Figure 9.3B shows the compositional variability of hercynite on an Mg–Fe^{3+}–(Fe^{2+} + Mn) plot. There is a large range of the Mg/(Fe^{2+} + Mn) ratio, with hercynite from the Armanda and Wilson Creek intrusions being the richest in iron, and that from the Wilagee intrusion being the richest in magnesium.

Disseminated magnetite analysed from the Toby and Springvale intrusions contains up to 2.2% V_2O_3 and 0.77% V_2O_3, respectively.

Origin of coronas and geothermobarometry

Corona textures around olivine have been reported in gabbroic rock from many parts of the world (see Joesten 1986a,b, Mongkoltip & Ashworth 1983, Griffin et al. 1985 and references therein, Ballhaus & Berry 1991, Acquafredda et al. 1992, etc). Since this study is focused on the geobarometry of layered intrusions, complex aspects of corona formation (e.g. diffusion models proposed by Grant 1988 and Johnson & Carlson 1990) are not considered here.

Corona textures in the East Kimberley intrusions were first described by Gemuts (1971), and later by Hamlyn (1977, 1980) and Mathison & Hamlyn (1987). These authors described orthopyroxene, green amphibole, spinel, and opaque minerals surrounding olivine in gabbroic rocks from the Armanda and McIntosh intrusions. This study has shown that the coronas and

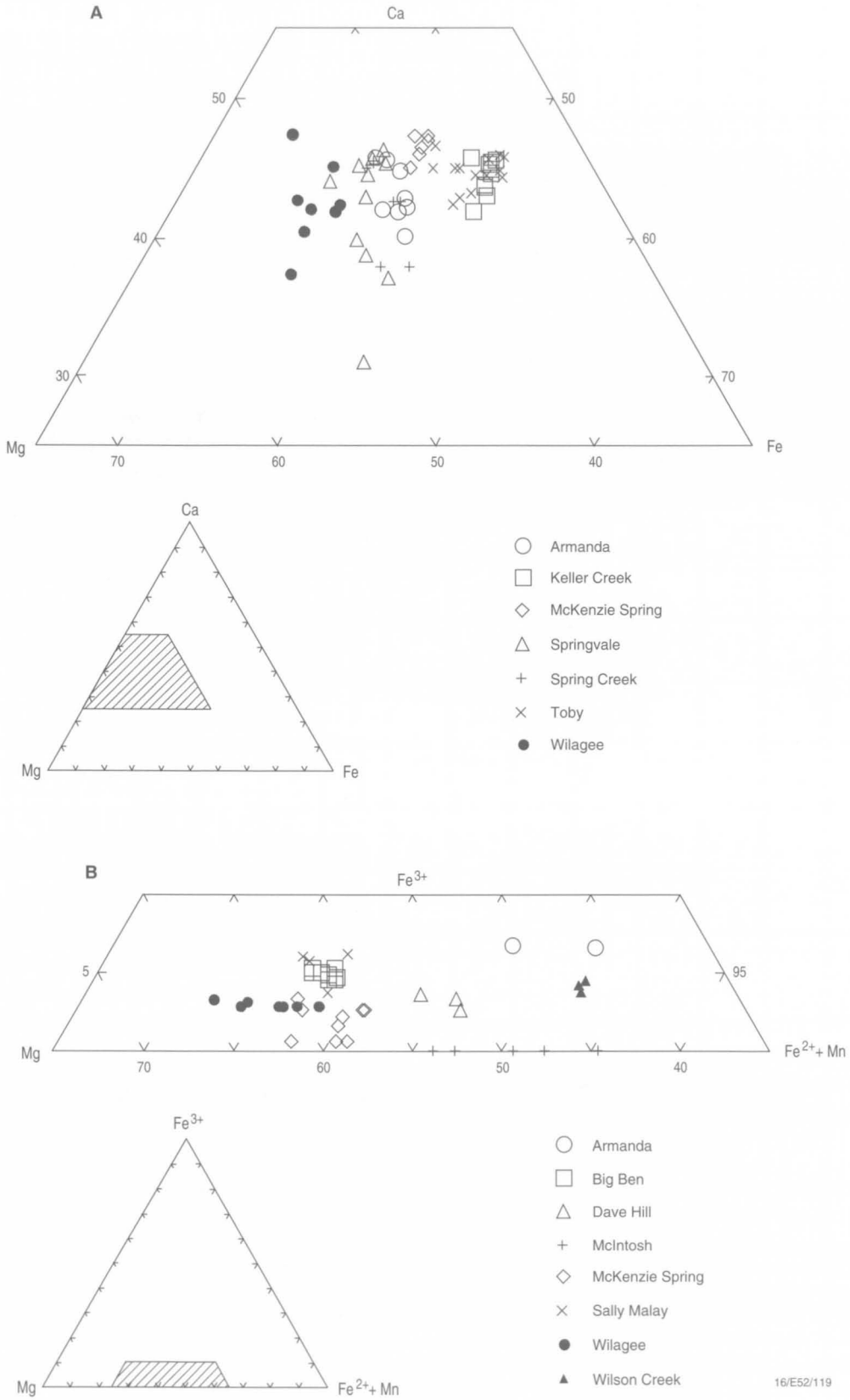


Figure 9.3. Variations of clinopyroxene and spinel compositions for the East Kimberley mafic–ultramafic intrusions.

A. Variation of Mg–Ca–Fe components for cumulus and intercumulus clinopyroxene.

B. Variation of Mg–Fe^{3+}–(Fe^{2+} + Mn) components for spinel in coronas surrounding cumulus olivine.

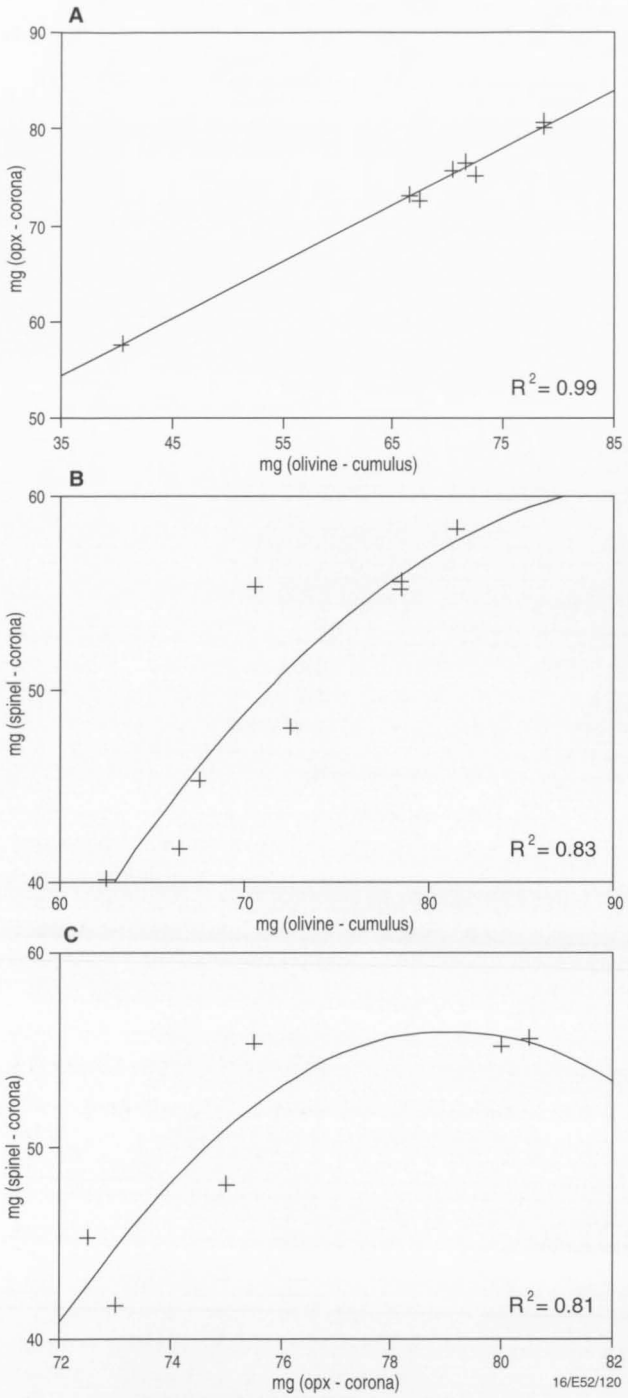


Figure 9.4. Relationships of mg in olivine and associated corona minerals. R^2 is the correlation coefficient for line of best fit (Hoel 1971).

A. Cumulus olivine versus corona orthopyroxene.
B. Cumulus olivine versus corona spinel.
C. Corona orthopyroxene versus corona spinel.

associated symplectites are much more widespread, being found in most mafic intrusions in a wide range of plagioclase-bearing rock types, especially leucogabbro, olivine gabbronorite, troctolite, anorthosite, and plagioclase-peridotite.

A late magmatic, rather than a metamorphic, origin is favoured for the East Kimberley coronas because: (1) both intercumulus orthopyroxene and corona orthopyroxene have the same mg, and there is a direct correlation between the mg of primary magmatic olivine and orthopyroxene in the adjacent corona (Fig. 9.4A). Weaker relationships also exist for the other mineral components of coronas (Figs 9.4B–C); (2) there is an apparent correlation between the type of corona and the different groups of intrusions, indicating a local compositional or depth of emplacement control rather than a regional metamorphic (amphibolite or granulite facies) control; and (3), the textures of the coronas closely resemble those of magmatic coronas described in intrusions elsewhere (Joesten 1986a,b; Acquafredda et al. 1992). Although coronas are disequilibrium textures, we think that amphiboles associated with them can be used for amphibole geothermobarometry, because the techniques used in this paper (Ti content in amphibole—Otten 1984, for temperatures; Al content in amphibole—Hammarstrom & Zen 1986 and Anderson & Smith 1995, for pressures) do not require cationic exchange between minerals, and the coronas and amphiboles are believed to represent the last phase of the magmatic event.

Otten (1984) requires that rock types suitable for Ti amphibole geothermometry have:

i) excess ilmenite to indicate Ti saturation of the magmas, and

ii) oxygen fugacity conditions falling near the fayalite–magnetite–quartz (FMQ) buffer.

In our study we have observed ilmenite in the oxide assemblages of fractionated mafic rocks. Haggerty (1976) has documented that the FMQ buffer falls within the centre of the field containing intrusions emplaced at about 5 kb pressure (similar to the East Kimberley and west Pilbara intrusions: Hoatson et al. 1992). Temperatures determined from the Ti content of the amphiboles in coronas (Otten 1984) of the East Kimberley gabbroic rocks range from 665 to 800°C, similar to the late magmatic to subsolidus temperatures (580–880°C) documented by Acquafredda et al. (1992) for amphibole in the gabbroic rocks of the Sila Massif, Italy. On the basis of exsolution features in pyroxenes, paragenesis of cumulus assemblages, and similarities with other tholeiitic mafic intrusions emplaced in the upper to middle crust (Hoatson et al. 1992), the liquidus temperatures for the mafic magmas that formed the East Kimberley intrusions are believed to be in the range 1050–1250°C. These temperatures are consistent with Thornett's (1981) average crystallisation temperatures obtained for two-pyroxene geothermometry of peridotites near the base of the Sally Malay intrusion (1175°C and 1146°C), Mathison & Hamlyn's (1987) estimation from pyroxene compositions for the McIntosh intrusion (1090–1200°C), and magmatic temperatures (1000–1124°C) for chromite from the Lamboo intrusion (see Chapter 13).

Calculated crystallisation pressures determined in this study from the Al content of the amphiboles in coronas (Anderson & Smith 1995) range from 2.4 to 6.7±0.6 kb (Table 9.7), which equate to upper–middle crustal depths of around 8–23 km, assuming a gradient of 3.5 km/kb for 'normal' continental crust. The pressures are generally consistent within each group of intrusions, but

Table 9.7. Estimated crystallisation pressures for the major layered intrusions in the East Kimberley.

	Intrusion U–Pb zircon age	*Thickness (km)*	*Pressure (kb)*	*Approximate depth of crystallisation (km)*
Group I	Panton 1856±2 Ma	1.6	3.2±0.6	11
	Big Ben	2	3.1±0.6	11
Group II	Springvale 1857±2 Ma	2	5.1±0.6	18
	Wilagee	1.3	2.8±0.6	10
Group III	Toby 1855±2 Ma	?2	2.4±0.6	8
Group V	Sally Malay 1844±3 Ma	1.7	6.3±0.6	22
	Dave Hill	0.8	5.6±0.6	20
	Keller Creek	0.3	6.0±0.6	21
	McKenzie Spring	?1	6.7±0.6	23
	Spring Creek	2.5	5.7±0.6?	20?
	Wilson Creek	?2	6.4±0.6	22
Group VI	McIntosh 1830±3 Ma	7.8	5.0±0.6	18
	Armanda	0.7	2.8±0.6	10

Estimated pressures were determined on the Al content of amphibole in coronas, using the geobarometer of Anderson & Smith (1995). Equivalent depths of crystallisation assumed a gradient of 3.5 km/kb for 'normal' continental crust.

differ between the groups. For example, the Cr–platinum-group elements (PGEs)–Ni–Cu-bearing Panton and Big Ben intrusions of group I have pressures of 3.2 and 3.1 kb, respectively. This is significantly lower than the 8–9 kb (~30 km) suggested for the Panton intrusion by Hamlyn (1980). A lower pressure of 2.4 kb for the group III Toby intrusion is consistent with the fine-grained subophitic texture and evolved mineralogy (apatite–biotite–magnetite–ilmenite–quartz–zircon) of the gabbros in this body. The adjacent Wilagee intrusion has a similar low crystallisation pressure of 2.8 kb, the difference in pressure between the two intrusions (~0.4 kb = 1.4 km) being approximately equal to the thickness of the Toby intrusion (2 km). A possible implication is that the southern fault-bounded part of the Wilagee intrusion represents an uplifted more primitive basal part of the Toby intrusion. This is supported by the similar trace-element geochemistry and Nd isotopes of both intrusions (see Chapter 11). If this hypothesis is correct, the Wilagee intrusion should be reclassified as a group III intrusion rather than a group II intrusion. The Springvale intrusion was emplaced at a depth of about 18 km at 1857±2 Ma, at about the same time, but 10 km deeper than the Toby intrusion, 14 km to the north. That these coeval intrusions are exposed on the present land surface, despite crystallising at very different depths, might indicate that tilting or differential uplift occurred after their emplacement, possibly during the Halls Creek Orogeny (Blake 1997, see Chapter 3). The Ni–Cu–Co-bearing intrusions of group V cluster at the upper end of the pressure spectrum at 5.7–6.7 kb, consistent with Joesten's (1986a,b) observations that well-developed coronas, such as that found in the group V intrusions, form at pressures greater than 5 kb. The different pressures for the McIntosh (5 kb) and Armanda (2.8 kb) intrusions of group VI can be explained if the Armanda intrusion correlates with the upper part of the McIntosh intrusion, as the McIntosh sample is from near the base of a 7.8 km thick body, whereas the Armanda sample is from the middle of a 0.7 km thick body.

Warren (AGSO, pers. comm. 1995) has estimated emplacement pressures for the Sally Malay, McIntosh, and Springvale intrusions from high-temperature assemblages in contact metamorphic rocks. Using Fe/Mg partitioning between coexisting garnet and cordierite in metapelites adjacent to the Sally Malay and McIntosh intrusions and the stability of cordierite in a metasomatised raft in the Springvale intrusion, pressures of 4–5 kb for Sally Malay, 5–6 kb for McIntosh, and about 4 kb for Springvale were obtained (Table 9.2). These pressures are the same (McIntosh) or about 0.5–1 kb lower (Sally Malay, Springvale) than the findings of this study.

Relationships between intrusions and country rock migmatites

Migmatites in the central zone of the HCO (see Chapter 3) are predominantly pelitic and quartzofeldspathic metasedimentary rocks of the Tickalara Metamorphics that show complexly folded banding and abundant leucosomes, indicative of partial melting. In McINTOSH[1], migmatites are locally developed (for distances of up to ~100 m) adjacent to the larger layered intrusions, such as the Panton and McIntosh bodies. With distance away from these intrusions the migmatites merge into hornfelses, which in turn grade into lower grade rocks, supporting the suggestion of Gemuts (1971) and Blake (in Blake & Hoatson 1993) that some migmatites in the central zone formed by contact metamorphism during the emplacement of the intrusions.

The presence of chilled and contaminated margins, comagmatic satellite intrusions, and narrow (100 m) contact aureoles indicates that most of the East Kimberley intrusions crystallised in situ (Hoatson & Tyler 1993). Blake (1997) has noted that the in-situ

[1] 1:100 000 sheet names throughout this *Bulletin* are in capital letters to avoid confusion with identical place names and to distinguish them from 1:250 000 sheet names.

crystallisation of the intrusions implies that the adjacent country rocks and coeval granitic plutons were at the same depth as the layered intrusions during emplacement. As the country rocks and granites were already very hot (~350–1100°C), only a small amount of extra heat from intruding mafic–ultramafic magma could have caused widespread melting of the country rocks. However, north of the Ord River in TURKEY CREEK and MOUNT REMARKABLE, migmatites are widely developed over tens of kilometres and are one of the most common country rocks to the mafic bodies of group V and the Corridor gabbro. Since these extensive migmatites are not spatially restricted to the margins of these intrusions and there appears to be an antipathetic relationship between the volume of migmatite and mafic material (at least for that exposed on the surface) towards the northeast of the HCO, we believe that most of these areally extensive migmatites have formed from regional metamorphic and/or anatectic melting events in the deeper parts of the crust (as implied by the group V intrusions emplaced at 20–23 km depth) rather than from contact metamorphism related to emplacement of the mafic intrusions. This is consistent with Thornett's (1981) finding for the 1845 Ma Sally Malay intrusion that, on the basis of phase changes at the migmatite contact and two-pyroxene thermometry on the intrusive rocks, the emplacement of the Sally Malay intrusion postdated the thermal peak of regional metamorphism. It is also supported by the massive sulphides near the basal contact of this intrusion, which show little indication of recrystallisation and are coarse grained (see Chapters 5 & 12). However, Bordorkos et al. (1998) have used U–Pb zircon ages of migmatites in the Ord River region to show that peak metamorphism occurred at 1845±3 Ma, the same age as the nearby Sally Malay intrusion.

Stratigraphic variations in mineral chemistry

A preliminary study of the variations in mineral chemistry across layering was carried out in the Toby, Springvale, and Wilagee intrusions. In the Toby intrusion, however, outcrop is poor, and the true thickness of the stratigraphy could not be measured. Since only a few samples were analysed in this study, only gross compositional variations can be documented. Further mineralogical studies, involving more samples, are required to determine the large and complex compositional variations that may be expected in these intrusions.

The variation in mg for the main mafic minerals of the Wilagee and Toby intrusions is shown in Figure 9.5A. Cumulates from the Wilagee intrusion show relatively high mg (>78), indicating fairly primitive compositions, whereas the subophitic rocks from the Toby intrusion are more evolved (mg 50–70), as is also reflected by the greater abundance of biotite–quartz–zircon–apatite assemblages in this intrusion. The lowermost two samples along the SE–NW sample traverse across the Toby intrusion (below arrow in Fig. 9.5A) have considerably lower mg, i.e. more evolved compositions, than those for the overlying two samples, suggesting that

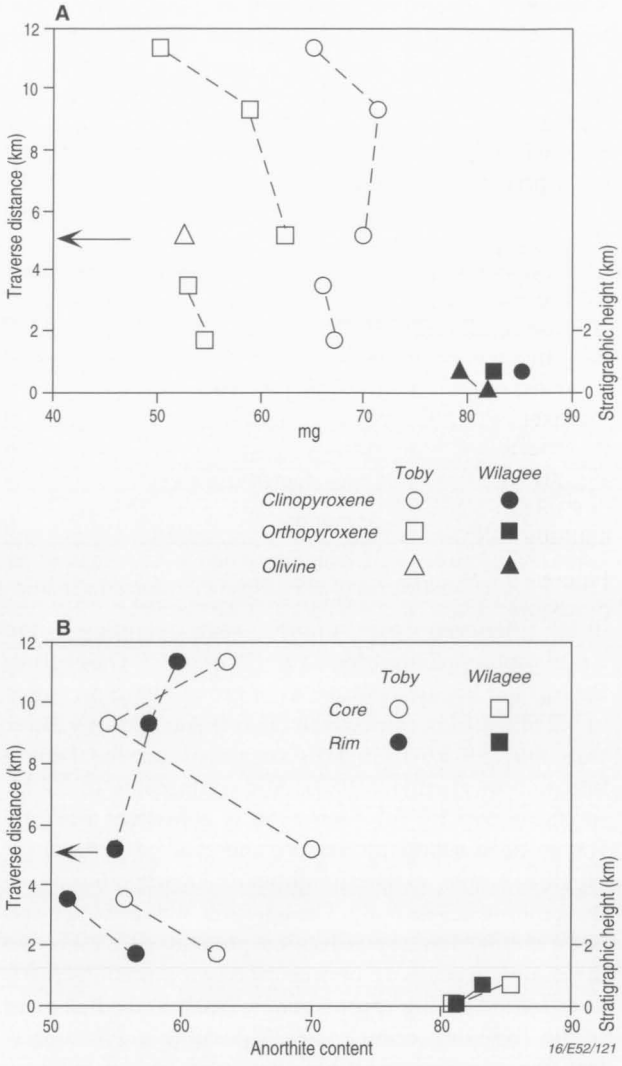


Figure 9.5. Variation of mineral chemistry for the Toby and Wilagee intrusions.

A. mg of clinopyroxene, orthopyroxene, and olivine.

B. Anorthite content of plagioclase.

In both diagrams the stratigraphic height for the Wilagee intrusion is shown on the right vertical axis and, since the true thickness of the stratigraphy could not be measured for the Toby intrusion, owing to poor outcrop, a traverse distance is used on the left vertical axis for this intrusion. The approximate position of a west-northwest-trending fault near the centre of the Toby intrusion is indicated by the arrow.

either the northern part of the intrusion represents a new primitive pulse of magma or a substantial vertical movement has taken place along a major west-northwest-trending fault cutting across the centre of the intrusion, exposing a lower part of the stratigraphy on the northern side. Large-scale concentric lineaments, which are continuous over much of the Toby intrusion (see Chapter 5), suggest it is unlikely that the northern part of this intrusion formed from a new pulse of magma. The latter interpretation agrees with the results of recent geological mapping of the area (Tyler et al. 1997), which indicate a sub-parallel series of west-northwest-trending faults across the centre of a shallowly dipping mafic body.

The variation in anorthite content of plagioclase, in the same samples as in Figure 9.5A, is shown in Figure 9.5B. The results for the Wilagee and the Toby intrusions are generally consistent with the mafic mineral data in Figure 9.5A, i.e. the high anorthite content of plagioclase from the Wilagee intrusion (>An_{80}) indicates more primitive crystallisation conditions than those for the Toby intrusion (<An_{70}). As with the mafic minerals (Fig. 9.5A), the anorthite content of both cores and rims of plagioclase in the lower part of the Toby intrusion (below the arrow in Fig. 9.5B) shows a trend to more evolved compositions, but these are reset to more primitive compositions near the 5 km traverse distance (near the arrow in Fig. 9.5B). In the upper part of the intrusion, the plagioclase rims show different trends to the mafic minerals (Fig. 9.5A), since they become slightly more calcic with traverse distance, owing to possible re-equilibration of the plagioclase margins with abutting calcic minerals, such as amphibole.

Figures 9.6A and 9.6B show the variations of mg of pyroxene and olivine and anorthite content of plagioclase with stratigraphic height for the Springvale intrusion. The overall patterns of the two plots are similar, but complex; most of the data fall approximately between those of the Wilagee and Toby intrusions (Figs 9.5A,B). The mineral chemistry patterns of the lower part, where the samples near the basal contact tend to be more evolved than those immediately above, are a feature often seen in layered intrusions (Hoatson et al. 1992). A likely reason for this reverse fractionation trend is contamination of the magma from the country rocks. Higher up the stratigraphy, the magmatic differentiation trend resumes its normal pattern towards lower mg and anorthite content. Although there are no data for the poorly exposed 1–2 km stratigraphic interval, there is an indication of a relatively less differentiated magma with higher mg and anorthite contents towards the top of the intrusion, possibly due to a new pulse or pulses of magma being emplaced into the upper parts of the chamber. This part of the intrusion equates with the cyclic troctolite, anorthosite, and olivine gabbro units that overly the more homogenous gabbroic rocks in the lower part of the intrusion. The Springvale intrusion appears to be a good example of a magma chamber changing from a largely closed system to a more open system with time.

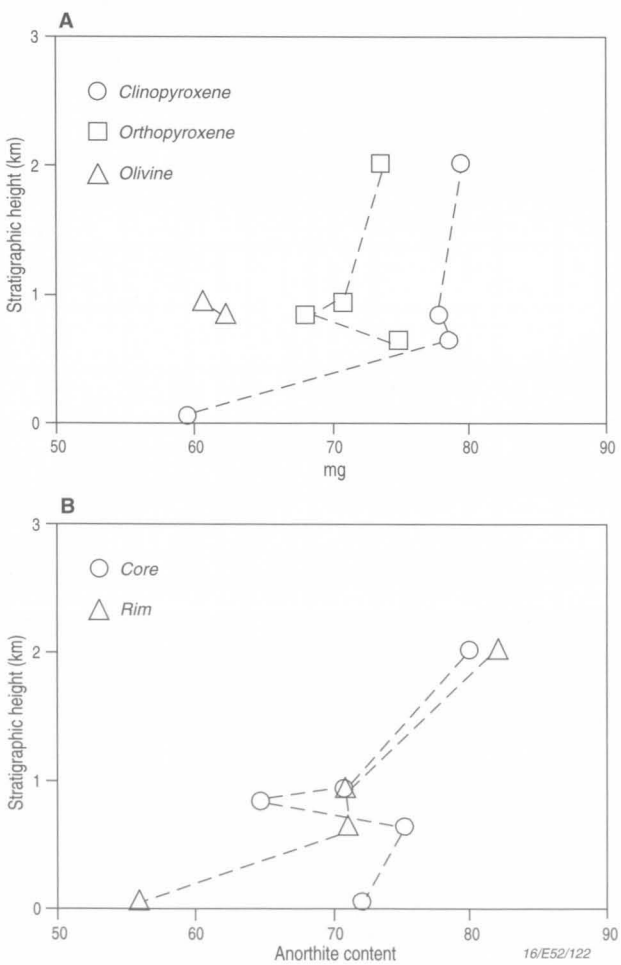


Figure 9.6. Variations of mineral chemistry versus stratigraphic height for the Springvale intrusion.

A. mg of clinopyroxene, orthopyroxene, and olivine.

B. Anorthite content of plagioclase (core and rim compositions).

Some regional implications and conclusions

The geobarometric results of this study provide better controls on the distribution of the mineralised layered intrusions and have important implications for the geological evolution of the East Kimberley.

1. Calculated crystallisation pressures of the East Kimberley intrusions, determined in this study from the Al content of the amphiboles in coronas, range from 2.4 to 6.7±0.6 kb, which equate to upper–middle crustal depths of around 8–23 km, assuming a gradient of 3.5 km/kb for 'normal' continental crust. These findings are generally similar to pressures reported for individual intrusions by Warren (pers. comm. 1995) and Thornett (1981).
2. Estimated crystallisation pressures and, hence, emplacement depths, for the layered intrusions generally increase from <5.5 kb in the southwest to >5.5 kb in the northeast of the study area (Fig. 9.7). Exposed deeper crustal levels (i.e. deeper erosional levels) northeastwards along the central zone of the Halls Creek Orogen (HCO: see Chapter 3) are consistent with the increase in metamorphic grade of the country rocks (mainly Tickalara Metamorphics) from greenschist to amphibolite to granulite facies and the increased development of migmatites. The deepening crustal levels to the northeast imply a regional differential uplift before ~1800 Ma (age of Kimberley Group: see Chapter 3) in the central zone of the HCO. Interestingly, the regional trend for the western zone appears to be the opposite of the central zone, with exposure levels for ~1855 Ma mafic and felsic rocks decreasing towards the northeast, i.e. 18 km for the Springvale intrusion, through 8 km for the Toby intrusion, to the subvolcanic Greenvale

Porphyry, and the extrusive Whitewater Volcanics further to the northeast. In this respect, the western zone appears to have had a different history of uplift compared to the central zone.

3. The presence of chilled and contaminated margins, comagmatic satellite intrusions, narrow (100 m) contact aureoles (Hoatson & Tyler 1993), and the relationship between individual intrusions in each group and their depth of emplacement (e.g. all group I intrusions emplaced at 11 km, group II at 10–18 km, group V at 20–23 km, and group VI at 10–18 km) indicate that most of the East Kimberley layered intrusions crystallised in situ and are not tectonically emplaced segments of larger bodies, as suggested by Hancock & Rutland (1984). This downgrades the potential for large-tonnage stratabound PGE deposits in the HCO, since economic deposits of this type elsewhere typically occur in large layered intrusions and the mineralised layers extend for great distances (hundreds of kilometres for the UG-2 Chromitite and Merensky Reef in the Bushveld Complex).
4. The temporal relationship of the intrusions to the migmatites in the central zone of the HCO indicates that the migmatites formed from both contact and regional metamorphic processes. However, the latter process was probably more important for the formation of the laterally extensive migmatites north of the Ord River in TURKEY CREEK and MOUNT REMARKABLE.

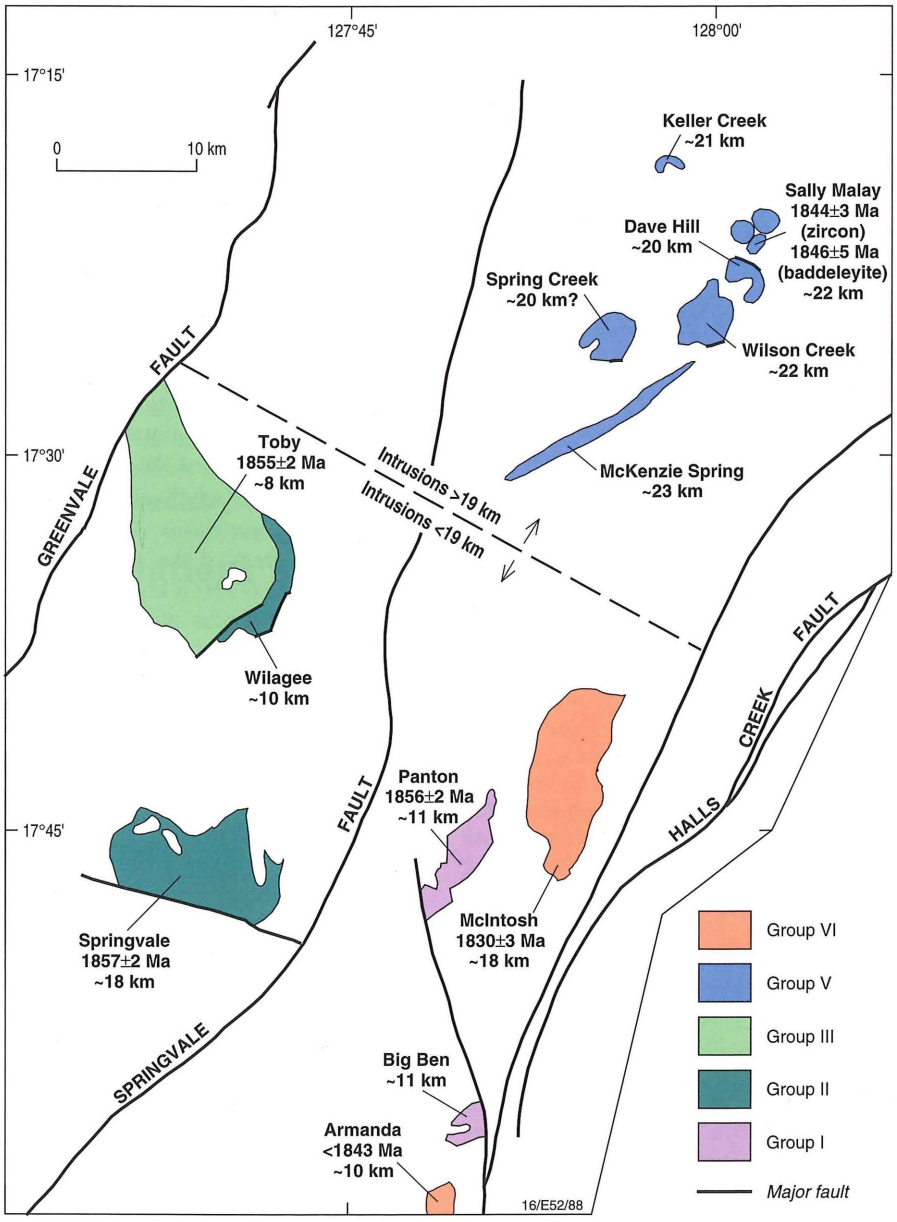


Figure 9.7. Calculated emplacement depths for the 13 layered mafic–ultramafic intrusions studied. The end of the pointer for each intrusion indicates the approximate location of the sample or samples.

5. A preliminary study of the variations in mineral chemistry across three mafic intrusions indicates that the Toby intrusion is significantly more evolved than the Springvale and Wilagee intrusions. Cryptic variation in the Springvale and Wilagee intrusions suggests that open fractionation systems, involving regular new pulses of magma into the chambers, generally prevailed over closed systems. More primitive mineral compositions in the Wilagee intrusion are consistent with the proposal in Chapters 5 and 11 that it may represent an uplifted basal part of the adjacent Toby intrusion.
6. The Ni–Cu–Co-bearing group V intrusions (e.g. Sally Malay) were emplaced at deeper crustal levels (20–23 km) than the Cr–PGE–Ni–Cu-bearing intrusions of group I (11 km: Panton). Thus, the depth of emplacement may be an important exploration guide for determining the Ni–Cu–Co or Cr–PGE–Ni–Cu prospectivity of layered intrusions in the East Kimberley.
7. The major mineralised intrusions of the world (Bushveld, Stillwater) were emplaced at fairly moderate pressures in the crust (<5 kb), indicating a possible correlation between mineralisation and depth of emplacement. This is consistent with the mineralised intrusions in the East Kimberley, which were emplaced at pressures of less than ~6 kb.
8. The similarity in emplacement depth, rock types, mineralogy, and mineralisation of the group I Panton and Big Ben intrusions supports the suggestion of Hoatson (1993) that the two bodies are part of the same intrusion, the Big Ben part being displaced sinistrally 15 km south along the Panton Fault relative to the Panton part. Strike-slip faulting has significantly disrupted the original distribution of other layered intrusions in the central zone, in particular the group I intrusions. The Greenvale Fault, which separates the 1855±2 Ma Toby intrusion (emplaced at 8 km depth) of the western zone from coeval felsic volcanics of the Whitewater Volcanics, may have had a vertical displacement of 8 km, upthrown to the east, accounting for why no Whitewater Volcanics are preserved east of the fault on McINTOSH and MOUNT REMARKABLE (Blake 1997).
9. The two parallel metallogenic corridors (Fig. 9.1) each contain mineralised intrusions that have similar depths of emplacement. The more northwestern Ni–Cu–Co-PGEs±Cr corridor contains the mineralised group II (18 km) and V (20–23 km) intrusions, whereas the Cr–PGEs–Ni–Cu±Au corridor to the southeast is represented by the mineralised group I (11 km) intrusions. These corridors appear to contain distinctive suites of mafic and mafic–ultramafic intrusions that were emplaced at different crustal levels between 1860 Ma and 1840 Ma. The petrogenetic significance of the two corridors is discussed by Hoatson in Chapter 5. The mineralised corridors will help focus future exploration programs for different styles of base-metal and precious-metal mineralisation and define prospective intrusions in areas that have little or no outcrop in the HCO.

Acknowledgements

The authors would like to thank David Blake, Morrie Duggan, John Sheraton, Alastair Stewart (all AGSO), Alan Butcher (CSIRO), Kurt Stuwe (Monash University), and Ian Tyler (GSWA) for their constructive comments of earlier drafts of the manuscript. Nick Ware (Research School of Earth Sciences, Australian National University, Canberra) and Wieslaw Jablonski (Central Science Laboratory, University of Tasmania) are thanked for their assistance with the electron probe microanalyses. Gladys Warren (previously AGSO) allowed us to use her unpublished data on the pressure estimates for the East Kimberley intrusions, and Jonathon Claoue-Long (AGSO) assisted with the photomicrographs.

References

Acquafredda, P., Caggiarelli, A. & Piccarreta, G., 1992. Late magmatic to subsolidus coronas in gabbroic rocks from the Sila Massif (Calabria, Italy). Mineralogy and Petrology, 46, 229–238.

Anderson, J.L. & Smith, D.R., 1995. The effects of temperature and fO_2 on the Al-in-hornblende barometer. American Mineralogist, 80, 549–559.

Ashworth, J.R. & Chinner, G.A., 1978. Coexisting garnet and cordierite in migmatites from the Scottish Caledonides. Contributions to Mineralogy and Petrology, 65, 379–394.

Ballhaus, C. & Berry, R.F., 1991. Crystallization pressure and cooling history of the Giles layered intrusion Complex, Central Australia. Journal of Petrology, 32, 1–28.

Berg, J.H., 1977. Regional geobarometry in the contact aureoles of the anorthositic Nain complex, Labrador. Journal of Petrology, 18, 399–430.

Bernstein, S., Kelemen, P.B. & Brooks, C.K., 1996. Evolution of the Kap Edvald Holm complex: a mafic intrusion at a rifted continental margin. Journal of Petrology, 37, 497–519.

Blake, D.H., 1997. Speculations relating to the layered mafic–ultramafic intrusions of the East Kimberley, Western Australia. AGSO Research Newsletter, 27 19–21.

Blake, D.H. & Hoatson, D.M., 1993. Granite, gabbro, and migmatite field relationships in the Proterozoic Lamboo Complex of the East Kimberley region, Western Australia. AGSO Journal of Australian Geology & Geophysics, 14, 319–330.

Bohlen, S.R. & Boettcher, A.L., 1981. Experimental investigations and geological applications of orthopyroxene geobarometry. American Mineralogist, 66, 951–964.

Bordorkos, S. Cawood, P.A. & Oliver, N.H.S., 1998. Thermal evolution of the central Halls Creek Orogen, Western Australia: field, petrological and geochronological constraints. Abstracts 49, 14th Australian Geological Convention, Townsville, Queensland, 6–10 July, 46.

Carey, J.W., 1995. A thermodynamic formulation of hydrous cordierite. Contributions to Mineralogy and Petrology, 119, 155–165.

Droop, G.T.R. & Charnley, N.R., 1985. Comparative geobarometry of pelitic hornfelses associated with the Newer Gabbros: a preliminary study. Journal of the Geological Society, London, 142, 53–62.

Ellis, D.J., 1980. Osumilite–sapphirine–quartz granulites from Enderby Land, Antarctica: P–T conditions of metamorphism, implications for garnet–cordierite equilibria and the evolution of the deep crust. Contributions to Mineralogy and Petrology, 74, 201–210.

Ellis, D.J. & Green, D.H., 1979. An experimental study of the effect of Ca upon garnet–clinopyroxene Fe–Mg exchange equilibria. Contributions to Mineralogy & Petrology, 71, 13–22.

Emslie, R.F., 1970. Liquidus relations and subsolidus reactions in some plagioclase-bearing systems. Carnegie Institution of Washington, Year Book 1969, 148–155.

Gaite, J.M. & Hafner, S.S., 1984. Environment of Fe^{3+} at the M2 and Si sites of forsterite obtained from EPR. Journal of Chemical Physics, 80, 2747–2751.

Gemuts, I., 1971. Metamorphic and igneous rocks of the Lamboo Complex, East Kimberley region, Western Australia. Bureau of Mineral Resources, Australia, Bulletin 107, 71 pp.

Geopeko Ltd. 1986–1989. Springvale platinum/chromite exploration. Geopeko Ltd internal report (unpublished) for the Department of Minerals and Energy, Western Australia (Item 4592, Fiche 6447–6448).

Geopeko Ltd. 1986–1990. Toby Sill platinum exploration. Geopeko Ltd internal report (unpublished) for the Department of Minerals and Energy, Western Australia (Item 4326, Fiche 5755-5757–M4713).

Grant, S.M., 1988. Diffusion models for corona formation in metagabbros from the Western Grenville Province, Canada. Contributions to Mineralogy and Petrology, 98, 49–63.

Greenwood, R.C., Donaldson, C.H. & Emeleus, C.H., 1990. The contact zone of the Rhum ultrabasic intrusion: evidence of peridotitic formation from magnesian magmas. Journal of the Geological Society, London, 147, 209–212.

Griffin, W.L., Mellini, M., Oberti, R. & Rossi, G., 1985. Evolution of coronas in Norwegian anorthosites: re-evaluation based on crystal-chemistry and microstructures. Contributions to Mineralogy and Petrology, 91, 330–339.

Haggerty, S.E., 1976. Opaque mineral oxides in terrestrial igneous rocks. In: Rumble, D. (editor), Reviews in mineralogy—oxide minerals. Volume 3. Mineralogical Society of America, Hg101–Hg300.

Hamlyn, P.R., 1977. Petrology of the Panton and McIntosh layered intrusions, Western Australia, with particular reference to the genesis of the Panton chromite deposits. PhD thesis, University of Melbourne, 390 pp.

Hamlyn, P.R., 1980. Equilibration history and phase chemistry of the Panton Sill, Western Australia. American Journal of Science, 280, 631–668.

Hammarstrom, J.M. & Zen, E-an, 1986. Aluminium in hornblende: an empirical igneous geobarometer. American Mineralogist, 71, 1297–1313.

Hancock, S.L. & Rutland, R.W.R., 1984. Tectonics of an Early Proterozoic geosuture—the Halls Creek orogenic sub-province, northern Australia. Journal of Geodynamics, 1, 397–432.

Harley, S.L., 1984. Comparison of the garnet–orthopyroxene geobarometer with recent experimental studies, and applications to natural assemblages. Journal of Petrology, 25, 697–712.

Harris, N.B.W. & Holland, T.J.B., 1984. The significance of cordierite–hypersthene assemblages from the Beitbridge region of the Central Limpopo Belt; evidence for rapid decompression in the Archean? American Mineralogist, 69, 1036–1049.

Helz, T.R., 1995. The Stillwater Complex, Montana: a subvolcanic magma chamber. American Mineralogist, 80, 1343–1346.

Hensen, B.J. & Green, D.H., 1972. Experimental study of the stability of cordierite and garnet in pelitic compositions at high pressures and temperatures. II. Compositions without excess aluminosilicate. Contributions to Mineralogy and Petrology, 35, 331–354.

Hensen, B.J. & Green, D.H., 1973. Experimental study of the stability of cordierite and garnet in pelitic compositions at high pressures and temperatures. III. Synthesis of experimental data and geological applications. Contributions to Mineralogy and Petrology, 38, 151–166.

Hoatson, D.M., 1993. Correlation of structurally disrupted layered mafic–ultramafic intrusions in the East Kimberley: is Big Ben part of the Panton intrusion? AGSO Research Newsletter 19, 9–10.

Hoatson, D., 1995. New mineral discoveries in the East Kimberley. AGSO Research Newsletter, 22, 9–11.

Hoatson, D. & Tyler, I., 1993. Prospective layered mafic–ultramafic intrusions in the East Kimberley. AGSO Research Newsletter, 18, 8–9.

Hoatson, D.M., Wallace, D.A., Sun, S-s., Macias, L.F., Simpson, C.J. & Keays, R.R., 1992. Petrology and platinum-group-element geochemistry of Archaean layered mafic–ultramafic intrusions, west Pilbara Block, Western Australia. Australian Geological Survey Organisation, Bulletin, 242, 319 pp.

Hoatson, D., Blake, D., Warren, G., Orth, K. & Tyler, I., 1995. Recent NGMA mapping highlights the metallogenic potential of the East Kimberley. AGSO Research Newsletter, 22, 1–2.

Hoatson, D.M., Sproule, R.A. & Lambert, D.D., 1997. Are there Voisey's Bay-type Ni–Cu–Co sulphide deposits in the East Kimberley of Western Australia? AGSO Research Newsletter, 27, 17–19.

Hoel, P.G., 1971. Introduction to mathematical statistics. Wiley & Sons, 409 pp.

Holland, T.J.B. & Powell, R., 1990. An enlarged and updated internally consistent thermodynamic dataset with uncertainties and corrections: the system K_2O, Na_2O–CaO–MgO–MnO–FeO–Fe_2O_3–Al_2O_3–TiO_2–SiO_2–C–H_2–O_2. Journal of Metamorphic Geology, 8, 89–124.

Joesten, R., 1986a. The role of magmatic reaction, diffusion and annealing in the evolution of coronitic microstructure in troctolitic gabbro from Risör, Norway. Mineralogical Magazine, 50, 441–467.

Joesten, R., 1986b. The role of magmatic reaction, diffusion and annealing in the evolution of coronitic

microstructure in troctolitic gabbro from Risör, Norway—a reply. Mineralogical Magazine, 50, 474–479.

Johnson, C.D. & Carlson, W.D., 1990. The origin of olivine–plagioclase coronas in metagabbros from the Adirondack Mountains, New York. Journal of Metamorphic Geology, 8, 697–717.

Kushiro, I. & Yoder, H.S., Jr., 1966. Anorthite–forsterite and anorthite–enstatite reactions and their bearing on the basalt–eclogite transformation. Journal of Petrology, 7, 337–362.

Labotka, T.C., 1985. Petrogenesis of metamorphic rocks beneath the Stillwater Complex: assemblages and conditions of metamorphism. In: Czamanske, G.K. & Zientek, M.L. (editors), The Stillwater Complex, Montana: geology and guide 92, Montana Bureau of Mines and Geology, Special Publication, Butte, Montana, 70–76.

Lindsley, D.H., 1983. Pyroxene thermometry. American Mineralogist, 68, 477–493.

Lonker, S.W. 1981. The P–T–X relations of the cordierite–garnet–sillimanite equilibrium. American Journal of Science, 281, 1056–1090.

Mathison, C.I. & Hamlyn, P.R., 1987. The McIntosh layered olivine troctolite–olivine gabbro intrusion, East Kimberley, Western Australia. Journal of Petrology, 28, 211–234.

McGuire, A.V. & Coleman, R.G., 1986. The Jabal Tirf layered gabbro and associated rocks of the Tihama Asir complex, SW Saudi Arabia. Journal of Geology, 94, 651–665.

Mongkoltip, P. & Ashworth, J.R., 1983. Quantitative estimation of an open-system symplectite-forming reaction: restricted diffusion of Al and Si in coronas around olivine. Journal of Petrology, 24, 635–661.

Morrison, D.A., Maczuge, D.E., Phinney, W.C. & Ashwal, L.D., 1986. Stratigraphy and petrology of the Mulcahy Lake layered gabbro: an Archean intrusion in the Wabigoon Subprovince, Ontario. Journal of Petrology, 27, 303–341.

Nell, J., 1985. The Bushveld metamorphic aureole in the Potgietersrus area: evidence for a two stage metamorphic event. Economic Geology, 80, 1129–1152.

Newton, R.C., 1983. Geobarometry of high-grade metamorphic rocks. American Journal of Science, 283A, 1–28.

Olesen, N., Hansen, E.S., Kristensen, L.H. & Thyrsted, T., 1973. A preliminary account on the geology of the Selbu–Tydal area, Trondheim region, central Norwegian Caledonides. Leidse Geologische Mededelingen, 49, 259–276.

Otten, M.T., 1984. The origin of brown hornblende in the Artfjället gabbro and dolerite. Contributions to Mineralogy and Petrology, 86, 189–199.

Page, R., Hoatson, D., Sun, S-s. & Foudoulis, C., 1995. High-precision geochronology of Palaeoproterozoic layered mafic–ultramafic intrusions in the East Kimberley. AGSO Research Newsletter, 22, 7–8.

Powell, R. & Holland, T.J.B., 1985. An internally consistent thermodynamic dataset with uncertainties and corrections: 1. Methods and worked example. Journal of Metamorphic Geology, 3, 327–342.

Powell, R. & Holland, T.J.B., 1988. An internally consistent thermodynamic dataset with uncertainties and corrections: 3. Applications to geobarometry, worked examples and a computer program. Journal of Metamorphic Geology, 6, 173–204.

Smith, D., 1971. Stability of the assemblage iron-rich orthopyroxene–olivine–quartz. American Journal of Science, 271, 370–382.

Thornett, J.R., 1981. The Sally Malay deposit: gabbroid-associated nickel–copper sulfide mineralization in the Halls Creek Mobile Zone. Economic Geology, 76, 1565–1580.

Thornett, J.R., 1986. Evolution of a high-grade metamorphic terrain in the Proterozoic Halls Creek Mobile Zone, Western Australia. PhD thesis, University of Western Australia, 311 pp.

Tyler, I.M., Hoatson, D.M., Griffin, T.J., Sheppard, S., Blake, D.H. & Warren, R.G., 1997. McIntosh, Western Australia, 1:100 000 geological map (sheet 4462) Geological Survey of Western Australia, Perth.

Wallmach, T., Hatton, C.J. & Droop, G.T.R., 1989. Extreme facies of contact metamorphism developed in calc-silicate xenoliths in the eastern Bushveld Complex. Canadian Mineralogist, 27, 509–523.

Wilkinson, J.F.G., Duggan, M.B., Herbert, H.K. & Kalocsai, G.I.Z., 1975. The Salt Lick Creek layered intrusion, East Kimberley region, Western Australia. Contributions to Mineralogy and Petrology, 50, 1–23.

CHAPTER 10

COMMENTS ON RELATIONSHIPS OF MAFIC AND FELSIC MAGMATISM

by LESLEY A.I. WYBORN & DAVID H. BLAKE

Introduction

The Palaeoproterozoic of the Halls Creek Orogen (HCO) is characterised by abundant felsic as well as mafic to ultramafic igneous rocks and a paucity of igneous rocks of intermediate composition. Most of the felsic rocks form part of the Bow River Batholith, which comprises the 1865–1850 Ma Paperbark supersuite and the 1835–1805 Ma Sally Downs supersuite (see Chapter 3).

Geochemical and isotopic data indicate that, although coeval, the felsic and mafic rocks were not comagmatic (e.g. Sheppard et al. 1997a). The mafic magmas originated in the mantle, whereas the felsic magmas were derived from melting in the lower crust. The distinct bimodal nature of the magmatism, in terms of silica content, is an important consideration for any tectonic model proposed for the Palaeoproterozoic in this part of northwestern Australia.

Bimodal magmatism

The recently completed program of geological mapping and U–Pb zircon geochronology in the East Kimberley by the Australian Geological Survey Organisation (AGSO) and the Geological Survey of Western Australia (GSWA), together with major and trace element geochemistry and isotope studies, shows that extensive mafic and felsic magmatism took place between about 1910 Ma and 1790 Ma in the western, central, and eastern zones of the HCO (Table 10.1). The layered mafic and ultramafic intrusions described in this *Bulletin* (see Chapter 5) were coeval with granitic intrusions, and widespread mafic volcanism was accompanied by equally widespread felsic volcanism.

Field evidence for contemporaneous intrusion of mafic and felsic magmas includes numerous net-veined complexes formed by the mingling of mafic and felsic magmas, and the presence of synplutonic mafic dykes in granite plutons (e.g. Blake & Hoatson 1993, and Chapters 3, 5, and 6 of this *Bulletin*). Interleaving of mafic and felsic volcanic rocks, common in the ~1910 Ma Ding Dong Downs Volcanics and ~1880 Ma Biscay Formation in the eastern zone of the HCO and in the ~1843 Ma Koongie Park Formation in the central zone, indicates contemporaneous mafic and felsic extrusive activity. Overall in the HCO, felsic igneous rocks are more voluminous and crop out over greater areas than the mafic igneous rocks.

Of the few igneous rocks of intermediate composition in the HCO, most are clearly hybrids that have resulted either from local mingling of mafic and felsic magmas, as in net-veined complexes, or from contamination of mafic magma by more felsic country rocks at intrusive contacts.

Bimodal magmatism like that evident in the HCO (Fig. 10.1) has long been taken to indicate extensional intracratonic tectonism (e.g. Christiansen & Lipman 1972, Martin & Piwinski 1972), and is certainly not typical of magmatism associated with subduction at continental margins, which is more intermediate in character.

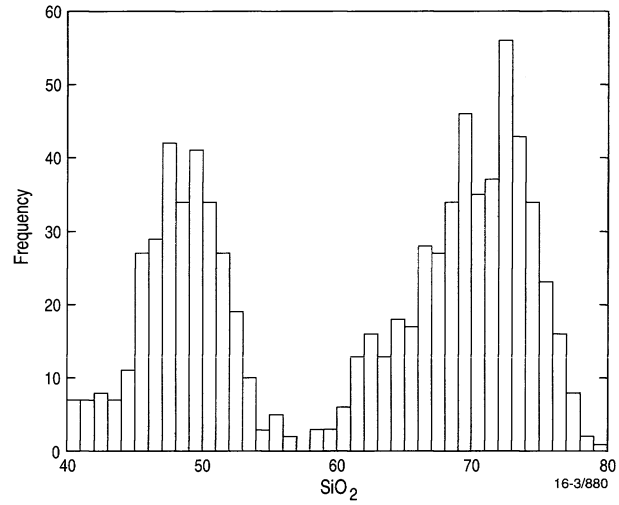


Figure 10.1. Histogram of igneous rocks (792 samples) from the Halls Creek Orogen, showing a distinct bimodal distribution and a paucity of rocks of intermediate SiO_2 composition (52–62 wt. %). Source of data: AGSO's OZCHEM database and GSWA data in Sheppard et al. 1997b.

Chemical characteristics of the granites

The Proterozoic granites of the HCO, like most Proterozoic granites in Australia, are predominantly I-(granodioritic) type (Chappell & Stevens 1988) with SiO_2 contents greater than 66 wt. %. They have higher K, Th, and U contents than typical Archaean and Palaeozoic granites and Nd model source ages that are significantly older than their emplacement ages. The majority have Sr-depleted, Y-undepleted mantle-normalised trace-element signatures (Fig. 10.2). Such magmas indicate a tonalitic source in the lower crust (Chappell & Stevens 1988, Johannes & Holz 1996).

Generation of the magmas

The mafic magmas of the HCO are considered to have come from the upper mantle (see Chapter 11), perhaps a result of asthenospheric upwelling (Oliver et al. 1998), with different basaltic parent magmas representing separate thermal pulses. The felsic magmas on the other hand are inferred to have been generated by melting of

Table 10.1. Palaeoproterozoic magmatism in the Halls Creek Orogen.

Age (Ma)	*Western zone*	*Central zone*	*Eastern zone*
~1790	**Mafic:** Hart Dolerite		**Felsic:** San Sou Monzogranite
~1800	**Mafic:** Carson Volcanics in Kimberley Group	**Mafic:** volcanics in Kimberley Group and correlatives	**Mafic:** volcanics in Kimberley Group and correlatives
~1810		**Felsic:** part of Mount Christine Granitoid of Sally Downs supersuite, Eastmans Granite	**Felsic:** part of Mount Christine Granitoid of Sally Downs supersuite
~1820	**Felsic:** ?plutons of Sally Downs supersuite	**Felsic:** Sally Downs Tonalite, part of Mount Christine Granitoid and other plutons of Sally Downs supersuite, felsic components of net-veined complexes **Mafic:** ?group VII layered intrusions (e.g. Black Hills Yard), mafic components of net-veined complexes	**Felsic:** part of Mount Christine Granitoid, ?unnamed granite in south
~1825	**Felsic:** ?plutons of Sally Downs supersuite	**Felsic:** Loadstone Monzogranite, McHale Granodiorite andother plutons of Sally Downs supersuite, felsic components of net-veined complexes **Mafic:** ?Corridor gabbro, mafic components of net-veined complexes	
~1830	**Felsic:** ?plutons of Sally Downs supersuite	**Felsic:** Mabel Downs Tonalite of Sally Downs supersuite, felsic components of net-veined complexes **Mafic:** group VI layered intrusions (e.g. McIntosh), mafic components of net-veined complexes (e.g. near Armanda)	
~1835	**Felsic:** minor volcanics in Speewah Group		
~1845		**Felsic:** volcanics in Koongie Park Formation **Mafic:** volcanics in Koongie Park Formation, group V layered intrusions (e.g. Sally Malay), intrusive sheets in Tickalara Metamorphics	**Felsic:** ?volcanics in Olympio Formation in north
~1850		**Felsic:** Tickalara Metamorphics (e.g. Dougalls Tonalite, Fletcher Creek Monzogranite) **Mafic:** ?group IV layered intrusions (e.g. Wild Dog Creek), intrusive sheets in Tickalara Metamorphics	**Alkaline:** volcanics in Olympio Formation (Butchers Gully Member) **Mafic:** ?some Woodward Dolerite

Table 10.1. (Cont.). Palaeoproterozoic magmatism in the Halls Creek Orogen.

Age (Ma)	*Western zone*	*Central zone*	*Eastern zone*
~1855	**Felsic:** Whitewater Volcanics, Castlereagh Hill Porphyry, Greenvale Porphyry, plutons of Paperbark supersuite of Bow River Batholith, felsic components of net-veined complexes **Mafic:** layered intrusions of group II (e.g. Springvale) and group III (e.g. Toby), Corridor gabbro and other mafic intrusions, mafic components of net-veined complexe	**Mafic–ultramafic:** group I layered intrusions (e.g. Panton)	**Mafic:** ?some Woodward Dolerite
~1860			**Alkaline:** volcanics in Olympio Formation (Maude Headley Member) **Mafic:** ?some Woodward Dolerite
~1865		**Felsic:** Rose Bore Granite (Tickalara Metamorphics) **Mafic:** ?Norton intrusion (Tickalara Metamorphics)	
~1880			**Felsic:** volcanics in Biscay Formation **Mafic:** volcanics in Biscay Formation, Woodward Dolerite
~1910			**Felsic:** Ding Dong Downs Volcanics (including Sophie Downs Granophyre Member), Junda Microgranite, **Mafic:** Ding Dong Downs Volcanics, ?Woodward Dolerite

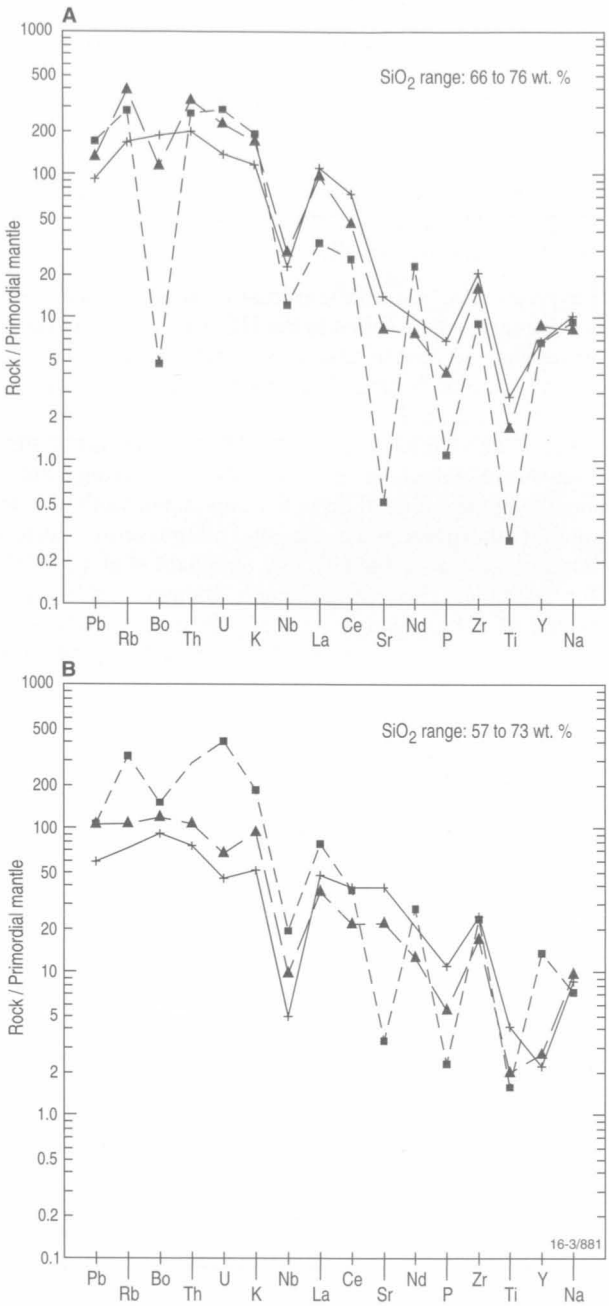


Figure 10.2. Spidergrams for typical Sr-depleted (A) and Sr-undepleted (B) granites from the Halls Creek Orogen. The solid line is for samples with lowest SiO_2 contents, the short dashed line for samples with the highest SiO_2 contents, and the long dashed line for samples with in-between SiO_2 contents. Note: the highest SiO_2 spidergram (short dashed line) in (B) is Sr-depleted because of high SiO_2 content. The mantle normalisation values are from McDonough & Sun (1995).

tonalitic material in the lower crust (see above). As discussed by many researchers (e.g. Huppert & Sparks 1988, Bergantz & Dawes 1994, Laube & Springer 1998, Koyaguchi & Kaneko 1999), felsic magmas are an expected consequence when hot mafic magma from the mantle is emplaced in the lower crust. Hence, the extensive felsic magmatism in the HCO can be regarded as a second-order effect of mantle underplating of mafic magma. The felsic magmas were emplaced as plutons in the middle and upper crust and reached the surface in volcanic eruptions.

Sun & Hoatson (see Chapter 11) have shown that the older layered mafic–ultramafic intrusions, those of groups I–V, which predate the main compressional event of the Halls Creek Orogeny at ~1835 Ma, have lower abundances of incompatible trace elements than younger layered intrusions, such as those of group VI, which were emplaced shortly after the ~1835 Ma event. They attribute this difference to the older magmas being generated by more asthenospheric mantle melting at shallower mantle depths and beneath a thinner lithosphere, compared to the younger intrusions. However, the youngest Palaeoproterozoic mafic intrusions in the HCO, those of the ~1790 Ma Hart Dolerite in the west, have incompatible-trace-element abundances comparable to those of the pre-1835 Ma mafic–ultramafic intrusions. This is inferred to indicate a return to higher mantle geothermal gradients, similar to those of the pre-1835 Ma magmas.

The granitic intrusions of the HCO also show a significant change in trace-element composition at ~1835 Ma. Most granites emplaced before 1835 Ma have Sr-depleted, Y-undepleted mantle-normalised trace-element signatures (Fig. 10.2), indicating source regions in which plagioclase was a stable phase. However, some of the granites emplaced shortly after 1835 Ma have Sr-undepleted, Y-depleted signatures, indicating source regions containing garnet instead of plagioclase. Source regions in which plagioclase is stable can be inferred to lie at depths of less than 35 km, whereas garnet-stable regions imply melting in source regions deeper than 35 km.

For melting to occur in the crust at depths less than 35 km, as suggested for the Sr-depleted granites, geothermal gradients of >30°C/km are required (e.g. Johannes & Holz 1996). Such geothermal gradients are in accord with the high-temperature/low-pressure metamorphism that characterises the Palaeoproterozoic rocks of the HCO (see Chapter 3). In contrast, normal crustal geothermal gradients are generally accepted as ~ 20°C/km. The above-average crustal geothermal gradients may be attributed, at least in part, to the large volume of hot mafic magma intruded from the upper mantle into the crust, as evidenced by the voluminous mafic–ultramafic intrusions and mafic volcanics. From the high K, Th, and U contents of the HCO granites (relative to average granites), it can be inferred that the source regions of these granites were enriched in these radioactive elements, and this could have contributed to the high crustal temperatures (Hand et al. 1999, McLaren et al. 1999).

In contrast, the Sr-undepleted granites, generated at depths greater than 35 km, imply a lower geothermal gradient, as indicated for contemporaneous mafic–ultramafic rocks (see Chapter 11). The ~1835 Ma compressional event of the Halls Creek Orogeny can be inferred to have thickened the crust, and this thickening would have lowered the crustal geothermal gradients. As shown in Figure 10.3, the difference between the Sr-depleted and Sr-undepleted granites could result from only minor changes in geothermal gradient and crustal thickness; radical changes in the tectonic setting are not necessary.

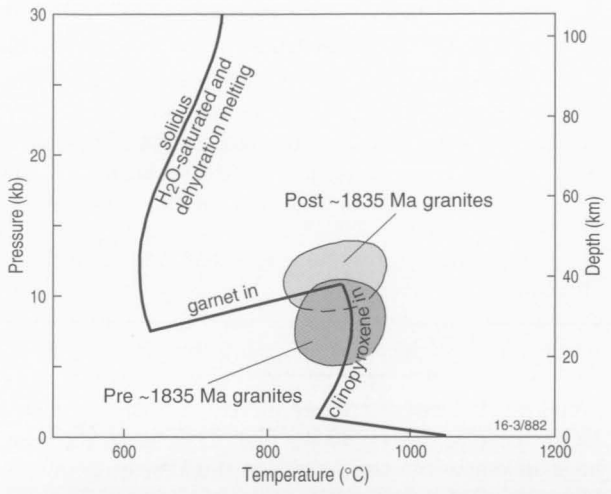


Figure 10.3. Pressure–temperature–depth diagram, showing solidus curves for dehydration melting of amphibolites based on Wyllie & Wolf (1993). Inferred P–T fields for post-1835 Ma and pre-1835 Ma granites from the Halls Creek Orogen show that the variation in granite type may be a result of a relatively minor difference in pressure. Modified from Johannes & Holtz 1996.

Inheritance

Isotopic evidence indicates that the lower crust from which the granitic magmas were derived was Archaean and/or early Palaeoproterozoic (older than 2000 Ma?). No Archaean rocks have been found within the HCO, but some are exposed in The Granites–Tanami block to the east (e.g. Page et al. 1994). There is also evidence for the existence of Archaean basement beneath the Little Mount Isa and Ilmars base-metal prospects in the HCO, northeast of Halls Creek township (Sun et al. 1996), and beneath the Palaeoproterozoic Speewah and Kimberley Basins of the Kimberley Block to the west of the HCO (Graham et al. 1999).

It might be expected that if the source ages of the I-type granites of the HCO were older than emplacement ages, these granites would contain abundant inherited zircon. That this is not so can be attributed to zircon being highly soluble in I-granodiorite-type (metaluminous) melts (e.g. Watson 1979). Any zircon inherited from the source regions of such granitic melts is likely to be completely resorbed before the melt begins to crystallise. In particular, inherited zircon cannot be expected in I-type granitic rocks with >75 wt. % SiO_2, as such rocks represent almost 100% melt. In contrast, zircon is almost insoluble in peraluminous melts like those forming S-type granites, accounting for the large amounts of inherited zircon typically present in S-type granites (e.g. Williams & Chappell 1998).

Tectonic models

Although the chemical signature of a granitic magma is commonly thought to be related to its specific tectonic setting, it can depend at least as much on the chemistry of the crust from which it was derived as on the processes involved in magma generation (e.g. Arculus 1987, Chappell & Stevens 1988, Roberts & Clemens 1993). For example, high-K, I-type magmas, like those that gave rise to most of the granites in the HCO, are documented in continental arcs and also in situations where melting is a consequence of decompression following crustal compression, and where crustal thickening is followed by substantial uplift (Robert & Clemens 1993). Hence, the composition of the felsic magmas cannot be used to uniquely define the tectonic setting of the HCO, either before or after 1835 Ma.

Layered mafic–ultramafic intrusions and bimodal magmatism of the type found in the HCO are normally taken to indicate an overall extensional, rather than compressional, tectonic setting. High geothermal gradients and high-temperature/low-pressure metamorphism evident in the Palaeoproterozoic of the HCO imply a hot thin lithosphere, which is also compatible with an extensional regime. None of these features support subduction of cold lithosphere at a continental margin setting, as has been suggested for the HCO by Sheppard et al. (1997a), for example. There is evidence, though, for a short period of compression at ~1835 Ma in the HCO—the compressional phase of the Halls Creek Orogeny. This phase could represent a period of cooling-induced lithospheric compression separating two longer periods of asthenospheric upwelling and extension.

A model proposed by Huppert & Sparks (1988) for the generation of granitic magma by intrusion of mafic magma into continental crust can account for the Palaeoproterozoic bimodal magmatism in the HCO, and provides a mechanism for the crustal contamination of the mafic magmas indicated by the isotopic studies described in chapters 11 and 12 of this *Bulletin*. In the initial phase of the Huppert & Sparks model, mafic magma from the upper mantle is intruded into overlying cold and brittle crust as dykes, some of which reach the surface as feeders for basaltic lava flows. As intrusion of mafic magma from the mantle continues, the crust becomes hotter and parts begin to melt. During this phase, much of the mafic magma forms intrusions in the now more ductile middle and upper crust, instead of continuing to the surface as dykes. Felsic melts generated in the lower crust rise to form voluminous plutons and also reach the surface in large caldera complexes.

In the HCO, underplating of mafic magma at the base of the crust appears to have slowed down or ceased at ~1840 Ma, with crustal extension being replaced by compressional tectonism and crustal thickening, as represented by the ~1835 Ma compressional phase of the Halls Creek Orogeny. Shortly after this phase, a resumption of asthenospheric upwelling resulted in a new cycle of crustal extension and bimodal magmatism, the last manifestations of which were the emplacement of mafic sills (Hart Dolerite) in the northwest and granite plutons (San Sou Granite suite) in the south at ~1790 Ma.

Acknowledgements

We would like to thank David Champion, Alastair Stewart, and Shen-Su Sun (all AGSO) for their constructive comments on an earlier draft of the manuscript. Terry Brown drafted the figures.

References

Arculus, R.J., 1987. The significance of source versus process in the tectonic controls of magma genesis. Journal of Volcanology and Geothermal Research, 32, 1–12.

Bergantz, G.W. & Dawes, R., 1994. Aspects of magma generation and ascent in continental lithosphere. In: Ryan, M. P. (editor), Magmatic systems. Academic Press, San Diego, 291–317.

Blake, D.H. & Hoatson D.M., 1993. Granite, gabbro and migmatite field relationships in the Proterozoic Lamboo Complex of the East Kimberley region, Western Australia. AGSO Journal of Australian Geology & Geophysics, 14(4), 319–330.

Chappell, B.W. & Stephens, W.E., 1988. Origin of infracrustal (I-type) granite magmas. Transactions of the Royal Society of Edinburgh, Earth Sciences, 79, 71–86.

Christiansen, R.L. & Lipman, P.W., 1972. Cenozoic volcanism and plate-tectonic evolution of the western United States. Philosophical Transactions of the Royal Society, London, Series A, 271, 249–284.

Graham, S., Lambert, D.D., Shee, S.R., Smith, C.B. & Reeves, S., 1999. Re–Os isotopic evidence for Archean lithospheric mantle beneath the Kimberley block, Western Australia. Geology, 27, 431–434.

Hand, M., Sandiford, M. & Wyborn, L., 1999. Some thermal consequences of high heat production in the Australian Proterozoic. AGSO Research Newsletter, 30, 20–23.

Huppert, H.E. & Sparks, R.S.J., 1988. The generation of granitic magmas by intrusion of basalt into continental crust. Journal of Petrology, 29, 599–624.

Johannes, W. & Holz, F., 1996. Petrogenesis and experimental petrology of granitic rocks. Springer, Berlin, 335 pp.

Koyaguchi, T. & Kaneko, K., 1999. A two-stage thermal evolution model of magmas in continental crust. Journal of Petrology, 40, 241–254.

Laube, N. & Springer, J., 1998. Crustal melting by ponding of mafic magmas: a numerical model. Journal of Volcanology and Geothermal Research, 81, 19–35.

Martin, R.F. & Piwinski, A.J., 1972. Magmatism and tectonic settings. Journal of Geophysical Research, 77, 4966–4976.

McDonough, W.F. & Sun S-s., 1995. The composition of the Earth. Chemical Geology, 120, 223–253.

McLaren, S., Neumann, N., Sandiford, M., & Wyborn, L., 1999. Post-intrusion heating associated with high-heat producing Proterozoic granites—implications for mineralisation? AGSO Research Newsletter, 30, 23–26.

Oliver, N.H.S., Bodorkos, S., Nemchin, A.A., Kinny, P.D. & Watt, G.R., 1998. Differential renewal of U–Pb patterns in zircons during anatexis of Kimberleys pelites: implications for granite genesis. Geological Society of Australia, Abstracts, 49, 339.

Page, R.W., Blake, D.H., Edgecombe, D.R. & Pearcey, D.P., 1995. Geochronology of an exposed late Archaean basement terrane in The Granites–Tanami Region. AGSO Research Newsletter, 22, 19–20.

Roberts, M.P. & Clemens, J.D., 1993. Origin of high-potassium, calc-alkaline, I-type granitoids. Geology, 21, 825–828.

Sheppard, S., Griffin, T.J. & Tyler, I.M., 1997a. The tectonic setting of granites in the Halls Creek and King Leopold Orogens, northwest Australia. In: Rutland, R.W.R. & Drummond, B.J. (editors), Palaeoproterozoic tectonics and metallogenesis: comparative analysis of parts of the Australian & Fennoscandian shields. Workshop, Darwin, September, 14–22, 1997. Australian Geological Survey Organisation, Record 1997/44, 107–109.

Sheppard, S., Griffin, T.J. & Tyler, I.M., 1997b. Compilation of whole-rock geochemical data for the King Leopold and Halls Creek Orogens. Geological Survey of Western Australia, Record 1997/4, 138 pp.

Sun, S-s., Carr, G.R. & Page, R.W., 1996. A continued effort to improve lead-isotope model ages. AGSO Research Newsletter, 24, 19–20.

Watson, E.B., 1979. Zircon saturation in felsic liquids: experimental results and applications to trace element geochemistry. Contributions to Mineralogy & Petrology, 70, 407–419.

Wyllie, P.J. & Wolf, M.B., 1993. Amphibole dehydration-melting: sorting out the solidus. In: Prichard, H.M., Alabaster, T., Harris, N.B.W. & Neary, C.R. (editors), Magmatic processes and plate tectonics. Geological Society of London, Special, 76, 405–416.

Williams, I.S. & Chappell, B.W., 1998. Crustal evolution in southeastern Australia: a zircon viewpoint. In: The Bruce Chappell symposium: granites, island arcs, the mantle and ore deposits. Canberra, November 23–24, 1998, Abstracts.. Australian Geological Survey Organisation, Record 1998/33, 44.

CHAPTER 11

TRACE-ELEMENT GEOCHEMICAL AND ND ISOTOPIC STUDY OF THE MAFIC–ULTRAMAFIC INTRUSIONS: IMPLICATIONS FOR THEIR PETROGENESIS AND TECTONIC ENVIRONMENT

by SHEN-SU SUN & DEAN M. HOATSON

Introduction

Mafic–ultramafic intrusions form a large and economically prospective component of the Halls Creek Orogen (HCO) in the East Kimberley of northern Western Australia (Fig. 11.1). The intrusions are composed of different types of mafic, mafic–ultramafic, and ultramafic rocks and they have different ages of emplacement, morphologies, metamorphic overprinting, relationships to country rocks, and styles of mineralisation. To understand the evolution and metallogenesis of these intrusions it is important to know how many different magma sources were involved, and the significance of crustal contamination, magma mixing, and chemical heterogeneity of the mantle. In this chapter we use trace-element geochemical and Nd isotope data for selected ~1860–1790 Ma mafic and ultramafic intrusive rocks in the HCO to determine:

1. the composition of parent magmas for the different groups of intrusions;
2. the significance of crustal contamination for magma genesis; and
3. the implications for tectonic setting and potential for platinum-group element (PGE) and Ni–Cu–Co mineralisation in the intrusions.

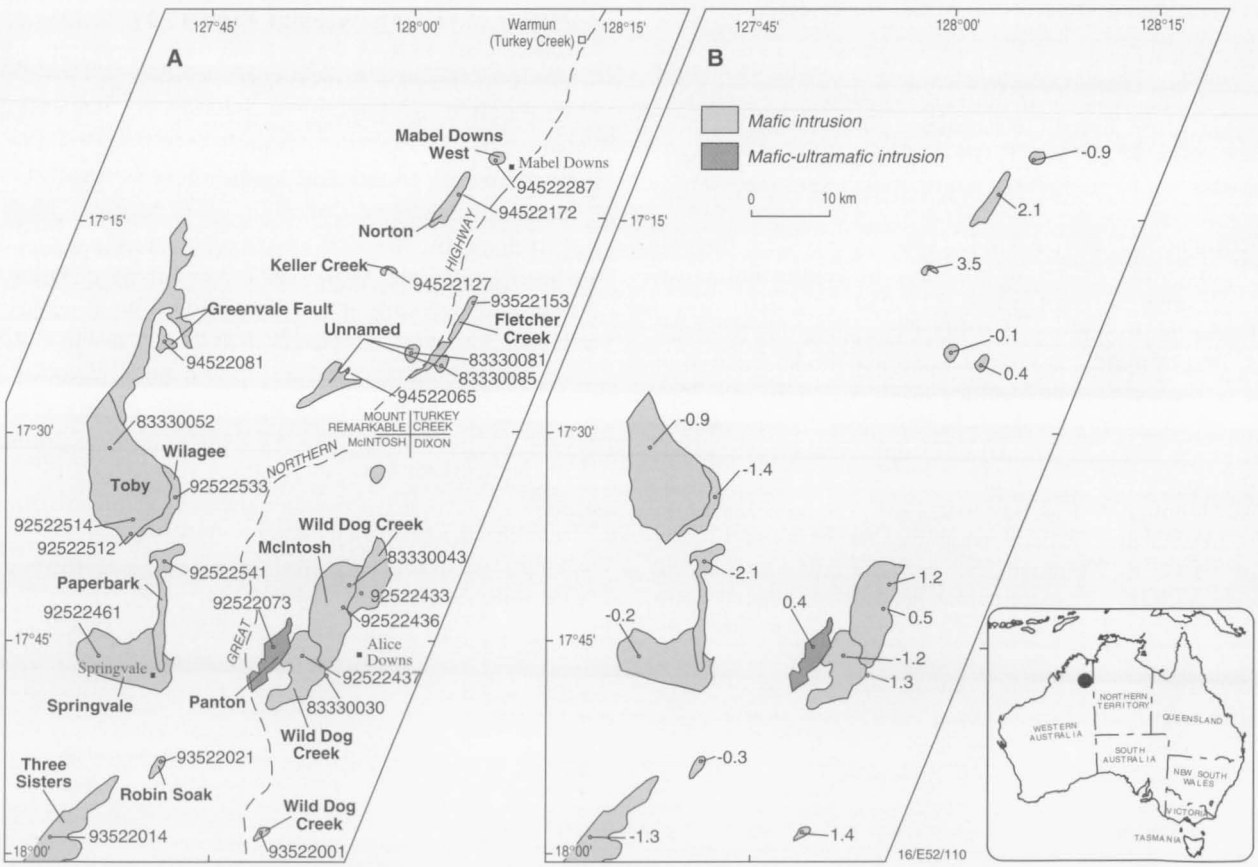


Figure 11.1. East Kimberley mafic–ultramafic intrusions investigated and isotopic results.

A. Intrusions studied and sample locations.

B. Initial ε_{Nd} values for those samples shown in A.

Following the approach adopted in an earlier study of the HCO (Sun et al. 1991), samples that best represent chilled marginal rocks, comagmatic dykes, and other melt-rich samples (with comparatively high Ti, Zr, P, and REE contents) have been used to quantify the chemical characteristics of the different groups of intrusions. These geochemical characteristics are used to test the validity of Hoatson's classification of the intrusions based on age, field, and petrological criteria (see Chapter 5). Other studies of layered intrusions (Sun et al. 1991, Hoatson et al. 1992) have shown that geochemical data on fine-grained marginal rocks should be used cautiously, since these rocks may contain various amounts of cumulus minerals and, therefore, may not truly represent the parent magma or magmas. For example, high Al_2O_3 and positive Eu anomalies reflect early crystallising plagioclase, and high Sc can be due to cumulus clinopyroxene. Furthermore, the margins of intrusions in the East Kimberley were frequently contaminated by country rocks during emplacement, were the focus for high water activity (amphibole replacement of pyroxene), and were often overprinted by post-intrusive metamorphic and igneous events. The 'chilled' samples used in this study were generally restricted to fine-grained marginal phases of magmas intruded into solidified rocks of their own kind.

There is general agreement that the emplacement of the mafic intrusions, generation of granites, and regional metamorphism from 1860 to 1830 Ma in the HCO are likely to be causally linked (e.g. Page et al. 1995). There is also a consensus regarding the occurrence and interpretation of light-REE-enriched basaltic andesite to rhyolite in the 1848 Ma Butchers Gully Member of the Olympio Formation east of the Halls Creek Fault (see Chapter 3). These geochemically distinctive volcanic rocks have intraplate-type chemistry and show no Nb depletion or Th enrichment. Rhyolites of the 1857 Ma Maude Headley Member of the Olympio Formation have a similar intraplate-type chemistry (Page & Hancock 1988, Taylor et al. 1995, Sun et al. 1995, Tyler et al. 1995, Page, pers. comm. 1997). Thus, an intraplate or passive continental margin environment can be suggested for these volcanics. However, the tectonic environment west of the Halls Creek Fault during this period is an issue of debate, with two major contrasting models being proposed, namely:

- all tectonic and magmatic activities were ensialic and the mafic intrusions were emplaced in an intraplate extensional environment (e.g. Hancock & Rutland 1984, Etheridge et al. 1987, Wyborn 1988, Blake et al. 1998, 1999); and
- there was a magmatic arc generated during northwestward subduction of oceanic crust beneath the Kimberley Craton (Ogasawara 1988, Tyler et al. 1995). Modifications of this plate tectonic model have been proposed by Sheppard et al. (1997).

Analytical methods

The twenty-one samples used in this study were analysed at AGSO for major and trace-element abundances by X-ray fluorescence spectrometry (XRF, for Ba, Cr, Cu, V, Zn, and Zr) and inductively coupled plasma-mass spectrometry (ICP-MS). Neodymium isotope work was carried out at the Research School of Earth Sciences, Australian National University, Canberra. The method used for ICP-MS analysis (see Appendix 1.1) is basically the same as that described in Eggins et al. (1997); analytical uncertainty is about 5%. Three samples—two from the Wild Dog Creek intrusion (92522433, 93522001), and one from the McIntosh intrusion (92522436)—that have unusually low abundance of Th and high Nb/Th were reanalysed by ICP-MS at the Department of Earth Sciences, University of Queensland (courtesy of Dr. Yaoling Niu). The repeat analyses confirmed AGSO's Th data (0.35 v. 0.34, 0.64 v. 0.65, and 0.18 v. 0.16 ppm, respectively).

For Sm–Nd isotope analyses, the chemical separation of Sm and Nd was carried out following the method of Maas & McCulloch (1991). Purified Sm and Nd were analysed by a multi-collector Finnigan MAT 261 mass spectrometer. All $^{143}Nd/^{144}Nd$ values were normalised to the 0.511872 (La Jolla) and 0.512653 (BCR-1) standards. Reproducibility of the $^{143}Nd/^{144}Nd$ value is about 0.002% (i.e. 0.2 ε_{Nd} unit); reproducibility of $^{147}Sm/^{144}Nd$ for separate decompositions of the same samples is generally better than 0.2%. The chemical and Nd isotope data are presented in Tables 11.1 and 11.2.

Chemical analyses and trace-element spidergrams

In order to show the chemical characteristics of the different intrusion groups, some selected incompatible trace elements are plotted on 'spidergram' diagrams (Fig. 11.2), using the mantle normalisation values of McDonough & Sun (1995), and chondrite-normalised diagrams for rare earth elements (Fig. 11.3). The trace elements used for these diagrams are generally considered to be immobile during metamorphism and mild hydrothermal alteration (e.g. Pearce 1987). The grouping classification of the intrusions adopted here follows that of Hoatson (see Chapter 5). Ages quoted below are those reported by Page & Hoatson (see Chapter 6). Sample locations are shown on Figure 11.1, and the major and trace-element chemistry of the samples analysed by ICP-MS and XRF is summarised in Table 11.1 and Appendix 2, respectively.

Group I

A fractionated and contaminated quartz gabbro sample (92522073) from the northwestern basal contact of the Ultramafic Series of the 1856±2 Ma Panton intrusion has low MgO (4.15%) and Al_2O_3 (12.3%), and a fairly flat mantle-normalised trace-element pattern, with the exception of high Th (Fig. 11.2). A nearby sample (92522072) analysed by XRF has the same geochemical features. Both samples have considerably higher Nb/La (0.9 v. 0.3) than another 'melt-like' Panton sample (PS-A13) quoted in Sun et al. (1991). The major element data of PS-A13 are from Hamlyn's thesis (1977) and the trace-element data are based on personal communication (Hamlyn 1989) of unpublished data. Unfortunately, no Th value is available for this sample. In contrast to

Table 11.1. Major and trace-element geochemistry and Nd isotopic data for melt-like mafic rocks from the East Kimberley.

Sample number	*92522073*	*92522461*	*92522533*	*83330052*	*92522512*	*92522514*	*92522433*
Intrusion	*Panton*	*Springvale*	*Wilagee*	*Toby*	*Toby*	*Toby*	*Wild Dog Creek*
Group	*I*	*II*	*II*	*III*	*III*	*III*	*IV*
Lithology	*Hornblende quartz gabbro*	*Olivine gabbronor.*	*Chilled biotite gabbro*	*Biotite gabbro*	*Quartz gabbro*	*Biotite gabbronor.*	*Magnetite gabbro*
Easting	*375790*	*354000*	*363340*	*354500*	*359120*	*357850*	*387900*
Northing	*8037070*	*8034300*	*8055550*	*8062300*	*8052200*	*8053850*	*8045100*
SiO_2	52.52	48.31	49.85	48.73	49.33	50.59	50.77
TiO_2	1.55	0.78	1.04	1.17	1.17	1.18	1.19
Al_2O_3	12.25	17.73	15.45	15.21	15.29	15.35	15.23
Fe_2O_3	2.79	1.51	1.03	1.86	1.95	1.63	1.39
FeO	12.81	7.48	9.42	9.48	8.82	9.11	9.30
MnO	0.18	0.12	0.15	0.16	0.16	0.15	0.15
MgO	4.15	9.04	7.51	7.50	7.75	7.21	7.89
CaO	8.33	10.70	10.95	11.52	10.53	10.26	10.00
Na_2O	2.67	1.86	2.11	2.22	1.75	1.83	2.46
K_2O	0.34	0.83	0.75	0.46	0.66	0.89	0.10
P_2O_5	0.15	0.15	0.17	0.21	0.19	0.17	0.21
LOI	1.65	1.22	1.33	1.03	2.00	1.16	0.93
Rest	0.18	0.26	0.30	0.20	0.31	0.31	0.31
Total	**99.57**	**99.99**	**100.06**	**99.75**	**99.91**	**99.84**	**99.93**
O=F,S,Cl	0.00	0.03	0.04	0.00	0.05	0.05	0.05
Total	**99.57**	**99.95**	**100.02**	**99.75**	**99.86**	**99.79**	**99.89**
Trace elements in parts per million							
Li	11	6	22	14	6	15	5
S	50	650	800	-	990	950	920
Sc	50	25	40	45	42	39	30
V	584	161	223	213	223	222	194
Cr	23	168	389	275	345	343	584
Ni	52	183	106	73	123	126	194
Cu	37	46	95	59	64	64	63
Zn	116	73	92	90	95	97	99
Ga	17.3	14.7	15.8	17.0	17.0	16.9	16.2
Rb	3.5	28.5	33.0	17.5	40.0	38.5	1.0
Sr	126	295	155	213	151	151	250
Y	34.5	18.0	25.5	27.5	29.5	29.5	15.0
Zr	109	91	122	106	126	122	49
Nb	5.85	7.90	6.42	6.89	7.98	6.93	5.91
Ba	64	283	228	267	202	242	70
La	6.20	20.0	18.1	21.4	20.3	20.0	7.95
Ce	17.6	41.5	38.5	46.2	43.3	42.0	18.9
Pr	2.62	4.92	4.78	5.76	5.34	5.26	2.60
Nd	12.0	18.4	18.6	23.0	21.0	20.5	11.4
Sm	3.58	3.42	4.02	4.80	4.60	4.54	2.78
Eu	1.18	1.03	1.19	1.49	1.37	1.36	1.10
Gd	5.00	3.46	4.46	5.15	5.15	5.11	3.18
Tb	0.91	0.55	0.74	0.83	0.87	0.86	0.50
Dy	5.58	3.12	4.45	4.87	5.17	5.10	2.90
Ho	1.31	0.70	1.02	1.10	1.19	1.17	0.63
Er	3.88	2.03	2.97	3.17	3.45	3.45	1.72
Yb	3.58	1.81	2.68	2.88	3.04	3.08	1.47
Lu	0.53	0.27	0.41	0.42	0.47	0.47	0.22
Pb	7.5	6.0	6.0	6.0	7.0	8.5	1.0
Th	3.83	3.46	2.83	0.84	2.70	4.68	0.34
U	0.93	0.63	0.61	0.20	0.54	1.10	0.11
ε_{Ndi}	0.4	-0.2	-1.4	-0.9	-	-	-
mg	32.6	64.6	56.4	54.5	56.6	54.8	57.1
Nb/La	0.9	0.4	0.4	0.3	0.4	0.4	0.7
Nb/Th	1.5	2.3	2.3	8.2	3.0	1.5	17.4
Ba/Nb	11.0	35.8	35.5	38.8	25.3	34.9	11.8
Sr/Nd	10.5	16.0	8.3	9.3	7.2	7.4	21.9
Ti/Zr	85.6	51.4	51.1	66.8	55.7	58.0	145.6

Table 11.1. (Cont.). Major and trace-element geochemistry and Nd isotopic data for melt-like mafic rocks from the East Kimberley.

Sample number	*92522437*	*93522001*	*93522153*	*94522065*	*94522127*	*92522436*	*92522541*
Intrusion	*Wild Dog*	*Wild Dog Creek*	*Fletcher Creek*	*Unnamed Creek*	*Keller Creek*	*McIntosh*	*Paperbark*
Group	*IV*	*IV*	*V*	*Undivided*	*V*	*VI*	*Corridor*
Lithology	*gabbro Magnetite quartz gabbronor.*	*Chilled mt quartz gabbro*	*Chilled magnetite gabbro*	*Gabbronor. gabbro*	*Olivine gabbro gabbronor.*	*Chilled quartz*	*Biotite*
Easting	*380900*	*374298*	*400000*	*384878*	*390440*	*387060*	*361900*
Northing	*8036300*	*8011885*	*8080075*	*8073260*	*8086585*	*8044060*	*8046400*
SiO_2	49.64	49.16	48.12	49.18	48.65	56.79	51.43
TiO_2	1.45	1.27	1.47	1.28	1.68	0.83	1.08
Al_2O_3	15.53	14.64	16.47	15.26	13.32	17.23	15.35
Fe_2O_3	1.18	1.84	1.92	1.00	2.46	1.20	0.57
FeO	11.18	10.52	9.62	10.03	13.94	7.24	9.41
MnO	0.17	0.18	0.16	0.15	0.25	0.10	0.13
MgO	7.15	6.67	7.38	8.43	5.66	3.82	7.78
CaO	10.03	11.45	11.67	9.95	10.37	8.82	9.13
Na_2O	1.44	2.00	1.19	2.00	1.74	2.55	1.61
K_2O	0.47	0.23	0.13	0.68	0.19	0.16	1.01
P_2O_5	0.18	0.12	0.22	0.24	0.14	0.22	0.32
LOI	1.14	1.60	1.36	1.23	1.21	0.79	1.75
Rest	0.31	0.28	0.31	0.36	0.48	0.13	0.34
Total	**99.87**	**99.96**	**100.02**	**99.79**	**100.09**	**99.88**	**99.91**
O=F,S,Cl	0.06	0.05	0.06	0.05	0.17	0.00	0.04
Total	**99.81**	**99.91**	**99.96**	**99.73**	**99.93**	**99.88**	**99.87**
Trace elements in parts per million							
Li	7	13	2	14	7	4	19
S	1170	1100	1190	1090	3320	60	740
Sc	39	45	41	33	46	24	32
V	270	327	255	208	457	142	173
Cr	187	195	108	498	13	27	451
Ni	111	72	123	174	43	44	94
Cu	94	125	172	62	74	110	26
Zn	103	109	109	103	135	60	103
Ga	18.1	16.6	18.0	15.8	17.9	18.7	17.0
Rb	18.5	7.0	1.0	18.0	4.0	1.5	50.0
Sr	193	181	245	182	153	204	201
Y	33.0	24.5	26.5	28.5	25.5	19.5	33.5
Zr	89	38	120	124	62	161	196
Nb	5.74	5.17	8.48	10.1	4.91	7.54	13.7
Ba	185	89	116	275	14	76	396
La	12.5	6.55	16.6	22.2	4.55	13.2	37.9
Ce	29.3	15.9	37.4	47.9	12.5	31.5	77.1
Pr	4.06	2.30	4.92	6.02	2.00	4.10	9.28
Nd	17.4	10.6	20.6	23.6	9.96	16.6	34.9
Sm	4.68	2.98	4.56	4.86	3.06	3.64	6.72
Eu	1.46	1.18	1.73	1.38	1.28	1.21	1.78
Gd	5.77	4.01	5.13	5.26	4.25	3.96	6.74
Tb	1.01	0.72	0.82	0.83	0.75	0.63	1.05
Dy	5.91	4.42	4.81	5.04	4.58	3.59	5.95
Ho	1.31	1.02	1.08	1.14	1.04	0.78	1.32
Er	3.75	2.90	3.05	3.13	2.93	2.18	3.79
Yb	3.08	2.58	2.63	2.89	2.59	1.87	3.36
Lu	0.45	0.38	0.40	0.44	0.40	0.27	0.5
Pb	7.0	2.0	4.0	6.0	4.0	0.5	12.00
Th	2.34	0.65	0.54	1.64	0.44	0.16	6.61
U	0.50	0.21	0.13	0.43	0.16	0.09	1.09
ε_{Ndi}	-1.2	1.4	-	-	3.5	0.5	-2.1
mg	51.0	49.4	53.7	57.9	38.4	45.0	58.3
Nb/La	0.5	0.8	0.5	0.5	1.1	0.6	0.4
Nb/Th	2.5	8.0	15.7	6.2	11.2	47.1	2.1
Ba/Nb	32.2	17.2	13.7	27.2	2.9	10.1	28.9
Sr/Nd	11.1	17.1	11.9	7.7	15.4	12.3	5.8
Ti/Zr	97.7	200.4	73.4	61.9	162.5	30.9	33.0

Table 11.1. (Cont.). Major and trace-element geochemistry and Nd isotopic data for melt-like mafic rocks from the East Kimberley.

Sample number	*94522081*	*94522287*	*94522172*	*93522014*	*93522021*	*83330081*	*83330074*
Intrusion	*Greenvale Fault*	*Mabel Downs West*	*Norton*	*Three Sisters*	*Robin Soak*	*Unnamed*	*dolerite ?Biscay Fm*
Group	*Corridor gabbro*	*Corridor gabbro*	*Tickalara Metamorph*	*Undivided gabbro*	*Undivided gabbro*		
Lithology	*Biotite melagabbro*	*Chilled magnetite gabbro*	*Metagabbro*	*Biotite quartz gabbro*	*Biotite quartz gabbro*	*Gabbro*	*Amphibol.*
Easting	*361930*	*404205*	*398174*	*346295*	*364582*	*395200*	*348300*
Northing	*8073884*	*8100958*	*8094102*	*8011535*	*8019328*	*8076100*	*7950300*
SiO_2	51.76	47.63	52.75	48.42	54.31	49.16	49.97
TiO_2	1.03	2.01	1.22	1.88	1.13	2.15	1.07
Al_2O_3	15.13	15.01	14.05	14.80	14.34	13.37	13.72
Fe_2O_3	1.31	1.54	0.29	1.38	1.03	2.76	1.90
FeO	8.11	12.09	12.24	11.46	8.79	11.07	9.71
MnO	0.14	0.18	0.19	0.17	0.14	0.18	0.14
MgO	8.24	7.00	6.59	6.93	6.15	5.26	7.03
CaO	9.69	10.00	10.75	10.30	8.82	9.02	11.51
Na_2O	1.87	1.98	0.58	1.88	2.21	2.46	1.85
K_2O	1.11	0.52	0.04	0.76	1.57	1.12	0.20
P_2O_5	0.15	0.41	0.11	0.40	0.21	0.31	0.10
LOI	1.02	1.27	1.21	1.12	1.02	2.25	1.92
Rest	0.25	0.28	0.28	0.40	0.32	0.28	0.33
Total	**99.81**	**99.92**	**100.30**	**99.90**	**100.04**	**99.39**	**99.45**
O=F,S,Cl	0.01	0.03	0.07	0.07	0.06	0.00	0.07
Total	**99.80**	**99.89**	**100.23**	**99.82**	**99.98**	**99.39**	**99.37**
Trace elements in parts per million							
Li	14	11	5	8	14	11	11
S	180	610	1470	1490	1110	-	1500
Sc	33	38	42	42	37	37	47
V	216	267	328	252	190	302	320
Cr	497	250	92	329	247	544	348
Ni	173	118	61	86	50	31	92
Cu	70	58	20	44	45	52	100
Zn	81	132	105	125	92	125	80
Ga	15.7	18.1	17.4	18.1	16.7	19.5	15.7
Rb	61.0	15.0	1.0	23.0	84.5	38.5	3.0
Sr	144	174	147	207	165	234	100
Y	26.0	31.5	28.5	42.0	35.5	31.0	24.0
Zr	105	114	63	177	139	149	64
Nb	6.15	11.0	4.60	15.3	11.0	13.4	2.91
Ba	197	306	25	342	312	366	37
La	20.1	21.0	5.80	35.9	30.9	23.4	5.20
Ce	42.0	45.7	15.7	79.1	65.7	51.8	12.7
Pr	5.14	5.96	2.36	10.2	7.92	6.74	1.90
Nd	19.5	24.0	10.9	39.7	29.7	26.7	9.22
Sm	4.08	5.14	3.20	7.90	6.02	5.86	2.58
Eu	1.11	1.78	1.00	2.12	1.45	1.80	0.99
Gd	4.57	5.70	4.40	8.11	6.28	6.14	3.61
Tb	0.77	0.93	0.80	1.31	1.05	0.98	0.65
Dy	4.51	5.50	4.94	7.24	6.01	5.61	4.00
Ho	1.01	1.24	1.12	1.64	1.38	1.23	0.94
Er	2.89	3.49	3.13	4.71	4.07	3.38	2.82
Yb	2.57	3.14	2.90	4.05	3.51	2.92	2.50
Lu	0.39	0.48	0.43	0.61	0.53	0.45	0.35
Pb	9.0	5.5	4.0	8.5	12.5	7.0	1.5
Th	7.12	1.61	0.59	1.74	10.20	3.85	0.77
U	1.70	0.39	0.86	0.42	2.80	0.99	0.19
ε_{Ndi}	-	-0.9	2.1	-1.3	-0.3	-0.1	4.5
mg	61.3	48.1	48.4	49.3	53.0	40.9	52.3
Nb/La	0.3	0.5	0.8	0.4	0.4	0.6	0.6
Nb/Th	0.9	6.8	7.8	8.8	1.1	3.5	3.8
Ba/Nb	32.0	27.8	5.4	22.4	28.4	27.3	12.7
Sr/Nd	7.4	7.3	13.5	5.2	5.6	8.8	10.9
Ti/Zr	58.8	105.7	116.1	63.9	48.7	86.5	100.2

92522073, sample PS-A13 has a slightly light-REE-enriched pattern and a strong Nb depletion, with Nb/La ~0.3. Since there is a lack of consistency between these two melt-like samples, it is difficult to determine the trace-element pattern of the original magma for the Panton intrusion. Nevertheless, we tend to think that the Panton intrusion probably had a parent magma with a flat light-REE pattern, Nb depletion and Th enrichment.

Group II

An olivine gabbronorite sample (92522461) from the 1857±2 Ma Springvale intrusion and a 'chilled' biotite gabbro sample (92522533) from the Wilagee intrusion show strong depletion of P relative to Nd, Ti relative to Sm, and Nb relative to La, and enrichment of Th on the spidergram plot. Both have a Nb/La ratio of 0.4 and a Nb/Th ratio of 2.3. These geochemical features can be produced by processes during subduction and/or crustal contamination (e.g. Sun & McDonough 1989). The enriched component (Ba, Th, U, light REE), in addition to crustal contamination, could have been introduced through contemporaneous subduction or subduction processes during an earlier phase of evolution of the region and was incorporated later into the lithospheric mantle source of the magma.

Group III

Three biotite gabbro samples (83330052, 92522512, 92522514) from the 1855±2 Ma Toby intrusion have very similar spidergram patterns, with the exception of Th (Fig. 11.2). As mentioned in the analytical methods section, we are confident that the Th data obtained by ICP-MS are accurate and, therefore, we suspect the variation in Th is likely to be caused by variable mobility during alteration and/or metamorphism. As most samples from the Toby intrusion have Th concentrations between 3 and 5 ppm (total 10 samples, see Appendix 2), the low Th concentration for sample 83330052 (0.84 ppm) is interpreted as being due to Th loss. The Nb/Th ratios of 3.0 and 1.5 for 92522512 and 92522514 are considered to be close to the magmatic value. Accordingly, the Toby intrusion samples have similar spidergram patterns to the group II samples, suggesting similar petrogenesis and, thus, they may be genetically related. This suggestion is consistent with the group II Wilagee body being spatially close to the Toby intrusion, i.e. both intrusions are separated by a fault (see Fig. 5.15). The Wilagee and Toby intrusions have similar initial ε_{Nd} values of about –1 (Table 11.2), consistent with the two intrusions being derived from the same parent magma.

Group IV

Three magnetite gabbro samples (92522433, 92522437, 93522001) in Table 11.1 from the Wild Dog Creek intrusion show considerable geochemical variation on the spidergram plot (Fig. 11.2), especially in terms of Nb/Th (2.5–17.4). Samples 93522001 (a 'chilled' phase) and 92522433 have low Zr content (38 and 49 ppm) and unusually high Ti/Zr (200 and 146) for mafic magmas. These features, along with high Nb/La (0.8 and 0.7) and Nb/Th (8.0 and 17.4), suggest a significant cumulus component in these samples, such as ilmenite rich in Ti and containing some Nb, rather than representing a melt composition. Sample 92522433 has a heavy-REE depleted pattern (Fig. 11.3) that is quite different from the other samples studied. Sample 92522437 has a melt-like composition that has much higher Zr (89 ppm), lower Ti/Zr = 98, Nb/La = 0.5, and Nb/Th = 2.5, and a spidergram pattern similar to groups II and III. Thus, sample 92522437 is probably more representative of the melt composition of the group IV intrusions than the other two samples. Samples 93522001 and 92522437 have different initial ε_{Nd} values (+1.4 and –1.2, respectively; see *Neodymium isotope data* section). They are located ~25 km from each other (see Chapter 5; Fig. 11.1) and their contrasting isotopic and trace-element compositions suggest they are unlikely to be genetically related.

Group V

A 'chilled' magnetite gabbro sample (93522153) from the Fletcher Creek intrusion and a gabbronorite (94522065) intruding the upper part of the Spring Creek intrusion have, with the exception of Th, similar spidergram patterns to rocks from groups II–IV described above (Fig. 11.2). The Fletcher Creek 'chilled' sample shows strong Th depletion, like the other samples of this study. A Spring Creek gabbro (94522050), reported in Appendix 2 with 7.1% MgO and high TiO_2 (1.48%), has considerably higher Nb (20 ppm), La (47 ppm), Th (5 ppm), and Zr (204 ppm) than the younger gabbronorite sample (94522065), and slightly lower Nb/Th (4.0 v. 6.2; Table 11.1). Both these samples may retain their magmatic Nb/Th values. Olivine gabbro (94522127) from the Keller Creek intrusion has low MgO (5.7%) and Al_2O_3 (13.3%), high S (3320 ppm), and unusually low Cr (13 ppm) compared to the two other Keller Creek olivine gabbro samples (94522089, 94522126; see Appendix 2). It has a very flat spidergram pattern with some depletion of Zr (62 ppm)—but still much higher than the other two samples (12 and 14 ppm)—and a slight positive Eu anomaly. As this sample is highly fractionated, it is expected to have experienced a considerable amount of plagioclase separation and to possess a negative Eu anomaly. Thus, either plagioclase cumulus crystallisation or some element mobility may have modified its trace-element pattern. The spidergram pattern of this Keller Creek sample is very similar to that of the Norton gabbro discussed below. Interestingly, the mafic rocks from both these intrusions have the highest initial ε_{Nd} values (+3.5 and +2.1) of all the samples studied. The chemical and Nd isotope data indicate that the Keller Creek intrusion probably belongs to the Norton metagabbro group, which is part of the Tickalara Metamorphics and, hence, is older (>1850 Ma) than the 1845 Ma age assigned to it in Chapter 5. The Sally Malay intrusion (1844±3 Ma), which contains significant amounts of Ni–Cu–Co sulphide mineralisation along its basal contact, is the type example of group V. Characterisation of this intrusion is not possible, since no chilled or fine-grained melt-like samples are available for analysis. Re–Os and Sm–Nd isotopic systematics on coarse-grained cumulate rocks from the Sally Malay intrusion are described by Sproule et al. in Chapter 12.

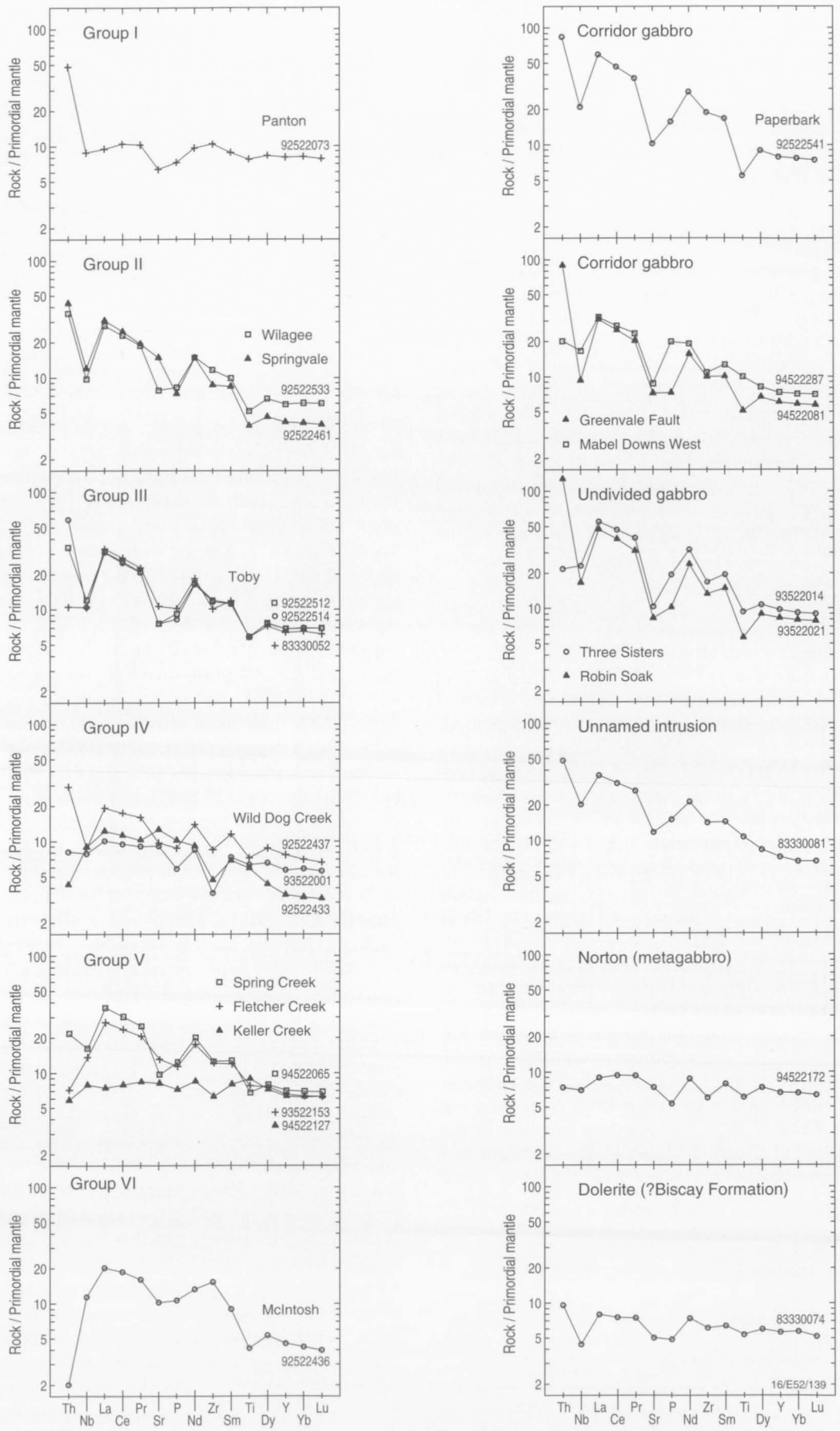


Figure 11.2. Mantle-normalised trace-element diagrams of melt-like samples from the East Kimberley mafic–ultramafic intrusions. The normalisation values are from McDonough & Sun (1995).

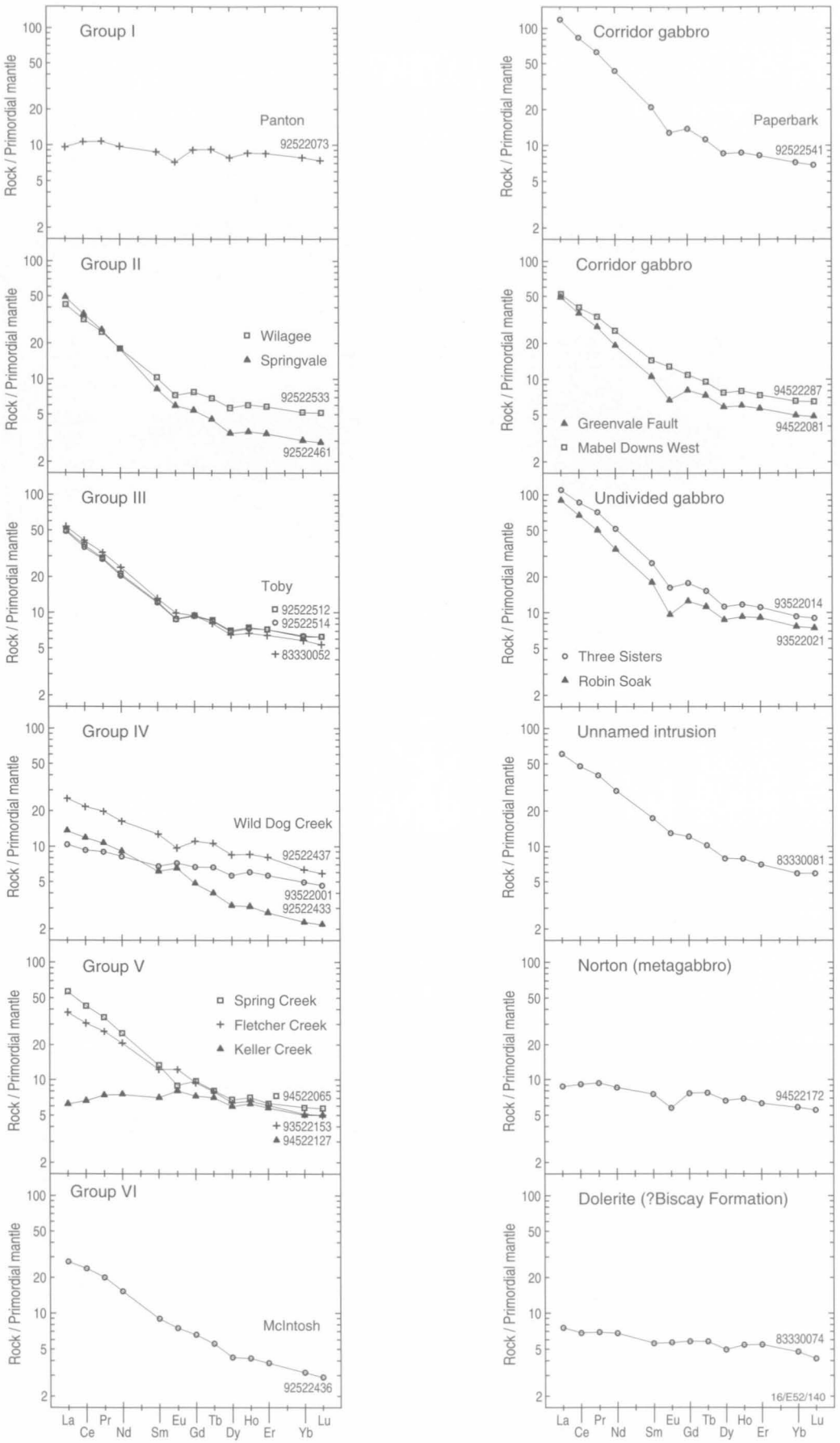


Figure 11.3. Chondrite-normalised rare earth element diagrams of melt-like samples from the East Kimberley mafic–ultramafic intrusions.

Table 11.2. Samarium and Nd whole rock and mineral data for samples from the East Kimberley.

Sample	*Intrusion (group)*	*Sm (ppm)*	*Nd (ppm)*	*$^{147}Sm/^{144}Nd$*	*$^{143}Nd/^{144}Nd$*	*±2σ*	*T(Ma)*	*ε_{Ndi}*	*T_{DM}*	*T (2-stage)*
92522073	Panton (I)	3.39	10.90	0.1880	0.512563	5	1856	0.4		
92522461	Springvale (II)	3.22	17.02	0.1144	0.511634	6	1857	-0.2		
92522533	Wilagee (II)	4.52	20.57	0.1328	0.511799	6	1857	-1.4		
83330052	Toby (III)	4.69	21.97	0.1292	0.511766	14	1855	-1.2		
83330052	Toby, clinopyroxene (III)	5.35	17.18	0.1884	0.512501	14	1855	-0.9		
83330052	Toby, plagioclase (III)	0.68	5.80	0.0710	0.511088	18	1855	-0.5		
92522437	Wild Dog Creek (IV)	4.66	16.84	0.1675	0.512236	8	1845	-1.2		
93522001	Wild Dog Creek (IV)	2.85	9.87	0.1744	0.512449	6	1845	1.4		
94522127	Keller Creek (V)	3.02	9.55	0.1911	0.512761	7	1850	3.5		
83330043	McIntosh (VI)	0.54	2.57	0.1272	0.511875	20	1830	1.2		
92522436	McIntosh (VI)	3.60	16.21	0.1344	0.511924	7	1830	0.5		
92522541	Paperbark (Corridor gabbro)	6.91	34.36	0.1215	0.511638	6	1830	-2.1		
94522287	Mabel Downs West (Corridor gabbro)	4.65	21.18	0.1328	0.511834	6	1830	-0.9		
94522172	Norton (Tickalara Metamorphics)	3.26	10.68	0.1844	0.512607	6	1850	2.1		
93522014	Three Sisters (Undivided gabbro)	7.14	34.74	0.1243	0.51171	6	1830	-1.3		
93522021	Robin Soak (Undivided gabbro)	6.26	29.69	0.1274	0.511801	7	1830	-0.3		
83330081	Unnamed	5.90	26.70	0.1336	0.511877	16	1845	-0.1		
83330030	Unnamed	2.61	9.42	0.1674	0.512363	20	1830	1.3		
83330085	Unnamed	3.00	11.68	0.1555	0.512171	7	1845	0.4		
	Other rock types									
83330074	Dolerite (?Biscay Formation)	2.47	8.52	0.1751	0.512614	8	1880	4.5		
83330072	Greywacke (Biscay Formation)	6.68	36.09	0.1120	0.511361	24	1880	-4.7	2682	2678
87598014	Greywacke (Olympio Formation)	4.40	24.60	0.1082	0.511333	6	1870	-4.5	2628	2651
83330014	Granite (Paperbark supersuite)	8.74	42.15	0.1254	0.511624	16	1850	-3.1	2639	2531
93526027	Tonalite (Dougalls Tonalite)	3.24	19.63	0.0997	0.511509	6	1850	0.8	2201	2240
93526003	Granodiorite (Mabel Downs Tonalite)	5.70	31.88	0.1080	0.511589	6	1840	0.3	2258	2271
51706	Tonalite (Sally Downs Tonalite)	3.90	21.70	0.1083	0.511525	20	1830	-1.2	2356	2371

$\varepsilon_{Ndi} = 10^4[(^{143}Nd/^{144}Nd_{sample}/^{143}Nd/^{144}Nd_{CHUR})-1]$ where $^{143}Nd/^{144}Nd_{CHUR} = 0.512653 - 0.1967(e^{\lambda t}-1)$, t = emplacement age of the intrusion and $\lambda = 6.54 \times 10^{-12}$ yr^{-1}.

T_{DM} = depleted mantle model age with mantle depletion beginning at 4.56 Ga (e.g. Sun et al. 1995).

T (2-stage) = Two-stage model age assuming $^{147}Sm/^{144}Nd = 0.11$ in the source rocks (e.g. Page & Sun 1998).

Group VI

A 'chilled' gabbro sample (92522436) from the 1830±3 Ma McIntosh intrusion has a low MgO content (3.8%), suggesting a highly fractionated magma, high Al_2O_3 (17.2%), low abundances of heavy REE and Ti, severe Th depletion, and a positive Zr anomaly on the spidergram plot (Fig. 11.2). These features have been confirmed by repeat ICP-MS analyses at the University of Queensland (courtesy of Dr. Yaoling Niu). The very low Th of the McIntosh sample again suggests Th loss by secondary mobility during post-magmatic processes. It is possible that as with some other 'chilled' rocks in this study, sample 92522436 also contains a cumulus component, so does not accurately represent a melt composition. The 'chilled' microgabbronorite (8.09% MgO, 0.89% TiO_2) from the contact of the McIntosh intrusion reported in Mathison & Hamlyn (1987; Table 8) may be a candidate for the melt composition. In this case, its low abundance of P_2O_5 (0.08%), comparable to many mid-ocean ridge basalts (MORB) and arc tholeiites, suggests that this melt was generated by similar degrees of mantle melting to MORB and arc tholeiites. Another 'chilled' olivine gabbro sample (92522321 in Appendix 2) from this intrusion has major element abundances (MgO = 9.99%, TiO_2 = 0.67%, P_2O_5 = 0.05%) similar to the Mathison & Hamlyn (1987) sample. However, it has very low Zr (18 ppm), indicating it is likely to contain a significant component of cumulus minerals and, therefore, it does not represent a melt composition. For the same reason, we suggest this may also be the case for the 'chilled margin' sample of Mathison & Hamlyn (1987).

Corridor gabbro

In contrast to groups I–VI, a biotite quartz gabbronorite sample (92522541) from the Paperbark intrusion has a distinctive spidergram pattern, with enrichment of light REE, Ba, and Th, and marked depletion of Nb, Sr, P, and Ti (Fig. 11.2). In a later section it is suggested that involvement of crustal components through melting of subduction-modified mantle sources and/or crustal contamination could be important in generating this trace-element pattern signature. Sample 92522541 also has the lowest initial ε_{Nd} (–2.1) documented in this study. A chilled magnetite gabbro sample (94522287) from the ?post-1830 Ma Mabel Downs West (Corridor gabbro) intrusion has 7.0% MgO, is enriched in light REE with Nb/La = 0.52, and shows no evidence of P and Ti depletion on the spidergram (Fig. 11.2). It is possible that the high Ti content (TiO_2 = 2.01%) is partly due to the presence of Ti–Fe magnetite, which can also lead to an increase in Nb/La. The P content of this sample is twice that of other similar samples (e.g. 94522283 in Appendix 2) from this intrusion. The possibility of cumulus apatite in sample 94522287 may account for the high P. The high Nb/Th ratio of this sample (6.8) is likely to be related to the Th mobility problem discussed above. XRF data (see Appendix 2) for a large proportion of the Corridor gabbro samples generally give Nb/Th values a factor of two lower. A biotite gabbro sample (94522081) from the Greenvale Fault intrusion has very high Rb (61 ppm), Th (7.1 ppm), and U (1.7 ppm), and very low Nb/Th (~1.0). This strongly enriched Rb, Th, and U character is shared by two other Greenvale Fault samples analysed by XRF (see Appendix 2). Field evidence indicates that magma mixing occurred between the Greenvale Fault intrusion and partial melts of 1865–1850 Ma granites of the Bow River batholith. Thus, enrichment of Rb, Th, and U in 94522081 could be related to assimilation of country rock and/or its melting products.

Undivided gabbro

The ?post-1830 Ma Robin Soak and Three Sisters (Fig. 11.1) mafic intrusions have not been assigned to the classification scheme of East Kimberley intrusions by Hoatson (see Chapter 5). The Robin Soak intrusion shows field evidence of in-situ melting, contamination of granite country rocks and hybridisation features similar to the intrusions of the Corridor gabbro intrusions. Also, biotite quartz gabbro (93522021: see Appendix 2) from the Robin Soak intrusion has a very similar spidergram pattern to that of biotite quartz gabbronorite from the Corridor gabbro intrusions (Fig. 11.2). The Robin Soak intrusion can, therefore, be tentatively classified as a Corridor group intrusion on the basis of both field relationships and trace-element geochemistry. When compared to the Robin Soak sample, the biotite quartz gabbro (93522014) from the Three Sisters intrusion has higher Ti and P, but much lower Th (1.74 v. 10.2 ppm) and lower SiO_2 (48.4 v. 54.3%). Its low Th is likely to be due to mobilisation of Th during alteration and metamorphism, like some other samples documented in this study.

Unnamed intrusion

A gabbro sample (83330081), previously studied by Sun et al. (1991), has a similar spidergram pattern (Fig. 11.2), except for Th, to the nearby group V gabbro that intrudes the Spring Creek intrusion (94522065). These two gabbros may be genetically related.

Mafic intrusions within the Tickalara Metamorphics

The Norton metagabbro intrusion is a mafic granulite sill of the Tickalara Metamorphics which that was probably intruded before a major metamorphic event at ~1850 Ma. A representative metagabbro sample (94522172) has a flat spidergram pattern, showing relative depletion of P, Zr, and Ti, and is very similar to that of the Keller Creek sample (Fig. 11.2) described above. This distinctive flat pattern, which is shared by other Norton metagabbro samples analysed by XRF (see Appendix 2), may in part be due to the presence of some cumulus minerals. XRF data show that another Norton sample (94522168, Appendix 2) has a geochemical pattern that reflects the presence of Ti–Fe oxides; as it has very high FeO (19.6%), TiO_2 (2.67%), and V (1009 ppm). This sample also has high Nb (10 ppm) and unusually high Nb/La (1.7), suggesting Nb enrichment in the oxide phase.

Dolerite in the ?Biscay Formation (~1880 Ma)

An amphibolite sample (83330074) previously studied by Sun et al. (1991) and considered to be part of the 'Woodward Dolerite' occurs about 40 km south of Halls Creek between the Halls Creek Fault and Angelo Fault. Recent mapping by AGSO and the Geological Survey of Western Australia (e.g. Blake et al., 1997, 1999) has confirmed that many of the mafic rocks previously assigned to the Woodward Dolerite belong to the Biscay Formation of the Halls Creek Group. Sample 83330074 has low abundances of Ti, P, Th, Ba, REE, and Y and a flat spidergram pattern with depletion of Nb, Sr, and P

(Fig. 11.2). Sun et al. (1991) suggested that the amphibolite was generated by large degrees of mantle melting in an ensialic intraplate setting with strong crustal thinning.

Discussion of geochemical results

Some general points can be made about the geochemical features of the melt-like mafic and ultramafic rocks in the East Kimberley.

1. Tectonic–trace-element discrimination diagrams provide little help in classifying the East Kimberley mafic magmas, since they fall within several compositional fields. On a Ti–Zr–Y diagram (Fig. 11.4), the samples fall into the low-potassium tholeiite, MORB, and calcalkaline basalt fields, whereas on a Nb–Zr–Y diagram (Fig. 11.5) they fall in the MORB, within plate tholeiite, and arc basalt fields. On the Ti–V plot (not shown) of Shervais (1982), most samples fall in the field of MORB and near axis seamount, with some overlap with the field of 'island arc tholeiite': two of the Panton melt-like samples fall within the island arc tholeiite field. These discrimination plots are not very useful unless they can be effectively combined with other geological and mineralogical criteria (e.g. Pearce 1987). Although Th is generally considered to be an 'immobile' element during secondary processes, this study has shown that there appears to have been significant movement of Th during hydrothermal alteration and metamorphism. Strong enrichment of Th relative to Nb has been observed in many East Kimberley samples, resulting in Nb/Th values as low as 1.0. In comparison, the Nb/Th value for the primitive mantle is 8.4, for the upper and lower continental crust, ~1.3 and ~4.5, respectively, and for MORB, ~20 (Sun & McDonough 1989, Rudnick & Fountain 1995, Plank & Langmuir 1998). This suggests that the magma sources of the East Kimberley intrusions are enriched in Th, induced by subduction-related processes, and/or the parental magma has assimilated material en route through the middle and upper

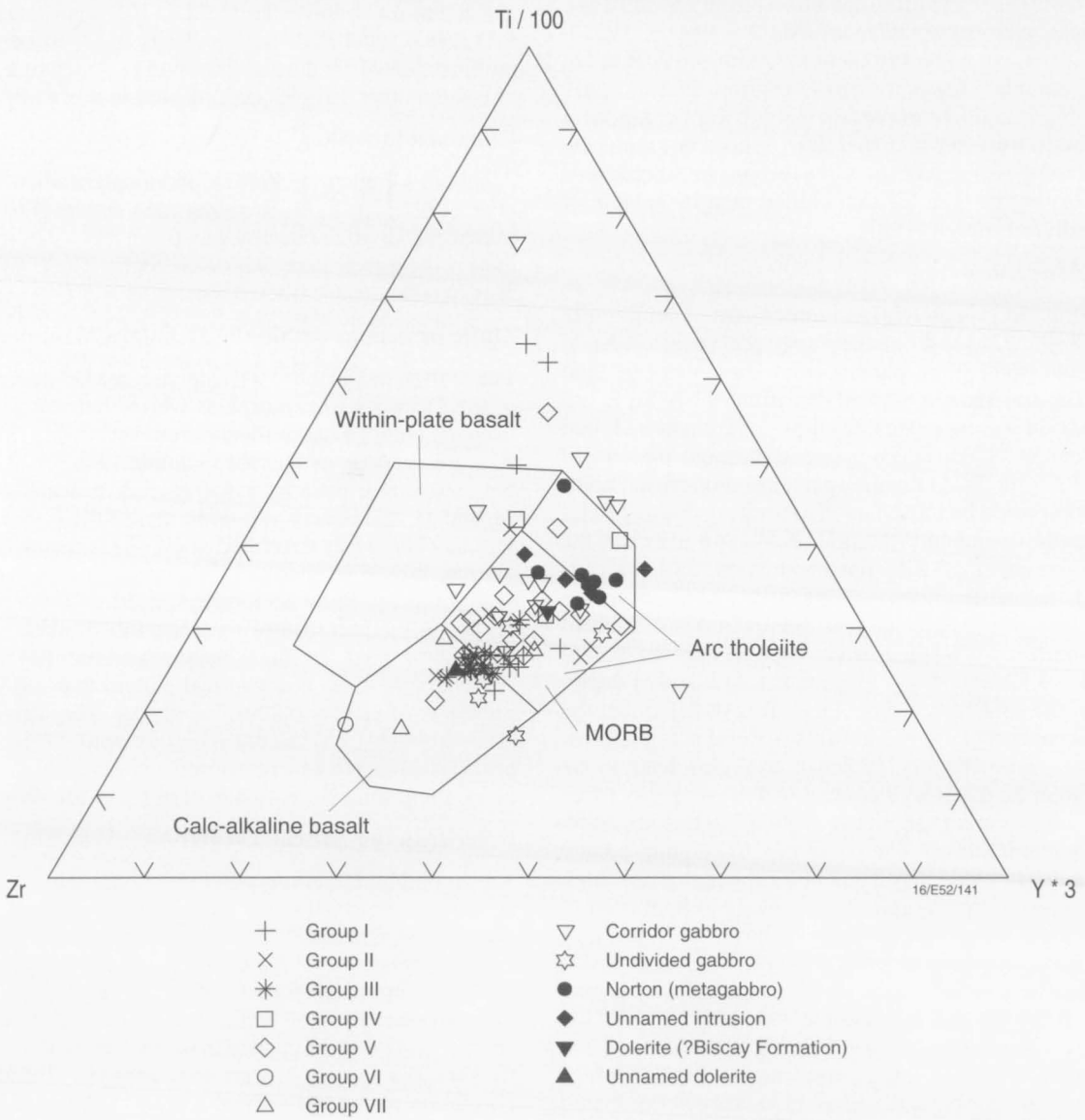


Figure 11.4. Ti–Zr–Y discrimination diagram for East Kimberley samples with Y ≥10 ppm and Zr ≥20 ppm. Fields for different types of basalt are from Pearce & Cann (1973).

crust. It is important to note that Th enrichment has often been observed in post-collisional, intraplate basalts derived from melting of lithospheric mantle previously modified by subduction zone enrichment processes (e.g. Sun & McDonough 1989). Thus, it is reasonable to conclude that the mantle source regions for most of the East Kimberley intrusions studied contain a 'subduction zone' component. However, this feature does not necessarily mean a general subduction environment for the generation of these magmas. Additional problems using tectonic–trace-element discrimination diagrams relate to the mobility of Th and the enrichment of Nb and Ti through the crystallisation of Ti–Fe oxides. The apparent mobile behaviour of Th in some of the samples in this study warrants further investigation.

2. Except for an olivine gabbronorite sample from the Springvale intrusion, which has high Al_2O_3 (17.7%) and, therefore, may contain a considerable amount of cumulus plagioclase, Sr depletion relative to Nd is a general feature of the melt-like samples (Table 11.1 and Appendix 2). The generally low Sr/Nd (less than the primitive mantle value of 15.6 for all but two samples) is distinctly different from that of island arc basalts, which generally have considerably higher Sr/Nd (e.g. 40). Higher Sr/Nd in island arc basalts is a result of addition of mobile alkali and alkaline earth elements from dehydration of the subducted oceanic crust during island arc magma generation. Nevertheless, it is possible that the observed Sr/Nd values are not a primary feature of the parent magmas of the East Kimberley intrusions, as Sr is mobile during alteration and metamorphism. Low Sr/Nd can also result from plagioclase fractionation, which reduces Sr in the magma, or from involvement of felsic crustal material in magma generation through sediment subduction or crustal contamination.
3. The geochemical and isotopic findings from this study generally support Hoatson's classification of the intrusions on the basis of field and petrological evidence (see Chapter 5). However, there are two examples where his classification is not consistent

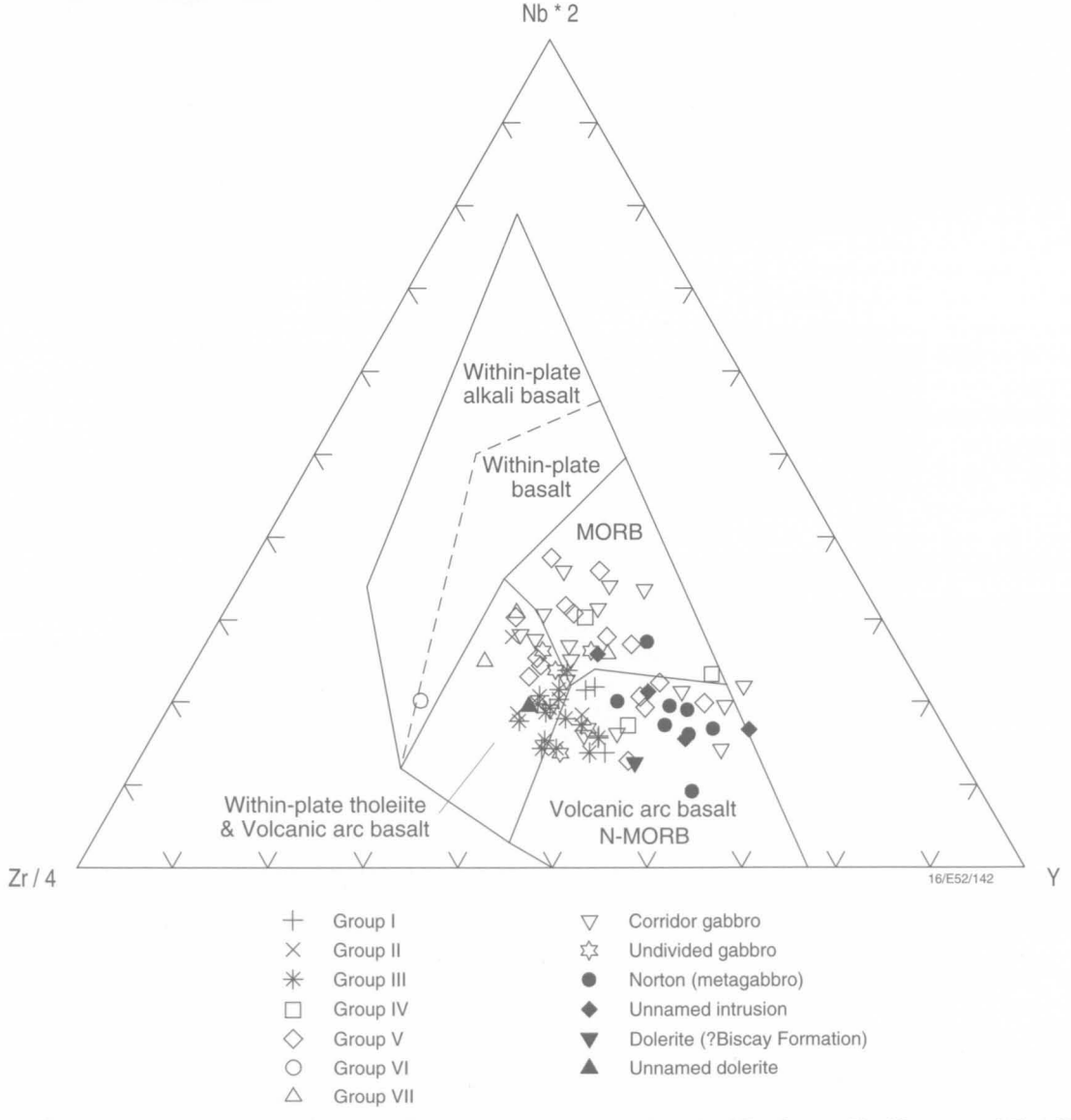


Figure 11.5. Nb–Zr–Y discrimination diagram for East Kimberley samples with Nb ≥2 ppm, Y ≥10 ppm and Zr ≥20 ppm. Fields for different types of basalt are from Meschede (1986).

with the data presented here. The first example concerns the strongly differentiated group II Wilagee mafic–ultramafic intrusion, which is separated by a fault from the more homogeneous group III Toby mafic intrusion. The geochemical and Nd isotope data (Tables 11.1 and 11.2) indicate that both intrusions are likely to be derived from the same parent magma. The second example concerns the group V Keller Creek intrusion. Its spidergram pattern and initial ε_{Nd} value (discussed below) are very similar to that of Norton metagabbro, indicating that the Keller Creek intrusion may belong to the Norton metagabbro group in the Tickalara Metamorphics and, therefore, be older than the currently assigned age of 1845 Ma for the group V intrusions. This may also be the case for the group V Corkwood mafic intrusion, described in Chapter 5, which has a very similar geological setting to the Keller Creek intrusion. Another point relating to the classification of the intrusions concerns two small unnamed intrusions (e.g. samples 8333081 and 8333085 on Fig. 11.1) that have similar geochemical compositions to the nearby Fletcher Creek intrusion. It can be suggested that all these intrusions are likely to be genetically related. In addition, the previously unassigned Robin Soak intrusion can, on the basis of field and geochemical evidence, be classified as a Corridor group intrusion.

4. A group of earlier intrusions in the central zone, including Panton (1856 Ma), Norton (pre-1850 Ma), and Keller Creek (probably of similar age to Norton) have flat spidergram and heavy-REE patterns and low abundance of incompatible elements. They share similar trace-element abundance patterns to metabasalts in the Tickalara Metamorphics (e.g. 94522216 and 94522320 in Appendix 2, and in Sheppard et al. 1999). They were generated by large degrees of mantle melting under low-pressure environments (see a later section on the composition of parent magma).
5. Mafic intrusions, ranging from 1855 Ma (Toby intrusion in the western zone) to post-1830 Ma (e.g. Three Sisters intrusion), have light-REE enriched patterns and higher abundances of incompatible trace elements. They show strong depletion of Nb and enrichment of Th (and Ba, not shown) on the spidergram plots (Fig. 11.2). The Paperbark intrusion has the same enriched spidergram pattern as the Three Sisters intrusion. Two representative samples of the Paperbark (Corridor gabbro) and Three Sisters intrusions with 7.8% and 6.9% MgO (Table 11.1) have relatively high Nb (~15 ppm), La (~35 ppm), and Zr (~180-200 ppm).

Neodymium isotope data

Sm and Nd whole-rock and mineral data and Nd isotopic data for this study are summarised in Table 11.2. Also included in this table are six 1983 samples that were published by Sun et al. (1991). $^{143}Nd/^{144}Nd$ values of these samples have been normalised using $^{146}Nd/^{144}Nd = 0.7219$ and checked by two new analyses of 83330074 and 83330085. The repeat analyses were found to be within +0.3 and –0.6 ε_{Nd} units, respectively, of the 1991 published data. Since the 1991 data have an uncertainty of around ±0.4 ε_{Nd} units and the new data have an uncertainty of ±0.2 ε_{Nd} units, we consider that the agreement is reasonable.

The initial ε_{Nd} values for the mafic and mafic–ultramafic intrusions (Table 11.2) range from +3.5 (Keller Creek intrusion) to –2.1 (Paperbark intrusion, Corridor gabbro). The age of these intrusions (~1865 and 1830 Ma) has only a minor effect on the initial ε_{Nd} values calculated to the same age. The Keller Creek sample is an olivine gabbro with low incompatible trace-element abundances and a flat spidergram pattern, whereas the Paperbark (Corridor gabbro) sample is a biotite quartz gabbronorite showing an enriched incompatible trace-element signature partially imposed by crustal contamination. Most other samples in Table 11.2 have initial ε_{Nd} values ranging from –1.4 (Wilagee) to +1.4 (Wild Dog Creek). In addition, Sproule et al. in Chapter 12 report initial ε_{Nd} values ranging from –0.2 to +0.7 for five samples from the Sally Malay intrusion, and from –1.1 to +0.3 for eight samples from the Panton intrusion.

The Keller Creek and Norton samples have high initial ε_{Nd} values, +3.5 and +2.1, respectively, but these values are somewhat lower than the value +4.5 for the ~1880 Ma dolerite in the ?Biscay Formation. A value +4.5 at 1880 Ma is close to that for depleted mantle at that time. The higher initial ε_{Nd} values for the Keller Creek and Norton samples relative to the other intrusions suggest they were less affected by continental felsic components either in the form of crustal contamination or sediment subduction. It is interesting to note that the Keller Creek and Norton intrusions were emplaced at deeper crustal levels (~20 km) than the other East Kimberley intrusions further south (see Chapter 9) and, apparently, were the least contaminated.

The only Panton intrusion sample we studied has a higher initial ε_{Nd} value (+0.4) than the initial value (-0.3) calculated from the whole-rock isochron (when normalised to the same standard value) reported by Sproule et al. in Chapter 12. However, it is within the range of variation (–1.1 to +0.4) calculated for individual samples.

The 'chilled' Wild Dog Creek magnetite quartz gabbro sample (92522001) has an initial ε_{Nd} value, +1.4, which is considerably higher than –1.2, the value for the melt-like gabbronorite sample (92522437). As discussed above, these samples are unlikely to be genetically related.

Mantle-source character versus crustal contamination

It is likely that parent magmas of many East Kimberley intrusions were contaminated by continental crust. This could have occurred in different places during their ascent from the mantle through the lower crust to their emplacement in chambers in the middle to upper crust. Three of the largest intrusions, Panton, Springvale, and Toby, were emplaced at around 1855 Ma (Page et al.

1995, see Chapter 6), contemporaneously with various granite plutons of the Bow River Batholith (see Chapter 3). The intimate spatial and temporal relationships of these intrusions in the HCO are highlighted by the widespread occurrence of hybrid rock types resulting from the mingling of felsic and mafic magmas (Blake & Hoatson 1993, Sheppard 1996, see Chapter 5). Contamination varies from the localised occurrence of olivine-poor orthopyroxene-bearing rocks (norite and harzburgite), such as near the basal contacts of Sally Malay and Panton, to the more contaminated and homogeneous orthopyroxene-bearing hybrid rocks that constitute the Corridor gabbro. The occurrence of these orthopyroxene-bearing rocks testifies to the more siliceous and contaminated character of the magma at the margins of the intrusions. Mixing 15% of felsic melt containing 70% SiO_2 with 85% of mafic melt containing 50% SiO_2 will produce a melt with 53% SiO_2. If the felsic component is increased to 30%, the SiO_2 content of the mixing product will increase by 6%, i.e. to 56%, which is enough to promote the crystallisation of orthopyroxene. Results of an Os isotopic study (see Chapter 12) support our suggestion that the basal norite of the Sally Malay intrusion resulted from significant crustal contamination, whereas the Panton intrusion suffered relatively less crustal contamination. It is intriguing to note that the more crustally contaminated Sally Malay intrusion samples, as indicated by high initial Os isotope values, have initial ε_{Nd} values slightly higher than those for the samples from the Panton intrusion (+0.7 to –0.2 compared to +0.3 to –1.1, respectively, see Chapter 12). The Nd data suggest slightly less contamination by felsic crust for the Panton intrusion. The lack of correlation between Nd and Os isotopes could be due to:

- differences in Os and Nd contents and isotopic compositions of the parent magmas of Sally Malay and Panton;
- the composition of the contaminants, e.g. Archaean crust in the western zone and Palaeoproterozoic crust in the central zone of the HCO ;
- decoupling of Os and Nd during crustal contamination and the preference of Os for immiscible sulphide; and/or
- magma chamber processes (see Chapter 12 for a more detailed discussion).

The measured initial ε_{Nd} of a mantle-derived melt that has been contaminated by continental crust depends on three major factors: 1, the ε_{Nd} values of the mantle and crust end members (ε_{Ndm} and ε_{Ndc}); 2, the abundance ratio of Nd in the contaminant to the mantle-derived magma (β); and 3, the relative amount of the contaminant to the parent magma. The assumption that the

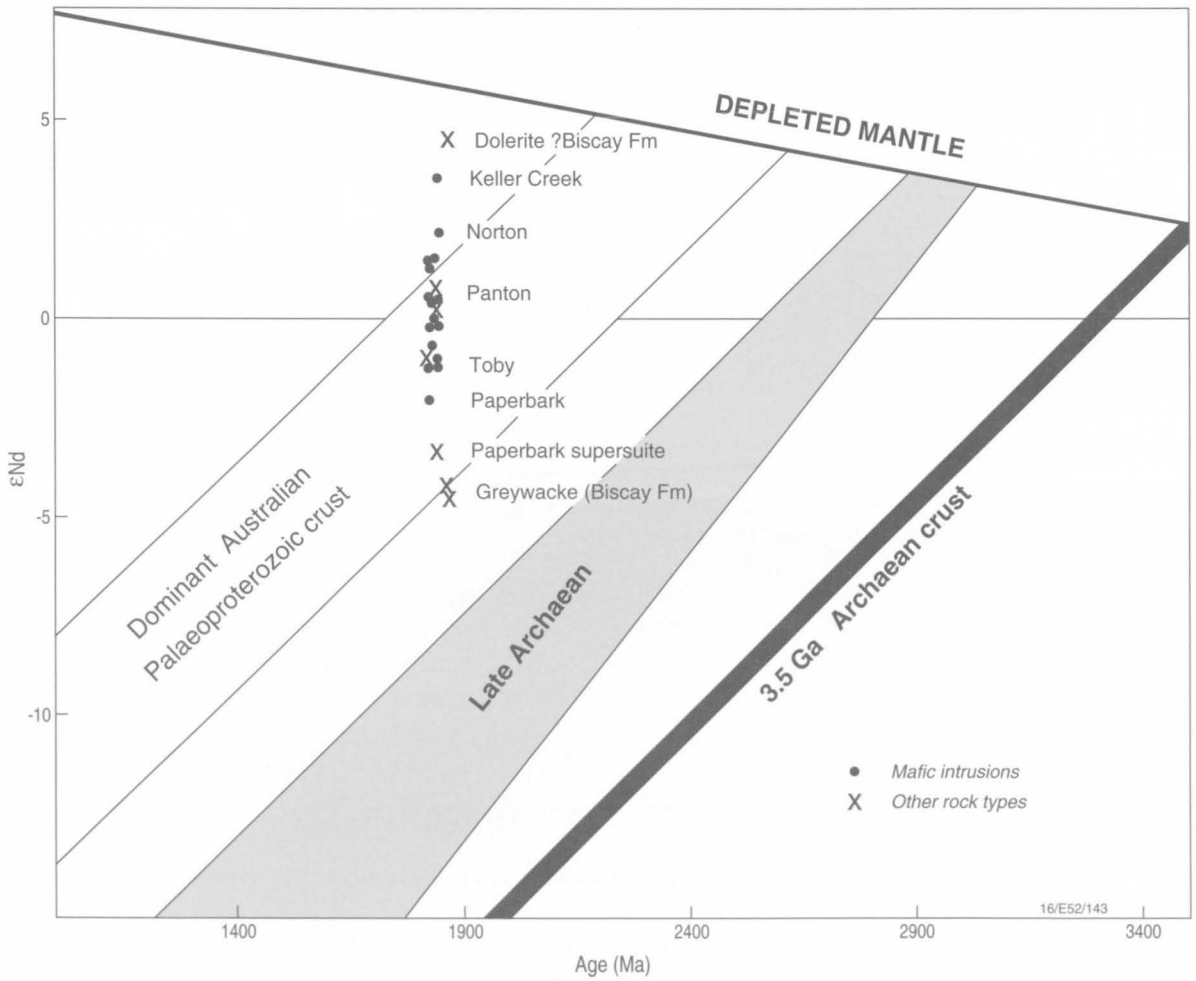


Figure 11.6. Plot of initial ε_{Nd} values versus geological age for samples of mafic–ultramafic intrusions and other rocks from the East Kimberley, and fields for dominant Australian Palaeoproterozoic and Archaean rocks.

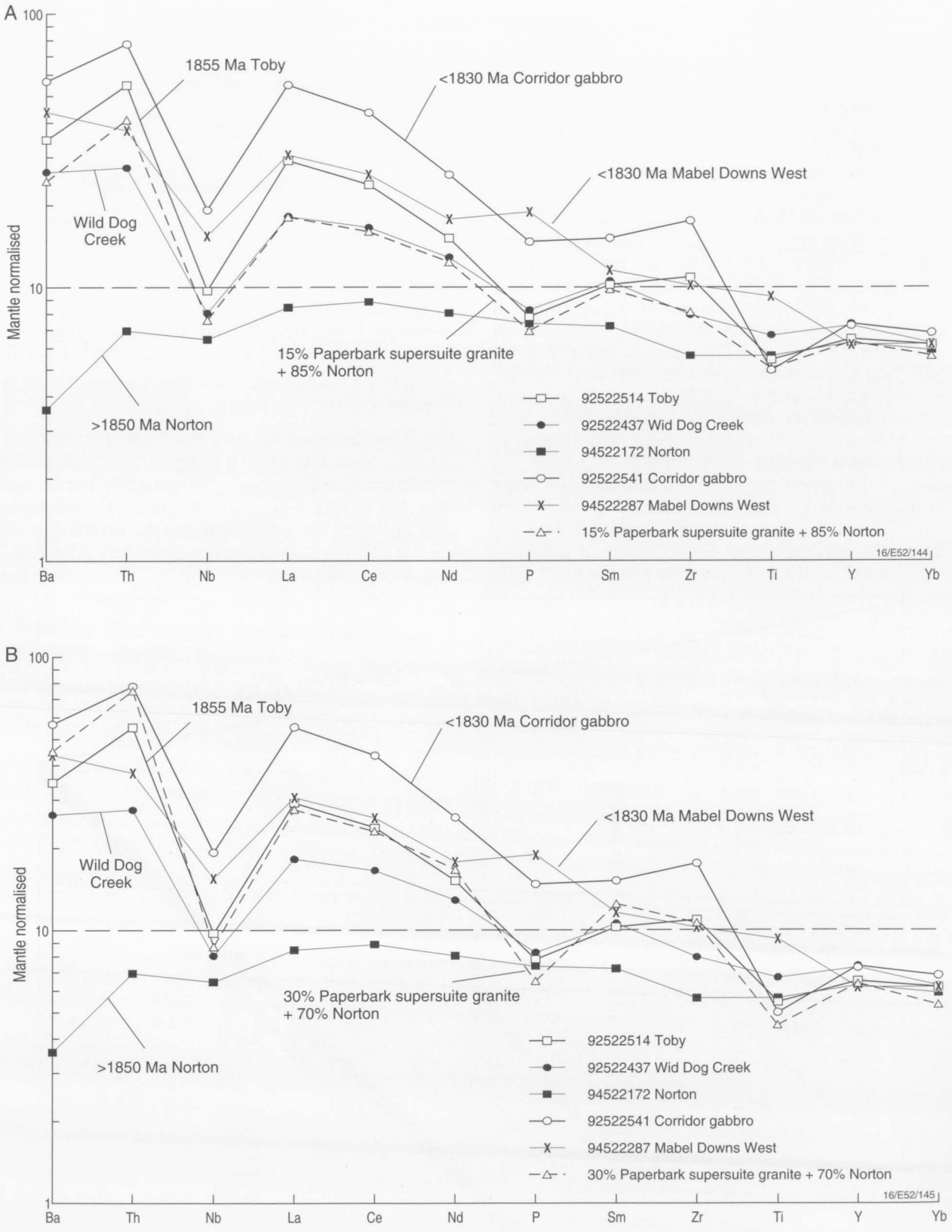
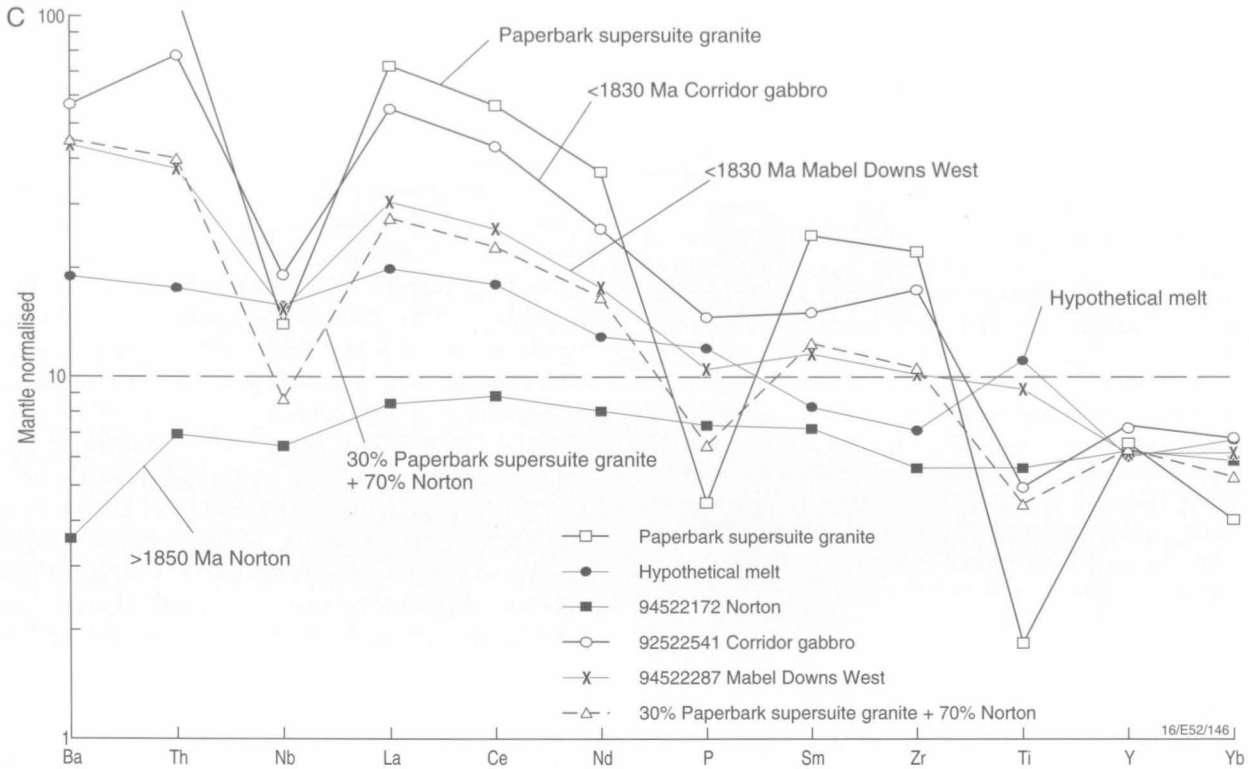
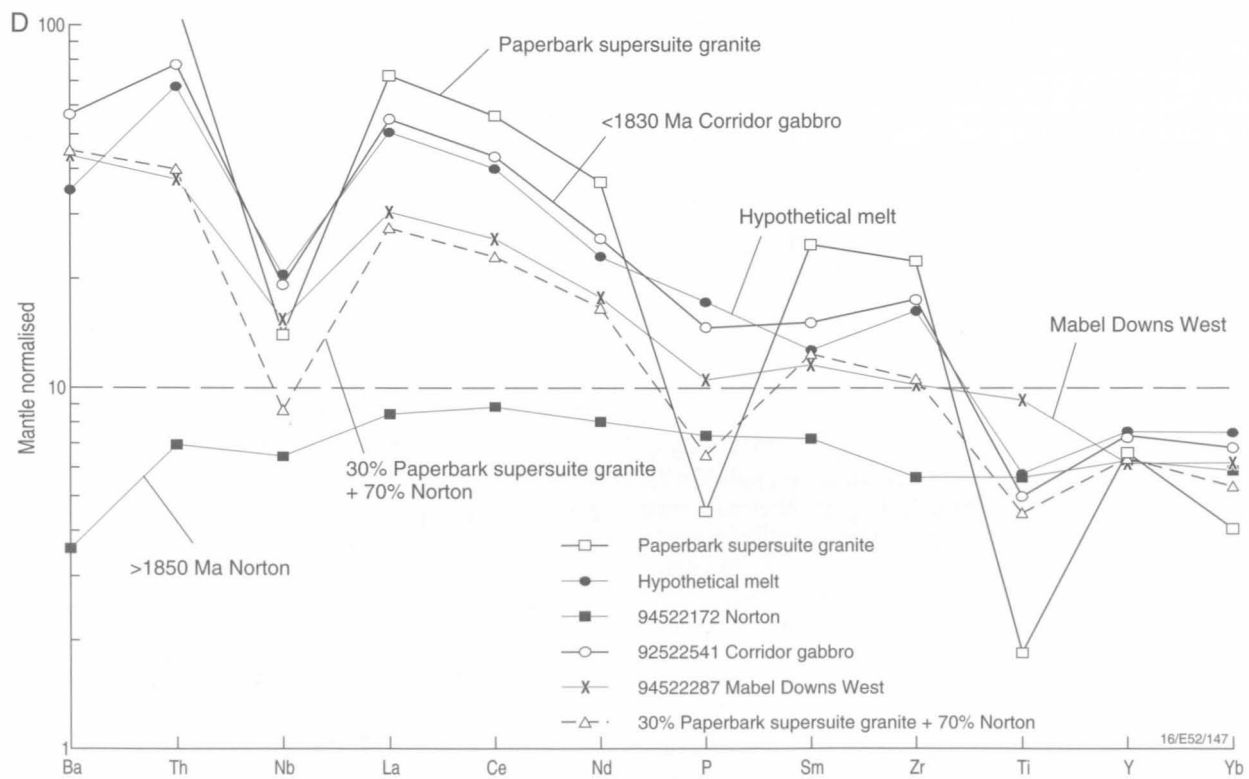


Figure 11.7. Mantle-normalised trace-element diagrams for East Kimberley mafic–ultramafic intrusions and Paperbark supersuite granite.

A. Contamination of Norton-type magma by 15% Paperbark supersuite granite of the Bow River Batholith can produce the trace-element abundances observed in the Wild Dog Creek intrusion magma.

B. Assimilation of 30% Paperbark supersuite granite by Norton-type magma is required to generate the trace-element abundances observed in Toby intrusion magma.





C. Mixing of 70% Norton-type melt with 30% Paperbark supersuite granite can produce some trace-element abundances similar to those observed in the Mabel Downs West sample, but there are serious discrepancies in Ti, P, and Nb.

D. 30% crustal contamination cannot generate the trace-element abundances observed in the magma for the Paperbark (Corridor gabbro) intrusion.

mantle component has an initial ε_{Nd} value that is the same as the depleted mantle (+5 at 1850 Ma) may not be valid, because the potential magma sources may be located in the lithospheric mantle and a subduction-modified mantle wedge. Thus, it may have considerably lower ε_{Nd} values than +5 at 1850 Ma. If the initial ε_{Nd} value of the crustal contaminant is similar to that of the Palaeoproterozoic felsic igneous rocks and sediments in the central and western zones of HCO with T_{DM} model ages of 2500–2700 Ma, then initial ε_{Nd} values of –3 to –5 at 1850 Ma can be expected (Table 11.2). Such values are commonly observed in other North Australian felsic igneous and sedimentary rocks of similar age (Fig. 11.6), suggesting that these rocks contain a large component of recycled material from Archaean source rocks. There is no clear evidence for the existence of Archaean basement rocks in the central and western zones of the HCO. However, if they did exist they may have had initial ε_{Nd} values considerably lower than –5 at ~1850 Ma. Thus, the ε_{Nd} values of mafic magmas contaminated by Archaean rocks could have been more strongly affected than those arising from contamination by Palaeoproterozoic crust (Fig. 11.6). On the other hand, if the contaminant is more-mafic lower crust with higher initial ε_{Nd} values and lower Nd contents, the effects of crustal contamination would be more difficult to recognise.

Abundance of Nd in felsic crustal contaminant relative to that in mantle-derived magma (β) is commonly 3–5; i.e. 10 ppm in mafic magma such as in the MORB-like Norton gabbro versus 30–50 ppm in the felsic contaminant. The lower the β value, the more contaminant is required to generate a specific ε_{Nd} value for the mixing product. Assuming the Nd composition of the two end members, calculations can be made to estimate the amount of crustal contamination needed to produce the observed ε_{Nd} value. Trace-element spidergrams and SiO_2 content of observed igneous rocks (the mixing product) can be used to evaluate the feasibility of the mixing model. If the mantle-derived magma has $\varepsilon_{Nd} = +5$ with a SiO_2 content of 50% and the felsic contaminant has $\varepsilon_{Nd} = -5$ with a SiO_2 content of 70% and the β value is 5, then 8% contaminant is required to produce a mixture with $\varepsilon_{Nd} = +2$, 17% contaminant is required for a mixing product with $\varepsilon_{Nd} = 0$, and 32% for a mixing product with $\varepsilon_{Nd} = -2$. In the last case the mixing product will have 56.4% SiO_2. If the felsic contaminant is Archaean felsic rock with $\varepsilon_{Nd} = -10$ and the β value is 5, then 9% contaminant is required to produce $\varepsilon_{Nd} = 0$, and 15% contaminant is required for $\varepsilon_{Nd} = -2$ with a 3% increase of SiO_2. If the β value is 3, then 23% contaminant is required to generate a mixture having $\varepsilon_{Nd} = -2$, and this would result in a 4.6% increase in the SiO_2 content of the contaminated magma. It is important to note that except for the basal rocks of the Sally Malay and Panton intrusions, orthopyroxene is not an important cumulus mineral in the intrusions we studied. Thus, it is unlikely that these two intrusions have suffered extensive contamination by felsic crust.

Figure 11.7A shows that it is possible to produce the trace-element spidergram of the Wild Dog Creek intrusion magma from a Norton intrusion-type magma by 15% contamination of incompatible element-enriched Paperbark supersuite (Bow River Batholith) granite-type crust (Sheppard et al. 1995) with a β value of 5. To generate the trace-element spidergram of the Toby intrusion magma, about 30% contamination of Paperbark supersuite granite-type crust is required (Fig. 11.7B), but the resulting mixing product is too siliceous and its ε_{Nd} value (–1.8) is lower than that of the Toby intrusion (–0.9). Thirty per cent crustal contamination by a Paperbark supersuite granite-like felsic crust is not able to generate incompatible trace-element abundances similar to the Paperbark intrusion (Corridor gabbro) magma (Fig. 11.7C) and the mixing product is again too siliceous. If the contaminant is an Archaean felsic rock with 30 ppm Nd and the β value is 3, the spidergram pattern will be more dissimilar. Figure 11.7C shows that in order to generate the spidergram pattern of the Mabel Downs West intrusion (Corridor gabbro), a Norton-intrusion-type magma and 30% crustal contamination by the Paperbark supersuite granite-like crust is required. However, as major anomalies in Ti, P, and Nb contents reflect intraplate features of the parent magma, the assumption of a mantle-derived magma having initial $\varepsilon_{Nd} = +5$ and incompatible trace-element contents similar to the Norton intrusion is probably not valid. As mentioned earlier, the Mabel Downs West and Paperbark intrusions (both Corridor gabbro) show chemical features characteristic of intraplate magmas. Thus, their mantle-derived parent magmas are likely to have initial ε_{Nd} values lower than +5 and to have higher incompatible trace-element contents than the assumed MORB-like gabbros of the Norton intrusion. This point can be demonstrated in the following way. If the magma that formed the Mabel Downs West intrusion experienced 20% crustal contamination by a Paperbark supersuite granite-like crust, the hypothetical uncontaminated magma would have a trace-element pattern similar to that of intraplate basalt (Fig. 11.7C). If the amount of crustal contamination is less than 20%, the hypothetical uncontaminated magma would have higher incompatible trace-element abundances with more marked Nb depletion and Th and Ba enrichment.

Figure 11.7D indicates that even 30% crustal contamination by felsic rocks of the Paperbark supersuite granite is not nearly enough to generate the Paperbark (Corridor gabbro) intrusion magma from a Norton-gabbro-type parent magma. Thus, a parent magma enriched in incompatible trace elements is required. If the Paperbark intrusion magma experienced 20% crustal contamination by a Paperbark supersuite granite-type crust then the hypothetical uncontaminated magma would have a trace-element enriched pattern similar to that of Paperbark intrusion sample (Fig. 11.7D). On this basis we suggest that the incompatible trace-element features of the parent magma of the Paperbark intrusion were most likely mainly derived from melting of lithospheric mantle that had previously been modified and enriched by subduction processes.

Compositions of parent magmas

On the basis of the composition of 'chilled margins' and cumulus mineral assemblages, many of the Palaeoproterozoic mafic–ultramafic intrusions in the East Kimberley can be inferred to have olivine tholeiite and quartz tholeiite parent magmas (e.g. Mathison & Hamlyn 1987, Sun et al. 1991). On a $Na_2O + K_2O$ versus SiO_2 plot (not shown here), all melt-like samples of East Kimberley intrusions with 48–52% SiO_2 fall in the field of tholeiite generated at pressures ranging from <10 kb to 20 kb (Kuno 1966, Hirose & Kushiro 1993, Kushiro 1994). However, problems associated with the mobility of Si, Na, and K during metamorphism mean that these pressure estimates need to be treated with caution. The presence of corona overgrowth of orthopyroxene on cumulus olivine (see Chapter 9) suggests rising silica activity in the melt during crystallisation, and implies a subalkaline basaltic parentage for the intrusions. The abundance of incompatible trace elements in the East Kimberley intrusions ranges from the MORB-like Norton intrusion to the more enriched Toby, Mabel Downs West, and Paperbark (Corridor gabbro) intrusions, which are similar to many continental tholeiites. The light-REE enriched samples from these intrusions have gently sloping heavy-REE patterns (Fig. 11.3), suggesting that garnet is not an important residual mineral during magma generation, and the depths of magma generation are <100 km, or <30 kb (e.g. Hirschmann & Stolper 1996). Samples of ?post-1830 Ma biotite quartz gabbronorite from the Paperbark (Corridor gabbro) intrusion are more enriched in alkalis and incompatible elements (e.g. Th, Nb, P, Zr, and light REE) than older intrusions of the HCO. As discussed later, this enrichment can be partly due to the effect of crustal contamination, but is mainly due to smaller degrees of mantle melting than in the pre-1830 Ma magmas.

The most primitive olivine compositions in the East Kimberley intrusions range from mg_{85} to mg_{42} (summarised in Table 11.3) with most intrusions having olivine composition between mg_{85} and mg_{70} (see Chapter 9). There is a general distinction between the mafic–ultramafic intrusions which contain the most primitive olivine (e.g. Panton, mg_{85}; Wilagee, mg_{84}; Salt Lick Creek, mg_{84}; and Sally Malay, mg_{82}), and the mafic intrusions which have more evolved olivine (e.g. McIntosh, mg_{79}; Spring Creek, mg_{74}; Dave Hill, mg_{73}; and McKenzie Spring, mg_{70}). Olivine compositions for the other intrusions (Armanda, mg_{67}; Wilson Creek, mg_{64}; and Toby mg_{63}) are even more evolved. These low mg compositions should be regarded as minima, since most samples analysed by electron microprobe analysis (Trudu & Hoatson 1996) were from the middle to upper parts of the intrusions, and it is most likely that more primitive olivine exists at lower stratigraphic levels in these intrusions. The extremely low mg in the Keller Creek intrusion (mg_{42}) may reflect metamorphic re-equilibration of the olivine.

When a partition coefficient (Kd) of 0.30 is used for $(Fe^{2+}/Mg)_{olivine}/(Fe^{2+}/Mg)_{liquid}$ for terrestrial tholeiites (Roeder & Emslie 1970, Kushiro & Walter 1998), the liquid in equilibrium with the most primitive olivine in the East Kimberley intrusions (Panton, mg_{85}) would have a $100Mg/(Mg + Fe^{2+})$ value of 63. We assume that the parent magma for the Panton intrusion has an mg value of 63 and has 9.5% FeO as the total Fe content (a value commonly observed in tholeiitic to picritic parent magmas), and that among the total Fe content there is 90% in the form of Fe^{2+}. In this case, the MgO content of the parent magma can be calculated to be 8.2%. If the

Table 11.3. Estimated mg number of parent magmas for the East Kimberley layered intrusions.

Intrusion (group)	*Most primitive olivine composition (mg number[1])*	*Estimated mg number of parent magma[2]*	*Reference for mg number of olivine*
Panton (I)	85	63	Hamlyn (1977)
Big Ben (I)	71	42	Chapter 9
Springvale (II)	82	58 (67)[3]	Geopeko (1986–1989)
Wilagee (II)	84	61 (59)[3]	Chapter 9
Toby (III)	63	34 (58)[3]	Geopeko (1986–1990)
Sally Malay (V)	82	58	Thornett (1981)
Dave Hill (V)	73	45	Chapter 9
Spring Creek (V)	74	46 (60)[3]	Chapter 9
McKenzie Spring (V)	70	41	Chapter 9
Wilson Creek (V)	64	35	Chapter 9
Keller Creek (V)	42	18 (41)[3]	Chapter 9
McIntosh (VI)	79	53	Mathison & Hamlyn (1987)
Armanda (VI)	67	38	Chapter 9
Salt Lick Creek	84	61	Wilkinson et al. (1975)

[1] mg number of olivine used in this study is 100 x $Mg/(Mg + Fe^{2+})$. Some of the other studies have used minor variations of this ratio (e.g. inclusion of Mn); see individual reference for details.

[2] Using Fe^{2+}/Mg partitioning between olivine and liquid ($(Fe^{2+}/Mg)_{olivine}/(Fe^{2+}/Mg)_{liquid}$) = 0.3 ± 0.03 (Roeder & Emslie 1970, Kushiro & Walter 1998).

[3] mg number (100 x $Mg/(Mg + Fe^{2+})$ of melts estimated from whole-rock compositions shown in Table 11.1.

Kd of $(Fe^{2+}/Mg)_{olivine}/(Fe^{2+}/Mg)_{liquid}$ is increased to 0.35, a value suitable for more ultramafic picritic and komatiitic melts (Kushiro & Walter 1998), then the MgO content calculated for the melt becomes 9.5%. If the total Fe in the parent magma is increased to 10.5% and the Kd of $(Fe^{2+}/Mg)_{olivine}/(Fe^{2+}/Mg)_{liquid}$ is 0.30, the calculated MgO content becomes 9.0%. Thus, we can conclude that the parent magma for the Panton intrusion is tholeiitic in composition and has a MgO content probably close to, but less than, 9%. The tholeiitic character of the parent magmas to the Panton and other East Kimberley intrusions is supported by the spinel composition of chromitite layers reported by Mernagh et al. in Chapter 13. Figure 11.8 shows that most analysed spinels occupy the tholeiitic series field on the Ti (ppm) versus Cr# [atomic ratio of Cr/(Cr+Al)] discrimination diagram constructed by Wayne Taylor (pers. comm. 1998). According to Mernagh et al., the spinels re-equilibrated with co-existing olivine at low temperatures during post-magmatic cooling, leading to a decrease in the mg numbers of the spinel and an increase in the mg numbers of the co-existing olivine. However, the Cr and Al contents (and Ti also) of the spinels are largely unaffected and reflect their original magmatic character.

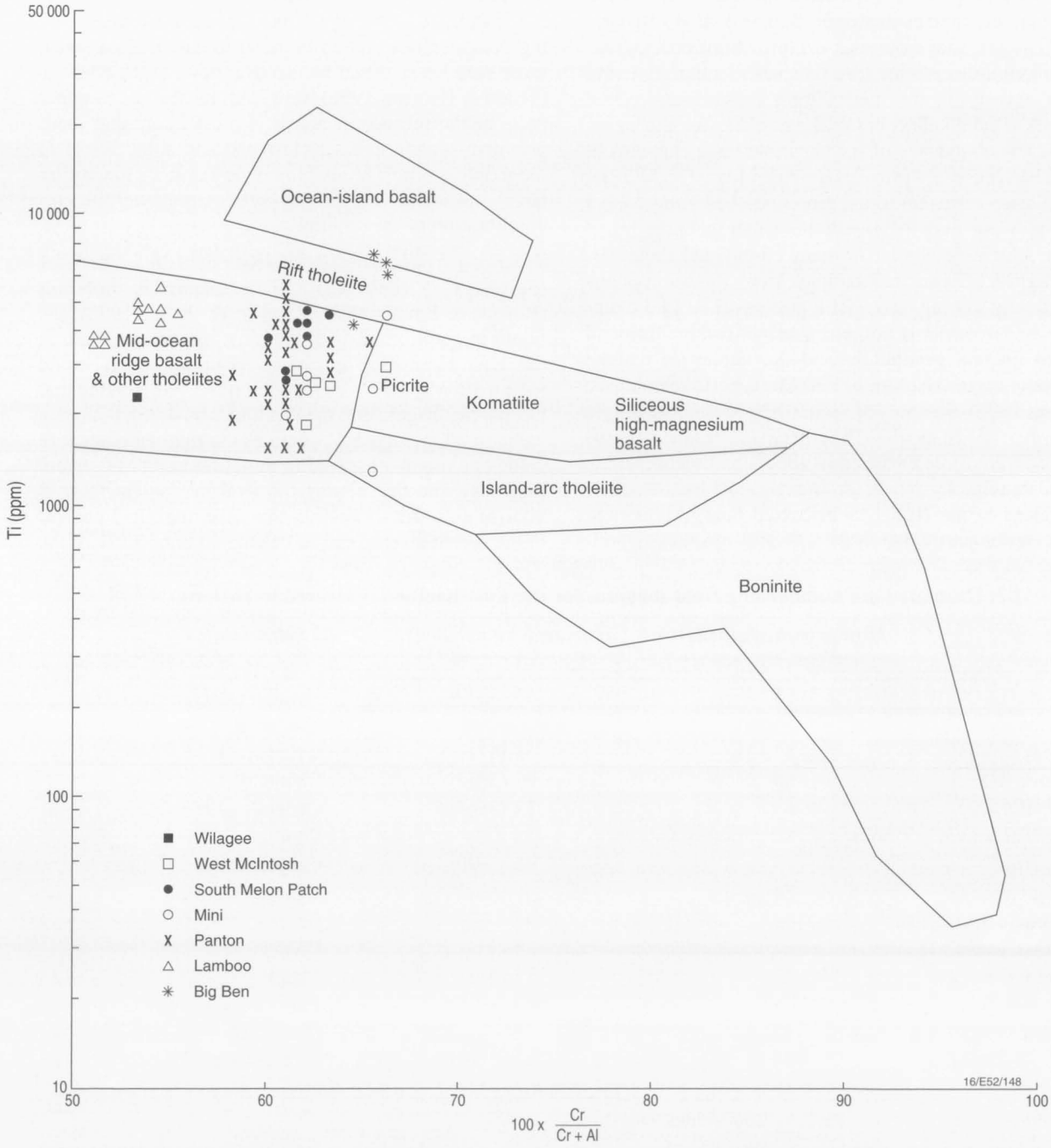


Figure 11.8. Discrimination diagram of Ti (ppm) content versus Cr# in spinel for different magma types defined by Wayne Taylor (pers. comm. 1998, Research School of Earth Sciences, ANU). Data for chromitite layers in the East Kimberley mafic–ultramafic intrusions lie mainly in the field of mid-ocean ridge basalts and other tholeiites.

The estimated mg numbers of parent magmas for the other East Kimberley intrusions are summarised in Table 11.3, with additional mg values based on whole-rock compositions of melt-like samples of Table 11.1 in brackets. The mg values for the Toby, Spring Creek, and Springvale intrusions estimated this way are significantly higher than those based on olivine compositions. In view of the very homogeneous chemical composition of the Toby intrusion, the mg value based on the whole-rock melt composition is probably more reliable than that based on olivine composition. Similarly, the Spring Creek sample, which has an extremely low mg value (46) for the parent magma, based on olivine composition, has a more reliable composition (mg_{60}) based on the whole-rock data. The extremely evolved olivine (mg_{18}) and whole-rock (mg_{41}) compositions for the parent magma of the Keller Creek intrusion may reflect re-equilibration processes during metamorphism.

Potential temperature of the asthenospheric upper mantle during the Palaeoproterozoic was hotter (by ~50°C?) than the present upper mantle, ~1300°C (Cordery et al. 1997). However, no high-temperature picritic ultramafic magmas or cumulus minerals with exceptionally high mg values have been observed in the HCO intrusions. Thus, there is no obvious evidence for the existence of magmas generated by high-temperature mantle plume activity. As discussed above, the most primitive magma documented for the East Kimberley intrusions has an mg of only 63, based on olivine composition, or 67, based on whole-rock melt composition (Table 11.3). These data are derived from several hundred probe analyses by a number of investigators. It is clear that the parent magmas of the East Kimberley intrusions were basaltic rather than ultramafic magmas, and they were considerably more fractionated than the high magnesian, high silica parent magmas that formed the Bushveld (mg = 71, Sharpe & Hulbert 1985), Great Dyke (mg = 74, Wilson 1982), and Stillwater (mg = 69, Longhi et al. 1983) intrusions. This is also illustrated by the most primitive olivine compositions documented in important Precambrian layered intrusions, namely: mg_{90}—Bushveld (Cameron 1980), mg_{92}—Great Dyke (Wilson 1982), mg_{88}—Stillwater (Todd et al. 1982), mg_{84}—Lac des Iles (Sutcliffe et al. 1989), and mg_{89}—Wingellina Hills (Ballhaus & Glikson 1989).

Since the parent magmas of the East Kimberley mafic and mafic–ultramafic intrusions were generated in response to tectono-thermal pulses ranging in age from ~1860 Ma to ~1800 Ma, it is probable that magma generation processes in the central, and western zones of the HCO were not the same. It can be envisaged that tholeiitic magmas were generated when the lithosphere was stretched and thinned by extension and/or thermal erosion and, thus, they were generated in the shallow asthenospheric mantle with temperatures of ~1350°C (?), possibly with involvement of the lithospheric mantle.

We conclude that the 1855 Ma Panton and possibly older Norton and Keller Creek intrusions in the central zone have low incompatible trace-element abundances and infer that they were generated by large degrees of asthenospheric mantle melting at shallow mantle depths with a thinned lithospheric lid. The 1855 Ma group II and III intrusions in the western zone, which are considerably more enriched in incompatible trace elements, have similar spidergram patterns and could be genetically related, especially for the adjoining Toby and Wilagee intrusions. The ~1845 Ma groups IV and V intrusions (not including Keller Creek) have trace-element spidergrams similar to those of the 1855 Ma Toby intrusion of the western zone. It is possible that at ~1845 Ma, the lithospheric mantle in the central zone became thicker and comparable to that of the western zone at 1855 Ma. There are no obvious geochemical differences between the post ?1830 Ma intrusions, including the Robin Soak, Three Sisters (both Undivided gabbro), and Paperbark (Corridor gabbro) in the central and western zones. These intrusions are more enriched in incompatible trace elements than earlier magmas of the HCO, except for the light-REE-enriched intraplate basaltic andesite to rhyolite in the ~1848 Ma Butchers Gully Member of the Olympio Formation in the eastern zone (see Chapter 3). The magmas for the post ?1830 Ma intrusions were generated by smaller degrees of mantle melting under a progressively thicker lithospheric lid than pre-1830 Ma magmas of the central and western zones. This trend was interrupted at ~1790 Ma with the intrusion of the Hart Dolerite in the Kimberley Basin farther to the west, possibly initiated by mantle plume activity.

Tectonic environments of the mafic–ultramafic intrusions

As discussed in the previous section, the geochemistry of the ?post-1830 Ma mafic intrusions in the East Kimberley suggests that their parent magmas were potentially derived from mantle sources modified by subduction processes. This is consistent with previous suggestions based on isotope modelling that such subduction modification in the Kimberley region probably occurred during the Palaeoproterozoic (Nelson et al. 1985, Sun et al. 1986, 1995), although the exact timing is not well defined.

There are no diagnostic petrological and geochemical indicators in the HCO, such as the occurrence of ophiolites, boninites, or shoshonites, to indicate a subduction environment between ~1860 and ~1800 Ma. It is possible that that the eastern zone of the HCO has an Archaean basement, similar to that of the Pine Creek Inlier to the east. However, the tectonic environment west of the Halls Creek Fault during this period is a contentious issue, as two contrasting models have been proposed:

- all tectonic and magmatic activities were ensialic, and the mafic and mafic–ultramafic intrusions were emplaced in an intraplate extensional environment (e.g. Hancock & Rutland 1984, Mathur & Shaw 1982, Etheridge et al. 1987, Wyborn 1988, Blake et al. 1998, 1999). Shaw & Macias (see Chapter 7) suggest that the mafic–ultramafic intrusions were emplaced into dilatational pockets during switches from compressional to transtensional fault movements in a complex tectonic setting; or

- the HCO was a zone of lithosphere subduction and magmatic arc formation on the eastern margin of the Archaean Kimberley Craton (e.g. Ogasawara 1988, Tyler et al. 1995, Sheppard et al. 1997). Shaw et al. (see Chapter 4) argue that the HCO represents a plate or subplate boundary with a complex history.

In the first model, upwelling of mafic magma from the mantle, perhaps due to mantle convection or hot-spot activity and/or regional tectonism, resulted in underplating of mafic magma at the base of the crust. Consequences of this include extension and thinning of the continental crust and lithospheric mantle, leading to basin formation and melting of the lower crust to produce felsic magma. The extension of the continental crust was insufficient to cause ocean-floor spreading and the generation of any oceanic crust. Compressional orogenies at around 1865 and 1835 Ma may be related to differential movements of Archaean cratons.

In the subduction-related model for the East Kimberley, granites were generated in the western and central zones during and after northwestward subduction of oceanic crust. Sheppard et al. (1997, 1999) suggest that the Bow River Batholith granite (Paperbark supersuite) and ~1855 Ma mafic intrusions (Toby and Springvale) in the western zone were emplaced in an extensional environment on the margin of the Kimberley Craton, and the 1856 Ma Panton and pre-1850 Ma Norton and Keller Creek intrusions in the central zone were emplaced into an oceanic island arc above an easterly dipping subduction zone. They suggest that this island arc was accreted to the Kimberley Craton at ~1850 Ma (Sheppard et al. 1999) and the eastern zone on the western edge of the North Australian craton collided with the Kimberley Craton, which then included the accreted central zone, at ~1820 Ma. This model involves the accretion of an island arc (the central zone) onto a continental margin to the west and the subduction of oceanic crust during collision of two continental masses previously widely separated. Tonalites of the Mabel Downs suite were emplaced between ~1835 and 1820 Ma in the central zone. These tonalites are depleted in heavy-REE and Y and have high Al_2O_3, Na_2O, Sr, and Sr/Y, similar to those found in Archaean tonalite–trondhjemite–granodiorite (TTG) associations. Sheppard et al. (1997) suggested that these tonalites were generated by melting of mafic rock with a garnet amphibolite residue in the deeper part of the newly accreted, thickened island arc crust above a westward-dipping subduction zone. This mechanism for tonalite formation is a variation of the idea originally proposed by Ogasawara (1988), who suggested that these heavy-REE-depleted tonalites were generated by partial melting of subducted oceanic crust in the garnet stability field. Magma generation in this field will have a large portion of heavy REE and Y held back in the residue by garnet, resulting in the depletion of these elements and a high Sr/Y in the tonalitic magmas. It is important to point out, however, that tonalites with strongly depleted heavy REE and Y and high Sr/Y values can also be generated in an intraplate compressional environment by melting of mafic granulite and eclogite in the lower part of thickened crust, where garnet is stable.

Neodymium isotope model ages and initial ε_{Nd} values of felsic igneous rocks in the HCO can provide constraints for petrogenetic models and give an insight into the tectonic environment of the mafic–ultramafic intrusions. Some felsic igneous rocks of the HCO, e.g. granites of the Bow River Batholith, are likely to be melting products of mafic to intermediate rocks previously underplated in the lower crust during intraplate rifting (Wyborn 1988) or lithosphere subduction (Sheppard et al. 1997). If the underplated materials contain Archaean crustal components from recycling, through subduction, of older crust, the magma generated from this underplate can have Nd T_{DM} model ages considerably older than the underplating event. In this context, Nd T_{DM} model ages of 2530–2600 Ma for the Bow River Batholith granite (~1865–1850 Ma) and Whitewater Volcanics (1855 Ma) in the western zone indicate the involvement of large amounts of Archaean-derived crustal material in their source region. However, as shown in Figure 11.6, it is unlikely that these felsic igneous rocks were derived simply from melting of Archaean crust, since Archaean rocks of North Australia generally have Nd T_{DM} model ages considerably older than 2600 Ma (Page & Sun 1994, 1998). Compared to felsic igneous rocks of the western zone of the HCO, samples of the ~1850 Ma Dougalls Tonalite suite in the central zone, farther from the Kimberley Craton, have younger Nd T_{DM} ages and higher initial ε_{Nd} values of 2234–2258 Ma and +0.3 to +0.8 (4 samples) and 2372 Ma and –1.0 (one sample), respectively. Two granitic samples from the ~1830 Ma Sally Downs Tonalite and Mabel Downs Tonalite in the central zone have similar T_{DM} ages and initial ε_{Nd} values—2371 Ma and –1.2, and 2271 Ma and +0.3, respectively. These T_{DM} ages are considerably younger than those of felsic igneous rocks in the western zone, but are still much older than the emplacement ages (1855–1820 Ma) and the expected model ages for a juvenile 'island arc' of ~1860 Ma. Thus, these felsic rocks cannot be derived by simply melting the mafic rocks of the Tickalara Metamorphics that formed in a juvenile oceanic island arc (see also Page & Sun 1998). Instead, it would seem that the source rocks contained a significant Archaean crustal component. Perhaps the source included subducted sediments derived from a nearby Archaean craton and/or Archaean crystalline rocks deep in the crust.

In spite of uncertainties regarding tectonic environment as discussed above, the incompatible trace-element abundances and spidergram patterns of mafic intrusions in the western zone of HCO and post-1850 Ma intrusions in the central zone are consistent with an intraplate environment. However, geochemical characteristics of pre-1850 Ma intrusions in the central zone (Panton, Norton, and possibly Keller Creek) and metabasalts in the Tickalara Metamorphics are not consistent with a simple island arc model. Some metabasalt samples in the Tickalara Metamorphics have Nb/La greater than 1.0 and high Nb/Th (Sheppard et al. 1999; see Appendix 2), and, hence, do not resemble magmas generated in a typical subduction environment. This does not rule out an atypical subduction environment, where windows and breaks in the subducted plate allow occurrence of intraplate-like basalts (e.g. DeLong et al. 1975).

Alternatively, these metabasalts may be related to a switch from a subduction to intraplate environment over a short time. The seemly conflicting geochemical features could also be related to emplacement of the ~1855 Ma mafic–ultramafic intrusions in a transtensional environment (see Chapter 4), where a thinned lithospheric mantle was modified by subduction processes. In summary, the geochemical data do not impose many constraints on the tectonic environment for pre-1850 Ma intrusions in the central zone of HCO.

Implications of magma chemistry for PGE and Ni–Cu–Co mineralisation potential

Palaeoproterozoic mafic–ultramafic intrusions in the East Kimberley have similar dimensions to the 1080 Ma Giles intrusions of the Musgrave Block (Glikson et al. 1996) and the mineralised 2925 Ma intrusions of the west Pilbara Craton (Hoatson et al. 1992). None of the Kimberley intrusions has any documented occurrences of stratabound PGE–sulphide (e.g. Merensky Reef-type) mineralisation, common in Precambrian provinces elsewhere. However, there are subeconomic concentrations of PGEs associated with cumulus chromite in ultramafic sequences of the group I intrusions (e.g. Panton intrusion; see Chapter 12), and there are low concentrations of PGEs associated with Ni–Cu–Co sulphide mineralisation along the basal contacts of group V intrusions and mafic bodies in the Tickalara Metamorphics (e.g. Sally Malay and Norton intrusions; see Chapter 12).

Sun et al. (1991) suggested that a major prerequisite for PGE-enriched mineralisation in a layered intrusion is the involvement of a S-undersaturated magma fertile in Pt, Pd (≥10 ppb), and Au (≥2 ppb). S-undersaturated magma can be generated through large degrees of melting of asthenospheric mantle containing ~250 ppm S or through smaller degrees of melting of refractory mantle with a S content much less than 250 ppm in the mantle wedge of a subduction zone (e.g. boninite and some arc tholeiite magmas). It can also be generated through melting of S-poor, refractory lithospheric mantle (e.g. some siliceous high-Mg basalt magmas). Some oxidised magmas that contain a large fraction of S in the oxidised form can remain S undersaturated during magma generation and differentiation.

There is no evidence that S-undersaturated magmas existed in the magma chambers of the Palaeoproterozoic mafic–ultramafic intrusions investigated in this study. The intrusions show evidence of S saturation throughout the mafic and ultramafic sequences, with S concentrations for most unaltered cumulates being in the range 300–800 ppm. Strongly serpentinised peridotite and chromitite often have S content less than 80 ppm, but this is probably due to loss of S during alteration. By determining the amount of trapped intercumulus liquid in unaltered cumulates (mostly adcumulates to mesocumulates) and normalising the S content of the cumulate to a rock comprising 100% melt (see method of Hoatson & Keays 1989), it can be shown that most intrusions in the HCO were formed from mafic magmas containing more than 1000 ppm S and were S saturated. This conclusion is reinforced by widespread occurrence of trace sulphides in thin section and outcrop. Thus, the intrusions in the HCO appear to have little potential for stratabound Merensky Reef or Munni Munni–type PGE mineralisation. On the other hand, it is encouraging to find that four samples representing the magma composition of the Toby intrusion have 2–4 ppb Pd and high, but variable, Au contents (4.5, 5.1, 6.4, and 21.7 ppb; Sun et al. 1991). It is likely that the unfractionated, primitive magma of the Toby intrusion was originally S undersaturated when it was generated in the mantle. Using incompatible trace-element abundance as a criterion for estimating degrees of mantle melting, we could infer that the parent magmas of the 1856 Ma Panton and 1845 Ma intrusions in the central zone, with lower than or similar abundances of incompatible elements to the Toby intrusion, were probably S undersaturated at the time they were generated in the mantle source region. Thus, the first stage of S saturation of the magma is likely to have occurred before the parent magma entered the magma chambers of these intrusions. This S saturation may have occurred in chambers deep in the crust or in feeder dykes associated with the intrusions. In the latter case, it offers some potential for Noril'sk or Voisey's Bay-style Ni–Cu mineralisation in magma conduits.

We conclude that the HCO has little potential for Merensky Reef-type PGE mineralisation. However, the HCO is a province characterised by high background values of Pt, Pd, and Au. Thus, it should not be dismissed as unprospective for hydrothermal and placer deposits of these elements.

Acknowledgements

The authors would like to acknowledge Alastair Stewart, David Blake (both AGSO), Steve Sheppard, Ian Tyler (both GSWA), and Rebecca Sproule (Monash University) for reviewing earlier versions of the manuscript. Wayne Taylor (Research School of Earth Sciences, ANU) kindly allowed us to use the chromite discrimination diagram (Fig. 11.8). We thank John Pyke, Bruce Cruikshank, and Bill Pappas for XRF and ICP-MS analyses and Angie Jaensch for drafting the figures. Shen-su Sun thanks Graham Mortimer for his help in the ANU isotope laboratories; and Yaoling Niu and Alan Greig (both University of Queensland) for reanalysing samples by ICP-MS.

References

Ballhaus, C.G. & Glikson, A.Y., 1989. Magma mixing and intraplutonic quenching in the Wingellina Hills intrusion, Giles Complex, central Australia. Journal of Petrology, 30, 1443–1469.

Blake, D.H. & Hoatson, D.M., 1993. Granite, gabbro, and migmatite field relationships in the Proterozoic Lamboo Complex of the East Kimberley region, Western Australia. AGSO Journal of Australian Geology & Geophysics, 14(4), 319–330.

Blake, D.H., Tyler, I.M. & Griffin, T.J., 1997. Ruby Plains, Western Australia, 1:100 000 geological map (sheet 4460; first edition). Australian Geological Survey Organisation, Canberra.

Blake, D.H., Hoatson, D.M. & Wyborn, L.A.I., 1998. Review of new data and interpretations for the Palaeoproterozoic of the East Kimberley, Western Australia. 14th Australian Geological Convention, Townsville, Queensland, 6-10 July, Geological Society of Australia, Abstracts, 49, 41.

Blake, D.H., Tyler, I.M., Griffin, T.J., Sheppard, S., Thorne, A.M. & Warren, R.G., 1999. Geology of the Halls Creek 1:100 000 sheet area (4461), Western Australia. Explanatory Notes. Australian Geological Survey Organisation, Canberra, 36 pp.

Cameron, E.N., 1980. Evolution of the Lower Critical Zone, central sector, Eastern Bushveld Complex, and its chromite deposits. Economic Geology, 75, 845–871.

Cordery, M.J., Davies, G.F. & Campbell, I.H., 1997. Genesis of flood basalts from eclogite-bearing mantle plumes. Journal of Geophysical Research, 102, 20179–20197.

DeLong, S.E., Hodges, F.N. & Arculus, R.J., 1975. Ultramafic and mafic inclusions, Kanaga Island, Alaska, and the occurrence of alkaline rocks in island arcs. Journal of Geology, 83, 721–736.

Eggins, S.M., Woodhead, J.D., Kinsley, L., Mortimer, G.E., Sylvester, P., McCulloch, M.T., Hergt, J.M. & Handler, M.R., 1997. A simple method for the precise determination of 40 trace elements in geological samples by ICP-MS using enriched isotope internal standardisation. Chemical Geology, 134, 311–326.

Etheridge, M.A., Rutland, R.W.R. & Wyborn, L.A.I., 1987. Orogenesis and tectonic process in the early to middle Proterozoic of Northern Australia. In: Kröner, A. (editor), Proterozoic lithospheric evolution. American Geophysical Union, Geodynamic Series, 17, 131–147.

Geopeko Ltd., 1986–1989. Springvale platinum/chromite exploration. Geopeko Ltd internal report (unpublished) for the Department of Minerals and Energy, Western Australia (Item 4592, Fiche 6447–6448).

Geopeko Ltd., 1986–1990. Toby intrusion platinum exploration. Geopeko Ltd internal report (unpublished) for the Department of Minerals and Energy, Western Australia (Item 4326, Fiche 5755-5757–M4713).

Glikson, A.Y., Stewart, A.J., Ballhaus, C.G., Clarke, G.L., Feeken, E.H.J., Leven, J.H., Sheraton, J.W. & Sun, S-s., 1996. Geology of the western Musgrave Block, central Australia, with particular reference to the mafic–ultramafic Giles Complex. Australian Geological Survey Organisation, Bulletin 239, 206 pp.

Hamlyn, P.R., 1977. Petrology of the Panton and McIntosh layered intrusions, Western Australia, with particular reference to the genesis of the Panton chromite deposit. PhD thesis, University of Melbourne, 389 pp.

Hancock, S.L. & Rutland, R.W.R., 1984. Tectonics of an early Proterozoic suture: the Halls Creek orogenic sub-province, Northern Australia. Journal of Geodynamics, 1, 387–432.

Hirose, K. & Kushiro, I., 1993. Partial melting of dry peridotites at high pressures: determination of compositions of melt segregated from peridotite using aggregates of diamond. Earth and Planetary Science Letters, 114, 477–489.

Hirschmann, M.M. & Stolper, E.M., 1996. A possible role for garnet pyroxenite in the origin of the "garnet signature" in MORB. Contributions to Mineralogy and Petrology, 124, 185–208.

Hoatson, D.M. & Keays, R.R., 1989. Formation of platiniferous sulfide horizons by crystal fractionation and magma mixing in the Munni Munni layered intrusion, west Pilbara Block, Western Australia. Economic Geology, 84, 1775–1804.

Hoatson, D.M., Wallace, D.A., Sun, S-s., Macias, L.F., Simpson, C.J. & Keays, R.R., 1992. Petrology and platinum-group-element geochemistry of Archaean layered mafic–ultramafic intrusions, west Pilbara block, Western Australia. Australian Geological Survey Organisation, Bulletin 242, 319 pp.

Kuno, H., 1966. Lateral variation of basalt magma type across continental margins and island arcs. Bulletin of Volcanology, 29, 195–222.

Kushiro, I., 1994. Recent experimental studies on partial melting of mantle peridotites at high pressures using diamond aggregates. Journal of Geological Society of Japan, 100, 103–110.

Kushiro, I. & Walter, M.J., 1998. Mg–Fe partitioning between olivine and mafic–ultramafic melts. Geophysical Research Letters, 25, 2337–2340.

Longhi, J., Wooden, J.L. & Coppinger, K.D., 1983. The petrology of high-Mg dikes from the Beartooth Mountains, Montana: a search for the parent magma of the Stillwater Complex. Journal of Geophysical Research, Supplement, 88, B53–B69.

Maas, R. & McCulloch, M.T., 1991. The provenance of Archaean clastic sediments in the Narryer Gneiss Complex, Western Australia: trace element geochemistry, Nd isotopes and U–Pb ages from detrital zircons. Geochimica et Cosmochimica Acta 55, 1915–1932.

Mathison, C.I. & Hamlyn, P.R., 1987. The McIntosh layered troctolite–olivine gabbro intrusion, east Kimberley, Western Australia. Journal of Petrology, 28, 211–234.

Mathur, S.P. & Shaw, R.D., 1982. Australian orogenic belts. Evidence of evolving plate tectonics. Earth Evolution Sciences, 4, 281–308.

McDonough, W.F. & Sun S-s., 1995. The composition of the Earth. Chemical Geology, 120, 223–253.

Meschede, M., 1986. A method of discriminating between different types of mid-ocean ridge basalts and continental tholeiites with the Nb–Zr–Y diagram. Chemical Geology, 56, 207–218.

Nelson, D.R., McCulloch, M.T. & Sun, S-s., 1985. The origins of ultrapotassic rocks as inferred from Sr, Nd and Pb isotopes. Geochimica et Cosmochimica Acta, 50, 231–245.

Ogasawara, M., 1988. Geochemistry of the Early Proterozoic granitoids in the Halls Creek orogenic subprovince, northern Australia. Precambrian Research, 40/41, 469–486.

Page, R.W. & Hancock, S.L., 1988. Geochronology of a rapid 1.85–1.86 Ga tectonic transition: Halls Creek Orogen, northern Australia. Precambrian Research, 40/41, 447–467.

Page, R.W. & Sun, S-s., 1994. Evolution of the Kimberley Region, W.A., and adjacent Proterozoic Inliers—new geochronological constraints. Geological Society of Australia, Abstracts, 37, 332–333.

Page, R.W. & Sun, S-s., 1998. Aspects of geochronology and crustal evolution in the Eastern Fold Belt, Mt Isa inlier. Australian Journal of Earth Sciences, 45, 343–361.

Page, R.W., Hoatson, D.M., Sun, S-s. & Foudoulis, C., 1995. High-precision geochronology of Palaeoproterozoic layered mafic–ultramafic intrusions in the East Kimberley. AGSO Research Newsletter, 22, 7–8.

Pearce, J.A., 1987. An expert system for the tectonic characterization of ancient volcanic rocks. Journal of Volcanology and Geothermal Research, 32, 51–65.

Pearce, J.A. & Cann, J.R., 1973. Tectonic setting of basic volcanic rocks determined using trace element analysis. Earth and Planetary Science Letters, 19, 290–300.

Plank, T. & Langmuir, C.H., 1998. The geochemical composition of subducting sediment and its consequences for the crust and mantle. Chemical Geology, 145, 325–394.

Roeder, P.L. & Emslie, R.F., 1970. Olivine–liquid equilibrium. Contributions to Mineralogy and Petrology, 29, 275–289.

Rudnick, R.L. & Fountain, D.M., 1995. Nature and composition of the continental crust: a lower crustal perspective. Reviews of Geophysics, 33, 267–309.

Sharpe, M.R. & Hulbert, L.J., 1985. Ultramafic sills beneath the Eastern Bushveld Complex: mobilized suspensions of early lower zone cumulates in a parental magma with boninitic affinities. Economic Geology, 80, 849–871.

Sheppard, S., 1996. Mafic–felsic magma mingling in the Bow River batholith of the Halls Creek Orogen. Geological Survey of Western Australia, 1995–96 Annual Review, 56–60.

Sheppard, S., Griffin, T. J. & Tyler, I.M., 1995. Geochemistry of felsic igneous rocks from the southern Halls Creek Orogen. Geological Survey of Western Australia, Record 1995/4, 81 pp.

Sheppard, S., Griffin, T.J. & Tyler, I.M., 1997. The tectonic setting of granites in the Halls Creek and King Leopold Orogens, northwest Australia. In: Rutland, R.W.R. & Drummond, B.J. (editors), Palaeoproterozoic tectonics and metallogenesis: comparative analysis of parts of the Australian & Fennoscandian shields. Workshop, Darwin, September, 14-22, 1997. Australian Geological Survey Organisation, Record 1997/44, 107–109.

Sheppard, S., Tyler, I.M., Griffin, T.J. & Taylor, W.R., 1999. Palaeoproterozoic subduction-related and passive margin basalts in the Halls Creek Orogen, northwest Australia. Australian Journal of Earth Sciences, 46, 679–690.

Shervais, J.W., 1982. Ti–V plots and the petrogenesis of modern and ophiolitic lavas. Earth and Planetary Science Letters, 59, 101–118.

Sun, S-s. & McDonough, W.F., 1989. Chemical and isotopic systematics of oceanic basalts: implications for mantle composition and processes. In: Sunders, A.D. & Norry, M.J. (editors), Magmatism in the ocean basins. Geological Society of London Special Publication, 42, 313–345.

Sun, S-s., Jaques, A.L. & McCulloch, M.T., 1986. Isotopic evolution of the Kimberley Block, Western Australia. Fourth International Kimberlite Conference, Geological Society of Australia Abstracts, 16, 346–348.

Sun, S-s., Wallace, D.A., Hoatson, D.M., Glikson, A.Y. & Keays, R.R., 1991. Use of geochemistry as a guide to platinum group element potential of mafic–ultramafic rocks: examples from the west Pilbara Block and Halls Creek Mobile Zone, Western Australia. Precambrian Research, 50, 1–35.

Sun, S-s., Warren, R.G. & Shaw, R.D., 1995. Nd isotope study of granites from the Arunta Inlier, central Australia: constraints on geological models and limitation of the method. Precambrian Research, 71, 301–314.

Sutcliffe, R.H., Sweeny, J.M. & Edgar, A.D., 1989. The Lac des Iles Complex, Ontario: petrology and platinum-group-elements mineralization in an Archean mafic intrusion. Canadian Journal of Earth Sciences, 26, 1408–1427.

Taylor, W.R., Esslemont, G. & Sun, S-s., 1995. Geology of the volcanic hosted Brockman rare-metals deposit, Halls Creek Mobile Zone, northwest Australia. II. Geochemistry and petrogenesis of the Brockman volcanics. Mineralogy and Petrology, 52, 231–255.

Thornett, J.R., 1981. The Sally Malay deposit: gabbroid associated nickel–copper sulfide mineralization in the Halls Creek Mobile Zone, Western Australia. Economic Geology, 76(6), 1565–1580.

Todd, S.G., Keith, D.W., Le Roy, L.W., Schissel, D.J., Mann, E.L. & Irvine, T.N., 1982. The J-M platinum-palladium reef of the Stillwater Complex, Montana: stratigraphy and petrology. Economic Geology, 77, 1454–1480.

Trudu, A. & Hoatson, D.M., 1996. Depths of emplacement of Precambrian layered intrusions in the East Kimberley. AGSO Research Newsletter, 25, 10–12.

Tyler, I.M., Griffin, T.J., Page, R.W. & Shaw, R.D., 1995. Are there terranes within the Lamboo Complex of the Halls Creek Orogen? Western Australia Geological Survey, Annual Review 1993-94, 37–46.

Wilkinson, J.F.G., Duggan, M.B., Herbert, H.K. & Kalocsai, G.I.Z., 1975. The Salt Lick Creek layered intrusion, East Kimberley region, Western Australia. Contributions to Mineralogy and Petrology, 50, 1–23.

Wilson, A.H., 1982. The geology of the Great 'Dyke', Zimbabwe: the ultramafic rocks. Journal of Petrology, 23, 240–292.

Wyborn, L.A.I., 1988. Petrology, geochemistry and origin of major Australian 1880-1840 Ma felsic volcano-plutonic suite: a model for intracontinental felsic magma generation. Precambrian Research, 40/41, 37–60.

CHAPTER 12

GEOCHEMICAL AND ISOTOPIC CONSTRAINTS ON THE PETROGENESIS OF THE PANTON AND SALLY MALAY INTRUSIONS: IMPLICATIONS FOR EXPLORATION

by REBECCA A. SPROULE[1], DAVID D. LAMBERT[1], & DEAN M. HOATSON

Introduction

In this chapter we present new platinum-group element (PGE) and isotope data to investigate the role of magma source region and the degree of crustal input in the petrogenesis of the Panton and Sally Malay mafic–ultramafic intrusions. These intrusions are 'type' examples from the two northeast-trending corridors (Hoatson 1993, Trudu & Hoatson 1996, see Chapter 5) that contain most of the mineralised Palaeoproterozoic mafic–ultramafic intrusions in the Halls Creek Orogen (HCO). The ~1855 Ma Panton intrusion is representative of the southeastern corridor, which is characterised by mafic–ultramafic intrusions containing PGE-bearing chromitites, and the ~1845 Ma Sally Malay intrusion is representative of the northwestern corridor, characterised by largely mafic intrusions hosting Ni–Cu–Co sulphides. Accurately delineating the source of the ore metals and mechanisms of concentration have important implications for PGE and Ni–Cu–Co exploration programs in the HCO.

Geological setting

Panton intrusion

The 1856±2 Ma Panton intrusion (Page et al. 1995, see Chapters 5 and 6) is an elongate mafic–ultramafic body 11 km in strike length with a maximum width of 2.5 km (Fig. 12.1). It consists of a lower rhythmically-layered, Ultramafic Series (UMS), 650 m thick, and an overlying Gabbroic Series (GS), 900 m thick. Olivine and subordinate chromite are the major cumulus phases in the UMS. Chemical and petrographic evidence indicates that cumulus orthopyroxene is absent in the UMS (Hamlyn 1980). This infers a fundamental difference in the crystallisation sequence of the Panton intrusion compared to that observed in the Stillwater Complex (Lambert et al. 1994), Bushveld Complex (Campbell et al. 1984), and Great Dyke (Podmore & Wilson 1987, Prendergast 1988), where bronzitites form a major lithological unit (Hamlyn 1980). The GS is marked by the first major appearance of cumulus plagioclase and consists of gabbro and gabbronorite packages (cumulus plagioclase, cumulus augite, and rare cumulus orthopyroxene), gradually grading upwards to anorthosite and Fe-rich gabbro packages (cumulus plagioclase and augite). The ratio of stratigraphic thickness of ultramafic rocks to mafic rocks in the Panton intrusion is 0.7:1, similar to the Great Dyke of Zimbabwe, but unlike the more mafic-dominated bodies, such as the Bushveld and Stillwater intrusions (Hamlyn 1980).

PGE-enriched sulphide mineralisation in the Panton intrusion is concentrated in chromitite seams, which are believed to have formed when new pulses of primitive basaltic magma entered the chamber and mixed with more-fractionated resident magma (Perring & Vogt 1991). Mixing between compositionally disparate magmas may result in a hybrid magma oversaturated with chromite and sulphide (Irvine 1975, 1977). This model is supported by reversals in fractionation trends in trace elements across major chromitite seams in the Panton intrusion (Hamlyn et al. 1988). The five thickest chromitite seams (A–E) occur in the UMS (Perring & Vogt 1991). Minor thin chromitites are hosted by dunite lenses in the GS. The A seam, ~120 m below the UMS–GS contact, is the thickest (0.8–2.5 m) and contains the highest PGE grades (~3.1 ppm Pt, ~3.7 ppm Pd, ~105 ppb Os). The Panton intrusion appears to be sulphide-saturated stratigraphically above and below the A seam, as small amounts of cumulus sulphides are present throughout the UMS and GS sequence. Hamlyn et al. (1988) noted that the high background S content of the UMS (742 ppm) is more than four times higher than the mean S content of the sulphide-undersaturated ultramafic sections of the Stillwater Complex.

Sally Malay intrusion

The 1844±3 Ma Sally Malay intrusion (see Chapters 5 and 6) consists of four layered bodies (Fig. 12.2) with a total surface area of about 2 km^2. It was intruded, after a major metamorphic event at about 1850 Ma, into variably metamorphosed sedimentary and igneous rocks of the Tickalara Metamorphics, including migmatites, granulites, and minor graphite–pyrrhotite-bearing gneiss horizons (Thornett 1981; see Chapter 5). The most economically important section of the intrusion is the southern body, which hosts a Ni–Cu–Co sulphide deposit (3.85 Mt @ 1.79% Ni, 0.73% Cu, and 0.10% Co: Shedden & Barnes 1996) within a thin gabbroic unit that separates overlying peridotite from underlying footwall migmatites (Thornett 1981). The gabbroic unit varies from 5 to 40 m in thickness, and has been divided by Thornett (1981) into a subordinate and, occasionally absent, upper unit, consisting of norite with euhedral pyroxene, and a lower unit with ophitic norite and olivine norite.

[1] Victorian Institute of Earth and Planetary Sciences, Department of Earth Sciences, Monash University, Clayton, Victoria 3168.

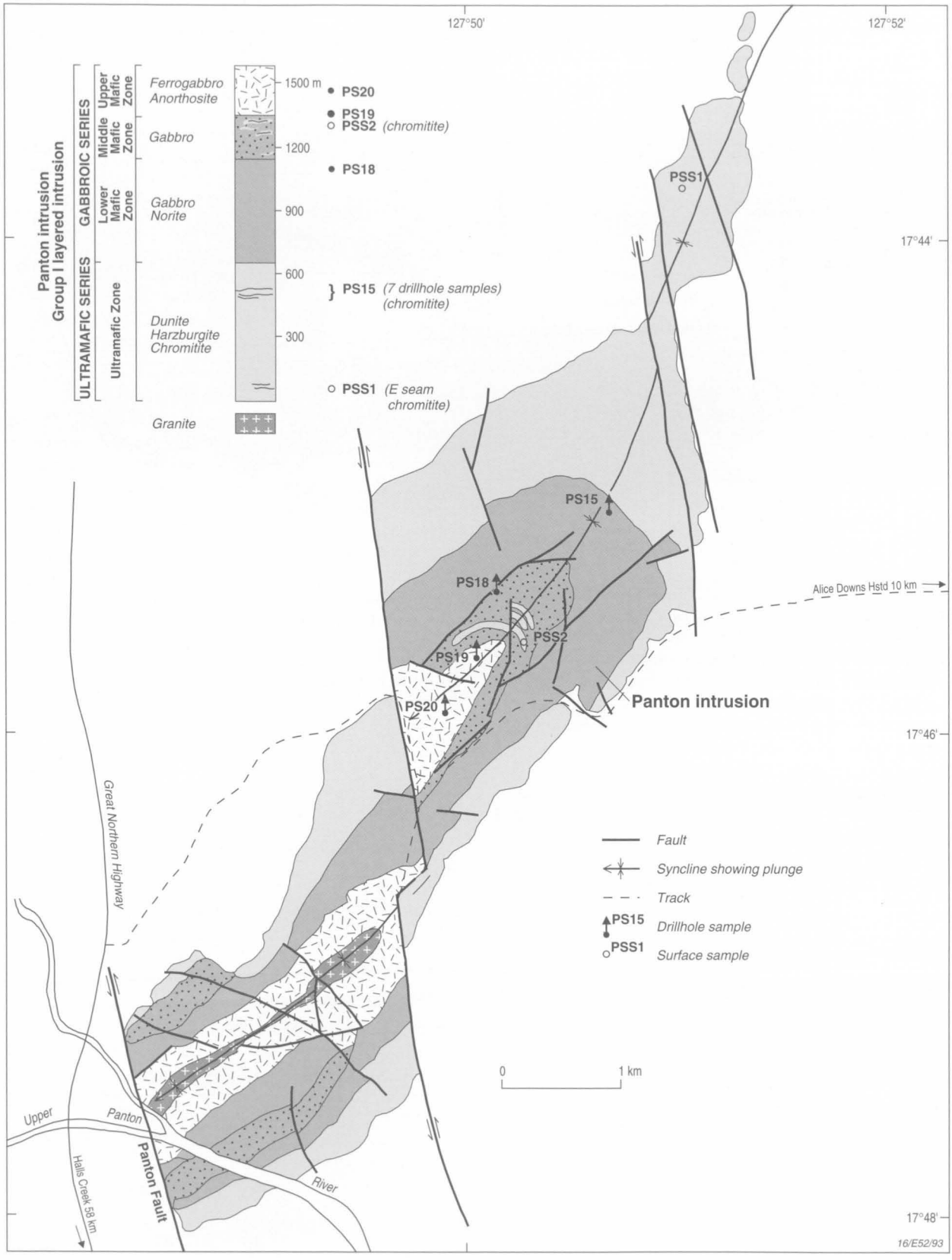


Figure 12.1. Geology of the Panton intrusion and locations of sampled diamond-drill holes and surface samples (PSS1, PSS2).

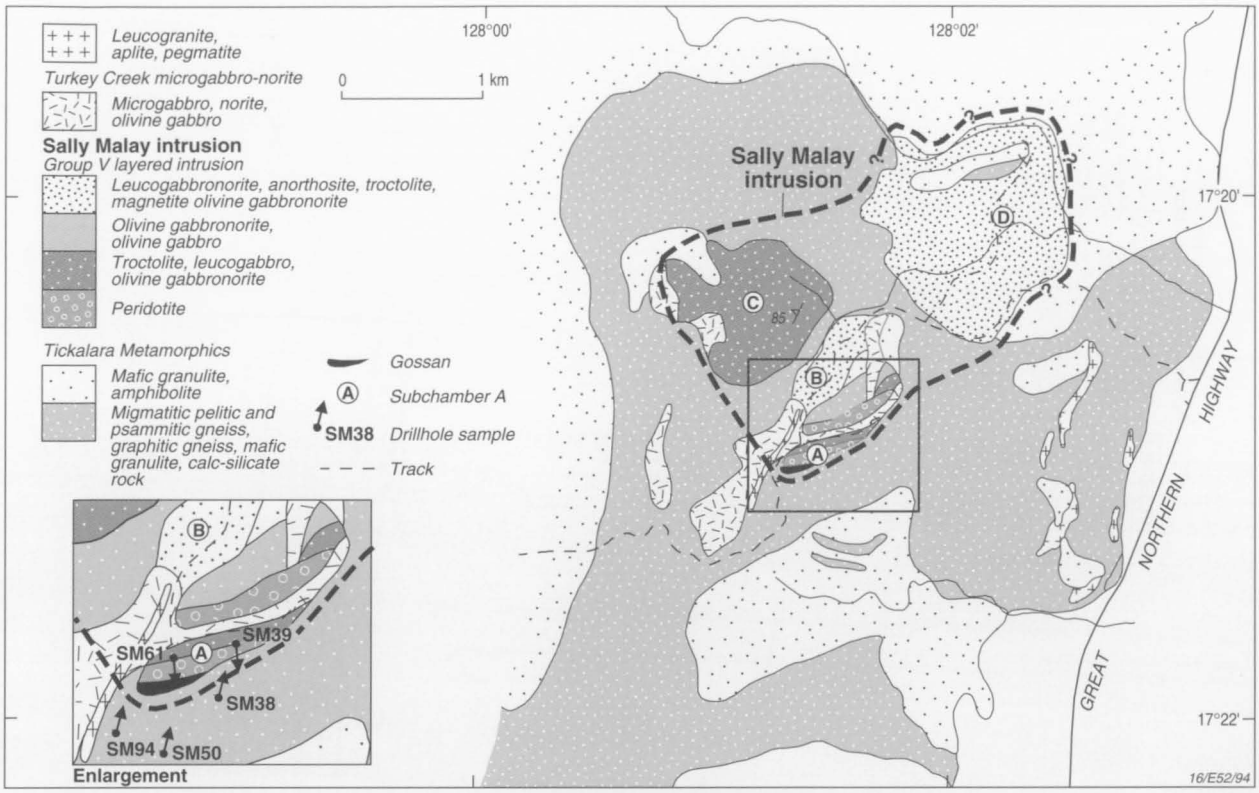


Figure 12.2. Geology of the Sally Malay intrusion and locations of sampled diamond-drill holes.

Sulphide mineralisation is of two major textural types: disseminated matrix sulphide (5–40 vol. %) and massive sulphide (90–100 vol. %). The massive sulphide consists of primary hexagonal pyrrhotite and minor granular pentlandite, chalcopyrite, and rounded magnetite (~1 mm across). It shows little indication of recrystallisation and is coarse grained (pyrrhotite ~1–3 mm diameter; pentlandite ~1 mm diameter). Matrix sulphides extend upward into the overlying basal peridotite and also form part of the matrix in breccias of the footwall migmatites.

The Sally Malay intrusion shows many similarities to the intrusion containing the recently discovered Voisey's Bay Ni–Cu–Co deposit in Labrador, Canada (Naldrett et al. 1996, Ryan et al. 1995, Hoatson et al. 1997, Lambert et al. 1997b). The two mineralised intrusions occupy similar tectonic settings, namely a Proterozoic 1.85 Ga collisional suture zone (Torngat orogen in Labrador, HCO in East Kimberley), and both contain troctolites (Naldrett et al. 1996, Ryan et al. 1995, see Chapter 14). The sulphide-hosting southern body of Sally Malay (Hoatson et al. 1997) may be analogous to the most mineralised section of Voisey's Bay, which is interpreted to represent a feeder conduit to other exposed sections of the intrusion (Naldrett et al. 1996, Ryan et al. 1995).

Methods

Eleven representative whole-rock cumulates were selected from the UMS and GS of the Panton intrusion for trace-element and Sm–Nd and Re–Os isotopic analysis (Fig. 12.1). Re–Os isotopic analyses were undertaken on chromite separates from three chromitite seams and one olivine–chromite cumulate. Sm–Nd and Re–Os iso-

Table 12.1. Platinum-group-element geochemistry of major rock types in the Panton intrusion.

Drillhole	*Depth (m)*	*Lithology*	*Ir (ppb)*	*Ru (ppb)*	*Pt (ppb)*	*Pd (ppb)*	*Au (ppb)*
PS20	108.4	Anorthosite	0.057	1.48	10.30	0.96	0.59
PS19	206.6	Gabbro	0.057	0.05	7.63	0.71	1.01
PS19	430.0	Gabbro	0.034	1.05	19.50	3.49	2.42
PS18	69.15	Gabbro	0.085	0.59	18.80	3.59	2.69
PS15	210.5	Dunite	1.010	3.83	25.40	43.10	3.67
PS15	232.0	Dunite	4.710	22.70	137.6	284.4	8.96
PS15	233.6	A seam chromitite	20.10	247.0	4499	1110	210.0
PS15	238.0	Dunite	5.850	9.92	353.1	226.9	32.60
PS15	265.8	Dunite	16.70	42.50	343.0	407.0	27.30
PSS1[1]	-	E seam chromitite	74.00	202.0	649.0	637.0	42.00

[1] Surface sample.

topic analyses were carried out on five whole-rock samples from the Sally Malay intrusion, including one of massive sulphide. We have also analysed pentlandite and pyrrhotite separates from the massive sulphide ore and a bulk sulphide separate from a matrix ore sample.

PGE analyses were determined by nickel sulphide fire assay and radiochemical neutron activation analysis (RNAA) at the University of Melbourne, using the method outlined in Reeves & Keays (1995). Sm–Nd isotopic data were obtained by isotope dilution, using a Finnigan MAT 262 multi-collector thermal ionisation mass spectrometer at La Trobe University and methods described in Elburg & Nicholls (1995), which are similar to those of Maas & McCulloch (1991). Re–Os isotopic data were obtained by isotope dilution negative thermal ionisation mass spectrometry (N-TIMS), using methods outlined in Lambert et al. (1998b). Selected chromitites were reanalysed on a Finnigan MAT 'Element' high resolution inductively coupled plasma mass spectrometer (HR-ICP-MS).

Geochemical and isotopic results

Panton intrusion

Platinum-group-element data. PGE data for the Panton intrusion are shown in Table 12.1. The mantle-normalised PGE abundances (Fig. 12.3) have distinctive arch-shaped patterns, similar to those observed for other reef-style PGE deposits (e.g. UG-2 and Merensky Reef from the Bushveld Complex: Barnes et al. 1988). This contrasts with the flat PGE patterns observed for ophiolite deposits (Barnes et al. 1988). The low concentrations of the IPGE (iridium group of PGEs = Ru, Os, and Ir) and high concentrations of the more chalcophilic PPGE (platinum group of PGEs = Rh, Pt, Pd, and 'Au') in the Panton intrusion infer a sulphide control of the PGE abundances (Naldrett 1989).

No systematic variation can be seen in the Pd/Ir ratio in the Panton intrusion (Fig. 12.4A), suggesting that the magma was continually sulphide saturated. This is supported by the high S content (Hamlyn et al. 1988) and the presence of minor amounts of cumulus sulphide throughout the intrusion. Cu/Pd and Cu/Pt are sensitive to R factor (= the effective mass of silicate melt with which a given mass of sulphide melt has equilibrated: Campbell et al. 1983, Naldrett 1989, 1997) and sulphide saturation. In numerous PGE reef-hosting intrusions, including the Munni Munni intrusion of the west Pilbara Craton, Western Australia, and the Bushveld Complex, the main ore zones coincide with sulphide saturation (Hoatson & Keays 1989, Barnes et al. 1993, Maier et al. 1996) and are marked by an abrupt increase in Cu/Pd ratio (Barnes et al. 1993, Fig. 12.4B). In the Panton intrusion, the increase in the Cu/Pd ratio above the A seam (Fig. 12.4B) is not as marked as in some other PGE-bearing intrusions, such as the Munni Munni intrusion (Fig. 12.4C), because the magma was continually sulphide saturated.

Sm–Nd isotopic data. Sm–Nd isotopic data for samples from the Panton intrusion are shown in Table 12.2. The data define a Model 1 errorchron (McIntyre et al. 1966)

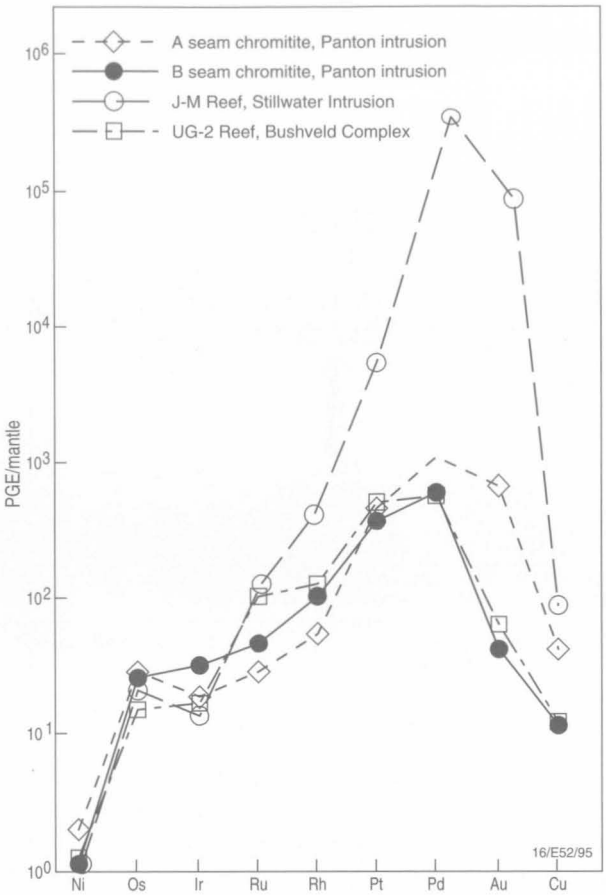


Figure 12.3. Primitive mantle-normalised PGE patterns for the A and B chromitite seams from the Panton intrusion, the J-M Reef from the Stillwater Intrusion, and the UG-2 chromitite from the Bushveld Intrusion. The primitive mantle values for normalising and the Stillwater and Bushveld plots are from Barnes et al. (1988). The PGE data for the Panton intrusion are based on multiple analyses from Perring & Vogt (1991).

giving an age of 1863±40 Ma and an initial ε_{Nd} value of –0.9 with a mean square of weighted deviates (MSWD) = 9.14 (Fig. 12.5). The high MSWD suggests that there is more scatter about the isochron than can be accounted for by analytical uncertainty (McIntyre et al. 1966). A Model 3 isochron regression yields an age of 1865±30 Ma and an initial ε_{Nd} of –0.9, within the uncertainty of the U–Pb SHRIMP zircon age of 1856±2 Ma (Page et al. 1995) for an anorthosite cyclic unit near the top of the GS. This suggests that the Sm–Nd isotopic system has remained closed and that there may have been subtle heterogeneity in initial Nd isotopic composition in the magma chamber. No systematic variation in the initial Nd isotopic composition is seen across the A chromitite seam. The initial Nd isotopic composition (ε_{Nd} = –0.9) is much less radiogenic than that of the depleted mantle at the time the Panton intrusion was emplaced (ε_{Nd} = +5, using values of Michard et al. 1985).

Re–Os isotopic data. Re–Os isotopic data for samples from the Panton intrusion are shown in Table 12.3. Chromitite whole-rock samples and chromite separates have a high Os concentration and low Re/Os ratio (Fig. 12.6A). This is characteristic of strong partitioning of Os

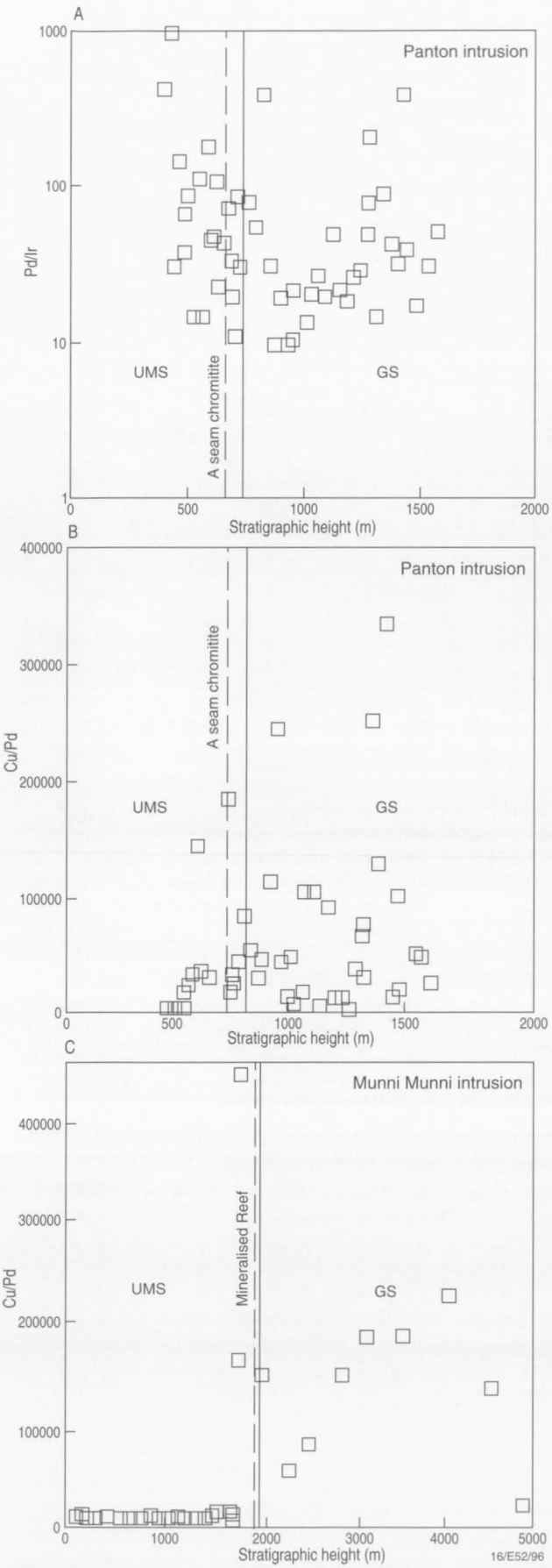


Figure 12.4. Trace-element geochemistry of the Panton and Munni Munni intrusions.

A. Variations in Pd/Ir with stratigraphic height (m) for the Panton intrusion (after Hamlyn et al. 1988).

B. Variations in Cu/Pd with stratigraphic height (m) for the Panton intrusion (after Hamlyn et al. 1988).

C. Variations in Cu/Pd with stratigraphic height (m) for the Munni Munni intrusion, west Pilbara Craton, Western Australia (after Barnes et al. 1993).

over Re during chromite crystallisation. The chromitite values overlap the field for Stillwater Complex chromitites and chromite separates, and lie near the field of J-M Reef sulphides (Stillwater Complex) (Fig. 12.6A). Whole-rock samples from the UMS (olivine ± chromite mesocumulates) and the GS (two gabbros and one anorthosite) form a continuum from a high Os and low Re/Os ratio to a low Os and high Re/Os ratio, and plot within the field of mafic and ultramafic magmas (Fig. 12.6A).

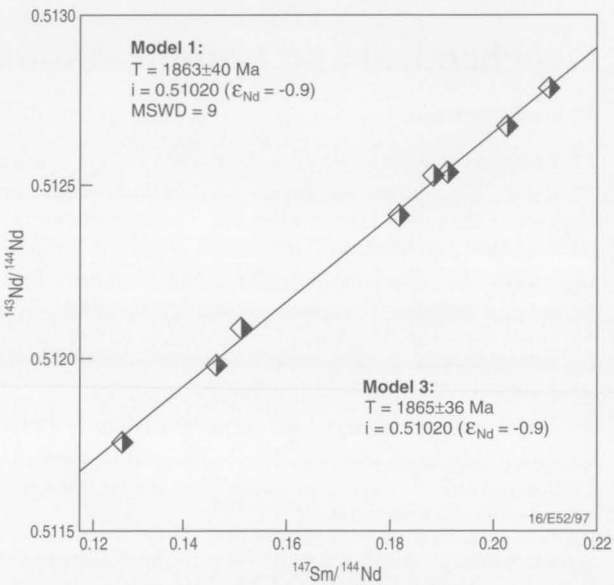


Figure 12.5. Sm–Nd isotopic evolution diagram for samples from the Panton intrusion. Isochron regressions are based on algorithms of McIntyre et al. (1966).

Re–Os isotopic data for samples from above and below the A chromitite seam (excluding one dunite whole-rock analysis) define a Model 1 errorchron (McIntyre et al. 1966) with an age of 1780±17 Ma and an MSWD of 1700. This suggests that there is again significant scatter about the isochron, more than can be accounted for by analytical uncertainty (McIntyre et al. 1966). A Model 3 isochron regression yields an age of 1850±40 Ma (Fig. 12.6B). This age is within error of the Sm–Nd isochron age and the magmatic SHRIMP U–Pb zircon age of 1856±2 Ma (see Chapter 6), inferring that the Re–Os isotopic system has remained closed, and an initial gOs value of +10 (per cent deviation of initial Os isotopic composition from chondritic asthenospheric mantle of the same age). One dunite sample deviates significantly from the isochron. This sample has extensively altered postcumulus phases and sulphides that are recrystallised along grain boundaries and along veinlets, and it may

Table 12.2. Sm-Nd isotopic data for the Panton and Sally Malay intrusions.

Drillhole	*Depth (m)*	*Lithology*	*Nd (ppm)*	*Sm (ppm)*	$^{143}Nd/^{144}Nd$[1]	$^{147}Sm/^{144}Nd$	ε_{Ndi}[2]	T_{DM} (Ga)[3]
Panton intrusion								
PS15	318.4	Dunite	0.966	0.238	0.512022	0.14910	-0.68	2.27
PS15	238.0	Dunite	1.485	0.458	0.512492	0.18655	-0.43	2.66
PS15	232.0	Dunite	2.023	0.616	0.512481	0.18421	-0.09	2.54
PS15	210.5	Dunite	1.337	0.337	0.512114	0.15250	0.31	2.18
PS19	430.0	Gabbro	1.211	0.393	0.512592	0.19622	-0.79	3.07
PS19	206.6	Gabbro	2.585	0.765	0.512364	0.17898	-1.13	2.64
PS20	108.4	Anorthosite	5.139	1.142	0.511830	0.13436	-0.92	2.22
Sally Malay intrusion								
SM38	205.0	Peridotite	2.879	0.736	0.512120	0.15459	-0.16	2.46
SM39	164.0	Troctolite	3.304	0.86	0.512173	0.15726	0.25	2.44
SM38	203.2	Peridotite	3.315	0.852	0.512172	0.15532	0.69	2.36
SM61	36.7	Troctolite	2.512	0.666	0.512196	0.16021	0.00	2.50
SM61	344.0	Troctolite	5.829	1.439	0.512069	0.14926	0.11	2.38

[1] 2σ external precision, based on repeat analyses of La Jolla Nd standards = ±0.000016.

[2] $\varepsilon_{Ndi} = 10^4[(^{143}Nd/^{144}Nd \text{ of the sample}/^{143}Nd/^{144}Nd_{CHUR})-1]$ where $^{143}Nd/^{144}Nd_{CHUR} = 0.512638–0.1966(e^{\lambda t}–1)$ (Wasserberg et al. 1981), t = time of intrusion and $\lambda = 6.54 \times 10^{-12}$ yr^{-1} (Lugmair & Marti 1978).

[3] Calculated using depleted mantle values from Michard et al. (1985).

have experienced Re loss, thus increasing the apparent initial Os isotopic composition. A systematic variation in the initial Os isotopic composition is not seen either side of the A chromitite seam (PGE ore zone).

Sally Malay intrusion

Sm–Nd isotopic data. Sm–Nd isotopic analyses for the Sally Malay intrusion are shown in Table 12.2. The data demonstrate a limited range of $^{147}Sm/^{144}Nd$ values (0.1493–0.1602), too narrow to determine a precise isochron. Tightly clustered initial Nd isotopic compositions (ε_{Nd} = +0.7 to –0.2) overlap those for the Nd isotopic data from the Panton intrusion.

Re–Os isotopic data. Re–Os isotopic data for samples from the Sally Malay intrusion are shown in Table 12.3. The data show an intermediate to high Re/Os ratio and intermediate to high Os concentration. The three sulphide-poor samples (troctolite and peridotite) lie in the ultramafic–mafic melts field (Fig. 12.7A). Sulphide-rich samples have a low to medium Os concentration (2–4 ppb) and a high Re/Os ratio (~20), similar to data for massive sulphide ores from the Duluth Complex, Minnesota, USA (Fig. 12.7A, Ripley et al. 1995, Lambert et al. 1997a), and Voisey's Bay, Labrador, Canada (Lambert et al. 1997b), but unlike the low Re/Os ratio and high Os concentration observed in the J-M Reef sulphides of the Stillwater Complex (Lambert et al. 1994).

Massive sulphide mineralisation from the Sally Malay intrusion yields an exceptionally radiogenic initial Os isotopic compositions (γ_{Os} = +1100 to +1300). Troctolites with matrix-disseminated sulphide (~40% sulphide) range from γ_{Os} = +450 to +470, whereas those from weakly mineralised troctolite and peridotite range from γ_{Os} = +60 to +369. Non-massive sulphide samples yield a Model 3 isochron (selected because of the small sample size; McIntyre et al. 1966) of ε_{Nd} 1893±57 Ma (Fig. 12.7B), within error of the magmatic SHRIMP U–Pb zircon age of 1844±3 Ma (see Chapter 6), suggesting that these samples have remained isotopically closed. The Re–Os isotopic data from the Sally Malay intrusion do not define an isochron, but lie between the 1845 Ma chondritic and enriched reference lines (Fig. 12.7B).

Petrogenesis of the Panton and Sally Malay intrusions

Enriched mantle versus crustal contamination

Sun et al. (1991) noted the similarity of the Panton intrusion and other intrusions in the HCO to continental flood basalts and proposed that they were derived dominantly from the convecting asthenospheric mantle, with some input from the lithospheric mantle and crust. In particular, the Nb depletion and LREE enrichment observed in the Panton intrusion may be attributed to crustal contamination.

The initial Nd isotopic composition (ε_{Nd} = –0.9) for samples from the Panton intrusion is much lower than depleted mantle of the same age (ε_{Nd} = +5: Michard et al. 1985). The initial Os isotopic composition is more radiogenic (γ_{Os} = +10) than that of asthenospheric upper mantle (γ_{Os} = 0). These data may be consistent with a magma source in the upper mantle, followed by contamination with continental lithosphere. The uniformly low ε_{Nd} values for the Panton intrusion imply that all parental magmas for the intrusions were equally contaminated and well mixed. The combination of near-chondritic Nd and Os isotopic compositions, though, is also characteristic of modern enriched mantle plume-derived ocean-island basalts (OIB: Martin 1991); hence magmas parental to the Panton intrusion may have been derived from a Proterozoic enriched mantle plume. We cannot clearly differentiate between a parental magma sourced from enriched portions of the mantle and a mantle-

Table 12.3. Re-Os isotopic data for the Panton and Sally Malay intrusions.

Drillhole-surface sample	*Depth (m)*	*Lithology*	*Stratigraphic height (m)*	*Re (ppb)*	*Os (ppb)*	*Common Os (ppb)*[1]	*Re/ common Os*	$^{187}Re/^{188}Os$	$^{187}Os/^{188}Os$ (2σ)[2]	$^{187}Os/^{188}Os(i)$ (2σ)[3]	$\gamma_{Os(i)}$[4] (2σ)[3]
Panton intrusion											
PS20	108.4	Anorthosite	1480	0.2034	0.0307	0.0263	6.625	37.21	1.2826 (1251)	0.1325 (495)	16.2 (43)
PS19	206.6	Gabbro	1295	0.1864	0.0429	0.0378	4.345	23.72	0.84158 (401)	0.1081 (317)	-5.51 (2740)
PSS2	-	Chromitite	1280	0.1166	34.55	34.15	0.003	.02231	0.17477 (35)	0.1741 (4)	52.0 (3)
PSS2	-	Chromite separate	1280	0.21225	49.04	48.56	0.004	0.009787	0.12329 (33)	0.1230 (3)	7.37 (29)
PSS2	-	Chromite separate	1280	0.3737	49.04	48.56	0.008	0.03769	0.12329 (33)	0.1222 (3)	6.62 (29)
PS18	69.15	Gabbro	995	0.1959	0.1460	0.1370	4.341	6.874	0.35946 (1029)	0.1469 (137)	28.1 (120)
PS15	210.5	Dunite	570	1.226	0.8362	0.7133	1.467	8.268	0.49354 (838)	0.2376 (138)	107 (12)
PS15	233.6	A seam chromitite	530	10.25	105.3	105.1	0.097	0.4716	0.12776 (39)	0.1132 (7)	-1.12 (60)
PS15	233.6	A seam chromitite	530	13.52	101.8	101.6	0.133	0.3994	0.12847 (26)	0.11610 (6)	1.29 (90)
PS15	233.6	A seam chromite separate	530		15.06	15.06			0.13043 (46)		
PS15	233.6	A seam chromite separate	530	1.5315	16.99	16.25	0.090	0.4531	0.12878 (81)	0.1149 (10)	0.283 (88)
PS15	265.8	Dunite	520	1.243	11.16	11.06	.112	.5404	0.15570 (324)	0.1390 (33)	21.3 (29)
PS15	318.4	Chromite separate	460	0.98975	23.16	22.97	0.0431	0.2072	0.13559 (53)	0.1292 (6)	12.8 (6)
PSS1	-	E seam chromitite	20	1.392	91.03	90.82	0.0153	0.07369	0.12787 (37)	0.1256 (3)	9.64 (34)
PSS1	-	E seam chromite separate	20	0.18685	13.43	13.02	0.0143	0.06898	0.15333 (100)	0.1512 (10)	32.9 (9)
Sally Malay intrusion											
SM94	428.5	Pentlandite separate	-	41.98	2.847	1.618	25.94	124.7	5.3550 (107)	1.5237 (1641)	1230 (143)
SM94	428.5	Pyrrhotite separate	-	50.62	3.265	1.876	26.99	129.7	5.5758 (225)	1.5893 (1720)	1290 (150)
SM94	428.5	Massive sulphide	-	43.85	7.416	4.655	9.421	45.20	2.7660 (209)	1.3777 (629)	1100 (55)
SM61	344.0	Troctolite	-	0.1501	0.3047	0.2797	0.537	2.580	0.61791 (124)	0.5388 (36)	369 (3)
SM61	36.7	Troctolite	-	0.1242	0.0904	0.0839	1.479	7.112	0.48509 (744)	0.2671 (119)	132 (10)
SM38	203.2	Peridotite	-	4.655	0.5596	0.4698	9.909	47.64	1.6443 (10)	0.1840 (632)	60.4 (55)
SM50	366.8	Sulphide separate	-	37.61	2.999	2.092	17.98	86.43	3.3067 (66)	0.6572 (1134)	473 (99)
SM50	366.8	Sulphide-troctolite	-	63.32	4.654	2.651	23.89	114.8	4.1544 (160)	0.6341 (1514)	453 (132)

[1] Common Os excludes ^{187}Os which results from decay of ^{187}Re after the intrusion age.

[2] Uncertainties are 2σ of the population (0.7%) for repeat DTM standard Os isotopic analyses (n = 22) or represent internal precision at 2 standard deviations of the mean if >0.7%.

[3] 2σ errors determined using the method from Sambridge & Lambert (1997).

[4] $\gamma_{Os(i)} = 10^2[(^{187}Os/^{188}Os_{initial}/^{187}Os/^{188}Os_{CHUR})-1]$ where $^{187}Os/^{188}Os_{CHUR} = 0.09600 + 0.4007(e^{\lambda(TE)}-e^{\lambda t})$ (Walker et al. 1994), TE = age of Earth = 4.56 x 10^9 Ma; t = time of intrusion in Ma and $\lambda = 1.64 \times 10^{-11}$ yr^{-1} (Lindner et al. 1989).

[5] Reanalysed using High Resolution ICP–MS.

PSS = surface sample from the Panton intrusion; PS or SM = drill core sample from the Panton (PS) or Sally Malay (SM) intrusions.

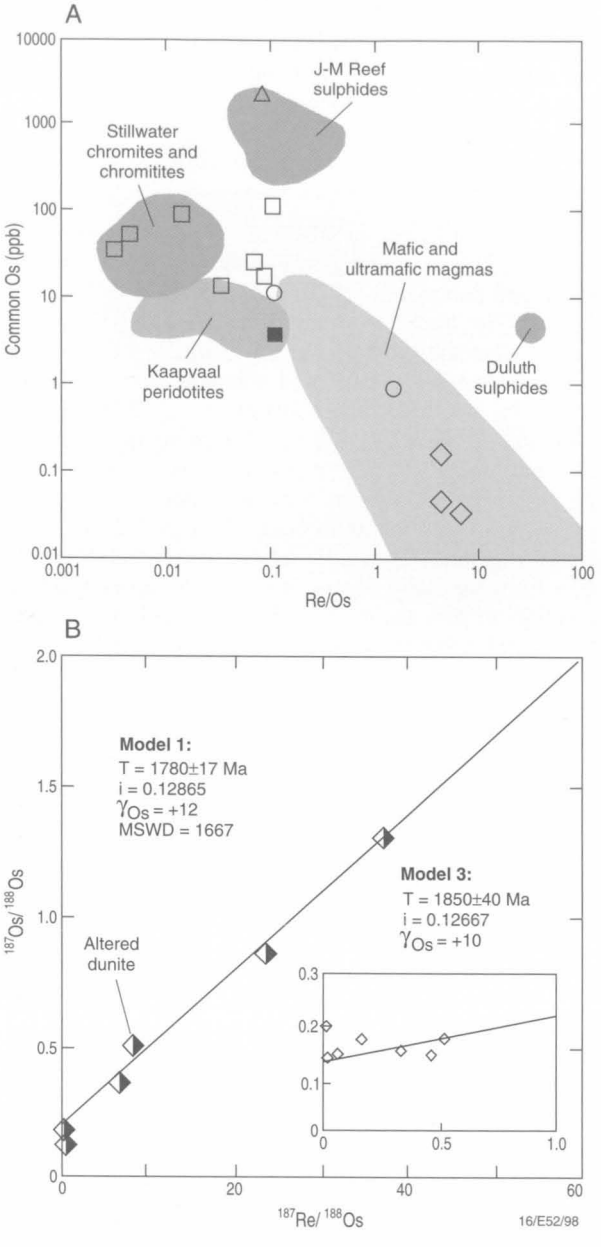


Figure 12.6. Re/Os versus Os isotope plots for the Panton and overseas intrusions.

A. Comparison of common Os concentration versus Re/Os ratio for the Panton intrusion with other mafic–ultramafic rocks and mineralised settings. Panton intrusion: chromitite seams & separates = open squares, Ultramafic Series cumulates = open circles, and Mafic Series cumulates = open diamonds. Stillwater Intrusion: J-M Reef chromitite = open triangle (Lambert et al. 1994). Duluth Complex: Babbitt Deposit Cu–Ni sulphide mineralisation = grey circle (Ripley et al. 1995). Kaapvaal peridotites = light grey field (Walker et al. 1989). Mafic and ultramafic magmas are a global compilation of data for Ocean Island Basalts (Martin 1991, Pegram & Allegre 1992, Hauri & Hart 1993, Reisberg et al. 1993, Marcantonio et al. 1995) and Pyke Hill and Gorgona komatiites and basalts (Walker et al. 1989, 1991). The primitive mantle value is shown as a filled black square (Morgan 1986, Walker & Morgan 1989).

B. Re–Os isotopic evolution diagram for the Panton intrusion. Inset shows an enlargement of the small scatter at low values of $^{187}Re/^{188}Os$ and $^{187}Os/^{188}Os$. Isochrons are based on all samples, excluding an altered dunite sample.

derived magma that assimilates crustal material en route to the mid-upper crust. Although the Panton and Sally Malay intrusions have near-identical initial Nd isotopic compositions, the Sally Malay intrusion has significantly more radiogenic Os isotopic signatures (γ_{Os} = +60 to +1300). This extreme range of Os isotopic compositions requires crustal contamination of a mantle-derived melt.

We have modelled the degree of crustal contamination required to produce the Os and Nd isotopic compositions observed in the Panton intrusion, using two-component mixing between mantle-derived basalt and average crust (Shirey 1991). The modelling of the Os data suggests that a minor amount of crustal contamination has occurred, with 5–20% assimilation of crust with an age of 3.6 and 2.7 Ga, respectively. This is less than is indicated by two-component mixing with Nd isotopic data, possibly suggesting that the Re–Os and Sm–Nd isotopic systems were decoupled during crustal assimilation and subsequent mineralisation (Fig. 12.8). We suggest that this variation may be attributed to the preference of Os for any immiscible sulphide and also to the effect of the R factor on the Os isotopic system. The Sally Malay intrusion (γ_{Os} = +60 to +1300) has a significantly more radiogenic Os isotopic composition than the Panton intrusion. The Os isotopic data indicate a higher (and variable) degree of crustal contamination than that indicated by the Nd isotopic data. Again, this may be ascribed to the effect of the R factor on Re–Os isotopic systematics.

R-factor modelling and ore genesis

When the sulphur solubility of a magma is exceeded, excess sulphur forms an immiscible sulphide melt, essentially an Fe–S–O melt, which coexists with the silicate magma (Fincham & Richardson 1954). PGEs, Cu, and Ni are strongly partitioned into the immiscible sulphide melt (Campbell et al. 1984, Peach et al. 1990, Fleet et al. 1996); hence, sulphide melts act as efficient metal concentrators. Sulphur solubility can be influenced by physical (e.g. pressure, temperature) and chemical changes (e.g. f_{O_2} composition) in the magma (Fincham & Richardson 1954, Haughton et al. 1974, Buchanan & Nolan 1979). In particular, the sulphur solubility of a magma can be reduced by assimilation of crustal material, a process which may be important in the formation of some magmatic sulphide ore deposits (Irvine 1975, Naldrett 1989). Geochemical evidence for crustal contamination in magmatic ore systems can include LREE enrichment, low initial ε_{Nd}, and γ_{Os} >>1 (Lambert et al. 1997a).

The R factor, which is not routinely included in isotopic modelling of sulphide ore genesis, can be crucial for radiogenic isotopes with a strong affinity (D >>1) for magmatic sulphide melts, in particular the Re–Os isotopic system (Foster et al. 1996). If the R factor is high (i.e. in dynamic magmatic systems), extensive equilibration can occur between immiscible sulphide melt and chondritic asthenospheric mantle melt (Lambert et al. 1997a). This equilibration can result in a decrease in the initial Os isotopic composition of crustally contaminated ores, if R is sufficiently large (i.e. R >500). Thus, crustal

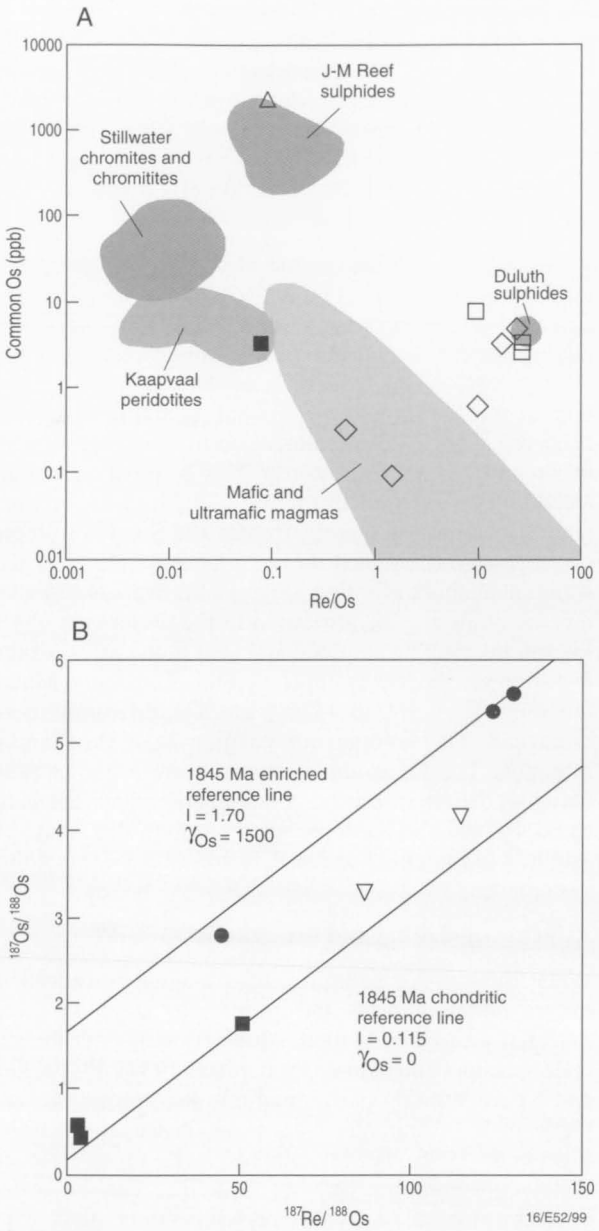


Figure 12.7. Re/Os versus Os isotopic plots for the Sally Malay and overseas intrusions.

A. Comparison of common Os concentration and Re/Os ratio for the Sally Malay intrusion with other mafic–ultramafic rocks and mineralised settings. Sally Malay intrusion: troctolite and peridotite = open diamonds, massive sulphide = open squares. Stillwater Intrusion: J-M Reef chromitite = open triangle (Lambert et al. 1994). Duluth Complex: Babbit Deposit Cu–Ni sulphide mineralisation = grey circle (Ripley et al. 1995). Kaapvaal peridotites = light grey field (Walker et al. 1989). Mafic and ultramafic magmas are a global compilation of data for Ocean Island Basalts (Martin 1991, Pegram & Allegre 1992, Hauri & Hart 1993, Reisberg et al. 1993, Marcantonio et al. 1995) and Pyke Hill and Gorgona komatiites and basalts (Walker et al. 1989, 1991). The primitive mantle value is shown as a filled square (Morgan 1986, Walker & Morgan 1989).

B. Re–Os isotopic evolution diagram for the Sally Malay intrusion. Massive sulphide and separate = filled circles; sulphide-rich troctolite = open triangles; troctolite and peridotite = filled squares.

contamination processes which may promote sulphide saturation are difficult to assess with Re–Os isotopes, as the effects of contamination can be masked in dynamic magmatic systems (Lambert et al. 1997a). Hence, consideration of R-factor processes during interpretation of Os isotopic data in mineralising environments is imperative.

We have modelled the R-factor process in the Sally Malay intrusion, using the equation developed by Campbell & Naldrett (1979). We found low estimates of R (~250) for the Sally Malay intrusion (Table 12.4), suggesting that the ore-forming environment in this intrusion was largely passive and stagnant. For the Panton intrusion, we found high estimates of R (~6125 to ~40 000, Table 12.4), inferring a more turbulent and dynamic magmatic ore system. Thus, high R-factor processes in the Panton intrusion may be potentially masking crustal contamination. On a global Os versus Re/Os diagram (Fig. 12.9), massive sulphide mineralisation from the Sally Malay intrusion occupies a similar position to low tenor ores from the Duluth Complex (medium Os, but high Re/Os, Lambert et al. 1997a). The Panton intrusion PGE mineralisation (calculated to 100% sulphide) occupies a similar position to the high tenor ores from the J-M Reef (i.e. high Os, but low Re/Os, Lambert et al. 1994). The Re and Os data, therefore, support the R-factor estimates based on PGE and Cu data for each intrusion (Table 12.4).

The Re–Os isotopic data for the Sally Malay intrusion sulphide mineralisation can be modelled with equations developed by Foster et al. (1996), whereby a basaltic magma is contaminated with old crustal sulphides

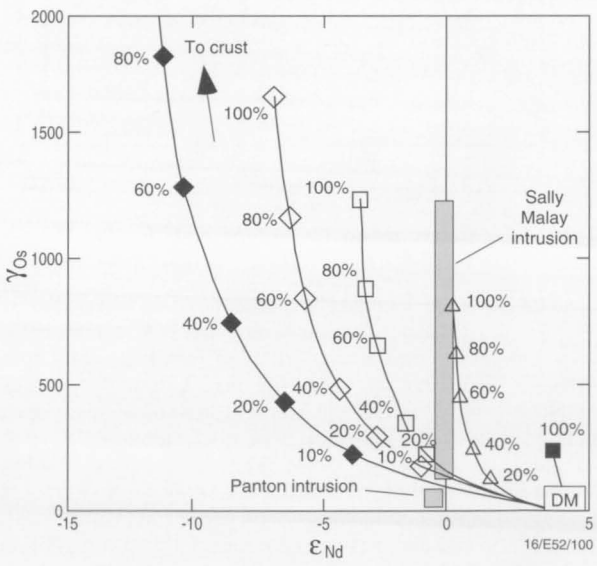


Figure 12.8. Two-component γ_{Os} versus ε_{Nd} contamination diagram, using depleted mantle (DM) melt (Os = 0.075 ppm and Nd = 10 ppm) and crust formed at 2.0–3.6 Ga. Crust values are from Taylor & McLennan (1995), and depleted mantle (DM) values are from Shirey (1991). The effect of the R factor is not shown on this diagram. Filled diamonds are 3.6 Ga crust; open diamonds are 3.0 Ga crust, open squares are 2.7 Ga crust; open triangles are 2.4 Ga crust, and filled squares are 2.0 Ga crust.

(Lambert et al. 1997a). In this model, Re and PGE abundances increase as the crustally contaminated immiscible sulphide melt equilibrates with host basalt, increasing the Os concentration and decreasing the Re/Os ratio of the sulphide mineralisation at R factors of 200–400. This low R-factor step may represent a transport phase, in which the sulphides are entrained upward in the magma conduit, similar to what occurred in the Celebration Dyke in the Widgemooltha Dyke Swarm (Purvis & Moeskops 1981). Hence, crustal assimilation may have occurred as the magma ascended to the mid–upper crust.

Significant variation in Os isotopic composition is observed in the Sally Malay intrusion. Massive sulphides yield exceptionally radiogenic initial Os isotopic compositions (γ_{Os} = +1100 to +1300). Matrix-disseminated sulphide mineralisation in troctolite (~40 sulphide vol. %) ranges in γ_{Os} from +450 to +470, whereas that of weakly mineralised troctolite and peridotite ranges from +60 to +369. As the R factor is low in the massive sulphide mineralisation zone, the crustal-like Os isotopic signature in this zone will be little diluted, as evidenced by the radiogenic nature of the ores (Fig. 12.10). Moreover, the variation observed in initial Os isotopic composition in different parts of the Sally Malay mineralising system may also be due to a variable R factor: massive sulphide mineralisation appears to have experienced a lower R factor (~200) than the matrix-disseminated mineralisation (~500–800). This demonstrates that Re–Os isochron systematics cannot be applied successfully in crustally contaminated sulphide-saturated igneous rocks that have experienced a low and variable R factor, such as in the Sally Malay intrusion.

Table 12.4. R-factor estimates based on Pd, Pt, and Cu concentrations from the Panton and Sally Malay intrusions (using equations from Campbell & Naldrett 1979).

Intrusion	*Pd*[1]	*Pt*[1]	*Cu*[1]
Sally Malay[2]			250[3]
Panton[2]	10 000[4]	40 000[4]	6 000[4]

[1] K_d = 35 000 was used for Pt and Pd (Peach et al. 1990) and K_d = 500 was used for Cu (Klöck & Palme 1988).

[2] Negri Volcanics and the Cooya Pooya Dolerite (Sun et al. 1991) were used for average values of the parental magma.

[3] R-factor caculation based on the Cu content of the massive ore (from Normandy Poseidon Ltd).

[4] Assuming 2 wt% sulphide in the Panton intrusion. Estimating the amount of sulphide is difficult in chromitites as Fe from the Fe–S–O sulphide melt is consumed during chromite formation (Naldrett 1989) and sulphide is easily mobilised. 2 wt% was the minimum which could be assumed to give reasonable (i.e. not excessively high) concentrations of PGEs in the sulphide.

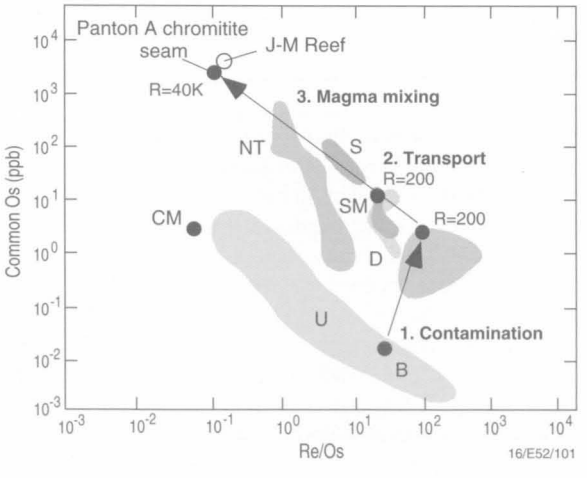


Figure 12.9. Common Os concentration versus Re/Os ratio for mantle-derived magmas and ores (adapted from Lambert et al. 1997a). All samples are calculated to 100% sulphide. SM = Sally Malay; NT = Noril'sk-Talnakh; S = Sudbury; D = Duluth; U = ultramafic magmas; B = basaltic magmas; CM = chondritic mantle. The R-factor paths assume D_{Re} = 500 and D_{Os} = 30 000.

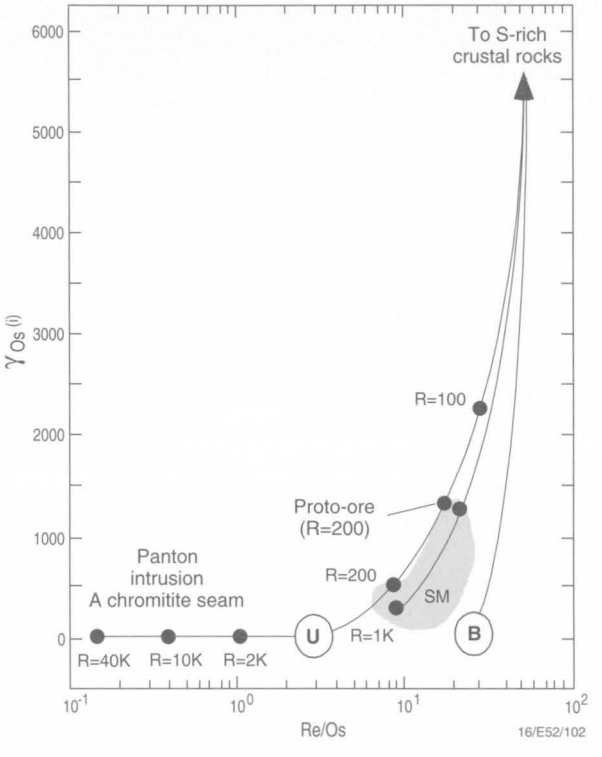


Figure 12.10. Initial γ_{Os} versus Re/Os for massive sulphides from the Sally Malay (SM) intrusion and chromitite from the Panton intrusion (A seam). Sulphide-rich crustal rocks are from Lambert et al. (1997a). B = basaltic magma with Re/Os = 25 (Foster et al. 1996) and U = ultramafic magma with Re/Os = 2 (Lambert et al. 1997a).

We prefer a two-stage model for the formation of Ni–Cu–Co mineralisation in the Sally Malay intrusion, which may be also appropriate for other magmatic sulphide ore systems (Duluth, Noril'sk-Talnakh, Sudbury, Voisey's Bay: Lambert et al. 1997a,b). In this model, sulphide-undersaturated basaltic melts assimilated crustal material en route to their mid-upper crustal magma chambers, and this promoted sulphide saturation in conduits or staging chambers. The immiscible sulphide 'proto-ores' became entrained in the silicate magmas and were transported to the crustal magma chambers, where the sulphide melts were passively deposited as a

result of fluid dynamic contrasts accompanying a change from narrow, near-vertical conduits to broader, open magma chambers. This process resulted in a low R factor, as the sulphide melts retained an old crustal γ_{Os} value inherited from the contaminant (Fig. 12.10). In contrast, the disseminated sulphide mineralisation preserves a record of higher R factors in some portions of the magmatic system, possibly as a result of greater transport or more extensive–effective mixing in a repeatedly replenished magma chamber.

For the Panton intrusion, our Re–Os modelling suggests that a two-stage contamination–R-factor process similar to that observed in the Sally Malay intrusion could not impart the necessary Os concentration and Re/Os ratio observed in the A chromitite seam. This process results in low–medium tenor ores, similar to sulphides from the Sally Malay intrusion and Noril'sk-Talnakh (Fig. 12.9). A possible way to achieve a better fit to the isotopic and geochemical data for the PGE mineralisation in the Panton intrusion is to add an extra R-factor step in the magma chamber. In this model, basaltic sulphide droplets, produced by crustal contamination deep in the crust, are entrained in a magma, resulting in a low R 'proto-ore'. The final magma mixing event in the upper crustal chamber resulted in a high R factor, producing the low Re/Os ratio and high Os concentration. This exceptionally high R factor produced the high-PGE tenor sulphide mineralisation in the A chromitite seam and increased Cu/Pd values near this seam (Fig. 12.4B). The A seam may be the thickest chromitite and have the highest PGE tenors because of the interplay of two factors. Firstly, a larger pulse of primitive magma may have mixed with the resident magma. Secondly, the formation of the A seam was close to the first major appearance of cumulus plagioclase in the Panton intrusion. This may have resulted in a resident magma with a density similar to the new magma pulse, permitting more extensive mixing, as proposed by Campbell et al. (1984) for the Merensky Reef in the Bushveld Complex and the J-M Reef in the Stillwater Complex. The high R factors and low γ_{Os} of the Panton intrusion (γ_{Os} = +10, Fig. 12.10) indicate that the initial crustal-like radiogenic Os isotopic signature was significantly diluted.

The Os isotopic composition and Re and Os concentrations of the Panton intrusion PGE-mineralisation are most closely matched with an R factor of 40 000, but only if the resident magma has a low Re/Os ratio (~2), like picrite and high MgO basalt melts (Bennett et al. 1996, Lambert et al. 1998). If the resident magma has a typical basaltic Re/Os value, then exceptionally high R factors are required (>>1 000 000). A three-stage model, which was also applied to the J-M Reef of the Stillwater Complex by Lambert et al. (1997a), requires a resident magma with lower Re/Os and higher Os concentration. However, Nd and Os isotopic data from the Stillwater Complex suggest the presence of two magma types (Lambert et al. 1994), as supported by a change in the crystallisation order of silicate minerals (i.e. olivine + chromite; bronzite; plagioclase; augite in the Ultramafic Series is replaced by plagioclase; olivine + chromite; bronzite; augite in the troctolite–anorthosite zones of the Banded Series: Irvine et al. 1983). Based on these observations, two compositionally different magma types have been designated at the Stillwater Complex by a high MgO and high SiO_2 'U–type' magma, and a high-Al 'A–type' tholeiitic magma. U–type magmas are characterised by the production of abundant cumulus orthopyroxene, a feature not observed in the Panton intrusion. Neither is there evidence for two isotopically distinct magma types in the Os and Nd isotopic data for the Panton intrusion. However, the available isotopic evidence does not preclude a high-MgO basaltic to picritic parental magma with low SiO_2, low Re/Os, and high Os concentration for the UMS of the Panton intrusion.

Implications for exploration

Mineralised intrusions in the HCO can be divided into two major types: high R factor, PGE–Cr-rich intrusions (e.g. Panton), and low R factor, Ni–Cu–Co-rich intrusions (Sally Malay) as shown in Figure 12.11. Geobarometric studies suggest that the Panton intrusion was emplaced at a relatively shallow depth (10–12 km) compared to the Sally Malay intrusion (20–23 km: Trudu & Hoatson 1996, see Chapter 9). If contamination and sulphide saturation occurred at depth, the shallow level of final sulphide accumulation may help to explain the high PGE tenor of magmatic sulphides. For example, large magma chambers in the shallower parts of the crust for the Panton and other similar intrusions (e.g. Bushveld, Stillwater) may have promoted higher R factors. The PGE-bearing intrusions (Panton, Big Ben, and South Melon Patch) are generally distinguished by larger magma chambers compared to the smaller Ni–Cu–Co-bearing intrusions (Sally Malay, Keller Creek, and Corkwood). Hence, the depth of emplacement, intrusion mechanisms, and size of intrusion appear to be important considerations in determining the tenor of magmatic sulphides and also the prospectivity of intrusions in the HCO. Maier et al. (1996) noted the sensitivity of Cu/Pt and Cu/Pd ratios to sulphide saturation and the R factor in PGE-reef ore genesis, and suggested that these ratios can be used to detect where the mineralisation is located within a vast section of magmatic stratigraphy. This is important, as PGE mineralisation is generally confined to narrow seams (<2 m). Increases in Cu/Pd ratio occur in the Panton intrusion at the A chromitite seam, but are not as marked as those observed in some other intrusions (e.g. Munni Munni), as the Panton magma was always sulphide saturated. Hence, Cu/Pd ratio may not be a useful geochemical indicator for ore zones in layered intrusions that have had an early history of sulphide saturation. Instead, the location of the ore zone near the appearance of cumulus plagioclase (marking the density contrast between the resident magma and newly injected magma in the intrusion, promoting more extensive mixing and higher R factor) may be used as an exploration guide.

Ni–Cu–Co mineralisation in the Sally Malay-type of intrusions is more likely to accumulate passively as basal sulphide layers or near (or in) feeders, being physically controlled by a widening or 'bending' of the magma conduit, which slows the magma flow rate and allows deposition (e.g. Voisey's Bay or Noril'sk-Talnakh). Ni–Cu–Co sulphide mineralisation is perhaps the more

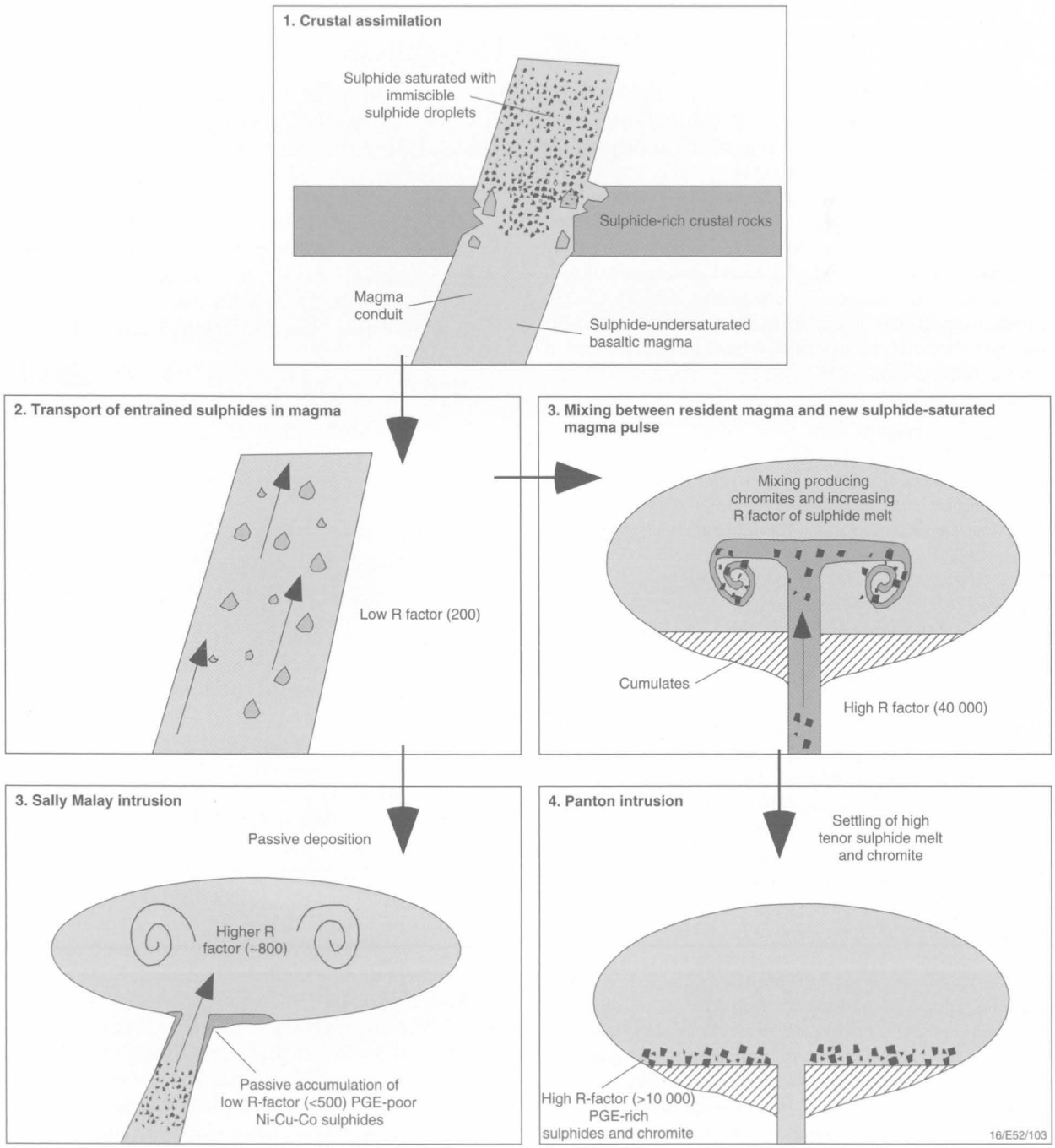


Figure 12.11. Model for the formation of magmatic mineralisation in the Sally Malay and Panton intrusions (see text for descriptions of various stages).

prospective target for explorers in the HCO, since it is often hosted by mafic intrusions, which are common in the HCO, and, unlike the PGE–Cr-type of mineralisation, it is less dependent on the volume of magma and high R-factor magma dynamics. The numerous narrow dyke-like intrusions and feeders to intrusions should be considered high priority for possible hosts for this style of mineralisation.

The occurrence of the Panton intrusion (which displays some similarities to the Bushveld and Stillwater complexes) and Sally Malay intrusion (which displays many similarities to Voisey's Bay) in the same province, and their similar age, indicate that these types of mineralised intrusions may also occur together elsewhere in the world. Based on observations from the HCO, PGE–Cr-bearing mineralisation may be found in large shallowly emplaced mafic–ultramafic intrusions, and Ni–Cu–Co mineralisation may occur in magma conduits and near the base of mafic intrusions that have been emplaced at deeper levels of the crust.

Conclusions

The parental magma or magmas to the Panton intrusion may be derived from enriched portions of the mantle or by crustal contamination of a mantle-derived magma. However, turbulent magma dynamics (high R factor) in the Panton intrusion have the potential to mask the crustal-like Os isotopic signatures. Crustal contamination is an important process in the petrogenesis of the Sally Malay intrusion and the magmatic Ni–Cu–Co sulphide mineralisation. This contamination probably occurred at deep levels in the crust, before the final stratigraphic level of sulphide accumulation. A two-stage model (Fig. 12.11) for the Sally Malay intrusion and its ores is indicated by the Re–Os isotopic data. The first stage requires crustal contamination of a basaltic melt at depth, promoting sulphide saturation and the formation of an immiscible sulphide melt phase. The second stage took place during transport of the sulphides in the host basaltic magma, resulting in a low R factor and low metal tenor. Passive deposition of the magma produced a basal sulphide layer with a very radiogenic crustal Re–Os isotopic composition (Fig. 12.11). The variable initial Os isotopic composition is likely to be caused by a variable R factor, which makes isochron systematics difficult to interpret. In the Panton intrusion, we envisage a three-stage model (Fig. 12.11). The first two stages (contamination and transport of sulphides) are common to the Sally Malay intrusion. The third stage requires a dynamic magma chamber process in which a new magma pulse carrying low-tenor sulphide droplets mixed with resident magma, resulting in a high R factor and PGE-enriched sulphides. The high R factor resulted in near-chondritic initial Os isotopic composition.

Acknowledgements

Financial and logistical support and permission to publish were kindly provided by Helix Resources NL. Access to diamond drill core from the Sally Malay intrusion was kindly provided by Normandy Exploration Limited. We thank Shane Reeves (University of Melbourne) for the PGE analyses, David Blake, Shen-su Sun (both AGSO), and Jeff Foster (BHP Minerals) for helpful reviews. R.A. Sproule is funded by an Australian Postgraduate Award (Industry).

References

Barnes, S-J., Boyd, R., Korneliussen, A., Nilsson, L-P., Often, M., Pedersen, R.B. & Robins, B., 1988. The use of mantle normalization and metal ratios in discriminating between the effects of partial melting, crystal fractionation and sulphide segregation on platinum-group elements, gold, nickel and copper: examples from Norway. In: Prichard, H.M., Potts, P.J., Bowles, J.F.W. & Cribb, S.J. (editors), Geoplatinum 87, 22–23 April 1987, Open University, Milton Keynes, United Kingdom, Elsevier, England, 113–143.

Barnes, S-J., Couture, J.F., Sawyer, E.W. & Bouchaib, C., 1993. Nickel–copper occurrences in the Belleterre–Angliers belt of the Pontiac subprovince and the use of Cu/Pd ratios in interpreting platinum-group element distributions: Economic Geology, 88, 1402–1418.

Bennett, V.C., Esat, T.M. & Norman, M.D., 1996. Two mantle-plume components in Hawaiian picrites inferred from correlated Os–Pb isotopes. Nature, 381, 221–224.

Buchanan, D.L. & Nolan, J., 1979. Solubility of sulfur and sulfide-immiscibility in synthetic tholeiitic melts and their relevance to Bushveld-Complex rocks. Canadian Mineralogist, 17, 483–494.

Campbell, I.H. & Naldrett, A.J., 1979. The influence of silicate:sulfide ratios on the geochemistry of magmatic sulfides. Economic Geology, 74, 1503–1506.

Campbell, I.H., Naldrett, A.J. & Barnes, S.J., 1983. A model for the origin of the platinum-rich sulphide horizons in the Bushveld and Stillwater Complexes. Journal of Petrology, 24, 133–165.

Campbell, I.H. Naldrett, A.J. & Barnes, S.J., 1984. A model for the origin of the platinum-group elements in magmatic sulfide deposits. Canadian Mineralogist, 22, 151–160.

Elburg, M.A. & Nicholls, I.A., 1995. Origin of microgranitoid enclaves in the S-type Wilson's Promontory Batholith, Victoria: evidence for magma mingling. Australian Journal of Earth Sciences, 42, 423–435.

Fincham, C.J. & Richardson, F.D., 1954. The behaviour of sulphur in silicate and aluminate melts. Philosophical Transactions of the Royal Society, London, 223, 40–62.

Fleet, M.E., Crocket, J.H. & Stone, W.E., 1996. Partitioning of platinum-group elements (Os, Ir, Ru, Pt, Pd) and gold between sulfide liquid and basalt melt. Geochimica et Cosmochimica Acta, 60, 2397–2412.

Foster, J.G., Lambert, D.D., Frick, L.R. & Maas, R., 1996. Re–Os isotopic evidence for genesis of Archaean nickel ores from uncontaminated komatiites: Nature, 382, 703–706.

Hamlyn, P.R., 1980. Equilibration history and phase chemistry of the Panton Sill, Western Australia. American Journal of Science, 280, 631–668.

Hamlyn, P.R., Keays, R.R., Peck, D.C. & Reeves, S.J. 1988. Geochemical criteria for platinum metal exploration (85/P228). Australian Mineral Industries Research Association report (unpublished), 215 pp.

Haughton, D.R., Roeder, P.L. & Skinner, B.J., 1974. Solubility of sulfur in mafic magmas. Economic Geology, 69, 451–467.

Hauri, E.H. & Hart S.R., 1993. Re-Os isotope systematics of HIMU and EMII oceanic island basalts from the south Pacific Ocean. Earth and Planetary Science Letters, 114, 353–371.

Hoatson, D.M., 1993. Correlation of structurally disrupted layered ultramafic–mafic intrusions in the East Kimberley. Is Big Ben part of the Panton Intrusion? AGSO Research Newsletter, 19, 9–10.

Hoatson, D.M. & Keays, R.R., 1989. Formation of platiniferous sulfide horizons by crystal fractionation and magma mixing in the Munni Munni layered intrusion, West Pilbara Block, Western Australia. Economic Geology, 84, 1775–1804.

Hoatson, D.M., Sproule, R.A. & Lambert, D.D., 1997. Are there Voisey's Bay-type Ni–Cu–Co sulphide deposits in the East Kimberley of Western Australia? AGSO Research Newsletter, 27, 17–19.

Irvine, T.N., 1975. Crystallization sequences of the Muskox intrusion and other layered intrusions—II. Origin of chromitite layers and similar deposits of other magmatic ores. Geochimica et Cosmochimica Acta, 39, 991–1020.

Irvine, T.N., 1977. Origin of chromitite layers in the Muskox intrusion and other stratiform intrusions: a new interpretation. Geology, 5, 273–277.

Irvine, T.N., Keith, D.W. & Todd, S.G., 1983. The J-M Reef platinum-palladium reef of the Stillwater Complex, Montana: II. Origin by double-diffusive convective magma mixing and the implications for the Bushveld Complex. Economic Geology, 78, 1287–1334.

Klöck, W. & Palme, H., 1988. Partitioning of siderophile and chalcophile elements between sulfide, olivine and glass in naturally reduced basalt from Disko Island, Greenland. Proceedings of the 18th Lunar and Planetary Scientific Conference, 471–483.

Lambert, D.D., Walker, R.J., Morgan, J.W., Shirey, S.B., Carlson, R.W., Zientek, M.L., Lipin, B.R., Koski, M.S. & Cooper, R.L., 1994. Rhenium–Osmium and Samarium–Neodymium isotope geochemistry of the Stillwater Complex, Montana: implications for the petrogenesis of the J-M Reef, Journal of Petrology, 35, 1717–1753.

Lambert, D.D., Foster, J.G., Frick, L.R., Ripley, E.M. & Zientek, M.L., 1997a. Geodynamics of magmatic Cu–Ni–PGE sulfide deposits: new insights from the Re–Os isotopic system: South American Symposium on Isotope Geology (Brazil), Conference Abstracts, 12–17.

Lambert, D.D., Foster, J.G., Frick, L.R., Li, C. & Naldrett, A.J., 1997b. Re–Os isotopic systematics of the Voisey's Bay Ni–Cu–Co magmatic ore system, Labrador, Canada. American Geophysical Union, 1997 Fall Meeting.

Lambert, D.D., Foster, J.G., Frick, L.R., Hoatson, D.M. & Purvis, A.C., 1998. Application of the Re–Os isotopic system to the study of Precambrian magmatic sulfide deposits of Western Australia. Australian Journal of Earth Sciences, 45, 265–284.

Lindner, M. Leich, D.A., Russ, G.P., Bazan, J.M. & Borg, R.J., 1989. Direct determination of the half life of ^{187}Re. Geochimica et Cosmochimica Acta, 53, 1597–1606.

Lugmair, G.W. & Marti, K., 1978. Lunar initial $^{143}Nd/^{144}Nd$: differential evolution of the lunar crust and mantle. Earth and Planetary Science Letters, 39, 349–357.

Maas, R. & McCulloch, M.T., 1991. The provenance of Archaean clastic metasediments in the Narryer Gneiss Complex, Western Australia: Trace element geochemistry, Nd isotopes, and U-Pb ages for detrital zircons. Geochimica et Cosmochimica Acta, 55, 1915–1932.

Maier, W.D., Barnes, S-J., De Klerk, W.J., Teigler, B. & Mitchell, A.A., 1996. Cu/Pd and Cu/Pt of silicate rocks in the Bushveld Complex: Implications for platinum-group element exploration. Economic Geology, 91, 1151–1158.

Marcantonio, F., Zindler, A., Elliot, T. & Staudigel, H., 1995. Os isotope systematics of La Palma, Canary Islands: Evidence for recycled crust in the mantle source of HIMU ocean islands. Earth and Planetary Science Letters, 133, 397–410.

Martin, C.E., 1991. Osmium isotopic characteristics of mantle-derived rocks. Geochimica et Cosmochimica Acta, 55, 1421–1434.

McIntyre G.A., Brooks C., Compston, W. & Turek, A. 1966. The statistical assessment of Rb-Sr isochrons: Journal of Geophysical Research, 71, 5459–5468.

Michard A., Gurriet, P., Soudant, M. & Albarede, F., 1985. Nd isotopes in French Phanerozoic shales; external versus internal aspects of crustal evolution. Geochimica et Cosmochimica Acta, 49, 601–610.

Morgan, J.W., 1986. Ultramafic xenoliths: clues to Earth's late accretionary history. Journal of Geophysical Research, 91, 12375–12387.

Naldrett, A.J., 1989. Magmatic sulfide deposits. Oxford University Press, 186 pp.

Naldrett, A.J., 1997. Key factors in the genesis of Noril'sk, Sudbury, Jinchuan, Voisey's Bay and other world-class Ni–Cu–PGE deposits: implications for exploration. Australian Journal of Earth Sciences, 44, 283–315.

Naldrett, A.J., Keats, H., Sparkes, K. & Moore, R., 1996. Geology of the Voisey's Bay Ni–Cu–Co deposit, Labrador, Canada. Exploration and Mining Journal, 5, 169–179.

Page, R., Hoatson, D, Sun, S-s. & Foudoulis, C., 1995. High precision geochronology of Palaeoproterozoic layered mafic–ultramafic intrusions in the East Kimberley. AGSO Research Newsletter, 22, 7–8.

Peach, C.L., Mathez, E.A. & Keays, R.R., 1990. Sulfide melt–silicate melt distribution coefficients for noble metals and other chalcophile elements as deduced from MORB: implications for partial melting. Geochimica et Cosmochimica Acta, 54, 3379–3389.

Pegram, W.J. & Allegre, C.J., 1992. Osmium isotopic compositions from oceanic basalts. Earth and Planetary Science Letters, 111, 59–68.

Perring, R.J. & Vogt, J.H., 1991. The Panton Sill. In: Barnes, S.J. & Hill, R.E.T. (editors), Guidebook for the post-symposium field excursion. Geological Society of Australia, Sydney, 97–106.

Podmore, F. & Wilson, A.H., 1987. A reappraisal of the structure, geology, and emplacement of the Great Dyke, Zimbabwe. In: Halls, H.C. & Fahrig, W.F. (editors), Mafic dyke swarms. Geological Society of Canada, Special Paper, 34, 317–330.

Prendergast, M.D., 1988. The geology and economic potential of the PGE-rich Main Sulphide Zone of the Great Dyke, Zimbabwe. In: Prichard, H.M., Potts, P.J., Bowles, J. F.W. & Cribb, S.J. (editors), Geoplatinum 87, 22–23 April, Open University, Milton Keynes, United Kingdom, Elsevier, England, 281–302.

Purvis, A.C. & Moeskops, P.G., 1981. Nickel–copper sulfide-rich Proterozoic dikes at Cowarna Rocks, Western Australia. Economic Geology, 76, 1597–1605.

Reeves, S.J. & Keays, R.R., 1995. The platinum-group element geochemistry of the Bucknalla Layered Complex, central Queensland. Australian Journal of Earth Sciences, 42, 187–201.

Reisberg, L., Zindler, A., Marcantonio, F., White, W., Wyman D. & Weaver, B., 1993. Os isotope systematics in ocean island basalts. Earth and Planetary Science Letters, 120, 149–167.

Ripley, E.M., Frick, L.R. & Lambert, D.D., 1995. Pb and Re–Os isotopic studies on Cu–Ni sulfide mineralization at the Babbitt Deposit, Duluth Complex, Minnesota: IGCP 336 International Field Conference and Symposium, Petrology and Metallogeny of Volcanic and Intrusive Rocks of the Midcontinent Rift System, Duluth, 159–160.

Ryan, B., Wardle, R., Gower, C. & Nunn, G., 1995. Nickel–copper sulphide mineralization in Labrador: The Voisey Bay discovery and its exploration implications. Current Research, Report 95-1, Geological Survey, Department of Natural Resources, Government of Newfoundland and Labrador, 177–204.

Sambridge, M. & Lambert, D.D., 1997. Propagating errors in decay equations: examples from the Re–Os isotopic system. Geochimica et Cosmochimica Acta, 61, 3019–3024.

Shedden, S.H. & Barnes, G.J., 1996. East Kimberley Nickel Province — Characteristics and origin of the Sally Malay Ni-Cu-Co deposit, East Kimberley, Western Australia. In: Grimsey, E.J. & Neuss, I. (editors), Nickel 96—Mineral to market. Australasian Institute of Mining and Metallurgy, Publication Series 6/96, November 27–29, Kalgoorlie, Western Australia, 145–155.

Shirey, S.B., 1991. The Rb–Sr, Sm–Nd and Re–Os isotopic systems: a summary and comparison of their application to the cosmochronology and geochronology of igneous rocks. In: Heaman, L. & Ludden, J.N. (editors), Application of radiogenic isotopes to geochemistry. Mineralogical Society of Canada, 103–166.

Sun, S-s., Wallace, D.A., Hoatson, D.M., Glikson, A.Y. & Keays, R.R., 1991. Use of geochemistry as a guide to platinum group element potential of mafic–ultramafic rocks: examples from the West Pilbara and the Halls Creek Mobile Zone, Western Australia. Precambrian Research, 50, 1–35.

Taylor, S.R. & McLennan, S.M., 1995. The geochemical evolution of the continental crust. Reviews in Geophysics, 33, 241–265.

Thornett, J.R., 1981. The Sally Malay deposit: gabbroid associated nickel–copper sulfide mineralization in the Halls Creek Mobile Zone, Western Australia. Economic Geology, 76, 1565–1580.

Trudu, A. & Hoatson, D.M., 1996. Depths of emplacement of Precambrian layered intrusions in the East Kimberley. AGSO Research Newsletter, 25, 10–12.

Walker, R.J. & Morgan, J.W., 1989. Rhenium–osmium isotope systematics of carbonaceous chondrites: Science, 243, 519–522.

Walker, R.J., Carlson, R.W., Shirey, S.B. & Boyd, F.R., 1989. Os, Sr, Nd and Pb isotope systematics of southern African peridotite xenoliths: Implications for the chemical evolution of subcontinental mantle. Geochimica et Cosmochimica Acta, 53, 1583–1595.

Walker, R.J., Echeverria, L.M., Shirey, S.B. & Horan, M.F., 1991. Re–Os isoptopic constraints on the origin of volcanic rocks, Gorgona Island, Colombia: Os isotopic evidence for ancient heterogeneities in the mantle. Contributions to Mineralogy and Petrology, 107, 150–162.

Wasserburg, G.J., Jacobsen, S.B., Depaolo, D.J., McCulloch, M.T. & Wen, T., 1981. Precise determinations of Sm/Nd ratios, Sm and Ni isotopic abundances in standard solutions. Geochimica et Cosmochimica Acta, 45, 2311–2323.

A LASER RAMAN AND ELECTRON PROBE MICROANALYSIS STUDY OF CHROMITE FROM PRECAMBRIAN LAYERED MAFIC–ULTRAMAFIC INTRUSIONS IN NORTHERN WESTERN AUSTRALIA

by TERRENCE P. MERNAGH, ALFONSO G. TRUDU[1], & DEAN M. HOATSON

Introduction

The spinel-group mineral chromite is economically significant because it is the most common source of chromium in ultramafic rocks and one of the few minerals that commonly has minor amounts of platinum-group elements associated with it. Chromite is a common accessory mineral in mafic and ultramafic igneous and metamorphic rocks. Over the past few decades, spinel chemistry has been recognised as showing systematic relationships with chemical zoning, bulk rock composition or mineral assemblages, and geological environments and processes (e.g. Irvine 1965, 1967, Hill & Roeder 1974, Sack 1982, Allan et al. 1988). The analysis of spinel-bearing assemblages also allows the calculation of Fe–Mg, Ni–Zn, and Ni–Mn exchange geothermometry, geobarometry of phase transitions, and the use of composition as an indicator of magmatic processes and fluid evolution in metamorphic systems. All these calculations depend critically on an adequate knowledge of relationships between structure, composition, and the pressure–temperature stability of spinels (Sack & Ghiorso 1991).

In this study, the chemical composition of chromites from five group I intrusions and one group II layered intrusion (see Chapter 5) was determined by electron probe microanalysis, and the results have been compared with those of other chromite occurrences worldwide. Chromite equilibration temperature has also been calculated using the Ni–Zn and Ni–Mn geothermometers recently developed by W.R. Taylor (personal communication, Australian National University, Canberra, 1997). Raman microprobe analyses were carried out to see if this technique could be used to identify and indicate the general chemical composition of chromites from layered mafic–ultramafic intrusions in northern Western Australia and to compare the results with previous Raman studies on natural and synthetic spinels.

[1] Department of Earth Sciences, Monash University, Clayton, Victoria 3168;

Present address: CSIRO Minerals, PO Box 883, Kenmore, Queensland 4069.

Occurrence of chromite in the layered mafic–ultramafic intrusions of the East Kimberley

Chromite, sensu stricto, in the East Kimberley has been a focus for exploration since Dow & Gemuts (1969) first reported platinum-group element (PGE)-bearing chromitite layers in the Palaeoproterozoic Panton mafic–ultramafic intrusion. The main exploration interest has been chromium and the associated metals, such as the PGEs, Au, Cu, and Ni. Massive chromitite layers and disseminated chromite occurrences are restricted to the coeval group I mafic–ultramafic intrusions (e.g. Panton, Big Ben, Highway, Mini, West McIntosh, Melon Patch group, West Robin Soak) and group II mafic intrusions (e.g. Wilagee, Springvale; see Fig. 13.1 and Chapter 5) in the central and western zones of the Halls Creek Orogen (see Chapters 3 and 5), respectively.

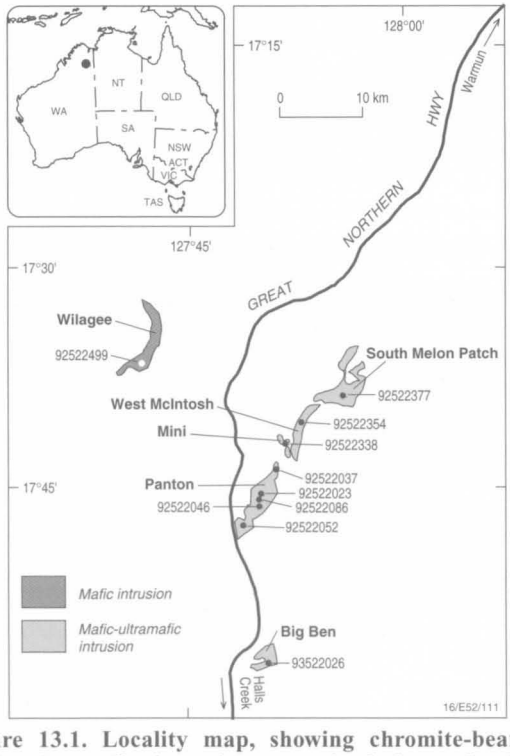


Figure 13.1. Locality map, showing chromite-bearing mafic–ultramafic intrusions examined from the East Kimberley, except for the Lamboo intrusion, which occurs further south on the ANGELO 1:100 000 Sheet (4361; at AMG coordinates ~235575).

The chromite-bearing 1856±2 Ma group I intrusions are concentrated in a narrow northeast-trending Cr–PGEs–Ni–Cu±Au metallogenic corridor that traverses the central eastern part of McINTOSH[1] (see Chapter 5). The only known mineralised group I intrusion outside this corridor is the Big Ben body, which is believed to be a tectonised fault-bounded block that was transposed from the southern part of the Panton intrusion (Hoatson 1993). Stratabound chromitite layers in the group I intrusions are associated with olivine-rich cumulates (dunite, lherzolite) in the upper parts of the ultramafic zones or with contaminated olivine–orthopyroxene-bearing ultramafic zone rocks (harzburgite) near the basal contact of the intrusions. In some intrusions, a few thin chromitite layers are also hosted by dunite lenses in the gabbroic zones (e.g. the Panton intrusion). The chromitite layers of greatest economic interest occur up to 150 m below the contact between the ultramafic zone and overlying gabbroic zone in all known group I intrusions.

The main mineralised chromitite in the Panton intrusion (belonging to the Middle Group; see Chapters 5 and 14) is a few centimetres to 2.4 m thick and continues along strike for at least 12 km. It varies in morphology from a single fine-grained massive layer to an interlayered package of several thin discontinuous layers and mineralised dunite (Perring & Vogt 1991). Chromitite layers and stringers also occur stratigraphically below the main mineralised layer, but these are generally less than 15 cm thick. The chromitite layers often show: rapid thinning and thickening along strike; marked deviations in strike, owing to offsets by high-angle faults; and are locally isoclinally folded. The thin character, lack of lateral continuity, and lower associated metal abundances of the thin layers below the main mineralised chromitite layer indicate that they have low economic potential.

The chromite-bearing 1857±2 Ma group II intrusions are situated in the central western and northwestern parts of McINTOSH. The chromite in these intrusions is hosted by mafic cumulates at high stratigraphic levels in the gabbroic zones. In the Wilagee intrusion (Fig. 13.1), a chromitite lens, 20 cm thick, occurs in a pegmatoidal troctolite just below the contact of two mafic–ultramafic megacyclic units, which consist of a thin basal unit of serpentinised peridotite overlain by thicker mafic units of olivine gabbro, troctolite, anorthosite, and leucogabbro. Wilagee is one of the few Precambrian layered intrusions in Australia where a chromitite layer is hosted by a mafic cumulate rather than an ultramafic cumulate. At least three arcuate-trending mafic cyclic units, consisting of troctolite, leucogabbro, and anorthosite, with lesser amounts of olivine gabbro and norite, occur in the upper part of the Springvale intrusion. Low abundances of PGEs have been reported by exploration companies (see Chapter 2) associated with disseminated chromite in the middle cyclic unit, but no chromitite layers have been identified in the Springvale intrusion.

[1] 1:100 000 sheet names throughout this *Bulletin* are in capital letters to avoid confusion with identical place names and to distinguish them from 1:250 000 sheet names

Chromite petrography

Chromite in mafic–ultramafic intrusions from the East Kimberley generally forms euhedral to subhedral cumulus grains, typically 0.05–0.5 mm across (Fig. 13.2A–F). Chromite in the Lamboo intrusion (Fig. 13.2A) occurs as tightly packed adcumulus grains in a groundmass of chlorite and serpentinised olivine. The chromite grains commonly show triple point junctions and lighter coloured rims, owing to partial oxidation and the development of more Fe-rich phases. Chromite in the Big Ben intrusion (Fig. 13.2B) occurs in a groundmass of chlorite and orthoamphibole as subhedral grains containing subrounded inclusions of serpentinised olivine. The small Mini intrusion (Fig. 13.2C) contains subhedral chromite grains in a groundmass of calcite, amphibole, and plagioclase. Chromite in the Panton intrusion (Fig. 13.2D) consists of subhedral to euhedral grains that have penetrative fracturing and small subrounded inclusions of serpentinised olivine (similar to the Big Ben intrusion). Sericite, calcite, chlorite, clinopyroxene, and clays are the major minerals in the groundmass. Anhedral to subhedral chromite grains occur in a groundmass of plagioclase, clinopyroxene, and sericite in the South Melon Patch intrusion (Fig. 13.2E). Chromite forms grains of variable size in a groundmass of plagioclase, clinopyroxene, and sericite in the West McIntosh intrusion (Fig. 13.2F). The Wilagee intrusion contains euhedral to subhedral grains of chromite in a groundmass of chlorite, plagioclase, and clinopyroxene.

The vibrational spectrum of spinels

The spinel structure (Fig. 13.3) has parallel chains of octahedra aligned along [110] and linked together by two oxygens, and there are isolated tetrahedra between the octahedral chains. It has been assigned to the Fd3m (O_h^7) space group, but several authors (Hwang et al. 1973, Heuer & Mitchell 1975, Samuelsen & Steinvoll 1975) have suggested that the structure is best represented by the sub-group F43m (T_d^2). A factor group analysis (Bhagavantam & Venkatarayudu 1951) predicts the following irreducible representations (Γ) for the optically active vibrational modes of these space groups:

Fd3m (O_h^7): $\Gamma opt. = A_{1g}\,(R) + 2\,A_{2u} + E_g\,(R) + 2\,E_u + T_{1g} + 2\,T_{2u} + 3\,T_{2g}\,(R) + 4\,T_{1u}\,(IR)$

F43m (T_d^2): $\Gamma opt. = 3\,A_1\,(R) + 3\,E\,(R) + 3\,T_1 + 7\,T_2\,(R, IR)$

where R denotes Raman active modes and IR denotes infrared active modes. Note that, if degeneracies are included, both space groups predict a total of 39 optical modes for the spinel structure, but the Fd3m (O_h^7) symmetry results in 5 Raman active modes (i.e. $A_{1g} + E_g + 3\,T_{2g}$), whilst the F43m (T_d^2) symmetry results in 13 Raman active modes (i.e. $3\,A_1 + 3\,E + 7\,T_2$).

In more complex spinels, two different cations may occupy the same symmetry site, which causes a lowering of the crystal symmetry. This results in a large number of possible superstructures for the spinel group. The num-

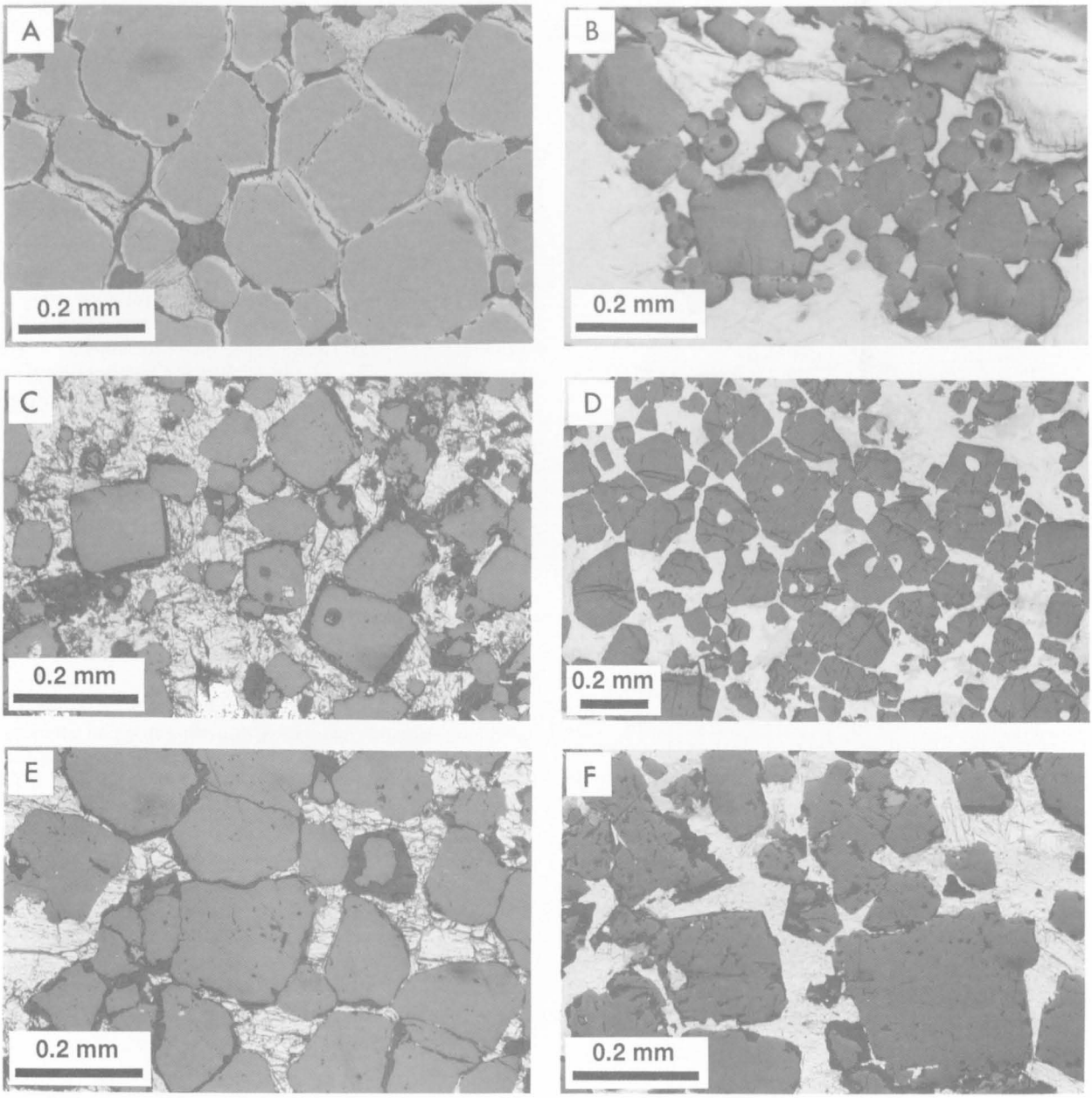


Figure 13.2. Combined reflected and transmitted light photomicrographs of cumulus chromite from the East Kimberley mafic–ultramafic intrusions.

A. Tightly packed subhedral to euhedral chromite grains displaying light-coloured grey rims representing partial oxidation of the chromite and the formation of Fe-rich phases, such as magnetite and hematite from the Lamboo intrusion.

B. Subhedral chromite (some rimmed by lighter coloured, Fe-rich phases) from the Big Ben intrusion.

C. Subhedral chromite from the Mini intrusion.

D. Subhedral to euhedral chromite containing small subrounded inclusions of serpentinised olivine from the Panton intrusion.

E. Anhedral to subhedral chromite from the South Melon Patch intrusion.

F. Euhedral chromite from the West McIntosh intrusion.

ber of possible space groups which may result was calculated by Malézieux & Piriou (1988) and the corresponding Raman active modes are listed in Table 13.1.

Experimental techniques

Marked-up, polished thin-sections of chromite were particle-coated with carbon prior to electron probe microanalyses. The composition of individual chromite grains was determined on a Camebax (Cameca) microbeam electron-probe (at the Research School of Earth Sciences, ANU, Canberra), using wavelength dispersive X-ray analysers. Note that Fe_2O_3 (and, hence, Fe^{3+}) is calculated by stoichiometry from the electron probe data. The chromite standard used for these analyses was from the Tiebaghi mine, New Caledonia. An accelerating voltage of 15 kV and a beam current of 40 nA (beam orientation and current determined on barium silicate) were used for all analyses.

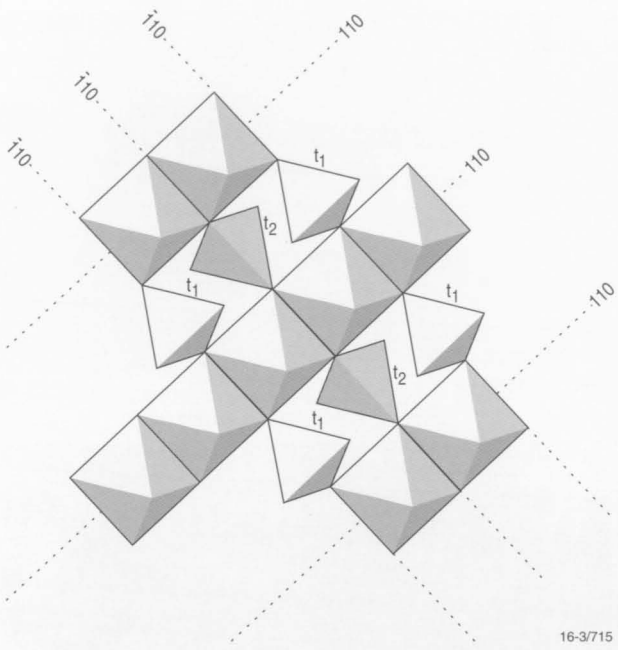


Figure 13.3. Part of the spinel structure, showing parallel chains of octahedra linked together by two oxygens and isolated tetrahedra (modified from Battey 1975).

Laser Raman spectra were recorded on a Microdil 28 Raman microprobe, manufactured by Dilor Co., Lille, France; a detailed description of the spectrometer is given in Liu & Mernagh (1990). The same thin sections of chromite analysed by the electron probe were placed on the stage of an Olympus BH-2 microscope and brought to focus in reflected light using a 100x (0.95 numerical aperture) Olympus objective. The 514.5 nm green line of a Spectra Physics 2020 3W argon ion laser was then directed through the same microscope objective to produce a focused spot 1 μm in diameter on the chromite grains. Care was taken to ensure that the position of the laser beam was always within 5 μm of the spot (usually a small burn mark) produced during the electron probe microanalysis, but laser powers had to be restricted to 5 mW or less at the sample to prevent damage to the chromite grains. Raman spectra were recorded from 340 to 800 cm^{-1}, using a spectral resolution of approximately 3 cm^{-1} and 15 accumulations with 30 seconds integration time. The spectrometer was calibrated with the emission lines from a neon lamp and was accurate to ±1 cm^{-1}.

All smoothing and peak-fitting of the Raman spectra data were done using the 'Razor for Grams' software (Spectrum Square Associates, Inc., Ithaca, New York, USA). The number of peaks in each spectrum was independently determined by the software from the raw data using a Bayesian 2nd derivative (Richardson 1972) and a Maximum Likelihood method (Dodd & DeNoyer 1985). All smoothing was carried out using Maximum Likelihood and Maximum Entropy methods. Peak-fitting was carried out on the raw spectral data using a least-squares algorithm and the Maximum Likelihood principle. The peak-fitting procedure was stopped when the minimum value of the Reduced Chisquare (calculated by the Levenberg-Marquardt method, see Press et al. 1988) was close to one.

Electron probe microanalysis and Laser Raman microprobe results

Electron probe microanalysis

Averaged electron probe analyses obtained for the East Kimberley chromites are summarised in Table 13.2. Location co-ordinates for the 1992 and 1993 samples are given in Appendix 2. The complete set of analyses is given in Appendix Table 3.14, and all data are presented in Figures 13.4–13.7. Table 13.2 shows that the chromites have relatively low calculated $Fe^{3+\prime}$ (= 100 x $Fe^{3+}/'Cr + Al + Fe^{3+}$) and a narrow range of Cr′ (44–59) and Al′ (30–48), but a relatively wide spread in mg number (8–57). In order to extend the range of Cr′ and Al′ for the Raman microprobe study, additional natural chromites from the Archaean Munni Munni layered mafic–ultramafic intrusion in the west Pilbara Craton, Western Australia have been included in this study. The composition of these chromites is listed in Hoatson et al. (1992, pp. 227–228).

The cumulus chromite from the East Kimberley layered intrusions can be divided into two separate geochemical subgroups:

Subgroup 1—those with high-Al and low-Cr; and

Subgroup 2—those with low-Al, high-Cr, and variable Fe^{3+}concentration.

Table 13.1. Possible superstructures in spinel (Joubert 1965) and the predicted Raman active modes for each structure.

Site	*Order*	*Space group*	*Raman active modes*
Octahedral	1/1	P4m2 (D_{2d}^5)	13 A_1 + 6 B_1 + 15 B_2 + 22 E
	1/1	$P4_122$ (D_4^3)	9 A_1 + 10 B_1 + 11 B_2 + 21 E
	1/1	Imma (D_{2h}^{28})	5 A_g + 2 B_{1g} + 4 B_{2g} + 4 B_{3g}
	1/3	O^6	6 A_1 + 14 E + 20 T_2
	1/3	D_{3d}^5	4 A_1 + 5 E_g
Tetrahedral	1/1	F43m (T_d^2)	3 A_1 + 3 E + 7 T_2
	1/1	$I4_122$ (D_4^{10})	*

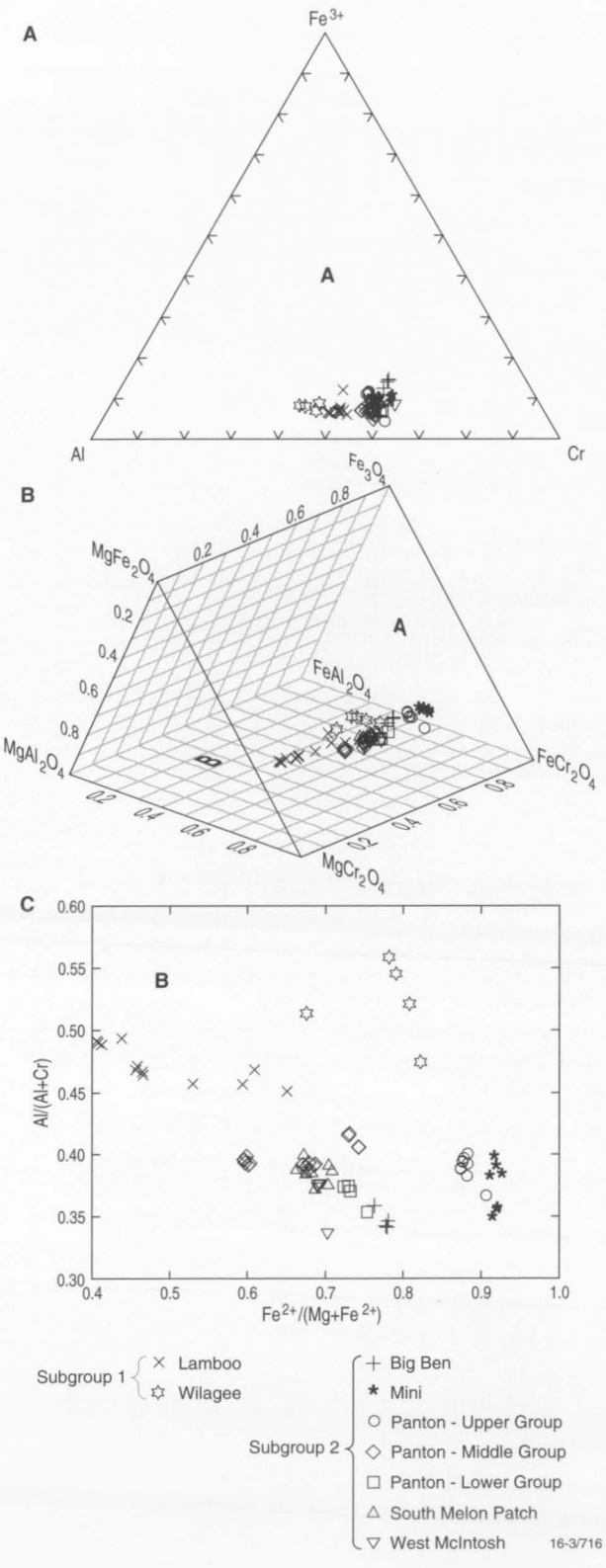
* No modes are listed as this corresponds to a gap in the spinel structure.

Table 13.2. Electron microprobe analyses of chromite from chromitite layers in East Kimberley layered mafic–ultramafic intrusions.

Sample no.	93522026	83330021	83330192	92522338	92522037	92522023	92522052	92522086	92522046	92522377	92522354	92522499
No. of anal.	4	7	5	7	4	4	6	6	8	8	5	5
Intrusion	Big Ben	Lamboo	Lamboo	Mini	Panton Lower Group	Panton Middle Group	Panton Middle Group	Panton Middle Group	Panton Upper Group	South Melon Patch	West McIntosh	Wilagee
Lithology	Peridotite	Peridotite	Peridotite	Peridotite	Peridotite	Peridotite	Peridotite	Peridotite	Peridotite	Peridotite	Peridotite	Troctolite
SiO_2	0.02	0.03	<0.02	0.04	0.04	<0.02	0.02	<0.02	<0.02	0.04	<0.02	0.02
TiO_2	1.01	0.76	0.70	0.45	0.52	0.51	0.81	0.50	1.06	0.64	0.42	0.31
Al_2O_3	14.66	22.79	24.66	16.62	17.20	19.40	18.37	19.05	17.07	17.82	17.39	25.43
V_2O_3	0.24	0.20	0.18	0.31	0.18	0.20	0.23	0.18	0.46	0.26	0.21	0.23
Cr_2O_3	41.01	39.41	38.88	42.62	44.01	41.41	42.62	43.54	39.79	42.39	43.99	34.63
FeO Total	38.43	26.67	22.41	37.89	32.29	32.28	29.95	27.65	38.63	32.22	31.36	35.30
Fe_2O_3 Calc[1]	10.64	6.23	5.69	6.03	5.85	5.62	5.15	5.54	7.50	7.07	6.36	6.37
FeO Calc[1]	27.79	20.44	16.72	31.86	26.44	26.66	24.80	22.11	31.13	25.15	25.00	28.93
MnO	0.35	0.56	0.19	0.49	0.35	0.29	0.34	0.34	0.87	0.29	0.31	0.31
NiO	0.07	0.17	0.17	0.02	0.07	0.07	0.04	0.06	0.05	0.07	0.04	0.14
MgO	4.53	9.94	12.65	1.58	5.36	5.35	6.56	8.31	2.32	6.43	6.31	4.71
ZnO	0.21	0.15	0.08	0.49	0.29	0.26	0.14	0.19	0.18	0.20	0.19	0.10
CaO	0.01	<0.01	<0.01	<0.01	0.01	0.02	0.03	0.01	0.01	<0.01	0.01	0.02
Total	100.54	100.68	99.92	100.51	100.32	99.79	99.11	99.83	100.44	100.36	100.23	101.20
Oxygens	32	32	32	32	32	32	32	32	32	32	32	32
Si	0.005	0.008	0.003	0.012	0.011	0.003	0.006	0.003	0.003	0.010	0.003	0.006
Ti	0.204	0.143	0.129	0.093	0.104	0.100	0.161	0.097	0.215	0.127	0.084	0.060
Al	4.649	6.707	7.120	5.326	5.363	6.020	5.710	5.797	5.437	5.501	5.385	7.631
V	0.052	0.039	0.036	0.068	0.038	0.042	0.048	0.037	0.099	0.054	0.045	0.047
Cr	8.726	7.781	7.530	9.163	9.205	8.619	8.886	8.889	8.502	8.779	9.140	6.970
Fe^{3+} Calc[1]	2.154	1.170	1.048	1.233	1.164	1.114	1.022	1.076	1.525	1.393	1.257	1.220
Fe^{2+} Calc[1]	6.254	4.269	3.425	7.246	5.848	5.870	5.470	4.776	7.035	5.509	5.495	6.158
Mn	0.079	0.119	0.039	0.113	0.078	0.064	0.075	0.075	0.198	0.064	0.070	0.066
Ni	0.015	0.034	0.033	0.005	0.015	0.015	0.008	0.012	0.011	0.014	0.008	0.028
Mg	1.816	3.700	4.620	0.642	2.113	2.099	2.578	3.199	0.936	2.509	2.473	1.789
Zn	0.042	0.027	0.014	0.098	0.057	0.051	0.028	0.036	0.035	0.039	0.038	0.019
Ca	0.004	0.001	0.001	0.001	0.004	0.005	0.009	0.002	0.004	0.001	0.003	0.005
mg	23	46	57	8	27	26	32	40	12	31	31	23
Cr'	56	50	48	58	59	55	57	56	55	56	58	44
Al'	30	43	45	34	34	38	37	37	35	35	34	48
Fe^{3+}'	14	7	7	8	7	7	7	7	10	9	8	8

[1] Fe_2O_3 Calc, FeO Calc, Fe^{2+} Calc, and Fe^{3+} Calc have been calculated by stoichiometry assuming 24 cations and 32 oxygens.

mg = 100 x Mg/(Mg + Fe^{2+}); Al' = 100 x Al/(Cr + Al + Fe^{3+}); Cr' = 100 x Cr/(Cr + Al + Fe^{3+}); Fe^{3+}' = 100 x Fe^{3+}/(Cr + Al + Fe^{3+}).



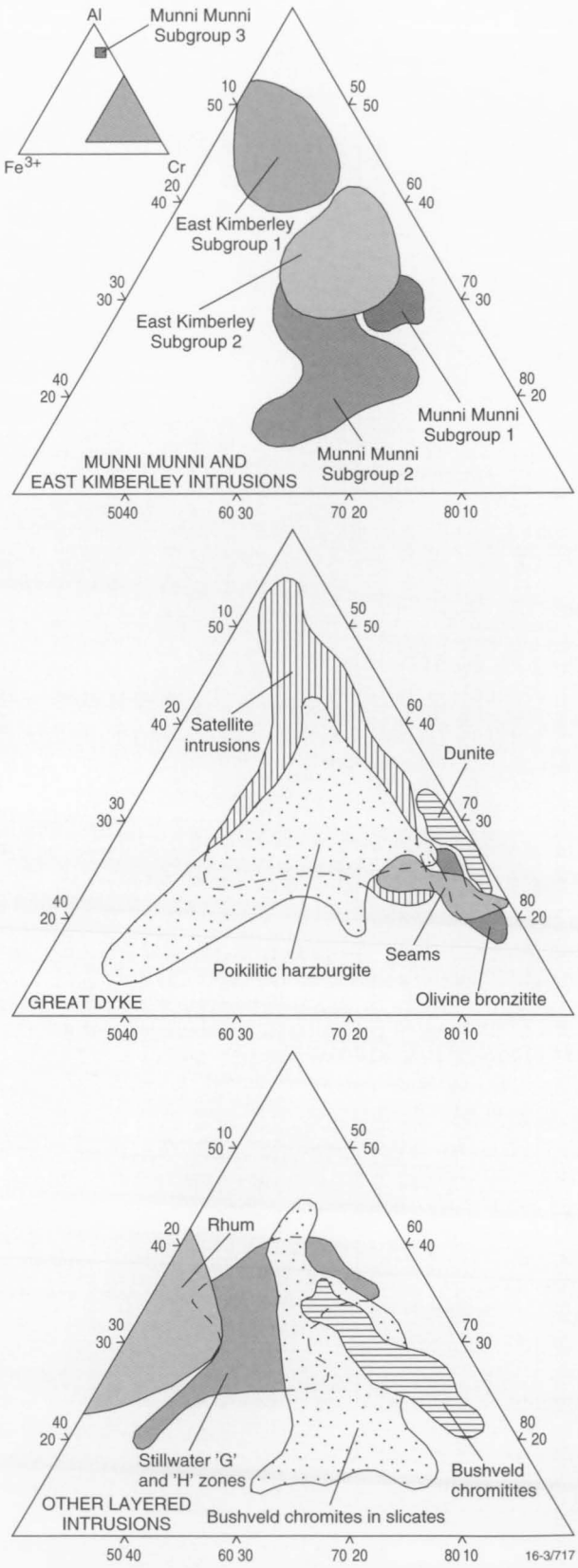


Figure 13.4A–C. Composition of chromite from the East Kimberley region in the oxidised-spinel prism (defined by the $MgCr_2O_4$–$FeCr_2O_4$–$FeAl_2O_4$–$MgAl_2O_4$–$MgFe_2O_4$–Fe_3O_4 components), and their projections on faces A (Al–Cr–Fe^{3+}) and B (Al/(Al + Cr)–Fe^{2+}/(Mg + Fe^{2+})).

Figure 13.5. Variations in Cr–Al–Fe^{3+} in Cr-bearing spinel from the two subgroups (see Fig. 13.4A–C) from the East Kimberley region, the subgroups from the Munni Munni intrusion, the Great Dyke, and other layered intrusions. The position of each ternary plot is represented by the shaded area in the small key diagram of Cr–Al–Fe^{3+}, which also includes subgroup 3 from the Munni Munni intrusion. The ternary diagrams are modified after Wilson (1982) and Hoatson et al. (1992).

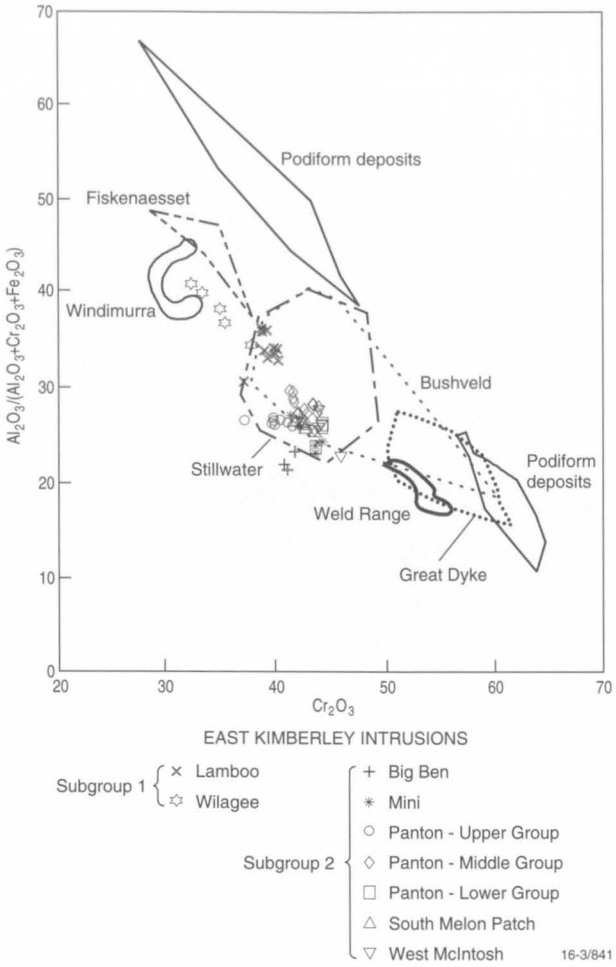


Figure 13.6. Cr_2O_3 versus $Al_2O_3/(Al_2O_3 + Cr_2O_3 + Fe_2O_3)$ diagram for intrusions from the Halls Creek Orogen–East Kimberley, Yilgarn Craton (Windimurra, Weld Range), and from overseas (Fiskenaesset–Greenland, Bushveld, Stillwater, Great Dyke, various podiform deposits). Variation diagram and source of data from Thayer (1970) and Parks (1998).

The compositions of the two subgroups are illustrated by their distribution in the oxidised-spinel prism in Figure 13.4A–C. Subgroup 1 chromites have a restricted distribution of the trivalent cations Cr^{3+}, Fe^{3+}, and Al^{3+} (side A), from $Cr_{41}Fe^{3+}{}_8Al_{51}$ to $Cr_{49}Fe^{3+}{}_7Al_{44}$, while subgroup 2 chromites have a slightly wider range of compositions, from $Cr_{50}Fe^{3+}{}_7Al_{43}$ through $Cr_{56}Fe^{3+}{}_{15}Al_{29}$ to $Cr_{60}Fe^{3+}{}_8Al_{32}$. With the exception of the samples from the Wilagee intrusion, the spinels from the two subgroups define a weak trend of increasing Al/(Al + Cr) with decreasing $Fe^{2+}/(Mg + Fe^{2+})$ (side B). The chromites from the Wilagee intrusion are appreciably higher in aluminium than chromites from other intrusions in the East Kimberley, which may be because these chromites are hosted by mafic rocks while all the other chromites are hosted by ultramafic rocks.

A comparison of the chemical composition of chromite from major overseas mafic–ultramafic intrusions with that from the East Kimberley and other Australian intrusions is given in Figures 13.5 and 13.6. Hoatson et al. (1992) considered the relationships between Munni Munni chromites and those from the Bushveld Complex and the Great Dyke, and this will not be repeated here. Subgroup 1 chromites from the East Kimberley have higher Al content than chromites from Munni Munni subgroups 1 and 2 and partly overlap the satellite intrusion chromite field of the Great Dyke (Fig. 13.5). When Al is compared with the $Al + Cr + Fe^{3+}$ (Fig. 13.6), it can be seen that chromites from the East Kimberley intrusions fall along a negative correlation trend, similar to the other layered intrusions, but well below the fields for podiform chromite deposits. Subgroup I chromites (Wilagee intrusion) have similar high aluminous compositions to the Windimurra and Fiskenaesset intrusions.

The East Kimberley subgroup 2 chromites have similar compositions to the Munni Munni subgroups 1 and 2 (Fig. 13.5). They fall into the same compositional fields as the silicate-hosted chromite from the Bushveld and Stillwater complexes and the poikilitic harzburgite chromite field of the Great Dyke (Figs 13.5, 13.6). However, the chromites for the Big Ben intrusion (Fig. 13.6) fall just below the fields of the Bushveld and Stillwater complexes, owing to their lower Al content. The separation of the Big Ben chromites from the tight cluster of other East Kimberley subgroup 2 chromites may be due to different magmatic and/or fractionation processes.

Geothermometry. Since the cation composition of chromites is temperature dependent (Sack & Ghiorso 1991), the electron probe data can be used to estimate the equilibration temperatures of chromite. W. Taylor (pers. comm., Research School of Earth Sciences, ANU, 1997) has recently developed semi-empirical Ni–Zn and Ni–Mn exchange geothermometers for chromites using data gathered from a large, world-wide suite of ultramafic and mafic volcanic rocks. The following geothermometers are applicable where chromite coexists with olivine, which is the case for all of the East Kimberley chromite:

Ni–Zn geothermometer:

$$T(^{\circ}C) = \frac{10000}{7.9182 - 1.240 \times 1n\left(\frac{Ni(ppm)}{Zn(ppm)}\right)} - 273.15 \qquad (1)$$

Ni–Mn geothermometer:

$$T(^{\circ}C) = \left(\frac{10000}{8.322 - 1.339 \times 1n\left(\frac{Ni(ppm)}{Mn(ppm)}\right)} - \left(1.914 \times \frac{Cr}{Cr+Al}\right) \right) - 273.15 \qquad (2)$$

Average temperature of crystallisation for the various East Kimberley chromites, calculated from the above equations, is listed in Table 13.3. The temperatures calculated with the Ni–Zn geothermometer are also shown in Figure 13.7, as a function of the Cr′. The classification of the chromites into two subgroups on the basis of

Table 13.3. Calculated equilibration temperatures for chromites from the East Kimberley region.

Sample number	*Intrusion*	*Ni–Zn geothermometer*[1] *Average temp. (°C)*	*Ni–Zn geothermometer*[1] *Standard deviation*	*Ni–Mn geothermometer*[1] *Average temp. (°C)*	*Ni–Mn geothermometer*[1] *Standard deviation*
83330192B	Lamboo	1023	37	1071	46
83330021A	Lamboo	932	25	909	156
92522499	Wilagee	1038	73	906	64
93522026	Big Ben	799	44	811	41
92522338	Mini	636		696	
92522037	Panton (Lower Group)	756	67	805	76
92522052	Panton (Middle Group)	819	110	755	111
92522086	Panton (Middle Group)	756	47	754	70
92522046	Panton (Upper Group)	807	29	678	19
92522377	South Melon Patch	792	38	835	60
92522354	West McIntosh	791	74	778	23

[1] Geothermometers were developed by W.R. Taylor (pers. comm., Research School of Earth Sciences, Australian National University, 1997).

geochemistry is supported by the subgroups plotting into two distinctive temperature fields. Calculated temperatures for subgroup 1 are much higher than those for subgroup 2. Subgroup 1 chromites range from 911 to 1103°C and are at the low end of expected liquidus temperatures, but are similar to the magmatic temperatures determined by pyroxene geothermometry for the Munni Munni layered intrusion (Hoatson et al. 1992). Subgroup 2 temperatures range from 630 to 897°C and are below the likely liquidus temperature. These intrusions have been overprinted (and folded) by, probably, at least two major deformation and metamorphic events in the central zone and, hence, the lower temperatures may be due to subsolidus or metamorphic re-equilibration of the chromite. Similar processes have been invoked to explain the low temperatures calculated for Fe–Ti oxides in the Munni Munni layered intrusion (Hoatson et al. 1992).

Figure 13.8 shows calculated temperature (using the Ni–Mn geothermometer) for chromite equilibration as a function of chromite number. The temperature difference between subgroup 1 and subgroup 2 is again readily apparent, but differs from that for the Ni–Zn geothermometer

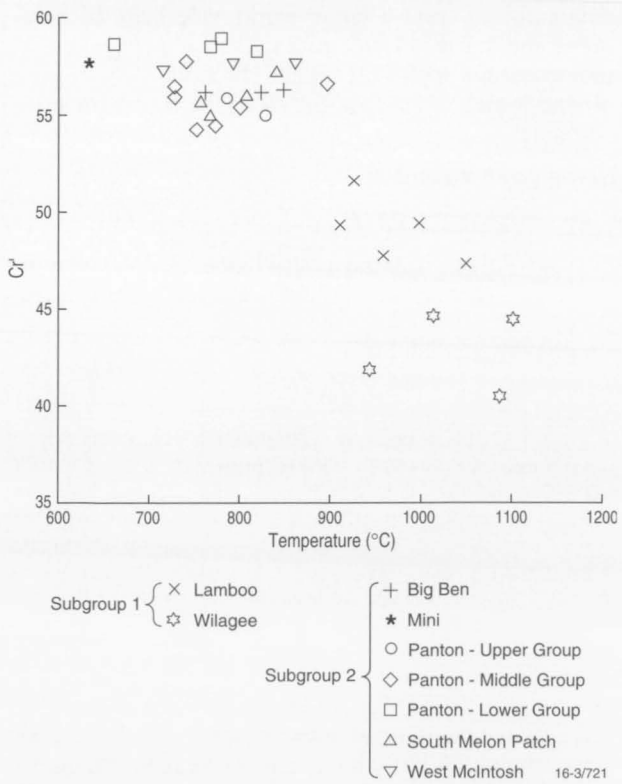


Figure 13.7. Equilibration temperatures for chromite from East Kimberley mafic–ultramafic intrusions, calculated with the Ni–Zn geothermometer and plotted as a function of Cr′ (see Table 13.2).

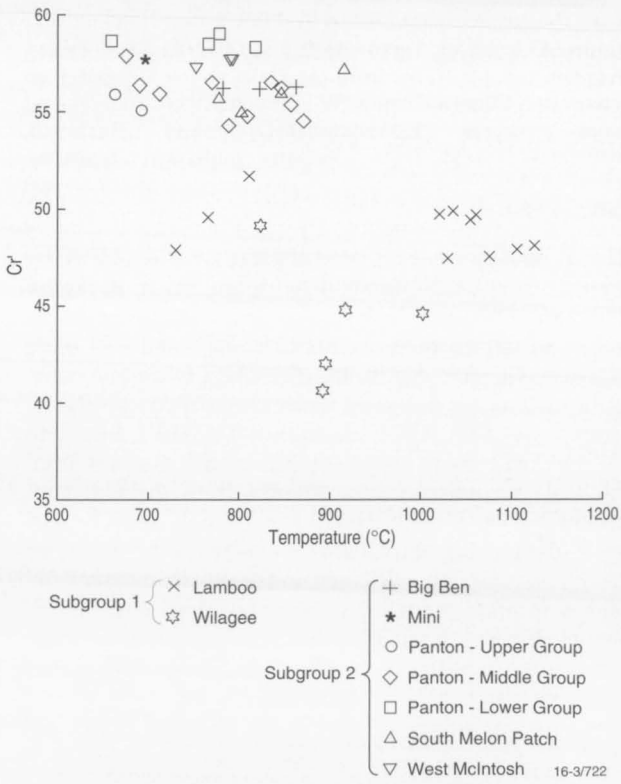


Figure 13.8. Equilibration temperatures for chromite from East Kimberley mafic–ultramafic intrusions calculated with the Ni–Mn geothermometer and plotted as a function of Cr′ (see Table 13.2).

(Fig. 13.7). For example, chromite from the Lamboo intrusion generally plots at higher temperatures than that from Wilagee in Figure 13.8, whereas the reverse occurs in Figure 13.7, and the Ni–Mn geothermometer also seems to produce a wider range of temperatures.

The spread of results for chromite from the Lamboo intrusion may lead to other interpretations. The low zinc concentration in the Lamboo chromites limited the number suitable for Ni–Zn geothermometry, but a larger number of chromite analyses could be included in the Ni–Mn geothermometry. As shown in Figure 13.8, the samples from Lamboo fall into two separate regions. The majority of samples plot in the range from 1000–1124°C, which is equivalent to the magmatic temperatures mentioned above, but three Lamboo samples plot between 765 and 811°C. This suggests that there has been partial re-equilibration of chromites in the Lamboo intrusion, but the process has not gone to completion, as in subgroup 2. Partial re-equilibration may also have occurred in the Wilagee intrusion, but more analyses are required to confirm this possibility.

Laser Raman microprobe studies

Selected laser Raman spectra of chromites from the East Kimberley intrusions are shown in Figure 13.9A–C. The spectra are relatively weak, as low laser powers had to be used to prevent damage to the chromite grains. In agreement with previous studies (Malézieux et al. 1983, Malézieux & Piriou 1988), the spectra of natural chromite show two broad bands at approximately 550–600 cm^{-1} and 680-720 cm^{-1}. Peak-fitting by the Maximum Likelihood method (Dodd & DeNoyer 1985) over the region from 340 to 800 cm^{-1} identified a minimum of eight lorentzian bands (Fig. 13.9A–C). The very weak bands around 380 and 480 cm^{-1} were, however, difficult to observe and measure accurately, owing to overlap with the other more intense bands, and will not be considered further. The two intense broad bands in Figure 13.9A–C are each adequately fitted by three lorentzian bands. Note that all six of these bands shift to higher wavenumbers as the aluminium content of the chromites increases and the chromium and iron contents decrease. At very high aluminium compositions the broad band at higher wave number splits into three peaks with two distinct side bands at around 687 and 763 cm^{-1} (Fig. 13.9A).

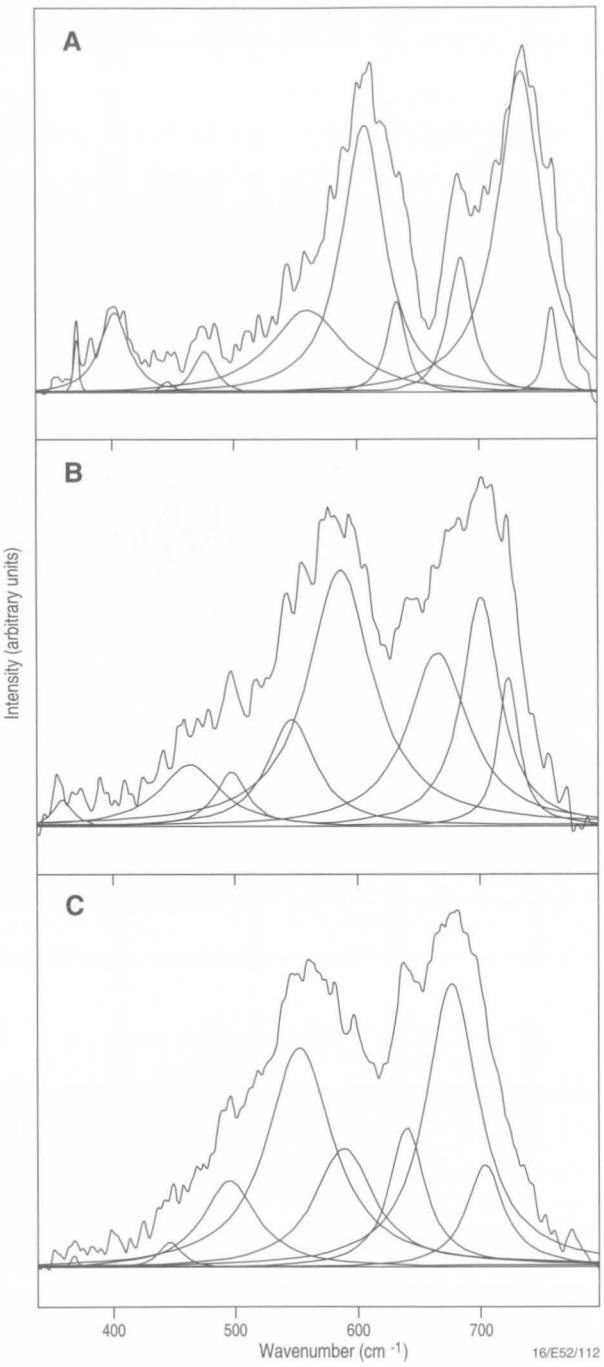


Figure 13.9. Selected laser Raman microprobe spectra of East Kimberley chromite with compositions of: A, Cr′ = 16, Al′ = 78, and $Fe^{3+\prime}$ = 6; B, Cr′ = 41, Al′ = 51, and $Fe^{3+\prime}$ = 8; and C, Cr′ = 56, Al′ = 30, and $Fe^{3+\prime}$ = 14. Each spectrum has been fitted with 8 lorentzian curves, using a Maximum Likelihood method. Note that all bands above 480 cm^{-1} shift to higher wave number with increasing Al content.

The frequency of the Raman spectral bands was plotted against the chemical composition of the natural chromites in order to investigate which compositional parameters have the greatest influence on the spectra. Plots of Raman frequency as a function of Cr′ are shown in Figure 13.10. There is some scatter in the data, owing to the poor signal to noise ratio of the spectra; however, the lines of best fit still define a definite relationship between the frequency of the Raman bands and Cr′. All six bands display a non-linear decrease in frequency with increasing Cr′. The two bands at 722 and 690 cm^{-1} (at high Cr′) have a similar dependence, indicated by a steadily decreasing change of slope with increasing Cr′. However, the band at 653 cm^{-1} (at high Cr′) appears to exhibit an almost linear decrease in frequency, within the error limits of this experiment. The three lorentzian bands used to fit the broad band at lower wave numbers also show a similar dependence on Cr′. The line of best fit for lowest frequency band at 490 cm^{-1} (at high Cr′) appears to have a greater curvature, but this is probably due to the greater scatter of data for this band. Note that this band is typically very weak and may also overlap with the other weak band near 480 cm^{-1}.

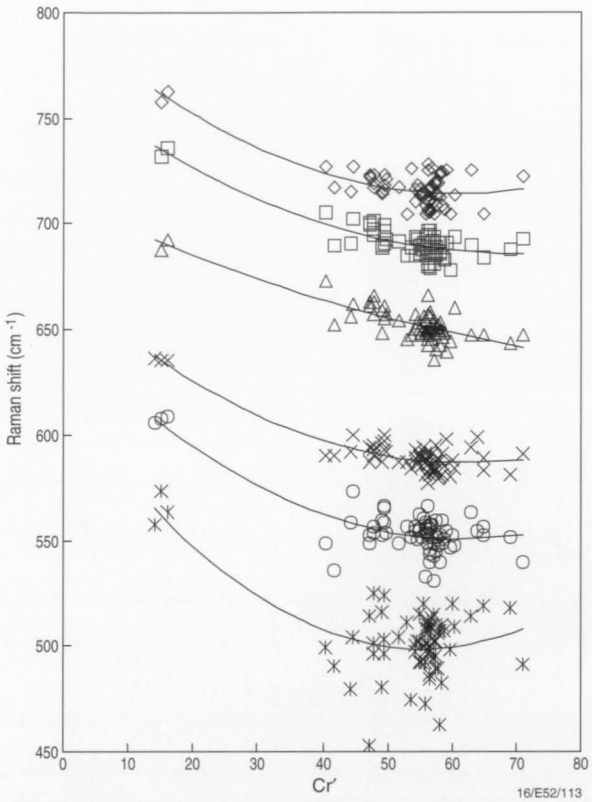


Figure 13.10. A plot of the six fitted lorentzian curves to the two most intense Raman peaks of chromite as a function of the Cr number (Cr′) for the East Kimberley intrusions (see Table 13.2) and the Munni Munni intrusion in the west Pilbara Craton (Hoatson et al. 1992).

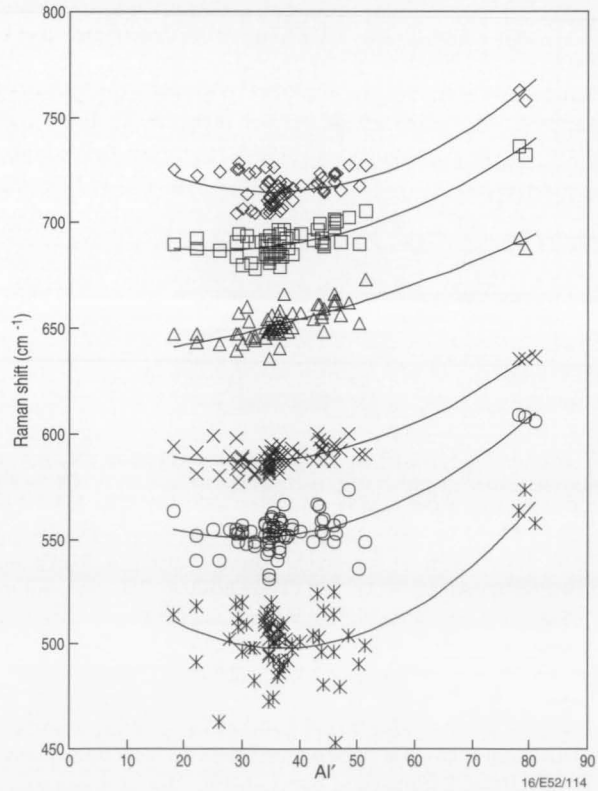


Figure 13.11. The non-linear frequency shift of the fitted lorentzian curves for the two most intense Raman peaks of chromite as a function of Al number (Al′) for the East Kimberley mafic–ultramafic intrusions (see Table 13.2) and the Munni Munni intrusion in the west Pilbara Craton (Hoatson et al. 1992).

Figure 13.11 shows frequency of the Raman bands as a function of Al′. The Raman bands exhibit a similar, but opposite trend to those in Figure 13.10, and frequency increases with increasing Al′. Once again the lowest band (at ~653 cm^{-1}) in the broad band at higher wave number shows an almost linear change in frequency with increasing Al′. Similarly, the three lorentzian curves fitted to the broad band at lower wave number have a similar non-linear increase in frequency with increasing Al′.

The plots of Raman frequency as a function of $Fe^{3+\prime}$ (Fig. 13.12) have been fitted with linear trend lines. However, this may be an artefact caused by the relatively small amount of Fe^{3+} (see Table 13.2) in these samples. The line of best fit for the band near 720 cm^{-1} shows a slight increase in frequency with increasing $Fe^{3+\prime}$, while most of the other peaks decrease in frequency with increasing $Fe^{3+\prime}$, but the change of frequency for all bands is less than the scatter of data, indicating that the Raman spectra are relatively independent of changes in $Fe^{3+\prime}$.

Malézieux & Piriou (1988) have previously reported that the symmetrical A_{1g} Raman mode (i.e. the band near 690 cm^{-1}) of both natural and synthetic spinels correlates well with the $(Cr + Fe^{3+})/(Cr + Al + Fe^{3+})$ ratio. In this study, we have plotted all six lorentzian peaks as a function of this ratio (Fig. 13.13). The main effect is a slight enhancement in the curvature of the lines of best fit (see Table 13.4) and a reduction in the errors involved with calculations based on the Raman measurements.

Discussion

The compositional variation of natural spinels may be explained by (1) variations in the physical or chemical parameters of the parent magma during the early crystallisation (cumulus) stage; and (2) reaction with adjacent silicates or intercumulus liquid, either during the post-cumulus stage or the subsolidus stage (Hamlyn & Keays 1979). Henderson (1975) found that spinels in chromite-rich layers or in peridotite adcumulates from the Rum (formerly Rhum) intrusion in Scotland show a reaction trend involving a marked increase in the Al/Cr ratio and little variation in Fe^{3+}, whereas chromite in cumulates that contain trapped liquid define a trend involving enrichment of Fe^{3+} and depletion of Al. However, as shown here, other variables, such as temperature, pressure, and f_{O_2} are also important in determining the composition of spinels.

The Raman spectra of natural chromites are difficult to fully interpret unless the precise atomic structure of each grain has been determined by X-ray diffraction or other crystallographic methods. Natural chromite contains variable amounts of divalent ions (Mg^{2+} and Fe^{2+}) and trivalent ions (Cr^{3+}, Al^{3+}, and Fe^{3+}). Previous studies on several series of chemically simpler, synthetic spinel by Malézieux et al. (1983), Cervelle et al. (1984), and Malézieux & Piriou (1988) have enabled a much better understanding of the Raman spectra of spinels, but some peculiarities still await further investigation. Malézieux & Piriou (1988) summarised their observations of the Raman spectra of synthetic spinel as follows: (a) the Raman bands above about 500 cm^{-1} shift to higher

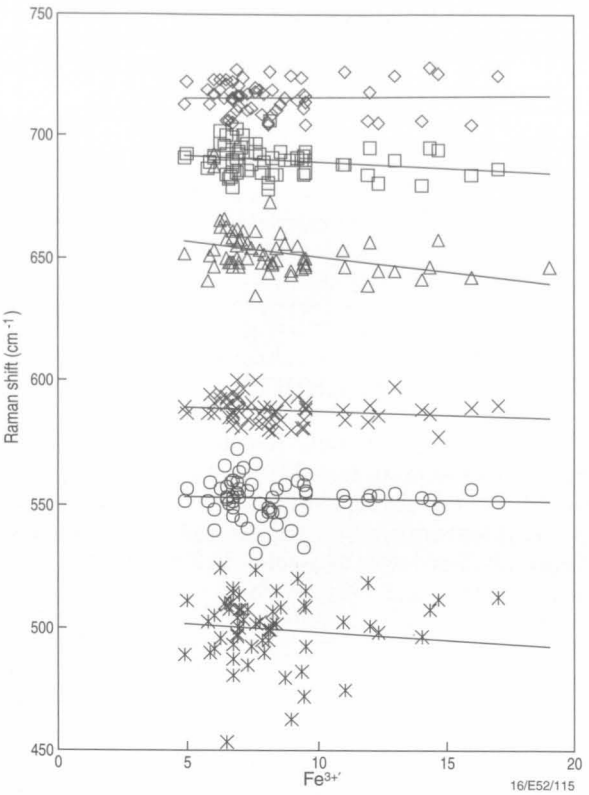


Figure 13.12. A plot of chromite from the East Kimberley mafic–ultramafic intrusions (see Table 13.2) and the Munni Munni intrusion (Hoatson et al. 1992), showing the linear frequency dependence of the fitted lorentzian curves for the two most intense Raman peaks of chromite as a function of Fe^{3+} number ($Fe^{3+\prime}$).

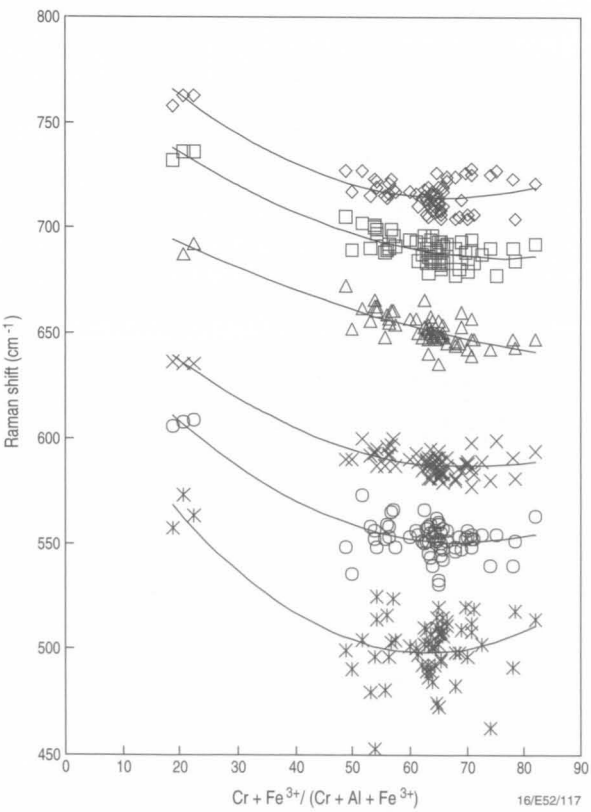


Figure 13.13. A plot of spectral data for chromite from the East Kimberley mafic–ultramafic intrusions and the Munni Munni intrusion, showing the fitted lorentzian curves for the two most intense Raman peaks of chromite as a function of $Cr + Fe^{3+}/(Cr + Al + Fe^{3+})$.

frequency as the aluminium content of the spinel increases, (b) the Raman bands at lower frequencies do not shift as a function of chemical composition, and (c) all Raman spectra contain more bands than predicted by factor group analysis.

Malézieux & Piriou (1988) suggested that the compositionally induced change of frequency of some bands, while others in the spectrum remain at fixed frequencies, may be explained by assuming both 'one mode' and 'two mode' behaviour, respectively. 'One mode' behaviour means that there is only one Raman mode for a particular vibration regardless of which cations (or anions) are substituted into the structure, and this mode will change in frequency according to the ratio of cations (or anions) associated with this vibration. For example, in classical theory, the simplest pure stretching vibration is the fundamental of a diatomic species given by the formula:

$$\bar{\nu} = 1303\sqrt{F\left(\frac{1}{m_1} + \frac{1}{m_2}\right)} \qquad (3)$$

Where $\bar{\nu}$ is the vibrational frequency (in cm^{-1}), F is the force constant for the atomic bond (in N/cm), and m_1 and m_2 are the atomic masses of the atoms. If we assume the force constant (F) for the B^{3+}–O vibration remains at 3.38 N/cm, then the above equation predicts a frequency of 685 cm^{-1} for the Cr–O vibration. However, substitution of Al^{3+}, which has an atomic mass approximately half that of Cr^{3+}, increases the frequency to 756 cm^{-1} for the Al–O vibration. Thus, if this vibration behaved as 'one mode', its frequency would vary between 685 and 756 cm^{-1} according to the Cr/Al ratio, but if the atomic motions behaved as a 'two mode' vibration, then two bands would be observed at 685 and 756 cm^{-1} and their relative intensities would be proportional to the Cr/Al ratio. Malézieux & Piriou (1988) reported that natural chromites display only 'one mode' behaviour. The present study confirms this observation, as all bands show some change in frequency over the available compositional range (Cr′ 14–71).

In agreement with previous studies (White & De Angelis 1967, Malézieux et al. 1983, Cervelle et al. 1984, Malézieux & Piriou 1988), the observed Raman spectra contain more Raman bands than predicted by factor group analysis. Only two Raman bands are predicted in the region above 500 cm^{-1} for chromites belonging to the Fd3m (O_h^7) space group; however, six lorentzian curves were needed to obtain a proper fit to the broad bands obtained from the chromites used in this study. Malézieux & Piriou (1988) suggested that the additional bands may be caused by either a localised decrease in symmetry or by some micro-heterogeneity due to the coexistence of both normal and inverse lattice arrangements on the scale of a few unit cells. Ordering of cations on the tetrahedral and octahedral sites will lead to a transition from the Fd3m (O_h^7) spinel structure to one or other of the superstructures listed in Table 13.1. 1/1 ordering on the tetrahedral sites results in 13 Raman active modes, while 1/1 ordering on the octahedral sites may result in up to 56 Raman modes, and 1/3 ordering on the octahedral sites produces up to 40 Raman modes.

Table 13.4. Raman frequencies (in cm^{-1}) as a function of ratioed compositions of chromite.

Raman spectral band	$X = (Cr + Fe^{3+})/(Cr + Al + Fe^{3+})$ *Line of best fit*	R^2
Band 8 (704–763 cm^{-1})	$0.022X^2 - 2.935X + 812.65$	0.69
Band 7 (680–736 cm^{-1})	$0.020X^2 - 2.318X + 776.46$	0.79
Band 6 (642–692 cm^{-1})	$0.007X^2 - 1.516X + 720.84$	0.70
Band 5 (580–636 cm^{-1})	$0.022X^2 - 3.017X + 691.59$	0.80
Band 4 (545–608 cm^{-1})	$0.025X^2 - 3.416X + 667.56$	0.62
Band 3 (495–564 cm^{-1})	$0.036X^2 - 4.601X + 644.32$	0.33

R – correlation coefficient for line of best fit (Hoel 1971).

Conclusions

1. Raman spectra from 340 to 800 cm^{-1} of natural spinels from Palaeoproterozoic layered intrusions in the East Kimberley and the Munni Munni layered intrusion of the west Pilbara Craton have weak bands around 380 and 480 cm^{-1} and more intense, but broad, bands at approximately 550–600 cm^{-1} and 680–720 cm^{-1}. Curve-fitting of these last two bands showed that they were composed of at least six lorentzian bands. The frequency of these six bands varies as a function of chemical composition and is particularly sensitive to the relative amount of trivalent cations in each chromite crystal.

2. This study has shown that Raman spectroscopy can be used as an alternative and rapid method for the general classification of chromite according to chemical composition. The shifts in the frequency of the lorentzian curves of chromite were found to correlate with Cr′, Al′, $Cr + Fe^{3+}/(Cr + Al + Fe^{3+})$ and are in agreement with previous studies of other natural and synthetic chromite (Malézieux et al. 1983, Cervelle et al. 1984, Malézieux & Piriou 1988).

3. Cumulus chromite from East Kimberley layered intrusions can be divided into the following two geochemical subgroups: subgroup 1 with high Al^{3+} and high Fe^{3+}, and subgroup 2 with high Cr and varying, but generally low, Fe^{3+} contents. These chromites also have chemical affinities with chromite from overseas layered intrusions, such as the Great Dyke and the Bushveld Complex.

4. Chromite from the Wilagee intrusion in the East Kimberley is appreciably higher in aluminium than chromite from other intrusions. This intrusion is largely undeformed and not significantly metamorphosed, but the higher aluminium content in the chromite may reflect the fact that these chromites are hosted by plagioclase-rich mafic rocks, while all other chromites in this study are hosted by ultramafic rocks.

5. Calculations using the recently developed Ni–Zn and Ni–Mn exchange geothermometers show a clear distinction between subgroup 1 and subgroup 2, with subgroup 1 having higher temperatures. The higher temperatures are close to the probable magmatic temperatures determined by pyroxene geothermometry for the Munni Munni layered intrusion (Hoatson et al. 1992). The lower temperatures obtained for subgroup 2 are attributed to subsolidus or metamorphic re-equilibration of the chromite.

Acknowledgements

The authors wish to thank Morrie Duggan and David Blake (both AGSO), Jean-Marie Malézieux (Université Michel de Montaigne, Bordeaux), and Steve Sheppard (GSWA) for reviewing this manuscript. We thank Wayne Taylor for allowing us to use the Ni–Zn and Ni–Mn geothermometers, and Nick Ware (both at the Research School of Earth Sciences, Australian National University) for assistance with the electron probe microanalyses.

References

Allan, J.F., Sack, R.O. & Batiza, R., 1988. Cr-rich spinels as petrogenetic indicators—MORB-type lavas from the Lamont seamount chain, Eastern Pacific, American Mineralogist, 73, 741–753.

Battey, M.H., 1975. Mineralogy for students. Longman Group Ltd, 323 pp.

Bhagavantam, S. & Venkatarayudu, T., 1951. Theory of groups and its application to physical problems. Bangalore Press. Bangalore city, India, 2nd edition.

Cervelle, B., Coutures, J.P., Malézieux, J.M. & Piriou, B., 1984. Cristallochimie des chromites: étude sur des produits de synthèse du système $Mg(Al, Cr)_2O_4$. Bulletin de Minéralogie, 107, 627–634.

Dodd, J.G. & DeNoyer, L.K., 1985. Deconvolution of spectra. In: Armstrong, J.T. (editor), Microbeam analysis, San Francisco Press, San Francisco, California, 1985, 7–14.

Dow, D.E. & Gemuts, I., 1969. Geology of the Kimberley Region, Western Australia: the East Kimberley. Bureau of Mineral Resources, Australia, Bulletin 106, 135 pp.

Hamlyn, P.R. & Keays, R.R., 1979. Origin of chromite compositional variation in the Panton Sill, Western Australia. Contributions to Mineralogy & Petrology, 69, 75–82.

Henderson, P., 1975. Reaction trends shown by chrome-spinels of the Rhum layered intrusion. Geochimica et Cosmochimica Acta, 39, 1035–1044.

Heuer, A.H. & Mitchell, T.E., 1975. Further discussion on the space group of spinel. Journal of Physics, Part C, Solid State Physics, 8, L543–L551.

Hill, R. & Roeder, P.L., 1974. The crystallization of spinel from basaltic liquids as a function of oxygen fugacity. Journal of Geology, 84, 709–929.

Hoatson, D.M., 1993. Correlation of structurally disrupted layered mafic–ultramafic intrusions in the

East Kimberley: Is Big Ben part of the Panton intrusion? AGSO Research Newsletter, 19, 9–10.

Hoatson, D.M., Wallace, D.A., Sun, S-s., Macias, L.F., Simpson, C.J. & Keays, R.R., 1992. Petrology and platinum-group-element geochemistry of Archaean layered mafic–ultramafic intrusions, west Pilbara Block, Western Australia. Australian Geological Survey Organisation, Bulletin 242, 319 pp.

Hoel, P.G., 1971. Introduction to mathematical statistics. Wiley & Sons, 409 pp.

Hwang, L., Heuer, A.H. & Mitchell, T.E., 1973. On the space group of $MgAl_2O_4$ spinel. Philosophical Magazine, 28, 241–243.

Irvine, T.N., 1965. Chromian spinel as a petrogenetic indicator. Part I, Theory. Canadian Journal of Earth Sciences, 2, 648–672.

Irvine, T.N., 1967. Chromian spinel as a petrogenetic indicator. Part II, Petrological applications. Canadian Journal of Earth Sciences, 4, 71–103.

Joubert, J.C., 1965. Contribution à la recherche et a l'étude des superstructures dans les oxydes mixtes du type spinelle. Préparation de composé spinelles lacunaires. PhD thesis, Grenoble, France.

Liu, L. & Mernagh, T.P., 1990. Phase transitions and Raman spectra of calcite at high pressures and room temperature. American Mineralogist, 75, 801–806.

Malézieux, J.M. & Piriou, B., 1988. Relation entre la composition chimique et le comportement vibrationnel de spinelles de synthèse et de chromites naturelles en microspectrométrie Raman. Bulletin de Minéralogie, 111, 649–669.

Malézieux, J.M., Barbillat, J., Cervelle, B. Coutures, J.P. Couzi, M. & Piriou, B., 1983. Étude de spinelles de synthèse de la série $Mg(Cr_xAl_{2-x})O_4$ et de chromites naturelles par microsonde Raman-Laser. TMPM Tschermaks Mineralogische und Petrographische Mitteilungen, 32, 171–185.

Parks, J., 1998. Weld Range platinum group element deposit. In: Berkman, D.A. & Mackenzie, D.H. (editors), Geology of Australian and Papua New Guinean mineral deposits. Australasian Institute of Mining and Metallurgy, Monograph 22, 279–286.

Perring, R.J. & Vogt, J.H., 1991. The Panton Sill. In: Barnes, S.J. & Hill, R.E.T. (editors), Mafic–ultramafic complexes of Western Australia. IAGOD and the Geological Society of Australia, Sixth International Platinum Symposium, July 1991, Perth, Western Australia, Excursion Guidebook 3, 97–106.

Press, W.H., Flannery, B.P., Teukolsky, S.A. & Vetterling, W.T., 1988. Numerical recipes, the art of scientific computing. Cambridge University Press.

Richardson, W.H., 1972. Bayesian iterative method of image restoration. Journal of the Optical Society of America, 62, 55–59.

Sack, R.O., 1982. Spinels as petrogenetic indicators: Activity–composition relations at low pressures. Contributions to Mineralogy and Petrology, 102, 41–68.

Sack, R.O. & Ghiorso, M.S., 1991. Chromian spinels as petrogenetic indicators: Thermodynamics and petrological applications. American Mineralogist, 76, 827–847.

Samuelsen, E.J. & Steinvoll, O., 1975. On the space group of spinel. Journal of Physics, Part C, Solid State Physics, 8, L427–L429.

Thayer, T.P., 1970. Chromite segregations as petrogenetic indicators. In: Vosser, D.J.L. & von Gruenewaldt, G. (editors), Symposium on the Bushveld Igneous Complex and other layered intrusions. Geological Society of South Africa, Special Publication No. 1, pp. 380–390.

White, W.B. & De Angelis, B.A., 1967. Interpretation of the vibrational spectra of spinels. Spectrochimica Acta, 23A, 985–995.

Wilson, A.H., 1982. The geology of the Great Dyke, Zimbabwe: the ultramafic rocks. Journal of Petrology, 23, 240–292.

CHAPTER 14

MINERALISATION AND ECONOMIC POTENTIAL OF THE MAFIC–ULTRAMAFIC INTRUSIONS

by DEAN M. HOATSON

Introduction

The Palaeoproterozoic layered mafic–ultramafic intrusions in the Halls Creek Orogen (HCO) of the East Kimberley represent one of the most extensively mineralised igneous associations of their type in Australia. The intrusions contain a range of magmatic and hydrothermal deposits of platinum-group elements (PGEs), chromium, nickel, copper, cobalt, titanium, vanadium, iron, and gold. Even after four decades of intensive exploration and research, important new types and environments of mineralisation are still being discovered. For example, the recent mapping by the Australian Geological Survey Organisation and the Geological Survey of Western Australia (see Chapter 1), as part of the National Geoscience Mapping Accord (NGMA), has extended the distribution of prospective layered intrusions and indicated that different styles of mineralisation with prominent surface expressions and geophysical–geochemical signatures are still to be found (Hoatson 1995, Hoatson et al. 1995). In recent years, the geological maps, reports, and databases derived from the NGMA program (see Chapter 1) and the discovery of world-class Ni–Cu–Co sulphide deposits overseas, such as Voisey's Bay in Canada, have renewed exploration interest in the metallogeny of mafic–ultramafic rocks in the HCO. Companies in the late 1990s evaluated large areas of prospective ground by sophisticated airborne geophysical and remote sensing techniques, and incorporating various computer-modelling programs into their exploration strategies. The East Kimberley is now recognised as one of the most prospective and actively explored mafic–ultramafic igneous provinces in Australia.

The main aims of this chapter are to summarise the major mineral deposits associated with the Palaeoproterozoic intrusions of the East Kimberley, compare these deposits with those of other Precambrian provinces in Australia and overseas, and provide exploration strategies for locating new deposits in the HCO.

Styles of platinum-group-element mineralisation associated with Precambrian layered mafic–ultramafic intrusions in Australia

Precambrian layered mafic–ultramafic intrusions in Australia have generated considerable exploration interest because of their PGE and Ni–Cu–Co potential (Fig. 14.1, Table 14.1). Exploration has generally focussed on large differentiated layered mafic–ultramafic intrusions in the Archaean Yilgarn and Pilbara cratons and the Proterozoic Halls Creek and Albany–Fraser Orogens. The Munni Munni, Andover, Radio Hill, and Mount Sholl (Pilbara Craton), Weld Range, Windimurra, Narndee (Yilgarn Craton), Panton, Eastmans Bore, and Lamboo (HCO) intrusions all contain significant, though subeconomic, concentrations of PGEs, Cr, Au, and associated base metals (Table 14.2). Despite the intensive efforts of many exploration companies and the expenditure of millions of dollars over the past few decades, an economic resource of PGEs associated with a layered intrusion has yet to be found in Australia. In the 1980s, the Munni Munni, Windimurra, and Panton intrusions were the most intensively explored intrusions for PGEs, whereas most interest in the 1990s has been generated by the Weld Range intrusion in the Murchison Province, northwest Yilgarn Craton (Fig. 14.1). In regard to Ni–Cu–Co–PGE sulphide mineralisation, the Radio Hill, Mount Sholl, Carr Boyd (Yilgarn Craton), and Sally Malay (HCO) intrusions have been considered the most prospective. PGE production in Australia is currently restricted to Ni–Cu sulphide deposits associated with komatiitic volcanism in the Eastern Goldfields Province of the Yilgarn Craton.

The five major styles of PGE mineralisation associated with the Precambrian intrusions described below have been the focus of exploration, with stratabound sulphide-bearing layers and chromitite layers being the most attractive targets since they generally display considerable lateral continuity (up to 22 km), have uniform grades (layers with 1–6 ppm Pt+Pd+Au) and thicknesses (0.5–3 m), contain a significant component of the more valuable precious metals (Pt, Pd, Ir, Rh, Au), and have potential for large tonnage (up to 30 Mt) multi-element deposits (PGEs, Cr, Cu, Ni, Co, Ti, V, Au). Mineralised stratabound layers in Australia would need to have grades of at least 8 ppm Pt+Pd for underground mining to be economic (Hoatson 1998).

The five major styles of PGE mineralisation are:

(i) Stratabound sulphide-bearing layers (e.g. Munni Munni, Weld Range: Hoatson & Keays 1989, Barnes et al. 1992, Barnes & Hoatson 1994, Parks 1998). Disseminated Cu–Ni sulphides (2–3 vol. %) enriched in PGEs occur in laterally extensive layers, 1–2 m thick, at particular stratigraphic levels in the mafic–ultramafic intrusions, as in the Merensky Reef of the Bushveld Complex, South Africa (Campbell et al. 1983) and the J-M Reef of the Stillwater Complex, Montana, USA (Todd et al. 1982). The mineralised layers, which are usually

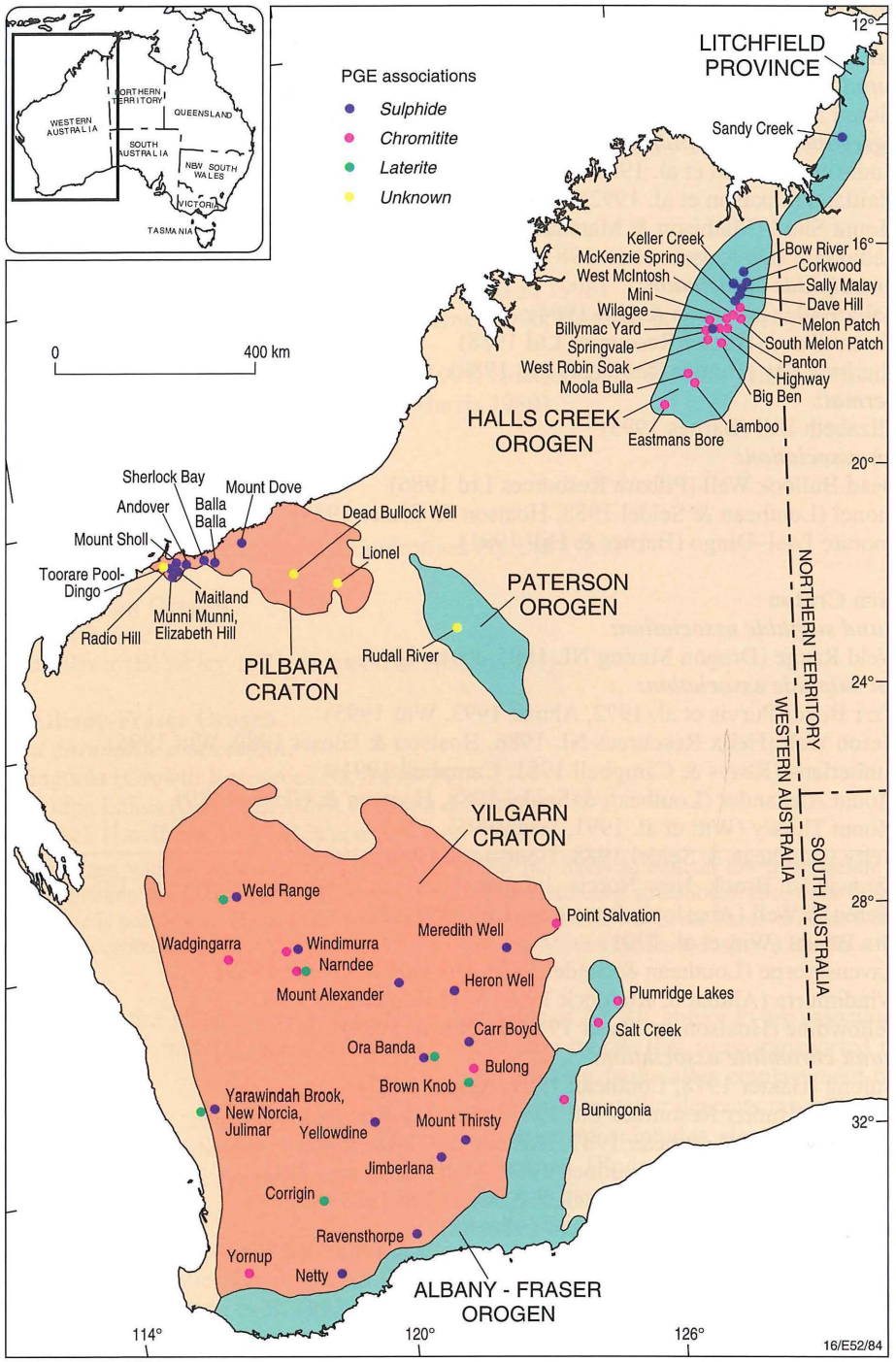


Figure 14.1. Distribution of platinum-group-element mineralisation related to Precambrian layered mafic–ultramafic intrusions in Australia. See Table 14.1 for further details.

pyroxenitic, generally form porphyritic or pegmatoidal 'reefs' up to about 20 m below (Munni Munni, Great Dyke of Zimbabwe) to 500 m above (Merensky Reef, J-M Reef) the lowest stratigraphic level where plagioclase first appears as a major cumulus mineral, i.e. the contact between the ultramafic zone and mafic zone.

No stratabound PGE-enriched sulphide layers have been documented in the HCO. This probably reflects the early S saturation of the mafic magmas (i.e. prior to emplacement in the magma chambers) and/or absence of favourable magmatic conditions, such as wide-scale turbulent mixing, in the magma chambers.

(ii) Stratabound chromitite layers (e.g. Panton, Eastmans Bore, Lamboo, Big Ben, Melon Patch: Perring & Vogt 1991, Trudu & Hoatson 1996). Stratabound chromitite layers a few centimetres to 2.4 m thick occur in dunite (Panton), troctolite (Wilagee), and at or near the base of cyclic dunite–bronzite units (Windimurra), similar to the UG-2 chromitites of the Bushveld Complex (Naldrett 1989). Most sulphide-enriched

Table 14.1. Precambrian layered mafic–ultramafic intrusions containing platinum–group elements.

Archaean Pilbara Craton

Stratabound sulphide association:

Munni Munni (Hoatson & Keays 1989, Barnes et al. 1992, Hoatson et al. 1992, Barnes 1995)

Basal segregations of sulphide:

Andover (Hoatson et al. 1992)
Maitland (Hoatson et al. 1992)
Mount Sholl (Mathison & Marshall 1981, Hoatson et al. 1992)
Radio Hill (De Angelis et al. 1987, 1988, Hoatson et al. 1992)

Unknown sulphide association:

Balla Balla (Louthean & Hill 1994)
Mount Dove (Hunter Resources Ltd 1988)
Sherlock Bay (Hunter Resources Ltd 1988)

Hydrothermal:

Elizabeth Hill (Barnes 1995)

Unknown association:

Dead Bullock Well (Pilbara Resources Ltd 1986)
Lionel (Louthean & Seidel 1988, Hoatson & Glaser 1989)
Toorare Pool–Dingo (Barnes & Hill 1991)

Archaean Yilgarn Craton

Stratabound sulphide association:

Weld Range (Dragon Mining NL 1995, Parks 1998)

Unknown sulphide association:

Carr Boyd (Purvis et al. 1972, Ahmat 1993, Witt 1995)
Heron Well (Helix Resources NL 1986, Hoatson & Glaser 1989, Witt 1995)
Jimberlana (Keays & Campbell 1981, Campbell 1991)
Mount Alexander (Louthean & Seidel 1988, Hoatson & Glaser 1989)
Mount Thirsty (Witt et al. 1991, Witt 1995)
Netty (Louthean & Seidel 1988, Hoatson & Glaser 1989)
Yarawindah Brook–New Norcia–Julimar (Harrison 1986, Cornelius et al. 1987)
Meredith Well (Aberfoyle Resources Ltd 1989–92)
Ora Banda (Witt et al. 1991)
Ravensthorpe (Louthean & Seidel 1988, Hoatson & Glaser 1989)
Windimurra (Ahmat & Ruddock 1990, Mathison et al. 1991)
Yellowdine (Hoatson & Glaser 1989, Louthean 1989)

Stratabound chromitite association:

Bulong (Baxter 1978, Louthean 1989, Ahmat 1993)
Narndee (Hunter Resources Ltd 1987, Ahmat & Ruddock 1990)
Point Salvation (Louthean 1987, Hoatson & Glaser 1989)
Windimurra (Ahmat & Ruddock 1990, Mathison et al. 1991)
Wadgingarra (International Nickel Australia Ltd 1981–82)
Yornup (West Coast Holdings Ltd 1985–88)

Laterite association:

Brown Knob (Newcrest Mining Ltd 1990–92)
Corrigin (Dragon Mining NL 1995)
Ora Banda (Witt et al. 1991, Witt 1995)
Narndee (Hunter Resources Ltd 1987)
Weld Range (Dragon Mining NL 1995, Parks 1998)
Yarawindah Brook (Harrison 1986, Cornelius et al. 1987)

Palaeoproterozoic Halls Creek Orogen

Stratabound chromitite association:

Big Ben (Hoatson 1993, Trudu & Hoatson 1996)
Eastmans Bore (Vogt 1989, Barnes & Hill 1991)
Highway (Hoatson & Tyler 1993, Trudu & Hoatson 1996)
Lamboo (Barnes & Hill 1991)
Melon Patch (Hoatson & Tyler 1993, Trudu & Hoatson 1996)
Mini (Hoatson & Tyler 1993, Trudu & Hoatson 1996)
Moola Bulla (Clarke et al. 1982)
Panton (Hamlyn & Keays 1979, Perring & Vogt 1991, Hoatson & Tyler 1993, Sproule et al. 1997a,b)
South Melon Patch (Hoatson & Tyler 1993, Trudu & Hoatson 1996)

Table 14.1. (Cont.). Precambrian layered mafic–ultramafic intrusions containing platinum–group elements.

Springvale (Barnes & Hill 1991, Hoatson & Tyler 1993, Trudu & Hoatson 1996)
West McIntosh (Hoatson & Tyler 1993, Trudu & Hoatson 1996)
West Robin Soak (Trudu & Hoatson 1996)
Wilagee – previously called Toby – (Barnes & Hill 1991, Hoatson & Tyler 1993, Trudu & Hoatson 1996)

Basal segregations of sulphide:

?Corkwood[1] (Nevill 1974, Wilding 1980, Barnes 1994)
?Keller Creek[1] (Gaunt 1977, Trudu & Hoatson 1996)
?McKenzie Spring[1] (McNeil 1991, Trudu & Hoatson 1996)
Sally Malay (Thornett 1981, Shedden & Barnes 1996, Hoatson et al. 1997, Sproule et al. in press)

Unknown sulphide association:

Billymac Yard (Sherrington 1985, Keeley 1991, Hoatson & Tyler 1993, Trudu & Hoatson 1996)
?Bow River[1] (Marston 1979, Halligan & Harris 1980)
Dave Hill (Trudu & Hoatson 1996)

Palaeoproterozoic Litchfield Province

Unknown sulphide association:

Sandy Creek (Eupene Exploration Enterprises Pty Ltd 1989)

Palaeoproterozoic Paterson Orogen

Unknown association:

Rudall River (Blockley 1971, Hoatson & Glaser 1989)

Mesoproterozoic Albany-Fraser Orogen

Stratabound chromitite association:

Buningonia (Growth Resources NL 1988–90)
Plumridge Lakes (Louthean 1987, Hoatson & Glaser 1989)
Salt Creek (Louthean 1987, Hoatson & Glaser 1989)

[1] sulphide-bearing intrusions with no published occurrences of PGEs, but likely to contain low to moderate concentrations of PGEs. The above compilation does not include Precambrian intrusions containing stratabound chromitite layers where the PGE content of the chromitite is not known. These intrusions include: Coobina, Nobs Well, Pear Creek (Pilbara Craton), Bridgetown, Bunbury, Imagi Well, Taccabba Well, West Bendering (Yilgarn Craton), Mount Davies (Musgrave Block).

chromitites near or above the level where plagioclase first appears as a cumulus mineral are particularly enriched in PGEs.

The HCO contains the largest concentration of, and some of the most PGE-rich, stratabound chromitite layers of any Precambrian province in Australia (discussed in next section).

(iii) Basal segregations of Ni–Cu–Co–PGE sulphides (e.g. Sally Malay, Corkwood, Keller Creek, Radio Hill, Mount Sholl: Thornett 1981, Hoatson et al. 1992, 1997). Layered mafic and mafic–ultramafic intrusions that underwent early S saturation before or during their emplacement contain massive and disseminated pyrrhotite–pentlandite–chalcopyrite±pyrite±magnetite assemblages with low to moderate concentrations of PGEs (<0.6 ppm). The sulphides are often localised in or over fault-controlled structural embayments or depressions in the footwall contact beneath the thickest sequence of mafic or mafic–ultramafic cumulates (Radio Hill, Mount Sholl) or in feeder conduits (Sally Malay?).

The HCO and the west Pilbara Craton host the most important examples of this style of mineralisation (discussed in next section).

(iv) Hydrothermal remobilisation (e.g. Elizabeth Hill, Yarawindah Brook: Barnes 1995). Subeconomic concentrations of Pd, Rh, and/or Pt are associated with precious and base metals that were transported by hydrothermal fluids along faults after emplacement of the intrusions. These polymetallic deposits range from localised remobilisation of sulphides along the basal contacts of the intrusions (Radio Hill, Sally Malay) to more distal deposits associated with shear zones in adjacent country rocks (Elizabeth Hill).

Hydrothermal PGE deposits appear to be rare in the HCO, perhaps because exploration programs have been focussed on more traditional targets, such as chromitite layers.

(v) Enrichment in the laterite profile (Weld Range, Ora Banda: Witt et al. 1991; Louthean & Hill 1994, Parks 1998). PGE-enriched laterite profiles overlying mafic–ultramafic sequences contain low-grade deposits (3–15 Mt @ ~1 ppm PGEs) that can be quickly brought into production during periods of favourable metal prices. However, low grades and metallurgical problems have inhibited mining. Lateritic–supergene PGE deposits appear to be restricted to the Yilgarn Craton, where the largest deposits are at Weld Range and Ora Banda (Table 14.2).

No PGE deposits associated with laterites have been documented in the HCO. This may reflect unfavourable palaeoclimatic or tectonic conditions for supergene

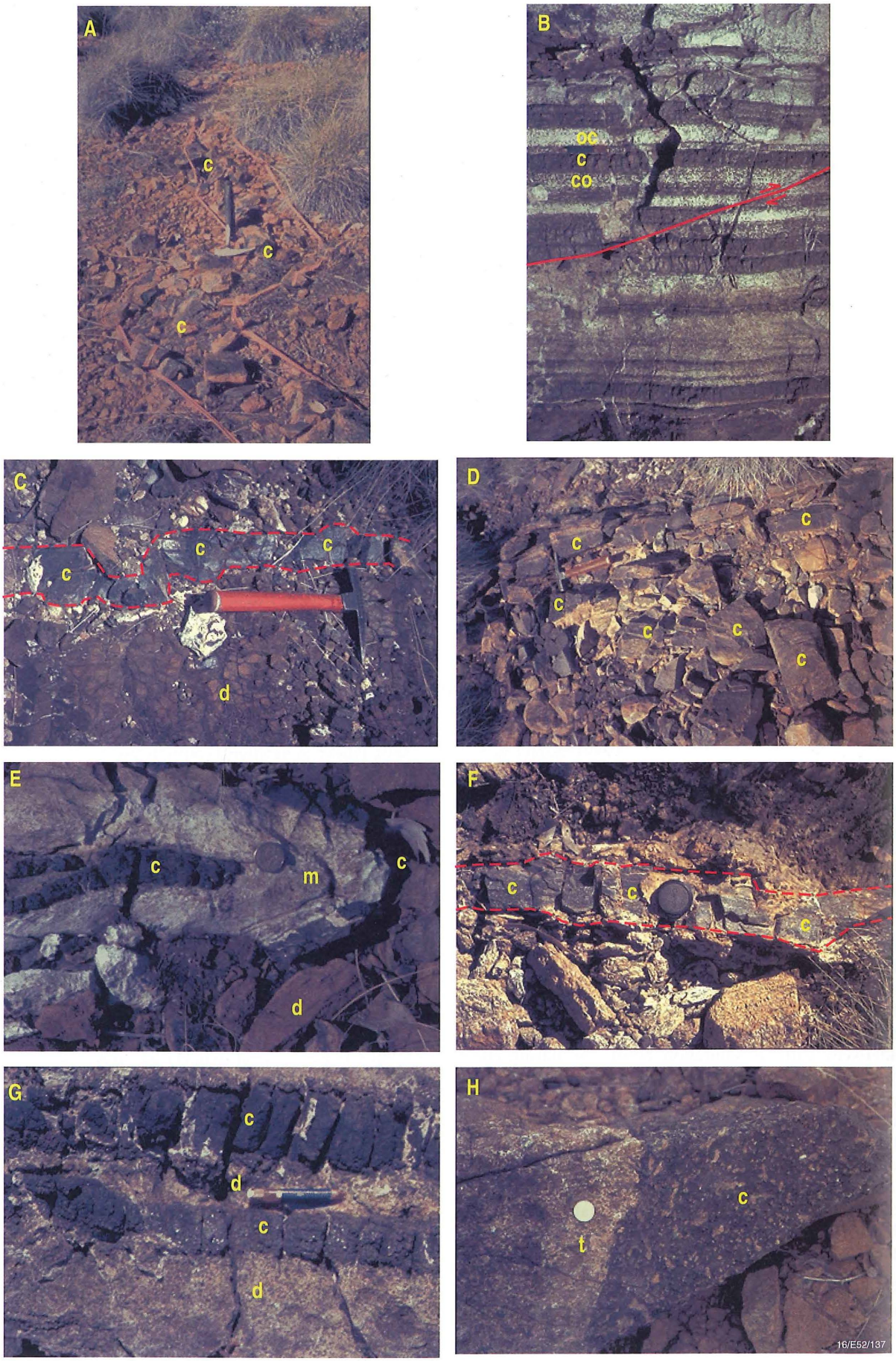


Figure 14.2. See page 284 for caption.

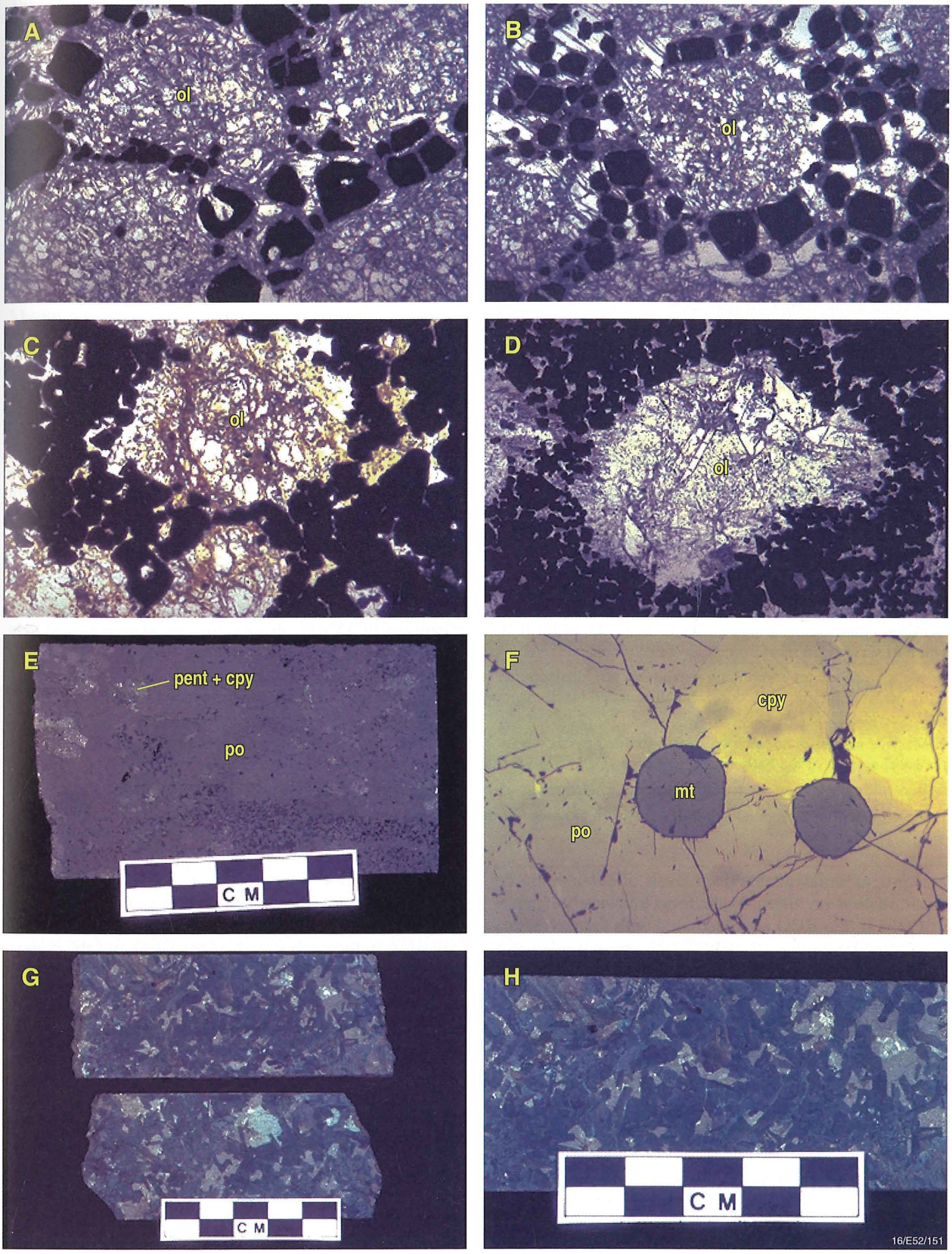


Figure 14.3. See page 284 for caption.

Figure 14.2. Chromitites from the East Kimberley layered mafic–ultramafic intrusions (photograph A by R. Perring, Normandy Exploration Ltd; B–H by D. Hoatson).

A. Massive A chromitite (c) layer, Middle Group chromitites of the Ultramafic Series of the group I Panton intrusion (near McINTOSH AMG ~762367). The irregular strike of the chromitite is indicated by the red flagging tape.

B. Stacked cyclic sequence comprising alternating thin chromite (c), chromite–olivine (co), and olivine–chromite (oc) cumulates, Middle Group chromitites of the Ultramafic Series of the Panton intrusion (McINTOSH AMG ~771372). The olivine has been replaced by white magnesite. A reverse fault with a displacement of a few centimetres is indicated by the red line.

C. Irregular chromitite (c) in dunite (d), Lower Group chromitites of the Ultramafic Series of the Panton intrusion (McINTOSH AMG ~779392).

D. Sheared and fragmented chromitite (c) in dunite lenses, Upper Group chromitites in the Middle Mafic Zone of the Panton intrusion (McINTOSH AMG ~766359).

E. Isoclinally folded chromitite (c) layers in dunite (d), Middle Group chromitites in the Ultramafic Series of the Panton intrusion (McINTOSH AMG ~755347). Olivine between the layers has been replaced by magnesite (m), whereas outside the layers, it is unaffected by the magnesite alteration.

F. Massive chromitite (c) layer in dunite near the base of the group I Big Ben intrusion (McINTOSH AMG ~766168).

G. Parallel chromitite (c) layers in dunite (d), group I West McIntosh intrusion (McINTOSH AMG ~821462).

H. Chromitite (c) in troctolite (t), group II Wilagee intrusion (McINTOSH AMG ~612526).

Figure 14.3. Mineralised rocks from the East Kimberley layered mafic–ultramafic intrusions (photographs A–D by A. Trudu, CSIRO Minerals; E–H by R. Sproule, Monash University).

A. Serpentinised olivine (ol)–chromite cumulate, group I Panton intrusion (92522023, photomicrograph, plane-polarised light, width of view is 2.6 mm).

B. Serpentinised olivine (ol)–chromite cumulate, group I Big Ben intrusion (93522026, photomicrograph, plane-polarised light, width of view is 2.6 mm).

C. Serpentinised olivine (ol)–chromite cumulate, group I West McIntosh intrusion (92522359, photomicrograph, plane-polarised light, width of view is 2.6 mm).

D. Serpentinised olivine (ol)–chromite cumulate, group II Wilagee intrusion (92522499, photomicrograph, plane-polarised light, width of view is 2.6 mm).

E. Massive sulphides comprising pyrrhotite (po), chalcopyrite (cpy), and pentlandite (pent), near the basal contact of the group V Sally Malay intrusion (drill core). Small rounded black magnetite grains (see Fig. 14.3F) are concentrated in the lower half of the drill core (DDH SM 94 428.5 m).

F. Massive sulphides comprising coarse-grained pyrrhotite (po) and chalcopyrite (cpy), and rounded chrome magnetite (mt), near the basal contact of the Sally Malay intrusion (DDH SM 94 428.5 m, photomicrograph, reflected light, width of view is 3 mm).

G. Troctolite containing interstitial pyrrhotite, chalcopyrite, and pentlandite, Sally Malay intrusion (DDH SM 50 366.9 m).

H. Enlargement of interstitial sulphides shown in top piece of drill core in Figure 14.3G.

enrichment, unfavourable deep levels of exhumation for the intrusions or, alternatively, most known occurrences of PGEs in the HCO are associated with thin refractory chromitite layers that are stable in the weathering profile and have weak dispersion haloes in the regolith. More widespread secondary dispersion of the PGEs might be expected under favourable climatic conditions if the PGEs were associated with sulphide-rich layers. The Lamboo and Eastmans Bore intrusions (see Chapter 2), which have widespread primary mineralisation and are close to the weathering surface, may be prospective for laterite-related PGE mineralisation.

Mineral deposits associated with mafic–ultramafic intrusions in the East Kimberley

Mineral deposits hosted by the layered intrusions can be broadly classified into three major orthomagmatic associations (chromite, sulphide, and Fe–Ti oxide) reflecting an apparent secular evolution of mineralising systems, i.e. Cr–PGEs–Ni–Cu±Au in 1856 Ma group I intrusions, Ni–Cu–Co±PGEs in 1845 Ma group V intrusions, and Fe–Ti–V in 1845 Ma group V and 1830 Ma group VI intrusions. A fourth association relates to hydrothermal polymetallic deposits. The concentration of PGE mineralisation in the central part of the HCO and the coexistence of the chromite and sulphide associations in this province are highlighted in Figure 14.1.

Chromite association (Cr–PGEs–Ni–Cu±Au)

Chromite, sensu stricto, is a ubiquitous cumulus mineral in the 1856 Ma group I (see Chapter 5 for the geological setting and classification of the intrusions) mafic–ultramafic intrusions (Panton, Big Ben, West Panton, Highway, Melon Patch, South Melon Patch, West McIntosh, Mini, West Robin Soak) and a rare accessory mineral in some coeval group II mafic intrusions (e.g. Springvale, Wilagee; see Figs 14.1 and 5.1). In the group I intrusions, concentrations of chromite form laterally continuous layers which, despite local irregularities, are generally conformable to, and form an integral part of, the ultramafic stratigraphy. Chromite in these intrusions occurs with cumulus olivine (dunite, lherzolite) in the middle and upper parts of the ultramafic stratigraphy and, more rarely, with cumulus orthopyroxene and olivine (harzburgite, dunite) near the contaminated basal

Table 14.2. Platinum-group element resources in Australian Precambrian layered mafic–ultramafic intrusions.

Intrusion	*Type of deposit*	*Resource*	*Reference/s*
Munni Munni, WA (western extent of mineralised layer)	Stratabound sulphide layer	20 to 30 Mt @ 2.9 ppm Pt+Pd+Au, 0.3% Cu, 0.2% Ni	Hoatson & Keays (1989) Williams et al. (1990) Barnes et al. (1992)
Munni Munni, WA (eastern extent of mineralised layer)	Stratabound sulphide layer	5 Mt @ 2.9 ppm Pt+Pd+Au,	Phaceas & Young (1996)
Radio Hill, WA	Basal segregations of sulphide	1.1 Mt @ 2.5% Ni, 1.8% Cu, ~0.3[1] ppm PGEs	De Angelis et al. (1987) Hoatson et al. (1992)
Mount Sholl, WA	Basal segregations of sulphide	4 Mt @ 0.5% Ni, 0.6% Cu, ~0.3[1] ppm PGEs	Mathison & Marshall (1981) Hoatson et al. (1992)
Sally Malay, WA	Basal segregations of sulphide	3.8 Mt @ 1.8% Ni, 0.7% Cu, 0.1% Co ~0.2[1] ppm PGEs	Barnes (1992) Frankcombe et al. (1994)
Panton, WA	Stratabound chromitite layer	2.0 Mt @ 6.02 ppm PGEs+Au, 0.28% Ni (Ind R+Inf R)	Perring & Vogt (1991) Hoatson (1993)
Yarawindah Brook, WA	Remobilised-laterite	2.9 Mt @ 0.79 ppm Pt+Pd (cut-off 0.5 ppm); 0.5 Mt @ 1.44 ppm Pt+Pd (cut-off 1.0 ppm)	Audax Resources NL (1986–90)
Weld Range, WA	Laterite	14.76 Mt @ 1.1 ppm Pt+Pd+Au (cut-off 0.5 ppm Pt+Pd+Au) (Inf R)	Louthean & Hill (1994) Parks (1998)
Mount Carnage (Ora Banda intrusion), WA	Laterite	10 Mt @ 1 ppm PGEs	Louthean & Hill (1994)

Ind R = Indicated resource; Inf R = Inferred resource.
[1] estimated PGE grades by author.

contacts of the intrusions. In the Panton intrusion it also occurs with cumulus olivine in a stacked sequence of ultramafic lenses in the Middle Mafic Zone. Cumulus chromite is associated with cumulus or intercumulus plagioclase and minor cumulus olivine (troctolite, anorthosite, leucogabbro) in the middle part of the group II Wilagee intrusion and also in the upper part of the group II Springvale intrusion: these occurrences are the only known examples in the East Kimberley where chromite is associated with plagioclase. Orthopyroxene and clinopyroxene, where present in the group I and II intrusions, are generally postcumulus to chromite.

Stratabound chromitite layers occur in all group I intrusions and in the group II Wilagee intrusion, where they are closely associated with cyclic units. In the ultramafic zones of group I intrusions, chromitite layers are associated with ultramafic cycles of dunite and lherzolite, whereas in the group II Wilagee intrusion they are hosted by troctolite in cycles comprising, in ascending stratigraphic order, peridotite, olivine gabbro, troctolite, anorthosite, and leucogabbro. Disseminated chromite occurs in cyclic mafic sequences of olivine gabbro, troctolite, leucogabbro, and anorthosite in the group II Springvale intrusion. In contrast to the Bushveld Complex, South Africa no chromitites in the HCO are hosted by pyroxenite.

The chromitite layers have different morphologies (Fig. 14.2A–H), ranging from very thin grain-size laminations, to single thick massive isomodal layers (Fig. 14.2A), to stacked cyclic packages comprising alternating thin chromitite layers and chromite-bearing dunite layers (Fig. 14.2B), to thin discontinuous stringers and lenses. A feature of the group I intrusions is the repeated occurrence of chromitite and chromite-bearing dunite layers throughout the ultramafic stratigraphy, indicating that open fractionation systems involved emplacement of new pulses of primitive magma into the evolving magma chambers. For example, in the Panton intrusion, there are three major stratigraphic levels of chromitite layers: in ascending order they are near the basal contact of the Ultramafic Series (Lower Group, Fig. 14.2C), just below the contact between the Ultramafic Series and

Table 14.3. Platinum-group-element and trace-element geochemistry of chromitites, sulphides, and other rock types from the East Kimberley layered intrusions.

Intrusion (Group)	*Sample number*	*Rock type/sulphides*	*Pt ppb*	*Pd ppb*	*Au ppb*	*Cu ppm*	*Ni ppm*	*S ppm*	*Cr ppm*	*Pt/Pd*	*Pdx10³/S*
Big Ben (I)	93522026	Chromitite	583	1080	8	44	664	70	>99 999	0.54	15.4
Big Ben (I)	BB1	Chromitite	520	580	7	20	640	-	140 000	0.90	-
Big Ben (I)	BB3	Chromitite	450	760	15	40	540	-	175 000	0.59	-
Big Ben (I)	BB2	Pyroxenite	40	33	13	130	440	-	4400	1.21	-
Big Ben (I)	93522029	Peridotite	2.4	1.9	2	88	343	410	1901	1.26	0.005
Mini (I)	92522338	Chromitite	43.4	122	1	54	637	220	>99 999	0.36	0.55
Panton (I)	92522046	Chromitite (UCG)	202	67.4	4	1	924	<10	>99 999	3.00	>6.74
Panton (I)	92522018	Chromitite (MCG)	2850	2375	153	272	971	60	>99 999	1.20	39.6
Panton (I)	92522023	Chromitite (MCG)	181	171	14	44	827	10	60 829	1.06	17.1
Panton (I)	92522086	Chromitite (MCG)	2565	2470	115	218	1174	50	>99 999	1.04	49.4
Panton (I)	92522037	Chromitite (LCG)	762	793	99	164	2986	50	>99 999	0.96	15.9
Panton (I)	92522072	Quartz gabbro chill	1.4	1	2	41	61	20	102	1.40	0.05
Panton (I)	92522076	Dunite (+chromite)	148	151	70	338	2164	1750	5149	0.98	0.09
Panton (I)	92522078	Dunite (+chromite)	120	112	119	886	2297	30	6022	1.07	3.73
Panton (I)	92522079	Dunite (+chromite)	53.8	37	36	625	2479	80	4742	1.45	0.46
South Melon Patch (I)	92522377	Chromitite	527	283	38	744	1785	100	>99 999	1.86	2.83
South Melon Patch (I)	92522380	Peridotite	91.6	179	3	182	1550	1350	7235	0.51	0.13
West McIntosh (I)	92522354	Chromitite	662	488	6	54	1263	20	>99 999	1.36	24.4
West McIntosh (I)	92522359	Chromitite	333	79	2	145	1088	90	>99 999	4.21	0.88
West Panton (I)	92522068	Chromitite	75.7	142	7	142	1512	40	>99 999	0.53	3.55
Springvale (II)	92522450	Olivine gabbro	1.9	4.2	2	53	314	530	1418	0.45	0.008
Springvale (II)	92522471	Olivine gabbro	0.5	<0.5	1	111	164	780	1302	>1.0	0.0006
Wilagee (II)	92522499	Chromitite	57.4	148	1	3	1082	<10	>99 999	0.39	>14.8
Wilagee (II)	92522506	Troctolite	6.9	21.7	2	57	1267	240	2256	0.32	0.09
Wilagee (II)	92522533	Gabbro chill	0.5	<0.5	3	95	106	800	389	>1.0	0.0006
Toby (III)	92522519	Biotite gabbronorite	0.6	<0.5	<1	57	103	1050	325	>1.2	0.0005
Wild Dog Creek (IV)	92522433	Magnetite gabbro	2.3	2.5	1	63	194	920	584	0.92	0.003
Dave Hill (V)	93522106	Olivine gabbro	1.4	2.1	4	268	402	2760	762	0.66	0.0008
Fletcher Creek (V)	93522153	Gabbro chill	0.5	2.8	1	172	123	1190	108	0.18	0.002
Sally Malay (V)	93522064	Olivine websterite	3.1	4.2	2	55	1537	450	1585	0.74	0.009
Sally Malay (V)	SMD30/36	Massive sulphides	0.8	102	16	-	-	-	-	0.008	-
Sally Malay (V)	SMD30/44	Dissem. sulphides	40.5	336	176	-	-	-	-	0.12	-
Sally Malay (V)	SMD88/45.5	Dissem. sulphides	3.7	8.3	10	-	-	-	-	0.45	-
Three Nuns (V)	93522080	Limonite	1.2	4.8	2	332	43	2560	141	0.25	0.002
Wilson Creek (V)	93522126	Troctolite	0.5	<0.5	1	40	127	1430	556	>1.0	0.0003
Armanda (VI)	92522489	Olivine gabbro	0.6	<0.5	2	221	242	590	1233	>1.2	<0.0008
Armanda (VI)	92522494	Gabbro	1.3	1	3	268	234	970	967	1.30	0.001
McIntosh (VI)	92522205	Magnetite gabbro	4.8	2.3	4	60	34	1590	162	2.09	0.001
McIntosh (VI)	92522267	Gabbro chill	2.2	1.1	1	97	114	1290	301	2.00	0.0008
McIntosh (VI)	92522293	Olivine gabbro	1.4	0.7	1	141	113	1160	517	2.00	0.0006
McIntosh (VI)	92522321	Olivine gabbro chill	1.9	1.6	2	108	178	1140	393	1.19	0.001
Black Hills Yard (VII)	92522517	Troctolite	8.5	16.1	2	47	851	280	3179	0.53	0.06
Three Sisters (U g)	93522007	Magnetite gabbro	0.9	<0.5	2	50	152	1220	397	>1.8	0.0004

Locations, stratigraphic heights, and major-trace-element geochemistry for the AGSO samples are listed in Appendix 2. For details of groups (I to VII, U g = Undivided gabbro) see Chapter 5. PGE and Au concentrations for individual chromitite layers in the Panton intrusion are shown in Table 5.2. UCG = Upper Chromitite Group in the Panton intrusion, MCG = Middle Chromitite Group, LCG = Lower Chromitite Group. - = not determined. The thickness for the Middle Chromitite Group layers are up to 2.4 m, but thicknesses for all other chromitites are less than 20 cm. Pt, Pd, and Au were determined by fire assay, lead concentration, and ICP-MS (method GS333 by Analabs Pty. Ltd., Welshpool, Western Australia), with detection limits 0.5 ppb Pt, 0.5 ppb Pd, and 1 ppb Au. Cu and Ni were determined by AAS (AGSO), and S

Gabbroic Series (Middle Group, Fig. 14.2A), and in ultramafic lenses (Upper Group, Fig. 14.2D) in the Middle Mafic Zone of the Gabbroic Series. Less persistent thin chromitite layers also occur between the Lower and Middle groups of the Ultramafic Series. Thicknesses of the chromitite layers in the three groups range from a few millimetres for the grain-size laminations to a maximum of 240 cm for massive isomodal layers, such as the A chromitite layer in the Middle Group of the Panton intrusion. The chromitites are generally thickest near the axial planes of the folded group I intrusions and thinnest along the limbs of the folds (e.g. Panton and South Melon Patch intrusions). This variation is believed to be due to a primary depositional control involving sagging of the cumulus pile rather than structural thickening during deformation. Most of the thin chromitite layers in the smaller group I intrusions can be traced along strike for hundreds of metres, whereas the A chromitite layer in the Panton intrusion crops out intermittently for at least 12 km along strike. The lateral continuity of the chromitite layers is locally disrupted by faults that crosscut at high angles and have displacements of a few centimetres to tens of metres. Dips of the chromitite layers range from shallow to steep, and in some of the larger intrusions, such as the Panton intrusion, they are locally overturned. Those in the deformed group I intrusions locally display heterogeneous strain partitioning. Chromitites near the axial plane region of the synclinal Panton intrusion are intensely schistose and fragmented (Fig. 14.2D), owing to a steeply dipping penetrative cleavage, and are also locally isoclinally folded (Fig. 14.2E) and boudinaged, whereas those on the limbs of the fold are less deformed. The contrasting physical characteristics of chromitites in different parts of an intrusion need to be considered when their economic viability is being evaluated.

The size of the chromite grains (0.2–2 mm) in the chromitites generally increases with increasing modal amounts of gangue olivine, which is invariably replaced by serpentine minerals, magnesite, and magnetite (Fig. 14.3A–D). Magnesite alteration is a characteristic feature of chromitite layers with a high olivine component in the upper part of the Ultramafic Series in the Panton intrusion, e.g. the C chromitite layer of the Middle Group. The alteration is generally confined to the matrix of the chromitite layer and may be due to late magmatic fluid movement along pathways or conduits with favourable porosities or chemistry. Rhythmic modal layering, comprising varying amounts of cumulus olivine and chromite, are common in the stacked chromitite layers, but size-grading of the cumulus grains is rarely developed.

The distribution of chromite in the layered intrusions of the East Kimberley is summarised in Figure 14.4. Of greatest economic significance are stratabound chromitite layers at comparable stratigraphic levels in the upper parts of the ultramafic stratigraphy in group I intrusions. As shown by the Panton intrusion, these chromitites are generally thicker, show greater lateral continuity, and are enriched in PGEs, Au, and Ni, relative to chromitites at other stratigraphic levels in the intrusions. Mixing between magmas of contrasting composition (Irvine 1975, 1977, see Chapter 12) is considered to be the major mechanism for the precipitation of chromite in these layers. This is supported by reversals in fractionation trends of trace elements across major chromitite layers in the Panton intrusion (Hamlyn et al. 1988). There is a correlation between the thickness of these chromitite layers and the thickness of the ultramafic sequence. The thickest layers are in the Panton and Big Ben intrusions, which contain the thickest sequences of olivine-bearing cumulates, 650 m and 1700 m, respectively. Some ultramafic sequences less than 200 m thick (e.g. Highway and Mini intrusions) host thin (1–5 cm) chromitite layers. The chromitites generally occur from 2 to 150 m below the contact of the ultramafic and overlying mafic zones and, hence, are useful stratigraphic and structural markers. In more detail there appears to be a relationship between the stratigraphic level of these chromitites and the relative thickness of the ultramafic sequence. For example, the distance of the major chromitite layer below the mafic–ultramafic contact increases progressively with increasing thickness of the ultramafic sequence. This spatial relationship is a useful predictive tool when the upper parts of the ultramafic stratigraphy are being explored.

The basal parts of the ultramafic zones in the thicker group I intrusions (Panton, Big Ben, and Melon Patch) host stratabound chromitite layers, but are absent from the thinner intrusions. This may indicate that the volume of the primitive magma may have been an important factor in the formation of these layers and that chromite precipitation—most likely initiated by crustal contamination—may have been more pronounced during emplacement of thicker and hotter bodies.

Stratabound chromitite layers are also hosted by ultramafic lenses in gabbroic sequences of group I intrusions (Panton, West McIntosh) and in troctolite rocks of group II intrusions (Wilagee). These layers have lateral extents of only a few hundred metres. Mafic cyclic units in the upper part of the group II Springvale intrusion contain only trace amounts of disseminated chromite with associated low abundances of PGEs and base metals. Exploration companies have reported Pt+Pd concentrations of up to 500 ppb (note: repeat analyses showed much lower PGE concentrations—see Chapter 2) and anomalous Ni and Cu concentrations in chromite-bearing troctolite and anorthosite layers, 1.5 m thick. Lack of lateral continuity and low grades indicate that the chromite-bearing layers in mafic rocks of the East Kimberley offer limited potential for a major PGE or Cr resource.

Table 14.3 summarises the Pt, Pd, Au, and trace-element geochemistry of chromitites, sulphides, and other rocks from the East Kimberley intrusions. With the exception of the A chromitite layer in the Panton intrusion (samples 92522018, 92522086), which has high abundances of Pt (2565–2850 ppb) and Pd (2375–2470 ppb), the chromitites from the other intrusions have subeconomic concentrations of Pt (43.4–762 ppb) and Pd (67.4–1080 ppb). Average Pt+Pd abundances in chromitites decrease in the order: Panton (Middle Group), Big Ben, Panton (Lower Group), South Melon Patch, West McIntosh, Panton (Upper Group), West Panton, Wilagee, and Mini.

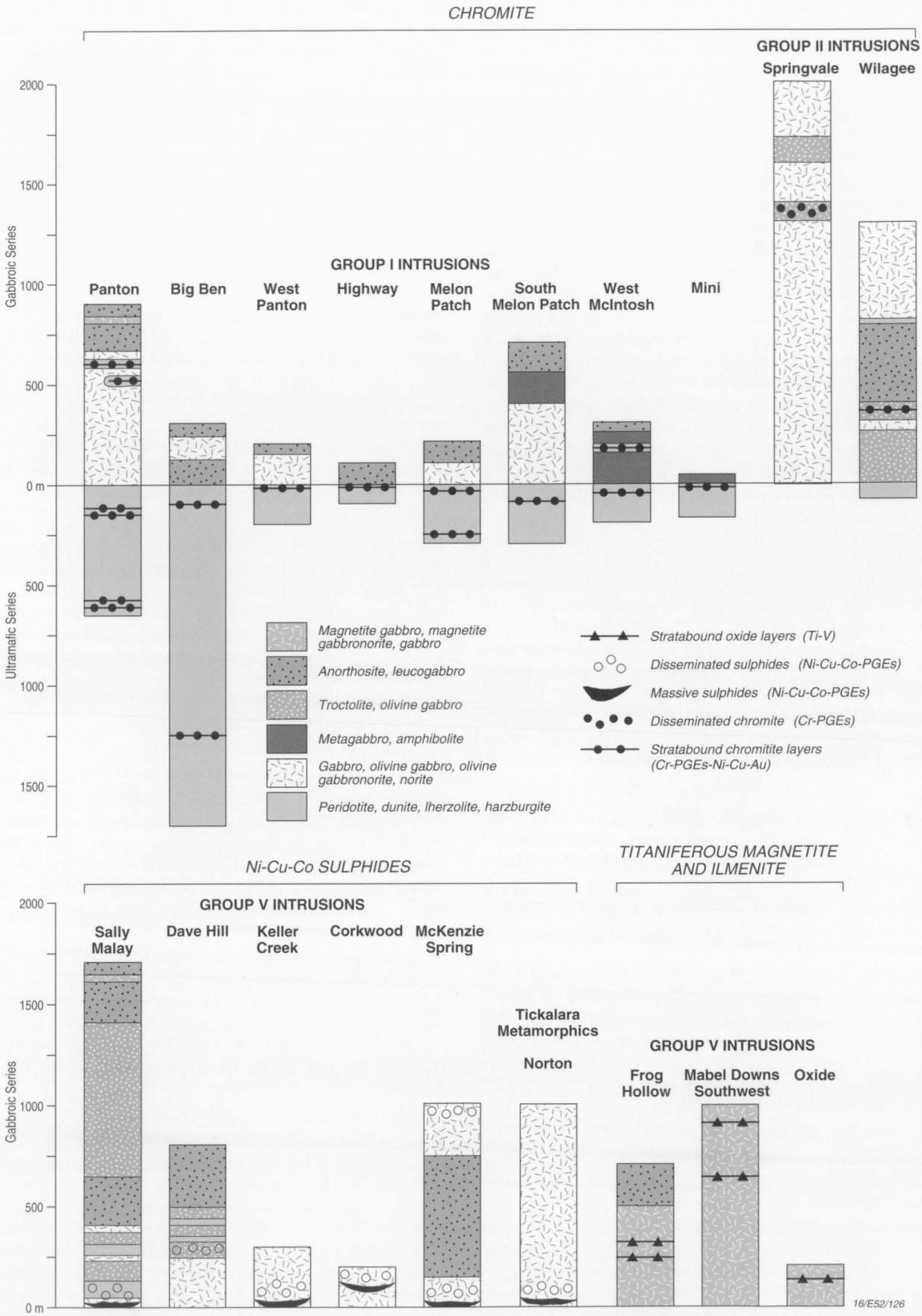


Figure 14.4. Stratigraphic distribution of chromite, Ni–Cu–Co sulphides, and titaniferous magnetite and ilmenite in the East Kimberley layered mafic–ultramafic intrusions. The vertical axis shows the thicknesses of the Ultramafic Series and Gabbroic Series for each intrusion.

This order generally correlates with decreasing thickness of the ultramafic component in the intrusion, implying that the precious-metal abundances of the chromitites are related to the volume of the ultramafic magma. The Pt/Pd ratio of the chromitites ranges from 0.36 to 4.2, with the intrusions containing the thinner ultramafic components (Mini, Wilagee, West Panton) having the lower ratios. Au (up to 153 ppb) and Cu (up to 744 ppm) show positive correlations with Pt and Pd, with the highest Cu abundances being in chromite-bearing dunite (886 ppm) from the Panton intrusion. Ni is most enriched in the Lower Group chromitite (2986 ppm) and chromite-bearing dunite (2479 ppm) of the Panton intrusion. A geochemical feature of the chromitites is their low S content. Sulphur reaches a maximum of 220 ppm in the Mini intrusion, but in most intrusions it is less than 100 ppm. This is rather surprising, given the S-saturated character of the surrounding ultramafic cumulates, and may indicate that significant amounts of S were mobilised during serpentinisation of olivine in the chromitites. Mineralogical and chemical features of chromite in the East Kimberley intrusions are discussed in some detail in Chapter 13.

In summary, group I layered mafic–ultramafic intrusions with the thickest sequence of olivine-bearing ultramafic cumulates host the thickest and most PGE-rich stratabound chromitite layers. The stratigraphic interval from 0 to 150 m below the Ultramafic Series and Gabbroic Series contact should be highest priority when exploring for PGE-enriched chromitite layers in these bodies. If the main exploration focus is just for Cr, then olivine-bearing cumulates in the mafic and ultramafic components of thick group I intrusions should be investigated. The paucity of thick sequences of orthopyroxene-dominant cumulates in the HCO suggests that chromite–orthopyroxene–olivine associations, often seen in overseas intrusions, are unlikely to occur in the East Kimberley.

Sulphide association (Ni–Cu–Co±PGEs)

The Ni–Cu–Co±PGEs sulphide association in the East Kimberley is exemplified by the 1845 Ma group V intrusions in the northern part of the study area (see Fig. 5.1). Most of those investigated (Corkwood, Dave Hill, Fletcher Creek, Keller Creek, McKenzie Spring, Sally Malay, Spring Creek, and Wilson Creek) contain subeconomic concentrations of massive and disseminated sulphides in the lower parts of their mafic-dominated stratigraphy (Fig. 14.4). The massive sulphides are generally hosted by fractionated gabbroic rocks, which form basal units, 5–40 m thick, between the overlying peridotite and paramigmatite footwall country rocks. Matrix sulphides persist into the overlying thin (tens of metres thick) peridotite and gabbroic rocks. Olivine gabbro, gabbro, norite, and metagabbro are the major host rocks to the sulphides in intrusions which have no ultramafic component. There is also significant sulphide mineralisation in the lower stratigraphic levels of some massive mafic granulite bodies in the Tickalara Metamorphics (e.g. Norton, ?Bow River), but preliminary studies indicate these sulphide deposits have lower Ni and Cu concentrations than those hosted by the group V intrusions.

The group V Sally Malay intrusion contains the largest sulphide deposit in the East Kimberley, with an indicated and inferred resource of 3.85 Mt @ 1.79% Ni, 0.73% Cu, and 0.10% Co (Shedden & Barnes 1996). Published resource statistics are not available for the other deposits, but in most cases they are believed to be about 1–3 Mt @ 1–2% combined Ni and Cu, with Co concentrations about 0.05–0.1 times the Ni concentrations, and less than 0.5 ppm total PGEs. The Ni/Cu ratio for mineralised drill-hole intersections from these intrusions generally ranges from 2:1 to 5:1, which is within the mid-range normally associated with gabbro-hosted deposits (Marston 1984). The Ni/Cu ratio for the granulite-hosted deposits appears to be lower, ranging from 0.5:1 to 2:1. The trace-element geochemistry of sulphides and other rock types from the Sally Malay and other group V intrusions is summarised in Table 14.3.

Most of the sulphide deposits were discovered in the 1970s (see Chapter 2) by locating linear ferruginous gossans near the basal contacts of the intrusions (Fig. 14.5A–C) or disseminated sulphides in gabbroic rocks (Fig. 14.5D). Other indicators were secondary Cu carbonates on fracture and cleavage planes, and remobilised sulphides in shear zones and along contacts with dolerite dykes and pegmatite veins. The gossans generally form discontinuous bouldery outcrops, 0.2–2 m high, and up to 5 m wide. The Sally Malay gossan is a notable exception, with widths attaining 20 m. Strike extent ranges from a few hundred metres for the group V intrusions (Corkwood, 220m; Sally Malay, 300 m; Keller Creek, 400 m; McKenzie Spring, 400 m) up to several kilometres for the granulite intrusions (Bow River, 750 m; Norton, 6.5 km). Gossanous veins at the Sally Malay, Keller Creek, Norton, and Bow River intrusions cut the footwall country rocks, indicating remobilisation of the sulphides. The Norton intrusion gossan contains goethite, hematite, limonite, and traces of magnetite and/or maghemite, with quartz and montmorillonite as the major silicate minerals. Diagnostic cellular boxwork textures are rarely present, owing to masking by lateritisation.

Sulphides in all mineralised intrusions of group V and the Tickalara Metamorphics show a clear association with the lower parts of the stratigraphy (Fig. 14.4). Massive and/or disseminated sulphides in the Sally Malay, Keller Creek, McKenzie Spring, and Norton intrusions occur along or very near the basal contact of the intrusion or in the feeder conduit. The geometry of the basal contact and conduit is important, because massive sulphide ores need to be concentrated in restricted environments in order to attain economic grades. For example, in the Sally Malay intrusion, sulphides are concentrated in a keel-shaped depression of the feeder conduit (Hoatson et al. 1997), and in the McKenzie Spring intrusion they occur in a 1600-m-long fault-controlled structural embayment of the basal contact that is transgressive to the footwall country rocks. The widespread, and thinness of, mineralisation in the Norton and Bow River granulite intrusions indicate that there may not have been a suitable basal depression for concentrating dense sulphides by gravitational processes. The Corkwood intrusion is one of the few intrusions that has

a major sulphide concentration a significant distance (~100 m) above the basal contact (Fig. 14.4). This may reflect metamorphic remobilisation of the sulphides towards the least recrystallised, low-stress areas of the metagabbro host.

Another important feature, as shown by most group V intrusions, is that the accumulation of sulphides is greatest below the thickest part of the overlying cumulates. These parts of the intrusions represent the thickest columns of magma with potentially the greatest abundance of metals. They will also have the greatest heat retention, which may be important for gravitational and contamination mineralising processes.

Four major textural types of sulphides (Fig. 14.3E–H) occur in the mineralised group V intrusions: massive basal sulphides (80–100 vol. % sulphide), matrix and disseminated sulphides (5–40 vol. %), breccia matrix sulphides, and remobilised sulphides. Massive sulphides at the base of the intrusions generally consist of coarse (1–4 mm) interlocking hexagonal pyrrhotite (50–90 vol. %), and spatially associated smaller granular pentlandite and chalcopyrite grains. Exsolved pentlandite flames occur along pyrrhotite grain boundaries. Accessory minerals include pyrite, chrome magnetite, aluminous spinel, ilmenite, garnet, biotite, and quartz. Violarite occurs to depths of 50 m. Sulphides directly above the massive sulphides range from finer grained matrix variants of the massive sulphides to more Cu-rich stringer, interstitial, and disseminated blebby sulphides for lower sulphide-bearing rocks. Pyrrhotite–chalcopyrite forms matrix sulphides to breccias in the basal parts of the intrusion and in the footwall migmatites. Remobilised sulphides rich in chalcopyrite occur as offset contact ores in the footwall migmatites and along contacts, fractures, and as veins. Some pentlandite-rich sulphides in the Keller Creek intrusion have been remobilised by later felsic intrusive bodies. Sulphide textures in the group V intrusions generally show little evidence of strain or recrystallisation, whereas those in granulite bodies are characterised by discontinuous massive recrystallised bands and thin lenticular segregations subparallel to the foliation of the host metagabbros.

The assimilation and contamination of mafic magmas with crustal components are considered crucial for the formation of economic deposits of magmatic Ni–Cu–Co sulphides (Peltonen 1995a, Naldrett 1997, Hoatson 1998, and see Chapters 1 & 12). Thornett (1981) used mineralogical and chemical evidence, such as the association of sulphide and alkali minerals, the differentiated nature of the mineralised basal zone, and the abundance of migmatite-derived xenoliths in this zone, to show that contamination of the Sally Malay magma by silica-rich Tickalara Metamorphic country rocks was instrumental in initiating S saturation of the magma. This precipitation of sulphide resulted in the formation of a basal accumulation of Ni–Cu–Co sulphide and an overlying relatively S-depleted zone. Persistent gossans along both the footwall and hangingwall contacts of the McKenzie Spring intrusion. indicate that silica and/or volatile contamination of the mafic magma with metasedimentary country rocks may have induced S saturation of the magma. Detailed isotopic and trace-element studies of the mineralised East Kimberley intrusions (see Chapters 11 & 12) reinforces the importance of crustal contamination processes. Significantly, the major footwall rocks for all mineralised group V and mafic granulite intrusions are high-grade metasediments (generally garnet–cordierite–sillimanite–spinel–biotite–feldspar–quartz paragneisses) of the Tickalara Metamorphics. The siliceous character and, presumably, ease of assimilation of these metasediments make them favourable country rocks for changing the sulphide solubility of the mafic magmas. Other potentially reactionary components in these metasediments (pyrrhotite, graphite) have also been reported (Thornett 1981). Intrusions with igneous footwall sequences should not be completely discounted, since ascending magmas may have been contaminated with favourable S-bearing rocks in the conduit before emplacement into the chamber.

It is concluded that the most prospective intrusions for magmatic Ni–Cu–Co±PGE sulphide deposits in the East Kimberley are those of group V. Restricted depositional environments for massive sulphide ores are required if economic grades are to be attained. Such favourable environments include local depressions or fault-controlled structural embayments along basal contacts in which dense sulphides can concentrate from gravitational and/or crustal contamination processes. Initial investigations should carefully reconstruct the configuration of the basal contact for such environments, particularly below the thickest part of the intrusion. Group V intrusions with mainly metasedimentary rocks in the footwall are considered more prospective than those with mainly igneous rocks. The feeder conduit environment is a high-priority exploration target for massive sulphide mineralisation. Fluid dynamic contrasts associated with the change from narrow vertical conduits to broad sub-horizontal open magma chambers (e.g. fast, slow, turbulent, passive) may be important for the deposition and concentration of sulphides (Lambert et al. 1998).

Fe–Ti oxide association (Fe–Ti–V)

Concentrations of titaniferous magnetite and ilmenite are hosted by gabbroic rocks in the middle to upper fractionated parts of some 1845 Ma group V (Frog Hollow, Mabel Downs Southwest, Oxide) and 1830 Ma group VI (McIntosh, see also Ord Crossing—Grid A North Ti–V in Chapter 2) mafic intrusions (Figs 14.5 E, F). Their distribution (Fig. 14.4) highlights the evolved and tholeiitic character of these bodies, and their association with the younger layered intrusions is consistent with the general progression from early, more primitive, mineralising magmatic systems to later, more evolved systems in the HCO.

Most Fe–Ti–V deposits appear to be small and have little or no potential for a large-tonnage resource. None of the deposits has been mined and few, if any, have been tested by drilling. The fact that one of the largest outcropping resources in the Kimberleys, the Frog Hollow deposit (Hoatson 1995), was discovered as late as 1994 attests to the low priority that exploration companies have placed on these deposits.

The Fe–Ti oxides are disseminated or form stacked sequences of thin (0.5–5 cm) cyclic units, thin discontinuous irregular layers, and thicker massive lenses. The

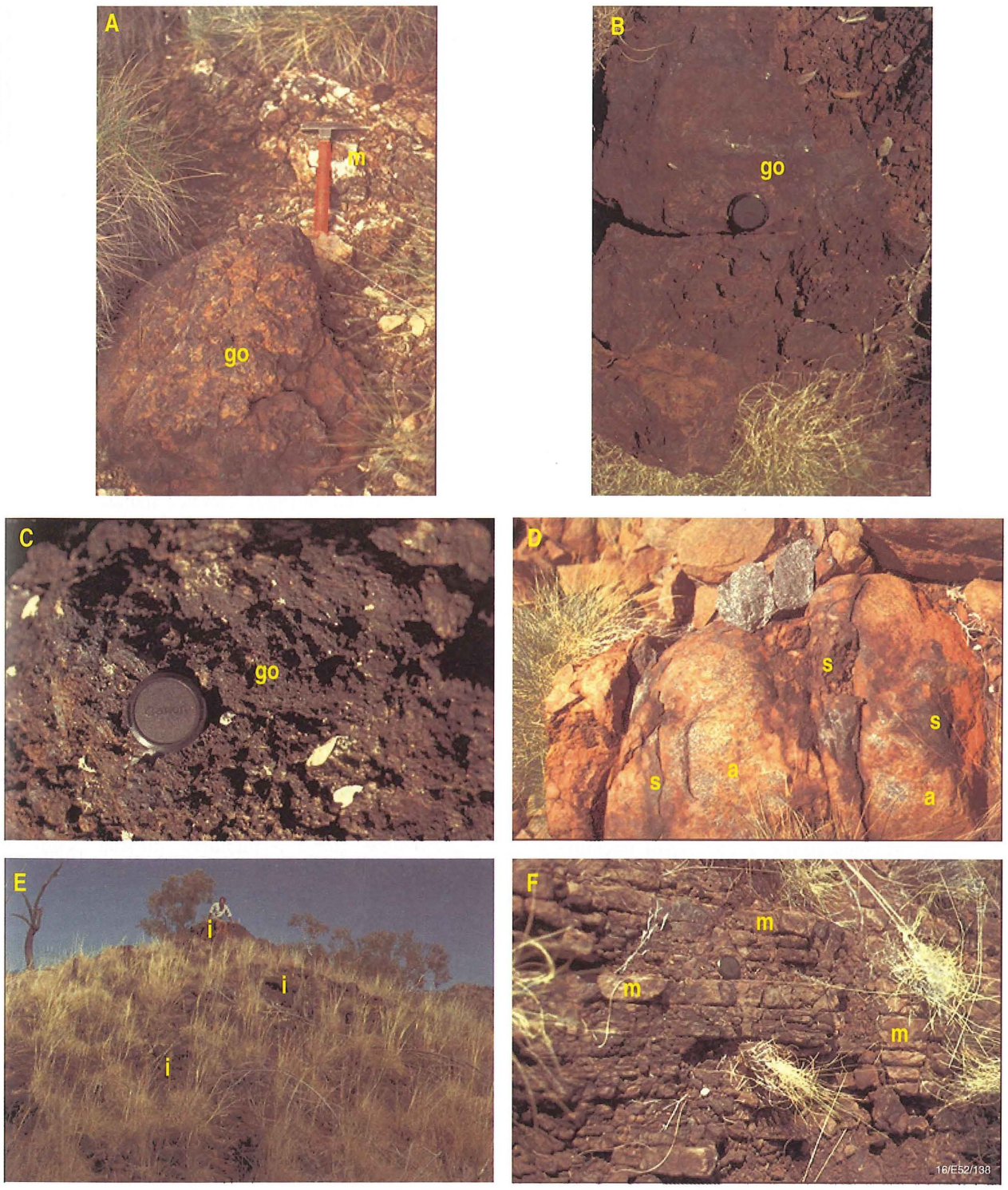


Figure 14.5. Gossans and Fe–Ti oxides from the group V East Kimberley mafic–ultramafic intrusions.

A. Ferruginous gossan (go) and magnesite (m) altered peridotite at the base of subchamber A of the Sally Malay intrusion (TURKEY CREEK AMG ~962816).

B. Massive goethite–hematite–limonite gossan (go) at the base of the Norton intrusion (TURKEY CREEK AMG ~983959).

C. Ferruginous gossan (go) at the base of the Keller Creek intrusion (MOUNT REMARKABLE AMG ~904866).

D. Partly oxidised Fe-sulphides (s) in leucogabbro and anorthosite (a) in the upper part of the Dave Hill intrusion (TURKEY CREEK AMG ~962791).

E. Massive lens of ilmenite (i) and minor titaniferous magnetite, Frog Hollow intrusion (TURKEY CREEK AMG ~984873).

F. Cyclic layers of titaniferous magnetite (m) and minor ilmenite in the Mabel Downs Southwest intrusion (TURKEY CREEK AMG ~032000).

Frog Hollow mafic intrusion (see Fig. 5.1) contains a number of massive oxide lenses hosted by ferrogabbro and leucogabbro. The lenses form prominent small hills (Fig. 14.5E), 5 to 15 m high, surrounded by recessive gabbroic rocks, and are drained by creeks containing abundant oxide alluvium. Deformed coarse-grained aggregates of ilmenite (~55 vol. %), secondary tremolite–actinolite (40%) after clinopyroxene, and minor titaniferous magnetite (5%) are the major components of the lenses, which contain a maximum of 39.4% TiO_2, 0.99% V, 60.6% total Fe as Fe_2O_3, and 0.93% Cr. These values compare favourably with those of other major Australian titaniferous magnetite deposits: 3–30% TiO_2 and 0.1–0.7% V (1986 Australian Mineral Industry Quarterly 39, 1, p.7). The deformation, coarse grain size, and high TiO_2 grades of the Frog Hollow deposit may reflect high-temperature subsolidus annealing and grain enlargement processes related to later metamorphism.

At the Oxide intrusion (see Fig. 5.1), massive oxides form rubble over an area of 15 m by 30 m; the size of this deposit and its relationship to the host gabbroic rocks are unknown, owing to poor exposure.

Stacked cyclic units of titaniferous magnetite and ilmenite crop out over a stratigraphic interval of about 150 m in the upper fractionated part of the Mabel Downs Southwest mafic intrusion (see Fig. 5.1). Individual cyclic layers are 2–5 cm thick and collectively form stacked units, 10 m thick, (Fig. 14.5F) that can be traced along strike for several hundreds of metres. They have a lower ratio of ilmenite to magnetite than the Frog Hollow deposit, as indicated by lower TiO_2 (15.5%) and V (0.17%) contents.

Mathison & Hamlyn (1987) stated that Fe–Ti oxides in the large McIntosh intrusion (see Fig. 5.1) form a minor disseminated component (<2 vol. %) of troctolite and olivine gabbro and are more abundant (up to 10 vol. %) in gabbronorite. Magnetite is the dominant phase and is cumulus, whereas ilmenite is postcumulus and commonly in contact with magnetite. The magnetite-bearing gabbronorite is characterised by low Ti (<1.44% TiO_2) and V (<0.04%) contents. Cyclic units of Fe–Ti oxides (up to 50 vol. %) characterise gabbroic and leucogabbroic rocks in the upper half of the body and at the northwestern margin of the intrusion. They range from wispy isomodal laminations about one grain thick, to thin (1–5 cm) isomodal layers, to similarly thin modally layered units, typically with sharp bases and gradational tops. The cyclic oxide units are separated by sequences of gabbro, gabbronorite, ferrogabbro, leucogabbro, and rare anorthosite. Although the units extend along strike for several hundreds of metres, they appear to have little economic potential.

Hydrothermal polymetallic association (Pd, Pt, Cu, Zn, Pb, Au)

Hydrothermally remobilised polymetallic deposits in the East Kimberley have historically not been a priority target for exploration. However, features such as extensive alteration systems indicated by widespread serpentinisation of ultramafic sequences, reactivated faults that cut rocks of different composition, multiple phases of metamorphism and deformation, potential heating by coeval gabbroic and granitic intrusions, and high regional background concentrations of PGEs indicate that this province contains many favourable ore-forming components (e.g. fluids, structural conduits, heat, and metals) for such deposits.

The Emull Zn–Cu–Pb–Ag prospect (ANGELO[1] at AMG coordinates ~204617), 5 km northwest of the Lamboo mafic–ultramafic intrusion (see Chapter 2), is an example of hydrothermal-remobilised mineralisation spatially associated with a mafic intrusion in the East Kimberley. The polymetallic prospect (demonstrated resource of 4.7 Mt @ 4.5% Zn, 0.33% Cu, 0.2% Pb, and 19 ppm Ag) occurs near the contact between the differentiated Emull Gabbro and poorly exposed lateritised metasediments of the Koongie Park Formation (Griffin et al. 1998). The mineralisation consists of a series of en echelon lenses and pods of disseminated and massive sulphides comprising sphalerite–galena–chalcopyrite–pyrite–pyrrhotite in 'serpentinite' and a diopside–carbonate–chlorite calc-silicate rock interpreted as assimilated country rock in the gabbro (Ferguson 1999). Elevated abundances of Ag, Au, Bi, and Cd are associated with the Zn-rich sulphides. The gabbro also contains low-grade disseminated sulphide mineralisation. Griffin et al. (1998) interpreted the mineralised 'serpentinite' and calc-silicate rocks to be formed by metasomatism of the gabbro by possible felsic intrusions. Ferguson (1999) cites the unusual metal and lithological associations to indicate that the base-metal sulphide phase was introduced into the partially crystallised gabbro. The coeval relationships of many mafic and felsic magmatic systems in the western and central zones of the HCO (see Chapter 10) highlight the potential for secondary redistribution of base and precious metals by volatiles or volatile-enriched magmas (breccia-type and constitutional zone refining mineralisation of Brügmann et al. 1989 and Barrie 1995).

Overseas hydrothermal deposits associated with mafic–ultramafic intrusions, such as those documented at Hitura, Finland (Hakli et al. 1976), the New Rambler mine, USA (McCallum et al. 1976), and the Hochgrössen massif, Austria (Thalhammer & Stumpfl 1988) demonstrate the effectiveness of serpentinisation as a concentrating mechanism for PGEs. Rathbun Lake, Ontario (Rowell & Edgar 1986) is an example of a fault-controlled hydrothermal mineralisation system that could be an exploration target in faulted and intensely serpentinised mafic–ultramafic intrusions and their country rocks, such as the group I Panton and Big Ben intrusions of the East Kimberley.

Investigations for hydrothermal mineralisation in the HCO should focus on zones of alteration, hybridisation, and brecciation near the contacts of coeval granite and gabbro bodies, and in thick sequences of serpentinised and faulted olivine-rich cumulates.

[1] 1:100 000 sheet names throughout this *Bulletin* are in capital letters to avoid confusion with identical place names and to distinguish them from 1:250 000 sheet names.

Comparison of the East Kimberley mafic–ultramafic intrusions with overseas intrusions

The layered mafic–ultramafic intrusions of the HCO cannot be readily classified according to the various schemes based on tectonic setting, composition of magma, and associated magmatic deposits (Naldrett & Cabri 1976, Macdonald 1987, Naldrett 1981, 1989, 1997). Intrusions in the HCO display some broad similarities to the major mineralised layered intrusions that characterise tectonically stable Precambrian granite–greenstone and metasedimentary cratonic terranes overseas (category III and subclass 2 of Naldrett 1989), such as the Bushveld Complex, Stillwater Complex, Sudbury Complex (Ontario, Canada), and the Great Dyke of Zimbabwe. These similarities include:

- medium to large layered mafic–ultramafic intrusions of dominantly tholeiitic affinity;
- emplacement between 1.85 Ga and 2.7 Ga;
- preferential location along major unconformities or at contacts between metasedimentary, metavolcanic, or granitic sequences that are >200 Ma older than the intrusion, implying a stable cratonic setting at the time of emplacement (Barrie 1995);
- geometry ranging from broad shallow-dipping basins (e.g. Bushveld and Toby) and funnel-shaped lopoliths (Muskox–Canada and McIntosh), to steeply dipping saucer-shaped bodies (Stillwater and West McIntosh) and elongated dyke-like bodies (Great Dyke and Corridor gabbro);
- thick, laterally continuous, cyclic sequences of mafic–ultramafic cumulates ranging in composition from dunite to ferrogabbro; and
- PGE mineralisation associated with chromite and/or sulphide near the base of cyclic units or near the interface of ultramafic and mafic parts of the intrusion.

However, in contrast to these large overseas intrusions, the East Kimberley mafic–ultramafic intrusions were emplaced near the centre of a Palaeoproterozoic orogenic belt that experienced several phases of metamorphism and deformation. Orogenic events are a feature of many early Proterozoic terranes overseas (e.g. Torngat and Wopmay Orogenies in Canada and Eburuian Orogeny in Africa) and elsewhere within Australia (e.g. Barramundi Orogeny in the Arunta, Gawler, Granites-Tanami, Mount Isa, Pine Creek, and Tennant Creek domains: Etheridge et al. 1987). In some respect the layered intrusions of the HCO show some affinities with synorogenic intrusions emplaced into orogenic belts, such as the Råna intrusion, Norway (Boyd & Mathiesen 1979), Moxie intrusion, USA (Thompson & Naldrett 1984), and Fongen–Hyllingen intrusion, Norway (Wilson et al. 1987). These intrusions, which belong to category IV and subclass 1 of Naldrett (1989), are characterised by syndeformational structures, irregular igneous layering, tectonic fabrics, irregular distribution of a wide variety of igneous rock types, and metamorphism and deformation in the late stages of tectonism. However, most East Kimberley intrusions lack pervasive deformational features, and many display well-preserved primary igneous features, such as cumulus textures and undisturbed compositional layering (see Chapter 5). Those layered bodies that are folded and show an axial-plane cleavage (e.g. group I in the central zone of the HCO: see Chapters 3 and 5) were probably deformed after their emplacement. The presence of laterally continuous cyclic layers and cumulate rocks containing delicate layering fabrics over several kilometres along strike indicate stable tectonic conditions during crystallisation.

The layered mafic–ultramafic intrusions of the HCO appear to show distinct temporal relationships with the main periods of orogenesis. The intrusions were generally emplaced in pulses soon after or between the main orogenic events that affected the central and western zones of the HCO. The first major phase of magmatism responsible for the layered intrusions (1855 Ma groups I, II, and III) followed the main period of deformation and metamorphism associated with the Hooper Orogeny at ~1860 Ma (Sheppard et al. 1997b). Another magmatic phase (≤1830 Ma groups VI and VII) took place shortly after the main period of the Halls Creek Orogeny at ~1835 Ma (Tyler & Page 1996, see Chapter 3). An economically important phase of magmatism (1845 Ma group V) characterises the period midway between these two major orogenic events. It should be kept in mind that this overall temporal relationship is more complicated than presented here since the duration and intensity of deformation and metamorphism associated with the orogenic events was different for the western, central, and eastern zones of the HCO.

In conclusion, the layered mafic–ultramafic intrusions of the HCO can be generally regarded as late orogenic to postorogenic Palaeoproterozoic bodies that were emplaced during relatively more quiescent periods between phases of active tectonism in a complex orogenic belt.

Some intrusions in the HCO have thicknesses of mafic rocks similar to those of major intrusions overseas (Fig. 14.6). For example, the thickness of mafic rocks in the McIntosh intrusion (7.8 km) is similar to that of one of the largest intrusions in the world, the Bushveld Complex (Naldrett 1989). However, only the group I intrusions (Panton group) have mafic to ultramafic ratios comparable to the overseas intrusions and, of the other groups in the East Kimberley, only group V (Sally Malay) has significant thicknesses of ultramafic rocks. A distinctive feature of the East Kimberley intrusions is the general paucity of ultramafic rocks, and in particular pyroxenites. Some of the group V intrusions which have been explored for Ni–Cu–Co sulphide mineralisation, e.g. Corkwood and Keller Creek, are small mafic bodies only 200 to 300 m thick. These thicknesses are comparable to some small economic Ni–Cu-bearing intrusions in southern Finland (Peltonen 1995a), but are much smaller than the major mineralised intrusions overseas, such as Sudbury and Voisey's Bay. If the group V East Kimberley intrusions are to contain a significant resource of base-metal sulphides, the parent magmas for

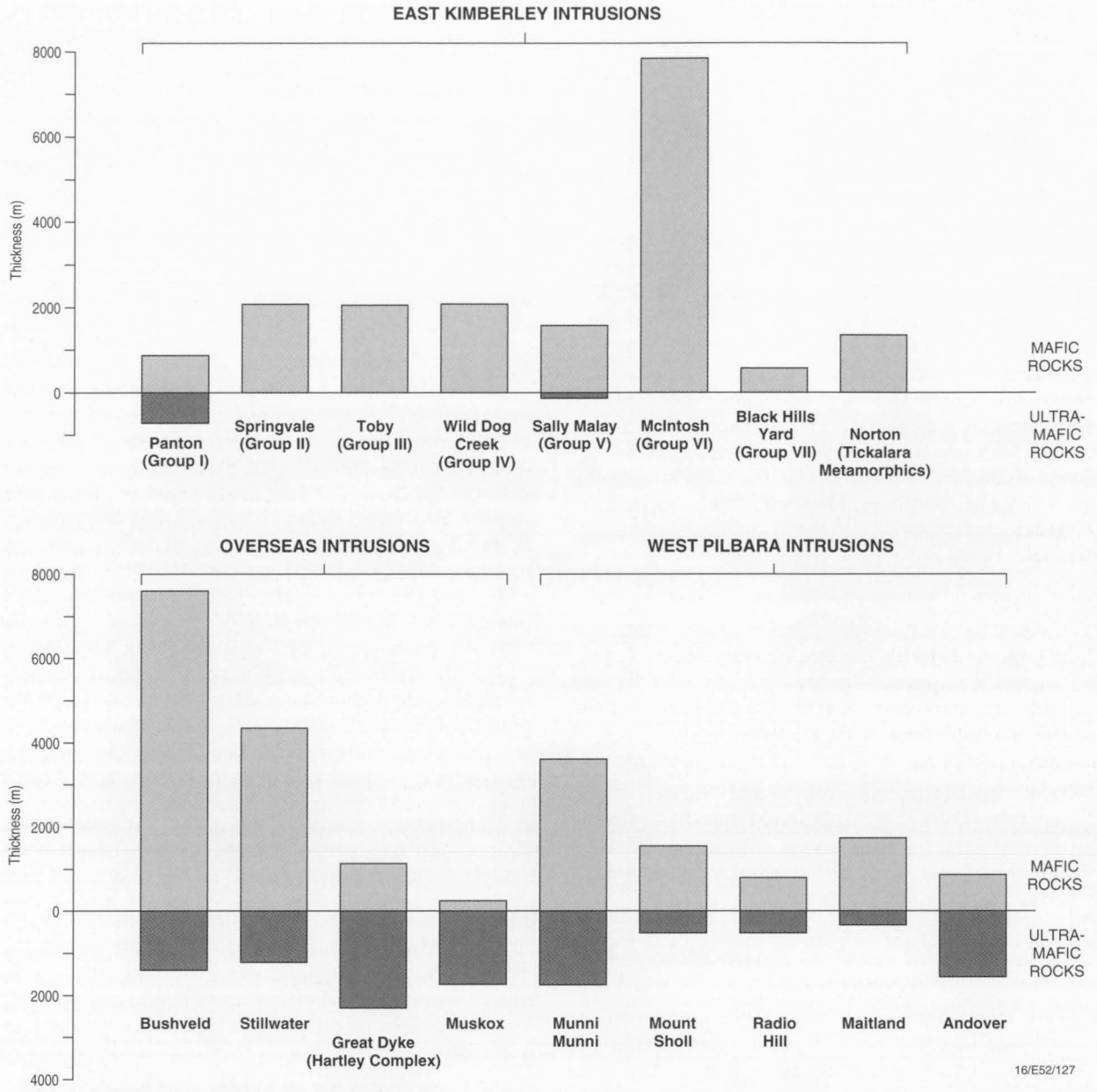


Figure 14.6. Comparative thicknesses of mafic and ultramafic rocks in layered intrusions from the East Kimberley, the west Pilbara Craton of Western Australia, and overseas.

these small bodies would have to be exceptionally rich in metals and/or the mineralising mechanisms would have to be very efficient, since the volumes of magma involved appear to be small. These intrusions would be more prospective if it could be shown that they represent parts of a much larger magmatic system, such as a feeder to other intrusive or extrusive bodies, or are associated with other bodies that have been removed by faulting, erosion, or are concealed at depth. It is recommended that in searching for these deposits, exploration companies should initially focus on the thickest group V intrusions.

The layered intrusions in the HCO display different erosional levels, ranging from near the top of areally large mafic bodies (Toby intrusion) to those that have the complete mafic–ultramafic sequence and the floor rocks and roof rocks exposed (Panton), to others which only have the basal keel of the ultramafic zone preserved (Springvale Track, West Robin Soak). Areally, most intrusions in the HCO are significantly smaller than the overseas intrusions listed in Table 14.4, with the largest being Toby (covering 240 km^2), McIntosh (84 km^2), and Springvale (78 km^2). The most important mineralised intrusions in the East Kimberley—Panton (28 km^2) and Sally Malay (5 km^2)—are several orders of magnitude smaller in area than the economically significant Bushveld (67 340 km^2), Great Dyke (3265 km^2), and Sudbury (1340 km^2) intrusions.

The crystallisation order of cumulus minerals in the East Kimberley intrusions (Table 14.5) contrasts with that of the major PGE-bearing intrusions overseas by the (1) late crystallisation of orthopyroxene and clinopyroxene relative to olivine, chromite, and plagioclase, and (2) clinopyroxene generally crystallising before orthopyroxene.

Table 14.4. Areal extent of layered mafic–ultramafic intrusions.

Intrusion	*Area (km²)*
East Kimberley intrusions:	
Black Hills Yard	0.5
Sally Malay	5
Norton	14
Panton	28
Springvale	78
McIntosh	84
Toby	240
West Pilbara intrusions:	
Radio Hill	4
Maitland	14
Mount Sholl	18
Andover	140
Munni Munni	225[1]
Overseas intrusions:	
Vammala, Finland	0.5
Rum[2], Scotland	30
Voisey's Bay, Canada	30
Skye, Scotland	72
Skaergaard, Greenland	105
Stillwater, USA	195
Dore Lake, Canada	470
Insizwa, South Africa	545
Sudbury, Canada	1340
Niquelândia, Brazil	1800
Great Dyke, Zimbabwe	3265
Muskox, Canada	3500[3]
Duluth, USA	4715
Kunene, Angola	7770
Dufek, Antarctica	50 000[4]
Bushveld, South Africa	67 340

Data for overseas intrusions modified from Willemse (1969), Peltonen & Huhma (1997), and Ryan (1997).

[1] Includes major part of intrusion inferred from geophysical surveys to exist beneath Fortescue Group platform rocks.

[2] Previously called Rhum.

[3] Includes minimum of 2000 km² of intrusion inferred from geophysical surveys to exist beneath cover rocks.

[4] Minimum estimate for the Dufek Intrusion.

The latter feature indicates that the primary magmas were for the most part silica undersaturated and that there was no widespread silica contamination from the crust during emplacement. Campbell (1985) suggested that the abundance of orthopyroxene in most continental layered intrusions indicates that these intrusions crystallised from magmas that have assimilated continental crust. Campbell (1985) believed that, since orthopyroxene was an early crystallising mineral in many layered intrusions, the assimilation took place before the magma entered the chamber. Cumulus orthopyroxene is rare in the East Kimberley intrusions. However, the mineralised Panton and Sally Malay intrusions contain orthopyroxene-bearing rocks (harzburgite, norite) near their basal contacts, probably as a result of localised crustal contamination processes. The Lower Group chromitites at Panton are hosted by harzburgite and dunite, and the basal massive sulphides at Sally Malay occur in orthopyroxene-bearing gabbroic rocks up to 40 m thick, implying that silica contamination of the primitive magmas may have been an important mechanism for both these types of mineralisation. The paucity of early crystallising clinopyroxene in the ultramafic cumulates of the East Kimberley intrusions was favourable for the formation of cumulus chromite. As Cr is partitioned less strongly into olivine or orthopyroxene than into clinopyroxene during crystal fractionation, this would have the effect of enriching the melt in Cr until chromite precipitation could be initiated by such processes as magma mixing or contamination.

The chromitite layers in the group I intrusions (Panton group) of the HCO are in a similar stratigraphic position to those in the lower parts of the Bushveld Complex (Lower Group chromitites), Stillwater Complex, and the Great Dyke. Typically, these chromitites are associated with cyclic units of olivine and/or orthopyroxene cumulates in the ultramafic zones. The most PGE-enriched chromitites in the group I intrusions (e.g. A chromitite in the Panton intrusion) occur below the contact between the ultramafic and mafic zones, i.e. before the introduction of cumulus plagioclase. This is similar to the PGE-enriched A chromitite of the Stillwater Complex, but contrasts with the main mineralised chromitites of the Bushveld Complex (Upper Group chromitites, such as the UG-2), which are closely associated with plagioclase-rich rocks a few hundred metres above the first appearance of cumulus plagioclase (Naldrett 1989).

The chromitite layers from the overseas intrusions described above typically have variable amounts and ratios of the PGEs, like the chromitite layers in the group I East Kimberley intrusions (Table 14.3). The mantle-normalised PGE patterns for the major chromitite layers from the Panton intrusion (Middle Group A and B chromitites in Fig. 12.3) have similar steep-sided arched patterns to those from the major overseas stratabound magmatic deposits, like the UG-2 chromitite (Bushveld Complex) and the J-M Reef (Stillwater Complex). These patterns contrast with the flatter PGE patterns typical of ophiolite and alpine deposits, and support the suggestion of Hamlyn (1980) that the Panton intrusion has 'stratiform', rather than alpine, intrusive affinities.

The sulphide-bearing group V intrusions (Sally Malay group) of the HCO (see Chapter 5) display similar tectonic, stratigraphic, and mineralisation features to the (i) world-class Voisey's Bay deposit in Labrador, Canada, and (ii) Palaeoproterozoic intrusions in the Svecofennian domain of Finland.

(i) The Voisey's Bay Ni–Cu–Co deposit (Fig. 14.7, Ryan et al. 1995, Naldrett et al. 1996, Naldrett 1997, Ryan 1997) is located in the 1.9–1.8 Ga collisional zone (Torngat Orogen) that separates the Palaeoproterozoic Churchill Province to the west from the Archaean Nain Province to the east (see inset on Fig. 14.7). The deposit occurs in a troctolite sheet, 30–100 m thick, that intrudes Archaean biotite–feldspar–quartz gneiss of the Nain Province. This sheet is interpreted to be a feeder for the nearby Reid Brook intrusion of the 1.34–1.29 Ga Nain

Table 14.5. Sequences of cumulus mineral assemblages in various mafic–ultramafic geological settings (modified after Naldrett & Cabri 1976).

Intrusion	*Cumulus assemblages*
Panton, Australia	ol, ol+chr, chr+ol, ol+chr(+plag), ol(+cpx+opx), plag+cpx, plag, plag+cpx+mt
McIntosh, Australia	plag+ol, ol+plag, plag+cpx+ol, plag+cpx+opx, plag+cpx+opx+mt(+ol)
Munni Munni, Australia	ol, ol+cpx, cpx+ol, cpx, cpx+opx, plag+opx+cpx, plag+cpx+opx+mt+ilm
Bushveld, South Africa	opx+ol, opx+ol+chr, plag+opx+chr+cpx(+ol), plag+cpx(+opx), plag+cpx+mt, plag+cpx+mt+ol
Stillwater, USA	ol, ol+opx, ol+opx+chr, plag+opx, plag+cpx+opx, plag+cpx(+opx+ol), plag+cpx+opx
Sudbury, Canada	plag+opx, plag+opx+cpx, plag+cpx, plag+cpx+mt
Duke Island, Alaska	ol+chr, ol+cpx, cpx+mt, cpx+mt, cpx+mt+plag
Pechenga, Russia	ol, cpx, cpx+mt, plag+cpx+mt
Dundonald, Canada	ol, cpx, plag+cpx+mt, plag+cpx(+opx?)
Komatiites, various	ol, ol+cpx(opx), cpx+plag(+ol)

Plutonic Suite. Gabbro and troctolite from the mineralised intrusion has a baddeleyite U–Pb age of 1333±1 Ma (Amen et al. 1999). Massive and disseminated sulphides are hosted by troctolite and a basal breccia sequence (BBS) in three different but closely related settings which are considered to reflect contrasting erosion levels—namely, the Western Extension, the Ovoid, and the Eastern Deeps. The BBS contains brecciated fragments of basement gneiss and unmineralised troctolite and peridotite cut by sulphide-bearing troctolite veins. Ore reserves for the Ovoid are 32 Mt @ 2.83% Ni, 1.68% Cu, and 0.12% Co (Canadian Mining Journal, February 1997, 24). The entire deposit is estimated to be 150 Mt of similar grade.

Although the Reid Brook intrusion (Fig. 14.7) is 500 Ma younger than the Sally Malay intrusion and was emplaced well after orogenesis, the two intrusions display several striking similarities:

- the Torngat Orogen and HCO are of comparable age (1.9–1.8 Ga), and may have formed from similar tectonic processes. The Torngat orogenic zone (Naldrett 1997) shows some parallels with the plate-tectonic model of Tyler et al. (1995) and Sheppard et al. (1997a) for the HCO, which involves modern-style collisional–subduction processes in a magmatic-arc environment;
- the Reid Brook and Sally Malay intrusions are Proterozoic multichambered bodies, whose nearby genetically related subchambers have different geometries;
- sulphides, generally hosted by mafic rocks near the basal contacts of both intrusions, occur as massive and disseminated forms and as a matrix to brecciated rock;
- both intrusions have similar ore mineralogy assemblages (hexagonal pyrrhotite–pentlandite–chalcopyrite±magnetite±?cubanite) and sulphide–silicate textures;
- troctolites are a substantial component of the mineralised stratigraphy, although their significance is not fully understood (Wiebe 1990);
- brecciation, xenoliths, xenocrysts, and hybridised magma, indicative of interaction and contamination of mafic magmas with country-rock gneisses, are present in both intrusions;
- xenolithic gneiss fragments in the brecciated basal parts of both intrusions contain green hercynitic spinel in reaction coronas; and
- S saturation in both intrusions could have been triggered by silicification of the magmas and/or by addition of external S from the crust. Re–Os isotopic-data modelling of the Sally Malay intrusion (see Chapter 12) suggests that crustal contamination of the magma played an important role for the sulphide mineralisation.

(ii) The Svecofennian domain of the Fennoscandian Shield (formerly called the Baltic Shield) in southern Finland contains a number of Palaeoproterozoic intrusions that are similar in their geology, tectonic setting, and mineralisation to the Ni–Cu–Co-bearing intrusions of the East Kimberley (Table 14.6). The following description of the Svecofennian intrusions is summarised from Papunen et al. (1979), Peltonen (1995a,b), and Peltonen & Huhma (1997).

The Fennoscandian Shield in Finland consists of orogenic belts and magmatic provinces of varying ages. The principal geological units are the 3.1–2.5 Ga Archaean basement and the 1.9–1.8 Ga Palaeoproterozoic Svecofennian domain. Mica schist, gneiss, and paramigmatite make up about 80% of the Svecofennian supracrustal rocks. Voluminous granite, quartz diorite, and trondhjemite plutons were intruded during syn-, late-, and postkinematic stages of the Svecofennian orogeny. The Palaeoproterozoic Svecofennian domain represents predominantly juvenile crust generated in a rapid succession of events of igneous activity, uplift, erosion, and redeposition as several microplates, subduction zones, and extensional regimes probably existed at the same time. Ophiolites have not been recognised from the Svecofennian domain.

Economically, the most important episode of mafic magmatism occurred near the peak of the Svecofennian

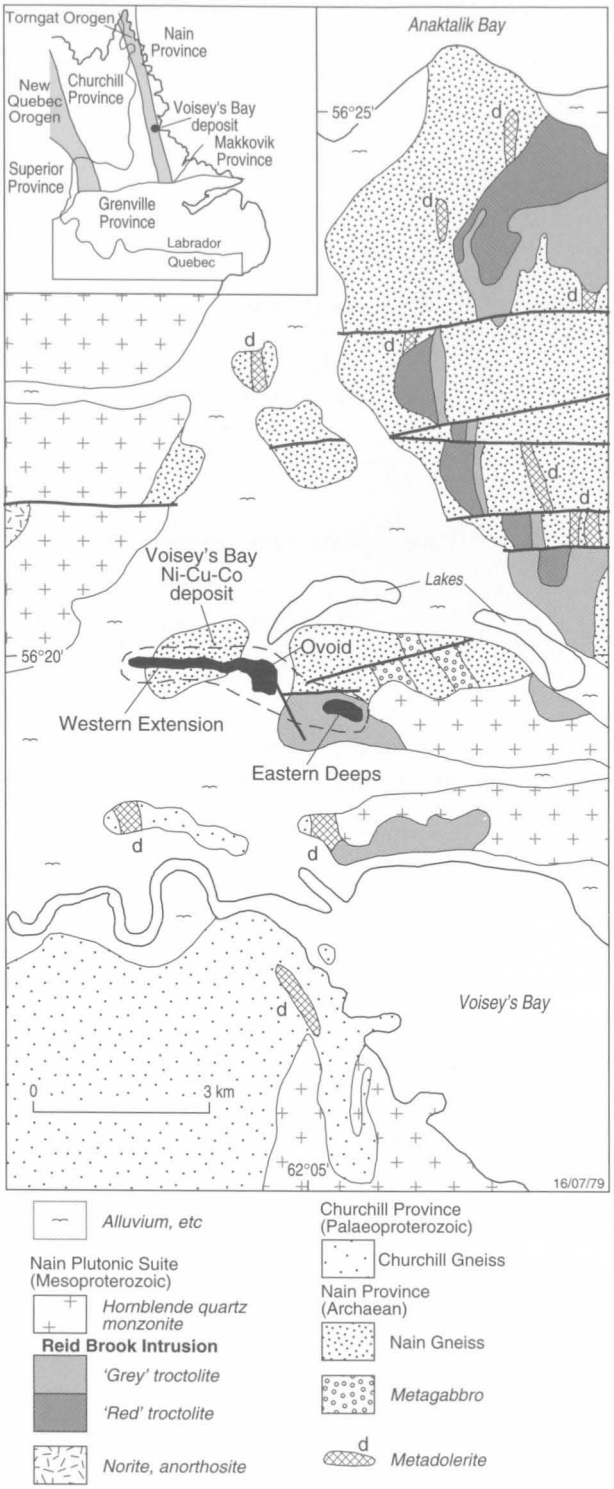


Figure 14.7. Geology and tectonic setting (inset) of the Voisey's Bay Ni–Cu–Co sulphide deposit, Labrador, Canada (modified after Naldrett 1997).

orogeny, when mantle-derived tholeiitic basaltic melts intruded the metasedimentary supracrustal rocks, giving rise to large gabbroic and pyroxenitic intrusions and smaller ultramafic intrusions. Ultramafic cumulate bodies are the economically important group as they host several small Ni–Cu±PGE deposits along a number of sublinear belts which collectively form a regional circular belt. Some of the larger deposits that have been mined are Vammala (7.6 Mt @ 0.67% Ni and 0.42% Cu), Kotalahti (12 Mt @ 0.66% Ni and 0.26% Cu), Enonkoski (6.7 Mt @ 0.78% Ni and 0.21% Cu), and Hitura (8 Mt @ 0.55% Ni and 0.2% Cu).

One of the more important mineralised sublinear belts is the Vammala Nickel Belt, which contains three economic and several subeconomic Ni–Cu deposits. It is 250 km long and generally parallels an arcuate polydeformed migmatite zone across southern Finland. Protoliths to the migmatites were arenaceous and argillaceous greywackes and arkosic sandstones locally rich in iron sulphides and carbon. Major shear zones separate the migmatite zone from lower grade schists to the north and south. The ultramafic cumulate bodies are small (100–1000 m long) boudins, lenses, plugs, and pipes interpreted as remnants of synorogenic feeder dykes and/or sills that crystallised at middle crustal levels. Rock types include peridotite, pyroxenite, hornblende pyroxenite, and minor poikilitic gabbro, ophitic gabbro, and diorite. Olivine, augite, and chrome spinel are generally cumulus, whereas enstatite, amphibole, and phlogopite are postcumulus.

Net-textured, disseminated, and vein sulphides occur at vertical contacts, close to basal contacts, in shear zones or at the contacts of intersecting dykes. The dominant sulphides are monoclinic pyrrhotite, pentlandite, chalcopyrite, cubanite, and mackinawite. The presence of minor phases, such as graphite, sphalerite, molybdenite, and galena, and the high Zn contents of the interstitial sulphides (280–450 ppm) and liquidus chrome spinels (0.7–1.0%) indicate that sedimentary sulphides and magma–country rock interaction played important roles during ore genesis. It has been proposed that the ascending magmas forming the mineralised bodies encountered metasedimentary rocks containing abundant sulphide-rich black schists near their final level of emplacement, and that assimilation of the external S led to the formation of a base-metal-enriched sulphide phase in the magmas. However, the magmas that formed the subeconomic intrusions assimilated S from the sediments at much lower crustal levels relative to their final level of emplacement, and consequently became depleted in base metals due to the early segregation of sulphides.

As indicated by the Finnish sulphide deposits (Table 14.6), the constraints of favourable S-bearing country rocks and the crustal levels at which these rocks interact with the invading magma may also partly determine why some group V intrusions in the East Kimberley are mineralised and others are not.

Status of sulphur saturation during magma evolution

The timing of S (and Cr) saturation in evolving mafic–ultramafic magmas is critical to the formation of PGE-enriched stratabound layers in layered intrusions. If a host magma attains S saturation too early in its evolution (i.e. at the time of its generation or during transport to high crustal levels), the PGEs will be rapidly depleted

Table 14.6. Comparison of Ni-Cu-Co layered intrusions in the East Kimberley and the Svecofennian domain of southern Finland.

	East Kimberley	*Svecofennian domain*
Intrusions:	Sally Malay (group V) Keller Creek (group V) Norton (Tickalara Metamorphics)	Vammala Kotalahti Enonkoski
Types:	Mafic–ultramafic, mafic	Ultramafic-mafic
Age:	~1870 Ma to 1845 Ma	1900 Ma to 1850 Ma
Regional province:	Linear belt (~400 km long by 120 km wide)	Several linear belts forming large circular belt (~1200 km long by 100 km wide)
Timing:	Some preorogenic (Norton), most late orogenic to postorogenic	Preorogenic and synorogenic
Form:	Folded sheets, lenses, composite chambers	Plugs, lenses, pipes, tectonic blocks
Area:	Most <5 km^2, some up to 20 km^2	All <4 km^2
Emplacement depths:	Middle crust to lower crust (~20 to 23 km)	Middle crust
Major rock types:	Peridotite, troctolite, olivine gabbro, gabbro leucogabbro, anorthosite, magnetite gabbro	Peridotite, pyroxenite, hornblende pyroxenite, olivine gabbro, gabbro, diorite
Country rocks:	Migmatitic paragneiss	Migmatitic paragneiss
Timing of granites:	Coeval	Coeval
Location of sulphides:	Basal contacts, feeder conduits, remobilised veins in country rocks	Basal contacts, vertical contacts, shear zones, contacts of dykes
Host rocks:	Gabbro, peridotite	Peridotite, gabbro
Textures of sulphides:	Massive, interstitial disseminations, round droplets, veinlets	Interstitial disseminations, round droplets, veinlets
Resources:	4 Mt @ 1.8% Ni, 0.7% Cu, 0.1% Co	6–12 Mt @ 0.6–0.8% Ni, 0.2–0.4% Cu
Important mineralisation mechanisms:	Country rock assimilation, timing of S saturation of tholeiitic basaltic magmas, fluid dynamics of magma flow	Country rock assimilation, timing of S saturation of high-Mg tholeiitic magmas
Status:	All subeconomic	Some economic, most subeconomic

Data for the intrusions in the Svecofennian Domain are from Papunen et al. (1979), Peltonen (1995a,b), and Peltonen & Huhma (1997).

in the magma, owing to their extremely high sulphide melt/silicate melt partition coefficients (about 10^3–10^5: Stone et al. 1990, Fleet et al. 1999). Consequently, early S saturation of a magma will inhibit the effectiveness of such mineralising processes as sulphide fractionation, crustal contamination, and magma mixing for the generation of high R-factor (effective mass of silicate melt with which a given mass of sulphide melt has equilibrated: see Chapter 14) sulphides in PGE-enriched layers. Favourable S-undersaturated PGE-enriched magmas are high temperature, high MgO primitive types that formed by high degrees of partial melting of the mantle. In addition, these magmas are chalcophile metal undepleted and show no indication of early crustal contamination (Brooks et al. 1999).

Sulphur solubility in a silicate melt increases with increasing temperature, FeO content, and f_{S_2}, and with decreasing f_{O_2} and pressure (Haughton et al. 1974, Wendlandt, 1982). Haughton et al. (1974) showed that the principal compositional control of S solubility is the ferrous iron content of the magma. They found that the maximum S-solubility for a basaltic melt at 1200°C varies from 0.05 to 0.2% as the FeO content increased from 5 to 20%. These results were confirmed by a study

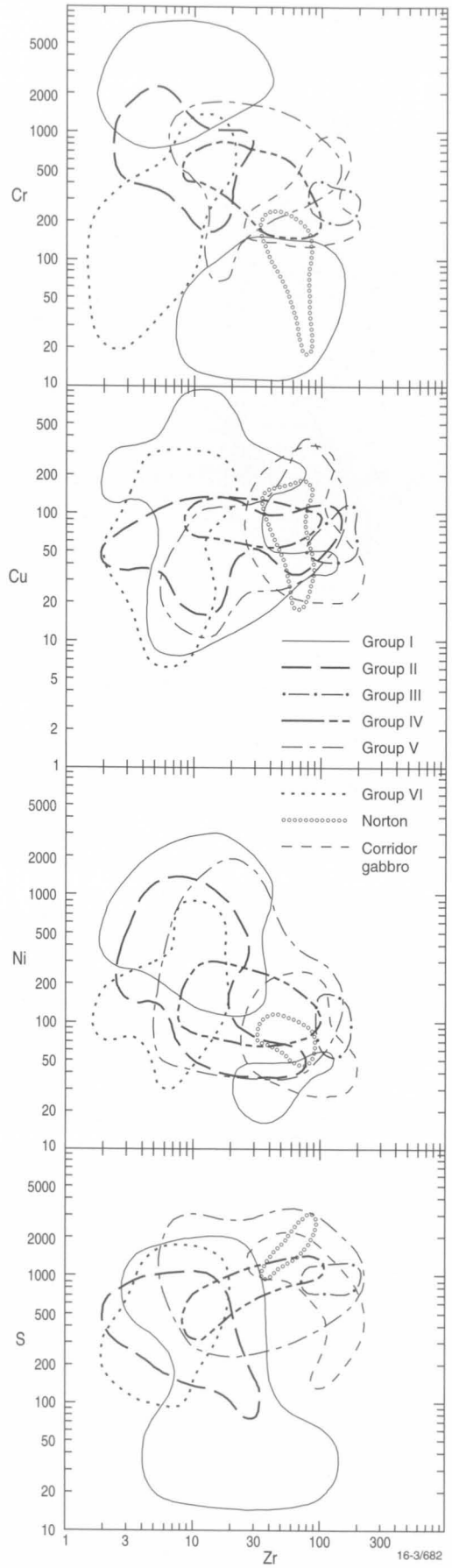


Figure 14.8. East Kimberley layered intrusions: logarithmic plots of S, Ni, Cu, and Cr against Zr (all ppm).

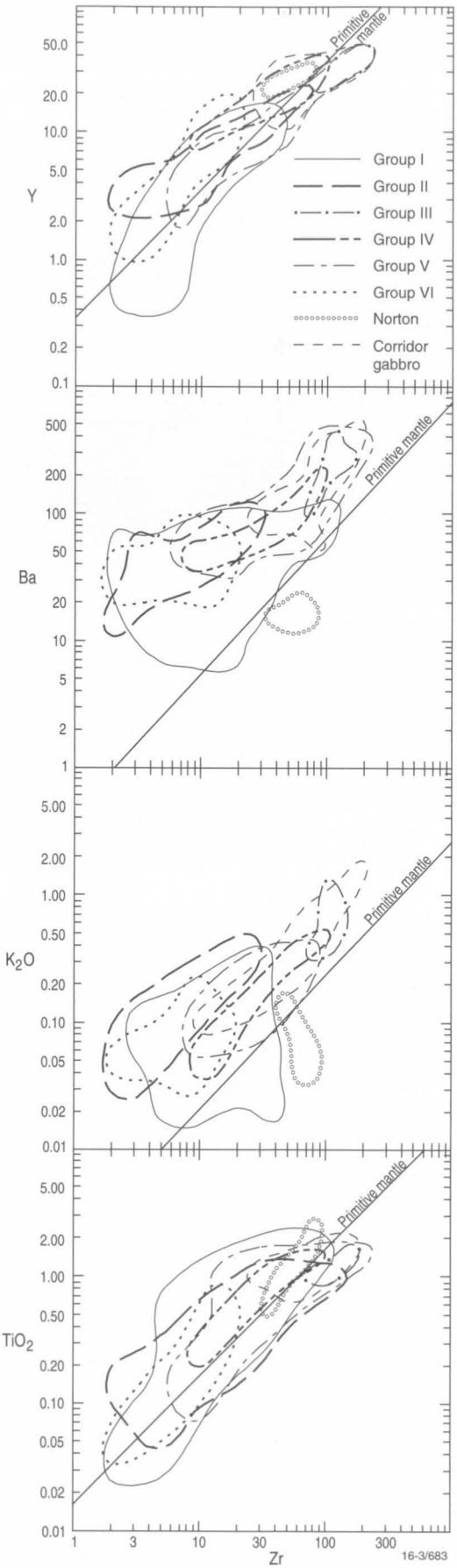


Figure 14.9. East Kimberley layered intrusions: logarithmic plots of TiO_2 and K_2O (in wt. %), Ba and Y (in ppm) against Zr (in ppm). Data for primitive mantle reference lines are from Sun & McDonough (1989).

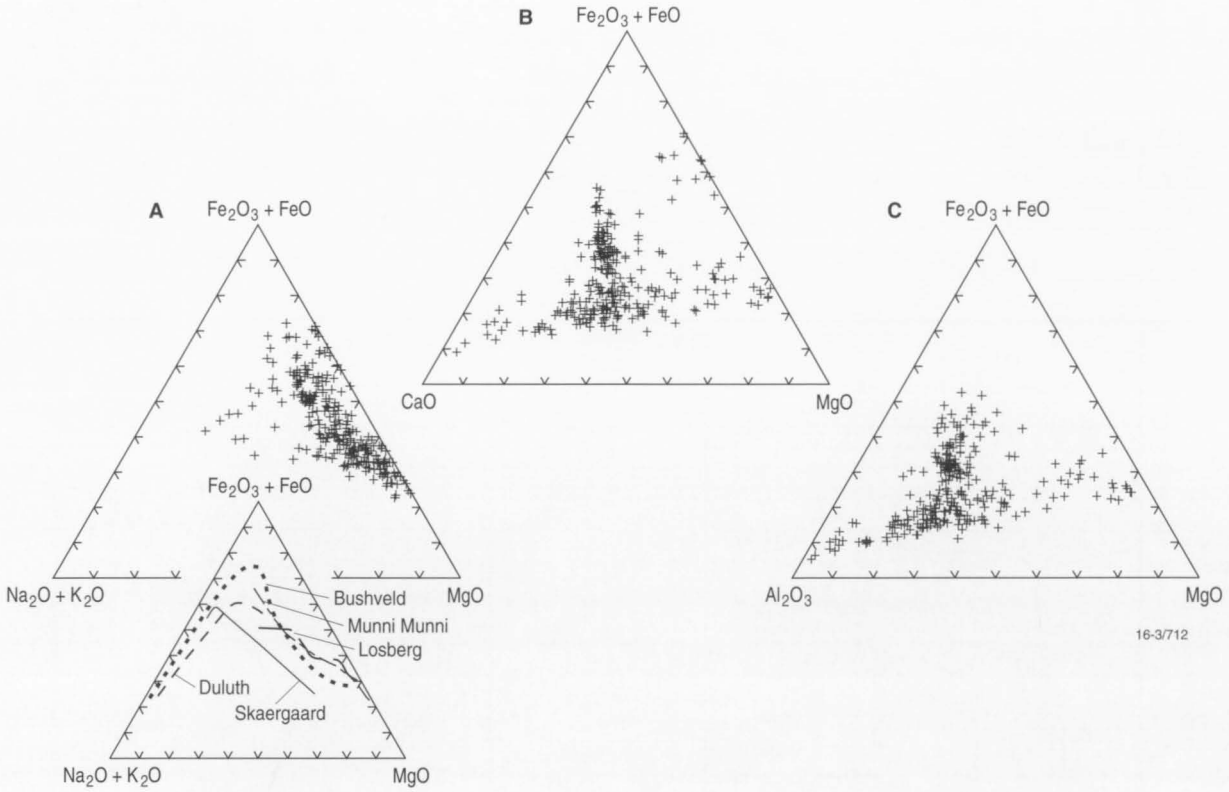


Figure 14.10. East Kimberley and other layered intrusions: ternary plots, showing variation in whole-rock major-element composition (in wt. %) and fractionation trends (inset). Bushveld and Losberg rock trends from Danchin & Ferguson (1970), Duluth rock trend from Taylor (1956), Skaergaard liquid trend from Wager & Brown (1968), and Munni Munni rock trend from Hoatson et al. (1992).

of the S contents of submarine basalts by Czamanske & Moore (1977). They found the S contents of these basalts increased from 0.084 to 0.137% as their FeO increased from 8.0 to 12.6%. Buchanan et al. (1983) found that at constant f_{O_2} and f_{S_2}, the dissolved S content in a basaltic melt that contained 17% FeO increased by a factor of about 8.5 times per 100°C at 1000°C, but by a factor of only 3 times per 100°C at 1400°C. These results are consistent with experiments by Haughton et al. (1974), which showed that with each temperature rise of 100°C from 1000°C to 1400°C, the S capacity of the magma increased by a factor of 5–7, assuming a constant ratio of f_{O_2} to f_{S_2}. In their study of the system Fe–Si–S–O at 32 kb, Huang & Williams (1980) found that the miscibility gap between sulphide and silicate liquids expands with increasing pressure. This is supported by Wendlandt's (1982) experiments, which indicated a negative relationship between S solubility and pressure for melts of different FeO contents at a temperature of 1420°C.

To determine whether a cumulate rock has formed from a S-saturated magma requires a knowledge of both the amount of trapped intercumulus melt and the S content of the cumulate. For example, an adcumulate mafic rock containing 5 vol. % intercumulus material and 100 ppm S, would form from a parent magma with 2000 ppm S, if all the S in the rock was contained in the intercumulus melt. Hence, the magma would have been S saturated. By contrast, a parent magma for a chilled magma with 100% melt and containing 500 ppm S would have been S undersaturated. In general, most mafic rocks are S saturated when the S content of the parent magma exceeds 1000 ppm (Hoatson & Keays 1989). This S tolerance increases for hotter more primitive parent magmas (e.g. picritic and komatiitic composition), but these appear not to be relevant to the East Kimberley intrusions (see Chapter 11). It should be emphasised that this normalisation method provides an approximate estimate of the original S content of the melt, since S is very mobile during alteration and post-cumulus processes. A more reliable semi-quantitative estimate of the S content of the primary magma can be obtained by evaluating porosities in association with S/Se ratios of cumulates (Hoatson & Keays 1989).

The average S contents of 150 unmineralised mafic and ultramafic cumulates from the type examples of the different groups of East Kimberley intrusions are: group I Panton (520 ppm, comprising 510 ppm for ultramafic cumulates and 530 ppm for mafic cumulates); group II Springvale (515 ppm); group III Toby (920 ppm); group IV Wild Dog Creek (760 ppm); group V Sally Malay (680 ppm); group VI McIntosh (555 ppm), group VII Black Hills Yard (280 ppm), Corridor gabbro (940 ppm), and Tickalara Metamorphics–Norton (1570 ppm). Trace-element geochemistry (see Chapter 11) has indi-

cated that the East Kimberley intrusions were derived from basaltic rather than ultramafic parent magmas. Therefore, the high average S contents suggest that all groups, with the possible exception of VII, were derived from S-saturated parent magmas. This is particularly apparent if one takes into account that the S concentrations are a minimum, since some cumulates (especially serpentinised dunites) lost significant amounts of S during alteration and, if one uses the normalisation process described above for the cumulates, which generally have 5–30% trapped melt, the S contents of the magmas for all groups are at least 1500–2000 ppm. The average S contents for the different groups also provide a general fractionation index, from the most primitive, relatively low-S groups (I, II, VI), to intermediate groups (V, IV), to evolved, high-S groups (III, Corridor gabbro), to anomalously high-S groups (Tickalara Metamorphics-Norton). The S-rich character of the latter intrusion may be attributed in part to enrichment processes (recrystallisation and mobilisation of sulphides) during granulite metamorphism. The Black Hills Yard intrusion of group VII may be a rare example of an East Kimberley intrusion derived from a S-undersaturated magma. This is supported by the absence of cumulus sulphides (low S content of 280 ppm) and above background concentrations of Pd (16 ppb) and Pt (8.5 ppb) for a primitive ($mg_{79.1}$) troctolite sample (92522517).

It is not surprising that most East Kimberley intrusions appear to be derived from S-saturated parent magmas, given the high ratio of mafic to ultramafic types, their evolved tholeiitic compositions (see below), and the extent of contamination from crustal rocks (see Chapters 11 &12). The ubiquitous occurrence of cumulus sulphides in both mafic and ultramafic cumulates testifies to their S-saturated origins. However, the 'PGE-fertile' character of the group I Panton-type intrusions, in particular, indicates that the S-saturation processes must have occurred late in the evolution of the magmas, either in the upper parts of the conduit or in the magma chamber.

The similar S-saturated character of the different groups of intrusions is shown by the distribution of chalcophile elements with an incompatible element (Zr) that provides an index of fractionation for unmineralised mafic and ultramafic cumulates (Fig. 14.8). With the exception of group I, all groups generally have overlapping fields defined by moderate to high abundances of S and Zr. The low S contents (<50 ppm) of some group I cumulates corresponds with intensely serpentinised ultramafics that have experienced significant loss of S. Interestingly, the intrusions with the greatest potential for Ni–Cu–Co sulphides (group V and Norton-type) have the highest concentrations of S. The moderately high S contents of the Corridor gabbro suggest these fractionated elongate bodies could be prospective for the accumulation of base-metal sulphides in their feeder conduits or associated magma chambers. The similar chalcophile compatible behaviour of Cu and Ni is indicated by their overlapping distributions in Figure 14.8. The most prospective intrusions in the East Kimberley—groups I (Panton) and V (Sally Malay)—have some of the highest, and most variable background concentrations of Cu and Ni (Fig. 14.8). A slight antipathetic trend of increasing Ni with decreasing Zr for groups I, II, and V is in response to olivine crystallisation. Chromium for most groups (Fig. 14.8) displays a wider distribution than the chalcophile elements, reflecting involvement of chromite and Cr-bearing silicate minerals (e.g. pyroxenes) in magma differentiation. Group I contains two separate fields either side of the main cluster of fields, corresponding to the bimodal distribution of high-Zr, chromite-poor mafic cumulates and more primitive, low-Zr, chromite-bearing ultramafic cumulates. Groups I–VII and the Corridor gabbro show similar increasing TiO_2, K_2O, Ba, and Y trends with increasing fractionation (Fig. 14.9). The low Zr part of the trend (<~30 ppm Zr) is dominated by mineral accumulation (e.g. clinopyroxene, orthopyroxene, olivine) and the upper part is controlled by crystal fractionation. The coherence of the different fields above the primitive mantle reference line of Sun & McDonough (1989) testifies to the similar compositions of the parent magmas (see Chapter 11). In contrast, the low Ba and K_2O contents for the Norton intrusion may be a primary magmatic feature that distinguishes it from the other groups of intrusions. However, since Ba and K are mobile during metamorphism and alteration, it is more likely that the very low abundance of these elements in the Norton samples containing 40–80 ppm Zr is due to mobility during granulite facies metamorphism.

Despite the limitations of using whole-rock major-element compositions of cumulates as petrogenetic indicators (because they do not represent parent liquid compositions: see Chapter 1) they are useful for defining gross geochemical features of layered intrusions. The thoeliitic fractionation trends of the East Kimberley cumulates are highlighted by the ternary plots of Figure 14.10. Dunite, lherzolite, peridotite, and rare pyroxenite have low alkali contents and plot on the Fe–Mg side of Figure 14.10A. Gabbroic cumulates show a pronounced enrichment in Fe_2O_3+FeO at the expense of MgO, over similar concentrations of Na_2O+K_2O. The prominent CaO and Al_2O_3 trends in Figure 14.10B&C indicate the paucity of plagioclase-bearing ultramafics and the dominance of leucogabbro and anorthosite in the upper stratigraphic levels of most mafic intrusions.

Major-element variation with stratigraphic height in the East Kimberley intrusions is generally similar to that of other layered intrusions of basaltic tholeiitic affinity. These include enrichment in FeO, Fe_2O_3, MnO, TiO_2, Al_2O_3, Na_2O, K_2O, and P_2O_5, and a decrease in mg, MgO, and CaO with fractionation. The MgO–Fe_2O_3+FeO–Na_2O+K_2O trends of the Bushveld and Losberg Intrusions of South Africa (Danchin & Ferguson 1970), the Duluth Complex (Taylor 1956), the Skaergaard Intrusion (Wager & Brown 1968), and the Munni Munni intrusion (Hoatson et al. 1992) are shown in the inset diagram of Figure 14.10A. The general fractionation trend of the East Kimberley cumulates initially parallels the Fe-fractionation trend of the Bushveld Intrusion, whereas the change in the fractionation trend to alkali enrichment is not as pronounced, and occurs at slightly more MgO-rich compositions, than those in the overseas intrusions.

Review of exploration strategies for layered intrusions in the East Kimberley

Exploration programs vary considerably for different styles of precious and base-metal mineralisation in layered mafic–ultramafic intrusions. This diversity of mineralisation is highlighted in Figure 14.11, which shows an idealised intrusion containing the major deposit types in the East Kimberley, other Precambrian provinces of Australia, and in overseas intrusions. Some of the more important considerations when planning exploration strategies in the East Kimberley for stratabound mineralised layers and basal sulphide segregations are summarised by Hoatson (in press) and are listed below.

Stratabound PGE-enriched chromitite and sulphide-bearing layers

- Group 1 differentiated layered mafic–ultramafic intrusions in the central zone of the HCO that display open fractionation systems with repeated large pulses of primitive magma into the chamber (Panton, Big Ben, West McIntosh, Melon Patch group) are considered to be the most prospective for stratabound PGE-enriched chromitite layers. Those intrusions formed from the most primitive magmas (mg >58, corresponding to olivine compositions with mg >82; see Table 11.3) and containing thick sequences of olivine cumulates in the ultramafic zone should be high priority.
- The general S-saturated character of most East Kimberley intrusions (see Chapter 5) downgrades the potential for stratabound sulphide layers. S-undersaturated, PGE-enriched, primitive magmas are considered most favourable for these deposits. With the possible exception of mid-ocean ridge basalts (MORB), there are few restrictions on the actual composition (e.g. mantle-derived, ultramafic, or tholeiitic) of the parent magma for mineralised intrusions. However, high-Mg, high-Cl primitive basaltic magmas with Pt and Pd concentrations >~10–30 ppb (>~0.01–0.03 g/t) appear to have the greatest potential for significant PGE deposits (Boudreau 1995). The primitive character of the magma may be indicated by high metal ratios (Ni/Cu, Ir/Pd) in the magmatic sulphides.
- Stratabound PGE-enriched sulphide layers (examples C and D in Fig. 14.11) are difficult targets to explore because they are narrow (1–2 m-thick layers in sequences up to 8 km thick), and they typically have weak geophysical (only ~2–3 vol. % disseminated sulphides) and geochemical signatures.
- To establish if the magma that formed the intrusion was ever S or Cr saturated, determine parent magma compositions (from chilled marginal rocks, comagmatic dykes and sills), document the modal distribution of sulphides and chromite in cumulates, normalise S content of the intercumulus liquid (trapped melt) in unaltered cumulates to 100% melt, or use S/Se ratios (Hoatson & Keays 1989). In general, most basaltic parent magmas with S contents exceeding 1000 ppm are S saturated. If the intrusion is S saturated throughout its stratigraphy, the basal contact region and feeder conduit should be investigated for Ni–Cu–Co–PGE sulphides (Sally Malay, Norton, Keller Creek); if the intrusion is in part S undersaturated, the stratigraphic level of S saturation will need to be determined for stratabound PGE-enriched sulphide layers.
- The composition of olivine (Ni content versus forsterite component) is a useful indicator of any Ni depletion in the magma from which the olivine has crystallised (Naldrett 1989). The Ni content of chromite, analogous to that of olivine, can also be used to indicate S saturation in magma (Brügmann et al. 1993, Peltonen 1995a).
- Detailed geological mapping and closely spaced sampling (initially 10–20 m spacing) through the entire stratigraphic succession of an intrusion are needed to determine the stratigraphic level of Cr and/or S saturation, and also for studies on:
  - the distribution trends of cumulus and intercumulus minerals;
  - crystal fractionation, magma mixing, and hydrothermal processes; and
  - the dynamics of magma input (Lambert et al. 1998), e.g. wide-scale turbulent magma mixing and/or rapid turbulent flow through a narrow conduit is required for sulphides to equilibrate with a large volume of magma to achieve a high R factor (the effective mass of silicate melt with which a given mass of sulphide melt has equilibrated: Campbell & Naldrett 1979, Naldrett 1989, 1997, see Chapter 12) and to scavenge PGEs, Ni, and Cu.
- Magma-chamber processes, such as the mixing of primitive magma with more fractionated magma and crystal fractionation, which are important for the formation of stratabound Cr and PGE deposits can be indicated by:
  - rapid changes in the composition of cumulus minerals and the volume of intercumulus melt in cumulates (rock porosity) across a layered sequence;
  - presence of sulphide, chromite, graphite, and halogen-bearing minerals (apatite, biotite, amphibole);
  - transitions from Fe-rich to Cu-rich sulphide mineral assemblages with crystal fractionation;
  - development of porphyritic, pegmatoidal, and orthocumulus textures;
  - occurrence of hybrid rocks and accidental blocks in slump deposits;
  - lateral variation of rock types, such as interfingering, thinning, or thickening; and
  - large magma influxes.
- Evidence for magma influxes into the chamber include:
  - unconformities representing magmatic erosion/disruption of footwall sequences;
  - recurrence of high-temperature primitive minerals, such as chromite and olivine;

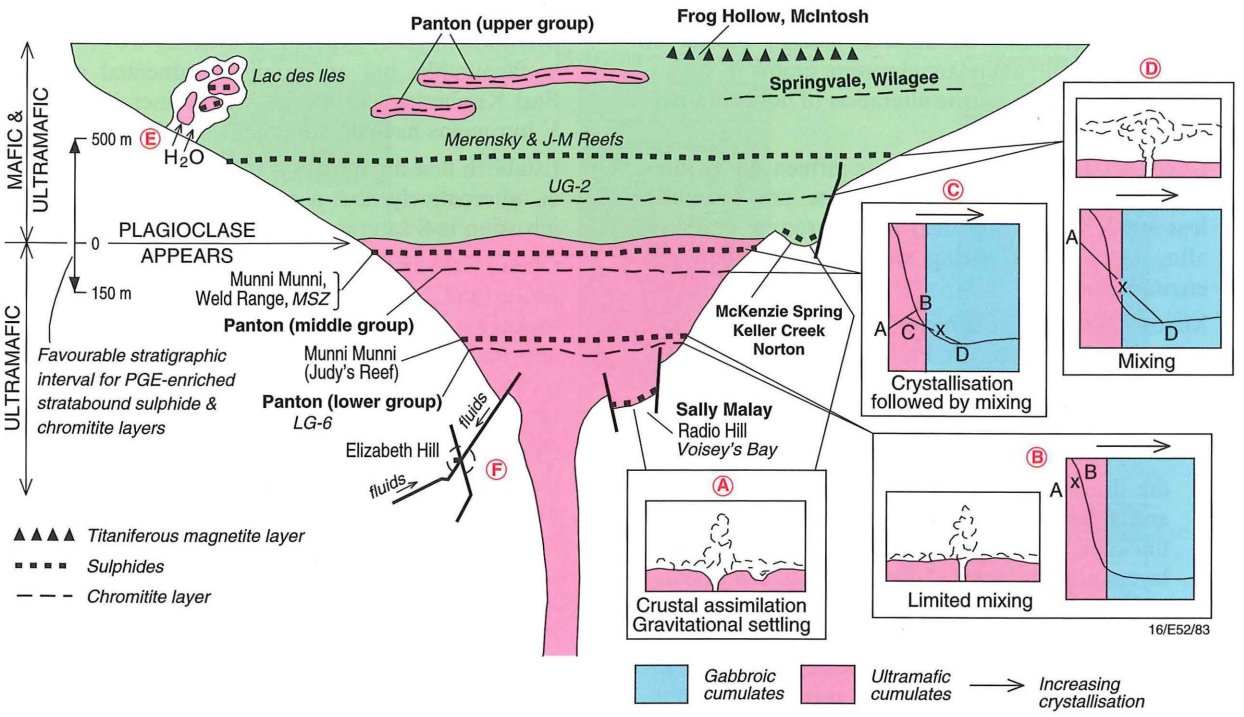


Figure 14.11. Summary of the different types of PGE–Cr and Ni–Cu–Co–PGE deposits related to crustal assimilation, crystal fractionation, magma mixing, constitutional zone refining, and hydrothermal fluid mineralising processes in an idealised layered mafic–ultramafic intrusion (modified after Naldrett 1993). Early S saturation of the primitive magma by crustal assimilation and gravitational settling of the sulphides can form PGE-poor massive sulphide deposits in embayments along the basal contact or in the feeder conduit (example A); localised fountain-type mixing (i.e. low R factor) of resident magma with primitive magma before plagioclase has appeared on the liquidus can give rise to a PGE-poor sulphide layer or chromitite (example B); crystal fractionation of a S-undersaturated PGE-bearing primitive resident magma and extensive magma mixing (i.e., high R factor) with a S-saturated gabbroic magma may give rise to a PGE-rich layer not associated with the base of a cyclic unit (example C); turbulent plume-type mixing of resident magma with a more primitive magma after the crystallisation of plagioclase may give rise to a PGE-enriched sulphide layer or chromitite layer (example D); volatile-induced partial melting of cumulates (constitutional zone refining) caused by the introduction of water into the hot cumulus pile can concentrate PGEs when the partial melt becomes S saturated (example E); and structurally controlled hydrothermal PGE–base-metal deposits can occur inside or outside the intrusion (example F). The relationship between crystallisation and magma mixing along sulphide solubility curves are also depicted for deposit types B, C, and D (for further details see Naldrett 1993). The arrows indicate direction of increasing crystallisation. Examples of East Kimberley deposits are shown in bold type, deposits from other Australian provinces are shown in normal type, and the major overseas deposits are shown in italics: Merensky Reef, UG-2 (Upper Group-2 Chromitite), and LG-6 (Lower Group-6 Chromitite) of the Bushveld Complex, South Africa; the J-M Reef of the Stillwater Complex, Montana, USA; the MSZ (Main Sulphide Zone) of the Great Dyke, Zimbabwe; and the Lac des Iles Complex, Ontario, Canada.

  - increase in mg number of mafic minerals; and
  - significant changes in radiogenic isotope initial ratios in whole rocks (Barrie 1995).
- Marked discontinuities in stratigraphic profiles of Cs, Zr, Rb, Sr, Y, S, Se, Cu, Pt/Pd, (Pt+Pd)/Cu, (Pt+Pd)/Se, (Pt+Pd)/S, (Pt+Pd)/Cs, (Pt+Pd)/(Zr+Y), (Pt+Pd)/Ir, Cu/Zr, and Mg/(Mg+Fe) in an intrusion may highlight major new pulses of magma, and indicate stratigraphic levels of S saturation and stratabound PGE layers formed from magma mixing (Hoatson & Keays 1989).
- Mineralised layers of greatest economic importance generally occur near major compositional interfaces involving the crystallisation of plagioclase in the intrusion (i.e. contacts between ultramafic and mafic sequences): PGE-enriched sulphide layers often lie between 20 m below and 500 m above the level where plagioclase first becomes a cumulus mineral, and most sulphide-enriched chromitites, particularly those enriched in PGEs, occur between 150 m below and several hundreds of metres above this same stratigraphic level.
- PGE-enriched sulphide layers can occur at the base of cyclic units (Merensky Reef, J-M Reef) or show no spatial relationship with cyclic units (Main Sulphide Zone (MSZ) in the Great Dyke).
- Thickness and PGE content of sulphide layers may vary between the margins and the centre of the intrusion (Great Dyke).
- S/Se ratios of the major PGE-rich stratabound sulphide layers overseas are generally lower than the inferred mantle value of ~3000. By contrast, magmatic sulphides with relatively low PGEs have a S/Se ratio above the mantle value, which may indicate a crustal source of S.
- Orthopyroxene and/or olivine cumulates are more favourable than clinopyroxene cumulates for hosting stratabound chromitite layers because of the relative high partitioning of Cr into clinopyroxene.

- Proximity of chromitite layers is indicated by disseminated chromite in adjacent rocks, blocks of chromite in soil, abundant chromite grains in stream sediments, and magnesite alteration of host ultramafic cumulates.
- Chemical dispersion of metals is influenced by mineralogy: PGE-sulphide associations are generally less stable chemically than PGE-chromite or PGE-alloy associations during weathering in semi-arid environments.
- Major pathfinder elements for rocks, soils, and stream sediments are: Cr, Pt, Pd, Cu, Ni, Co, Au, Mg, As, and Hg.
- Geophysical and remote sensing techniques have different applications:
  - the disseminated nature, low primary magnetite and sulphide content (~2–3 vol. %), and narrow thickness (<2 m) of PGE-enriched stratabound layers means electrical methods (e.g. electromagnetics, induced polarisation) have limited application in locating these deposits (in contrast to basal Ni–Cu–Co sulphide deposits); aeromagnetics, gamma-ray spectrometry, gravity, and remote sensing are more useful for defining macroscopic features of intrusions rather than mineralised layers;
  - aeromagnetics and gravity can delineate regional extent, geometry, and major structures of poorly exposed intrusions; gravity, subject to sufficient density contrast with the country rocks, can define feeder conduits;
  - aeromagnetics can help determine gross younging directions in gabbroic zones (coarse-grained primary Fe–Ti oxides) and the intensity of serpentinisation in ultramafic zones (fine-grained magnetite after olivine);
  - composite gamma-ray spectrometry can define the regional distribution of mafic-ultramafic rocks, since these have low concentrations of K, Th, and U; and
- Landsat 5 Thematic Mapper imagery (in particular, the directed principal component 2(4/3,5/7), 5/4, and 1+7 image, displayed as red, green, and blue, enhancing clays, iron oxides, and silica, respectively) is extremely useful for discriminating ultramafic, mafic, and felsic rock types, and identifying favourable contacts between ultramafic and gabbroic sequences.

Basal segregations of Ni–Cu–Co sulphides

- Differentiated mafic–ultramafic intrusions of group V (Sally Malay, Corkwood, Keller Creek, Wilson Creek, McKenzie Creek, etc) and large mafic granulite bodies of the Tickalara Metamorphics (Norton) west of the Highway Shear Zone (see Chapters 4, 5, and Fig. 7.3) are considered the most prospective for hosting segregations of Ni–Cu–Co±PGE sulphides near basal contacts and in feeder conduits.
- Favourable country rocks are paramigmatites (Tickalara Metamorphics) and metasediments (Halls Creek Group), rather than metavolcanics or granites. Metasediments containing S-bearing minerals (e.g. pyrrhotite, pyrite, gypsum, anhydrite) are particularly favourable, but are rarely documented near the East Kimberley intrusions. Most mineralised group V intrusions have paramigmatites as footwall units.
- Establish that the intrusion is S saturated throughout or, alternatively, that a significant thickness of the intrusion is S saturated.
- Obtain field evidence for thermal and chemical interaction and contamination of magma with country rocks, e.g. association of sulphides and alkali minerals, fractionated character of mineralised marginal rocks, alteration, and abundance of accidental xenoliths and xenocrysts in the basal zones.
- Chemical indications of sulphide contamination include: 1) S-isotope compositions outside normal magmatic values; 2) mixed Sm–Nd and Re–Os isotopes; 3) S/Se ratios of PGE-poor magmatic sulphides much higher than those of the mantle; 4) anomalously high Zn contents in chromite, indicating possible assimilation of Zn-bearing sulphidic metasediments; 5) different crystal fractionation trends in the same magmatic province; and 6) variable compatible versus incompatible elemental ratios in an intrusion (Papunen 1996).
- Massive Ni–Cu–Co–PGE sulphide ores need to be concentrated in restricted environments to attain economic grades. Such environments include depressions and fault-controlled structural embayments at basal contacts beneath the thickest sequences of mafic–ultramafic cumulates. Disseminated sulphide ores may occur for several hundred metres above the massive sulphides.
- Remobilised discordant and fractionated ores enriched in Cu–Au–Pd may occur away from basal contacts or in country rocks.
- Feeder conduits (Sally Malay) to the intrusions are particularly favourable for the concentration of sulphides and, with basal contacts, are priority exploration targets.
- The dynamics of the magma flow (e.g. fast, slow, turbulent, passive) are important for the deposition of sulphides, e.g. fluid dynamic contrasts associated with the change from narrow vertical conduits to broad sub-horizontal open magma chambers (Lambert et al. 1998).
- Gossan search, stream sediment sampling, and rock geochemistry are recommended geochemical techniques.
- Electromagnetics, ground magnetics, and induced polarisation are useful since most deposits have massive and disseminated ores containing pyrrhotite and magnetite.

The East Kimberley layered mafic–ultramafic intrusions are generally regarded as having greater potential for hosting an economic resource of Ni–Cu–Co sulphides rather than for PGEs associated with stratabound chromitite layers. Economic chromitite layers such as those in the Great Dyke of Zimbabwe and the UG-2 in the Bushveld Complex (Naldrett 1989) typically have

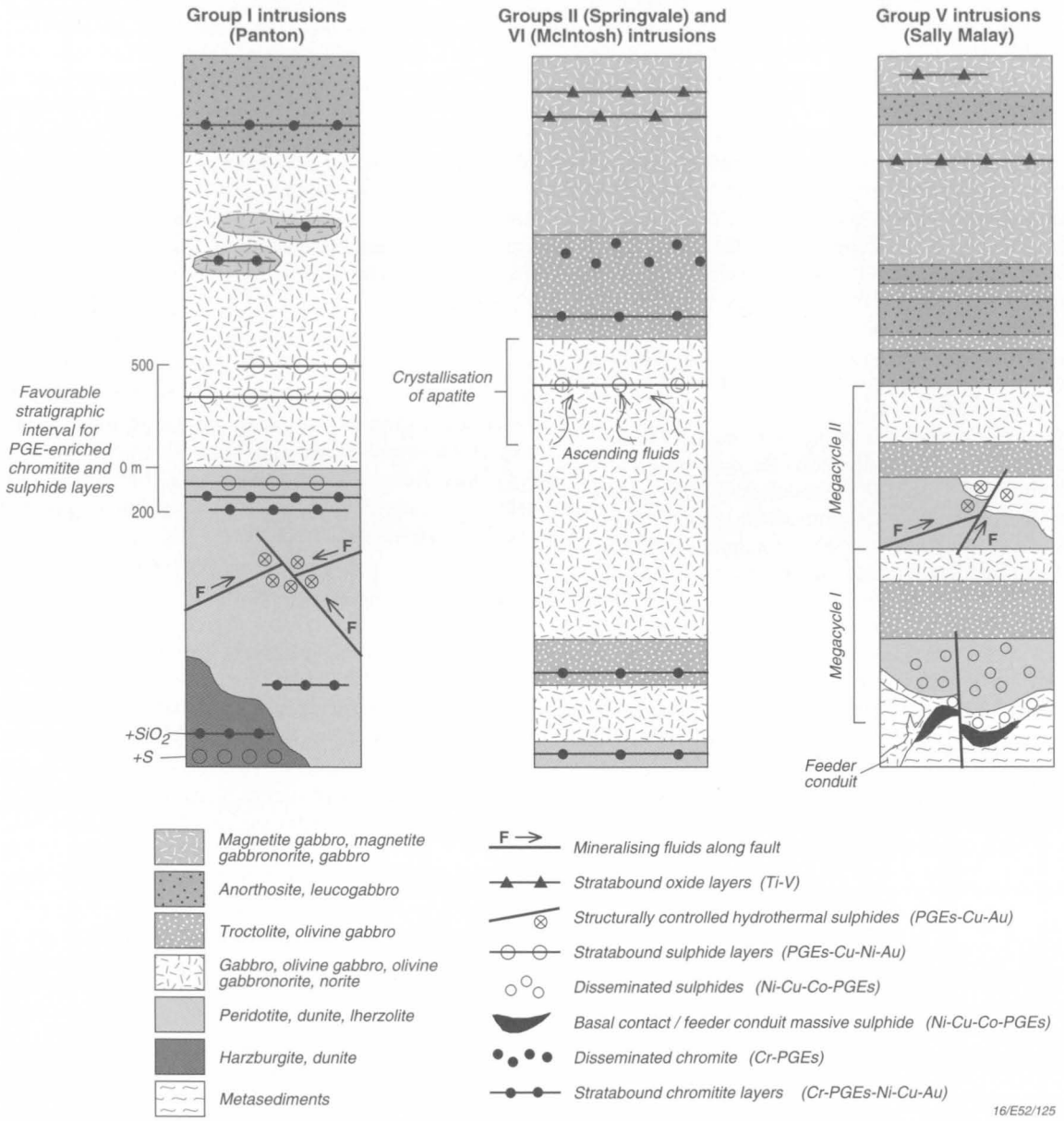


Figure 14.12. Stratigraphic levels of potential orthomagmatic and hydrothermal mineralisation in the groups I, II, V, and VI mafic–ultramafic intrusions of the East Kimberley.

strike lengths of tens to hundreds of kilometres and are hosted by large layered bodies containing thick sequences of olivine and orthopyroxene cumulates; features which are not typical of the East Kimberley intrusions. The economic viability of these deposits is usually dependent on the uniformity of PGE and Cr grades over long strike extents. A major problem relating to the chromitite layers in the East Kimberley is their variable morphology along strike. For example, the A chromitite layer in the Panton intrusion (the largest chromitite layer in the HCO) varies in thickness from a few centimetres to 240 cm over a few hundred metres, is locally tightly folded, varies from a single massive layer to a package of several thin layers, and is displaced by high-angle cross-cutting faults; all these features potentially affect the lateral continuity of ore grades and hinder mining operations. In contrast, economic Ni–Cu–Co sulphide deposits are often hosted by small to medium sized mafic intrusions that may be layered or massive (common in the HCO), and are less dependent on the volume of magma and high R-factor magma dynamics. Crustal contamination of evolving mafic magmas—an important mineralising process for these deposits—is also a common feature of the East Kimberley intrusions (see Chapters 11 and 12).

The major challenge in exploring for Ni–Cu–Co sulphide deposits in the HCO is to locate feeder conduits or depressions within the basal contact, as these may be poorly exposed or underlie thick sequences of mafic–ultramafic cumulates. Large prospective areas are covered by shallow alluvium cover within the corridors containing the mineralised intrusions (see Chapter 5) and also in the southern part of the HCO between the Eastmans Bore intrusion in the southwest and the Big Ben intrusion in the northeast (see Chapters 2 and 5). The identification of favourable environments in these areas will most likely be achieved through advanced

geophysical (airborne electromagnetic and gravity) and remote-sensing (e.g. ASTER-Advanced Spaceborne Thermal Emission and Reflection Radiometer) techniques in association with closely-spaced grid drilling, mapping, and possibly an element of luck. For example, the Discovery Hill gossan at Voisey's Bay in Canada was found fortuitously during a regional stream-sampling program for diamond indicator minerals. A follow-up horizontal-loop electromagnetic survey of the gossan indicated a 1200-m long continuous conductor at depth. Intrusions in the HCO with basal sulphide mineralisation (Sally Malay, Keller Creek, McKenzie Spring, Corkwood, and Norton) are characterised by prominent gossans. Frankcombe et al. (1994) showed that electromagnetic, ground magnetic, and induced polarisation were the most useful methods for locating concentrations of Ni–Cu–Co sulphides at depth in the Sally Malay intrusion. However, the small size of the deposits means that the mineralisation may miss detection during airborne surveys if the line spacing of the survey is too broad. Sophisticated airborne electromagnetic, remote sensing (see Chapter 8), and gravity (see Chapter 7) techniques also have application in the HCO. Large mafic intrusions, such as McIntosh (~84 km^2, 7.8 km thick), Springvale, and Toby are characterised by gravity anomalies. Detailed gravity surveys over these and other large intrusions might identify superimposed anomalies that could define feeder conduits similar to that of the Cadgerina feeder dyke of the mineralised Munni Munni intrusion in the west Pilbara Craton (Barnes & Hoatson 1994). The relatively unexplored McIntosh intrusion has potential for sulphide mineralisation in the feeder conduit and along the basal contact (both presently undefined) because of its large size, multiple magma pulses, and S-saturated character. Other mafic intrusions in the HCO (McKenzie Spring, Fletcher Creek, Norton, and the Corridor gabbro), which have narrow and long (some in excess of 70 km) dyke-like forms, could represent the feeder systems of concealed or erosionally removed subchambers.

Hoatson et al. (1997) and Hoatson (1998, in press) have highlighted the potential of the East Kimberley and other Proterozoic provinces in Australia, such as the Musgrave Block of central Australia, for Ni–Cu–Co sulphide mineralisation associated with mafic–ultramafic intrusions.

Other potential styles of mineralisation in the HCO which should be considered include: structurally controlled hydrothermal and constitutional zone refining and breccia-type mineralisation (Lac des Iles Intrusion, Ontario: Brügmann et al. 1989, Barrie 1995), Ni–Cu–PGE sulphides in mafic sills related to flood basalts (Noril'sk-Talnakh, Russia: Naldrett 1989, 1997, Barnes et al. 1997), and 'stratabound' Platinova Reef-type Au–PGE mineralisation (Skaergaard Intrusion: East Greenland: Bird et al. 1991, Nielsen & Brooks 1995) related to ascending fluids in the upper parts of thick mafic intrusions.

Concluding statements

The Palaeoproterozoic layered intrusions in the East Kimberley represent one of the most extensively mineralised mafic–ultramafic igneous associations in Australia. The intrusions host a range of deposits containing different associations of precious and base metals. When exploring these intrusions, it is important to maintain a flexible innovative approach rather than being 'blinkered' to a particular model and consider unusual styles of orthomagmatic and hydrothermal mineralisation at different stratigraphic levels in the intrusion. A summary of the potential styles of mineralisation in the intrusions considered to be the most prospective (groups I, II, V, and VI) in the East Kimberley is shown in Figure 14.12.

In searching for economic deposits in mafic–ultramafic intrusions, it should be borne in mind that it took more than 20 years of intensive exploration to define the J-M Reef of the Stillwater Complex, and it was not until late in the 1990s, that a significant Au–PGE layer (Platinova Reef) was found in the Skaergaard Intrusion, East Greenland—an intrusion which has been investigated in great detail for more than 60 years.

Acknowledgements

The author thanks David Blake, Greg Ewers, Roger Skirrow, Alastair Stewart, Shen-su Sun (all AGSO), and Ian Tyler (GSWA) for their constructive comments of earlier drafts of the manuscript. Lana Murray drafted the figures.

References

Aberfoyle Resources Ltd, 1989–92. Meredith Well PGE and gold exploration. Reports on various exploration licences (5 volumes). Western Australia Geological Survey M-series Open File, I 6560 (unpublished).

Ahmat, A.L., 1993. Mafic/ultramafic rocks of the Gindalbie Terrane: a review of the Bulong and Carr Boyd Complexes. In: An international conference on crustal evolution, metallogeny and exploration of the Eastern Goldfields. Extended Abstracts. Australian Geological Survey Organisation, Record 1993/54, 23–27.

Ahmat, A.L. & Ruddock, I., 1990. Windimurra and Narndee layered complexes. In: Geology and mineral resources of Western Australia. Western Australia Geological Survey, Memoir 3, 119–126.

Amen, Y., Chusi, Li. & Naldrett, A.J., 1999. Geochronology of the Voisey's Bay intrusion, Labrador, Canada by precise U-Pb dating of coexisting baddeleyite, zircon, and apatite. Lithos, 47, 33–51.

Audax Resources NL, 1986–1990. Yarawindah Brook PGE/gold exploration. Reports on exploration licence E 70/320 (8 volumes). Western Australia Geological Survey M-series Open File, I 5589 (unpublished).

Barnes, G.J., 1992. Sally Malay final resource estimate. Poseidon Exploration Limited, internal report 1094, (unpublished).

Barnes, G.J., 1994. Surrender report E80/1450—Corkwood Project. Poseidon Group Trading Ltd, internal report 6490 (unpublished) for the

Department of Minerals and Energy, Western Australia (Item 7511, AN40093).

Barnes, G.B., 1995. Silver mineralisation at Elizabeth Hill, Munni Munni Complex, Western Australia. In: Ho, S.E. & Amann, W.J. (editors), Recent developments in base metal geology and exploration. Australian Institute of Geoscientists, Bulletin 16, 89–94.

Barnes, S.J. & Hill, R.E.T. (editors), 1991. Mafic–ultramafic complexes of Western Australia. Excursion Guidebook No. 3. Sixth International Platinum Symposium, July 1991, Perth, WA. IAGOD and the Geological Society of Australia, 111 pp.

Barnes, S.J. & Hoatson, D.M., 1994. The Munni Munni Complex, Western Australia: Stratigraphy, structure and petrogenesis. Journal of Petrology, 35, 715–751.

Barnes, S.J., Keays, R.R. & Hoatson, D.M., 1992. Distribution of sulphides and PGE within the porphyritic websterite zone of the Munni Munni Complex, Western Australia. Australian Journal of Earth Sciences, 39, 289–302.

Barnes, S-J., Zientek, M.L. & Severson, M.J., 1997. Ni, Cu, Au, and platinum-group element contents of sulphides associated with intraplate magmatism: a synthesis. Canadian Journal of Earth Sciences, 34, 337–351.

Barrie, C.T., 1995. Magmatic platinum group elements. In: Eckstrand, O.R., Sinclair, W.D. & Thorpe, R.I. (editors), Geology of Canadian Mineral Deposit Types. Geological Survey of Canada, 8, 605–614.

Baxter, J.L., 1978. Molybdenum, tungsten, vanadium and chromium in Western Australia. Western Australia Geological Survey, Mineral Resources Bulletin 11, 140 pp.

Bird, D.K., Brooks, C.K., Gannicott, R.A. & Turner, P.A., 1991. A gold-bearing horizon in the Skaergaard intrusion, East Greenland. Economic Geology, 86, 1083–1092.

Blockley, J.G., 1971. A reported platinum find in the Rudall River area. Geological Survey of Western Australia, Annual Report 1971, 59–61.

Boudreau, A.E., 1995. Some geochemical considerations for platinum-group element exploration in layered intrusions. Exploration and Mining Geology, 4, 215–225.

Boyd, R. & Mathiesen, C.O., 1979. The nickel mineralization of the Råna mafic intrusion, Nordland, Norway. Canadian Mineralogist, 17, 287–298.

Brooks, C.K., Keays, R.R., Lambert, D.D., Frick, L.R. & Nielsen, T.F.D., 1999. Re–Os isotope geochemistry of Tertiary picritic and basaltic magmatism of East Greenland: constraints on plume–lithosphere interactions and the genesis of the Platinova reef, Skaergaard intrusion. Lithos, 47, 107–126.

Brügmann, G.E., Naldrett, A.J. & Macdonald, A.J., 1989. Magma mixing and constitutional zone refining in the Lac des Iles Complex, Ontario: genesis of platinum-group element mineralization. Economic Geology, 84, 1557–1573.

Brügmann, G.E., Hanski, E.J. & Naldrett, A.J. 1993. The nickel content of chromites as an indicator of sulfide segregation in ultramafic lava flows and intrusions. Terra abstracts, 5, 6.

Buchanan, D.L., Nolan, J., Wilkinson, N. & De Villiers, J.R.R., 1983. An experimental investigation of sulfur solubility as a function of temperature in synthetic silicate melts. Geological Society of South Africa, Special Publication 7, 383–391.

Campbell, I.H., 1985. The difference between oceanic and continental tholeiites: a fluid dynamic explanation. Contributions to Mineralogy and Petrology, 91, 37–43.

Campbell, I.H., 1991. The Jimberlana intrusion. In: Barnes, S.J. & Hill, R.E.T. (editors), Mafic–ultramafic complexes of Western Australia, Excursion Guidebook No. 3. Sixth International Platinum Symposium, July 1991, Perth, WA. IAGOD and Geological Society of Australia, 15–18.

Campbell, I.H. & Naldrett, A.J., 1979. The influence of silicate:sulfide ratios on the geochemistry of magmatic sulfides. Economic Geology, 74, 1503–1506.

Campbell, I.H., Naldrett, A.J. & Barnes, S.J., 1983. A model for the origin of the platinum-rich sulphide horizons in the Bushveld and Stillwater Complexes. Journal of Petrology, 24, 133–165.

Clarke, C.J. Anderson, G.A. & Gibson, B.G., 1982. Moola Bulla platinum exploration. Union Corporation (Aust) Proprietary Limited and Pontifex Associates Proprietary Limited internal report on TR 7066H and TR 7067H. Western Australia Geological Survey M-series Open File, item 1536, roll 479, M2522/1, 321 pp, (unpublished).

Cornelius, M., Stumpfl, E.F., Gee, D. & Prochaska, W., 1987. Platinum group elements in mafic–ultramafic rocks of the Western Gneiss Terrain, Western Australia. Mineralogy and Petrology, 36, 247–265.

Czamanske, G.K. & Moore, J.G., 1977. Composition and phase chemistry of sulfide globules in basalt from the Mid-Atlantic Ridge rift valley near 37°N latitude. Bulletin of the Geological Society of America, 88, 587–599.

Danchin, R.V. & Ferguson, J., 1970. The geochemistry of the Losberg Intrusion, Fochville, Transvaal. In: Visser, D.J.L. & von Gruenewaldt, G. (editors), Symposium on the Bushveld Igneous Complex and other layered intrusions. Geological Society of South Africa, Special Publication 1, 689–714.

De Angelis, M., Hoyle, M.W.H., Peters, W.S. & Wightman, D., 1987. The nickel–copper deposit at Radio Hill, Karratha, Western Australia. Australasian Institute of Mining & Metallurgy, Bulletin & Proceedings, 292, 61–74.

De Angelis, M., Hoyle, M.W.H. & Voermans, F.M., 1988. The Radio Hill Ni–Cu deposit and the Mount Sholl–Munni Munni mafic–ultramafic metallogenic province: a case of integrated exploration technique. In: Second international conference on prospecting in arid terrain, April 1988, Perth, Western Australia. Australasian Institute of Mining & Metallurgy, 51–58.

Dragon Mining NL, 1995. Annual Report 1995 (unpublished).

Etheridge, M.A, Rutland, R.W.R. & Wyborn, L.A.I., 1987. Orogenesis and tectonic process in the early to middle Proterozoic of northern Australia. In: Kröner, A. (editor), Proterozoic lithospheric evolution.

American Geophysical Union, Geodynamic Series, 17, 131–147.

Eupene Exploration Enterprises Pty Ltd., 1989. Platinum group metals in the Northern Territory. Department of Mines and Energy, Northern Territory Geological Survey, 16 pp.

Ferguson, K.M., 1999. Lead, zinc and silver deposits of Western Australia. Western Australia Geological Survey, Mineral Resources Bulletin 15, 314 pp.

Fleet, M.E., Crocket, J.H., Liu, M. & Stone, W.E. 1999. Laboratory partitioning of platinum-group elements (PGE) and gold with application to magmatic sulfide-PGE deposits. Lithos, 47, 127–142.

Frankcombe, K., Barnes, G. & Trussell, D., 1994. Geophysical signature of the Sally Malay nickel deposit, Western Australia. In: Dentith, M.C. et al. (editors), Geophysical signatures of Western Australian mineral deposits. Geology and Geophysics Department & UWA Extension, University of Western Australia, 26, 157–168.

Gaunt, F. McA., 1977. Keller Creek final report. Results of exploration of Mineral Claims 80/5209, 5302–5319 inclusive. Australian Anglo American Limited internal report (unpublished) for the Department of Minerals and Energy, Western Australia (Item 742, AN7692).

Griffin, T.J., Tyler, I.M., Orth, K. & Sheppard, S., 1998. Geology of the Angelo 1:100 000 sheet: Western Australia Geological Survey, 1:100 000 Geological Series Explanatory Notes, 27 pp.

Growth Resources NL, 1988–90. Buningonia platinum/nickel/chromite exploration. Report on Exploration Licences E 28/281, E 28/308, and E 28/324. Western Australia Geological Survey M-series Open File, I 6068 (unpublished).

Hakli, T.A., Hanninen, E., Vuorelainen, Y. & Papunen, H., 1976. Platinum-group minerals in the Hitura nickel deposit, Finland. Economic Geology, 71, 1206–1213.

Halligan, R. & Harris, J.L., 1980. Bow River Cu–Ni deposit, Halls Creek Province, Western Australia. Journal of Geochemical Exploration, 12 (2/3), 214–217.

Hamlyn, P.R., 1980. Equilibration history and phase chemistry of the Panton Sill, Western Australia. American Journal of Science, 280/7, 631–668.

Hamlyn, P.R. & Keays, R.R., 1979. Origin of chromite compositional variation in the Panton Sill, Western Australia. Contributions to Mineralogy and Petrology, 69/1, 75–82.

Hamlyn, P.R., Keays, R.R., Peck, D.C. & Reeves, S.J. 1988. Geochemical criteria for platinum metal exploration. Australian Mineral Industries Research Association Limited, Final Report 85/P228 (unpublished), 215 pp.

Harrison, P.H., 1986. The mineral potential of layered igneous complexes within the Western Gneiss Terrane. Geological Survey of Western Australia Professional Paper 1984, 19, 37–54.

Haughton, D.R., Roeder, P.L. & Skinner, B.J., 1974. Solubility of sulfur in mafic magmas. Economic Geology, 69, 451–467.

Helix Resources NL,. 1986. Prospectus.

Hoatson, D.M., 1993. Correlation of structurally disrupted layered mafic–ultramafic intrusions in the East Kimberley: Is Big Ben part of the Panton intrusion? AGSO Research Newsletter, 19, 9–10.

Hoatson, D.M., 1995. New mineral discoveries in the East Kimberley. AGSO Research Newsletter, 22, 9–11.

Hoatson, D.M., 1998. Platinum-group element mineralisation in Australian Precambrian layered mafic–ultramafic intrusions. AGSO Journal of Australian Geology & Geophysics, 17(4), 139–151.

Hoatson, D.M., in press. Exploration strategies for Precambrian layered mafic–ultramafic intrusions in the East Kimberley. AGSO Research Newsletter, 32.

Hoatson, D.M. & Glaser, L.M., 1989. The geology and economics of platinum-group metals in Australia. Bureau of Mineral Resources, Australia, Resource Report 5, 81 pp.

Hoatson, D.M. & Keays, R.R., 1989. Formation of platiniferous sulfide horizons by crystal fractionation and magma mixing in the Munni Munni layered intrusion, west Pilbara Block, Western Australia. Economic Geology, 84, 1775–1804.

Hoatson, D.M. & Tyler, I., 1993. Prospective layered mafic–ultramafic intrusions in the East Kimberley. AGSO Research Newsletter, 18, 8–9.

Hoatson, D.M., Wallace, D.A., Sun, S-s., Macias, L.F., Simpson, C.J. & Keays, R.R., 1992. Petrology and platinum-group-element geochemistry of Archaean layered mafic–ultramafic intrusions, west Pilbara block, Western Australia. Australian Geological Survey Organisation, Bulletin 242, 319 pp.

Hoatson, D.M., Blake, D., Warren, G., Orth, K. & Tyler, I.M., 1995. Recent NGMA mapping highlights the metallogenic potential of the East Kimberley. AGSO Research Newsletter, 22, 1–2.

Hoatson, D.M., Sproule, R.A. & Lambert, D.D., 1997. Are there Voisey's Bay-type Ni–Cu–Co sulphide deposits in the East Kimberley of Western Australia? AGSO Research Newsletter, 27, 17–19.

Huang, W.L. & Williams, R.J., 1980. Melting relations of portions of the system Fe-S-Si-O to 32 kb with implications for the nature of the mantle/core boundary. Abstract. Lunar & Planet Sc. XI, Lunar & Planetary Institute, Houston, 486–488.

Hunter Resources Limited, 1987. Report to the Australian Stock Exchange for the quarter ended December 31 1987 (unpublished).

Hunter Resources Limited, 1988. Report to the Australian Stock Exchange for the quarter ended September 30 1988 (unpublished).

International Nickel Australia Ltd., 1981–82. Wadgingarra platinum–chromite exploration. Report on Exploration Licence TR 70/8424. Western Australia Geological Survey M-series Open File, Item 1828, Roll 569 (unpublished).

Irvine, T.N., 1975. Crystallization sequences of the Muskox intrusion and other layered intrusions—II. Origin of chromitite layers and similar deposits of other magmatic ores. Geochimica et Cosmochimica Acta, 39, 991–1020.

Irvine, T.N., 1977. Origin of chromitite layers in the Muskox intrusion and other stratiform intrusions: a new interpretation. Geology, 5, 273–277.

Keays, R.R. & Campbell, I.H., 1981. Precious metals in the Jimberlana Intrusion, Western Australia: implications for the genesis of platiniferous ores in layered intrusions. Economic Geology, 76, 1118–1141.

Keeley, G., 1991. Billymac Prospect E80/1393, Kimberley Mineral Field, Western Australia. Internal report (unpublished) for the Department of Minerals and Energy, Western Australia (Item 6425, AN34824).

Lambert, D.D., Foster, J.G. & Frick, L.R., 1998. Geodynamics of magmatic Cu-Ni-PGE sulfide deposits: new insights from the Re-Os isotope system. Economic Geology, 93, 121–136.

Louthean, R., 1987. Platinum. In: Louthean, R. (editor), Register of Australian mining, 1987. Resource Information Unit Ltd, Perth, 202–219.

Louthean, R., 1989. Platinum. In: Louthean, R. (editor), Register of Australian mining, 1989/90. Resource Information Unit Ltd, Perth, 255–268.

Louthean, R. & Hill, J., 1994. Platinum. In: Wilkinson, D. (editor), Register of Australian mining, 1994–95. Resource Information Unit Ltd, Perth, 300–304.

Louthean, R. & Seidel, H., 1988. Platinum. In: Louthean, R. (editor), Register of Australian mining, 1988–89. Resource Information Unit Ltd, Perth, 212–232.

Macdonald, A.J., 1987. The platinum group element deposits: classification and genesis. Geoscience Canada, 14, 155–166.

Marston, R.J., 1979. Copper mineralization in Western Australia. Western Australia Geological Survey, Mineral Resources Bulletin 13, 208 pp.

Marston, R.J., 1984. Nickel mineralization in Western Australia. Geological Survey of Western Australia, Mineral Resources Bulletin 14, 271 pp.

Mathison, C.I. & Hamlyn, P.R., 1987. The McIntosh layered troctolite–olivine gabbro intrusion, east Kimberley, Western Australia. Journal of Petrology, 28, 211–234.

Mathison, C.I. & Marshall, A.E., 1981. Ni–Cu sulfides and their host mafic–ultramafic rocks in the Mt. Sholl intrusion, Pilbara region, Western Australia. Economic Geology, 76, 1581–1596.

Mathison, C.I., Perring, R.J., Vogt, J.H., Parks, J., Hill, R.E.T. & Ahmat, A.L., 1991. The Windimurra Complex. In: Barnes, Stephen J. & Hill, R.E.T. (editors), Mafic–ultramafic complexes of Western Australia, Excursion Guidebook No. 3. Sixth International Platinum Symposium, July 1991, Perth, WA. IAGOD and the Geological Society of Australia, 45–76.

McCallum, M.E., Loucks, R.R., Carlson, R.R., Cooley, E.F. & Doerge, T.A., 1976. Platinum metals associated with hydrothermal copper ores of the New Rambler Mine, Medicine Bow Mountains, Wyoming. Economic Geology, 71, 1429–1450.

McNeil, P., 1991. McKenzie Bore—report on work completed May–December 1991. Western Australia Geological Survey M-series Open File, item 6425, AN34826 (unpublished).

Naldrett, A.J., 1981. Nickel sulfide deposits: classification, composition, and genesis. Economic Geology, 75th Anniversary Volume, 628–685.

Naldrett, A.J., 1989. Magmatic sulfide deposits. Clarendon Press; Oxford University Press, New York, 177 pp.

Naldrett, A.J., 1993. Models for the formation of stratabound concentrations of platinum-group elements in layered intrusions. In: Kirkham et al. (editors), Mineral deposit modeling. Geological Association of Canada, Special Paper 40, 373–387.

Naldrett, A.J., 1997. Key factors in the genesis of Noril'sk, Sudbury, Jinchuan, Voisey's Bay and other world-class Ni–Cu–PGE deposits: implications for exploration. Australian Journal of Earth Sciences, 44, 283–315.

Naldrett, A.J. & Cabri, L.J., 1976. Ultramafic and related mafic rocks: Their classification and genesis with special reference to the concentration of nickel sulfides and platinum-group elements. Economic Geology, 71, 1131–1158.

Naldrett, A.J., Keats, H., Sparkes, K. & Moore, R., 1996. Geology of the Voisey's Bay Ni–Cu–Co deposit, Labrador, Canada. Journal of Exploration of Mining and Geology. Canadian Institute of Mining, Metallurgy, and Petroleum, 5, 169–179.

Nevill, M.W., 1974. The geology and mineralisation of the Corkwood prospect area, Lamboo Complex, East Kimberley, Western Australia. BSc (Honours) thesis, University of Western Australia (unpublished), 72 pp.

Newcrest Mining Ltd., 1990–92. Brown Knob PGE/gold exploration. Report on Exploration Licence M 26/334. Western Australia Geological Survey M-series Open File, I 6427 (unpublished).

Nielsen, T.F.D. & Brooks, C.K., 1995. Precious metals in magmas of East Greenland: Factors important to the mineralization in the Skaergaard Intrusion. Economic Geology, 90, 1911–1917.

Papunen, H., 1996. Ni-Cu deposits in intrusive mafic–ultramafic rocks - a review. In: Grimsey, E.J. & Neuss, I. (editors), Nickel 96 - Mineral to market. Australasian Institute of Mining and Metallurgy, Publication Series 6/96, November 27–29, Kalgoorlie, Western Australia, 123–129.

Papunen, H., Häkli, T.A. & Idman, H., 1979. Geological, geochemical and mineralogical features of sulfide-bearing ultramafic rocks in Finland. Canadian Mineralogist, 17, 217–232.

Parks, J., 1998. Weld Range platinum group element deposit. In: Berkman, D.A. & Mackenzie, D.H. (editors), Geology of Australian and Papua New Guinean mineral deposits. The Australasian Institute of Mining and Metallurgy, Melbourne, Monograph 22, 279–286.

Peltonen, P., 1995a. Magma–country rock interaction and the genesis of Ni–Cu deposits in the Vammala nickel belt, Southwest Finland. Mineralogy & Petrology, 52, 1–24.

Peltonen, P., 1995b. Petrogenesis of ultramafic rocks in the Vammala Nickel Belt: implications for crustal evolution of the early Proterozoic Svecofennian arc terrane. Lithos, 34, 253–274.

Peltonen, P. & Huhma, H., 1997. Overview of the Svecofennian mafic magmatism in Finland. In: Rutland, R.W.R. & Drummond, B.J. (editors), Palaeoproterozoic tectonics and metallogenesis: comparative analysis of parts of the Australian & Fennoscandian shields. Workshop, Darwin, September, 14–22, 1997. Australian Geological Survey Organisation, Record 1997/44, 95–97.

Perring, R.J. & Vogt, J.H., 1991. The Panton Sill. In: Barnes, S.J. & Hill, R.E.T. (editors), Mafic–ultramafic complexes of Western Australia. Excursion Guidebook 3. Sixth International Platinum Symposium, July 1991, Perth, Western Australia. IAGOD and the Geological Society of Australia, 97–106.

Phaceas, J. & Young, P., 1996. Platinum. In: Wilkinson, D. (editor), Register of Australian mining, 1996–97. Resource Information Unit Ltd, Perth, 295–297.

Pilbara Resources Limited, 1986. Interim report by Pilbara Gold Trust, March 1986 (unpublished).

Purvis, A.C., Nesbitt, R.W. & Hallberg, J.A., 1972. The geology of part of the Carr-Boyd Rocks complex, and its associated nickel mineralisation, WA. Economic Geology, 67, 1093–1113.

Rowell, W.F. & Edgar, A.D., 1986. Platinum-group element mineralization in a hydrothermal Cu-Ni sulfide occurrence, Rathbun Lake, northeastern Ontario. Economic Geology, 81, 1272–1277.

Ryan, B. 1997. The Mesoproterozoic Nain Plutonic Suite in eastern Canada, and the setting of the Voisey's Bay Ni-Cu-Co sulphide deposit. Geoscience Canada, 24, 173–188.

Ryan, B., Wardle, R.J., Gower, C.F. & Nunn, G.A.G., 1995. Nickel–copper sulphide mineralization in Labrador: The Voisey Bay discovery and its implications. Current Research Newfoundland and Labrador Department of Natural Resources, Geological Survey, Report 95-1, 177–204.

Shedden, S.H. & Barnes, G.J., 1996. East Kimberley Nickel Province — Characteristics and origin of the Sally Malay Ni-Cu-Co deposit, East Kimberley, Western Australia. In: Grimsey, E.J. & Neuss, I. (editors), Nickel 96—mineral to market. Australasian Institute of Mining and Metallurgy, Publication Series 6/96, November 27–29, Kalgoorlie, Western Australia, 145–155.

Sheppard, S., Griffin, T.J. & Tyler, I.M., 1997a. The tectonic setting of granites in the Halls Creek and King Leopold Orogens, northwest Australia. In: Rutland, R.W.R. & Drummond, B.J. (editors), Palaeoproterozoic tectonics and metallogenesis: comparative analysis of parts of the Australian & Fennoscandian shields. Workshop, Darwin, September, 14–22, 1997. Australian Geological Survey Organisation, Record 1997/44, 107–109.

Sheppard, S., Tyler, I.M. & Hoatson, D.M., 1997b. Geology of the Mount Remarkable 1:100 000 sheet, Western Australia. Western Australia Geological Survey, 1:100 000 Geological Series Explanatory Notes, 27 pp.

Sherrington, G.H., 1985. Final report on the Exploration Licence 80/368 - Billymac Yard, for the period 30 March 1984 to 14 September 1984. Geopeko, Division of Peko-Wallsend Operations Limited internal report. Western Australia Geological Survey M-series Open File, item 2177, AN15391 (unpublished).

Sproule, R., Lambert, D.D. & Hoatson, D.M., 1997a. Re–Os and Sm–Nd isotopic constraints on the genesis of magmatic ores in the Palaeoproterozoic Panton Intrusion, East Kimberley. New Developments in Research for Ore Deposit Exploration. Third National Conference of the Specialist Group in Economic Geology, Canberra, January 30–31 1997. Geological Society of Australia, Abstracts, 44, 67.

Sproule, R.A., Lambert, D.D. & Hoatson, D.M., 1997b. Guides to PGE and Ni-Cu-Co exploration in the East Kimberley, Western Australia. In: Burroughs, A. (editor), Student and young professionals conference. Australasian Institute of Mining and Metallurgy, Abstract, Ballarat 1997.

Sproule, R.A., Lambert, D.D. & Hoatson, D.M., 1999. Re–Os isotopic constraints on the genesis of the Sally Malay Ni–Cu–Co deposit, East Kimberley, Western Australia. Lithos, 47, 89–106.

Stone, W.E., Crockett, J.H. & Fleet, M.E., 1990. Partitioning of palladium, iridium, platinum, and gold between sulfide liquid and basalt melt at 1200°C. Geochimica et Cosmochimica Acta, 54, 2341–2344.

Sun, S-s. & McDonough, W.F., 1989. Chemical and isotopic systematics of oceanic basalts: implication for mantle composition and processes. In: Saunders, A.D. & Norry, M. J. (editors), Magmatism in the ocean basins. Geological Society Special Publication 42. Blackwell Scientific Publications, Oxford, 313–345.

Taylor, R.B., 1956. The Duluth gabbro complex, Duluth, Minnesota. Annual Meeting, GSA, Guidebook, Field Trip No. 1, 42–66.

Thalhammer, O.A.R. & Stumpfl, E.F., 1988. Platinum-group minerals from Hochgrössen ultramafic massif, Styria: first reported occurrence of PGM in Austria. Transactions of the Institution of Mining & Metallurgy, London, 97, B77–82.

Thompson, J.F.H. & Naldrett, A.J., 1984. Sulfide–silicate reactions as a guide. In: Buchanan, D.L. & Jones, M.L. (editors), Sulfide deposits in mafic and ultramafic rocks. Proceedings of IGCP Projects 161 & 91, Third Nickel Sulphide Field Conference, Perth, WA, 23–25 May 1982. Institution of Mining & Metallurgy, London, 103–113.

Thornett, J.R., 1981. The Sally Malay deposit: gabbroid associated nickel–copper sulfide mineralization in the Halls Creek Mobile Zone, Western Australia. Economic Geology, 76 (6), 1565–1580.

Todd, S.G., Keith, D.W., Le Roy, L.W., Schissel, D.J., Mann, E.L. & Irvine, T.N., 1982. The J-M platinum–palladium reef of the Stillwater Complex, Montana: I. Stratigraphy and petrology. Economic Geology, 77, 1454–1480.

Trudu, A. & Hoatson, D.M., 1996. Depths of emplacement of Precambrian layered intrusions in the East Kimberley. AGSO Research Newsletter, 25, 10–12.

Tyler, I.M. & Page, R.W. 1996. Palaeoproterozoic deformation, metamorphism and igneous intrusion in the

central zone of the Lamboo Complex, Halls Creek Orogen. Geological Society of Australia, Abstracts, 41, 450–451.

Tyler, I.M., Griffin, T.J., Page, R.W. & Shaw, R.D., 1995. Are there terranes within the Lamboo Complex of the Halls Creek Orogen? Western Australia Geological Survey, Annual Review 1993–94, 37–46.

Vogt, J.H., 1989. Third Annual Report E80/685 - Louisa Downs. Pancontinental Mining, Degussa Exploration, Helix Resources NL Report to Western Australia Geological Survey (unpublished).

Wager, L.R. & Brown, G.M., 1968. Layered igneous rocks. Oliver & Boyd, Edinburgh & New York, 588 pp.

Wendlandt, R.F., 1982. Sulfide saturation of basalt and andesite melts at high pressures and temperatures. American Mineralogist, 67, 877–885.

West Coast Holdings Ltd., 1985–88. Yornup chromitite/PGE exploration. Report on Exploration Licence E 70/161. Western Australia Geological Survey M-series Open File, I 3491, Fiche 3572 to 3574 (unpublished).

Wiebe, R.A., 1990. Evidence for unusually feldspathic liquids in the Nain complex, Labrador. American Mineralogist, 73, 1–12.

Wilding, I.G.P., 1980. Corkwood Cu-Ni prospect, Halls Creek Province, WA. In: Butt, C. R.M. & Smith, R.E. (editors), Conceptual models in exploration geochemistry. Journal of Geochemical Exploration, 12, 220–224.

Willemse, J., 1969. The geology of the Bushveld Igneous Complex, the largest repository of magmatic ore deposits in the world. In: Wilson, H.D.B. (editor), Magmatic ore deposits. Economic Geology, Monograph 4, 1–22.

Williams, C.R., Nisbet, B.W. & Hoatson, D.M., 1990. Munni Munni Complex platinum group mineralisation. In: Hughes, F.E. (editor), Geology of the mineral deposits of Australia and Papua New Guinea. Australasian Institute of Mining & Metallurgy, Melbourne, Monograph 14, 145–150.

Wilson, J.R., Menuge, J.F., Pedersen, S. & Engell-Sørensen, O., 1987. The southern part of the Fongen–Hyllingen layered mafic complex, Norway: emplacement and crystallization of compositionally stratified magma. In: Parsons, I. (editor), Origins of igneous layering. NATO Advanced Science Series, 196. D. Reidel Publishing Company, Dordrecht, 145–184.

Witt, W.K., 1995. Tholeiitic and high-Mg mafic/ultramafic sills in the Eastern Goldfields Province, Western Australia: implications for tectonic settings. Australian Journal of Earth Sciences, 42, 407–422.

Witt, W.K., Hill, R.E.T., Gole, M.J., Barnes, S.J. & Perring, R.J., 1991. Layered mafic–ultramafic complexes of the Norseman–Wiluna Greenstone Belt. In: Barnes, S.J. & Hill, R.E.T. (editors), Mafic–ultramafic complexes of Western Australia. Excursion Guidebook No. 3. Sixth International Platinum Symposium, July 1991, Perth, WA. IAGOD and the Geological Society of Australia, 27–44.

CHAPTER 15

SUMMARY OF CONCLUSIONS AND SUGGESTIONS FOR FURTHER STUDIES

by DEAN M. HOATSON & DAVID H. BLAKE

Introduction

The Australian Geological Survey Organisation (AGSO) and the Geological Survey of Western Australia (GSWA) began investigating the Palaeoproterozoic layered mafic–ultramafic intrusions of the Halls Creek Orogen (HCO) in 1992 as part of the National Geoscience Mapping Accord (NGMA) Kimberley–Arunta project. The main aims of the investigations were to determine the geological setting and evolution of the layered mafic–ultramafic intrusions and assess their economic potential. Detailed studies of individual intrusions, involving their stratigraphy, mineralisation, geochronology, fluid dynamic modelling, and depth of emplacement, as well as isotope, mineral, and whole-rock geochemistry, have been integrated with studies of the regional geology, geophysics, and tectonic processes. The results of these studies, reported in this *Bulletin*, should be of interest to those involved in the:

- exploration of layered mafic–ultramafic intrusions in the HCO;
- application of geochemical, geochronological, geophysical, geothermobarometric, and remote sensing studies in the assessment of the metallogenesis of mafic–ultramafic magmatic systems;
- modelling of isotopic systematics, dynamics of magma emplacement and crustal contamination, and the interaction of mafic and felsic magmas; and
- regional geology and tectonics of the East Kimberley and other Precambrian provinces.

Significant results of the AGSO–GSWA study of the Palaeoproterozoic layered mafic–ultramafic intrusions of the HCO, together with some of the more important outstanding problems relating to geology, geophysics, geochronology, and geochemistry, are summarised in this chapter. The objectives and framework of the different studies of the intrusions are outlined in the individual chapters. A comprehensive list (up to June 2000) of published articles and maps produced as part of the NGMA investigations in the East Kimberley is given in Appendix 6.

Summary of major points and conclusions

Chapter 2 (exploration history of the East Kimberley)

- The first systematic regional investigations of the mafic–ultramafic intrusions in the HCO of the East Kimberley were made in 1962–64, during the geological mapping of the Precambrian rocks of the Kimberley region by the Bureau of Mineral Resources (now AGSO) and the GSWA. The intrusive mafic and ultramafic rocks were divided into three distinct units: tightly folded narrow sills and dykes of dolerite and gabbro (Woodward Dolerite), and broadly warped thick sills of ultramafic rocks (Alice Downs Ultrabasics) and mafic rocks (McIntosh Gabbro).
- The layered mafic–ultramafic intrusions have been explored for platinum-group elements (PGEs), Cr, Ni, Cu, Co, Ti, V, and Au since the early 1960s. Significant amounts of these metals have been found associated with the intrusions, but no economic deposits have been located to date. However, the HCO is regarded as one of the more prospective geological provinces in Australia for these commodities.
- Four major phases of exploration have taken place during the last four decades in the HCO:
  1. *mid 1960s:* stimulated by the first systematic geological survey of the region by BMR (now AGSO) and GSWA, with the focus mainly on Cr–PGEs, Ti–V, and Ni–Cu–Co;
  2. *early 1970s (the 'nickel boom years'):* stimulated by the discovery of komatiite-hosted Ni–Cu sulphide deposits in the Yilgarn Craton of Western Australia, and focussing on Ni–Cu–Co;
  3. *mid–late 1980s:* stimulated by buoyant world PGE metal prices and the general interest of PGEs in Australia, and focussing on Cr–PGEs; and
  4. *mid–late 1990s:* stimulated by the NGMA geological mapping by AGSO and GSWA in the region and the discovery overseas of world-class deposits (e.g. Voisey's Bay in Canada), and focussing on Ni–Cu–Co and Cr–PGEs.

Chapter 3 (regional geology of the Halls Creek Orogen)

- The HCO consists of variably deformed and metamorphosed sedimentary, volcanic, and intrusive Palaeoproterozoic rocks, including the layered mafic–ultramafic intrusions, and overlapping Proterozoic and Palaeozoic basinal sequences.
- The HCO is divided into three north-northeasterly trending zones separated from one another by major strike-slip faults. Layered intrusions are present in the central and western zones, west of the Halls Creek Fault, but none are known in the eastern zone.
- Major tectonism, involving deformation and metamorphism, affected the western zone between 1870 and 1850 Ma (Hooper Orogeny), the central zone between 1863 and 1845 Ma (unnamed orogeny), and both the central and eastern zones between 1840 and 1805 Ma (Halls Creek Orogeny). Later deformations, but only minor metamorphism, took place at ~1000 Ma (Yampi Orogeny), ~560 Ma (King

Leopold Orogeny), and ~300 Ma (Alice Springs Orogeny).

- Layered mafic–ultramafic intrusions predating the Halls Creek Orogeny form part of what is termed the basement, which ranges in age from ~1910 to 1840 Ma. The basement in the western zone includes layered intrusions and coeval granitic plutons of the 1865–1850 Ma Paperbark supersuite of the Bow River Batholith. Younger layered intrusions, mainly in the central zone, are coeval with granitic plutons of the 1835–1805 Ma Sally Downs supersuite of the Bow River Batholith.
- In many places, the layered intrusions appear to have locally melted the country rocks to form migmatite (Panton and McIntosh intrusions) and net-vein complexes (Toby and Armanda intrusions) during emplacement of the mafic–ultramafic magma.
- Three contrasting interpretations have been proposed for the tectonic evolution of the HCO between ~1910 and 1800 Ma:
  1. An island arc, represented by high-grade Tickalara Metamorphics of the central zone of the HCO, accreted onto the eastern margin of the Kimberley craton, forming the western zone by 1850 Ma. This accretion was followed by northwestward subduction of oceanic crust at ~1835 Ma, during collision between the Kimberley craton, which included the accreted island arc, and a continental plate, which contained the eastern zone of the HCO.
  2. Palaeoproterozoic orogenesis and magmatism took place in an intracratonic setting and was essentially ensialic, being a result of underplating of mafic magma at the base of the crust below the HCO. Heating and melting of the lower crust caused crustal extension and thinning and led to bimodal magmatism. Cooling of underplated magma triggered crust–mantle delamination, providing a driving force for compressional orogenesis.
  3. Development of a complex orogenic wedge above a Palaeoproterozoic plate or sub-plate boundary, perhaps dominated by transpressional and transtensional tectonism. Layered mafic–ultramafic intrusions may occupy dilational pockets formed during complex transcurrent movements.

Chapter 4 (regional geophysical setting and tectonic implications)

- A dipole gravity anomaly along the eastern margin of the HCO is of a type commonly associated with a sub-plate boundary, and could represent a major collisional suture, possibly involving basement reactivation.
- Marked gravity highs along the HCO can be attributed to mafic intrusions and high-grade (granulite facies) metamorphic rocks. The mafic–ultramafic intrusions generally show moderate to high magnetic susceptibilities.
- A regional magnetic trough, corresponding to the western zone of the HCO, shows many geophysical similarities to the King Leopold Orogen.
- The geophysical expression of the Highway Shear Zone appears to be more evident than the northern splay of the Springvale Fault, which has been previously regarded as the boundary between the western and central zones of the HCO.
- Transpressional and transtensional tectonism played an important part in the evolution of the HCO.

Chapter 5 (classification and geological setting of the mafic–ultramafic intrusions)

- The layered mafic–ultramafic intrusions of the HCO are assigned to seven major groups (designated I–VII) on the basis of rock types, U–Pb geochronology, contact relationships with country rocks, metamorphic–structural history, types of mineralisation, assemblages of cumulus minerals, trace-element chemistry, and Sm–Nd isotopic composition. Intrusions that show no primary compositional layering and generally form irregular massive bodies (Corridor gabbro, Turkey Creek microgabbro-norite) or belong to the Tickalara Metamorphics (Norton metagabbro) are not included in this classification.
- The well-preserved mafic–ultramafic intrusions form folded sheets, shallowly dipping basins, composite multi-chambered bodies, large funnel-shaped bodies, steeply plunging plugs, fault-bounded blocks, and narrow dyke-like bodies and screens between granite plutons. Most intrusions crosscut structural fabrics in the country rocks and some are up to 7.8 km thick; thus, the previously used term, 'sill', is generally not applicable.
- The layered mafic–ultramafic intrusions in the HCO appear to be unique in their abundance, size, and styles of mineralisation with respect to other intrusions of similar age in Australia.
- The presence of chilled and contaminated margins, contact aureoles, ribbon-like comagmatic satellite intrusions, associated net-vein complexes (resulting from mingling of mafic and felsic magmas), and possible feeder conduits indicate that most layered mafic–ultramafic intrusions crystallised in situ, rather than being tectonically emplaced segments of large bodies that crystallised at greater depths.
- Major-element variations with stratigraphic height in the East Kimberley intrusions are comparable to those recorded in other layered mafic–ultramafic intrusions of basaltic tholeiitic affinity (Bushveld, Skaergaard).
- The major mineralised layered mafic–ultramafic intrusions (groups I, II, and V) are located in two northeast-trending 'metallogenic corridors', one characterised by a chromite association (Cr–PGEs–Ni–Cu±Au), and the other, to the northwest, by a sulphide association (Ni–Cu–Co±PGEs).
- High average S contents for all groups, with the possible exception of group VII, indicate derivation from S-saturated parent magmas.

- Restoration of the same rock units across the Panton Fault, and similarities in stratigraphy, mineralogy, and chemistry indicate that the group I Big Ben mafic–ultramafic intrusion is probably a transposed fault-bounded block that was originally part of the mineralised Panton intrusion.
- The identification of a possible mineralised feeder conduit in the Sally Malay intrusion, similar to that of Voisey's Bay in Canada, has important implications for the exploration of Palaeoproterozoic layered mafic–ultramafic intrusions in the HCO.

Chapter 6 (geochronology of the mafic–ultramafic intrusions)

- Fractionated anorthositic and gabbroic cumulates in four of the layered mafic–ultramafic intrusions contain magmatic zircon and, in one case, coexisting baddeleyite. Zircon from the group I Panton intrusion is dated at 1856±2 Ma, that from the group II Springvale intrusion, at 1857±2 Ma, and that from the group III Toby intrusion, at 1855±2 Ma. The age of zircon from the group V Sally Malay intrusion, 1844±3 Ma, is in good agreement with an age of 1846±5 Ma for baddeleyite from the same rock sample. An age of 1830±3 Ma for the younger of two groups of zircons from a migmatitic hornfels in the contact aureole of the group VI McIntosh intrusion is inferred to be the emplacement age of this intrusion.
- The geochronological data indicate at least three main periods of mafic–ultramafic magmatism in the HCO: ~1855 Ma, ~1845 Ma and ~1830 Ma.
- With the exception of the massive granulite mafic bodies in the Tickalara Metamorphics, there is no apparent relationship between intensity of deformation and age of the layered mafic–ultramafic intrusion.
- The emplacement of groups I–III layered intrusions in the central and western zones of the HCO was contemporaneous with the emplacement of large granitic plutons of the Paperbark supersuite in the Bow River Batholith and the eruption of the felsic Whitewater Volcanics in the western zone. This mafic, mafic–ultramafic, and felsic magmatism represents a large flux of heat into the Earth's crust at around 1855 Ma, and probably contributed to the amphibolite–granulite facies metamorphism that affected this part of the East Kimberley.

Chapter 7 (geophysical expression of the mafic–ultramafic intrusions)

- Magnetic data show that magnetic highs in the western zone of the HCO correlate with the Springvale and Toby intrusions, and that the Corridor gabbro intrusions are closely aligned with a magnetic ridge. Layered mafic–ultramafic intrusions in the central zone are moderately to highly magnetic, reflecting their highly evolved tholeiitic character. Some have a complex magnetic expression, owing to the variable shape, size, and thickness of the body, and the irregular distribution of secondary magnetite in the ultramafic rocks.
- Some intense magnetic highs may correspond to large buried intrusions which may be connected to outcropping layered intrusions.
- Most prominent Bouguer gravity anomalies in the HCO correspond to outcropping garnet-bearing metapelites. Layered mafic–ultramafic intrusions with related gravity anomalies are the Toby, Springvale, and McIntosh intrusions, although none of them is directly centred over an individual gravity high. The eastern part of the Toby intrusion overlies a gravity high which could reflect a large, related magma chamber at depth. The Springvale intrusion corresponds to the southern edge of a gravity ridge which may link to the anomaly that partly overlaps the Toby intrusion. The McIntosh intrusion corresponds to the northern part of a gravity ridge, but not to the peak of the anomaly, which is to the southwest and could reflect a related larger parent magma chamber at depth.
- Small layered mafic–ultramafic intrusions in the HCO have no obvious expression in regional magnetic or gravity data.
- Major faults, along which mafic–ultramafic intrusions are sometimes concentrated, correspond to marked gravity gradients and lineaments.
- The two metallogenic corridors containing most mineralised intrusions in the HCO correspond to two geophysical zones which may have different tectonic and metamorphic histories. The geophysical zones are separated by the Highway Shear Zone.
- The East Kimberley layered mafic–ultramafic intrusions are late tectonic to post-tectonic bodies which appear to occupy transtensional pockets in an evolving, transcurrent, crustal-scale deformed zone.

Chapter 8 (remote sensing of mafic–ultramafic rocks)

- Landsat–5 Thematic Mapper imagery using band ratios, and directed principal component analysis (DPCA) has proved to be very useful in distinguishing mafic from ultramafic rocks in the layered intrusions and in mapping the extent of the intrusions, especially where they are surrounded by rocks of different mineralogy.
- DPCA directs an input of two specific band-ratio images, in particular, ratio 4/3, which enhances vegetation, and ratio 5/7, which enhances the mixed response of clay materials and vegetation. Band-ratio 5/4 was used to discriminate iron oxides and bands 1 and 7 were added to discriminate silica.
- The interpretation of band-ratio imagery is hampered by the mixed spectral responses of weathered rocks, surficial cover, vegetation (spinifex, lichen), variable terrain, and fire burn patterns. The masking effects of these factors are significantly reduced using DPCA.
- Gamma-ray spectrometry (K, Th, and U) provides a quick method of discriminating mafic–ultramafic rocks from granitic, metamorphic, and sedimentary rocks, owing to their low spectrometric response (dark brown to black).

Chapter 9 (depths of emplacement of the mafic–ultramafic intrusions)

- The depth of emplacement for 13 layered mafic–ultramafic intrusions in the HCO was determined using electron probe microanalyses of Ca-bearing amphibole from magmatic coronas around olivine and from magmatic amphibole replacing clinopyroxene. Crustal depth ranged from about 8 km (2.4 kb) to 23 km (6.7 kb), with the deepest intrusions being in the northern part of the central zone.
- Exposure of deeper erosional levels northwards in the central zone is consistent with increasing metamorphic grade in this zone, from greenschist facies in the south through to granulite facies in the north. The opposite appears to be the case for ~1855 Ma units in the western zone, where the emplacement depth of the Springvale intrusion, 18 km, is appreciably more than that of the Toby intrusion, 8 km, to the north, and the regional metamorphism of the coeval Whitewater Volcanics and Greenvale and Castlereagh Hill Porphyries further north is generally no more than greenschist facies.
- The same emplacement depth of 11 km for the group I Panton and Big Ben intrusions supports the suggestion that the two bodies were once part of the same intrusion.
- The Ni–Cu–Co-bearing group V intrusions (e.g. Sally Malay) were emplaced at deeper crustal levels (20–23 km) than the Cr–PGE–Ni–Cu-bearing intrusions of group I (e.g. Panton, at 11 km).
- Cryptic chemical variations of cumulus minerals in the Springvale and Wilagee intrusions indicate that open fractionation systems, involving regular pulses of magma into the chambers, prevailed over closed systems.

Chapter 10 (relationships of mafic and felsic magmatism)

- Palaeoproterozoic magmatism in the HCO is distinctly bimodal. Mafic intrusions are spatially associated with voluminous coeval granites of the Bow River Batholith, and mafic volcanism was often accompanied by felsic volcanism. The granites were emplaced between 1860 and 1850 Ma (Paperbark supersuite in the western zone) and between 1835 and 1805 Ma (Sally Downs supersuite, mainly in the central zone).
- The HCO granitic rocks are predominantly I-(granodioritic) types with mantle-normalised trace-element signatures indicative of a tonalitic source in the lower crust, crustal thicknesses of less than 35 km, and high crustal geothermal gradients.
- Both the layered mafic–ultramafic intrusions and the granitic intrusions show significant changes in trace-element compositions at ~1835 Ma. These changes can be accounted for by minor changes in crustal thickness and geothermal gradient, and do no necessarily imply a radical change in tectonic setting.
- The mafic and ultramafic rocks are attributed to intrusions of basaltic magma from the mantle. The felsic rocks, on the other hand, crystallised from magma formed by melting of Archaean and/or early Palaeoproterozoic lower crust by the mafic magma.
- Palaeoproterozoic features of the HCO, such as bimodal magmatism, layering in mafic–ultramafic intrusions, granitic rocks with compositions indicating hot thin crust and high geothermal gradients, and prevailing high temperature/low pressure metamorphism, suggest an overall extensional rather than compressional tectonic setting.

Chapter 11 (geochemistry, isotopes, and tectonic environment of the mafic–ultramafic intrusions)

- The parent magma for many of the layered mafic–ultramafic intrusions was probably contaminated by continental crust. This contamination could have occurred in the mantle and during ascent of magma from the mantle, through the lower crust, to emplacement as layered intrusions in the middle–upper crust.
- The parent magma for the post 1835 Ma layered intrusion could have been derived from mantle sources modified by Palaeoproterozoic subduction processes.
- Incompatible trace-element abundances and spidergram patterns of mafic cumulates in the western zone and post-1850 Ma intrusions in the central zone are consistent with an intraplate environment. However, geochemical characteristics of pre-1850 Ma intrusions in the central zone (Panton, Norton, ?Keller Creek) and metabasalts in the Tickalara Metamorphics are not consistent with a simple island arc model.
- Many of the layered mafic–ultramafic intrusions are inferred to have olivine tholeiite and quartz tholeiite parent magmas, and all were basaltic (i.e. relatively fractionated with mg = 67 or less) rather than ultramafic. Abundances of incompatible trace elements indicate compositions ranging from mid-ocean ridge basalt to continental tholeiite.
- The layered mafic–ultramafic intrusions show evidence of S saturation throughout their mafic and ultramafic sequences; thus, they appear to have little potential for stratabound Merensky Reef or Munni Munni-type PGE mineralisation.
- Some layered mafic–ultramafic intrusions have high background values of Pt, Pd, and Au; hence, the HCO should not be dismissed as unprospective for hydrothermal and placer deposits of these elements.

Chapter 12 (geochemistry, isotopes, and petrogenesis of the Panton and Sally Malay intrusions)

- The parental magma or magmas for the group I Panton intrusion may be derived from enriched portions of the mantle or from a mantle-derived magma contaminated by crustal material. Crustal contamination is an important process in the petrogenesis of the Sally Malay intrusion and its associated magmatic Ni–Cu–Co sulphide mineralisation.
- Mineralisation in the group V Sally Malay type of intrusions is likely to accumulate passively as basal sulphide layers or in feeders, being physically controlled by a widening or bending of the magma

conduit, which slows the magma flow rate and allows deposition.

- Re–Os isotopic data indicate a two-stage model for the petrogenesis of the Sally Malay intrusion and its associated sulphide mineralisation. The first stage involved contamination of a basaltic (tholeiitic) melt–magma at depth (mantle?), promoting S saturation and formation of an immiscible sulphide melt phase. The second stage took place during transport of the sulphides in the host basaltic magma, resulting in a low metal tenor. Crystallisation in passive conditions followed emplacement of the magma as a layered intrusion and resulted in a basal sulphide layer with highly radiogenic crustal Re–Os isotopic composition. The same two stages are envisaged for the Panton intrusion, but in this case, the crystallisation of the magma in the intrusion was a dynamic process in which new magma pulses carrying low-tenor sulphide droplets mixed with resident magma. This resulted in PGE-enriched sulphides and near-chondrite initial Os isotopic compositions.
- The depth of emplacement, intrusion mechanisms, degree of contamination, and size of intrusion appear to be important considerations in determining the prospectivity of the layered intrusions in the HCO.

Chapter 13 (geochemistry of chromite in Precambrian layered intrusions of northern Western Australia)

- Raman spectra from 340 to 800 cm^{-1} of natural spinels from layered intrusions in the East Kimberley and the west Pilbara Craton have weak bands around 380 and 480 cm^{-1} and more intense, but broad bands at approximately 550–600 cm^{-1} and 680–720 cm^{-1}. Curve-fitting of these last two bands showed that they were composed of at least six lorentzian bands. The frequencies of these six bands vary as a function of chemical composition, and are particularly sensitive to the relative amount of trivalent cations in each chromite crystal.
- Raman spectroscopy is a rapid method for classifying chromite according to chemical composition and temperature. Two subgroups of cumulus chromite can be distinguished geochemically in the layered mafic–ultramafic intrusions of the HCO: a high Al^{3+} and Fe^{3+}, higher temperature subgroup 1 (group II Wilagee and Lamboo intrusions), and a high Cr and generally low Fe^{3+}, lower temperature subgroup 2 (group I intrusions).
- The high aluminium content of subgroup 1 chromite from the Wilagee intrusion may reflect the association of plagioclase-rich mafic rocks, whereas chromite of subgroup II is hosted by ultramafic rocks.
- Lower temperatures obtained for chromites from subgroup 2 are attributed to subsolidus or metamorphic re-equilibration processes.
- Subgroup 2 chromite has chemical affinities with chromite from overseas layered intrusions, such as the Great Dyke and the Bushveld Complex.

Chapter 14 (mineralisation and economic potential of the mafic–ultramafic intrusions in the Halls Creek Orogen)

- The layered intrusions of the HCO are one of the most extensively mineralised mafic–ultramafic igneous associations in Australia. They contain a range of magmatic and hydrothermal deposits with various associations of precious and base metals.
- Deposits characterised by prominent surface expressions and geophysical–geochemical signatures are still to be found, despite the intensity of past exploration.
- Mineral deposits related to the layered intrusions can be broadly divided into a:
  - chromite association (Cr–PGEs–Ni–Cu±Au);
  - sulphide association (Ni–Cu–Co±PGEs);
  - Fe–Ti oxide association (Fe–Ti–V); and
  - hydrothermal polymetallic association (Pd, Pt, Cu, Zn, Pb, Au).
- The different associations in the HCO—Cr–PGEs–Ni–Cu±Au in 1856 Ma group I intrusions, Ni–Cu–Co±PGEs in 1845 Ma group V intrusions, and Fe–Ti–V in 1845 Ma group V and 1830 Ma group VI intrusions—reflect a general progression from early, more primitive, magmatic mineralising systems to later, more evolved systems.
- The layered mafic–ultramafic intrusions cannot be readily classified according to previous schemes based on tectonic setting, composition of magma, and associated magmatic deposits.
- Most layered mafic–ultramafic intrusions are late orogenic to postorogenic bodies that were emplaced during quiescent phases between periods of active tectonism in a complex orogenic belt.
- The sulphide-bearing group V Sally Malay intrusion displays similar tectonic, stratigraphic, and feeder conduit mineralisation features to those in the Voisey's Bay deposit in Canada and in Palaeoproterozoic intrusions in the Svecofennian domain of Finland.
- Exploration programs vary considerably for different styles of precious and base-metal mineralisation. It is important not to be 'blinkered' by a particular model, but to maintain a flexible innovative approach and consider different styles of orthomagmatic and hydrothermal mineralisation at different stratigraphic levels in the intrusion.

Suggestions for further studies

Geology and geophysics

- More comprehensive regional geological and geophysical investigations to constrain models for the tectonic evolution of the East Kimberley intrusions and to determine the timing and pressure–temperature conditions of regional and contact metamorphism.
- Determine the regional extent of the metallogenic corridors in the HCO. There is potential for further

mineralised intrusions of groups I, II, and V to be found along strike of the presently defined corridors.

- Detailed mapping and geophysics, to define the geometry of embayments and structural traps along the basal contacts of potential Ni–Cu–Co sulphide-bearing intrusions in groups V and VI and in the Tickalara Metamorphics.
- Detailed geophysical surveys (airborne electromagnetic, ground magnetic, induced polarisation), to identify prospective magma chambers and feeder conduits that may be poorly exposed or at depth.
- Assess the potential for other styles of PGE mineralisation, e.g. (1) structurally controlled hydrothermal Au–PGEs; (2) contaminated rocks along the basal contact—Platreef type; (3) transgressive pipe-like bodies; and (4) Au–Pd–Cu mineralisation in fractionated mafic rocks—Platinova Reef type (see Chapter 14), rather than focussing on the more commonly explored targets, such as stratabound chromitite layers in ultramafic sequences.
- Determine the significance of the Highway Shear Zone, which may be the boundary between the central and western zones in the HCO. This has important implications for the regional distribution and uplift history of the intrusions, in particular, the mineralised group V intrusions.

Geochronology

- Further studies to determine: (1) other periods of magmatism in the HCO and to constrain the emplacement ages of mineralised intrusions, particularly those in the two metallogenic corridors (by U–Pb zircon, baddeleyite, and Sm–Nd); and (2) the ages of fault movements younger than 1830 Ma, to help constrain the uplift history of the intrusions (by Ar–Ar and Rb–Sr).
- Ascertain if all the mineralised group I intrusions are similar in age (as favoured by Hoatson) or if some, like the Eastmans Bore, Lamboo, and Big Ben intrusions, are much younger (i.e. intruding 1843 Ma Koongie Park Formation; see Lamboo entry in Chapter 2). Also, are the Corridor gabbro intrusions that are associated with granites of the 1865–1850 Ma Paperbark supersuite in the western zone much older than those associated with the granites of the 1835–1805 Ma Sally Downs supersuite in the western and central zones?

Geochemistry

- More comprehensive compositional studies of minerals across the total stratigraphic sequences, to document cryptic layering, parent magma composition, open versus closed fractionation systems, fluid dynamics of magma emplacement, and the importance of potential mineralisation processes, such as crustal contamination, crystal fractionation, and magma mixing.
- Detailed mineralogical (e.g. olivine and chromite composition) and structural studies, to ascertain if the group I intrusions along the western margin of the McIntosh intrusion represent tectonised fragments of a single intrusion or are separate unrelated bodies.
- Use S and Re–Os isotopes with trace-element geochemistry to assess the source of S (magmatic versus crustal) and the importance of crustal contamination in the Ni–Cu–Co sulphide-bearing intrusions of group V and in the Tickalara Metamorphics.

Acknowledgements

The authors would like to thank John Bain, Greg Ewers, Jim Jackson, Peter Southgate, and Shen-su Sun (all AGSO) for their constructive comments on earlier drafts of the manuscript.

APPENDICES

APPENDIX 1. ANALYTICAL PROCEDURES

1.1. X-ray fluorescence spectrometry (XRFS), atomic-absorption spectrophotometry (AAS), and inductively coupled plasma-mass spectrometry (ICP–MS) for major- and trace-element analysis

Major and trace elements were determined from 1992 to 1994 by X-ray fluorescence spectrometry (XRFS) and atomic-absorption spectrophotometry (AAS) at AGSO in Canberra. Instruments used were Philips PW1404 and PW1450 sequential X-ray spectrometers and a Varian AA-975 atomic absorption spectrophotometer. Ferrous oxide was determined by a titrimetric method, and gravimetric analysis was used to determine H_2O^+ and CO_2. The chemical techniques and the instrumental operating conditions used in the analyses are described by Cruikshank & Pyke (1993). In 1996 a number of samples were reanalysed for trace elements by inductively coupled plasma-mass spectrometry (ICP–MS). A brief summary of the procedures is given below.

Major-element oxides (SiO_2, TiO_2, Al_2O_3, Fe_2O_3 (total), MnO, MgO, CaO, K_2O, and P_2O_5) and S were determined by XRFS on glass fusion discs using the method of Norrish & Hutton (1969). Finely ground rock powder (0.36 g) was mixed with Norrish Formula flux (1.95 g - lithium tetraborate, lithium carbonate, and lanthanum oxide) and heated at 460°C for 15 minutes in an electric furnace to convert S^{2-} to SO_4^{2-}. The powder was fused into a homogeneous melt in a rocking furnace at a temperature of 1050°C and then pressed in a preheated (180°C) graphite platten, forming a glass disc measuring 1 by 30 mm. Matrix corrections, with alpha factors calculated for the rhodium tube, were applied to all major oxides. Calibration of the major oxides was against USGS and AGSO rock standards, using SiO_2 and CaO blanks. The USGS standards included: GSP—1(granodiorite), AGV—1(andesite), BCR—1(basalt), W—1(diabase), PCC—1(peridotite), and DTS—1(dunite).

A combined HF (10 mL, 40%)-$HClO_4$ (5 mL, 1:1) acid digestion on 0.4 g of rock powder was used for the atomic-absorption analysis of Na_2O. The analyte solution contained controlled amounts of HCl and K^+, and calibration was against identical solutions prepared from AGSO rock standards.

For the determination of FeO, a 0.5 g sample was digested in H_2SO_4 (10 mL, 1:3) and HF (5 mL, 40%) acid on a hotplate for 10 minutes. The digested solution was transferred into a beaker containing H_2O (300 mL), H_3BO_3 (15 g), and H_3PO_4 (10 mL, 1:1) before being titrated with standard $K_2Cr_2O_7$ solution (1 mL = 2.00 mg Fe^{2+}) using a Metrohm E536 potentiograph with a platinum reference electrode.

Moisture water (H_2O^-) was measured by determining the loss in weight of a sample dried for two hours at 110°C. Lattice water (H_2O^+) and CO_2 content were determined using the gravimetric method described by Hughes & Hannaker (1978). A 0.5 g powder sample was heated to 1100°C in a purified oxygen stream, with the evolved H_2O and CO_2 being trapped and weighed respectively on $MgClO_4.H_2O$ and soda-asbestos.

The trace elements (**As**, Ba, Ce, Cr, Cs, **Ga**, La, **Nb**, Nd, **Pb**, Pr, **Rb**, Sc, **Se**, **Sr**, **Th**, **U**, V, **Y**, and **Zr**) were determined by XRFS using pressed-powder pellets. A mixture of 12 g of sample powder and approximately 30 drops of 7% aqueous alcohol PVA binding agent was pressed into a 40 x 6 mm pellet using a Specac hydraulic press at 2 ton pressure. Molybdenum, rhodium, and gold target X-ray tubes were used to give optimum excitation for different groups of elements. The elements indicated above in bold were determined using a mass-absorption correction by the Compton Scatter method, whereas the determination of the other elements involved calculated mass-absorption coefficients. Count-rates were converted into element concentrations using a modification of the Norrish & Chappell (1977) method, and calibration was by synthetic standards with verification against international and AGSO secondary standards.

The trace elements Cu, Li, Ni, and Zn were determined by AAS after the digestion of a 1.0 g sample with HF (10 mL, 40%) and $HClO_4$ (6 mL, 1:1) on a waterbath. The solution was taken to dryness on a hotplate, taken up with HCl (10 mL, 1:1), made up to 50 mL, and analysed by AAS using direct calibration against standard solutions.

Estimated detection limits are given in Appendix Table 1.1. Those for elements determined by XRFS were based on the method of Jenkins & Vries (1967), which uses peak and background count rates. The detection limits given are twice these calculated theoretical values, and are considered to be more realistic. Detection limits for elements for which there are significant inter-element corrections (e.g. Ba, Ce, Sc, and Y) will probably be even higher. Those for AAS are for an absorbance of 0.004 (equivalent to 99% transmission).

The precision of the XRFS technique is generally good, as the effects of all but very short-term drift in machine response is effectively eliminated by ratioing each measurement to an internal monitor standard. The precision (1 standard deviation level) for major elements was better than ± 1% for concentrations greater than 5%, and for trace-element analyses was typically ± 3% at the 30 to 100 ppm level. The corresponding precision for AAS analyses was between ± 4% and ± 6%.

Accuracy was assessed by analysing international rock standards. Comparisons of XRFS and AAS results for two standard rocks (GSP–1 and BCR–1) are given in Appendix Table 1.2.

The ICP–MS analytical program included a number of elements formerly analysed by XRFS, plus and a number of additional elements, most notably a suite of Rare-Earth Elements. The instrument used was a Perkin Elmer Elan 6000 with AS–91 sample changer, and interfaced with a micro-computer running Perkin Elmer Elan software.

Samples were digested using a modification of the method of Eggins et al. (1997). Each sample (0.1g) was weighed into a 22 mL Savillex Teflon vessel and 5.00

mL of an internal standard solution containing a mix of enriched isotopes and low-abundance elements (Li–6, Ni–61, Rh, Sm–147, Tm and Tl), was added. This was evaporated to incipient dryness, and redistilled HNO_3 (2 mL) and HF (6 mL) were added. The vessel was capped tightly and then heated on a hotplate at 150°C overnight. The acid mixture was evaporated off, 6M HNO_3 (10 mL) was added, and the vessel capped and heated overnight. The acid was evaporated off and 6 mL of concentrated HNO_3, with a trace of HF, was added; the walls of the vessel were washed down with water. The vessel was then heated to dissolve the residue, and the resulting solution was transferred to a plastic 200 mL volumetric flask, and made up to a 1:2000 dilution in 2% HNO_3. Each batch of samples included a reagent blank and a number of international and secondary rock standards.

The spectrometer was optimised and factors for significant isobaric, double-ion and oxide interferences were estimated. The spectrometer was then calibrated against artificial solution standards and the samples analysed. A list of elements, detection limits, and analyses for RGM–1 and BHVO–1, is given in Appendix Table 1.2.

Precision was typically ± 2% at the high end of the mass range (e.g. U, Pb) and ± 3-4% at the low end (e.g. Li and Be).

Pt, Pd, and Au abundances of selected samples were determined by fire assay, lead concentration, and ICP–MS (method GS333 by Analabs Pty. Ltd., Welshpool, Western Australia), with detection limits 0.5 ppb Pt, 0.5 ppb Pd, and 1 ppb Au.

Appendix Table 1.1. Accuracy of XRFS and AAS data: comparison of analyses of standard rocks with the recommended values of Abbey (1983). Detection limits (in % or ppm) are shown in parenthesis after the element/oxide symbol.

	GSP–1 (see text)		BCR–1 (see text)	
	AGSO	Recommended	AGSO	Recommended
SiO_2 (0.006 %)	67.97 (0.29)[1]	67.32	54.42 (0.16)[1]	54.53
TiO_2 (0.008 %)	0.67 (0.004)[1]	0.66	2.26 (0.015)[1]	2.26
Al_2O_3 (0.007 %)	15.16 (0.08)[1]	15.28	13.51 (0.06)[1]	13.72
Fe_2O_3 (t) (0.005 %)	4.26 (0.016)[1]	4.28	13.39 (0.03)[1]	13.44
FeO (0.05 %)	2.25	2.32	8.89	8.96
MnO (0.004 %)	0.04	0.04	0.17	0.18
MgO (0.006 %)	0.99 (0.015)[1]	0.97	3.53 (0.012)[1]	3.48
CaO (0.0014 %)	1.97 (0.006)[1]	2.03	6.97 (0.06)[1]	6.97
Na_2O (0.02 %)	2.74	2.81	3.27 (0.05)[1]	3.30
K_2O (0.0004 %)	5.56 (0.012)[1]	5.51	1.71 (0.010)[1]	1.70
P_2O_5 (0.003 %)	0.28	0.28	0.36	0.36
Ba (4 ppm)	1300	1300	702	680
Li (1 ppm)	25	30	11	14
Rb (1 ppm)	253	250	46	47
Sr (2 ppm)	237	240	329	330
Pb (1 ppm)	54	54	14	14
Th (1 ppm)	104	105	6	6
U (0.5 ppm)	2.0	2.1	1.5	1.7
Zr (2 ppm)	507	500	187	185
Nb (1 ppm)	25	?23	13	?19
Y (2 ppm)	28	29	37	40
La (2 ppm)	165	195	29	27
Ce (2 ppm)	391	360	55	53
Nd (2 ppm)	187	?190	32	?26
Pr (3 ppm)	46	?50	4	?7
Sc (3 ppm)	8	7	31	33
V (2 ppm)	49	54	416	420
Cr (1 ppm)	11	12	6	15
Ni (2 ppm)	7	9	7	10
Cu (2 ppm)	30	33	17	16
Zn (1 ppm)	91	105	117	125
Ga (1 ppm)	24	23	21	22
As (0.5 ppm)	< 0.5	< 0.5	1.0	?0.8
S (12 ppm)	400	?300	400	?400
F (100 ppm)			500	500

[1] standard deviation. See text for elements analysed respectively by XRFS and AAS.

Appendix Table 1.2. Accuracy of ICP–MS data: comparison of analyses of standard rocks with recommended values of Govindaraju (1994). Detection limits (in ppm) are shown in parenthesis after the element symbol.

	RGM-1		BHVO-1	
	AGSO	Recommended	AGSO	Recommended
Li (0.5)	58.0	57	4.5	4.6
Ga (0.1)	16.4	15	22.0	21
Rb (0.5)	152	149	10.0	11
Sr (1.0)	101	108	392	403
Y (0.5)	23.5	25	26.9	27.6
Nb (0.1)	8.4	8.9	17.2	19
La (0.05)	23.3	24	15.7	15.8
Ce (0.05)	47.4	47	39.4	39
Pr (0.01)	5.25	4.7	5.34	5.7
Nd (0.01)	19.0	19	24.4	25.2
Sm (0.01)	3.9	4.3	6.08	6.2
Eu (0.01)	0.64	0.66	2.15	2.06
Tb (0.01)	0.57	0.66	0.92	0.96
Gd (0.01)	3.61	3.7	6.43	6.4
Dy (0.01)	3.65	4.08	5.34	5.2
Ho (0.01)	0.76	0.95	0.99	0.99
Er (0.01)	2.36	2.6	2.58	2.4
Yb (0.01)	2.49	2.6	2.00	2.02
Lu (0.01)	0.38	0.41	0.27	0.29
Pb (0.5)	23.5	24	2.0	2.6
Th (0.01)	14.3	15.1	1.19	1.08
U (0.01)	5.73	5.8	0.42	0.42

1.2. Electron probe microanalysis

Electron probe microanalyses of minerals from the East Kimberley intrusions were carried out by A.G. Trudu on a Cameca Camebax electron probe in energy dispersive mode at the Research School of Earth Sciences, Australian National University, Canberra. Accelerating voltage was 15 kV, beam current between 5 and 6 nA, and the counting time was 80 seconds per analysis. The San Carlos olivine standard was used to monitor calibration and adjust correction factors. A small number of olivine analyses were carried out by W. Jablonski on a Cameca electron probe at the Central Science Laboratory, University of Tasmania, under similar operating conditions to those above.

References

Abbey, S., 1983. Studies in 'standard samples' of silicate rocks and minerals, 1969-1982. Geological Survey of Canada, Paper 83, 15.

Cruikshank, B.I. & Pyke, J.G. 1993. Analytical methods used in Mineral and Land Use Program's geochemical laboratory. Australian Geological Survey Organisation, Record 1993/26, 22 pp.

Eggins, S.M., Woodhead, J.D., Kinsley, L.P.J., Mortimer, G.E., Sylvester, P., McCulloch, M.T., Hergt, J.M. & Handler, M.R., 1997. A simple method for the precise determination of >= 40 trace elements in geological samples by ICPMS using enriched isotope internal standardisation. Chemical Geology, 134, 311–326.

Govindaraju, K., 1994. 1994 compilation of working values and sample description for 383 geostandards. Geostandards Newsletter, 18, 1–158.

Hughes, T.C. & Hannaker, P., 1978. The determination of carbon and hydrogen in geological materials by thermal decomposition. Chemical Geology, 22, 331–339.

Jenkins, R. & De Vries, J.L., 1967. Practical x-ray spectrometry. Philips, Eindhoven, Macmillan Press Ltd, London, 181 pp.

Norrish, K. & Chappell, B., 1977. X-ray fluorescence spectrography. In: Zussman, J. (editor), Physical methods in determinative mineralogy, Academic Press, London, 161–214.

Norrish, K. & Hutton, J.T. 1969. An accurate X-ray spectrographic method for the analysis of a wide range of geological samples. Geochimica et Cosmochimica Acta, 33, 431–453.

APPENDIX 2. WHOLE-ROCK (MAJOR, TRACE, PGES) GEOCHEMICAL TABLES

Sample collection

Samples of 272 mafic and ultramafic rocks were collected for whole-rock geochemistry by D.M. Hoatson during the systematic regional mapping of the layered intrusions. Sample sites were located using a Global Positioning System (GPS) instrument (accuracy of ± 50 to 80 m) and 1:25 000 colour aerial photographs. Ten samples collected in 1983 were located using aerial photographs and topographic maps. Approximately 3 to 5 kg of material was obtained with a sledge hammer at about 50 to 100 m spacing along traverses across the major intrusions (including the type example of each intrusion group) and from random locations on the less significant intrusions. Strongly layered rocks with variable compositions at a hand specimen scale were avoided and any weathering surfaces or veins were removed in the field with a geological pick. The samples were analysed for 11 major-elements and 25 trace elements in the AGSO laboratories (see Appendix 1). Some mineralised and 'chilled' surface samples were also analysed for Pt, Pd, and Au and for Sm and Nd isotopes. Mineralised diamond drill core from the Panton and Sally Malay intrusions were sampled for trace-element and Sm–Nd and Re–Os isotopic analysis (see Chapter 12), and chromitites from several group I intrusions were sampled for trace-element analysis (see Chapter 13). Large (20 to 30 kg) samples of fractionated gabbro and anorthosite from the Panton, Springvale, Toby, and Sally Malay intrusions, and gabbro from the contact aureole of the McIntosh intrusion, were collected for U–Pb geochronology (see Chapter 6) by drilling and blasting fresh surface material.

The geochemical and field data can be purchased in digital or hard-copy formats from AGSO's geological databases, including whole-rock geochemistry (OZCHEM), structural and field data (OZROX), and geochronology (OZCHRON).

Explanation of attribute data and ratio used in the whole-rock geochemical tables

Sample no: Eight-digit, comprising year of collection (83, 92, 93, 94), BMR/AGSO project code (33 or 52), and four-digit sample number. Most samples are arranged in order of increasing sample number and stratigraphic height. The locations of the samples are given as Australian Map Grid (AMG) co-ordinates and in AGSO's geological database OZROX.

Intrusion: As indicated.

Group: Classification of intrusion from I to VII, Undivided gabbro, Corridor gabbro, Turkey Creek microgabbro-norite (see Chapter 5 for details of different groups).

Lithology: As indicated. Abbreviations used are amphibol = amphibolite, anorthos = anorthosite, biot = biotite, gabbronor = gabbronorite, hbl = hornblende, microgabb = microgabbro, mt = magnetite = mt, plg = plagioclase, qtz = quartz, suboph = subophitic.

Strat. ht (m): Estimated stratigraphic height in metres above the base of the intrusion. A traverse distance in metres is used for the Toby intrusion (*) since the true thickness of the stratigraphy could not be measured due to poor outcrop.

Easting & Northing: Sample locations are given as Australian Map Grid (AMG) co-ordinates comprising 6 digit easting and 7 digit northing.

Ratio used: mg = mg number = (100 x MgO/40.32)/(FeO/71.85 + Fe_2O_3/79.85 + MgO/40.32).

Sample number	92522018	92522023	92522037	92522044	92522046	92522068	92522072	92522073
Intrusion	Panton	Panton	Panton	Panton	Panton	West Panton	Panton	Panton
Group	I	I	I	I	I	I	I	I
Lithology	Chromitite	Chromitite	Chromitite	Chromitite	Chromitite	Chromitite	Hornblende quartz gabbro	Hornblende quartz gabbro
Strat. ht (m)	-	-	-	-	-	-	1	3
Easting	376240	377150	377860	375700	376640	374460	375790	375790
Northing	8036550	8037230	8039120	8035000	8035980	8035570	8037070	8037070
SiO2	6.81	12.44	10.84	15.88	17.61	15.99	53.09	52.52
TiO2	0.58	0.18	0.67	1.34	0.73	0.56	1.30	1.55
Al2O3	16.39	5.42	13.91	19.93	21.77	18.31	12.82	12.25
Fe2O3	21.82	8.22	23.65	21.18	21.07	19.72	2.68	2.79
FeO	0.73	0.95	1.07	4.72	3.98	1.93	11.58	12.81
MnO	0.42	0.16	0.35	0.38	0.48	0.35	0.18	0.18
MgO	13.15	25.15	14.15	11.68	10.04	14.15	4.51	4.15
CaO	0.03	10.01	0.04	2.39	3.84	1.50	8.24	8.33
Na2O	0.02	0.02	0.01	0.27	0.44	0.08	2.63	2.67
K2O	<0.01	<0.01	<0.01	0.04	0.09	0.03	0.51	0.34
P2O5	<0.01	0.01	<0.01	0.01	0.02	0.02	0.14	0.15
LOI	1.30	27.23	2.78	2.59	1.28	3.05	1.93	1.65
Rest	15.10	9.10	15.37	15.12	15.16	15.10	0.19	0.20
Total	76.35	98.89	82.84	95.53	96.51	90.79	99.80	99.59
O=F,S,Cl	0.00	0.00	0.00	0.00	0.00	0.00	0.00	0.00
Total	76.34	98.89	82.84	95.53	96.51	90.79	99.80	99.59
	Trace elements in parts per million							
Ba	<4	7	<4	<4	21	43	119	59
Li	-	2	2	1	3	4	11	12
Rb	<1	<1	<1	<1	2	2	12	3
Sr	3	31	3	8	17	10	130	123
Pb	5	<2	7	<2	<2	4	7	6
Th	<2	<2	<2	<2	<2	<2	5	5
U	<0.5	<0.5	<0.5	2.5	<0.5	<0.5	2.5	2
Zr	5	7	15	11	7	13	108	109
Nb	<2	<2	<2	<2	<2	<2	5	6
Y	<1	1	1	3	<1	3	35	35
La	4	<2	9	9	4	7	6	8
Ce	6	6	10	22	10	8	19	19
Nd	6	<2	4	6	2	3	10	11
Pr	3	<2	<2	<2	2	4	5	6
Sc	8	14	11	13	15	12	49	55
V	934	301	755	1321	1447	807	432	584
Cr	>99999	60829	>99999	>99999	>99999	>99999	102	23
Ni	971	827	2986	855	924	1512	61	52
Cu	272	44	164	10	1	142	41	37
Zn	1037	251	1519	1160	1187	828	95	116
Ga	40	13	35	51	61	38	17	16
As	34	1.5	56	4	1.5	15	0.5	<0.5
S	60	10	50	<10	<10	40	20	50
Cs	<3	<3	<3	<3	<3	<3	<3	<3
Se	1	<1	<1	<1	<1	<1	<1	<1
	Trace elements in parts per billion							
Pd	2375	171	793	-	67.4	142	1	-
Pt	2850	181	762	-	202	75.7	1.4	-
Au	153	14	99	-	4	7	2	-
εNd	-	-	-	-	-	-	-	0.4
mg	53.5	84.3	53.0	46.7	43.8	56.2	36.5	32.6

Sample number	92522074	92522075	92522076	92522077	92522078	92522079	92522080	92522081
Intrusion	Panton	Panton	Panton	Panton	Panton	Panton	Panton	Panton
Group	I	I	I	I	I	I	I	I
Lithology	Dunite	Dunite	Dunite	Dunite	Dunite	Dunite	Dunite	Peridotite
Strat. ht (m)	10	80	100	130	190	240	280	360
Easting	376050	375960	375940	375970	375990	376010	376020	376000
Northing	8037150	8037100	8037070	8037000	8036920	8036940	8036860	8036820
SiO2	43.87	40.48	39.34	34.72	33.89	35.33	36.78	39.79
TiO2	0.43	0.30	0.24	0.12	0.12	0.14	0.13	0.01
Al2O3	8.27	4.86	4.17	2.17	2.37	2.31	2.39	19.11
Fe2O3	2.85	3.36	3.88	9.32	9.05	8.98	10.39	1.06
FeO	8.74	6.99	6.43	1.95	2.76	2.40	1.99	5.98
MnO	0.17	0.14	0.13	0.14	0.15	0.13	0.14	0.09
MgO	23.81	31.23	32.67	33.46	32.52	33.39	32.84	16.34
CaO	3.43	3.59	2.98	1.39	1.96	1.25	0.47	10.39
Na2O	0.10	0.15	0.09	0.01	0.01	<0.02	0.01	1.59
K2O	0.02	0.03	0.05	<0.01	0.01	<0.01	<0.01	0.27
P2O5	0.04	0.04	0.03	0.01	0.01	0.01	0.01	0.01
LOI	7.51	7.98	9.01	15.84	16.12	15.19	14.06	4.57
Rest	0.65	1.12	1.28	1.05	1.35	1.12	1.11	0.58
Total	99.89	100.27	100.30	100.18	100.32	100.25	100.32	99.79
O=F,S,Cl	0.00	0.08	0.09	0.00	0.00	0.00	0.00	0.01
Total	99.89	100.20	100.22	100.18	100.32	100.25	100.32	99.78
Trace elements in parts per million								
Ba	9	13	11	8	<4	<4	<4	66
Li	10	7	4	2	2	3	2	33
Rb	1	2	3	<1	<1	<1	<1	4
Sr	16	44	28	10	34	15	2	309
Pb	4	5	7	<2	<2	3	<2	6
Th	<2	<2	<2	<2	<2	<2	<2	<2
U	1.0	1.0	<0.5	<0.5	<0.5	<0.5	1.0	<0.5
Zr	40	26	22	9	9	11	9	2
Nb	3	<2	<2	2	<2	<2	<2	<2
Y	12	7	6	3	4	4	3	<1
La	<2	<2	2	<2	<2	<2	<2	2
Ce	7	8	10	6	<5	<5	<5	<5
Nd	<2	3	<2	<2	<2	<2	<2	<2
Pr	2	<2	<2	<2	2	<2	<2	<2
Sc	21	17	14	10	10	10	7	12
V	141	93	84	54	65	58	49	28
Cr	3072	4443	5149	4697	6022	4742	4731	2661
Ni	893	1918	2164	2297	2426	2479	2506	632
Cu	204	272	338	343	886	625	595	149
Zn	86	52	48	43	79	52	47	116
Ga	8	4	4	2	2	2	1	8
As	14	1.5	<0.5	14	150	32	2.0	5.5
S	20	1530	1750	80	30	80	40	190
Cs	<3	<3	<3	<3	<3	<3	<3	<3
Se	<1	<1	1	<1	<1	<1	<1	<1
Trace elements in parts per billion								
Pd	-	-	151	-	112	37	-	-
Pt	-	-	148	-	120	53.8	-	-
Au	-	-	70	-	119	36	-	-
εNd	-	-	-	-	-	-	-	-
mg	79.0	84.8	85.4	85.2	84.2	85.0	83.8	80.8

Sample number	92522082	92522083	92522084	92522085	92522086	92522087	92522088	92522089
Intrusion	Panton	Panton	Panton	Panton	Panton	Panton	Panton	Panton
Group	I	I	I	I	I	I	I	I
Lithology	Plg peridotite	Plg peridotite	Dunite	Dunite	Chromitite	Dunite	Dunite	Gabbronor.
Strat. ht (m)	375	420	440	480	550	600	640	670
Easting	376050	376100	376100	376100	376240	376200	376200	376160
Northing	8036770	8036730	8036700	8036700	8036550	8036600	8036600	8036560
SiO2	38.12	41.98	41.74	35.00	10.44	39.24	39.67	41.33
TiO2	0.03	0.03	0.01	0.09	0.57	0.03	0.06	0.05
Al2O3	15.20	21.82	18.58	4.33	15.00	15.97	12.81	18.91
Fe2O3	2.35	0.72	3.22	5.87	20.39	1.43	2.10	1.55
FeO	6.11	3.76	2.98	7.18	0.55	6.25	6.98	4.86
MnO	0.08	0.05	0.07	0.18	0.33	0.08	0.11	0.08
MgO	21.81	14.31	19.08	34.15	14.63	20.38	24.39	16.70
CaO	6.93	11.32	10.49	1.90	0.05	8.31	6.91	10.33
Na2O	1.02	0.86	1.01	0.05	0.01	1.27	0.67	0.75
K2O	0.11	0.08	0.08	0.01	0.01	0.27	0.08	0.08
P2O5	0.01	0.02	0.01	0.01	<0.01	0.01	0.01	0.02
LOI	7.01	4.55	2.19	8.96	2.77	6.25	5.37	4.68
Rest	1.04	0.41	0.42	2.06	15.08	0.39	0.67	0.50
Total	99.82	99.91	99.88	99.79	79.83	99.88	99.83	99.84
O=F,S,Cl	0.05	0.02	0.03	0.03	0.00	0.00	0.05	0.03
Total	99.76	99.88	99.85	99.76	79.82	99.87	99.78	99.81
Trace elements in parts per million								
Ba	24	7	55	<4	<4	38	7	50
Li	10	23	8	4	1	10	8	11
Rb	<1	2	<1	<1	<1	2	<1	<1
Sr	39	138	68	11	2	80	49	119
Pb	6	12	46	3	9	<2	<2	<2
Th	<2	<2	<2	<2	<2	<2	<2	<2
U	<0.5	<0.5	<0.5	0.5	0.5	<0.5	0.5	<0.5
Zr	3	5	4	5	6	2	5	4
Nb	<2	<2	<2	<2	<2	<2	<2	<2
Y	<1	<1	<1	2	2	<1	1	2
La	<2	<2	<2	<2	11	<2	6	<2
Ce	<5	<5	<5	<5	<5	<5	<5	<5
Nd	<2	<2	<2	<2	4	<2	<2	3
Pr	<2	2	<2	<2	<2	<2	<2	<2
Sc	10	13	14	9	8	9	12	15
V	37	28	18	56	745	16	23	35
Cr	5194	879	995	11600	>99999	1622	2873	2203
Ni	812	369	403	2172	1174	632	704	403
Cu	267	144	188	13	218	251	242	150
Zn	80	1033	925	87	1020	26	77	35
Ga	8	13	10	5	35	7	6	10
As	3.5	3.5	<0.5	4.0	33.5	14.5	5.0	28.0
S	1080	500	590	530	50	100	1000	640
Cs	<3	<3	<3	<3	<3	<3	<3	<3
Se	<1	1	<1	<1	2	<1	<1	<1
Trace elements in parts per billion								
Pd	-	-	-	-	2470	-	-	-
Pt	-	-	-	-	2565	-	-	-
Au	-	-	-	-	115	-	-	-
εNd	-	-	-	-	-	-	-	-
mg	82.5	85.3	85.3	83.0	58.0	82.8	83.1	82.6

Sample number	92522090	92522091	92522092	92522093	92522094	92522095	92522096	92522097
Intrusion	Panton	Panton	Panton	Panton	Panton	Panton	Panton	Panton
Group	I	I	I	I	I	I	I	I
Lithology	Gabbronor.	Gabbro	Gabbro	Gabbro	Norite	Gabbro	Gabbro	Gabbro
Strat. ht (m)	720	780	820	900	980	1020	1060	1080
Easting	376160	376160	376260	376310	376310	376440	376440	376440
Northing	8036560	8036560	8036380	8036380	8036380	8036230	8036230	8036190
SiO2	44.92	49.47	49.71	42.92	45.63	43.48	47.82	44.80
TiO2	0.08	0.12	0.13	0.08	0.08	0.06	0.10	0.12
Al2O3	18.65	16.57	15.79	19.53	18.17	21.05	18.24	14.62
Fe2O3	0.91	0.37	0.27	0.78	1.42	2.05	0.40	1.20
FeO	4.02	5.29	5.78	5.80	5.24	3.99	5.61	5.75
MnO	0.07	0.11	0.11	0.09	0.10	0.09	0.10	0.11
MgO	12.68	12.88	13.44	13.93	15.80	11.87	13.49	15.49
CaO	14.30	12.05	11.74	11.43	10.12	13.23	10.87	12.65
Na2O	0.81	0.73	0.70	0.83	0.76	0.75	0.72	0.67
K2O	0.06	0.04	0.04	0.08	0.07	0.06	0.03	0.12
P2O5	0.02	0.02	0.01	0.02	0.02	0.02	0.01	0.02
LOI	2.93	1.92	1.98	4.21	2.22	2.07	2.41	3.78
Rest	0.43	0.44	0.41	0.33	0.37	1.00	0.32	0.44
Total	99.88	100.01	100.11	100.03	100.00	99.72	100.12	99.77
O=F,S,Cl	0.03	0.04	0.03	0.03	0.02	0.04	0.00	0.02
Total	99.85	99.98	100.08	100.00	99.98	99.68	100.12	99.75
Trace elements in parts per million								
Ba	14	9	8	14	12	15	11	16
Li	5	8	5	9	7	4	7	4
Rb	1	<1	<1	1	<1	<1	<1	2
Sr	112	105	94	140	114	169	142	77
Pb	<2	<2	<2	<2	<2	2	<2	<2
Th	2	<2	<2	<2	<2	<2	<2	<2
U	<0.5	<0.5	1.0	<0.5	<0.5	<0.5	<0.5	<0.5
Zr	3	6	5	7	5	3	6	6
Nb	<2	<2	<2	<2	<2	<2	<2	<2
Y	2	2	3	2	3	2	2	4
La	2	<2	<2	3	<2	<2	5	<2
Ce	6	5	<5	<5	<5	<5	<5	<5
Nd	<2	<2	<2	<2	<2	<2	<2	<2
Pr	<2	<2	<2	<2	<2	<2	<2	<2
Sc	31	38	40	20	21	24	29	37
V	77	88	99	44	52	86	75	105
Cr	1804	1837	1744	1132	1574	5447	1633	1937
Ni	311	223	228	411	440	375	258	434
Cu	169	211	128	110	43	190	2	181
Zn	22	30	35	44	53	53	24	42
Ga	10	11	10	12	12	12	13	9
As	33	12	1.0	<0.5	<0.5	<0.5	<0.5	<0.5
S	560	730	650	560	350	840	20	340
Cs	<3	<3	<3	<3	<3	<3	<3	<3
Se	<1	<1	<1	<1	<1	1	<1	<1
Trace elements in parts per billion								
Pd	-	-	-	-	-	-	-	-
Pt	-	-	-	-	-	-	-	-
Au	-	-	-	-	-	-	-	-
εNd	-	-	-	-	-	-	-	-
mg	82.4	80.3	79.9	79.2	81.2	78.4	80.1	80.2

Sample number	92522098	92522099	92522100	92522101	92522102	92522103	92522104	92522105
Intrusion	Panton	Panton	Panton	Panton	Panton	Panton	Panton	Panton
Group	I	I	I	I	I	I	I	I
Lithology	Gabbro	Gabbro	Gabbro	Dunite	Wehrlite	Gabbro	Gabbro	Gabbro
Strat. ht (m)	1120	1160	1180	1240	1280	1300	1320	1330
Easting	376370	376370	376390	376360	376380	376380	376360	376360
Northing	8036170	8036170	8036060	8036010	8035910	8035910	8035820	8035820
SiO2	46.35	46.85	43.24	40.07	39.00	50.41	49.65	48.91
TiO2	0.11	0.12	0.08	0.20	0.12	0.29	0.35	0.29
Al2O3	17.50	17.99	24.01	9.25	11.64	12.48	15.34	11.37
Fe2O3	1.31	1.00	0.83	6.02	4.09	1.00	0.95	1.32
FeO	4.05	4.22	4.78	6.60	8.71	6.15	4.97	6.35
MnO	0.09	0.08	0.08	0.09	0.12	0.11	0.10	0.13
MgO	12.45	11.65	9.58	23.92	22.69	13.94	10.03	13.71
CaO	14.66	15.09	12.80	5.75	5.39	12.07	15.63	14.12
Na2O	0.82	0.82	0.83	0.03	0.09	0.75	0.75	0.54
K2O	0.07	0.09	0.06	<0.01	0.02	0.06	0.08	0.21
P2O5	0.02	0.01	0.02	0.02	0.01	0.03	0.03	0.03
LOI	2.06	1.98	3.13	7.34	7.95	2.10	1.61	2.29
Rest	0.39	0.28	0.57	0.85	0.41	0.56	0.46	0.34
Total	99.88	100.18	100.01	100.14	100.24	99.95	99.95	99.61
O=F,S,Cl	0.03	0.03	0.03	0.00	0.00	0.05	0.04	0.03
Total	99.86	100.15	99.98	100.14	100.24	99.91	99.92	99.58
Trace elements in parts per million								
Ba	34	23	17	<4	<4	7	26	14
Li	4	2	6	1	<1	8	4	4
Rb	2	2	1	<1	<1	<1	<1	4
Sr	128	103	196	4	8	78	107	84
Pb	<2	<2	<2	<2	<2	2	3	2
Th	<2	<2	<2	<2	<2	<2	<2	<2
U	<0.5	<0.5	<0.5	<0.5	<0.5	<0.5	<0.5	<0.5
Zr	5	7	6	11	5	17	25	15
Nb	<2	<2	<2	<2	<2	<2	<2	<2
Y	4	5	1	5	3	8	10	10
La	4	<2	<2	<2	<2	<2	<2	<2
Ce	7	<5	<5	8	<5	11	10	5
Nd	2	<2	<2	<2	<2	2	4	4
Pr	<2	4	2	<2	<2	<2	<2	3
Sc	39	45	17	19	14	58	63	66
V	105	116	55	96	66	214	228	235
Cr	1634	930	2605	4745	2071	2460	1784	1156
Ni	273	206	391	952	613	159	134	155
Cu	134	95	209	32	15	154	209	136
Zn	24	27	26	36	90	49	48	49
Ga	10	13	17	7	9	10	11	8
As	<0.5	<0.5	<0.5	<0.5	<0.5	<0.5	<0.5	<0.5
S	510	550	690	20	30	920	790	540
Cs	<3	<3	<3	<3	<3	<3	<3	<3
Se	<1	<1	<1	<1	<1	<1	<1	<1
Trace elements in parts per billion								
Pd	-	-	-	-	-	-	-	-
Pt	-	-	-	-	-	-	-	-
Au	-	-	-	-	-	-	-	-
εNd	-	-	-	-	-	-	-	-
mg	80.9	80.2	75.5	78.0	76.5	77.9	75.4	76.4

Sample number	92522106	92522107	92522108	92522109	92522110	92522111	92522112	92522113
Intrusion	Panton	Panton	Panton	Panton	Panton	Panton	Panton	Panton
Group	I	I	I	I	I	I	I	I
Lithology	Anorthos.	Anorthos.	Anorthos.	Anorthos.	Mt hbl gabbro	Mt hbl gabbro	Anorthos.	Gabbro
Strat. ht (m)	1400	1420	1480	1490	1500	1510	1520	1530
Easting	376340	376340	376340	375930	375930	376030	375120	375120
Northing	8035800	8035800	8035720	8035160	8035160	8035180	8033630	8033630
SiO2	48.01	47.53	47.12	46.67	42.53	41.86	46.46	41.43
TiO2	0.33	0.36	0.29	0.36	2.07	1.83	0.24	0.06
Al2O3	28.53	28.74	28.58	27.20	12.77	17.73	29.17	15.93
Fe2O3	0.68	1.19	1.25	1.52	5.21	4.67	0.63	3.73
FeO	1.81	2.18	2.42	3.92	13.36	12.00	2.55	7.52
MnO	0.03	0.04	0.03	0.07	0.19	0.14	0.03	0.13
MgO	2.29	1.44	1.84	2.51	8.15	6.21	2.45	18.05
CaO	14.95	15.09	15.31	13.63	11.63	11.46	15.23	8.63
Na2O	2.33	2.33	1.87	2.32	0.99	1.39	1.55	0.65
K2O	0.06	0.12	0.16	0.12	0.35	0.20	0.26	0.13
P2O5	0.06	0.05	0.05	0.06	0.05	0.05	0.04	0.02
LOI	0.93	0.93	1.07	1.42	2.18	1.92	1.40	3.61
Rest	0.11	0.10	0.08	0.13	0.42	0.42	0.10	0.09
Total	100.12	100.10	100.07	99.93	99.90	99.88	100.11	99.98
O=F,S,Cl	0.01	0.01	0.00	0.00	0.00	0.03	0.01	0.01
Total	100.11	100.09	100.07	99.92	99.90	99.85	100.10	99.97
Trace elements in parts per million								
Ba	36	53	48	88	55	17	79	27
Li	6	6	7	9	14	23	7	3
Rb	2	1	9	5	5	2	15	3
Sr	277	245	269	326	110	222	244	98
Pb	6	4	3	6	2	<2	3	<2
Th	2	3	<2	<2	<2	<2	<2	<2
U	<0.5	1.0	<0.5	<0.5	1.5	<0.5	0.5	<0.5
Zr	37	33	32	27	34	31	24	8
Nb	3	<2	<2	<2	<2	<2	<2	<2
Y	7	9	9	8	14	10	7	2
La	5	<2	5	6	4	8	5	<2
Ce	13	12	13	11	9	8	9	<5
Nd	6	6	6	4	<2	4	5	<2
Pr	3	<2	3	<2	<2	<2	<2	3
Sc	23	25	25	20	71	43	18	15
V	76	102	75	170	1737	1415	55	28
Cr	48	3	27	16	129	44	6	47
Ni	42	34	13	36	156	88	30	272
Cu	27	40	5	97	40	237	16	9
Zn	14	19	21	41	131	77	15	70
Ga	20	21	22	26	18	22	21	10
As	<0.5	<0.5	<0.5	<0.5	<0.5	<0.5	<0.5	<0.5
S	270	200	60	60	70	590	270	110
Cs	<3	<3	<3	<3	<3	<3	8	<3
Se	<1	<1	<1	<1	<1	<1	<1	<1
Trace elements in parts per billion								
Pd	-	-	-	-	-	-	-	-
Pt	-	-	-	-	-	-	-	-
Au	-	-	-	-	-	-	-	-
εNd	-	-	-	-	-	-	-	-
mg	62.8	44.1	48.1	45.8	44.6	40.6	58.3	74.7

Sample number	92522114	92522115	92522116	92522205	92522206	92522207	92522242	92522267
Intrusion	Panton	Panton	Highway	McIntosh	McIntosh	McIntosh	McIntosh	McIntosh
Group	I	I	I	VI	VI	VI	VI	VI
Lithology	Anorthos.	Mt hbl gabbro	Anorthos.	Magnetite gabbro	Magnetite gabbro	Mt olivine gabbronor.	Olivine gabbronor.	Chilled gabbro
Strat. ht (m)	1540	1550	-	7540	7710	7790	6890	1
Easting	375170	375250	373290	384500	384660	384660	384200	383140
Northing	8033610	8033470	8036880	8043350	8043860	8044060	8041500	8033950
SiO2	46.57	46.22	48.25	47.90	48.72	48.29	51.09	48.30
TiO2	0.11	1.98	0.44	1.44	0.42	0.29	0.20	0.79
Al2O3	31.61	15.13	26.50	17.17	18.97	20.63	19.50	15.44
Fe2O3	0.89	4.18	0.90	3.75	1.46	1.00	1.30	1.72
FeO	0.89	11.80	2.49	7.97	5.41	5.93	4.14	9.13
MnO	0.02	0.19	0.05	0.14	0.10	0.10	0.09	0.16
MgO	0.74	5.43	2.32	6.92	8.13	8.31	7.92	9.02
CaO	16.94	10.26	13.75	11.00	13.34	11.97	12.17	11.07
Na2O	1.40	1.72	2.62	2.32	2.16	2.16	2.45	1.42
K2O	0.07	0.40	0.26	0.11	0.09	0.10	0.09	0.09
P2O5	0.03	0.08	0.11	0.02	0.03	0.03	0.02	0.02
LOI	0.85	2.08	2.14	0.72	0.65	0.72	0.53	2.21
Rest	0.07	0.28	0.11	0.33	0.23	0.20	0.20	0.30
Total	100.19	99.75	99.94	99.79	99.71	99.73	99.70	99.67
O=F,S,Cl	0.00	0.00	0.00	0.08	0.03	0.03	0.04	0.06
Total	100.19	99.75	99.93	99.71	99.69	99.71	99.66	99.61
Trace elements in parts per million								
Ba	52	53	80	43	48	54	54	28
Li	4	17	10	4	4	3	4	8
Rb	1	6	10	<1	2	1	<1	<1
Sr	296	152	301	322	376	403	365	179
Pb	3	4	4	<2	<2	<2	<2	<2
Th	<2	2	<2	<2	<2	<2	<2	<2
U	<0.5	1.5	<0.5	<0.5	<0.5	<0.5	<0.5	1.0
Zr	10	63	35	7	10	7	5	12
Nb	<2	<2	<2	<2	<2	<2	<2	<2
Y	4	19	9	5	7	5	5	12
La	<2	4	6	3	3	<2	<2	<2
Ce	6	14	12	<5	11	8	<5	<5
Nd	<2	8	7	<2	5	5	<2	<2
Pr	<2	<2	<2	<2	<2	<2	<2	3
Sc	20	59	28	48	41	27	38	48
V	35	960	134	417	98	58	68	289
Cr	16	13	29	162	457	292	154	301
Ni	4	35	21	34	99	113	89	114
Cu	19	217	1	60	94	84	86	97
Zn	11	124	31	63	38	41	28	77
Ga	23	20	20	18	15	15	16	15
As	<0.5	<0.5	<0.5	<0.5	<0.5	<0.5	<0.5	<0.5
S	70	40	50	1590	550	540	770	1290
Cs	<3	<3	7	3	<3	<3	<3	<3
Se	<1	<1	<1	<1	<1	<1	<1	<1
Trace elements in parts per billion								
Pd	-	-	-	2.3	-	-	-	1.1
Pt	-	-	-	4.8	-	-	-	2.2
Au	-	-	-	4	-	-	-	1
εNd	-	-	-	-	-	-	-	-
mg	43.8	38.3	55.6	52.1	68.3	68.4	72.7	60.1

Sample number	92522268	92522269	92522270	92522271	92522272	92522273	92522274	92522275
Intrusion	McIntosh	McIntosh	McIntosh	McIntosh	McIntosh	McIntosh	McIntosh	McIntosh
Group	VI	VI	VI	VI	VI	VI	VI	VI
Lithology	Troctolite	Olivine gabbronor.	Olivine gabbronor.	Olivine gabbronor.	Gabbro	Olivine gabbronor.	Magnetite gabbronor.	Olivine gabbronor.
Strat. ht (m)	250	520	770	850	930	1100	1330	1470
Easting	383320	383450	383660	383740	383740	383860	383370	383310
Northing	8034250	8034540	8034750	8034780	8034780	8035050	8035400	8035690
SiO2	42.58	41.20	42.84	41.93	44.94	45.26	47.31	48.12
TiO2	0.17	0.13	0.12	0.21	0.11	0.11	1.10	0.29
Al2O3	9.02	6.27	12.62	6.90	22.60	21.62	17.57	15.74
Fe2O3	1.96	2.58	1.59	2.74	0.83	0.77	1.95	1.21
FeO	13.15	14.33	9.10	11.02	4.36	5.47	8.84	5.84
MnO	0.19	0.21	0.13	0.18	0.06	0.08	0.15	0.11
MgO	22.70	27.67	21.64	26.47	9.31	11.55	7.87	11.39
CaO	7.16	4.79	7.69	6.20	11.50	11.21	11.74	14.75
Na2O	0.85	0.52	0.94	0.60	1.87	1.67	1.86	1.05
K2O	0.05	0.04	0.05	0.07	0.15	0.08	0.04	0.03
P2O5	0.03	0.02	0.02	0.03	0.02	0.03	0.02	0.02
LOI	1.99	2.18	2.93	3.25	4.09	1.86	1.10	0.81
Rest	0.28	0.22	0.22	0.31	0.13	0.14	0.24	0.35
Total	100.13	100.16	99.89	99.91	99.97	99.85	99.79	99.71
O=F,S,Cl	0.04	0.02	0.02	0.04	0.00	0.01	0.05	0.04
Total	100.09	100.14	99.87	99.86	99.97	99.84	99.75	99.67
Trace elements in parts per million								
Ba	21	23	28	23	43	37	23	26
Li	4	4	4	4	11	5	4	3
Rb	<1	1	<1	2	5	1	<1	<1
Sr	138	110	201	114	419	283	239	306
Pb	<2	<2	<2	2	3	<2	<2	<2
Th	<2	<2	<2	<2	<2	<2	<2	<2
U	<0.5	<0.5	<0.5	1.0	<0.5	<0.5	<0.5	<0.5
Zr	10	8	9	15	7	10	9	9
Nb	<2	<2	<2	<2	<2	<2	<2	<2
Y	5	4	3	6	3	3	13	8
La	2	<2	4	<2	<2	4	4	3
Ce	<5	<5	6	6	<5	<5	9	6
Nd	<2	<2	<2	4	<2	<2	3	<2
Pr	<2	<2	<2	<2	<2	<2	<2	<2
Sc	26	18	17	25	17	16	43	45
V	64	47	35	64	35	26	272	142
Cr	301	170	290	425	101	99	199	999
Ni	641	773	605	670	271	361	79	220
Cu	121	64	62	181	12	11	52	114
Zn	99	119	71	90	38	44	80	43
Ga	5	4	8	4	12	12	18	11
As	<0.5	<0.5	<0.5	<0.5	<0.5	<0.5	<0.5	<0.5
S	870	460	380	870	40	190	910	760
Cs	<3	4	<3	<3	<3	<3	<3	<3
Se	<1	<1	<1	<1	<1	<1	<1	<1
Trace elements in parts per billion								
Pd	-	-	-	-	-	-	-	-
Pt	-	-	-	-	-	-	-	-
Au	-	-	-	-	-	-	-	-
εNd	-	-	-	-	-	-	-	-
mg	73.1	74.8	78.5	77.8	76.5	77.0	57.0	74.6

Sample number	92522276	92522277	92522278	92522279	92522280	92522281	92522282	92522283
Intrusion	McIntosh	McIntosh	McIntosh	McIntosh	McIntosh	McIntosh	McIntosh	McIntosh
Group	VI	VI	VI	VI	VI	VI	VI	VI
Lithology	Olivine gabbro	Olivine gabbro	Olivine gabbronor.	Troctolite	Troctolite	Olivine gabbro	Troctolite	Olivine gabbro
Strat. ht (m)	1575	1680	1835	1915	2550	2900	3245	3400
Easting	383350	383370	383410	383380	383160	383210	383180	383270
Northing	8035940	8036120	8036390	8036640	8036760	8037100	8037360	8037450
SiO2	45.91	47.59	47.33	45.39	46.74	46.21	45.97	47.05
TiO2	0.09	0.27	0.19	0.05	0.10	0.05	0.06	0.11
Al2O3	25.13	19.36	17.54	24.62	26.89	27.04	27.25	24.80
Fe2O3	0.96	1.07	1.05	0.73	1.07	0.84	0.72	0.78
FeO	3.31	4.11	4.83	4.50	2.30	2.67	2.95	2.80
MnO	0.06	0.08	0.09	0.06	0.04	0.04	0.04	0.05
MgO	7.41	9.28	12.17	8.54	4.65	4.78	5.03	6.29
CaO	13.64	15.04	13.70	12.81	14.92	14.50	14.23	15.59
Na2O	1.60	1.35	1.09	1.57	1.72	1.78	1.78	1.42
K2O	0.05	0.07	0.03	0.05	0.06	0.05	0.07	0.06
P2O5	0.02	0.02	0.02	0.02	0.02	0.02	0.02	0.02
LOI	1.57	1.23	1.22	1.32	1.18	1.78	1.59	0.78
Rest	0.14	0.37	0.31	0.13	0.15	0.12	0.11	0.20
Total	99.89	99.84	99.57	99.79	99.83	99.88	99.82	99.95
O=F,S,Cl	0.01	0.03	0.04	0.01	0.02	0.01	0.01	0.01
Total	99.88	99.81	99.53	99.78	99.82	99.87	99.81	99.94
Trace elements in parts per million								
Ba	41	69	21	33	44	43	37	35
Li	4	5	3	5	6	4	3	4
Rb	<1	1	<1	<1	<1	<1	<1	1
Sr	428	373	347	355	373	382	394	371
Pb	<2	<2	<2	<2	<2	<2	<2	<2
Th	<2	<2	<2	<2	<2	<2	<2	<2
U	<0.5	<0.5	<0.5	<0.5	<0.5	<0.5	<0.5	0.5
Zr	4	10	8	3	5	3	3	7
Nb	<2	<2	<2	<2	<2	<2	<2	<2
Y	2	8	6	<1	3	<1	1	4
La	<2	<2	3	<2	<2	<2	4	4
Ce	6	6	10	<5	6	<5	7	10
Nd	3	<2	<2	<2	3	<2	<2	2
Pr	2	<2	2	<2	<2	<2	<2	<2
Sc	18	37	34	17	22	20	17	28
V	25	95	86	16	28	20	14	45
Cr	149	1271	764	157	191	120	59	529
Ni	240	241	293	183	98	105	133	132
Cu	9	107	102	45	45	28	40	73
Zn	30	32	35	31	21	20	24	21
Ga	14	12	11	14	17	18	18	16
As	<0.5	<0.5	<0.5	<0.5	<0.5	<0.5	<0.5	<0.5
S	130	590	730	160	320	170	180	280
Cs	<3	<3	<3	<3	<3	<3	<3	<3
Se	<1	<1	<1	<1	<1	<1	<1	<1
Trace elements in parts per billion								
Pd	-	-	-	-	-	-	-	-
Pt	-	-	-	-	-	-	-	-
Au	-	-	-	-	-	-	-	-
εNd	-	-	-	-	-	-	-	-
mg	76.0	76.5	79.0	74.7	71.7	70.8	71.4	76.2

Sample number	92522284	92522285	92522286	92522287	92522288	92522289	92522290	92522291
Intrusion	McIntosh	McIntosh	McIntosh	McIntosh	McIntosh	McIntosh	McIntosh	McIntosh
Group	VI	VI	VI	VI	VI	VI	VI	VI
Lithology	Olivine gabbro	Olivine gabbro	Olivine gabbro	Olivine gabbro	Olivine gabbronor.	Olivine gabbro	Olivine gabbro	Olivine gabbro
Strat. ht (m)	3525	3700	3945	4090	4245	4395	4525	4740
Easting	383360	383430	383500	383650	383660	383700	383690	383680
Northing	8037620	8037750	8037920	8038130	8038220	8038510	8038670	8038800
SiO2	45.44	45.95	46.56	47.12	47.61	48.07	48.92	47.07
TiO2	0.04	0.05	0.14	0.20	0.24	0.37	0.32	0.11
Al2O3	24.00	23.03	20.48	18.57	19.61	19.62	19.06	27.51
Fe2O3	1.14	0.61	0.82	0.99	0.79	1.30	1.23	0.90
FeO	4.77	5.75	4.62	5.87	5.07	4.65	4.74	2.94
MnO	0.07	0.07	0.08	0.09	0.09	0.08	0.09	0.04
MgO	9.12	9.82	10.58	10.39	9.29	7.73	8.43	4.65
CaO	12.37	11.51	13.89	13.98	14.58	15.49	14.39	13.93
Na2O	1.55	1.90	1.26	1.48	1.55	1.57	1.92	2.02
K2O	0.06	0.05	0.05	0.04	0.05	0.07	0.07	0.08
P2O5	0.02	0.03	0.02	0.02	0.02	0.03	0.02	0.03
LOI	1.11	0.91	1.10	0.69	0.91	0.76	0.63	0.76
Rest	0.11	0.23	0.21	0.25	0.20	0.28	0.18	0.11
Total	99.80	99.91	99.81	99.69	100.01	100.02	100.00	100.15
O=F,S,Cl	0.01	0.05	0.02	0.04	0.00	0.01	0.02	0.01
Total	99.79	99.86	99.79	99.65	100.00	100.00	99.98	100.14
Trace elements in parts per million								
Ba	45	28	40	30	41	41	38	45
Li	4	5	3	3	3	3	3	3
Rb	<1	1	<1	<1	<1	1	1	<1
Sr	421	438	422	295	350	308	341	402
Pb	<2	<2	<2	<2	<2	<2	<2	<2
Th	<2	<2	<2	<2	<2	<2	<2	<2
U	<0.5	<0.5	<0.5	<0.5	<0.5	<0.5	<0.5	<0.5
Zr	2	4	7	7	7	14	10	6
Nb	<2	<2	<2	<2	<2	<2	<2	<2
Y	2	2	4	6	6	7	7	2
La	<2	<2	<2	<2	5	<2	3	3
Ce	<5	9	<5	10	7	12	8	6
Nd	<2	<2	<2	<2	<2	3	4	<2
Pr	<2	<2	<2	<2	<2	<2	<2	<2
Sc	15	16	31	40	40	49	45	17
V	15	10	56	85	87	124	110	23
Cr	25	49	448	284	579	1027	304	46
Ni	84	149	179	180	168	108	57	75
Cu	59	256	91	265	7	25	50	24
Zn	35	37	34	37	33	32	32	22
Ga	17	15	13	12	12	13	15	18
As	<0.5	<0.5	<0.5	<0.5	<0.5	<0.5	<0.5	<0.5
S	230	1000	320	870	100	290	340	200
Cs	7	<3	<3	<3	<3	5	<3	<3
Se	<1	<1	<1	<1	<1	<1	<1	<1
Trace elements in parts per billion								
Pd	-	-	-	-	-	-	-	-
Pt	-	-	-	-	-	-	-	-
Au	-	-	-	-	-	-	-	-
εNd	-	-	-	-	-	-	-	-
mg	73.7	73.5	77.9	73.3	74.1	70.3	72.0	68.8

Sample number	92522292	92522293	92522294	92522295	92522296	92522297	92522298	92522299
Intrusion	McIntosh	McIntosh	McIntosh	McIntosh	McIntosh	McIntosh	McIntosh	McIntosh
Group	VI	VI	VI	VI	VI	VI	VI	VI
Lithology	Olivine gabbro	Olivine gabbro	Olivine gabbronor.	Olivine gabbro	Olivine gabbro	Olivine gabbro	Olivine gabbronor.	Troctolite
Strat. ht (m)	4860	5030	5195	5320	5520	5740	6065	6245
Easting	383780	383900	383950	383990	384010	384060	384140	384020
Northing	8038970	8039150	8039380	8039580	8039730	8039860	8040270	8040440
SiO2	47.19	47.04	48.35	46.46	49.13	46.27	46.24	47.29
TiO2	0.29	0.43	0.25	0.13	0.24	0.11	0.10	0.07
Al2O3	17.56	14.74	17.69	21.06	20.19	19.99	25.98	25.04
Fe2O3	1.11	1.54	1.00	1.35	1.45	1.03	0.88	0.81
FeO	6.32	8.47	6.60	5.49	4.22	7.44	3.83	4.40
MnO	0.11	0.14	0.11	0.09	0.09	0.11	0.05	0.06
MgO	10.01	11.28	10.48	9.48	6.99	10.73	6.86	6.76
CaO	14.72	13.74	12.60	12.45	14.50	11.45	13.20	12.32
Na2O	1.33	1.20	1.63	1.71	1.96	1.72	1.74	2.25
K2O	0.04	0.05	0.08	0.08	0.08	0.07	0.08	0.06
P2O5	0.02	0.02	0.02	0.02	0.02	0.02	0.02	0.02
LOI	0.83	0.82	0.83	1.20	0.73	0.83	0.79	0.87
Rest	0.26	0.31	0.23	0.23	0.22	0.19	0.14	0.12
Total	99.79	99.78	99.87	99.75	99.82	99.96	99.91	100.07
O=F,S,Cl	0.04	0.06	0.03	0.03	0.03	0.02	0.01	0.02
Total	99.76	99.72	99.84	99.72	99.79	99.94	99.90	100.06
Trace elements in parts per million								
Ba	39	41	36	32	46	39	43	31
Li	3	4	3	2	2	5	4	3
Rb	<1	<1	<1	1	<1	<1	1	<1
Sr	301	247	219	309	310	287	322	348
Pb	<2	<2	<2	<2	<2	<2	<2	<2
Th	<2	<2	<2	<2	<2	<2	<2	<2
U	1.0	<0.5	<0.5	<0.5	<0.5	<0.5	<0.5	<0.5
Zr	12	9	10	6	9	4	4	4
Nb	<2	<2	<2	<2	<2	<2	<2	<2
Y	9	8	7	3	6	4	2	2
La	4	<2	<2	<2	3	<2	5	<2
Ce	10	<5	<5	6	8	5	<5	6
Nd	<2	<2	<2	4	3	<2	<2	<2
Pr	<2	<2	<2	<2	<2	<2	<2	<2
Sc	44	51	37	25	40	22	16	16
V	110	169	88	40	92	40	19	15
Cr	532	517	509	530	442	388	259	61
Ni	132	113	133	174	63	193	157	120
Cu	99	141	116	99	109	52	31	47
Zn	45	61	45	41	28	50	30	32
Ga	11	12	11	13	14	11	16	16
As	<0.5	<0.5	<0.5	<0.5	<0.5	<0.5	<0.5	<0.5
S	760	1160	590	570	620	440	220	330
Cs	<3	<3	<3	<3	<3	<3	<3	<3
Se	<1	<1	<1	<1	<1	<1	<1	<1
Trace elements in parts per billion								
Pd	-	0.7	-	-	-	-	-	-
Pt	-	1.4	-	-	-	-	-	-
Au	-	1	-	-	-	-	-	-
εNd	-	-	-	-	-	-	-	-
mg	70.9	67.1	71.3	71.6	69.3	69.6	72.6	70.1

Sample number	92522300	92522301	92522302	92522303	92522304	92522311	92522321	92522338
Intrusion	McIntosh	McIntosh	McIntosh	McIntosh	McIntosh	McIntosh	McIntosh	Mini
Group	VI	VI	VI	VI	VI	VI	VI	I
Lithology	Olivine gabbro	Olivine gabbronor.	Olivine gabbronor.	Olivine gabbronor.	Olivine gabbronor.	Magnetite olivine gabbro	Chilled olivine gabbro	Chromitite
Strat. ht (m)	6410	6490	6570	6650	6765	7100	1	-
Easting	384000	384090	384090	384230	384290	385450	384500	378840
Northing	8040580	8040730	8040830	8040960	8041090	8044020	8035750	8043140
SiO2	46.25	45.60	46.16	48.04	47.93	45.84	46.96	19.97
TiO2	0.08	0.05	0.15	0.25	0.23	0.12	0.67	0.89
Al2O3	22.58	25.44	20.55	20.54	19.94	21.82	15.11	15.93
Fe2O3	0.74	0.71	0.71	0.69	0.85	0.83	2.14	21.21
FeO	5.11	3.98	5.48	4.15	4.16	6.96	8.51	2.73
MnO	0.08	0.06	0.08	0.07	0.08	0.09	0.16	0.37
MgO	9.67	8.24	11.10	8.58	9.11	10.18	9.99	9.96
CaO	12.47	12.88	12.83	15.08	14.94	11.53	13.43	3.52
Na2O	1.68	1.66	1.44	1.49	1.45	1.77	1.11	0.24
K2O	0.04	0.05	0.04	0.05	0.04	0.06	0.11	0.05
P2O5	0.02	0.02	0.02	0.02	0.02	0.02	0.05	0.01
LOI	0.96	1.24	1.02	0.73	0.77	0.75	1.01	1.12
Rest	0.19	0.13	0.27	0.27	0.32	0.17	0.30	15.27
Total	99.87	100.06	99.85	99.96	99.84	100.14	99.55	91.27
O=F,S,Cl	0.02	0.01	0.03	0.03	0.03	0.02	0.06	0.01
Total	99.85	100.05	99.81	99.93	99.81	100.12	99.50	91.26
Trace elements in parts per million								
Ba	21	25	24	29	23	43	36	83
Li	3	2	2	3	4	2	4	2
Rb	<1	<1	<1	<1	<1	<1	1	3
Sr	317	289	326	402	380	360	149	11
Pb	<2	<2	<2	<2	<2	<2	<2	4
Th	<2	<2	<2	<2	<2	<2	<2	<2
U	<0.5	<0.5	<0.5	<0.5	<0.5	<0.5	1.5	1.5
Zr	3	2	7	10	8	6	18	25
Nb	<2	<2	<2	<2	<2	<2	<2	<2
Y	3	3	4	8	8	2	18	7
La	<2	5	5	<2	<2	2	<2	10
Ce	6	<5	<5	7	5	<5	12	12
Nd	<2	<2	<2	2	<2	<2	7	6
Pr	<2	<2	<2	<2	3	<2	3	<2
Sc	21	13	26	40	40	19	52	23
V	30	15	56	93	94	25	257	1104
Cr	366	228	602	692	1040	214	393	>99999
Ni	156	152	218	75	109	195	178	637
Cu	104	47	179	116	80	58	108	54
Zn	35	29	36	27	28	45	81	2538
Ga	15	16	14	13	14	15	11	39
As	<0.5	<0.5	<0.5	<0.5	<0.5	<0.5	<0.5	<0.5
S	490	230	630	560	590	430	1140	220
Cs	<3	<3	<3	<3	6	3	<3	<3
Se	<1	<1	<1	<1	<1	<1	<1	<1
Trace elements in parts per billion								
Pd	-	-	-	-	-	-	1.6	122
Pt	-	-	-	-	-	-	1.9	43.4
Au	-	-	-	-	-	-	2	1
εNd	-	-	-	-	-	-	-	-
mg	74.9	76.1	76.4	76.2	76.7	70.2	63.0	44.9

Sample number	92522354	92522359	92522374	92522375	92522377	92522378	92522379	92522380
Intrusion	West McIntosh	West McIntosh	South Melon Patch	South Melon Patch	South Melon Patch	South Melon Patch	South Melon Patch	South Melon Patch
Group	I	I	I	I	I	I	I	I
Lithology	Chromitite	Chromitite	Leuco gabbro	Gabbro	Chromitite	Gabbro	Peridotite	Peridotite
Strat. ht (m)	-	-	-	-	-	-	-	-
Easting	380830	382000	385510	385790	386560	386160	385880	386170
Northing	8044240	8046070	8049130	8048980	8049080	8049140	8048630	8049080
SiO2	16.57	4.04	47.15	47.76	7.43	44.39	45.75	40.50
TiO2	0.71	0.52	0.18	0.21	0.81	0.09	0.42	0.15
Al2O3	11.49	13.38	31.14	16.69	15.26	20.27	7.23	4.04
Fe2O3	20.40	16.55	0.65	1.21	27.33	2.25	2.85	5.19
FeO	1.28	0.67	1.52	5.17	1.18	5.12	10.05	8.20
MnO	0.30	0.24	0.02	0.11	0.39	0.10	0.16	0.19
MgO	18.18	9.11	0.86	10.15	11.44	14.43	26.04	32.95
CaO	0.73	17.25	15.59	15.74	0.25	10.94	4.86	2.47
Na2O	0.01	0.06	2.13	0.73	0.04	0.45	0.33	0.16
K2O	0.02	0.01	0.06	0.09	0.01	0.05	0.06	0.02
P2O5	0.01	0.04	0.04	0.02	0.01	0.01	0.05	0.02
LOI	5.00	14.84	0.64	1.73	0.11	1.53	1.67	4.90
Rest	15.00	15.11	0.10	0.24	15.41	0.39	0.65	1.45
Total	89.70	91.82	100.08	99.85	79.67	100.02	100.12	100.24
O=F,S,Cl	0.00	0.00	0.01	0.03	0.00	0.00	0.05	0.07
Total	89.70	91.82	100.07	99.83	79.67	100.02	100.06	100.17
	Trace elements in parts per million							
Ba	7	<4	51	19	6	15	<4	7
Li	-	1	8	4	2	4	2	4
Rb	2	1	2	<1	2	1	<1	<1
Sr	5	51	336	138	2	197	5	10
Pb	<2	3	4	<2	<2	<2	<2	<2
Th	<2	<2	<2	<2	<2	<2	2	<2
U	<0.5	1.5	<0.5	<0.5	2	<0.5	1.5	0.5
Zr	5	6	14	8	16	5	38	10
Nb	<2	<2	<2	<2	<2	<2	3	<2
Y	1	<1	4	7	2	2	12	4
La	<2	2	<2	3	<2	<2	<2	2
Ce	12	14	11	<5	9	8	14	<5
Nd	2	<2	4	3	6	<2	5	<2
Pr	4	<2	<2	<2	<2	<2	3	4
Sc	14	19	20	58	12	19	28	13
V	732	1024	60	173	1252	56	138	83
Cr	>99999	>99999	10	636	>99999	1951	2438	7235
Ni	1263	1088	4	114	1785	421	836	1550
Cu	54	145	28	106	744	10	233	182
Zn	609	1019	9	40	1807	28	72	77
Ga	31	30	29	13	47	13	7	3
As	1.5	2.0	<0.5	<0.5	1.0	<0.5	<0.5	<0.5
S	20	90	190	530	100	40	1030	1350
Cs	<3	<3	8	<3	<3	5	<3	<3
Se	<1	1	<1	<1	<1	<1	1	<1
	Trace elements in parts per billion							
Pd	488	79	-	-	283	-	-	179
Pt	662	333	-	-	527	-	-	91.6
Au	6	2	-	-	38	-	-	3
εNd	-	-	-	-	-	-	-	-
mg	62.3	51.5	42.1	74.3	44.2	78.3	78.6	82.0

Sample number	92522394	92522428	92522430	92522433	92522436	92522437	92522438	92522439
Intrusion	South Melon Patch	Wild Dog Creek	Wild Dog Creek	Wild Dog Creek	McIntosh	Wild Dog Creek	Springvale	Springvale
Group	I	IV	IV	IV	VI	IV	II	II
Lithology	Gabbro	Olivine gabbronor.	Gabbro	Magnetite gabbro	Chilled gabbro	Mt quartz gabbronor.	Gabbro	Gabbronor.
Strat. ht (m)	-	-	-	-	1	-	-	-
Easting	387680	388500	387500	387900	387060	380900	362080	361720
Northing	8049070	8043160	8045850	8045100	8044060	8036300	8031750	8031550
SiO2	47.97	49.48	48.23	50.77	56.79	49.64	47.64	50.27
TiO2	0.77	0.24	0.26	1.19	0.83	1.45	0.36	0.33
Al2O3	20.19	17.00	21.09	15.23	17.23	15.53	22.76	15.88
Fe2O3	1.60	1.18	0.90	1.39	1.20	1.18	1.44	0.72
FeO	6.35	5.27	5.54	9.30	7.24	11.18	4.57	6.84
MnO	0.12	0.11	0.10	0.15	0.10	0.17	0.08	0.13
MgO	5.89	10.54	6.35	7.89	3.82	7.15	5.78	10.80
CaO	13.66	13.48	15.16	10.00	8.82	10.03	11.86	11.76
Na2O	1.55	1.59	1.28	2.46	2.55	1.44	2.02	1.21
K2O	0.22	0.04	0.05	0.10	0.16	0.47	0.21	0.19
P2O5	0.06	0.02	0.02	0.21	0.22	0.18	0.04	0.03
LOI	1.55	0.69	0.81	0.93	0.79	1.14	2.98	1.28
Rest	0.15	0.25	0.24	0.32	0.14	0.32	0.15	0.27
Total	100.08	99.89	100.03	99.94	99.89	99.88	99.89	99.71
O=F,S,Cl	0.01	0.02	0.03	0.05	0.00	0.06	0.01	0.04
Total	100.07	99.87	100.00	99.89	99.89	99.82	99.88	99.67
Trace elements in parts per million								
Ba	51	25	39	74	84	218	116	63
Li	6	3	3	4	3	5	8	3
Rb	6	<1	<1	1	2	18	5	8
Sr	196	157	184	249	207	195	236	155
Pb	<2	<2	<2	<2	<2	4	8	3
Th	<2	<2	<2	<2	<2	<2	<2	<2
U	<0.5	<0.5	<0.5	0.5	<0.5	<0.5	<0.5	<0.5
Zr	24	12	9	49	161	89	23	18
Nb	<2	<2	<2	7	8	5	<2	<2
Y	9	10	8	16	20	36	11	9
La	3	<2	<2	4	11	15	2	3
Ce	9	<5	6	20	34	35	15	7
Nd	<2	<2	4	6	16.21	16.84	4	4
Pr	<2	<2	3	2	3	2	5	<2
Sc	44	46	44	33	29	43	41	42
V	302	138	164	194	142	270	163	191
Cr	112	687	529	584	27	187	121	603
Ni	41	286	102	194	44	111	65	108
Cu	38	124	86	63	110	94	112	85
Zn	60	35	48	99	60	103	63	54
Ga	15	10	14	17	20	18	19	14
As	<0.5	<0.5	<0.5	<0.5	<0.5	1.00	<0.5	<0.5
S	140	360	590	920	60	1170	110	720
Cs	4	<3	<3	<3	<3	4	<3	<3
Se	<1	<1	<1	<1	<1	<1	<1	<1
Trace elements in parts per billion								
Pd	-	-	-	2.5	-	-	-	-
Pt	-	-	-	2.3	-	-	-	-
Au	-	-	-	1	-	-	-	-
εNd	-	-	-	-	0.5	-1.2	-	-
mg	57.4	74.8	64.1	57.1	45.0	51.0	63.7	72.0

Sample number	92522441	92522443	92522444	92522445	92522446	92522448	92522450	92522454
Intrusion	Springvale	Springvale	Springvale	Springvale	Springvale	Springvale	Springvale	Springvale
Group	II	II	II	II	II	II	II	II
Lithology	Gabbro	Gabbronor.	Gabbro	Gabbro	Olivine gabbronor.	Olivine gabbronor.	Olivine gabbro	Norite
Strat. ht (m)	-	-	-	-	940	1160	1250	50
Easting	361160	360160	359800	359920	354200	354200	354520	354390
Northing	8031200	8031080	8030980	8032230	8034650	8035050	8035200	8032050
SiO2	48.86	50.46	49.21	48.41	48.54	47.89	44.70	49.55
TiO2	0.41	0.35	1.47	0.33	0.59	0.16	0.09	0.90
Al2O3	18.77	16.63	16.58	14.73	16.07	18.21	21.89	13.30
Fe2O3	1.26	1.07	1.61	1.49	1.42	1.04	0.98	0.94
FeO	5.10	8.55	10.34	7.50	8.73	7.24	5.40	11.92
MnO	0.11	0.16	0.17	0.14	0.15	0.12	0.08	0.19
MgO	7.29	8.58	6.32	12.88	9.86	10.36	10.13	9.73
CaO	13.55	11.25	9.59	11.07	12.17	12.82	13.91	8.00
Na2O	1.53	1.54	2.02	1.02	1.31	1.03	0.90	1.39
K2O	0.30	0.18	0.50	0.15	0.07	0.07	0.03	0.47
P2O5	0.04	0.02	0.15	0.03	0.02	0.02	0.02	0.11
LOI	2.51	1.21	1.70	1.95	0.87	0.81	1.52	3.27
Rest	0.23	0.17	0.20	0.24	0.30	0.23	0.37	0.23
Total	99.96	100.17	99.86	99.94	100.10	100.00	100.02	100.00
O=F,S,Cl	0.00	0.02	0.01	0.01	0.05	0.03	0.03	0.03
Total	99.96	100.15	99.85	99.92	100.05	99.97	99.99	99.97
Trace elements in parts per million								
Ba	97	66	220	66	48	48	48	161
Li	2	2	13	3	3	4	3	5
Rb	12	4	15	6	1	<1	<1	20
Sr	160	183	201	134	184	200	238	152
Pb	3	3	22	2	<2	<2	<2	5
Th	<2	<2	2	<2	<2	<2	<2	2
U	<0.5	<0.5	<0.5	0.5	1.5	<0.5	<0.5	0.5
Zr	29	11	65	19	9	5	3	65
Nb	<2	<2	4	<2	<2	<2	<2	<2
Y	13	8	19	9	8	5	3	17
La	8	<2	17	7	5	<2	<2	7
Ce	10	6	31	<5	<5	<5	<5	17
Nd	4	<2	12	3	3	<2	<2	6
Pr	<2	<2	5	<2	<2	3	<2	3
Sc	45	45	40	38	46	38	29	43
V	209	210	281	175	233	117	74	249
Cr	739	226	154	776	577	446	1418	201
Ni	82	60	45	139	147	230	314	51
Cu	69	24	14	12	85	58	53	39
Zn	50	69	129	62	75	56	42	111
Ga	15	16	19	13	14	14	14	16
As	<0.5	<0.5	3.5	<0.5	<0.5	<0.5	<0.5	1.5
S	90	350	230	280	930	620	530	660
Cs	<3	<3	4	<3	5	<3	<3	5
Se	<1	1	<1	<1	<1	<1	<1	<1
Trace elements in parts per billion								
Pd	-	-	-	-	-	-	4.2	-
Pt	-	-	-	-	-	-	1.9	-
Au	-	-	-	-	-	-	2	-
εNd	-	-	-	-	-	-	-	-
mg	67.6	61.6	48.9	72.2	63.7	69.3	74.2	57.6

Sample number	92522457	92522458	92522459	92522460	92522461	92522462	92522471	92522472
Intrusion	Springvale	Springvale	Springvale	Springvale	Springvale	Springvale	Springvale	Springvale
Group	II	II	II	II	II	II	II	II
Lithology	Gabbronor.	Olivine gabbronor.	Gabbro	Gabbro	Olivine gabbronor.	Biotite olivine gabbronor.	Olivine gabbronor.	Gabbro
Strat. ht (m)	220	298	430	580	840	1300	1400	1450
Easting	354150	354150	354280	354100	354000	354150	354120	354010
Northing	8032580	8032900	8033200	8033620	8034300	8035260	8035480	8035680
SiO2	49.18	47.58	49.91	49.02	48.31	43.41	47.43	50.09
TiO2	0.23	0.16	0.23	0.67	0.78	0.08	0.19	0.29
Al2O3	23.00	22.59	16.27	16.67	17.73	16.31	17.82	16.33
Fe2O3	0.98	0.89	0.93	1.57	1.51	1.35	1.18	0.82
FeO	4.65	6.26	10.02	8.77	7.48	7.68	6.04	5.26
MnO	0.08	0.09	0.17	0.14	0.12	0.12	0.11	0.11
MgO	6.28	8.05	9.78	8.64	9.04	18.07	10.99	9.12
CaO	12.76	11.73	10.00	11.59	10.70	9.85	13.37	15.49
Na2O	1.74	1.66	1.25	1.54	1.86	0.64	0.96	1.14
K2O	0.24	0.17	0.12	0.16	0.83	0.05	0.06	0.08
P2O5	0.03	0.02	0.02	0.03	0.15	0.02	0.02	0.03
LOI	0.66	0.61	1.02	0.89	1.22	2.10	1.19	0.73
Rest	0.15	0.19	0.26	0.27	0.27	0.29	0.37	0.18
Total	99.98	100.00	99.98	99.96	100.00	99.97	99.73	99.67
O=F,S,Cl	0.01	0.04	0.04	0.04	0.03	0.02	0.04	0.02
Total	99.96	99.96	99.94	99.92	99.96	99.95	99.69	99.65
Trace elements in parts per million								
Ba	84	68	62	101	310	49	44	51
Li	4	5	4	3	4	4	4	6
Rb	6	2	<1	2	26	<1	2	1
Sr	209	231	154	144	286	258	191	191
Pb	<2	2	2	2	6	2	2	2
Th	<2	<2	<2	<2	3	<2	<2	<2
U	<0.5	<0.5	<0.5	<0.5	0.5	<0.5	0.5	<0.5
Zr	13	8	3	15	91	4	8	16
Nb	<2	<2	<2	<2	10	<2	<2	<2
Y	5	3	5	11	18	3	5	10
La	<2	<2	<2	5	22	<2	<2	3
Ce	11	<5	<5	<5	54	<5	<5	10
Nd	2	<2	<2	2	17.02	<2	<2	5
Pr	4	<2	<2	2	4	3	<2	<2
Sc	26	21	36	38	29	20	39	59
V	90	67	154	212	161	36	124	201
Cr	285	125	503	441	168	753	1302	203
Ni	57	137	189	169	183	561	164	53
Cu	20	100	71	66	46	50	111	81
Zn	39	47	86	78	73	64	50	38
Ga	18	19	16	15	15	10	13	15
As	<0.5	<0.5	<0.5	<0.5	<0.5	<0.5	<0.5	<0.5
S	250	800	810	800	650	440	780	500
Cs	<3	<3	<3	<3	<3	<3	<3	<3
Se	<1	<1	<1	<1	<1	<1	<1	<1
Trace elements in parts per billion								
Pd	-	-	-	-	-	-	<0.5	-
Pt	-	-	-	-	-	-	0.5	-
Au	-	-	-	-	-	-	1	-
εNd	-	-	-	-	-0.2	-	-	-
mg	66.9	67.0	61.6	60.2	64.6	78.4	73.4	73.0

Sample number	92522473	92522474	92522475	92522483	92522489	92522490	92522491	92522492
Intrusion	Springvale	Springvale	Springvale	Springvale	Armanda	Armanda	Armanda	Armanda
Group	II	II	II	II	VI	VI	VI	VI
Lithology	Troctolite	Gabbronor.	Gabbronor.	Gabbro	Olivine gabbro	Gabbro	Gabbro	Gabbro
Strat. ht (m)	1660	1970	2020	2200	30	100	220	320
Easting	353910	353750	353030	352920	373880	374010	374150	374350
Northing	8035900	8036480	8036420	8036200	8010400	8010380	8010200	8010220
SiO2	46.38	48.87	49.70	49.93	46.80	47.24	46.31	45.94
TiO2	0.11	0.12	0.18	0.60	0.28	0.29	0.20	0.11
Al2O3	25.17	23.61	17.76	15.59	13.48	22.04	22.54	23.34
Fe2O3	0.74	0.65	0.50	0.87	1.07	1.21	0.93	1.30
FeO	5.17	3.15	5.74	9.68	7.52	4.27	4.33	3.98
MnO	0.07	0.07	0.12	0.16	0.12	0.07	0.08	0.09
MgO	6.32	5.79	9.49	8.61	13.07	5.97	6.95	6.85
CaO	13.23	14.88	14.30	11.58	14.27	14.91	14.86	14.95
Na2O	1.58	1.46	1.03	1.55	0.86	1.33	1.31	1.20
K2O	0.10	0.18	0.04	0.07	0.05	0.61	0.12	0.22
P2O5	0.03	0.02	0.01	0.01	0.03	0.03	0.04	0.02
LOI	0.84	1.09	0.73	0.98	1.43	1.85	1.86	1.77
Rest	0.10	0.12	0.19	0.26	0.37	0.20	0.25	0.21
Total	99.84	100.01	99.79	99.89	99.35	100.02	99.78	99.98
O=F,S,Cl	0.01	0.01	0.03	0.04	0.03	0.01	0.01	0.01
Total	99.83	100.00	99.77	99.85	99.32	100.01	99.77	99.97
Trace elements in parts per million								
Ba	62	50	12	26	20	78	28	48
Li	3	8	5	9	3	6	5	8
Rb	2	21	1	1	1	36	4	11
Sr	285	269	151	143	142	192	212	227
Pb	<2	<2	<2	2	2	<2	3	9
Th	<2	<2	<2	<2	<2	<2	<2	<2
U	<0.5	<0.5	<0.5	<0.5	<0.5	1.5	<0.5	<0.5
Zr	10	8	2	<1	12	14	12	10
Nb	<2	<2	<2	<2	<2	<2	<2	<2
Y	3	6	3	6	8	8	5	4
La	<2	6	<2	<2	<2	<2	<2	<2
Ce	7	<5	6	<5	<5	<5	9	<5
Nd	<2	4	<2	<2	<2	<2	3	<2
Pr	<2	<2	<2	2	<2	<2	<2	<2
Sc	21	34	48	44	51	39	33	29
V	35	89	210	239	165	132	92	71
Cr	29	86	313	434	1233	470	882	616
Ni	73	26	115	130	242	94	160	144
Cu	19	36	47	70	221	120	106	118
Zn	35	30	35	78	48	39	41	48
Ga	18	19	16	16	11	13	13	15
As	<0.5	0.5	<0.5	<0.5	<0.5	<0.5	2	1
S	220	230	520	850	590	240	270	190
Cs	<3	15	<3	<3	<3	4	<3	<3
Se	<1	<1	<1	<1	<1	<1	<1	<1
Trace elements in parts per billion								
Pd	-	-	-	-	<0.5	-	-	-
Pt	-	-	-	-	0.6	-	-	-
Au	-	-	-	-	2	-	-	-
εNd	-	-	-	-	-	-	-	-
mg	65.9	73.4	73.2	59.5	73.3	66.5	70.6	70.3

Sample number	92522493	92522494	92522495	92522499	92522500	92522501	92522502	92522504
Intrusion	Armanda	Armanda	Armanda	Wilagee	Wilagee	Wilagee	Wilagee	Wilagee
Group	VI	VI	VI	II	II	II	II	II
Lithology	Olivine gabbronor.	Gabbro	Gabbro	Chromitite	Gabbro	Leuco gabbro	Olivine gabbronor.	Gabbro
Strat. ht (m)	400	470	600	390	390	460	710	190
Easting	374600	374800	375000	361000	361000	361050	361200	360610
Northing	8010200	8010190	8010180	8052750	8052750	8052600	8052300	8052800
SiO2	46.95	47.19	47.42	23.98	43.67	44.82	45.61	43.63
TiO2	0.33	0.30	0.15	0.59	0.19	0.25	0.18	0.13
Al2O3	16.10	14.89	23.22	22.88	21.43	22.82	23.36	23.63
Fe2O3	1.42	1.48	0.92	15.53	1.50	1.54	0.90	1.09
FeO	7.06	6.26	3.96	1.30	4.76	4.70	3.60	3.43
MnO	0.12	0.12	0.07	0.22	0.07	0.08	0.06	0.05
MgO	10.19	11.82	5.67	11.27	10.41	9.87	9.19	9.16
CaO	14.21	14.06	14.47	4.15	11.91	12.76	14.23	12.38
Na2O	1.32	0.99	1.29	0.72	1.09	1.10	1.12	1.28
K2O	0.08	0.12	0.52	0.49	0.44	0.13	0.09	0.74
P2O5	0.03	0.04	0.02	0.02	0.04	0.04	0.03	0.03
LOI	1.25	2.02	1.88	2.26	4.43	1.26	1.39	4.06
Rest	0.31	0.37	0.18	14.98	0.27	0.55	0.23	0.22
Total	99.37	99.66	99.77	98.39	100.21	99.92	99.99	99.83
O=F,S,Cl	0.04	0.05	0.00	0.00	0.01	0.02	0.01	0.01
Total	99.3	99.6	99.8	98.4	100.2	99.9	100.0	99.8
Trace elements in parts per million								
Ba	53	32	91	73	104	59	40	174
Li	3	3	11	15	9	4	5	10
Rb	3	3	26	39	27	4	2	42
Sr	200	140	211	45	147	154	162	193
Pb	<2	<2	3	3	8	<2	<2	11
Th	<2	<2	<2	<2	<2	<2	<2	<2
U	<0.5	0.5	<0.5	<0.5	<0.5	<0.5	<0.5	<0.5
Zr	17	16	7	11	25	21	14	12
Nb	<2	<2	<2	2	<2	<2	<2	<2
Y	8	8	5	3	7	7	5	4
La	<2	<2	4	2	<2	<2	<2	8
Ce	<5	<5	<5	16	13	<5	8	10
Nd	4	<2	3	7	2	<2	3	4
Pr	<2	<2	<2	<2	2	<2	<2	<2
Sc	43	49	34	13	18	20	24	16
V	131	156	85	763	55	82	63	35
Cr	658	967	608	>99999	959	2843	716	502
Ni	199	234	97	1082	362	318	376	364
Cu	198	268	18	3	70	54	20	103
Zn	61	55	37	411	33	42	30	39
Ga	13	11	14	40	11	12	12	11
As	<0.5	1	<0.5	7	7.5	<0.5	<0.5	1
S	890	970	20	<10	140	370	240	180
Cs	4	<3	<3	<3	<3	<3	<3	<3
Se	<1	<1	<1	<1	<1	<1	<1	<1
Trace elements in parts per billion								
Pd	-	1.0	-	148	-	-	-	-
Pt	-	1.3	-	57.4	-	-	-	-
Au	-	3	-	1	-	-	-	-
εNd	-	-	-	-	-	-	-	-
mg	68.5	73.5	67.8	56.8	75.2	74.3	78.8	78.7

Sample number	92522505	92522506	92522507	92522512	92522513	92522514	92522517	92522518
Intrusion	Wilagee	Wilagee	Wilagee	Toby	Toby	Toby	Black Hills Yard	Toby
Group	II	II	II	III	III	III	VII	III
Lithology	Troctolite	Troctolite	Troctolite	Quartz gabbro	Biot qtz gabbronor.	Biotite gabbronor.	Troctolite	Biot qtz gabbronor.
Strat. ht (m)	90	70	20	600*	1750*	2600*	-	3500*
Easting	360580	360450	360300	359120	358400	357850	361320	357600
Northing	8053000	8052900	8053000	8052200	8053130	8053850	8048140	8054700
SiO2	42.06	40.35	40.53	49.33	50.89	50.59	43.66	50.81
TiO2	0.15	0.05	0.08	1.17	1.09	1.18	0.37	1.36
Al2O3	22.55	10.59	11.46	15.29	15.34	15.35	5.11	14.77
Fe2O3	1.43	1.89	3.59	1.95	1.94	1.63	1.62	1.59
FeO	3.94	9.36	7.04	8.82	8.58	9.11	11.01	9.90
MnO	0.07	0.14	0.14	0.16	0.15	0.15	0.20	0.16
MgO	9.93	27.09	24.66	7.75	6.73	7.21	26.52	6.77
CaO	13.21	5.60	6.68	10.53	10.21	10.26	8.13	10.03
Na2O	0.94	0.56	0.45	1.75	1.77	1.83	0.66	1.86
K2O	0.15	0.05	0.06	0.66	1.30	0.89	0.25	0.91
P2O5	0.04	0.02	0.02	0.19	0.19	0.17	0.06	0.19
LOI	4.98	3.70	5.06	2.00	1.22	1.16	1.73	1.16
Rest	0.38	0.56	0.23	0.32	0.34	0.32	0.70	0.32
Total	99.83	99.96	100.00	99.92	99.75	99.85	100.02	99.83
O=F,S,Cl	0.03	0.01	0.01	0.05	0.05	0.05	0.01	0.05
Total	99.80	99.94	99.99	99.87	99.70	99.81	100.00	99.78
Trace elements in parts per million								
Ba	46	23	21	217	403	273	119	277
Li	18	4	4	6	19	16	5	17
Rb	10	<1	3	37	51	36	8	42
Sr	219	81	87	146	246	151	164	137
Pb	7	<2	<2	7	10	8	2	9
Th	<2	<2	<2	2	7	5	<2	5
U	<0.5	0.5	<0.5	<0.5	1.5	2	<0.5	1.5
Zr	12	5	8	126	110	122	29	123
Nb	<2	<2	<2	10	9	10	3	7
Y	3	3	3	31	30	30	10	33
La	5	<2	3	18	26	20	13	18
Ce	10	6	<5	43	59	42	20	44
Nd	<2	<2	<2	20	22	20	9	18
Pr	<2	<2	<2	7	4	8	<2	7
Sc	16	12	13	40	42	46	38	44
V	42	35	27	223	239	222	152	245
Cr	303	2256	337	345	282	343	3179	310
Ni	1155	1267	996	123	93	126	851	68
Cu	593	57	20	64	55	64	47	62
Zn	35	68	70	95	96	97	76	103
Ga	11	6	6	15	17	17	4	16
As	2.5	0.5	0.5	0.5	1.5	0.5	<0.5	0.5
S	590	240	160	990	960	950	280	980
Cs	<3	<3	<3	6	5	3	<3	6
Se	1	<1	<1	<1	<1	<1	<1	<1
Trace elements in parts per billion								
Pd	-	21.7	-	-	-	-	16.1	-
Pt	-	6.9	-	-	-	-	8.5	-
Au	-	2	-	-	-	-	2	-
εNd	-	-	-	-	-	-	-	-
mg	77.2	81.4	81.1	56.6	53.7	54.8	79.1	51.6

Sample number	92522519	92522520	92522522	92522523	92522524	92522525	92522533	92522541
Intrusion	Toby	Toby	Toby	Toby	Toby	Toby	Wilagee	Paperbark
Group	III	III	III	III	III	III	II	Corridor gabbro
Lithology	Biotite quartz gabbronor.	Biotite gabbronor.	Biotite gabbronor.	Biotite gabbronor.	Biotite gabbronor.	Biotite quartz gabbronor.	Chilled biotite gabbro	Biotite quartz gabbronor.
Strat. ht (m)	4100*	5200*	7000*	9300*	11400*	13500*	1	-
Easting	358160	357650	356880	355700	355280	353960	363340	361900
Northing	8055620	8056450	8058150	8060200	8062150	8064000	8055550	8046400
SiO2	49.72	49.04	49.36	49.77	50.59	48.45	49.85	51.43
TiO2	1.41	0.99	1.07	1.00	1.43	1.11	1.04	1.08
Al2O3	15.02	16.04	15.86	15.96	14.20	16.36	15.45	15.35
Fe2O3	1.87	1.30	1.21	1.32	1.66	1.23	1.03	0.57
FeO	9.92	9.64	9.38	9.00	10.61	9.89	9.42	9.41
MnO	0.16	0.15	0.15	0.14	0.18	0.16	0.15	0.13
MgO	6.99	8.27	7.87	7.65	6.40	7.94	7.51	7.78
CaO	10.46	10.73	10.80	10.37	10.58	10.77	10.95	9.13
Na2O	1.85	1.98	1.84	1.78	1.97	2.02	2.11	1.61
K2O	0.82	0.44	0.83	0.93	0.69	0.36	0.75	1.01
P2O5	0.27	0.14	0.18	0.15	0.20	0.12	0.17	0.32
LOI	1.01	0.97	0.99	1.12	1.06	1.29	1.33	1.75
Rest	0.35	0.31	0.34	0.30	0.34	0.25	0.31	0.35
Total	99.85	100.00	99.88	99.49	99.91	99.95	100.07	99.92
O=F,S,Cl	0.05	0.05	0.05	0.04	0.06	0.05	0.04	0.04
Total	99.80	99.95	99.83	99.45	99.86	99.90	100.03	99.88
Trace elements in parts per million								
Ba	387	172	327	232	269	107	268	440
Li	15	11	18	15	13	9	23	20
Rb	26	12	27	29	24	10	31	47
Sr	198	149	218	167	150	183	155	206
Pb	7	3	7	6	8	<2	6	12
Th	3	<2	4	4	4	<2	4	7
U	1.5	<0.5	2	1	<0.5	1.5	<0.5	<0.5
Zr	124	90	112	100	141	76	122	196
Nb	7	4	5	7	6	4	6	15
Y	36	27	27	26	36	24	28	38
La	27	7	22	17	18	8	22	42
Ce	58	26	51	39	43	19	41	74
Nd	27	15	21	18	21	10	21	35
Pr	<2	7	5	<2	6	2	4	7
Sc	43	41	40	40	48	40	40	35
V	235	228	233	219	271	232	223	173
Cr	325	381	341	331	321	138	389	451
Ni	103	141	139	139	61	82	106	94
Cu	57	69	60	62	72	50	95	26
Zn	111	89	90	88	112	86	92	103
Ga	17	17	18	17	18	19	16	18
As	<0.5	<0.5	<0.5	<0.5	<0.5	<0.5	<0.5	1.0
S	1050	970	990	830	1150	970	800	740
Cs	4	3	<3	3	5	3	13	4
Se	<1	<1	<1	<1	<1	<1	<1	<1
Trace elements in parts per billion								
Pd	<0.5	-	-	-	-	-	<0.5	-
Pt	0.6	-	-	-	-	-	0.5	-
Au	<1	-	-	-	-	-	3	-
εNd	-	-	-	-	-	-	-1.4	-2.1
mg	51.8	57.7	57.3	57.2	48.5	56.3	56.4	58.3

Sample number	93522001	93522007	93522014	93522015	93522020	93522021	93522022	93522024
Intrusion	Wild Dog Creek	Three Sisters	Three Sisters	Three Sisters	Three Sisters	Robin Soak	Robin Soak	Robin Soak
Group	IV	Undivided	Undivided	Undivided	Undivided	Undivided	Undivided	Undivided
Lithology	Chilled mt quartz gabbro	Magnetite gabbro	Biotite quartz gabbro	Gabbro	Gabbronor.	Biotite quartz gabbro	Biotite quartz gabbro	Biotite olivine gabbronor.
Strat. ht (m)	-	-	-	-	-	-	-	-
Easting	374298	345622	346295	351600	350585	364582	364582	363890
Northing	8011885	8010508	8011535	8015172	8014808	8019328	8019328	8017840
SiO2	49.16	47.75	48.42	50.56	51.02	54.31	60.66	47.22
TiO2	1.27	1.24	1.88	0.29	0.48	1.13	1.00	0.68
Al2O3	14.64	15.33	14.80	16.76	15.68	14.34	14.18	16.88
Fe2O3	1.84	1.67	1.38	0.92	0.79	1.03	1.49	2.10
FeO	10.52	9.51	11.46	6.22	7.09	8.79	6.24	6.89
MnO	0.18	0.15	0.17	0.13	0.14	0.14	0.11	0.12
MgO	6.67	8.29	6.93	9.86	9.60	6.15	3.64	10.71
CaO	11.45	10.37	10.30	11.87	11.77	8.82	6.07	10.16
Na2O	2.00	1.68	1.88	1.75	1.80	2.21	2.40	1.75
K2O	0.23	0.61	0.76	0.11	0.20	1.57	2.84	0.61
P2O5	0.12	0.20	0.40	0.01	0.05	0.21	0.19	0.13
LOI	1.60	2.62	1.12	1.32	1.24	1.02	0.94	2.18
Rest	0.30	0.35	0.41	0.26	0.21	0.33	0.24	0.40
Total	99.98	99.77	99.91	100.06	100.07	100.05	100.00	99.83
O=F,S,Cl	0.05	0.06	0.07	0.03	0.03	0.06	0.01	0.07
Total	99.92	99.71	99.84	100.03	100.04	99.99	99.99	99.77
Trace elements in parts per million								
Ba	97	218	396	43	64	353	525	177
Li	14	14	8	4	6	15	14	7
Rb	7	20	22	2	7	78	144	21
Sr	189	179	211	154	150	167	143	244
Pb	5	7	10	4	4	14	21	6
Th	<2	<2	<2	<2	<2	12	16	4
U	-	-	-	-	-	4	4	-
Zr	38	90	177	12	27	139	150	73
Nb	5	5	16	<2	<2	12	15	3
Y	27	27	44	8	14	37	47	19
La	5	18	40	3	5	35	40	15
Ce	18	45	92	<5	15	66	81	31
Nd	9.87	23	40	<2	3	29.69	39	14
Pr	4	5	8	3	<2	5	10	3
Sc	46	41	43	37	45	33	24	27
V	327	221	252	165	199	190	144	148
Cr	195	397	329	680	309	247	121	676
Ni	72	152	86	97	82	50	27	337
Cu	125	50	44	73	52	45	27	95
Zn	109	106	125	48	56	92	81	73
Ga	18	16	20	13	15	18	19	14
As	3	2	3	2	1	3	4	3
S	1100	1220	1490	700	640	1110	210	1340
Cs	<3	<3	<3	3	3	8	10	<3
Se	<1	<1	<1	<1	<1	<1	<1	<1
Trace elements in parts per billion								
Pd	-	<0.5	-	-	-	-	-	-
Pt	-	0.9	-	-	-	-	-	-
Au	-	2	-	-	-	-	-	-
εNd	1.4	-	-1.3	-	-	-0.3	-	-
mg	49.4	57.3	49.3	71.4	68.7	53.0	46.1	68.5

Sample number	93522026	93522028	93522029	93522030	93522030	93522060	93522061	93522062
Intrusion	Big Ben	Big Ben	Big Ben	Big Ben	Big Ben	Sally Malay	Sally Malay	Sally Malay
Group	I	I	I	I	I	V	V	V
Lithology	Chromitite	Anorthos.	Peridotite	Pyroxenite	Plg peridotite	Microgabb.	Troctolite	Troctolite
Strat. ht (m)	-	-	-	-	-	50	100	140
Easting	376088	375672	375780	375898	375838	396130	396135	396212
Northing	8015348	8015438	8015475	8015530	8015722	8081500	8081520	8081668
SiO2	22.87	47.77	46.26	45.15	42.67	51.46	45.57	47.28
TiO2	0.61	0.32	0.23	0.31	0.15	0.77	0.20	0.42
Al2O3	16.08	28.78	13.63	15.78	16.03	13.43	20.43	19.30
Fe2O3	19.49	0.60	2.34	1.85	2.22	0.89	0.71	0.79
FeO	3.72	2.10	5.04	7.07	9.97	9.67	5.94	6.98
MnO	0.31	0.03	0.12	0.14	0.16	0.16	0.09	0.10
MgO	13.44	1.73	15.52	14.99	17.52	8.86	13.33	10.99
CaO	3.54	14.91	13.03	10.09	9.09	13.01	10.84	11.32
Na2O	0.23	2.34	0.88	0.83	0.59	0.49	1.32	1.78
K2O	0.06	0.12	0.15	0.40	0.24	0.11	0.13	0.17
P2O5	<0.01	0.01	<0.01	0.02	0.01	0.05	0.01	0.04
LOI	0.02	1.14	2.14	2.71	1.35	0.95	0.98	0.89
Rest	15.01	0.10	0.44	0.36	0.10	0.20	0.24	0.22
Total	95.38	99.95	99.78	99.70	100.10	100.05	99.79	100.28
O=F,S,Cl	0.00	0.01	0.02	0.05	0.00	0.00	0.04	0.04
Total	95.39	99.94	99.76	99.65	100.10	100.05	99.75	100.24
	Trace elements in parts per million							
Ba	<4	43	40	66	84	80	58	91
Li	2	5	5	15	8	6	4	3
Rb	1	4	2	22	20	5	3	4
Sr	7	285	112	111	163	148	210	213
Pb	5	6	4	6	5	7	<2	3
Th	<2	<2	<2	<2	<2	<2	<2	<2
U	-	1.0	-	-	1.0	1.0	-	1.0
Zr	12	36	12	31	12	44	14	33
Nb	<2	<2	<2	<2	<2	2	<2	<2
Y	4	10	8	9	4	16	4	10
La	<2	6	<2	4	<2	10	<2	2
Ce	<5	19	<5	9	<5	17	<5	<5
Nd	<2	7	<2	3	4	8	5	<2
Pr	<2	2	<2	3	4	2	<2	2
Sc	19	16	41	25	15	52	17	26
V	822	60	133	108	47	305	57	117
Cr	>99999	21	1901	827	26	279	226	180
Ni	664	31	343	428	252	211	502	273
Cu	44	19	88	173	13	26	70	56
Zn	1091	18	69	87	80	86	46	57
Ga	38	21	9	12	7	15	12	14
As	12	3	3	5	3	9	3	3
S	70	220	410	910	20	100	800	720
Cs	3	<3	<3	<3	3	<3	<3	<3
Se	<1	<1	<1	<1	<1	<1	<1	<1
	Trace elements in parts per billion							
Pd	1080	-	1.9	-	-	-	-	-
Pt	583	-	2.4	-	-	-	-	-
Au	8	-	2	-	-	-	-	-
εNd	-	-	-	-	-	-	-	-
mg	53.0	53.9	79.5	75.4	72.3	60.1	78.3	71.8

Sample number	93522063	93522064	93522065	93522066	93522067	93522068	93522069	93522070
Intrusion	Sally Malay	Sally Malay	Sally Malay	Sally Malay	Sally Malay	Sally Malay	Sally Malay	Sally Malay
Group	V	V	V	V	V	V	V	V
Lithology	Olivine gabbro	Olivine websterite	Plg lherzolite	Troctolite	Leuco gabbro	Leuco gabbro	Leuco gabbro	Troctolite
Strat. ht (m)	190	250	300	350	550	590	630	740
Easting	396520	396438	396488	396590	396300	396210	396115	395945
Northing	8081820	8081862	8082010	8082045	8082280	8082225	8082360	8082385
SiO2	43.07	46.58	40.94	42.43	48.76	49.25	48.62	45.83
TiO2	0.21	0.33	0.27	0.10	0.35	0.23	0.36	0.31
Al2O3	18.47	3.03	6.67	19.09	18.68	20.58	19.93	19.96
Fe2O3	1.55	2.18	2.47	1.15	0.94	0.83	0.78	0.53
FeO	7.92	15.25	13.75	7.74	8.13	6.11	6.38	6.57
MnO	0.11	0.22	0.20	0.10	0.14	0.11	0.11	0.09
MgO	15.79	28.93	27.43	16.61	8.67	9.52	9.08	12.85
CaO	10.12	1.94	5.26	10.07	11.46	11.13	11.63	11.34
Na2O	0.93	0.22	0.43	0.81	1.36	1.25	1.27	1.39
K2O	0.12	0.07	0.06	0.08	0.13	0.10	0.13	0.14
P2O5	0.02	0.02	0.01	0.01	0.02	0.03	0.06	0.02
LOI	1.26	0.75	1.93	1.12	1.06	0.66	1.29	0.88
Rest	0.38	0.54	0.51	0.35	0.34	0.29	0.28	0.20
Total	99.95	100.06	99.93	99.66	100.04	100.09	99.92	100.11
O=F,S,Cl	0.03	0.02	0.03	0.01	0.07	0.04	0.04	0.02
Total	99.92	100.04	99.90	99.65	99.97	100.05	99.87	100.08
Trace elements in parts per million								
Ba	94	38	42	61	66	66	89	61
Li	7	7	6	6	7	8	6	4
Rb	2	2	1	2	1	<1	2	2
Sr	462	26	143	416	323	453	445	198
Pb	3	5	4	3	5	3	2	3
Th	<2	<2	<2	<2	<2	<2	<2	<2
U	-	-	-	-	1	-	-	-
Zr	12	20	12	7	17	9	16	24
Nb	<2	<2	<2	<2	<2	<2	<2	<2
Y	4	6	5	2	8	5	7	7
La	4	4	2	<2	8	3	5	<2
Ce	15	11	7	11	12	13	14	7
Nd	6	3	<2	<2	6	3	6	<2
Pr	5	<2	<2	<2	2	<2	<2	<2
Sc	13	26	21	9	38	26	28	20
V	76	126	105	34	188	99	120	81
Cr	976	1585	1431	1077	496	514	424	279
Ni	645	1537	1324	730	121	168	140	337
Cu	42	55	74	18	110	72	47	28
Zn	65	136	112	58	72	57	59	48
Ga	12	4	6	12	16	16	14	12
As	1	1	2	2	2	3	3	1
S	510	450	540	190	1320	860	840	500
Cs	<3	<3	<3	<3	<3	<3	<3	3
Se	<1	<1	<1	<1	<1	<1	<1	<1
Trace elements in parts per billion								
Pd	-	4.2	-	-	-	-	-	-
Pt	-	3.1	-	-	-	-	-	-
Au	-	2	-	-	-	-	-	-
εNd	-	-	-	-	-	-	-	-
mg	75.1	75.0	75.4	77.1	63.3	71.2	69.6	76.5

Sample number	93522071	93522072	93522073	93522074	93522075	93522076	93522077	93522080
Intrusion	Sally Malay	Sally Malay	Sally Malay	Sally Malay	Sally Malay	Sally Malay	Unnamed	Three Nuns
Group	V	V	V	V	V	V	Turkey Creek microgabb.	V
Lithology	Olivine gabbronor.	Troctolite	Olivine gabbronor.	Leuco gabbro	Leuco gabbro	Magnetite gabbronor.	Gabbronor.	Limonitic gossan
Strat. ht (m)	940	1140	1440	1500	1700	-	-	-
Easting	395832	395510	395445	396865	396955	397062	396495	394240
Northing	8082670	8082855	8082808	8082995	8083168	8083110	8082206	8081144
SiO2	44.67	46.69	48.02	47.12	47.05	46.94	47.86	11.86
TiO2	0.28	0.33	0.28	0.59	1.53	1.17	1.10	0.36
Al2O3	16.23	20.07	17.84	26.53	27.77	17.40	12.80	2.50
Fe2O3	0.83	0.71	0.76	1.92	1.12	3.64	1.29	72.73
FeO	8.38	6.79	8.27	3.40	3.29	8.87	11.62	0.29
MnO	0.12	0.10	0.12	0.06	0.04	0.14	0.20	0.06
MgO	17.44	11.45	11.45	2.83	1.74	8.49	9.06	0.32
CaO	8.98	11.11	10.71	14.54	14.86	11.21	13.77	0.21
Na2O	1.26	1.55	1.19	1.79	1.91	1.28	1.16	0.14
K2O	0.11	0.22	0.30	0.08	0.13	0.10	0.08	0.47
P2O5	0.02	0.02	0.02	0.03	0.03	0.04	0.03	0.02
LOI	1.15	0.81	0.88	1.04	0.58	0.46	0.78	10.72
Rest	0.22	0.20	0.25	0.17	0.18	0.37	0.33	0.43
Total	99.69	100.05	100.09	100.10	100.23	100.11	100.08	100.11
O=F,S,Cl	0.03	0.03	0.03	0.01	0.02	0.08	0.07	0.13
Total	99.66	100.02	100.05	100.08	100.20	100.03	100.01	99.99
	Trace elements in parts per million							
Ba	44	88	105	82	120	69	11	316
Li	6	4	3	7	8	4	5	1
Rb	2	4	7	1	3	1	2	20
Sr	169	204	192	380	441	249	128	32
Pb	4	3	4	9	6	5	3	17
Th	<2	<2	<2	<2	<2	<2	<2	<2
U	-	-	-	-	-	-	1	1
Zr	19	20	19	15	28	25	27	74
Nb	<2	<2	<2	2	3	3	3	6
Y	6	6	9	7	6	10	18	6
La	2	5	2	6	11	8	<2	13
Ce	9	11	9	12	18	15	5	21
Nd	<2	6	2	7	6	6	4	4
Pr	2	<2	2	<2	2	2	5	3
Sc	17	20	26	27	26	39	55	3
V	68	85	99	264	163	485	398	203
Cr	198	190	426	76	14	189	217	141
Ni	512	291	275	42	11	148	103	43
Cu	43	32	29	37	33	109	147	332
Zn	62	54	75	34	30	91	92	69
Ga	12	13	14	25	27	19	15	5
As	1	1	2	1	1	3	4	11
S	610	620	690	230	490	1540	1470	2560
Cs	<3	4	<3	<3	<3	<3	<3	4
Se	<1	<1	<1	<1	<1	<1	<1	5
	Trace elements in parts per billion							
Pd	-	-	-	-	-	-	-	4.8
Pt	-	-	-	-	-	-	-	1.2
Au	-	-	-	-	-	-	-	2
εNd	-	-	-	-	-	-	-	-
mg	77.3	73.3	69.5	49.6	41.9	55.5	55.8	0.9

Sample number	93522103	93522104	93522106	93522107	93522126	93522133	93522153	94522050
Intrusion	Dave Hill	Dave Hill	Dave Hill	Dave Hill	Wilson Creek	Wilson Creek	Fletcher Creek	Spring Creek
Group	V	V	V	V	V	V	V	V
Lithology	Leuco gabbronor.	Olivine gabbronor.	Olivine gabbronor.	Troctolite	Olivine gabbronor.	Troctolite	Chilled mt gabbro	Gabbro
Strat. ht (m)	-	-	-	-	-	-	-	10
Easting	396022	396098	396222	396312	394142	393850	400000	387668
Northing	8078692	8078845	8079065	8078980	8077448	8077208	8080075	8075072
SiO2	50.18	45.35	48.59	45.07	45.40	45.97	48.12	50.22
TiO2	0.21	0.15	0.17	0.08	0.25	0.66	1.47	1.48
Al2O3	16.40	16.46	18.39	22.30	11.91	21.72	16.47	15.04
Fe2O3	1.04	1.44	0.67	0.69	1.33	0.80	1.92	0.71
FeO	7.21	8.01	5.98	4.93	13.18	6.49	9.62	9.69
MnO	0.13	0.12	0.10	0.07	0.18	0.08	0.16	0.15
MgO	13.02	14.68	11.58	11.21	15.81	9.42	7.38	7.11
CaO	9.72	10.51	11.72	12.55	8.95	11.56	11.67	10.77
Na2O	1.06	1.03	1.14	1.20	1.10	1.61	1.19	1.99
K2O	0.07	0.10	0.13	0.10	0.09	0.36	0.13	0.79
P2O5	<0.01	0.01	<0.01	0.01	0.01	0.05	0.22	0.37
LOI	0.73	1.89	0.97	1.61	1.35	0.75	1.36	0.99
Rest	0.37	0.31	0.56	0.29	0.33	0.24	0.32	0.40
Total	100.14	100.06	100.00	100.11	99.89	99.71	100.03	99.71
O=F,S,Cl	0.07	0.06	0.14	0.05	0.07	0.02	0.06	0.05
Total	100.07	100.00	99.86	100.06	99.82	99.69	99.97	99.66
Trace elements in parts per million								
Ba	62	79	90	80	62	188	125	403
Li	5	3	5	3	9	9	3	23
Rb	<1	2	2	1	1	11	1	32
Sr	376	364	355	396	144	229	253	180
Pb	5	5	5	3	5	6	3	12
Th	<2	<2	<2	<2	<2	<2	<2	5
U	1.0	-	-	-	-	-	-	<0.5
Zr	8	11	9	9	11	51	120	204
Nb	<2	<2	<2	<2	<2	4	9	20
Y	4	4	4	3	6	12	30	41
La	<2	2	4	3	2	12	16	47
Ce	5	7	<5	10	5	23	36	91
Nd	3	2	3	2	<2	9	19	42
Pr	<2	<2	<2	2	<2	<2	5	10
Sc	31	24	28	16	34	20	45	42
V	106	61	87	39	184	96	255	242
Cr	559	406	762	389	556	535	108	534
Ni	232	349	402	348	127	190	123	58
Cu	165	80	268	105	40	12	172	33
Zn	60	66	45	37	100	58	109	109
Ga	13	12	13	11	11	16	19	19
As	3.0	2.0	5.0	2.0	2.0	1.0	2.0	<0.5
S	1460	1130	2760	1030	1430	360	1190	1100
Cs	<3	4	<3	<3	<3	<3	<3	3
Se	<1	<1	<1	<1	<1	<1	<1	<1
Trace elements in parts per billion								
Pd	-	-	2.1	-	<0.5	-	2.8	-
Pt	-	-	1.4	-	0.5	-	0.5	-
Au	-	-	4	-	1	-	1	-
εNd	-	-	-	-	-	-	-	-
mg	74.0	73.8	75.8	78.3	66.2	70.0	53.7	55.1

Sample number	94522051	94522052	94522053	94522054	94522055	94522056	94522057	94522058
Intrusion	Spring Creek	Spring Creek	Spring Creek	Spring Creek	Spring Creek	Spring Creek	Spring Creek	Spring Creek
Group	V	V	V	V	V	V	V	V
Lithology	Mela gabbro	Leuco gabbro	Olivine gabbronor.	Olivine gabbro	Leuco gabbro	Olivine gabbro	Gabbronor.	Gabbronor.
Strat. ht (m)	200	400	610	790	970	1260	1385	1525
Easting	387460	387208	386922	386865	386630	386478	386258	386084
Northing	8075034	8074894	8074798	8074726	8074592	8074558	8074448	8074252
SiO2	48.74	48.78	49.52	46.26	48.72	47.63	50.25	49.17
TiO2	0.30	0.30	0.22	0.21	0.20	0.14	0.19	0.42
Al2O3	18.44	22.44	16.89	17.72	26.05	21.81	18.30	18.25
Fe2O3	0.32	1.95	0.50	0.75	0.49	0.74	0.69	0.85
FeO	5.19	3.07	5.34	9.92	2.84	4.89	7.91	7.11
MnO	0.09	0.08	0.10	0.13	0.05	0.08	0.13	0.12
MgO	8.84	5.90	10.91	12.30	3.78	6.94	9.56	8.48
CaO	15.22	13.98	14.09	9.99	15.00	14.93	10.50	12.50
Na2O	1.44	1.60	1.05	1.49	1.80	1.53	1.50	1.53
K2O	0.10	0.18	0.06	0.08	0.14	0.06	0.06	0.09
P2O5	0.02	0.03	0.01	0.02	0.02	0.01	0.01	0.02
LOI	0.71	1.25	0.68	1.03	0.92	1.01	0.85	0.75
Rest	0.32	0.22	0.29	0.26	0.13	0.18	0.31	0.21
Total	99.73	99.78	99.66	100.16	100.14	99.95	100.26	99.50
O=F,S,Cl	0.05	0.02	0.04	0.03	0.00	0.02	0.05	0.01
Total	99.68	99.76	99.62	100.12	100.14	99.93	100.20	99.49
Trace elements in parts per million								
Ba	91	107	49	61	92	53	51	71
Li	5	11	5	6	7	2	5	4
Rb	2	6	<1	<1	5	<1	<1	2
Sr	393	422	282	197	462	388	354	359
Pb	2	3	<2	<2	<2	<2	<2	<2
Th	<2	2	<2	<2	<2	<2	<2	<2
U	<0.5	<0.5	<0.5	0.5	<0.5	<0.5	<0.5	<0.5
Zr	15	15	9	7	15	6	6	13
Nb	2	3	<2	<2	<2	<2	<2	<2
Y	8	7	6	4	5	5	3	7
La	5	<2	<2	4	5	2	2	4
Ce	10	9	<5	6	6	<5	<5	<5
Nd	5	5	4	<2	3	2	<2	2
Pr	<2	3	2	<2	4	<2	<2	<2
Sc	39	31	40	20	27	35	30	42
V	135	114	150	79	93	121	114	264
Cr	624	388	666	572	139	241	633	291
Ni	132	59	127	301	16	63	157	145
Cu	113	19	87	28	5	18	40	13
Zn	37	40	40	86	28	34	68	55
Ga	13	16	12	16	18	15	16	17
As	<0.5	<0.5	<0.5	<0.5	<0.5	<0.5	<0.5	<0.5
S	950	470	800	650	90	450	1010	300
Cs	<3	<3	<3	<3	<3	<3	<3	<3
Se	<1	1	<1	<1	<1	<1	<1	<1
Trace elements in parts per billion								
Pd	-	-	-	-	-	-	-	-
Pt	-	-	-	-	-	-	-	-
Au	-	-	-	-	-	-	-	-
εNd	-	-	-	-	-	-	-	-
mg	74.2	68.5	77.1	65.6	67.2	69.0	66.6	65.7

Sample number	94522059	94522060	94522061	94522062	94522063	94522064	94522065	94522066
Intrusion	Spring Creek	Spring Creek	Spring Creek	Spring Creek	Spring Creek	Spring Creek	Unnamed	Unnamed
Group	V	V	V	V	V	V	Undivided gabbro	Undivided gabbro
Lithology	Troctolite	Olivine gabbro	Olivine gabbro	Olivine gabbronor.	Gabbronor.	Olivine gabbronor.	Gabbronor.	Gabbro
Strat. ht (m)	1690	1840	2000	2080	2230	2360	2500	2680
Easting	385868	385734	385548	385528	385308	385130	384878	384694
Northing	8073978	8073860	8073775	8073550	8073430	8073320	8073260	8073006
SiO2	47.05	47.54	45.72	46.90	50.02	45.59	49.18	49.73
TiO2	0.18	0.29	0.28	0.22	0.36	0.50	1.28	0.67
Al2O3	20.17	19.09	23.79	23.65	17.93	20.73	15.26	17.81
Fe2O3	0.69	0.45	0.68	0.38	0.63	0.69	1.00	0.68
FeO	7.16	5.09	5.55	5.01	5.70	7.70	10.03	6.97
MnO	0.10	0.09	0.07	0.07	0.11	0.10	0.15	0.12
MgO	9.79	8.72	7.60	7.75	9.39	9.60	8.43	7.30
CaO	12.51	15.73	12.94	12.85	12.78	11.40	9.95	12.40
Na2O	1.23	1.22	1.54	1.59	1.41	1.65	2.00	1.87
K2O	0.09	0.09	0.14	0.13	0.13	0.23	0.68	0.31
P2O5	0.02	0.03	0.06	0.04	0.04	0.13	0.24	0.07
LOI	0.94	0.90	1.16	1.04	0.98	1.47	1.23	1.59
Rest	0.31	0.40	0.25	0.25	0.29	0.25	0.37	0.28
Total	100.24	99.64	99.78	99.88	99.77	100.04	99.80	99.80
O=F,S,Cl	0.05	0.06	0.03	0.03	0.04	0.03	0.05	0.04
Total	100.19	99.58	99.75	99.85	99.73	100.01	99.74	99.76
Trace elements in parts per million								
Ba	82	87	101	88	83	135	295	146
Li	3	7	5	8	7	11	15	11
Rb	<1	2	2	2	3	5	17	11
Sr	520	589	359	346	276	329	182	271
Pb	<2	<2	<2	<2	<2	2	6	3
Th	<2	<2	<2	<2	<2	2	3	<2
U	1.5	<0.5	0.5	0.5	2	<0.5	0.5	<0.5
Zr	7	13	21	16	23	40	124	42
Nb	<2	<2	2	3	3	6	12	5
Y	4	7	6	5	8	10	31	12
La	4	7	5	5	6	11	24	10
Ce	5	16	13	9	8	14	52	17
Nd	3	11	4	3	3	9	27	11
Pr	2	<2	<2	<2	<2	3	8	<2
Sc	24	41	17	19	38	18	36	41
V	61	106	57	55	141	62	208	179
Cr	551	892	552	507	649	319	498	459
Ni	238	178	218	202	119	322	174	79
Cu	45	65	36	55	95	36	62	69
Zn	54	34	46	39	47	66	103	63
Ga	15	16	17	16	15	14	17	16
As	<0.5	<0.5	<0.5	<0.5	<0.5	<0.5	<0.5	<0.5
S	920	1150	550	600	810	640	1090	770
Cs	<3	<3	<3	4	<3	<3	<3	4
Se	<1	<1	<1	<1	<1	<1	<1	<1
Trace elements in parts per billion								
Pd	-	-	-	-	-	-	-	-
Pt	-	-	-	-	-	-	-	-
Au	-	-	-	-	-	-	-	-
εNd	-	-	-	-	-	-	-	-
mg	69.2	73.9	68.7	72.1	72.8	67.3	57.9	63.2

Sample number	94522067	94522068	94522069	94522070	94522076	94522081	94522082	94522083
Intrusion	Unnamed	Unnamed	Unnamed	Unnamed	Amphithea.	Greenvale Fault	Greenvale Fault	Greenvale Fault
Group	Undivided gabbro	Undivided gabbro	Undivided gabbro	Corridor gabbro	VII	Corridor gabbro	Corridor gabbro	Corridor gabbro
Lithology	Gabbro	Biotite gabbro	Biotite olivine gabbro	Biotite quartz diorite	Olivine gabbronor.	Biotite gabbro	Biotite gabbro	Biotite quartz gabbro
Strat. ht (m)	2810	3030	3290	-	-	-	-	-
Easting	384478	384212	383988	384134	381064	361930	361030	362288
Northing	8072865	8072738	8072578	8075756	8074900	8073884	8081580	8089466
SiO2	50.25	50.60	49.90	52.66	46.40	51.76	49.02	50.58
TiO2	0.58	0.83	0.92	1.89	1.18	1.03	0.68	1.17
Al2O3	13.47	14.71	16.19	14.30	15.91	15.13	19.19	15.10
Fe2O3	0.92	1.13	1.43	2.19	1.16	1.31	1.07	1.30
FeO	8.39	8.68	7.84	8.55	11.07	8.11	6.10	9.19
MnO	0.16	0.15	0.13	0.15	0.15	0.14	0.11	0.15
MgO	9.25	8.93	8.04	5.33	11.01	8.24	6.90	7.22
CaO	14.16	11.37	10.57	8.86	9.21	9.69	11.72	10.56
Na2O	1.41	1.69	1.88	2.06	1.55	1.87	2.09	1.92
K2O	0.13	0.36	0.42	1.82	0.62	1.11	0.43	0.83
P2O5	0.04	0.16	0.12	0.39	0.30	0.15	0.08	0.15
LOI	0.84	0.93	1.63	1.18	1.09	1.02	2.17	1.16
Rest	0.29	0.24	0.32	0.30	0.43	0.26	0.26	0.33
Total	99.89	99.78	99.39	99.68	100.08	99.82	99.82	99.66
O=F,S,Cl	0.04	0.02	0.03	0.02	0.06	0.01	0.06	0.06
Total	99.86	99.76	99.35	99.66	100.02	99.81	99.76	99.60
Trace elements in parts per million								
Ba	97	171	214	503	264	223	78	193
Li	10	7	6	19	9	11	4	8
Rb	2	10	11	90	21	59	25	43
Sr	197	271	326	240	215	147	134	120
Pb	<2	2	5	16	5	8	6	6
Th	<2	3	4	11	3	9	3	7
U	<0.5	<0.5	<0.5	0.5	1.5	2	0.5	1.5
Zr	29	52	66	185	109	105	58	118
Nb	3	6	8	20	11	8	3	9
Y	17	18	18	44	22	28	17	32
La	7	14	12	53	22	19	8	16
Ce	8	31	28	104	45	43	15	36
Nd	9	15	14	51	19	22	8	20
Pr	3	4	<2	10	6	5	4	3
Sc	61	47	38	35	25	35	35	40
V	283	205	182	235	114	216	160	245
Cr	488	404	632	185	805	497	181	366
Ni	95	92	87	48	349	173	131	94
Cu	113	67	56	30	81	70	66	69
Zn	67	78	82	117	106	81	55	90
Ga	16	17	17	19	16	17	16	17
As	<0.5	<0.5	<0.5	1.0	<0.5	1.0	1.0	1.0
S	790	310	690	340	1280	180	1180	1130
Cs	<3	<3	<3	8	5	6	3	4
Se	<1	<1	<1	<1	<1	<1	<1	<1
Trace elements in parts per billion								
Pd	-	-	-	-	-	-	-	-
Pt	-	-	-	-	-	-	-	-
Au	-	-	-	-	-	-	-	-
εNd	-	-	-	-	-	-	-	-
mg	64.1	62.1	61.1	47.4	61.8	61.3	63.5	55.4

Sample number	94522089	94522126	94522127	94522129	94522138	94522147	94522148	94522152
Intrusion	Keller Creek	Keller Creek	Keller Creek	Nine Mile	Norton	Norton	Norton	Frog Hollow
Group	V	V	V	Corridor gabbro	Tickalara Metamorph.	Tickalara Metamorph.	Tickalara Metamorph.	V
Lithology	Olivine gabbronor.	Olivine gabbro	Olivine gabbro	Mela gabbro	Limonitic gossan	Metagabbro	Limonitic gossan	Ti-Fe oxide lens
Strat. ht (m)	-	-	-	-	1	-	2	-
Easting	390275	390440	390440	394265	396970	398280	398618	398550
Northing	8086600	8086555	8086585	8095195	8094040	8095930	8096150	8090020
SiO2	47.02	48.18	48.65	48.05	29.40	47.59	21.37	7.50
TiO2	1.13	0.98	1.68	1.26	0.53	1.22	0.23	22.14
Al2O3	14.47	13.29	13.32	17.89	3.43	13.24	4.26	0.89
Fe2O3	0.55	0.40	2.46	1.51	56.23	1.28	62.95	43.27
FeO	12.03	11.11	13.94	8.68	0.26	12.73	0.38	15.62
MnO	0.19	0.19	0.25	0.14	0.08	0.22	0.06	0.32
MgO	8.32	8.98	5.66	5.88	0.77	7.62	0.11	1.13
CaO	13.96	14.44	10.37	12.25	0.20	12.29	0.11	0.14
Na2O	1.25	1.07	1.74	1.90	0.03	1.25	0.11	0.31
K2O	0.01	0.02	0.19	0.21	0.40	0.15	1.52	0.06
P2O5	0.02	0.01	0.14	0.05	0.11	0.11	0.05	0.10
LOI	1.19	1.01	1.21	1.76	8.26	1.51	8.79	5.14
Rest	0.30	0.40	0.50	0.30	0.32	0.35	0.34	3.40
Total	100.44	100.08	100.11	99.88	100.02	99.56	100.28	100.02
O=F,S,Cl	0.07	0.11	0.17	0.06	0.05	0.07	0.08	0.06
Total	100.37	99.97	99.94	99.81	99.97	99.49	100.20	99.97
Trace elements in parts per million								
Ba	8	4	17	78	16	269	491	14
Li	6	4	6	7	4	9	3	1
Rb	<1	<1	3	4	108	2	34	1
Sr	142	141	155	207	18	212	35	8
Pb	<2	<2	3	5	7	<2	34	3
Th	3	<2	<2	<2	4	<2	9	<2
U	1.0	<0.5	<0.5	0.5	6	<0.5	3.5	<0.5
Zr	12	14	62	29	34	47	67	58
Nb	2	2	5	3	7	4	7	17
Y	14	15	27	15	21	28	10	3
La	6	<2	6	6	2	16	17	<2
Ce	<5	<5	<5	12	5	14	28	9
Nd	3	<2	9	5	6	20	16	2
Pr	<2	<2	6	2	<2	2	3	31
Sc	53	55	51	45	40	25	3	48
V	398	376	457	343	281	344	170	9943
Cr	118	298	13	180	147	161	43	9271
Ni	85	108	43	53	79	91	17	490
Cu	106	65	74	57	139	78	62	280
Zn	83	85	135	88	655	135	305	244
Ga	15	15	22	19	11	18	8	27
As	<0.5	<0.5	<0.5	1.0	1.0	<0.5	3.0	<0.5
S	1410	2200	3320	1300	1010	1390	1610	1160
Cs	<3	<3	4	<3	<3	13	<3	<3
Se	<1	<1	<1	<1	3	<1	3	5
Trace elements in parts per billion								
Pd	-	-	-	-	-	-	-	-
Pt	-	-	-	-	-	-	-	-
Au	-	-	-	-	-	-	-	-
εNd	-	-	-	-	-	-	-	-
mg	54.2	58.2	38.4	51.1	2.6	49.4	0.3	3.6

Sample number	94522167	94522168	94522169	94522170	94522171	94522172	94522173	94522178
Intrusion	Norton	Norton	Norton	Norton	Norton	Norton	Norton	Frog Hollow V
Group	Tickalara Metamorph.	Tickalara Metamorph.	Tickalara Metamorph.	Tickalara Metamorph.	Tickalara Metamorph.	Tickalara Metamorph.	Tic kalara Metamorph.	
Lithology	Hornblende metagabbro	Hornblende metagabbro	Hornblende metagabbro	Hornblende metagabbro	Metagabbro	Metagabbro	Hornblende metagabbro	Ti-Fe oxide lens
Strat. ht (m)	20	100	300	550	700	850	1000	-
Easting	397510	397626	397806	397965	398095	398174	398280	398400
Northing	8094360	8094378	8094398	8094398	8094275	8094102	8093980	8087280
SiO2	48.42	44.78	47.99	48.41	47.96	52.75	48.40	3.88
TiO2	0.96	2.67	1.32	1.19	1.58	1.22	0.96	39.41
Al2O3	14.12	12.14	13.04	14.00	13.92	14.05	14.80	0.55
Fe2O3	1.44	1.81	0.92	0.80	0.08	0.29	0.81	19.12
FeO	10.79	18.03	12.93	12.86	14.63	12.24	10.67	30.00
MnO	0.19	0.24	0.21	0.21	0.22	0.19	0.19	0.43
MgO	8.15	5.77	7.60	7.15	7.60	6.59	7.96	2.35
CaO	12.35	10.55	12.30	12.06	11.90	10.75	13.07	0.13
Na2O	1.63	1.84	1.92	1.76	0.54	0.58	1.53	0.28
K2O	0.14	0.07	0.09	0.12	0.04	0.04	0.12	0.02
P2O5	0.08	0.16	0.12	0.11	0.14	0.11	0.09	0.19
LOI	1.37	1.73	1.27	1.24	1.39	1.21	1.06	3.28
Rest	0.18	0.55	0.33	0.35	0.41	0.29	0.29	0.70
Total	99.82	100.34	100.04	100.26	100.41	100.31	99.95	100.34
O=F,S,Cl	0.01	0.13	0.08	0.09	0.12	0.07	0.06	0.02
Total	99.81	100.21	99.96	100.17	100.30	100.24	99.89	100.31
Trace elements in parts per million								
Ba	15	14	23	13	18	23	<4	<4
Li	7	7	5	7	4	4	6	4
Rb	2	<1	<1	1	<1	1	<1	<1
Sr	121	134	163	132	162	148	131	4
Pb	<2	<2	<2	<2	5	3	<2	4
Th	<2	<2	<2	<2	<2	<2	<2	<2
U	<0.5	<0.5	1.0	<0.5	0.5	<0.5	1.5	<0.5
Zr	44	77	57	53	79	63	41	114
Nb	4	10	5	2	6	6	3	56
Y	23	34	27	26	28	30	21	2
La	5	6	5	4	3	7	<2	<2
Ce	7	18	11	11	7	18	12	7
Nd	<2	17	12	9	6	9	9	4
Pr	<2	<2	3	2	4	<2	<2	83
Sc	55	54	53	53	51	45	54	70
V	354	1009	386	403	398	328	351	2335
Cr	186	19	171	119	163	92	226	833
Ni	101	54	80	78	85	61	100	61
Cu	70	167	53	95	45	20	81	266
Zn	101	152	125	106	129	105	91	135
Ga	17	21	18	18	21	20	16	7
As	<0.5	<0.5	<0.5	<0.5	<0.5	<0.5	<0.5	<0.5
S	160	2700	1550	1810	2310	1470	1160	480
Cs	<3	<3	<3	3	<3	<3	<3	<3
Se	<1	<1	<1	<1	<1	<1	1	4
Trace elements in parts per billion								
Pd	-	-	-	-	-	-	-	-
Pt	-	-	-	-	-	-	-	-
Au	-	-	-	-	-	-	-	-
εNd	-	-	-	-	-	-	-	-
mg	54.6	34.3	49.6	48.4	47.9	48.4	55.4	8.1

Sample number	94522193	94522198	94522199	94522200	94522214	94522216	94522217	94522226
Intrusion	Unnamed	Corkwood	Corkwood	Corkwood	Corkwood	Unnamed	Fletcher Creek	Unnamed
Group	Tickalara Metamorph.	V	V	V	V	Tickalara Metamorph.	V	Tickalara Metamorph.
Lithology	Amphibol.	Mela gabbro	Limonitic gossan	Chilled gabbro	Metagabbro	Amphibol.	Chilled biotite gabbro	Amphibol.
Strat. ht (m)	-	-	-	-	-	-	-	-
Easting	413265	413480	413480	413912	413204	413520	398972	415102
Northing	8087588	8087770	8087820	8088850	8087525	8087640	8078715	8110385
SiO2	51.54	51.23	36.12	49.29	50.25	48.15	44.35	48.27
TiO2	0.84	0.48	0.53	0.30	1.08	1.40	0.82	0.64
Al2O3	15.89	5.41	6.07	18.50	13.69	13.71	14.93	14.99
Fe2O3	0.92	0.69	30.01	0.35	1.37	1.51	2.89	1.26
FeO	7.83	8.79	4.03	7.39	10.62	11.77	8.11	8.18
MnO	0.13	0.15	0.15	0.12	0.20	0.21	0.13	0.15
MgO	7.48	17.07	6.95	8.47	6.91	7.68	7.87	8.72
CaO	10.79	11.85	3.66	12.10	11.35	11.77	18.31	14.15
Na2O	2.18	0.72	0.48	1.53	2.41	1.93	0.54	1.25
K2O	0.27	0.26	0.35	0.17	0.30	0.36	0.05	0.12
P2O5	0.08	0.05	0.10	0.03	0.10	0.13	0.08	0.05
LOI	1.42	2.24	8.37	1.16	1.08	1.29	1.65	1.70
Rest	0.26	0.60	3.31	0.35	0.27	0.22	0.27	0.29
Total	99.63	99.54	100.13	99.76	99.63	100.13	100.00	99.77
O=F,S,Cl	0.04	0.10	0.05	0.09	0.05	0.01	0.03	0.04
Total	99.59	99.44	100.07	99.67	99.58	100.12	99.96	99.73
Trace elements in parts per million								
Ba	55	56	148	71	58	144	12	11
Li	11	8	10	10	13	10	6	7
Rb	2	4	25	1	2	3	<1	1
Sr	279	95	79	424	154	149	177	108
Pb	3	<2	<2	<2	2	3	<2	<2
Th	<2	<2	2	<2	<2	<2	<2	<2
U	1.0	0.5	2.0	1.5	<0.5	0.5	1.5	<0.5
Zr	40	40	48	15	59	66	47	20
Nb	4	<2	3	<2	6	6	4	2
Y	13	13	9	7	27	28	19	15
La	5	9	7	4	5	4	3	5
Ce	12	24	21	12	13	14	<5	8
Nd	9	14	10	6	8	12	7	5
Pr	<2	4	3	<2	4	3	<2	<2
Sc	29	58	23	34	53	54	50	52
V	177	219	304	158	346	389	331	293
Cr	272	1503	1261	174	75	222	359	538
Ni	195	525	14650	227	69	114	155	163
Cu	64	120	8240	95	172	78	86	103
Zn	83	74	115	60	99	116	70	67
Ga	17	9	12	17	16	17	16	14
As	<0.5	<0.5	<0.5	<0.5	<0.5	<0.5	0.5	<0.5
S	880	2090	1070	1720	960	120	670	880
Cs	<3	<3	<3	<3	<3	<3	4	<3
Se	<1	<1	11	<1	<1	<1	<1	<1
Trace elements in parts per billion								
Pd	-	-	-	-	-	-	-	-
Pt	-	-	-	-	-	-	-	-
Au	-	-	-	-	-	-	-	-
εNd	-	-	-	-	-	-	-	-
mg	60.6	76.4	28.5	66.2	51.0	51.0	56.7	62.5

Sample number	94522237	94522238	94522239	94522240	94522276	94522278	94522282	94522283
Intrusion	Faulted	Faulted	Faulted	Faulted	Unnamed	Unnamed	Unnamed	Mabel Downs West
Group	Corridor gabbro	Corridor gabbro	Corridor gabbro	Corridor gabbro	Tickalara Metamorph.	Corridor gabbro	Turkey Creek microgabb.	Corridor gabbro
Lithology	Biotite gabbronor.	Biot-mt-gabbronor.	Biot-mt-gabbronor.	Biot-mt-gabbronor.	Amphibol.	Olivine gabbro	Magnetite microgabb.	Biot-mt-gabbro
Strat. ht (m)	-	-	-	-	-	-	-	-
Easting	411992	412088	412274	412432	413160	412780	417560	405618
Northing	8115884	8115320	8114480	8114040	8107110	8108220	8120155	8101735
SiO2	49.82	49.44	49.41	51.18	47.79	47.33	51.24	50.22
TiO2	0.79	0.21	0.95	1.11	0.54	0.84	1.69	1.96
Al2O3	11.03	16.64	17.16	15.97	16.65	16.53	13.61	15.24
Fe2O3	0.89	0.76	1.07	0.71	1.16	1.72	1.03	2.45
FeO	12.01	7.68	11.24	10.55	7.08	9.69	13.12	10.43
MnO	0.20	0.13	0.18	0.18	0.13	0.15	0.20	0.17
MgO	13.51	10.94	6.90	8.89	8.77	9.94	7.69	6.34
CaO	7.98	11.39	9.66	7.39	14.39	10.19	9.58	9.01
Na2O	1.00	0.91	1.46	1.78	1.12	1.77	0.33	2.08
K2O	0.43	0.10	0.23	0.88	0.30	0.27	0.04	0.75
P2O5	0.47	0.03	0.19	0.21	0.04	0.16	0.11	0.23
LOI	1.31	1.44	1.29	1.08	1.75	1.14	1.31	1.14
Rest	0.59	0.33	0.32	0.38	0.22	0.27	0.38	0.21
Total	100.03	100.00	100.06	100.31	99.94	100.00	100.33	100.23
O=F,S,Cl	0.10	0.05	0.06	0.04	0.03	0.05	0.07	0.01
Total	99.92	99.95	100.00	100.27	99.90	99.95	100.25	100.22
Trace elements in parts per million								
Ba	138	63	140	367	13	120	57	282
Li	8	8	9	14	6	6	5	15
Rb	11	2	4	36	3	6	3	24
Sr	308	150	289	382	127	171	141	170
Pb	3	3	5	6	3	2	3	6
Th	4	<2	2	<2	<2	3	<2	3
U	1.0	1.0	<0.5	<0.5	0.5	0.5	1.5	1
Zr	48	10	50	79	15	45	88	88
Nb	7	<2	9	7	<2	6	14	8
Y	38	9	23	22	13	15	32	20
La	29	8	14	20	3	8	8	18
Ce	69	17	37	43	8	19	26	31
Nd	50	4	19	24	3	11	14	15
Pr	8	2	6	7	2	<2	<2	4
Sc	49	39	48	35	50	31	37	35
V	299	236	205	210	256	143	282	248
Cr	1252	857	341	690	222	320	438	223
Ni	147	80	56	82	127	207	198	87
Cu	50	24	31	34	101	55	109	29
Zn	143	75	160	133	60	94	145	107
Ga	17	15	22	22	14	15	20	20
As	<0.5	<0.5	<0.5	<0.5	<0.5	<0.5	<0.5	<0.5
S	2090	920	1120	840	660	930	1450	130
Cs	5	<3	<3	<3	<3	<3	<3	<3
Se	<1	<1	<1	<1	<1	<1	<1	<1
Trace elements in parts per billion								
Pd	-	-	-	-	-	-	-	-
Pt	-	-	-	-	-	-	-	-
Au	-	-	-	-	-	-	-	-
εNd	-	-	-	-	-	-	-	-
mg	65.3	70.0	50.2	58.6	65.8	61.2	49.4	47.2

Sample number	94522285	94522287	94522288	94522311	94522319	94522320	83330026	83330030
Intrusion	Mabel Downs West	Mabel Downs West	Mabel Downs Southwest	Wilson Creek	Unnamed dolerite	Unnamed	Lamboo	Unnamed
Group	Corridor gabbro	Corridor gabbro	V	V		Tickalara Metamorph.	I	Undivided gabbro
Lithology	Biot-mt-gabbro	Chilled mt gabbro	Ti-Fe oxide lens	Gabbronor.	Dolerite dyke	Amphibol.	Microgabb.	Gabbro
Strat. ht (m)	-	-	-	-	-	-	-	-
Easting	405192	404205	403282	392338	403370	392958	321500	382700
Northing	8101255	8100958	8100095	8075192	8094050	8081720	8057300	8032700
SiO2	45.40	47.63	27.86	48.52	52.31	48.71	48.71	49.08
TiO2	4.72	2.01	15.46	1.22	1.46	1.26	0.80	1.09
Al2O3	13.43	15.01	6.08	15.93	13.73	13.25	15.82	16.24
Fe2O3	2.68	1.54	16.96	1.33	3.13	0.87	4.48	1.18
FeO	12.92	12.09	19.89	11.20	10.36	13.97	5.82	9.57
MnO	0.18	0.18	0.30	0.18	0.18	0.22	0.13	0.15
MgO	7.11	7.00	6.49	7.82	4.60	6.66	7.56	8.00
CaO	9.71	10.00	3.78	10.17	8.83	11.27	9.25	11.33
Na2O	1.96	1.98	0.66	1.62	2.47	2.01	2.29	1.97
K2O	0.39	0.52	0.11	0.13	1.13	0.04	0.06	0.15
P2O5	0.14	0.41	0.04	0.14	0.19	0.12	0.05	0.08
LOI	1.22	1.27	2.19	1.43	1.40	1.39	4.26	1.09
Rest	0.48	0.30	0.46	0.29	0.31	0.34	0.17	0.14
Total	100.34	99.94	100.28	99.98	100.10	100.11	99.40	100.07
O=F,S,Cl	0.10	0.03	0.00	0.02	0.04	0.08	0.00	0.00
Total	100.24	99.90	100.28	99.96	100.06	100.03	99.40	100.07
Trace elements in parts per million								
Ba	127	349	29	445	394	17	301	105
Li	15	12	5	15	12	14	7	3
Rb	10	14	3	3	39	<1	2	2
Sr	146	176	70	156	187	136	149	213
Pb	4	5	<2	4	7	2	3	4
Th	3	2	<2	<2	6	<2	1	<1
U	0.5	<0.5	<0.5	1.5	2.0	<0.5	1.0	1.0
Zr	48	114	46	90	158	58	43	28
Nb	7	15	9	15	9	4	2	2
Y	13	34	7	31	35	29	17	17
La	6	23	<2	16	23	<2	5	8
Ce	14	48	<5	30	46	9	6	13
Nd	9	26	3	20	22	7	5	9.42
Pr	3	7	22	4	8	3	-	-
Sc	49	43	58	46	38	59	36	33
V	761	267	1693	220	322	428	212	192
Cr	271	250	495	347	68	119	296	167
Ni	120	118	48	142	54	72	57	89
Cu	72	58	107	125	141	103	32	54
Zn	106	132	141	110	127	124	61	80
Ga	20	20	22	19	22	20	15	14
As	<0.5	<0.5	<0.5	<0.5	1.0	<0.5	<1.0	<1.0
S	2040	610	100	450	800	1590	-	-
Cs	3	<3	<3	<3	<3	<3	-	-
Se	<1	<1	<1	<1	<1	<1	-	-
Trace elements in parts per billion								
Pd	-	-	-	-	-	-	-	-
Pt	-	-	-	-	-	-	-	-
Au	-	-	-	-	-	-	-	-
εNd	-	-	-	-	-	-	-	1.3
mg	45.2	48.1	24.8	52.9	38.4	44.6	57.8	57.3

Sample number	83330043	83330047	83330050	83330052	83330054	83330060	83330081	83330085
Intrusion	McIntosh	Toby	Toby	Toby	Toby	Toby	Unnamed	Unnamed
Group	VI	III	III	III	III	III		
Lithology	Troctolite	Gabbro	Biotite gabbro	Biotite gabbro	Biotite gabbro	Gabbro	Gabbro	Biotite gabbro
Strat. ht (m)	-	-	-	-	-	-	-	-
Easting	386300	356600	357200	354500	357400	358600	395200	396100
Northing	8045600	8054100	8054600	8062300	8054400	8051900	8076100	8074700
SiO2	47.69	49.10	49.19	48.73	49.06	47.28	49.16	48.19
TiO2	0.17	1.07	1.20	1.17	1.40	1.71	2.15	1.15
Al2O3	26.55	16.23	15.60	15.21	15.36	14.47	13.37	15.50
Fe2O3	0.94	1.71	1.82	1.86	1.87	1.81	2.76	1.06
FeO	2.64	8.71	9.27	9.48	9.51	11.74	11.07	10.53
MnO	0.04	0.13	0.14	0.16	0.14	0.17	0.18	0.16
MgO	4.49	7.70	7.73	7.50	7.67	8.15	5.26	8.56
CaO	14.12	10.87	10.41	11.52	10.42	6.43	9.02	12.15
Na2O	2.51	2.07	1.91	2.22	2.03	3.10	2.46	1.35
K2O	0.09	0.78	0.74	0.46	0.76	0.19	1.12	0.24
P2O5	0.03	0.16	0.18	0.21	0.24	0.27	0.31	0.14
LOI	0.60	1.09	0.97	1.03	0.87	4.34	2.25	1.28
Rest	0.10	0.29	0.30	0.21	0.31	0.21	0.29	0.18
Total	99.97	99.91	99.46	99.76	99.64	99.87	99.40	100.49
O=F,S,Cl	0.00	0.05	0.05	0.00	0.05	0.00	0.00	0.00
Total	99.97	99.86	99.41	99.76	99.59	99.87	99.40	100.49
Trace elements in parts per million								
Ba	51	295	275	297	284	73	406	150
Li	3	8	11	9	10	14	6	3
Rb	2	38	32	17	32	7	36	6
Sr	477	213	143	218	143	61	246	163
Pb	2	5	7	6	10	3	8	3
Th	<1	2	3	1	3	4	4	1
U	<1.0	1.0	1.0	<1.0	1.0	2.0	<1.0	<1.0
Zr	7	101	122	106	161	168	149	69
Nb	<2	6	5	6	8	10	12	4
Y	3	25	29	28	34	39	31	24
La	4	19	20	25	25	29	25	9
Ce	7	33	35	45	44	53	47	18
Nd	2.57	19	20	21.97	25	26	26.70	11.68
Pr	-	-	-	-	-	-	-	-
Sc	8	27	29	34	29	34	30	37
V	23	178	181	213	175	228	302	227
Cr	106	254	276	275	274	348	544	260
Ni	41	107	122	73	126	96	31	128
Cu	53	54	56	59	53	109	52	61
Zn	19	80	87	90	90	110	125	91
Ga	17	16	17	20	19	13	21	16
As	<1.00	1.00	1.00	<1.00	<1.00	1.00	<1.00	1.00
S	-	950	1000	-	1000	90	-	-
Cs	-	-	-	-	-	-	-	-
Se	-	-	-	-	-	-	-	-
Trace elements in parts per billion								
Pd	-	-	-	-	-	-	-	-
Pt	-	-	-	-	-	-	-	-
Au	-	-	-	-	-	-	-	-
εNd	1.2	-	-	-0.9	-	-	-0.1	0.5
mg	69.7	57.2	55.8	54.5	55.0	52.1	40.9	57.1

APPENDIX 3. MINERAL CHEMICAL TABLES

Electron probe microanalyses were carried out on the cores and rims of cumulus minerals, intercumulus minerals, and corona minerals from thirteen intrusions. The tables of data (3.1 to 3.13) have been arranged alphabetically (intrusion and mineral names) and have been divided into silicate minerals (amphibole, biotite, clinopyroxene, olivine, orthopyroxene, plagioclase), and oxide minerals (ilmenite, magnetite, spinel). Appendix Table 3.14 is a compilation of chromite data from the East Kimberley intrusions (including data from the Lamboo intrusion).

Appendix Table 3.1.	Silicate minerals from the Armanda intrusion
Appendix Table 3.1a.	Oxide minerals from the Armanda intrusion
Appendix Table 3.2.	Silicate minerals from the Big Ben intrusion
Appendix Table 3.2a.	Oxide minerals from the Big Ben intrusion
Appendix Table 3.3.	Silicate minerals from the Dave Hill intrusion
Appendix Table 3.3a.	Oxide minerals from the Dave Hill intrusion
Appendix Table 3.4.	Silicate minerals from the Keller Creek intrusion
Appendix Table 3.5.	Silicate minerals from the McKenzie Spring intrusion
Appendix Table 3.5a.	Oxide minerals from the McKenzie Spring intrusion
Appendix Table 3.6.	Silicate minerals from the McIntosh intrusion
Appendix Table 3.6a.	Oxide minerals from the McIntosh intrusion
Appendix Table 3.7.	Silicate minerals from the Norton intrusion
Appendix Table 3.8.	Silicate minerals from the Sally Malay intrusion
Appendix Table 3.8a.	Oxide minerals from the Sally Malay intrusion
Appendix Table 3.9.	Silicate minerals from the Spring Creek intrusion
Appendix Table 3.10.	Silicate minerals from the Springvale intrusion
Appendix Table 3.10a.	Oxide minerals from the Springvale intrusion
Appendix Table 3.11.	Silicate minerals from the Toby intrusion
Appendix Table 3.11a.	Oxide minerals from the Toby intrusion
Appendix Table 3.12.	Silicate minerals from the Wilagee intrusion
Appendix Table 3.12a.	Oxide minerals from the Wilagee intrusion
Appendix Table 3.13.	Silicate minerals from the Wilson Creek intrusion
Appendix Table 3.13a.	Oxide minerals from the Wilson Creek intrusion
Appendix Table 3.14.	Chromite from the East Kimberley intrusions

Explanation of attribute data and atomic ratios used in the mineral tables

Sample no: Eight-digit, comprising year of collection (92, 93, 94), AGSO project code (52), and four-digit sample number. Appendix Table 3.14 also includes two samples collected in 1983 from the Lamboo intrusion. Most samples are arranged in order of increasing sample number. Sample locations are given as Australian Map Grid (AMG) co-ordinates in the whole-rock geochemical tables in Appendix 2 and in AGSO's geological database OZROX.

Analysis no: Analyses undertaken at the Research School of Earth Sciences, Australian National University have a five-digit number, whereas those undertaken at the University of Tasmania are indicated by a number and Tas (e.g. 1 – Tas).

Mineral: As indicated.

Description: Cumulus, intercumulus, corona, core of grain (c), rim of grain (r), alteration (alter), inclusion (incl), metamorphic (metam), repl = replacement of, cpx = clinopyroxene, oliv = olivine, plag = plagioclase.

Lithology: As indicated. Abbreviations used are biot = biotite, gabbronor = gabbronorite, qtz = quartz, suboph = subophitic.

Strat. ht (m): Estimated stratigraphic height in metres above the base of the intrusion. A traverse distance in metres is used for the Toby intrusion since the true thickness of the stratigraphy could not be measured due to poor outcrop.

Atomic ratios used:

Amphibole:

mg number = mg = 100 x Mg/(Mg + Fe^{2+})

(Amphibole classification after Hawthorne, F.C., 1983. The crystal chemistry of the amphiboles. Canadian Mineralogist, 21, 173–480)

Biotite:

mg number = mg = 100 x Mg/(Mg + Fe), where Fe = total Fe

Chromite:

mg number = mg = 100 x Mg/(Mg + Fe^{2+})

Cr ' = 100 x Cr/(Cr + Al + Fe^{3+})

Al ' = 100 x Al/(Cr + Al + Fe^{3+})

$Fe^{3+'} = 100 \times Fe^{3+}/(Cr + Al + Fe^{3+})$

Olivine:

mg number = mg = $100 \times Mg/(Mg + Fe^{2+})$

Plagioclase:

Albite = $100 \times Ca/(Ca + Na + K)$

Anorthite = $100 \times Na/(Ca + Na + K)$

Orthoclase = $100 \times K/(Ca + Na + K)$

Pyroxene:

mg number = mg = $100 \times Mg/(Mg + Fe^{2+})$

Enstatite = $100 \times Mg/(Mg + Fe^{2+} + Ca)$

Ferrosilite = $100 \times Fe^{2+}/(Mg + Fe^{2+} + Ca)$

Wollastonite = $100 \times Ca/(Mg + Fe^{2+} + Ca)$

Spinel:

mg number = mg = $100 \times Mg/(Mg + Fe^{2+})$

For all minerals:

FeO* = total iron calculated as FeO

Appendix Table 3.1. Electron microprobe analyses of silicate minerals from the Armanda layered intrusion.

Sample no.	92522493	92522493	92522493	92522493	92522493	92522493
Analysis no.	71706	71707	71718	71729	72171	72172
Mineral	Amphibole	Amphibole	Amphibole	Amphibole	Amphibole	Amphibole
Description	Corona	Corona	Corona	Corona	Alter. of cpx	Alter. of cpx
Lithology	Olivine gabbronorite	Olivine gabbronorite	Olivine gabbronorite	Olivine gabbronorite	Olivine gabbronorite	Olivine gabbronorite
Strat. ht. (m)	400	400	400	400	400	400
SiO_2	50.71	53.87	47.72	42.05	47.60	46.61
TiO_2	0.00	0.17	0.00	0.00	0.59	0.48
Al_2O_3	6.82	2.59	9.31	15.78	6.08	7.98
Cr_2O_3	0.00	0.00	0.00	0.00	0.00	0.00
FeO*	8.17	7.24	9.16	10.11	13.13	14.19
MnO	0.00	0.00	0.00	0.00	0.12	0.17
MgO	18.61	20.35	18.02	14.79	13.95	13.33
CaO	11.36	11.71	10.54	11.48	11.79	11.72
Na_2O	1.00	0.15	1.62	2.49	0.70	1.12
K_2O	0.00	0.00	0.06	0.24	0.06	0.19
Total	96.67	96.08	96.43	96.94	94.02	95.79
Oxygens	23	23	23	23	23	23
Si	7.064	7.495	6.656	5.998	7.106	6.866
Ti	0.000	0.018	0.000	0.000	0.066	0.053
Al	1.120	0.425	1.530	2.652	1.070	1.354
Cr	0.000	0.000	0.000	0.000	0.000	0.000
Fe^{3+}	0.952	0.842	1.068	1.112	1.601	0.722
Fe^{2+}	0.000	0.000	0.000	0.094	1.038	1.026
Mn	0.000	0.000	0.000	0.000	0.015	0.021
Mg	3.874	4.220	3.746	3.144	3.104	2.927
Ca	1.695	1.745	1.575	1.754	1.886	1.850
Na	0.270	0.040	0.438	0.689	0.203	0.320
K	0.000	0.000	0.011	0.044	0.011	0.036
Total Cations	14.975	14.785	15.024	15.487	16.100	15.175
mg	100.0	100.0	100.0	97.1	74.9	74.0
Classification	Ferrian Magnesio Hornblende	Ferrian Tremolitic Hornblende	Ferri Magnesio Hornblende	Ferri Tschermakite	Magnesio Hornblende	Magnesio Hornblende

Sample no.	92522493	92522493	92522493
Analysis no.	71709	71710	71711
Mineral	Clinopyroxene	Clinopyroxene	Clinopyroxene
Description	Intercumulus	Intercumulus	Intercumulus
Lithology	Olivine gabbronorite	Olivine gabbronorite	Olivine gabbronorite
Strat. ht. (m)	400	400	400
SiO_2	51.70	51.70	52.24
TiO_2	0.00	0.40	0.56
Al_2O_3	2.75	2.86	2.20
Cr_2O_3	0.26	0.36	0.10
FeO*	9.03	8.84	9.67
MnO	0.18	0.00	0.26
MgO	14.93	15.15	15.56
CaO	20.33	20.19	19.59
Na_2O	0.00	0.17	0.00
K_2O	0.00	0.00	0.00
Total	99.18	99.68	100.18
Oxygens	6	6	6
Si	1.935	1.922	1.937
Ti	0.000	0.011	0.016
Al	0.121	0.125	0.096
Cr	0.008	0.011	0.003
Fe^{3+}	0.002	0.010	0.000
Fe^{2+}	0.281	0.265	0.300
Mn	0.006	0.000	0.008
Mg	0.833	0.840	0.860
Ca	0.815	0.804	0.778
Na	0.000	0.012	0.000
K	0.000	0.000	0.000
Total Cations	4.001	4.000	3.998
mg	74.8	76.0	74.1
Enstatite	43.2	44.0	44.4
Ferrosilite	14.6	13.9	15.5
Wollastonite	42.2	42.1	40.1

Appendix Table 3.1 (cont.). Electron microprobe analyses of silicate minerals from the Armanda layered intrusion.

Sample no.	92522493	92522493	92522493	92522493	92522493	92522493
Analysis no.	71720	71721	71722	72166	72167	72169
Mineral	Clinopyroxene	Clinopyroxene	Clinopyroxene	Clinopyroxene	Clinopyroxene	Clinopyroxene
Description	Intercumulus	Intercumulus	Intercumulus	Intercumulus	Intercumulus	Intercumulus
Lithology	Olivine gabbronorite	Olivine gabbronorite	Olivine gabbronorite	Olivine gabbronorite	Olivine gabbronorite	Olivine gabbronorite
Strat. ht. (m)	400	400	400	400	400	400
SiO_2	51.36	52.11	52.57	53.33	53.93	52.65
TiO_2	0.50	0.28	0.51	0.14	0.11	0.24
Al_2O_3	2.55	2.55	1.91	0.85	0.50	2.05
Cr_2O_3	0.16	0.28	0.00	0.00	0.00	0.19
FeO*	9.22	8.57	8.98	7.42	6.99	8.10
MnO	0.17	0.15	0.00	0.10	0.00	0.09
MgO	14.88	15.72	15.55	15.27	15.59	15.02
CaO	20.60	20.48	20.69	22.64	22.94	21.88
Na_2O	0.00	0.00	0.00	0.00	0.00	0.00
K_2O	0.00	0.00	0.00	0.00	0.00	0.00
Total	99.45	100.16	100.21	99.75	100.06	100.22
Oxygens	6	6	6	6	6	6
Si	1.920	1.926	1.945	1.979	1.990	1.948
Ti	0.014	0.008	0.014	0.004	0.003	0.007
Al	0.112	0.111	0.083	0.037	0.022	0.089
Cr	0.005	0.008	0.000	0.000	0.000	0.006
Fe^{3+}	0.014	0.013	0.000	0.000	0.000	0.000
Fe^{2+}	0.274	0.252	0.278	0.230	0.216	0.251
Mn	0.005	0.005	0.000	0.003	0.000	0.003
Mg	0.829	0.866	0.858	0.845	0.858	0.828
Ca	0.825	0.811	0.820	0.900	0.907	0.867
Na	0.000	0.000	0.000	0.000	0.000	0.000
K	0.000	0.000	0.000	0.000	0.000	0.000
Total Cations	3.998	4.000	3.998	3.998	3.996	3.999
mg	75.2	77.5	75.5	78.6	79.9	76.7
Enstatite	43.0	44.9	43.9	42.8	43.3	42.5
Ferrosilite	14.2	13.1	14.2	11.6	10.9	12.9
Wollastonite	42.8	42.0	41.9	45.6	45.8	44.6

Sample no.	92522493	92522493	92522493
Analysis no.	71696	71697	71698
Mineral	Olivine	Olivine	Olivine
Description	Cumulus (c)	Cumulus (r)	Cumulus (r)
Lithology	Olivine gabbronorite	Olivine gabbronorite	Olivine gabbronorite
Strat. ht. (m)	400	400	400
SiO_2	36.66	36.27	36.36
TiO_2	0.00	0.00	0.00
Al_2O_3	0.00	0.00	0.00
Cr_2O_3	0.00	0.00	0.00
FeO*	29.85	30.10	30.11
MnO	0.27	0.33	0.25
MgO	33.05	32.24	32.20
CaO	0.00	0.00	0.00
Na_2O	0.00	0.00	0.00
K_2O	0.00	0.00	0.00
Total	99.83	98.94	98.92
Oxygens	4	4	4
Si	0.990	0.991	0.994
Ti	0.000	0.000	0.000
Al	0.000	0.000	0.000
Cr	0.000	0.000	0.000
Fe^{3+}	0.021	0.017	0.012
Fe^{2+}	0.653	0.671	0.676
Mn	0.006	0.008	0.006
Mg	1.330	1.313	1.312
Ca	0.000	0.000	0.000
Na	0.000	0.000	0.000
K	0.000	0.000	0.000
Total Cations	3.000	3.000	3.000
mg	67.1	66.2	66.0

Appendix Table 3.1 (cont.). Electron microprobe analyses of silicate minerals from the Armanda layered intrusion.

Sample no.	92522493	92522493	92522493	92522493	92522493	92522493	92522493
Analysis no.	71699	71700	71714	71715	71725	71726	71727
Mineral	Olivine	Olivine	Olivine	Olivine	Olivine	Olivine	Olivine
Description	Cumulus (r)	Cumulus (r)	Cumulus (r)	Cumulus (r)	Cumulus (r)	Cumulus (r)	Cumulus (c)
Lithology	Olivine gabbronorite	Olivine gabbronorite	Olivine gabbronorite	Olivine gabbronorite	Olivine gabbronorite	Olivine gabbronorite	Olivine gabbronorite
Strat. ht. (m)	400	400	400	400	400	400	400
SiO_2	36.26	36.22	36.51	36.70	36.60	36.80	36.72
TiO_2	0.00	0.00	0.00	0.00	0.00	0.00	0.00
Al_2O_3	0.00	0.00	0.00	0.00	0.00	0.00	0.00
Cr_2O_3	0.00	0.00	0.00	0.00	0.00	0.00	0.00
FeO*	30.28	30.28	30.26	29.84	29.36	30.04	29.93
MnO	0.19	0.23	0.29	0.25	0.33	0.23	0.27
MgO	32.49	32.49	32.34	32.61	33.10	32.58	32.92
CaO	0.00	0.00	0.00	0.00	0.00	0.00	0.00
Na_2O	0.00	0.00	0.00	0.00	0.00	0.00	0.00
K_2O	0.00	0.00	0.00	0.00	0.00	0.00	0.00
Total	99.22	99.22	99.40	99.40	99.39	99.65	99.84
Oxygens	4	4	32	4	4	4	4
Si	0.987	0.986	0.993	0.997	0.991	0.997	0.992
Ti	0.000	0.000	0.000	0.000	0.000	0.000	0.000
Al	0.000	0.000	0.000	0.000	0.000	0.000	0.000
Cr	0.000	0.000	0.000	0.000	0.000	0.000	0.000
Fe^{3+}	0.025	0.028	0.013	0.007	0.017	0.005	0.016
Fe^{2+}	0.664	0.662	0.675	0.671	0.648	0.676	0.660
Mn	0.004	0.005	0.007	0.006	0.008	0.005	0.006
Mg	1.319	1.319	1.311	1.320	1.336	1.316	1.326
Ca	0.000	0.000	0.000	0.000	0.000	0.000	0.000
Na	0.000	0.000	0.000	0.000	0.000	0.000	0.000
K	0.000	0.000	0.000	0.000	0.000	0.000	0.000
Total Cations	3.000	3.000	3.000	3.000	3.000	3.000	3.000
mg	66.5	66.6	66.0	66.3	67.3	66.1	66.8

Sample no.	92522493	92522493
Analysis no.	71705	71708
Mineral	Orthopyroxene	Orthopyroxene
Description	Corona	Corona
Lithology	Olivine gabbronorite	Olivine gabbronorite
Strat. ht. (m)	400	400
SiO_2	53.44	54.18
TiO_2	0.00	0.00
Al_2O_3	0.91	0.51
Cr_2O_3	0.00	0.00
FeO*	18.83	18.97
MnO	0.21	0.28
MgO	25.73	25.91
CaO	0.00	0.08
Na_2O	0.00	0.00
K_2O	0.00	0.00
Total	99.12	99.93
Oxygens	6	6
Si	1.965	1.978
Ti	0.000	0.000
Al	0.039	0.022
Cr	0.000	0.000
Fe^{3+}	0.031	0.023
Fe^{2+}	0.548	0.556
Mn	0.007	0.009
Mg	1.410	1.410
Ca	0.000	0.003
Na	0.000	0.000
K	0.000	0.000
Total Cations	4.000	4.000
mg	72.0	71.7
Enstatite	72.0	71.6
Ferrosilite	28.0	28.2
Wollastonite	0.0	0.2

Appendix Table 3.1 (cont.). Electron microprobe analyses of silicate minerals from the Armanda layered intrusion.

Sample no.	92522493	92522493	92522493
Analysis no.	71728	71731	71732
Mineral	Orthopyroxene	Orthopyroxene	Orthopyroxene
Description	Corona	Corona	Corona
Lithology	Olivine gabbronorite	Olivine gabbronorite	Olivine gabbronorite
Strat. ht. (m)	400	400	400
SiO_2	54.25	53.48	54.74
TiO_2	0.00	0.13	0.00
Al_2O_3	0.31	0.82	0.00
Cr_2O_3	0.00	0.00	0.00
FeO*	18.69	18.48	18.03
MnO	0.30	0.27	0.22
MgO	26.23	26.15	26.86
CaO	0.12	0.78	0.00
Na_2O	0.00	0.00	0.00
K_2O	0.00	0.00	0.00
Total	99.90	100.11	99.85
Oxygens	6	6	6
Si	1.978	1.944	1.990
Ti	0.000	0.004	0.000
Al	0.013	0.035	0.000
Cr	0.000	0.000	0.000
Fe^{3+}	0.031	0.070	0.020
Fe^{2+}	0.539	0.492	0.528
Mn	0.009	0.008	0.007
Mg	1.425	1.417	1.455
Ca	0.005	0.031	0.000
Na	0.000	0.000	0.000
K	0.000	0.000	0.000
Total Cations	4.000	4.000	4.000
mg	72.6	74.2	73.4
Enstatite	72.3	73.0	73.4
Ferrosilite	27.4	25.4	26.6
Wollastonite	0.3	1.6	0.0

Sample no.	92522493	92522493	92522493
Analysis no.	71701	71702	71703
Mineral	Plagioclase	Plagioclase	Plagioclase
Description	Cumulus (r)	Cumulus (r)	Cumulus (c)
Lithology	Olivine gabbronorite	Olivine gabbronorite	Olivine gabbronorite
Strat. ht. (m)	400	400	400
SiO_2	49.15	49.02	49.40
TiO_2	0.00	0.00	0.00
Al_2O_3	33.79	33.71	33.35
Cr_2O_3	0.00	0.00	0.00
FeO*	0.14	0.09	0.15
MnO	0.00	0.00	0.00
MgO	0.00	0.00	0.00
CaO	15.10	15.08	14.98
Na_2O	2.40	2.50	2.51
K_2O	0.00	0.00	0.10
Total	100.58	100.40	100.49
Oxygens	8	8	8
Si	2.226	2.225	2.240
Ti	0.000	0.000	0.000
Al	1.803	1.803	1.782
Cr	0.000	0.000	0.000
Fe^{3+}	0.000	0.000	0.000
Fe^{2+}	0.005	0.003	0.006
Mn	0.000	0.000	0.000
Mg	0.000	0.000	0.000
Ca	0.733	0.733	0.728
Na	0.211	0.220	0.220
K	0.000	0.000	0.006
Total Cations	4.978	4.984	4.982
Albite	22.4	23.1	23.1
Anorthite	77.6	76.9	76.3
Orthoclase	0.0	0.0	0.6

Sample no.	92522493
Analysis no.	71704
Mineral	Plagioclase
Description	Cumulus (c)
Lithology	Olivine gabbronorite
Strat. ht. (m)	400
SiO_2	49.07
TiO_2	0.00
Al_2O_3	33.39
Cr_2O_3	0.00
FeO*	0.00
MnO	0.00
MgO	0.00
CaO	15.02
Na_2O	2.55
K_2O	0.00
Total	100.03
Oxygens	8
Si	2.234
Ti	0.000
Al	1.792
Cr	0.000
Fe^{3+}	0.000
Fe^{2+}	0.000
Mn	0.000
Mg	0.000
Ca	0.733
Na	0.225
K	0.000
Total Cations	4.983
Albite	23.5
Anorthite	76.5
Orthoclase	0.0

Appendix Table 3.1 (cont.). Electron microprobe analyses of silicate minerals from the Armanda layered intrusion.

Sample no.	92522493	92522493	92522493	92522493
Analysis no.	71716	71717	71730	72170
Mineral	Plagioclase	Plagioclase	Plagioclase	Plagioclase
Description	Cumulus (r)	Cumulus (r)	Cumulus (r)	Cumulus
Lithology	Olivine gabbronorite	Olivine gabbronorite	Olivine gabbronorite	Olivine gabbronorite
Strat. ht. (m)	400	400	400	400
SiO_2	49.26	47.76	49.23	47.92
TiO_2	0.00	0.00	0.00	0.00
Al_2O_3	33.62	34.97	33.50	34.09
Cr_2O_3	0.00	0.00	0.00	0.00
FeO*	0.13	0.11	0.12	0.14
MnO	0.00	0.00	0.00	0.00
MgO	0.00	0.00	0.00	0.00
CaO	15.12	16.23	15.08	15.88
Na_2O	2.80	2.03	2.53	2.13
K_2O	0.05	0.00	0.00	0.00
Total	100.98	101.10	100.46	100.16
Oxygens	8	8	8	8
Si	2.226	2.161	2.233	2.187
Ti	0.000	0.000	0.000	0.000
Al	1.790	1.865	1.791	1.834
Cr	0.000	0.000	0.000	0.000
Fe^{3+}	0.005	0.000	0.000	0.000
Fe^{2+}	0.000	0.004	0.004	0.005
Mn	0.000	0.000	0.000	0.000
Mg	0.000	0.000	0.000	0.000
Ca	0.732	0.787	0.733	0.776
Na	0.245	0.178	0.223	0.188
K	0.003	0.000	0.000	0.000
Total Cations	5.001	4.995	4.983	4.991
Albite	25.0	18.4	23.3	19.5
Anorthite	74.7	81.6	76.7	80.5
Orthoclase	0.3	0.0	0.0	0.0

Appendix Table 3.1a. Electron microprobe analyses of oxide minerals from the Armanda layered intrusion.

Sample no.	92522493	92522493	92522493	92522493
Analysis no.	71723	71724	71712	71713
Mineral name	Ilmenite	Ilmenite	Spinel	Spinel
Description	Intercumulus	Intercumulus	Corona	Corona
Lithology	Olivine gabbronorite	Olivine gabbronorite	Olivine gabbronorite	Olivine gabbronorite
Strat. ht. (m)	400	400	400	400
SiO_2	0.00	0.00	1.04	0.00
TiO_2	49.64	48.95	0.00	0.00
Al_2O_3	0.00	0.00	58.21	59.57
V_2O_3	0.00	0.00	0.00	0.00
Cr_2O_3	0.12	0.22	0.00	0.00
FeO*	47.27	47.71	28.34	29.37
MnO	1.54	1.68	0.26	0.30
MgO	0.45	0.47	11.14	9.52
CaO	0.00	0.00	0.00	0.00
Total	99.58	99.73	98.99	98.76
Oxygens	3	3	32	32
Si	0.000	0.000	0.227	0.000
Ti	0.946	0.932	0.000	0.000
Al	0.000	0.000	14.946	15.428
Cr	0.002	0.004	0.000	0.000
Fe^{3+}	0.106	0.132	0.601	0.572
Fe^{2+}	0.896	0.878	4.561	4.826
Mn	0.033	0.036	0.049	0.057
Mg	0.017	0.018	3.617	3.117
Ca	0.000	0.000	0.000	0.000
Total Cations	2.000	2.000	24.001	24.000
mg			44.2	39.2

Appendix Table 3.2. Electron microprobe analyses of silicate minerals from the Big Ben layered intrusion.

Sample no.	93522031	93522031	93522031	93522031	93522031	93522031	93522031	93522031	93522031	93522031
Analysis no.	70699	70700	70709	70718	70719	70726	70727	70732	70733	70744
Mineral	Amphibole	Amphibole	Amphibole	Amphibole	Amphibole	Amphibole	Amphibole	Amphibole	Amphibole	Amphibole
Description	Corona	Corona	Corona	Corona	Corona	Corona	Corona	Corona	Corona	Corona
Lithology	Plagioclase peridotite	Plagioclase peridotite	Plagioclase peridotite	Plagioclase peridotite	Plagioclase peridotite	Plagioclase peridotite	Plagioclase peridotite	Plagioclase peridotite	Plagioclase peridotite	Plagioclase peridotite
SiO_2	46.21	45.64	48.13	47.71	48.03	47.38	47.23	46.11	45.95	48.66
TiO_2	0.14	0.00	0.10	0.10	0.10	0.22	0.00	0.12	0.11	0.00
Al_2O_3	13.71	13.15	11.08	11.10	10.21	11.42	11.89	11.94	12.98	10.07
Cr_2O_3	0.00	0.00	0.00	0.00	0.00	0.00	0.00	0.00	0.00	0.00
FeO*	8.40	7.77	7.44	7.18	7.34	7.32	7.54	9.09	8.40	7.70
MnO	0.00	0.00	0.00	0.00	0.00	0.00	0.00	0.00	0.00	0.00
MgO	15.93	15.57	17.22	16.94	17.36	16.96	16.92	16.30	16.25	17.86
CaO	11.83	11.84	12.05	11.88	12.11	11.91	11.83	11.43	11.64	11.39
Na_2O	1.25	1.17	0.98	0.88	0.92	1.04	1.07	1.00	1.16	0.92
K_2O	0.29	0.33	0.31	0.29	0.30	0.31	0.13	0.26	0.31	0.22
Total	98.69	96.33	98.14	96.88	97.18	97.37	97.44	97.27	97.73	97.68
Oxygens	23	23	23	23	23	23	23	23	23	23
Si	6.443	6.531	6.717	6.733	6.776	6.666	6.619	6.504	6.453	6.759
Ti	0.015	0.000	0.010	0.011	0.011	0.023	0.000	0.013	0.012	0.000
Al	2.253	2.218	1.822	1.846	1.697	1.893	1.964	1.985	2.148	1.649
Cr	0.000	0.000	0.000	0.000	0.000	0.000	0.000	0.000	0.000	0.000
Fe^{3+}	0.909	0.704	0.799	0.782	0.763	0.799	0.884	1.072	0.986	0.894
Fe^{2+}	0.071	0.226	0.069	0.066	0.102	0.062	0.000	0.000	0.000	0.000
Mn	0.000	0.000	0.000	0.000	0.000	0.000	0.000	0.000	0.000	0.000
Mg	3.306	3.321	3.582	3.563	3.650	3.556	3.534	3.427	3.401	3.698
Ca	1.767	1.815	1.802	1.796	1.830	1.795	1.776	1.727	1.751	1.695
Na	0.338	0.325	0.265	0.241	0.252	0.284	0.291	0.274	0.316	0.248
K	0.052	0.060	0.055	0.052	0.054	0.056	0.023	0.047	0.056	0.039
Total Cations	15.154	15.200	15.121	15.090	15.135	15.134	15.091	15.049	15.123	14.982
mg	97.9	93.6	98.1	98.2	97.3	98.3	100.0	100.0	100.0	100.0
Classification	Ferrian Tschermakitic Hornblende	Magnesio Hornblende	Ferrian Magnesio Hornblende	Ferrian Magnesio Hornblende	Ferrian Magnesio Hornblende	Ferrian Magnesio Hornblende	Ferrian Magnesio Hornblende	Ferri Magnesio Hornblende	Ferrian Tschermakitic Hornblende	Ferrian Magnesio Hornblende

Appendix Table 3.2 (cont.). Electron microprobe analyses of silicate minerals from the Big Ben layered intrusion.

Sample no.	93522031	93522031	93522031	93522031	93522031	93522031	93522031	93522031	93522031	93522031	93522031	93522031
Analysis no.	70693	70694	70695	70698	70701	70702	70703	70704	70714	70715	70716	70730
Mineral	Olivine	Olivine	Olivine	Olivine	Olivine	Olivine	Olivine	Olivine	Olivine	Olivine	Olivine	Olivine
Description	Cumulus	Cumulus	Cumulus	Cumulus	Cumulus (c)	Cumulus (c)	Cumulus (r)	Cumulus (r)	Cumulus (c)	Cumulus (c)	Cumulus (r)	Cumulus (c)
Lithology	Plagioclase peridotite	Plagioclase peridotite	Plagioclase peridotite	Plagioclase peridotite	Plagioclase peridotite	Plagioclase peridotite	Plagioclase peridotite	Plagioclase peridotite	Plagioclase peridotite	Plagioclase peridotite	Plagioclase peridotite	Plagioclase peridotite
SiO_2	36.83	37.31	37.04	37.20	36.90	36.90	36.94	37.06	36.86	37.30	37.18	36.97
TiO_2	0.00	0.00	0.00	0.00	0.00	0.00	0.00	0.00	0.00	0.00	0.00	0.00
Al_2O_3	0.00	0.00	0.00	0.00	0.00	0.00	0.00	0.00	0.00	0.00	0.00	0.00
Cr_2O_3	0.00	0.00	0.00	0.00	0.00	0.00	0.00	0.00	0.00	0.00	0.00	0.00
FeO*	27.45	27.69	27.59	27.11	27.22	27.51	26.99	27.23	26.93	27.25	27.35	27.13
MnO	0.34	0.33	0.26	0.22	0.22	0.21	0.33	0.21	0.31	0.19	0.22	0.21
MgO	35.43	35.33	35.09	35.19	34.87	34.91	35.03	35.13	35.11	35.00	35.05	34.95
CaO	0.00	0.00	0.00	0.00	0.00	0.00	0.00	0.00	0.00	0.00	0.00	0.00
Na_2O	0.00	0.00	0.00	0.00	0.00	0.00	0.00	0.00	0.00	0.00	0.00	0.00
K_2O	0.00	0.00	0.00	0.00	0.00	0.00	0.00	0.00	0.00	0.00	0.00	0.00
Total	100.05	100.66	99.98	99.72	99.21	99.53	99.29	99.63	99.21	99.74	99.80	99.26
Oxygens	4	4	4	4	4	4	4	4	4	4	4	4
Si	0.979	0.987	0.987	0.992	0.990	0.987	0.989	0.989	0.987	0.996	0.992	0.991
Ti	0.000	0.000	0.000	0.000	0.000	0.000	0.000	0.000	0.000	0.000	0.000	0.000
Al	0.000	0.000	0.000	0.000	0.000	0.000	0.000	0.000	0.000	0.000	0.000	0.000
Cr	0.000	0.000	0.000	0.000	0.000	0.000	0.000	0.000	0.000	0.000	0.000	0.000
Fe^{3+}	0.042	0.026	0.027	0.016	0.020	0.025	0.021	0.021	0.025	0.009	0.017	0.018
Fe^{2+}	0.568	0.587	0.588	0.588	0.591	0.590	0.584	0.587	0.578	0.599	0.594	0.590
Mn	0.008	0.007	0.006	0.005	0.005	0.005	0.007	0.005	0.007	0.004	0.005	0.005
Mg	1.404	1.393	1.393	1.399	1.394	1.392	1.398	1.398	1.402	1.392	1.393	1.396
Ca	0.000	0.000	0.000	0.000	0.000	0.000	0.000	0.000	0.000	0.000	0.000	0.000
Na	0.000	0.000	0.000	0.000	0.000	0.000	0.000	0.000	0.000	0.000	0.000	0.000
K	0.000	0.000	0.000	0.000	0.000	0.000	0.000	0.000	0.000	0.000	0.000	0.000
Total Cations	3.000	3.000	3.000	3.000	3.000	3.000	3.000	3.000	3.000	3.000	3.000	3.000
mg	71.2	70.4	70.3	70.4	70.2	70.2	70.5	70.4	70.8	69.9	70.1	70.3

Appendix Table 3.2 (cont.). Electron microprobe analyses of silicate minerals from the Big Ben layered intrusion.

Sample no.	93522031	93522031
Analysis no.	70731	70742
Mineral	Olivine	Olivine
Description	Cumulus (r)	Cumulus (c)
Lithology	Plagioclase peridotite	Plagioclase peridotite
SiO_2	37.07	37.26
TiO_2	0.00	0.00
Al_2O_3	0.00	0.00
Cr_2O_3	0.00	0.00
FeO*	27.50	27.70
MnO	0.27	0.26
MgO	34.80	35.39
CaO	0.00	0.00
Na_2O	0.00	0.00
K_2O	0.00	0.00
Total	99.64	100.61
Oxygens	4	4
Si	0.991	0.986
Ti	0.000	0.000
Al	0.000	0.000
Cr	0.000	0.000
Fe^{3+}	0.017	0.028
Fe^{2+}	0.598	0.585
Mn	0.006	0.006
Mg	1.387	1.395
Ca	0.000	0.000
Na	0.000	0.000
K	0.000	0.000
Total Cations	3.000	3.000
mg	69.9	70.5

Sample no.	93522031	93522031	93522031	93522031	93522031	93522031
Analysis no.	70710	70711	72904	72905	72906	72907
Mineral	Orthopyroxene	Orthopyroxene	Orthopyroxene	Orthopyroxene	Orthopyroxene	Orthopyroxene
Description	Corona	Corona	Intercumulus	Intercumulus	Intercumulus	Intercumulus
Lithology	Plagioclase peridotite	Plagioclase peridotite	Plagioclase peridotite	Plagioclase peridotite	Plagioclase peridotite	Plagioclase peridotite
SiO_2	54.14	53.81	52.36	53.34	53.85	53.62
TiO_2	0.00	0.00	0.00	0.00	0.00	0.00
Al_2O_3	1.08	1.39	1.44	1.10	1.41	1.05
Cr_2O_3	0.00	0.00	0.00	0.00	0.00	0.00
FeO*	16.40	15.66	15.74	16.14	16.03	15.30
MnO	0.14	0.26	0.21	0.21	0.24	0.20
MgO	27.05	27.16	26.12	26.61	27.00	27.27
CaO	0.00	0.00	0.08	0.00	0.00	0.00
Na_2O	0.00	0.00	0.00	0.00	0.00	0.00
K_2O	0.00	0.00	0.00	0.00	0.00	0.00
Total	99.63	99.73	96.49	98.14	99.40	99.21
Oxygens	6	6	6	6	6	6
Si	1.966	1.951	1.961	1.966	1.958	1.953
Ti	0.000	0.000	0.000	0.000	0.000	0.000
Al	0.046	0.059	0.063	0.048	0.060	0.045
Cr	0.000	0.000	0.000	0.000	0.000	0.000
Fe^{3+}	0.022	0.040	0.015	0.021	0.024	0.048
Fe^{2+}	0.498	0.475	0.493	0.497	0.487	0.466
Mn	0.004	0.008	0.007	0.007	0.007	0.006
Mg	1.464	1.468	1.458	1.462	1.463	1.481
Ca	0.000	0.000	0.003	0.000	0.000	0.000
Na	0.000	0.000	0.000	0.000	0.000	0.000
K	0.000	0.000	0.000	0.000	0.000	0.000
Total Cations	4.000	4.000	4.000	4.000	4.000	4.000
mg	74.6	75.6	74.7	74.6	75.0	76.1
Enstatite	74.6	75.6	74.6	74.6	75.0	76.1
Ferrosilite	25.4	24.4	25.2	25.4	25.0	23.9
Wollastonite	0.0	0.0	0.2	0.0	0.0	0.0

Appendix Table 3.2 (cont.). Electron microprobe analyses of silicate minerals from the Big Ben layered intrusion.

Sample no.	93522031	93522031	93522031	93522031	93522031	93522031	93522031	93522031	93522031
Analysis no.	70696	70697	70705	70712	70713	70717	70728	70729	70743
Mineral	Plagioclase	Plagioclase	Plagioclase	Plagioclase	Plagioclase	Plagioclase	Plagioclase	Plagioclase	Plagioclase
Description	Cumulus	Cumulus	Cumulus	Cumulus (c)	Cumulus (c)	Cumulus (r)	Cumulus (c)	Incl. in plag.	Cumulus (r)
Lithology	Plagioclase peridotite	Plagioclase peridotite	Plagioclase peridotite	Plagioclase peridotite	Plagioclase peridotite	Plagioclase peridotite	Plagioclase peridotite	Plagioclase peridotite	Plagioclase peridotite
SiO_2	46.65	45.94	44.44	43.47	45.19	44.80	44.29	45.65	46.18
TiO_2	0.00	0.00	0.00	0.00	0.00	0.00	0.00	0.00	0.00
Al_2O_3	36.04	35.48	36.15	37.41	35.81	36.26	36.87	35.69	35.65
Cr_2O_3	0.00	0.00	0.00	0.00	0.00	0.00	0.00	0.00	0.00
FeO*	0.20	0.18	0.00	0.00	0.00	0.15	0.00	0.00	0.13
MnO	0.00	0.00	0.00	0.00	0.00	0.00	0.00	0.00	0.00
MgO	0.00	0.00	0.00	0.00	0.00	0.00	0.00	0.00	0.00
CaO	17.62	17.47	18.56	19.47	17.93	18.21	18.73	17.50	17.43
Na_2O	1.22	1.14	0.46	0.00	0.73	0.47	0.40	0.98	1.16
K_2O	0.00	0.06	0.00	0.00	0.00	0.00	0.00	0.00	0.00
Total	101.73	100.27	99.61	100.35	99.66	99.89	100.28	99.83	100.55
Oxygens	8	8	8	8	8	8	8	8	8
Si	2.106	2.105	2.054	1.999	2.082	2.062	2.034	2.098	2.108
Ti	0.000	0.000	0.000	0.000	0.000	0.000	0.000	0.000	0.000
Al	1.917	1.916	1.969	2.028	1.945	1.967	1.995	1.933	1.917
Cr	0.000	0.000	0.000	0.000	0.000	0.000	0.000	0.000	0.000
Fe^{3+}	0.000	0.000	0.000	0.000	0.000	0.000	0.000	0.000	0.000
Fe^{2+}	0.007	0.007	0.000	0.000	0.000	0.006	0.000	0.000	0.005
Mn	0.000	0.000	0.000	0.000	0.000	0.000	0.000	0.000	0.000
Mg	0.000	0.000	0.000	0.000	0.000	0.000	0.000	0.000	0.000
Ca	0.852	0.857	0.919	0.959	0.885	0.898	0.921	0.862	0.852
Na	0.107	0.101	0.041	0.000	0.065	0.042	0.035	0.087	0.102
K	0.000	0.004	0.000	0.000	0.000	0.000	0.000	0.000	0.000
Total Cations	4.989	4.990	4.983	4.987	4.978	4.975	4.986	4.980	4.985
Albite	11.2	10.5	4.3	0.0	6.8	4.5	3.7	9.2	10.7
Anorthite	88.8	89.1	95.7	100.0	93.2	95.5	96.3	90.8	89.3
Orthoclase	0.0	0.4	0.0	0.0	0.0	0.0	0.0	0.0	0.0

Appendix Table 3.2a. Electron microprobe analyses of oxide minerals from the Big Ben layered intrusion.

Sample no.	93522031	93522031	93522031	93522031	93522031	93522031	93522031	93522031
Analysis no.	70707	70708	70720	70721	70722	70723	70724	70736
Mineral	Spinel	Spinel	Spinel	Spinel	Spinel	Spinel	Spinel	Spinel
Description	Corona	Corona	Corona	Corona	Corona	Granular aggregate	Granular aggregate	Corona
Lithology	Plagioclase peridotite	Plagioclase peridotite	Plagioclase peridotite	Plagioclase peridotite	Plagioclase peridotite	Plagioclase peridotite	Plagioclase peridotite	Plagioclase peridotite
Al_2O_3	62.44	62.60	62.78	63.06	63.06	62.80	62.87	62.50
FeO*	22.32	22.67	22.47	23.18	22.68	22.45	22.44	22.70
MnO	0.14	0.16	0.21	0.18	0.21	0.00	0.21	0.00
MgO	13.92	13.83	14.12	14.02	14.07	14.25	14.30	13.83
Total	98.81	99.26	99.59	100.43	100.02	99.50	99.82	99.03
Oxygens	32	32	32	32	32	32	32	32
Al	15.615	15.603	15.578	15.544	15.585	15.577	15.550	15.609
Fe^{3+}	0.385	0.397	0.422	0.456	0.415	0.423	0.450	0.391
Fe^{2+}	3.576	3.613	3.534	3.598	3.563	3.530	3.489	3.631
Mn	0.024	0.028	0.036	0.032	0.037	0.000	0.037	0.000
Mg	4.401	4.359	4.430	4.370	4.400	4.470	4.473	4.369
Total Cations	24.001	24.000	24.000	24.000	24.000	24.000	23.999	24.000
mg	55.2	54.7	55.6	54.8	55.3	55.9	56.2	54.6

Appendix Table 3.3. Electron microprobe analyses of silicate minerals from the Dave Hill layered intrusion.

Sample no.	93522114	93522114	93522114	93522114	93522114
Analysis no.	71077	71078	71094	71095	71103
Mineral	Amphibole	Amphibole	Amphibole	Amphibole	Amphibole
Description	Corona	Corona	Corona	Corona	Corona
Lithology	Troctolite	Troctolite	Troctolite	Troctolite	Troctolite
SiO_2	46.19	46.84	47.53	46.56	45.71
TiO_2	0.00	0.00	0.00	0.00	0.00
Al_2O_3	13.59	12.50	11.02	12.55	14.33
Cr_2O_3	0.00	0.00	0.00	0.00	0.00
FeO*	8.33	8.28	8.13	7.70	8.11
MnO	0.00	0.09	0.00	0.00	0.00
MgO	16.31	16.82	17.67	17.09	16.42
CaO	11.83	11.96	11.61	11.83	11.71
Na_2O	1.59	1.45	1.39	1.47	1.66
K_2O	0.08	0.07	0.05	0.12	0.10
Total	97.92	98.01	97.40	97.32	98.04
Oxygens	23	23	23	23	23
Si	6.423	6.503	6.598	6.490	6.332
Al	2.227	2.045	1.803	2.067	2.339
Fe^{3+}	0.958	0.961	0.944	0.898	0.939
Fe^{2+}	0.011	0.000	0.000	0.000	0.000
Mn	0.000	0.011	0.000	0.000	0.000
Mg	3.381	3.480	3.656	3.551	3.390
Ca	1.762	1.779	1.727	1.767	1.738
Na	0.492	0.390	0.374	0.397	0.446
K	0.014	0.012	0.009	0.021	0.018
Total Cations	15.268	15.181	15.111	15.191	15.202
mg	99.7	100.0	100.0	100.0	100.0
Classification	Ferrian Tschermakitic Hornblende	Ferrian Magnesio Hornblende	Ferrian Magnesio Hornblende	Ferrian Tschermakitic Hornblende	Ferrian Tschermakitic Hornblende

Sample no.	93522114	93522114	93522114	93522114
Analysis no.	71069	71070	71071	71072
Mineral	Olivine	Olivine	Olivine	Olivine
Description	Cumulus (c)	Cumulus (c)	Cumulus (r)	Cumulus (r)
Lithology	Troctolite	Troctolite	Troctolite	Troctolite
SiO_2	37.29	37.35	37.35	37.40
TiO_2	0.00	0.00	0.00	0.00
Al_2O_3	0.00	0.00	0.00	0.00
Cr_2O_3	0.00	0.00	0.00	0.00
FeO*	25.86	25.66	25.85	25.38
MnO	0.14	0.17	0.15	0.23
MgO	36.35	36.39	36.37	36.53
CaO	0.00	0.00	0.00	0.00
Na_2O	0.00	0.00	0.00	0.00
K_2O	0.00	0.00	0.00	0.00
Total	99.75	99.65	99.82	99.64
Oxygens	4	4	4	4
Si	0.988	0.990	0.989	0.990
Al	0.000	0.000	0.000	0.000
Fe^{3+}	0.024	0.020	0.022	0.019
Fe^{2+}	0.549	0.549	0.551	0.543
Mn	0.003	0.004	0.003	0.005
Mg	1.436	1.438	1.435	1.442
Ca	0.000	0.000	0.000	0.000
Na	0.000	0.000	0.000	0.000
K	0.000	0.000	0.000	0.000
Total Cations	3.000	3.001	3.000	2.999
mg	72.3	72.4	72.3	72.6

Appendix Table 3.3 (cont.). Electron microprobe analyses of silicate minerals from the Dave Hill layered intrusion.

Sample no.	93522114	93522114	93522114	93522114	93522114	93522114
Analysis no.	71073	71074	71090	71091	71100	71101
Mineral	Olivine	Olivine	Olivine	Olivine	Olivine	Olivine
Description	Cumulus (r)	Cumulus (r)	Cumulus (r)	Cumulus (r)	Cumulus (r)	Cumulus (r)
Lithology	Troctolite	Troctolite	Troctolite	Troctolite	Troctolite	Troctolite
SiO_2	37.56	37.68	37.59	37.42	37.73	37.94
TiO_2	0.00	0.00	0.00	0.00	0.00	0.00
Al_2O_3	0.00	0.00	0.00	0.00	0.00	0.00
Cr_2O_3	0.00	0.00	0.00	0.00	0.00	0.00
FeO*	25.02	25.40	25.62	25.99	26.25	26.47
MnO	0.15	0.09	0.19	0.11	0.22	0.11
MgO	36.60	36.45	36.65	36.50	36.61	36.26
CaO	0.00	0.00	0.00	0.00	0.00	0.00
Na_2O	0.00	0.00	0.00	0.00	0.00	0.00
K_2O	0.00	0.00	0.00	0.00	0.00	0.00
Total	99.36	99.65	100.14	100.14	100.92	100.81
Oxygens	4	4	4	4	4	4
Si	0.996	0.997	0.991	0.988	0.989	0.997
Al	0.000	0.000	0.000	0.000	0.000	0.000
Fe^{3+}	0.009	0.005	0.018	0.024	0.022	0.007
Fe^{2+}	0.546	0.557	0.547	0.549	0.554	0.575
Mn	0.003	0.002	0.004	0.002	0.005	0.002
Mg	1.446	1.438	1.440	1.436	1.430	1.419
Ca	0.000	0.000	0.000	0.000	0.000	0.000
Na	0.000	0.000	0.000	0.000	0.000	0.000
K	0.000	0.000	0.000	0.000	0.000	0.000
Total Cations	3.000	2.999	3.000	2.999	3.000	3.000
mg	72.6	72.1	72.5	72.3	72.1	71.2

Sample no.	93522114	93522114	93522114
Analysis no.	71075	71076	71089
Mineral	Orthopyroxene	Orthopyroxene	Orthopyroxene
Description	Corona	Corona	Corona
Lithology	Troctolite	Troctolite	Troctolite
SiO_2	53.97	54.00	54.14
TiO_2	0.00	0.00	0.00
Al_2O_3	1.64	1.64	1.59
Cr_2O_3	0.00	0.00	0.00
FeO*	16.40	16.51	17.01
MnO	0.20	0.15	0.00
MgO	27.62	27.47	26.42
CaO	0.57	0.57	0.38
Na_2O	0.00	0.00	0.00
K_2O	0.00	0.00	0.00
Total	100.40	100.34	99.54
Oxygens	6	6	6
Si	1.935	1.939	1.967
Al	0.069	0.069	0.068
Fe^{3+}	0.061	0.053	0.000
Fe^{2+}	0.431	0.442	0.517
Mn	0.006	0.004	0.000
Mg	1.476	1.470	1.431
Ca	0.022	0.022	0.015
Na	0.000	0.000	0.000
K	0.000	0.000	0.000
Total Cations	4.000	3.999	3.998
mg	77.4	76.9	73.5
Enstatite	76.6	76.0	72.9
Ferrosilite	22.3	22.9	26.3
Wollastonite	1.1	1.1	0.8

Appendix Table 3.3 (cont.). Electron microprobe analyses of silicate minerals from the Dave Hill layered intrusion.

Sample no.	93522114	93522114	93522114	93522114	93522114
Analysis no.	71092	71093	71096	71097	71102
Mineral	Orthopyroxene	Orthopyroxene	Orthopyroxene	Orthopyroxene	Orthopyroxene
Description	Corona	Corona	Cumulus (c)	Cumulus (r)	Corona
Lithology	Troctolite	Troctolite	Troctolite	Troctolite	Troctolite
SiO_2	53.86	54.01	53.96	54.21	54.91
TiO_2	0.00	0.00	0.00	0.00	0.00
Al_2O_3	1.73	1.68	1.96	1.72	0.77
Cr_2O_3	0.00	0.00	0.00	0.00	0.00
FeO*	16.88	17.00	16.00	15.60	16.88
MnO	0.11	0.20	0.14	0.12	0.17
MgO	27.23	27.10	27.60	27.31	27.47
CaO	0.43	0.51	0.51	1.30	0.00
Na_2O	0.00	0.00	0.00	0.00	0.00
K_2O	0.00	0.00	0.00	0.00	0.00
Total	100.24	100.50	100.17	100.26	100.20
Oxygens	6	6	6	6	6
Si	1.938	1.941	1.937	1.945	1.978
Al	0.073	0.071	0.083	0.073	0.033
Fe^{3+}	0.051	0.047	0.044	0.037	0.011
Fe^{2+}	0.458	0.464	0.436	0.431	0.498
Mn	0.003	0.006	0.004	0.004	0.005
Mg	1.461	1.451	1.476	1.460	1.475
Ca	0.016	0.020	0.020	0.050	0.000
Na	0.000	0.000	0.000	0.000	0.000
K	0.000	0.000	0.000	0.000	0.000
Total Cations	4.000	4.000	4.000	4.000	4.000
mg	76.1	75.8	77.2	77.2	74.8
Enstatite	75.5	75.0	76.4	75.2	74.8
Ferrosilite	23.7	24.0	22.6	22.2	25.2
Wollastonite	0.8	1.0	1.0	2.6	0.0

Sample no.	93522114	93522114	93522114	93522114
Analysis no.	71079	71080	71081	71083
Mineral	Plagioclase	Plagioclase	Plagioclase	Plagioclase
Description	Cumulus (r)	Cumulus (r)	Cumulus (c)	Cumulus (c)
Lithology	Troctolite	Troctolite	Troctolite	Troctolite
SiO_2	46.31	46.21	46.31	46.48
TiO_2	0.00	0.00	0.00	0.00
Al_2O_3	35.27	35.02	34.85	35.19
Cr_2O_3	0.00	0.00	0.00	0.00
FeO*	0.00	0.00	0.00	0.10
MnO	0.00	0.00	0.00	0.00
MgO	0.00	0.00	0.00	0.00
CaO	16.98	17.02	17.01	16.74
Na_2O	1.43	1.35	1.49	1.50
K_2O	0.00	0.00	0.00	0.00
Total	99.99	99.59	99.65	100.02
Oxygens	8	8	8	8
Si	2.123	2.126	2.131	2.129
Al	1.905	1.899	1.890	1.900
Fe^{3+}	0.000	0.000	0.000	0.000
Fe^{2+}	0.000	0.000	0.000	0.004
Mn	0.000	0.000	0.000	0.000
Mg	0.000	0.000	0.000	0.000
Ca	0.833	0.839	0.838	0.822
Na	0.126	0.120	0.132	0.134
K	0.000	0.000	0.000	0.000
Total Cations	4.987	4.984	4.991	4.989
Albite	13.1	12.5	13.6	14.0
Anorthite	86.9	87.5	86.4	86.0
Orthoclase	0.0	0.0	0.0	0.0

Appendix Table 3.3 (cont.). Electron microprobe analyses of silicate minerals from the Dave Hill layered intrusion.

Sample no.	93522114	93522114	93522114	93522114
Analysis no.	71087	71088	71104	71105
Mineral	Plagioclase	Plagioclase	Plagioclase	Plagioclase
Description	Cumulus (r)	Cumulus (r)	Cumulus (r)	Cumulus (r)
Lithology	Troctolite	Troctolite	Troctolite	Troctolite
SiO_2	46.07	46.03	46.38	46.22
TiO_2	0.00	0.00	0.00	0.00
Al_2O_3	35.41	35.28	35.31	35.37
Cr_2O_3	0.00	0.00	0.00	0.00
FeO*	0.00	0.12	0.00	0.11
MnO	0.00	0.00	0.00	0.00
MgO	0.00	0.00	0.00	0.00
CaO	16.97	16.85	16.96	16.91
Na_2O	1.51	1.20	1.39	1.33
K_2O	0.00	0.00	0.00	0.00
Total	99.97	99.48	100.04	99.94
Oxygens	8	8	8	8
Si	2.114	2.119	2.124	2.119
Al	1.915	1.915	1.906	1.912
Fe^{3+}	0.000	0.000	0.000	0.000
Fe^{2+}	0.000	0.004	0.000	0.004
Mn	0.000	0.000	0.000	0.000
Mg	0.000	0.000	0.000	0.000
Ca	0.834	0.831	0.832	0.830
Na	0.134	0.107	0.123	0.117
K	0.000	0.000	0.000	0.000
Total Cations	4.997	4.976	4.985	4.982
Albite	13.8	11.4	12.9	12.4
Anorthite	86.2	88.6	87.1	87.6
Orthoclase	0.0	0.0	0.0	0.0

Appendix Table 3.3a. Electron microprobe analyses of oxide minerals from the Dave Hill layered intrusion.

Sample no.	93522114	93522114	93522114
Analysis no	71085	71086	71098
Mineral	Spinel	Spinel	Spinel
Description	Corona	Corona	Corona
Lithology	Troctolite	Troctolite	Troctolite
Al_2O_3	63.06	62.46	63.37
FeO*	25.00	24.98	24.69
MnO	0.00	0.11	0.00
MgO	11.91	11.90	12.62
Total	99.97	99.45	100.68
Oxygens	32	32	32
Al	15.788	15.725	15.705
Fe^{3+}	0.212	0.275	0.295
Fe^{2+}	4.229	4.189	4.046
Mn	0.000	0.021	0.000
Mg	3.771	3.791	3.954
Total Cations	24.000	24.000	24.000
mg	47.1	47.5	49.4

Appendix Table 3.4. Electron microprobe analyses of silicate minerals from the Keller Creek layered intrusion.

Sample no.	94522089	94522089
Analysis no.	72125	72126
Mineral	Amphibole	Amphibole
Description	Corona	Corona
Lithology	Olivine gabbronorite	Olivine gabbronorite
SiO_2	42.80	43.63
TiO_2	1.62	1.47
Al_2O_3	12.88	12.72
Cr_2O_3	0.00	0.00
FeO*	13.67	13.87
MnO	0.00	0.00
MgO	12.57	12.66
CaO	11.10	11.15
Na_2O	2.35	2.32
K_2O	0.14	0.10
Total	97.13	97.92
Oxygens	23	23
Si	6.226	6.185
Ti	0.177	0.156
Al	2.208	2.126
Cr	0.000	0.000
Fe^{3+}	0.836	1.621
Fe^{2+}	0.827	0.000
Mn	0.000	0.000
Mg	2.725	2.676
Ca	1.730	1.694
Na	0.663	0.637
K	0.025	0.018
Total Cations	15.417	15.113
mg	76.7	76.2
Classification	Ferrian Tschermakite	Ferrian Tschermakitic Hornblende

Sample no.	94522089	94522089	94522089	94522089	94522089	94522089	94522089
Analysis no.	72127	72128	72129	72130	72131	72140	72141
Mineral	Clinopyroxene	Clinopyroxene	Clinopyroxene	Clinopyroxene	Clinopyroxene	Clinopyroxene	Clinopyroxene
Description	Intercumulus	Intercumulus	Intercumulus	Intercumulus	Intercumulus	Intercumulus	Intercumulus
Lithology	Olivine gabbronorite	Olivine gabbronorite	Olivine gabbronorite	Olivine gabbronorite	Olivine gabbronorite	Olivine gabbronorite	Olivine gabbronorite
SiO_2	51.56	51.31	51.56	51.71	50.97	51.57	51.40
TiO_2	0.23	0.21	0.12	0.30	0.23	0.25	0.22
Al_2O_3	1.21	1.30	1.12	1.38	1.62	1.58	1.47
Cr_2O_3	0.00	0.00	0.00	0.09	0.00	0.00	0.00
FeO*	11.30	11.32	11.48	11.33	11.29	11.92	11.38
MnO	0.19	0.13	0.11	0.19	0.16	0.17	0.13
MgO	12.56	12.38	12.60	12.62	12.41	13.05	12.84
CaO	21.81	21.87	21.43	21.84	21.33	20.68	20.69
Na_2O	0.00	0.00	0.00	0.00	0.00	0.00	0.00
K_2O	0.00	0.00	0.00	0.00	0.00	0.00	0.00
Total	98.86	98.52	98.42	99.46	98.01	99.22	98.13
Oxygens	6	6	6	6	6	6	6
Si	1.967	1.965	1.974	1.960	1.959	1.958	1.968
Ti	0.007	0.006	0.003	0.008	0.007	0.007	0.006
Al	0.055	0.059	0.051	0.061	0.073	0.071	0.067
Cr	0.000	0.000	0.000	0.003	0.000	0.000	0.000
Fe^{3+}	0.000	0.000	0.000	0.000	0.000	0.000	0.000
Fe^{2+}	0.360	0.362	0.368	0.359	0.363	0.378	0.365
Mn	0.006	0.004	0.003	0.006	0.005	0.005	0.004
Mg	0.714	0.706	0.719	0.713	0.711	0.739	0.733
Ca	0.891	0.897	0.879	0.887	0.879	0.841	0.849
Na	0.000	0.000	0.000	0.000	0.000	0.000	0.000
K	0.000	0.000	0.000	0.000	0.000	0.000	0.000
Total Cations	4.000	4.000	3.997	3.999	3.997	3.999	3.992
mg	66.5	66.1	66.1	66.5	66.2	66.2	66.8
Enstatite	36.3	35.9	36.6	36.4	36.4	37.7	37.7
Ferrosilite	18.3	18.4	18.7	18.3	18.6	19.3	18.7
Wollastonite	45.3	45.7	44.7	45.3	45.0	43.0	43.6

Appendix Table 3.4 (cont.). Electron microprobe analyses of silicate minerals from the Keller Creek layered intrusion.

Sample no.	94522089	94522089	94522089
Analysis no.	72142	72143	72144
Mineral	Clinopyroxene	Clinopyroxene	Clinopyroxene
Description	Intercumulus	Intercumulus	Intercumulus
Lithology	Olivine gabbronorite	Olivine gabbronorite	Olivine gabbronorite
SiO_2	51.23	51.40	51.69
TiO_2	0.35	0.26	0.16
Al_2O_3	1.75	1.71	1.08
Cr_2O_3	0.00	0.00	0.00
FeO*	12.74	11.36	10.42
MnO	0.23	0.17	0.13
MgO	13.23	12.78	12.91
CaO	19.70	20.80	22.04
Na_2O	0.23	0.00	0.00
K_2O	0.00	0.00	0.00
Total	99.46	98.48	98.43
Oxygens	6	6	6
Si	1.939	1.962	1.973
Ti	0.010	0.007	0.005
Al	0.078	0.077	0.048
Cr	0.000	0.000	0.000
Fe^{3+}	0.041	0.000	0.000
Fe^{2+}	0.362	0.363	0.332
Mn	0.007	0.005	0.004
Mg	0.746	0.727	0.734
Ca	0.799	0.851	0.901
Na	0.017	0.000	0.000
K	0.000	0.000	0.000
Total Cations	4.000	3.992	3.998
mg	67.3	66.7	68.9
Enstatite	39.1	37.5	37.3
Ferrosilite	19.0	18.7	16.9
Wollastonite	41.9	43.8	45.8

Sample no.	94522089	94522089	94522089	94522089	94522089	94522089	94522089
Analysis no.	72119	72120	72121	72122	72132	72133	72134
Mineral	Olivine	Olivine	Olivine	Olivine	Olivine	Olivine	Olivine
Description	Cumulus (c)	Cumulus (c)	Cumulus (r)	Cumulus (r)	Cumulus (c)	Cumulus (c)	Cumulus (r)
Lithology	Olivine gabbronorite	Olivine gabbronorite	Olivine gabbronorite	Olivine gabbronorite	Olivine gabbronorite	Olivine gabbronorite	Olivine gabbronorite
SiO_2	33.11	33.11	33.04	33.24	33.26	33.17	33.18
TiO_2	0.00	0.00	0.00	0.00	0.00	0.00	0.00
Al_2O_3	0.00	0.00	0.00	0.00	0.00	0.00	0.00
Cr_2O_3	0.00	0.00	0.00	0.00	0.00	0.00	0.00
FeO*	47.46	47.72	47.74	47.39	46.87	46.88	46.93
MnO	0.50	0.44	0.52	0.44	0.55	0.58	0.56
MgO	18.16	17.81	17.90	18.02	18.08	18.66	18.31
CaO	0.00	0.00	0.00	0.00	0.00	0.00	0.00
Na_2O	0.00	0.00	0.00	0.00	0.00	0.00	0.00
K_2O	0.00	0.00	0.00	0.00	0.00	0.00	0.00
Total	99.23	99.08	99.20	99.09	98.76	99.29	98.98
Oxygens	4	4	4	4	4	4	4
Si	0.990	0.994	0.990	0.996	0.999	0.988	0.993
Ti	0.000	0.000	0.000	0.000	0.000	0.000	0.000
Al	0.000	0.000	0.000	0.000	0.000	0.000	0.000
Cr	0.000	0.000	0.000	0.000	0.000	0.000	0.000
Fe^{3+}	0.019	0.012	0.019	0.008	0.002	0.023	0.013
Fe^{2+}	1.168	1.186	1.177	1.180	1.175	1.145	1.162
Mn	0.013	0.011	0.013	0.011	0.014	0.015	0.014
Mg	0.810	0.797	0.800	0.805	0.810	0.829	0.817
Ca	0.000	0.000	0.000	0.000	0.000	0.000	0.000
Na	0.000	0.000	0.000	0.000	0.000	0.000	0.000
K	0.000	0.000	0.000	0.000	0.000	0.000	0.000
Total Cations	3.0	3.0	3.0	3.0	3.0	3.0	3.0
mg	41.0	40.2	40.5	40.6	40.8	42.0	41.3

Appendix Table 3.4 (cont.). Electron microprobe analyses of silicate minerals from the Keller Creek layered intrusion.

Sample no.	94522089	Sample no.	94522089	94522089	Sample no.	94522089	94522089	94522089	94522089	94522089
Analysis no.	72137	Analysis no.	72138	72139	Analysis no.	72123	72124	72135	72136	72145
Mineral	Olivine	Mineral	Orthopyroxene	Orthopyroxene	Mineral	Plagioclase	Plagioclase	Plagioclase	Plagioclase	Plagioclase
Description	Cumulus (r)	Description	Corona	Corona	Description	Cumulus	Cumulus	Incl. in oliv.	Incl. in oliv.	Cumulus
Lithology	Olivine gabbronorite	Lithology	Olivine gabbronorite	Olivine gabbronorite	Lithology	Olivine gabbronorite	Olivine gabbronorite	Olivine gabbronorite	Olivine gabbronorite	Olivine gabbronorite
SiO_2	33.50	SiO_2	51.23	51.55	SiO_2	48.33	48.19	49.35	49.44	48.54
TiO_2	0.00	TiO_2	0.00	0.00	TiO_2	0.00	0.00	0.00	0.00	0.00
Al_2O_3	0.00	Al_2O_3	0.52	0.69	Al_2O_3	34.19	34.31	33.43	33.58	34.16
Cr_2O_3	0.00	Cr_2O_3	0.00	0.00	Cr_2O_3	0.00	0.00	0.00	0.00	0.00
FeO*	49.00	FeO*	27.57	27.33	FeO*	0.26	0.23	0.42	0.43	0.14
MnO	0.49	MnO	0.34	0.44	MnO	0.00	0.00	0.00	0.00	0.00
MgO	18.37	MgO	19.44	19.76	MgO	0.00	0.00	0.00	0.00	0.00
CaO	0.00	CaO	0.52	0.53	CaO	15.58	15.83	14.84	14.94	15.63
Na_2O	0.00	Na_2O	0.00	0.00	Na_2O	2.33	2.15	2.74	2.70	2.23
K_2O	0.00	K_2O	0.00	0.00	K_2O	0.00	0.00	0.00	0.00	0.00
Total	101.36	Total	99.62	100.30	Total	100.69	100.71	100.78	101.09	100.70
Oxygens	4	Oxygens	6	6	Oxygens	8	8	8	8	8
Si	0.983	Si	1.957	1.953	Si	2.193	2.187	2.234	2.232	2.200
Ti	0.000	Ti	0.000	0.000	Ti	0.000	0.000	0.000	0.000	0.000
Al	0.000	Al	0.023	0.031	Al	1.829	1.835	1.784	1.787	1.825
Cr	0.000	Cr	0.000	0.000	Cr	0.000	0.000	0.000	0.000	0.000
Fe^{3+}	0.035	Fe^{3+}	0.063	0.064	Fe^{3+}	0.000	0.000	0.000	0.000	0.000
Fe^{2+}	1.167	Fe^{2+}	0.817	0.802	Fe^{2+}	0.010	0.009	0.016	0.016	0.005
Mn	0.012	Mn	0.011	0.014	Mn	0.000	0.000	0.000	0.000	0.000
Mg	0.803	Mg	1.107	1.115	Mg	0.000	0.000	0.000	0.000	0.000
Ca	0.000	Ca	0.021	0.021	Ca	0.757	0.770	0.720	0.722	0.759
Na	0.000	Na	0.000	0.000	Na	0.205	0.189	0.240	0.236	0.196
K	0.000	K	0.000	0.000	K	0.000	0.000	0.000	0.000	0.000
Total Cations	3.0	Total Cations	4.000	4.000	Total Cations	4.995	4.990	4.994	4.993	4.985
mg	40.8	mg	57.5	58.2	Albite	21.3	19.7	25.0	24.6	20.5
		Enstatite	56.9	57.5	Anorthite	78.7	80.3	75.0	75.4	79.5
		Ferrosilite	42.0	41.4	Orthoclase	0.0	0.0	0.0	0.0	0.0
		Wollastonite	1.1	1.1						

Appendix Table 3.5. Electron microprobe analyses of silicate minerals from the McKenzie Spring layered intrusion.

Sample no.	94522022	94522022	94522022	94522022
Analysis no.	72869	72870	72892	72893
Mineral	Amphibole	Amphibole	Amphibole	Amphibole
Description	Corona	Corona	Corona	Corona
Lithology	Olivine gabbronorite	Olivine gabbronorite	Olivine gabbronorite	Olivine gabbronorite
SiO_2	42.29	40.83	43.73	42.91
TiO_2	0.00	0.00	0.00	0.00
Al_2O_3	15.73	17.18	15.38	16.02
FeO*	9.94	10.28	9.07	9.13
MnO	0.00	0.09	0.00	0.00
MgO	14.73	13.74	15.13	15.30
CaO	11.31	10.99	11.51	11.63
Na_2O	2.06	2.38	1.88	2.05
K_2O	0.26	0.39	0.09	0.13
Total	96.32	95.88	96.79	97.17
Oxygens	23	23	23	23
Si	6.035	5.883	6.180	6.048
Ti	0.000	0.000	0.000	0.000
Al	2.646	2.917	2.561	2.661
Fe^{3+}	1.186	1.188	1.062	1.076
Fe^{2+}	0.000	0.000	0.010	0.000
Mn	0.000	0.011	0.000	0.000
Mg	3.133	2.951	3.187	3.214
Ca	1.729	1.696	1.743	1.756
Na	0.570	0.665	0.515	0.560
K	0.047	0.072	0.016	0.023
Total Cations	15.346	15.383	15.274	15.338
mg	100.0	98.3	99.7	100.0
Classification	Ferri Tschermakite	Ferri Tschermakite	Ferri Tschermakite	Ferri Tschermakite

Sample no.	94522022	94522022	94522022	94522022
Analysis no.	72872	72873	72874	72875
Mineral	Clinopyroxene	Clinopyroxene	Clinopyroxene	Clinopyroxene
Description	Intercumulus	Intercumulus	Intercumulus	Intercumulus
Lithology	Olivine gabbronorite	Olivine gabbronorite	Olivine gabbronorite	Olivine gabbronorite
SiO_2	51.66	51.45	51.63	51.41
TiO_2	0.72	0.66	0.56	0.53
Al_2O_3	3.22	3.35	3.22	4.09
FeO*	7.75	8.37	8.24	8.26
MnO	0.00	0.16	0.00	0.00
MgO	13.82	13.59	13.74	14.24
CaO	22.70	22.59	22.23	21.40
Na_2O	0.00	0.00	0.00	0.00
K_2O	0.00	0.00	0.00	0.00
Total	99.87	100.17	99.62	99.93
Oxygens	6	6	6	6
Si	1.925	1.916	1.930	1.910
Ti	0.020	0.018	0.016	0.015
Al	0.141	0.147	0.142	0.179
Fe^{3+}	0.000	0.000	0.000	0.000
Fe^{2+}	0.241	0.260	0.257	0.256
Mn	0.000	0.005	0.000	0.000
Mg	0.767	0.753	0.765	0.789
Ca	0.906	0.901	0.890	0.851
Na	0.000	0.000	0.000	0.000
K	0.000	0.000	0.000	0.000
Total Cations	4.000	4.000	4.000	4.000
mg	76.0	74.3	74.8	75.5
Enstatite	40.1	39.4	40.0	41.6
Ferrosilite	12.6	13.6	13.5	13.5
Wollastonite	47.3	47.0	46.5	44.9

Appendix Table 3.5 (cont.). Electron microprobe analyses of silicate minerals from the McKenzie Spring layered intrusion.

Sample no.	94522022	94522022	94522022
Analysis no.	72876	72877	72878
Mineral	Clinopyroxene	Clinopyroxene	Clinopyroxene
Description	Intercumulus	Intercumulus	Intercumulus
Lithology	Olivine gabbronorite	Olivine gabbronorite	Olivine gabbronorite
SiO_2	51.33	51.37	51.6
TiO_2	0.66	0.73	0.61
Al_2O_3	3.13	3.48	3.33
FeO*	7.71	8.22	7.87
MnO	0.00	0.14	0.11
MgO	13.79	13.50	14.12
CaO	22.59	22.61	22.26
Na_2O	0.00	0.00	0.00
K_2O	0.00	0.00	0.00
Total	99.21	100.05	99.89
Oxygens	6	6	6
Si	1.920	1.910	1.919
Ti	0.019	0.021	0.017
Al	0.138	0.152	0.148
Fe^{3+}	0.000	0.000	0.000
Fe^{2+}	0.241	0.256	0.263
Mn	0.000	0.004	0.003
Mg	0.769	0.748	0.783
Ca	0.905	0.901	0.887
Na	0.000	0.000	0.000
K	0.000	0.000	0.000
Total Cations	3.992	3.993	4.020
mg	76.1	74.5	74.9
Enstatite	40.2	39.3	40.5
Ferrosilite	12.6	13.4	13.6
Wollastonite	47.2	47.3	45.9

Sample no.	94522022	94522022	94522022	94522022	94522022	94522022
Analysis no.	71106	71107	71112	71113	71114	71115
Mineral	Olivine	Olivine	Olivine	Olivine	Olivine	Olivine
Description	Cumulus (c)	Cumulus (c)	Cumulus (c)	Cumulus (c)	Cumulus (c)	Cumulus (c)
Lithology	Olivine gabbronorite	Olivine gabbronorite	Olivine gabbronorite	Olivine gabbronorite	Olivine gabbronorite	Olivine gabbronorite
SiO_2	36.66	36.45	36.94	36.94	36.77	36.34
TiO_2	0.00	0.00	0.00	0.00	0.00	0.00
Al_2O_3	0.00	0.00	0.00	0.00	0.00	0.00
FeO*	29.05	28.97	29.61	30.04	29.87	28.85
MnO	0.16	0.23	0.21	0.15	0.21	0.18
MgO	33.42	33.74	33.66	33.94	33.69	32.99
CaO	0.00	0.00	0.00	0.00	0.00	0.00
Na_2O	0.00	0.00	0.00	0.00	0.00	0.00
K_2O	0.00	0.00	0.00	0.00	0.00	0.00
Total	99.29	99.39	100.42	101.07	100.54	98.36
Oxygens	4	4	4	4	4	4
Si	0.992	0.984	0.989	0.983	0.984	0.993
Ti	0.000	0.000	0.000	0.000	0.000	0.000
Al	0.000	0.000	0.000	0.000	0.000	0.000
Fe^{3+}	0.017	0.032	0.022	0.035	0.033	0.014
Fe^{2+}	0.640	0.621	0.641	0.633	0.636	0.645
Mn	0.004	0.005	0.005	0.003	0.005	0.004
Mg	1.348	1.357	1.343	1.346	1.343	1.344
Ca	0.000	0.000	0.000	0.000	0.000	0.000
Na	0.000	0.000	0.000	0.000	0.000	0.000
K	0.000	0.000	0.000	0.000	0.000	0.000
Total Cations	3.000	3.000	3.000	3.000	3.000	3.000
mg	67.8	68.6	67.7	68.0	67.9	67.6

Appendix Table 3.5 (cont.). Electron microprobe analyses of silicate minerals from the McKenzie Spring layered intrusion.

Sample no.	94522022	94522022	94522022	94522022	94522022	94522022	94522022	94522022	94522022
Analysis no.	71116	71117	72863	72864	72885	72886	72887	72888	72903
Mineral	Olivine	Olivine	Olivine	Olivine	Olivine	Olivine	Olivine	Olivine	Olivine
Description	Cumulus (c)	Cumulus (c)	Cumulus (r)	Cumulus (r)	Cumulus (c)	Cumulus (c)	Cumulus (r)	Cumulus (r)	Cumulus
Lithology	Olivine gabbronorite	Olivine gabbronorite	Olivine gabbronorite	Olivine gabbronorite	Olivine gabbronorite	Olivine gabbronorite	Olivine gabbronorite	Olivine gabbronorite	Olivine gabbronorite
SiO_2	36.70	37.07	36.66	36.64	37.02	36.72	36.81	36.92	36.82
TiO_2	0.00	0.00	0.00	0.00	0.00	0.00	0.00	0.00	0.00
Al_2O_3	0.00	0.00	0.00	0.00	0.00	0.00	0.00	0.00	0.00
FeO*	29.88	29.75	29.79	30.12	29.20	28.98	29.16	29.34	28.39
MnO	0.27	0.32	0.23	0.23	0.11	0.19	0.14	0.18	0.25
MgO	33.54	33.65	33.23	33.18	34.22	34.08	33.68	33.68	34.73
CaO	0.00	0.00	0.00	0.00	0.00	0.00	0.00	0.00	0.00
Na_2O	0.00	0.00	0.00	0.00	0.00	0.00	0.00	0.00	0.00
K_2O	0.00	0.00	0.00	0.00	0.00	0.00	0.00	0.00	0.00
Total	100.39	100.79	99.91	100.17	100.55	99.97	99.79	100.12	100.19
Oxygens	4	4	4	4	4	4	4	4	4
Si	0.984	0.990	0.988	0.986	0.987	0.984	0.990	0.991	0.982
Ti	0.000	0.000	0.000	0.000	0.000	0.000	0.000	0.000	0.000
Al	0.000	0.000	0.000	0.000	0.000	0.000	0.000	0.000	0.000
Fe^{3+}	0.032	0.021	0.023	0.028	0.026	0.031	0.020	0.019	0.037
Fe^{2+}	0.637	0.643	0.648	0.650	0.625	0.618	0.636	0.640	0.596
Mn	0.006	0.007	0.005	0.005	0.002	0.004	0.003	0.004	0.006
Mg	1.340	1.339	1.335	1.331	1.360	1.362	1.350	1.347	1.380
Ca	0.000	0.000	0.000	0.000	0.000	0.000	0.000	0.000	0.000
Na	0.000	0.000	0.000	0.000	0.000	0.000	0.000	0.000	0.000
K	0.000	0.000	0.000	0.000	0.000	0.000	0.000	0.000	0.000
Total Cations	3.000	3.000	3.000	3.000	3.000	3.000	3.000	3.000	3.000
mg	67.8	67.6	67.3	67.2	68.5	68.8	68.0	67.8	69.8

Appendix Table 3.5 (cont.). Electron microprobe analyses of silicate minerals from the McKenzie Spring layered intrusion.

Sample no.	94522022	94522022	94522022	94522022	94522022
Analysis no.	72867	72868	72889	72890	72891
Mineral	Orthopyroxene	Orthopyroxene	Orthopyroxene	Orthopyroxene	Orthopyroxene
Description	Corona	Corona	Corona	Corona	Corona
Lithology	Olivine gabbronorite	Olivine gabbronorite	Olivine gabbronorite	Olivine gabbronorite	Olivine gabbronorite
SiO_2	53.19	53.90	53.52	53.46	53.27
TiO_2	0.00	0.00	0.00	0.00	0.00
Al_2O_3	0.75	0.56	0.50	0.70	0.73
FeO*	18.53	18.74	17.68	18.17	18.03
MnO	0.19	0.19	0.24	0.13	0.20
MgO	25.81	26.31	26.15	26.30	26.17
CaO	0.08	0.00	0.07	0.08	0.00
Na_2O	0.00	0.00	0.00	0.00	0.00
K_2O	0.00	0.00	0.00	0.00	0.00
Total	98.55	99.70	98.16	98.84	98.40
Oxygens	6	6	6	6	6
Si	1.965	1.967	1.980	1.964	1.966
Ti	0.000	0.000	0.000	0.000	0.000
Al	0.033	0.024	0.022	0.030	0.032
Fe^{3+}	0.038	0.042	0.019	0.041	0.036
Fe^{2+}	0.534	0.530	0.528	0.517	0.520
Mn	0.006	0.006	0.008	0.004	0.006
Mg	1.421	1.431	1.441	1.440	1.440
Ca	0.003	0.000	0.003	0.003	0.000
Na	0.000	0.000	0.000	0.000	0.000
K	0.000	0.000	0.000	0.000	0.000
Total Cations	4.000	4.000	4.000	4.000	4.000
mg	72.7	71.4	73.2	73.6	73.5
Enstatite	72.5	71.4	73.0	73.4	73.5
Ferrosilite	27.3	28.6	26.8	26.4	26.5
Wollastonite	0.2	0.0	0.2	0.2	0.0

Sample no.	94522022	94522022	94522022	94522022
Analysis no.	72865	72866	72896	72897
Mineral	Plagioclase	Plagioclase	Plagioclase	Plagioclase
Description	Cumulus (c)	Cumulus (c)	Cumulus (r)	Cumulus (r)
Lithology	Olivine gabbronorite	Olivine gabbronorite	Olivine gabbronorite	Olivine gabbronorite
SiO_2	49.01	50.89	44.28	43.46
TiO_2	0.00	0.00	0.00	0.00
Al_2O_3	33.59	32.38	37.17	36.30
FeO*	0.00	0.00	0.00	0.13
MnO	0.00	0.00	0.00	0.00
MgO	0.00	0.00	0.00	0.00
CaO	15.05	13.84	18.82	18.32
Na_2O	2.46	3.02	0.40	0.22
K_2O	0.00	0.00	0.00	0.00
Total	100.11	100.13	100.67	98.43
Oxygens	8	8	8	8
Si	2.229	2.303	2.026	2.033
Ti	0.000	0.000	0.000	0.000
Al	1.800	1.727	2.005	2.001
Fe^{3+}	0.000	0.000	0.000	0.000
Fe^{2+}	0.000	0.000	0.000	0.005
Mn	0.000	0.000	0.000	0.000
Mg	0.000	0.000	0.000	0.000
Ca	0.733	0.671	0.923	0.918
Na	0.217	0.265	0.035	0.020
K	0.000	0.000	0.000	0.000
Total Cations	4.980	4.966	4.989	4.977
Albite	22.8	28.3	3.7	2.1
Anorthite	77.2	71.7	96.3	97.9
Orthoclase	0.0	0.0	0.0	0.0

Appendix Table 3.5 (cont.). Electron microprobe analyses of silicate minerals from the McKenzie Spring layered intrusion.

Sample no.	94522022	94522022	94522022
Analysis no.	72898	72899	72900
Mineral	Plagioclase	Plagioclase	Plagioclase
Description	Cumulus (c)	Cumulus (c)	Cumulus (c)
Lithology	Olivine gabbronorite	Olivine gabbronorite	Olivine gabbronorite
SiO_2	50.65	51.03	52.09
TiO_2	0.00	0.00	0.00
Al_2O_3	32.57	32.26	31.72
FeO*	0.00	0.00	0.00
MnO	0.00	0.00	0.00
MgO	0.00	0.00	0.00
CaO	13.89	13.68	13.01
Na_2O	3.31	3.43	3.81
K_2O	0.00	0.00	0.00
Total	100.42	100.40	100.63
Oxygens	8	8	8
Si	2.290	2.306	2.343
Ti	0.000	0.000	0.000
Al	1.735	1.718	1.681
Fe^{3+}	0.000	0.000	0.000
Fe^{2+}	0.000	0.000	0.000
Mn	0.000	0.000	0.000
Mg	0.000	0.000	0.000
Ca	0.673	0.662	0.627
Na	0.290	0.300	0.332
K	0.000	0.000	0.000
Total Cations	4.988	4.986	4.983
Albite	30.1	31.2	34.6
Anorthite	69.9	68.8	65.4
Orthoclase	0.0	0.0	0.0

Appendix Table 3.5a. Electron microprobe analyses of oxide minerals from the McKenzie Spring layered intrusion.

Sample no.	94522022	94522022	94522022	94522022	94522022	94522022	94522022	94522022
Analysis no.	72879	72880	72881	72882	72883	72884	72894	72895
Mineral	Spinel	Spinel	Spinel	Spinel	Spinel	Spinel	Spinel	Spinel
Description	Corona	Corona	Corona	Corona	Corona	Corona	Corona	Corona
Lithology	Olivine gabbronorite	Olivine gabbronorite	Olivine gabbronorite	Olivine gabbronorite	Olivine gabbronorite	Olivine gabbronorite	Olivine gabbronorite	Olivine gabbronorite
Al_2O_3	64.10	62.65	61.85	61.85	63.85	63.23	63.19	63.40
FeO*	24.85	25.03	26.63	26.63	25.88	25.86	24.24	24.21
MgO	11.61	11.53	10.80	10.80	10.92	10.78	11.61	11.65
Na_2O	0.00	0.00	0.00	0.00	0.00	0.21	0.00	0.25
Total	100.57	99.21	99.28	99.28	100.65	100.08	99.04	99.51
Oxygens	32	32	32	32	32	32	32	32
Al	15.956	15.827	15.940	15.724	15.956	15.881	15.952	15.898
Fe^{3+}	0.044	0.173	0.128	0.275	0.044	0.206	0.048	0.204
Fe^{2+}	4.346	4.315	4.265	4.528	4.546	4.404	4.294	4.103
Mg	3.654	3.685	3.599	3.472	3.454	3.423	3.706	3.693
Na	0.000	0.000	0.068	0.000	0.000	0.087	0.000	0.102
Total Cations	24.000	24.000	24.000	24.000	24.000	24.000	24.000	24.000
mg	45.7	46.1	45.8	43.4	43.2	43.7	46.3	47.4

Appendix Table 3.6. Electron microprobe analyses of silicate minerals from the McIntosh layered intrusion.

Sample no.	92522273	92522273	Sample no.	92522273	92522273	92522273	92522273	92522273	92522273	92522273
Analysis no.	70817	70818	Analysis no.	70791	70792	70793	70794	70795	70815	70816
Mineral	Amphibole	Amphibole	Mineral	Olivine	Olivine	Olivine	Olivine	Olivine	Olivine	Olivine
Description	Corona	Corona	Description	Cumulus (r)	Cumulus (r)	Cumulus (c)	Cumulus (c)	Cumulus (c)	Cumulus (r)	Cumulus (r)
Lithology	Olivine gabbronorite	Olivine gabbronorite	Lithology	Olivine gabbronorite	Olivine gabbronorite	Olivine gabbronorite	Olivine gabbronorite	Olivine gabbronorite	Olivine gabbronorite	Olivine gabbronorite
Strat. ht. (m)	1100	1100	Strat. ht. (m)	1100	1100	1100	1100	1100	1100	1100
SiO_2	42.27	41.99	SiO_2	38.51	38.55	38.36	38.37	38.70	38.63	38.32
TiO_2	2.10	2.23	TiO_2	0.00	0.00	0.00	0.00	0.00	0.00	0.00
Al_2O_3	13.84	14.54	Al_2O_3	0.00	0.00	0.00	0.00	0.00	0.00	0.00
Cr_2O_3	0.00	0.00	Cr_2O_3	0.00	0.00	0.00	0.00	0.00	0.00	0.00
FeO*	8.31	8.58	FeO*	20.68	20.79	20.38	20.40	20.36	20.38	20.24
MnO	0.00	0.00	MnO	0.15	0.15	0.12	0.13	0.12	0.00	0.00
MgO	15.51	14.97	MgO	40.38	40.49	40.45	40.72	40.80	40.77	40.65
CaO	11.39	11.89	CaO	0.00	0.00	0.00	0.00	0.00	0.00	0.00
Na_2O	1.96	1.95	Na_2O	0.00	0.00	0.00	0.00	0.00	0.00	0.00
K_2O	0.91	1.01	K_2O	0.00	0.00	0.00	0.00	0.00	0.00	0.00
Total	96.29	97.16	Total	99.73	99.98	99.31	99.62	99.99	99.79	99.21
Oxygens	23	23	Oxygens	4	4	4	4	4	4	4
Si	6.090	6.046	Si	0.995	0.993	0.994	0.990	0.995	0.995	0.992
Ti	0.228	0.241	Ti	0.000	0.000	0.000	0.000	0.000	0.000	0.000
Al	2.350	2.467	Al	0.000	0.000	0.000	0.000	0.000	0.000	0.000
Cr	0.000	0.000	Cr	0.000	0.000	0.000	0.000	0.000	0.000	0.000
Fe^{3+}	0.783	0.560	Fe^{3+}	0.010	0.013	0.012	0.019	0.009	0.010	0.015
Fe^{2+}	0.218	0.473	Fe^{2+}	0.437	0.435	0.429	0.421	0.429	0.430	0.423
Mn	0.000	0.000	Mn	0.003	0.003	0.003	0.003	0.003	0.000	0.000
Mg	3.331	3.213	Mg	1.555	1.555	1.562	1.567	1.564	1.566	1.569
Ca	1.758	1.834	Ca	0.000	0.000	0.000	0.000	0.000	0.000	0.000
Na	0.547	0.544	Na	0.000	0.000	0.000	0.000	0.000	0.000	0.000
K	0.167	0.185	K	0.000	0.000	0.000	0.000	0.000	0.000	0.000
Total Cations	15.472	15.563	Total Cations	3.000	3.000	3.000	3.000	3.000	3.000	3.000
mg	0.938	0.872	mg	78.1	78.1	78.5	78.8	78.5	78.5	78.8
Classification	Ferrian Tschermakite	Magnesio Hastingsite								

Appendix Table 3.6 (cont.). Electron microprobe analyses of silicate minerals from the McIntosh layered intrusion.

Sample no.	92522273	92522273
Analysis no.	70819	70821
Mineral	Olivine	Olivine
Description	Cumulus (r)	Cumulus (r)
Lithology	Olivine gabbronorite	Olivine gabbronorite
Strat. ht. (m)	1100	1100
SiO_2	38.67	38.46
TiO_2	0.00	0.00
Al_2O_3	0.00	0.00
Cr_2O_3	0.00	0.00
FeO*	20.52	20.35
MnO	0.00	0.12
MgO	40.77	40.28
CaO	0.00	0.00
Na_2O	0.00	0.00
K_2O	0.00	0.00
Total	99.97	99.21
Oxygens	4	4
Si	0.995	0.998
Ti	0.000	0.000
Al	0.000	0.000
Cr	0.000	0.000
Fe^{3+}	0.010	0.004
Fe^{2+}	0.431	0.437
Mn	0.000	0.003
Mg	1.563	1.558
Ca	0.000	0.000
Na	0.000	0.000
K	0.000	0.000
Total Cations	3.000	3.000
mg	78.4	78.1

Sample no.	92522273	92522273	92522273	92522273
Analysis no.	70804	70806	70807	70808
Mineral	Orthopyroxene	Orthopyroxene	Orthopyroxene	Orthopyroxene
Description	Corona	Corona	Corona	Corona
Lithology	Olivine gabbronorite	Olivine gabbronorite	Olivine gabbronorite	Olivine gabbronorite
Strat. ht. (m)	1100	1100	1100	1100
SiO_2	55.38	56.08	55.01	55.52
TiO_2	0.00	0.00	0.00	0.00
Al_2O_3	0.00	0.00	0.14	0.00
Cr_2O_3	0.00	0.00	0.00	0.00
FeO*	14.32	14.57	14.44	14.61
MnO	0.12	0.19	0.14	0.10
MgO	30.16	29.60	29.95	29.68
CaO	0.00	0.00	0.00	0.00
Na_2O	0.00	0.00	0.00	0.00
K_2O	0.00	0.00	0.00	0.00
Total	99.98	100.44	99.68	99.91
Oxygens	6	6	6	6
Si	1.971	1.993	1.964	1.982
Ti	0.000	0.000	0.000	0.000
Al	0.000	0.000	0.006	0.000
Cr	0.000	0.000	0.000	0.000
Fe^{3+}	0.059	0.013	0.066	0.037
Fe^{2+}	0.368	0.420	0.366	0.399
Mn	0.004	0.006	0.004	0.003
Mg	1.599	1.568	1.594	1.579
Ca	0.000	0.000	0.000	0.000
Na	0.000	0.000	0.000	0.000
K	0.000	0.000	0.000	0.000
Total Cations	4.000	4.000	4.000	4.000
mg	81.3	78.9	81.3	79.8
Enstatite	81.3	78.9	81.3	79.8
Ferrosilite	18.7	21.1	18.7	20.2
Wollastonite	0.0	0.0	0.0	0.0

Sample no.	92522273
Analysis no.	70796
Mineral	Plagioclase
Description	Cumulus (r)
Lithology	Olivine gabbronorite
Strat. ht. (m)	1100
SiO_2	48.79
TiO_2	0.00
Al_2O_3	33.85
Cr_2O_3	0.00
FeO*	0.00
MnO	0.00
MgO	0.00
CaO	15.48
Na_2O	2.50
K_2O	0.00
Total	100.62
Oxygens	8
Si	2.212
Ti	
Al	1.809
Cr	
Fe^{3+}	0.000
Fe^{2+}	0.000
Mn	0.000
Mg	0.000
Ca	0.752
Na	0.220
K	0.000
Total Cations	4.993
Albite	22.6
Anorthite	77.4
Orthoclase	0.0

Appendix Table 3.6 (cont.). Electron microprobe analyses of silicate minerals from the McIntosh layered intrusion.

Sample no.	92522273	92522273	92522273	92522273	92522273	92522273	92522273
Analysis no.	70797	70798	70799	70813	70814	70822	70823
Mineral	Plagioclase	Plagioclase	Plagioclase	Plagioclase	Plagioclase	Plagioclase	Plagioclase
Description	Cumulus (r)	Cumulus (c)	Cumulus (c)	Cumulus (r)	Cumulus (r)	Cumulus (r)	Cumulus (r)
Lithology	Olivine gabbronorite	Olivine gabbronorite	Olivine gabbronorite	Olivine gabbronorite	Olivine gabbronorite	Olivine gabbronorite	Olivine gabbronorite
Strat. ht. (m)	1100	1100	1100	1100	1100	1100	1100
SiO_2	48.37	48.28	47.92	49.23	48.78	48.89	50.03
TiO_2	0.00	0.00	0.00	0.00	0.00	0.00	0.00
Al_2O_3	33.66	33.86	33.76	33.60	33.41	33.60	32.83
Cr_2O_3	0.00	0.00	0.00	0.00	0.00	0.00	0.00
FeO*	0.15	0.15	0.11	0.00	0.00	0.00	0.00
MnO	0.00	0.00	0.00	0.00	0.00	0.00	0.00
MgO	0.00	0.00	0.00	0.00	0.00	0.00	0.00
CaO	15.54	15.39	15.44	15.06	15.18	15.14	14.39
Na_2O	2.33	2.36	2.25	2.55	2.48	2.70	2.89
K_2O	0.00	0.00	0.00	0.05	0.00	0.00	0.00
Total	100.05	100.04	99.48	100.49	99.85	100.33	100.14
Oxygens	8	8	8	8	8	8	8
Si	2.208	2.203	2.199	2.231	2.226	2.222	2.270
Ti							
Al	1.811	1.821	1.826	1.795	1.797	1.800	1.756
Cr				0.000	0.000	0.000	0.000
Fe^{3+}	0.000	0.000	0.000	0.000	0.000	0.000	0.000
Fe^{2+}	0.006	0.006	0.004	0.000	0.000	0.000	0.000
Mn	0.000	0.000	0.000	0.000	0.000	0.000	0.000
Mg	0.000	0.000	0.000	0.000	0.000	0.000	0.000
Ca	0.760	0.753	0.759	0.732	0.742	0.737	0.700
Na	0.206	0.209	0.200	0.224	0.220	0.238	0.255
K	0.000	0.000	0.000	0.003	0.000	0.000	0.000
Total Cations	4.990	4.991	4.988	4.984	4.985	4.997	4.980
Albite	21.3	21.7	20.9	23.4	22.9	24.4	26.7
Anorthite	78.7	78.3	79.1	76.6	77.1	75.6	73.3
Orthoclase	0.0	0.0	0.0	0.0	0.0	0.0	0.0

Appendix Table 3.6a. Electron microprobe analyses of oxide minerals from the McIntosh layered intrusion.

Sample no.	92522273	92522273	92522273	92522273	92522273
Analysis no.	72931	72932	72933	72934	72935
Mineral	Spinel	Spinel	Spinel	Spinel	Spinel
Description	Corona	Corona	Corona	Corona	Corona
Lithology	Olivine gabbronorite	Olivine gabbronorite	Olivine gabbronorite	Olivine gabbronorite	Olivine gabbronorite
Strat. ht. (m)	1100	1100	1100	1100	1100
Al_2O_3	65.91	66.56	65.54	65.51	64.90
FeO*	20.10	18.16	19.65	21.34	22.02
MgO	14.14	15.55	14.82	13.17	12.90
Total	100.16	100.28	100.01	100.02	99.81
Oxygens	32	32	32	32	32
Al	16.098	16.087	16.010	16.118	16.064
Fe^{3+}	0.000	0.000	0.000	0.000	0.000
Fe^{2+}	3.484	3.115	3.407	3.726	3.867
Mg	4.369	4.754	4.579	4.097	4.038
Total Cations	23.951	23.956	23.995	23.941	23.968
mg	55.6	60.4	57.3	52.4	51.1

Appendix Table 3.7. Electron microprobe analyses of silicate minerals from the Norton intrusion.

Sample no.	94522167	94522167	94522167	94522167	94522167	94522167	94522167	94522167
Analysis no.	72158	72159	72161	72155	72156	72157	72164	72165
Mineral	Amphibole	Amphibole	Amphibole	Amphibole	Amphibole	Amphibole	Amphibole	Amphibole
Description	Metam.	Metam.	Metam.	Metam. (c)	Metam. (c)	Metam. (c)	Metam.	Metam.
Lithology	Metagabbro	Metagabbro	Metagabbro	Metagabbro	Metagabbro	Metagabbro	Metagabbro	Metagabbro
Strat. ht. (m)	20	20	20	20	20	20	20	20
SiO_2	45.95	45.98	45.88	50.17	52.05	52.45	51.82	51.87
TiO_2	1.74	1.79	1.69	0.92	0.00	0.00	0.00	0.00
Al_2O_3	8.39	8.47	7.94	0.94	0.82	0.54	0.26	0.57
FeO*	16.20	15.93	16.82	27.36	27.02	26.35	25.79	24.68
MnO	0.10	0.00	0.00	0.57	0.62	0.57	0.55	0.56
MgO	12.14	12.28	11.80	15.88	16.10	16.78	16.27	15.99
CaO	10.96	11.09	11.13	1.16	1.04	1.25	0.39	0.47
Na_2O	1.00	1.06	1.17	0.00	0.00	0.00	0.00	0.00
K_2O	0.27	0.31	0.19	0.00	0.00	0.00	0.00	0.00
Total	98.55	98.67	98.49	97.00	97.63	97.95	97.96	96.89
Oxygens	23	23	23	23	23	23	23	23
Si	6.722	6.721	6.765	7.507	7.713	7.716	7.865	7.940
Ti	0.191	0.197	0.187	0.103	0.000	0.000	0.000	0.000
Al	1.446	1.459	1.380	0.166	0.142	0.094	0.047	0.103
Fe^{3+}	0.959	0.873	0.828	0.613	0.433	0.473	0.224	0.017
Fe^{2+}	1.023	1.074	1.246	2.811	2.915	2.768	3.049	3.142
Mn	0.012	0.000	0.000	0.073	0.077	0.071	0.071	0.072
Mg	2.647	2.676	2.593	3.541	3.555	3.680	3.680	3.649
Ca	1.718	1.737	1.758	0.186	0.165	0.197	0.064	0.076
Na	0.284	0.300	0.334	0.000	0.000	0.000	0.000	0.000
K	0.050	0.058	0.036	0.000	0.000	0.000	0.000	0.000
Total Cations	15.052	15.095	15.127	15.000	15.000	15.000	15.000	15.000
mg	72.1	71.3	67.5	55.7	54.9	57.1	54.7	53.7
Classification	Ferrian Magnesio Hornblende	Ferrian Magnesio Hornblende	Ferrian Magnesio Hornblende	Cummingtonite	Cummingtonite	Cummingtonite	Cummingtonite	Cummingtonite

Appendix Table 3.7 (cont.). Electron microprobe analyses of silicate minerals from the Norton intrusion.

Sample no.	94522167	94522167	94522167
Analysis no.	72148	72149	72150
Mineral	Orthopyroxene	Orthopyroxene	Orthopyroxene
Description	Metam. (c)	Metam. (c)	Metam.
Lithology	Metagabbro	Metagabbro	Metagabbro
Strat. ht. (m)	20	20	20
SiO_2	51.42	50.91	50.78
TiO_2	0.00	0.00	0.00
Al_2O_3	0.37	0.34	0.48
FeO*	29.36	30.00	29.95
MnO	0.62	0.55	0.55
MgO	17.39	17.41	16.99
CaO	0.58	0.52	0.69
Na_2O	0.00	0.00	0.00
K_2O	0.00	0.00	0.00
Total	99.76	99.88	99.54
Oxygens	6	6	6
Si	1.988	1.970	1.973
Ti	0.000	0.000	0.000
Al	0.017	0.016	0.022
Fe^{3+}	0.008	0.045	0.031
Fe^{2+}	0.941	0.926	0.942
Mn	0.020	0.018	0.018
Mg	1.002	1.004	0.984
Ca	0.024	0.021	0.029
Na	0.000	0.000	0.000
K	0.000	0.000	0.000
Total Cations	4.000	4.000	4.000
mg	51.6	52.0	51.1
Enstatite	51.0	51.4	50.3
Ferrosilite	47.8	47.5	48.2
Wollastonite	1.2	1.1	1.5

Sample no.	94522167	94522167	94522167	94522167
Analysis no.	72151	72152	72153	72154
Mineral	Plagioclase	Plagioclase	Plagioclase	Plagioclase
Description	Metam. (r)	Metam. (r)	Metam. (c)	Metam. (c)
Lithology	Metagabbro	Metagabbro	Metagabbro	Metagabbro
Strat. ht. (m)	20	20	20	20
SiO_2	50.40	49.86	50.01	49.88
TiO_2	0.00	0.00	0.00	0.00
Al_2O_3	33.30	32.97	32.64	32.66
FeO*	0.00	0.17	0.00	0.00
MnO	0.00	0.00	0.00	0.00
MgO	0.00	0.00	0.00	0.00
CaO	14.49	14.47	14.33	14.32
Na_2O	3.31	2.93	2.98	2.90
K_2O	0.06	0.05	0.00	0.00
Total	101.74	100.46	99.95	99.76
Oxygens	8	8	8	8
Si	2.257	2.260	2.274	2.272
Ti	0.000	0.000	0.000	0.000
Al	1.757	1.761	1.749	1.753
Fe^{3+}	0.006	0.000	0.000	0.000
Fe^{2+}	0.000	0.007	0.000	0.000
Mn	0.000	0.000	0.000	0.000
Mg	0.000	0.000	0.000	0.000
Ca	0.695	0.703	0.698	0.699
Na	0.288	0.258	0.262	0.256
K	0.003	0.003	0.000	0.000
Total Cations	5.007	4.990	4.983	4.980
Albite	29.2	26.8	27.3	26.8
Anorthite	70.5	72.9	72.7	73.2
Orthoclase	0.3	0.3	0.0	0.0

Appendix Table 3.8. Electron microprobe analyses of silicate minerals from the Sally Malay layered intrusion.

Sample no.	93522066	93522066	93522066	93522066	93522066
Analysis no.	70761	70762	70775	70776	70790
Mineral	Amphibole	Amphibole	Amphibole	Amphibole	Amphibole
Description	Corona	Incl. in plag.	Corona	Corona	Corona
Lithology	Troctolite	Troctolite	Troctolite	Troctolite	Troctolite
Strat. ht. (m)	350	350	350	350	350
SiO_2	42.17	42.04	42.48	41.93	41.88
TiO_2	0.96	0.99	0.72	0.54	0.89
Al_2O_3	15.41	15.90	15.59	15.72	15.49
Cr_2O_3	0.34	0.00	0.18	0.12	0.21
FeO*	7.64	8.41	8.14	7.44	8.09
MnO	0.00	0.00	0.09	0.00	0.00
MgO	16.37	15.38	16.48	16.41	16.11
CaO	11.89	11.61	11.59	11.80	11.26
Na_2O	2.21	2.24	2.62	2.47	2.37
K_2O	0.66	0.63	0.65	0.65	0.69
Total	98.50	98.15	99.45	97.91	97.90
Oxygens	23	23	23	23	23
Si	5.969	5.974	5.948	5.955	5.945
Ti	0.102	0.106	0.076	0.058	0.095
Al	2.571	2.663	2.573	2.631	2.591
Cr	0.038	0.000	0.020	0.013	0.024
Fe^{3+}	0.841	0.910	0.953	0.883	0.960
Fe^{2+}	0.064	0.000	0.000	0.000	0.000
Mn	0.000	0.000	0.011	0.000	0.000
Mg	3.454	3.258	3.439	3.473	3.408
Ca	1.803	1.768	1.739	1.795	1.712
Na	0.606	0.617	0.711	0.680	0.652
K	0.119	0.617	0.116	0.118	0.125
Total Cations	15.567	15.913	15.586	15.606	15.512
mg	98.2	100.0	100.0	100.0	100.0
Classification	Ferrian Magnesio Hastingsite	Tschermakite	Ferrian Magnesio Hastingsite	Ferrian Magnesio Hastingsite	Ferrian Tschermakite

Sample no.	93522066	93522066	93522066	93522066
Analysis no.	70748	70749	70750	70767
Mineral	Olivine	Olivine	Olivine	Olivine
Description	Cumulus (c)	Cumulus (c)	Corona (r)	Corona (r)
Lithology	Troctolite	Troctolite	Troctolite	Troctolite
Strat. ht. (m)	350	350	350	350
SiO_2	38.64	38.48	38.27	38.87
TiO_2	0.00	0.00	0.00	0.00
Al_2O_3	0.00	0.00	0.00	0.00
Cr_2O_3	0.00	0.00	0.00	0.00
FeO*	20.52	20.92	20.53	20.50
MnO	0.13	0.11	0.00	0.00
MgO	40.39	39.98	40.50	40.82
CaO	0.00	0.00	0.00	0.00
Na_2O	0.00	0.00	0.00	0.00
K_2O	0.00	0.00	0.00	0.00
Total	99.69	99.51	99.38	100.22
Oxygens	4	4	4	4
Si	0.998	0.998	0.991	0.998
Ti	0.000	0.000	0.000	0.000
Al	0.000	0.000	0.000	0.000
Cr	0.000	0.000	0.000	0.000
Fe^{3+}	0.003	0.004	0.017	0.004
Fe^{2+}	0.440	0.450	0.428	0.436
Mn	0.003	0.002	0.000	0.000
Mg	1.555	1.546	1.564	1.562
Ca	0.000	0.000	0.000	0.000
Na	0.000	0.000	0.000	0.000
K	0.000	0.000	0.000	0.000
Total Cations	3.000	3.000	3.000	3.000
mg	77.9	77.5	78.5	78.2

Appendix Table 3.8 (cont.). Electron microprobe analyses of silicate minerals from the Sally Malay layered intrusion.

Sample no.	93522066	93522066	93522066	93522066	93522066	93522066	93522066
Analysis no.	70768	70769	70770	70785	70786	70787	70788
Mineral	Olivine	Olivine	Olivine	Olivine	Olivine	Olivine	Olivine
Description	Corona (r)	Cumulus (c)	Cumulus (c)	Cumulus (r)	Cumulus (r)	Cumulus (c)	Cumulus (c)
Lithology	Troctolite	Troctolite	Troctolite	Troctolite	Troctolite	Troctolite	Troctolite
Strat. ht. (m)	350	350	350	350	350	350	350
SiO_2	38.16	38.19	38.27	38.08	38.39	38.22	38.01
TiO_2	0.00	0.00	0.00	0.00	0.00	0.00	0.00
Al_2O_3	0.00	0.00	0.00	0.00	0.00	0.00	0.00
Cr_2O_3	0.00	0.00	0.00	0.00	0.00	0.00	0.00
FeO*	20.30	21.19	20.76	20.71	21.01	20.92	20.80
MnO	0.13	0.12	0.12	0.11	0.00	0.00	0.09
MgO	40.52	39.98	40.13	40.55	40.51	40.45	40.06
CaO	0.00	0.00	0.00	0.00	0.00	0.00	0.00
Na_2O	0.00	0.00	0.00	0.00	0.00	0.00	0.00
K_2O	0.00	0.00	0.00	0.00	0.00	0.00	0.00
Total	99.22	99.57	99.34	99.60	100.01	99.71	99.07
Oxygens	4	4	4	4	4	4	4
Si	0.990	0.991	0.994	0.985	0.990	0.988	0.990
Ti	0.000	0.000	0.000	0.000	0.000	0.000	0.000
Al	0.000	0.000	0.000	0.000	0.000	0.000	0.000
Cr	0.000	0.000	0.000	0.000	0.000	0.000	0.000
Fe^{3+}	0.020	0.018	0.013	0.029	0.020	0.023	0.020
Fe^{2+}	0.420	0.442	0.438	0.419	0.433	0.429	0.433
Mn	0.003	0.003	0.003	0.002	0.000	0.000	0.002
Mg	1.567	1.546	1.553	1.564	1.557	1.559	1.555
Ca	0.000	0.000	0.000	0.000	0.000	0.000	0.000
Na	0.000	0.000	0.000	0.000	0.000	0.000	0.000
K	0.000	0.000	0.000	0.000	0.000	0.000	0.000
Total Cations	3.000	3.000	3.000	3.000	3.000	3.000	3.000
mg	78.9	77.8	78.0	78.9	78.2	78.4	78.2

Sample no.	93522066	93522066
Analysis no.	70777	70778
Mineral	Orthopyroxene	Orthopyroxene
Description	Corona	Corona
Lithology	Troctolite	Troctolite
Strat. ht. (m)	350	350
SiO_2	53.66	53.74
TiO_2	0.00	0.00
Al_2O_3	2.88	3.00
Cr_2O_3	0.00	0.00
FeO*	14.17	13.83
MnO	0.00	0.10
MgO	29.19	28.74
CaO	0.10	0.07
Na_2O	0.00	0.00
K_2O	0.00	0.00
Total	100.23	99.57
Oxygens	6	6
Si	1.908	1.922
Ti	0.000	0.000
Al	0.121	0.126
Cr	0.000	0.000
Fe^{3+}	0.064	0.029
Fe^{2+}	0.357	0.385
Mn	0.000	0.003
Mg	1.547	1.532
Ca	0.004	0.003
Na	0.000	0.000
K	0.000	0.000
Total Cations	4.000	4.000
mg	81.3	79.9
Enstatite	81.1	79.7
Ferrosilite	18.7	20.1
Wollastonite	0.2	0.2

Appendix Table 3.8 (cont.). Electron microprobe analyses of silicate minerals from the Sally Malay layered intrusion.

Sample no.	93522066	Sample no.	93522066	93522066	93522066	93522066	93522066	93522066	93522066	93522066
Analysis no.	70789	Analysis no.	70752	70754	70755	70771	70772	70773	70774	70782
Mineral	Orthopyroxene	Mineral	Plagioclase	Plagioclase	Plagioclase	Plagioclase	Plagioclase	Plagioclase	Plagioclase	Plagioclase
Description	Corona	Description	Cumulus (r)	Cumulus (r)	Cumulus (c)	Cumulus (r)	Cumulus (c)	Cumulus (c)	Cumulus (c)	Cumulus (r)
Lithology	Troctolite	Lithology	Troctolite	Troctolite	Troctolite	Troctolite	Troctolite	Troctolite	Troctolite	Troctolite
Strat. ht. (m)	350	Strat. ht. (m)	350	350	350	350	350	350	350	350
SiO_2	55.45	SiO_2	45.79	45.91	46.53	46.78	45.39	45.40	45.09	45.73
TiO_2	0.00	TiO_2	0.00	0.00	0.00	0.00	0.00	0.00	0.00	0.00
Al_2O_3	0.73	Al_2O_3	35.39	35.62	35.37	36.42	35.92	35.65	36.21	35.94
Cr_2O_3	0.00	Cr_2O_3	0.00	0.00	0.00	0.00	0.00	0.00	0.00	0.00
FeO*	14.23	FeO*	0.12	0.15	0.00	0.10	0.11	0.00	0.00	0.00
MnO	0.16	MnO	0.00	0.00	0.00	0.00	0.00	0.00	0.00	0.00
MgO	29.84	MgO	0.00	0.00	0.00	0.00	0.00	0.00	0.00	0.00
CaO	0.00	CaO	17.44	17.36	17.13	17.44	17.80	17.70	18.14	17.75
Na_2O	0.00	Na_2O	1.22	1.12	1.51	1.17	1.06	0.97	0.79	1.27
K_2O	0.00	K_2O	0.00	0.00	0.07	0.00	0.00	0.00	0.00	0.05
Total	100.56	Total	99.96	100.16	100.60	101.92	100.29	99.72	100.23	100.84
Oxygens	6	Oxygens	8	8	8	8	8	8	8	8
Si	1.966	Si	2.104	2.104	2.122	2.104	2.081	2.091	2.068	2.086
Ti	0.000	Ti	0.000	0.000	0.000	0.000	0.000	0.000	0.000	0.000
Al	0.030	Al	1.917	1.924	1.901	1.931	1.941	1.935	1.958	1.932
Cr	0.000	Cr	0.000	0.000	0.000	0.000	0.000	0.000	0.000	0.000
Fe^{3+}	0.038	Fe^{3+}	0.000	0.000	0.000	0.000	0.000	0.000	0.000	0.004
Fe^{2+}	0.384	Fe^{2+}	0.004	0.006	0.000	0.004	0.004	0.000	0.000	0.000
Mn	0.005	Mn	0.000	0.000	0.000	0.000	0.000	0.000	0.000	0.000
Mg	1.577	Mg	0.000	0.000	0.837	0.000	0.000	0.000	0.000	0.000
Ca	0.000	Ca	0.858	0.852	0.133	0.841	0.874	0.873	0.892	0.867
Na	0.000	Na	0.109	0.099	0.004	0.102	0.094	0.087	0.070	0.112
K	0.000	K	0.000	0.000	0.000	0.000	0.000	0.000	0.000	0.003
Total Cations	4.000	Total Cations	4.992	4.984	4.996	4.982	4.995	4.985	4.988	5.004
mg	80.4	Albite	11.3	10.4	2.9	10.8	9.7	9.1	7.3	11.4
Enstatite	80.4	Anorthite	88.7	89.6	97.1	89.2	90.3	90.9	92.7	88.3
Ferrosilite	19.6	Orthoclase	0.0	0.0	0.0	0.0	0.0	0.0	0.0	0.3
Wollastonite	0.0									

Appendix Table 3.8 (cont.). Electron microprobe analyses of silicate minerals from the Sally Malay layered intrusion.

Sample no.	93522066	93522066
Analysis no.	70783	70784
Mineral	Plagioclase	Plagioclase
Description	Cumulus (r)	Cumulus (c)
Lithology	Troctolite	Troctolite
Strat. ht. (m)	350	350
SiO_2	45.41	45.66
TiO_2	0.00	0.00
Al_2O_3	35.90	35.79
Cr_2O_3	0.00	0.00
FeO*	0.18	0.00
MnO	0.00	0.00
MgO	0.00	0.00
CaO	18.06	17.59
Na_2O	0.87	1.04
K_2O	0.00	0.00
Total	100.41	100.07
Oxygens	8	8
Si	2.080	2.094
Ti	0.000	0.000
Al	1.938	1.934
Cr	0.000	0.000
Fe^{3+}	0.000	0.000
Fe^{2+}	0.007	0.000
Mn	0.000	0.000
Mg	0.000	0.000
Ca	0.886	0.864
Na	0.078	0.092
K	0.000	0.000
Total Cations	4.989	4.985
Albite	8.1	9.6
Anorthite	91.9	90.4
Orthoclase	0.0	0.0

Appendix Table 3.8a. Electron microprobe analyses of oxide minerals from the Sally Malay layered intrusion.

Sample no.	93522066	93522066	93522066	93522066
Analysis no.	70763	70765	70779	70780
Mineral name	Spinel	Spinel	Spinel	Spinel
Description	Corona	Corona	Corona	Corona
Lithology	Troctolite	Troctolite	Troctolite	Troctolite
Strat. ht. (m)	350	350	350	350
Al_2O_3	60.93	58.21	58.24	58.66
Cr_2O_3	2.43	4.65	4.77	4.62
FeO*	21.88	23.41	22.17	22.29
MnO	0.15	0.19	0.16	0.16
MgO	13.86	13.51	14.17	14.14
Total	99.25	99.97	99.51	99.87
Oxygens	32	32	32	32
Al	15.277	14.681	14.682	14.730
Cr	0.409	0.787	0.807	0.779
Fe^{3+}	0.315	0.532	0.512	0.491
Fe^{2+}	3.579	3.657	3.454	3.480
Mn	0.028	0.034	0.029	0.028
Mg	4.393	4.309	4.517	4.492
Total Cations	24.000	24.000	24.000	24.000
mg	55.1	54.1	56.7	56.3

Appendix Table 3.9. Electron microprobe analyses of silicate minerals from the Spring Creek layered intrusion.

Sample no.	94522062	94522062	94522062	94522062	94522062	94522062	94522062
Analysis no.	71746	71747	72915	72916	71744	71748	71749
Mineral	Amphibole	Amphibole	Amphibole	Amphibole	Amphibole	Amphibole	Amphibole
Description	Corona	Corona	Repl. cpx	Repl. cpx	Corona	Corona	Corona
Lithology	Olivine gabbronorite	Olivine gabbronorite	Olivine gabbronorite	Olivine gabbronorite	Olivine gabbronorite	Olivine gabbronorite	Olivine gabbronorite
Strat. ht. (m)	2080	2080	2080	2080	2080	2080	2080
SiO_2	44.18	45.43	43.98	43.98	56.74	55.71	55.90
TiO_2	0.00	0.00	2.48	2.43	0.00	0.00	0.00
Al_2O_3	14.68	13.12	12.12	11.99	0.00	0.30	0.00
Cr_2O_3	0.00	0.00	0.44	0.48	0.00	0.00	0.00
FeO*	8.26	8.18	11.71	12.02	11.05	13.87	14.40
MnO	0.00	0.00	0.00	0.00	0.00	0.31	0.23
MgO	16.16	17.04	13.46	13.37	24.26	25.32	24.99
CaO	11.59	11.55	11.95	12.00	4.69	0.62	0.34
Na_2O	2.06	1.72	0.66	0.54	0.00	0.00	0.00
K_2O	0.29	0.18	0.68	0.69	0.00	0.00	0.00
Total	97.22	97.22	97.48	97.50	96.74	96.13	95.86
Oxygens	23	23	23	23	23	23	23
Si	6.210	6.342	6.295	6.359	7.942	7.859	7.930
Ti	0.000	0.000	0.267	0.264	0.000	0.000	0.000
Al	2.432	2.158	2.045	2.043	0.000	0.050	0.000
Cr	0.000	0.000	0.050	0.055	0.000	0.000	0.000
Fe^{3+}	0.971	0.955	0.709	0.551	0.115	0.232	0.141
Fe^{2+}	0.000	0.000	0.813	0.902	1.178	1.404	1.568
Mn	0.000	0.000	0.000	0.000	0.000	0.037	0.028
Mg	3.388	3.545	2.822	2.881	5.061	5.324	5.283
Ca	1.745	1.727	1.833	1.859	0.703	0.094	0.052
Na	0.561	0.465	0.183	0.151	0.000	0.000	0.000
K	0.052	0.032	0.124	0.127	0.000	0.000	0.000
Total Cations	15.359	15.224	15.141	15.192	15.000	15.000	15.000
mg	100.0	100.0	77.9	76.2	81.1	79.1	77.1
Classification	Ferrian Tschermakite	Ferrian Tschermakite	Titanian Tschermakitic Hornblende	Titanian Tschermakitic Hornblende	Magnesio Cummingtonite	Magnesio Cummingtonite	Magnesio Cummingtonite

Sample no.	94522062
Analysis no.	71768
Mineral	Clinopyroxene
Description	Cumulus
Lithology	Olivine gabbronorite
Strat. ht. (m)	2080
SiO_2	50.76
TiO_2	1.37
Al_2O_3	2.58
Cr_2O_3	0.48
FeO*	10.42
MnO	0.14
MgO	15.70
CaO	18.21
Na_2O	0.00
K_2O	0.00
Total	99.67
Oxygens	6
Si	1.898
Ti	0.039
Al	0.114
Cr	0.014
Fe^{3+}	0.000
Fe^{2+}	0.326
Mn	0.005
Mg	0.875
Ca	0.730
Na	0.000
K	0.000
Total Cations	3.999
mg	72.9
Enstatite	45.3
Ferrosilite	16.9
Wollastonite	37.8

Appendix Table 3.9 (cont.). Electron microprobe analyses of silicate minerals from the Spring Creek layered intrusion.

Sample no.	94522062	94522062	94522062	94522062	94522062	94522062
Analysis no.	71769	72909	72911	72912	72913	72914
Mineral	Clinopyroxene	Clinopyroxene	Clinopyroxene	Clinopyroxene	Clinopyroxene	Clinopyroxene
Description	Cumulus	Intercumulus	Intercumulus	Intercumulus	Intercumulus	Intercumulus
Lithology	Olivine gabbronorite	Olivine gabbronorite	Olivine gabbronorite	Olivine gabbronorite	Olivine gabbronorite	Olivine gabbronorite
Strat. ht. (m)	2080	2080	2080	2080	2080	2080
SiO_2	51.24	50.93	51.29	51.48	51.80	51.24
TiO_2	0.74	1.03	0.64	0.85	0.61	0.68
Al_2O_3	3.56	3.35	2.89	3.06	2.74	3.04
Cr_2O_3	0.46	0.55	0.60	0.54	0.43	0.64
FeO*	6.65	7.28	8.84	9.81	7.53	8.40
MnO	0.00	0.21	0.00	0.16	0.15	0.17
MgO	14.90	14.84	15.06	16.22	15.14	15.17
CaO	21.46	21.42	20.54	18.06	21.40	20.46
Na_2O	0.28	0.25	0.00	0.19	0.30	0.00
K_2O	0.00	0.00	0.00	0.00	0.00	0.00
Total	100.16	99.86	99.85	100.37	100.10	99.80
Oxygens	6	6	6	6	6	6
Si	1.904	1.888	1.909	1.900	1.912	1.906
Ti	0.021	0.029	0.018	0.024	0.017	0.019
Al	0.156	0.146	0.127	0.133	0.119	0.133
Cr	0.014	0.016	0.018	0.016	0.013	0.019
Fe^{3+}	0.002	0.022	0.003	0.018	0.031	0.000
Fe^{2+}	0.205	0.204	0.272	0.285	0.202	0.261
Mn	0.000	0.007	0.000	0.005	0.005	0.005
Mg	0.825	0.820	0.835	0.892	0.833	0.841
Ca	0.854	0.851	0.819	0.714	0.847	0.815
Na	0.020	0.018	0.000	0.013	0.022	0.000
K	0.000	0.000	0.000	0.000	0.000	0.000
Total Cations	4.000	4.000	4.000	4.000	4.000	3.999
mg	80.1	80.1	75.4	75.8	80.5	76.3
Enstatite	43.8	43.7	43.4	47.1	44.3	43.9
Ferrosilite	10.9	10.9	14.1	15.1	10.7	13.6
Wollastonite	45.3	45.4	42.5	37.8	45.0	42.5

Sample no.	94522062	94522062	94522062
Analysis no.	71735	71736	71737
Mineral	Olivine	Olivine	Olivine
Description	Cumulus (c)	Cumulus (c)	Cumulus (r)
Lithology	Olivine gabbronorite	Olivine gabbronorite	Olivine gabbronorite
Strat. ht. (m)	2080	2080	2080
SiO_2	38.35	37.66	37.52
TiO_2	0.00	0.00	0.00
Al_2O_3	0.00	0.00	0.00
Cr_2O_3	0.00	0.00	0.00
FeO*	23.48	26.12	26.13
MnO	0.13	0.20	0.16
MgO	38.25	36.74	36.52
CaO	0.00	0.00	0.00
Na_2O	0.00	0.00	0.00
K_2O	0.00	0.00	0.00
Total	100.21	100.72	100.33
Oxygens	4	4	4
Si	1.000	0.987	0.988
Ti	0.000	0.000	0.000
Al	0.000	0.000	0.000
Cr	0.000	0.000	0.000
Fe^{3+}	0.001	0.026	0.024
Fe^{2+}	0.511	0.547	0.551
Mn	0.003	0.004	0.004
Mg	1.486	1.436	1.433
Ca	0.000	0.000	0.000
Na	0.000	0.000	0.000
K	0.000	0.000	0.000
Total Cations	3.000	3.000	3.000
mg	74.4	72.4	72.2

Appendix Table 3.9 (cont.). Electron microprobe analyses of silicate minerals from the Spring Creek layered intrusion.

Sample no.	94522062	94522062	94522062	94522062	94522062	94522062	94522062	94522062
Analysis no.	71738	71750	71751	71752	71757	71758	71759	71760
Mineral	Olivine	Olivine	Olivine	Olivine	Olivine	Olivine	Olivine	Olivine
Description	Cumulus (r)	Cumulus (r)	Cumulus (r)	Cumulus (c)	Cumulus (r)	Cumulus (r)	Cumulus (c)	Cumulus (c)
Lithology	Olivine gabbronorite	Olivine gabbronorite	Olivine gabbronorite	Olivine gabbronorite	Olivine gabbronorite	Olivine gabbronorite	Olivine gabbronorite	Olivine gabbronorite
Strat. ht. (m)	2080	2080	2080	2080	2080	2080	2080	2080
SiO_2	37.53	37.69	37.68	37.55	37.79	37.54	37.66	37.50
TiO_2	0.00	0.00	0.00	0.00	0.00	0.00	0.00	0.00
Al_2O_3	0.00	0.00	0.00	0.00	0.00	0.00	0.00	0.00
Cr_2O_3	0.00	0.00	0.00	0.00	0.00	0.00	0.00	0.00
FeO*	26.48	25.98	26.24	26.05	26.17	26.09	25.99	26.13
MnO	0.14	0.11	0.19	0.16	0.18	0.24	0.20	0.22
MgO	36.19	36.51	36.01	36.53	35.92	36.58	36.34	36.54
CaO	0.00	0.00	0.00	0.00	0.00	0.00	0.00	0.00
Na_2O	0.00	0.00	0.00	0.00	0.00	0.00	0.00	0.00
K_2O	0.00	0.00	0.00	0.00	0.00	0.00	0.00	0.00
Total	100.34	100.29	100.12	100.29	100.06	100.45	100.19	100.39
Oxygens	4	4	4	4	4	4	4	4
Si	0.990	0.992	0.996	0.989	1.000	0.987	0.993	0.987
Ti	0.000	0.000	0.000	0.000	0.000	0.000	0.000	0.000
Al	0.000	0.000	0.000	0.000	0.000	0.000	0.000	0.000
Cr	0.000	0.000	0.000	0.000	0.000	0.000	0.000	0.000
Fe^{3+}	0.020	0.015	0.008	0.022	0.000	0.025	0.013	0.026
Fe^{2+}	0.564	0.557	0.573	0.551	0.579	0.548	0.560	0.549
Mn	0.003	0.002	0.004	0.003	0.004	0.005	0.004	0.005
Mg	1.423	1.433	1.419	1.434	1.417	1.434	1.429	1.433
Ca	0.000	0.000	0.000	0.000	0.000	0.000	0.000	0.000
Na	0.000	0.000	0.000	0.000	0.000	0.000	0.000	0.000
K	0.000	0.000	0.000	0.000	0.000	0.000	0.000	0.000
Total Cations	3.000	3.000	3.000	3.000	3.000	3.000	3.000	3.000
mg	71.6	72.0	71.2	72.2	71.0	72.4	71.8	72.3

Sample no.	94522062
Analysis no.	71765
Mineral	Orthopyroxene
Description	Corona
Lithology	Olivine gabbronorite
Strat. ht. (m)	2080
SiO_2	53.93
TiO_2	0.19
Al_2O_3	1.02
Cr_2O_3	0.00
FeO*	16.80
MnO	0.16
MgO	28.04
CaO	0.47
Na_2O	0.00
K_2O	0.00
Total	100.61
Oxygens	6
Si	1.930
Ti	0.005
Al	0.043
Cr	0.000
Fe^{3+}	0.086
Fe^{2+}	0.417
Mn	0.005
Mg	1.496
Ca	0.018
Na	0.000
K	0.000
Total Cations	4.000
mg	78.2
Enstatite	77.5
Ferrosilite	21.6
Wollastonite	0.9

Appendix Table 3.9 (cont.). Electron microprobe analyses of silicate minerals from the Spring Creek layered intrusion.

Sample no.	94522062	94522062
Analysis no.	71766	71767
Mineral	Orthopyroxene	Orthopyroxene
Description	Corona	Corona
Lithology	Olivine gabbronorite	Olivine gabbronorite
Strat. ht. (m)	2080	2080
SiO_2	54.23	53.96
TiO_2	0.12	0.16
Al_2O_3	1.03	1.22
Cr_2O_3	0.00	0.00
FeO*	16.46	16.62
MnO	0.23	0.23
MgO	27.33	26.65
CaO	0.82	1.12
Na_2O	0.00	0.00
K_2O	0.00	0.00
Total	100.22	99.96
Oxygens	6	6
Si	1.952	1.953
Ti	0.003	0.004
Al	0.044	0.052
Cr	0.000	0.000
Fe^{3+}	0.045	0.034
Fe^{2+}	0.450	0.469
Mn	0.007	0.007
Mg	1.467	1.438
Ca	0.031	0.043
Na	0.000	0.000
K	0.000	0.000
Total Cations	4.000	4.000
mg	76.5	75.4
Enstatite	75.3	73.7
Ferrosilite	23.1	24.1
Wollastonite	1.6	2.2

Sample no.	94522062	94522062	94522062	94522062	94522062	94522062	94522062
Analysis no.	71739	71740	71741	71742	71753	71754	71755
Mineral	Plagioclase	Plagioclase	Plagioclase	Plagioclase	Plagioclase	Plagioclase	Plagioclase
Description	Cumulus (r)	Cumulus (r)	Cumulus (c)	Cumulus (c)	Cumulus (r)	Cumulus (r)	Cumulus (c)
Lithology	Olivine gabbronorite	Olivine gabbronorite	Olivine gabbronorite	Olivine gabbronorite	Olivine gabbronorite	Olivine gabbronorite	Olivine gabbronorite
Strat. ht. (m)	2080	2080	2080	2080	2080	2080	2080
SiO_2	48.02	48.09	47.38	48.74	48.07	48.14	49.05
TiO_2	0.00	0.00	0.34	0.00	0.00	0.00	0.00
Al_2O_3	34.19	33.72	33.28	33.79	34.01	34.20	33.53
Cr_2O_3	0.00	0.00	0.00	0.00	0.00	0.00	0.00
FeO*	0.00	0.14	0.99	0.00	0.22	0.25	0.00
MnO	0.00	0.00	0.00	0.00	0.00	0.00	0.00
MgO	0.00	0.00	0.00	0.00	0.00	0.00	0.00
CaO	15.96	15.66	15.23	15.18	15.63	15.72	15.09
Na_2O	1.99	2.07	2.25	2.40	2.01	2.10	2.61
K_2O	0.00	0.00	0.00	0.00	0.00	0.00	0.00
Total	100.16	99.68	99.47	100.10	99.94	100.42	100.29
Oxygens	8	8	8	8	8	8	8
Si	2.189	2.202	2.186	2.218	2.196	2.190	2.229
Ti	0.000	0.000	0.012	0.000	0.000	0.000	0.000
Al	1.837	1.820	1.809	1.812	1.830	1.834	1.795
Cr	0.000	0.000	0.000	0.000	0.000	0.000	0.000
Fe^{3+}	0.000	0.000	0.000	0.000	0.008	0.010	0.000
Fe^{2+}	0.000	0.005	0.038	0.000	0.000	0.000	0.000
Mn	0.000	0.000	0.000	0.000	0.000	0.000	0.000
Mg	0.000	0.000	0.000	0.000	0.000	0.000	0.000
Ca	0.779	0.768	0.752	0.740	0.765	0.766	0.734
Na	0.176	0.184	0.201	0.212	0.178	0.185	0.230
K	0.000	0.000	0.000	0.000	0.000	0.000	0.000
Total Cations	4.981	4.980	4.998	4.982	4.978	4.985	4.989
Albite	18.4	19.3	21.1	22.3	18.9	19.5	23.9
Anorthite	81.6	80.7	78.9	77.7	81.1	80.5	76.1
Orthoclase	0.0	0.0	0.0	0.0	0.0	0.0	0.0

Appendix Table 3.9 (cont.). Electron microprobe analyses of silicate minerals from the Spring Creek layered intrusion.

Sample no.	94522062	94522062	94522062	94522062	94522062	94522062	94522062	94522062	94522062
Analysis no.	71756	71761	71762	71763	71764	72917	72918	72919	72920
Mineral	Plagioclase	Plagioclase	Plagioclase	Plagioclase	Plagioclase	Plagioclase	Plagioclase	Plagioclase	Plagioclase
Description	Cumulus (c)	Cumulus (r)	Cumulus (r)	Cumulus (c)	Cumulus (c)	Cumulus (r)	Cumulus (r)	Cumulus (c)	Cumulus (c)
Lithology	Olivine gabbronorite	Olivine gabbronorite	Olivine gabbronorite	Olivine gabbronorite	Olivine gabbronorite	Olivine gabbronorite	Olivine gabbronorite	Olivine gabbronorite	Olivine gabbronorite
Strat. ht. (m)	2080	2080	2080	2080	2080	2080	2080	2080	2080
SiO_2	48.77	45.63	47.96	47.66	47.71	48.17	47.74	47.94	48.12
TiO_2	0.00	0.00	0.00	0.00	0.00	0.00	0.00	0.00	0.00
Al_2O_3	32.93	35.65	34.08	33.65	33.61	33.77	34.12	33.96	33.71
Cr_2O_3	0.00	0.00	0.00	0.00	0.00	0.00	0.00	0.00	0.00
FeO*	0.73	0.00	0.18	0.17	0.34	0.11	0.00	0.09	0.00
MnO	0.00	0.00	0.00	0.00	0.00	0.00	0.00	0.00	0.00
MgO	0.00	0.00	0.00	0.00	0.48	0.48	0.48	0.48	0.48
CaO	15.08	17.53	15.75	15.35	15.16	15.46	15.33	15.53	15.52
Na_2O	2.34	1.03	2.20	2.29	2.05	2.08	2.30	2.22	2.15
K_2O	0.00	0.00	0.00	0.00	0.00	0.00	0.00	0.11	0.06
Total	99.84	99.84	100.16	99.11	99.34	100.07	99.95	100.32	100.04
Oxygens	8	8	8	8	8	8	8	8	8
Si	2.232	2.097	2.188	2.196	2.193	2.206	2.189	2.193	2.205
Ti	0.000	0.000	0.000	0.000	0.000	0.000	0.000	0.000	0.000
Al	1.776	1.931	1.833	1.828	1.821	1.822	1.844	1.831	1.820
Cr	0.000	0.000	0.000	0.000	0.000	0.000	0.000	0.000	0.000
Fe^{3+}	0.028	0.000	0.007	0.000	0.000	0.000	0.000	0.000	0.000
Fe^{2+}	0.000	0.000	0.000	0.007	0.013	0.004	0.000	0.003	0.000
Mn	0.000	0.000	0.000	0.000	0.000	0.000	0.000	0.000	0.000
Mg	0.000	0.000	0.000	0.000	0.033	0.000	0.000	0.000	0.000
Ca	0.739	0.863	0.770	0.758	0.746	0.759	0.753	0.761	0.762
Na	0.208	0.091	0.194	0.204	0.183	0.185	0.204	0.197	0.191
K	0.000	0.000	0.000	0.000	0.000	0.000	0.000	0.006	0.003
Total Cations	4.984	4.983	4.992	4.992	4.988	4.976	4.991	4.993	4.982
Albite	22.0	9.5	20.1	21.2	19.7	19.6	21.3	20.4	20.0
Anorthite	78.0	90.5	79.9	78.8	80.3	80.4	78.7	79.0	79.7
Orthoclase	0.0	0.0	0.0	0.0	0.0	0.0	0.0	0.6	0.3

Appendix Table 3.10. Electron microprobe analyses of silicate minerals from the Springvale layered intrusion.

Sample no.	92522454	92522454	92522454	92522454	92522454	92522454	92522454	92522454	92522454	92522454	92522454
Analysis no.	57316	57319	57320	57322	57323	57324	57326	57327	57340	57341	57343
Mineral	Amphibole	Amphibole	Amphibole	Amphibole	Amphibole	Amphibole	Amphibole	Amphibole	Amphibole	Amphibole	Amphibole
Description	Alter. of cpx	Alter. of cpx	Alter. of cpx	Alter. of cpx	Alter. of cpx	Alter. of cpx	Alter. of cpx	Alter. of cpx	Alter. of cpx	Alter. of cpx	Alter. of cpx
Lithology	Norite	Norite	Norite	Norite	Norite	Norite	Norite	Norite	Norite	Norite	Norite
Strat. ht. (m)	50	50	50	50	50	50	50	50	50	50	50
SiO_2	53.88	53.92	54.74	52.93	52.32	53.39	54.15	54.66	53.54	54.00	53.66
TiO_2	0.00	0.00	0.34	0.00	0.00	0.00	0.51	0.00	0.00	0.00	0.60
Al_2O_3	0.26	1.57	0.52	0.49	0.67	0.85	0.94	0.59	0.44	0.34	0.46
Cr_2O_3	0.00	0.00	0.00	0.00	0.00	0.00	0.00	0.00	0.00	0.00	0.00
FeO*	21.89	17.14	20.22	22.12	21.79	22.24	19.01	21.44	23.18	23.27	23.10
MnO	0.32	0.17	0.29	0.35	0.30	0.34	0.33	0.41	0.33	0.46	0.27
NiO	0.00	0.00	0.00	0.00	0.00	0.00	0.00	0.00	0.00	0.00	0.00
MgO	18.84	18.50	20.21	19.21	18.72	18.81	20.49	19.66	18.58	18.58	18.85
CaO	0.33	4.96	0.21	0.36	0.48	0.46	0.59	0.29	0.38	0.98	0.70
Na_2O	0.00	0.00	0.00	0.00	0.00	0.00	0.00	0.00	0.00	0.00	0.00
K_2O	0.00	0.00	0.00	0.00	0.15	0.00	0.26	0.00	0.00	0.00	0.00
Total	95.52	96.26	96.53	95.46	94.43	96.09	96.28	97.05	96.45	97.63	97.64
Oxygens	23	23	23	23	23	23	23	23	23	23	23
Si	7.983	7.842	7.948	7.836	7.833	7.866	7.861	7.941	7.887	7.864	7.811
Ti	0.000	0.000	0.037	0.000	0.000	0.000	0.056	0.000	0.000	0.000	0.066
Al	0.045	0.269	0.089	0.085	0.118	0.148	0.161	0.101	0.076	0.058	0.079
Cr	0.000	0.000	0.000	0.000	0.000	0.000	0.000	0.000	0.000	0.000	0.000
Fe^{3+}	0.000	0.047	0.000	0.243	0.245	0.120	0.053	0.017	0.149	0.213	0.168
Fe^{2+}	2.712	2.038	2.455	2.496	2.483	2.620	2.255	2.588	2.706	2.622	2.644
Ni	0.000	0.000	0.000	0.000	0.000	0.000	0.000	0.000	0.000	0.000	0.000
Mn	0.040	0.021	0.036	0.044	0.038	0.042	0.041	0.050	0.041	0.057	0.033
Mg	4.161	4.010	4.374	4.239	4.177	4.131	4.434	4.257	4.080	4.033	4.090
Ca	0.052	0.773	0.033	0.057	0.077	0.073	0.092	0.045	0.060	0.153	0.109
Na	0.000	0.000	0.000	0.000	0.000	0.000	0.000	0.000	0.000	0.000	0.000
K	0.000	0.000	0.000	0.000	0.029	0.000	0.048	0.000	0.000	0.000	0.000
Total Cations	14.994	15.000	14.971	15.000	15.000	15.000	15.000	15.000	15.000	15.000	15.000
mg	60.5	66.3	64.0	62.9	62.7	61.2	66.2	62.2	60.1	60.6	60.7
Classification	Cummingtonite	Cummingtonite	Cummingtonite	Cummingtonite	Cummingtonite	Cummingtonite	Cummingtonite	Cummingtonite	Cummingtonite	Cummingtonite	Cummingtonite

Appendix Table 3.10 (cont.). Electron microprobe analyses of silicate minerals from the Springvale layered intrusion.

Sample no.	92522454	92522461	92522461	92522461	92522461
Analysis no.	57344	57497	57504	57516	57517
Mineral	Amphibole	Amphibole	Amphibole	Amphibole	Amphibole
Description	Alter. of cpx	Alter. of cpx	Alter. of cpx	Alter. of cpx	Alter. of cpx
Lithology	Norite	Biot. olivine gabbronorite	Biot. olivine gabbronorite	Biot. olivine gabbronorite	Biot. olivine gabbronorite
Strat. ht. (m)	50	840	840	840	840
SiO_2	53.46	42.85	43.51	42.17	42.40
TiO_2	0.00	1.79	1.66	1.69	1.59
Al_2O_3	0.66	11.91	11.61	12.09	12.37
Cr_2O_3	0.00	0.00	0.00	0.00	0.00
FeO*	22.19	12.65	12.78	13.23	13.23
MnO	0.34	0.00	0.00	0.00	0.00
NiO	0.00	0.00	0.00	0.00	0.00
MgO	19.53	14.19	14.71	13.76	13.84
CaO	0.46	11.51	11.40	11.48	11.54
Na_2O	0.00	2.12	2.33	2.30	2.06
K_2O	0.00	0.82	0.90	0.91	0.87
Total	96.64	97.84	98.90	97.63	97.90
Oxygens	23	23	23	23	23
Si	7.809	6.192	6.212	6.142	6.134
Ti	0.000	0.195	0.178	0.185	0.173
Al	0.114	2.028	1.954	2.075	2.109
Cr	0.000	0.000	0.000	0.000	0.000
Fe^{3+}	0.268	0.889	0.969	0.870	0.963
Fe^{2+}	2.443	0.639	0.226	0.741	0.638
Ni	0.000	0.000	0.000	0.000	0.000
Mn	0.042	0.000	0.000	0.000	0.000
Mg	4.252	3.056	3.130	2.987	2.984
Ca	0.072	1.782	1.744	1.791	1.788
Na	0.000	0.594	0.645	0.649	0.578
K	0.000	0.151	0.164	0.169	0.161
Total Cations	15.000	15.526	15.222	15.609	15.528
mg	63.5	82.7	85.4	80.1	82.4
Classification	Cummingtonite	Ferrian Magnesio Hastingsite	Ferrian Magnesio Hastingsite	Ferrian Magnesio Hastingsite	Ferrian Magnesio Hastingsite

Sample no.	92522439	92522439	92522454	92522454	92522461	92522461
Analysis no.	57371	57372	57317	57318	57511	57512
Mineral	Biotite	Biotite	Biotite	Biotite	Biotite	Biotite
Description	Intercumulus	Intercumulus	Intercumulus	Intercumulus	Intercumulus	Intercumulus
Lithology	Gabbronorite	Gabbronorite	Norite	Norite	Biot. olivine gabbronorite	Biot. olivine gabbronorite
Strat. ht. (m)	650	650	50	50	840	840
SiO_2	37.60	37.59	37.24	36.62	37.16	36.55
TiO_2	3.73	3.29	1.96	2.18	2.20	4.32
Al_2O_3	15.52	15.26	16.60	16.15	16.16	15.60
Cr_2O_3	0.10	0.00	0.00	0.00	0.00	0.00
FeO*	13.63	12.99	19.63	18.81	12.51	14.26
MnO	0.00	0.00	0.00	0.00	0.00	0.00
NiO	0.00	0.00	0.00	0.00	0.00	0.00
MgO	15.90	16.57	13.29	12.80	18.72	15.94
CaO	0.00	0.00	0.00	0.00	0.00	0.00
Na_2O	0.00	0.00	0.00	0.00	0.00	0.16
K_2O	9.93	9.85	9.23	9.09	9.53	9.42
Total	96.41	95.55	97.95	95.65	96.28	96.25
Oxygens	22	22	22	22	22	22
Si	5.522	5.552	5.503	5.530	5.427	5.396
Ti	0.412	0.365	0.218	0.248	0.242	0.480
Al	2.686	2.656	2.891	2.875	2.782	2.714
Cr	0.012	0.000	0.000	0.000	0.000	0.000
Fe	1.674	1.605	2.426	2.376	1.528	1.761
Ni	0.000	0.000	0.000	0.000	0.000	0.000
Mn	0.000	0.000	0.000	0.000	0.000	0.000
Mg	3.481	3.648	2.927	2.881	4.075	3.507
Ca	0.000	0.000	0.000	0.000	0.000	0.000
Na	0.000	0.000	0.000	0.000	0.000	0.046
K	1.860	1.856	1.740	1.751	1.775	1.774
Total Cations	15.647	15.682	15.704	15.660	15.828	15.677
mg	67.5	69.5	54.7	54.8	72.7	66.6

Appendix Table 3.10 (cont.). Electron microprobe analyses of silicate minerals from the Springvale layered intrusion.

Sample no.	92522461	92522461	92522461
Analysis no.	57513	57520	57521
Mineral	Biotite	Biotite	Biotite
Description	Intercumulus	Intercumulus	Intercumulus
Lithology	Biot. olivine gabbronorite	Biot. olivine gabbronorite	Biot. olivine gabbronorite
Strat. ht. (m)	840	840	840
SiO_2	36.78	36.18	36.10
TiO_2	3.84	5.22	5.26
Al_2O_3	15.80	15.08	14.97
Cr_2O_3	0.00	0.00	0.00
FeO*	13.22	15.68	15.61
MnO	0.00	0.00	0.00
NiO	0.00	0.00	0.00
MgO	17.06	15.21	14.89
CaO	0.00	0.00	0.00
Na_2O	0.19	0.00	0.00
K_2O	9.34	9.47	9.53
Total	96.23	96.84	96.36
Oxygens	22	22	22
Si	5.398	5.353	5.370
Ti	0.424	0.581	0.588
Al	2.733	2.630	2.624
Cr	0.000	0.000	0.000
Fe	1.623	1.940	1.942
Ni	0.000	0.000	0.000
Mn	0.000	0.000	0.000
Mg	3.732	3.354	3.301
Ca	0.000	0.000	0.000
Na	0.054	0.000	0.000
K	1.749	1.787	1.808
Total Cations	15.713	15.645	15.634
mg	69.7	63.4	63.0
Classification			

Sample no.	92522439	92522461	92522461	92522461	92522475	92522475	92522475
Analysis no.	57374	57505	57506	57507	57351	57353	57354
Mineral	Clinopyroxene	Clinopyroxene	Clinopyroxene	Clinopyroxene	Clinopyroxene	Clinopyroxene	Clinopyroxene
Description	Intercumulus	Intercumulus	Intercumulus	Intercumulus	Intercumulus	Intercumulus	Intercumulus
Lithology	Gabbronorite	Biot. olivine gabbronorite	Biot. olivine gabbronorite	Biot. olivine gabbronorite	Gabbronorite	Gabbronorite	Gabbronorite
Strat. ht. (m)	650	840	840	840	2020	2020	2020
SiO_2	52.19	51.40	52.01	51.89	53.49	52.43	52.37
TiO_2	0.50	0.39	0.26	0.45	0.30	0.30	0.40
Al_2O_3	1.96	3.10	1.72	2.22	1.03	1.85	1.50
Cr_2O_3	0.21	0.69	0.00	0.11	0.09	0.00	0.00
FeO*	7.60	7.64	8.10	7.80	9.44	8.04	7.36
MnO	0.12	0.00	0.17	0.11	0.00	0.00	0.19
NiO	0.00	0.00	0.00	0.00	0.00	0.00	0.00
MgO	15.11	15.74	14.68	15.93	16.79	16.79	15.75
CaO	22.20	20.66	22.18	20.46	19.51	19.51	22.15
Na_2O	0.00	0.00	0.18	0.25	0.00	0.00	0.00
K_2O	0.00	0.00	0.00	0.00	0.00	0.00	0.00
Total	99.89	99.62	99.98	99.78	100.31	100.46	99.73
Oxygens	6	6	6	6	6	6	6
Si	1.937	1.906	1.939	1.925	1.949	1.930	1.940
Ti	0.014	0.011	0.007	0.013	0.008	0.008	0.011
Al	0.086	0.135	0.076	0.097	0.044	0.080	0.066
Cr	0.006	0.020	0.000	0.003	0.003	0.000	0.000
Fe^{3+}	0.007	0.011	0.031	0.038	0.039	0.043	0.031
Fe^{2+}	0.229	0.226	0.312	0.213	0.174	0.247	0.197
Ni	0.000	0.000	0.000	0.000	0.000	0.000	0.000
Mn	0.004	0.000	0.008	0.005	0.003	0.000	0.006
Mg	0.835	0.870	0.909	0.812	0.921	0.921	0.870
Ca	0.882	0.821	0.718	0.881	0.859	0.770	0.879
Na	0.000	0.000	0.000	0.013	0.000	0.000	0.000
K	0.000	0.000	0.000	0.000	0.000	0.000	0.000
Total Cations	4.000	4.000	4.000	4.000	4.000	4.000	4.000
mg	78.5	79.4	74.5	79.2	84.1	78.8	81.6
Enstatite	42.9	45.4	46.9	42.5	47.1	47.5	44.7
Ferrosilite	11.8	11.8	16.1	11.2	8.9	12.8	10.1
Wollastonite	45.3	42.8	37.0	46.3	44.0	39.7	45.2

Appendix Table 3.10 (cont.). Electron microprobe analyses of silicate minerals from the Springvale layered intrusion.

Sample no.	92522475	92522475	92522475	92522475
Analysis no.	57355	57356	57360	57361
Mineral	Clinopyroxene	Clinopyroxene	Clinopyroxene	Clinopyroxene
Description	Intercumulus	Intercumulus	Intercumulus	Intercumulus
Lithology	Gabbronorite	Gabbronorite	Gabbronorite	Gabbronorite
Strat. ht. (m)	2020	2020	2020	2020
SiO_2	51.90	51.93	51.80	51.89
TiO_2	0.36	0.35	0.44	0.53
Al_2O_3	1.92	1.93	1.96	1.60
Cr_2O_3	0.00	0.17	0.10	0.09
FeO*	9.99	7.61	7.88	11.94
MnO	0.00	0.12	0.12	0.25
NiO	0.00	0.00	0.00	0.00
MgO	16.61	15.24	15.50	17.94
CaO	18.80	22.18	21.61	15.07
Na_2O	0.00	0.00	0.00	0.00
K_2O	0.00	0.00	0.00	0.00
Total	99.59	99.54	99.41	99.31
Oxygens	6	6	6	6
Si	1.928	1.931	1.928	1.934
Ti	0.010	0.010	0.012	0.015
Al	0.084	0.085	0.086	0.070
Cr	0.000	0.005	0.003	0.003
Fe^{3+}	0.040	0.028	0.030	0.030
Fe^{2+}	0.270	0.209	0.215	0.343
Ni	0.000	0.000	0.000	0.000
Mn	0.000	0.004	0.004	0.008
Mg	0.920	0.845	0.860	0.997
Ca	0.748	0.884	0.862	0.602
Na	0.000	0.000	0.000	0.000
K	0.000	0.000	0.000	0.000
Total Cations	4.000	4.000	4.000	4.000
mg	77.3	80.2	80.0	74.4
Enstatite	47.5	43.6	44.4	51.4
Ferrosilite	13.9	10.8	11.1	17.6
Wollastonite	38.6	45.6	44.5	31.0

Sample no.	92522446	92522446	92522446	92522446	92522446	92522446
Analysis no.	57375	57376	57380	57381	57382	57383
Mineral	Olivine	Olivine	Olivine	Olivine	Olivine	Olivine
Description	Cumulus (r)	Cumulus (c)	Cumulus (c)	Cumulus (c)	Cumulus (c)	Cumulus (r)
Lithology	Olivine gabbronorite	Olivine gabbronorite	Olivine gabbronorite	Olivine gabbronorite	Olivine gabbronorite	Olivine gabbronorite
Strat. ht. (m)	940	940	940	940	940	940
SiO_2	35.24	34.99	35.50	35.26	35.69	35.24
TiO_2	0.00	0.00	0.00	0.00	0.00	0.00
Al_2O_3	0.00	0.00	0.00	0.00	0.00	0.00
Cr_2O_3	0.00	0.00	0.00	0.00	0.00	0.00
FeO*	34.60	35.64	34.91	35.17	35.11	34.22
MnO	0.28	0.38	0.38	0.25	0.28	0.21
NiO	0.00	0.00	0.00	0.00	0.00	0.00
MgO	29.69	29.69	30.25	30.12	29.78	29.57
CaO	0.00	0.00	0.00	0.00	0.00	0.00
Na_2O	0.00	0.00	0.00	0.00	0.00	0.00
K_2O	0.00	0.00	0.00	0.00	0.00	0.00
Total	99.80	100.70	101.04	100.79	100.86	99.23
Oxygens	4	4	4	4	4	4
Si	0.973	0.960	0.967	0.964	0.976	0.978
Ti	0.000	0.000	0.000	0.000	0.000	0.000
Al	0.000	0.000	0.000	0.000	0.000	0.000
Cr	0.000	0.000	0.000	0.000	0.000	0.000
Fe^{3+}	0.054	0.080	0.065	0.072	0.048	0.044
Fe^{2+}	0.745	0.737	0.730	0.731	0.755	0.750
Ni	0.000	0.000	0.000	0.000	0.000	0.000
Mn	0.007	0.009	0.009	0.006	0.007	0.005
Mg	1.222	1.214	1.228	1.227	1.214	1.223
Ca	0.000	0.000	0.000	0.000	0.000	0.000
Na	0.000	0.000	0.000	0.000	0.000	0.000
K	0.000	0.000	0.000	0.000	0.000	0.000
Total Cations	3.001	3.000	2.999	3.000	3.000	3.000
mg	62.1	62.2	62.7	62.7	61.7	62.0

Appendix Table 3.10 (cont.). Electron microprobe analyses of silicate minerals from the Springvale layered intrusion.

Sample no.	92522446	92522446	92522446	92522446	92522446	92522446	92522446	92522446	92522461	92522461	92522461	92522461
Analysis no.	57384	57385	65003	65004	65005	65006	65007	65008	57501	57502	57503	57518
Mineral	Olivine	Olivine	Olivine	Olivine	Olivine	Olivine	Olivine	Olivine	Olivine	Olivine	Olivine	Olivine
Description	Cumulus (c)	Cumulus (r)	Cumulus (r)	Cumulus (c)	Cumulus (c)	Cumulus (c)	Cumulus	Cumulus (c)	Cumulus (c)	Cumulus (c)	Cumulus (r)	Cumulus (c)
Lithology	Olivine gabbronorite	Olivine gabbronorite	Olivine gabbronorite	Olivine gabbronorite	Olivine gabbronorite	Olivine gabbronorite	Olivine gabbronorite	Olivine gabbronorite	Biot. olivine gabbronorite	Biot. olivine gabbronorite	Biot. olivine gabbronorite	Biot. olivine gabbronorite
Strat. ht. (m)	940	940	940	940	940	940	940	940	840	840	840	840
SiO_2	35.44	35.30	35.58	35.43	35.60	35.59	35.37	35.17	35.14	35.20	35.65	35.38
TiO_2	0.00	0.00	0.00	0.00	0.00	0.00	0.00	0.00	0.00	0.00	0.00	0.00
Al_2O_3	0.00	0.00	0.00	0.00	0.00	0.00	0.00	0.00	0.00	0.00	0.00	0.00
Cr_2O_3	0.00	0.00	0.00	0.00	0.00	0.00	0.00	0.00	0.00	0.00	0.00	0.00
FeO*	35.38	34.84	35.41	35.36	35.19	35.49	35.03	35.33	34.08	34.27	32.86	34.53
MnO	0.31	0.38	0.36	0.25	0.24	0.30	0.29	0.29	0.36	0.36	0.37	0.25
NiO	0.00	0.00	0.00	0.00	0.00	0.00	0.00	0.00	0.00	0.00	0.00	0.00
MgO	29.76	29.53	29.56	29.59	29.54	29.65	29.74	29.42	30.31	30.23	31.18	30.29
CaO	0.00	0.00	0.00	0.00	0.00	0.00	0.00	0.00	0.00	0.00	0.00	0.00
Na_2O	0.00	0.00	0.00	0.00	0.00	0.00	0.00	0.00	0.00	0.00	0.00	0.00
K_2O	0.00	0.00	0.00	0.00	0.00	0.00	0.00	0.00	0.00	0.00	0.00	0.00
Total	100.90	100.06	100.91	100.63	100.57	101.03	100.43	100.22	99.88	100.07	100.05	100.46
Oxygens	4	4	4	4	4	4	4	4	4	4	4	4
Si	0.970	0.974	0.974	0.972	0.977	0.973	0.971	0.970	0.966	0.967	0.973	0.968
Ti	0.000	0.000	0.000	0.000	0.000	0.000	0.000	0.000	0.000	0.000	0.000	0.000
Al	0.000	0.000	0.000	0.000	0.000	0.000	0.000	0.000	0.000	0.000	0.000	0.000
Cr	0.000	0.000	0.000	0.000	0.000	0.000	0.000	0.000	0.000	0.000	0.000	0.000
Fe^{3+}	0.061	0.053	0.051	0.055	0.045	0.054	0.057	0.061	0.068	0.066	0.054	0.064
Fe^{2+}	0.749	0.751	0.759	0.756	0.763	0.758	0.747	0.754	0.715	0.721	0.696	0.727
Ni	0.000	0.000	0.000	0.000	0.000	0.000	0.000	0.000	0.000	0.000	0.000	0.000
Mn	0.007	0.009	0.008	0.006	0.006	0.007	0.007	0.007	0.008	0.008	0.009	0.006
Mg	1.214	1.214	1.206	1.210	1.209	1.208	1.217	1.209	1.242	1.238	1.268	1.236
Ca	0.000	0.000	0.000	0.000	0.000	0.000	0.000	0.000	0.000	0.000	0.000	0.000
Na	0.000	0.000	0.000	0.000	0.000	0.000	0.000	0.000	0.000	0.000	0.000	0.000
K	0.000	0.000	0.000	0.000	0.000	0.000	0.000	0.000	0.000	0.000	0.000	0.000
Total Cations	3.001	3.001	2.998	2.999	3.000	3.000	2.999	3.001	2.999	3.000	3.000	3.001
mg	61.8	61.8	61.4	61.5	61.3	61.4	62.0	61.6	63.5	63.2	64.6	63.0

Appendix Table 3.10 (cont.). Electron microprobe analyses of silicate minerals from the Springvale layered intrusion.

Sample no.	92522461	Sample no.	92522439	92522439	92522439	92522439	92522439	92522439	92522446	92522446	92522446
Analysis no.	57519	Analysis no.	57364	57365	57367	57366	57367	57370	57386	57388	57389
Mineral	Olivine	Mineral	Orthopyroxene	Orthopyroxene	Orthopyroxene	Orthopyroxene	Orthopyroxene	Orthopyroxene	Orthopyroxene	Orthopyroxene	Orthopyroxene
Description	Cumulus (r)	Description	Cumulus (r)	Cumulus	Cumulus	Cumulus	Cumulus	Cumulus	Intercumulus	Intercumulus	Intercumulus
Lithology	Biot. olivine gabbronorite	Lithology	Gabbronorite	Gabbronorite	Gabbronorite	Gabbronorite	Gabbronorite	Gabbronorite	Olivine gabbronorite	Olivine gabbronorite	Olivine gabbronorite
Strat. ht. (m)	840	Strat. ht. (m)	650	650	650	650	650	650	940	940	940
SiO_2	35.53	SiO_2	53.41	53.25	53.12	52.94	53.12	53.29	52.34	52.27	52.29
TiO_2	0.00	TiO_2	0.10	0.00	0.24	0.00	0.24	0.09	0.36	0.00	0.33
Al_2O_3	0.00	Al_2O_3	1.06	0.72	0.60	0.87	0.60	1.00	0.76	0.82	0.78
Cr_2O_3	0.00	Cr_2O_3	0.00	0.00	0.00	0.00	0.00	0.00	0.00	0.00	0.00
FeO*	32.94	FeO*	18.39	17.15	18.38	18.17	18.38	16.62	21.02	21.14	20.38
MnO	0.46	MnO	0.21	0.27	0.20	0.21	0.20	0.28	0.33	0.26	0.32
NiO	0.00	NiO	0.00	0.00	0.00	0.00	0.00	0.00	0.00	0.00	0.00
MgO	31.41	MgO	26.27	25.58	26.09	25.96	26.09	25.29	23.98	24.24	23.61
CaO	0.00	CaO	0.72	2.73	0.74	0.99	0.74	2.81	1.50	1.16	2.71
Na_2O	0.00	Na_2O	0.00	0.00	0.00	0.00	0.00	0.00	0.00	0.00	0.00
K_2O	0.00	K_2O	0.00	0.00	0.00	0.00	0.00	0.00	0.00	0.00	0.00
Total	100.34	Total	100.43	100.02	99.37	99.43	99.63	99.58	100.64	100.29	100.80
Oxygens	4	Oxygens	6	6	6	6	6	6	6	6	6
Si	0.967	Si	1.938	1.941	1.945	1.941	1.945	1.949	1.926	1.927	1.921
Ti	0.000	Ti	0.003	0.000	0.007	0.000	0.007	0.002	0.010	0.000	0.009
Al	0.000	Al	0.045	0.031	0.026	0.038	0.026	0.043	0.033	0.036	0.034
Cr	0.000	Cr	0.000	0.000	0.000	0.000	0.000	0.000	0.000	0.000	0.000
Fe^{3+}	0.067	Fe^{3+}	0.073	0.087	0.070	0.080	0.070	0.054	0.096	0.111	0.105
Fe^{2+}	0.683	Fe^{2+}	0.486	0.436	0.493	0.477	0.493	0.454	0.551	0.541	0.521
Ni	0.000	Ni	0.000	0.000	0.000	0.000	0.000	0.000	0.000	0.000	0.000
Mn	0.011	Mn	0.006	0.008	0.006	0.007	0.006	0.009	0.010	0.008	0.010
Mg	1.273	Mg	1.421	1.390	1.424	1.419	1.424	1.379	1.315	1.332	1.293
Ca	0.000	Ca	0.028	0.107	0.029	0.039	0.029	0.110	0.059	0.046	0.107
Na	0.000	Na	0.000	0.000	0.000	0.000	0.000	0.000	0.000	0.000	0.000
K	0.000	K	0.000	0.000	0.000	0.000	0.000	0.000	0.000	0.000	0.000
Total Cations	3.001	Total Cations	4.000	4.000	4.000	4.000	4.000	4.000	4.000	4.000	4.000
mg	65.6	mg	74.5	76.1	74.3	74.9	74.3	75.2	70.5	71.1	71.3
		Enstatite	73.5	71.9	73.2	73.3	73.2	70.9	68.3	69.4	67.3
		Ferrosilite	25.1	22.6	25.3	24.7	25.3	23.4	28.6	28.2	27.1
		Wollastonite	1.5	5.5	1.5	2.0	1.5	5.7	3.1	2.4	5.6

Appendix Table 3.10 (cont.). Electron microprobe analyses of silicate minerals from the Springvale layered intrusion.

Sample no.	92522461	92522461	92522461	92522461	92522461	92522475	92522475	92522475	92522475	92522475	92522475
Analysis no.	57500	57502	57514	57522	57523	57346	57350	57352	57357	57362	57363
Mineral	Orthopyroxene	Orthopyroxene	Orthopyroxene	Orthopyroxene	Orthopyroxene	Orthopyroxene	Orthopyroxene	Orthopyroxene	Orthopyroxene	Orthopyroxene	Orthopyroxene
Description	Intercumulus	Intercumulus	Intercumulus	Intercumulus	Intercumulus	Intercumulus	Intercumulus	Intercumulus	Intercumulus	Intercumulus	Intercumulus
Lithology	Biot. olivine gabbronorite	Biot. olivine gabbronorite	Biot. olivine gabbronorite	Biot. olivine gabbronorite	Biot. olivine gabbronorite	Gabbronorite	Gabbronorite	Gabbronorite	Gabbronorite	Gabbronorite	Gabbronorite
Strat. ht. (m)	840	840	840	840	840	2020	2020	2020	2020	2020	2020
SiO_2	53.14	52.69	52.52	52.69	52.33	53.73	53.47	53.90	53.35	53.46	53.54
TiO_2	0.00	0.29	0.15	0.09	0.11	0.12	0.13	0.00	0.27	0.00	0.13
Al_2O_3	0.62	1.69	1.58	0.77	0.71	0.68	0.64	0.63	0.73	0.44	0.68
Cr_2O_3	0.00	0.00	0.00	0.00	0.00	0.00	0.00	0.00	0.00	0.00	0.00
FeO*	21.65	20.30	20.70	23.35	23.22	18.62	18.63	18.55	19.55	19.23	19.04
MnO	0.32	0.18	0.27	0.21	0.39	0.22	0.28	0.28	0.36	0.28	0.22
NiO	0.00	0.00	0.00	0.00	0.00	0.00	0.00	0.00	0.00	0.00	0.00
MgO	23.94	23.95	23.38	22.53	22.49	25.78	25.63	25.98	25.00	26.18	26.12
CaO	0.65	2.16	2.06	1.15	1.29	1.26	1.48	1.05	1.44	0.54	0.91
Na_2O	0.00	0.00	0.00	0.00	0.00	0.00	0.00	0.00	0.00	0.00	0.00
K_2O	0.00	0.00	0.00	0.00	0.00	0.00	0.00	0.00	0.00	0.00	0.00
Total	100.54	101.56	100.92	101.02	100.84	100.64	100.53	100.62	100.95	100.46	100.96
Oxygens	6	6	6	6	6	6	6	6	6	6	6
Si	1.957	1.915	1.926	1.948	1.940	1.951	1.946	1.956	1.942	1.946	1.939
Ti	0.000	0.008	0.004	0.003	0.003	0.003	0.004	0.000	0.007	0.000	0.004
Al	0.027	0.072	0.068	0.034	0.031	0.029	0.027	0.027	0.031	0.019	0.029
Cr	0.000	0.000	0.000	0.000	0.000	0.000	0.000	0.000	0.000	0.000	0.000
Fe^{3+}	0.060	0.081	0.072	0.065	0.083	0.062	0.074	0.062	0.069	0.090	0.086
Fe^{2+}	0.607	0.536	0.563	0.657	0.637	0.503	0.493	0.501	0.526	0.496	0.490
Ni	0.000	0.000	0.000	0.000	0.000	0.000	0.000	0.000	0.000	0.000	0.000
Mn	0.010	0.006	0.008	0.007	0.012	0.007	0.009	0.009	0.011	0.009	0.007
Mg	1.314	1.298	1.278	1.242	1.243	1.395	1.390	1.405	1.357	1.420	1.410
Ca	0.026	0.084	0.081	0.046	0.051	0.049	0.058	0.041	0.056	0.021	0.035
Na	0.000	0.000	0.000	0.000	0.000	0.000	0.000	0.000	0.000	0.000	0.000
K	0.000	0.000	0.000	0.000	0.000	0.000	0.000	0.000	0.000	0.000	0.000
Total Cations	4.000	4.000	4.000	4.000	4.000	4.000	4.000	4.000	4.000	4.000	4.000
mg	68.4	70.8	69.4	65.4	66.1	73.5	73.8	73.7	72.1	74.1	74.2
Enstatite	67.5	67.7	66.5	63.8	64.3	71.5	71.6	72.2	70.0	73.3	72.9
Ferrosilite	31.2	27.9	29.3	33.8	33.0	25.8	25.4	25.7	27.1	25.6	25.3
Wollastonite	1.3	4.4	4.2	2.4	2.7	2.5	3.0	2.1	2.9	1.1	1.8

Appendix Table 3.10 (cont.). Electron microprobe analyses of silicate minerals from the Springvale layered intrusion.

Sample no.	92522439	92522439	92522446	92522446	92522446	92522446	92522446	92522446	92522454	92522454	92522454
Analysis no.	57369	57373	57375	57391	65009	65010	65011	65012	57320	57328	57329
Mineral	Plagioclase	Plagioclase	Plagioclase	Plagioclase	Plagioclase	Plagioclase	Plagioclase	Plagioclase	Plagioclase	Plagioclase	Plagioclase
Description	Cumulus	Cumulus	Cumulus	Cumulus	Cumulus (r)	Cumulus (c)	Cumulus (r)	Cumulus (r)	Cumulus	Cumulus (c)	Cumulus (c)
Lithology	Gabbronorite	Gabbronorite	Olivine gabbronorite	Olivine gabbronorite	Olivine gabbronorite	Olivine gabbronorite	Olivine gabbronorite	Olivine gabbronorite	Norite	Norite	Norite
Strat. ht. (m)	650	650	940	940	940	940	940	940	50	50	50
SiO_2	48.23	49.28	46.96	50.82	48.77	48.38	49.66	49.58	51.59	49.00	49.79
TiO_2	0.00	0.00	0.00	0.00	0.00	0.00	0.00	0.00	0.00	0.00	0.00
Al_2O_3	33.39	33.03	34.45	33.14	34.11	34.07	33.24	33.62	30.83	33.25	32.47
Cr_2O_3	0.00	0.00	0.00	0.00	0.00	0.00	0.00	0.00	0.00	0.00	0.00
FeO*	0.52	0.11	0.39	0.00	0.37	0.21	0.15	0.22	0.35	0.25	0.20
MnO	0.00	0.00	0.00	0.00	0.00	0.00	0.00	0.00	0.00	0.00	0.00
NiO	0.00	0.00	0.00	0.00	0.00	0.00	0.00	0.00	0.00	0.00	0.00
MgO	0.00	0.00	0.00	0.00	0.00	0.00	0.00	0.00	0.30	0.00	0.00
CaO	14.82	14.39	16.08	14.35	15.51	15.27	14.72	14.82	12.02	14.69	13.98
Na_2O	2.70	2.95	2.02	3.25	2.49	2.36	2.97	2.89	4.38	2.88	3.26
K_2O	0.00	0.00	0.00	0.11	0.07	0.00	0.12	0.08	0.08	0.00	0.00
Total	99.66	99.76	99.90	101.67	101.32	100.29	100.86	101.21	99.55	100.07	99.70
Oxygens	8	8	8	8	8	8	8	8	8	8	8
Si	2.212	2.249	2.155	2.274	2.201	2.201	2.245	2.234	2.350	2.233	2.272
Ti	0.000	0.000	0.000	0.000	0.000	0.000	0.000	0.000	0.000	0.000	0.000
Al	1.805	1.776	1.863	1.747	1.815	1.827	1.771	1.786	1.655	1.786	1.747
Cr	0.000	0.000	0.000	0.000	0.014	0.008	0.006	0.008	0.013	0.010	0.008
Fe^{3+}	0.000	0.000	0.000	0.000	0.000	0.000	0.000	0.000	0.000	0.000	0.000
Fe^{2+}	0.020	0.004	0.015	0.000	0.000	0.000	0.000	0.000	0.000	0.000	0.000
Ni	0.000	0.000	0.000	0.000	0.000	0.000	0.000	0.000	0.000	0.000	0.000
Mn	0.000	0.000	0.000	0.000	0.000	0.000	0.000	0.000	0.000	0.000	0.000
Mg	0.000	0.000	0.000	0.000	0.000	0.000	0.000	0.000	0.000	0.000	0.000
Ca	0.728	0.704	0.791	0.688	0.750	0.744	0.713	0.716	0.587	0.717	0.684
Na	0.240	0.261	0.180	0.282	0.218	0.208	0.260	0.253	0.387	0.255	0.288
K	0.000	0.000	0.000	0.006	0.004	0.000	0.007	0.005	0.005	0.000	0.000
Total Cations	5.005	4.994	5.003	4.997	5.002	4.989	5.003	5.001	5.018	5.001	4.999
Albite	24.8	27.1	18.5	28.9	22.4	21.9	26.6	26.0	39.5	26.2	29.7
Anorthite	75.2	72.9	81.5	70.4	77.2	78.1	72.7	73.5	60.0	73.8	70.3
Orthoclase	0.0	0.0	0.0	0.7	0.4	0.0	0.7	0.5	0.5	0.0	0.0

Appendix Table 3.10 (cont.). Electron microprobe analyses of silicate minerals from the Springvale layered intrusion.

Sample no.	92522454	92522454	92522461	92522461	92522461	92522461	92522475	92522475	92522475	92522475
Analysis no.	57330	57345	57496	57509	57515	57524	57347	57349	57358	57359
Mineral	Plagioclase	Plagioclase	Plagioclase	Plagioclase	Plagioclase	Plagioclase	Plagioclase	Plagioclase	Plagioclase	Plagioclase
Description	Cumulus (r)	Cumulus (c)	Cumulus	Cumulus	Cumulus	Cumulus	Cumulus	Cumulus (c)	Cumulus (c)	Cumulus (r)
Lithology	Norite	Norite	Biot. olivine gabbronorite	Biot. olivine gabbronorite	Biot. olivine gabbronorite	Biot. olivine gabbronorite	Gabbronorite	Gabbronorite	Gabbronorite	Gabbronorite
Strat. ht. (m)	50	50	840	840	840	840	2020	2020	2020	2020
SiO_2	52.79	53.12	52.53	51.17	51.36	53.86	47.47	47.49	47.43	46.84
TiO_2	0.00	0.00	0.00	0.00	0.00	0.00	0.00	0.08	0.00	0.00
Al_2O_3	30.83	30.50	31.25	32.10	31.71	30.01	34.43	34.20	34.49	33.62
Cr_2O_3	0.00	0.00	0.00	0.00	0.00	0.00	0.00	0.00	0.00	0.00
FeO*	0.38	0.31	0.00	0.21	0.18	0.21	0.27	0.00	0.29	0.33
MnO	0.00	0.00	0.00	0.00	0.00	0.00	0.00	0.00	0.00	0.00
NiO	0.00	0.00	0.00	0.00	0.00	0.00	0.00	0.00	0.00	0.00
MgO	0.00	0.00	0.00	0.00	0.00	0.00	0.00	0.00	0.00	0.00
CaO	11.86	11.27	12.21	13.17	13.04	10.92	15.82	15.91	16.26	15.80
Na_2O	4.80	5.15	4.66	3.91	4.00	5.31	2.24	2.28	2.06	1.87
K_2O	0.11	0.06	0.10	0.08	0.10	0.10	0.00	0.10	0.05	0.05
Total	100.77	100.41	100.75	100.64	100.39	100.40	100.23	100.06	100.58	98.51
Oxygens	8	8	8	8	8	8	8	8	8	8
Si	2.375	2.394	2.361	2.310	2.323	2.423	2.168	2.172	2.162	2.177
Ti	0.000	0.000	0.000	0.000	0.000	0.000	0.000	0.003	0.000	0.000
Al	1.635	1.620	1.656	1.708	1.691	1.591	1.853	1.844	1.853	1.841
Cr	0.014	0.012	0.000	0.000	0.000	0.000	0.000	0.000	0.000	0.000
Fe^{3+}	0.000	0.000	0.000	0.000	0.000	0.000	0.000	0.000	0.000	0.000
Fe^{2+}	0.000	0.000	0.000	0.008	0.007	0.008	0.010	0.000	0.011	0.013
Ni	0.000	0.000	0.000	0.000	0.000	0.000	0.000	0.000	0.000	0.000
Mn	0.000	0.000	0.000	0.000	0.000	0.000	0.000	0.000	0.000	0.000
Mg	0.000	0.000	0.000	0.000	0.000	0.000	0.000	0.000	0.000	0.000
Ca	0.572	0.544	0.588	0.637	0.632	0.526	0.774	0.780	0.794	0.787
Na	0.419	0.450	0.407	0.342	0.351	0.463	0.198	0.202	0.182	0.168
K	0.006	0.003	0.006	0.005	0.006	0.006	0.000	0.006	0.003	0.003
Total Cations	5.020	5.023	5.017	5.010	5.009	5.016	5.004	5.007	5.004	4.989
Albite	42.0	45.1	40.7	34.8	35.5	46.6	20.4	20.5	18.6	17.6
Anorthite	57.4	54.6	58.7	64.7	63.9	52.8	79.6	78.9	81.1	82.1
Orthoclase	0.6	0.3	0.6	0.5	0.6	0.6	0.0	0.6	0.3	0.3

Appendix Table 3.10a. Electron microprobe analyses of oxide minerals from the Springvale layered intrusion.

Sample no.	92522446	92522446	92522446	92522454	92522454	92522454	92522454	92522454	92522461	92522461
Analysis no.	57397	57398	57399	57334	57335	57336	57337	57338	57493	57495
Mineral	Ilmenite	Ilmenite	Ilmenite	Ilmenite	Ilmenite	Ilmenite	Ilmenite	Ilmenite	Ilmenite	Ilmenite
Description										
Lithology	Olivine gabbronorite	Olivine gabbronorite	Olivine gabbronorite	Norite	Norite	Norite	Norite	Norite	Biot. olivine gabbronorite	Biot. olivine gabbronorite
Strat. ht. (m)	940	940	940	50	50	50	50	50	840	840
SiO_2	0.00	0.00	0.00	0.00	0.00	0.00	0.00	0.00	0.12	0.00
TiO_2	52.53	53.03	51.84	51.76	51.76	52.18	51.79	51.44	51.59	51.38
Al_2O_3	0.00	0.00	0.00	0.00	0.00	0.00	0.00	0.12	0.00	0.00
V_2O_3	0.00	0.00	0.00	0.00	0.00	0.00	0.00	0.00	0.00	0.00
Cr_2O_3	0.00	0.10	0.00	0.00	0.10	0.00	0.00	0.00	0.00	0.00
FeO*	44.46	44.51	45.37	48.45	47.58	47.74	47.79	47.25	45.46	45.16
MnO	0.57	0.63	0.91	0.86	0.80	0.84	0.83	0.69	1.49	1.39
MgO	2.54	2.49	0.18	0.13	0.16	0.26	0.15	0.11	1.37	1.14
Total	100.10	100.76	98.30	101.20	100.40	101.02	100.56	99.61	100.03	99.07
Oxygens	3	3	3	3	3	3	3	3	3	3
Si	0.000	0.000	0.000	0.000	0.000	0.000	0.000	0.000	0.003	0.000
Ti	0.976	0.980	0.974	0.973	0.977	0.978	0.976	0.979	0.967	0.975
Al	0.000	0.000	0.000	0.000	0.000	0.000	0.000	0.002	0.000	0.000
V	0.000	0.000	0.000	0.000	0.000	0.000	0.000	0.000	0.000	0.000
Cr	0.000	0.002	0.000	0.000	0.002	0.000	0.000	0.000	0.000	0.000
Fe^{3+}	0.048	0.039	0.052	0.055	0.045	0.044	0.049	0.040	0.060	0.051
Fe^{2+}	0.870	0.875	0.948	0.950	0.954	0.950	0.952	0.960	0.888	0.902
Mn	0.012	0.013	0.019	0.018	0.017	0.018	0.018	0.015	0.031	0.030
Mg	0.094	0.091	0.007	0.005	0.006	0.010	0.006	0.004	0.051	0.043
Total Cations	2.000	2.000	2.000	2.000	2.000	2.000	2.000	2.000	2.000	2.000

Appendix Table 3.10a (cont.). Electron microprobe analyses of oxide minerals from the Springvale layered intrusion.

Sample no.	92522446	92522461	92522461	92522461	92522461	92522461	92522461
Analysis no.	57396	57488	57489	57490	57491	57492	57494
Mineral	Spinel	Magnetite	Magnetite	Magnetite	Magnetite	Magnetite	Magnetite
Description							
Lithology	Olivine gabbronorite	Biot. olivine gabbronorite	Biot. olivine gabbronorite	Biot. olivine gabbronorite	Biot. olivine gabbronorite	Biot. olivine gabbronorite	Biot. olivine gabbronorite
Strat. ht. (m)	940	840	840	840	840	840	840
SiO_2	0.00	0.12	0.16	0.10	0.15	0.00	0.35
TiO_2	36.24	0.16	0.66	0.00	0.21	0.00	0.00
Al_2O_3	0.46	0.25	0.44	0.14	0.43	0.41	0.14
V_2O_3	0.46	0.38	0.46	0.12	0.77	0.26	0.00
Cr_2O_3	0.90	0.00	0.00	0.00	0.00	0.00	0.00
FeO*	59.45	92.13	92.90	93.96	93.08	93.31	93.18
MnO	0.46	0.22	0.17	0.10	0.17	0.00	0.00
MgO	1.69	0.00	0.00	0.00	0.00	0.00	0.12
Total	99.66	93.26	94.79	94.42	94.81	93.98	93.79
Oxygens	32	32	32	32	32	32	32
Si	0.000	0.037	0.048	0.030	0.045	0.000	0.107
Ti	7.960	0.037	0.150	0.000	0.048	0.000	0.000
Al	0.158	0.091	0.157	0.050	0.153	0.147	0.050
V	0.108	0.094	0.112	0.029	0.187	0.064	0.000
Cr	0.208	0.000	0.000	0.000	0.000	0.000	0.000
Fe^{3+}	0.000	15.669	15.336	15.861	15.475	15.790	15.737
Fe^{2+}	14.521	8.016	8.155	8.005	8.049	8.000	8.052
Mn	0.114	0.057	0.044	0.026	0.044	0.000	0.000
Mg	0.736	0.000	0.000	0.000	0.000	0.000	0.055
Total Cations	23.804	24.001	24.001	24.001	24.001	24.001	24.001

Appendix Table 3.11. Electron microprobe analyses of silicate minerals from the Toby layered intrusion.

Sample no.	92522513	92522513	92522513	92522518	92522518	92522518	92522523	92522523	92522523
Analysis no.	65047	65048	65049	65102	65103	65104	65116	65118	65119
Mineral	Amphibole	Amphibole	Amphibole	Amphibole	Amphibole	Amphibole	Amphibole	Amphibole	Amphibole
Description	Alter. of cpx	Alter. of cpx	Alter. of cpx	Alter. of cpx	Alter. of cpx	Alter. of cpx	Alter. of cpx	Alter. of cpx	Alter. of cpx
Lithology	Suboph. biot qtz gabbronor.	Suboph. biot qtz gabbronor.	Suboph. biot qtz gabbronor.	Suboph. biot qtz gabbronor.	Suboph. biot qtz gabbronor.	Suboph. biot qtz gabbronor.	Suboph. biot gabbronorite	Suboph. biot gabbronorite	Suboph. biot gabbronorite
Trav. dist. (m)	1750	1750	1750	3500	3500	3500	9300	9300	9300
SiO_2	48.12	45.73	46.53	47.22	47.77	48.17	48.29	47.19	47.49
TiO_2	0.62	1.40	1.30	1.02	0.75	0.94	0.95	1.06	0.97
Al_2O_3	5.85	7.92	7.20	6.51	6.38	5.90	6.49	7.01	6.96
Cr_2O_3	0.00	0.00	0.00	0.00	0.00	0.00	0.00	0.00	0.26
FeO*	16.57	17.71	17.17	16.36	16.82	16.18	14.47	15.14	15.74
MnO	0.00	0.15	0.15	0.00	0.15	0.10	0.11	0.09	0.13
NiO	0.00	0.00	0.00	0.00	0.00	0.00	0.00	0.00	0.00
MgO	13.40	11.89	12.41	12.97	13.01	13.69	14.56	13.69	13.68
CaO	11.06	11.30	11.17	11.23	11.22	11.19	11.36	11.27	11.18
Na_2O	0.29	0.88	0.62	0.39	0.37	0.45	0.66	0.69	0.54
K_2O	0.39	0.79	0.67	0.48	0.52	0.39	0.54	0.57	0.52
Total	96.30	97.77	97.22	96.18	96.99	97.01	97.43	96.71	97.47
Oxygens	23	23	23	23	23	23	23	23	23
Si	7.005	6.697	6.799	6.923	6.944	6.970	6.933	6.863	6.853
Ti	0.068	0.154	0.143	0.112	0.082	0.102	0.103	0.116	0.105
Al	1.004	1.367	1.240	1.125	1.093	1.006	1.093	1.201	1.184
Cr	0.000	0.000	0.000	0.000	0.000	0.000	0.000	0.000	0.030
Fe^{3+}	1.248	0.988	1.000	1.076	1.161	1.183	1.053	1.029	1.106
Fe^{2+}	0.769	1.180	1.018	0.930	0.884	0.775	0.684	0.812	0.793
Ni	0.000	0.000	0.000	0.000	0.000	0.000	0.000	0.000	0.000
Mn	0.000	0.019	0.019	0.000	0.018	0.012	0.013	0.011	0.016
Mg	2.907	2.595	2.703	2.834	2.819	2.952	3.116	2.967	2.942
Ca	1.725	1.773	1.748	1.764	1.747	1.735	1.747	1.756	1.728
Na	0.082	0.250	0.176	0.111	0.104	0.126	0.184	0.195	0.151
K	0.072	0.148	0.125	0.090	0.096	0.072	0.099	0.106	0.096
Total Cations	14.880	15.171	14.971	14.965	14.948	14.933	15.025	15.056	15.004
mg	79.1	68.7	72.6	75.3	76.1	79.2	82.0	78.5	78.8
Classification	Ferri Magnesio Hornblende	Ferrian Magnesio Hornblende	Ferrian Magnesio Hornblende	Ferrian Magnesio Hornblende	Ferrian Magnesio Hornblende	Ferrian Magnesio Hornblende	Ferrian Magnesio Hornblende	Ferrian Magnesio Hornblende	Ferrian Magnesio Hornblende

Appendix Table 3.11 (cont.). Electron microprobe analyses of silicate minerals from the Toby layered intrusion.

Sample no.	92522513	92522513	92522518	92522518	92522520	92522520	92522520	92522520	92522520	92522523
Analysis no.	65050	65051	65097	65098	57538	57539	57544	57545	57547	65121
Mineral	Biotite	Biotite	Biotite	Biotite	Biotite	Biotite	Biotite	Biotite	Biotite	Biotite
Description										
Lithology	Suboph. biot qtz gabbronor.	Suboph. biot qtz gabbronor.	Suboph. biot qtz gabbronor.	Suboph. biot qtz gabbronor.	Suboph. biot gabbronorite	Suboph. biot gabbronorite	Suboph. biot gabbronorite	Suboph. biot gabbronorite	Suboph. biot gabbronorite	Suboph. biot gabbronorite
Trav. dist. (m)	1750	1750	3500	3500	5200	5200	5200	5200	5200	9300
SiO_2	35.25	35.80	36.55	35.34	36.04	35.81	35.59	36.57	35.96	35.81
TiO_2	4.66	4.55	4.97	5.21	6.05	6.62	6.37	5.97	6.57	5.31
Al_2O_3	14.55	14.54	15.00	14.04	14.49	14.32	14.56	14.13	14.67	14.87
Cr_2O_3	0.00	0.00	0.00	0.00	0.15	0.24	0.34	0.24	0.22	0.00
FeO*	19.58	18.20	19.69	19.34	19.12	18.95	19.21	19.35	19.60	17.60
MnO	0.00	0.00	0.00	0.00	0.00	0.00	0.00	0.00	0.00	0.00
NiO	0.00	0.00	0.00	0.00	0.00	0.00	0.00	0.00	0.00	0.00
MgO	11.36	12.81	12.21	11.41	12.12	11.65	11.29	11.93	11.27	13.15
CaO	0.00	0.00	0.09	0.00	0.00	0.00	0.00	0.00	0.00	0.00
Na_2O	0.00	0.00	0.00	0.00	0.00	0.00	0.00	0.00	0.00	0.00
K_2O	9.82	10.00	9.42	9.93	9.94	9.95	10.02	9.42	10.07	10.08
Total	95.22	95.90	97.93	95.27	97.91	97.54	97.38	97.61	98.36	96.82
Oxygens	22	22	22	22	22	22	22	22	22	22
Si	5.431	5.438	5.438	5.443	5.380	5.369	5.356	5.460	5.360	5.372
Ti	0.540	0.520	0.556	0.603	0.679	0.746	0.721	0.670	0.736	0.599
Al	2.642	2.603	2.630	2.548	2.549	2.530	2.582	2.486	2.577	2.629
Cr	0.000	0.000	0.000	0.000	0.018	0.028	0.040	0.028	0.026	0.000
Fe	2.523	2.312	2.450	2.491	2.387	2.376	2.418	2.416	2.443	2.208
Ni	0.000	0.000	0.000	0.000	0.000	0.000	0.000	0.000	0.000	0.000
Mn	0.000	0.000	0.000	0.000	0.000	0.000	0.000	0.000	0.000	0.000
Mg	2.609	2.900	2.708	2.619	2.697	2.603	2.532	2.655	2.504	2.941
Ca	0.000	0.000	0.014	0.000	0.000	0.000	0.000	0.000	0.000	0.000
Na	0.000	0.000	0.000	0.000	0.000	0.000	0.000	0.000	0.000	0.000
K	1.930	1.938	1.788	1.951	1.893	1.903	1.924	1.794	1.915	1.929
Total Cations	15.674	15.710	15.585	15.655	15.603	15.557	15.573	15.510	15.560	15.678
mg	50.8	55.6	52.5	51.3	53.1	52.3	51.2	52.4	50.6	57.1

Appendix Table 3.11 (cont.). Electron microprobe analyses of silicate minerals from the Toby layered intrusion.

Sample no.	92522523	92522524	92522524
Analysis no.	65122	65076	65077
Mineral	Biotite	Biotite	Biotite
Description			
Lithology	Suboph. biot gabbronorite	Suboph. biot qtz gabbronor.	Suboph. biot qtz gabbronor.
Trav. dist. (m)	9300	11400	11400
SiO_2	35.53	35.74	35.16
TiO_2	5.57	5.59	5.75
Al_2O_3	14.93	14.44	14.50
Cr_2O_3	0.00	0.00	0.00
FeO*	17.65	20.63	20.27
MnO	0.00	0.00	0.00
NiO	0.00	0.00	0.00
MgO	12.64	10.96	10.91
CaO	0.00	0.00	0.00
Na_2O	0.00	0.00	0.00
K_2O	10.06	10.00	9.73
Total	96.38	97.36	96.32
Oxygens	22	22	22
Si	5.359	5.408	5.371
Ti	0.632	0.636	0.661
Al	2.654	2.575	2.610
Cr	0.000	0.000	0.000
Fe	2.227	2.611	2.589
Ni	0.000	0.000	0.000
Mn	0.000	0.000	0.000
Mg	2.842	2.472	2.484
Ca	0.000	0.000	0.000
Na	0.000	0.000	0.000
K	1.936	1.930	1.896
Total Cations	15.650	15.633	15.611
mg	56.1	48.6	49.0

Sample no.	92522513	92522513	92522518	92522518	92522520	92522520	92522520
Analysis no.	65053	65054	65099	65100	57532	57533	57534
Mineral	Clinopyroxene	Clinopyroxene	Clinopyroxene	Clinopyroxene	Clinopyroxene	Clinopyroxene	Clinopyroxene
Description	Subophitic	Subophitic	Subophitic	Subophitic	Subophitic	Subophitic	Subophitic
Lithology	Suboph. biot qtz gabbronor.	Suboph. biot qtz gabbronor.	Suboph. biot qtz gabbronor.	Suboph. biot qtz gabbronor.	Suboph. biot gabbronorite	Suboph. biot gabbronorite	Suboph. biot gabbronorite
Trav. dist. (m)	1750	1750	3500	3500	5200	5200	5200
SiO_2	51.63	51.65	51.97	51.37	51.73	51.54	51.43
TiO_2	0.00	0.15	0.00	0.14	0.26	0.42	0.45
Al_2O_3	0.67	0.80	0.60	0.95	1.44	1.45	1.56
Cr_2O_3	0.00	0.00	0.00	0.00	0.00	0.00	0.00
FeO*	12.28	11.98	11.97	12.41	11.29	11.80	11.62
MnO	0.34	0.22	0.16	0.16	0.13	0.18	0.22
NiO	0.00	0.00	0.00	0.00	0.00	0.00	0.00
MgO	12.75	13.03	12.62	12.39	13.74	13.93	13.39
CaO	21.30	21.45	22.09	21.49	20.72	20.43	20.78
Na_2O	0.00	0.00	0.00	0.00	0.00	0.00	0.00
K_2O	0.00	0.00	0.00	0.00	0.00	0.00	0.00
Total	98.97	99.28	99.41	98.91	99.31	99.75	99.45
Oxygens	6	6	6	6	6	6	6
Si	1.971	1.962	1.974	1.964	1.955	1.941	1.946
Ti	0.000	0.004	0.000	0.004	0.007	0.012	0.013
Al	0.030	0.036	0.027	0.043	0.064	0.064	0.070
Cr	0.000	0.000	0.000	0.000	0.000	0.000	0.000
Fe^{3+}	0.029	0.032	0.025	0.020	0.012	0.031	0.014
Fe^{2+}	0.363	0.348	0.355	0.377	0.345	0.341	0.354
Ni	0.000	0.000	0.005	0.005	0.004	0.006	0.007
Mn	0.011	0.007	0.000	0.000	0.000	0.000	0.000
Mg	0.725	0.738	0.715	0.706	0.774	0.782	0.755
Ca	0.871	0.873	0.899	0.880	0.839	0.824	0.842
Na	0.000	0.000	0.000	0.000	0.000	0.000	0.000
K	0.000	0.000	0.000	0.000	0.000	0.000	0.000
Total Cations	4.000	4.000	4.000	4.000	4.000	4.000	4.000
mg	66.6	67.9	66.8	65.2	69.2	69.6	68.1
Enstatite	37.0	37.7	36.3	36.0	39.5	40.2	38.7
Ferrosilite	18.5	17.8	18.1	19.2	17.6	17.5	18.2
Wollastonite	44.5	44.6	45.7	44.9	42.8	42.3	43.2

Appendix Table 3.11 (cont.). Electron microprobe analyses of silicate minerals from the Toby layered intrusion.

Sample no.	92522520	92522523	92522523	92522523	92522524	92522524	92522524
Analysis no.	57548	65120	65123	65124	65080	65081	65082
Mineral	Clinopyroxene	Clinopyroxene	Clinopyroxene	Clinopyroxene	Clinopyroxene	Clinopyroxene	Clinopyroxene
Description	Subophitic	Subophitic	Subophitic	Subophitic	Subophitic	Subophitic	Subophitic
Lithology	Suboph. biot gabbronorite	Suboph. biot gabbronorite	Suboph. biot gabbronorite	Suboph. biot gabbronorite	Suboph. biot qtz gabbronor.	Suboph. biot qtz gabbronor.	Suboph. biot qtz gabbronor.
Trav. dist. (m)	5200	9300	9300	9300	11400	11400	11400
SiO_2	51.29	51.83	51.84	52.04	51.52	50.91	51.76
TiO_2	0.45	0.00	0.18	0.22	0.20	0.23	0.00
Al_2O_3	2.06	0.67	1.13	1.05	0.93	0.90	0.76
Cr_2O_3	0.29	0.00	0.00	0.00	0.00	0.00	0.00
FeO*	10.28	10.30	10.08	10.65	12.27	12.31	12.04
MnO	0.11	0.13	0.19	0.17	0.26	0.21	0.11
NiO	0.00	0.00	0.00	0.00	0.00	0.00	0.00
MgO	13.88	13.43	13.63	13.43	12.45	12.08	12.21
CaO	21.64	21.66	22.54	21.86	21.28	21.87	22.07
Na_2O	0.00	0.00	0.00	0.00	0.00	0.00	0.00
K_2O	0.00	0.00	0.00	0.00	0.00	0.00	0.00
Total	100.00	98.02	99.59	99.42	98.91	98.51	98.95
Oxygens	6	6	6	6	6	6	6
Si	1.920	1.983	1.950	1.965	1.970	1.957	1.978
Ti	0.013	0.000	0.005	0.006	0.006	0.007	0.000
Al	0.091	0.030	0.050	0.047	0.042	0.041	0.034
Cr	0.009	0.000	0.000	0.000	0.000	0.000	0.000
Fe^{3+}	0.035	0.005	0.041	0.011	0.006	0.032	0.009
Fe^{2+}	0.287	0.325	0.276	0.326	0.386	0.364	0.375
Ni	0.000	0.000	0.000	0.000	0.000	0.000	0.000
Mn	0.003	0.004	0.006	0.005	0.008	0.007	0.004
Mg	0.774	0.766	0.764	0.756	0.710	0.692	0.696
Ca	0.868	0.888	0.908	0.884	0.872	0.901	0.904
Na	0.000	0.000	0.000	0.000	0.000	0.000	0.000
K	0.000	0.000	0.000	0.000	0.000	0.000	0.000
Total Cations	4.000	4.000	4.000	4.000	4.000	4.000	4.000
mg	73.0	70.2	73.4	69.9	64.8	65.5	65.0
Enstatite	40.1	38.7	39.2	38.5	36.1	35.4	35.2
Ferrosilite	14.9	16.4	14.2	16.6	19.6	18.6	19.0
Wollastonite	45.0	44.9	46.6	44.9	44.3	46.0	45.8

Sample no.	92522520	92522520	92522520
Analysis no.	57550	57551	57552
Mineral	Olivine	Olivine	Olivine
Description	Cumulus		
Lithology	Suboph. biot gabbronorite	Suboph. biot gabbronorite	Suboph. biot gabbronorite
Trav. dist. (m)	5200	5200	5200
SiO_2	34.42	34.43	34.21
TiO_2	0.00	0.00	0.00
Al_2O_3	0.00	0.00	0.00
Cr_2O_3	0.00	0.00	0.00
FeO*	41.97	41.36	41.01
MnO	0.45	0.43	0.41
NiO	0.00	0.00	0.00
MgO	24.28	24.66	25.13
CaO	0.00	0.00	0.00
Na_2O	0.00	0.00	0.00
K_2O	0.00	0.00	0.00
Total	101.13	100.88	100.75
Oxygens	4	4	4
Si	0.973	0.973	0.965
Ti	0.000	0.000	0.000
Al	0.000	0.000	0.000
Cr	0.000	0.000	0.000
Fe^{3+}	0.053	0.054	0.069
Fe^{2+}	0.939	0.924	0.899
Ni	0.000	0.000	0.000
Mn	0.011	0.010	0.010
Mg	1.023	1.039	1.057
Ca	0.000	0.000	0.000
Na	0.000	0.000	0.000
K	0.000	0.000	0.000
Total Cations	2.999	3.000	3.000
mg	52.1	52.9	54.0

Appendix Table 3.11 (cont.). Electron microprobe analyses of silicate minerals from the Toby layered intrusion.

Sample no.	92522520	92522520
Analysis no.	57553	57554
Mineral	Olivine	Olivine
Description		
Lithology	Suboph. biot gabbronorite	Suboph. biot gabbronorite
Trav. dist. (m)	5200	5200
SiO_2	34.48	34.32
TiO_2	0.00	0.00
Al_2O_3	0.00	0.00
Cr_2O_3	0.00	0.00
FeO*	39.78	40.45
MnO	0.28	0.41
NiO	0.00	0.00
MgO	25.75	25.38
CaO	0.00	0.00
Na_2O	0.00	0.00
K_2O	0.00	0.00
Total	100.30	100.57
Oxygens	4	4
Si	0.972	0.968
Ti	0.000	0.000
Al	0.000	0.000
Cr	0.000	0.000
Fe^{3+}	0.055	0.063
Fe^{2+}	0.883	0.891
Ni	0.000	0.000
Mn	0.007	0.010
Mg	1.083	1.067
Ca	0.000	0.000
Na	0.000	0.000
K	0.000	0.000
Total Cations	3.000	2.999
mg	55.1	54.5

Sample no.	92522513	92522518	92522518	92522518	92522520	92522520	92522520	92522520
Analysis no.	65052	65101	65105	65106	57536	57537	57542	57543
Mineral	Orthopyroxene	Orthopyroxene	Orthopyroxene	Orthopyroxene	Orthopyroxene	Orthopyroxene	Orthopyroxene	Orthopyroxene
Description	Subophitic	Subophitic	Subophitic	Subophitic	Subophitic	Subophitic	Subophitic	Subophitic
Lithology	Suboph. biot qtz gabbronor.	Suboph. biot qtz gabbronor.	Suboph. biot qtz gabbronor.	Suboph. biot qtz gabbronor.	Suboph. biot gabbronorite	Suboph. biot gabbronorite	Suboph. biot gabbronorite	Suboph. biot gabbronorite
Trav. dist. (m)	1750	3500	3500	3500	5200	5200	5200	5200
SiO_2	50.91	51.06	51.14	50.94	51.67	51.85	51.90	50.90
TiO_2	0.00	0.00	0.00	0.00	0.28	0.16	0.29	0.40
Al_2O_3	0.37	0.29	0.33	0.31	0.84	0.73	0.78	0.84
Cr_2O_3	0.00	0.00	0.00	0.00	0.00	0.00	0.00	0.00
FeO*	29.17	29.60	30.71	29.99	24.78	24.53	24.21	25.96
MnO	0.71	0.46	0.53	0.53	0.42	0.30	0.41	0.38
NiO	0.00	0.00	0.00	0.00	0.00	0.00	0.00	0.00
MgO	18.05	17.98	17.43	17.66	20.68	21.07	21.47	20.36
CaO	0.87	0.92	0.85	0.79	1.58	1.66	1.84	1.72
Na_2O	0.00	0.00	0.00	0.00	0.00	0.00	0.00	0.00
K_2O	0.00	0.00	0.00	0.00	0.00	0.00	0.00	0.00
Total	100.34	100.56	101.24	100.45	100.48	100.56	101.23	100.96
Oxygens	6	6	6	6	6	6	6	6
Si	1.955	1.958	1.957	1.959	1.941	1.942	1.929	1.913
Ti	0.000	0.000	0.000	0.000	0.008	0.005	0.008	0.011
Al	0.017	0.013	0.015	0.014	0.037	0.032	0.034	0.037
Cr	0.000	0.000	0.000	0.000	0.000	0.000	0.000	0.000
Fe^{3+}	0.074	0.072	0.072	0.068	0.064	0.074	0.091	0.114
Fe^{2+}	0.863	0.877	0.911	0.897	0.714	0.694	0.662	0.703
Ni	0.000	0.000	0.000	0.000	0.000	0.000	0.000	0.000
Mn	0.023	0.015	0.017	0.017	0.013	0.010	0.013	0.012
Mg	1.033	1.027	0.994	1.012	1.158	1.176	1.190	1.141
Ca	0.036	0.038	0.035	0.033	0.064	0.067	0.073	0.069
Na	0.000	0.000	0.000	0.000	0.000	0.000	0.000	0.000
K	0.000	0.000	0.000	0.000	0.000	0.000	0.000	0.000
Total Cations	4.000	4.000	4.000	4.000	4.000	4.000	4.000	4.000
mg	54.5	53.9	52.2	53.0	61.9	62.9	64.3	61.9
Enstatite	53.5	52.8	51.2	52.1	59.8	60.8	61.8	59.7
Ferrosilite	44.7	45.2	47.0	46.2	36.9	35.8	34.4	36.7
Wollastonite	1.9	2.0	1.8	1.7	3.3	3.4	3.8	3.6

Appendix Table 3.11 (cont.). Electron microprobe analyses of silicate minerals from the Toby layered intrusion.

Sample no.	92522520	92522520	92522520	92522523	92522523	92522524	92522524	92522524	92522524	Sample no.	92522513
Analysis no.	57555	57556	57557	65125	65126	65074	65075	65078	65079	Analysis no.	65029
Mineral	Orthopyroxene	Orthopyroxene	Orthopyroxene	Orthopyroxene	Orthopyroxene	Orthopyroxene	Orthopyroxene	Orthopyroxene	Orthopyroxene	Mineral	Plagioclase
Description	Subophitic	Subophitic	Subophitic	Subophitic	Subophitic	Subophitic	Subophitic	Subophitic	Subophitic	Description	Subophitic (r)
Lithology	Suboph. biot gabbronorite	Suboph. biot gabbronorite	Suboph. biot gabbronorite	Suboph. biot gabbronorite	Suboph. biot gabbronorite	Suboph. biot gabbronorite	Suboph. biot gabbronorite	Suboph. biot gabbronorite	Suboph. biot gabbronorite	Lithology	Suboph. biot qtz gabbronor.
Trav. dist. (m)	5200	5200	5200	9300	9300	11400	11400	11400	11400	Trav. dist. (m)	1750
SiO_2	51.62	51.74	51.83	51.66	51.65	50.75	50.28	50.63	50.79	SiO_2	51.07
TiO_2	0.26	0.34	0.30	0.00	0.00	0.19	0.00	0.00	0.00	TiO_2	0.00
Al_2O_3	0.81	0.83	0.78	0.32	0.43	0.41	0.29	0.35	0.46	Al_2O_3	32.06
Cr_2O_3	0.00	0.00	0.00	0.00	0.00	0.00	0.00	0.00	0.00	Cr_2O_3	0.00
FeO*	26.17	24.56	25.51	27.47	26.70	31.30	31.21	31.22	30.75	FeO*	0.17
MnO	0.31	0.28	0.45	0.43	0.41	0.67	0.54	0.53	0.52	MnO	0.00
NiO	0.00	0.00	0.00	0.00	0.00	0.00	0.00	0.00	0.00	NiO	0.00
MgO	20.36	21.07	20.72	19.73	20.30	16.35	16.49	16.74	16.85	MgO	0.00
CaO	1.38	1.67	1.72	0.86	0.41	0.95	0.78	0.82	0.93	CaO	13.33
Na_2O	0.00	0.00	0.00	0.00	0.00	0.00	0.00	0.00	0.00	Na_2O	3.78
K_2O	0.00	0.00	0.00	0.00	0.00	0.00	0.00	0.00	0.00	K_2O	0.00
Total	101.20	100.75	101.63	100.74	100.13	100.78	99.82	100.52	100.50	Total	100.41
Oxygens	6	6	6	6	6	6	6	6	6	Oxygens	8
Si	1.934	1.935	1.930	1.955	1.958	1.961	1.960	1.958	1.961	Si	2.309
Ti	0.007	0.010	0.008	0.000	0.000	0.006	0.000	0.000	0.000	Ti	0.000
Al	0.036	0.037	0.034	0.014	0.019	0.019	0.013	0.016	0.021	Al	1.709
Cr	0.000	0.000	0.000	0.000	0.000	0.000	0.000	0.000	0.000	Cr	0.000
Fe^{3+}	0.081	0.074	0.089	0.076	0.065	0.048	0.066	0.068	0.057	Fe^{3+}	0.000
Fe^{2+}	0.739	0.694	0.706	0.793	0.781	0.964	0.952	0.942	0.936	Fe^{2+}	0.006
Ni	0.000	0.000	0.000	0.000	0.000	0.000	0.000	0.000	0.000	Ni	0.000
Mn	0.010	0.009	0.014	0.014	0.013	0.022	0.018	0.017	0.017	Mn	0.000
Mg	1.137	1.175	1.150	1.113	1.147	0.942	0.958	0.965	0.970	Mg	0.000
Ca	0.055	0.067	0.069	0.035	0.017	0.039	0.033	0.034	0.038	Ca	0.646
Na	0.000	0.000	0.000	0.000	0.000	0.000	0.000	0.000	0.000	Na	0.331
K	0.000	0.000	0.000	0.000	0.000	0.000	0.000	0.000	0.000	K	0.000
Total Cations	4.000	4.000	4.000	4.000	4.000	4.000	4.000	4.000	4.000	Total Cations	5.002
mg	60.6	62.9	62.0	58.4	59.5	49.4	50.2	50.6	50.9	Albite	33.9
Enstatite	58.8	60.6	59.7	57.3	59.0	48.4	49.3	49.7	49.9	Anorthite	66.1
Ferrosilite	38.3	35.9	36.7	40.9	40.1	49.6	49.0	48.5	48.1	Orthoclase	0.0
Wollastonite	2.9	3.5	3.6	1.8	0.9	2.0	1.7	1.8	2.0		

Appendix Table 3.11 (cont.). Electron microprobe analyses of silicate minerals from the Toby layered intrusion.

Sample no.	92522513	92522513	92522513	92522513	92522513	92522513	92522513	92522513	92522513	92522513	92522513
Analysis no.	65030	65031	65032	65033	65034	65035	65036	65037	65038	65039	65040
Mineral	Plagioclase	Plagioclase	Plagioclase	Plagioclase	Plagioclase	Plagioclase	Plagioclase	Plagioclase	Plagioclase	Plagioclase	Plagioclase
Description	Subophitic (c)	Subophitic (r)	Subophitic (c)	Subophitic (r)	Subophitic (r)	Subophitic (r)	Subophitic (c)	Subophitic (r)	Subophitic (c)	Subophitic (r)	Subophitic (c)
Lithology	Suboph. biot qtz gabbronor.	Suboph. biot qtz gabbronor.	Suboph. biot qtz gabbronor.	Suboph. biot qtz gabbronor.	Suboph. biot qtz gabbronor.	Suboph. biot qtz gabbronor.	Suboph. biot qtz gabbronor.	Suboph. biot qtz gabbronor.	Suboph. biot qtz gabbronor.	Suboph. biot qtz gabbronor.	Suboph. biot qtz gabbronor.
Trav. dist. (m)	1750	1750	1750	1750	1750	1750	1750	1750	1750	1750	1750
SiO_2	53.70	49.67	54.44	54.53	54.04	55.81	54.05	54.24	46.22	53.07	50.54
TiO_2	0.00	0.00	0.00	0.00	0.00	0.00	0.00	0.00	0.00	0.00	0.00
Al_2O_3	29.84	32.71	29.23	29.50	29.80	28.27	29.49	29.34	35.10	30.21	32.51
Cr_2O_3	0.00	0.00	0.00	0.00	0.00	0.00	0.00	0.00	0.00	0.00	0.00
FeO*	0.25	0.31	0.23	0.33	0.20	0.25	0.20	0.19	0.17	0.25	0.31
MnO	0.00	0.00	0.00	0.00	0.00	0.00	0.00	0.00	0.00	0.00	0.00
NiO	0.00	0.00	0.00	0.00	0.00	0.00	0.00	0.00	0.00	0.00	0.00
MgO	0.00	0.00	0.00	0.00	0.00	0.00	0.00	0.00	0.00	0.00	0.00
CaO	10.92	13.95	10.18	10.41	10.68	9.20	10.75	10.59	16.77	11.48	13.86
Na_2O	5.00	3.16	5.52	5.54	5.39	6.19	5.31	5.10	1.53	4.86	3.67
K_2O	0.10	0.08	0.17	0.19	0.10	0.12	0.16	0.08	0.00	0.12	0.08
Total	99.81	99.88	99.77	100.50	100.21	99.84	99.96	99.54	99.79	99.99	100.97
Oxygens	8	8	8	8	8	8	8	8	8	8	8
Si	2.427	2.264	2.459	2.449	2.433	2.512	2.441	2.454	2.124	2.401	2.281
Ti	0.000	0.000	0.000	0.000	0.000	0.000	0.000	0.000	0.000	0.000	0.000
Al	1.590	1.757	1.556	1.561	1.582	1.500	1.569	1.564	1.901	1.611	1.729
Cr	0.000	0.000	0.000	0.000	0.000	0.000	0.000	0.000	0.000	0.000	0.000
Fe^{3+}	0.000	0.000	0.000	0.000	0.000	0.000	0.000	0.000	0.000	0.000	0.000
Fe^{2+}	0.009	0.012	0.009	0.012	0.008	0.009	0.008	0.007	0.007	0.009	0.012
Ni	0.000	0.000	0.000	0.000	0.000	0.000	0.000	0.000	0.000	0.000	0.000
Mn	0.000	0.000	0.000	0.000	0.000	0.000	0.000	0.000	0.000	0.000	0.000
Mg	0.000	0.000	0.000	0.000	0.000	0.000	0.000	0.000	0.000	0.000	0.000
Ca	0.529	0.681	0.493	0.501	0.515	0.444	0.520	0.513	0.826	0.556	0.670
Na	0.438	0.279	0.483	0.482	0.471	0.540	0.465	0.447	0.136	0.426	0.321
K	0.006	0.005	0.010	0.011	0.006	0.007	0.009	0.005	0.000	0.007	0.005
Total Cations	5.000	4.999	5.010	5.017	5.014	5.012	5.012	4.990	4.994	5.011	5.018
Albite	45.0	28.9	49.0	48.5	47.4	54.5	46.8	46.3	14.2	43.1	32.2
Anorthite	54.4	70.6	50.0	50.4	52.0	44.8	52.3	53.2	85.8	56.2	67.3
Orthoclase	0.6	0.5	1.0	1.1	0.6	0.7	0.9	0.5	0.0	0.7	0.5

Appendix Table 3.11 (cont.). Electron microprobe analyses of silicate minerals from the Toby layered intrusion.

Sample no.	92522513	92522513	92522513	92522513	92522513	92522513	92522518	92522518	92522518	92522518	92522518
Analysis no.	65041	65042	65043	65044	65045	65046	65083	65084	65085	65086	65087
Mineral	Plagioclase	Plagioclase	Plagioclase	Plagioclase	Plagioclase	Plagioclase	Plagioclase	Plagioclase	Plagioclase	Plagioclase	Plagioclase
Description	Subophitic (r)	Subophitic (c)	Subophitic (r)	Subophitic (c)	Subophitic (r)	Subophitic (c)	Subophitic (r)	Subophitic (c)	Subophitic (r)	Subophitic (c)	Subophitic (r)
Lithology	Suboph. biot qtz gabbronor.	Suboph. biot qtz gabbronor.	Suboph. biot qtz gabbronor.	Suboph. biot qtz gabbronor.	Suboph. biot qtz gabbronor.	Suboph. biot qtz gabbronor.	Suboph. biot qtz gabbronor.	Suboph. biot qtz gabbronor.	Suboph. biot qtz gabbronor.	Suboph. biot qtz gabbronor.	Suboph. biot qtz gabbronor.
Trav. dist. (m)	1750	1750	1750	1750	1750	1750	3500	3500	3500	3500	3500
SiO_2	50.78	50.29	54.67	49.44	53.39	54.73	54.77	51.26	54.61	54.36	53.02
TiO_2	0.00	0.00	0.00	0.00	0.00	0.00	0.00	0.00	0.00	0.00	0.00
Al_2O_3	31.89	32.50	30.01	32.68	29.96	29.45	28.94	31.16	29.15	29.20	30.38
Cr_2O_3	0.00	0.00	0.00	0.00	0.00	0.00	0.00	0.00	0.00	0.00	0.00
FeO*	0.23	0.21	0.39	0.20	0.39	0.12	0.26	0.14	0.28	0.17	0.18
MnO	0.00	0.00	0.00	0.00	0.00	0.00	0.00	0.00	0.00	0.00	0.00
NiO	0.00	0.00	0.00	0.00	0.00	0.00	0.00	0.00	0.00	0.00	0.00
MgO	0.00	0.00	0.00	0.00	0.00	0.00	0.00	0.00	0.00	0.00	0.00
CaO	13.26	13.84	10.83	14.25	11.22	10.38	10.18	12.62	10.21	10.36	11.49
Na_2O	3.75	3.25	5.42	3.03	4.91	5.58	5.56	4.01	5.60	5.52	4.79
K_2O	0.09	0.05	0.18	0.11	0.08	0.18	0.15	0.09	0.19	0.18	0.10
Total	100.00	100.14	101.50	99.71	99.95	100.44	99.86	99.28	100.04	99.79	99.96
Oxygens	8	8	8	8	8	8	8	8	8	8	8
Si	2.308	2.283	2.434	2.259	2.414	2.456	2.471	2.341	2.462	2.456	2.398
Ti	0.000	0.000	0.000	0.000	0.000	0.000	0.000	0.000	0.000	0.000	0.000
Al	1.708	1.739	1.575	1.760	1.597	1.558	1.539	1.677	1.549	1.555	1.619
Cr	0.000	0.000	0.000	0.000	0.000	0.000	0.000	0.000	0.000	0.000	0.000
Fe^{3+}	0.000	0.000	0.000	0.000	0.000	0.000	0.000	0.000	0.000	0.000	0.000
Fe^{2+}	0.009	0.008	0.015	0.008	0.015	0.005	0.010	0.005	0.011	0.006	0.007
Ni	0.000	0.000	0.000	0.000	0.000	0.000	0.000	0.000	0.000	0.000	0.000
Mn	0.000	0.000	0.000	0.000	0.000	0.000	0.000	0.000	0.000	0.000	0.000
Mg	0.000	0.000	0.000	0.000	0.000	0.000	0.000	0.000	0.000	0.000	0.000
Ca	0.646	0.673	0.517	0.698	0.544	0.499	0.492	0.617	0.493	0.502	0.557
Na	0.330	0.286	0.468	0.268	0.431	0.486	0.486	0.355	0.489	0.484	0.420
K	0.005	0.003	0.010	0.006	0.005	0.010	0.009	0.005	0.011	0.010	0.006
Total Cations	5.006	4.992	5.018	4.999	5.005	5.013	5.007	5.001	5.014	5.013	5.006
Albite	33.7	29.7	47.0	27.6	44.0	48.8	49.3	36.3	49.3	48.6	42.8
Anorthite	65.8	70.0	52.0	71.7	55.5	50.2	49.8	63.2	49.6	50.4	56.6
Orthoclase	0.5	0.3	1.0	0.7	0.5	1.0	0.9	0.5	1.1	1.0	0.6

Appendix Table 3.11 (cont.). Electron microprobe analyses of silicate minerals from the Toby layered intrusion.

Sample no.	92522518	92522518	92522518	92522518	92522518	92522518	92522520	92522520	92522520	92522520	92522520
Analysis no.	65088	65089	65090	65091	65092	65093	57535	57540	57541	57546	57547
Mineral	Plagioclase	Plagioclase	Plagioclase	Plagioclase	Plagioclase	Plagioclase	Plagioclase	Plagioclase (c)	Plagioclase (r)	Plagioclase	Plagioclase
Description	Subophitic (c)	Subophitic (r)	Subophitic (r)	Subophitic (r)	Subophitic (c)	Subophitic	Subophitic	Subophitic (c)	Subophitic (r)	Subophitic (c)	Subophitic (r)
Lithology	Suboph. biot qtz gabbronor.	Suboph. biot qtz gabbronor.	Suboph. biot qtz gabbronor.	Suboph. biot qtz gabbronor.	Suboph. biot qtz gabbronor.	Suboph. biot qtz gabbronor.	Suboph. biot gabbronorite	Suboph. biot gabbronorite	Suboph. biot gabbronorite	Suboph. biot gabbronorite	Suboph. biot gabbronorite
Trav. dist. (m)	3500	3500	3500	3500	3500	3500	5200	5200	5200	5200	5200
SiO_2	52.05	54.45	53.61	55.74	54.76	53.44	53.79	49.70	54.20	49.92	52.36
TiO_2	0.00	0.00	0.00	0.00	0.00	0.00	0.00	0.00	0.00	0.00	0.00
Al_2O_3	30.66	29.23	29.99	28.60	29.12	30.11	30.04	32.82	29.98	32.99	31.12
Cr_2O_3	0.00	0.00	0.00	0.00	0.00	0.00	0.00	0.00	0.00	0.00	0.00
FeO*	0.00	0.00	0.00	0.33	0.13	0.16	0.16	0.00	0.11	0.15	0.25
MnO	0.00	0.00	0.00	0.00	0.00	0.00	0.00	0.00	0.00	0.00	0.00
NiO	0.00	0.00	0.00	0.00	0.00	0.00	0.00	0.00	0.00	0.00	0.00
MgO	0.00	0.00	0.00	0.00	0.00	0.00	0.00	0.00	0.00	0.00	0.00
CaO	12.03	10.24	11.14	9.52	9.99	11.20	10.99	14.22	10.84	14.24	12.23
Na_2O	4.31	5.42	4.95	5.98	5.75	5.04	5.30	3.27	5.19	3.35	4.68
K_2O	0.05	0.19	0.15	0.19	0.20	0.10	0.18	0.08	0.20	0.06	0.08
Total	99.10	99.79	99.84	100.36	99.95	100.05	100.45	100.09	100.52	100.70	100.73
Oxygens	8	8	8	8	8	8	8	8	8	8	8
Si	2.374	2.459	2.422	2.499	2.468	2.413	2.420	2.261	2.432	2.259	2.358
Ti	0.000	0.000	0.000	0.000	0.000	0.000	0.000	0.000	0.000	0.000	0.000
Al	1.648	1.556	1.597	1.511	1.547	1.602	1.592	1.760	1.586	1.759	1.652
Cr	0.000	0.000	0.000	0.000	0.000	0.000	0.000	0.000	0.000	0.000	0.000
Fe^{3+}	0.000	0.000	0.000	0.000	0.000	0.000	0.000	0.000	0.000	0.000	0.000
Fe^{2+}	0.000	0.010	0.000	0.012	0.005	0.006	0.006	0.000	0.004	0.006	0.010
Ni	0.000	0.000	0.000	0.000	0.000	0.000	0.000	0.000	0.000	0.000	0.000
Mn	0.000	0.000	0.000	0.000	0.000	0.000	0.000	0.000	0.000	0.000	0.000
Mg	0.000	0.000	0.000	0.000	0.000	0.000	0.000	0.000	0.000	0.000	0.000
Ca	0.588	0.495	0.539	0.457	0.482	0.542	0.529	0.693	0.521	0.690	0.590
Na	0.381	0.475	0.434	0.520	0.502	0.441	0.462	0.289	0.452	0.294	0.409
K	0.003	0.011	0.009	0.011	0.011	0.006	0.010	0.005	0.011	0.003	0.005
Total Cations	4.994	5.006	5.001	5.011	5.016	5.010	5.020	5.006	5.006	5.011	5.023
Albite	39.2	48.4	44.2	52.6	50.4	44.6	46.2	29.3	45.9	29.8	40.8
Anorthite	60.5	50.5	54.9	46.3	48.4	54.8	52.8	70.2	53.0	69.9	58.7
Orthoclase	0.3	1.1	0.9	1.1	1.2	0.6	1.0	0.5	1.1	0.3	0.5

Appendix Table 3.11 (cont.). Electron microprobe analyses of silicate minerals from the Toby layered intrusion.

Sample no.	92522523	92522523	92522523	92522523	92522523	92522523	92522524	92522524	92522524	92522524	92522524
Analysis no.	65107	65108	65109	65110	65111	65112	65059	65060	65061	65062	65064
Mineral	Plagioclase	Plagioclase	Plagioclase	Plagioclase	Plagioclase	Plagioclase	Plagioclase	Plagioclase	Plagioclase	Plagioclase	Plagioclase
Description	Subophitic (r)	Subophitic (c)	Subophitic (r)	Subophitic (c)	Subophitic (r)	Subophitic (c)	Subophitic (r)	Subophitic (c)	Subophitic (c)	Subophitic (r)	Subophitic (c)
Lithology	Suboph. biot gabbronorite	Suboph. biot gabbronorite	Suboph. biot gabbronorite	Suboph. biot gabbronorite	Suboph. biot gabbronorite	Suboph. biot gabbronorite	Suboph. biot qtz gabbronor.	Suboph. biot qtz gabbronor.	Suboph. biot qtz gabbronor.	Suboph. biot qtz gabbronor.	Suboph. biot qtz gabbronor.
Trav. dist. (m)	9300	9300	9300	9300	9300	9300	11400	11400	11400	11400	11400
SiO_2	52.49	52.49	52.63	54.45	52.31	53.82	52.95	50.87	52.59	54.45	53.41
TiO_2	0.00	0.00	0.00	0.00	0.00	0.00	0.00	0.00	0.00	0.00	0.00
Al_2O_3	29.96	30.80	30.59	29.16	31.04	29.40	29.98	31.35	30.59	29.32	29.77
Cr_2O_3	0.00	0.00	0.00	0.00	0.00	0.00	0.00	0.00	0.00	0.00	0.00
FeO*	0.23	0.20	0.26	0.27	0.20	0.00	0.31	0.12	0.21	0.13	0.00
MnO	0.00	0.00	0.00	0.00	0.00	0.00	0.00	0.00	0.00	0.00	0.00
NiO	0.00	0.00	0.00	0.00	0.00	0.00	0.00	0.00	0.00	0.00	0.00
MgO	0.00	0.00	0.00	0.00	0.00	0.00	0.00	0.00	0.00	0.00	0.00
CaO	11.26	11.99	11.86	10.30	12.08	10.94	10.97	12.77	11.57	10.20	11.07
Na_2O	5.08	4.41	4.76	5.64	4.39	5.06	4.97	3.86	4.66	5.41	4.98
K_2O	0.12	0.14	0.13	0.26	0.11	0.16	0.12	0.13	0.14	0.16	0.06
Total	99.13	100.03	100.23	100.08	100.13	99.38	99.30	99.10	99.76	99.67	99.29
Oxygens	8	8	8	8	8	8	8	8	8	8	8
Si	2.397	2.375	2.379	2.456	2.365	2.442	2.409	2.329	2.385	2.459	2.425
Ti	0.000	0.000	0.000	0.000	0.000	0.000	0.000	0.000	0.000	0.000	0.000
Al	1.612	1.642	1.630	1.550	1.654	1.572	1.608	1.691	1.635	1.561	1.593
Cr	0.000	0.000	0.000	0.000	0.000	0.000	0.000	0.000	0.000	0.000	0.000
Fe^{3+}	0.000	0.000	0.000	0.000	0.000	0.000	0.000	0.000	0.000	0.000	0.000
Fe^{2+}	0.009	0.008	0.010	0.010	0.008	0.000	0.012	0.005	0.008	0.005	0.000
Ni	0.000	0.000	0.000	0.000	0.000	0.000	0.000	0.000	0.000	0.000	0.000
Mn	0.000	0.000	0.000	0.000	0.000	0.000	0.000	0.000	0.000	0.000	0.000
Mg	0.000	0.000	0.000	0.000	0.000	0.000	0.000	0.000	0.000	0.000	0.000
Ca	0.551	0.581	0.574	0.498	0.585	0.532	0.535	0.626	0.562	0.494	0.539
Na	0.449	0.387	0.417	0.493	0.385	0.445	0.438	0.343	0.410	0.474	0.438
K	0.007	0.008	0.007	0.015	0.006	0.009	0.007	0.008	0.008	0.009	0.003
Total Cations	5.025	5.001	5.018	5.023	5.003	5.000	5.009	5.001	5.007	5.002	4.999
Albite	44.6	39.6	41.8	49.0	39.4	45.1	44.7	35.1	41.8	48.5	44.7
Anorthite	54.7	59.6	57.4	49.5	59.9	54.0	54.6	64.1	57.4	50.6	54.9
Orthoclase	0.7	0.8	0.8	1.5	0.7	0.9	0.7	0.8	0.8	0.9	0.4

Appendix Table 3.11 (cont.). Electron microprobe analyses of silicate minerals from the Toby layered intrusion.

Sample no.	92522524	92522524	92522524	92522524	92522524	92522524
Analysis no.	65065	65066	65067	65068	65069	65070
Mineral	Plagioclase	Plagioclase	Plagioclase	Plagioclase	Plagioclase	Plagioclase
Description	Subophitic (r)	Subophitic (c)	Subophitic (r)	Subophitic (c)	Subophitic (r)	Subophitic (c)
Lithology	Suboph. biot qtz gabbronor.	Suboph. biot qtz gabbronor.	Suboph. biot qtz gabbronor.	Suboph. biot qtz gabbronor.	Suboph. biot qtz gabbronor.	Suboph. biot qtz gabbronor.
Trav. dist. (m)	11400	11400	11400	11400	11400	11400
SiO_2	49.09	45.85	51.47	53.48	52.67	50.82
TiO_2	0.00	0.00	0.00	0.00	0.00	0.00
Al_2O_3	32.99	35.19	31.37	29.99	30.57	31.92
Cr_2O_3	0.00	0.00	0.00	0.00	0.00	0.00
FeO*	0.14	0.24	0.13	0.00	0.23	0.21
MnO	0.00	0.00	0.00	0.00	0.00	0.00
NiO	0.00	0.00	0.00	0.00	0.00	0.00
MgO	0.00	0.00	0.00	0.00	0.00	0.00
CaO	14.48	16.76	12.50	11.11	11.82	13.10
Na_2O	2.87	1.56	4.27	5.04	4.54	3.80
K_2O	0.05	0.00	0.05	0.12	0.14	0.11
Total	99.62	99.60	99.79	99.74	99.97	99.96
Oxygens	8	8	8	8	8	8
Si	2.245	2.113	2.339	2.419	2.384	2.310
Ti	0.000	0.000	0.000	0.000	0.000	0.000
Al	1.778	1.911	1.680	1.599	1.631	1.710
Cr	0.000	0.000	0.000	0.000	0.000	0.000
Fe^{3+}	0.000	0.000	0.000	0.000	0.000	0.000
Fe^{2+}	0.005	0.009	0.005	0.000	0.009	0.008
Ni	0.000	0.000	0.000	0.000	0.000	0.000
Mn	0.000	0.000	0.000	0.000	0.000	0.000
Mg	0.000	0.000	0.000	0.000	0.000	0.000
Ca	0.709	0.828	0.609	0.538	0.573	0.638
Na	0.254	0.139	0.376	0.442	0.398	0.335
K	0.003	0.000	0.003	0.007	0.008	0.006
Total Cations	4.995	5.001	5.011	5.006	5.004	5.006
Albite	26.3	14.4	38.1	44.8	40.7	34.2
Anorthite	73.4	85.6	61.6	54.5	58.5	65.1
Orthoclase	0.3	0.0	0.3	0.7	0.8	0.7

Appendix Table 3.11a. Electron microprobe analyses of oxide minerals from the Toby layered intrusion.

Sample no.	92522513	92522513	92522513	92522518	92522518	92522518	92522520	92522520	92522520	92522523
Analysis no.	65055	65056	65057	65094	65095	65096	57527	57529	57530	65113
Mineral	Ilmenite	Ilmenite	Ilmenite	Ilmenite	Ilmenite	Ilmenite	Ilmenite	Ilmenite	Ilmenite	Ilmenite
Description										
Lithology	Suboph. biot qtz gabbronor.	Suboph. biot qtz gabbronor.	Suboph. biot qtz gabbronor.	Suboph. biot qtz gabbronor.	Suboph. biot qtz gabbronor.	Suboph. biot qtz gabbronor.	Suboph. biot gabbronorite	Suboph. biot gabbronorite	Suboph. biot gabbronorite	Suboph. biot gabbronorite
Trav. dist. (m)	1750	1750	1750	3500	3500	3500	5200	5200	5200	9300
SiO_2	0.00	0.00	0.00	0.00	0.00	0.00	0.21	0.00	0.00	0.00
TiO_2	50.27	50.14	50.17	50.09	49.95	50.76	51.20	50.61	51.43	48.18
Al_2O_3	0.00	0.00	0.00	0.00	0.00	0.00	0.00	0.00	0.00	0.00
V_2O_3	0.00	0.00	0.00	0.00	0.00	0.00	0.00	0.00	0.00	0.00
Cr_2O_3	0.00	0.00	0.10	0.00	0.11	0.10	0.00	0.11	0.11	0.00
FeO	46.90	46.89	46.60	47.10	47.52	47.55	45.26	46.29	47.41	49.46
MnO	1.38	1.37	1.43	0.55	0.57	0.58	1.18	0.65	0.62	0.80
MgO	0.00	0.00	0.36	0.19	0.19	0.00	0.87	0.52	0.15	0.21
CaO	0.00	0.00	0.00	0.00	0.00	0.00	0.00	0.77	0.00	0.00
Total	98.55	98.40	98.66	97.93	98.34	98.99	98.72	98.95	99.72	98.65
Oxygens	3	3	3	3	3	3	3	3	3	3
Si	0.000	0.000	0.000	0.000	0.000	0.000	0.005	0.000	0.000	0.000
Ti	0.967	0.966	0.961	0.968	0.961	0.973	0.976	0.963	0.977	0.922
Al	0.000	0.000	0.000	0.000	0.000	0.000	0.000	0.000	0.000	0.000
V	0.000	0.000	0.000	0.000	0.000	0.000	0.000	0.000	0.000	0.000
Cr	0.000	0.000	0.002	0.000	0.002	0.002	0.000	0.002	0.002	0.000
Fe^{3+}	0.066	0.068	0.076	0.064	0.075	0.053	0.036	0.071	0.043	0.156
Fe^{2+}	0.937	0.936	0.916	0.949	0.942	0.960	0.924	0.909	0.958	0.897
Mn	0.030	0.030	0.031	0.012	0.012	0.013	0.025	0.014	0.013	0.017
Mg	0.000	0.000	0.014	0.007	0.007	0.000	0.033	0.020	0.006	0.008
Ca	0.000	0.000	0.000	0.000	0.000	0.000	0.000	0.021	0.000	0.000
Total Cations	2.000	2.000	2.000	2.000	2.000	2.000	2.000	2.000	2.000	2.000

Appendix Table 3.11a (cont.). Electron microprobe analyses of oxide minerals from the Toby layered intrusion.

Sample no.	92522523	92522524	92522524	Sample no.	92522513	92522520	92522520	92522520	92522520	92522524
Analysis no.	65115	65071	65072	Analysis no.	65058	57525	57526	57528	57531	65073
Mineral	Ilmenite	Ilmenite	Ilmenite	Mineral	Magnetite	Magnetite	Magnetite	Magnetite	Magnetite	Magnetite
Description				Description						
Lithology	Suboph. biot gabbronorite	Suboph. biot qtz gabbronor.	Suboph. biot qtz gabbronor.	Lithology	Suboph. biot qtz gabbronor.	Suboph. biot gabbronorite	Suboph. biot gabbronorite	Suboph. biot gabbronorite	Suboph. biot gabbronorite	Suboph. biot qtz gabbronor.
Trav. dist. (m)	9300	11400	11400	Trav. dist. (m)	1750	5200	5200	5200	5200	11400
SiO_2	0.00	0.00	0.00	SiO_2	0.00	0.17	0.00	0.09	0.00	0.00
TiO_2	49.27	50.46	50.23	TiO_2	0.16	0.26	0.12	0.15	0.25	0.25
Al_2O_3	0.00	0.00	0.00	Al_2O_3	0.00	0.22	0.65	0.23	0.28	0.00
V_2O_3	0.00	0.00	0.00	V_2O_3	1.36	1.84	0.55	0.55	2.19	1.31
Cr_2O_3	0.00	0.10	0.00	Cr_2O_3	0.43	1.59	0.74	0.95	4.13	1.75
FeO	48.78	46.91	46.77	FeO	91.29	90.48	92.26	91.70	89.13	89.88
MnO	0.69	0.77	0.70	MnO	0.00	0.14	0.16	0.00	0.11	0.14
MgO	0.18	0.23	0.18	MgO	0.00	0.00	0.00	0.00	0.00	0.00
CaO	0.00	0.00	0.00	CaO	0.00	0.00	0.00	0.00	0.00	0.00
Total	98.92	98.47	97.88	Total	93.24	94.71	94.48	93.66	96.08	93.34
Oxygens	3	3	3	Oxygens	32	32	32	32	32	32
Si	0.000	0.000	0.000	Si	0.000	0.054	0.000	0.028	0.000	0.000
Ti	0.942	0.970	0.972	Ti	0.037	0.061	0.027	0.035	0.058	0.060
Al	0.000	0.000	0.000	Al	0.000	0.082	0.243	0.087	0.102	0.000
V	0.000	0.000	0.000	V	0.343	0.466	0.138	0.137	0.546	0.331
Cr	0.000	0.002	0.000	Cr	0.107	0.397	0.184	0.235	1.015	0.436
Fe^{3+}	0.117	0.058	0.057	Fe^{3+}	15.477	14.824	15.381	15.418	14.222	15.114
Fe^{2+}	0.920	0.944	0.950	Fe^{2+}	8.037	8.077	7.984	8.062	8.030	8.024
Mn	0.015	0.017	0.015	Mn	0.000	0.038	0.044	0.000	0.028	0.037
Mg	0.007	0.009	0.007	Mg	0.000	0.000	0.000	0.000	0.000	0.000
Ca	0.000	0.000	0.000	Ca	0.000	0.000	0.000	0.000	0.000	0.000
Total Cations	2.000	2.000	2.000	Total Cations	24.001	24.001	24.001	24.001	24.001	24.001

Appendix Table 3.12. Electron microprobe analyses of silicate minerals from the Wilagee layered intrusion.

Sample no.	92522506	92522506	92522506	92522506	92522506	92522506	92522506
Analysis no.	57466	57467	57468	57469	57470	57471	57476
Mineral	Amphibole	Amphibole	Amphibole	Amphibole	Amphibole	Amphibole	Amphibole
Description	Alter. of cpx	Alter. of cpx	Alter. of cpx (r)	Alter. of cpx (r)	Alter. of cpx (c)	Alter. of cpx (c)	Alter. of cpx
Lithology	Troctolite	Troctolite	Troctolite	Troctolite	Troctolite	Troctolite	Troctolite
Strat. ht. (m)	70	70	70	70	70	70	70
SiO_2	52.87	50.31	45.92	48.17	48.98	50.11	50.44
TiO_2	0.16	0.35	1.85	0.41	0.40	0.28	0.00
Al_2O_3	4.48	7.75	10.70	9.53	8.72	7.66	8.25
Cr_2O_3	0.28	0.42	0.41	0.51	0.41	0.36	0.00
FeO*	5.09	5.82	6.13	6.00	5.79	5.85	5.82
MnO	0.00	0.00	0.00	0.00	0.00	0.00	0.00
NiO	0.00	0.00	0.00	0.00	0.00	0.00	0.00
MgO	21.78	19.96	18.34	19.34	19.50	20.02	20.68
CaO	11.89	12.17	12.29	12.11	12.29	12.07	11.41
Na_2O	0.38	1.14	1.86	1.40	1.54	1.26	1.32
K_2O	0.00	0.08	0.45	0.23	0.20	0.05	0.05
Total	96.93	98.00	97.95	97.70	97.83	97.66	97.97
Oxygens	23	23	23	23	23	23	23
Si	7.236	6.934	6.462	6.694	6.813	6.924	6.841
Ti	0.016	0.036	0.196	0.043	0.042	0.029	0.000
Al	0.723	1.259	1.774	1.561	1.429	1.247	1.319
Cr	0.030	0.046	0.046	0.056	0.045	0.039	0.000
Fe^{3+}	0.582	0.671	0.480	0.697	0.613	0.676	0.660
Fe^{2+}	0.000	0.000	0.242	0.000	0.061	0.000	0.000
Ni	0.000	0.000	0.000	0.000	0.000	0.000	0.000
Mn	0.000	0.000	0.000	0.000	0.000	0.000	0.000
Mg	4.443	4.100	3.847	4.006	4.043	4.123	4.180
Ca	1.743	1.797	1.853	1.803	1.831	1.787	1.658
Na	0.101	0.305	0.507	0.377	0.415	0.338	0.347
K	0.000	0.014	0.081	0.041	0.035	0.009	0.009
Total Cations	14.874	15.162	15.488	15.278	15.327	15.172	15.014
mg	100.0	100.0	94.1	100.0	98.5	100.0	100.0
Classification	Magnesio Hornblende	Magnesio Hornblende	Tschermakit Hornblende	Magnesio Hornblende	Magnesio Hornblende	Magnesio Hornblende	Magnesio Hornblende

Sample no.	92522502	92522502	92522502
Analysis no.	57563	57564	57566
Mineral	Clinopyroxene	Clinopyroxene	Clinopyroxene
Description	Intercumulus	Intercumulus	Intercumulus
Lithology	Olivine gabbronorite	Olivine gabbronorite	Olivine gabbronorite
Strat. ht. (m)	710	710	710
SiO_2	51.18	51.55	52.09
TiO_2	1.27	0.98	0.34
Al_2O_3	2.67	2.26	2.48
Cr_2O_3	0.00	0.00	0.65
FeO*	6.62	6.56	6.81
MnO	0.16	0.00	0.00
NiO	0.00	0.00	0.00
MgO	16.49	16.81	18.60
CaO	20.55	20.44	18.22
Na_2O	0.00	0.00	0.00
K_2O	0.00	0.00	0.00
Total	98.94	98.60	99.19
Oxygens	6	6	6
Si	1.903	1.920	1.916
Ti	0.036	0.027	0.009
Al	0.117	0.099	0.108
Cr	0.000	0.000	0.019
Fe^{3+}	0.005	0.006	0.022
Fe^{2+}	0.201	0.199	0.188
Ni	0.000	0.000	0.000
Mn	0.005	0.000	0.000
Mg	0.914	0.933	1.020
Ca	0.819	0.816	0.718
Na	0.000	0.000	0.000
K	0.000	0.000	0.000
Total Cations	4.000	4.000	4.000
mg	82.0	82.5	84.5
Enstatite	47.3	47.9	52.9
Ferrosilite	10.4	10.2	9.8
Wollastonite	42.3	41.9	37.3

Table 3.12 (cont). Electron microprobe analyses of silicate minerals from the Wilagee layered intrusion.

Sample no.	92522502	92522502	92522502	92522502	92522502
Analysis no.	57567	57568	57569	57571	57579
Mineral	Clinopyroxene	Clinopyroxene	Clinopyroxene	Clinopyroxene	Clinopyroxene
Description	Intercumulus	Intercumulus	Intercumulus	Intercumulus	Intercumulus
Lithology	Olivine gabbronorite	Olivine gabbronorite	Olivine gabbronorite	Olivine gabbronorite	Olivine gabbronorite
Strat. ht. (m)	710	710	710	710	710
SiO_2	52.16	51.98	52.11	53.56	51.12
TiO_2	0.38	0.35	0.36	0.21	0.98
Al_2O_3	2.00	2.28	2.41	0.88	2.79
Cr_2O_3	0.54	0.67	0.67	0.18	0.53
FeO*	5.95	6.46	5.59	4.03	5.66
MnO	0.12	0.00	0.00	0.00	0.15
NiO	0.00	0.00	0.00	0.00	0.00
MgO	17.30	17.69	17.49	17.18	16.08
CaO	20.52	19.70	20.89	23.76	21.81
Na_2O	0.00	0.00	0.00	0.00	0.00
K_2O	0.00	0.00	0.00	0.00	0.00
Total	98.97	99.13	99.52	99.80	99.12
Oxygens	6	6	6	6	6
Si	1.930	1.919	1.914	1.960	1.898
Ti	0.011	0.010	0.010	0.006	0.027
Al	0.087	0.099	0.104	0.038	0.122
Cr	0.016	0.020	0.019	0.005	0.016
Fe^{3+}	0.015	0.023	0.027	0.026	0.013
Fe^{2+}	0.169	0.176	0.144	0.097	0.163
Ni	0.000	0.000	0.000	0.000	0.000
Mn	0.004	0.000	0.000	0.000	0.005
Mg	0.954	0.974	0.958	0.937	0.890
Ca	0.814	0.779	0.822	0.931	0.867
Na	0.000	0.000	0.000	0.000	0.000
K	0.000	0.000	0.000	0.000	0.000
Total Cations	4.000	4.000	4.000	4.000	4.000
mg	84.9	84.7	86.9	90.6	84.5
Enstatite	49.3	50.5	49.8	47.7	46.3
Ferrosilite	8.7	9.1	7.5	4.9	8.5
Wollastonite	42.0	40.4	42.7	47.4	45.2

Sample no.	92522502	92522502	92522502	92522502	92522502
Analysis no.	1 - Tas	2 - Tas	3 - Tas	4 - Tas	5 - Tas
Mineral	Olivine	Olivine	Olivine	Olivine	Olivine
Description	Cumulus	Cumulus	Cumulus	Cumulus	Cumulus
Lithology	Olivine gabbronorite	Olivine gabbronorite	Olivine gabbronorite	Olivine gabbronorite	Olivine gabbronorite
Strat. ht. (m)	710	710	710	710	710
SiO_2	38.79	38.32	38.63	38.74	38.88
TiO_2	0.02	0.00	0.01	0.00	0.01
Al_2O_3	0.01	0.01	0.01	0.01	0.00
Cr_2O_3	0.00	0.05	0.06	0.00	0.01
FeO*	18.40	18.35	18.26	19.29	18.46
MnO	0.28	0.32	0.27	0.28	0.28
NiO	0.23	0.18	0.27	0.20	0.23
MgO	41.89	42.18	42.03	41.63	41.69
CaO	0.02	0.01	0.02	0.03	0.00
Na_2O	0.01	0.00	0.00	0.00	0.00
K_2O	0.00	0.00	0.00	0.00	0.00
Total	99.65	99.43	99.57	100.18	99.56
Oxygens	4	4	4	4	4
Si	0.994	0.982	0.990	0.990	0.998
Ti	0.000	0.000	0.000	0.000	0.000
Al	0.000	0.000	0.000	0.000	0.000
Cr	0.000	0.001	0.001	0.000	0.000
Fe^{3+}	0.012	0.034	0.018	0.019	0.004
Fe^{2+}	0.382	0.360	0.373	0.393	0.392
Ni	0.006	0.007	0.006	0.006	0.006
Mn	0.005	0.004	0.006	0.004	0.005
Mg	1.599	1.612	1.605	1.586	1.595
Ca	0.001	0.000	0.001	0.001	0.000
Na	0.001	0.000	0.000	0.000	0.000
K	0.000	0.000	0.000	0.000	0.000
Total Cations	3.000	3.000	3.000	2.999	3.000
mg	80.7	81.7	81.1	80.1	80.6

Table 3.12 (cont). Electron microprobe analyses of silicate minerals from the Wilagee layered intrusion.

Sample no.	92522502	92522502	92522502	92522502	92522502	92522502	92522502	92522502	92522502	92522502	92522502	92522502
Analysis no.	6 - Tas	7 - Tas	8 - Tas	9 - Tas	10 - Tas	11 - Tas	12 - Tas	13 - Tas	14 - Tas	15 - Tas	16 - Tas	18 - Tas
Mineral	Olivine	Olivine	Olivine	Olivine	Olivine	Olivine	Olivine	Olivine	Olivine	Olivine	Olivine	Olivine
Description	Cumulus	Cumulus	Cumulus	Cumulus	Cumulus	Cumulus	Cumulus	Cumulus	Cumulus	Cumulus	Cumulus	Cumulus
Lithology	Olivine gabbronorite	Olivine gabbronorite	Olivine gabbronorite	Olivine gabbronorite	Olivine gabbronorite	Olivine gabbronorite	Olivine gabbronorite	Olivine gabbronorite	Olivine gabbronorite	Olivine gabbronorite	Olivine gabbronorite	Olivine gabbronorite
Strat. ht. (m)	710	710	710	710	710	710	710	710	710	710	710	710
SiO_2	38.66	38.19	38.48	38.06	38.48	39.00	38.83	38.92	38.90	38.80	38.76	38.55
TiO_2	0.00	0.03	0.02	0.03	0.01	0.03	0.02	0.00	0.02	0.02	0.04	0.02
Al_2O_3	0.01	0.02	0.02	0.00	0.01	0.00	0.01	0.01	0.01	0.00	0.00	0.00
Cr_2O_3	0.00	0.00	0.00	0.00	0.01	0.01	0.00	0.03	0.05	0.00	0.01	0.01
FeO*	19.34	19.47	19.13	19.33	19.35	19.33	18.86	18.94	19.40	18.91	19.95	19.99
MnO	0.30	0.28	0.23	0.23	0.36	0.29	0.26	0.29	0.24	0.27	0.28	0.23
NiO	0.22	0.20	0.24	0.23	0.28	0.19	0.28	0.18	0.29	0.29	0.24	0.27
MgO	41.51	41.09	41.23	41.20	41.38	42.02	41.63	42.05	41.47	41.87	41.15	41.37
CaO	0.00	0.00	0.07	0.01	0.06	0.05	0.00	0.00	0.17	0.01	0.00	0.01
Na_2O	0.00	0.00	0.00	0.00	0.00	0.00	0.00	0.00	0.00	0.00	0.00	0.00
K_2O	0.00	0.00	0.00	0.00	0.00	0.00	0.00	0.00	0.00	0.00	0.00	0.00
Total	100.05	99.28	99.43	99.09	99.95	100.92	99.90	100.43	100.56	100.17	100.43	100.46
Oxygens	4	4	4	4	4	4	4	4	4	4	4	4
Si	0.990	0.986	0.991	0.984	0.987	0.989	0.994	0.991	0.992	0.990	0.992	0.985
Ti	0.000	0.001	0.000	0.001	0.000	0.001	0.000	0.000	0.000	0.000	0.001	0.000
Al	0.000	0.001	0.001	0.000	0.000	0.000	0.000	0.000	0.000	0.000	0.000	0.000
Cr	0.000	0.000	0.000	0.000	0.000	0.000	0.000	0.001	0.001	0.000	0.000	0.000
Fe^{3+}	0.020	0.026	0.016	0.031	0.025	0.020	0.010	0.018	0.014	0.018	0.015	0.028
Fe^{2+}	0.395	0.395	0.397	0.387	0.390	0.390	0.394	0.385	0.400	0.386	0.412	0.399
Ni	0.007	0.006	0.005	0.005	0.008	0.006	0.006	0.006	0.005	0.006	0.006	0.005
Mn	0.005	0.004	0.005	0.005	0.006	0.004	0.006	0.004	0.006	0.006	0.005	0.006
Mg	1.584	1.582	1.583	1.587	1.582	1.588	1.589	1.595	1.576	1.593	1.569	1.576
Ca	0.000	0.000	0.002	0.000	0.002	0.001	0.000	0.000	0.005	0.000	0.000	0.000
Na	0.000	0.000	0.000	0.000	0.000	0.000	0.000	0.000	0.000	0.000	0.000	0.000
K	0.000	0.000	0.000	0.000	0.000	0.000	0.000	0.000	0.000	0.000	0.000	0.000
Total Cations	3.001	3.001	3.000	3.000	3.000	2.999	2.999	3.000	2.999	2.999	3.000	2.999
mg	80.0	80.0	79.9	80.4	80.2	80.3	80.1	80.6	80.0	80.5	79.2	79.9

Table 3.12 (cont). Electron microprobe analyses of silicate minerals from the Wilagee layered intrusion.

Sample no.	92522502	92522502	92522502	92522502	92522502	92522502	92522502	92522502	92522502	92522502	92522502	92522502
Analysis no.	19 - Tas	20 - Tas	30 - Tas	57572	57573	57575	57576	57577	57578	64988	64989	64990
Mineral	Olivine	Olivine	Olivine	Olivine	Olivine	Olivine	Olivine	Olivine	Olivine	Olivine	Olivine	Olivine
Description	Cumulus	Cumulus	Cumulus	Cumulus	Cumulus (c)	Cumulus	Cumulus	Cumulus (r)	Cumulus (c)	Cumulus	Cumulus	Cumulus
Lithology	Olivine gabbronorite	Olivine gabbronorite	Olivine gabbronorite	Olivine gabbronorite	Olivine gabbronorite	Olivine gabbronorite	Olivine gabbronorite	Olivine gabbronorite	Olivine gabbronorite	Olivine gabbronorite	Olivine gabbronorite	Olivine gabbronorite
Strat. ht. (m)	710	710	710	710	710	710	710	710	710	710	710	710
SiO_2	38.54	38.75	38.82	38.11	37.91	38.27	38.34	38.36	38.38	38.51	38.60	38.38
TiO_2	0.05	0.03	0.03	0.00	0.00	0.00	0.00	0.00	0.00	0.00	0.00	0.00
Al_2O_3	0.00	0.00	0.00	0.00	0.00	0.00	0.00	0.00	0.00	0.00	0.00	0.00
Cr_2O_3	0.00	0.05	0.00	0.00	0.00	0.00	0.00	0.00	0.00	0.00	0.00	0.00
FeO*	19.79	19.50	19.27	21.13	20.83	19.86	20.09	19.38	19.40	19.56	19.19	19.38
MnO	0.27	0.34	0.34	0.15	0.15	0.20	0.10	0.23	0.17	0.16	0.13	0.15
NiO	0.22	0.22	0.23	0.00	0.00	0.00	0.00	0.00	0.00	0.00	0.00	0.00
MgO	41.21	41.23	42.02	40.96	40.53	41.81	41.68	42.18	41.86	41.97	41.98	42.23
CaO	0.03	0.01	0.02	0.00	0.00	0.00	0.00	0.00	0.00	0.00	0.00	0.00
Na_2O	0.00	0.01	0.00	0.00	0.00	0.00	0.00	0.00	0.00	0.00	0.00	0.00
K_2O	0.00	0.00	0.00	0.00	0.00	0.00	0.00	0.00	0.00	0.00	0.00	0.00
Total	100.12	100.14	100.73	100.34	99.42	100.15	100.21	100.15	99.81	100.20	99.90	100.14
Oxygens	4	4	4	4	4	4	4	4	4	4	4	4
Si	0.988	0.993	0.986	0.978	0.982	0.978	0.980	0.978	0.983	0.983	0.987	0.979
Ti	0.001	0.001	0.001	0.000	0.000	0.000	0.000	0.000	0.000	0.000	0.000	0.000
Al	0.000	0.000	0.000	0.000	0.000	0.000	0.000	0.000	0.000	0.000	0.000	0.000
Cr	0.000	0.001	0.000	0.000	0.000	0.000	0.000	0.000	0.000	0.000	0.000	0.000
Fe^{3+}	0.021	0.012	0.026	0.045	0.037	0.043	0.039	0.043	0.034	0.035	0.026	0.043
Fe^{2+}	0.403	0.405	0.383	0.408	0.414	0.381	0.390	0.370	0.381	0.383	0.384	0.370
Ni	0.006	0.007	0.007	0.003	0.003	0.004	0.002	0.005	0.004	0.003	0.003	0.003
Mn	0.005	0.005	0.005	0.000	0.000	0.000	0.000	0.000	0.000	0.000	0.000	0.000
Mg	1.575	1.575	1.591	1.566	1.564	1.593	1.588	1.603	1.598	1.596	1.600	1.605
Ca	0.001	0.000	0.001	0.000	0.000	0.000	0.000	0.000	0.000	0.000	0.000	0.000
Na	0.000	0.001	0.000	0.000	0.000	0.000	0.000	0.000	0.000	0.000	0.000	0.000
K	0.000	0.000	0.000	0.000	0.000	0.000	0.000	0.000	0.000	0.000	0.000	0.000
Total Cations	3.000	3.000	3.000	3.000	3.000	2.999	2.999	2.999	3.000	3.000	3.000	3.000
mg	79.6	79.5	80.6	79.3	79.1	80.7	80.4	81.2	80.7	80.6	80.6	81.3

Table 3.12 (cont). Electron microprobe analyses of silicate minerals from the Wilagee layered intrusion.

Sample no.	92522502	92522502	92522502	92522502	92522502	92522506	92522506	92522506	92522506	92522506	92522506	92522506	92522506
Analysis no.	64991	64992	64993	64994	65001	57402	57403	57404	57405	57457	57458	57459	57460
Mineral	Olivine	Olivine	Olivine	Olivine	Olivine	Olivine	Olivine	Olivine	Olivine	Olivine	Olivine	Olivine	Olivine
Description	Cumulus	Cumulus	Cumulus	Cumulus	Cumulus	Cumulus	Cumulus (r)	Cumulus (c)	Cumulus (c)	Cumulus	Cumulus	Cumulus	Cumulus
Lithology	Olivine gabbronorite	Olivine gabbronorite	Olivine gabbronorite	Olivine gabbronorite	Olivine gabbronorite	Troctolite	Troctolite	Troctolite	Troctolite	Troctolite	Troctolite	Troctolite	Troctolite
Strat. ht. (m)	710	710	710	710	710	70	70	70	70	70	70	70	70
SiO_2	38.35	38.15	38.26	38.20	38.17	39.11	38.71	39.03	38.48	39.03	38.98	38.55	38.56
TiO_2	0.00	0.00	0.00	0.00	0.00	0.00	0.00	0.00	0.00	0.00	0.00	0.00	0.00
Al_2O_3	0.00	0.00	0.00	0.00	0.00	0.00	0.00	0.00	0.00	0.00	0.00	0.00	0.00
Cr_2O_3	0.00	0.00	0.00	0.00	0.00	0.00	0.00	0.00	0.00	0.00	0.00	0.00	0.00
FeO*	20.69	20.69	20.57	20.65	20.38	17.21	17.63	17.19	17.44	17.24	17.38	18.76	18.80
MnO	0.12	0.11	0.13	0.17	0.19	0.00	0.00	0.11	0.00	0.12	0.00	0.11	0.12
NiO	0.00	0.00	0.00	0.00	0.00	0.00	0.00	0.00	0.00	0.00	0.00	0.00	0.00
MgO	40.69	40.65	41.30	40.68	41.31	43.95	43.43	43.92	43.52	43.91	43.82	42.69	42.43
CaO	0.00	0.00	0.00	0.00	0.00	0.00	0.00	0.05	0.00	0.00	0.00	0.00	0.00
Na_2O	0.00	0.00	0.00	0.00	0.00	0.00	0.00	0.05	0.00	0.00	0.00	0.00	0.00
K_2O	0.00	0.00	0.00	0.00	0.00	0.00	0.00	0.00	0.00	0.00	0.00	0.00	0.00
Total	99.85	99.60	100.26	99.70	100.05	100.26	99.76	100.34	99.44	100.29	100.19	100.11	99.91
Oxygens	4	4	4	4	4	4	4	4	4	4	4	4	4
Si	0.988	0.985	0.980	0.986	0.979	0.986	0.983	0.983	0.979	0.984	0.984	0.980	0.983
Ti	0.000	0.000	0.000	0.000	0.000	0.000	0.000	0.000	0.000	0.000	0.000	0.000	0.000
Al	0.000	0.000	0.000	0.000	0.000	0.000	0.000	0.000	0.000	0.000	0.000	0.000	0.000
Cr	0.000	0.000	0.000	0.000	0.000	0.000	0.000	0.000	0.000	0.000	0.000	0.000	0.000
Fe^{3+}	0.023	0.029	0.040	0.028	0.042	0.028	0.035	0.036	0.042	0.032	0.032	0.039	0.033
Fe^{2+}	0.423	0.418	0.400	0.417	0.396	0.334	0.339	0.326	0.329	0.331	0.335	0.360	0.368
Ni	0.003	0.002	0.003	0.004	0.004	0.000	0.000	0.000	0.000	0.000	0.000	0.000	0.000
Mn	0.000	0.000	0.000	0.000	0.000	0.000	0.000	0.002	0.000	0.003	0.000	0.002	0.003
Mg	1.563	1.565	1.577	1.565	1.580	1.651	1.643	1.649	1.650	1.650	1.649	1.618	1.613
Ca	0.000	0.000	0.000	0.000	0.000	0.000	0.000	0.001	0.000	0.000	0.000	0.000	0.000
Na	0.000	0.000	0.000	0.000	0.000	0.000	0.000	0.002	0.000	0.000	0.000	0.000	0.000
K	0.000	0.000	0.000	0.000	0.000	0.000	0.000	0.000	0.000	0.000	0.000	0.000	0.000
Total Cations	3.000	2.999	3.000	3.000	3.001	2.999	3.000	2.999	3.000	3.000	3.000	2.999	3.000
mg	78.7	78.9	79.8	79.0	80.0	83.2	83.0	83.5	83.4	83.3	83.1	81.8	81.4

Table 3.12 (cont). Electron microprobe analyses of silicate minerals from the Wilagee layered intrusion.

Sample no.	92522506	92522506	92522506	92522506	92522506	92522506	92522506	92522506	92522506	92522506	92522506	92522506	92522506
Analysis no.	57461	57462	57463	57464	57465	65014	65016	65017	65018	65019	65020	65021	65022
Mineral	Olivine	Olivine	Olivine	Olivine	Olivine	Olivine	Olivine	Olivine	Olivine	Olivine	Olivine	Olivine	Olivine
Description	Cumulus (c)	Cumulus (r)	Cumulus (c)	Cumulus (r)	Cumulus (c)	Cumulus (r)	Cumulus (c)	Cumulus (r)	Cumulus (c)	Cumulus (r)	Cumulus (c)	Cumulus (c)	Cumulus (c)
Lithology	Troctolite	Troctolite	Troctolite	Troctolite	Troctolite	Troctolite	Troctolite	Troctolite	Troctolite	Troctolite	Troctolite	Troctolite	Troctolite
Strat. ht. (m)	70	70	70	70	70	70	70	70	70	70	70	70	70
SiO_2	38.94	38.85	38.87	38.72	39.11	38.85	39.15	38.97	39.08	39.09	39.01	38.84	38.65
TiO_2	0.00	0.00	0.00	0.00	0.00	0.00	0.00	0.00	0.00	0.00	0.00	0.00	0.00
Al_2O_3	0.00	0.00	0.00	0.00	0.00	0.00	0.00	0.00	0.00	0.00	0.00	0.00	0.00
Cr_2O_3	0.00	0.00	0.00	0.00	0.00	0.00	0.00	0.00	0.00	0.00	0.00	0.00	0.00
FeO*	17.23	17.75	17.81	17.86	17.60	16.81	17.36	17.52	17.57	17.98	17.29	17.82	18.32
MnO	0.00	0.24	0.00	0.10	0.23	0.13	0.12	0.14	0.00	0.12	0.13	0.00	0.10
NiO	0.00	0.00	0.00	0.00	0.00	0.00	0.00	0.00	0.00	0.00	0.00	0.00	0.00
MgO	43.93	43.67	43.70	43.73	44.53	43.63	43.68	43.49	43.57	42.69	43.41	43.05	42.84
CaO	0.00	0.00	0.00	0.00	0.00	0.00	0.00	0.00	0.00	0.08	0.00	0.00	0.00
Na_2O	0.00	0.00	0.00	0.00	0.00	0.00	0.00	0.00	0.00	0.00	0.00	0.00	0.00
K_2O	0.00	0.00	0.00	0.00	0.00	0.00	0.00	0.00	0.00	0.00	0.00	0.00	0.00
Total	100.10	100.50	100.38	100.40	101.46	99.42	100.31	100.12	100.22	99.96	99.84	99.71	99.91
Oxygens	4	4	4	4	4	4	4	4	4	4	4	4	4
Si	0.983	0.980	0.981	0.977	0.975	0.987	0.988	0.986	0.988	0.994	0.989	0.988	0.983
Ti	0.000	0.000	0.000	0.000	0.000	0.000	0.000	0.000	0.000	0.000	0.000	0.000	0.000
Al	0.000	0.000	0.000	0.000	0.000	0.000	0.000	0.000	0.000	0.000	0.000	0.000	0.000
Cr	0.000	0.000	0.000	0.000	0.000	0.000	0.000	0.000	0.000	0.000	0.000	0.000	0.000
Fe^{3+}	0.034	0.041	0.038	0.046	0.051	0.025	0.024	0.028	0.025	0.011	0.021	0.024	0.033
Fe^{2+}	0.330	0.334	0.337	0.330	0.316	0.332	0.342	0.343	0.346	0.371	0.346	0.356	0.357
Ni	0.000	0.000	0.000	0.000	0.000	0.000	0.000	0.000	0.000	0.000	0.000	0.000	0.000
Mn	0.000	0.005	0.000	0.002	0.005	0.003	0.003	0.003	0.000	0.003	0.003	0.000	0.002
Mg	1.653	1.641	1.643	1.644	1.654	1.653	1.643	1.640	1.641	1.618	1.641	1.633	1.625
Ca	0.000	0.000	0.000	0.000	0.000	0.000	0.000	0.000	0.000	0.002	0.000	0.000	0.000
Na	0.000	0.000	0.000	0.000	0.000	0.000	0.000	0.000	0.000	0.000	0.000	0.000	0.000
K	0.000	0.000	0.000	0.000	0.000	0.000	0.000	0.000	0.000	0.000	0.000	0.000	0.000
Total Cations	3.000	3.001	2.999	2.999	3.001	3.000	3.000	3.000	3.000	2.999	3.000	3.001	3.000
mg	83.4	83.1	83.0	83.3	84.0	83.3	82.8	82.7	82.8	81.3	82.6	82.1	82.0

Table 3.12 (cont). Electron microprobe analyses of silicate minerals from the Wilagee layered intrusion.

Sample no.	92522506	92522506
Analysis no.	65023	65024
Mineral	Olivine	Olivine
Description	Cumulus	Cumulus
Lithology	Troctolite	Troctolite
Strat. ht. (m)	70	70
SiO_2	38.99	39.24
TiO_2	0.00	0.00
Al_2O_3	0.00	0.00
Cr_2O_3	0.00	0.00
FeO*	17.99	17.66
MnO	0.00	0.00
NiO	0.00	0.00
MgO	43.08	43.74
CaO	0.00	0.00
Na_2O	0.00	0.00
K_2O	0.00	0.00
Total	100.06	100.64
Oxygens	4	4
Si	0.989	0.988
Ti	0.000	0.000
Al	0.000	0.000
Cr	0.000	0.000
Fe^{3+}	0.022	0.025
Fe^{2+}	0.360	0.347
Ni	0.000	0.000
Mn	0.000	0.000
Mg	1.629	1.641
Ca	0.000	0.000
Na	0.000	0.000
K	0.000	0.000
Total Cations	3.000	3.001
mg	81.9	82.5

Sample no.	92522502	92522502	92522502	92522502	92522502	92522502
Analysis no.	57560	57561	57570	57580	57581	57582
Mineral	Orthopyroxene	Orthopyroxene	Orthopyroxene	Orthopyroxene	Orthopyroxene	Orthopyroxene
Description	Cumulus (r)	Cumulus (c)	Cumulus (c)	Cumulus (r)	Cumulus (c)	Cumulus (c)
Lithology	Olivine gabbronorite	Olivine gabbronorite	Olivine gabbronorite	Olivine gabbronorite	Olivine gabbronorite	Olivine gabbronorite
Strat. ht. (m)	710	710	710	710	710	710
SiO_2	54.44	55.09	54.48	54.42	54.45	54.54
TiO_2	0.48	0.32	0.36	0.24	0.31	0.33
Al_2O_3	1.02	1.00	1.22	0.99	1.15	1.32
Cr_2O_3	0.00	0.00	0.00	0.00	0.00	0.00
FeO*	12.83	12.94	12.78	12.74	12.94	12.55
MnO	0.18	0.00	0.28	0.10	0.13	0.18
NiO	0.00	0.00	0.00	0.00	0.00	0.00
MgO	29.18	29.63	29.58	28.97	29.48	29.02
CaO	1.59	1.28	1.12	2.00	1.49	1.90
Na_2O	0.00	0.00	0.00	0.00	0.00	0.00
K_2O	0.00	0.00	0.00	0.00	0.00	0.00
Total	99.89	100.40	100.01	99.65	100.19	99.99
Oxygens	6	6	6	6	6	6
Si	1.943	1.952	1.939	1.947	1.936	1.943
Ti	0.013	0.009	0.010	0.006	0.008	0.009
Al	0.043	0.042	0.051	0.042	0.048	0.055
Cr	0.000	0.000	0.000	0.000	0.000	0.000
Fe^{3+}	0.046	0.036	0.052	0.052	0.063	0.041
Fe^{2+}	0.337	0.347	0.328	0.329	0.321	0.333
Ni	0.000	0.000	0.000	0.000	0.000	0.000
Mn	0.005	0.000	0.008	0.003	0.004	0.005
Mg	1.552	1.565	1.569	1.545	1.562	1.541
Ca	0.061	0.049	0.043	0.077	0.057	0.073
Na	0.000	0.000	0.000	0.000	0.000	0.000
K	0.000	0.000	0.000	0.000	0.000	0.000
Total Cations	4.000	4.000	4.000	4.000	4.000	4.000
mg	82.2	81.9	82.7	82.5	82.9	82.2
Enstatite	79.6	79.8	80.9	79.2	80.5	79.2
Ferrosilite	17.3	17.7	16.9	16.9	16.6	17.1
Wollastonite	3.1	2.5	2.2	3.9	2.9	3.7

Table 3.12 (cont). Electron microprobe analyses of silicate minerals from the Wilagee layered intrusion.

Sample no.	92522502	92522502	92522502	92522502	92522502	92522502	92522502	92522502	92522502	92522502	92522502	92522502
Analysis no.	21 - Tas	22 - Tas	23 - Tas	24 - Tas	25 - Tas	26 - Tas	27 - Tas	28 - Tas	29 - Tas	57558	57559	57561
Mineral	Plagioclase	Plagioclase	Plagioclase	Plagioclase	Plagioclase	Plagioclase	Plagioclase	Plagioclase	Plagioclase	Plagioclase	Plagioclase	Plagioclase
Description	Cumulus	Cumulus	Cumulus	Cumulus	Cumulus	Cumulus	Cumulus	Cumulus	Cumulus	Cumulus	Cumulus	Cumulus
Lithology	Olivine gabbronorite	Olivine gabbronorite	Olivine gabbronorite	Olivine gabbronorite	Olivine gabbronorite	Olivine gabbronorite	Olivine gabbronorite	Olivine gabbronorite	Olivine gabbronorite	Olivine gabbronorite	Olivine gabbronorite	Olivine gabbronorite
Strat. ht. (m)	710	710	710	710	710	710	710	710	710	710	710	710
SiO_2	45.61	45.49	46.46	46.71	46.21	47.24	46.49	46.26	46.53	46.29	45.83	46.50
TiO_2	0.01	0.02	0.04	0.01	0.00	0.01	0.00	0.04	0.06	0.00	0.00	0.00
Al_2O_3	34.41	34.90	34.11	34.35	34.27	33.91	34.31	34.14	34.31	34.60	35.20	34.74
Cr_2O_3	0.00	0.00	0.01	0.07	0.00	0.00	0.00	0.00	0.01	0.00	0.00	0.00
FeO*	0.29	0.33	0.24	0.34	0.28	0.33	0.42	0.28	0.30	0.21	0.14	0.27
MnO	0.01	0.00	0.04	0.03	0.03	0.00	0.00	0.02	0.02	0.00	0.00	0.00
NiO	0.00	0.00	0.00	0.00	0.00	0.00	0.00	0.00	0.00	0.00	0.00	0.00
MgO	0.00	0.01	0.00	0.00	0.06	0.07	0.04	0.04	0.03	0.00	0.00	0.00
CaO	17.48	17.66	17.00	16.97	17.25	16.70	17.23	17.37	17.55	16.55	16.98	16.51
Na_2O	1.64	1.39	1.81	1.88	1.88	2.09	1.78	1.69	1.60	1.58	1.27	1.76
K_2O	0.01	0.07	0.04	0.04	0.04	0.17	0.05	0.07	0.03	0.00	0.08	0.09
Total	99.46	99.87	99.75	100.40	100.02	100.52	100.32	99.91	100.44	99.23	99.51	99.88
Oxygens	8	8	8	8	8	8	8	8	8	8	8	8
Si	2.113	2.100	2.142	2.140	2.128	2.161	2.134	2.133	2.133	2.138	2.113	2.137
Ti	0.000	0.001	0.001	0.000	0.000	0.000	0.000	0.001	0.002	0.000	0.000	0.000
Al	1.879	1.899	1.853	1.855	1.860	1.829	1.856	1.855	1.854	1.884	1.913	1.881
Cr	0.000	0.000	0.000	0.003	0.000	0.000	0.000	0.000	0.000	0.000	0.000	0.000
Fe^{3+}	0.000	0.000	0.000	0.000	0.000	0.000	0.000	0.000	0.000	0.000	0.000	0.000
Fe^{2+}	0.011	0.013	0.009	0.013	0.011	0.013	0.016	0.011	0.012	0.008	0.005	0.011
Ni	0.000	0.000	0.000	0.000	0.000	0.000	0.000	0.000	0.000	0.000	0.000	0.000
Mn	0.000	0.000	0.002	0.001	0.001	0.000	0.000	0.001	0.001	0.000	0.000	0.000
Mg	0.000	0.001	0.000	0.000	0.004	0.005	0.003	0.003	0.002	0.000	0.000	0.000
Ca	0.868	0.873	0.840	0.833	0.851	0.819	0.847	0.858	0.862	0.819	0.839	0.813
Na	0.147	0.124	0.162	0.167	0.168	0.185	0.158	0.151	0.142	0.141	0.114	0.157
K	0.001	0.004	0.002	0.002	0.002	0.010	0.003	0.004	0.002	0.000	0.005	0.005
Total Cations	5.021	5.014	5.012	5.015	5.026	5.022	5.018	5.016	5.010	4.991	4.989	5.004
Albite	14.5	12.4	16.1	16.7	16.4	18.3	15.7	14.9	14.1	14.7	11.9	16.1
Anorthite	85.4	87.2	83.7	83.1	83.4	80.7	84.0	84.7	85.7	85.3	87.6	83.4
Orthoclase	0.1	0.4	0.2	0.2	0.2	1.0	0.3	0.4	0.2	0.0	0.5	0.5

Table 3.12 (cont). Electron microprobe analyses of silicate minerals from the Wilagee layered intrusion.

Sample no.	92522502	92522502	92522502	92522502	92522502	92522502	92522502	92522506	92522506	92522506	92522506	92522506
Analysis no.	57565	57574	64995	64996	64997	64998	64999	57472	57473	57474	57475	65025
Mineral	Plagioclase	Plagioclase	Plagioclase	Plagioclase	Plagioclase	Plagioclase	Plagioclase	Plagioclase	Plagioclase	Plagioclase	Plagioclase	Plagioclase
Description	Cumulus	Cumulus	Cumulus (c)	Cumulus (r)	Cumulus (r)	Cumulus (c)	Cumulus (c)	Cumulus (r)	Cumulus (c)	Cumulus	Cumulus	Cumulus (r)
Lithology	Olivine gabbronorite	Olivine gabbronorite	Olivine gabbronorite	Olivine gabbronorite	Olivine gabbronorite	Olivine gabbronorite	Olivine gabbronorite	Troctolite	Troctolite	Troctolite	Troctolite	Troctolite
Strat. ht. (m)	710	710	710	710	710	710	710	70	70	70	70	70
SiO_2	45.95	45.95	46.74	46.91	47.07	46.88	47.03	47.29	47.51	48.19	48.09	47.75
TiO_2	0.00	0.00	0.00	0.00	0.00	0.00	0.00	0.00	0.00	0.00	0.00	0.00
Al_2O_3	35.21	35.38	34.87	34.99	34.53	34.85	34.65	34.59	34.30	34.66	34.45	34.81
Cr_2O_3	0.00	0.00	0.00	0.00	0.00	0.00	0.00	0.00	0.00	0.00	0.00	0.00
FeO*	0.13	0.21	0.18	0.24	0.24	0.19	0.32	0.28	0.55	0.13	0.21	0.18
MnO	0.00	0.00	0.00	0.00	0.00	0.00	0.00	0.00	0.00	0.00	0.00	0.00
NiO	0.00	0.00	0.00	0.00	0.00	0.00	0.00	0.00	0.00	0.00	0.00	0.00
MgO	0.00	0.00	0.00	0.00	0.00	0.00	0.00	0.00	0.00	0.00	0.00	0.00
CaO	17.30	17.00	16.77	16.35	16.30	16.51	16.33	16.25	16.09	16.12	15.93	16.07
Na_2O	1.43	1.40	1.66	1.79	1.85	1.56	1.84	1.91	1.94	2.26	2.30	2.19
K_2O	0.06	0.49	0.07	0.00	0.00	0.00	0.09	0.07	0.19	0.09	0.00	0.00
Total	100.08	100.43	100.29	100.28	99.99	99.99	100.26	100.39	100.58	101.45	100.98	101.00
Oxygens	8	8	8	8	8	8	8	8	8	8	8	8
Si	2.110	2.107	2.138	2.143	2.156	2.146	2.151	2.158	2.167	2.174	2.179	2.164
Ti	0.000	0.000	0.000	0.000	0.000	0.000	0.000	0.000	0.000	0.000	0.000	0.000
Al	1.906	1.911	1.880	1.884	1.864	1.881	1.868	1.861	1.844	1.844	1.840	1.859
Cr	0.000	0.000	0.000	0.000	0.000	0.000	0.000	0.000	0.000	0.000	0.000	0.000
Fe^{3+}	0.000	0.000	0.000	0.000	0.000	0.000	0.000	0.000	0.000	0.000	0.000	0.000
Fe^{2+}	0.005	0.008	0.007	0.009	0.009	0.007	0.012	0.011	0.021	0.005	0.008	0.007
Ni	0.000	0.000	0.000	0.000	0.000	0.000	0.000	0.000	0.000	0.000	0.000	0.000
Mn	0.000	0.000	0.000	0.000	0.000	0.000	0.000	0.000	0.000	0.000	0.000	0.000
Mg	0.000	0.000	0.000	0.000	0.000	0.000	0.000	0.000	0.000	0.000	0.000	0.000
Ca	0.851	0.835	0.822	0.800	0.800	0.810	0.800	0.795	0.787	0.779	0.774	0.780
Na	0.127	0.125	0.147	0.159	0.164	0.138	0.163	0.169	0.172	0.198	0.202	0.192
K	0.003	0.029	0.004	0.000	0.000	0.000	0.005	0.004	0.011	0.005	0.000	0.000
Total Cations	5.002	5.014	4.998	4.995	4.994	4.983	4.999	4.998	5.002	5.005	5.002	5.003
Albite	13.0	12.6	15.1	16.5	17.0	14.6	16.9	17.5	17.7	20.2	20.7	19.8
Anorthite	86.6	84.5	84.5	83.5	83.0	85.4	82.5	82.1	81.2	79.3	79.3	80.2
Orthoclase	0.4	2.9	0.4	0.0	0.0	0.0	0.6	0.4	1.1	0.5	0.0	0.0

Table 3.12 (cont). Electron microprobe analyses of silicate minerals from the Wilagee layered intrusion.

Sample no.	92522506	92522506	92522506
Analysis no.	65026	65027	65028
Mineral	Plagioclase	Plagioclase	Plagioclase
Description	Cumulus (c)	Cumulus (r)	Cumulus (c)
Lithology	Troctolite	Troctolite	Troctolite
Strat. ht. (m)	70	70	70
SiO_2	47.54	47.70	47.69
TiO_2	0.00	0.00	0.00
Al_2O_3	34.60	34.64	34.39
Cr_2O_3	0.00	0.00	0.00
FeO*	0.15	0.00	0.24
MnO	0.00	0.00	0.00
NiO	0.00	0.00	0.00
MgO	0.00	0.00	0.00
CaO	15.96	15.92	16.06
Na_2O	2.05	2.06	2.08
K_2O	0.12	0.00	0.08
Total	100.42	100.32	100.54
Oxygens	8	8	8
Si	2.167	2.172	2.172
Ti	0.000	0.000	0.000
Al	1.858	1.859	1.846
Cr	0.000	0.000	0.000
Fe^{3+}	0.000	0.000	0.000
Fe^{2+}	0.006	0.000	0.009
Ni	0.000	0.000	0.000
Mn	0.000	0.000	0.000
Mg	0.000	0.000	0.000
Ca	0.779	0.777	0.784
Na	0.181	0.182	0.184
K	0.007	0.000	0.005
Total Cations	4.998	4.989	4.999
Albite	18.7	19.0	18.9
Anorthite	80.6	81.0	80.6
Orthoclase	0.7	0.0	0.5

Appendix Table 3.12a. Electron microprobe analyses of oxide minerals from the Wilagee layered intrusion.

Sample no.	92522502	92522502	92522502	92522502
Analysis no.	57594	57595	57598	57599
Mineral	Ilmenite	Ilmenite	Ilmenite	Ilmenite
Description	Intercumulus	Intercumulus	Intercumulus	Intercumulus
Lithology	Olivine gabbronorite	Olivine gabbronorite	Olivine gabbronorite	Olivine gabbronorite
Strat. ht. (m)	710	710	710	710
TiO_2	51.10	51.08	50.74	50.72
Al_2O_3	0.00	0.00	0.00	0.00
V_2O_3	0.00	0.00	0.00	0.00
Cr_2O_3	0.73	0.68	1.26	0.86
FeO*	43.86	43.76	44.15	43.85
MnO	0.85	0.83	0.94	0.84
MgO	1.83	1.63	1.69	1.78
CaO	0.14	0.00	0.00	0.00
Total	98.51	97.99	98.78	98.06
Oxygens	3	3	3	3
Ti	0.969	0.976	0.961	0.967
Al	0.000	0.000	0.000	0.000
V	0.000	0.000	0.000	0.000
Cr	0.014	0.014	0.025	0.017
Fe^{3+}	0.047	0.033	0.053	0.048
Fe^{2+}	0.878	0.897	0.878	0.882
Mn	0.018	0.018	0.020	0.018
Mg	0.069	0.062	0.064	0.067
Ca	0.004	0.000	0.000	0.000
Total Cations	2.000	2.000	2.000	2.000

Sample no.	92522502	92522502	92522502	92522502	92522502
Analysis no.	57588	57589	57590	57591	57592
Mineral	Spinel	Spinel	Spinel	Spinel	Spinel
Description	Cumulus	Cumulus	Cumulus	Cumulus	Cumulus
Lithology	Olivine gabbronorite	Olivine gabbronorite	Olivine gabbronorite	Olivine gabbronorite	Olivine gabbronorite
Strat. ht. (m)	710	710	710	710	710
TiO_2	0.45	0.58	0.62	0.10	0.87
Al_2O_3	12.00	11.73	9.26	28.54	29.59
V_2O_3	1.09	1.08	1.03	0.31	0.25
Cr_2O_3	30.54	31.04	26.78	27.84	26.89
FeO*	51.51	51.53	58.58	32.35	32.29
MnO	0.65	0.44	0.38	0.25	0.24
MgO	1.91	1.87	1.35	8.76	8.13
CaO	0.00	0.00	0.00	0.00	0.00
Total	98.14	98.26	98.01	98.16	98.26
Oxygens	32	32	32	32	32
Ti	0.095	0.121	0.132	0.018	0.163
Al	3.947	3.862	3.092	8.382	8.689
V	0.243	0.241	0.234	0.063	0.051
Cr	6.741	6.855	5.999	5.486	5.298
Fe^{3+}	4.880	4.800	6.412	2.032	1.636
Fe^{2+}	7.146	7.238	7.469	4.710	5.093
Mn	0.153	0.104	0.092	0.054	0.050
Mg	0.795	0.779	0.571	3.255	3.021
Ca	0.000	0.000	0.000	0.000	0.000
Total Cations	24.000	24.000	24.000	24.000	24.000
mg	10.0	9.7	7.1	40.9	37.2

Appendix Table 3.12a (cont.). Electron microprobe analyses of oxide minerals from the Wilagee layered intrusion.

Sample no.	92522502	92522502	92522506	92522506	92522506	92522506	92522506	92522506	92522506	92522506	92522506
Analysis no.	57593	57596	57408	57411	57412	57414	57415	57416	57417	57418	57419
Mineral	Spinel	Spinel	Spinel	Spinel	Spinel	Spinel	Spinel	Spinel	Spinel	Spinel	Spinel
Description	Cumulus	Cumulus	Alteration	Cumulus	Alteration	Cumulus	Cumulus	Cumulus	Cumulus	Alteration	Alteration
Lithology	Olivine gabbronorite	Olivine gabbronorite	Troctolite	Troctolite	Troctolite	Troctolite	Troctolite	Troctolite	Troctolite	Troctolite	Troctolite
Strat. ht. (m)	710	710	70	70	70	70	70	70	70	70	70
TiO_2	0.00	0.96	0.00	1.15	0.00	1.50	2.31	0.00	1.13	0.00	0.00
Al_2O_3	30.03	16.64	63.03	15.58	63.37	15.97	15.85	33.79	16.28	63.40	63.01
V_2O_3	0.31	0.72	0.00	0.61	0.00	0.70	0.74	0.11	0.75	0.00	0.00
Cr_2O_3	27.22	34.08	0.00	40.26	0.00	37.19	36.81	27.77	37.09	0.00	0.00
FeO*	34.05	43.99	21.46	37.99	20.94	40.28	40.56	30.12	40.20	20.48	20.73
MnO	0.24	0.26	0.00	0.25	0.12	0.50	0.36	0.17	0.48	0.00	0.00
MgO	8.11	2.21	14.03	3.15	14.34	2.57	2.32	6.85	2.86	14.68	15.15
CaO	0.00	0.00	0.00	0.00	0.00	0.00	0.00	0.00	0.00	0.00	0.00
Total	99.96	98.87	98.52	98.98	98.77	98.70	98.93	98.81	98.80	98.56	98.89
Oxygens	32	32	32	32	32	32	32	32	32	32	32
Ti	0.000	0.196	0.000	0.235	0.000	0.308	0.474	0.000	0.231	0.000	0.000
Al	8.674	5.340	15.757	4.994	15.769	5.142	5.106	9.813	5.218	15.768	15.757
V	0.061	0.157	0.000	0.133	0.000	0.153	0.163	0.021	0.164	0.000	0.000
Cr	5.274	7.334	0.000	8.660	0.000	8.033	7.956	5.409	7.976	0.000	0.000
Fe^{3+}	1.991	2.778	0.243	1.743	0.231	2.057	1.826	0.757	2.181	0.232	0.243
Fe^{2+}	4.988	7.237	3.564	6.901	3.466	7.147	7.448	5.448	6.962	3.383	3.210
Mn	0.050	0.061	0.000	0.058	0.021	0.115	0.083	0.035	0.111	0.000	0.000
Mg	2.962	0.898	4.436	1.276	4.513	1.046	0.944	2.517	1.158	4.617	4.790
Ca	0.000	0.000	0.000	0.000	0.000	0.000	0.000	0.000	0.000	0.000	0.000
Total Cations	24.000	24.000	24.000	24.000	24.000	24.000	24.000	24.000	24.000	24.000	24.000
mg	37.3	11.0	55.5	15.6	56.6	12.8	11.2	31.6	14.3	57.7	59.9

Appendix Table 3.12a (cont.). Electron microprobe analyses of oxide minerals from the Wilagee layered intrusion.

Sample no.	92522506	92522506	92522506	92522506	92522506	92522506	92522506	92522506	92522506
Analysis no.	57477	57478	57479	57480	57481	57482	57483	57486	57487
Mineral	Spinel	Spinel	Spinel	Spinel	Spinel	Spinel	Spinel	Spinel	Spinel
Description	Alteration	Alteration	Alteration	Cumulus	Cumulus (r)	Cumulus (c)	Cumulus (c)	Cumulus (c)	Cumulus (r)
Lithology	Troctolite	Troctolite	Troctolite	Troctolite	Troctolite	Troctolite	Troctolite	Troctolite	Troctolite
Strat. ht. (m)	70	70	70	70	70	70	70	70	70
TiO_2	0.00	0.00	0.00	0.41	1.11	6.96	1.26	1.50	1.43
Al_2O_3	63.24	63.35	63.67	23.54	16.34	13.58	15.96	13.96	16.01
V_2O_3	0.00	0.00	0.00	0.44	0.72	0.56	0.66	0.67	0.64
Cr_2O_3	0.00	0.00	0.00	33.72	37.08	35.57	38.41	38.94	39.55
FeO*	20.58	19.75	19.19	36.50	40.14	38.80	38.88	40.71	38.49
MnO	0.00	0.10	0.00	0.35	0.41	0.47	0.45	0.57	0.49
MgO	14.59	15.19	15.75	3.75	2.98	2.83	2.78	1.84	2.08
CaO	0.00	0.00	0.00	0.00	0.00	0.00	0.00	0.00	0.00
Total	98.41	98.39	98.61	98.71	98.77	98.77	98.39	98.19	98.68
Oxygens	32	32	32	32	32	32	32	32	32
Ti	0.000	0.000	0.000	0.082	0.228	1.446	0.259	0.314	0.294
Al	15.762	15.732	15.720	7.278	5.232	4.423	5.148	4.582	5.182
V	0.000	0.000	0.000	0.093	0.157	0.123	0.145	0.150	0.141
Cr	0.000	0.000	0.000	6.994	7.964	7.768	8.312	8.574	8.584
Fe^{3+}	0.238	0.268	0.280	1.471	2.192	0.794	1.877	2.067	1.505
Fe^{2+}	3.401	3.212	3.082	6.537	6.927	8.170	7.022	7.415	7.332
Mn	0.000	0.018	0.000	0.077	0.095	0.110	0.104	0.134	0.113
Mg	4.599	4.770	4.918	1.468	1.205	1.166	1.134	0.765	0.849
Ca	0.000	0.000	0.000	0.000	0.000	0.000	0.000	0.000	0.000
Total Cations	24.000	24.000	24.000	24.000	24.000	24.000	24.000	24.000	24.000
mg	57.5	59.8	61.5	18.3	14.8	12.5	13.9	9.4	10.4

Appendix Table 3.13. Electron microprobe analyses of silicate minerals from the Wilson Creek intrusion.

Sample no.	93522126	93522126	93522126	93522126	93522126	93522126	93522126	93522126
Analysis no.	71420	71421	71422	71433	71440	71441	71442	71443
Mineral	Amphibole	Amphibole	Amphibole	Amphibole	Amphibole	Amphibole	Amphibole	Amphibole
Description	Corona	Corona	Corona	Corona	Corona	Corona	Corona	Corona
Lithology	Olivine gabbronorite	Olivine gabbronorite	Olivine gabbronorite	Olivine gabbronorite	Olivine gabbronorite	Olivine gabbronorite	Olivine gabbronorite	Olivine gabbronorite
SiO_2	42.75	43.02	42.57	42.07	42.57	41.73	42.08	42.09
TiO_2	0.75	0.88	0.66	0.00	1.03	0.00	0.00	0.00
Al_2O_3	14.69	14.32	14.27	17.09	14.69	16.39	16.57	16.60
FeO*	10.18	10.17	10.50	11.16	10.89	10.93	10.71	10.81
MnO	0.00	0.00	0.12	0.00	0.00	0.00	0.00	0.00
MgO	15.05	15.00	14.92	13.75	13.70	14.20	14.29	14.18
CaO	11.11	11.23	11.21	11.06	10.86	11.11	11.18	11.14
Na_2O	2.20	2.28	2.38	2.57	2.02	2.60	2.67	2.54
K_2O	0.41	0.40	0.30	0.19	0.40	0.20	0.13	0.25
Total	98.28	98.42	98.08	99.15	97.36	98.37	98.83	98.80
Oxygens	23	23	23	23	23	23	23	23
Si	6.064	6.118	6.081	5.942	6.137	5.939	5.955	5.959
Ti	0.080	0.094	0.071	0.000	0.112	0.000	0.000	0.000
Al	2.458	2.400	2.402	2.845	2.496	2.749	2.764	2.770
Fe^{3+}	1.185	1.054	1.148	1.185	1.016	1.233	1.180	1.192
Fe^{2+}	0.024	0.155	0.106	0.133	0.299	0.068	0.087	0.088
Mn	0.000	0.000	0.015	0.000	0.000	0.000	0.000	0.000
Mg	3.185	3.179	3.177	2.895	2.943	3.012	3.014	2.992
Ca	1.690	1.711	1.716	1.674	1.677	1.694	1.695	1.690
Na	0.606	0.629	0.629	0.704	0.565	0.717	0.733	0.697
K	0.074	0.073	0.055	0.034	0.074	0.036	0.023	0.045
Total Cations	15.366	15.413	15.400	15.412	15.319	15.448	15.451	15.433
mg	99.3	95.3	96.8	95.6	90.8	97.8	97.2	97.1
Classification	Ferri Tschermakite	Ferri Tschermakite	Ferri Tschermakite	Ferri Tschermakite	Ferri Tschermakite	Ferri Tschermakite	Ferri Tschermakite	Ferri Tschermakite

Appendix Table 3.13 (cont.). Electron microprobe analyses of silicate minerals from the Wilson Creek intrusion.

Sample no.	93522126	93522126	93522126	93522126	93522126	93522126	93522126	93522126	93522126	93522126	93522126
Analysis no.	71408	71409	71410	71411	71412	71413	71414	71415	71434	71435	71436
Mineral	Olivine	Olivine	Olivine	Olivine	Olivine	Olivine	Olivine	Olivine	Olivine	Olivine	Olivine
Description	Cumulus (c)	Cumulus (c)	Cumulus (c)	Cumulus (c)	Cumulus (c)	Cumulus (c)	Cumulus (r)	Cumulus (c)	Cumulus (r)	Cumulus (r)	Cumulus (c)
Lithology	Olivine gabbronorite	Olivine gabbronorite	Olivine gabbronorite	Olivine gabbronorite	Olivine gabbronorite	Olivine gabbronorite	Olivine gabbronorite	Olivine gabbronorite	Olivine gabbronorite	Olivine gabbronorite	Olivine gabbronorite
SiO_2	35.78	35.88	35.93	36.33	36.17	36.25	36.39	35.98	35.87	35.70	35.78
TiO_2	0.00	0.00	0.00	0.00	0.00	0.00	0.00	0.00	0.00	0.00	0.00
Al_2O_3	0.00	0.00	0.00	0.00	0.00	0.00	0.00	0.00	0.00	0.00	0.00
FeO*	33.70	32.98	32.72	33.16	33.01	33.06	33.43	33.35	34.18	34.25	34.24
MnO	0.31	0.25	0.23	0.29	0.18	0.24	0.35	0.27	0.27	0.23	0.25
MgO	30.26	30.55	30.81	30.68	31.09	30.41	30.90	31.00	30.01	29.71	29.84
CaO	0.00	0.00	0.00	0.00	0.00	0.00	0.00	0.00	0.00	0.00	0.00
Na_2O	0.00	0.00	0.00	0.00	0.00	0.00	0.00	0.00	0.00	0.00	0.00
K_2O	0.00	0.00	0.00	0.00	0.00	0.00	0.00	0.00	0.00	0.00	0.00
Total	100.23	99.81	99.82	100.55	100.60	100.02	101.22	100.80	100.50	100.05	100.27
Oxygens	4	4	4	4	4	4	4	4	4	4	4
Si	0.982	0.986	0.985	0.990	0.984	0.994	0.986	0.979	0.983	0.984	0.984
Ti	0.000	0.000	0.000	0.000	0.000	0.000	0.000	0.000	0.000	0.000	0.000
Al	0.000	0.000	0.000	0.000	0.000	0.000	0.000	0.000	0.000	0.000	0.000
Fe^{3+}	0.036	0.029	0.030	0.019	0.032	0.012	0.028	0.043	0.033	0.032	0.033
Fe^{2+}	0.737	0.729	0.721	0.737	0.719	0.746	0.730	0.716	0.751	0.758	0.755
Mn	0.007	0.006	0.005	0.007	0.004	0.006	0.008	0.006	0.006	0.005	0.006
Mg	1.238	1.251	1.259	1.247	1.261	1.243	1.248	1.257	1.226	1.221	1.223
Ca	0.000	0.000	0.000	0.000	0.000	0.000	0.000	0.000	0.000	0.000	0.000
Na	0.000	0.000	0.000	0.000	0.000	0.000	0.000	0.000	0.000	0.000	0.000
K	0.000	0.000	0.000	0.000	0.000	0.000	0.000	0.000	0.000	0.000	0.000
Total Cations	3.000	3.000	3.000	3.000	3.000	3.000	3.000	3.000	3.000	3.000	3.000
mg	62.7	63.2	63.6	62.9	63.7	62.5	63.1	63.7	62.0	61.7	61.8

Appendix Table 3.13 (cont.). Electron microprobe analyses of silicate minerals from the Wilson Creek intrusion.

Sample no.	93522126	93522126	93522126	93522126	93522126	93522126	93522126	93522126
Analysis no.	71437	71446	71447	71448	71449	71450	71458	71459
Mineral	Olivine	Olivine	Olivine	Olivine	Olivine	Olivine	Olivine	Olivine
Description	Cumulus (c)	Cumulus (r)	Cumulus (r)	Cumulus (c)	Cumulus (c)	Cumulus (c)	Cumulus (r)	Cumulus (r)
Lithology	Olivine gabbronorite	Olivine gabbronorite	Olivine gabbronorite	Olivine gabbronorite	Olivine gabbronorite	Olivine gabbronorite	Olivine gabbronorite	Olivine gabbronorite
SiO_2	35.95	35.72	35.73	35.68	35.93	36.07	35.56	35.63
TiO_2	0.00	0.00	0.00	0.00	0.00	0.00	0.00	0.00
Al_2O_3	0.00	0.00	0.00	0.00	0.00	0.00	0.00	0.00
FeO*	34.27	33.83	34.29	33.56	33.20	32.82	34.16	33.99
MnO	0.15	0.17	0.25	0.21	0.25	0.20	0.27	0.29
MgO	29.79	30.01	29.65	30.05	30.23	30.40	29.86	29.83
CaO	0.00	0.00	0.00	0.00	0.00	0.00	0.00	0.00
Na_2O	0.00	0.00	0.00	0.00	0.00	0.00	0.00	0.00
K_2O	0.00	0.00	0.00	0.00	0.00	0.00	0.00	0.00
Total	100.27	99.89	100.06	99.66	99.72	99.56	100.05	99.91
Oxygens	4	4	4	4	4	4	4	4
Si	0.988	0.984	0.985	0.985	0.989	0.993	0.980	0.983
Ti	0.000	0.000	0.000	0.000	0.000	0.000	0.000	0.000
Al	0.000	0.000	0.000	0.000	0.000	0.000	0.000	0.000
Fe^{3+}	0.024	0.032	0.030	0.031	0.022	0.015	0.040	0.035
Fe^{2+}	0.764	0.747	0.761	0.744	0.743	0.741	0.747	0.749
Mn	0.004	0.004	0.006	0.005	0.006	0.005	0.006	0.007
Mg	1.220	1.233	1.219	1.236	1.241	1.247	1.227	1.226
Ca	0.000	0.000	0.000	0.000	0.000	0.000	0.000	0.000
Na	0.000	0.000	0.000	0.000	0.000	0.000	0.000	0.000
K	0.000	0.000	0.000	0.000	0.000	0.000	0.000	0.000
Total Cations	3.000	3.000	3.000	3.000	3.000	3.000	3.000	3.000
mg	61.5	62.3	61.6	62.4	62.6	62.7	62.2	62.1

Appendix Table 3.13 (cont.). Electron microprobe analyses of silicate minerals from the Wilson Creek intrusion.

Sample no.	93522126	93522126	93522126	93522126	93522126	93522126	93522126	Sample no.	93522126
Analysis no.	71426	71427	71432	71444	71445	71455	71456	Analysis no.	71416
Mineral	Orthopyroxene	Orthopyroxene	Orthopyroxene	Orthopyroxene	Orthopyroxene	Orthopyroxene	Orthopyroxene	Mineral	Plagioclase
Description	Cumulus	Cumulus	Corona	Corona	Corona	Intercumulus	Intercumulus	Description	Cumulus (r)
Lithology	Olivine gabbronorite	Olivine gabbronorite	Olivine gabbronorite	Olivine gabbronorite	Olivine gabbronorite	Olivine gabbronorite	Olivine gabbronorite	Lithology	Olivine gabbronorite
SiO_2	53.06	53.13	53.70	53.55	53.77	52.38	53.37	SiO_2	50.85
TiO_2	0.00	0.00	0.00	0.00	0.00	0.19	0.00	TiO_2	0.00
Al_2O_3	1.09	0.89	0.27	0.32	0.49	2.54	0.88	Al_2O_3	32.41
FeO*	21.43	21.34	20.54	21.19	20.63	18.51	20.46	FeO*	0.15
MnO	0.30	0.28	0.19	0.24	0.27	0.20	0.15	MnO	0.00
MgO	23.84	24.12	25.21	24.92	25.40	23.22	24.82	MgO	0.00
CaO	0.30	0.56	0.00	0.00	0.00	2.74	0.44	CaO	13.38
Na_2O	0.00	0.00	0.00	0.00	0.00	0.00	0.00	Na_2O	3.24
K_2O	0.00	0.00	0.00	0.00	0.00	0.00	0.00	K_2O	0.00
Total	100.16	100.51	100.06	100.43	100.76	99.87	100.30	Total	100.03
Oxygens	6	6	6	6	6	6	6	Oxygens	8
Si	1.958	1.953	1.972	1.965	1.961	1.927	1.957	Si	2.303
Ti	0.000	0.000	0.000	0.000	0.000	0.005	0.000	Ti	0.000
Al	0.047	0.038	0.012	0.014	0.021	0.110	0.038	Al	1.730
Fe^{3+}	0.037	0.055	0.044	0.056	0.057	0.025	0.049	Fe^{3+}	0.000
Fe^{2+}	0.625	0.601	0.587	0.595	0.572	0.545	0.578	Fe^{2+}	0.006
Mn	0.010	0.009	0.006	0.008	0.008	0.006	0.005	Mn	0.000
Mg	1.312	1.322	1.380	1.363	1.381	1.273	1.356	Mg	0.000
Ca	0.012	0.022	0.000	0.000	0.000	0.108	0.017	Ca	0.650
Na	0.000	0.000	0.000	0.000	0.000	0.000	0.000	Na	0.285
K	0.000	0.000	0.000	0.000	0.000	0.000	0.000	K	0.000
Total Cations	4.000	4.000	4.000	4.000	4.000	4.000	4.000	Total Cations	4.974
mg	67.7	68.7	70.2	69.6	70.7	70.0	70.1	Albite	30.5
Enstatite	67.3	68.0	70.2	69.6	70.7	66.1	69.5	Anorthite	69.5
Ferrosilite	32.1	30.9	29.8	30.4	29.3	28.3	29.6	Orthoclase	0.0
Wollastonite	0.6	1.1	0.0	0.0	0.0	5.6	0.9		

Appendix Table 3.13 (cont.). Electron microprobe analyses of silicate minerals from the Wilson Creek intrusion.

Sample no.	93522126	93522126	93522126	93522126	93522126	93522126
Analysis no.	71417	71418	71451	71452	71453	71454
Mineral	Plagioclase	Plagioclase	Plagioclase	Plagioclase	Plagioclase	Plagioclase
Description	Cumulus (r)	Cumulus (c)	Cumulus (r)	Cumulus (r)	Cumulus (c)	Cumulus (c)
Lithology	Olivine gabbronorite	Olivine gabbronorite	Olivine gabbronorite	Olivine gabbronorite	Olivine gabbronorite	Olivine gabbronorite
SiO_2	51.59	50.05	49.77	50.27	50.43	51.12
TiO_2	0.00	0.00	0.00	0.00	0.00	0.00
Al_2O_3	31.62	32.85	32.65	32.98	32.52	31.95
FeO*	0.00	0.00	0.00	0.00	0.00	0.00
MnO	0.00	0.00	0.00	0.00	0.00	0.00
MgO	0.00	0.00	0.00	0.00	0.00	0.00
CaO	12.83	14.18	14.25	14.39	13.80	13.25
Na_2O	3.65	2.83	3.02	3.05	3.17	3.56
K_2O	0.00	0.00	0.05	0.05	0.00	0.05
Total	99.69	99.91	99.72	100.73	99.92	99.93
Oxygens	8	8	8	8	8	8
Si	2.340	2.274	2.282	2.269	2.290	2.319
Ti	0.000	0.000	0.000	0.000	0.000	0.000
Al	1.690	0.000	1.745	1.754	1.740	1.707
Fe^{3+}	0.000	1.759	0.000	0.000	0.000	0.000
Fe^{2+}	0.000	0.000	0.000	0.000	0.000	0.000
Mn	0.000	0.000	0.000	0.000	0.000	0.000
Mg	0.000	0.000	0.000	0.000	0.000	0.000
Ca	0.623	0.690	0.684	0.696	0.671	0.644
Na	0.321	0.249	0.270	0.267	0.279	0.313
K	0.000	0.000	0.000	0.003	0.000	0.003
Total Cations	4.975	4.972	4.981	4.989	4.980	4.986
Albite	34.0	26.5	28.3	27.7	29.4	32.6
Anorthite	66.0	73.5	71.7	72.0	70.6	67.1
Orthoclase	0.0	0.0	0.0	0.3	0.0	0.3

Appendix Table 3.13a. Electron microprobe analyses of oxide minerals from the Wilson Creek intrusion.

Sample no.	93522126	93522126	93522126
Analysis no.	71428	71429	71430
Mineral	Spinel	Spinel	Spinel
Description	Corona	Corona	Corona
Lithology	Olivine gabbronorite	Olivine gabbronorite	Olivine gabbronorite
Al_2O_3	60.33	61.58	61.50
FeO*	28.08	27.38	27.40
MnO	0.13	0.00	0.13
MgO	9.73	9.99	9.95
Total	98.28	98.95	98.98
Oxygens	32	32	32
Al	15.628	15.656	15.685
Fe^{3+}	0.372	0.344	0.315
Fe^{2+}	4.789	4.786	4.767
Mn	0.024	0.000	0.024
Mg	3.187	3.214	3.208
Total Cations	24.000	24.000	24.000
mg	40.0	40.2	40.2

Appendix Table 3.14. Electron microprobe analyses of chromite from chromitite layers in East Kimberley intrusions.

Sample no.	93522026	93522026	93522026	93522026	83330021	83330021	83330021	83330021	83330021	83330021	83330021	83330192	83330192	83330192
Analysis no.	124357	124359	124361	124363	124441	124442	124443	124444	124445	124446	124447	124247	124248	124250
Intrusion	Big Ben	Big Ben	Big Ben	Big Ben	Lamboo	Lamboo	Lamboo	Lamboo	Lamboo	Lamboo	Lamboo	Lamboo	Lamboo	Lamboo
Lithology	Peridotite	Peridotite	Peridotite	Peridotite	Peridotite	Peridotite	Peridotite	Peridotite	Peridotite	Peridotite	Peridotite	Peridotite	Peridotite	Peridotite
SiO_2	<.02	<.02	0.03	0.03	<.02	0.05	0.10	<.02	<.02	<.02	0.03	<.02	0.03	<.02
TiO_2	1.03	1.24	1.07	0.70	0.74	0.70	0.75	0.76	0.81	0.80	0.78	0.66	0.64	0.96
Al_2O_3	14.25	14.47	14.30	15.61	22.98	20.93	22.07	23.69	23.38	23.76	22.71	24.91	25.26	22.75
V_2O_3	0.24	0.24	0.24	0.24	0.18	0.19	0.20	0.19	0.21	0.19	0.22	0.18	0.17	0.20
Cr_2O_3	40.95	40.61	40.90	41.60	38.85	37.11	40.05	40.10	39.80	39.70	40.25	38.86	39.13	39.13
Fe_2O_3	11.27	10.67	11.01	9.62	5.72	9.82	4.90	5.54	6.01	5.71	5.85	5.34	5.38	6.33
FeO	27.87	28.08	27.82	27.37	22.79	21.53	24.29	17.89	18.21	17.93	20.47	16.19	16.17	18.01
MnO	0.39	0.33	0.37	0.30	0.81	1.50	0.70	0.21	0.20	0.25	0.26	0.15	0.18	0.24
NiO	0.06	0.07	0.10	0.05	0.14	0.20	0.16	0.16	0.17	0.21	0.16	0.17	0.19	0.17
MgO	4.43	4.43	4.47	4.78	8.20	8.27	7.31	11.97	11.77	11.88	10.19	12.96	13.18	11.58
ZnO	0.24	0.18	0.22	0.20	0.21	0.23	0.22	<.07	<.08	0.07	0.22	<.08	<.08	0.16
CaO	<.01	<.01	0.02	0.02	<.01	<.01	<.01	<.01	<.01	<.01	<.01	<.01	<.01	<.01
Total	100.74	100.31	100.53	100.52	100.61	100.54	100.75	100.51	100.55	100.50	101.13	99.42	100.33	99.52
Oxygens	32	32	32	32	32	32	32	32	32	32	32	32	32	32
Si	-	-	0.007	0.008	-	0.012	0.025	-	-	-	0.008	-	0.007	-
Ti	0.209	0.252	0.217	0.140	0.141	0.135	0.144	0.140	0.150	0.148	0.145	0.122	0.118	0.180
Al	4.525	4.606	4.545	4.921	6.839	6.294	6.622	6.864	6.789	6.889	6.650	7.199	7.225	6.691
V	0.051	0.051	0.053	0.052	0.037	0.040	0.041	0.037	0.042	0.037	0.043	0.035	0.033	0.040
Cr	8.721	8.672	8.720	8.794	7.757	7.486	8.061	7.794	7.754	7.721	7.907	7.535	7.509	7.721
Fe^{3+}	2.285	2.168	2.234	1.936	1.087	1.885	0.938	1.024	1.114	1.056	1.093	0.986	0.983	1.189
Fe^{2+}	6.278	6.341	6.274	6.122	4.813	4.593	5.171	3.678	3.754	3.689	4.253	3.321	3.281	3.759
Mn	0.090	0.075	0.084	0.067	0.174	0.325	0.151	0.043	0.041	0.052	0.054	0.030	0.038	0.051
Ni	0.014	0.016	0.021	0.010	0.029	0.041	0.032	0.033	0.034	0.041	0.031	0.033	0.037	0.035
Mg	1.780	1.785	1.795	1.904	3.086	3.145	2.773	4.386	4.321	4.354	3.774	4.738	4.769	4.306
Zn	0.049	0.036	0.044	0.040	0.039	0.043	0.042	-	-	-	-	-	-	0.029
Ca	-	-	0.006	0.005	-	-	-	-	-	0.013	0.041	-	-	-
Total Cations	24.000	24.000	24.000	24.000	24.000	24.000	24.000	24.000	24.000	24.000	24.000	24.000	24.000	24.000
mg	22	22	22	24	39	41	35	54	54	54	47	59	59	53
Cr'	56	56	57	57	49	48	52	50	50	49	51	48	48	49
Al'	29	30	29	31	44	40	42	44	43	44	42	46	46	43
Fe^{3+}'	15	14	14	12	7	12	6	7	7	7	7	6	6	8

Appendix Table 3.14 (cont.). Electron microprobe analyses of chromite from chromitite layers in East Kimberley intrusions.

Sample no.	83330192	83330192	92522338	92522338	92522338	92522338	92522338	92522338	92522338	92522037	92522037	92522037	92522037
Analysis no.	124251	124252	124427	124428	124430	124431	124433	124435	124436	124346	124347	124350	124354
Intrusion	Lamboo	Lamboo	Mini	Mini	Mini	Mini	Mini	Mini	Mini	Panton	Panton	Panton	Panton
Chrom. gp.										Lower Group	Lower Group	Lower Group	Lower Group
Lithology	Peridotite	Peridotite	Peridotite	Peridotite	Peridotite	Peridotite	Peridotite	Peridotite	Peridotite	Peridotite	Peridotite	Peridotite	Peridotite
SiO_2	<.02	<.02	0.21	<.02	<.02	<.02	<.02	<.02	0.05	<.02	0.06	<.02	0.08
TiO_2	0.61	0.64	0.20	0.44	0.41	0.71	0.64	0.46	0.32	0.53	0.48	0.60	0.49
Al_2O_3	25.12	25.27	16.04	15.64	17.02	15.27	17.05	17.52	17.79	15.95	17.74	17.70	17.42
V_2O_3	0.19	0.18	0.34	0.31	0.32	0.30	0.30	0.31	0.30	0.20	0.18	0.18	0.16
Cr_2O_3	38.68	38.59	44.22	43.52	42.12	43.53	41.89	41.84	41.19	43.48	44.22	44.16	44.20
Fe_2O_3	5.81	5.54	5.28	6.20	6.07	6.61	6.27	5.35	6.40	7.30	5.56	5.31	5.23
FeO	16.00	17.25	31.96	31.66	31.58	31.89	32.31	31.74	31.86	26.61	26.55	26.25	26.33
MnO	0.16	0.22	0.47	0.50	0.44	0.50	0.54	0.48	0.49	0.41	0.29	0.35	0.35
NiO	0.15	0.17	<.03	<.03	0.04	<.03	<.03	0.04	<.03	0.04	0.09	0.06	0.09
MgO	13.12	12.42	1.54	1.55	1.72	1.65	1.45	1.57	1.61	4.89	5.52	5.62	5.41
ZnO	0.11	<.08	0.47	0.44	0.47	0.43	0.56	0.50	0.56	0.37	0.24	0.23	0.32
CaO	<.01	<.01	<.01	<.01	<.01	<.01	<.01	<.01	<.01	<.01	0.02	0.02	<.01
Total	99.96	100.29	100.72	100.26	100.18	100.89	101.01	99.81	100.57	99.78	100.94	100.48	100.09
Oxygens	32	32	32	32	32	32	32	32	32	32	32	32	32
Si	-	-	0.057	-	-	-	-	-	0.013	-	0.015	-	0.022
Ti	0.112	0.118	0.040	0.090	0.084	0.145	0.130	0.094	0.064	0.106	0.095	0.119	0.097
Al	7.217	7.266	5.141	5.048	5.459	4.907	5.437	5.629	5.671	5.044	5.481	5.488	5.435
V	0.038	0.035	0.073	0.067	0.070	0.067	0.066	0.067	0.065	0.043	0.039	0.038	0.035
Cr	7.455	7.445	9.510	9.426	9.060	9.382	8.960	9.017	8.808	9.226	9.164	9.186	9.250
Fe^{3+}	1.065	1.018	1.081	1.279	1.243	1.355	1.277	1.098	1.303	1.475	1.098	1.051	1.041
Fe^{2+}	3.263	3.520	7.270	7.253	7.185	7.271	7.310	7.236	7.206	5.972	5.820	5.776	5.827
Mn	0.034	0.046	0.107	0.115	0.101	0.117	0.123	0.112	0.112	0.094	0.063	0.078	0.078
Ni	0.029	0.034	-	-	0.008	-	-	0.009	-	0.009	0.018	0.013	0.019
Mg	4.767	4.517	0.625	0.632	0.696	0.670	0.585	0.636	0.647	1.957	2.157	2.203	2.133
Zn	0.020	-	0.095	0.090	0.095	0.086	0.112	0.100	0.112	0.074	0.046	0.044	0.063
Ca	-	-	-	-	-	-	-	-	-	-	0.004	0.005	-
Total Cations	24.000	24.000	24.000	24.000	24.000	24.000	24.000	24.000	24.000	24.000	24.000	24.000	24.000
mg	59	56	8	8	9	8	7	8	8	25	27	28	27
Cr'	47	47	60	60	57	60	57	57	56	59	58	58	58
Al'	46	46	33	32	35	31	35	36	36	32	35	35	35
Fe^{3+}'	7	6	7	8	8	9	8	7	8	9	7	7	7

Appendix Table 3.14 (cont.). Electron microprobe analyses of chromite from chromitite layers in East Kimberley intrusions.

Sample no.	92522023	92522023	92522023	92522023	92522052	92522052	92522052	92522052	92522052	92522052	92522086
Analysis no.	124314	124315	124316	124317	124257	124258	124260	124261	124262	124263	124450
Intrusion	Panton	Panton	Panton	Panton	Panton	Panton	Panton	Panton	Panton	Panton	Panton
Chrom. gp.	Middle Group	Middle Group	Middle Group	Middle Group	Middle Group	Middle Group	Middle Group	Middle Group	Middle Group	Middle Group	Middle Group
Lithology	Peridotite	Peridotite	Peridotite	Peridotite	Peridotite	Peridotite	Peridotite	Peridotite	Peridotite	Peridotite	Peridotite
SiO_2	<.02	<.02	<.02	<.02	<.02	0.09	<.02	<.02	<.02	<.02	<.02
TiO_2	0.49	0.40	0.33	0.81	0.97	0.93	0.85	0.68	0.72	0.72	0.61
Al_2O_3	19.76	19.07	19.77	19.01	18.09	18.37	18.48	18.63	18.35	18.32	19.05
V_2O_3	0.18	0.19	0.20	0.22	0.23	0.25	0.25	0.22	0.21	0.20	0.16
Cr_2O_3	41.18	41.55	41.46	41.46	41.93	42.42	42.49	43.12	42.78	43.01	43.79
Fe_2O_3	5.56	6.21	5.51	5.31	6.03	5.41	5.33	3.84	5.84	4.53	5.01
FeO	26.45	26.72	26.28	27.10	25.05	25.39	24.86	24.15	24.77	24.53	22.08
MnO	0.32	0.33	0.29	0.21	0.32	0.30	0.33	0.38	0.33	0.36	0.35
NiO	0.06	0.07	0.09	0.06	0.06	<.03	0.08	0.03	<.03	<.03	0.11
MgO	5.47	5.20	5.46	5.27	6.46	6.49	6.59	6.64	6.68	6.50	8.36
ZnO	0.26	0.27	0.33	0.18	0.14	0.14	0.13	0.14	0.15	0.15	0.12
CaO	0.03	0.03	<.01	<.01	0.05	0.02	0.02	0.03	0.03	0.04	<.01
Total	99.74	100.05	99.71	99.62	99.35	99.80	99.41	97.84	99.85	98.35	99.63
Oxygens	32	32	32	32	32	32	32	32	32	32	32
Si	-	-	-	-	-	0.023	-	-	-	-	-
Ti	0.097	0.079	0.065	0.160	0.193	0.183	0.168	0.135	0.142	0.143	0.118
Al	6.118	5.919	6.124	5.918	5.624	5.676	5.725	5.843	5.664	5.735	5.805
V	0.037	0.041	0.041	0.046	0.048	0.053	0.052	0.046	0.044	0.042	0.033
Cr	8.553	8.652	8.616	8.661	8.745	8.794	8.831	9.072	8.857	9.032	8.953
Fe^{3+}	1.098	1.231	1.090	1.055	1.197	1.067	1.055	0.769	1.151	0.905	0.974
Fe^{2+}	5.812	5.884	5.776	5.988	5.525	5.568	5.465	5.374	5.425	5.450	4.775
Mn	0.071	0.075	0.065	0.048	0.073	0.066	0.073	0.085	0.072	0.081	0.076
Ni	0.013	0.016	0.019	0.012	0.014	-	0.016	0.007	-	-	0.024
Mg	2.141	2.043	2.140	2.076	2.541	2.538	2.581	2.633	2.607	2.573	3.221
Zn	0.050	0.052	0.064	0.036	0.028	0.027	0.026	0.028	0.029	0.029	-
Ca	0.010	0.009	-	-	0.014	0.006	0.007	0.008	0.008	0.011	0.022
Total Cations	24.000	24.000	24.000	24.000	24.000	24.000	24.000	24.000	24.000	24.000	24.000
mg	27	26	27	26	32	31	32	33	32	32	40
Cr'	54	55	54	55	56	56	56	58	57	57	57
Al'	39	37	39	38	36	37	37	37	36	37	37
Fe^{3+}'	7	8	7	7	8	7	7	5	7	6	6

Appendix Table 3.14 (cont.). Electron microprobe analyses of chromite from chromitite layers in East Kimberley intrusions.

Sample no.	92522086	92522086	92522086	92522086	92522086	92522046	92522046	92522046	92522046	92522046	92522046
Analysis no.	124451	124452	124453	124454	124455	124298	124300	124302	124304	124305	124306
Intrusion	Panton	Panton	Panton	Panton	Panton	Panton	Panton	Panton	Panton	Panton	Panton
Chrom. gp.	Middle Group	Middle Group	Middle Group	Middle Group	Middle Group	Upper Group	Upper Group	Upper Group	Upper Group	Upper Group	Upper Group
Lithology	Peridotite	Peridotite	Peridotite	Peridotite	Peridotite	Peridotite	Peridotite	Peridotite	Peridotite	Peridotite	Peridotite
SiO_2	<.02	<.02	<.02	<.02	0.03	<.02	<.02	<.02	0.03	<.02	<.02
TiO_2	0.43	0.43	0.60	0.40	0.52	0.27	0.37	0.24	6.04	0.23	0.60
Al_2O_3	18.91	18.94	19.33	18.87	19.18	17.42	17.54	17.24	14.44	17.82	17.49
V_2O_3	0.19	0.19	0.16	0.18	0.19	0.48	0.50	0.46	0.36	0.47	0.45
Cr_2O_3	43.55	43.12	43.45	43.70	43.61	40.83	39.71	41.43	37.11	39.72	40.31
Fe_2O_3	5.75	6.06	5.24	5.94	5.28	7.35	8.60	7.43	2.79	8.69	7.35
FeO	22.23	21.86	22.19	22.20	22.08	30.13	30.66	30.50	35.42	30.64	30.72
MnO	0.34	0.38	0.34	0.35	0.31	0.89	0.89	0.85	0.89	0.82	0.89
NiO	0.03	0.04	0.09	<.03	0.05	0.06	<.03	0.06	<.03	0.05	0.08
MgO	8.20	8.32	8.33	8.26	8.40	2.44	2.38	2.30	2.05	2.29	2.30
ZnO	0.16	0.21	0.23	0.18	0.22	0.19	0.10	0.20	0.11	0.30	0.20
CaO	<.01	0.02	<.01	<.01	<.01	<.01	0.02	0.02	0.02	0.02	<.01
Total	99.80	99.58	99.96	100.08	99.86	100.06	100.77	100.75	99.26	101.04	100.39
Oxygens	32	32	32	32	32	32	32	32	32	32	32
Si	-	-	-	-	0.008	-	-	-	0.009	-	-
Ti	0.083	0.084	0.116	0.078	0.100	0.056	0.075	0.049	1.256	0.046	0.121
Al	5.767	5.781	5.869	5.740	5.828	5.553	5.560	5.474	4.703	5.632	5.565
V	0.039	0.040	0.034	0.036	0.038	0.104	0.107	0.100	0.080	0.100	0.097
Cr	8.907	8.830	8.849	8.915	8.892	8.735	8.442	8.822	8.107	8.421	8.602
Fe^{3+}	1.120	1.181	1.015	1.154	1.024	1.497	1.741	1.505	0.580	1.754	1.493
Fe^{2+}	4.810	4.734	4.781	4.791	4.761	6.817	6.895	6.871	8.184	6.871	6.935
Mn	0.075	0.083	0.075	0.076	0.067	0.204	0.203	0.195	0.208	0.185	0.203
Ni	0.007	0.009	0.018	-	0.010	0.012	-	0.013	-	0.010	0.017
Mg	3.161	3.212	3.199	3.176	3.228	0.985	0.952	0.924	0.845	0.916	0.926
Zn	0.030	0.041	0.044	0.035	0.043	0.038	0.020	0.040	0.022	0.059	0.040
Ca	-	0.004	-	-	-	-	0.005	0.006	0.005	0.005	-
Total Cations	24.000	24.000	24.000	24.000	24.000	24.000	24.000	24.000	24.000	24.000	24.000
mg	40	40	40	40	40	13	12	12	9	12	12
Cr'	56	56	56	56	56	56	54	55	61	53	54
Al'	37	37	37	36	37	35	35	35	35	36	36
Fe^{3+}'	7	7	6	7	7	9	11	10	4	11	10

Appendix Table 3.14 (cont.). Electron microprobe analyses of chromite from chromitite layers in East Kimberley intrusions.

Sample no.	92522046	92522046	92522377	92522377	92522377	92522377	92522377	92522377	92522377	92522377
Analysis no.	124307	124308	124235	124236	124237	124238	124239	124240	124242	124243
Intrusion	Panton	Panton	South Melon	South Melon	South Melon	South Melon	South Melon	South Melon	South Melon	South Melon
Chrom. gp.	Upper Group	Upper Group	Patch	Patch	Patch	Patch	Patch	Patch	Patch	Patch
Lithology	Peridotite	Peridotite	Peridotite	Peridotite	Peridotite	Peridotite	Peridotite	Peridotite	Peridotite	Peridotite
SiO_2	<.02	<.02	<.02	0.23	<.02	<.02	<.02	<.02	<.02	<.02
TiO_2	0.40	0.32	0.69	0.63	0.68	0.80	0.48	0.64	0.81	0.43
Al_2O_3	17.34	17.29	17.86	18.08	17.92	17.12	17.80	18.69	17.23	17.85
V_2O_3	0.45	0.49	0.27	0.26	0.24	0.24	0.27	0.27	0.26	0.26
Cr_2O_3	39.70	39.54	42.66	42.60	41.57	42.46	42.13	41.86	43.34	42.50
Fe_2O_3	9.09	8.77	7.59	6.74	7.62	6.55	7.36	7.42	6.92	6.40
FeO	30.69	30.22	24.90	24.64	25.72	25.42	25.76	24.79	25.28	24.61
MnO	0.78	0.92	0.36	0.31	0.30	0.24	0.27	0.33	0.25	0.26
NiO	0.07	0.04	0.06	0.08	0.06	0.09	<.03	0.11	0.08	0.05
MgO	2.43	2.40	6.72	7.01	6.04	6.01	5.96	6.79	6.47	6.42
ZnO	0.15	0.17	0.25	0.23	0.23	0.21	0.12	0.26	0.20	0.10
CaO	<.01	<.01	<.01	<.01	<.01	<.01	<.01	<.01	<.01	<.01
Total	101.09	100.16	101.37	100.79	100.38	99.14	100.14	101.15	100.85	98.86
Oxygens	32	32	32	32	32	32	32	32	32	32
Si	-	-	-	0.059	-	-	-	-	-	-
Ti	0.081	0.064	0.134	0.123	0.134	0.161	0.095	0.124	0.159	0.085
Al	5.484	5.516	5.455	5.529	5.546	5.373	5.524	5.695	5.309	5.582
V	0.097	0.107	0.057	0.054	0.051	0.052	0.056	0.057	0.054	0.055
Cr	8.423	8.462	8.741	8.737	8.629	8.941	8.772	8.557	8.957	8.915
Fe^{3+}	1.835	1.787	1.480	1.315	1.505	1.312	1.459	1.443	1.362	1.277
Fe^{2+}	6.887	6.841	5.397	5.345	5.647	5.662	5.674	5.362	5.526	5.460
Mn	0.177	0.211	0.079	0.068	0.067	0.055	0.059	0.072	0.056	0.058
Ni	0.014	0.009	0.014	0.016	0.013	0.018	-	0.023	0.016	0.011
Mg	0.973	0.970	2.596	2.709	2.363	2.385	2.338	2.619	2.522	2.537
Zn	0.030	0.034	0.048	0.044	0.045	0.041	0.023	0.049	0.038	0.019
Ca	-	-	-	-	-	-	-	-	-	-
Total Cations	24.000	24.000	24.000	24.000	24.000	24.000	24.000	24.000	24.000	24.000
mg	12	12	32	34	30	30	29	33	31	32
Cr'	53	54	56	57	55	58	56	55	57	57
Al'	35	35	35	35	35	34	35	36	34	35
Fe^{3+}'	12	11	9	8	10	8	9	9	9	8

Appendix Table 3.14 (cont.). Electron microprobe analyses of chromite from chromitite layers in East Kimberley intrusions.

Sample no.	92522354	92522354	92522354	92522354	92522354	92522499	92522499	92522499	92522499	92522499
Analysis no.	124321	124322	124323	124324	124328	124332	124333	124336	124338	124339
Intrusion	West McIntosh	West McIntosh	West McIntosh	West McIntosh	West McIntosh	Wilagee	Wilagee	Wilagee	Wilagee	Wilagee
Lithology	Peridotite	Peridotite	Peridotite	Peridotite	Peridotite	Troctolite	Troctolite	Troctolite	Troctolite	Troctolite
SiO_2	<.02	<.02	<.02	<.02	<.02	<.02	0.02	<.02	0.05	0.03
TiO_2	0.48	0.31	0.50	0.42	0.41	0.29	0.23	0.39	0.37	0.29
Al_2O_3	18.53	17.56	15.59	17.76	17.49	27.36	26.65	25.00	22.81	25.35
V_2O_3	0.18	0.23	0.24	0.20	0.21	0.21	0.24	0.24	0.23	0.22
Cr_2O_3	43.66	43.27	45.61	43.85	43.54	32.23	33.14	35.33	37.68	34.77
Fe_2O_3	4.66	7.61	6.79	6.12	6.61	6.84	6.60	7.30	5.43	5.65
FeO	24.29	25.21	25.41	25.09	25.00	29.45	29.56	25.55	30.25	29.83
MnO	0.33	0.32	0.30	0.29	0.33	0.30	0.30	0.27	0.35	0.32
NiO	0.06	<.03	<.03	0.04	0.06	0.13	0.13	0.19	0.09	0.15
MgO	6.68	6.27	6.02	6.30	6.29	4.62	4.39	6.91	3.67	3.98
ZnO	0.19	0.23	0.20	0.23	0.12	0.08	0.16	0.11	<.07	0.13
CaO	<.01	0.02	<.01	<.01	0.02	0.04	0.03	<.01	<.01	0.02
Total	99.06	101.03	100.66	100.31	100.06	101.54	101.45	101.29	100.95	100.74
Oxygens	32	32	32	32	32	32	32	32	32	32
Si	-	-	-	-	-	-	0.006	-	0.013	0.007
Ti	0.095	0.061	0.100	0.083	0.081	0.056	0.045	0.074	0.072	0.057
Al	5.754	5.404	4.860	5.491	5.425	8.127	7.956	7.403	6.982	7.675
V	0.039	0.049	0.051	0.042	0.044	0.042	0.048	0.048	0.049	0.044
Cr	9.093	8.931	9.537	9.093	9.060	6.422	6.638	7.020	7.736	7.061
Fe^{3+}	0.924	1.494	1.352	1.208	1.308	1.298	1.257	1.380	1.062	1.092
Fe^{2+}	5.351	5.503	5.620	5.503	5.503	6.207	6.263	5.370	6.568	6.407
Mn	0.073	0.072	0.067	0.065	0.073	0.064	0.065	0.057	0.078	0.071
Ni	0.012	-	-	0.008	0.012	0.026	0.026	0.038	0.020	0.032
Mg	2.622	2.439	2.373	2.463	2.466	1.734	1.658	2.589	1.420	1.524
Zn	0.037	0.044	0.040	0.044	0.022	0.014	0.030	0.020	-	0.024
Ca	-	0.004	-	-	0.005	0.011	0.008	-	-	0.007
Total Cations	24.000	24.000	24.000	24.000	24.000	24.000	24.000	24.000	24.000	24.000
mg	33	31	30	31	31	22	21	33	18	19
Cr'	58	57	60	57	58	41	42	44	49	45
Al'	36	34	31	35	34	51	50	47	44	48
Fe^{3+}'	6	9	9	8	8	8	8	9	7	7

APPENDIX 4. U-PB GEOCHRONOLOGICAL TABLES

Appendix Table 4.1. Panton intrusion

Appendix Table 4.2. Rose Bore Granite and pegmatite cutting Panton intrusion

Appendix Table 4.3. Springvale intrusion

Appendix Table 4.4. Toby intrusion

Appendix Table 4.5. Sally Malay intrusion (zircon data)

Appendix Table 4.6. Sally Malay intrusion (baddeleyite data)

Appendix Table 4.7. McIntosh intrusion

Appendix Table 4.1. Zircon U-Pb SHRIMP data for a mottled anorthosite (93526033) from the Panton intrusion.

Grain-analysis	*U ppm*	*Th/U*	$^{206}Pb/^{204}Pb$	* *f206%*	$^{208}Pb/^{206}Pb$	$^{206}Pb/^{238}U$	±	$^{207}Pb/^{235}U$	±	$^{207}Pb/^{206}Pb$	±	$^{207}Pb/^{206}Pb$ *age*	±
200.1	2356	1.62	543478	0.00	0.4494	0.3347	0.0074	5.237	0.116	0.1135	0.0000	1856	1
201.1	3224	1.82	330033	0.00	0.4956	0.3333	0.0073	5.218	0.116	0.1135	0.0001	1857	2
202.1	2897	2.04	244499	0.00	0.5687	0.3336	0.0073	5.224	0.116	0.1136	0.0001	1857	2
203.1	3742	2.33	671141	0.00	0.6423	0.3369	0.0074	5.278	0.117	0.1136	0.0001	1858	2
204.1	5930	3.10	1204819	0.00	0.8489	0.3412	0.0075	5.343	0.118	0.1136	0.0000	1858	1
205.1	3529	2.26	444444	0.00	0.6268	0.3274	0.0072	5.114	0.113	0.1133	0.0001	1853	2
206.1	4732	2.19	591716	0.00	0.6195	0.3460	0.0076	5.421	0.120	0.1136	0.0000	1858	1
207.1	4651	2.61	2439024	0.00	0.7300	0.3254	0.0072	5.049	0.112	0.1126	0.0000	1841	1
208.1	3167	1.38	303030	0.00	0.3772	0.3203	0.0071	5.016	0.111	0.1136	0.0001	1857	2
209.1	3580	2.24	371747	0.00	0.6183	0.3318	0.0073	5.183	0.115	0.1133	0.0001	1853	2
210.1	3555	2.39	411523	0.00	0.6552	0.3246	0.0071	5.072	0.112	0.1133	0.0001	1853	2
211.1	3672	1.87	546448	0.00	0.5191	0.3357	0.0074	5.256	0.116	0.1136	0.0000	1857	1
212.1	2874	0.99	255102	0.00	0.2731	0.3284	0.0072	5.141	0.114	0.1136	0.0001	1857	2
213.1	3202	1.68	500000	0.00	0.4790	0.3319	0.0073	5.188	0.115	0.1134	0.0001	1854	2
214.1	4420	2.30	36873	0.04	0.6445	0.3522	0.0078	5.506	0.122	0.1134	0.0000	1855	1
215.1	2400	2.42	171233	0.00	0.6575	0.3326	0.0073	5.203	0.115	0.1135	0.0001	1855	2

* denotes the percentage of common ^{206}Pb in the total measured ^{206}Pb.

Appendix Table 4.2. Zircon U-Pb SHRIMP data for the Rose Bore Granite (113439) and a pegmatite (93526031) cutting the Panton intrusion.

Grain-analysis	*U ppm*	*Th/U*	$^{206}Pb/^{204}Pb$	* *f206%*	$^{208}Pb/^{206}Pb$	$^{206}Pb/^{238}U$	±	$^{207}Pb/^{235}U$	±	$^{207}Pb/^{206}Pb$	±	$^{207}Pb/^{206}Pb$ *age*	±
Rose Bore Granite													
1.1	276	0.36	10062	0.15	0.0983	0.3263	0.0059	5.069	0.098	0.1127	0.0006	1843	9
1.2	302	0.30	30581	0.05	0.0850	0.3205	0.0058	5.016	0.096	0.1135	0.0005	1856	8
2.1	547	0.49	45662	0.03	0.1356	0.3332	0.0060	5.236	0.098	0.1140	0.0003	1864	5
3.1	771	0.27	39231	0.04	0.0701	0.3278	0.0059	5.152	0.096	0.1140	0.0003	1864	4
4.1	270	0.81	26144	0.06	0.2270	0.3339	0.0061	5.262	0.101	0.1143	0.0005	1869	8
5.1	315	0.49	42070	0.04	0.1403	0.3212	0.0058	5.052	0.096	0.1141	0.0004	1865	7
6.1	223	0.52	133156	0.01	0.1469	0.3307	0.0060	5.213	0.102	0.1143	0.0006	1869	9
7.1	460	0.42	7402	0.21	0.1236	0.3098	0.0056	4.837	0.092	0.1133	0.0005	1852	7
7.2	190	0.62	14449	0.11	0.1720	0.3285	0.0060	5.152	0.102	0.1137	0.0007	1860	10
8.1	969	0.27	14453	0.11	0.0781	0.3255	0.0059	5.055	0.094	0.1126	0.0003	1842	4
8.2	1072	0.55	203252	0.00	0.1590	0.3218	0.0058	5.027	0.093	0.1133	0.0002	1853	4
9.1	606	0.32	36819	0.04	0.0868	0.3286	0.0059	5.166	0.096	0.1140	0.0003	1865	5
10.1	350	0.37	57110	0.03	0.1024	0.3309	0.0060	5.187	0.098	0.1137	0.0004	1859	6
11.1	971	0.03	85324	0.02	0.0083	0.3680	0.0067	6.414	0.118	0.1264	0.0002	2048	3
12.1	2185	0.03	14843	0.10	0.0097	0.3335	0.0060	5.268	0.096	0.1146	0.0002	1873	3
13.1	780	0.19	35932	0.04	0.0419	0.3286	0.0059	5.187	0.096	0.1145	0.0003	1872	4
14.1	813	0.50	523560	0.00	0.1400	0.3302	0.0060	5.213	0.097	0.1145	0.0003	1872	4
15.1	232	0.42	41271	0.04	0.1202	0.3233	0.0059	5.054	0.099	0.1134	0.0006	1854	9
16.1	97	0.37	6261	0.25	0.1037	0.3169	0.0059	4.944	0.111	0.1131	0.0012	1850	19
17.1	536	0.37	41322	0.04	0.1036	0.3235	0.0059	5.079	0.095	0.1139	0.0004	1862	6
18.1	403	0.38	69589	0.02	0.1070	0.3328	0.0060	5.227	0.099	0.1139	0.0004	1863	6
19.1	102	0.48	9077	0.17	0.1131	0.3225	0.0060	5.015	0.112	0.1128	0.0012	1845	19
Muscovite pegmatite													
51.1	2179	0.00	1978	0.78	0.0005	0.2967	0.0059	4.553	0.093	0.1113	0.0003	1821	6
52.1	3733	0.00	545	2.83	0.0061	0.3265	0.0064	5.025	0.103	0.1116	0.0004	1826	7

* denotes the percentage of common ^{206}Pb in the total measured ^{206}Pb.

Appendix Table 4.3. Zircon U-Pb SHRIMP data for a leucogabbro (93526022) from the Springvale intrusion.

Grain-analysis	*U ppm*	*Th/U*	*$^{206}Pb/^{204}Pb$*	** f206%*	*$^{208}Pb/^{206}Pb$*	*$^{206}Pb/^{238}U$*	±	*$^{207}Pb/^{235}U$*	±	*$^{207}Pb/^{206}Pb$*	±	*$^{207}Pb/^{206}Pb$ age*	±
300.1	232	1.38	15053	0.10	0.3816	0.3293	0.0073	5.123	0.116	0.1128	0.0003	1846	5
301.1	1314	1.21	106724	0.01	0.3534	0.3330	0.0073	5.213	0.115	0.1135	0.0000	1857	1
302.1	3145	0.66	371747	0.00	0.1813	0.3335	0.0073	5.226	0.115	0.1137	0.0000	1859	1
303.1	566	0.14	46642	0.03	0.0414	0.3329	0.0073	5.209	0.116	0.1135	0.0002	1856	3
304.1	2668	2.00	312500	0.00	0.5487	0.3296	0.0073	5.160	0.114	0.1136	0.0000	1857	1
305.1	795	0.58	72046	0.02	0.1624	0.3318	0.0073	5.181	0.115	0.1133	0.0002	1852	2
306.1	562	0.35	53022	0.03	0.1104	0.3370	0.0074	5.277	0.118	0.1136	0.0002	1857	3
307.1	2527	1.04	51073	0.03	0.2917	0.3291	0.0072	5.154	0.114	0.1136	0.0000	1857	1
308.1	413	1.17	17331	0.09	0.3393	0.3307	0.0073	5.179	0.118	0.1136	0.0004	1857	6
309.1	1050	1.72	45331	0.03	0.4832	0.3248	0.0072	5.083	0.114	0.1135	0.0002	1857	3
310.1	533	1.02	48473	0.03	0.2850	0.3271	0.0072	5.126	0.116	0.1137	0.0003	1859	5
311.1	517	1.14	13321	0.12	0.3626	0.3266	0.0072	5.079	0.115	0.1128	0.0003	1845	5
312.1	962	0.95	42553	0.04	0.2716	0.3245	0.0072	5.069	0.113	0.1133	0.0002	1853	3
313.1	1242	1.34	81699	0.02	0.3635	0.3164	0.0070	4.940	0.110	0.1133	0.0002	1852	3
314.1	1051	1.33	35549	0.04	0.3753	0.3259	0.0072	5.093	0.114	0.1134	0.0002	1854	3
315.1	491	1.09	38536	0.04	0.3120	0.3250	0.0072	5.085	0.115	0.1135	0.0003	1856	5
316.1	286	0.78	19113	0.08	0.2580	0.3189	0.0070	4.984	0.114	0.1134	0.0004	1854	6
317.1	780	1.36	30665	0.05	0.3716	0.3206	0.0071	5.012	0.112	0.1134	0.0002	1854	3

* denotes the percentage of common ^{206}Pb in the total measured ^{206}Pb.

Appendix Table 4.4. Zircon U-Pb SHRIMP data for a quartz gabbro (93526017) from the Toby intrusion.

Grain-analysis	*U ppm*	*Th/U*	*$^{206}Pb/^{204}Pb$*	** f206%*	*$^{208}Pb/^{206}Pb$*	*$^{206}Pb/^{238}U$*	±	*$^{207}Pb/^{235}U$*	±	*$^{207}Pb/^{206}Pb$*	±	*$^{207}Pb/^{206}Pb$ age*	±
1.1	309	0.66	152672	0.01	0.1812	0.3301	0.0073	5.161	0.115	0.1134	0.0002	1854	3
2.1	117	0.50	36536	0.04	0.1372	0.3327	0.0074	5.214	0.119	0.1137	0.0004	1859	7
3.1	85	0.47	32321	0.05	0.1269	0.3374	0.0075	5.259	0.122	0.1131	0.0005	1849	8
4.1	192	0.66	157233	0.01	0.1807	0.3380	0.0075	5.312	0.119	0.1140	0.0003	1864	4
5.1	129	0.57	124224	0.01	0.1569	0.3282	0.0073	5.122	0.118	0.1132	0.0005	1851	8
6.1	150	0.71	56818	0.03	0.1933	0.3301	0.0073	5.188	0.117	0.1140	0.0003	1864	5
7.1	155	0.59	42717	0.04	0.1631	0.3392	0.0075	5.297	0.120	0.1133	0.0003	1853	5
8.1	177	0.59	24242	0.06	0.1619	0.3218	0.0071	5.017	0.114	0.1131	0.0003	1849	6
9.1	118	0.48	31676	0.05	0.1351	0.3312	0.0073	5.195	0.120	0.1138	0.0005	1860	8
10.1	378	0.60	71225	0.02	0.1678	0.3275	0.0072	5.114	0.115	0.1133	0.0002	1852	4
11.1	157	0.62	35448	0.04	0.1684	0.3212	0.0071	4.999	0.114	0.1129	0.0004	1847	6
12.1	454	1.01	523560	0.00	0.2807	0.3271	0.0072	5.122	0.114	0.1136	0.0002	1857	3
13.1	321	0.92	60496	0.03	0.2527	0.3331	0.0073	5.187	0.116	0.1130	0.0003	1847	4
13.2	459	0.93	77101	0.02	0.2558	0.3235	0.0071	5.066	0.113	0.1136	0.0002	1857	3
14.1	425	0.99	431034	0.00	0.2738	0.3245	0.0072	5.096	0.114	0.1139	0.0002	1862	4
15.1	389	0.81	143678	0.01	0.2247	0.3318	0.0073	5.199	0.116	0.1137	0.0002	1859	4
16.1	111	0.52	16321	0.09	0.1423	0.3251	0.0072	5.042	0.117	0.1125	0.0005	1840	9
17.1	219	0.62	42827	0.04	0.1732	0.3330	0.0074	5.164	0.117	0.1125	0.0004	1840	6
18.1	111	0.52	69156	0.02	0.1422	0.3257	0.0072	5.089	0.118	0.1134	0.0005	1854	8
19.1	385	0.95	65189	0.02	0.2621	0.3336	0.0074	5.211	0.117	0.1133	0.0003	1853	4
20.1	179	0.63	22920	0.07	0.1751	0.3328	0.0074	5.179	0.118	0.1129	0.0004	1846	6
21.1	188	0.59	21061	0.07	0.1627	0.3292	0.0073	5.135	0.117	0.1131	0.0004	1850	6
22.1	99	0.51	12158	0.13	0.1400	0.3277	0.0073	5.088	0.120	0.1126	0.0006	1842	10
23.1	169	0.55	27108	0.06	0.1504	0.3229	0.0071	5.046	0.116	0.1133	0.0005	1853	8

* denotes the percentage of common ^{206}Pb in the total measured ^{206}Pb.

Appendix Table 4.5. Zircon U-Pb SHRIMP data for a mottled anorthosite (94522307) from the Sally Malay intrusion.

Grain-analysis	*U ppm*	*Th/U*	$^{206}Pb/^{204}Pb$	* *f206%*	$^{208}Pb/^{206}Pb$	$^{206}Pb/^{238}U$	±	$^{207}Pb/^{235}U$	±	$^{207}Pb/^{206}Pb$	±	$^{207}Pb/^{206}Pb$ *age*	±
2.1	59	0.77	INF	-0.00	0.2249	0.3216	0.0064	5.000	0.111	0.1128	0.0009	1845	14
3.1	73	0.61	38926	0.04	0.1773	0.3210	0.0064	4.981	0.104	0.1125	0.0005	1841	8
4.1	113	0.51	35423	0.04	0.1451	0.3165	0.0063	4.913	0.100	0.1126	0.0004	1841	6
5.1	582	0.89	149254	0.01	0.2564	0.3227	0.0064	5.011	0.100	0.1126	0.0001	1842	2
5.2	411	0.75	INF	-0.00	0.2156	0.3119	0.0215	4.871	0.338	0.1133	0.0002	1853	4
6.1	105	1.14	29412	0.05	0.3310	0.3236	0.0064	5.002	0.103	0.1121	0.0004	1834	7
7.1	98	0.81	22548	0.07	0.2364	0.3183	0.0063	4.926	0.102	0.1123	0.0005	1836	7
8.1	164	1.07	INF	-0.01	0.3081	0.3139	0.0062	4.907	0.099	0.1134	0.0003	1854	4
8.2	199	1.19	INF	-0.03	0.3469	0.3311	0.0229	5.147	0.358	0.1127	0.0005	1844	7
9.1	82	1.00	30618	0.05	0.2869	0.3253	0.0065	5.063	0.106	0.1129	0.0005	1847	8
10.1	107	0.53	65104	0.02	0.1498	0.3242	0.0064	5.019	0.103	0.1123	0.0004	1836	6
10.2	132	0.38	35002	0.04	0.1085	0.3026	0.0060	4.687	0.096	0.1123	0.0004	1838	6
11.1	80	0.98	77160	0.02	0.2834	0.3229	0.0064	5.009	0.103	0.1125	0.0004	1840	6
12.1	107	0.93	46598	0.03	0.2677	0.3192	0.0063	4.972	0.103	0.1130	0.0005	1848	7
12.2	99	0.78	17649	0.09	0.2248	0.3366	0.0067	5.232	0.108	0.1127	0.0004	1844	7
13.1	1316	2.21	746269	0.00	0.6334	0.3208	0.0063	4.975	0.099	0.1125	0.0000	1840	1
13.2	1096	2.34	136799	0.01	0.6787	0.3212	0.0222	5.006	0.346	0.1130	0.0002	1849	3
13.3	975	1.36	77220	0.02	0.3945	0.3596	0.0248	5.604	0.388	0.1130	0.0002	1849	3
14.1	108	0.84	19881	0.08	0.2413	0.3220	0.0064	4.993	0.103	0.1125	0.0004	1839	7
15.1	100	1.07	24863	0.06	0.3165	0.3061	0.0061	4.734	0.098	0.1122	0.0005	1835	8
16.1	165	0.95	64977	0.02	0.2761	0.3165	0.0063	4.907	0.099	0.1125	0.0003	1839	4
18.1	70	0.66	17277	0.09	0.1899	0.3168	0.0063	4.931	0.104	0.1129	0.0006	1847	9
25.1	1279	1.01	60716	0.03	0.2904	0.3348	0.0231	5.220	0.361	0.1131	0.0001	1850	2

* denotes the percentage of common ^{206}Pb in the total measured ^{206}Pb.
INF = very low ^{204}Pb, not measurable.

Appendix Table 4.6. Baddeleyite U-Pb SHRIMP data for a mottled anorthosite (94522307) from the Sally Malay intrusion.

Grain-analysis	*U ppm*	*Th/U*	$^{206}Pb/^{204}Pb$	* *f206%*	$^{208}Pb/^{206}Pb$	$^{206}Pb/^{238}U$	±	$^{207}Pb/^{235}U$	±	$^{207}Pb/^{206}Pb$	±	$^{207}Pb/^{206}Pb$ *age*	±
1.1	124	0.00	243309	0.00	0.0010	0.2878	0.0057	4.464	0.093	0.1125	0.0006	1840	9
19.1	32	0.00	9741	0.16	0.0004	0.3307	0.0228	5.078	0.370	0.1114	0.0018	1822	30
20.1	61	0.00	19223	0.08	0.0041	0.2993	0.0207	4.720	0.340	0.1144	0.0015	1870	24
21.1	61	0.02	45704	0.03	0.0074	0.3736	0.0258	5.820	0.411	0.1130	0.0010	1848	16
22.1	89	0.02	19253	0.08	0.0057	0.3143	0.0217	4.904	0.343	0.1132	0.0007	1851	11
23.1	42	0.00	5493	0.28	-0.0005	0.3295	0.0228	5.078	0.368	0.1118	0.0017	1828	28
24.1	47	0.00	8283	0.19	0.0013	0.3255	0.0225	5.054	0.358	0.1126	0.0011	1842	17
26.1	66	0.00	15380	0.10	0.0011	0.3103	0.0214	4.771	0.334	0.1115	0.0007	1825	11
27.1	71	0.00	21983	0.07	0.0018	0.3104	0.0214	4.858	0.342	0.1135	0.0009	1857	14
27.2	58	0.00	22085	0.07	0.0011	0.3008	0.0208	4.668	0.333	0.1126	0.0013	1841	21
28.1	61	0.01	9813	0.16	0.0022	0.3229	0.0223	4.994	0.352	0.1122	0.0009	1835	14
29.1	54	0.00	29595	0.05	0.0039	0.3075	0.0212	4.773	0.336	0.1126	0.0009	1841	15
31.1	41	0.00	11130	0.14	0.0023	0.3222	0.0222	4.931	0.349	0.1110	0.0010	1816	17
32.1	67	0.00	INF	-0.07	0.0042	0.3334	0.0230	5.221	0.370	0.1136	0.0011	1857	18
32.2	41	0.00	15470	0.10	-0.0002	0.3500	0.0242	5.453	0.391	0.1130	0.0014	1848	22
33.1	29	0.00	283286	0.00	0.0052	0.2952	0.0204	4.573	0.323	0.1123	0.0010	1838	16
34.1	30	0.00	16375	0.09	0.0014	0.3550	0.0245	5.504	0.391	0.1124	0.0012	1839	19
35.1	47	0.00	74019	0.02	0.0018	0.3252	0.0224	5.056	0.354	0.1128	0.0007	1845	11
36.1	41	0.00	14808	0.10	0.0007	0.3569	0.0246	5.574	0.395	0.1133	0.0011	1853	17
37.1	68	0.01	32300	0.05	0.0039	0.3379	0.0233	5.231	0.366	0.1123	0.0007	1837	10
38.1	173	0.00	INF	-0.00	0.0032	0.3125	0.0216	4.874	0.338	0.1131	0.0003	1850	5
39.1	57	0.00	36510	0.04	0.0007	0.3543	0.0245	5.520	0.388	0.1130	0.0008	1848	13
40.1	37	0.00	17182	0.09	0.0023	0.3166	0.0219	4.922	0.348	0.1128	0.0010	1844	16
41.1	59	0.01	23618	0.07	0.0103	0.3089	0.0213	4.835	0.339	0.1135	0.0008	1857	12
42.1	47	0.00	12726	0.12	0.0000	0.3205	0.0221	4.966	0.350	0.1124	0.0009	1838	14
43.1	60	0.00	10326	0.15	0.0008	0.3374	0.0233	5.200	0.366	0.1118	0.0009	1829	14
44.1	39	0.00	INF	-0.03	0.0052	0.2974	0.0205	4.610	0.329	0.1124	0.0013	1839	20
45.1	107	0.00	21209	0.07	0.0024	0.3231	0.0223	5.036	0.351	0.1131	0.0005	1849	8
46.1	57	0.00	13401	0.12	-0.0002	0.3266	0.0225	4.997	0.353	0.1110	0.0009	1815	15
48.1	139	0.01	42626	0.04	0.0052	0.3199	0.0221	5.017	0.349	0.1138	0.0004	1860	6

* denotes the percentage of common ^{206}Pb in the total measured ^{206}Pb.
INF = very low ^{204}Pb, not measurable.

Appendix Table 4.7. Zircon U-Pb SHRIMP data for a paramigmatite (93525043) from the McIntosh intrusion.

Grain-analysis	*U ppm*	*Th/U*	$^{206}Pb/^{204}Pb$	* *f206%*	$^{208}Pb/^{206}Pb$	$^{206}Pb/^{238}U$	±	$^{207}Pb/^{235}U$	±	$^{207}Pb/^{206}Pb$	±	$^{207}Pb/^{206}Pb$ *age*	±
Leucosome—younger zircons													
111.1	369	1.18	14285714	0.00	0.3264	0.3221	0.0071	4.979	0.111	0.1121	0.0002	1834	3
111.2	351	1.04	102775	0.02	0.2917	0.3225	0.0071	4.966	0.112	0.1117	0.0003	1827	4
114.1	362	0.98	81566	0.02	0.2697	0.3131	0.0069	4.820	0.109	0.1116	0.0003	1826	5
114.2	293	0.59	108225	0.01	0.1603	0.3119	0.0069	4.800	0.108	0.1116	0.0003	1826	5
114.3	374	0.81	34423	0.05	0.2285	0.3275	0.0072	5.088	0.116	0.1127	0.0004	1843	6
115.1	221	0.33	4558	0.34	0.0929	0.3227	0.0071	4.963	0.115	0.1115	0.0005	1825	8
116.1	424	0.90	65189	0.02	0.2476	0.3259	0.0072	5.020	0.113	0.1117	0.0002	1827	4
116.2	376	0.90	51546	0.03	0.2486	0.3069	0.0068	4.729	0.107	0.1118	0.0004	1828	6
120.1	444	1.07	65189	0.02	0.2971	0.3246	0.0072	5.026	0.113	0.1123	0.0002	1837	4
125.1	350	0.93	17513	0.09	0.2603	0.3311	0.0073	5.122	0.118	0.1122	0.0004	1835	7
126.1	179	0.67	22302	0.07	0.1892	0.3133	0.0070	4.829	0.113	0.1118	0.0006	1828	10
126.2	173	0.40	21160	0.07	0.1118	0.3072	0.0068	4.731	0.109	0.1117	0.0005	1827	8
131.1	232	0.34	18889	0.08	0.0962	0.3101	0.0069	4.776	0.110	0.1117	0.0005	1827	7
131.2	254	0.93	271003	0.00	0.2584	0.3140	0.0069	4.849	0.110	0.1120	0.0004	1832	6
Palaeosome—older zircons													
100.1	210	0.28	INF	-0.01	0.0768	0.3456	0.0076	5.486	0.126	0.1151	0.0005	1882	8
101.1	201	0.29	47348	0.03	0.0785	0.3429	0.0076	5.425	0.122	0.1147	0.0003	1876	4
102.1	231	0.57	55249	0.03	0.1579	0.4115	0.0091	8.066	0.180	0.1422	0.0003	2254	3
103.1	393	0.47	168919	0.00	0.1290	0.3306	0.0073	5.193	0.116	0.1139	0.0002	1863	3
104.1	369	0.35	163399	0.00	0.1018	0.3259	0.0072	5.140	0.115	0.1144	0.0002	1870	3
105.1	193	0.22	71633	0.02	0.0625	0.3319	0.0073	5.266	0.119	0.1151	0.0003	1881	5
106.1	382	0.70	273224	0.00	0.1948	0.3387	0.0075	5.321	0.119	0.1139	0.0002	1863	4
107.1	202	0.40	35855	0.04	0.1121	0.3285	0.0073	5.151	0.116	0.1137	0.0003	1860	5
108.1	377	0.37	119760	0.01	0.1030	0.3353	0.0074	5.287	0.118	0.1144	0.0002	1870	4
109.1	260	0.45	46882	0.03	0.1258	0.3270	0.0072	5.141	0.116	0.1140	0.0003	1865	5
110.1	360	0.54	56786	0.03	0.1475	0.3205	0.0071	5.037	0.113	0.1140	0.0002	1864	4
112.1	349	0.43	39124	0.04	0.1205	0.3270	0.0072	5.147	0.115	0.1142	0.0002	1867	4
113.1	449	0.46	38447	0.04	0.1287	0.3258	0.0072	5.131	0.115	0.1142	0.0002	1867	3
117.1	513	0.68	195313	0.00	0.1914	0.3304	0.0073	5.180	0.116	0.1137	0.0002	1859	4
118.1	990	0.39	94162	0.02	0.1092	0.4857	0.0107	11.754	0.261	0.1755	0.0002	2611	2
119.1	476	0.25	32394	0.05	0.0687	0.3315	0.0073	5.201	0.117	0.1138	0.0003	1860	4
121.1	271	0.48	775194	0.00	0.1369	0.3326	0.0073	5.218	0.118	0.1138	0.0003	1861	5
122.1	218	0.40	33580	0.05	0.1086	0.3291	0.0073	5.153	0.117	0.1136	0.0004	1857	6
123.1	576	0.91	72622	0.02	0.2534	0.3211	0.0071	5.023	0.112	0.1135	0.0002	1855	3
124.1	281	0.18	657895	0.00	0.0498	0.3241	0.0072	5.127	0.117	0.1147	0.0004	1876	6
127.1	336	0.59	16946	0.09	0.1648	0.3234	0.0071	5.058	0.115	0.1134	0.0004	1855	6
128.1	229	0.42	31201	0.05	0.1173	0.3345	0.0074	5.397	0.124	0.1170	0.0004	1911	7
129.1	270	0.32	7610	0.20	0.0949	0.2928	0.0065	4.595	0.106	0.1138	0.0005	1862	7
130.1	176	0.41	58207	0.03	0.1139	0.3273	0.0073	5.190	0.120	0.1150	0.0005	1880	8

* denotes the percentage of common ^{206}Pb in the total measured ^{206}Pb. INF = very low ^{204}Pb, not measurable.

APPENDIX 5. MAGNETIC SUSCEPTIBILITY TABLES

Code: Four-digit number, comprising year of collection (92), and AGSO project code (52; LAB for some samples).

Sample: Four-digit sample number.

Fr: Fraction of sample used.

E-AMG: Australian Map Grid (AMG) co-ordinates comprising 6 digit easting.

N-AMG: Australian Map Grid (AMG) co-ordinates comprising 7 digit northing.

Lithology: Simplified field description of lithology.

Unit: Name of formation, intrusion, informal rock unit.

Magnetic susceptibility [Field] (SI [10^{-6}]): As measured by R.D. Shaw on exposures of rock in the field. Commonly, in this particular terrain, the wide variation between field and laboratory measurements is a result of heterogeneous variations in the content of the magnetic mineral, which is generally magnetite.

Estimated magnetite content %: Approximate estimate of the content of 'magnetite' in percent; assumes 31 415 [SI *10^{-6}] = 1% of 'magnetite'; uses field values.

Magnetic susceptibility [Laboratory] (SI [10^{-6}]): Normalised SI*10^{-6}; measured in AGSO Laboratory Black Mountain, Canberra, on cored samples.

NRM (mA/m): Normal Remanent Magnetism; measured in AGSO Laboratory Black Mountain, Canberra, on cored samples.

NRM inclination: Normal Remanent Magnetism (NRM) measured with respect to the foliation on hand specimens oriented with a Brunton compass. Basic cleaning of 2.5 cm drilll core samples only; not suitable for palaeomagnetic studies; used to give an indication of whether NRM is an important parameter or not.

Bulk specific gravity: Equivalent to dry density; units are g/cc; 1.0 g/cm^3 is equivalent to one tonne per cubic metre; analyses by K. Rouse & S. Burrows, AMDEL Report L5863/94; ASTM C97–83 standard test method by water absorption.

Gamma–ray (c/s): Total counts/second; relative spectrometric (radiometric) measurement made in field by hand-held instrument while in a standing position.

Notes: Information that could be important to understanding the measured sample/site values.

Appendix Table 5. Measured physical properties of rock samples from the Dixon Range and Gordon Downs 1:250 000 Sheet areas.

Code	*Sample*	*Fr*	*E-AMG*	*N-AMG*	*Lithology*	*Unit*	*Magnetic suscept. [Field] (SI [10^{-6}])*	*Estimated magnetite content (%)*	*Magnetic suscept. [Laborat.] (SI [10^{-6}])*	*NRM (mA/m)*	*NRM inclin.*	*Bulk specific gravity*	*Gamma-ray (c/s)*	*Notes*
9252	2048		377750	8035380	Amphibolite	Tickalara Metamorphics	430	0.01						
9252	2057		374080	8033260	Gabbro	Panton intrusion	410	0.01						
9252	2070		373580	8036190	Magnetite gabbro	Panton intrusion	12 800	0.4						
9252	2082	8	376050	8036770	Plagioclase peridotite	Panton intrusion	510	0.02				2.97		SiO_2 - 38.1 wt%, MgO - 21.8%, $FeO+Fe_2O_3$ - 8.4%, Al_2O_3 - 15.2%
9252	2085	8	376100	8036700	Serpentinised dunite	Panton intrusion	4470	0.15				2.95		SiO_2 - 35 wt%, MgO - 43.1%, $FeO+Fe_2O_3$ - 13.1%, Al_2O_3 - 4.3%
9252	2087	2	376200	8036600	Tremolite-actinolite ultramafic rock	Panton intrusion						2.98		
9252	2097	1	376440	8036190	Gabbro	Panton intrusion	340	0.01						
9252	2106	7	376340	8035800	Anorthosite	Panton intrusion	50	0.00						SiO_2 - 48 wt%, MgO - 2.2%, $FeO+Fe_2O_3$ - 2.5%, Al_2O_3 - 28.5%
9252	2108	5	376340	8035720	Anorthosite	Panton intrusion	250	0.01						
9252	2109	7	375930	8035160	Anorthosite	Panton intrusion	1020	0.05				2.80		SiO_2 - 46.7 wt%, MgO - 2.5, $FeO+Fe_2O_3$ - 5.4%, Al_2O_3 - 27.2%

9252	2159		376860	8031070	Peridotite	Unnamed intrusion	11 000	0.35	3.02	
9252	2205	9	384500	8043350	Magnetite gabbro	McIntosh intrusion	42 500	1.35		SiO_2 - 47.9 wt%, MgO - 6.9%, $FeO+Fe_2O_3$ - 11.7%, Al_2O_3 - 17.2%
9252	2206		384660	8043860	Magnetite gabbro	McIntosh intrusion	6970	0.22		
9252	2262		382990	8032080	Metabasalt	Tickalara Metamorphics	600	0.02		
9252	2263		382990	8032080	Hybrid granite	Tickalara Metamorphics	160	0.01		
9252	2268	8	383320	8034250	Troctolite	McIntosh intrusion	1520	0.05	3.24	SiO_2 - 42.6 wt%, MgO - 22.7%, $FeO+ Fe_2O_3$ - 15.1%, Al_2O_3 - 9%
9252	2269	9	383450	8034540	Olivine gabbronorite	McIntosh intrusion	2030	0.06	3.22	SiO_2 - 41.2 wt%, MgO - 27.7%, $FeO+ Fe_2O_3$ - 16.9%, Al_2O_3 - 6.3%
9252	2270	9	383660	8034750	Olivine gabbronorite	McIntosh intrusion	1800	0.06		
9252	2287	9	383650	8038130	Olivine gabbro	McIntosh intrusion	1760	0.06		SiO_2 - 47.1 wt%, MgO - 10.4%, $FeO+ Fe_2O_3$ - 6.9%, Al_2O_3 - 18.6%
9252	2288	9	383660	8038220	Olivine gabbronorite	McIntosh intrusion	1770	0.06		
9252	2358	8	381060	8043640	Anorthosite	West McIntosh intrusion	70	>0.01		
9252	2398		388120	8051380	Gabbro	Melon Patch intrusion	520	0.02		

9252	2435		387000	8043620	Gabbro	Wild Dog Creek intrusion	210	0.01						
9252	2447		354200	8034900	Cordierite-magnetite -sillimanite metasediment	Raft in Springvale intrusion	15 400	0.5						Cordierite, magnetite, sillimanite
9252	2452	5	360050	8033090	Biotite granite	Paperbark supersuite	210	0.01						SiO_2 - 70.3 wt % MgO - 0.4%, FeO+ Fe_2O_3 - 4.1%, Al_2O_3 - 13.3%
9252	2486		360220	8032490	Granite	Paperbark supersuite	13 100	0.42						
9252	2510		362350	8052150	Biotite granite	Paperbark supersuite	170	0.01						
9252	2520	9	357650	8056450	Biotite olivine gabbro	Toby intrusion	12 000	0.38						SiO_2 - 49 wt %, MgO - 8.3%, FeO+ Fe_2O_3 - 10.9%, Al_2O_3 - 16.0%
9252	2546		374060	8022260	Magnetite gabbro	Panton River intrusion	11 400	0.35						
9252	5018	A	376900	7975000	Felsic volcaniclastic rock	Biscay Formation	350	0.01				27		
9252	5025	A	377600	7971000	Black chert	Biscay Formation	100	0.00				2		
9252	5029		377200	7962900	Turbiditic sandstone	Olympio Formation	300	0.01	338.41	0.2583	-0.7	2.69	14	
9252	5044		378000	7961000	Siltstone	Ranford Formation	300	0.01					19	
9252	5064		408300	7963900	Basalt	Antrim Plateau Basalt	20 000	0.65					13	With biotite and chlorite, auto-metamorphism?
9252	5071		375270	7955800	Metabasalt	Biscay Formation	800	0.03	1520.15	21981	44.7	2.99	5	
9252	5073	A	371240	8049400	Gabbro	Togo intrusion	400	0.01					27	Sheared; within Springvale Fault Zone

9252	5073	B	371240	8049400	Granite	Sandy Dam Monzogranite	50	>0.01						
9252	5106	A	402800	8064500	Deformed metabasalt	Tickalara Metamorphics	600	0.02	410.27	0.9678	-57	2.72		
9252	5121		372200	8032700	Granite	Togo Monzogranite	6000	0.20	9204.81	404.82	-33.9	2.68	7	
9252	5122		370700	8033500	Leucogranite	Corrara Granite	1300	0.04					7	Sally Downs supersuite
9252	5126		364900	8029900	Deformed granite	Mussell Creek Granite	250	0.01	117.65	18.168	-20.9	2.64	16	Sheared, porphyritic
9252	5128		363000	80310500	Granite	Mussell Creek Granite	500	0.02					15	Sheared, porphyritic
9252	5129		363330	80311400	Deformed granite	Mussell Creek Granite	900	0.03	129.84	0.08379	0	2.60	15	Sheared, porphyritic
9252	5133		357800	8032200	Olivine gabbro	Springvale intrusion (east)	1700	0.05	2874.25	5808.9	73.5	3.17	2	
9252	5136		350100	8035100	Granite	Top Water Tonalite	300	0.01	220.87	0.2436	-57.1	2.69	14.5	
9252	5138	A	342000	8048500	Felsic Volcanics	Whitewater Volcanics	100	>0.01						
9252	5138	B	345500	8036200	Metasediments	Marboo Formation	100	>0.01					10	
9252	5143		370500	7982000	Turbiditic sandstone	Biscay Formation	800	0.03	1017.83	47.899	-60.3	3.04	2	
9252	5145		368600	7982000	Black siltstone	Olympio Formation	400	0.01	293.06	1.368	-57	2.99	20	
9252	5148		363600	7980700	Sandstone	Moola Bulla Formation	200	0.01	86.28	1.0796	-37.8		19	
9252	5150		362600	7982800	Metabasalt	Carson Volcanics	25 000	0.80	54 434.72	3832.7	-49.8	2.98	4	
9252	5154	D	347800	7974800	Ironstone	Koongie Park Formation	60 000	1.90					13	Rockhole Prospect; weathered samples can be low (200-400)

9252	5157		397200	8070800	Metadolerite	Woodward Dolerite?	400	0.01	777.56	15.128	8.7	2.95	2	Post-tectonic, of the Woodward Dolerite type
9252	5158		397200	8070800	Sillimanite gneiss	Tickalara Metamorphics	60 000	1.90	76 706.75	13 862	-61.3	2.79	4	
9252	5160		387000	8068700	Tonalite	Mabel Downs Tonalite	40 000	1.28	33 939.35	35 688	-74.8	2.71	3.5	Foliated
9252	5162		403700	8074700	Granodiorite	Mabel Downs Tonalite	20 000	0.65	24 277.69	282.13	-14.7	2.72	3	
9252	5169		412800	8073900	Basalt	'Fish Hole Dolerite'	6500	0.20	846.26	9.658	-23.6	3.04	3	
9252	5173		418700	8076900	Turbiditic sandstone	Olympio Formation	500	0.02	1863.97	36.965	-10.8	2.67	19	
9252	5175		423800	8061500	Basalt	Antrim Plateau Basalt	15 000	0.48	34 839.53	3578.3	-16.3	2.83	4	
9252	5179	A	422815	8058289	Basalt	Antrim Plateau Basalt	30 000	0.95	34 697.40	747.45	12.3	2.92	5	
9252	5180	A	422800	8058300	Amydaloidal basalt	Antrim Plateau Basalt	2500	0.08	1191.66	54.712	-52.6	2.28	13	Weathered?
9252	5181		422800	8058300	Amydaloidal basalt	Antrim Plateau Basalt	1750	0.06	35 304.28	1216.09	-54.2	2.89	8	
9252	5188		407500	8077600	Diorite	Mabel Downs Tonalite	2500	0.08						Foliated, with leucosomes
9252	5192	A	400600	8081500	Sillimanite gneiss	Tickalara Metamorphics	6000	0.20	1532.44	335.86	25.6	2.74	5	
9252	5192	B	400600	8081500	Sillimanite gneiss	Tickalara Metamorphics	5000	0.16	13 173.26	4290.9	-3		4	
9252	5194		419600	8114200	Hornblende tonalite	Mabel Downs Tonalite	3500	0.1	3600.93	1687.6	-76.7	2.80	6	Foliated, with leucosomes
9252	5195		420600	8094500	Dolerite	Tickalara Metamorphics	600	0.02	838.02	0.0347	-63	3.02	5	Foliated, Woodward Dolerite'

9252	5197		420300	8095600	Diorite	McHale Granite	10 000	0.32					Hornblende
9252	5199	A	400500	8081600	Pyroxene granulite	Tickalara Metamorphics	400	0.01	367.35	88.43	-9.4	2.75	Fine-grained, hybrid rock; +biotite
9252	5199	B	400500	8081600	Pyroxene granulite	Tickalara Metamorphics	400	0.01	1282.13	176.88	41.4	3.07	Hybrid rock
9252	5210	A	407100	8096090	Sillimanite gneiss	Tickalara Metamorphics	15 000	0.48				2	
9252	5210	B	407100	8096090	Garnet-sillimanite gneiss	Tickalara Metamorphics	100	>0.01				2	
9252	5210	C	407100	8096090	Para-amphibolite	Tickalara Metamorphics	200	>0.01	239.48	4.43	-6.6	2.77	2
9252	5211		408100	8061550	Para-amphibolite	Tickalara Metamorphics	300	0.01	782.97	3.5283	5.9	2.85	2
9252	5212		408500	8061500	Metabasalt	'Fish Hole Dolerite'	400	0.01	792.90	3.718	-62.2	2.80	1
9252	5215	A	409300	8064000	Metabasalt	'Fish Hole Dolerite'	300	0.01	989.07	6735	71.1		6
9252	5216	A	409400	8064000	Para-amphibolite	Tickalara Metamorphics	700	0.02	822.79	0.0243	9	2.93	2
9252	5217		410300	8067400	Banded magnetite quartzite	Tickalara Metamorphics	325 000	10.35					2
9252	5219		410600	8069000	Vein quartz	Halls Creek Fault	>50	>0.01					0.1
9252	5223		373400	8057300	Granite	Togo Monzogranite	50	>0.01					13 Sheared, porphyritic
9252	5224		373700	8057200	Biotite gabbronorite	Toby intrusion	700	0.02					4 Dolerite
9252	5226	A	373300	8057600	Granite	Togo Monzogranite	50	>0.01					16
9252	5226	B	373300	8057600	Granite eluvium	Togo Monzogranite	100	>0.01					14
9252	5227		371900	8058000	Granite	Togo Monzogranite	300	>0.01					16 Sheared, porphyritic

9252	5228	A	373700	8059000	Biotite gabbronorite	Toby intrusion	200	>0.01				6	Dolerite
9252	5231		373800	8061900	Granite	Togo Monzogranite	400	0.01				5	Sheared, porphyritic
9252	5232		373600	8061900	Granite	Togo Monzogranite	300	0.01				12	Sheared, porphyritic
9252	5234		283170	8063000	Metadiorite	Tickalara Metamorphics	750	0.02	1079.87	10.857	49.6	3.08	
9252	5235		283170	8063000	Tonalite	Mabel Downs Tonalite	2500	0.08				5	
9252	5160	C	387000	8068700	Tonalite	Mabel Downs Tonalite	40 000	1.27	34 340.00			2.71	3.5	Duplicate analyses
LAB	5160	C	387000	8068700	Tonalite	Mabel Downs Tonalite	40 000	1.28	34 680.00			2.71	3.5	Duplicate analyses
LAB	5158	C	397200	8070800	Sillimanite gneiss	Tickalara Metamorphics	60 000	1.9	77 310.00			2.79	4	Duplicate analyses
LAB	5158	C	397200	8070800	Sillimanite gneiss	Tickalara Metamorphics	60 000	1.9	77 780.00			2.79	4	Duplicate analyses
LAB	5211	C	408100	8061550	Para-amphibolite	Tickalara Metamorphics	300	0.01	746.80			2.85	2	Duplicate analyses
LAB	5211	C	408100	8061550	Para-amphibolite	Tickalara Metamorphics	300	0.01	741.50			2.85	2	Duplicate analyses
LAB	5126	C	364900	8029900	Granite	Musell Creek Granite	250	0.01	117.30			2.64	16	Duplicate analyses
LAB	5126	C	364900	8029900	Granite	Musell Creek Granite	250	0.01	115.40			2.64	16	Duplicate analyses
LAB	5071	C	375270	7955800	Metabasalt	Biscay Formation	800	0.03	1583.00				5	Duplicate analyses
LAB	5071	C	375270	7955800	Metabasalt	Biscay Formation	800	0.03	1594.00				5	Duplicate analyses

APPENDIX 6. NATIONAL GEOSCIENCE MAPPING ACCORD BIBLIOGRAPHY OF THE EAST KIMBERLEY

The following publications (including abstracts), maps, and commentaries relating to the East Kimberley have been produced by AGSO and GSWA within the framework of the National Geoscience Mapping Accord Kimberley–Arunta project. The 118 entries are post-1991 and have been alphabetically grouped into seven categories:

- geochemistry
- geochronology
- geological maps and map commentaries
- geophysics and remote sensing
- mineralisation
- regional geology
- structure and tectonics

Geochemistry

Sheppard, S., Griffin, T.J. & Tyler, I.M., 1995. Geochemistry of felsic igneous rocks from the southern Halls Creek Orogen. Geological Survey of Western Australia, Record 1995/4, 81 pp.

Sheppard, S., Griffin, T.J. & Tyler, I.M., 1997. Compilation of whole-rock geochemical data for the King Leopold and Halls Creek Orogens. Geological Survey of Western Australia, Record 1997/4, 138 pp.

Sun, S-s., 1997. Chemical and isotopic features of Palaeoproterozoic mafic igneous rocks of Australia: implications for tectonic processes. In: Rutland, R.W.R. & Drummond, B.J. (editors), Palaeoproterozoic tectonics and metallogenesis: comparative analysis of parts of the Australian & Fennoscandian shields. Workshop, Darwin, September, 14-22, 1997. Australian Geological Survey Organisation, Record 1997/44, 119–122.

Sun, S-s. & Hoatson, D.M. 2000. Chapter 11. Trace-element geochemical and Nd isotopic study of the mafic-ultramafic intrusions: implications for their petrogenesis and tectonic environment. In: Hoatson, D.M. & Blake D.H. (editors), Geology and economic potential of the Palaeoproterozoic layered mafic–ultramafic intrusions in the East Kimberley, Western Australia. Australian Geological Survey Organisation Bulletin 246, 226–249.

Taylor, W.R., Esslemont, G. & Sun, S-s., 1995. Geology of the volcanic-hosted Brockman rare-metals deposit, Halls Creek Mobile Belt, northwest Australia, Part II - Geochemistry and petrogenesis of the Brockman volcanics. Mineralogy and Petrology, 52, 231–255.

Geochronology

Page, R.W., 1997. Some key geochronological constraints for Palaeoproterozoic crustal evolution in northern Australia. In: Rutland, R.W.R. & Drummond, B.J. (editors), Palaeoproterozoic tectonics and metallogenesis: comparative analysis of parts of the Australian & Fennoscandian shields. Workshop, Darwin, September, 14-22, 1997. Australian Geological Survey Organisation, Record 1997/44, 87–90.

Page, R.W. & Hoatson, D.M., 1997. SHRIMP U-Pb geochronology of Palaeoproterozoic layered mafic-ultramafic intrusions, East Kimberley, Western Australia. Abstract GAC/MAC Annual Meeting Ottawa '97, 9-21 May 1997, A 111.

Page, R.W. & Hoatson, D.M., 2000. Chapter 6. Geochronology of the mafic-ultramafic intrusions. In: Hoatson, D.M. & Blake D.H. (editors), Geology and economic potential of the Palaeoproterozoic layered mafic–ultramafic intrusions in the East Kimberley, Western Australia. Australian Geological Survey Organisation Bulletin 246, 163–172.

Page, R.W. & Sun, S-s., 1994. Evolution of the Kimberley region, WA and adjacent Proterozoic inliers — new chronological constraints. Geological Society of Australia, Abstracts, 37, 12th Australian Geological Convention, Perth, 26-30 September, 332–333.

Page, R.W., Sun, S-s. & Carr, G., 1994. Proterozoic sediment-hosted lead-zinc-silver deposits in northern Australia - U-Pb zircon and Pb isotope studies. Geological Society of Australia, Abstracts, Abstracts, 37, 12th Australian Geological Convention, Perth, 26-30 September, 334–335.

Page, R.W., Blake, D.H., Sun, S-s., Tyler, I.M., Griffin, T.J. & Thorne A.M., 1994. New geological and geochronological constraints on volcanogenic massive sulphide prospectivity near Halls Creek, W.A. AGSO Research Newsletter, 20, 5–7.

Page, R.W., Blake, D.H., Edgecombe, D.R. & Pearcey, D.P, 1995. Geochronology of an exposed late Archaean basement terrane in The Granites–Tanami Region. AGSO Research Newsletter, 22, 19–20.

Page, R.W., Hoatson, D.M., Sun, S-s. & Foudoulis, C., 1995. High–precision geochronology of Palaeoproterozoic layered mafic-ultramafic intrusions in the East Kimberley. AGSO Research Newsletter, 22, 7–8.

Page, R.W., Tyler, I.M. & Blake, D.H., 1995. Geochronology of magmatism and high-grade metamorphism, Kimberley region, W.A. (abstract) 3rd Australian Conference on Geochronology (ACOG-3); Perth, November 1995, 3, 25.

Page, R.W., Sun, S-s., Blake, D.H., Edgecombe, D.R. & Pearcey, D.P., 1996. Exposed late-Archaean basement terrains in The Granites–Tanami Region, Northern Territory. Abstracts, 41, 13th Australian Geological Convention, Canberra, 19-23 February, 334.

Shaw, R.D., Tyler, I.M., Griffin, T.J. & Webb. A., 1992. New K-Ar constraints on the onset of subsidence in the Canning Basin, Western Australia. BMR Journal of Australian Geology and Geophysics, 13, 31–35.

Sun, S-s., Carr, G.R. & Page, R.W., 1996. A continued effort to improve lead-isotope model ages. AGSO Research Newsletter, 24, 19–20.

Taylor, W.R., Page, R.W., Esslemont, G., Rock, N.H.S. & Chalmers, D.I., 1995. Geology of the volcanic-hosted Brockman rare-metals deposit, Halls Creek Mobile Belt, northwest Australia, Part I—Volcanic environment, geochronology and petrography of the Brockman volcanics. Mineralogy and Petrology, 52, 209–230.

Geological maps and map commentaries

Blake, D.H., 1996. Cow Creek, Western Australia, preliminary 1:100 000 geological map (sheet 4560). Australian Geological Survey Organisation, Canberra.

Blake, D.H., 1996. Gordon Downs, Western Australia, preliminary 1:100 000 geological map (sheet 4660). Australian Geological Survey Organisation, Canberra.

Blake, D.H. & Warren, R.G., 1996. Antrim, Western Australia, preliminary 1:100 000 geological map (sheet 4561). Australian Geological Survey Organisation, Canberra.

Blake, D.H. & Warren, R.G., 1996. Nicholson, Western Australia, preliminary 1:100 000 geological map (sheet 4661). Australian Geological Survey Organisation, Canberra.

Blake, D.H., Tyler, I.M. & Griffin, T.J., 1997. Ruby Plains, Western Australia, 1:100 000 geological map (sheet 4460). Australian Geological Survey Organisation, Canberra.

Blake, D.H., Tyler, I.M. & Sheppard, S., 1997. Geology of the Ruby Plains 1:100 000 Sheet area (4460), Western Australia. Australian Geological Survey Organisation, Canberra, 15 pp.

Blake, D.H., Griffin, T.J., Tyler, I.M., Thorne, A.M. & Warren, R.G., 1999. Halls Creek, Western Australia, 1:100 000 geological map (sheet 4461). Australian Geological Survey Organisation, Canberra.

Blake, D.H., Tyler, I.M., Griffin, T.J., Sheppard, S., Thorne, A.M. & Warren, R.G., 1999. Geology of the Halls Creek 1:100 000 sheet area (4461), Western Australia. Explanatory Notes. Australian Geological Survey Organisation, 36 pp.

Griffin, T.J. & Tyler, I.M., 1994. Angelo, Western Australia, 1:100 000 geological map (sheet 4361). Geological Survey of Western Australia, Perth.

Griffin, T.J., Tyler, I.M., Orth, K. & Sheppard, S., 1998. Geology of the Angelo 1:100 000 sheet: Western Australia Geological Survey, 1:100 000 Geological Series Explanatory Notes, 27 pp.

Sheppard, S., Tyler, I.M. & Hoatson, D.M., 1996. Mount Remarkable, Western Australia, 1:100 000 geological map (sheet 4463). Geological Survey of Western Australia, Perth.

Sheppard, S., Thorne, A.M. & Tyler, I.M. 1997. Bow, Western Australia, 1:100 000 geological map (sheet 4564). Geological Survey of Western Australia, Perth.

Sheppard, S., Tyler, I.M. & Hoatson, D.M., 1997. Geology of the Mount Remarkable 1:100 000 sheet: Western Australia Geological Survey, 1:100 000 Geological Series Explanatory Notes, 27 pp.

Sheppard, S., Thorne, A.M. & Tyler, I.M. 1999. Geology of the Bow 1:100 000 sheet: Western Australia Geological Survey, 1:100 000 Geological Series Explanatory Notes, 36 pp.

Thorne, A.M., Sheppard, S. & Tyler, I.M. 1998. Lissadell, Western Australia, 1:250 000 geological map (sheet SE 52-2). Geological Survey of Western Australia, Perth.

Thorne, A.M., Sheppard, S. & Tyler, I.M. 1999. Lissadell, Western Australia (second edition): Western Australia Geological Survey, 1:250 000 Geological Series Explanatory Notes, 68 pp.

Tyler, I.M. & Griffin, T.J., 1994. Dockrell, Western Australia, 1:100 000 geological map (sheet 4360). Geological Survey of Western Australia, Perth.

Tyler, I.M., Hoatson, D.M. Griffin, T.J., Sheppard, S., Blake, D.H. & Warren, R.G., 1997. McIntosh, Western Australia, 1:100 000 geological map (sheet 4462). Geological Survey of Western Australia, Perth.

Tyler, I.M., Thorne, A.M., Hoatson, D.M. & Blake, D.H., 1997. Turkey Creek, Western Australia, 1:100 000 geological map (sheet 4563). Geological Survey of Western Australia, Perth.

Tyler, I.M., Griffin, T.J. & Sheppard, S., 1998. Geology of the Dockrell 1:100 000 sheet: Western Australia Geological Survey, 1:100 000 Geological Series Explanatory Notes 24 pp.

Tyler, I.M., Thorne, A.M., Sheppard, S., Hoatson, D.M., Griffin, T.J., Blake, D.H. & Warren, R.G., 1998. Dixon Range, Western Australia, 1:250 000 geological map (sheet SE 52–6). Geological Survey of Western Australia, Perth.

Tyler, I.M., Warren, R.G. & Blake, D.H., 1998. Dixon, Western Australia, 1:100 000 geological map (sheet 4562). Geological Survey of Western Australia, Perth.

Geophysics and remote sensing

Macias, L.F., 1995. Remote sensing of mafic-ultramafic rocks: examples from Australian Precambrian terranes. AGSO Journal of Australian Geology & Geophysics, 16/1&2, 163–171.

Macias, L.F., 2000. Chapter 8. Remote sensing of mafic and ultramafic rocks in the McIntosh 1:100 000 sheet area. In: Hoatson, D.M. & Blake D.H. (editors), Geology and economic potential of the Palaeoproterozoic layered mafic–ultramafic intrusions in the East Kimberley, Western Australia. Australian Geological Survey Organisation Bulletin 246, 190–200.

Shaw, R.D. & Macias, L. F., 2000. Chapter 7. Geophysical expression of the mafic-ultramafic intrusions and implications for exploration. In: Hoatson, D.M. & Blake D.H. (editors), Geology and economic potential of the Palaeoproterozoic layered mafic–ultramafic intrusions in the East Kimberley, Western Australia. Australian Geological Survey Organisation Bulletin 246, 173–189.

Shaw, R.D., Meixner, A.S. & Murray, A.S., 2000. Chapter 4. Regional geophysical setting and tectonic implications of the mafic-ultramafic intrusions. In: Hoatson, D.M. & Blake D.H. (editors), Geology and economic potential of the Palaeoproterozoic layered mafic–ultramafic intrusions in the East Kimberley, Western Australia. Australian Geological Survey Organisation Bulletin 246, 63–98.

Mineralisation

Hoatson, D.M., 1994. Geological setting and mineral potential of early Proterozoic layered mafic-ultramafic intrusions, East Kimberley, Western Australia. Geological Society of Australia, Abstracts, 37, 12th Australian Geological Convention, Perth, 26-30 September, 179–180.

Hoatson, D.M., 1995. New mineral discoveries in the East Kimberley. AGSO Research Newsletter, 22, 9–11.

Hoatson, D.M., 1997. Geology and mineralisation of the Palaeoproterozoic layered mafic-ultramafic intrusions in the Halls Creek Orogen, Western Australia. In: Rutland, R.W.R. & Drummond, B.J. (editors), Palaeoproterozoic tectonics and metallogenesis: comparative analysis of parts of the Australian & Fennoscandian shields. Workshop, Darwin, September, 14-22, 1997. Australian Geological Survey Organisation, Record 1997/44, 61–64.

Hoatson, D.M., 1998. The geology and economic potential of the Palaeoproterozoic layered mafic-ultramafic intrusions in the East Kimberley, Western Australia. The Geological Society of South Africa and The South African Institute of Mining and Metallurgy, Symposium Series S18. Extended

Abstract 8th International Platinum Symposium, Rustenburg, 28 June-3 July 1998, 153–156.

Hoatson, D.M., 1998. Platinum-group-element mineralisation in Australian Precambrian layered mafic-ultramafic intrusions. Special Issue of AGSO Journal of Australian Geology & Geophysics, 17(4), 139–151.

Hoatson, D.M., 2000. Chapter 14. Mineralisation and economic potential of the mafic-ultramafic intrusions. In: Hoatson, D.M. & Blake D.H. (editors), Geology and economic potential of the Palaeoproterozoic layered mafic–ultramafic intrusions in the East Kimberley, Western Australia. Australian Geological Survey Organisation Bulletin 246, 278-311.

Hoatson, D.M., in press. Exploration strategies for Precambrian layered mafic–ultramafic intrusions in the East Kimberley. AGSO Research Newsletter, 32.

Hoatson, D.M. & Tyler, I.M., 1993. Prospective layered mafic–ultramafic intrusions in the East Kimberley. AGSO Research Newsletter, 18, 8–9.

Hoatson, D.M., Blake, D.H., Warren, R.G., Orth, K. & Tyler, I.M., 1995. Recent NGMA mapping highlights the metallogenic potential of the East Kimberley. AGSO Research Newsletter, 22, 1–2.

Hoatson, D.M., Sproule, R.A. & Lambert, D.D., 1997. Are there Voisey's Bay-type Ni-Cu-Co sulphide deposits in the East Kimberley of Western Australia? AGSO Research Newsletter, 27, 17–19 (also published in the Canadian publication - The Gangue Newsletter).

Mernagh, T.P., Trudu, A.G. & Hoatson. D.M., 2000. Chapter 13. A Laser Raman and electron probe microanalysis study of chromite from Precambrian layered mafic-ultramafic intrusions in northern Western Australia. In: Hoatson, D.M. & Blake D.H. (editors), Geology and economic potential of the Palaeoproterozoic layered mafic–ultramafic intrusions in the East Kimberley, Western Australia. Australian Geological Survey Organisation Bulletin 246, 265–277.

Pirajno, F., Rugless, C.S., Griffin, T.J. & Tyler, I.M., 1994. Hydrothermal vein gold and base metal deposits in the Halls Creek province, East Kimberley, Western Australia. Geological Society of Australia, Abstracts, 37, 12th Australian Geological Convention, Perth, 26-30 September, 347.

Sanders T.S., 1999. Mineralization of the Halls Creek Orogen, east Kimberley region, Western Australia. Geological Survey of Western Australia, Report 66,44 pp.

Sproule, R. A., Lambert, D. D. & Hoatson, D.M., 1997. Sally Malay intrusion: A Voisey's Bay analogue? Guides to magmatic Ni-Cu-Co mineralisation in the East Kimberley. Geological Society of Australia Abstracts 46, 11th Universities Geoscience Conference, Monash University, Melbourne, 10th October 1997, 39.

Sproule, R. A., Lambert, D. D. & Hoatson, D.M., 1997. Rhenium-osmium isotopic constraints on the genesis of magmatic nickel-copper-cobalt-platinum-group element ores, East Kimberley, Western Australia. Seventh Annual V. M. Goldschmidt Conference, June 2-6, 1997, Tucson, Arizona, 195–196.

Sproule, R.A., Lambert, D.D. & Hoatson, D.M., 1997. Guides to PGE and Ni-Cu-Co exploration in the East Kimberley, Western Australia. In Burroughs, A. (editor), AUSIMM Student and Young Professionals Conference, Abstracts, Ballarat, Victoria, 42–43.

Sproule, R.A., Lambert, D.D. & Hoatson, D.M., 1997. Re-Os and Sm-Nd isotopic constraints on the genesis of magmatic ores in the Palaeoproterozoic Panton intrusion, East Kimberley. New developments in research for ore deposit exploration, Canberra, ACT. Geological Society of Australia, Abstracts 44, 67.

Sproule, R.A., Lambert, D.D. & Hoatson, D.M., 1998. Genesis of Voisey's Bay-style Ni-Cu-Co mineralisation on the east Kimberley, Western Australia. Abstracts 49, 14th Australian Geological Convention, Geoscience for the Millennium, 6-10 July, Townsville, Queensland, 422.

Sproule, R.A., Lambert, D.D., and Hoatson, D.M., 1998. Genesis of Merensky Reef-type PGE and Voisey's Bay-type Ni-Cu-Co mineralisation in the East Kimberley, Western Australia: Perspectives from the Re-Os isotopic system. The Geological Society of South Africa and The South African Institute of Mining and Metallurgy, Symposium Series S18. Extended Abstract 8th International Platinum Symposium, Rustenburg, 28 June-3 July 1998, 385–388.

Sproule, R.A., Lambert, D.D. & Hoatson, D.M., 1999. Re-Os isotopic constraints on the genesis of the Sally Malay Ni-Cu-Co deposit, East Kimberley, Western Australia. Lithos, 47, 89–106.

Sproule, R.A., Lambert, D.D. & Hoatson, D.M., 2000. Chapter 12. Geochemical and isotopic constraints on the petrogenesis of the Panton and Sally Malay intrusions: implications for exploration. In: Hoatson, D.M. & Blake D.H. (editors), Geology and economic potential of the Palaeoproterozoic layered mafic–ultramafic intrusions in the East Kimberley, Western Australia. Australian Geological Survey Organisation Bulletin 246, 250–264.

Tyler, I.M., Pirajno, F. Bagas, L. Myers, J.S. & Preston, W.A. 1998. The geology and mineral deposits of the Proterozoic in Western Australia. AGSO Journal of Australian Geology & Geophysics, 17 (3), 223–244.

Warren, R.G., 1994. Gold mineralisation in the northern East Kimberley gold district, Western Australia. The AIMM Annual Conference, Darwin, 5–9 August 1994, 117–121.

Regional geology

Blake, D.H., 1991. Notes on the geology of the Halls Creek 1:100 000 Sheet area, East Kimberley, Western Australia: results of 1990 fieldwork. Bureau of Mineral Resources, Record, 1991/94, 12 pp.

Blake, D,H., 1994. Migmatites, magma mingling, mylonites and other myths in the east Kimberley, W.A. Geological Society of Australia, Abstracts, 37, 12th Australian Geological Convention, Perth, 26-30 September, 29–30.

Blake, D.H., 1996. How ancient is the Bungle Bungle Range of the East Kimberley, Western Australia? AGSO Research Newsletter, 24, 4–6.

Blake, D.H., 1997. Proterozoic thrusting in the Osmand Range area of the East Kimberley, Western Australia. AGSO Research Newsletter, 26, 4–7.

Blake, D.H., 1997. Speculations relating to the layered mafic-ultramafic intrusions of the East Kimberley. AGSO Research Newsletter, 27, 19–21.

Blake, D.H., 1997. Evolution of the Bungle Bungle Range, East Kimberley. Abstracts 49, 14th Australian Geological Convention, Townsville, Queensland, 6-10 July, 40.

Blake, D.H., 1997. Palaeoproterozoic of the Kimberley to Granites-Tanami region, northwestern Australia. In: Rutland, R.W.R. & Drummond, B.J. (editors), Palaeoproterozoic tectonics and metallogenesis: comparative analysis of parts of the Australian & Fennoscandian shields. Workshop, Darwin, September, 14-

22, 1997. Australian Geological Survey Organisation, Record 1997/44, 21–24.

Blake, D.H. & Hoatson D.M., 1993. Granite, gabbro and migmatite field relationships in the Proterozoic Lamboo Complex of the East Kimberley region, Western Australia. AGSO Journal of Australian Geology and Geophysics, 14/4, 319–330.

Blake, D.H., Griffin, T.J., Tyler, I.M., Young, D.N., Edgoose, C., Shaw, R.D., Black, L.P. & Warren, R.G. 1991. National Geoscience Mapping Accord. Preliminary results of the Kimberley-Arunta project. BMR Research Newsletter, 14, 9–12.

Blake, D.H., Shaw, R.D., Warren, R.G., Sun, S-s., Black, L.P., Hoatson, D.M., Macias L. F. & Page, R. W. 1993. Kimberley-Arunta Mapping Accord Project. AGSO Yearbook 1992, 77–82.

Blake, D.H., Page, R.W., Shaw, R.D. & Warren, R.G., 1994. Correlating geological events between the Proterozoic Arunta and east Kimberley regions. Geological Society of Australia, Abstracts, 37, 12th Australian Geological Convention, Perth, 26–30 September, 31.

Blake, D.H., Shaw, R.D., Warren, R.G., Sun, S-s., Black, L.P., Hoatson, D.M. & Macias L.F. 1994. Kimberley-Arunta Mapping Accord Project. AGSO Yearbook 1993, 71–74.

Blake, D.H., Hoatson, D.M. & Wyborn, L.A.I., 1998. Review of new data and interpretations for the Palaeoproterozoic of the East Kimberley, Western Australia. Abstracts 49, 14th Australian Geological Convention, Townsville, Queensland, 6-10 July, 41.

Blake, D.H., Tyler, I.M. & Page, R.W., 2000. Chapter 3. Regional geology of the Halls Creek Orogen. In: Hoatson, D.M. & Blake D.H. (editors), Geology and economic potential of the Palaeoproterozoic layered mafic–ultramafic intrusions in the East Kimberley, Western Australia. Australian Geological Survey Organisation Bulletin 246, 35–62.

Grey, K. & Blake, D.H., 1999. Neoproterozoic (Cryogenian) stromatolites from the Wolfe Basin, east Kimberley, Western Australia: correlation with the Centralian Superbasin. Australian Journal of Earth Sciences, 46, 329–341.

Grey, K. & Corkeron, M., 1998. Late Neoproterozoic stromatolites in glacigenic successions of the Kimberley region, Western Australia: evidence for a younger Marinoan glaciation. Precambrian Research, 92, 65–87.

Griffin, T.J. & Tyler, I.M., 1992. Geology of the southern Halls Creek Orogen - summary of field work in 1992. Geological Survey of Western Australia, Record, 1992/17, 28 pp.

Hoatson, D.M., 1993. Correlations of structurally disrupted layered ultramafic-mafic intrusions in the East Kimberley. Is Big Ben part of the Panton intrusion? AGSO Research Newsletter, 19, 9–10.

Hoatson, D.M., 1993. Summary of geoscientific information for the East Kimberley, Western Australia, with specific reference to the Dixon Range 1:250 000 Sheet (SE/52-6) and Gordon Downs 1:250 000 Sheet (SE /52-10). Australian Geological Survey Organisation, Record, 1993/32, 76 pp.

Hoatson, D.M., 2000. Chapter 1. Introduction. In: Hoatson, D.M. & Blake D.H. (editors), Geology and economic potential of the Palaeoproterozoic layered mafic–ultramafic intrusions in the East Kimberley, Western Australia. Australian Geological Survey Organisation Bulletin 246, 1–12.

Hoatson, D.M., 2000. Chapter 2. Exploration history of the East Kimberley, Western Australia. In: Hoatson, D.M. & Blake D.H. (editors), Geology and economic potential of the Palaeoproterozoic layered mafic–ultramafic intrusions in the East Kimberley, Western Australia. Australian Geological Survey Organisation Bulletin 246, 13-34.

Hoatson, D.M., 2000. Chapter 5. Geological setting, petrography, and geochemistry of the mafic-ultramafic intrusions. In: Hoatson, D.M. & Blake D.H. (editors), Geology and economic potential of the Palaeoproterozoic layered mafic–ultramafic intrusions in the East Kimberley, Western Australia. Australian Geological Survey Organisation Bulletin 246, 99-162.

Hoatson, D.M. & Blake, D.H., 2000. Chapter 15. Summary of conclusions and suggestions for further studies. In: Hoatson, D.M. & Blake D.H. (editors), Geology and economic potential of the Palaeoproterozoic layered mafic–ultramafic intrusions in the East Kimberley, Western Australia. Australian Geological Survey Organisation Bulletin 246, 312–317.

Hoatson, D.M., Blake, D.H., Mory, A.J., Tyler, I.M., Pittavino, M., Allen, B.K. & Kamprad, J., 1997. Bungle Bungle Range, Purnululu National Park, East Kimberley, Western Australia: a guide to the rocks, landforms, plants, animals, and human impact. Australian Geological Survey Organisation, Canberra, 83 pp.

Orth, K., 1997. Notes on the geology of the Koongie Park Formation southwest of Halls Creek, Western Australia. Australian Geological Survey Organisation, Record 1997/25.

Shaw, R.D., Blake, D.H., Warren, R.G., Sun, S-s. & Young D.N., 1992. Geological investigations in the Kimberley-Arunta region. BMR Research Newsletter, 16, 10–11.

Shaw, R.D., Blake, D.H., Hoatson, D.M., Warren, R.G., Page, R.W. & Macias, L.F., 1995. Project 211.12 Kimberley-Arunta (NGMA project). AGSO 94, 70–72.

Sheppard, S., 1996. Mafic-felsic magma mingling in the Bow River batholith of the Halls Creek Orogen. Geological Survey of Western Australia, 1995–96 Annual Review, 56–60.

Trudu, A. & Hoatson, D.M., 1996. Depths of emplacement of Precambrian layered intrusions in the East Kimberley. AGSO Research Newsletter, 25, 10–12.

Trudu, A.G. & Hoatson. D.M., 2000. Chapter 9. Depths of emplacement of the mafic-ultramafic intrusions. In: Hoatson, D.M. & Blake D.H. (editors), Geology and economic potential of the Palaeoproterozoic layered mafic–ultramafic intrusions in the East Kimberley, Western Australia. Australian Geological Survey Organisation Bulletin 246, 201–219.

Tyler, I.M. & Page, R.W., 1996. Palaeoproterozoic deformation, metamorphism and igneous intrusion in the central zone of the Lamboo Complex, Halls Creek Orogen. Geological Society of Australia, Abstracts, 41, 13th Australian Geological Convention, Canberra, 19-23 February, 450.

Warren, R.G., 1992. District surrounding the Armanda Sill, Halls Creek Inlier, Western Australia. Australian Geological Survey Organisation, Record 1992/70, 16 pp.

Warren, R.G., 1994. Landscape evolution in the East Kimberley region, Western Australia. AGSO Research Newsletter, 20, 14–16.

Warren, R.G., 1997. Reconnaissance geological mapping in Dixon, SE McIntosh and northernmost Halls Creek 1:100 000 Sheet areas, East Kimberley, W.A. 1992-3. Australian Geological Survey Organisation, Record 1997/26, 54 pp.

Witt, W.K. & Sanders, T., 1996. Magmatic-hydrothermal breccia dykes and hydrothermal alteration in the McHale Granodiorite, Halls Creek Orogen: a possible porphyry

system. Geological Survey of Western Australia, Annual Review 1994-95, 104–110.

Wyborn, L.A.I. & Blake, D.H., 2000. Chapter 10. Comments on relationships of mafic and felsic magmatism. In: Hoatson, D.M. & Blake D.H. (editors), Geology and economic potential of the Palaeoproterozoic layered mafic–ultramafic intrusions in the East Kimberley, Western Australia. Australian Geological Survey Organisation Bulletin 246, 220–225.

Structure and tectonics

Griffin, T.J., Sheppard, S. & Tyler, I.M. 1994. Geochemical constraints on the tectonic evolution of the Early Proterozoic orogens in the Kimberley region of Western Australia. Abstracts, 37, 12th Australian Geological Convention, Perth, 26-30 September, 151–152.

Griffin, T.J., Page, R.W., Sheppard, S., Thorne, A.M. & Tyler, I.M., 1995. Tectonics of a Palaeoproterozoic collision in the Kimberley region of Western Australia. Precambrian '95 Abstracts - International Conference on Tectonics and Metallogeny of Early/Mid Precambrian Orogenic Belts, Montreal, 27.

Myers, J.S., Shaw, R.D. & Tyler, I.M., 1996. Tectonic evolution of Proterozoic Australia. Tectonics, 15, 1431–1446.

Shaw, R.D., Sexton, M.J. & Zeilinger, I., 1994. The tectonic framework of the Canning Basin, W.A., including the 1:2 million structural elements map of the Canning Basin. Australian Geological Survey Organisation, Record 1994/48.

Shaw, R.D., Wellman, P., Whitaker, A.J., Tarlowski, C. & Morse, M.P. 1994. Implications of the basement tectonic elements map of Australia for reconstructions of Proto-Gondwanaland. Abstracts, 37, 12th Australian Geological Convention, Perth, 26-30 September, 401.

Shaw, R.D., Wellman, P., Gunn, P., Whitaker, A.J., Tarlowski, C. & Morse, M.P., 1995. 'Australian Crustal Elements' map: a geophysical model for the tectonic framework of the continent. AGSO Research Newsletter, 23, 1–3.

Shaw, R.D., Wellman, P., Gunn, P., Whitaker, A.J., Tarlowski, C. & Morse, M.P., 1996. Guide to using the Australian Crustal Elements map. Australian Geological Survey Organisation, Record 1996/30, 49 pp.

Sheppard, S., Griffin, T.J. & Tyler, I.M., 1997. The tectonic setting of granites in the Halls Creek and King Leopold Orogens, northwest Australia. In: Rutland, R.W.R. & Drummond, B.J. (editors), Palaeoproterozoic tectonics and metallogenesis: comparative analysis of parts of the Australian & Fennoscandian shields. Workshop, Darwin, September, 14-22, 1997. Australian Geological Survey Organisation, Record 1997/44, 107–109.

Sheppard, S., Tyler, I.M., Griffin, T.J. & Taylor, W.R., 1999. Palaeoproterozoic subduction-related and passive margin basalts in the Halls Creek Orogen, northwest Australia. Australian Journal of Earth Sciences, 46, 679–690.

Thorne, A.M. & Tyler, I.M., 1996. Mesoproterozoic and Phanerozoic sedimentary basins in the northern Halls Creek Orogen: constraints on the timing of strike-slip movement on the Halls Creek Fault system. Geological Survey of Western Australia, Annual Review 1995-96, 156–168.

Tyler, I.M. & Griffin, T.J., 1994. The Yampi Orogeny in the Kimberley region of Western Australia: an intracratonic response to the assembly of proto-Gondwanaland. Abstracts, 37, 12th Australian Geological Convention, Perth, 26-30 September, 436.

Tyler, I.M., Griffin, T.J., Page, R.W. & Shaw, R.D., 1994. The Halls Creek fault-zone: repeated reactivation of a major north Australian tectonic boundary. Geological Society of Australia, Abstracts, 36, 167–168.

Tyler, I.M., Griffin, T.J., Page, R.W. & Shaw, R.D., 1995. Are there terranes within the Lamboo Complex of the Halls Creek Orogen? Geological Survey of Western Australia, Annual Review 1993-94, 37–46.

Tyler, I.M., Page, R.W. & Griffin, T.J., 1999. Depositional age and provenance of the Marboo Formation from SHRIMP U-Pb zircon geochronology: Implications for the early Palaeoproterozoic tectonic evolution of the Kimberley region, Western Australia. Precambrian Research, 95, 225–243.

Warren, R.G., 1994. Role of early extensional faults in the Grants Patch district, East Kimberley, Western Australia. Geological Society of Australia, Abstracts, 37, 12th Australian Geological Convention, Perth, 26-30 September, 453–454.

NOTES

NOTES

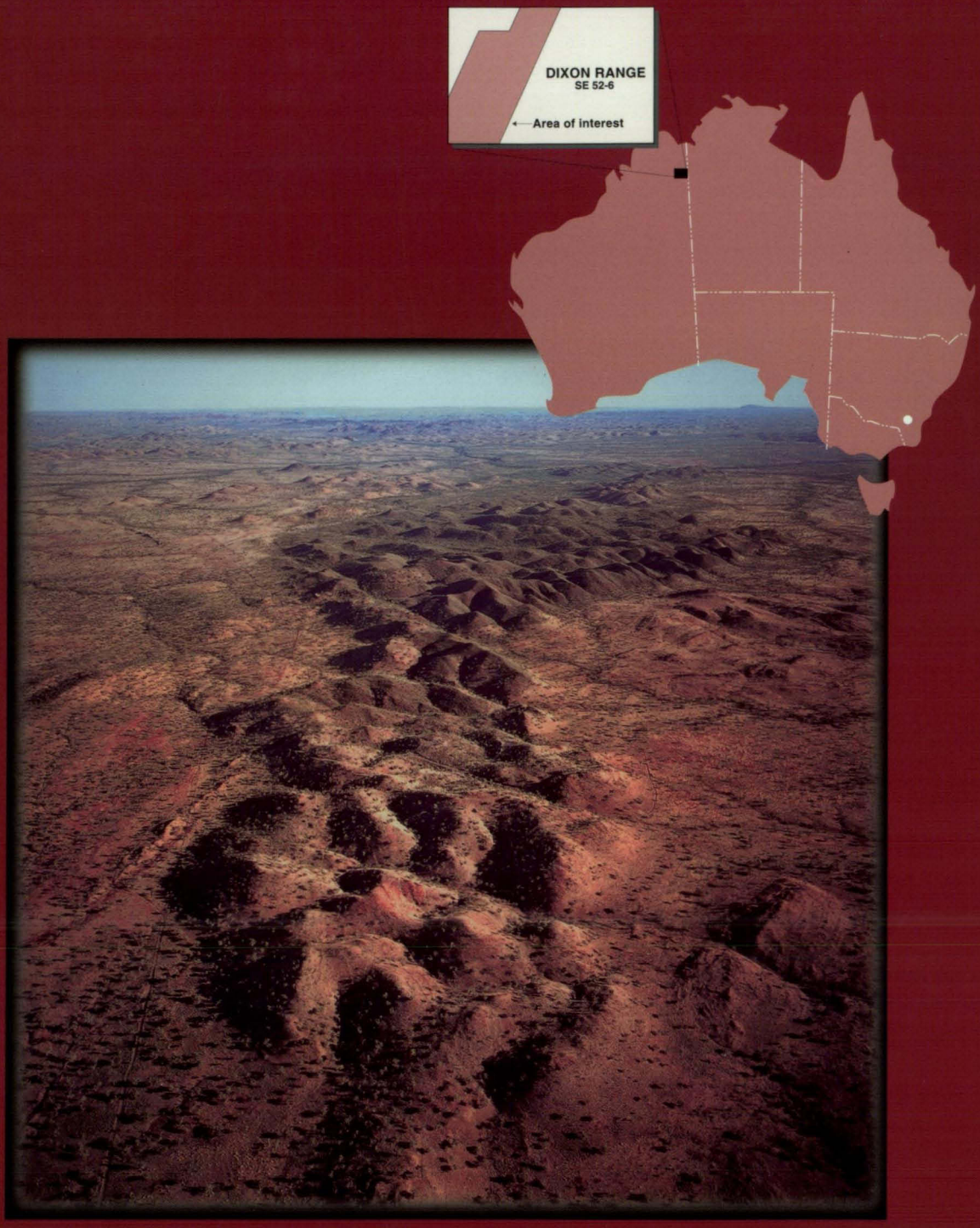
NOTES

NOTES

NOTES

NOTES

NOTES



The Palaeoproterozoic layered mafic–ultramafic intrusions in the Halls Creek Orogen of the East Kimberley, Western Australia, represent one of the most extensively mineralised igneous associations of their type in Australia. They contain a range of magmatic and hydrothermal deposits of platinum-group elements, chromium, nickel, copper, cobalt, titanium, vanadium, iron, and gold.

This *Bulletin* presents the results of a collaborative AGSO/GSWA/Monash University/minerals industry study of the geology and mineral potential of these intrusions. It is an essential reference for those involved in the exploration of layered mafic–ultramafic intrusions, the geology of the Halls Creek Orogen and its environs, or the study of Precambrian orogenic terranes.